DESIGN, SYNTHESIS, AND BIOLOGICAL EVALUATION OF $GABA_AR$ SUBTYPE SELECTIVE (α6, α2/3, AND α5) LIGANDS TO TREAT MIGRAINE, NEUROPATHIC PAIN, TRIGEMINAL PAIN, TOURETTE SYNDROME, EPILEPSY, ANXIETY AND COGNITIVE DISORDERS AS WELL AS ASTHMA

by

Dishary Sharmin

A Dissertation Submitted in

Partial Fulfillment of the

Requirements for the Degree of

Doctor of Philosophy

in Chemistry

at

The University of Wisconsin-Milwaukee

December 2023

ABSTRACT

DESIGN, SYNTHESIS, AND BIOLOGICAL EVALUATION OF $GABA_AR$ SUBTYPE SELECTIVE (α6, α2/3, AND α5) LIGANDS TO TREAT MIGRAINE, NEUROPATHIC PAIN, TRIGEMINAL PAIN, TOURETTE SYNDROME, EPILEPSY, ANXIETY AND COGNITIVE DISORDERS AS WELL AS ASTHMA

by

Dishary Sharmin

The University of Wisconsin-Milwaukee, 2023
Under the Supervision of Professor James M. Cook

Part I: Development of α6-$GABA_AR$ Subtype-Selective Pyrazoloquinolinones for Treating Tourette Syndrome, Migraine, and Trigeminal Pain

The α6β2/3γ2 $GABA_AR$ selective ligands have the potential for treating trigeminal orofacial pain and neuropsychiatric disorders with sensori-motor gating deficits. The positive allosteric modulators (PAMs) specifically targeting α6$GABA_ARs$ hold promise as effective interventions for treating essential tremor (ET). A number of α6β2/3γ2 $GABA_AR$ selective pyrazoloquinolinones were synthesized and extensively studied. The deuterated pyrazoloquinolinone **DK-I-56-1** emerged as the lead compound with significantly improved pharmacokinetics. Importantly, the ligands modulated diazepam-insensitive α6β2/3γ2 $GABA_ARs$, displaying no sedation and were not cytotoxic. **PZ-II-029 and DK-I-56-1** demonstrate the ability to mitigate the motor-impairing effects caused by diazepam**.** These effects were moderately mitigated by **DS-I-78.** The α6$GABA_AR$-selective PAMs **DK-I-56-1, PZ-II-029,** and **LAU 463** significantly attenuated action tremor and restored physical well-being in a mouse model mimicking ET by acting in the cerebellum.

Part-II: The Development of a Scalable Synthesis, and Assessment of Bioactivity of Imidazodiazepines Targeting α2/3-$GABA_AR$ Subtypes for the Treatment of Epilepsy, Anxiety, and Neuropathic Pain

KRM-II-81 is an imidazodiazepine that acts as a potentiator for $GABA_A$ receptors. It is currently in preparation for clinical development, showing potential for targeted modulation of receptor activity. It demonstrates widespread effectiveness in preventing seizures and is associated with minimal sedative effects. We outlined an innovative, revised, and refined synthetic pathway for **KRM-II-81** suitable for the large-scale production of kilogram quantities of the compound. The recent biological and chemical findings represent crucial advancements in the progress of **KRM-II-81** for individuals facing treatment-resistant epilepsy. These developments offer hope for improving the condition of patients who have not responded well to conventional treatments. A brominated analog, **DS-II-73** , was synthesized and pharmacologically characterized as a potential back-up compound as KRM-II-81 moves forward into development. The synthesis from 2-amino-5-bromophenyl)(pyridin-2yl)methanone was processed in five steps with an overall yield of 38% and without the need for a palladium catalyst. $GABA_AR$ binding occurred with a *Ki* of 150 nM and only 3 of 41 screened binding sites produced inhibition > 50% at 10 mM and the potency to induce cytotoxicity was > 240 mM. DS-II-73 was selective for α2/3/5- over that of a1-containing $GABA_ARs$. Oral exposure of plasma and brain of rats was more than sufficient to functionally impact $GABA_ARs$. Tonic convulsions in mice and lethality induced by pentylenetetrazol were suppressed by **DS-II-73** after oral administration and latencies to clonic and tonic seizures were prolonged. Cortical slice preparations from a patient with pharmacoresistant epilepsy (mesial temporal lobe) showed decreases in the frequency of local field potentials by **DS-II-73**. As with **KRM-II-81**, the

sedative liabilities of **DS-II-73** were low compared to diazepam. Molecular docking studies of **DS-II-73** with the α1β3γ2L configured $GABA_AR$ showed low interaction with a1His102 that is suggested as a potential molecular mechanism for its low sedative side effects. These findings support the viability of **DS-II-73** as a back-up molecule for its ethynyl analog, KRM-II-81, with the human tissue data providing translational credibility.

Part-III: The Design and Synthesis of Chiral α5 Subtype BzR/$GABA_AR$ Modulators for Treating Anxiety, Depression, and Schizophrenia as well as Asthma

Gamma (γ)-amino butyric acid is a natural neurotransmitter with inhibitory functions in the brain. Benzodiazepines bind to specific subunits of GABA receptors, influencing brain activities. Different subunits contribute to various effects like sedation, anxiolysis, and cognition. Dysfunctional GABA receptors relate to CNS disorders. The search for improved treatments for anxiety, depression, and cognitive issues is vital. A series of α5-preferring ligands, including GL-II-73, were synthesized to address these needs. **GL-II-73** showed promise in anxiolytic, antidepressant, and cognitive effects. A scalable synthesis method was developed and synthesized more than 40 grams for evaluation. Further studies are ongoing by DAMONA PHARMACEUTICALS to move this ligand toward the clinic for depression and potentially Alzheimer's disease. The α5-$GABA_AR$ subtype selective ligand **MP-III-022**, a monomethyl amide, is active in low doses in several psychiatric disorders including autism, antipsychotic activity, and cognitive disorders. **MP-III-022** resulted in a reduction in slow wave power in mice with Angelman syndrome. Due to the results obtained with **GL-II-73** and **MP-III-022** in animal models, several analogs were synthesized to extend the structure–activity relationship and

screened for pro-cognitive efficacy in Y-maze assay. GL-II-73 is the best ligand till date for this project.

The α5-selective ligand MIDD0301 (GL-II-93) is currently in development by PANTHERICS for asthma treatment. Notably, this lead compound, **MIDD0301**, demonstrates relaxation effects on human, guinea pig, and mouse airway smooth muscle (ASM) in *ex vivo* studies. The imine migrated MIDD0301 known as **MYM-III-100** showed better activity in guinea pig airway smooth muscle (ASM) *ex vivo* studies. Several analogs were synthesized based on the structures of **MIDD0301**, **MYM-III-100**, and evaluated on ASM assay. Several analogs including **DS-II-67** showed better ASM relaxation profiles than MIDD0301 in the *ex vivo* ASM relaxation assay. The recently developed ligands need additional testing to fully characterize their profiles and assess whether they hold advantages over MIDD0301 for treating asthma. Further evaluation is necessary to determine their potential efficacy and safety in comparison to the established lead compound.

To

Allah (the Creator)

To

My mother Halima Kabir

TABLE OF CONTENTS

LIST OF FIGURES……..xx

LIST OF TABLES……xIviii

LIST OF SCHEMES……..……Ii

LIST OF ABBREVIATIONS……Iiv

ACKNOWLEDGEMENTS…….Iviii

Chapter 1. Introduction……1

1.1.The $GABA_A$ receptors……...1

1.2.Benzodiazepines……8

1.3.The pharmacology of $GABA_AR$ associated with different subunits…….…..10

1.4.Molecular modeling…….18

1.5.Research Objectives…….35

Chapter 2. Development of α6-GABAAR Subtype-Selective Pyrazoloquinolinones for Treating Tourette Syndrome, Migraine, and Trigeminal Pain……...36

2.1. Introduction…….36

2.2. Chemistry……41

2.3. Biology of α6 subtype selective pyrazoquinolinones ……50

2.3.1. PZ-II-029 (i.p.) mitigated tremor and reinstated burrowing activity in harmaline treated mice with Dr Huang, Ming Tatt Lee, Dr LC Chiou, and colleagues [116]……50

2.3.2. The administration of furosemide (intracerebellar, i.cb.) counteracted the effects of PZ-II-029 (i.p.) on both tremor and burrowing activities in mice treated with harmaline with Huang, Dr Ming Tatt Lee, Dr LC Chiou, and colleagues[116] ……56

2.3.3. Analogues and deuterated derivatives of PZ-II-029 exhibited comparable anti-tremor and burrowing-restorative effects in mice subjected to harmaline treatment with Huang, Dr Ming Tatt Lee, Dr LC Chiou, and colleagues…….59

2.3.4. PZ-II-026 analogues exert a complete flumazenil-like preventative effect on diazepam-induced incapatication in the rotarod with Brianka, Dr Miroslav Savic, and colleagues (Unpublished data)…….60

2.3.5. Effects of DK-I-56-1 on Frequency-Rate Intracranial Self-Stimulation in Rats (NIH, Unpublished data)……..62

2.4. Methods……..68

2.4.1. Intra-cerebellar (i.cb), intraperitoneal (i.p.) and subcutaneous (s.c.) injections …….68

2.4.2. Tremor induction and measurement……68

2.4.3. Burrowing activity assessment……....69

2.4.4. Statistical analysis……71

2.4.5. Method to evaluate the effect of DK-I-56-1 on frequency-rate intracranial self-stimulation in Rats (NIH)……..71

2.5. Experimental……...76

2.5.1. General……76

2.5.2. Ethyl 7-methoxy-4-oxo-1,4-dihydroquinoline-3-carboxylate (14) …….77

2.5.3. Ethyl 7-bromo-4-oxo-1,4-dihydroquinoline-3-carboxylate (15)…….77

2.5.4. Ethyl 6-bromo-8-fluoro-4-oxo-1,4-dihydroquinoline-3-carboxylate (16)…….78

2.5.5. Ethyl 6-bromo-4-oxo-1,4-dihydroquinoline-3-carboxylate (17)…….79

2.5.6. Ethyl 6-fluoro-4-oxo-1,4-dihydroquinoline-3-carboxylate (18)……..80

2.5.7. Ethyl 6-fluoro-4-oxo-1,4-dihydroquinoline-3-carboxylate (19)……..81

2.5.8. Ethyl 4-chloro-7-methoxyquinoline-3-carboxylate (20)……..81

2.5.9. Ethyl 4-chloro-7-bromoquinoline-3-carboxylate (21)…….83

2.5.10. Ethyl 6-bromo-4-chloro-8-fluoroquinoline-3-carboxylate (22)……84

2.5.11. Ethyl 6-bromo-4-chloro-1,4-dihydroquinoline-3-carboxylate (23)……...85

2.5.12. Ethyl 6-fluoro-4-chloro-1,4-dihydroquinoline-3-carboxylate (24)……86

2.5.13. Ethyl 7-fluoro-4-chloro-1,4-dihydroquinoline-3-carboxylate (24)……87

2.5.14. 7-Methoxy-2-(4-methoxyphenyl)-2,5-dihydro-3H-pyrazolo[4,3-c]quinolin-3-one (PZ-II-029, 3)……..89

2.5.15. 7-Methoxy-2-(4-methoxyphenyl)-2,5-dihydro-3H-pyrazolo[4,3-c]quinolin-3-one (LAU 463, 6)……90

2.5.16. 8-Chloro-2-(3-methoxyphenyl)-2,5-dihydro-3H-pyrazolo[4,3-c]quinolin-3-one (LAU 159, 5)……91

2.5.17. 7-methoxy-6-methyl-2-(4-(trifluoromethoxy)phenyl)-2,5-dihydro-3H-pyrazolo[4,3-c]quinolin-3-one (CW-02-79, 32)…….92

2.5.18. 8-Bromo-2-(4-methoxyphenyl)-2,5-dihydro-3H-pyrazolo[4,3-c]quinolin-3-one (DS-I-78, 33)…….93

2.5.19. 7-fluoro-2-(4-methoxyphenyl)-2,5-dihydro-3H-pyrazolo[4,3-c]quinolin-3-one (DS-I-84, 34)……..94

2.5.20. 8-Fluoro-2-(4-methoxyphenyl)-2,5-dihydro-3H-pyrazolo[4,3-c]quinolin-3-one (DS-I-83, 35)……..95

2.5.21. 8-Bromo-6-fluoro-2-(4-methoxyphenyl)-2,5-dihydro-3H-pyrazolo[4,3-c]quinolin-3-one (MM-I-03, 36)……..96

2.5.22. 7-Bromo-2-(2-methoxyphenyl)-2,5-dihydro-3H-pyrazolo[4,3-c]quinolin-3-one (DS-II-04, 37)……97

2.5.23. 7-Bromo-2-(3-methoxyphenyl)-2,5-dihydro-3H-pyrazolo[4,3-c]quinolin-3-onene (DS-II-05, 38)……..98

2.5.24. 7-Methoxy-2-(2-methoxyphenyl)-2,5-dihydro-3H-pyrazolo[4,3-c]quinolin-3-one (DS-II-08, 39)…….99

2.5.25. 8-Chloro-2-(2-methoxyphenyl)-2,5-dihydro-3H-pyrazolo[4,3-c]quinolin-3-one (DS-I-97, 41)……100

2.5.26. 4-Methoxy-d3-phenylhydrazine (43)……..101

2.5.27. 7-Methoxy-2-(4-methoxy-d3-phenyl)-2,5-dihydro-3H-pyrazolo[4,3-c]quinoline-3-one (DK-I-56-1, 44)……103

Chapter 3. The Development of a Scalable Synthesis, and Assessment of Bioactivity of Imidazodiazepines Targeting α2/3-GABAAR Subtypes for the Treatment of Epilepsy, Anxiety, and Neuropathic Pain……104

3.1 Introduction ……..…….104

3.2 Chemistry…….. ……121

3.2.1. Synthesis of KRM-II-81……..121

3.2.2. Synthesis of DS-II-73, a brominated analog of KRM-II-81 ……..…….140

3.2.3. Synthesis of MP-III-080 (1, 2, 4-oxadizole bioisostere of HZ-166)……142

3.2.4. Synthesis of MP-III-24 and DS-II-27……..……...143

3.2.5. Synthesis of salt analogs of Hz-166…….144

3.3. Biological studies of α2/3-selective imidazodiazepines: Results and discussions ……..……145

3.3.1. Biological studies of KRM-II-81.....145

3.3.1.2. Motor impairment effects of KRM-II-81 and MP-III-080 (Inverted screen test, A. Biggerstaff, J.M. Witkin and others).....148

3.3.1.3. Effects of KRM-II-81 and MP-III-080 on acute and chronic neuropathic pain (Paclitaxel induced pain, A. Biggerstaff, J.M. Witkin and others).....148

3.3.1.4. Effects of KRM-II-81 (p.o., bid) on the cumulative handling-induced seizure burden in mice inoculated with TMEV (with Jeff Witkin, Rok Cerne, and others).....154

3.3.1.5. Effects of KRM-II-81 Dravet syndrome (with Dr Kyoshi, ETSP, and others)…….158

3.3.2. Biological studies of DS-II-73……..166

3.3.3. Biological studies of MP-III-024 (18).....176

3.4. Methods ……187

3.4.1. *In vivo* studies……187

3.4.2. Receptor binding studies with PDSP program (Dr Bryan Roth)……...190

3.4.3. Electrophysiology studies with Dr Jeffrey M Witkin and coworkers …….190

3.4.5. Theiler's murine encephalomyelitis virus (TMEV) model handling-induced seizures with Dr Jeffrey M Witkin and coworkers ……190

3.4.6. Experimental procedures for Harmaline-Induced Tremor and Locomotor Activity Analysis with Dr Kuter, Barbara, and others……..195

3.4.7. Synergistic antihyperalgesic and antinociceptive effects of morphine and MP-III-024 with Atiqur Rahman, Dr Fisher, and others…….....201

3.5. Experimental…….205

3.5.1. General……..205

3.5.2. N-(4-Bromo-2-picolinoylphenyl)-2-chloroacetamide (10)……205

3.5.3.7-Bromo-5-(pyridin-2-yl)-1,3-dihydro-2H-benzo[e][1,4]diazepin-2-one (6)……206

3.5.4. Ethyl 8-bromo-6-(pyridin-2-yl)-4H-benzo[f]imidazo[1,5-a][1,4]diazepine-3-carboxylate (7)……..208

3.5.5. Ethyl 6-(pyridin-2-yl)-8-((triisopropylsilyl)ethynyl) 4H benzo[f]imidazo[1,5a][1,4] diazepine-3-carboxylate (8)……210

3.5.6. Ethyl-6-(pyridin-2-yl)-8-((trimethylsilyl)ethynyl)-4H-benzo[f] imidazo[1,5a]-[1,4]dia zepine-3-carboxylate (7a)……212

3.5.7. Ethyl 8-ethynyl-6-(pyridin-2-yl)-4H-benzo[f]imidazo[1,5-a][1,4]diazepine-3-carboxylate (Hz-166, 1)……213

3.5.8. 8-Ethynyl-6-(pyridin-2-yl)-4H-benzo[f]imidazo[1,5-a][1,4] diazepine-3-carbaldehyde (9)……..214

3.5.9. 5-(8-Ethynyl-6-(pyridin-2-yl)-4H-benzo[f]imidazo[1,5-a][1,4] diazepin-3-yl)oxazole (KRM-II-81, 3)…….216

3.5.10. 8-bromo-6-(pyridin-2-yl)-4H-benzo[f]imidazo[1,5-a][1,4]diazepine-3-carbaldehyde (17)…….217

3.5.11. 5-(8-Bromo-6-(pyridin-2-yl)-4H-benzo[f]imidazo[1,5-a][1,4]diazepin-3-yl)oxazole (DS-II-73, 16)……..218

3.5.12. Methyl 8-ethynyl-6-(pyridin-2-yl)-4H-benzo[f]imidazo[1,5-a][1,4]diazepine-3-carboxylate (MP-III-024,18)…….……..220

3.5.13. 2-(8-ethynyl-3-(oxazol-5-yl)-4H-benzo[f]imidazo[1,5-a][1,4]diazepin-6-yl)pyridin-1-ium chloride (MYM-V-26, KRM-II-81.HCl, 20)……..221

3.5.14. 2-(3-(Ethoxycarbonyl)-8-ethynyl-4H-benzo[f]imidazo[1,5-a][1,4]diazepin-6-yl)pyridin-1-ium hydrochloride (DS-II-47, 21)……222

3.5.15.2-(8-Ethynyl-3-(methoxycarbonyl)-4H-benzo[f]imidazo[1,5-a][1,4]diazepin-6-yl)pyridin-1-ium chloride (DS-II-48, 22)……223

Chapter 4. The Design and Synthesis of Chiral α5 Subtype BzR/GABAAR Modulators for Treating Anxiety, Depression, and Schizophrenia as well as Asthma……..224

4.1 Introduction and background…..……...224

4.2. Chemistry: Results and Discussion……..239

4.2.1. Improved scalable synthesis of SH-053-2'F-*R*-CH_3 and SH-053-2'F-*S*-CH_3 ……239

4.2.2. Synthesis of GL-II-73…….254

4.2.3. Synthesis of analogs of GL-II-73……257

4.3.Results and Discussion: Biological Activity……..268

4.3.1. Systemic administration of selective α5-PAM, MP-III-022, reverses hippocampal activity impairments in AAV-AD rats by S.M Perez, Daniel Lodge and colleagues…….268

4.3.2. Systemic administration of the selective α5-PAM, MP-III-022, effectively reverses the aberrant dopamine system function observed in AAV-AD rats by S.M Perez, Daniel Lodge and colleagues…….269

4.3.3. AAV-AD Rats Exhibit Intact Cognitive Function but Selective Impairment in Dopamine-Dependent Behavior, Reversed by Systemic Administration of the Selective α5-PAM, MP-III-022 by S.M Perez, Daniel Lodge and colleagues……271

4.3.4. Reduction of Parvalbumin-Positive Interneurons in AAV-AD Rats by MP-III-022 with S.M Perez, Daniel Lodge and colleagues……273

4.3.5. Significant amelioration of social impairments in VPA animals achieved by MP-III-022 with Anja Santrac, Dr Miroslav Savic, and colleagues……..275

4.3.6. MP-III-022 demonstrated efficacy in ameliorating hyperactivity and repetitive behavior, with notable effects observed particularly in male VPA animals with Anja Santrac, Dr Miroslav Savic, and colleagues……277

4.3.7. The efficacy of MP-III-022 was demonstrated in enhancing cognitive flexibility in male VPA animals with Anja Santrac, Dr Miroslav Savic, and colleagues…….279

4.3.8. Neurons affected by VPA exhibited compromised GABA-switch functionality and altered spontaneous neuronal activity, both of which were restored to normal levels following treatment with MP-III-022 with Anja Santrac, Dr Miroslav Savic, and colleagues…….282

4.3.9. The impact of MP-022 on the expression of GABRA5, NKCC1, and KCC2 genes exhibited variations depending on both the sex and prenatal administration conditions with Anja Santrac, Dr Miroslav Savic, and colleagues……...……284

4.3.10. 4.3.10. In 5xFAD mice, both MP-III-022 and PWZ-029 were observed to negatively affect social recognition and social interaction, respectively with Jovana Abandelovic, Dr Miroslav M Savic, and colleagues……..……286

4.3.11. Treatment with MP-III-022 was found to hinder procedural learning specifically in transgenic females with Arandelovic, Dr Miroslav M Savic, and colleagues…….288

4.3.12. Effects of MP-III-022 on Angelman syndrome with Dr Kyoshi, and colleagues (Unpublished data)……..292

4.4.Methods……317

4.5.Experimental section…….333

4.5.1. General…….333

4.5.2. *Tert*-Butyl-(*R*)-(1-((4-bromo-2-(2-fluorobenzoyl)phenyl)amino)-1-oxopropan-2-yl) carbamate (3)……...…334

4.5.3. *N*-Carboxy-D-Alanine Anhydride (14)…….335

4.5.4. (*R*)-7-Bromo-5-(2-fluorophenyl)-3-methyl-1,3-dihydro-2*H*-benzo[*e*][1,4]diazepin-2-one (4)…….337

4.5.5. Ethyl (*R*)-8-bromo-6-(2-fluorophenyl)-4-methyl-4*H*-benzo[*f*]imidazo[1,5-*a*][1,4] diazepine-3-carboxylate (5)…….340

4.5.6. Ethyl (*R*)-6-(2-fluorophenyl)-4-methyl-8-((triisopropylsilyl)ethynyl)-4*H*-benzo[*f*] imidazo[1,5-*a*][1,4]diazepine-3-carboxylate (6)……342

4.5.7. Ethyl (*R*)-8-ethynyl-6-(2-fluorophenyl)-4-methyl-4*H*-benzo[*f*]imidazo[1,5-*a*][1,4] diazepine-3-carboxylate (SH-053-2'F-*R*-CH_3, 7)……....344

4.5.8. *Tert*-Butyl (*S*)-(1-((4-bromo-2-(2-fluorobenzoyl)phenyl)amino)-1-oxopropan-2-yl) carbamate (9)……345

4.5.9. (*S*)-7-Bromo-5-(2-fluorophenyl)-3-methyl-1,3-dihydro-2*H*-benzo[*e*][1,4]diazepin-2-one (10)……..347

4.5.10. Ethyl (*S*)-8-bromo-6-(2-fluorophenyl)-4-methyl-4*H*-benzo[*f*]imidazo[1,5-*a*][1,4] diazepine-3-carboxylate (11)……348

4.5.11. Ethyl(S)-6-(2-fluorophenyl)-4-methyl-8-((triisopropylsilyl)ethynyl)-4Hbenzo[f] imidazo [1,5-a][1,4]diazepine-3-carboxylate (12)…….350

4.5.12. Ethyl (*S*)-8-ethynyl-6-(2-fluorophenyl)-4-methyl-4*H*-benzo[*f*]imidazo[1,5-*a*][1,4] diazepine-3-carboxylate (SH-053-2'F-*S*-CH_3, 13)……351

4.5.13. (*R*)-8-ethynyl-6-(2-fluorophenyl)-4-methyl-4H-benzo[f]imidazo[1,5-a][1,4]diazepine-3-carboxylic acid (15)…….353

4.5.14. *(R*)-8-Ethynyl-6-(2-fluorophenyl)-*N*,*N*,4-trimethyl-4*H*-benzo[*f*]imidazo[1,5 *a*][1,4]diazepine-3-carboxamide [GL-II-73,16]…….354

4.5.15. *(R)*-8-ethynyl-6-(2-fluorophenyl)-N,4-dimethyl-4H-benzo[f]imidazo[1,5-a][1,4] diazepine-3-carboxamide [MP-III-022,17]…….357

4.5.16. *Tert*-butyl-(*R*)-(1-((4-bromo-2-picolinoylphenyl)amino)-1-oxopropan-2-yl)carbamate (19)…….359

4.5.17. (*R*)-7-bromo-3-methyl-5-(pyridin-2-yl)-1,3-dihydro-2H-benzo[e][1,4]diazepin-2-one (20)…….360

4.5.18. Ethyl (*R*)-8-bromo-4-methyl-6-(pyridin-2'-yl)-4H-benzo[f]imidazo[1,5-a][1,4] diazepine-3-carboxylate(21)…….362

4.5.19. Ethyl (R)-4-methyl-6-(pyridin-2-yl)-8-((triisopropylsilyl)ethynyl)-4H-benzo[f] imidazo[1,5-a][1,4]diazepine-3-carboxylate (22)……363

4.5.20. Ethyl (S)-8-ethynyl-4-methyl-6-(pyridin-2-yl)-4H-benzo[f]imidazo [1,5-a][1,4] diazepine-3-carboxylate(23)……....365

4.5.21. (*R*)-8-Ethynyl-4-methyl-6-(pyridin-2-yl)-4H-benzo[f]imidazo[1,5-a][1,4]diazepine-3-carboxylic acid (24)…….366

4.5.22. (*R*)-8-Ethynyl-N,N,4-trimethyl-6-(pyridin-2-yl)-4H-benzo[f]imidazo[1,5-a][1,4] diazepine-3-carboxamide (25)……367

4.5.23. (*R*)-8-Ethynyl-N,N,4-trimethyl-6-(pyridin-2-yl)-4H-benzo[f]imidazo[1,5-a][1,4] diazepine-3-carboxamide (26)…….369

4.5.24. Ethyl (*R*)-6-(2'-fluorophenyl)-4-methyl-8-methyl-4H-benzo[f]imidazo[1,5-a][1,4] diazepine-3-carboxylate (27)……...370

4.5.25. Ethyl (*R*)-6-(2'-fluorophenyl)-4-methyl-8-methyl-4H-benzo[f]imidazo[1,5-a][1,4] diazepine-3-carboxylic acid (28)……372

4.5.26. Ethyl (*R*)-6-(2'-fluorophenyl)-4-methyl-8-methyl-4H-benzo[f]imidazo[1,5-a][1,4] diazepine-3-carboxylic acid (28)……..…373

4.5.27. (*R*)-8-bromo-6-(2'-fluorophenyl)-4-methyl-4H-benzo[f]imidazo[1,5-a][1,4]diazepine-3-carboxylic acid (29)……375

4.5.28. *(R)*-8-Bromo-6-(2-fluorophenyl)-*N*,*N*,4-trimethyl-4*H*-benzo[*f*]imidazo[1,5][1,4] diazepine-3-carboxamide [DS-III-97, 31]……376

4.5.29. *(R)-N*-ethyl-8-ethynyl-6-(2-fluorophenyl)-N,4-dimethyl-4H-benzo[f]imidazo[1,5-a][1,4]diazepine-3-carboxamide (DS-I-49, 32)…….378

4.5.30. (*R*)-5-(8-ethynyl-6-(2-fluorophenyl)-4-methyl-4*H*-benzo[*f*]imidazo[1,5-*a*][1,4]diazepin-3-yl)-3-methyl-1,2,4-oxadiazole (34)……380

4.5.31. (*R*)-5-(8-ethynyl-6-(2-fluorophenyl)-4-methyl-4*H*-benzo[*f*]imidazo[1,5-*a*][1,4]diazepin-3-yl)-3-methyl-1,2,4-oxadiazole (DS-IV-41, 35)……..381

4.5.32. 8-Ethynyl-6-(2-fluorophenyl)-4-methyl-3-(3-methyl-1H-1,2,4-triazol-5-yl)-4H-benzo[f]imidazo[1,5-a][1,4]diazepine (DS-III-69, 36)…….382

4.6.α5 Subtype $GABA_AR$ Modulators and Asthma……..384

4.6.1. Introduction……384

4.6.2. Chemistry……392

4.6.3. Evaluation of ex vivo ASM relaxation of analogs of MIDD0301 with Dr Charles Emala, Gene T. Yocum, and coworkers (unpublished data)……..393

4.6.4. Methods and Experimental……397

4.6.4.1. Relaxation of *ex vivo* airway smooth muscle with Dr Charles Emala, Gene Yocum and coworkers…….397

4.6.4.2. (*R*)-8-Ethynyl-4-methyl-6-(pyridin-2-yl)-4H-benzo[f]imidazo[1,5-a][1,4]diazepine-3-carboxylic acid (24)…….398

4.6.4.3. Ethyl (*R*)-6-(2'-fluorophenyl)-4-methyl-8-methyl-4H-benzo[f]imidazo[1,5-a][1,4] diazepine-3-carboxylic acid (28)……..400

4.6.4.4.(*R*)-Ethyl-cyclopropyl-6-(2-fluorophenyl)-4-methyl-4*H*-benzo[*f*]imidazo[1,5-*a*][1,4]diazepine-3-carboxylate (37)……401

4.6.4.5.(*R*)-8-cyclopropyl-6-(2-fluorophenyl)-4-methyl-4H-benzo[f]imidazo[1,5-a][1,4] diazepine-3-carboxylic acid (38)……403

4.6.4.6. Ethyl 8-bromo-6-(2-fluorophenyl)-4-methyl-6H-benzo[f]imidazo[1,5-a][1,4] diazepine -3-carboxylate (39)……404

4.6.4.7. 8-bromo-6-(2-fluorophenyl)-4-methyl-6H-benzo[f]imidazo[1,5-a][1,4]diazepine-3-carboxylic acid (42)…….405

4.6.4.8. 8-Bromo-4-methyl-6-(pyridin-2'-yl)-6H-benzo[f]imidazo[1,5-a][1,4]diazepine-3-carboxylic acid (44)…….406

4.6.4.9. 8-cyclopropyl-6-(2-fluorophenyl)-4-methyl-6H-benzo[f]imidazo[1,5-a][1,4]diazepine-3-carboxylic acid (43)……407

4.6.4.10. 8-cyclopropyl-6-(2'-fluorophenyl)-N-(2,5,8,11,14-pentaoxahexadecan-16-yl)-4-methyl-6H-benzo[f]imidazo[1,5-a][1,4]diazepine-3-carboxamide (45)……408

References……..411

LIST OF FIGURES

Chapter 1. Introduction

Figure 1. γ-Aminobutyric acid ……..2

Figure 2. The GABAAR is a type of pentameric ligand-gated chloride channel composed of two α subunits, two β subunits, and one γ subunit. The figure illustrating this structure was adapted from a publication by Jacob and colleagues in the journal Nature Reviews Neuroscience, 2008…….3

Figure 3. The figure depicts the potential configuration of a GABAA receptor subunit, with the N-terminus located in the extracellular domain and the M1-M4 representing the four transmembrane domains. This diagram has been adapted from the original figure in Burt *et al.*[21] and Clayton *et a*l.[22].....……...5

Figure 4. The schematic representation of a ligand-gated ion channel, both in longitudinal (A) and cross-sectional (B) views, is depicted in the figure. The segments M1, M2, M3, and M4 are indicated by the numbers 1, 2, 3, and 4, respectively. This image has been modified from the original figure provided by Keramidas *et al.* [23] and Clayton *et al.* [22], who have extensively studied the topic. By presenting the structural arrangement of the ligand-gated ion channel, this figure aids in understanding the spatial orientation of its various components and contributes to our comprehension of its functional properties……..6

Figure 5. The schematic representation of the arrangement of the α1β2γ2 GABAA receptor when viewed from the synaptic cleft. This figure shows that the β+α- subunit interfaces house the GABA binding sites, while the α+γ- subunit interface contains the benzodiazepine modulatory binding site. The presence of loop C in the respective subunits is indicated by the '+'

sign. This image has been adapted from the original figure presented in the works of Clayton *et al.* [17] and Ernst *et al.* [34]……..8

Figure 6. The structures of classical 1,4-benzodiazepines, including diazepam, chlordiazepoxide, the triazolobenzodiazepine alprazolam, and the imidazobenzodiazepine midazolam. Each of these benzodiazepines has a distinct chemical structure, contributing to their unique pharmacological properties and effects……..…10

Figure 7. The membrane potential changes over time during the transmission of a nerve signal. It represents the fluctuations in electrical potential across the neuronal membrane as the signal propagates. The Figure, which is adapted from Teny Clayton's Ph.D. thesis [67], likely demonstrates the dynamic nature of the membrane potential during the initiation and propagation of an action potential. Typically, at resting state, the membrane potential of a neuron is negative, indicating a polarized state. As the nerve signal is transmitted, there is a depolarization phase where the membrane potential becomes less negative, moving towards a positive charge. This depolarization triggers an action potential, which is characterized by a rapid and substantial increase in the membrane potential, reaching a peak. Following the peak of the action potential, there is a repolarization phase, during which the membrane potential returns to its resting state by becoming negative again. This repolarization phase is crucial for the neuron to restore its readiness for subsequent signaling..[67]……..17

Figure 8. The representation of the complex of diazepam (shown in yellow) with the α1 subunit (aquamarine) and γ2 subunit (orchid) of the α1β3γ2L GABAA receptor (6HUP). In the modified figure, various interactions are highlighted by dashed lines, representing π–π interactions, hydrogen bonding interactions, and a halogen bonding interaction. These interactions play a crucial role in the binding and stabilization of diazepam within the receptor complex. The π–π

interactions refer to the stacking interactions between certain aromatic residues, such as α1Tyr210 and α1Phe100, and the diazepam molecule. These interactions contribute to the overall stability of the binding complex. Additionally, hydrogen bonding interactions are observed between diazepam and specific amino acid residues within the receptor, facilitating further stabilization. The specific amino acid residues involved in these hydrogen bonding interactions are not specified in the provided information. Furthermore, a halogen bonding interaction is indicated in the Figure. This involves the interaction between a halogen atom, likely chlorine in the case of diazepam, and the carbonyl oxygen of a specific amino acid residue, α1His102. This interaction contributes to the specific binding orientation and affinity of diazepam within the GABAA receptor complex. The Figure, as modified from the work of Golani and Mian et al. 2022 [75], provides a visual representation of the molecular interactions between diazepam and the α1 and γ2 subunits of the GABAA receptor. It helps to illustrate the structural basis of diazepam's binding and its interactions within the receptor complex, contributing to our understanding of the pharmacological properties of benzodiazepines…….…….23

Figure 9. The complex of alprazolam (orange) with α1 (aquamarine) and γ2 (orchid) subunits of α1β3γ2L GABAA receptor 6HUO. The dashed lines (- - -) indicate π–π interactions, hydrogen bonding interactions, and a halogen bonding interaction. The image is modified from Golani and Mian et. al. 2022.[75] ……..…...24

Figure 10. The overlay diagram of flumazenil (grey) and diazepam (yellow) in the ion complex with α1 (aquamarine) and γ2 (orchid) subunits of α1β3γ2L $GABA_AR$ (6HUO and 6HUP). The image is modified from Golani and Mian et. al. 2022.[75]……...26

Figure 11. The docking studies revealed the docking pose of QH-II-066 5 (shown in deep sky blue) with the α1 (aquamarine) and γ2 (orchid) subunits of the α1β3γ2L GABAA receptor

6HUP. In this docking pose, no halogen bond is observed due to the presence of an ethinyl group. The modified image showcasing this docking pose is adapted from Golani and Mian et al., 2022 [75]. The absence of a halogen bond in the case of the ethinyl group substitution suggests that the molecular interactions between QH-II-066 and the α1β3γ2L GABAA receptor may differ compared to compounds with halogen groups. These interactions play a crucial role in the binding affinity and functional outcomes of ligand at the receptor……..…….....34

Chapter 2. Development of α6-GABAAR Subtype-Selective Pyrazolo-quinolinones for Treating Tourette Syndrome, Migraine, and Trigeminal Pain

Figure 1. The GABAAR α6β3γ2 subtype represents a pentameric chloride channel that operates as a ligand-gated structure, consisting of two α6, two β3, and one γ2 subunit. Pyrazoloquinolinones (PQs), such as PZ-II-029 (compound 6), exert their influence at the α6+β3- interface, recognized as the PQ Site, serving as positive allosteric modulators. Moreover, they interact at the α6+γ2- interface, identified as the DI-Bz site, exerting null modulation effects. This configuration showcases the PQ site, the DI-Bz binding site, and the binding sites for the endogenous ligand (GABA) at the β3+α6- interfaces. Image modified from Jacob et al., Nature Reviews Neuroscience, 2008.……...38

Figure 2. Structure of CGS 8216 and CGS 9896……..39

Figure 3. Lead α6-selective ligands for this project ……....40

Figure 4. Frequency domain-based motion power spectra and motion power spectrograms in mice treated with saline, harmaline and PZ-II-029 plus harmaline. (A) The motion waves

recorded from mice using a Tremor Monitor (San Diego Instruments, CA, USA) were transformed into frequency domain motion power spectra (upper panels) and motion power heatmap spectrograms (lower panels) via a fast Fourier transformer. It's notable that the administration of harmaline induced a tremor response in ICR mice, specifically at the frequency range of 10-16 Hz. However, the inclusion of Compound 6 in conjunction with harmaline exhibited a mitigating effect on harmaline-induced tremor activity. (B) In a distinct scenario, a sample of 10-minute motion power spectrograms (lower panel) is juxtaposed with concurrently detected motor activity identified by the SMART motion detector. This visual correlation highlights that tremor activity occurs during periods of movement (red region), while it is notably absent during phases of immobility (black region). This observation provides strong evidence that harmaline-induced tremor in mice is categorized as an action tremor, rather than a rest tremor. Figure was modified from Huang et al. 2021…….52

Figure 5: Dose-dependent effects of harmaline on tremor activity and burrowing activity in mice. (A) The illustration of the time-dependent progression of tremor activity prompted by saline, as well as doses of 10, 20, and 30 mg/kg (s.c.) of harmaline. Over the course of 120 minutes, the tremor activity was gauged for intervals of 10 minutes (pink shade). This included a 15-minute period before harmaline injection, a 5-minute interval following injection, and subsequent measurements taken every 20 minutes. Concurrently, the mouse's burrowing activity was evaluated for 10 minutes, right after each tremor activity assessment (grey shade). The alternating measurements of tremor and burrowing activity unfolded across the entire 120-minute duration. The means of tremor activity for each 10-minute segment were plotted against time, and comparisons were drawn among the treatment groups. Statistical significance levels were indicated as *$P < 0.05$, **$P < 0.01$, ***$P < 0.001$ in relation to the Saline group. These

comparisons were executed using a two-way ANOVA with repeated measures over time, followed by Holm-Sidak's post hoc test. (B) The cumulative tremor activity, quantified as the area under the curve (AUC) of tremor activity against time. (C) Concurrently, the cumulative burrowing activity is presented as the total displaced pellets throughout the 120-minute recording period. Statistical analysis indicated significance levels as *P < 0.05 and **P < 0.01 when compared to the Saline group. The statistical assessment utilized the Kruskal-Wallis test followed by Dunn's post hoc test. The numbers provided in parentheses indicate the number (n) of mice tested within each respective group. The data are expressed as mean ± S.E.M. Figure was modified from Huang et al. 2021…….54

Figure 6: The impacts of PZ-II-029, an α6GABAAR-selective PAM, and propranolol on harmaline-induced tremor and burrowing impairment in mice. (A) The time-dependent profiles of the effects of 3 mg/kg and 10 mg/kg (i.p.) doses of PZ-II-029, alongside its vehicle, as well as propranolol (20 mg/kg), on tremor induced by harmaline (20 mg/kg, s.c.) The sequence of measuring tremor activity and burrowing activity was conducted alternately over an 80-minute duration. Noteworthy, PZ-II-029 and its vehicle were intraperitoneally administered 5 minutes prior to the administration of harmaline. Statistical significance was indicated as *P < 0.05 and ***P < 0.001 in comparison to the Saline group. This evaluation was conducted through a two-way ANOVA with repeated measures over time, followed by the Holm-Sidak's post hoc test. (B) The cumulative tremor activity and (C) burrowing activity in mice subjected to harmaline treatment across various intervention groups. The statistical comparison demonstrated significance levels of *P < 0.05, **P < 0.01, and ***P < 0.001 relative to the Vehicle group. This analysis encompassed a one-way ANOVA followed by the Holm-Sidak's post hoc test. The numerical values in parentheses indicate the quantity (n) of mice examined within each specific

group. The data are presented as mean ± S.E.M. Notation: Veh= vehicle, C6= PZ-II-029. Figure was modified from Huang et al. 202……..……56

Figure 7: The impact of intra-cerebellar microinjection (i.cb.) of furosemide, an α6GABAAR antagonist, and its effects on the anti-tremor and burrow-restorative properties of Compound 6 in harmaline-treated mice. (A) The temporal progression of effects stemming from the administration of a 10 mg/kg (i.p.) dose of Compound 6, along with its corresponding vehicle, both in isolation and in conjunction with an intra-cerebellar microinjection (i.cb.) of furosemide (10 nmol) co-treatment, were assessed in terms of their influence on tremor activity in harmaline-treated mice. Statistical significance was noted as *P < 0.05 and ***P < 0.001 compared to the Saline group. This evaluation was conducted through a two-way ANOVA with repeated measures over time, succeeded by the Holm-Sidak's post hoc test. (B) The cumulative tremor activity and (C) burrowing activity pertaining to harmaline-treated mice who were pre-treated either with PZ-II-029 in isolation or in tandem with an intra-cerebellar microinjection (i.cb.) of furosemide. Statistical significance was denoted as *P < 0.05, **P < 0.01, and ***P < 0.001 relative to the Vehicle group, whereas #P < 0.05 indicated significance in comparison to the Veh (i.cb.)+C6 group. This analysis involved a one-way ANOVA followed by the Holm-Sidak's post hoc test. "Furo"=furosemide, "Veh" = vehicle, "C6" =PZ-II-029. Figure was modified from Huang et al. 2021……..…58

Figure 8: Effects of DK-I-56-1, LAU463 and DK-I-58-1, structural analogues of PZ-II-029, on harmaline-treated mice. (A) DK-I-56-1 (represented by half-filled square symbols), (B) LAU463 (indicated by diamond symbols), or (C) DK-I-58-1 (depicted by half-filled diamond symbols) were administered at doses of 3 and 10 mg/kg (i.p.). The statistical significance denoted by *P < 0.05, **P < 0.01, and ***P < 0.001 was observed compared to the Saline group, employing two-

way ANOVA with repeated measures over time followed by Holm-Sidak's post hoc test. The total tremor activity (D) and burrowing activity (E) were measured alternatively for 80 minutes, following the procedure outlined in Figure 3, within various treatment groups. The statistical comparison indicated *P < 0.05, **P < 0.01, and ***P < 0.001 versus the Vehicle group, performed using one-way ANOVA followed by Holm-Sidak's post hoc test. Notations used: Veh for vehicle, and PAM for positive allosteric modulator……..…….60

Figure 9: Effects of PZ-II-029 analogues on diazepam-induced incapatication in the rotarod. PZ-II-029, DK-I-56-1, RV-I-029, and DK-I-60-3 demonstrate the ability to mitigate the motor-impairing effects caused by diazepam. DS-I-78 displayed an effect that falls between the outcomes observed in the two groups.……..……...62

Figure 10: Frequency-rate response curves showing the effects of DK-I-56-1 (0.1, 1, 3, and 10 mg/kg) and vehicle (2% methylcellulose) administered i.p. 30 min pre-session. Values represent the mean + SEM normalized response rate (% of maximum control responding) across 10 frequency presentations (1.75 – 2.20 log/Hz) of 10 rats. Significant differences compared to vehicle at a respective frequency are denoted by asterisks (* p<0.0001). ADP34,282 = DK-I-56-1.…….65

Figure 11. Effects of 0.1, 1 3, and 10 mg/kg ATDP 34,282 and vehicle on % baseline T0 and M50 Values represent the mean (± SEM) of calculated % baseline T0 (top panel) or M50 (bottom panel) in 8 rats (n.b., 2 rats had marked rate decreases that precluded determination of T0 and M50). Significant differences compared to vehicle are denoted by asterisks (* p<0.0001). ADP34,282 = DK-I-56-1.…….66

Chapter 3. The Development of a Scalable Synthesis, and Assessment of Bioactivity of Imidazodiazepines Targeting α2/3-GABAAR Subtypes for the Treatment of Epilepsy, Anxiety, and Neuropathic Pain

Figure 1: Structures of Hz-166 (1), MP-III-080 (2), and KRM-II-81 (3)……104

Figure 2: The GABAAR α2/3β3γ2 subtypes represent a class of pentameric chloride channels that are regulated by specific ligands. Importantly, certain compounds known as IBDZs (such as HZ-166, MP-III-080, and KRM-II-81) act as positive allosteric modulators (PAMs) at the DS-Bz site, which is located at the interface of the α2/3 and γ2 subunits. These modulators play a role in mediating the effects of GABAAR α2/3β3γ2 subtypes. The accompanying image has been adapted from Jacob et al., Nature Reviews Neuroscience, 2008.[136]……106

Figure 3: The average enhancement of the current evoked by GABA EC3. Diazepam and KRM-II-81 are compounds that enhance the current response to GABA EC3 in GABAA receptors. Diazepam interacts with a broader range of receptor subtypes, including α1, α2, α3, α4, α5, and α6, while KRM-II-81 selectively activates α2 and α3-containing GABAA receptors. At a concentration of 0.1 μM, both compounds enhance the current response in GABAA receptors containing α1, α2, α3, and α5 subunits. At a concentration of 1 μM, diazepam enhances the response in α4 and α6-containing receptors, while KRM-II-81 affects α4 and α6-containing receptors as well. These findings highlight the differential selectivity and potency of diazepam and KRM-II-81 on various GABAA receptor subtypes. 100% base line just GABA-no activity of KRM-II-81 or diazepam itself…**……**……108

Figure 4 : Alprazolam vs KRM-II-81 at the $\alpha^{+}\gamma^{-}$ interface of the $GABA_A$ receptor. Alprazolam (orange) in the complex with the α1β3γ2L $GABA_A$ receptor 6HUO. Dashed lines indicate π-π,

hydrogen bond and halogen bond interactions. Data are modified from (Witkin et al., 2020, Golani, Mian et al 2021)[75,140]**……**.....110

Figure 5: Alprazolam vs KRM-II-81 at the $\alpha^{+}\gamma^{-}$ interface of the $GABA_A$ receptor. KRM-II-81 docked (sandy brown) in the complex with the α1β3γ2L $GABA_A$ receptor 6HUO. α1 (aquamarine); γ2 (orchid) subunit. Dashed lines indicate π-π, hydrogen bond and halogen bond interactions. Data are modified from Witkin et al., 2020, Golani, Mian et al 2021[75,140].....111

Figure 6: Flow reaction to synthesize Hz-166 aldehyde.....137

Figure 7: Structures of KRM-II-81 (**3**) and some structural analogs 140

Figure 8: The anxiolytic and motor impairment effects of KRM-II-81 and MP-III-80, compared to the reference anxiolytic drug, chlordiazepoxide. The figure shows the results of two behavioral assays conducted in mice: the marble-burying behavior and the inverted-screen performance. The experiment involved using the same group of 10 mice for both tests. The inverted-screen test was conducted first, followed immediately by the marble-burying test. Each mouse received either the vehicle or one of the drugs (KRM-II-81, MP-III-80, or chlordiazepoxide). The figure includes statistical analysis, showing significance levels denoted by asterisks ($*p < 0.05$; $***p < 0.001$) based on Dunnett's test following a one-way ANOVA for each behavioral assay. Error bars indicating the standard error of the mean (± SEM) are also included in the figure. The figure presented in this text is adapted from the study conducted by Biggerstaff Witkin et al. in 2020.....147

Figure 9: The dose response curves for mechanical hyperalgesia in paclitaxel-treated mice are depicted in the figure. The antinociceptive effects of KRM-II-81 are shown in green, MP-III-80 in blue, gabapentin in red, and vehicle in black. The analysis was performed on experimental day

15, with a sample size (n) ranging from 6 to 7. The error bars represent the standard error of the mean (± SEM), indicating the variability of the measurements around the mean values. The figure presented in this text is adapted from the study conducted by Biggerstaff Witkin et al. in 2020.....150

Figure 10. The figure presents the dose response curves for thermal allodynia in paclitaxel-treated mice. The antinociceptive effects of KRM-II-81 are depicted in green, MP-III-80 in blue, gabapentin in red, and vehicle in black. The analysis, with a sample size (n) of 6-7, was conducted on experimental day 15. The figure illustrates the varying responses of the different treatments in mitigating thermal allodynia. The error bars represent the standard error of the mean (± SEM), indicating the variability of the measurements around the mean values. The figure presented in this text is adapted from the study conducted by Biggerstaff Witkin et al. in 2020……..150

Figure 11: In the chronic neuropathic pain study conducted from days 18 to 40, mechanical hyperalgesia data were collected and analyzed for the effects of KRM-II-81, MP-III-80, gabapentin, and vehicle treatments. The data, obtained from a sample size of 6-7 mice, were measured 30 minutes after the administration of the respective treatments. In the figure, KRM-II-81 is represented by green, MP-III-80 by blue, gabapentin by red, and vehicle by black. Additionally, there is a Vehicle-Vehicle group shown in brown, which did not undergo paclitaxel pretreatment. The error bars in the figure represent the standard error of the mean (± SEM). Above the data points, any significant differences are indicated with asterisks corresponding to the respective significance levels: * < 0.05, ** < 0.01, *** < 0.001, **** < 0.0001. The figure presented in this text is adapted from the study conducted by Biggerstaff Witkin et al. in 2020……..152

Figure 12: In the chronic neuropathic pain study conducted from days 18 to 40, thermal allodynia data were collected and analyzed for the effects of KRM-II-81, MP-III-80, gabapentin, and vehicle treatments. The data were collected from a sample size of 6-7 mice and measured 30 minutes after the administration of the respective treatments. The color green represents KRM-II-81, blue represents MP-III-80, red represents gabapentin, and black represents the vehicle. Additionally, there is a Vehicle-Vehicle group shown in brown, which did not undergo paclitaxel pretreatment. The error bars in the figure represent the standard error of the mean (± SEM). Above the data points, any significant differences are indicated with asterisks corresponding to the respective significance levels: * < 0.05, ** < 0.01, *** < 0.001, **** < 0.0001. The figure presented in this text is adapted from the study conducted by Biggerstaff Witkin et al. in 2020……..153

Figure 13: Effects of KRM-II-81 (p.o., bid) on the cumulative handling-induced seizure burden in mice inoculated with TMEV on day 0. Data for the occurrence of seizures in the vehicle and KRM-II-81 groups are shown for the time periods 2 h post injection. Each data point represents the cumulative mean + SEM for N = 16-20 mice due to attrition in the initial N=20 due to criteria weight loss or death (see Results). * P < 0.05 compared to day 3 values; ## P < 0.01, ### P < 0.0001 by ANOVA and Šidák's multiple comparison test. (Unpublished data)……155

Figure 14: Heat map characterization of handling-induced behavioral seizure observations following TMEV inoculation. Effects of 15 mg/kg (left) and 30 mg/kg (right) KRM-II-81 are shown relative to vehicle with dosing bid. DI represents seizures observed during dosing and AM and PM designate handling-induced seizures observed 2 h post dosing for days 3-7 post viral inoculation on day 0. Behavioral seizures are illustrated according to the Racine seizure score (Racine, 1972) with stages 1-3 (green), 4 (yellow), 5 (orange), and no seizure (blank cell).

Only the highest scoring seizure during each observation period is shown. On average in such studies, 70-80% of all animals infected with TMEV experience handling-induced seizures. (Unpublished

data)……156

Figure 15: Miniature IPSCs. Voltage-clamp whole-cell patch clamp recordings were performed on CA1 pyramidal neurons in acute slices obtained from wild-type (WT) mice. mIPSCs with longer decay times were more significantly affected by KRM-II-81. (Unpublished data)……..160

Figure 16: Effects of KRM-II-081 on hyperthermia-induced seizure in DS mice. Acute administration of KRM-II-081 demonstrated protective effect against hyperthermia-induced seizure in DS mice. (Unpublished data)……161

Figure 17*:* Chromic administration of KRM-II-081 (10mg/kg, once per day) did not improve mortality rate in DS. (Unpublished data) ……..162

Figure 18: Survival curve evaluating percentage of animals not seizing as core temperature increases. There was a significant difference (Log-rank (Mantel-Cox) (P= 0.0113) between the vehicle and drug groups. (Unpublished data)…….……..163

Figure 19*:* Cytotoxicity data of DS-II-73 (Unpublished data)…….167

Figure 20*:* Selectivity of DS-II-73 for α2/3/5-containing GABAARs over that of α1-containing GABAARs. Data are means + S.E.M. for N = 5 (a1) or N = 4 (other cell lines). *P < 0.05 by Dunnett's post-hoc test. (Unpublished data)……...168

Figure 21 *:* Concentrations of DS-II-73 in plasma and brain of rats after oral dosing of 2 mg/kg. Each point represents the mean + S.E.M. of 3 rats. Left Axis: ng/mL or ng/g; Right Axis: nmol/L or nmol/Kg. AUC: area under the curve for concentration from 0-24 h; Cmax: maximum concentration achieved; Tmax: time of maximum concentration; T1/2: half-life. (Unpublished data)……169

Figure 22: Effects of DS-II-73 (5) on PTZ-induced seizure latencies. Data were evaluated by un-paired Student's t-test. ** $P < 0.01$; *** $P < 0.001$. (Unpublished data)……..171

Figure 23 *:* . Effects of DS-II-73 on electrical activity in a slice from freshly transected cortical tissue from a patient with pharmacoresistant epilepsy. A. Representative tracings showing the local field potentials (LFPs) on 10 s and 1 s time scale. B. Quantification of the LFP frequency across the 60 m periods of Baseline, DS-II-73 application, and washout. C. Data as per Panel B. with a second independent tissue slice from the same patient. ***, $p < 0.001$, Kruskal-Wallis test followed by Dunn's multiple comparisons test. (Unpublished data)……172

Figure 24: Comparative effects of diazepam and DS-II-73 on rotorod performance of mice. *** $P < 0.001$ compared to diazepam; ** $P < 0.01$ compared to diazepam by Tukey's multiple comparison test after ANOVA. The overall effect of treatment was significant ($F_{4,144} = 12.6$, $P < 0.0001$) as was the effect of time ($F_{2,144} = 5.42$, $P < 0.01$). There was not a significant treatment x time interction ($F_{8,144} = 1.00$, $P = 0.44$). (Unpublished data)……..173

Figure 25: . KRM-II-81 (1) vs. DS-II-73 (5) at the $\alpha^{+}\gamma^{-}$ interface of GABAAR. **A.** KR-II-81 (1) (brown) in complex with α1 (aquamarine) and γ2 (orchid) subunits of α1β3γ2L $GABA_A$ receptor 6HUO. **B.** Docked DS-II-73 (5) (yellow) in complex with α1 (aquamarine) and γ2 (orchid) subunits of α1β3γ2L $GABA_A$ receptor 6HUO. Dashed lines indicate π–π interactions, hydrogen bonds and halogen bonds. ……174

Figure 26: Overlay of KRM-II-81 (**1**) vs. DS-II-73 (**5**) at the $\alpha^{+}\gamma^{-}$ interface of $GABA_AR$ ….175

Figure 27: Timelines of drug administration and harmaline-induced tremor measurement…..177

Figure 28: Effects of MP-III-024 at different doses (3.2 mg/kg and 10 mg/kg) on harmaline-induced tremors in rats. The graph (A) displays the power spectrum, averaged over two intervals (0-30 and 30-60 min) for all animals in each group within a frequency range of 0-20 Hz. The specific tremor parameters are represented as means ± SEM: (B) AP2, (C) tremor index, and (D) AP1, along with (E) locomotor activity (distance) of the rats. The results show that both doses of MP-III-024 (3.2 mg/kg and 10 mg/kg) significantly reduced harmaline-induced tremors, as indicated by the effects on AP2 in graph (B). However, the anti-tremor effect of the higher dose (10 mg/kg) was comparatively weaker, as it only affected AP2 and did not show a significant impact on the tremor index parameter. Nonetheless, this effect lasted for the entire 60-minute measurement period. On the other hand, the lower dose (3.2 mg/kg) had a stronger and more observable effect on both AP2 and the tremor index but was limited to the initial 30 minutes after administration. Regarding locomotor activity (graph E), MP-III-024 at both doses increased the distance parameter compared to animals treated with harmaline alone. The effect was observed in the first 30 minutes after administration for the 3.2 mg/kg dose and throughout the 60-minute measurement period for the 10 mg/kg dose. The statistical analysis was performed using ANOVA for repeated measures, taking into account the effects of harmaline and MP-III-024 on AP2, tremor index, AP1, and distance parameters, as well as the impact of time. LSD post-hoc tests were conducted, with * indicating $p \leq 0.05$, ** $p \leq 0.01$, and *** $p \leq 0.001$ significance levels. Additionally, 'a' represented $p = 0.077$, 'b' denoted $p = 0.060$ compared to SOLV, and 'c' indicated $p = 0.090$ compared to HARM 15 mg. The figure was modified from Barbara *et al.* 2022…….179

Figure 29: MP-III-024 (at doses of 3.2 mg/kg and 10 mg/kg) effectively reversed the pimozide-induced tremulous jaw movements (TJMs). The data are presented as the mean (± SEM) number of tremulous jaw movements per 10-minute observation period. The study included the following number of animals in each group: SOLV, n = 7; PIM 1 mg/kg, n = 8; MP 3.2 mg/kg, n = 8; MP 10 mg/kg, n = 8; PIM 1 mg/kg + MP 3.2 mg/kg, n = 6; PIM 1 mg/kg + MP 10 mg/kg, n = 7. Statistical analysis using Factorial ANOVA revealed significant effects of pimozide (PIM effect: $F[1,38] = 41.736$, $p = 0.001$) and MP-III-024 (MP effect: $F[2,38] = 3.919$, $p = 0.028$) on the number of TJMs. LSD post-hoc test further confirmed the significance of the results (** $p \leq 0.01$, *** $p \leq 0.001$)…**……**180

Figure 30: Structures of MP-III-024 and morphine ……182

Figure 31: The dose-response curves for both morphine and MP-III-024 when administered individually in the von Frey mechanical hyperalgesia and thermal nociception procedures. In the mechanical hyperalgesia assay (panel A), injection of zymosan A into the right hind paw resulted in increased mechanical sensitivity compared to the non-injected left hind paw. The paw withdrawal thresholds of the non-injected paw were not affected by drug administration (data not shown). Each compound demonstrated dose- and time-dependent increases in mechanical sensitivity, expressed as %MPE (Maximum Possible Effect). The mean ED50 (Effective Dose 50) values for MP-III-024 and morphine were 9.96 (8.81–11.26) mg/kg and 10.72 (9.68–11.86) mg/kg, respectively. These potency values were used to determine the relative proportions of the compounds in subsequent studies that assessed MP-III-024/morphine mixtures. In panel B, the antinociceptive effects of MP-III-024 and morphine in the thermal nociceptive assay are shown. Morphine induced dose-dependent increases in latency to respond on the hotplate, resulting in an ED50 value of 14.98 (14.39–15.60) mg/kg. On the other hand, MP-III-024 had no effect in this

assay. Thus, the relative potencies determined in the von Frey procedure were also used to determine the proportions of the compounds in each MP-III-024/morphine mixture for subsequent combination studies in the hotplate test……183

Figure 32: Dose-response curves for morphine alone, MP-III-024 alone and a 0.94:1 mixture of MP-III-024:morphine for both the von Frey. Figure is modified from Atiqur Rahman et al. 2021.……184

Figure 33: MP-III-024 alone and a 0.94:1 mixture of MP-III-024: morphine for hot plate …….185

Figure 34: Isobolograms for MP-III024/morphine mixtures, mechanical hyperalgesia (panel a) and in the assay of thermal nociception (panel b). The abscissae represent the ED50 value for morphine in mg/kg, while the ordinates represent the ED50 value for MP-III024 in mg/kg. Each point in the isobolograms represents the mean (± S.E.M.) from 8 mice. In the mechanical hyperalgesia assay (panel a), some points fall above the line of additivity (marked as *), indicating supra-additive (synergistic) effects. These points demonstrate that the combination of MP-III024 and morphine produces stronger antihyperalgesic effects than would be expected if their effects were merely additive. In the thermal nociception assay (panel b), all points fall to the left of the line of additivity (marked as *), indicating supra-additive effects. This implies that the combination of MP-III024 and morphine produces more potent antinociceptive effects than predicted based on additivity. The asterisks (*) indicate that the observed effects of the drug combinations are significantly different from additivity, further confirming the presence of synergistic interactions……..186

Figure 35: The timelines of drug administration and the measurement or observation of tremor induced by different compounds. The timelines are as follows: (A, B) For harmaline-induced

tremor measurement using the Force Plate Actimeter (FPA), the measurement duration was 30 minutes. (C, D) For observation and counting of Tremulous Jaw Movements (TJMs) induced by pimozide, the observation period was not specified in the provided information. (E) For observation and counting of Tremulous Jaw Movements (TJMs) induced by TBZ, the observation period was not specified in the provided information. The abbreviations used in the figure are FPA for Force Plate Actimeter, TBZ for tetrabenazine, and TJMs for Tremulous Jaw Movements. Figure is modified from Barbara et al.2023……198

Chapter 4. D The Design and Synthesis of Chiral α5 Subtype BzR/GABAAR Modulators for Treating Anxiety, Depression, and Schizophrenia as well as Asthma

Figure 1: The α5β3γ2 subtype GABAAR. Several IBDZs such as SH-2'F-R-CH3, GL-II-73, and MP-III-22 have been identified as positive allosteric modulators (PAMs) that exert their effects specifically at the α5+γ2- interface (Jacob et al., Nature Reviews Neuroscience, 2008). These compounds have shown the ability to enhance the activity of α5β3γ2 GABAARs through allosteric modulation, leading to potential therapeutic applications. The modified image can be referred to in Jacob et al., Nature Reviews Neuroscience, 2008……..……..…….230

Figure 2 : Lead α5-Selective Ligands of this Work ……..231

Figure 3: Figure 3: The figure visually represents the relative potentiation of GL-II-73 at different GABAA receptor subtypes, highlighting its greater affinity for the α5 subtype compared to α1, α2, and α3 subtypes. At a concentration of 1 μM, the potentiation of GL-II-73 at α1, α2, and α3 subtypes was comparatively lower than its potentiation at the α5 subtype, suggesting that this ligand exhibits a preference for α5-containing GABAA receptors. This

modified figure provides a graphical representation of GL-II-73's α5 preference, as supported by the experimental data presented in the PhD thesis of Guanguan Li, University of Wisconsin – Milwaukee, 2019…….236

Figure 4. Analogs of GL-II-73[··]…….…….259

Figure 5: Impaired ventral hippocampal oscillatory activity reversed by MP-III-022 in AAV-AD rats. In Figure A (left), a representative brain slice is shown with an electrode track indicated by a black arrow, targeting the ventral hippocampus (vHipp). The corresponding schematic of the brain section is depicted in Figure A (right). The average firing rate of spontaneously active putative pyramidal neurons in the vHipp remains unchanged between different treatment groups and is not affected by treatment with the selective α5-GABAA positive allosteric modulator (PAM), MP-III-022, as illustrated in Figure B. AAV-AD rats exhibit a significant decrease in oscillatory power compared to eGFP controls, which is then reversed by the systemic administration of MP-III-022, as depicted in Figures C and D. Figure E shows a representative trace of spontaneous local field potential oscillations filtered for delta frequency in the vHipp of a control rat, while Figure F shows the same for an AAV-AD rat. It is noteworthy that the symbol "†" denotes a significant main effect with p=0.014, and the symbol "‡" denotes another significant main effect with p=0.006. The figure was modified from Eassa et al. 2023.[280]…….269

Figure 6. Aberrant ventral tegmental area activity is restored by MP-III-022 in AAV-AD rats. In Figure A, a representative brain slice is shown with electrode tracks indicated by black arrows targeting the ventral tegmental area (VTA). The dopamine neuron population activity, represented by the average number of spontaneously active dopamine neurons per electrode track, is significantly increased in AAV-AD rats compared to controls. However, this increase is

reversed by systemic administration of the selective α5-GABAA positive allosteric modulator (PAM), MP-III-022, as demonstrated in Figure B. Notably, there were no alterations observed in the average firing rate (Figure C) or bursting pattern (Figure D) in either control or AAV-AD rats, nor were there any effects of systemic MP-III-022 administration on these parameters. Figure E presents a representative dopamine recording and action potential from a control rat, while Figure F shows the same from an AAV-AD rat. The figure was modified from Eassa et al. 2023.[280] ……271

Figure 7. AAV-AD rats distinctly manifest a notable reduction in the count of parvalbumin-positive (PV) interneurons within the ventral hippocampus (vHipp). The AAV-AD rat group demonstrates a considerably lower presence of inhibitory interneurons that are parvalbumin-positive in the vHipp (A). A representative coronal brain section highlighting the ventral hippocampus (vHipp) showcases the presence of parvalbumin (rendered in greyscale and indicated by black arrows; (B)). Furthermore, a scatterplot illustrates the correlation between the activity of the dopamine neuron population and the quantity of PV interneurons in the vHipp. The black dots on the plot represent individual rats (C). * p = 0.032……..274

Figure 8: Impact of Treatment (Vehicle [VEH], MP-III-022 0.33 mg/kg [MP0.3], or MP-III-022 1 mg/kg [MP1]) on Social Behavior in Prenatally Treated Animals (Control [CTRL] or Valproate [VPA]):(A) Time dedicated to allogrooming and allosniffing;(B) Time spent in crawling over/under a conspecific;(C) Time allocated to following a conspecific;(D) Time devoted to tail manipulation of a conspecific. Group Pair Count: Males CTRL VEH 6, CTRL MP0.3 7, CTRL MP1 6, VPA VEH 6, VPA MP0.3 6, VPA MP1 7; females CTRL VEH 8, CTRL MP0.3 8, CTRL MP1 7, VPA VEH 7, VPA MP0.3 6, VPA MP1 8. *p < 0.05, **p < 0.01, ***p < 0.001. Figure was modified from Anja *et al*. 2021. [284]…….276

Figure 9: Effect of Treatment (Vehicle [VEH], MP-III-022 0.33 mg/kg [MP0.3], or MP-III-022 1 mg/kg [MP1]) on Spontaneous Locomotor Activity in Prenatally Treated Animals (Control [CTRL] or Valproate [VPA]):(a) Duration of activity; (b) Count of rotations; (c) Count of clockwise rotations; (d) Count of anticlockwise rotations; (e) Comparison between clockwise and anticlockwise rotations - statistical analysis conducted via paired t-test (solely significant difference observed in VPA VEH males: $p = 0.011$). (f) Time allocated to self-grooming. Group Size: Males CTRL VEH 11, CTRL MP0.3 11, CTRL MP1 11, VPA VEH 9, VPA MP0.3 9, VPA MP1 12; females CTRL VEH 11, CTRL MP0.3 9, CTRL MP1 11, VPA VEH 9, VPA MP0.3 11, VPA MP1 9. *$p < 0.05$, **$p < 0.01$, ***$p < 0.001$, ~ $0.05 < p < 0.01$. Figure was modified from Anja *et al*. 2021. [284]…….……278

Figure 10: Effect of Treatment (Vehicle [VEH], MP-III-022 0.33 mg/kg [MP0.3], or MP-III-022 1 mg/kg [MP1]) on Morris Water Maze (MWM) Performance in Prenatally Treated Animals (Control [CTRL] or Valproate [VPA]):(a) Latency during standard MWM; (b) Path efficiency during standard MWM; (c) Latency during reverse MWM; (d) Path efficiency during reverse MWM; (e) Count of entries to the previous target zone during reverse MWM. Group Size: Males CTRL VEH 11, CTRL MP0.3 10, CTRL MP1 10, VPA VEH 10, VPA MP0.3 9, VPA MP1 10; females CTRL VEH 11, CTRL MP0.3 11, CTRL MP1 11, VPA VEH 11, VPA MP0.3 10, VPA MP1 10. *$p < 0.05$, **$p < 0.01$, ***$p < 0.001$ compared to CTRL VEH; ^ $p < 0.05$, ^^$p < 0.01$ compared to CTRL MP0.3, $ $p < 0.05$, $$ $p < 0.01$ compared to CTRL MP1, #$p < 0.05$, ##$p < 0.01$ compared to VPA VEH, + $p < 0.05$, ++ $p < 0.01$ compared to VPA MP0.3. Figure was modified from Anja *et al*. 2021. [284] ……...281

Figure 11: MP-III-022 at a concentration of 30 nM (referred to as "MP") exhibited the ability to enhance the timing of the GABA switch, as well as improve spontaneous neuronal activity which

had been disrupted by the administration of valproate (referred to as "VPA"). This improvement was observed through various parameters: (a) the frequency and (b) amplitude of spontaneous calcium oscillations, (c) the amplitude of GABA-induced calcium transient at day in vitro (DIV) 13, and (d) the amplitude of spontaneous calcium oscillations at DIV 15. Additionally, (e) representative recordings of all experimental groups were obtained during constant perfusion and GABA application. The cells were loaded with Fluo-4 AM at a concentration of 5 μM and subsequently imaged at a frequency of 1 Hz. The data presented included comparisons with the control group (referred to as "CTRL") and the saline-treated group (referred to as "SAL"). Statistical significance was indicated as follows: *p < 0.05, ***p < 0.001. Figure was modified from Anja *et al*. 2021. [284]…….283

Figure 12: Hippocampal mRNA expression was assessed in response to different treatments (vehicle [VEH], MP-III-022 at 0.33 mg/kg [MP0.3], or MP-III-022 at 1 mg/kg [MP1]) administered to animals with prenatal exposure (control [CTRL] or valproate [VPA]). The expression levels of three genes were measured: (a) GABRA5, (b) NKCC1, and (c) KCC2. The sample sizes per group were as follows: For males in CTRL VEH and VPA VEH groups, there were 7 samples for GABRA5 and KCC2, and 6 samples for NKCC1. In the VPA MP0.3 group, there were 7 samples for GABRA5 and NKCC1, and 8 samples for KCC2. For males in CTRL MP0.3, CTRL MP1, VPA MP1, and females in each group, there were 6 samples for each gene expression. Statistical significance was denoted as follows: *p < 0.05, **p < 0.01, and 0.05 < p < 0.01. Figure was modified from Anja *et al*. 2021. [284]……..286

Figure 13: The outcomes of the Novel Object Recognition Test for short-term memory (NORT short-term), the Social Interaction Test (SIT), and the Social Recognition Test (SRT) are depicted for both transgenic and non-transgenic 5xFAD animals of both sexes, subjected to

treatments with PWZ-029, MP-III-022, or solvent. The analysis involves evaluating the time spent with the new versus old object for NORT short-term, the time spent with an empty cage versus a cage with a conspecific in SIT, and the time spent with cages containing a new versus old mouse in SRT (designated as A, B, and C, respectively). The levels of statistical significance are indicated on the graphs: * signifies significance within the range of $0.01 < p < 0.05$, ** indicates significance within the range of $0.001 < p < 0.01$, and *** signifies $p < 0.001$. Figure was modified from Arandelovic *et al.* 2022 [285] ……287

Figure 14 : The results from the Morris Water Maze (MWM) are presented for both transgenic and non-transgenic 5xFAD animals of both sexes, subjected to treatments with PWZ-029, MP-III-022, or the solvent. The time spent in the peripheral zone during the probe test (Figure A); Latencies to reach the new platform in trials 1 vs. 2 during the reversal cued phase (Figure B); In the reversal probe, the latency to find the new platform zone vs. the old platform zone (Figure C); The number of entries in the new platform zone vs. the old platform zone (Figure D); The time spent in the peripheral zone (Figure E). For the analyses involving trials (B, C, D), a three-way ANOVA with repeated measures was used. For the analyses without repeated measures (A, E), a three-way ANOVA was employed. In both cases, Sidak's post hoc test was applied. The levels of statistical significance are displayed on the graphs as follows: * for $0.01 < p < 0.05$, ** for $0.001 < p < 0.01$, and *** for $p < 0.001$. The abbreviations used are: "g" for genotype, "s" for sex, "t" for treatment, and "p" for platform. Figure was modified from Arandelovic *et al.* 2022 [285]……291

Figure 15: Patient with AS. Image was collected from google……..293

Figure 17. AS mice Vs WT mice. In mice with Angelman syndrome (AS), there was an observable increase in the power of slow-wave frequencies during their awake EEG recordings.……294

Figure 18. The varying doses of MP-III-022 (1.25 mg/kg, 2.5 mg/kg, and 5 mg/kg) exhibited a consistent trend of reducing slow wave power in mice with Angelman syndrome (AS), with the reduction being absent at the 0.5 mg/kg dose……..295

Figure 19. Induction of seizures by fluorothyl inhalation……296

Figure 20. The susceptibility of AS mice to experiencing seizures was effectively reduced by administering a lower dose of MP-III-022. #### and ## mean p < 0.0001 and <0.01 for comparison between WT and AS vehicle. *, **, *** and **** mean p <0.05, <0.01 , p <0.001 and <0.0001 in compared to vehicle of the same genotype……297

Figure 21. Open Field Test. Mice with Angelman syndrome (AS) exhibit behaviors that resemble anxiety-like behavior. A decreased tendency to explore the center field area is indicative of heightened anxiety in the mice under consideration……298

Figure 22. Improvement of anxiety-like behavior with MP-III-022. Specifically, the administration of a lower dose of MP-III-022 (0.5 mg/kg followed by 1.25 mg/kg intraperitoneal injection) led to a notable improvement in anxiety-like behavior in mice with Angelman syndrome (AS). This improvement was particularly evident when compared to the response observed at the higher dose levels (1.25 mg/kg, 2.5 mg/kg, and 5 mg/kg). #### and ## mean p < 0.0001 and <0.01 for comparison between WT and AS vehicle. *, **, *** and **** mean p <0.05, <0.01 , p <0.001 and <0.0001 in compared to vehicle of the same genotype……..299

Figure 23. (A) Exposure to valproic acid (VPA) during prenatal development resulted in heightened self-grooming behavior among both male and female rats during early adolescence. (B) However, this increase in self-grooming behavior was not sustained into adulthood. (C) Notably, adult male and female rats exposed to VPA exhibited a notable reduction in social interaction. (D) In terms of cognitive function, only male rats exposed to VPA displayed a decline in recognition memory, as evidenced by their performance in the Novel Object Recognition (NOR) test (n=8-10 rats per group). Statistical analysis using a two-way ANOVA followed by Tukey's post-test demonstrated statistical significance (*p<0.05) when comparing the results of the VPA-exposed rats to the saline-exposed rats. Image was modified from Adriana et al.2023 [287]……301

Figure 24. The effects of *in utero* valproic acid (VPA) exposure were observed in both male and female rats. (A) An augmented count of spontaneously active ventral tegmental area dopamine (VTA DA) neurons was evident, as indicated by significantly increased numbers in both males and females (n= 6 animals per group). (B) Importantly, despite the heightened activity, the firing rate of these VTA DA neurons remained unaffected. (C) Additionally, the percentage of spikes occurring within bursts of activity demonstrated no significant change. This analysis encompassed 56 DA neurons in male saline-exposed rats and 63 DA neurons in male VPA-exposed rats, as well as 57 DA neurons in female saline-exposed rats and 82 DA neurons in female VPA-exposed rats. Notably, statistical analysis was conducted using a two-way ANOVA followed by Tukey's post-test, with statistical significance indicated by *p<0.05 when comparing VPA-exposed rats to the saline-exposed rats. Image was modified from Adriana *et al*.2023 [287]……..303

Figure 25. (A) SH-053-2'F-R-CH_3 effectively mitigated the impaired social interaction test performance in male rats exposed to VPA. (B) However, this ameliorating effect was not observed in female rats exposed to VPA. (C) Additionally, SH-053-2'F-R-CH_3 was capable of reversing deficits in novel object recognition memory specifically in male rats with VPA exposure. (D) Notably, female rats exposed to VPA did not exhibit deficits in the novel object recognition test. (E) Despite these improvements, the heightened population activity of VTA DA neurons in (E) male and (F) female VPA-exposed rats remained unaltered by SH-053-2'F-R-CH_3 intervention. These findings were consistent across the behavioral tests (n=5-10 animals per group) and VTA recordings (n=5 animals per group). The statistical significance of these results was denoted by *p<0.05, as determined by a two-way ANOVA followed by Tukey's post-test. Image was modified from Adriana *et al*.2023 [287]……305

Figure 26. Verification of electrode placements and the response to pilocarpine. (A, Left) A representative brain slice displaying an electrode track within the ventral tegmental area (VTA; black arrow) and a cannula track within the ventral hippocampus (vHipp; white arrow) is presented, accompanied by the corresponding schematic of the brain section (right, positioned at -5.40 mm posterior to bregma. (B) Rats treated with pilocarpine exhibited a notably higher average Racine rating in comparison to controls treated with saline, **** $p < 0.0001$, n = 6–16/group; circles represent male subjects, while squares represent females. Image was modified from Alexandra *et al*.2023 [291]……..……308

Figure 27. GL-II-73 effectively counteracts the heightened VTA dopamine neuron activity induced by pilocarpine. (A) Administration of intraventral hippocampal (vHipp) pilocarpine led to a substantial rise in the number of spontaneously active dopamine cells per track (population activity), which was then reversed through the intra-vHipp application of GL-II-73 (100 ng/µL;

0.75 µL). However, average firing rate (B) and percent burst firing (C) remained unaffected by pilocarpine or drug treatment. Additionally, (D) the representative trace of dopamine neuron firing and action potential for saline-treated (left) and pilocarpine-treated (right) rats. ** p < 0.005, n = 6–13/group; circles represent male subjects and squares denote females. Figure was modified from Alexandra *et al.*2023……310

Figure 28. GL-II-73 exhibited an inability to reinstate proper dopamine system function in situations where radixin had been knocked down. In panel A, on the left, exposure to inescapable shock was observed to markedly elevate the count of spontaneously active cells per track, indicating an increase in population activity. However, this effect was counteracted by the administration of GL-II-73 (100ng/µL; 0.75 µL) into the ventral hippocampus, but this restoration was not observed in cases where radixin had been knocked down. On the right of panel A, a representative brain slice was displayed, with electrode placement highlighted in the ventral tegmental area (VTA) (marked by a black arrow), and the cannula's position for drug delivery in the ventral hippocampus (vHipp, indicated by a white arrow). Corresponding brain section schematics were provided for the region -5.40 mm posterior to bregma, with a box outlining the specific area containing the tracks. Analysis of (B) firing rate and (C) burst firing showed no significant effects resulting from siRNA, shock exposure, or drug treatment. Finally, panel (D) featured representative traces from both control (on the left) and shocked (on the right) rats. The study consisted of 6 to 8 individuals per group, with males represented by circles and females by squares. Statistical significance was denoted as ***P = 0.0001 and ****P < 0.0001. "RDX" refers to radixin. Figure was modified from Alexandra *et al.*2023 [294]……..…312

Figure 29. The reduction of radixin expression does not bring about any changes in prepulse inhibition. A period of two days involving inescapable shock demonstrated a notable overall impact on prepulse inhibition, as did the administration of GL-II-73 (with a significance level of p = 0.0042). Nevertheless, when subsequent detailed examinations were conducted, no significant differences among the groups were observed. Each group encompassed a total of 9 to 11 individuals, with males and females represented by circles and squares, respectively. **P < 0.005, and RDX= radixin. Figure was modified from Alexandra *et al.*2023 [294]……..…..314

Figure 30. The structures of Hz-166, SH-I-048A, SH-053-2'F-*R*-CH_3-acid, MP-III-004, and MP-III-058, and SH-053-2'F-*R*-CH_3……..387

Figure 31. Discovery of GL-II-93 (MIDD0301)……389

Figure 32: *Ex vivo* smooth muscle force in guinea pig tracheal rings. Rings were pre-contracted with 1 µM substance P and then treated with vehicle (0.1% DMSO) or 100 µM of indicated compounds and resulting relaxation was measured at 15 min, 30 min, 45 min, and 60 min. Data is expressed as the amount of muscle force remaining at indicated time points (n=4-7). Unpublished data (confidential)…… …394

Figure 33. Relaxation of *Ex vivo* guinea pig smooth muscle. Rings were pre-contracted with 1 µM substance P and then treated with vehicle (0.1% DMSO) or 100 µM of indicated compounds and resulting relaxation was measured at 15 min, 30 min, 45 min, and 60 min. Data is expressed as the amount of muscle force remaining at indicated time points (n=3). DS-II-67 produced comparable activity with MIDD0301. Unpublished data (confidential)…….. …….395

LIST OF TABLES

Chapter 1. Introduction

Table 1: The pharmacological effects at $GABA_A$ $\alpha_{1-6}\beta_{1-3}\gamma_2$ receptor subtypes.[18, 46-58]…….12

Table 2. Binding affinities at α1-3 and α5 human $GABA_A$ R subtypes……..26

Table 3. Binding affinities at α1-3 and α5 human $GABA_A$ R subtypes……..28

Table 4. The sequence alignment of α1-6 subunits…….……30

Chapter 2. Development of α6-GABAAR Subtype-Selective Pyrazoloquinolinones for Treating Tourette Syndrome, Migraine, and Trigeminal Pain

Table 1 : Summary table of log threshold (T0) values in rats tested with ATDP 34,282 (10 and 30 mg/kg) or vehicle. Data represent the mean baseline log T0 frequency (log/Hz) ± SEM of 10 rats. Test log T0 values were excluded from 2 rats due to due to marked rate suppression produced by the 10 mg/kg ATDP 34,282 dose. A significant difference in test T0 values compared to vehicle is denoted by asterisks (* $p<0.01$). ADP34,282 = DK-I-56-1.……..…..67

Table 2: Summary table of frequencies that sustained half-maximal responding (M50) in rats tested with ATDP 34,282 (10 and 30 mg/kg) or vehicle. Data represent the mean baseline log M50 frequency (log/Hz) ± SEM of 10 rats. Test log M50 values were excluded from 2 rats due to due to marked rate suppression produced by the 10 mg/kg ATDP 34,282 dose. There was no significant difference between baseline M50 values preceding ATDP 34,282 tests compared to vehicle. A significant difference in test M50 values compared to vehicle is denoted by asterisks (** $p<0.0001$). ADP34,282 = DK-I-56-1.……..…..67

Chapter 3. The Development of a Scalable Synthesis, and Assessment of Bioactivity of Imidazodiazepines Targeting α2/3-GABAAR Subtypes for the Treatment of Epilepsy, Anxiety, and Neuropathic Pain

Table 1: Effect of KRM-II-81 and it's analogs in different pain model…….114

Table 2: Effects of KRM-II-81 and it's analogs in different models of epilepsy…….115

Table 3: Yield improvement for Step 2…….…….126

Table 4: Emax/min and ED50 values for KRM-II-81, MP-III-80 and gabapentin from acute neuropathic pain dose response experiments ……...149

Table 5: Mean seizure severity during injection (DI) periods and in the AM or PM 2 h after injections.…….156

Table 6: Table 6. Number of stage 5 seizures during injection (DI) periods and in the AM or PM 2 h after injections ……157

Table 7: Table 7: Baseline and End Temperatures for ETSP #490011 tested at 30mg/kg for 2.0 hours in the Dravet Hyperthermia Assay …….…….164

Table 8: Ability of ETSP #490011 to Elevate the Temperature Threshold of Induced Seizures ……....165

Table 9. Ability of ETSP#490011 to Prevent Hyperthermia-Induced Seizures ……..…..165

Table 10 : Table 10. Primary and secondary binding data for DS-II-73 (Unpublished data)……..……..166

Table 11: Binding concentration-inhibition functions for DS-II-73 (16)……..168

Table 12: Effects of DS-II-73 (16) against PTZ-induced seizures and lethality after oral administration in mice……..170

Table 13: Opioid receptor binding of α5 selective imidazodiazepines (PDSP). Unpublished data……..328

Table 14: Binding affinities at BZP rat brain site (PDSP) for the novel compounds. Unpublished data……..331

Chapter 4. D The Design and Synthesis of Chiral α5 Subtype BzR/GABAAR Modulators for Treating Anxiety, Depression, and Schizophrenia as well as Asthma

Table 1: Binding affinity of SH-053-2'F-R-CH_3 at αxβ3γ2 $GABA_A$/benzodiazepine site subtypes. Measurements were made in duplicate. Ki values are reported in nM …….…..232

Table 2 : Efficacy of SH-053-2'F-R-CH3 at αxβ3γ2GABAA receptor subtypes as % of control current at 100 nM and 1 mM concentrations.……233

Table 3 : Binding affinity of GL-II-73 at αxβ3γ2 GABAA/benzodiazepine site subtypes …….….235

Table 4: Peptide coupling trials …….249

Table 5: Attempts to synthesize DS-III-69…….267

Table 7 : Pro-cognitive activity of GL-II-73 analogues in the Y-maze assay……..316

LIST OF SCHEMES

Chapter 2. Development of α6-GABAAR Subtype-Selective Pyrazoloquinolinones for Treating Tourette Syndrome, Migraine, and Trigeminal Pain

Scheme 1: Synthesis of 4-oxo-1,4-dihydro-quinolines by Gould Jacob cyclization……..42

Scheme 2: Probable mechanism of Gould-Jacob cyclization [114]……..43

Scheme 3: Vilsmeier chlorination of 4-oxo-1,4-dihydroquinolines …….45

Scheme 4: Probable mechanism for Vilsmeier chlorination of 4-oxo-1,4-dihydroquinolines……..……46

Scheme 5: Synthesis of pyrazoquinolinones…….47

Scheme 6: Synthesis of DK-I-56-1……...……49

Scheme-7 : Probable mechanism for arylhydrazine formation ……49

Chapter 3. The Development of a Scalable Synthesis, and Assessment of Bioactivity of Imidazodiazepines Targeting α2/3-GABAAR Subtypes for the Treatment of Epilepsy, Anxiety, and Neuropathic Pain

Scheme 1. Synthesis of KRM-II-81 by Li et al. 2018 [151]…….…….121

Scheme 2. Possible Route to Bromoacetamide via the Pyridium Salt……122

Scheme 3: Formation Pathway of Imidate Impurity during Synthesis ……..123

Scheme 4: Formation of Benzodiazepine by Delepine Reaction [152-154]……..124

Scheme 5: Probable mechanism of Delepine Reaction ……...127

Scheme 6: Step 3: Synthesis of imidazodiazepine …….....128

Scheme 7: Possible mechanism of imidazole top installation on benzodiazepine …….130

Scheme 8: Copper free Sonogashira coupling: earlier chemistry ……..131

Scheme 9: Probable mechanism for copper free Sonogashira coupling…….132

Scheme 10: Probable mechanism for fluoride mediated deprotection of TIPS group …..…….133

Scheme 11: Scheme 10: Reduction of Hz-166 by PDBBA……..…..134

Scheme 12: Probable mechanism of reduction of Hz-166 by PDBBA…….135

Scheme 13: Synthesis of KRM-II-81……..137

Scheme 14: Possible mechanism for the conversion of aldehyde function to oxazole …….138

Scheme 15: Improved and scalable synthesis of Hz-166 by Sharmin ……...139

Scheme 16 : Synthesis of DS-II-73 [158]……..……..142

Scheme 17: Synthesis of MP-III-080……..143

Scheme 18: Synthesis of MP-III-024 and DS-II-27……144

Scheme 19: Synthesis of MYM-V-26, DS-II-47, and DS-II-48……..……..145

Chapter 4. D The Design and Synthesis of Chiral α5 Subtype BzR/GABAAR Modulators for Treating Anxiety, Depression, and Schizophrenia as well as Asthma

Scheme 1: Synthesis of SH-053-2'F-R-CH_3…….242

Scheme 2: Synthesis of SH-053-2'F-S-CH_3…….244

Scheme 3: Cyclization of free amine to form benzodiazepine 4 using NaOH as base ……...245

Scheme 4: Probable mechanism of NCA formation ……..….246

Scheme 5: Synthesis of benzodiazepine intermediate by NCA route)……..247

Scheme 6: Peptide coupling and cyclization for formation of benzodiazepine, 4…….249

Scheme 7: Possible mechanism of imidazole top installation on benzodiazepine …….252

Scheme 8: Synthesis of GL-II-73……255

Scheme 9: Improved scalable synthesis of GL-II-73 by the modified Boc-route……..257

Scheme 10: Synthesis of MP-III-022……..…...258

Scheme 11. Synthesis of DS-I-19 and DS-I-93……...……261

Scheme 12. Synthesis of DS-II-30……..262

Scheme 13. Synthesis of DS-I-49……263

Scheme 14: Synthesis of DS-I-16……...…264

Scheme 15. Synthesis of DS-IV-41 and MP-IV-04……266

Scheme 16 : Synthesis of DS-III-69……267

Scheme 17. Synthesis of 8-cyclopropyl carboxylic acid 38……391

Scheme 18. Synthesis of imine migrated analogs of GL-II-93……392

LIST OF ABBREVIATIONS

ACh	acetylcholine
AHR	airway hyperresponsiveness
AP-4	4-Aminopyridine
ASM	airway smooth muscle
AUC	area under curve
BALF	bronchoalveolar lavage fluid
BBB	blood-brain-barrier
BQL	below the quantification limit
BZD	benzodiazepine
BzR	benzodiazepine receptor
CFA	complete Freund's adjuvant
CDAP	chlordiazepoxide
CINP	Chemotherapy-induced neuropathic pain
CMC	carboxymethyl cellulose
CNS	central nervous system
COPD	chronic obstructive pulmonary disease
CRS	chronic restraint stress
DI	diazepam-insensitive
DLM	dog liver microsomes
DNP-KLH	dinitrophenyl hapten-keyhole limpet hemocyanin
DS	diazepam-sensitive
ETSP	Epilepsy Therapy Screening Program

FDA	Food and Drug Administration
FST	forced swim test
GABA	gamma-aminobutyric acid
$GABA_AR$	gamma-aminobutyric acid type A receptors
$GABA_BR$	gamma-aminobutyric acid type B receptors
GINA	Global Initiative for Asthma
hERG	human Ether-à-go-go-Related Gene
HEK	human embryonic kidney cells
HDM	house dust mite
HLM	human liver microsomes
HPLC	high-performance liquid chromatography
HT	hydroxyl tryptamine
ICSS	ICSS
IMDZ	imidazodiazepine
IgG	immunoglobulin G
IP	intraperitoneal
IV	intravenously
KA	kainic acid
KOR	kappa opioid receptors
LABA	long-acting β_2 agonist
LR	Lawesson's reagent
LTG	lamotrigine
MAM	methylazoxymethanol acetate

MCh	methacholine
MDD	major depressive disorder
MED	minimal effective dose
MES	maximal electroshock
MLM	mouse liver microsomes
MOE	Molecular Operating Environment
MPE	maximum possible effect
MRM	multiple reaction monitoring
MTD	minimal toxic dose
mTLE	mesial temporal lobe epilepsy
MW	molecular weight
NAM	negative allosteric modulator
NIMH	National Institute of Mental Health
NO	nitric oxide
NMDA	*N*-methyl-D-aspartate
Ova s/c	ovalbumin sensitized challenged
PAM	positive allosteric modulator
PQ	pyrazoquinolinones
PBR	peripheral benzodiazepine receptor
PCLS	precision-cut lung slice
PCP	phencyclidine
PDSP	Psychoactive Drug Screening Program
PEG	polyethylene glycol

PFC	mouse prefrontal cortex
PI	protective indices
PK	pharmacokinetics
PPI	prepulse inhibition
PTZ	pentylenetetrazole
PWT	paw withdrawal threshold
PO	oral administration
RLM	rat liver microsomes
SABA	short-acting β_2 agonist
SAR	structure-activity relationship
scMET	subcutaneous pentylenetetrazole
SE	severe epilepsy
SEM	standard error of the mean
SLA	spontaneous locomotor activity
SNL	sciatic nerve ligation
SSRI	selective serotonin reuptake inhibitors
sRaw	specific airway resistance
SST	somatostatin
TLC	thin-layer chromatography
TLE	temporal lobe epilepsy
TPE	time of peak effect
TSPO	translocator protein

ACKNOWLEDGEMENTS

I extend my heartfelt appreciation and gratitude to my advisor, Professor James M. Cook, for his invaluable guidance and unwavering support throughout my journey in completing my doctorate in organic and synthetic medicinal chemistry. His mentorship has been pivotal in shaping both my professional and personal growth. I am genuinely thankful for his exceptional assistance in steering my research, as well as in refining my papers and thesis. I also wish to acknowledge the members of my doctoral committee: Dr Alexander E Arnold, Dr Alan W Schwabacher, Dr Arsenio Andy Pacheco, Dr Jorg C Woehl, and Dr Jarett M Wilcoxen. Their insightful advice, meaningful discussions, and constructive critiques have played a vital role in enhancing the quality and depth of my work.

I would like to thank our numerous collaborators. I have personally benefitted greatly and gained vast knowledge in the field of pharmacology, and medicinal chemistry, especially Miroslav M Savić (University of Belgrade, Serbia), Dr. Etienne Sibille (CAHM, University of Toronto, Canada), Dr Tom Prevot (CAHM, University of Toronto, Canada), Dr. Jeff Witkin (Ascension St. Vincent Hospital, Indianapolis, IN), Dr. Donna M. Platt (Mississippi Medical School, USA), Dr. Jun-Xu Li (University at Buffalo, USA), Dr. Charles W. Emala (Columbia University, USA) Dr LC Chiou (Taiwan University, Taiwan), Dr Kiyoshi Egawa (Hokkaido University, Japan), Dr Bradford Fisher (Cooper Medical School of Rowan University, USA), Dr Katarzyna Kuter (Polish Academy of Sciences, Polland), Dr David White (NIH).

I extend my gratitude to both past and current members of the Cook group who have been an integral part of my journey. A special thank you goes to Dr. Knutson for imparting the knowledge of large-scale synthesis and compound purification without chromatography. I am truly appreciative of Dr. Anna Benko, Dr. Holger, Mr. Neal Korfhage, Mr. Kevin Blackburn,

Ms. Elise D. Nicks, Ms. Wendy Grober, and Ms. Shelley Hagen for their unwavering support and willingness to assist whenever I needed guidance or help.

I express my heartfelt gratitude to my parents, in-laws, siblings, friends, and loved ones for their unwavering prayers, support, and affection throughout my entire life, especially during my PhD journey. A profound and exceptional thank you is reserved for my mother and grandmother, whose sacrifices have shaped the person I am today. I hold a special place of appreciation and acknowledgment for my husband, Yeunus Mian, who has been my best friend, co-worker, and a constant source of support throughout these years. Lastly, I attribute all the credit and honor of this work to Allah (the creator). It is through His divine guidance and assistance that I have achieved what I have. Without Him, none of this would have been possible.

Chapter 1

Introduction

1.1. The $GABA_A$ receptors

Gamma (γ)-amino butyric acid (GABA) is a naturally occurring amino acid that functions as the principal inhibitory neurotransmitter in the central nervous system (CNS), as well as the cerebellum of the mammalian brain.[1] GABA is known to inhibit the excess increase in the neuronal activity.[1] The inhibitory activity of GABA is mediated through the binding of GABA to GABA receptors. GABA receptors are classified into two major classifications, GABAA receptors and GABAB receptors.[2] GABAA receptors are found in the family of ligand-gated chloride ion channels. Once the allosteric benzodiazepines bind, the GABAA receptor is locked into a conformation where the neurotransmitter GABA has much higher affinity for the GABAA receptor. Once bound to GABA, the protein receptor changes conformation within the membrane, increasing the frequency of the opening of the pore to permit chloride anions (Cl^-) to pass down an electrochemical gradient.[3]

The potentiation of the inhibitory effect of GABA by benzodiazepines leads to anxiolytic, anticonvulsant, sedatives, ataxic, and a host of other CNS effects.3 GABAB receptors, on the other hand, are G-protein-coupled, slow-acting receptors that are involved in the activity of potassium and calcium channels.[4] The function of GABAAR is disrupted in various CNS disorders, including depression[5], schizophrenia[6], major depressive disorder (MDD)[5], anxiety[7], bipolar disorder [8,9], epilepsy [10], neuropathic pain [11], and Alzheimer's disease [12].

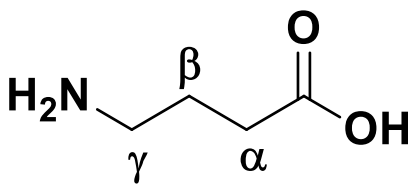


Figure 1. γ-Aminobutyric acid

GABAARs are heteropentameric ion channels composed of a variety of subunits. To date, 19 subunits have been identified in human GABAARs, including α1-6, β1-3, γ1-3, δ, ε, θ, π, and ρ1-3.[13] However, not all subunit combinations form functional receptors, and the exact subunit composition can vary depending on the location in the brain, developmental stage, and other factors. Among the subunits, the α, β, and γ subunits are the most commonly expressed in the brain and are essential for forming a functional receptor. The α subunits contribute to the binding site for GABA, while the β and γ subunits form the ion channel through which chloride ions flow when the receptor is activated.[14]

The stoichiometry of subunits in a functional GABAAR can vary, but a fully functional benzodiazepine-mediated chloride ion channel consists of α1-6β1-3γ2 subunits in a 2:2:1 stoichiometric ratio (**Figure 2**).[2,15] The specific combination of subunits in the GABAAR determines its pharmacological and physiological characteristics, such as its sensitivity to drugs like benzodiazepines. Although there is still much to learn about the roles that individual subunits play in GABAAR function, ongoing research is focused on elucidating these functions and identifying potential new drug targets for neurological and psychiatric disorders.

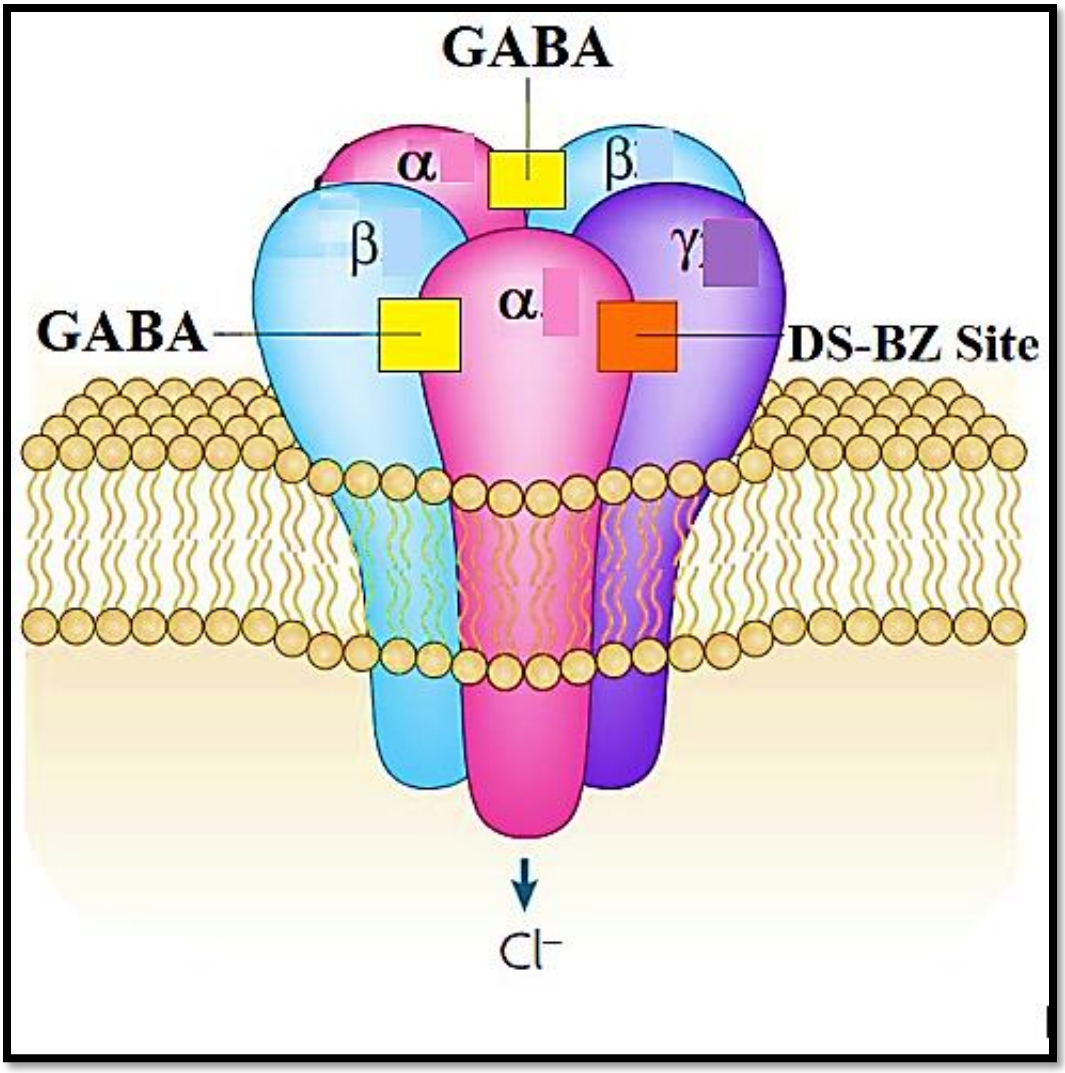


Figure 2. The GABAAR is a type of pentameric ligand-gated chloride channel composed of two α subunits, two β subunits, and one γ subunit. The figure illustrating this structure was adapted from a publication by Jacob and colleagues in the journal Nature Reviews Neuroscience, 2008.

Immunocytochemistry studies have been used to examine the occurrence and distribution of different subunits of GABAAR in the CNS of rodents[16]. These studies have revealed that α1, β1-3, and γ2 subunits are widely expressed in the brain, both synaptically and extrasynaptically[17]. In fact, the α1β2γ2 subunit combination is the most abundant in the rat brain, comprising

approximately 50% of the total GABAAR population. [15,18,1] Furthermore, the prevalence of α2 and α3 subunits in the rat brain is relatively equal, with each comprising 20-30% of the total GABAAR population.[15,18,19] This suggests that these subunits play an important role in GABAAR function in the CNS. Overall, the use of immunocytochemistry studies has provided important insights into the expression patterns of different subunits of GABAAR in the rodent brain, which has implications for our understanding of GABAAR function and the development of novel therapeutic strategies for neurological and psychiatric disorders.

The hippocampus is the primary location for GABAAR ion channels containing the α5 subunit, which accounts for only 5% of the total GABAAR population.[18,19] Although α5-containing GABAARs have also been found in the spinal cord[20], the prevalence of α5 subunits is much lower than that of α1, α2, and α3 subunits in the rat brain [18-20], suggesting that these other subunits play a more prominent role in GABAAR function. It is important to note that GABAARs are not limited to the central nervous system, and they have also been found in other parts of the body, such as the lungs, stomach, and heart sinus node.[1] This indicates that GABAARs may have a broader physiological role beyond their well-known function in the brain.

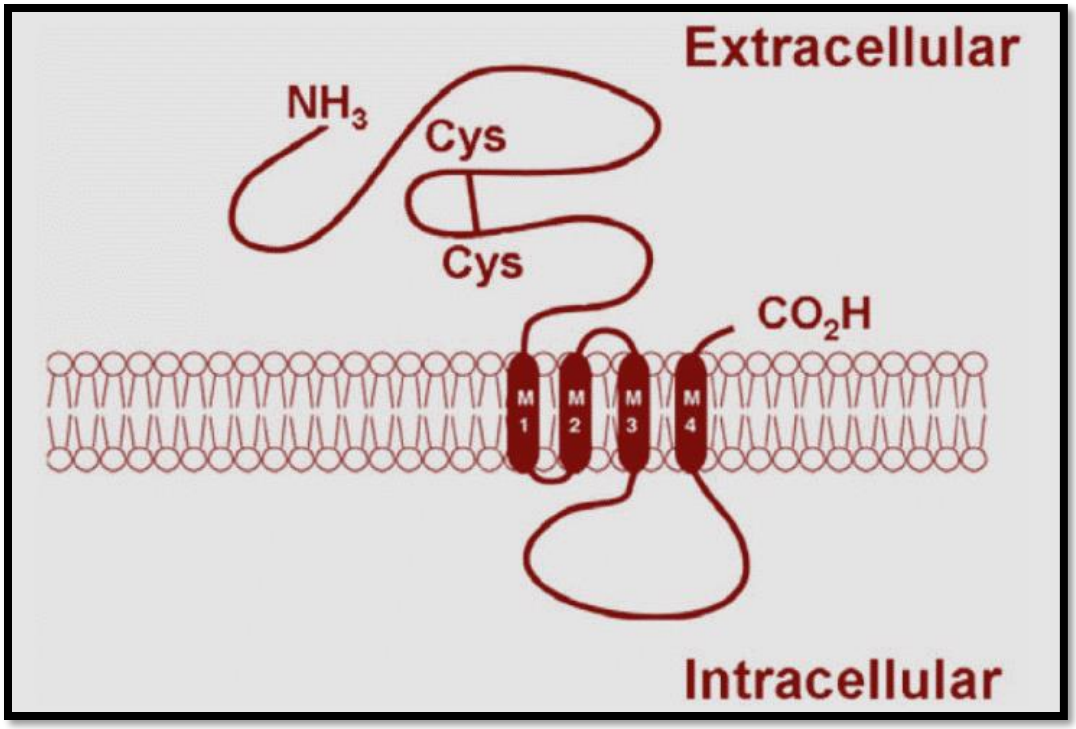


Figure 3. The figure depicts the potential configuration of a GABAA receptor subunit, with the N-terminus located in the extracellular domain and the M1-M4 representing the four transmembrane domains. This diagram has been adapted from the original figure in Burt et al.[21] and Clayton et al.[22]

The polypeptide GABAAR has an approximate mass of around 50 kD, and its structure exhibits significant similarity among each subunit. Different classes of subunits, such as α and β, display approximately 20% sequence identity or 50% sequence similarity, while subunits within the same class exhibit about 70% homology.[16] **Figure 3** illustrates that the potential glycosylation sites are located at the N-terminal end of each subunit, situated in the extracellular region of the chloride ion pore. [22-24]

Within the GABAAR structure, a crucial feature is the presence of two conserved cysteine residues that form a covalent bond, creating a loop commonly referred to as the "Cys-loop". Additionally, a substantial intracellular loop can be observed between the transmembrane regions 3 and 4, denoted as M3 and M4, respectively. It is worth noting that the chloride ion pore is formed through the combination of five individual subunits, as depicted in **Figure 4**.

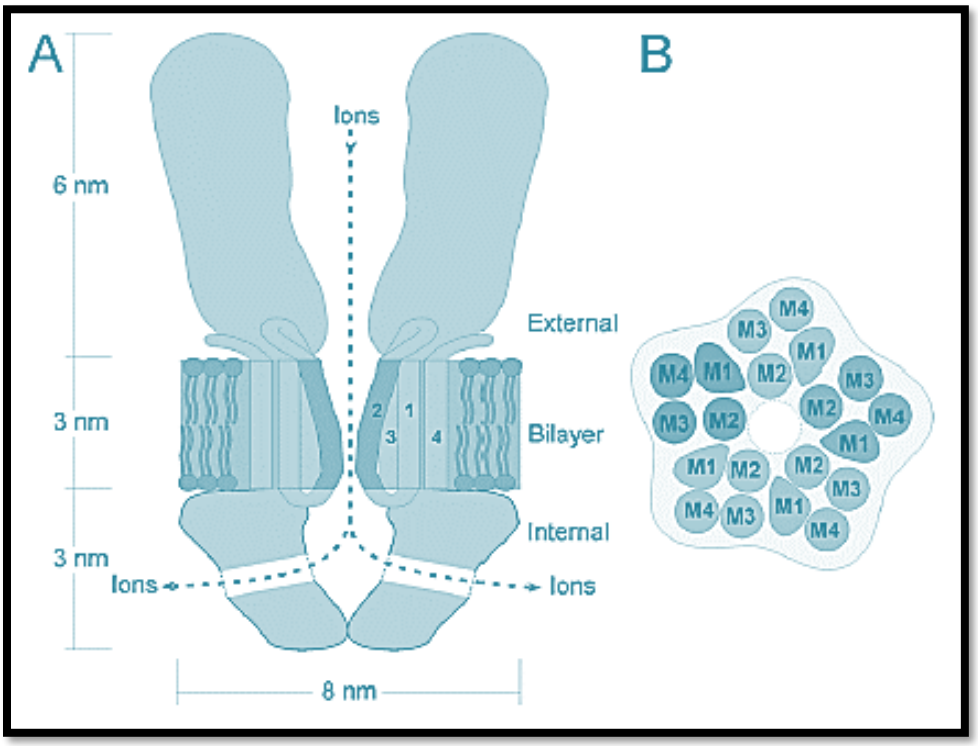


Figure 4. The schematic representation of a ligand-gated ion channel, both in longitudinal (A) and cross-sectional (B) views, is depicted in the figure. The segments M1, M2, M3, and M4 are indicated by the numbers 1, 2, 3, and 4, respectively. This image has been modified from the original figure provided by Keramidas et al. [23] and Clayton et al. [22], who have extensively studied the topic. By presenting the structural arrangement of the ligand-gated ion channel, this figure aids in understanding the spatial orientation of its various components and contributes to our comprehension of its functional properties.

Within the synaptic cleft and the pore of GABAAR, there are multiple binding sites available. These binding sites play a crucial role in the activation of the GABAAR complex when they interact with different classes of compounds, including β-carbolines, barbiturates, ethanol, benzodiazepines, and endogenous steroids. [2,24]

The synaptic cleft is notably enriched with the α1-6β1-3γ2 GABAR, which are arranged in a specific pattern known as αβαβγ clockwise when viewed from the extracellular region (**Figure 4**). GABA binds orthosterically at the two α-β+ interfaces, contributing to the activation of the GABAAR complex. Additionally, the γ-α+ interface serves as the allosteric benzodiazepine binding site (BzR) [3,25]. These important binding interactions are illustrated in **Figure 2** and **Figure 5**.

In the 1990s, studies revealed that the compound CGS 9895 binds specifically at the β-α+ interface of GABAAR [26,27]. Additionally, certain pyrazoloquinolines have been found to bind to the GABAAR, particularly targeting the α6 subunit at the PQ side. It is worth noting that the positive modulation of GABAAR by the CGS series may not solely stem from its tight activity at the BzR (benzodiazepine binding site). In some cases, it is possible that the agonist efficacy of these compounds arises from their interaction at the PQ site [2,15,28].

Furthermore, the interior pore of the GABAR also serves as a binding site for various compounds, including neurosteroids, ethanol, picrotoxin, barbiturates, and others. [29,30,31] Numerous studies have reported the binding of ethanol and its interactions with Bz/GABAAergic subtypes [32,^3] , and this has been a topic of ongoing research.

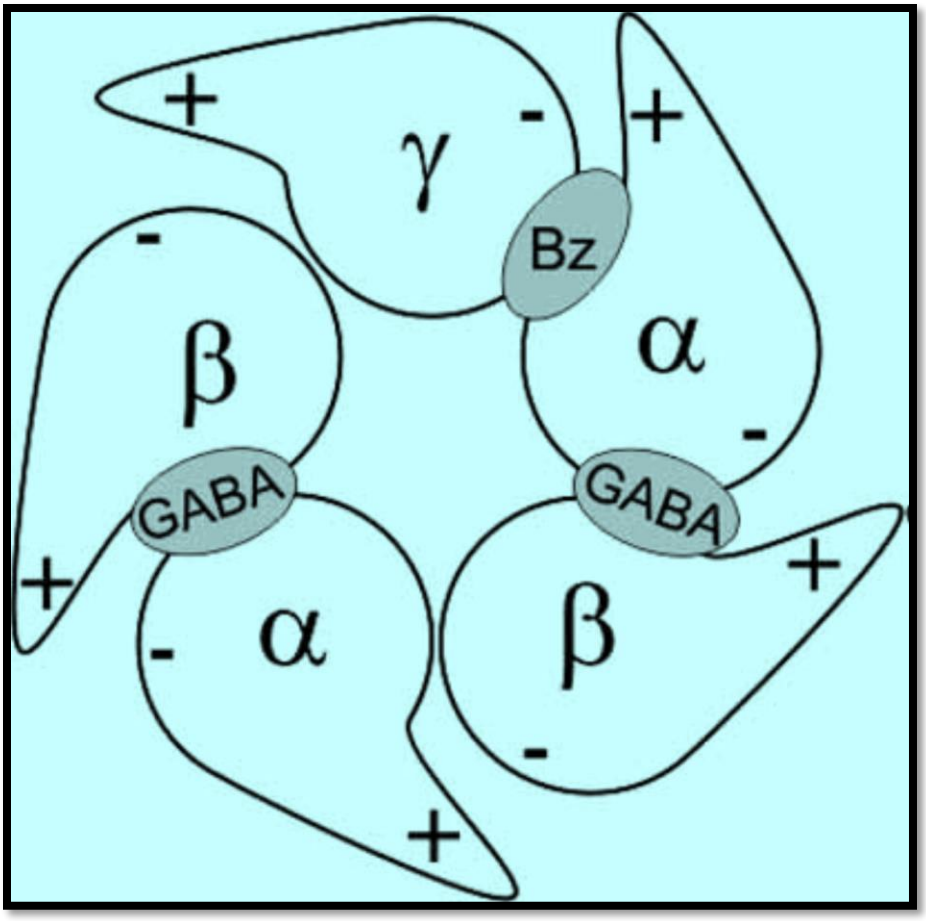


Figure 5. The schematic representation of the arrangement of the α1β2γ2 GABAA receptor when viewed from the synaptic cleft. This figure shows that the β+α- subunit interfaces house the GABA binding sites, while the α+γ- subunit interface contains the benzodiazepine modulatory binding site. The presence of loop C in the respective subunits is indicated by the '+' sign. This image has been adapted from the original figure presented in the works of Clayton *et al.* [17] and Ernst *et al.* [34]

1.2. Benzodiazepines

The psychoactive drugs known as benzodiazepines (BZDs) were first discovered by Dr. Leo Sternbach. These drugs have been prescribed for more than 50 years to treat various central nervous system (CNS) disorders, including seizures, anxiety, and insomnia. [35,36].

Benzodiazepines have high absorption in the gastrointestinal tract and can easily penetrate the blood-brain barrier (BBB) [37-39]. Benzodiazepines (BZDs) are commonly prescribed to alleviate symptoms associated with anxiety, insomnia, seizures, and muscle spasms. Benzodiazepines exert their effects by enhancing the activity of the neurotransmitter gamma-aminobutyric acid (GABA) in the brain. By binding to specific receptors on GABA receptors, benzodiazepines increase the inhibitory effects of GABA, leading to sedative, anxiolytic, muscle relaxant, amnesia and anticonvulsant dependance activities.

These medications are known for their rapid onset of action and effectiveness in providing short-term relief for acute symptoms. However, due to their potential for tolerance, dependence, and withdrawal, benzodiazepines are typically prescribed for short durations. Prolonged or excessive use of benzodiazepines can lead to various adverse effects, including drowsiness, dizziness, confusion, impaired coordination, memory problems, and in rare cases, paradoxical reactions.

It is essential to use benzodiazepines under medical supervision, according to prescribed guidelines. Gradual tapering off the medication is often recommended to minimize withdrawal symptoms and potential rebound effects. Furthermore, it is crucial to be aware of potential interactions with other medications or substances, as combining benzodiazepines with certain substances can amplify their sedative effects and increase the risk of respiratory depression.

While benzodiazepines remain valuable therapeutic options for specific conditions, ongoing research and medical advancements aim to develop alternative treatments with improved safety profiles and reduced risks associated with long-term use.

Traditional benzodiazepines, such as diazepam (also known as Valium), have a core structure consisting of a benzene-A ring fused with a seven-membered diazepine ring. They also feature a

pendant phenyl C ring (**Figure 6**) [40]. These traditional benzodiazepines bind non-selectively to the α1-3,5β1-3γ2 GABAA receptors at the benzodiazepine modulatory binding site (BzR). As a result, they exhibit certain adverse effects, including ataxia, drowsiness, muscle relaxation, sedation, amnesia, dependence, withdrawal issues, and tolerance to the anticonvulsant and antinociceptive effects [24,41,42].

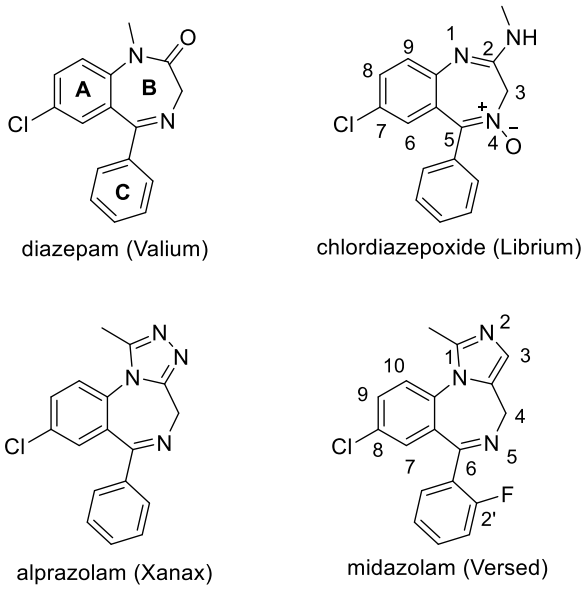


Figure 6. The structures of classical 1,4-benzodiazepines, including diazepam, chlordiazepoxide, the triazolobenzodiazepine alprazolam, and the imidazobenzodiazepine midazolam. Each of these benzodiazepines has a distinct chemical structure, contributing to their unique pharmacological properties and effects.

1.3. The pharmacology of $GABA_AR$ associated with different subunits

The different subtypes of GABAARs are associated with distinct pharmacological effects, largely influenced by the specific types of α(x) subunits present within the receptor complex. The α subunit plays a crucial role in determining the functional properties, ligand specificity, and pharmacological responses of GABAARs.

Different α subunits confer unique characteristics to GABAARs, leading to variations in their sensitivity to agonists, antagonists, and modulators. For example, GABAARs containing the α1 subunit are primarily associated with sedative and anxiolytic effects, while those with the α2 subunit are implicated in the regulation of anxiety, seizures, and sleep. The α3 subunit is commonly found in extrasynaptic GABAARs and is linked to tonic inhibition and anxiolytic effects. GABAARs containing the α4 and α6 subunits are predominantly expressed in cerebellar granule cells and contribute to motor coordination and control.

Furthermore, the presence of different α subunits can influence the receptor's sensitivity to specific drugs, such as benzodiazepines and other allosteric modulators. Variations in the α subunit composition of GABAARs can result in different affinities for these compounds, leading to diverse pharmacological responses.

Understanding the role of α (x) subunits in GABAAR subtypes provides insights into the functional diversity and specificity of GABAergic signaling in the brain. It also has implications for the development of targeted pharmacological interventions that selectively modulate GABAAR subtypes, potentially leading to more tailored treatments for various neurological and psychiatric conditions.

The identification of the associated effects of different subunits in GABAARs has been achieved through a combination of receptor binding studies, pharmacological investigations, and molecular genetic approaches. Numerous research groups, including the works of Mohler, Sieghart, McKernan, Sigel, Seeburg, Squires, and Haefely, have made significant contributions to this field.

Their collective efforts have led to the characterization of various GABAAR subtypes, such as α1β3γ2, α2β3γ2, α3β3γ2, α4β3γ2, α5β3γ2, and α6β3γ2, and the identification of their specific effects. These effects have been summarized in Table 1, representing the culmination of many years of research by scientists like Mohler, Rudolph, McKernan, Sieghart, Siegel,Cook and others.

The extensive body of work conducted by these researchers has advanced our understanding of GABAAR subunit composition, functional diversity, and their implications in neurological and psychiatric disorders. This knowledge serves as a foundation for further research and the development of targeted therapeutic interventions that can selectively modulate specific GABAAR subtypes for improved clinical outcomes.

Table 1: The pharmacological effects at $GABA_A$ $\alpha_{1-6}\beta_{1-3}\gamma_2$ receptor subtypes.[18, 46-58]

Subunits	Associated effects
α_1	Anxiolysis,,sedation, anterograde amnesia, some **anticonvulsant** action, ataxia, involved in the development of tolerance, addiction
α_2	**Anxiolytic**, some **anticonvulsant** action, **antihyperalgesia**
α_3	**Anxiolytic, antihyperalgesia** action,anticonvulsant action may be some muscle relaxation at higher doses
α_4	Diazepam-insensitive site; asthma, **important in lung disorders in the periphery**
α_5	**Cognition**, temporal and spatial memory, **depression, schizophrenia, asthma**

α_6	Diazepam-insensitive site; **migraine, trigeminal orofacial pain, active in a model of Tourettes syndrome, PPI model**
The green indicated pharmacology was discovered by pharmacologists in collaboration with the Milwaukee group. Presented at the BBC meeting, Cook et al. Feb 28 to March 2nd (2017).	

The α1-subunit of GABAAR is the most prevalent among all the α subunits in the brain, constituting approximately 40-50% of the α GABAA subtypes. [43,44] This high abundance of α1-containing GABAARs is associated with a diverse range of pharmacological effects. These effects include anxiolysis (reduction of anxiety), anticonvulsant action (prevention of seizures), ataxia (impaired muscle coordination), sedation, anterograde amnesia (inability to form new memories), the development of tolerance (reduced response to repeated administration), addiction, dependence, and muscle relaxation [45,46]. The prevalence and pharmacological effects of α1-containing GABAARs highlight their significance in the regulation of anxiety, sedation, and other related processes within the central nervous system. The understanding of the functional roles of α subunits, particularly α1, provides valuable insights into the mechanisms of action and therapeutic applications of drugs targeting GABAARs.

The α2 and α3 subunits are the second most abundant subunits throughout the brain, collectively comprising approximately 30-35% of the α GABAA subtypes [3]. The α2-subunit of GABAARs is primarily associated with anxiolytic (anxiety-reducing), antinociceptive (pain-relieving), and some anticonvulsant effects. [47,48] At higher doses of ligands, the α2-subunit can also induce hypnotic effects (inducing sleep) and muscle relaxation. Studies, including a triple-point mutation study and the work conducted by Zeilhofer, Cook, and others using the ligand Hz-166, have provided evidence suggesting and confirming the antihyperalgesic effects (reduction of

heightened sensitivity to pain) mediated by the GABAAR α2-subunit, primarily occurring in the spinal cord [49,50] . These findings highlight the involvement of the α2-subunit in modulating pain perception and the potential therapeutic implications for targeting α2-containing GABAARs in the management of pain conditions. Understanding the roles and pharmacological effects of α2-containing GABAAR subtypes contributes to our knowledge of the complex mechanisms underlying anxiety, pain modulation, and the development of novel treatment approaches targeting these specific subunits.

The α3 subtype of GABAAR accounts for approximately 14% of all subunits and is predominantly found in the limbic region of the brain [3]. GABAARs containing the α3 subunit contribute to various pharmacological effects. These effects include anxiolytic-like effects (reducing anxiety), anticonvulsant action (preventing seizures), and antinociceptive effects (relieving pain) [47,48]. Moreover, the α3-containing GABAARs are likely involved in muscle relaxation, particularly at higher doses of ligands. [51,52] This suggests that activation of α3 subunit-mediated GABAARs may contribute to the sedative and muscle relaxant effects observed in certain situations. Understanding the distribution and functional properties of the α3 subunit in GABAAR subtypes provides valuable insights into the regulation of anxiety, pain perception, and muscle relaxation. Further research on the α3-containing GABAARs can contribute to the development of targeted therapies for anxiety disorders, epilepsy, and pain management.

The hippocampus, a region of the brain involved in memory and spatial learning, is the primary location of the α5 subunit in the central nervous system (CNS) [51]. The α5 subunit represents approximately 5% of all GABAAR subunits. The α5-GABAAR subtype is known to play a significant role in cognitive functions, particularly in relation to memory processes. Research has

implicated the α5-GABAAR subtype in various cognitive disorders, including Alzheimer's disease, Huntington's disease, Down syndrome, schizophrenia, and depression [54,55]. Dysregulation or dysfunction of the α5-GABAAR subtype has been linked to impairments in memory formation and cognitive deficits observed in these disorders.

The diazepam-insensitive α4- and α6-containing GABAAR subtypes do not exhibit ataxia or sedation due to their lack of a large binding pocket for the pendant C ring of benzodiazepines (BZDs). [56,57] These subtypes are not as responsive to the sedative effects of BZDs due to structural differences in their binding sites. The α4 GABAAR subtype accounts for approximately 6% of all GABAAR subtypes [58]. It is primarily expressed in the cerebellum, trigeminal ganglia, and olfactory bulb [59]. Interestingly, α4-containing GABAARs have also been reported to be expressed in the peripheral nervous system (PNS), specifically in the lungs, which has been associated with asthma. [60-62] Similarly, the lung is also the site of expression for alpha-5, beta-2, beta-3, and gamma-2 subtypes, which appear to contribute to bronchodilation observed in asthma models when activated by compounds like GL-II-93, P1320, and ethinyl analogs. The PQ site discovered by Werner, Sieghert et al. using some of our analogs is located between the α andβ subunits. It is unique in that pyrazoquinolines bind very tightly to the DS (α1, α2, α3, α5) and DI (α4 and α6) benzodiazepines. They are antagonist at BZ sites. The unique activity of CGS-8216, CGS-9885, and CGS-9896 was achieved by modulation of GABA ion channels via this PQ site. The PQ site of α6 Bz/GABAergic subtypes has been implicated in various conditions, including trigeminal neuropathic pain, migraine, Tourette's syndrome, obsessive-compulsive disorder (OCD), and potentially schizophrenia [63-65]. Understanding the involvement of these subtypes in these disorders may offer insights into the development of targeted therapeutic interventions for their management. The expression and functional roles of α4 and α6

subtypes in both the central and peripheral nervous systems highlight their significance in mediating specific neurological and respiratory processes. Further research is needed to elucidate the precise mechanisms and potential therapeutic applications related to these subtypes in various disorders.

Benzodiazepine (BZD) modulated pharmacological responses occur through the facilitation of chloride ion influx via the GABAA receptor pore. This process leads to hyperpolarization of the neuron, which plays a crucial role in regulating neuronal signaling and action potential firing (**Figure 7**).

The mechanism of chloride ion influx and subsequent hyperpolarization is central to the pharmacological actions of benzodiazepines, which potentiate the inhibitory effects of GABA on GABAA receptors. By enhancing chloride ion conductance, benzodiazepines further inhibit neuronal activity, contributing to their anxiolytic, sedative, anticonvulsant, amnesia and muscle relaxant effects.

Positive allosteric modulators (PAMs) of the GABAA receptor play a significant role in enhancing receptor activity by increasing the influx chloride ions. This increased influx of chloride ions leads to further inhibition of neuronal firing, thereby promoting the overall inhibitory effects of GABA neurotransmission. [66] PAMs bind to distinct sites on the GABAA receptor, separate from the orthosteric agonist GABA. By binding to these allosteric sites, PAMs positively modulate the receptor's response to GABA, amplifying its inhibitory effects. In contrast, negative allosteric modulators (NAMs), also known as inverse agonists, exhibit the opposite effect on GABAA receptor activity. NAMs bind to the benzodiazepine binding site (BzR) of the receptor, but instead of enhancing chloride ion influx, they reduce it. By decreasing

the influx of chloride ions, NAMs disrupt the inhibitory effect of GABA neurotransmission and increase the likelihood of action potentials and neuronal firing. [66]

Antagonists, known as null modulators, do not produce any discernible effect on the influx of chloride ions through the GABAA receptor. However, they exhibit a strong binding affinity for specific BzR sites, effectively limiting the binding ability of other benzodiazepines, such as diazepam and alprazolam. As a result, these antagonists influence the membrane potential by preventing the potentiation of GABAA receptor activity by other ligands [66]. Flumazenil, a classic antagonist, is a commonly used benzodiazepine receptor antagonist that blocks the actions of benzodiazepines at the BzR. On the other hand, BCCT is an antagonist with a preference for α1, β2, β3, and γ2 subunit-containing receptors, and it exhibits distinct characteristics in its interaction with the receptor. [66]Understanding the modulation of GABAA receptor activity by positive, negative, and null modulators provides valuable insights into the complex regulation of neuronal excitability and the pharmacological effects of various compounds [66].

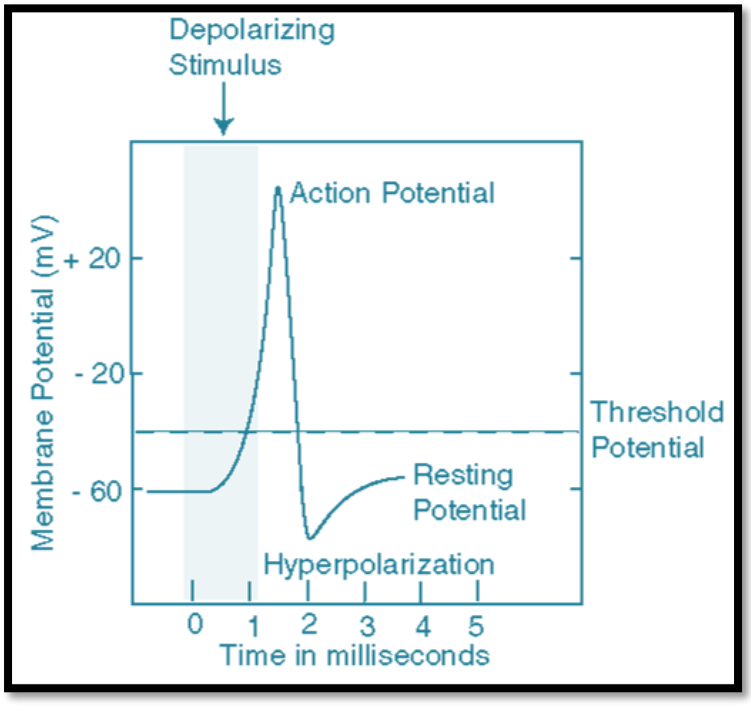


Figure 7. The membrane potential changes over time during the transmission of a nerve signal. It represents the fluctuations in electrical potential across the neuronal membrane as the signal propagates. The Figure, which is adapted from Teny Clayton's Ph.D. thesis 67, likely demonstrates the dynamic nature of the membrane potential during the initiation and propagation of an action potential. Typically, at resting state, the membrane potential of a neuron is negative, indicating a polarized state. As the nerve signal is transmitted, there is a depolarization phase where the membrane potential becomes less negative, moving towards a positive charge. This depolarization triggers an action potential, which is characterized by a rapid and substantial increase in the membrane potential, reaching a peak. Following the peak of the action potential, there is a repolarization phase, during which the membrane potential returns to its resting state by becoming negative again. This repolarization phase is crucial for the neuron to restore its readiness for subsequent signaling.

1.4. Molecular modeling

Rational structure-based drug design is a valuable approach that relies on understanding the key binding domains within GABAA receptors (Rs) to facilitate the discovery of subtype-selective drugs with therapeutic potential. In recent years, cryo-electron microscopy (cryo-EM) studies have played a crucial role in providing significant insights into the structure of heteropentameric GABAARs. [68-72] These cryo-EM studies have shed light on the overall architecture of heteropentameric GABAARs, revealing the arrangement and interactions of the protein subunits. This structural information is crucial for understanding the binding sites of various ligands and their modes of interaction. For example, these studies have provided insights into the protein-ligand interactions involving GABA, the endogenous agonist of GABAARs, as well as positive

allosteric modulators (PAMs) like diazepam and alprazolam, which are commonly used benzodiazepines.[73] By mapping the binding domains and understanding the molecular interactions of ligands within GABAARs, researchers can gain valuable insights into the mechanisms of receptor activation, allosteric modulation, and ligand selectivity. This knowledge serves as a foundation for the design and development of novel drugs that specifically target and modulate GABAARs subtypes, potentially leading to improved therapeutic outcomes for various neurological and psychiatric conditions. The application of cryo-EM studies in elucidating the structural details of GABAARs and their interactions with ligands represents a significant advancement in the field of drug discovery, providing valuable tools for rational drug design and the development of subtype-selective drugs with enhanced therapeutic efficacy and reduced side effects.

The "lock and pull" mechanism is a signaling mechanism employed by GABAA receptors. When the neurotransmitter GABA binds at the β3+/α1- interface of the receptor, it triggers a conformational change that involves the movement of a structural component called the C-loop. This movement of the C-loop initiates a coordinated global anti-clockwise motion in the extracellular domain (ECD) of the receptor.[73] Furthermore, this motion in the extracellular domain (ECD) is facilitated by the binding of benzodiazepines (BZDs) at the α1+/γ2- ECD interface of the receptor.[73] BZDs act as positive allosteric modulators, enhancing the receptor's response to GABA. Their binding at this interface promotes and stabilizes the conformational changes initiated by GABA binding, thereby amplifying the overall inhibitory signaling of GABAA receptors.

The examination of cryo-electron microscopy (cryo-EM) structures of the α1β3γ2L GABAA receptor (6HUP and 6HUO) has provided insights into the active conformations of diazepam

(DZP) and alprazolam (ALP), two benzodiazepines (BZDs) that act as positive allosteric modulators (PAMs) of the receptor. These cryo-EM structures have revealed three important interactions that are essential for the PAM activity of BZDs [74].

The first interaction involves the formation of a bifurcated hydrogen bond with α1Ser205. This hydrogen bonding interaction contributes to the stabilization of the BZD binding and modulates the receptor activity. The second crucial feature is a halogen bonding interaction between the BZD and the backbone of α1His102. This interaction further enhances the binding affinity and allosteric effects of the BZDs. It is worth noting that flunitrazepam and clonazepam, which contain nitro groups at the C7 position, utilize these groups to form hydrogen bonds with the histidine side chain, compensating for the absence of the C7 halogen bond interaction observed in diazepam. The third important feature is pi-pi stacking interactions between the BZDs and α1Tyr210 and α1Phe100. These pi-pi stacking interactions contribute to the stabilization of the BZD binding and facilitate their PAM activity [74.]

Importantly, the cryo-EM structures highlight that diazepam can bind to two different sites within the GABAA receptor complex, further demonstrating the structural diversity and flexibility of BZD binding in modulating receptor function [74].

The classical benzodiazepines, such as diazepam (DZP) and alprazolam (ALP), interact with the GABAA receptor through halogen bonding interactions with the backbone carbonyl group of α1His102 (**Figures 8 and 9**). In the cryo-EM structure bound to DZP (6HUP), the distance between the chlorine atom of DZP and the carbonyl oxygen of α1His102 is measured at 3.8 Å. In the cryo-EM structure bound to ALP (6HUO), this distance is shorter at 2.9 Å. Both cryo-EM structures exhibit a σ-hole angle of 165-167°, which is characteristic of halogen bonding interactions. Additionally, the bifurcated hydrogen bond formed by DZP with α1Ser205 is larger

than that observed with bound ALP (alprazolam). The shorter halogen bond and stronger bifurcated hydrogen bond interaction in ALP contribute to its more potent binding affinity toward α1 GABA-R as compared to DZP. This enhanced affinity toward α1 receptors leads to increased sedative effects for alprazolam compared to diazepam, as demonstrated in **Table 2** and **Table 3**. However, it is important to note that both DZP and ALP are potent modulators of the α1β3γ2 ion channel, contributing to their efficacy as benzodiazepines. The detailed understanding of the specific interactions and binding affinities of benzodiazepines with GABAA receptor subunits, as revealed by cryo-EM structures, provides valuable insights into their pharmacological properties and helps elucidate the structural basis of their differential effects. This knowledge can guide the development of novel benzodiazepine-based compounds with improved selectivity, efficacy, and reduced side effects for the treatment of various CNS disorders.

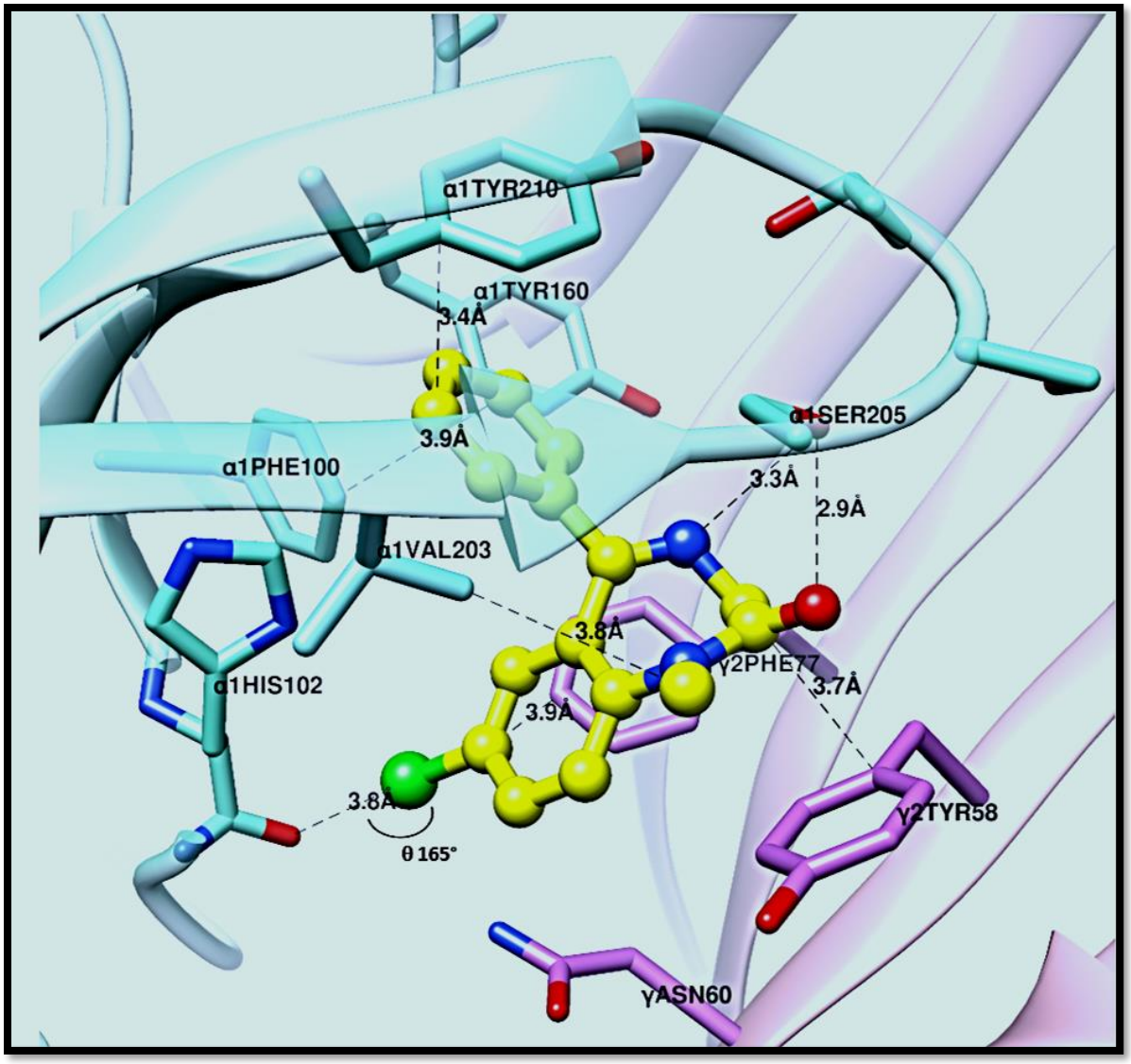


Figure 8. The representation of the complex of diazepam (shown in yellow) with the α1 subunit (aquamarine) and γ2 subunit (orchid) of the α1β3γ2L GABAA receptor (6HUP). In the modified figure, various interactions are highlighted by dashed lines, representing π–π interactions, hydrogen bonding interactions, and a halogen bonding interaction. These interactions play a crucial role in the binding and stabilization of diazepam within the receptor complex. The π–π interactions refer to the stacking interactions between certain aromatic residues, such as α1Tyr210 and α1Phe100, and the diazepam molecule. These

interactions contribute to the overall stability of the binding complex. Additionally, hydrogen bonding interactions are observed between diazepam and specific amino acid residues within the receptor, facilitating further stabilization. The specific amino acid residues involved in these hydrogen bonding interactions are not specified in the provided information. Furthermore, a halogen bonding interaction is indicated in the Figure. This involves the interaction between a halogen atom, likely chlorine in the case of diazepam, and the carbonyl oxygen of a specific amino acid residue, α1His102. This interaction contributes to the specific binding orientation and affinity of diazepam within the GABAA receptor complex. The Figure, as modified from the work of Golani and Mian et al. 2022 [75], provides a visual representation of the molecular interactions between diazepam and the α1 and γ2 subunits of the GABAA receptor. It helps to illustrate the structural basis of diazepam's binding and its interactions within the receptor complex, contributing to our understanding of the pharmacological properties of benzodiazepines.

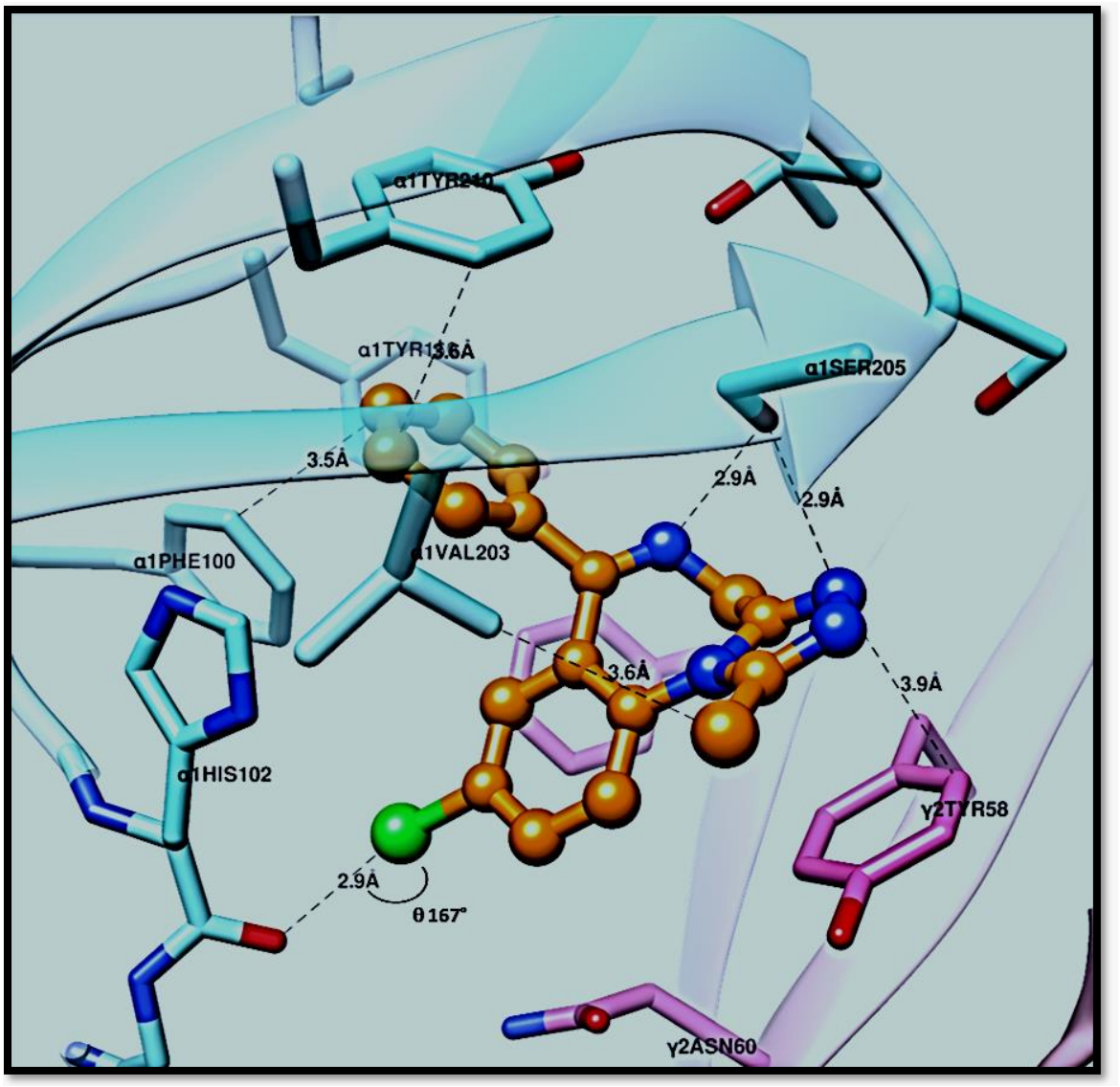


Figure 9. The complex of alprazolam (orange) with α1 (aquamarine) and γ2 (orchid) subunits of α1β3γ2L $GABA_A$ receptor 6HUO. The dashed lines (- - -) indicate π–π interactions, hydrogen bonding interactions, and a halogen bonding interaction. The image is modified from Golani and Mian et. al. 2022.[75]

Flumazenil, an antagonist of benzodiazepines (BZDs), serves as a crucial antidote in the treatment of benzodiazepine overdose [19]. The cryo-electron microscopy (cryo-EM) structure of the flumazenil-GABAA receptor complex (6HUO) reveals a distinct binding conformation

compared to diazepam (DZP) or alprazolam (ALP), particularly at the α+γ- interface[16]. **Figure 9** illustrates the differential binding mode of flumazenil. In the cryo-EM structure (6HUO), flumazenil adopts a different binding conformation wherein the bifurcated hydrogen bond and halogen bond interactions observed with DZP or ALP are absent. These interactions, which play a critical role in the binding of BZDs to the GABAA receptor, are not formed by flumazenil in the cryo-EM structure. Consequently, flumazenil does not induce the movement of the C-loop at the α+γ- interface, an essential step for receptor activation facilitated by BZDs. Instead, flumazenil acts as a competitive antagonist at this binding site, as depicted in **Figure 10**. It partially overlaps with the binding site of BZDs but lacks the specific interactions required for receptor activation. Without the bifurcated hydrogen bond and halogen bond interactions, flumazenil is unable to facilitate the conformational changes necessary for receptor activation. By competitively binding to the α+γ- interface, flumazenil effectively blocks the actions of BZDs, reversing their effects and acting as an antagonist. The unique binding mechanism of flumazenil, as revealed by the cryo-EM structure, highlights its role as a specific competitive antagonist at the α+γ- interface of the GABAA receptor. The absence of key interactions observed with BZDs prevents flumazenil from activating the receptor and enables it to counteract the effects of BZDs. Understanding the structural differences and mode of action of flumazenil contributes to its therapeutic application as an antidote for benzodiazepine overdose and related conditions. (Golani and Mian et al., 2022). [75]

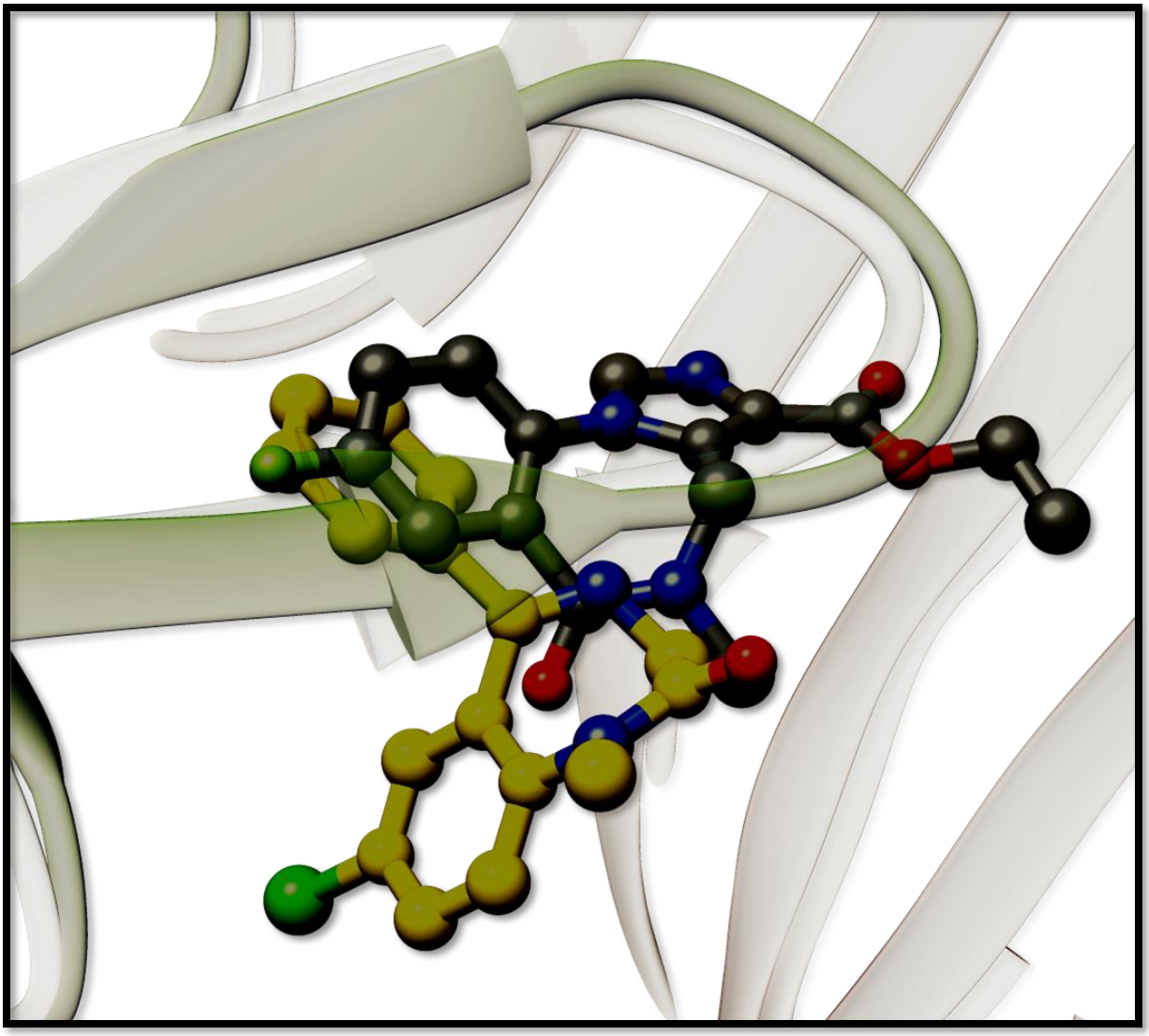


Figure 10. The overlay diagram of flumazenil (grey) and diazepam (yellow) in the ion complex with α1 (aquamarine) and γ2 (orchid) subunits of α1β3γ2L $GABA_AR$ (6HUO and 6HUP). The image is modified from Golani and Mian et. al. 2022.[75]

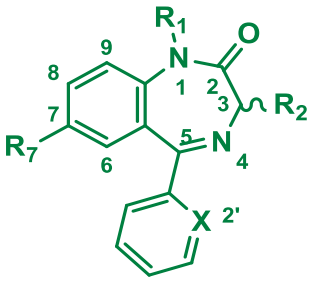


Table 2. Binding affinities at α1-3 and α5 human $GABA_A$ R subtypes

Comp	Code	R_1	R_2	R_7	X	K_i (nM)			
						α1	α2	α3	α5
1.	Diazepam	CH_3	H	Cl	C-H	14	20	15	11
2.	QH-II-059	CH_3	H	H	C-H	81	138	318	98
3.	QH-II-063	CH_3	H	Br	C-H	9.4	9.3	31	7.7
4.	QH-II-058b	H	H	H	C-H	288	233	350	140
5.	QH-II-066	CH_3	H	C≡CH	C-H	76.3	42.1	47.4	6.8
6.	XLi-352	CH_3	H	C≡CH	C-Cl	1.6	0.99	ND	1.96
7.	KRM-II-08	CH_3	H	C≡CH	C-F	3.9	1.2	3.4	0.8
8.	XLI-286	H	H	Br	C-Cl	0.05	0.06	0.12	0.68
9.	JYI-42	H	H	Br	C-F	0.26	0.15	0.28	0.26
10.	flunitrazepam[36]	CH_3	H	NO_2	C-F	2.2	2.5	4.5	2.1
11.	SH-I-030	H	*S*-CH_3	Br	C-H	14.4	11	19.1	1.89

12.	SH-I-035B	H	*R*-CH_3	Br	C-H	>3000	>3000	>3000	>3000

The affinity of compounds at $GABA_A$ recombinant subtypes was measured by competition of [^{3}H] flunitrazepam binding to HEK cell membranes expressing human $\alpha x\beta 2\gamma 2$ receptors. Data represent the average of at least three determinations with a SEM of ±5%. ND: not determined. The Table is modified from Golani and Mian et. al. 2022.[75]

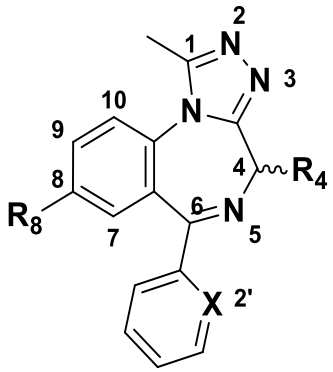


Table 3**. Binding affinities at α1-3 and α5 human $GABA_A$ R subtypes**

Comp.	**Code**	**R_4**	**R_8**	**X**	**K_i (nM)**			
					α1	**α2**	**α3**	**α5**
1.	alprazolam[36]	H	Cl	C-H	0.8	0.6	1.4	1.5
2**.**	Xli-2TC	H	Br	C-H	2.8	0.7	ND	0.6
3**.**	DM-II-90	H	Br	C-Cl	0.5	1	0.6	0.4
4**.**	SH-I-04	H	Br	N	7.3	6.1	5.1	7.7
5**.**	XLi-270	H	C≡CH	C-H	36.4	25.8	ND	5.3

6.	XLi-296	H	C≡CH	C-Cl	3.3	0.6	1.9	4.4
7.	JYI-70	H	C≡CH	C-F	6.3	2.1	ND	0.6
8.	SH-TRI-108	H	C≡CH	N	143.9	81.3	103.9	45.6
9.	SH-TS-CH3	*S*-CH_3	C≡CH	C-H	107.2	50.1	20.9	8.1

The affinity of compounds at $GABA_A$ recombinant subtypes was measured by competition of [^{3}H] flunitrazepam binding to HEK cell membranes expressing human $\alpha x\beta 2\gamma 2$ receptors. Data represent the average of at least three determinations with a SEM of ±5%. ND: not determined. The Table is modified from Golani and Mian et. al. 2022.[75]

The sequence alignment studies of α1-6 subunits reveal an interesting difference in the amino acid residue at position 102. Specifically, the α1His102 residue, which is present in the α1-3 and α5 subunits, is absent in the α4 and α6 subtypes, where it is replaced by an arginine residue (**Table 4**). This substitution of histidine with arginine results in a larger side chain in the protein for the α4 and α6 subunits. Consequently, the larger arginine side chain sterically clashes with classical 1,4-benzodiazepines such as diazepam (DZP) and alprazolam (ALP). This steric interaction prevents the binding of DZP and ALP to GABAA receptor subtypes containing the α4 or α6 subunits. [22] In contrast, the conserved histidine residue at position 102 in the α1-3 and α5 subunits enables these subunits to interact with the pendant ring of DZP and ALP. The specific amino acid residues involved in the interaction between DZP or ALP and the α1-3 and α5 subunits are provided in **Table 4**. These conserved residues contribute to the binding of DZP and ALP to the GABAA receptor and play a role in mediating their pharmacological effects.

The loop-C region of the α subunits within the benzodiazepine (BZD) binding site displays subtle differences in amino acid residues, as shown in **Table 4**. Notably, there are variations in specific residues among different α subunits. For instance, Thr205 in α5 subunits is replaced by Ser205 in the α1 subunit. Additionally, Ile203 is present in α2-3 and α5 subunits, whereas the α1 subunit has a Val203 residue in this position. These small differences in amino acid residues lead to distinct three-dimensional shapes of the BZD binding pockets within the α subunits. These unique shapes play a crucial role in subtype selectivity, as they contribute to the topography of lipophilic pockets known as H1, H2, L1, L2, L3, and LDi in previous homology models. The topography of these lipophilic pockets is important for the binding and interaction of BZDs with the α subunits of the GABAA receptor. These subtle differences in amino acids contribute to the structural diversity and specificity of the BZD binding sites among the different α subunits. Understanding the topography and specific residues within these binding pockets is essential for designing subtype-selective drugs and elucidating the mechanisms underlying the diverse pharmacological effects of BZDs.

Table 4. The s**equence alignment of α1-6 subunits.**

α subunits	**Halogen bond interaction with αHis102**	**Pendent ring pi-pi stacking interactions region**	**Bifurcated hydrogen bond interaction region (Loop-C)**
α1	**FFHN**	**GSYAY**	**GIVQSSTGEYV**
α2	**FFHN**	**GSYAY**	**ETIKSSTGEYT**
α3	**FFHN**	**GSYAY**	**EIIRSSTGEYV**

α4	**FFRN**	**GSYAY**	**ETIKSITGEYI**
α5	**FFHN**	**GSYAY**	**ENISTSTGEYT**
α6	**FFRN**	**GSYAY**	**ETIKSNTGEYV**

Each single letter represents an amino acid residue. The red colored amino acids are involved in the interaction with the ligand. The table **is modified from Golani and Mian et. al. 2022.**[75]

A series of novel subtype-selective positive allosteric modulators (PAMs) have been developed in Milwaukee, as reported in previous studies. [76-82] These compounds were designed to target and interact with specific subunits of the GABAA receptors. In this research group, we have also synthesized analogs of diazepam (DZP) and alprazolam (ALP) for further investigation of their molecular interactions and binding affinities at the α1-3+γ- and α5+γ- interfaces of the GABAA receptors. These analogs are listed in **Table 2** (entry 1) for DZP and **Table 3** (entry 1) for ALP. To explore the role of the halogen atom at the C7 position, several compounds with different substitutions were designed and synthesized, as shown in **Table 2** (entries 2, 3, and 5). Additionally, ligands with various substitutions on the pendant phenyl ring of DZP were also designed to investigate their molecular interactions (**Table 2**, entries 6-9). Ligands **11** and **12** were specifically designed to assess the impact of a chiral methyl group in the seven-membered ring of DZP.

The interaction of the halogen bond with the backbone of the α1His102 residue, as maintained, plays a critical role in the binding of diazepam (DZP) and alprazolam (ALP) to the GABAA receptor, as well as efficacy by the movement of the loop-C region, which acts as a positive

allosteric modulator (PAM). This loop-C movement can prolong the opening of the chloride ion channel leading to increased sedation and ataxia. A significant change in the molecular structure can be achieved through bioisosteric replacement, such as substituting the halogen group at the C-7 or C-8 position with an ethinyl group. This substitution has important implications. While the halogen group is involved in halogen bonding interactions [83-86], the ethinyl group does not participate in such interactions. This alteration in the chemical structure affects the specific interactions and binding characteristics of the ligand with the receptor. The absence of halogen bonding interactions in the case of substitution of the ethinyl group for the halogen atom results in distinct ligand-receptor interactions and altered pharmacological effects. The replacement of the halogen group by an ethinyl group represents a significant change in the molecular properties, potentially impacting the binding affinity, selectivity, and functional outcomes of the ligand at the GABAA receptor. As a result less sedation and ataxia is observed in case of C-7 ethinyl compounds. The chlorine atom at C7 of DZP was replaced with the ethinyl group (**Table 2**, entry 5). The docking pose of ligand 5 (QH-II-066) in the α1β3γ2L cryo-EM structure 6HUP is illustrated in **Figure 11**. The docking studies have demonstrated that the compound exhibits a similar docking pose to that of diazepam (DZP). Importantly, compared to diazepam, QH-II-066 (US Patent,2006) exhibited the same anxiolytic activity but much less sedation as compared to diazepam. The similarity in the docking pose indicates that the compound can bind to the α1 subunit of the GABAA receptor and modulate its activity in a manner similar to diazepam. However, the reduced sedation and ataxia suggest that the compound may have a more favorable pharmacological profile, potentially resulting in a more desirable therapeutic effect.[87] In another series, the investigation of ligand **10**, which contains a C7 nitro group (**Table 2**, entry 10), has revealed that it adopts a conformation similar to diazepam (DZP). Notably, two hydrogen

bonding interactions are observed between the nitro group at C7 and the side chains of α1His102 and γ21Asn60 (not shown). The presence of these hydrogen bonding interactions with α1His102 contributes to the strong sedative effects of this nitro ligand in vivo.

In the docking studies of compounds **11** and **12** at the α1β3γ2L GABAA receptor (6HUP and 6HUO), it was found that there was sufficient space to accommodate the (S)-methyl group in the alpha 2, 3, and 5 subtypes. However, the (R)-methyl group in compound **12** does not fit due to steric hindrance. This observation highlights the difference in subtype selectivity between the (S) and (R) enantiomers, as reported. [88,89] It should be noted that the R-enantiomer still exhibits binding affinity and efficacy at the alpha 5 subtype, indicating potential interactions and effects at this specific receptor subtype.

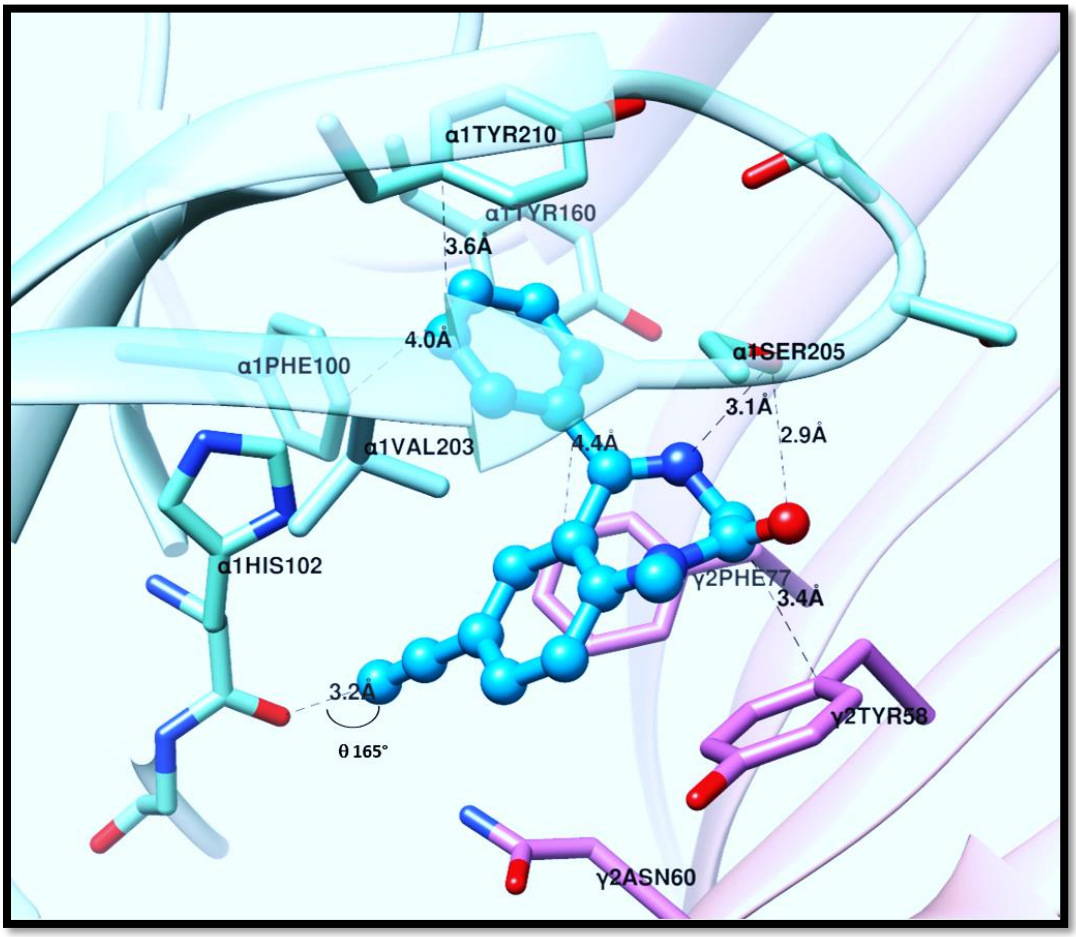


Figure 11. The docking studies revealed the docking pose of QH-II-066 # 5 (shown in deep sky blue) with the α1 (aquamarine) and γ2 (orchid) subunits of the α1β3γ2L GABAA receptor 6HUP. In this docking pose, no halogen bond is observed due to the presence of an ethinyl group. The modified image showcasing this docking pose is adapted from Golani and Mian et al., 2022 [75]. The absence of a halogen bond in the case of the ethinyl group substituent suggests that the molecular interactions between QH-II-066 5 and the α1β3γ2L GABAA receptor are less as compared to compounds with a halogen groups(DIA,ALP). These interactions play a crucial role in the binding affinity and functional outcomes of the activity of QH-II-066 the GABA/ BZ ion channel .

1.5 Research Objectives

The research presented in this study utilizes homology-derived pharmacophore models and cryo-EM structures to guide the development and synthesis of novel benzodiazepines and imidazodiazepines. The primary objective is to design compounds that exhibit improved binding affinity and efficacy at the benzodiazepine receptor (BzR) compared to existing agents. Importantly, these newly synthesized ligands are designed to mitigate the side effects associated with benzodiazepines, such as sedation and ataxia, by reducing their affinity for the α1 subtypes of the receptor. The synthesized ligands were subjected to extensive pharmacological evaluation using various in vitro assays and in vivo animal models. These evaluations aimed to assess their therapeutic potential for the treatment of diverse disorders, including asthma, schizophrenia, major depressive disorder (MDD), anxiety, non-sedative neuropathic pain, epilepsy, and other pain disorders. This includes complex regional pain disorder, back pain, and diabetic neuropathy. By targeting specific receptor subtypes and modulating their activity, these ligands hold promise for addressing a range of medical conditions.

Another important aspect of this research is the development of an optimal synthetic route to produce the key ligands in multigram to kilogram quantities. These large-scale syntheses are crucial for conducting comprehensive animal studies, including evaluating the ligands in a significant number of animal species including primates and conducting absorption, distribution, metabolism, excretion (ADME), and toxicity studies. By combining computational modeling, insights into structural biology insights, and thorough preclinical assessments, this research aims to advance the development of novel benzodiazepine and imidazodiazepine derivatives with improved therapeutic profiles into the clinic to treat patients.The ultimate goal is to provide safer and more effective treatment options for a variety of disorders, thereby addressing unmet medical needs and improving patient outcomes.

Chapter 2

Development of α6-GABAAR Subtype-Selective Pyrazoloquinolinones for Treating Tourette Syndrome, Migraine, and Trigeminal Pain

2.1. Introduction

GABA-A receptors ($GABA_ARs$) serve as the principal inhibitory neurotransmitter receptors within the mammalian brain and are targeted by a range of clinically significant medications designed to interact with GABAAR binding sites. These receptors are made up of ligand-gated pentameric chloride channels, consisting mainly of combinations of 19 distinct subunits ($\alpha_{1–6}$, $\beta_{1–3}$, $\gamma_{1–3}$, δ, ε, π, θ, ρ_{1-3}).[90, 14] In the classical composition, GABAARs consist of two α, two β, and one of the "tertiary" subunits (γ, δ, ε, θ, or π).[90, 91] The extensive variety of subunit combinations and their diverse distribution across regions, cells, and subcellular structures imply that these ion channels could potentially mediate a broad spectrum of pharmacological properties.[14],[17],[20],[92]

Various GABAergic drugs, such as benzodiazepines (Bzs) and barbiturates, exert their effects on GABAARs by interacting with allosteric binding sites.[93] However, many of the existing GABAergic drugs lack specificity for particular alpha subtypes leading to unwanted side effects (such as sedation, ataxia, amnesia, tolerance, and dependence) alongside their intended therapeutic advantages. In recent times, a renewed exploration into the development of GABAAR subtype-selective ligands has emerged[7], triggered by the identification of a new ligand binding site at the interface of GABAAR α_x+β_y-.[26] This discovery by Sieghart et al. has spurred the search for novel ligands tailored to interact precisely with this binding site,

potentially opening avenues for innovative therapeutic agents and prompting significant interest in this research area.[27, 94,95]

$GABA_AR$s incorporating the α6 subunit (α6βγ2, **Figure 1**) are predominantly observed within the granule cells of the cerebellum,[93] where their presence is distributed either synaptically or extrasynaptically[96], depending on the context, with the latter being the case in the cerebellum's granule cells especially the trigeminal ganglia. Additionally, these receptors are also detected in the olfactory bulb and the cochlear nucleus.[97]

A more limited expression of α6-GABAARs has been recently documented in the hippocampus, where they could potentially contribute to depressive behaviors.[98] Emerging findings also propose that receptors containing the α6 subunit might have implications in neuropsychiatric conditions characterized by deficits in sensori-motor gating (such as tic disorders, specific aspects of schizophrenia, obsessive-compulsive disorder, and attention deficit disorders),[99,100] as well as in migraine,[101]and trigeminal orofacial pain.[102] Nevertheless, our comprehension of the functional role of α6-containing receptors within the central nervous system is still limited. Currently, it remains uncertain whether α6βγ2, α6βδ, or both receptor types significantly influence the mentioned disorders. Irrespective of this uncertainty, the synthesis of ligands with selectivity for GABAARs containing the α6 subunit holds substantial significance. Such ligands could aid in elucidating the physiological processes that may be modulated by these specific ion channels, thus contributing to the assessment of their suitability as targets for drug development.

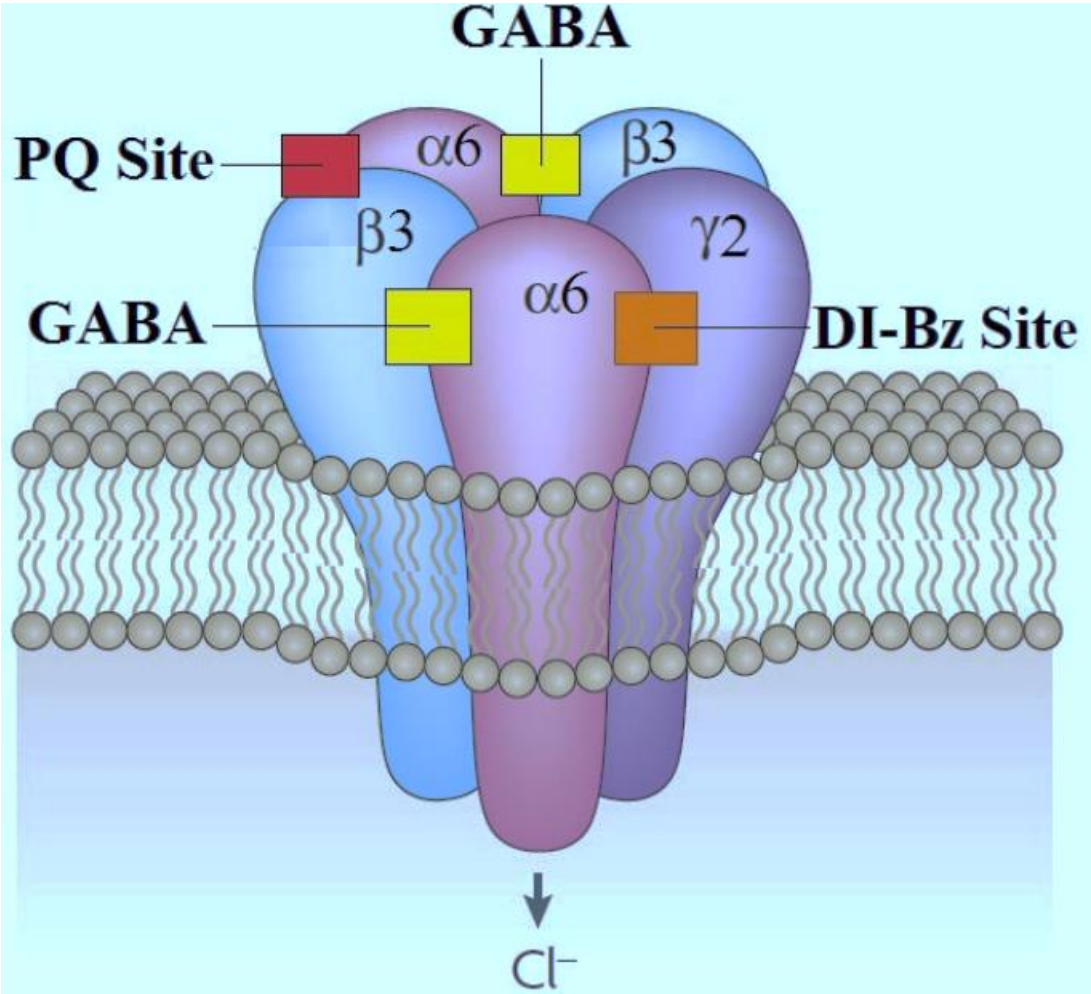
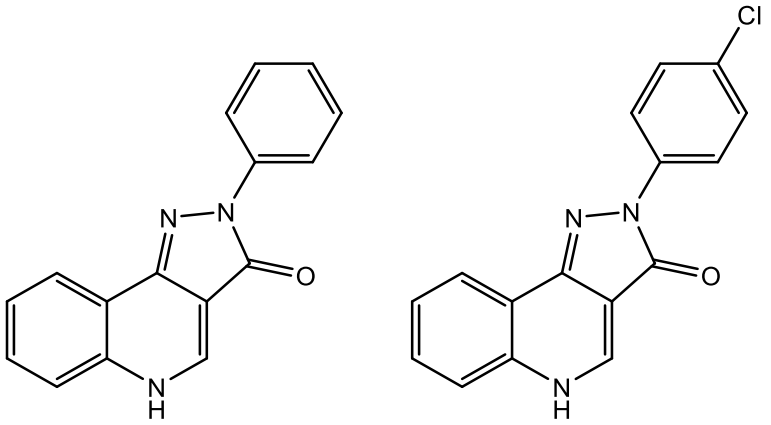


Figure 1. The GABAAR α6β3γ2 subtype represents a pentameric chloride channel that operates as a ligand-gated structure, consisting of two α6, two β3, and one γ2 subunit. Pyrazoloquinolinones (PQs), such as PZ-II-029 (compound 6), exert their influence at the α6+β3- interface, recognized as the PQ Site, serving as positive allosteric modulators. Moreover, they interact at the α6+γ2- interface, identified as the DI-Bz site, exerting null modulation effects. This configuration showcases the PQ site, the DI-Bz binding site diazepam site, and the binding sites for the endogenous ligand (GABA) at the β3+α6- interfaces. Image modified from Jacob et al., Nature Reviews Neuroscience, 2008.

The Ciba-Geigy Corporation unveiled pyrazoloquinolinones (PQs) such as CGS 8216, CGS-9895, and CGS 9896 (**Figure 2**) as pioneering nonbenzodiazepine ligands that engage with the Bz site of $GABA_ARs$.[103.104] These compounds demonstrated dual properties of being agonists (positive allosteric modulators) and antagonists (null modulators) at the Bz site of $GABA_ARs$. However, their selectivity in binding to receptors exhibited suboptimal discrimination between the diazepam-sensitive (DS) $GABA_AR$ subtypes (containing α1, α2, α3, or α5 subunits) and the diazepam-insensitive (DI) $GABA_AR$ subtypes (containing α4 or α6 subunits).[105]



CGS 8216 **CGS 9896**

1 **2**

Figure 2. Structure of CGS 8216 and CGS 9896

The addition of a 7-methoxy substituent on the "A-ring" (**Figure 3**) of PQs, as carried out by the Puwen Zhang, Ian Fvya and Phil Skolnick research team, led to enhanced affinity for the diazepam-insensitive (DI) subtype.[24] Utilizing the pharmacophore/receptor model specific to GABAAR subtypes, the deconstruction of CGS-related compounds guided the integration of structural alterations (illustrated in Scheme 1) in both the "A-ring" and "D-ring" (**Figure 3**) of PQs by He, Cook et al.[22, 106]

These modifications led to the creation of **PZ-II-029** and several other ligands that displayed a strong binding affinity to the Bz/GABAAR α6 subtype, comparable to that of imidazodiazepines.[107] The arrangement and size of substituents on the "D-ring" played a pivotal role in influencing the affinity toward the Bz/GABAAR α6 subtype.[108,109] In more recent times, analogous structures, including compound **6**, were not only found to bind to α6β2/3γ2 GABAARs, but also to amplify the effects of these receptors. This marked the first instance of functionally selective ligands for the α6β3γ2 subtype.[107] These prototypical ligands exerted their physiological influence via the recently discovered α_6+β_3- interface of GABAARs, operating as positive allosteric modulators. Additionally, they acted as antagonists (null modulators) at the Bz sites (α+γ2- interface) of $\alpha_{1\text{-}6}\beta\gamma_2$ receptors as mentioned above.[107,108]

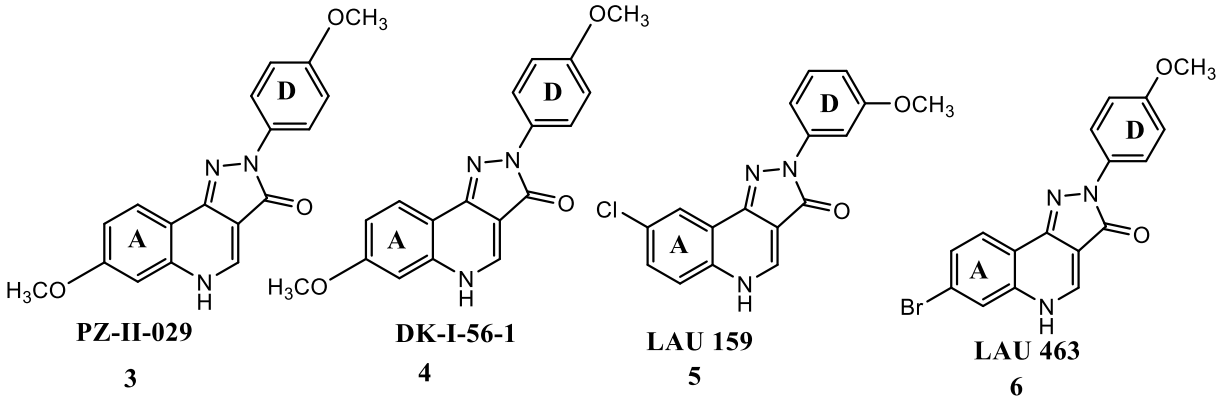


Figure 3. Lead α6-selective ligands for this project

Concurrently, the Ernst and Treven research group conducted a parallel investigation to the group at Milwaukee, resulting in the synthesis of closely related analogs, namely **LAU 159** (**4**)[110] and **LAU 463** (**5**).[111] These compounds also demonstrated functional selectivity at α6β2/3γ2 GABAARs similar to **PZ-II-029 (3)**, specifically within the spectrum of α1-6β2/3γ2 receptors. Hence, compounds **PZ-II-029**, **LAU 159**, and **LAU 463** emerged as the lead compounds highlighted in this study (**Figure 3**).[112] Given that all these PQs elicit their positive allosteric

modulation through the α6+β3- interface[100] of $GABA_A$Rs, they also possess the capability to modulate α1-6β2/3δ receptors, or any receptors featuring an α1-6β2/3 interface.[113]

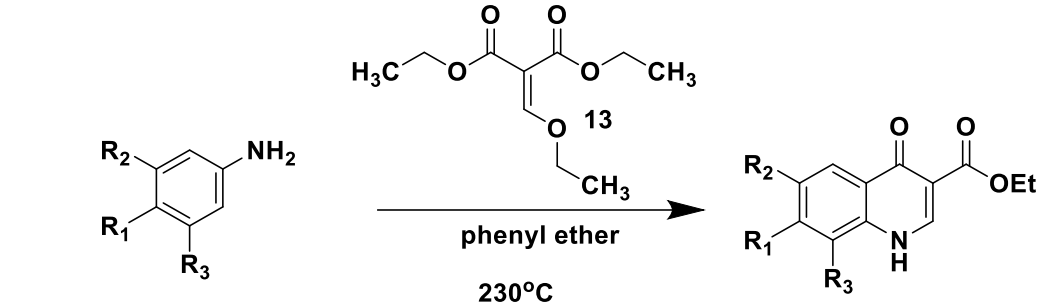
2.2. Chemistry

The synthesis of the key α6β2/3γ2-subtype selective ligand PZ-II-029 along with other key ligands DK-I-56-1**, LAU 463**, and **LAU159** is reported here. PZ-II-029 is a promising compound with positive allosteric modulation effects on α6β3γ2 GABA receptors, as described earlier. However, the aim is to enhance its bioactivity and potentially address any challenges related to patent protection. In order to expand the structure-activity relationship (SAR) and enhance bioactivity beyond that of **PZ-II-029**, as well as to counter potential patent challenges, a series of analogs derived from **PZ-II-029** were strategically designed. These modifications primarily involved altering various substituents in both the A ring and the D ring of the compound. Once synthesized, these analogs were subjected to thorough biological evaluation to determine their efficacy and other biological interactions.

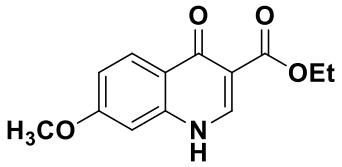
The pyrazoquinolinones were synthesized in three steps. The first step of the synthesis is to prepare the 4-oxo-1,4-dihydro-quinolines by Gould-Jacobs cyclization.[114] Different substituted anilines were treated with ethylethoxymethylenemalonate at 230°C in diphenyl ether in order to produce 4-oxo-1,4-dihydro-quinolines bearing different substituents in A ring (**Scheme 1**). The ethanol, evolved in this process, was collected in a Dean-Stark trap. The crude products were purified by washing with ethanol followed by hexane. The reactions gave moderate yields (61-75%) depending on the various substituents in the aniline. During the isolation phase, the undesired byproducts encompassing 5-substituted 4-oxo-1,4-dihydroquinolines and quinoline

derivatives stemming from the destructive pathway were effectively eliminated. This was achieved through a targeted approach using ethanol to differentially dissolve and remove these undesired isomers and byproducts earlier discovered by Knutson and Sharmin.

Scheme 1. Synthesis of 4-oxo-1,4-dihydro-quinolines by Gould Jacobs cyclization

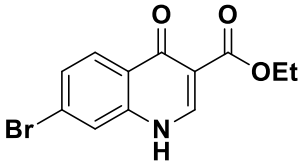


R_1= H, R_2 = H, R_3 = OCH_3, **7**
R_1= H, R_2 = H, R_3 = Br, **8**
R_1= Br, R_2=H, R_3 = F, **9**
R_1= Br, R_2 = H, R_3 = H, **10**
R_1= H, R_2 = F, R_3 = H, **11**
R_1= F, R_2 = H, R_3 = H, **12**



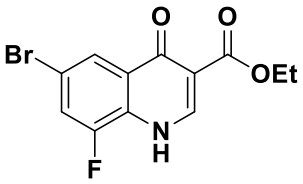
61%

14



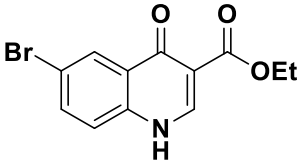
75%

15



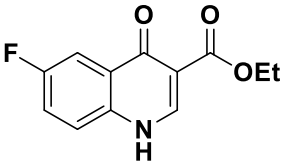
72%

16



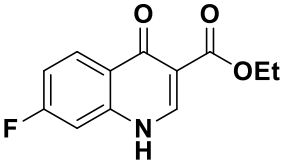
73%

17



68%

18

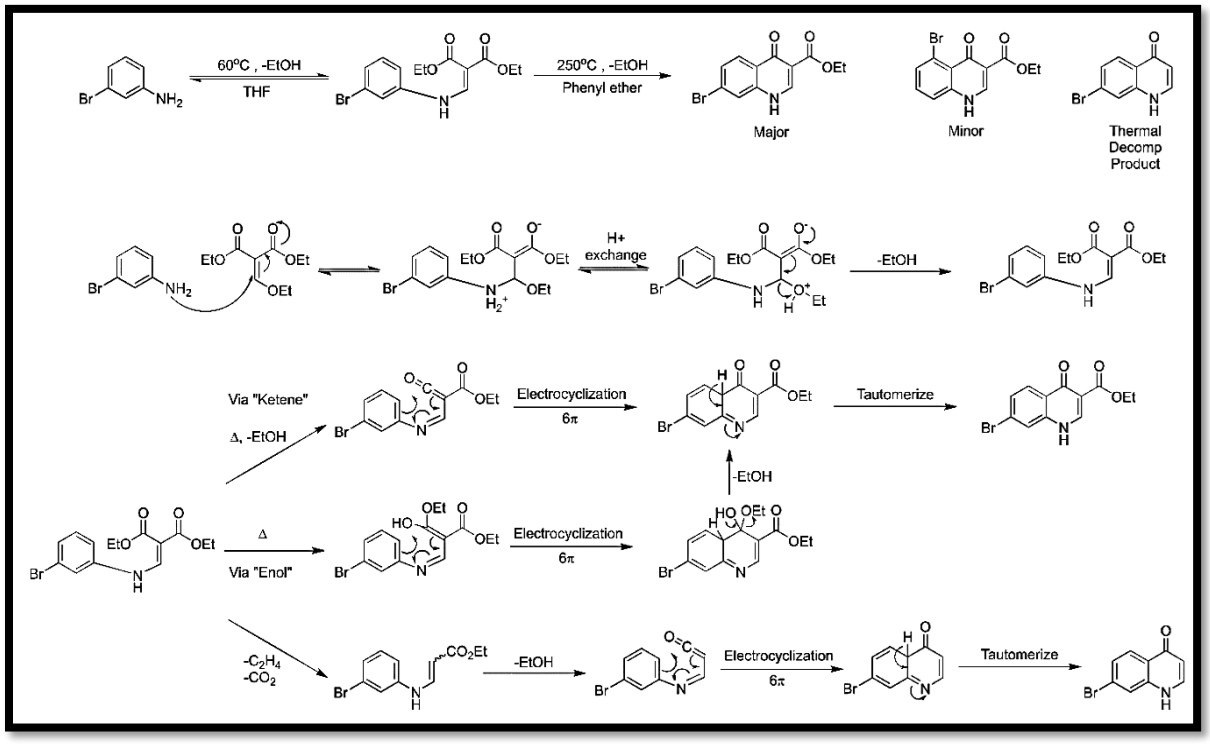


70%

19

The Gould-Jacobs cyclization is a complex chemical transformation that relies on multiple steps and possible pathways to produce quinoline compounds. The process begins with the reaction between substituted anilines and diethyl ethoxy methylenemalonate. This initial reaction leads to the formation of an intermediate compound known as an anilinomethylenemalonic ester (**Scheme 2**). Subsequently, this ester undergoes thermal cyclization, triggered by heat, which results, in the formation of the desired substituted quinoline . To further understand the intricate details of this reaction mechanism, researchers employed flash vacuum pyrolysis (FVP), as an experimental technique. [114] The FVP experiment offered insights into the proposed mechanism (**Scheme 2**).[114] The findings indicated that the anilinomethylenemalonic ester intermediate follows several potential pathways.

Scheme 2. Probable mechanism of Gould-Jacob cyclization [114]

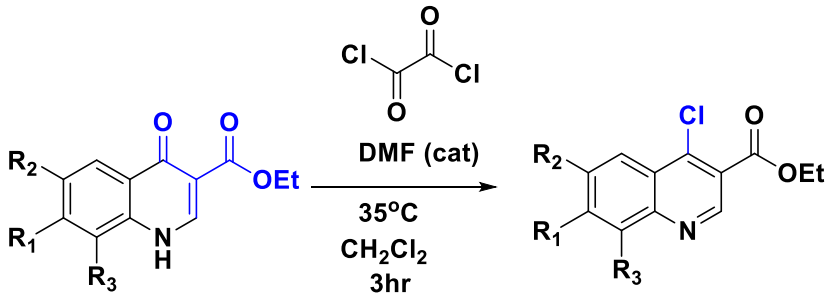


The first pathway involves the intermediate going through either a ketene or an enol pathway, followed by an electrocyclization process (a type of chemical reaction involving multiple bonds) and tautomerization steps. These steps ultimately result in the formation of the quinoline core, a key structural element of the final product. Apart from these productive pathways, a third option exists, referred to as the destructive pathway. In this scenario, the intermediate compound can undergo a process in which carbon dioxide (CO^2) and ethene are lost from the molecule, leading to a different outcome.

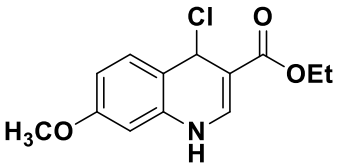
The second step of the synthesis is to prepare the 4-chloro-quinolines from 4-oxo-1,4-dihydro-quinolines using a catalytic Vilsmeier-related chlorination. The Vilsmeier reagent was harnessed in a catalytic manner to facilitate the chlorination of 4-oxo-1,4-dihydroquinolines (**14-19**), resulting in the generation of the intended 4-chloroquinolines (**20-25**, **Scheme 3**). The crude products were purified by making a slurry with hexane, followed by filtration and washing with hexane. These reactions gave moderate to good (75%-90%) yields of quinolones.

The approach employed for generating the Vilsmeier reagent involved an *in situ* process utilizing oxalyl chloride along with catalytic amounts of *N*,*N*-dimethylformamide. This strategy offers distinct advantages when compared to the previously reported techniques involving phosphorus oxychloride and thionyl chloride. Notably, the use of the catalytic Vilsmeier reagent permits the reaction to be carried out at a lower temperature range (35-40°C). Additionally, it affords to regulate the reaction rate by carefully controlling the rate at which the oxalyl chloride reagent is added. The innovation here lies in the capability to generate the Vilsmeier reagent *in situ*, which streamlines the process by avoiding the need for separate preparation steps. Oxalyl chloride and catalytic *N*,*N*-dimethylformamide combine to form the reagent, making it readily available for the subsequent chlorination reaction

.**Scheme 3. Vilsmeier-related chlorination of 4-oxo-1,4-dihydroquinolines**

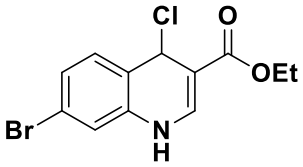


R_1= OCH_3, R_2 = H, R_3 = H, **14**
R_1= Br, R_2 = H, R_3 = H, **15**
R_1= H, R_2=Br, R_3 = F, **16**
R_1= H, R_2 = Br, R_3 = H, **17**
R_1= H, R_2 = F, R_3 = H, **18**
R_1= F, R_2 = H, R_3 = H, **19**



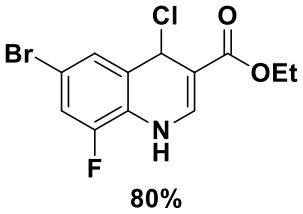
77%

20



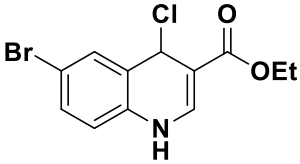
75%

21



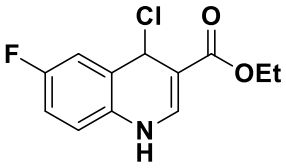
80%

22



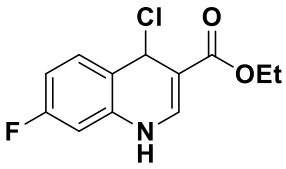
83%

23



90%

24

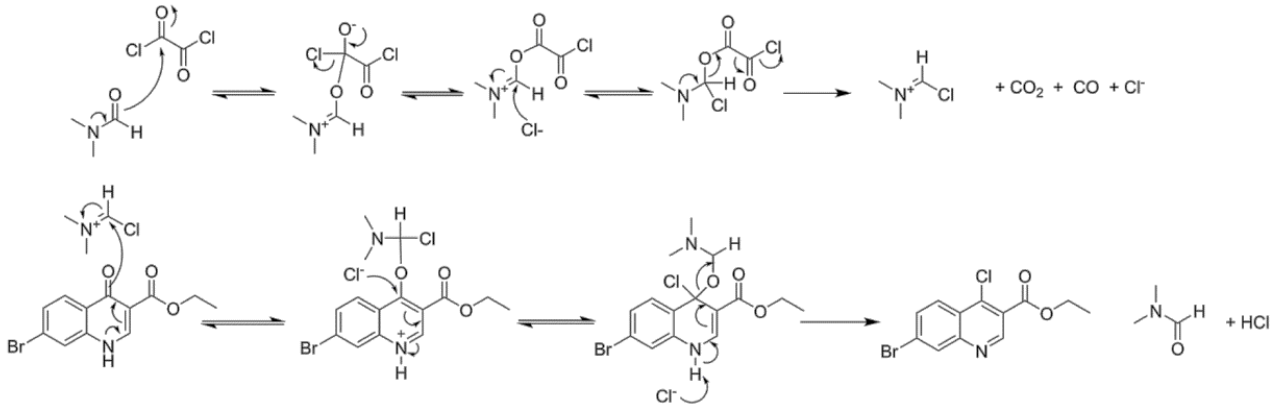


88%

25

Scheme 4 Illustrated in scheme 4 the suggested reaction mechanism, depicting the process by which the dimethylformamide (DMF) catalyst is regenerated. This mechanism outlines the sequence of steps that lead to the renewal of the DMF catalyst, shedding light on how it participates in the reaction cycle.

Scheme 4. Probable mechanism for The Vilsmeier-related chlorination of 4-oxo-1,4-dihydroquinolines

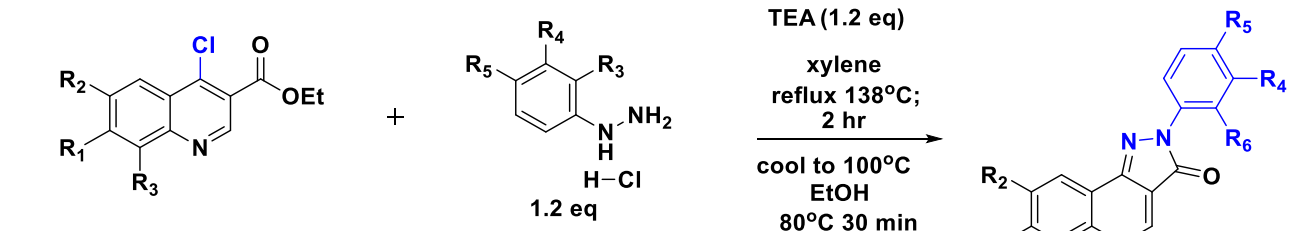


The third step of the synthesis is to produce the pyrazoquinolinones. The PQs (8a-t) were synthesized through a convergent coupling process. This method involved the combination of phenylhydrazines (4a-e) with suitable chloroquinolines (7a-e) through a straightforward adjustment of the previous procedure established by Ciba-Geigy. The reaction was conducted in mixed xylenes at a temperature range of 135-140 °C (**Scheme 5**). In every instance, an excess of triethylamine (1.2 equivalents) was employed to effectively neutralize the hydrogen chloride generated as a result of the nucleophilic aromatic substitution (SNAr) process. This SNAr reaction involved the replacement of chlorine by the primary amino group within the respective phenylhydrazines. Following this step, a thermal cyclization ensued through the secondary amine of the phenylhydrazine. This cyclization was succeeded by the elimination of ethanol, ultimately

leading to the formation of the PQ core. Once the cyclization process reached completion, the reaction mixtures were promptly introduced into ethanol and then filtered to yield the desired PQs ligands in yields ranging from 49% to 67s%. Notably, this improved approach eliminated the need for further purification, contrasting with the methods reported earlier.

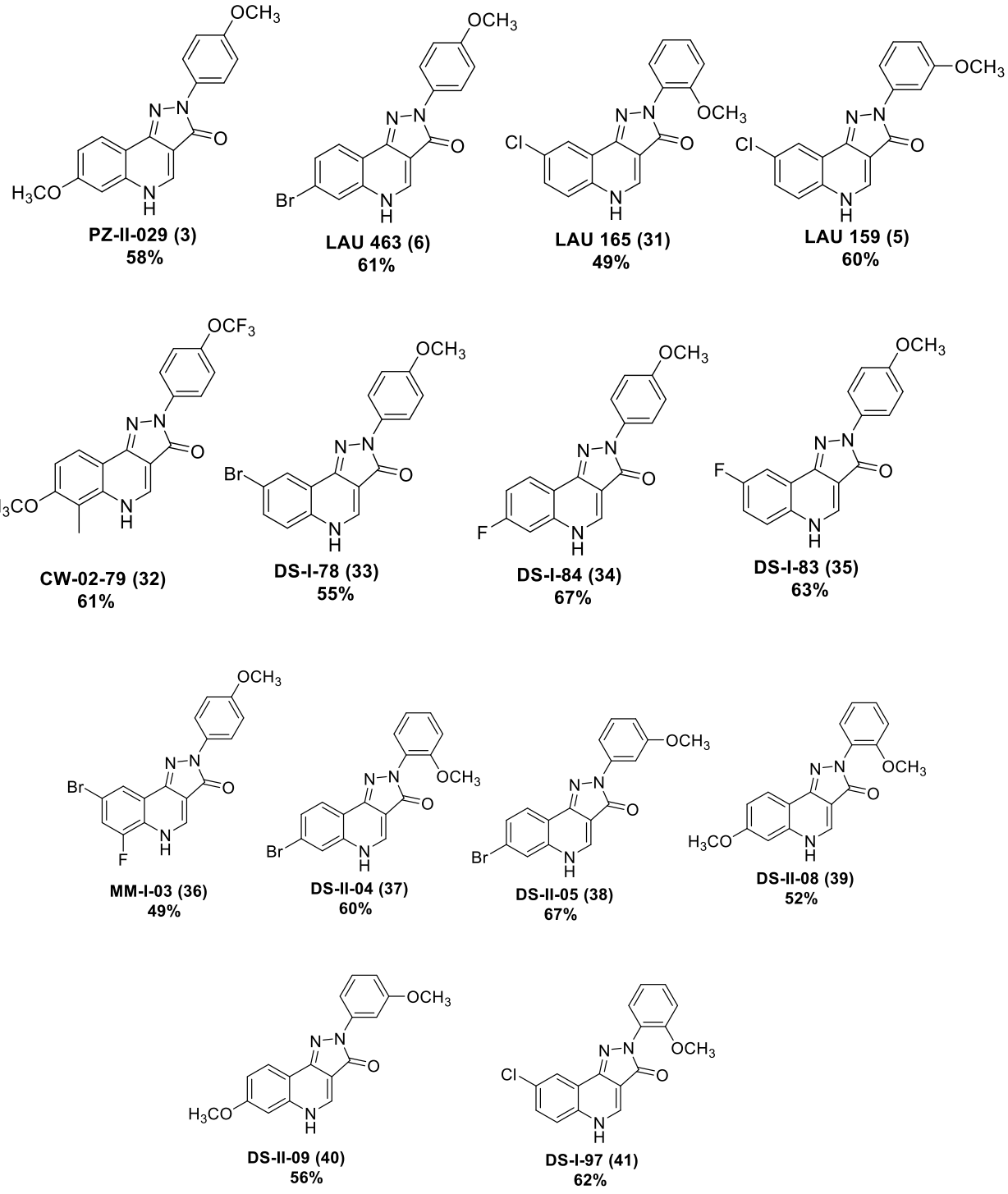
In scenarios where phenylhydrazine hydrochloride salts were incorporated, the quantity of triethylamine was adjusted to account for the additional mole of hydrogen chloride introduced.

Scheme 5. Synthesis of pyrazoquinolinones



R_1= OCH_3, R_2 = H, R_3 = H, **20**
R_1= Br, R_2 = H, R_3 = H, **21**
R_1= H, R_2=Br, R_3 = F, **22**
R_1= H, R_2 = Br, R_3 = H, **23**
R_1= H, R_2 = F, R_3 = H, **24**
R_1= F, R_2 = H, R_3 = H, **25**

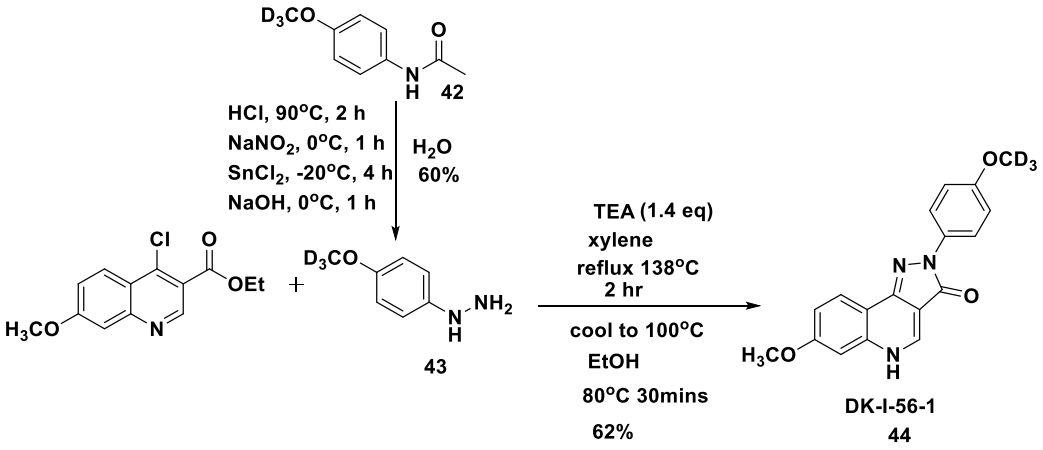
R_4= H, R_5 =OCH_3, R_6 = H, **26**
R_4= H, R_5 = H, R_6 = OCH_3, **27**
R_4= OCH_3, R_5 = H, R_6 = H, **28**
R_4= H, R_5 = OCF_3, R_6 = H, **29**
R_4= H, R_5 = H, R_6 = OCH_3, **30**



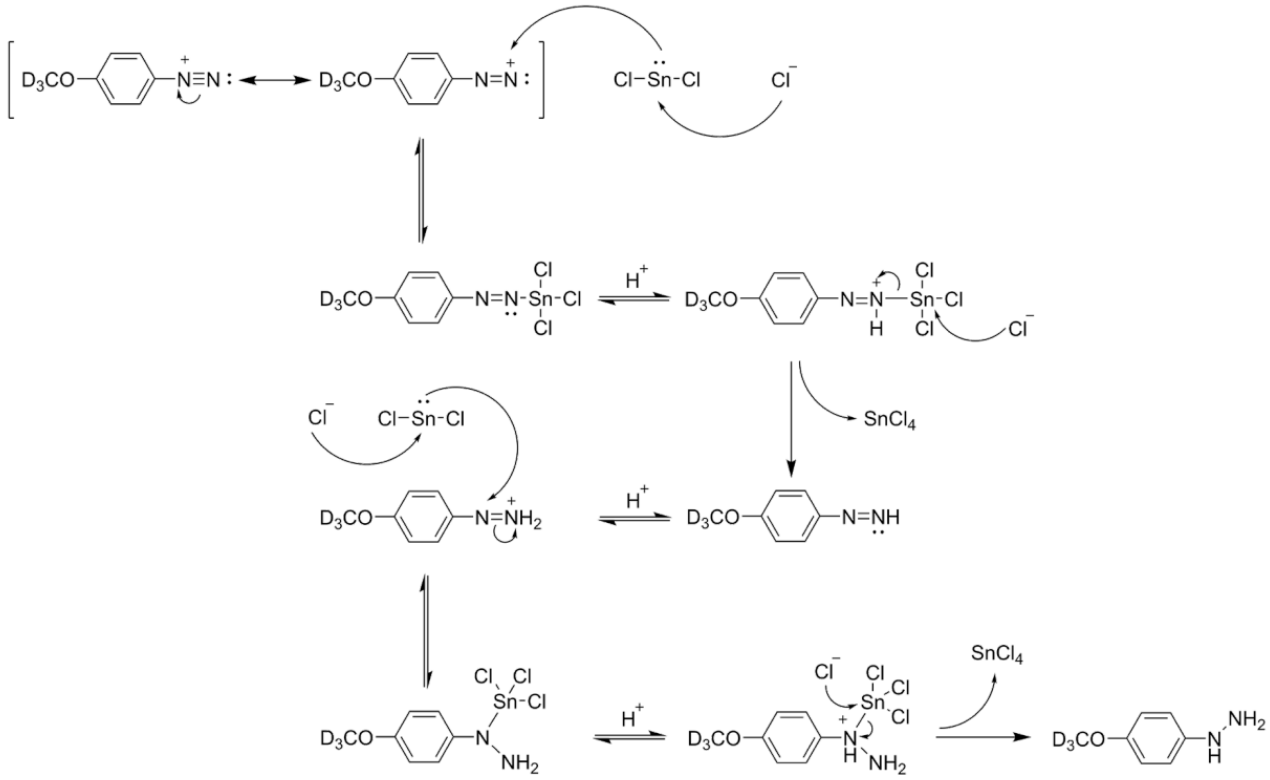
DK-I-56-1 (**4**), the deuterated counterpart of PZ-II-029, was synthesized using a comparable approach. However, instead of utilizing commercially available phenyl hydrazine, the deuterated phenyl hydrazine was produced through a distinct process developed earlier by Knutson et al. In

this method, the amine was subjected to hydrolytic removal of the amide group via hydrochloric acid. Following the deprotection step, diazonium salt formation was facilitated using sodium nitrite. Subsequently, the reduction process **(Scheme 7**) of the diazonium salts was undertaken to yield the intended hydrazines. This reduction was achieved through a one-pot procedure employing tin (II) chloride. This method, as documented by Frahn and Illman,[70] involved maintaining precise control over the temperature (-20°C) during both the diazotization and reduction stages. This temperature control was essential to prevent the undesirable elimination of nitrogen arising from the decomposition of the diazonium salt. This was especially critical for the series with para- and ortho-methoxy substitutions. To fulfill the requirement of preparing the aryl hydrazines in a moisture-free manner for the final pyrazoloquinolinone cyclization step, the aryl hydrazines were isolated as free bases rather than as HCl salts.

Scheme 6. Synthesis of DK-I-56-1



Scheme 7. Probable mechanism for arylhydrazine formation



2.3. Biology of α6 subtype selective pyrazoquinolinones

2.3.1. PZ-II-029 (i.p.) mitigated tremor and reinstated burrowing activity in harmaline treated mice with Dr Huang, Ming Tatt Lee, Dr LC Chiou, and colleagues [116]

Action tremor was induced in mice by treating with harmaline. As illustrated in **Figure 5**, 10 minutes after the subcutaneous administration of harmaline, the mouse was introduced into the tremor chamber for a duration of 10 minutes (depicted in pink shade). During this period, the extent of tremor activity was recorded. Immediately after the 10-minute tremor measurement, the mouse was transferred to a designated cage containing a burrowing tube that held 200 grams of

food pellets. The subsequent 10-minute interval involved measuring the mouse's burrowing activity (depicted in grey shade). Following the burrowing activity measurement, the mouse was returned to the tremor chamber for another round of tremor measurement.

This alternating pattern of tremor and burrowing activity measurement was repeated for multiple cycles, as indicated within each specific experiment. This arrangement was devised considering the nature of harmaline-induced tremor, categorized as an action tremor. The alternating cycles were meticulously structured to refresh the mouse's alertness upon re-entering the tremor chamber. This design aimed to bolster tremor consistency by replacing the rest period traditionally employed with the measurement of burrowing activity.

The administration of harmaline at doses of 10, 20, and 30 mg/kg (s.c.) resulted in a significant induction of tremor activity in mice. This effect was clearly illustrated through the application of a two-way analysis of variance (ANOVA) with repeated measures over time. This analysis revealed notable main effects for Time [$F(6,114) = 12.89$, $P < 0.001$] and Treatment [$F(3,19) = 12.73$, $P < 0.001$], in addition to a significant interaction between time and treatment [$F(18,114) = 2.778$, $P < 0.001$]. The tremor activity exhibited a peak at the frequency range of 10-16 Hz, a pattern discernible in both the motion power-frequency distribution plot and the heatmap spectrogram (**Figure 4A**). Interestingly, the analysis presented in **Figure 4B** demonstrated that tremor activity was evident during mobile phases (highlighted in red) while being notably absent during immobile phases (represented by black periods) in the harmaline-treated mice. This observation strongly indicates that the tremor induced by harmaline is classified as an action tremor.

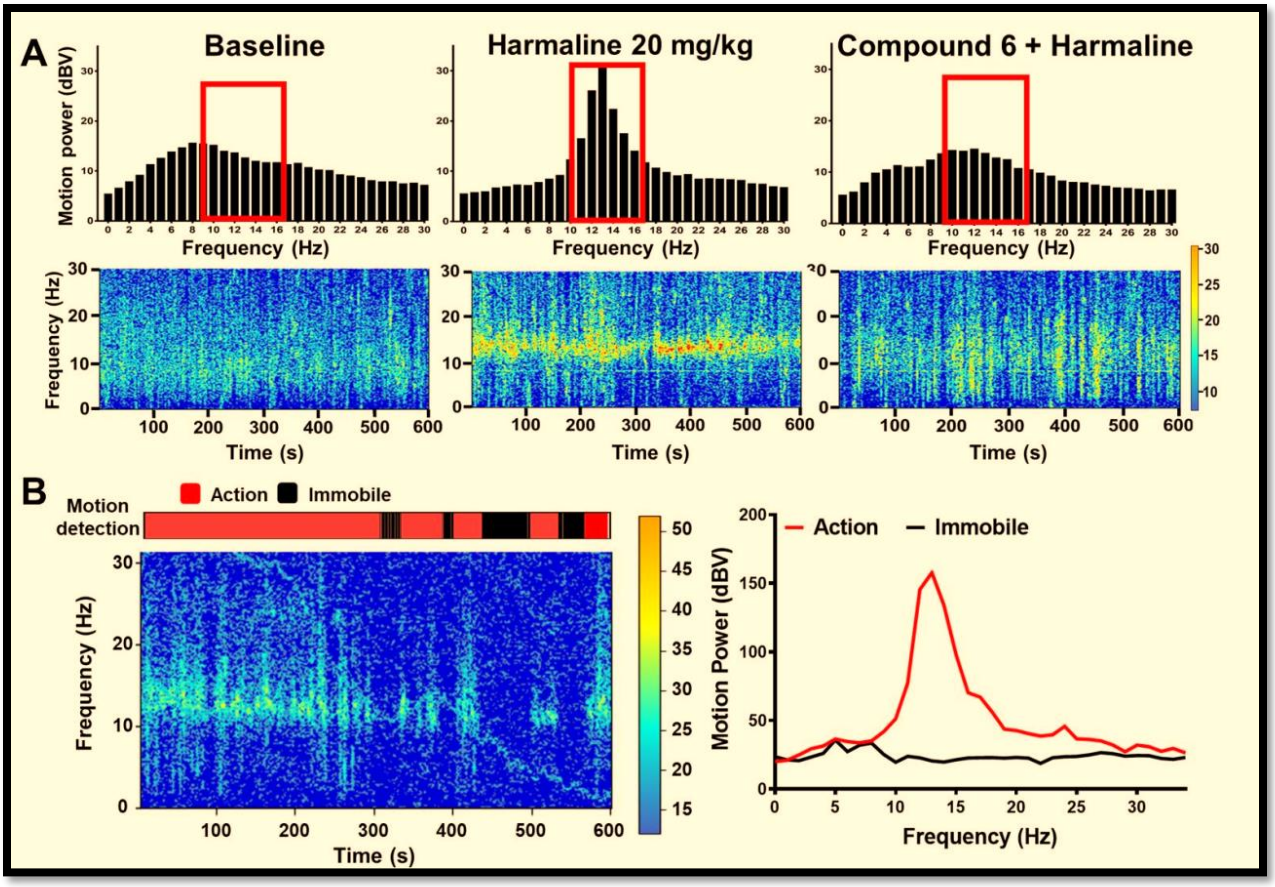


Figure 4. Frequency domain-based motion power spectra and motion power spectrograms in mice treated with saline, harmaline and PZ-II-029 plus harmaline. (A) The motion waves recorded from mice using a Tremor Monitor (San Diego Instruments, CA, USA) were transformed into frequency domain motion power spectra (upper panels) and motion power heatmap spectrograms (lower panels) via a fast Fourier transformer. It's notable that the administration of harmaline induced a tremor response in ICR mice, specifically at the frequency range of 10-16 Hz. However, the inclusion of Compound 6 in conjunction with harmaline exhibited a mitigating effect on harmaline-induced tremor activity. (B) In a distinct scenario, a sample of 10-minute motion power spectrograms (lower panel) is juxtaposed with concurrently detected motor activity identified by the SMART motion

detector. This visual correlation highlights that tremor activity occurs during periods of movement (red region), while it is notably absent during phases of immobility (black region). This observation provides strong evidence that harmaline-induced tremor in mice is categorized as an action tremor, rather than a rest tremor. This Figure was modified from Huang et al. 2021

The tremor activity induced by harmaline reached its peak during the initial assessment interval, specifically 10-20 minutes after the administration of harmaline. Notably, this peak activity was consistent across various dosage groups. However, a time-dependent analysis employing one-way ANOVA unveiled a significant distinction among the treatment groups [$F(3,19) = 6.472$, $P = 0.003$] (**Figure 5A**). Subsequently, the tremor activity demonstrated a gradual and dose-dependent decline. In particular, the heightened tremor activity persisted for at least 50, 75, and 115 minutes, respectively, for the dosages of 10, 20, and 30 mg/kg of harmaline. Furthermore, the area under the curve (AUC) representing the tremor activity over the 120-minute measurement period illustrated a clear dose-dependent trend for the tremor-inducing effect of harmaline (**Figure 5B**). Beyond its tremor-inducing impact, harmaline at doses of 10 and 20 mg/kg significantly suppressed the burrowing activity in mice (**Figure 5C**), except at the 30 mg/kg dose. This discrepancy in the latter case might be attributed to a smaller number of mice within this experimental group or potential undesirable effects stemming from the higher harmaline dose. Harmaline, acting as a neurotoxin that influences various ion channels and neurotransmitter receptors could potentially evoke unintended detrimental effects. As a result, the dose of 20 mg/kg (s.c.) was selected for subsequent pharmacological investigations targeting tremor and burrowing activity impairment. The measurement window was confined to the initial 75 minutes following harmaline injection. This choice was influenced by the desired balance

between inducing pronounced effects and minimizing the potential for unwanted side effects associated with higher doses.

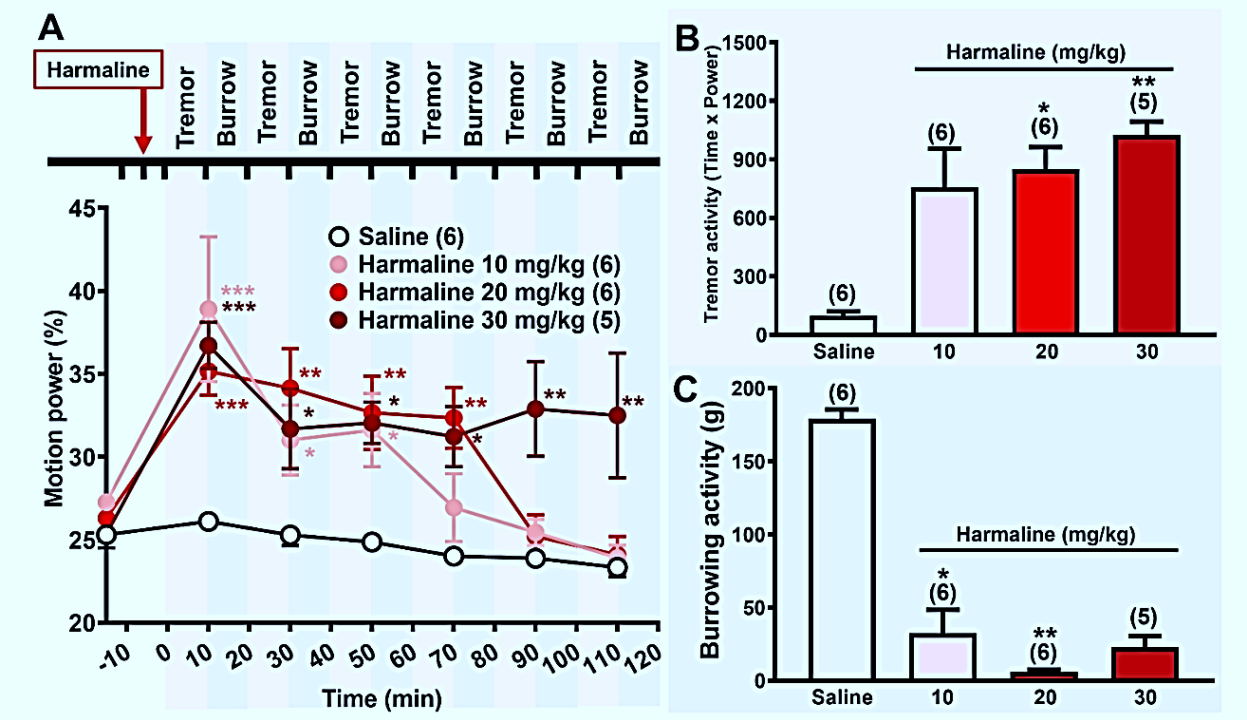


Figure 5. Dose-dependent effects of harmaline on tremor activity and burrowing activity in mice. (A) The illustration of the time-dependent progression of tremor activity prompted by saline, as well as doses of 10, 20, and 30 mg/kg (s.c.) of harmaline. Over the course of 120 minutes, the tremor activity was gauged for intervals of 10 minutes (pink shade). This included a 15-minute period before harmaline injection, a 5-minute interval following injection, and subsequent measurements taken every 20 minutes. Concurrently, the mouse's burrowing activity was evaluated for 10 minutes, right after each tremor activity assessment (grey shade). The alternating measurements of tremor and burrowing activity unfolded across the entire 120-minute duration. The means of tremor activity for each 10-minute segment were plotted against time, and comparisons were drawn among the treatment groups. Statistical significance levels were indicated as *P < 0.05, **P < 0.01,

*****P < 0.001 in relation to the saline group. These comparisons were executed using a two-way ANOVA with repeated measures over time, followed by Holm-Sidak's post hoc test. (B) The cumulative tremor activity,was quantified as the area under the curve (AUC) of tremor activity against time. (C) Concurrently, the cumulative burrowing activity is presented as the total displaced pellets throughout the 120-minute recording period. Statistical analysis indicated significance levels as *P < 0.05 and **P < 0.01 when compared to the saline group. The statistical assessment utilized the Kruskal-Wallis test followed by Dunn's post hoc test. The numbers provided in parentheses indicate the number (n) of mice tested within each respective group. The data are expressed as mean ± S.E.M. This Figure was modified from Huang et al. 2021**

Following a protocol similar to that outlined in **Figure 5A**, various interventions were administered intraperitoneally (i.p.) 5 minutes prior to the injection of harmaline (20 mg/kg, s.c.). These interventions encompassed the vehicle, **PZ-II-029** at doses of 3 mg/kg or 10 mg/kg, and propranolol at a dosage of 20 mg/kg (**Figure 6A**). A comprehensive analysis utilizing a two-way analysis of variance (ANOVA) with repeated measures over time revealed main effects pertaining to time [$F(4,164) = 41.59$, $P < 0.001$] and treatment [$F(3,41) = 12.57$, $P < 0.001$], alongside a noteworthy interaction between time and treatment [$F(12,164) = 8.327$, $P < 0.001$]. Significant reductions in tremor activity were observed across all time points for both doses of PZ-II-029 (3 and 10 mg/kg, i.p.) and propranolol (20 mg/kg) when compared to the vehicle-treated group (**Figure 6A**). Calculated from the time-dependent analysis, the area under the curve (AUC) highlighted substantial anti-tremor effects for both doses of PZ-II-029, with propranolol displaying the most pronounced suppressive impact (**Figure 6B**).

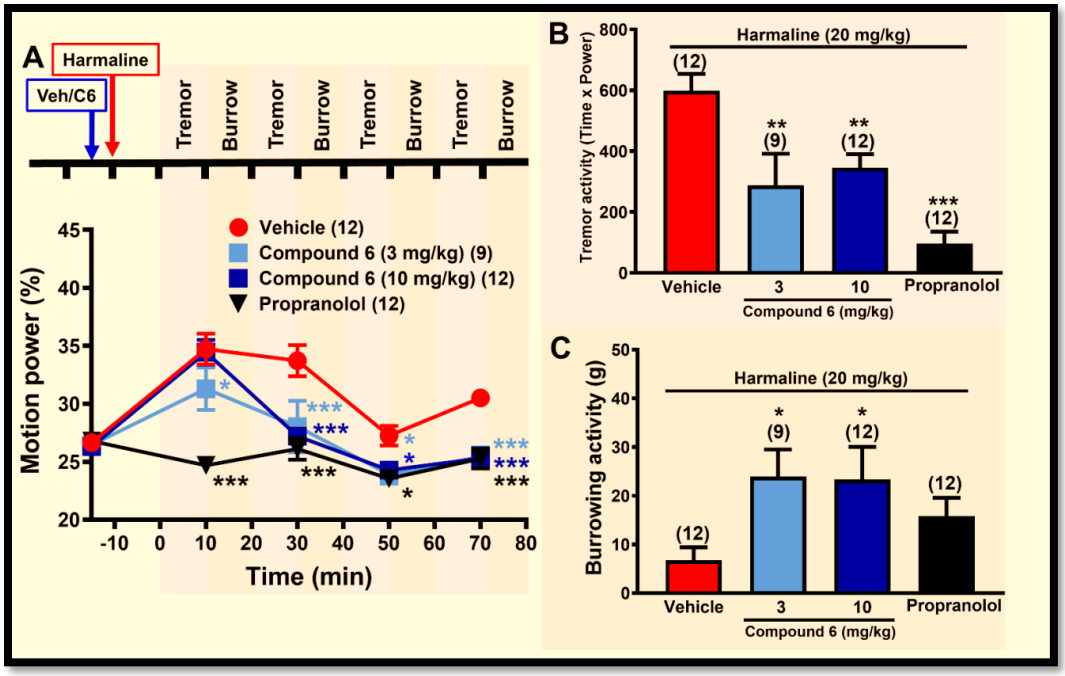


Figure 6. The impacts of PZ-II-029, an α6GABAAR-selective PAM, and propranolol on harmaline-induced tremor and burrowing impairment in mice. (A) The time-dependent profiles of the effects of 3 mg/kg and 10 mg/kg (i.p.) doses of PZ-II-029, alongside its vehicle, as well as propranolol (20 mg/kg), on tremor induced by harmaline (20 mg/kg, s.c.) The sequence of measuring tremor activity and burrowing activity was conducted alternately over an 80-minute duration. Noteworthy, PZ-II-029 and its vehicle were intraperitoneally administered 5 minutes prior to the administration of harmaline. Statistical significance was indicated as *P < 0.05 and ***P < 0.001 in comparison to the saline group. This evaluation was conducted through a two-way ANOVA with repeated measures over time, followed by the Holm-Sidak's post hoc test. (B) The cumulative tremor activity and (C) burrowing activity in mice subjected to harmaline treatment across various intervention groupsis illistrated. The statistical comparison demonstrated significance levels of *P < 0.05, **P < 0.01, and ***P < 0.001 relative to the Vehicle group. This analysis encompassed a one-way ANOVA followed by the Holm-Sidak's post hoc test.

The numerical values in parentheses indicate the quantity (n) of mice examined within each specific group. The data are presented as mean ± S.E.M. Notation: Veh= vehicle, C6= PZ-II-029. This Figure was modified from Huang et al. 2021

Further investigation through one-way ANOVA revealed a noteworthy distinction among treatment groups [$F(3,41) = 12.85$, $P < 0.001$]. However, a more detailed exploration employing one-way ANOVA followed by the Holm-Sidak post hoc test delineated specific outcomes: while the tremor-suppressant dose of propranolol didn't yield a significant restoration of burrowing activity in harmaline-induced mice ($P = 0.18$), **PZ-II-029** at both 3 mg/kg ($P = 0.05$) and 10 mg/kg ($P = 0.05$) exhibited a notable ability to reinstate burrowing activity.

2.3.2. The administration of furosemide (intracerebellar, i.cb.) counteracted the effects of PZ-II-029 (i.p.) on both tremor and burrowing activities in mice treated with harmaline with Mr. Huang, Dr Ming Tatt Lee, Dr LC Chiou, and colleagues[116]

To discern the potential involvement of cerebellar α6GABAARs in the anti-tremor effect mediated by PZ-II-029, a treatment strategy was executed involving the co-administration of intracerebellar (i.cb.) furosemide (10 nmol) and intraperitoneal (i.p.) PZ-II-029 (10 mg/kg), both administered 5 minutes before harmaline injection (**Figure 7A**).Furosemide not cross the BBB but is known as an α6 receptor antagonist, here it was administered directly into the brain(intracerebellam,i.cb.).

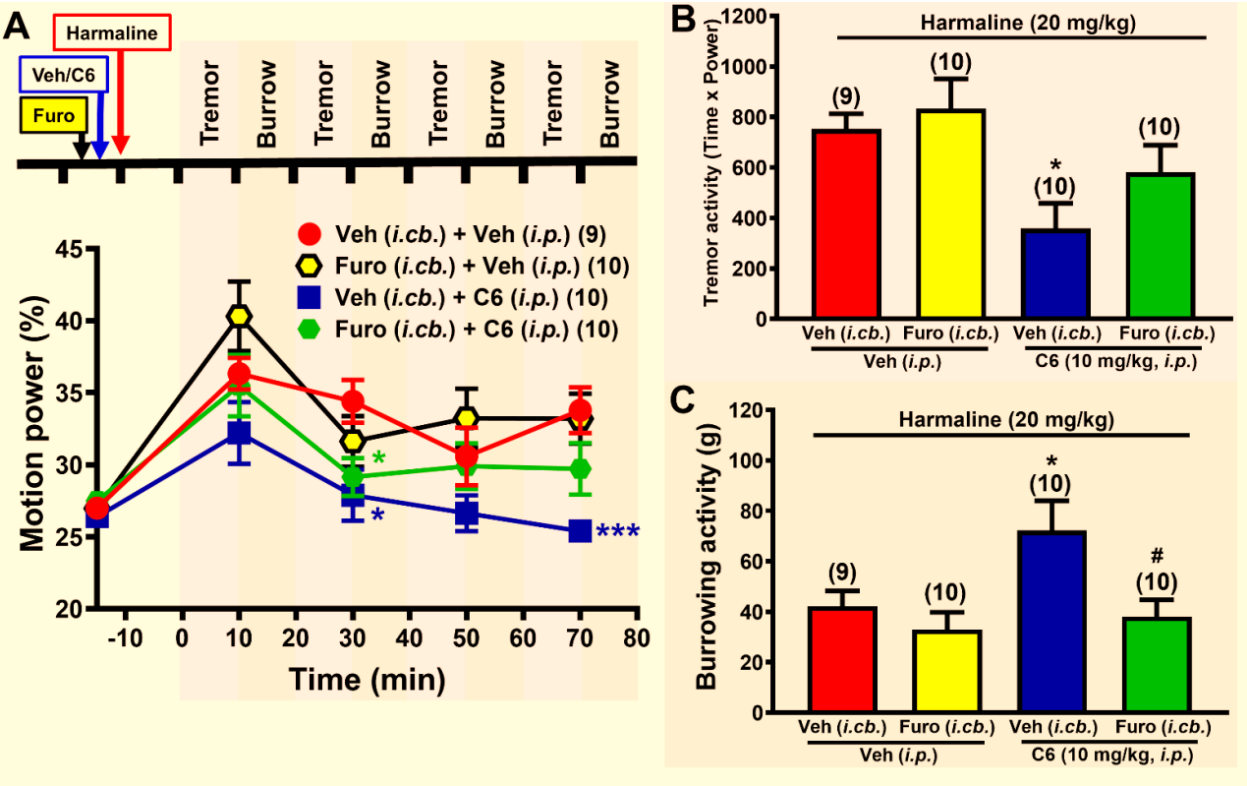


Figure 7. The impact of intra-cerebellar microinjection (i.cb.) of furosemide, an α6GABAAR antagonist, and its effects on the anti-tremor and burrow-restorative properties of α6 ligands PZ-II-029 (Compound 6) in harmaline-treated mice. (A) The temporal progression of effects stemming from the administration of a 10 mg/kg (i.p.) dose of compound 6, along with its corresponding vehicle, both in isolation and in conjunction with an intra-cerebellar microinjection (i.cb.) of furosemide (10 nmol) co-treatment, were assessed in terms of their influence on tremor activity in harmaline-treated mice. Statistical significance was noted as *P < 0.05 and ***P < 0.001 compared to the saline group. This evaluation was conducted through a two-way ANOVA with repeated measures over time, succeeded by the Holm-Sidak's post hoc test. (B) The cumulative tremor activity and (C) burrowing activity pertaining to harmaline-treated mice, who were pre-treated either with PZ-II-029 in isolation or in tandem with an intra-cerebellar microinjection (i.cb.) of

furosemide is illastrated. Statistical significance was denoted as *P < 0.05, **P < 0.01, and ***P < 0.001 relative to the vehicle group, whereas #P < 0.05 indicated significance in comparison to the Veh (i.cb.)+C6 group. This analysis involved a one-way ANOVA followed by the Holm-Sidak's post hoc test. "Furo"=furosemide, "Veh" = vehicle, "C6" =PZ-II-029. The Figure was modified from Huang et al. 2021

upon analysis, a two-way ANOVA with repeated measures over time highlighted key effects: time [$F(4,164) = 41.59$, $P < 0.001$] and treatment [$F(3,41) = 12.57$, $P < 0.001$], alongside a noteworthy interaction between time and treatment [$F(12,164) = 8.327$, $P < 0.001$] (**Figure 7A**). Examining both the time-dependent analysis (yellow diamonds, **Figure 7A**) and the calculated area under the curve (AUC) of motion power (yellow bar, **Figure 7B**) in harmaline-treated mice, it was observed that i.cb. furosemide alone had no discernible impact on tremor activity. Interestingly, co-administration of PZ-II-029 with i.cb. microinjection of furosemide (green bar, **Figure 7B**), in contrast to its vehicle (blue bar, **Figure 7A**), didn't exhibit a substantial anti-tremor effect. This implies that i.cb. furosemide, at a dose that doesn't inherently influence tremor activity, effectively counteracts the anti-tremor effect of PZ-II-029. Moreover, it is noteworthy that the reversal of the burrowing-restorative effect induced by PZ-II-029 in harmaline-treated mice was fully realized through i.cb. furosemide (green bar, **Figure 7C**). Importantly, the administration of i.cb. furosemide by itself didn't elicit any influence on burrowing activity (yellow bar, **Figure 7C**), which is important vs the positive effect of PZ-II-029.

2.3.3. Analogues and deuterated derivatives of PZ-II-029 exhibited comparable anti-tremor and burrowing-restorative effects in mice subjected to harmaline treatment with Mr.Huang, Dr Ming Tatt Lee, Dr LC Chiou, and colleagues

PZ-II-029 and its structural analogue, **LAU463**, alongside their corresponding deuterated derivatives, DK-I-56-1 were shown to exhibit comparable selectivity towards α6GABAAR as positive allosteric modulators. In this current investigation, the administration of **DK-I-56-1** (square, **Figure 8A**) and LAU-463 (diamond, **Figure 8B**), at doses of 3 and 10 mg/kg (i.p.) showcased a time and treatment-dependent reduction of harmaline-induced tremors in mice, with the effect persisting for approximately 1 hour.

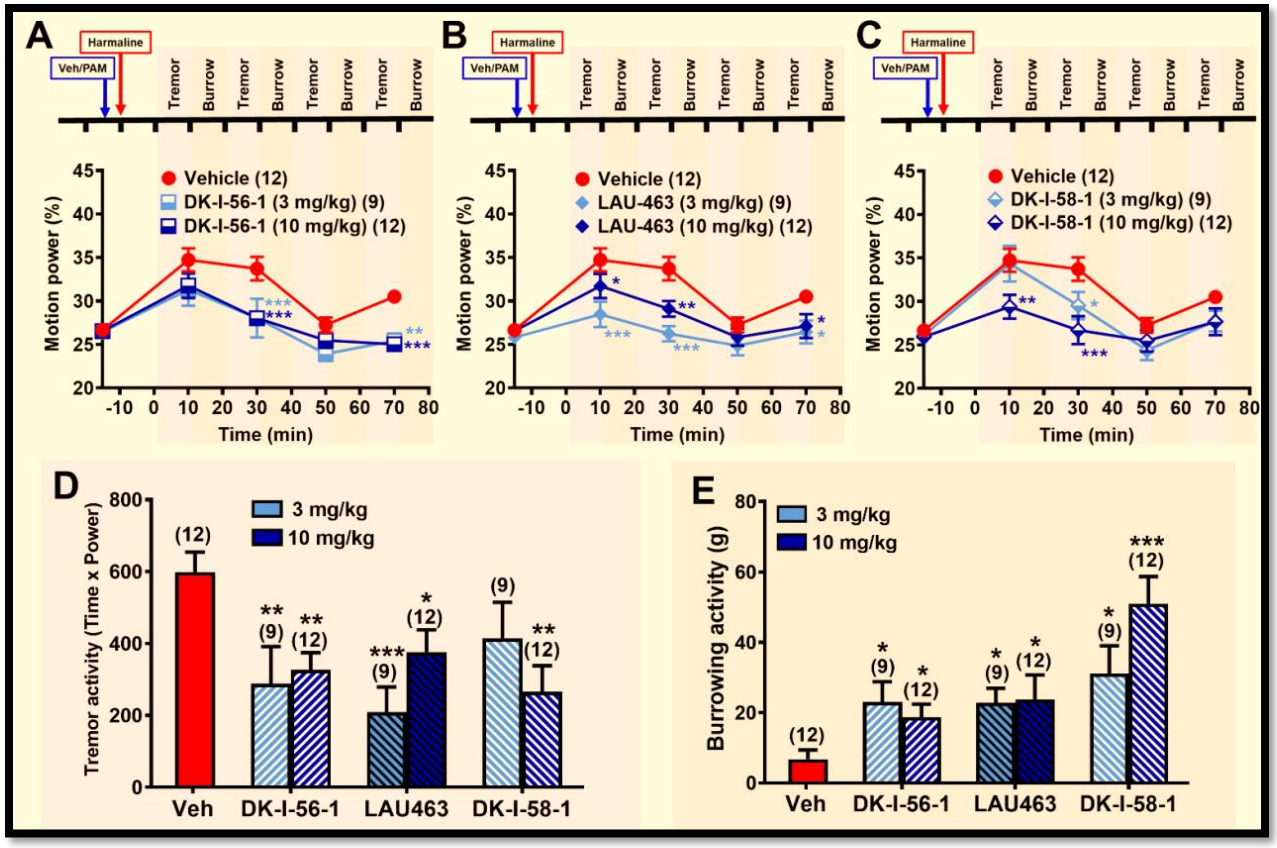


Figure 8. Effects of DK-I-56-1, LAU463 and DK-I-58-1, structural analogues of PZ-II-029, on harmaline-treated mice. (A) DK-I-56-1 (represented by half-filled square symbols), (B)

LAU463 (indicated by diamond symbols), or (C) DK-I-58-1 (depicted by half-filled diamond symbols the deuterated analogs of Lau 463) were administered at doses of 3 and 10 mg/kg (i.p.). The statistical significance denoted by *P < 0.05, **P < 0.01, and ***P < 0.001 was observed compared to the Saline group, employing two-way ANOVA with repeated measures over time followed by Holm-Sidak's post hoc test. The total tremor activity (D) and burrowing activity (E) were measured alternatively for 80 minutes, following the procedure outlined in Figure 3, within various treatment groups. The statistical comparison indicated *P < 0.05, **P < 0.01, and ***P < 0.001 versus the vehicle group, performed using one-way ANOVA followed by Holm-Sidak's post hoc test. Notations used: Veh for vehicle, and PAM for positive allosteric modulator.

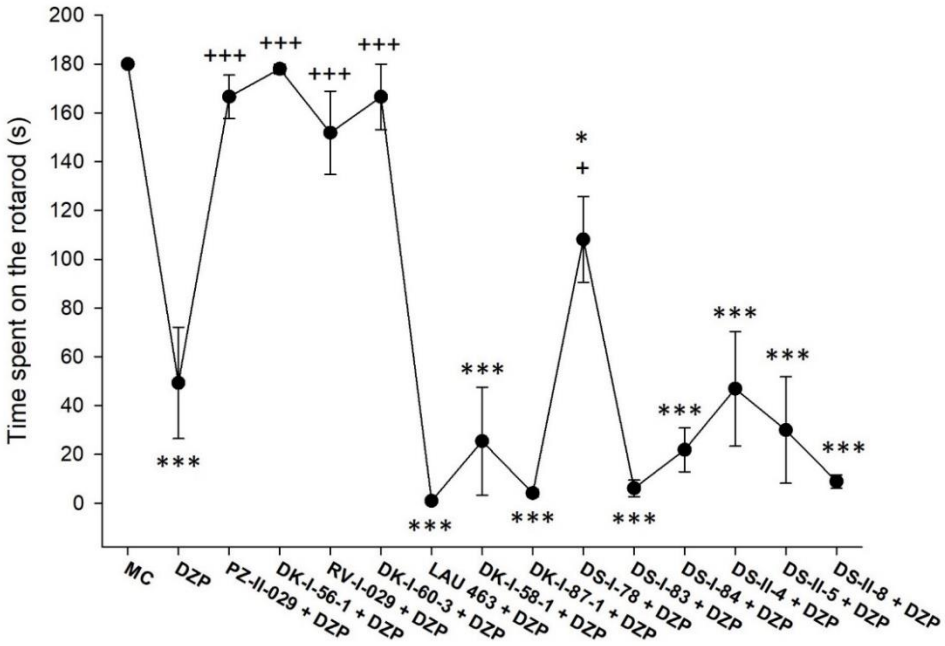
By assessing the area under the curve (AUC) obtained from the time-dependent analysis, it was evident that each drug group significantly suppressed tremor activity when compared to the vehicle group, except for DK-I-58-1 at the dose of 3 mg/kg. Interestingly, a consistent pattern was observed across all treatment groups, where they effectively restored burrowing activity in harmaline-treated mice (**Figure 8E**) as opposed to the vehicle group. This effect resembled that of **PZ-II-029** but was distinct from the influence of propranolol.

2.3.4. PZ-II-026 analogues exert a complete flumazenil-like preventative effect on diazepam-induced incapatication in the rotarod with Brianka, Dr Miroslav Savic, and colleagues (Unpublished data)

A variety of ligands were administered to Sprague-Dawley rats through oral gavage at a dosage of 30 mg/kg, suspended in 0.25% methylcellulose at a concentration of 3 mg/ml. This dosage was selected to prevent the motor incapacitating effect of diazepam (administered

intraperitoneally at 5 mg/kg) as evaluated using the rotarod test. Extensive pilot studies were conducted to fine-tune the routes and doses, and the reported results are consistently robust and reproducible.

The key observation of this study is that PZ-II-029, DK-I-56-1, RV-I-029, and DK-I-60-3 all exhibit the capability to counteract the motor-impairing impact of diazepam. Importantly, their efficacy in this regard is comparable to that of flumazenil. In contrast, a range of previously known and novel pyrazoloquinolinone compounds, including LAU463, DK-I-58-1, DK-I-87-1, DS-I-83, DS-I-84, DS-II-4, DS-II-5, and DS-II-8, did not demonstrate any influence on the effects of diazepam. Among these compounds, **DS-I-78** showed an intermediate effect between the two groups (**Figure 9**).



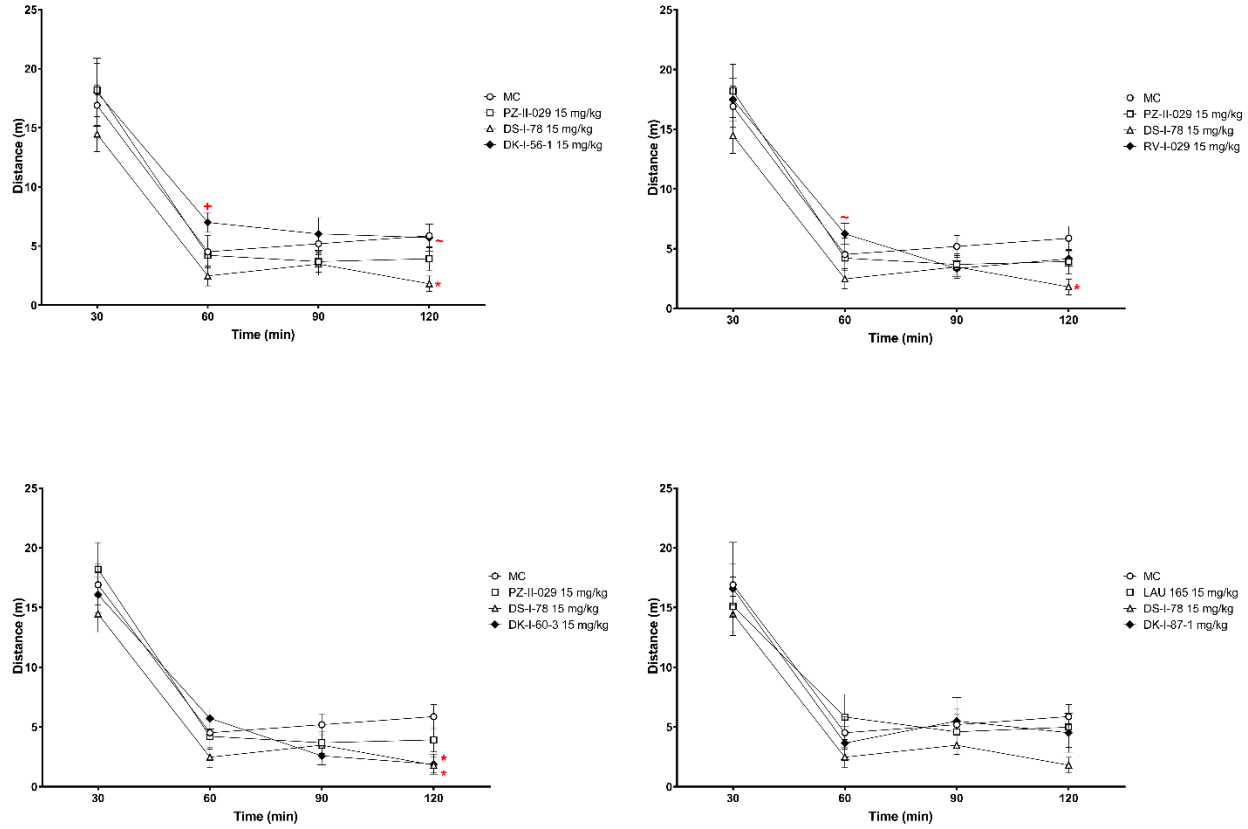


Figure 9. Effects of PZ-II-029 analogues on diazepam-induced incapatication in the rotarod. PZ-II-029, DK-I-56-1, RV-I-029, and DK-I-60-3 demonstrate the ability to mitigate the motor-impairing effects caused by diazepam. DS-I-78 displayed an effect that falls between the outcomes observed in the two groups.

2.3.5. Effects of DK-I-56-1 on Frequency-Rate Intracranial Self-Stimulation in Rats (NIH, Unpublished data)

The present study evaluated the effects of **DK-I-56-1** on lever pressing rates maintained by intracranial self-stimulation (ICSS) in rats using a frequency-rate procedure. **DK-I-56-1** (0.1, 1, 3, and 10 mg/kg) or its vehicle (2% methylcellulose) were administered i.p. 30 min prior to ICSS testing. Compared to vehicle, all of the **DK-I-56-1** doses tested significantly decreased response rates at one or more frequencies, with doses of 1 mg/kg and higher significantly decreasing

response rates at the frequency that supported maximal response rates under control conditions. Generally, the frequency-rate curve was downwardly displaced by effective doses of **DK-I-56-1** relative to vehicle control suggesting that decreased ICSS-reinforced responding, at least in part, was attributable to nonspecific motoric impairment. When normalized as a percent of the test day's baseline, 3 and 10 mg/kg **DK-I-56-1** significantly increased the estimated frequency supporting half-maximal response rate (M50), and the 10 mg/kg dose also significantly increased the estimated frequency supporting threshold responding (T0). Overall, these data indicate that **DK-I-56-1** produces dose dependent decreases in lever pressing reinforced by medial forebrain bundle stimulation in rats under these conditions.

ICSS involving electrical stimulation of the medial forebrain bundle is thought to result in the activation of myelinated neurons that engage dopaminergic dendrites or cell bodies of the ventral tegmental area and substantia nigra that subsequently send efferent, ascending projections throughout the mesocorticolimbic system. Drugs of abuse, such as nicotine, amphetamine, and the opiates, enhance ICSS by reducing the threshold frequency or intensity that supports this behavior, and this effect is hypothesized to correlate with their abuse-related effects. Conversely, drugs that produce anhedonia or dysphoria, such as the neuroleptics, lithium, or κ-opioid agonists, increase the threshold frequency or intensity that supports this behavior.

Frequency-rate curves from tests with **DK-I-56-1** (0.1, 1, 3, and 10 mg/kg) and vehicle are presented in **Figure 10**. There were significant main effects of frequency [$F(9, 81)=77.08$, $p<0.0001$], and **DK-I-56-1** treatment [$F(4, 36)=19.80$, $p<0.0001$], and a significant interaction [$F(36, 324)=2.551$, $p<0.0001$]. Post-hoc analysis indicated that all **DK-I-56-1** doses significantly decreased responding compared to vehicle. Specifically, responding was decreased at two

frequencies by the 0.1 mg/kg dose, six frequencies by 1 mg/kg, and seven frequencies each by 3 and 10 mg/kg. Generally, response rates at frequencies above 1.9 were downwardly displaced by **DK-I-56-1** doses relative to control conditions, suggesting that nonspecific motoric impairment may have contributed to the decreased responding produced by these doses. A vehicle control test conducted at the end of testing with 1-10 mg/kg **DK-I-56-1** did not significantly differ from the initial vehicle test (data not shown). Furthermore, analysis of baseline frequency-rate curves across test sessions showed no significant main effect of treatment day or interaction between stimulation frequency and day (data not shown), indicating that ICSS behavior was stable over the course of the study.

The effects of **DK-I-56-1** on T0 and M50 levels for all test conditions are presented in **Figure 11** and **Tables 1-2**. Two rats had non-calculable T0 and M50 values at the 10 mg/kg dose and were excluded from within-subjects analyses. When normalized to percent baseline, T0, and M50 were analyzed as separate one-way repeated measures ANOVAs (**Figure 11**). Analysis of % baseline T0 data (top panel) revealed there was no significant main effect of **DK-I-56-1** treatment [$F(4, 28)=2.161$, $p=0.0996$]. Planned comparisons using Fisher's LSD test indicated that 10 mg/kg **DK-I-56-1** significantly increased % baseline T0 values compared to vehicle ($p=0.0182$). Analysis of % baseline M50 data (bottom panel) revealed there was a significant and $p<0.0001$, respectively).

Log frequency values for ATDP 34,282 and baselines are displayed on **Tables 1 and 2**. There were no significant main effects of day on baseline T0 [$F(4, 36)=0.317$, $p=0.8646$) or M50 [$F(4, 36)=0.407$, $p=0.8022$) values. In contrast, there were significant main effects of treatment on test T0 [$F(4, 28)=3.34$, $p=0.0234$] and M50 values [$F(4, 28)=9.868$, $p<0.0001$]. Planned comparisons

indicated that 3 and 10 mg/kg **DK-I-56-1** significantly increased T0, and 1, 3, and 10 mg/kg **DK-I-56-1** significantly increased M50.

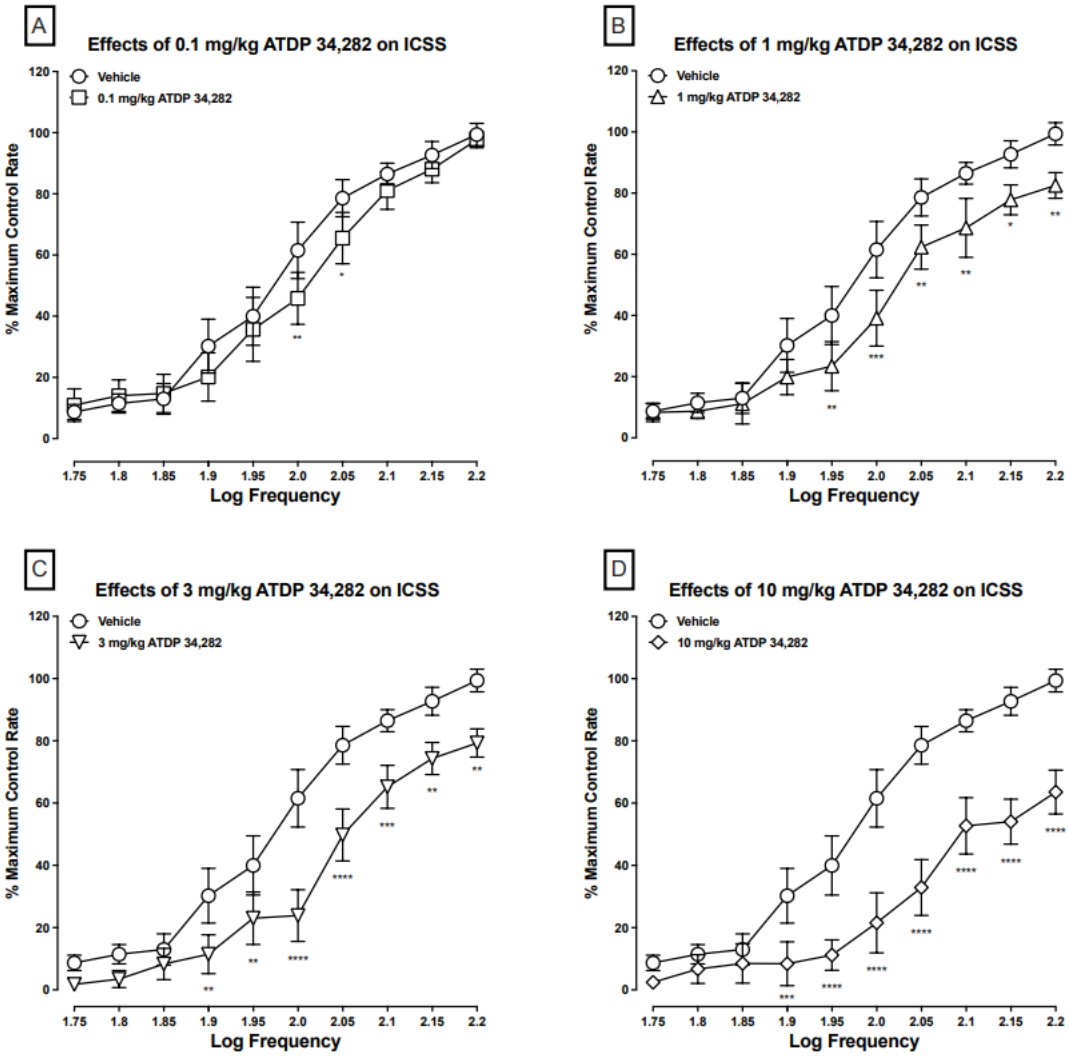


Figure 10: Frequency-rate response curves showing the effects of DK-I-56-1 (0.1, 1, 3, and 10 mg/kg) and vehicle (2% methylcellulose) administered i.p. 30 min pre-session. Values represent the mean + SEM normalized response rate (% of maximum control responding) across 10 frequency presentations (1.75 – 2.20 log/Hz) of 10 rats. Significant differences compared to vehicle at a respective frequency are denoted by asterisks (* p<0.0001). ADP34,282 = DK-I-56-1.

Overall, the results of this study demonstrate that the doses of **DK-I-56-1** tested significantly decreased ICSS frequency-rate curve responding and sufficiently high doses produced concomitant increases in T0 and M50 analyses. Generally, the frequency-rate curve was downwardly displaced by **DK-I-56-1** doses relative to control conditions, suggesting that nonspecific motoric impairment may have contributed to the decreased responding produced by effective doses. Overall, these data indicate that **DK-I-56-1** produces dose-dependent decreases in lever pressing reinforced by medial forebrain bundle stimulation in rats under these conditions.

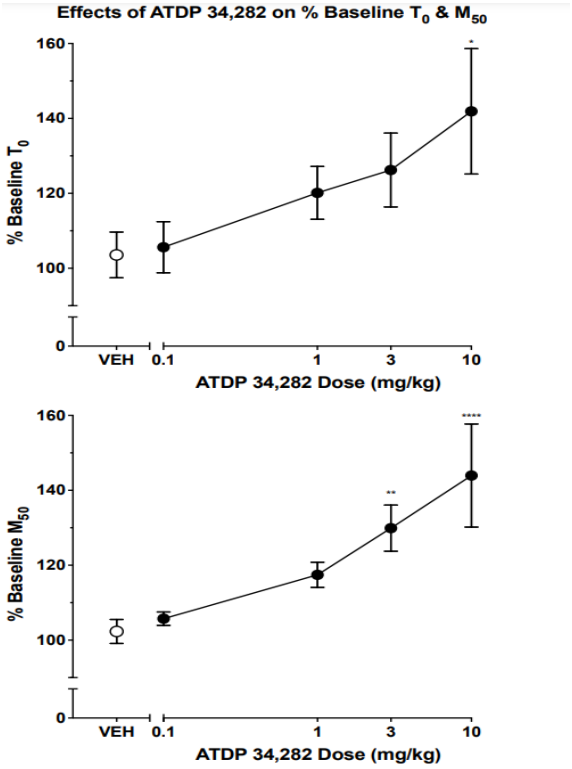


Figure 11: Effects of 0.1, 1 3, and 10 mg/kg ATDP 34,282 and vehicle on % baseline T0 and M50 Values represent the mean (± SEM) of calculated % baseline T0 (top panel) or M50 (bottom panel) in 8 rats (n.b., 2 rats had marked rate decreases that precluded

determination of T0 and M50). Significant differences compared to vehicle are denoted by asterisks (* p<0.0001). ADP34,282 = DK-I-56-1.

Threshold (T_0)	Baseline	Test	Test N
Vehicle	1.85 (0.03)	1.85 (0.04)	8
0.1 mg/kg ATDP 34,282	1.87 (0.03)	1.88 (0.04)	8
1 mg/kg ATDP 34,282	1.84 (0.03)	1.90 (0.04)	8
3 mg/kg ATDP 34,282	1.84 (0.03)	1.92 (0.03) *	8
10 mg/kg ATDP 34,282	1.85 (0.03)	1.96 (0.04) **	8

Table 1. Summary table of log threshold (T0) values in rats tested with ATDP 34,282 (10 and 30 mg/kg) or vehicle. Data represent the mean baseline log T0 frequency (log/Hz) ± SEM of 10 rats. Test log T0 values were excluded from 2 rats due to due to marked rate suppression produced by the 10 mg/kg ATDP 34,282 dose. A significant difference in test T0 values compared to vehicle is denoted by asterisks (* p<0.01). ADP34,282 = DK-I-56-1.

M_{50}	Baseline	Test	Test N
Vehicle	1.96 (0.02)	1.95 (0.02)	8
0.1 mg/kg ATDP 34,282	1.97 (0.02)	1.98 (0.03)	8
1 mg/kg ATDP 34,282	1.97 (0.02)	2.02 (0.03) **	8
3 mg/kg ATDP 34,282	1.96 (0.02)	2.05 (0.03) ***	8
10 mg/kg ATDP 34,282	1.96 (0.03)	2.08 (0.04) ****	8

Table 2. Summary table of frequencies that sustained half-maximal responding (M50) in rats tested with ATDP 34,282 (10 and 30 mg/kg) or vehicle. Data represent the mean baseline log M50 frequency (log/Hz) ± SEM of 10 rats. Test log M50 values were excluded from 2 rats due to due to marked rate suppression produced by the 10 mg/kg ATDP 34,282 dose. There was no significant difference between baseline M50 values preceding ATDP 34,282 tests compared to vehicle. A significant difference in test M50 values compared to vehicle is denoted by asterisks (p<0.0001). ADP34,282 = DK-I-56-1.**

2.4. Methods for Biological study with Huang, Dr Ming Tatt, Dr LC Chiou, Dr Miuroslav Savic, and colleagues

2.4.1. *Intra-cerebellar (i.cb), intraperitoneal* (*i.p.*) and subcutaneous (*s.c.*) *injections*

Mice were anesthetized using sodium pentobarbital (60 mg/kg, i.p.) and then placed in a stereotaxic frame to maintain the bregma-lambda axis in a horizontal position. Following hair removal and exposure of the skull surface, each mouse was implanted with a 24-gauge stainless-steel guide cannula that was directed towards the vermis (-7.0 mm caudal, -0.4 mm ventral from bregma) as per the stereotaxic coordinates for mice (Franklin and Paxinos, 1997). A recovery period of at least 1 week was allowed for each mouse after implantation.

During the behavioral testing day, a 30-gauge injection cannula, connected to a 1-µl Hamilton syringe via a 50 cm polyethylene tube, was inserted into the guide cannula for drug administration. A 0.5 µl drug solution was slowly infused using a microinfusion pump (KDS311, KD Scientific Inc.) over a period of 3 minutes, followed by a 2-minute "hold" time, while the mouse was allowed to move freely within an open field arena. To confirm the microinjection site, trypan blue was injected through the cannula after the behavioral tests, and data from mice with injections at offsite locations were excluded. For intraperitoneal (i.p.) and subcutaneous (s.c.) injections, the drug solution was administered at a volume of 10 ml/kg.

2.4.2. Tremor induction and measurement

To induce action tremor in mice, the harmaline-induced tremor protocol was followed with minor adjustments based on previous methods (Handforth et al., 2018; Martin et al., 2005). Tremor frequency and intensity were assessed using a Tremor Monitor (San Diego Instruments, SDI, CA, USA), a technique previously employed for accurate differentiation between tremor

activity and other types of movement (White et al., 2016). This instrument has been demonstrated to effectively discriminate between tremor and ambulatory/stereotyped motions, as well as overall motion activity (Paterson et al., 2009).

Each mouse underwent an acclimatization phase within the chamber, after which baseline motion power was recorded over a 10-minute period. Prior to harmaline administration, the test drugs were given through intraperitoneal (i.p.) or intra-cerebellar (i.cb.) injections, with the interval set at 5 minutes before the harmaline injection. The raw traces of movement activity, captured by the Tremor Monitor, were then subjected to fast Fourier transform to produce a frequency domain-based motion power spectrum, employing a bin size of 1 Hz. Tremor activity in each mouse was quantified by the ratio of motion power within the 10-16 Hz frequency range, divided by the tremor frequency (0-34 Hz) of the overall motion power. This assessment was conducted over a 10-minute span (**Figure 4A**). The overall extent of tremor activity was summarized by calculating the area under the curve (AUC) from the time-dependent tremor responses. In order to verify that the harmaline-induced tremor recorded within our experimental setup was indeed action tremor, the locomotor activity of the harmaline-treated mice was video-recorded within the tremor chamber. This footage was subsequently analyzed to distinguish between action-based movement and periods of immobility, using the SMART Video Tracking System (Harvard Apparatus, MA, USA) (**Figure 4B**).

2.4.3. Burrowing activity assessment

The measurement of a mouse's burrowing activity was conducted following previously established procedures (Ballon Romero et al., 2020; Deacon, 2012), with certain modifications.

To facilitate adaptation, an empty tube was introduced into the home cage, ensuring that all five mice in the cage encountered the tube. On the day of the actual testing, individual cages were arranged for each mouse to undergo isolated evaluation. The burrowing tube was loaded with 200 g of food pellets. To determine the burrowing activity, the weight of the expelled food pellet was calculated by deducting the weight of the remaining food pellet (at the conclusion of the experiment) from the initial weight of 200 g. This approach allowed for the quantification of the extent of burrowing undertaken by the mouse during the experiment.

As illustrated in **Figure 5A**, a sequence of events unfolded after the administration of harmaline (via subcutaneous injection). Ten minutes post-injection, the mouse was introduced into the tremor chamber, where its tremor activity was observed and measured for a span of 10 minutes (depicted by the pink shaded region). Subsequent to this tremor assessment, the mouse was transferred to a specified enclosure equipped with a burrowing tube containing 200 g of food pellets. Over the following 10-minute period (indicated by the grey shade), the mouse's burrowing activity was monitored. Subsequently, the mouse was returned to the tremor chamber for another round of tremor measurement. This alternating pattern of tremor and burrowing activity assessment was recurrently carried out for a series of cycles, as outlined in each experiment. This experimental design was motivated by the fact that harmaline-induced tremor is classified as an action tremor. The alternating sequence was meticulously devised to invigorate the mouse's attentiveness when placed back in the tremor chamber, thereby promoting the consistency of tremor readings. This innovative approach replaced the conventional resting period found in earlier studies (Handforth *et al*., 2018; Martin *et al*., 2005) with the burrowing activity assessment, ensuring improved stability in the observed tremor effects.

2.4.4. Statistical analysis

The data were presented as the mean ± S.E.M., and the 'n' value denoted the number of animals included in the study. To assess the variance in tremor intensity across different treatment groups over time, a two-way ANOVA was performed, followed by Holm-Sidak's post hoc test. For analyzing differences among treatment groups, a one-way ANOVA was used, along with Holm-Sidak's post hoc test. However, in cases where there was heterogeneity identified in the one-way ANOVA, which was indicated by a significant Brown-Forsythe test, a non-parametric Kruskal-Wallis test was applied, followed by Dunn's post hoc test. Statistically significant distinctions were acknowledged when the p-value was less than 0.05.

2.4.5. Method to evaluate the effect of DK-I-56-1 on frequency-rate intracranial self-stimulation in Rats (NIH)

Subjects

Eleven adult male Sprague-Dawley rats (Envigo, Dublin, VA) were individually housed in a temperature-regulated (20–22°C) AAALAC-accredited facility in which they had ad libitum access to water and controlled access to food (7012 Teklad LM-485 Mouse/Rat Sterilizable Diet; Envigo, Indianapolis, IN) that maintained the rats within a weight range of 380-420 g. The rats were maintained on a 12 h/12 h light-dark cycle (0600-1800 lights on) for the duration of testing, and they were trained and tested during the light segment of this cycle. Rats (360-420 g at the time of surgery) were anesthetized via isoflurane inhalation (~3%), and an electrode was implanted into the medial forebrain bundle at stereotaxic coordinates described by Paxinos & Watson (2007) (anteroposterior, −2.8 mm from bregma; lateral, 1.7 mm from the midline; ventrodorsal, −8.8 mm from the skull). Rats were administered 1 mg/kg buprenorphine SR-LAB

(ZooPharm, Laramie, WY) s.c. during surgery to provide relief from potential postoperative pain.

Apparatus

Experimental sessions were conducted in commercially obtained operant test chambers enclosed in sound-attenuating cubicles. The test chambers were each equipped with a ventilation fan, two retractable levers mounted on the front intelligence panel, a stimulus lamp positioned above each lever, and a 5-w house light (Med Associates, Inc., St. Albans, VT). A counterbalanced tether (Plastics One, Roanoke, VA) connected the electrode to an ICSS stimulator (#PHM-152/2, Med Associates, Inc., St. Albans, VT) and allowed free movement within the operant chamber. Control of stimuli and recording of data were arranged by computer-controlled software (MedPC IV; Med Associates, Inc., St. Albans, VT) interfaced with the operant test chambers.

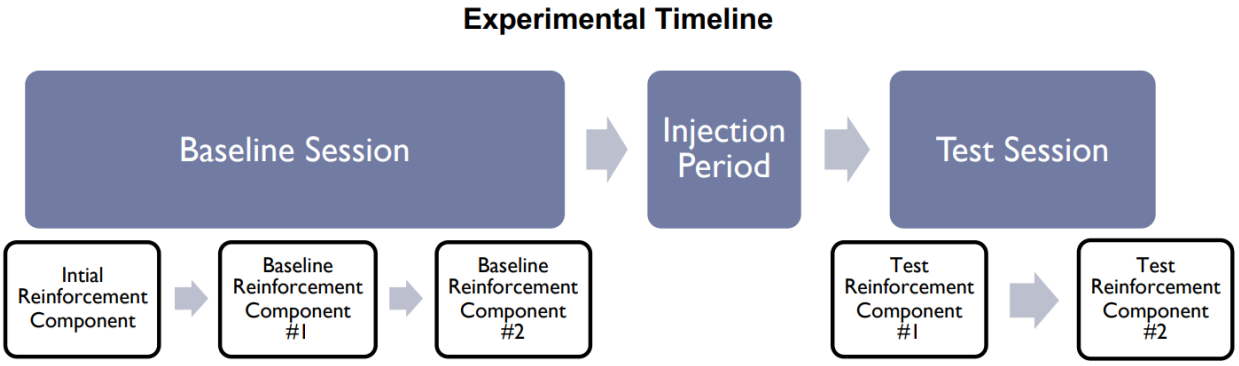
Procedure

The rats began fixed ratio 1 (FR1) self-stimulation training one week after surgery. Initially, only the right lever was extended, the house light illuminated, and each press of the right-side lever (i.e., FR1) resulted in the delivery of stimulation (70 µA, 158 Hz). During the delivery of stimulation (500 ms), the house light was extinguished, and the cue lights above each lever flashed at 3 Hz. The current intensity was individually adjusted when necessary to maximize the stability and the rates of behavior (>30 responses/min) at the highest frequency. This intensity level was held constant for the remainder of the experiment. The frequency-rate procedure (modified from Carlezon & Wise, 1996) consisted of multiple (see below) components, each composed of 10, 1-min FR 1 reinforcement periods. During each 1-min reinforcement period, a

single, scheduled frequency was available for delivery contingent upon FR 1 responding at the right-side lever. Frequencies were progressively decreased in 0.05 log increments from 158-56 Hz (i.e., 2.2–1.75 log Hz) during each component. Each 1-min reinforcement period was preceded by a 5-s sample period during which five response-independent stimulations were delivered at the scheduled stimulation frequency. Each response period was followed by a 5-s timeout (TO) period during which the house light was extinguished, and ICSS was unavailable. During frequency-rate training, both the left and right levers were extended. Presses of the left lever were without scheduled consequences, although they were recorded. Rats were trained daily (M-F) using the described procedure. Training sessions were conducted in the morning and consisted of three consecutive components. Threshold (T0), as defined by the theoretical frequency at which the linear portion of the frequency-rate curve intersected with the abscissa (i.e., zero responses), and M50, as defined by the estimated frequency that supported half-maximal response rates, were determined (see Data Analysis). Once stable behavior was established as demonstrated by ≤ +/- 20% variation of the five-day running mean of total stimulations during four out of five consecutive baseline sessions, animals began testing. Baseline response stability continued to be monitored throughout the experiment.

On test days, two ICSS experimental sessions were conducted. During the baseline session, each rat was tested during three consecutive components identical to training days. After completing this baseline determination, rats were returned to their home cages and received i.p. administration of either **DK-I-56-1** (0.1, 1, 3, or 10 mg/kg) or vehicle (2% methylcellulose). Following the 30-min pretreatment period, rats were returned to their operant chambers for the test session that consisted of two consecutive components (i.e., two complete frequency sweeps). Once vehicle control tests were completed, 1, 3, and 10 mg/kg **DK-I-56-1** were tested in

ascending dose order. Lastly, a test with vehicle was repeated to assess the stability of control responding over the duration of the experiment. Given the degree of rate- decreasing effects produced by all doses initially tested, a lower dose (0.1 mg/kg) was subsequently authorized for testing. The sequence of events and timeline during test sessions are depicted below.



Subjects were tested at most twice weekly (typically Tuesday and Friday), with a minimum of 72 h between test sessions. Training sessions were conducted during the week on non-test days to maintain stability in frequency-rate responding, and that also allowed its evaluation to determine testing eligibility. Rats were required to meet stability criteria (< 20% variation in total baseline stimulations compared to stable, pre-test total baseline stimulations) to be scheduled for testing. One to two frequency-rate training sessions were conducted between test sessions to assess behavioral stability and permit drug washout.

Data Analysis

One rat was removed from the study due to unstable baseline responding. Thus, the results included in this report are from ten rats. Results from the initial component during baseline sessions on test days were excluded from the data analysis as it has been shown that behavior is less stable during the first daily experimental component relative to subsequent components

(Carlezon & Chartoff, 2007). Results obtained at each frequency during the two subsequent baseline components were averaged to determine a baseline response rate for each frequency. The maximum control rate (MCR) was defined as the maximum averaged baseline response rate that occurred across all frequencies during the baseline session. For subsequent data analyses, baseline and test stimulation rates were normalized to each rat's daily baseline MCR to produce expressions of the percent maximum control rate (%MCR). These values were calculated by dividing the mean number of responses obtained at each frequency by the rat's MCR as determined during the associated (i.e., same-day) baseline session, then multiplying this quotient by 100 for both baseline and test sessions.

Frequency-rate response data were analyzed using two-way (treatment x frequency) repeated measures ANOVAs. Significant main effects of treatment or interactions of treatment and frequency were followed by Holm-Šídák multiple comparisons tests to identify treatmentrelated differences in responding at each frequency compared to vehicle (**Figure 10**). Parallel leftward shifts in the frequency-rate curve are inferred as reward facilitation, and parallel rightward shifts in the frequency-rate curve are inferred as reward attenuation. Downward displacement of the frequency-rate curve is often indicative of nonspecific motoric effects.

In addition to frequency-rate curves, additional summary dependent measures were calculated and analyzed. Threshold (T0), the theoretical frequency at which the linear portion of the frequency-rate curve intersects the abscissa (i.e., zero responses), and M50, the estimated frequency that supports half-maximal responding (i.e., 50% MCR), were calculated. Linear regression analysis was used to calculate T0 and M50 frequencies, and were normalized to baseline values (percent baseline T0 and M50) and subsequently analyzed using one-way repeated measures ANOVA. Planned comparisons of each **DK-I-56-1** dose versus vehicle were

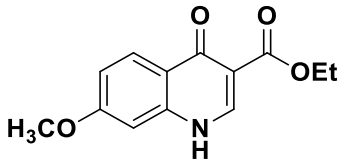
conducted using Fisher's LSD test (Figure 2). In addition, log transformations of T0 and M50 values were calculated using linear regression for each condition tested and analyzed using separate one-way repeated measures ANOVA for each condition (baseline and test). In instances where a treatment reduced responding at all frequencies below 50% MCR, T0, and M50 values were not calculated for that subject. Multiple comparisons were made using Fisher's LSD test to compare all **ATDP 34,282** doses to vehicle (Tables 1 and 2). All statistical tests were conducted using microcomputer software (Prism 9.5, GraphPad Software, Inc., San Diego, CA), and all comparisons were considered statistically significant if $p<0.05$.

2.5. Experimental

2.5.1. General

All reactions were conducted in oven-dried round-bottom flasks, utilizing magnetic stir bars or overhead mechanical stirrers, all done under an argon atmosphere. Whenever necessary, organic solvents were purified using standard methods or were procured from Sigma-Aldrich™. The chemicals used were sourced from suppliers including Sigma Aldrich™, Oakwood Chemical, Alfa Aesar, Matrix Scientific, or Acros Organic. The progression of the reactions was tracked by thin-layer chromatography (TLC) on silica gel plates (employing 25% EtOAc in hexanes or 10% MeOH in DCM as the mobile phase). The nuclear magnetic resonance (NMR) spectroscopic data for ^{1}HNMR and ^{13}CNMR were collected using Bruker Spectrospin 300 MHz and 500 MHz instruments, with chemical shifts denoted in δ (ppm). High-resolution mass spectrometry (HRMS) data were obtained using an LCMS-IT-TOF instrument by Shimadzu Scientific.

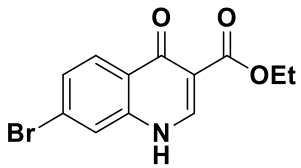
2.5.2. Ethyl 7-methoxy-4-oxo-1,4-dihydroquinoline-3-carboxylate (14)



14

A round bottom flask was charged with 3-methoxyaniline **7** (15.0 g, 122.0 mmol), diethyl ethoxymethylenemalonate (27.7 g, 128.0 mmol), and diphenyl ether (75 mL) and stirred for 5 min. The mixture was gradually heated to 230°C. The evolved ethanol (EtOH) was collected in a Dean-Stark trap. Once the formation of EtOH ceased, the reaction mixture was further heated for 30 minutes at 230°C. Afterward, the reaction mixture was cooled to 80°C and diluted with ethanol (EtOH) (200 mL). As the temperature decreased to 20-25°C, the resulting solid was collected through filtration, then washed using EtOH (50 mL x 2) and hexanes (50 mL x 2). The obtained solid was dried under vacuum conditions at 40°C, resulting in the formation of compound **14** as a light brown solid (16.5 g, 55%). **^{1}H NMR** (500 MHz, TFA-d) δ 11.66 (s, 1H), 9.13 (s, 1H), 8.47 (d, J = 9.3 Hz, 1H), 7.49 (dd, J = 9.3, 2.2 Hz, 1H), 7.38 (d, J = 2.1 Hz, 1H), 4.60 (t, J = 7.2 Hz, 2H), 4.03 (s, 3H), 1.47 (t, J = 7.2 Hz, 3H). **^{13}C NMR** (126 MHz, TFA-d) δ 171.78 (s), 167.78 (s), 167.52 (s), 144.41 (s), 142.32 (s), 126.19 (s), 121.82 (s), 113.97 (s), 103.73 (s), 99.18 (s), 64.16 (s), 55.38 (s), 11.95 (s); **HRMS (ESI)** m/z calculated for $C_{13}H_{14}NO_4$ $(M+H)^+$ 248.0917; found 248.0907.

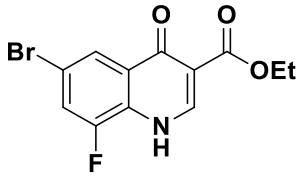
2.5.3. Ethyl 7-bromo-4-oxo-1,4-dihydroquinoline-3-carboxylate (15)



15

A mixture containing 3-bromoaniline **8** (30.0 g, 174.4 mmol), diethyl ethoxymethylenemalonate (39.6 g, 183 mmol), and diphenyl ether (150 mL) was gradually heated to 230°C. The evolved ethanol (EtOH) was collected in a Dean-Stark trap. Once the formation of EtOH ceased, the reaction mixture was further heated for 30 minutes at 230°C. Afterward, the reaction mixture was cooled to 80°C and diluted with ethanol (EtOH) (200 mL). As the temperature decreased to 20-25°C, the resulting solid was collected through filtration, then washed using EtOH (10 mL x 50) and hexanes (10 mL x 50). The obtained solid was dried under vacuum conditions at 40°C, resulting in the formation of compound **15** as a light brown solid (43.88 g, 75%). **^{1}H NMR** (500 MHz, TFA-d) δ 11.66 (s, 1H), 9.27 (dd, *J* = 8.7, 3.4 Hz, 1H), 8.47 (dt, *J* = 9.8, 4.9 Hz, 1H), 8.36 – 8.31 (m, 1H), 8.09 – 8.02 (m, 1H), 4.67 – 4.64 (m, 2H), 1.50 (q, *J* = 12.3, 7.0 Hz, 3H). **^{13}C NMR** (126 MHz, TFA-d) δ 173.37 (s), 167.19 (s), 145.64 (s), 139.59 (s), 134.02 (s), 133.76 (s), 125.55 (s), 122.58 (s), 118.40 (s), 105.01 (s), 64.62 (s), 11.94 (s). HRMS (ESI) m/z calculated for $C_{12}H_{10}BrNO_3$ (M+H)+ 295.9917; found 295.9893.

2.5.4. Ethyl 6-bromo-8-fluoro-4-oxo-1,4-dihydroquinoline-3-carboxylate (16)

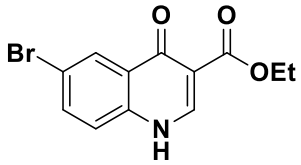


16

A round bottom flask was charged with 2-fluoro-4-bromoanniline **9** (25.0 g, 132.0 mmol), diethyl ethoxymethylenemalonate (30.3 g, 140.0 mmol), and diphenyl ether (125 mL) and stirred for 5 min. The mixture was gradually heated to 230°C. The evolved ethanol (EtOH) was collected in a Dean-Stark trap. Once the formation of EtOH ceased, the reaction mixture was further heated for 30 minutes at 230°C. Afterward, the reaction mixture was cooled to 80°C and

diluted with ethanol (EtOH) (100 mL). As the temperature decreased to 20-25°C, the resulting solid was collected through filtration, then washed using EtOH (50 mL x 2) and hexanes (50 mL x 2). The obtained solid was dried under vacuum conditions at 40°C, resulting in the formation of compound **16** as a white solid (34 g, 72%). **^{1}H NMR** (500 MHz, TFA-d) δ 11.64 (s, 1H), 9.44 – 9.42 (m, 1H), 8.66 (s, 1H), 8.12 (dd, *J* = 9.3, 1.8 Hz, 1H), 4.74 (dt, *J* = 9.5, 6.0 Hz,2H), 1.58 (dd, *J* = 8.3, 6.0 Hz, 3H).**^{13}C NMR** (126 MHz, TFA-d) δ 172.55 (d, *J* = 3.1 Hz), 167.00 (s), 151.53 (d, *J* = 261.7 Hz), 145.54 (s), 128.14 (d, *J* = 14.9 Hz), 125.50 (d, *J* = 19.1 Hz), 124.29 (d, *J* = 8.1 Hz), 123.04 (d, *J* = 4.7 Hz), 121.91 (s), 106.23 (s), 65.07 (s), 11.97 (s). **HRMS (ESI)** m/z calculated for $C_{12}H_{10}BrFNO_3$ (M+H)+ 313.9822; found 313.9823.

2.5.5. Ethyl 6-bromo-4-oxo-1,4-dihydroquinoline-3-carboxylate (17)

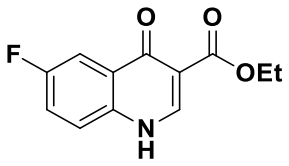


17

A mixture containing 4-bromoaniline **10** (20.0 g, 116 mmol), diethyl ethoxymethylenemalonate (26.35 g, 120 mmol), and diphenyl ether (100 mL) was gradually heated to 230°C. The evolved ethanol (EtOH) was collected in a Dean-Stark trap. Once the formation of EtOH ceased, the reaction mixture was further heated for 30 minutes at 230°C. Afterward, the reaction mixture was cooled to 80°C and diluted with ethanol (EtOH) (100 mL). As the temperature decreased to 20-25°C, the resulting solid was collected through filtration, then washed using EtOH (10 mL x 50) and hexanes (10 mL x 50). The obtained solid was dried under vacuum conditions at 40°C, resulting in the formation of compound **17** as an off-white solid (29.4 g, 85%). **^{1}H NMR** (500 MHz, D_2O) δ 6.09 (s, 1H), 5.60 (d, J = 2.0 Hz, 1H), 5.13 (s, 6H), 5.08 (dd, J = 9.0, 2.1 Hz, 1H), 4.83 (d, J = 9.0 Hz, 1H), 1.47 (q, J = 7.2 Hz, 2H), -1.69 (t, J = 7.2 Hz, 3H). **^{13}C NMR** (126 MHz,

D2O) δ 169.00 (s), 164.00 (s), 141.75 (s), 137.77 (s), 134.86 (s), 123.85 (s), 121.45 (s), 118.06 (s), 117.80 (s), 102.17 (s), 61.50 (s), 8.88 (s).

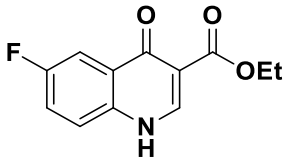
2.5.6. Ethyl 6-fluoro-4-oxo-1,4-dihydroquinoline-3-carboxylate (18)



18

A round bottom flask was charged with 4-fluoro-anniline **11** (30.0 g, 270 mmol), diethyl ethoxymethylenemalonate (61.3 g, 280.0 mmol), and diphenyl ether (150 mL) and stirred for 5 min. The mixture was gradually heated to 230°C. The evolved ethanol (EtOH) was collected in a Dean-Stark trap. Once the formation of EtOH ceased, the reaction mixture was further heated for 30 minutes at 230°C. Afterward, the reaction mixture was cooled to 80°C and diluted with ethanol (EtOH) (200 mL). As the temperature decreased to 20-25°C, the resulting solid was collected through filtration, then washed using EtOH (50 mL x 2) and hexanes (50 mL x 2). The obtained solid was dried under vacuum conditions at 40°C, resulting in the formation of compound **18** as an off-white solid (48.0 g, 68%). **^{1}H NMR** (500 MHz, D_2O) δ 6.03 (s, 1H), 5.15 (s, 5H), 5.01 (dd, *J* = 7.9, 2.7 Hz, 1H), 4.97 (dd, *J* = 9.3, 4.2 Hz, 1H), 4.72 (ddd, *J* = 9.6, 7.8, 2.7 Hz, 1H), 1.42 (q, *J* = 7.2 Hz, 2H), -1.73 (t, *J* = 7.2 Hz, 3H). **^{13}C NMR** (126 MHz, D_2O) δ 169.33 (d, *J* = 4.5 Hz), 164.03 (s), 159.09 (d, *J* = 256.7 Hz), 141.20 (s), 133.00 (s), 124.09 (d, *J* = 26.7 Hz), 119.64 (d, *J* = 9.3 Hz), 118.34 (d, *J* = 10.2 Hz), 105.89 (d, *J* = 25.3 Hz), 101.71 (s), 61.39 (s), 8.85 (s). **HRMS (ESI)** m/z calculated for $C_{12}H_{10}NO_3F$ (M+H)+ 236.0717; found 236.0710.

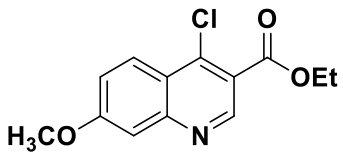
2.5.7. Ethyl 6-fluoro-4-oxo-1,4-dihydroquinoline-3-carboxylate (19)



19

A mixture containing 3-fluoroaniline **12** (15.0 g, 134 mmol), diethyl ethoxymethylenemalonate (30.0 g, 140 mmol), and diphenyl ether (75 mL) was gradually heated to 230°C. The evolved ethanol (EtOH) was collected in a Dean-Stark trap. Once the formation of EtOH ceased, the reaction mixture was further heated for 30 minutes at 230°C. Afterward, the reaction mixture was cooled to 80°C and diluted with ethanol (EtOH) (100 mL). As the temperature decreased to 20-25°C, the resulting solid was collected through filtration, then washed using EtOH (10 mL x 50) and hexanes (10 mL x 50). The obtained solid was dried under vacuum conditions at 40°C, resulting in the formation of compound **19** as an off-white crystalline solid (23.8 g, 76%). **^{1}H NMR** (500 MHz, D_2O) δ 6.08 (s, 1H), 5.51 (dd, *J* = 9.3, 5.3 Hz, 1H), 5.13 (s, 8H), 4.62 (dd, *J* = 8.3, 2.2 Hz, 1H), 4.53 – 4.49 (m, 1H), 1.46 (q, *J* = 7.2, 3.5 Hz, 2H), -1.69 (t, *J* = 7.2 Hz, 3H). **HRMS (ESI)** m/z calculated for $C_{12}H_{10}NO_3F$ (M+H)+ 236.0717; found 236.0736.

2.5.8. Ethyl 4-chloro-7-methoxyquinoline-3-carboxylate (20)



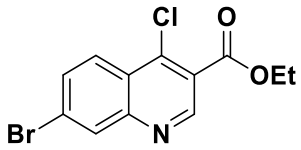
20

A round bottom flask was charged with ethyl 7-methoxy-4-oxo-1,4-dihydroquinoline-3-carboxylate **14** (8.5 g, 34.4 mmol), *N*,*N*-dimethylformamide (0.1 mL, 1.5 mmol), and DCM (70

mL) and stirred to make a solution. The mixture was gently heated to a temperature range of 35-40°C. Over a span of 30 minutes, oxalyl chloride (4.8 g, 37.8 mmol) was gradually added drop by drop to the reaction mixture. This mixture was allowed to reflux (38-40°C) for a duration of 2 h. Following this, the resulting solution turned brown and was allowed to cool to room temperature, around 20-25°C.

Upon cooling, the reaction mixture was diluted using DCM (150 mL) and the pH was adjusted to approximately 10 using pH paper. This was achieved by gradually introducing a 25% solution of aqueous K_2CO_3 (75 g) in water (300 mL). After separation of the layers, the aqueous layer was subjected to extraction using DCM (100 mL). The combined organic layers were further washed with a 25% solution of aqueous K_2CO_3 (75 g) in water (300 mL). The organic layers were then treated with magnesium sulfate (MgSO4) for drying. The solvents were removed under reduced pressure and it resulted a residue, which was then treated with hexanes (200 mL) to form a slurry. The solid material that formed was isolated through filtration and then washed with hexanes (50 mL x 2). The final solid product was dried under vacuum conditions at a temperature of 40°C, yielding compound **20** in the form of an off-white solid (6.85 g, 75%). **^{1}H NMR** (300 MHz, $CDCl_3$) δ 9.15 (s, 1H), 8.26 (d, *J* = 9.3 Hz, 1H), 7.40 (d, *J* = 2.4 Hz, 1H), 7.29 (dd, *J* = 9.3, 2.5 Hz, 1H), 4.48 (q, *J* = 7.1 Hz, 2H), 3.97 (s, 3H), 1.45 (t, *J* = 7.1 Hz, 3H); **^{13}C NMR** (75 MHz, $CDCl_3$) δ 164.56 (s), 162.62 (s), 151.69 (s), 150.89 (s), 143.40 (s), 126.71 (s), 121.44 (s), 121.21 (s), 120.66 (s), 107.60 (s), 61.81 (s), 55.78 (s), 14.25 (s). **HRMS (ESI)** m/z calculated for $C_{13}H_{13}ClNO_3$ $(M+H)^+$ 266.0578; found 266.0578.

2.5.9. Ethyl 4-chloro-7-bromoquinoline-3-carboxylate (21)

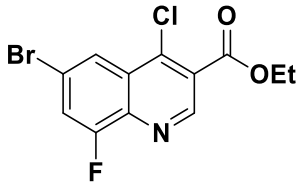


21

A round bottom flask was charged with ethyl 7-bromo-4-oxo-1,4-dihydroquinoline-3-carboxylate **15** (20 g, 67.5 mmol), *N*,*N*-dimethylformamide (0.25 mL, 6.7 mmol), and DCM (165 mL) and stirred to make a solution. The mixture was gently heated to a temperature range of 35-40°C. Over a span of 30 minutes, oxalyl chloride (9.4 g, 74.3 mmol) was gradually added drop by drop to the reaction mixture. This mixture was allowed to reflux (38-40°C) for a duration of 2 h. Following this, the resulting solution turned brown and was allowed to cool to room temperature, around 20-25°C. Upon cooling, the reaction mixture was diluted using DCM (150 mL) and the pH was adjusted to approximately 10 using pH paper. This was achieved by gradually introducing a 25% solution of aqueous K_2CO_3 (150 g) in water (600 mL). After separation of the layers, the aqueous layer was subjected to extraction using DCM (100 mL). The combined organic layers were further washed with a 25% solution of aqueous K_2CO_3 (150 g) in water (600 mL). The organic layers were then treated with magnesium sulfate (MgSO4) for drying. The solvents were removed under reduced pressure and it resulted in a residue, which was then treated with hexanes (300 mL) to form a slurry. The solid material that formed was isolated through filtration and then washed with hexanes (50 mL x 2). The final solid product was dried under vacuum conditions at a temperature of 40°C, yielding compound **21** in the form of an off-white solid (19.0 g, 90%). **^{1}H NMR** (500 MHz, $CDCl_3$) δ 9.25 – 9.08 (m, 1H), 8.32 (t, *J* = 4.9 Hz, 1H), 8.26 (dd, *J* = 13.1, 5.5 Hz, 1H), 7.82 – 7.73 (m, 1H), 4.51 (q, *J* = 7.1 Hz, 2H),

1.48 (t, *J* = 7.1 Hz, 3H). **^{13}C NMR** (126 MHz, $CDCl_3$) δ 164.16 (s), 151.26 (s), 149.92 (s), 143.63 (s), 132.12 (s), 131.93 (s), 126.82 (s), 126.70 (s), 124.99 (s), 123.17 (s), 62.24 (s), 14.25 (s). **HRMS (ESI)** m/z calculated for $C_{12}H_{10}BrClNO_2(M+H)^+$ 313.9578; found 313.9567.

2.5.10. Ethyl 6-bromo-4-chloro-8-fluoroquinoline-3-carboxylate (22)

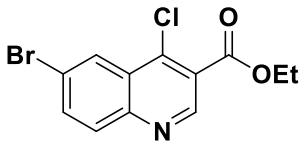


22

A mixture containing ethyl 6-bromo-8-fluoro-4-oxo-1,4-dihydroquinoline-3-carboxylate **16** (5.9 g, 18.7 mmol), *N*,*N*-dimethylformamide (0.1 mL, 1.3 mmol), and DCM (200 mL) was heated to an internal temperature of 35-40°C. Gradually, over a period of 30 minutes, oxalyl chloride (1.78 g, 2.6 mmol) was added dropwise to the reaction mixture. The reaction mixture was then heated at reflux (38-40°C) for a duration of 6 h. The resulting solution appeared as a pale yellow color and was subsequently allowed to cool to a temperature of 20-25°C. Upon cooling, the reaction mixture's pH was adjusted to approximately 10 using pH paper. This adjustment was achieved by gradually introducing a 25% solution of aqueous potassium carbonate (12.5 g) in water (50 mL). The separated layers were further treated, with the aqueous layer being subjected to extraction using DCM (100 mL). The combined organic layers were then washed with a 25% solution of aqueous potassium carbonate (12.5 g) in water (50 mL). Following this, the organic layers were dried using magnesium sulfate (MgSO4). Solvent removal under reduced pressure led to the formation of a residue, which was subsequently slurried with cold hexanes (25 mL). The solid material that resulted was isolated through filtration and washed with cold hexanes (5 mL x 2). The final solid product, compound **22**, was dried under vacuum conditions at a

temperature of 40°C to yield a pale yellow solid (1.5 g, 80% yield). **^{1}H NMR** (300 MHz, $CDCl_3$) δ 9.21 (s, 1H), 8.36 (d, J = 1.3 Hz, 1H), 7.68 (dd, J = 9.1, 1.6 Hz, 1H), 4.52 (q, J = 7.1 Hz, 2H), 1.48 (t, J = 7.1 Hz, 3H); **^{13}C NMR** (75 MHz, $CDCl_3$) δ 163.78 (s), 157.55 (d, *J* = 263.7 Hz), 150.38 (s), 142.17 (s), 138.63 (d, *J* = 12.4 Hz), 128.50 (s), 124.90 (s), 123.64 (d, *J* = 5.0 Hz), 121.59 (d, *J* = 9.4 Hz), 120.15 (d, *J* = 22.0 Hz), 62.54 (s), 14.21 (s); **HRMS (ESI)** m/z calculated for $C_{12}H_9BrClFNO_2$ $(M+H)^+$ 331.9483; found 331.9484.

2.5.11. Ethyl 6-bromo-4-chloro-1,4-dihydroquinoline-3-carboxylate (23)

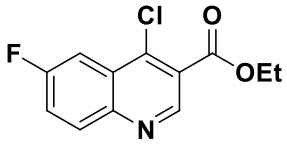


23

A round bottom flask was charged with ethyl 6-bromo-4-oxo-1,4-dihydroquinoline-3-carboxylate **17** (8.0 g, 27 mmol), *N*,*N*-dimethylformamide (0.1 mL, 1.5 mmol), and DCM (65 mL) and stirred to make a solution. The mixture was gently heated to a temperature range of 35-40°C. Over a span of 30 minutes, oxalyl chloride (2.6 mL, 29 mmol) was gradually added drop by drop to the reaction mixture. This mixture was allowed to reflux (38-40°C) for a duration of 2 h. Following this, the resulting solution turned brown and was allowed to cool to room temperature, around 20-25°C. Upon cooling, the reaction mixture was diluted using DCM (150 mL) and the pH was adjusted to approximately 10 using pH paper. This was achieved by gradually introducing a 25% solution of aqueous K_2CO_3 (50 g) in water (200 mL). After separation of the layers, the aqueous layer was subjected to extraction using DCM (100 mL). The

combined organic layers were further washed with a 25% solution of aqueous K_2CO_3 (50 g) in water (200 mL). The organic layers were then treated with magnesium sulfate (MgSO4) for drying. The solvents were removed under reduced pressure and it resulted in a residue, which was then treated with hexanes (100 mL) to form a slurry. The solid material that formed was isolated through filtration and then washed with hexanes (20 mL x 2). The final solid product was dried under vacuum conditions at a temperature of 40°C, yielding compound **21** in the form of an off-white solid (7.6 g, 90%). **^{1}H NMR** (500 MHz, $CDCl_3$) δ 9.19 (s, 1H), 8.55 (d, *J* = 2.1 Hz, 1H), 8.55 (d, *J* = 2.1 Hz, 1H), 8.00 (d, *J* = 8.9 Hz, 1H), 7.90 (dd, *J* = 8.9, 2.1 Hz, 1H), 4.52 (q, *J* = 7.1 Hz, 2H), 1.48 (t, *J* = 7.1 Hz, 3H). **^{13}C NMR** (126 MHz,$CDCl_3$) δ 164.14 (s), 150.42 (s), 148.09 (s), 142.22 (s), 135.37 (s), 131.47 (s), 127.66 (s), 127.33 (s), 123.68 (s), 122.85 (s), 62.30 (s), 14.24 (s).

2.5.12. Ethyl 6-fluoro-4-chloro-1,4-dihydroquinoline-3-carboxylate (24)

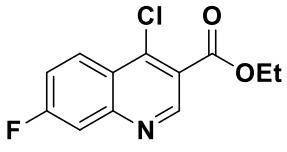


24

A round bottom flask was charged with ethyl 6-fluoro-4-oxo-1,4-dihydroquinoline-3-carboxylate **18** (8.5 g, 36 mmol), *N*,*N*-dimethylformamide (0.1 mL, 1.5 mmol), and DCM (70 mL) and stirred to make a solution. The mixture was gently heated to a temperature range of 35-40°C. Over a span of 30 minutes, oxalyl chloride (5.0 g, 39.7 mmol) was gradually added drop by drop

to the reaction mixture. This mixture was allowed to reflux (38-40°C) for a duration of 2 h. Following this, the resulting solution turned brown and was allowed to cool to room temperature, around 20-25°C. Upon cooling, the reaction mixture was diluted using DCM (150 mL) and the pH was adjusted to approximately 10 using pH paper. This was achieved by gradually introducing a 25% solution of aqueous K_2CO_3 (50 g) in water (200 mL). After separation of the layers, the aqueous layer was subjected to extraction using DCM (100 mL). The combined organic layers were further washed with a 25% solution of aqueous K_2CO_3 (50 g) in water (200 mL). The organic layers were then treated with magnesium sulfate (MgSO4) for drying. The solvents were removed under reduced pressure and it resulted in a residue, which was then treated with hexanes (100 mL) to form a slurry. The solid material that formed was isolated through filtration and then washed with hexanes (20 mL x 2). The final solid product was dried under vacuum conditions at a temperature of 40°C, yielding compound **23** in the form of an off-white solid (7.96 g, 87%). **HRMS (ESI)** m/z calculated for $C_{12}H_{10}ClFNO_2$ $(M+H)^+$ 254.0378; found 254.0372.

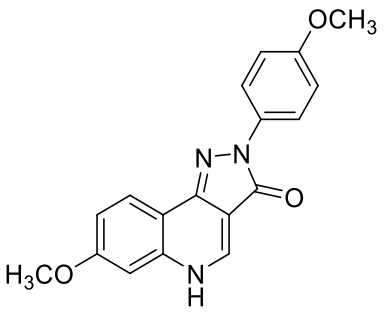
2.5.13. Ethyl 7-fluoro-4-chloro-1,4-dihydroquinoline-3-carboxylate (24)



25

A round bottom flask was charged with ethyl 7-fluoro-4-oxo-1,4-dihydroquinoline-3-carboxylate **19** (18.0 g, 76.5 mmol), *N*,*N*-dimethylformamide (0.2 mL, 3.0 mmol), and DCM (150 mL) and stirred to make a solution. The mixture was gently heated to a temperature range of 35-40°C. Over a span of 30 minutes, oxalyl chloride (10.7 g, 84.2 mmol) was gradually added drop by drop to the reaction mixture. This mixture was allowed to reflux (38-40°C) for a duration of 2 h. Following this, the resulting solution turned brown and was allowed to cool to room temperature, around 20-25°C. Upon cooling, the reaction mixture was diluted using DCM (250 mL) and the pH was adjusted to approximately 10 using pH paper. This was achieved by gradually introducing a 25% solution of aqueous K_2CO_3 (75 g) in water (300 mL). After separation of the layers, the aqueous layer was subjected to extraction using DCM (100 mL). The combined organic layers were further washed with a 25% solution of aqueous K_2CO_3 (75 g) in water (300 mL). The organic layers were then treated with magnesium sulfate (MgSO4) for drying. The solvents were removed under reduced pressure and it resulted in a residue, which was then treated with hexanes (200 mL) to form a slurry. The solid material that formed was isolated through filtration and then washed with hexanes (50 mL x 2). The final solid product was dried under vacuum conditions at a temperature of 40°C, yielding compound **23** in the form of an off-white solid (14.9 g, 79%). **^{1}H NMR** (500 MHz, DMSO-*d6*) δ 8.94 (d, J = 5.9 Hz, 1H), 8.37 (dd, J = 9.1, 6.1 Hz, 1H), 7.61 (dd, J = 9.7, 2.4 Hz, 1H), 7.50 (td, J = 8.8, 2.5 Hz, 1H), 4.22 (q, J = 7.1 Hz, 2H), 1.28 (t, J = 7.1 Hz, 3H).**HRMS (ESI)** m/z calculated for $C_{12}H_{10}ClFNO_2$ $(M+H)^+$ 255.0378; found 255.0399.

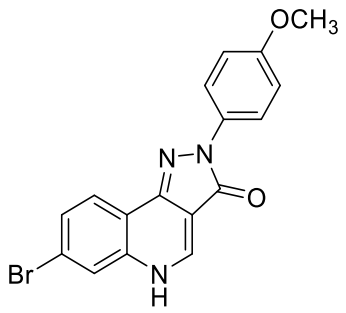
2.5.14. 7-Methoxy-2-(4-methoxyphenyl)-2,5-dihydro-3H-pyrazolo[4,3-c]quinolin-3-one (PZ-II-029, 3)



PZ-II-029 (3)

A round bottom flask was charged with a mixture of ethyl-4-chloro-7-methoxyquinoline-3-carboxylate **20** (8.0 g, 30.2 mmol), 4-methoxyphenylhydrazine hydrochloride **26** (6.31 g, 36.1 mmol), triethylamine (10.5 mL, 75.3 mmol), and xylenes (58 mL). The mixture was heated to reflux conditions (138°C) and maintained at reflux for a duration of 2 h. The yellow-orange slurry, which resulted was then cooled to a temperature of 100°C and subsequently diluted with ethanol (EtOH) (32 mL). The reaction mixture was then stirred at 80°C for 30 min. The mixture was allowed to cool down to a temperature of 20-25°C. The solid material that formed was collected by filtration and was subsequently washed with a 1:1 mixture of ethanol (2.5 mL x 2) and hexanes (2.5 mL x 2), followed by additional washing with hexanes (5 mL x 2). The solid was dried under vacuum temperature of 50°C to afford **PZ-II-029 (3)** as a yellow powder (5.6 g, 58%). **^{1}H NMR** (500 MHz, DMSO) δ 12.60 (s, 1H), 8.65 (s, 1H), 8.10 (dd, *J* = 13.6, 9.3 Hz, 3H), 7.17 (d, *J* = 6.5 Hz, 2H), 7.01 (d, *J* = 9.1 Hz, 2H), 3.88 (s, 3H), 3.79 (s, 3H). **^{13}C NMR** (126 MHz, DMSO) δ 161.45 (s), 160.84 (s), 156.21 (s), 143.11 (s), 139.33 (s), 137.41 (s), 134.10 (s), 124.05 (s), 120.69 (s), 115.78 (s), 114.25 (s), 112.67 (s), 106.87 (s), 102.26 (s), 55.99 (s), 55.68 (s). **HRMS (ESI)** m/z calculated for $C_{18}H_{16}N_3O_3$ (M+H)+ 322.1186; found 322.1178

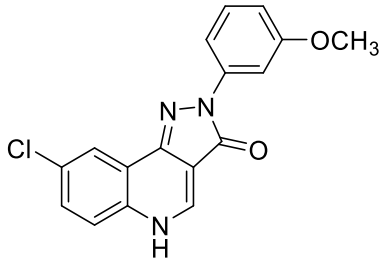
2.5.15. 7-Methoxy-2-(4-methoxyphenyl)-2,5-dihydro-3H-pyrazolo[4,3-c]quinolin-3-one (LAU 463, 6)



LAU 463 (6)

A round bottom flask was charged with a mixture of ethyl-4-chloro-7-bromoquinoline-3-carboxylate **21** (4.0 g, 12.6 mmol), 4-methoxyphenylhydrazine hydrochloride **26** (2.6 g, 15.1 mmol), triethylamine (4.2 mL, 13.6 mmol), and xylenes (75 mL). The mixture was heated to reflux conditions (138°C) and maintained at reflux for a duration of 2 h. The yellow-orange slurry, which resulted was then cooled to a temperature of 100°C and subsequently diluted with ethanol (EtOH) (32 mL). The reaction mixture was then stirred at 80°C for 30 min. The mixture was allowed to cool down to a temperature of 20-25°C. The solid material that formed was collected by filtration and was subsequently washed with a 1:1 mixture of ethanol (5.0 mL x 2) and hexanes (5.0 mL x 2), followed by additional washing with hexanes (5 mL x 2). The solid was dried under vacuum temperature of 50°C to afford **LAU463 (6)** as a yellow powder (2.9 g, 61%); **^{1}H NMR** (500 MHz, DMSO-d6) δ 12.76 (s, 1H), 8.73 (s, 1H), 8.10 (dd, J = 17.7, 8.8 Hz, 3H), 7.89 (d, J = 1.6 Hz, 1H), 7.68 (dd, J = 8.6, 1.6 Hz, 1H), 7.02 (d, J = 9.1 Hz, 2H), 3.79 (s, 3H); **^{13}C NMR** (126 MHz, DMSO-d6) δ 161.38, 156.48, 142.38, 140.08, 136.98, 133.85, 129.65, 124.51, 122.95, 122.22, 120.87, 118.22, 114.31, 107.21, 55.72; **HRMS (ESI)** m/z calculated for $C_{17}H_{13}BrN_3O_2$ $(M+H)^+$ 370.0186; found 370.0175.

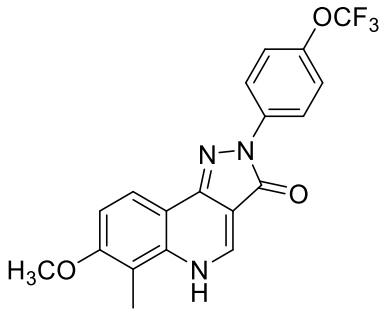
2.5.16. 8-Chloro-2-(3-methoxyphenyl)-2,5-dihydro-3H-pyrazolo[4,3-c]quinolin-3-one (LAU 159, 5)



LAU 159 (5)

A round bottom flask was charged with a mixture of ethyl-4,6-dichloro-quinoline-3-carboxylate (4.0 g, 14.8 mmol), 3-methoxyphenylhydrazine hydrochloride **28** (3.1 g, 17.8 mmol), triethylamine (5 mL, 35.6 mmol), and xylenes (100 mL). The mixture was heated to reflux conditions (138°C) and maintained at reflux for a duration of 2 h. The yellow-orange slurry, which resulted was then cooled to a temperature of 100°C and subsequently diluted with ethanol (EtOH) (50 mL). The reaction mixture was then stirred at 80°C for 30 min. The mixture was allowed to cool down to a temperature of 20-25°C. The solid material that formed was collected by filtration and was subsequently washed with a 1:1 mixture of ethanol (10.0 mL x 2) and hexanes (10.0 mL x 2), followed by additional washing with hexanes (10 mL x 2). The solid was dried under vacuum temperature of 50°C to afford **LAU 159 (5)** as a yellow powder (2.6 g, 60%); **^{1}H NMR** (500 MHz, DMSO) δ 12.92 (s, 1H), 8.75 (s, 1H), 8.20 (dd, J = 23.1, 1.8 Hz, 1H), 7.90 – 7.78 (m, 2H), 7.78 – 7.66 (m, 2H), 7.35 (t, J = 8.1 Hz, 1H), 6.76 (dt, J = 26.0, 12.7 Hz, 1H), 3.82 (s, 3H); **^{13}C NMR** (126 MHz, DMSO) δ 162.00 (s), 160.00 (s), 142.41 (s), 141.54 (s), 140.10 (s), 134.77 (s), 131.13 (s), 130.70 (s), 130.00 (s), 122.14 (s), 121.66 (s), 120.44 (s), 111.43 (s), 106.86 (s), 104.94 (s), 55.61 (s). **HRMS (ESI)** m/z calculated for $C_{17}H_{13}ClN_3O_2$ $(M+H)^+$ 326.0691; found 326.0692.

2.5.17. 7-methoxy-6-methyl-2-(4-(trifluoromethoxy)phenyl)-2,5-dihydro-3H-pyrazolo[4,3-c]quinolin-3-one (CW-02-79, 32)

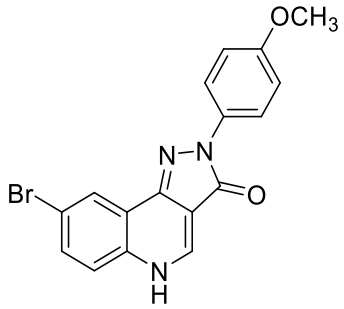


CW-02-79 (32)

A round bottom flask was charged with a mixture of ethyl-3-methoxy-2-methyl-quinoline-3-carboxylate (15.0 g, 53.5 mmol), 4-trifluoromethoxyphenylhydrazine hydrochloride **29** (14.7 g, 64 mmol), triethylamine (8.9 mL, 64.0 mmol), and xylenes (130 mL). The mixture was heated to reflux conditions (138°C) and maintained at reflux for a duration of 2 h. The yellow-orange slurry, which resulted was then cooled to a temperature of 100°C and subsequently diluted with ethanol (EtOH) (130 mL). The reaction mixture was then stirred at 80°C for 30 min. The mixture was allowed to cool down to a temperature of 20-25°C. The solid material that formed was collected by filtration and was subsequently washed with a 1:1 mixture of ethanol (20.0 mL x 2) and hexanes (20.0 mL x 2), followed by additional washing with hexanes (20 mL x 2). The solid was dried under vacuum temperature of 50°C to afford **CW-02-79 (32)** as a yellow powder (12.7 g, 61%); **^{1}H NMR** (300 MHz, DMSO-d6) δ 11.87 (s, 1H), 8.35 (dd, J = 16.0, 11.7 Hz, 3H), 8.08 (d, J = 8.7 Hz, 1H), 7.44 (d, J = 8.0 Hz, 2H), 7.29 (d, J = 8.8 Hz, 1H), 3.92 (s, 3H), 2.35 (s, 3H); **^{13}C NMR** (75 MHz, DMSO-d6) δ 162.10 (s), 158.48 (s), 144.48 (s), 144.41 (s), 139.63 (s), 139.57 (s), 135.45 (s), 121.97 (s), 121.29 (s), 120.67 (q, J = 256.8 Hz), 120.09 (s), 114.44 (s),

112.60 (s), 111.22 (s), 106.09 (s), 56.64 (s), 10.01 (s); **HRMS (ESI)** m/z calculated for $C_{19}H_{15}F_3N_3O_3$ $(M+H)^+$ 390.1066; found 390.1067.

2.5.18. 8-Bromo-2-(4-methoxyphenyl)-2,5-dihydro-3H-pyrazolo[4,3-c]quinolin-3-one (DS-I-78, 33)

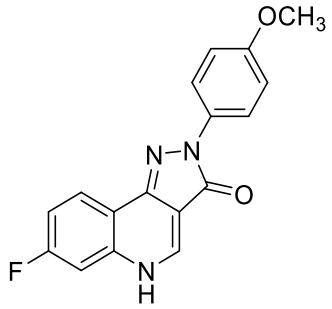


DS-I-78 (33)

A mixture of ethyl 6-bromo-4-chloro-1,4-dihydroquinoline-3-carboxylate **23** (5.5 g, 17.5 mmol), 4-methoxyphenylhydrazine hydrochloride **26** (3.66 g, 20.9 mmol), triethylamine (6.1 mL, 44.0 mmol), and xylenes (40 mL) was charged in a round bottom flask. The mixture was heated to reflux conditions (138°C) and maintained at reflux for a duration of 2 h. The yellow-orange slurry, which resulted was then cooled to a temperature of 100°C and subsequently diluted with ethanol (EtOH) (40 mL). The reaction mixture was then stirred at 80°C for 30 min. The mixture was allowed to cool down to a temperature of 20-25°C. The solid material that formed was collected by filtration and was subsequently washed with a 1:1 mixture of ethanol (10.0 mL x 2) and hexanes (10.0 mL x 2), followed by additional washing with hexanes (10 mL x 2). The solid was dried under vacuum temperature of 50°C to afford **DS-I-78 (33)** as a yellow powder (3.56 g, 55%). **^{1}H NMR** (500 MHz, DMSO-d6) δ 8.70 (s, 1H), 8.27 (d, *J* = 2.2 Hz, 1H), 8.08 – 8.06 (m, 2H), 7.79 (dd, *J* = 8.8, 2.2 Hz, 1H), 7.63 (d, *J* = 8.8 Hz, 1H), 7.03 – 6.99 (m, 2H), 3.79 (s, 3H).

^{13}C NMR (126 MHz, DMSO-d6) δ 161.37 (s), 156.49 (s), 141.79 (s), 139.81 (s), 134.84 (s), 133.81 (s), 133.13 (s), 124.56 (s), 122.17 (s), 120.93 (s), 120.79 (s), 119.21 (s), 114.27 (s), 106.99 (s), 55.70 (s). **HRMS (ESI)** m/z calculated for $C_{17}H_{12}N_3O_2Br$ $(M+H)^+$ 370.0185; found 370.0216.

2.5.19. 7-fluoro-2-(4-methoxyphenyl)-2,5-dihydro-3H-pyrazolo[4,3-c]quinolin-3-one (DS-I-84, 34)

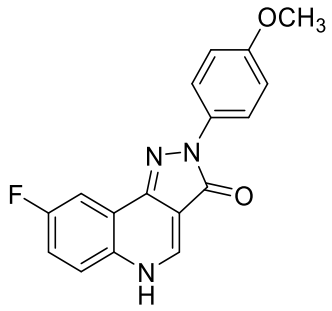


DS-I-84 (34)

A mixture of ethyl 7-fluoro-4-chloro-1,4-dihydroquinoline-3-carboxylate **25** (6.0 g, 23.6 mmol), 4-methoxyphenylhydrazine hydrochloride **26** (4.95 g, 28.4 mmol), triethylamine (8.2 mL, 59.1 mmol), and xylenes (45 mL) was charged in a round bottom flask. The mixture was heated to reflux conditions (138°C) and maintained at reflux for a duration of 2 h. The yellow-orange slurry, which resulted was then cooled to a temperature of 100°C and subsequently diluted with ethanol (EtOH) (45 mL). The reaction mixture was then stirred at 80°C for 30 min. The mixture was allowed to cool down to a temperature of 20-25°C. The solid material that formed was collected by filtration and was subsequently washed with a 1:1 mixture of ethanol (15.0 mL x 2) and hexanes (15.0 mL x 2), followed by additional washing with hexanes (15 mL x 2). The solid was dried under vacuum temperature of 50°C to afford **DS-I-84 (34)** as a yellow powder (4.9 g,

67%). **^{1}H NMR** (500 MHz, DMSO-d6) δ 12.78 (s, 1H), 8.69 (d, *J* = 11.7 Hz, 1H), 8.22 (dd, *J* = 8.6, 6.1 Hz, 1H), 8.05 (d, *J* = 8.9 Hz, 2H), 7.46 (d, *J* = 8.4 Hz, 1H), 7.40 (t, *J* = 8.6 Hz, 1H), 7.01 (d, *J* = 9.0 Hz, 2H), 3.78 (s, 3H). **^{13}C NMR** (126 MHz, DMSO-d6) δ 162.74 (d, *J* = 246.8 Hz), 161.34 (s), 156.39 (s), 142.52 (s), 139.98 (s), 137.13 (d, *J* = 11.7 Hz), 133.84 (s), 125.10 (d, *J* = 9.9 Hz), 120.86 (s), 115.93 (s), 115.14 (d, *J* = 23.3 Hz), 114.26 (s), 107.17 (s), 105.77 (d, *J* = 25.4 Hz), 55.68 (s). **HRMS (ESI)** m/z calculated for $C_{17}H_{12}N_3O_2F$ $(M+H)^+$ 310.0986; found 310.1009.

2.5.20. 8-Fluoro-2-(4-methoxyphenyl)-2,5-dihydro-3H-pyrazolo[4,3-c]quinolin-3-one (DS-I-83, 35)

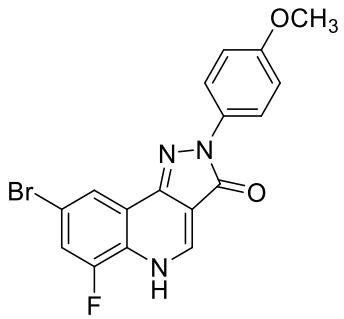


DS-I-83 (35)

A mixture of ethyl 6-fluoro-4-chloro-1,4-dihydroquinoline-3-carboxylate **24** (4.0 g, 17 mmol), 4-methoxyphenylhydrazine hydrochloride **26** (3.3 g, 21.2 mmol), triethylamine (6.2 mL, 39.4 mmol), and xylenes (30 mL) was charged in a round bottom flask. The mixture was heated to reflux conditions (138°C) and maintained at reflux for a duration of 2 h. The yellow-orange slurry, which resulted was then cooled to a temperature of 100°C and subsequently diluted with ethanol (EtOH) (30 mL). The reaction mixture was then stirred at 80°C for 30 min. The mixture was allowed to cool down to a temperature of 20-25°C. The solid material that formed was collected by filtration and was subsequently washed with a 1:1 mixture of ethanol (10.0 mL x 2)

and hexanes (10.0 mL x 2), followed by additional washing with hexanes (10 mL x 2). The solid was dried under vacuum temperature of 50°C to afford **DS-I-83 (35)** as a yellow powder (3.0 g, 63%). **^{1}H NMR** (500 MHz, DMSO-d6) δ 12.89 (s, 1H), 8.74 (s, 1H), 8.11 – 8.07 (m, 2H), 7.89 (dd, *J* = 8.9, 2.8 Hz, 1H), 7.78 (dd, *J* = 9.1, 4.8 Hz, 1H), 7.56 (td, *J* = 8.8, 2.9 Hz, 1H), 7.04 – 7.00 (m, 2H), 3.79 (s, 3H). **^{13}C NMR** (126 MHz, DMSO-d6) δ 161.44 (s), 160.17 (d, *J* = 245.1 Hz), 156.46 (s), 142.60 (d, *J* = 3.1 Hz), 139.53 (s), 133.91 (s), 132.62 (s), 122.63 (d, *J* = 9.1 Hz), 120.93 (s), 120.72 (d, *J* = 9.1 Hz), 118.74 (d, *J* = 24.8 Hz), 114.29 (s), 107.50 (d, *J* = 23.3 Hz), 105.99 (s), 55.71 (s). **HRMS (ESI)** m/z calculated for $C_{17}H_{12}N_3O_2F$ $(M+H)^+$ 310.0986; found 310.1009

2.5.21. 8-Bromo-6-fluoro-2-(4-methoxyphenyl)-2,5-dihydro-3H-pyrazolo[4,3-c]quinolin-3-one (MM-I-03, 36)

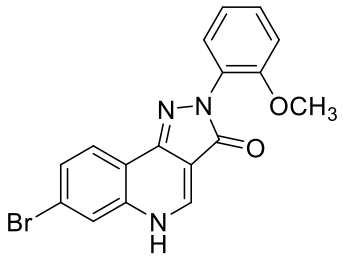


MM-I-03 (36)

A mixture of ethyl 6-bromo-4-chloro-8-fluoroquinoline-3-carboxylate **22** (7.0 g, 21 mmol), 4-methoxyphenylhydrazine hydrochloride **26** (4.4 g, 25 mmol), triethylamine (3.5 mL, 25 mmol), and xylenes (60 mL) was charged in a round bottom flask. The mixture was heated to reflux conditions (138°C) and maintained at reflux for a duration of 2 h. The yellow-orange slurry, which resulted was then cooled to a temperature of 100°C and subsequently diluted with ethanol (EtOH) (30 mL). The reaction mixture was then stirred at 80°C for 30 min. The mixture was

allowed to cool down to a temperature of 20-25°C. The solid material that formed was collected by filtration and was subsequently washed with a 1:1 mixture of ethanol (10.0 mL x 2) and hexanes (10.0 mL x 2), followed by additional washing with hexanes (10 mL x 2). The solid was dried under vacuum temperature of 50°C to afford **MM-I-03 (36)** as a yellow powder (1.9 g, 22%). **^{1}H NMR** (500 MHz, DMSO-d6) δ 13.43 (s, 1H), 8.93 (d, *J* = 2.3 Hz, 1H), 8.51 (d, *J* = 15.3 Hz, 1H), 8.49 (d, *J* = 9.1 Hz, 2H), 8.33 (dd, *J* = 10.2, 1.6 Hz, 1H), 7.45 (d, *J* = 9.1 Hz, 2H), 4.23 (s, 3H); **^{13}C NMR** (126 MHz, DMSO-d6) δ 161.12 (s), 156.67 (s), 152.72 (d, *J* = 254.3 Hz), 140.93 (s), 139.49 (s), 133.57 (s), 124.28 (d, *J* = 13.7 Hz), 122.02 (s), 121.00 (s), 120.62 (d, *J* = 2.4 Hz), 118.96 (d, *J*= 20.5 Hz), 118.28 (d, *J* = 9.0 Hz), 114.32 (s), 107.83 (s), 55.74 (s); **HRMS (ESI)** m/z calculated for $C_{17}H_{12}BrFN_3O_2$ $(M+H)^+$ 388.0097; found 388.0094

2.5.22. 7-Bromo-2-(2-methoxyphenyl)-2,5-dihydro-3H-pyrazolo[4,3-c]quinolin-3-one (DS-II-04, 37)

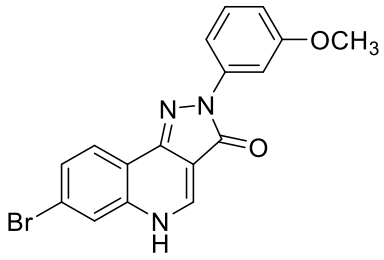


DS-II-04 (37)

A mixture of ethyl 7-bromo-4-chloro-1,4-dihydroquinoline -3-carboxylate **21** (7.0 g, 19.1 mmol), 2-methoxyphenylhydrazine hydrochloride **30** (4.0 g, 22.8 mmol), triethylamine (6.6 mL, 47 mmol), and xylenes (45 mL) was charged in a round bottom flask. The mixture was heated to reflux conditions (138°C) and maintained at reflux for a duration of 2 h. The yellow-orange slurry, which resulted was then cooled to a temperature of 100°C and subsequently diluted with ethanol (EtOH) (15 mL). The reaction mixture was then stirred at 80°C for 30 min. The mixture

was allowed to cool down to a temperature of 20-25°C. The solid material that formed was collected by filtration and was subsequently washed with a 1:1 mixture of ethanol (10.0 mL x 2) and hexanes (10.0 mL x 2), followed by additional washing with hexanes (10 mL x 2). The solid was dried under vacuum temperature of 50°C to afford **DS-II-04 (37)** as a yellow powder (4.2 g, 60%). **^{1}H NMR** (500 MHz, DMSO-d6) δ 12.60 (s, 1H), 8.67 (s, 1H), 8.01 (d, *J* = 8.5 Hz, 1H), 7.86 (d, *J* = 1.9 Hz, 1H), 7.65 (dd, *J* = 8.5, 1.9 Hz, 1H), 7.42 (ddd, *J* = 8.3, 7.6, 1.7 Hz, 1H), 7.32 (dd, *J* = 7.7, 1.7 Hz, 1H), 7.18 (dd, *J* = 8.4, 1.0 Hz, 1H), 7.05 (td, *J* = 7.6, 1.2 Hz, 1H), 3.75 (s, 3H). **^{13}C NMR** (126 MHz, DMSO) δ 162.13 (s), 155.63 (s), 142.22 (s), 139.80 (s), 136.89 (s), 129.90 (s), 129.84 (s), 129.44 (s), 128.23 (s), 124.36 (s), 122.64 (s), 122.03 (s), 120.71 (s), 118.50 (s), 113.00 (s), 106.17(s),56.11(s). **HRMS (ESI)** m/z calculated for $C_{17}H_{12}N_3O_2Br$ $(M+H)^+$ 370.0185; found 370.0178.

2.5.23. 7-Bromo-2-(3-methoxyphenyl)-2,5-dihydro-3H-pyrazolo[4,3-c]quinolin-3-onene (DS-II-05, 38)

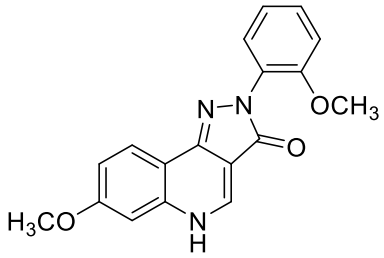


DS-II-05 (38)

A mixture of ethyl 7-bromo-4-chloro-1,4-dihydroquinoline -3-carboxylate **21** (6.0 g, 19.1 mmol), 3-methoxyphenylhydrazine hydrochloride **28** (4.0 g, 22.8 mmol), triethylamine (6.6 mL, 47 mmol), and xylenes (45 mL) was charged in a round bottom flask. The mixture was heated to reflux conditions (138°C) and maintained at reflux for a duration of 2 h. The yellow-orange slurry, which resulted was then cooled to a temperature of 100°C and subsequently diluted with

ethanol (EtOH) (15 mL). The reaction mixture was then stirred at 80°C for 30 min. The mixture was allowed to cool down to a temperature of 20-25°C. The solid material that formed was collected by filtration and was subsequently washed with a 1:1 mixture of ethanol (10.0 mL x 2) and hexanes (10.0 mL x 2), followed by additional washing with hexanes (10 mL x 2). The solid was dried under vacuum temperature of 50°C to afford **DS-II-05 (38)** as a yellow powder (4.17 g, 58%). **^{1}H NMR** (500 MHz, DMSO-d6) δ 12.79 (s, 1H), 8.76 (s, 1H), 8.16 (d, *J* = 8.5 Hz, 1H), 7.89 (d, *J* = 1.8 Hz, 1H), 7.85 (t, *J* = 2.2 Hz, 1H), 7.82 (dd, *J* = 4.9, 4.3 Hz, 1H), 7.71 (dd, *J* = 8.5, 1.9 Hz, 1H), 7.35 (t, *J* = 8.2 Hz, 1H), 6.79 – 6.76 (m, 1H), 3.81 (s, 3H). **^{13}C NMR** (126 MHz, DMSO-d6) δ 162.00 (s), 159.99 (s), 142.82 (s), 141.51 (s), 140.37 (s), 137.13 (s), 130.03 (s), 129.75 (s), 124.65 (s), 123.21 (s), 122.28 (s), 118.16 (s), 111.40 (s), 109.98 (s), 107.19 (s), 104.91 (s), 55.60 (s). **HRMS (ESI)** m/z calculated for $C_{17}H_{12}N_3O_2Br$ $(M+H)^+$ 370.0185; found 370.0214.

2.5.24. 7-Methoxy-2-(2-methoxyphenyl)-2,5-dihydro-3H-pyrazolo[4,3-c]quinolin-3-one (DS-II-08, 39)

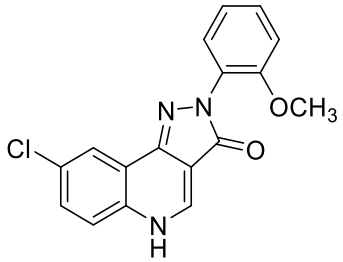


DS-II-08 (39)

A mixture of ethyl 7-methoxy-4-chloro-1,4-dihydroquinoline -3-carboxylate **20** (4.0 g, 15.0 mmol), 2-methoxyphenylhydrazine hydrochloride **30** (3.15 g, 18.1 mmol), triethylamine (5.2 mL, 37.6 mmol), and xylenes (40 mL) was charged in a round bottom flask. The mixture was heated to reflux conditions (138°C) and maintained at reflux for a duration of 2 h. The yellow-

orange slurry, which resulted was then cooled to a temperature of 100°C and subsequently diluted with ethanol (EtOH) (15 mL). The reaction mixture was then stirred at 80°C for 30 min. The mixture was allowed to cool down to a temperature of 20-25°C. The solid material that formed was collected by filtration and was subsequently washed with a 1:1 mixture of ethanol (10.0 mL x 2) and hexanes (10.0 mL x 2), followed by additional washing with hexanes (10 mL x 2). The solid was dried under vacuum temperature of 50°C to afford **DS-II-08 (39)** as a yellow powder (2.5 g, 52%). **^{1}H NMR** (500 MHz, DMSO-d6) δ 12.45 (s, 1H), 8.57 (d, *J* = 6.1 Hz, 1H), 7.99 (d, *J* = 8.7 Hz, 1H), 7.40 (td, *J* = 8.4, 1.7 Hz, 1H), 7.31 (dd, *J* = 7.6, 1.6 Hz, 1H), 7.17 (d, *J* = 8.5 Hz, 2H), 7.13 (dd, *J* = 8.8, 2.5 Hz, 1H), 7.04 (td, *J* = 7.5, 1.0 Hz, 1H), 3.88 (s, 3H), 3.75 (s, 3H). **^{13}C NMR** (126 MHz, DMSO-d6) δ 162.17 (s), 160.61 (s), 155.65 (s), 142.94 (s), 139.04 (s), 137.25 (s), 129.87 (s), 129.66 (s), 128.52 (s), 123.88 (s), 120.67 (s), 115.49 (s), 112.97 (s), 112.93 (s), 105.83 (s), 102.14 (s), 56.08 (s), 55.95 (s). **HRMS (ESI)** m/z calculated for $C_{18}H_{15}N_3O_3$ $(M+H)^+$ 322.1186; found 322.1213.

2.5.25. 8-Chloro-2-(2-methoxyphenyl)-2,5-dihydro-3H-pyrazolo[4,3-c]quinolin-3-one (DS-I-97, 41)

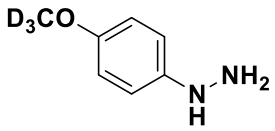


DS-I-97 (41)

A round bottom flask was charged with a mixture of ethyl-4,6-dichloro-quinoline-3-carboxylate (6.0 g, 22.2 mmol), 2-methoxyphenylhydrazine hydrochloride **30** (4.65 g, 26.7 mmol), triethylamine (7.7 mL, 55.5 mmol), and xylenes (100 mL). The mixture was heated to reflux

conditions (138°C) and maintained at reflux for a duration of 2 h. The yellow-orange slurry, which resulted was then cooled to a temperature of 100°C and subsequently diluted with ethanol (EtOH) (50 mL). The reaction mixture was then stirred at 80°C for 30 min. The mixture was allowed to cool down to a temperature of 20-25°C. The solid material that formed was collected by filtration and was subsequently washed with a 1:1 mixture of ethanol (20.0 mL x 2) and hexanes (20.0 mL x 2), followed by additional washing with hexanes (20 mL x 2). The solid was dried under vacuum temperature of 50°C to afford **DS-I-97 (41)** as a yellow powder (4.26 g, 59%). **^{1}H NMR** (500 MHz, DMSO) δ 12.75 (s, 1H), 8.67 (d, *J* = 5.8 Hz, 1H), 8.03 (d, *J* = 2.2 Hz, 1H), 7.69 (dt, *J* = 8.9, 5.5 Hz, 2H), 7.45 – 7.40 (m, 1H), 7.32 (dd, *J* = 7.5, 1.4 Hz, 1H), 7.20 – 7.17 (m, 1H), 7.05 (td, *J* = 7.6, 1.0 Hz, 1H), 3.75 (s, 3H). **^{13}C NMR** (126 MHz, DMSO) δ 162.13 (s), 155.63 (s), 141.86 (s), 139.61 (s), 134.49 (s), 130.82 (s), 130.24 (s), 129.91 (s), 129.84 (s), 128.23 (s), 121.91 (s), 121.39 (s), 120.76 (s), 120.71 (s), 113.01 (s), 105.80 (s), 56.12 (s). **HRMS (ESI)** m/z calculated for $C_{17}H_{13}ClN_3O_2$ $(M+H)^+$ 326.0691; found 326.0691.

2.5.26. 4-Methoxy-*d*$_3$-phenylhydrazine (43)

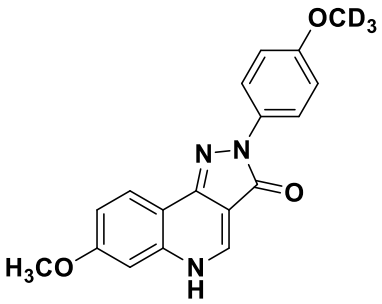


43

A mixture containing *N*-(4-methoxy-*d*$_3$-phenyl)acetamide **42** (20 g, 118.0 mmol), concentrated hydrochloric acid (40 mL), and water (40 mL) was heated to 90°C and maintained at that temperature for a period of 2 h, allowing for the hydrolysis of the amide functional group. Subsequently, the reaction mixture was cooled to a temperature range of 0 to 5°C, and a solution of sodium nitrite (8.54 g, 124 mmol) in water (20 mL) was gradually introduced drop-wise to the reaction mixture. After the complete addition of the sodium nitrite solution, the reaction mixture

was stirred for an additional 15 minutes at 0 to 5°C. Following this, the reaction mixture was cooled down further to a temperature range of -25 to -20°C. Then, a solution composed of tin (II) chloride (48 g, 262 mmol) and concentrated hydrochloric acid (100 mL) was introduced drop-wise into the reaction mixture over a 30-min period. After the complete addition of this solution, the reaction mixture was stirred for a further 4 h within the temperature range of -25 to -20°C. The reaction mixture was then diluted with diethyl ether (300 mL), and the resulting solid material was isolated through filtration and subsequently washed with diethyl ether (100 mL x 3). The obtained tin adduct of the product was dissolved in a mixture of sodium hydroxide (60 g), water (250 mL), and DCM (250 mL). The resulting mixture was stirred for 2 hours at a temperature range of 0 to 5°C, ensuring complete dissolution of the solids. After separation of the layers, the aqueous layer was subjected to extraction with dichloromethane (100 mL x 3). The combined organic layers were then treated with drying agent magnesium sulfate (MgSO4). The solvents were subsequently removed under reduced pressure, resulting in a residue that was slurried with hexanes (50 mL). The solid material was then collected by filtration, washed with hexanes (50 mL x 2), and dried under vacuum at room temperature, leading to the isolation of compound **43** as an orange-colored crystalline solid (11.1 g, 65%). **^{1}H NMR** (300 MHz, MeOD) δ 6.91 – 6.85 (m, 2H), 6.85 – 6.78 (m, 2H), 4.88 (s, 3H); **^{13}C NMR** (75 MHz, DMSO-d6) δ 152.05, 147.27, 114.60, 113.38; HRMS (ESI) m/z calculated for $C_7H_8D_3N_2O$ (M+H)+ 142.1054; found 142.1063.

2.5.27. 7-Methoxy-2-(4-methoxy-d3-phenyl)-2,5-dihydro-3H-pyrazolo[4,3-c]quinoline-3-one (DK-I-56-1, 44)



DK-I-56-1 (44)

A mixture containing ethyl-4-chloro-7-methoxyquinoline-3-carboxylate **21** (10 g, 37.6 mmol), 4-methoxy-d3-phenylhydrazine **43** (8.0 g, 45.1 mmol), triethylamine (6.3 mL, 45.1 mmol), and xylenes (80 mL) was subjected to heating at reflux temperature (138°C) and maintained at that temperature for a duration of 2 h. The resulting yellow-orange slurry was subsequently cooled to 100°C and then diluted with ethanol (EtOH) (80 mL). The reaction mixture was heated again at reflux temperature (80°C) for an additional 30 min and then allowed to cool down to a range of 20-25°C. Following this, the solids that remained were collected through filtration and subjected to washing using a mixture of ethanol (50 mL x 2) and hexanes (50 mL x 2), followed by additional washing with hexanes (50 mL x 2). The solid material was then dried under vacuum conditions at a temperature of 50°C, resulting in the isolation of compound **DK-I-56-1 (44)** as a yellow powder (7.6 g, 65%). **^{1}H NMR** (500 MHz, DMSO) δ 12.59 (s, 1H), 8.63 (s, 1H), 8.09 (dd, *J* = 16.4, 9.3 Hz, 3H), 7.16 (dd, *J* = 6.1, 2.4 Hz, 2H), 7.00 (d, *J* = 9.1 Hz, 2H), 3.86 (s, 3H). **^{13}C NMR** (126 MHz, DMSO) δ 161.47 (s), 160.86 (s), 156.27 (s), 143.14 (s), 139.33 (s), 137.37 (s), 134.01 (s), 124.07 (s), 120.82 (s), 115.83 (s), 114.24 (s), 112.65 (s), 106.83 (s), 102.22 (s), 55.97 (s). **HRMS (ESI)** m/z calculated for $C_{18}H_{13}D_3N_3O_3$ $(M+H)^+$ 325.1374; found 325.1373.

Chapter 3. The Development of a Scalable Synthesis, and Assessment of Bioactivity of Imidazodiazepines Targeting α2/3-GABAAR Subtypes for the Treatment of Epilepsy, Anxiety, and Neuropathic Pain

3.1 Introduction

Gamma-aminobutyric acid type A receptors (GABAARs) are pentameric ligand-gated ionotropic channels located in the central nervous system (CNS) and play a crucial role as the major inhibitory neurotransmitter receptors.[117] These receptors are involved in a wide range of brain functions, and their activity is influenced by various ligands that selectively target GABAA receptors.[118] Classical benzodiazepines (BZDs) are well-known positive allosteric modulators of GABAARs, binding specifically to the α+γ- interface of the receptor.[22,119-121] While these BZDs are commonly used to treat CNS disorders such as anxiety, convulsions, and insomnia, they are accompanied by unwanted side effects including sedation, ataxia, amnesia, and addiction.[120,122-125] These adverse reactions pose challenges for their long-term usage as prescribed medications. Despite these drawbacks, classical BZDs continue to be employed for the treatment of various CNS disorders due to the lack of alternative options that offer both subtype selectivity and efficacy. For instance, selective serotonin reuptake inhibitors (SSRIs) are associated with sexual dysfunction, while barbiturates carry a risk of easy overdose and fatalities.[22,119,125] The absence of suitable alternatives further contributes to the continued utilization of classical BZDs in managing CNS disorders.

The development of novel subtype-selective ligands targeting α2β2/3γ2 and α3β2/3γ2 subtypes of GABAARs is significant, as evidenced by multiple publications in various journals.[119,125] These newly designed ligands aim to achieve improved agonistic efficacy while demonstrating anxiolytic, antinociceptive, and anticonvulsant activity. Crucially, they are expected to exhibit limited or no efficacy at α1-subtypes, provided that the desired pharmacological profile is achieved.[119,122,126-133] By selectively targeting α2 or α3 subunits, these ligands hold promise for the treatment of anxiety disorders, epilepsy, and non-sedative neuropathic pain without the unwanted side effects of sedation, ataxia, amnesia, or dependence.

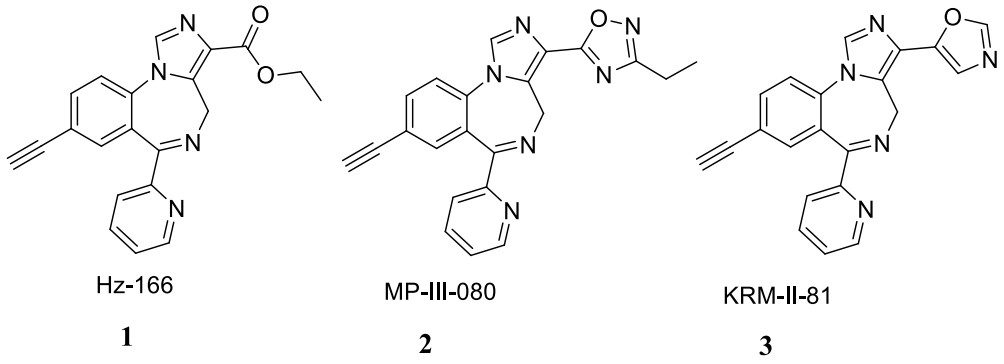


Figure 1: Structures of Hz-166 (1), MP-III-080 (2), and KRM-II-81 (3)

The lead compound in this study, 5-(8-ethynyl-6-(pyridin-2-yl)-4H-benzo[f]imidazo[1,5-a][1,4]diazepin-3-yl)oxazole, also referred to as KRM-II-81 (**Figure 1**), belongs to a novel series of orally-bioavailable imidazodiazepines derived from the initial lead compound, HZ-166. HZ-166, an imidazodiazepine ester, possessed an acetylene group at the C(8) position and demonstrated reduced efficacy and/or binding affinity at the α1-subtype.[22,104] To enhance its pharmacokinetic properties, the ester functionality of HZ-166 was bioisosterically replaced, leading to the development of a new compound named MP-III-080. This compound exhibited

significantly improved pharmacokinetic properties when tested in human, mouse, rat, and dog liver microsomes, surpassing those of the parent compound HZ-166. KRM-II-81, along with its structural analog MP-III-080, functions as positive allosteric modulators (PAM) specifically targeting α2/3-containing GABAA receptors (**Figure 2**). These compounds have exhibited analgesic effects in various pain models involving rodents, including acid-induced pain behaviors and inflammatory. [76,133-135] Additionally, KRM-II-81 has shown efficacy in treating pharmacoresistant epilepsies, traumatic brain injury, and neuropathic pain. Notably, it produces anxiolytic and anti-nociceptive, and anticonvulsant effects in rodent models. Remarkably, this imidazodiazepine exhibits low sedation potential, lacks tolerance development, and possesses the ability to prevent seizure sensitization, making it stand out due to its unique pharmacological characteristics. It is important to remember benzodiazepines are effective against status epilepticus in the ER , but develop tolerance in 2 or 3 days rendering them useless against epileptic seizures.

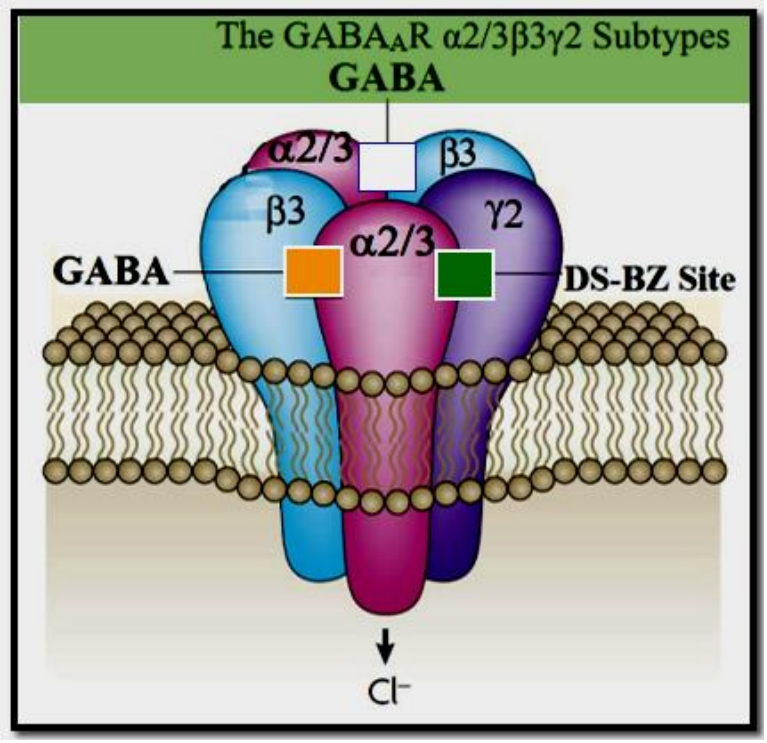


Figure 2. The GABAAR α2/3β3γ2 subtypes represent a class of pentameric chloride channels that are regulated by specific ligands. Importantly, certain compounds known as IBDZs (such as HZ-166, MP-III-080, and KRM-II-81) act as positive allosteric modulators (PAMs) at the DS-Bz site, which is located at the interface of the α2/3 and γ2 subunits. These modulators play a role in mediating the effects of GABAAR α2/3β3γ2 subtypes. The accompanying image has been adapted from Jacob et al., Nature Reviews Neuroscience, 2008.[136]

The α2/3-potentiating GABAkines (imidazodiazepines) possess a notable characteristic of inducing relatively low or sedation and ataxia compared to classical GABAkines like diazepam. In a comparative analysis between diazepam and KRM-II-81, researchers focused on examining their 'therapeutic index' and discovered that KRM-II-81 exhibited a greater separation or protective index than diazepam across various assessments.[137] Notably, KRM-II-81 demonstrated antinociceptive effects at doses lower than those required to induce decreases in rates of food-maintained behavior or muscle relaxation, as evaluated through a horizontal wire test in rodent pain models.[138] In terms of receptor selectivity, KRM-II-81 exhibits a specific activation of GABAA receptors that contain the α2 and α3 subunits as mentioned above. On the other hand, diazepam interacts non-selectively with GABAA receptors that contain the α1, α2, α3, and α5 subunits, as depicted in **Figure 3**.[139] This distinction highlights the differential binding and efficacy of KRM-II-81 and diazepam on various subtypes of GABAA receptors.

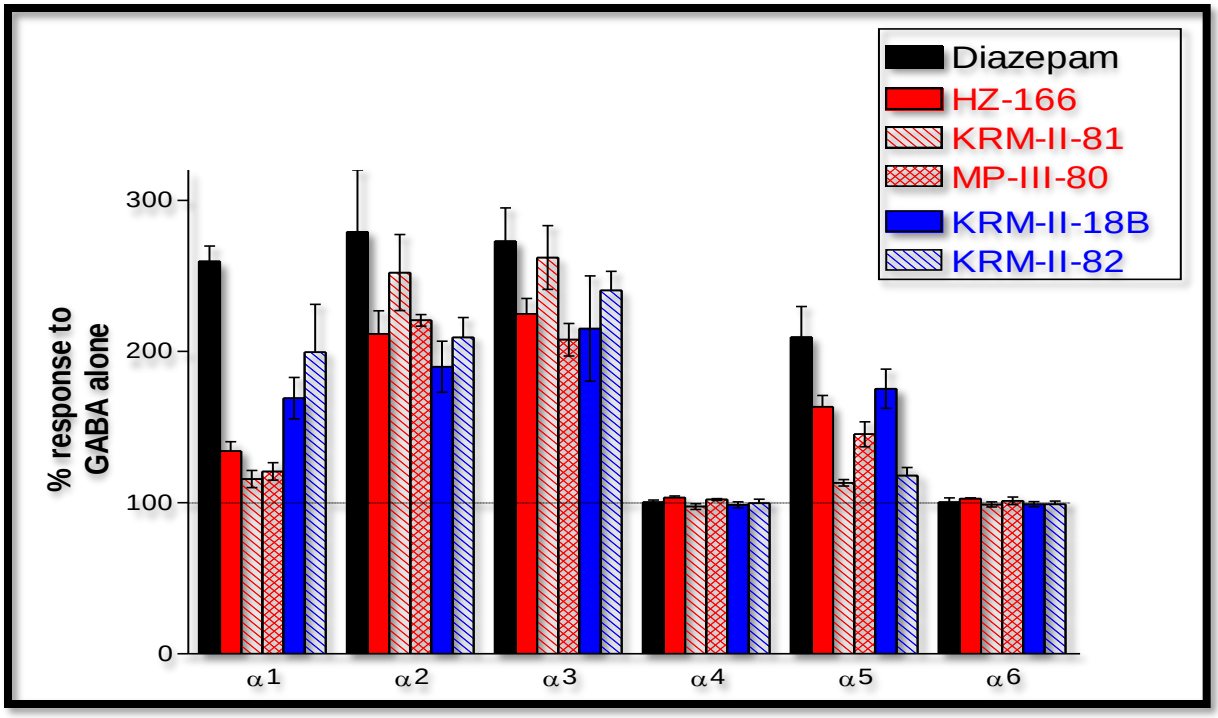


Figure 3: The average enhancement of the current evoked by GABA EC3. Diazepam and KRM-II-81 are compounds that enhance the current response to GABA EC3 in GABAA receptors. Diazepam interacts with a broader range of receptor subtypes, including α1, α2, α3, α4, α5, and α6, while KRM-II-81 selectively activates α2 and α3-containing GABAA receptors. At a concentration of 0.1 µM, both compounds enhance the current response in GABAA receptors containing α1, α2, α3, and α5 subunits. At a concentration of 1 µM, diazepam enhances the response in α4 and α6-containing receptors, while KRM-II-81 affects α4 and α6-containing receptors as well. These findings highlight the differential selectivity and potency of diazepam and KRM-II-81 on various GABAA receptor subtypes. 100% base line just GABA-no activity of KRM-II-81 or diazepam itself.

Docking studies conducted on the GABA(A) α1 receptor provided insights into the distinctive features contributing to the reduced sedative profile of KRM-II-81 compared to alprazolam. By overlaying the docking conformation of alprazolam bound to the CryoER structure (6HUO) and the best pose of KRM-II-81, it was observed that both compounds exhibited similar bound conformations for the pendant ring. However, the interactions between the diazepine ring and triazole/imidazole rings differed between the two compounds in their interactions with the protein.[28] These findings, outlined by Witkin et al. in 2020 [28], shed light on the structural basis underlying the distinct pharmacological properties of KRM-II-81 and alprazolam at the GABA(A) α1 receptor. During the docking studies, a halogen bond was observed between the chlorine atoms present at the C-8 position of alprazolam and the carbonyl oxygen of the α1His102 amino acid backbone. This interaction was not observed with KRM-II-81, as its docking conformation lacked a chlorine atom at the C-8 position, instead featuring an ethinyl moiety.

The docking scores for alprazolam and KRM-II-81 were -10.8 kcal/mol and -9.4 kcal/mol, respectively. This indicates that alprazolam had a tighter binding to the α1β3γ2L GABAA receptor compared to KRM-II-81, as depicted in **Figure 4 and Figure 5**. The differential interactions and binding affinities illustrates structural distinctions that contribute to the varied pharmacological properties of alprazolam and KRM-II-81 at the GABA(A) α1 receptor.

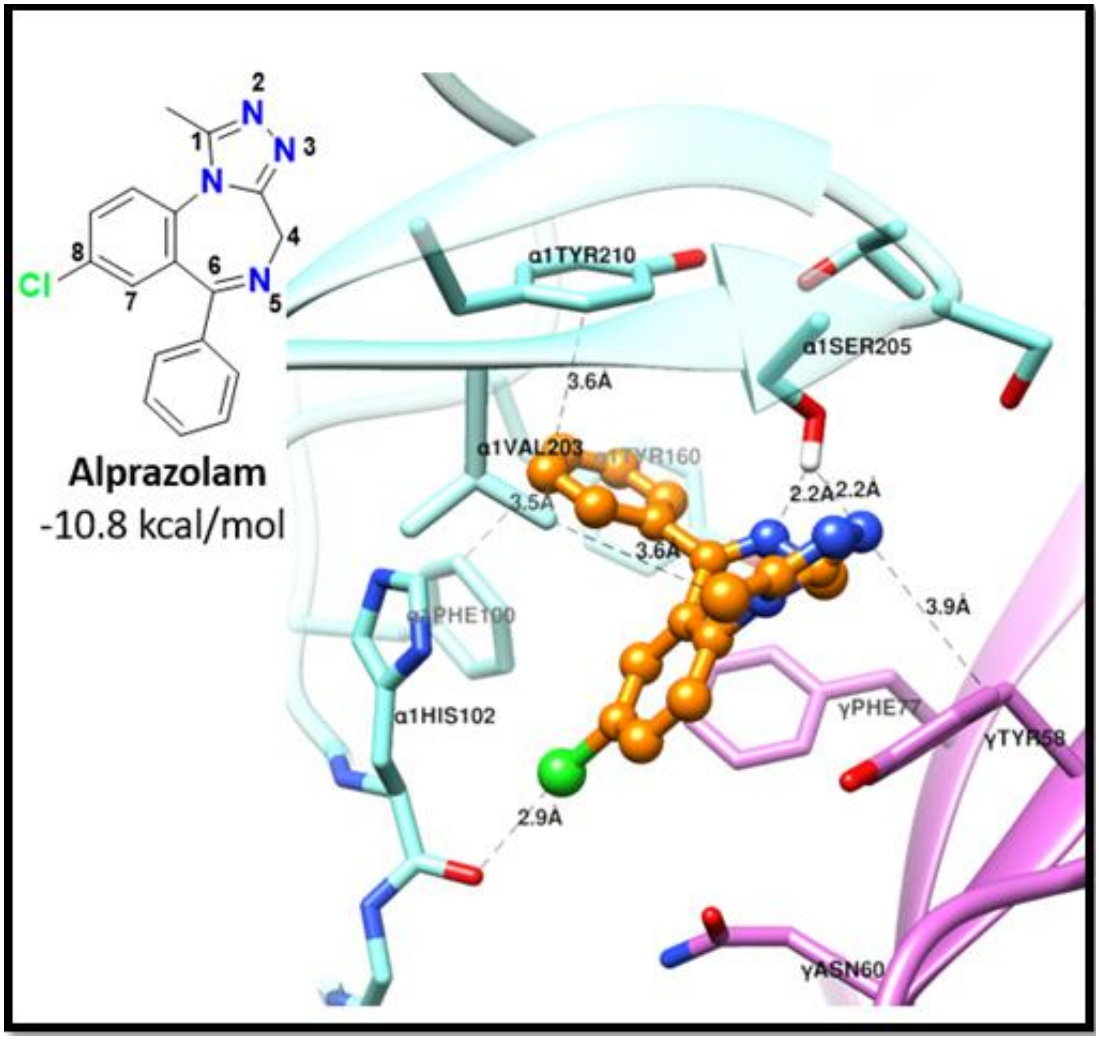


Figure 4. Alprazolam vs KRM-II-81 at the $\alpha^{+}\gamma^{-}$ interface of the $GABA_A$ receptor. Alprazolam (orange) in the complex with the α1β3γ2L $GABA_A$ receptor 6HUO. Dashed lines indicate π-π, hydrogen bond and halogen bond interactions. Data are modified from (Witkin et al., 2020, Golani, Mian et al 2021)[75,140]

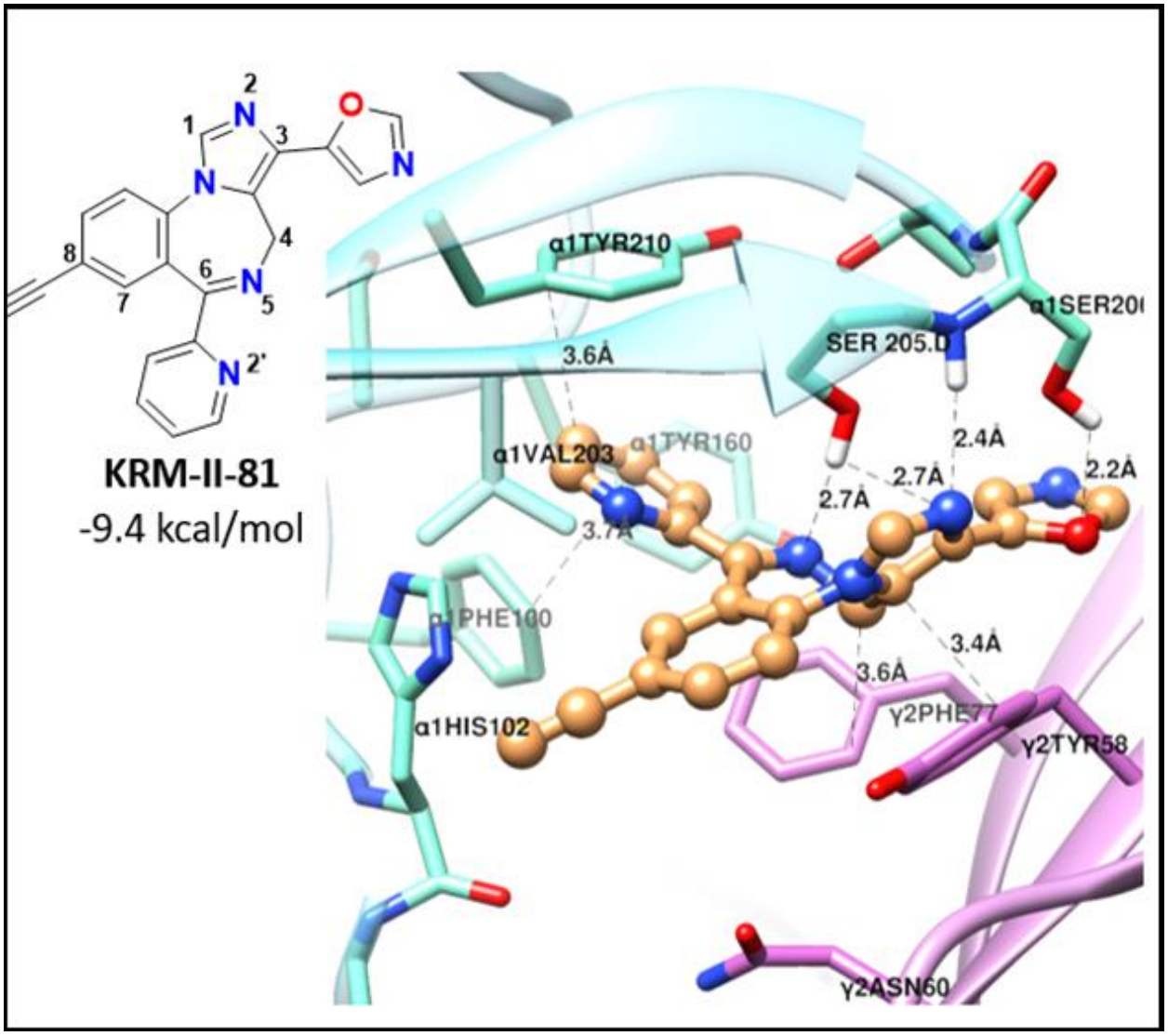


Figure 5. Alprazolam vs KRM-II-81 at the $\alpha^{+}\gamma^{-}$ interface of the $GABA_A$ receptor. KRM-II-81 docked (sandy brown) in the complex with the α1β3γ2L $GABA_A$ receptor 6HUO. α1 (aquamarine); γ2 (orchid) subunit. Dashed lines indicate π-π, hydrogen bond and halogen bond interactions. Data are modified from Witkin et al., 2020, Golani, Mian et al 2021[75,140]

KRM-II-81 has demonstrated efficacy in reducing pain behaviors across various acute and chronic pain models in rodents. In acid-induced writhing models [138], intracranial self-stimulation behaviors [141], and nest-building tests [138], KRM-II-81 showed a reduction in pain-related behaviors. Furthermore, KRM-II-81 was effective in alleviating neonatal inflammatory bladder

pain. In contrast, diazepam failed to attenuate nociceptive behaviors in formalin-treated rats even at doses up to 10 mg/kg orally. KRM-II-81 also exhibited notable activity in models of mechanical hyperalgesia induced by L5/6 nerve ligation (Witkin et al., 2019)[76] and against both mechanical and thermal hyperalgesia. Additionally, in mouse models of neuropathic pain induced by paclitaxel chemotherapy, the structurally similar analog of KRM-II-81, MP-III-080, showed equal efficacy in reducing pain as the active KRM-II-81 [134]. These findings highlight the analgesic potential of KRM-II-81 in various pain-related conditions.

Furthermore, an intriguing aspect observed in these studies was the development of tolerance with Gabapentin, whereas KRM-II-81 and its analog MP-III-080 did not exhibit such tolerance (Witkin et al., 2018a) [137]. This distinction highlights the potential advantage of KRM-II-81 in terms of sustained efficacy over time. Extensive preclinical data have underscored the therapeutic potential of KRM-II-81 in neurological pharmacology, particularly in the context of epilepsy. In vitro investigations demonstrated that KRM-II-81 effectively suppressed hyper-excitation in a network of rat cortical neurons without affecting spontaneous neuronal activity, suggesting a specific modulation of excessive neuronal firing (Witkin et al., 2018a). [137] This finding supports the notion that KRM-II-81 possesses a targeted mechanism of action, inhibiting aberrant neuronal excitability while maintaining normal neuronal function. This was carried out in two pediatric patients who had the epileptic tissue removed with their consent.

Regarding its anxiolytic effects, KRM-II-81 and its structural analog MP-III-080 exhibited favorable outcomes in rodent models. Notably, marble-burying assays conducted in mice indicated the anxiolytic potential of KRM-II-81 and MP-III-080 (Poe et al., 2016; Knutson et al., 2020) [119, 142]. Additionally, in a robust Vogel conflict test performed in rats, both compounds demonstrated anxiolytic properties (Poe et al., 2016; Witkin et al., 2017) [119,129]. Moreover, KRM-

II-81 exhibited a significant reduction in marble burying activity, comparable to the well-established clinical anti-anxiety drug chlordiazepoxide (Librium).

Furthermore, the antidepressant-like effects of KRM-II-81 and MP-III-080 were explored in mice (Witkin et al., 2018b).[137] Notably, KRM-II-81 displayed antidepressant-like properties in the forced-swim test, an experimental paradigm used to assess antidepressant activity. However, it did not elicit similar effects in the tail-suspension test. In contrast, diazepam did not exhibit any activity in the forced-swim test, possibly due to its sedative properties. The collective findings from these studies highlight the promising pharmacological profile of KRM-II-81, which encompasses anti-seizure effects, anxiolytic properties, and potential antidepressant-like activity. Its ability to suppress hyper-excitation in neuronal networks, sustained efficacy without tolerance development, and distinct pharmacological effects compared to diazepam further support its potential as a valuable target in neurological pharmacology (Witkin et al., 2018a) [137]. **Table 1** summarizes the effects of KRM-II-81 and related analogs on different models of pain versus controls.

Table 1: Effect of KRM-II-81 and it's analogs in different pain models

Compound	Models	Species	Activity	Comparator	References
KRM-II-81	Acetic acid induced writhing	Mice	Yes	Morphine	Lewter et al. (2017)
KRM-II-81	Lactic acid induced writhing	Mice	Yes	Morphine	Lewter et al. (2017)
KRM-II-81	Nesting	Mice	Yes	Morphine	Lewter et al. (2017)

KRM-II-81	Intracranial self-stimulation behaviors	Rats	Yes	Ketorolac and diazepam	Moerke et al (2019)
KRM-II-81	Tactile hyperalgesia (formalin induced)	Rats	Yes	Tramadol and diazepam	Witkin, et al. (2019)
KRM-II-81	Tactile hyperalgesia (L5/6 nerve ligation induced)	Rats	Yes	Gabapentin	Witkin, et al. (2019)
KRM-II-81	Thermal hyperalgesia (chemotherapy induced)	Mice	Yes	Gabapentin	Biggerstaff et al. (2020)
KRM-II-81	Tactile hyperalgesia (chemotherapy induced)	Mice	Yes	Gabapentin	Biggerstaff et al. (2020)
KRM-II-81B	Acetic acid induced writhing	Mice	Yes	Morphine	Lewter et al. (2017)
KRM-II-81B	Lactic acid induced writhing	Mice	Yes	Morphine	Lewter et al. (2017)
KRM-II-81B	Nesting	Mice	Yes	Morphine	Lewter et al. (2017)

MP-III-024	Mechanical hyperalgesia	Mice	Yes		Fischer et al. (2017)
MP-III-080	Thermal hyperalgesia (chemotherapy induced)	Mice	Yes	Gabapentin	Biggerstaff et al. (2020)
MP-III-080	Tactile hyperalgesia (chemotherapy induced)	Mice	Yes	Gabapentin	Biggerstaff et al. (2020)

Moreover, the studies clearly demonstrated that Gabapentin developed tolerance, while both KRM-II-81 and MP-III-080 did not exhibit such tolerance (reference not provided). This suggests that KRM-II-81 and MP-III-080 may have advantages in terms of long-term effectiveness. A substantial amount of preclinical data is available, highlighting the potential therapeutic activity of KRM-II-81 in neurological pharmacology, particularly in epilepsy (**Table 2**).

Table 2 : Effects of KRM-II-81 and it's analogs in different models of epilepsy

Compound	Models	Species	Activity	Efficacy	References
KRM-II-81	Dissociated cortical neurons	Rat	Yes, suppression of hyper-excitation of cortical neurons		Witkin et al., 2018a
KRM-II-81	Clonic seizure-Convulsant, cocaine (COC)	Rat	Yes, Blockade of convulsion	KRM-II-81 efficacious, DZP not	Knutson et al., 2020

KRM-II-81	Clonic seizure- (4-aminopyridine or 4-AP)	Rat	Yes, Blockade of convulsion	KRM-II-81 efficacious, DZP not	Knutson et al., 2020
KRM-II-81	Clonic seizure- Strychnine	Rat	Yes, Blockade of convulsion	KRM-II-81 efficacious, DZP not	Knutson et al., 2020
KRM-II-81	Pentylenetetrazol – clonic seizures	Rat	Yes, Blockade of convulsion	KRM-II-81= Diazepam	Knutson et al., 2020; Witkin et al., 2018
KRM-II-81	Electrical seizure provocation models 6Hz stimulation – 44mA	Mouse	Yes		Knutson et al., 2020; Witkin et al., 2018
KRM-II-81	Electroconvulsive Shock (Electrical seizure provocation model)	Mouse	Yes		Knutson et al., 2020; Witkin et al., 2018
KRM-II-81	Corneal kindling- (Seizure sensitization)	Mouse	Yes	KRM-II-81> Topiramate	Knutson et al., 2020; Witkin et al., 2018
KRM-II-81	Amygdala kindling- ADT (Seizure sensitization)	Rat	Yes	KRM-II-81> Diazepam	Knutson et al., 2020; Witkin et al., 2018

KRM-II-81	Amygdala kindling-ADD (Seizure sensitization)	Rat	Yes	KRM-II-81= Diazepam	Knutson et al., 2020; Witkin et al., 2018
KRM-II-81	Amygdala kindling-Seizure Severity (Seizure sensitization)	Rat	Yes	KRM-II-81= Diazepam	Knutson et al., 2020; Witkin et al., 2018
KRM-II-81	Mesial temporal lobe epilepsy (Pharmacoresistant epilepsy model)	Mouse	Yes	KRM-II-81> Lamotrigine, Valproate	Witkin et al., 2020
KRM-II-81	Lamotrigine − insensitive kindling (Pharmacoresistant epilepsy model)	Rat	Yes	KRM-II-81> Lamotrigine, Topiramate	Witkin et al., 2020
KRM-II-81	Kainate-induced chronic epilepsy (Pharmacoresistant epilepsy model)	Rat	Yes	KRM-II-81> Lamotrigine, Levetiracetam	Witkin et al., 2020
KRM-II-81	Picrotoxin stimulation (Human epileptic tissue)	Human	Yes		Witkin et al., 2018

ADT – After-discharge threshold, ADD- After-discharge duration

The ligand is in column 1, the model is in column, the organism is in column 3, in column 4the word 'yes' means active, the comparative activity of the ligand is in column 5

Salt selection of a drug is a critical aspect during the preformulation stage of drug development .[143-144] Creating a salt form of an ionizable molecule offers a solution to address non-optimal physicochemical and/or biopharmaceutical properties associated with such molecules.[145] Early selection of an optimal salt form in the drug development process can significantly improve the compound's developability, and this is facilitated by a well-defined salt screening strategy. This strategy involves assessing various factors such as crystallinity, hygroscopicity, solubility, stability, purity, polymorphism/hydrate formation, and powder flowability, in addition to practical considerations like cost and reaction yield.[146-147] It is widely recognized that creating a salt form of a compound can enhance its physicochemical and biopharmaceutical properties.[148] Furthermore, the improvement of compound bioavailability has been demonstrated through the use of salt formation.[149] These findings highlight the importance of salt selection in optimizing drug properties and improving the overall performance of a compound during the drug development process.

A hydrochloride salt at the 2'-N position of the pyridine ring of KRM-II-81 was designed and synthesized to explore the potential benefits of salt formation, such as improved solubility, enhanced absorption and distribution, and more efficient bulk synthesis methods.[150] The hydrochloride salt (KRM-II-81.HCl) was obtained by treating the free base of KRM-II-81 with anhydrous hydrochloric acid, resulting in the precipitation of the salt, which was then filtered off. The formation of the monohydrochloride salt was confirmed through various analyses, including X-ray crystallography, ^{1}H NMR, and ^{13}C NMR.

The physical characterization and solubility of KRM-II-81.HCl salt were determined. The salts are 13 times more soluble in water than their free base. Additionally, a comparative pharmacokinetics study was conducted, comparing KRM-II-81.HCl with the free base of KRM-

II-81 after oral dosing in an anticonvulsant activity study. The in vivo efficacy of both compounds as anticonvulsants against pentylenetetrazole-induced seizures was also investigated, and their activities were found to be similar. Oral administration of KRM-II-81.HCl showed a comparable brain-to-plasma ratio to the free base of KRM-II-81, with high concentrations of both compounds observed in plasma and brain, reaching approximately 1 μM in plasma and 0.5 μM in the brain at the maximum concentration (Cmax).

Moreover, oral dosing of KRM-II-81.HCl in mice significantly increased the latency to both clonic and tonic convulsions and reduced pentylenetetrazole-induced lethality. The anticonvulsant effects for clonic seizures lasted for at least 8 hours. Notably, the anticonvulsant activity of KRM-II-81 and its hydrochloride salt were very similar, demonstrating comparable efficacy in the studied anticonvulsant models. As the hydrochloride salt of KR-II-81 showed improved physical and chemical properties hydrochloride salts of MP-III-024, MP-III-080, and Hz-166 were prepared.

A significant requirement for testing ADME toxicity of KRM-II-81 is the availability of a large quantity of the compound. To address this need, an improved synthetic route was developed by Knutson et al. in 2020.

The precursor molecule, HZ-166, was previously synthesized by Li et al. in 2018. Knutson et al. modified and improved the synthetic method in several steps, resulting in a more efficient process. One of the notable advancements in the newly developed method is the elimination of chromatographic purification steps, which were replaced with recrystallization purification in the five synthetic steps involved in preparing HZ-166. This modification streamlines the purification

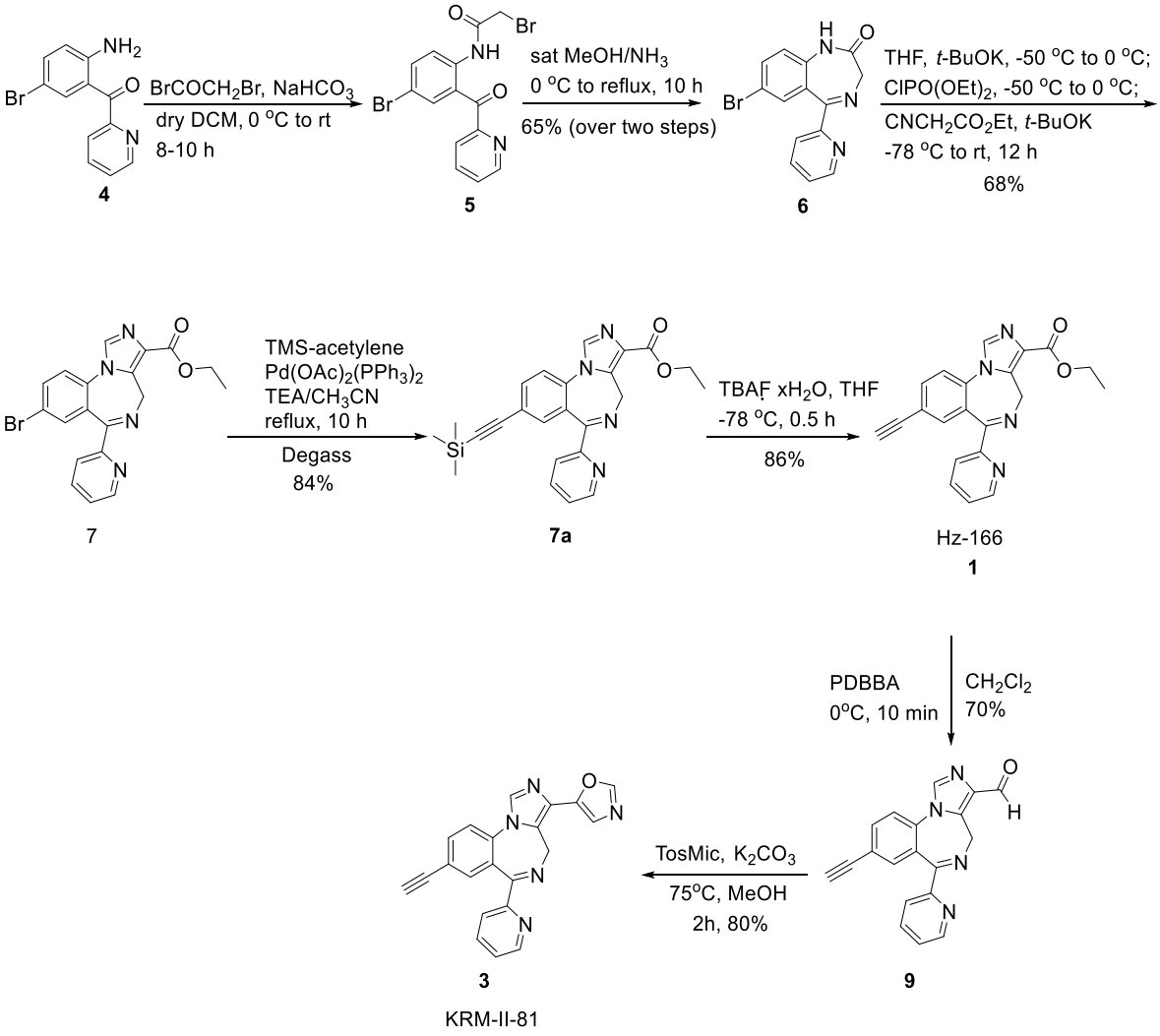
process and simplifies the overall synthesis. Additionally, the modified method exhibits reduced formation of side products, shorter process times, and improved overall yield. These features contribute to the practicality and efficiency of the newly developed synthetic route. Knutson, Mian, and Sharmin executed the method described here, enabling the production of large quantities of both HZ-166 and KRM-II-81. This advancement in synthetic methodology facilitates the availability of sufficient quantities of the compounds, making them more accessible for ADME toxicity testing and other research purposes.

3.2. Chemistry

3.2.1. Synthesis of KRM-II-81

In light of the aforementioned therapeutic potentials of KRM-II-81 [119,137,142,129], a more scalable synthesis approach has been developed. Initially, the synthesis of KRM-II-81 followed the procedure published by Li et al. in 2018 (**Scheme 1**).[151]

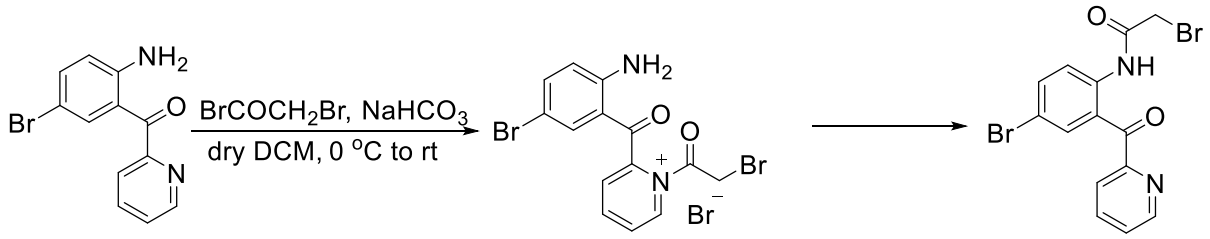
Scheme 1. Synthesis of KRM-II-81 by Li et al. 2018 [151]



However, to enhance efficiency and yield, the method underwent significant improvements. These improvements included a reduction in reaction time, mitigation of side products, implementation of crystallization-purification techniques, and overall enhancement of the yield achieved during synthesis.

In the synthesis of KRM-II-81, the commercially available amine, 2-amino-5-bromo-benzyl-2'-pyridyl ketone, was subjected to a reaction with bromoacetyl bromide in the presence of sodium bicarbonate in anhydrous dichloromethane. To facilitate the reaction, the reaction mixture was cooled to 0°C before the addition of bromoacetyl bromide. However, during the addition of bromoacetyl bromide at this low temperature, a red-thick solid was formed, making it challenging to stir the reaction mixture effectively. Upon further investigation and analysis of a potential reaction mechanism (**Scheme 2**), it was proposed that the formation of a 2'-pyridinum salt of the bromoacetamide was responsible for the formation of the red, thick mass observed in the reaction mixture.

Scheme 2 : Possible Route to Bromoacetamide via the Pyridium Salt



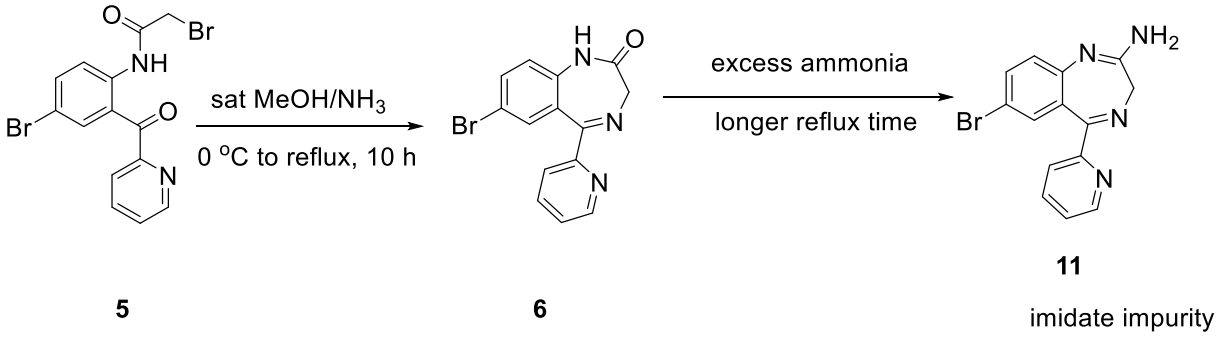
4 **10** **5**

In the updated procedure developed by Knutson et al. in 2020 (**Scheme 4**), the issue of agitation was effectively resolved. Instead of using bromoacetyl bromide, which posed challenges during stirring, they opted for chloroacetyl chloride, a more cost-effective reagent. The addition of chloroacetyl chloride was carried out at a slightly higher temperature, specifically at 25-30°C,

over a period of 60 minutes. Remarkably, the reaction was determined to be complete based on TLC analysis immediately after the addition of chloroacetyl chloride. The elevated temperature significantly accelerated the reaction rate. In the previous synthesis reported by Li et al. in 2019 [151], the acetamide product (**5**) was directly used for the subsequent step without undergoing any purification. However, in the improved procedure by Knutson et al. in 2020[142], the halo-acetamide underwent purification through ethanol recrystallization, resulting in a pure product. Interestingly, the substitution of chloroacetyl chloride for bromoacetyl bromide did not have any detrimental effects on the reaction, and the yield achieved was an impressive 99%.

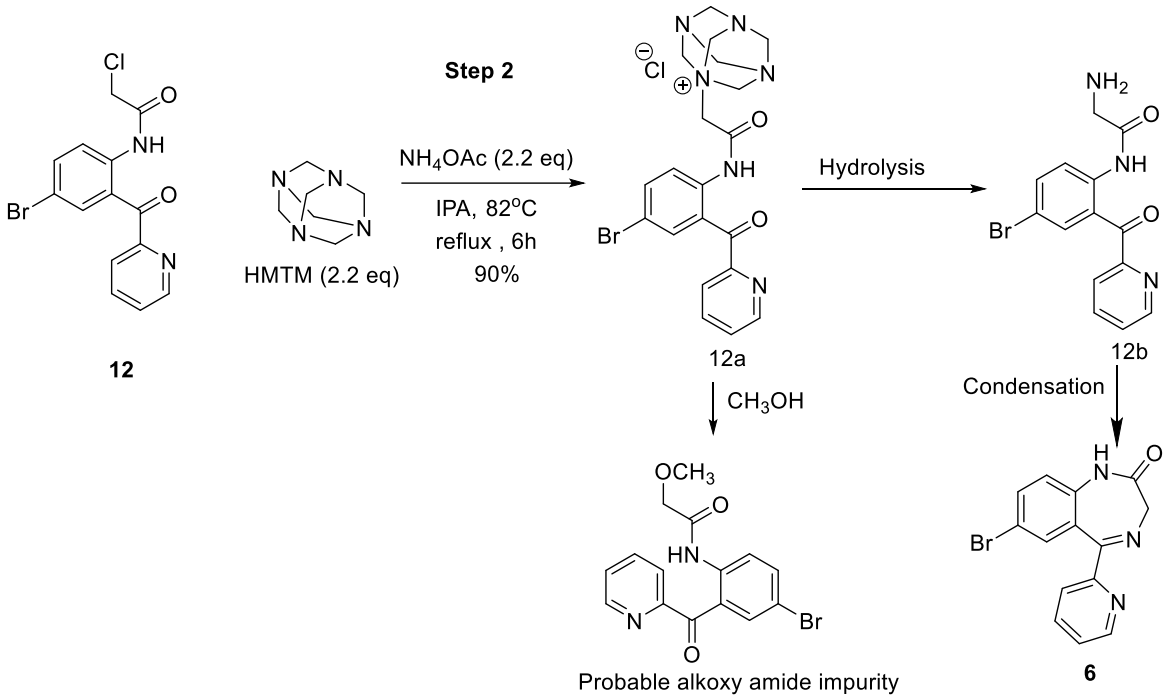
In the second step of the reaction, the benzodiazepine, specifically 7-bromo-5-(pyridin-2-yl)-1,3-dihydro-2H-benzo[e][1,4]diazepin-2-one (**6**), is formed. This transformation involves treating 2-bromo-N-(4-bromo-2-picolinoylphenyl) acetamide (**5**) with a saturated ammonia/methanol mixture, as described in the work of Li et al. in 2019[151]. However, it should be noted that the saturated ammonia/methanol system used in larger-scale quantities was found to result in the formation of an impurity known as β-amino imidate intermediate (**11**). This imidate impurity was subsequently isolated and characterized by Knutson et al. in 2020.[142]

Scheme 3 : Formation Pathway of Imidate Impurity during Synthesis



Following the observations made by Knutson, Mian, and Sharmin, they proceeded to utilize a hexamethylenetetramine (HMTM)-based cyclization, commonly known as the Delepine reaction. The HMTM-based cyclization, as depicted in **Scheme 4**, involved several steps. Firstly, the alkyl halide **12** underwent nucleophilic aliphatic substitution, resulting in the formation of the quaternary ammonium salt **12a**. This intermediate was then subjected to in situ hydrolysis, leading to the formation of the β-amino amide intermediate **12b**. Subsequently, **12b** was condensed with the carbonyl group, ultimately yielding the desired 2'-pyridyl-benzodiazepine **6**.

Scheme 4 : Formation of Benzodiazepine by Delepine Reaction [152-154]



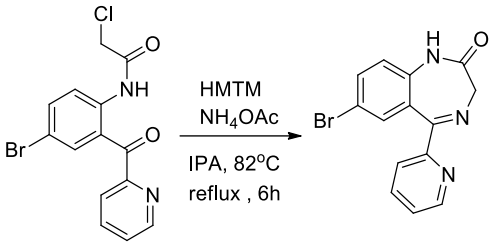
Although this new approach showed satisfactory performance, the yields obtained were slightly lower (around 60-65%) compared to those reported in the literature.[154] Upon further investigation, it was discovered that a minor impurity, identified as β-alkoxy amide , was present in the reaction mixture at a level of 5-10%. This impurity was believed to arise from the possible SN^2 addition of a primary alcohol (such as methanol or ethanol) used as a solvent, displacing the

tetramine. To address the issue of the undesired side reaction resulting in the formation of β-alkoxy amide impurity, a modification was introduced in the reaction by replacing the primary alcohol solvent (methanol or ethanol) with a secondary alcohol, specifically 2-propanol (IPA). This modification proved effective in eliminating the side reaction and suppressing the formation of the impurity. The substitution of methanol with IPA as the solvent in the reaction brought about a significant improvement in the yield. The yield of the reaction increased from the previous range of 60-65% to a higher range of 70-75%. This solvent switch proved to be a valuable modification, resulting in a notable enhancement in the overall efficiency of the synthesis process.

In recent developments (by Sharmin), there has been a specific focus on optimizing the isolation process to further increase the yield. Recognizing the importance of maximizing the yield of the desired product, our group has directed their efforts towards refining the techniques employed during the isolation step. By implementing advanced purification methods, and carefully controlling the parameters involved in the isolation process, it has become possible to achieve even higher yields than before. This increased attention to the isolation process has proven instrumental in maximizing the overall yield of the synthesis.

In the previously developed method by Knutson et al. in 2020[142], the isolation of the benzodiazepine product was achieved through a specific procedure. After the completion of the reaction, the reaction mixture was cooled to -5 °C using IPA as the cooling agent. Subsequently, the solids were filtered and washed with IPA and water. The obtained filtrate wash was kept separate from the initial filtrate. Notably, the analysis of the filtrate using HNMR revealed a substantial amount of the desired product present. To further utilize this unisolated product, the filtrate was concentrated to approximately 1/6th of its original volume. The resulting

concentrated mixture was then heated to 80 °C, and an equal volume of water (compared to the concentrated filtrate) was added dropwise at that temperature.

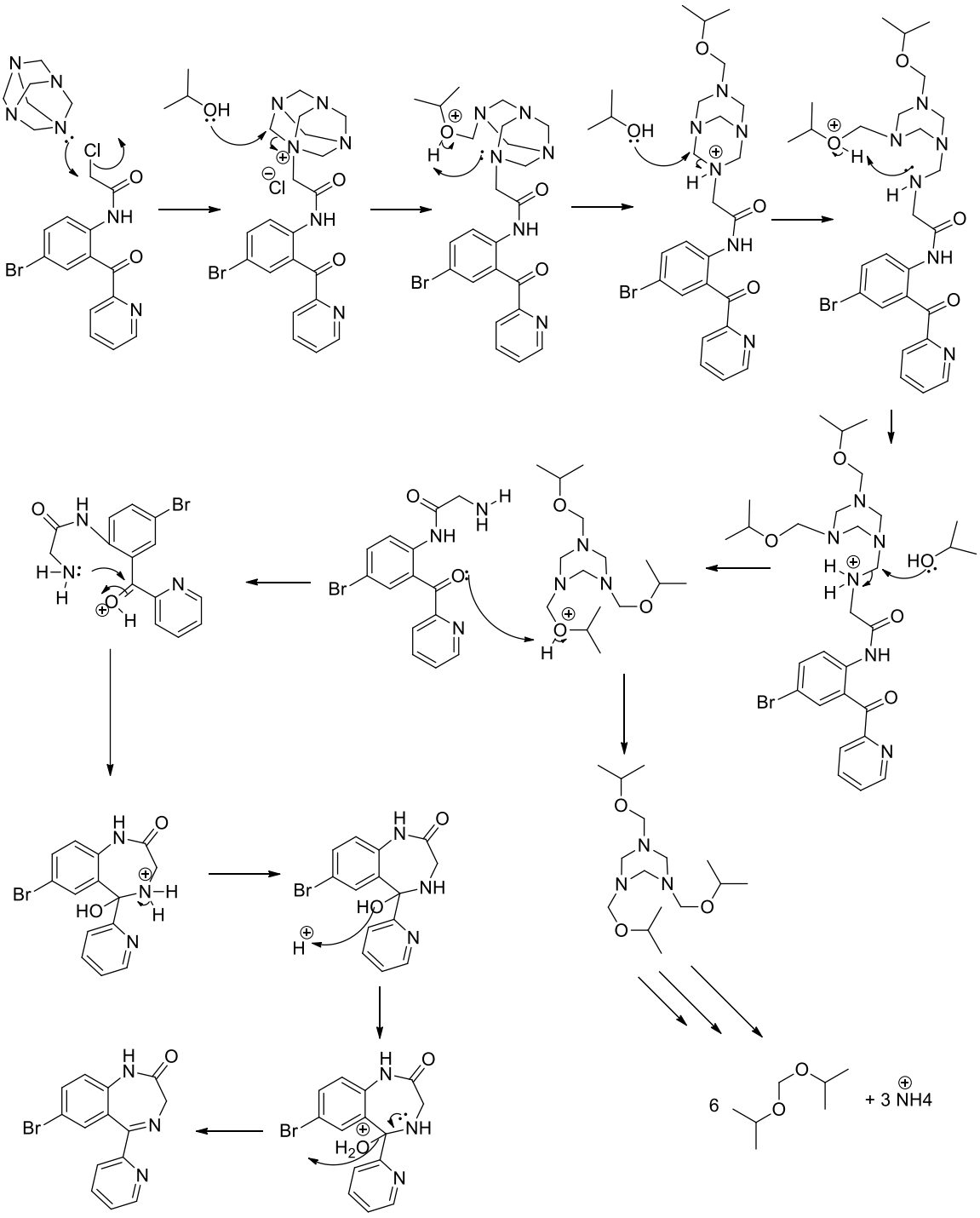
Table 3. Yield improvement for Step 2	
Synthetic step :2	
Previous yield	70-75%
Current yield*	88-91%
Yield improvement*	18-20%
Yield varies according to scale	

The mixture was subsequently cooled slowly to room temperature, allowing for the further isolation of the desired product with excellent purity. This modified procedure enabled to maximize the yield and purity of the benzodiazepine product by effectively capturing and isolating the remaining product present in the filtrate, thereby optimizing the overall synthesis process. The **Table 3** summarizes the overall yield improvement for this step.

It is indeed gratifying to note that the utilization of the Delépine reaction on a large scale, specifically in a 12 L flask, resulted in the production of 514 g (631 g scale starting material) of the desired 2'-pyridyl-benzodiazepine (**6**). This yield corresponds to an impressive 91% yield, demonstrating the scalability and efficiency of the reaction. The proposed Delépine reaction mechanism, depicted in **Scheme 5**, provides insights into the series of steps involved in the transformation. This mechanism serves as a valuable guide for understanding the reaction

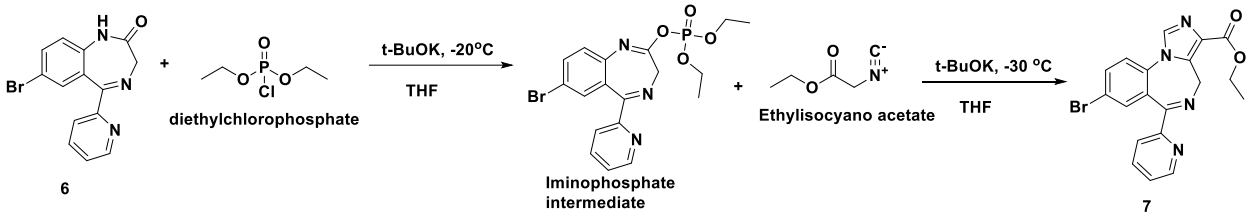
pathway and further optimizing the synthesis process of the 2'-pyridyl-benzodiazepine compound.

Scheme 5. Probable mechanism of Delepine Reaction



In the third step of the synthesis of KRM-II-81, the objective was to introduce the imidazole ring on the top of benzodiazepine to yield the imidazodiazepine compound (**Scheme 6**).

Scheme 6. Step 3: Synthesis of imidazodiazepine



Several enhancements have been implemented in this particular synthetic step. To clarify, in accordance with the initially developed synthetic procedure, the benzodiazepine intermediate (**6**) was dissolved in anhydrous THF and subsequently treated with 1.5 equivalents of solid potassium t-butoxide. This treatment was performed once the reaction mixture reached a temperature of -50°C. The mixture was then warmed up to 0°C and stirred for 30 minutes at that temperature. In the new procedure, the benzodiazepine intermediate (**6**) was subjected to a modified treatment. A solution containing 1.3 equivalents of potassium t-butoxide in THF was added to the reaction mixture at a temperature range of -20°C. The reaction mixture was then stirred between -20°C and -15°C for a duration of 30-40 minutes to ensure complete deprotonation of the benzodiazepine N-H function.

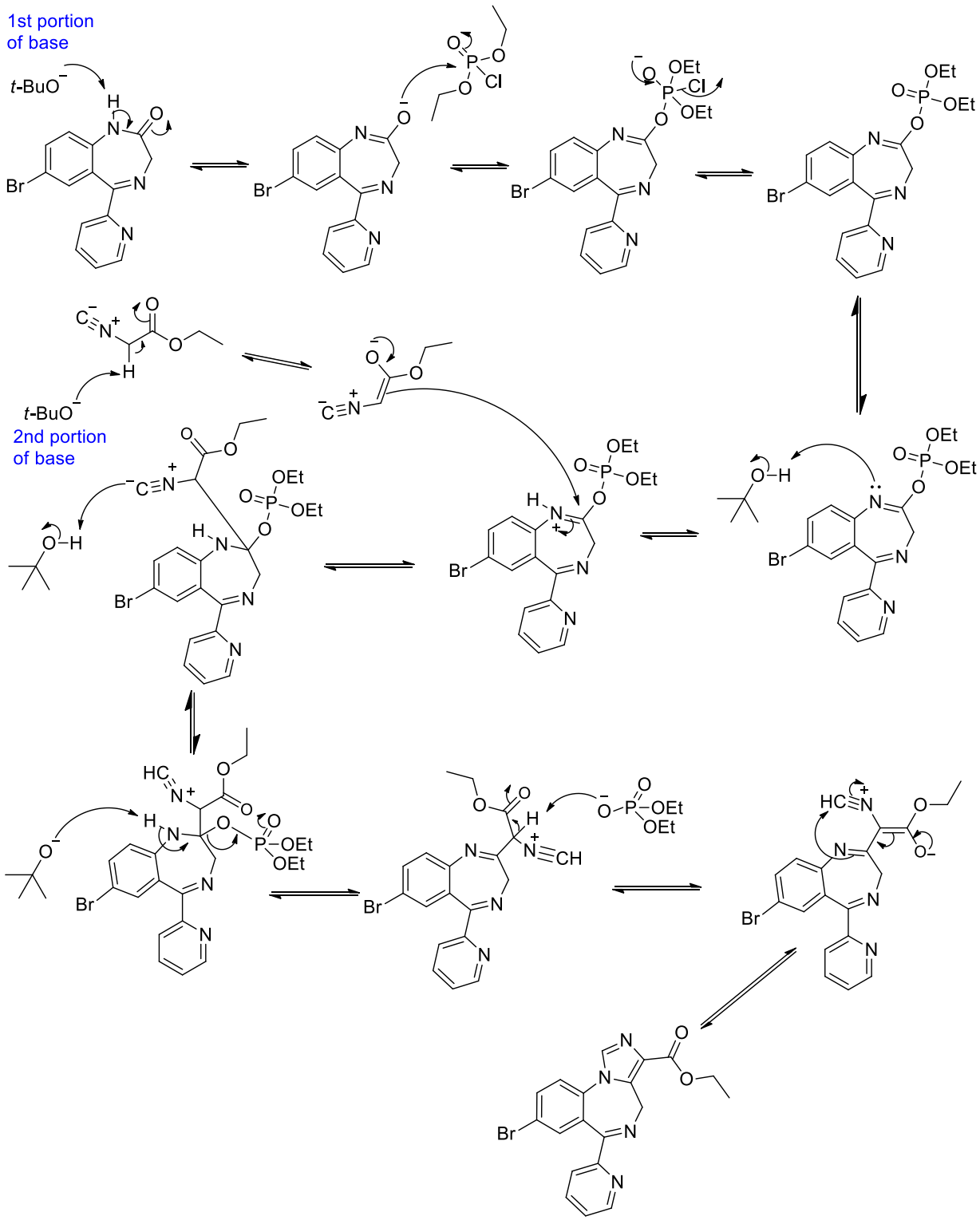
Following this, diethyl chlorophosphate (1.5 equivalents) was introduced to the reaction mixture at -20°C. In the previous procedure, the mixture was allowed to warm up to 0°C and stirred for 2 hours. However, in the new process, diethyl chlorophosphate (1.3 equivalents) was added drop wise over a period of 15 minutes to the reaction mixture at -20°C. The mixture was then stirred for 2 hours. The progress of the reaction was monitored and confirmed by TLC (thin-layer

chromatography), ensuring the consumption of the starting material. These modifications aim to optimize the reaction conditions and improve the efficiency of the reaction in the synthesis of HZ-166.

In the previous route, the synthesis of imidazodiazepine **7** involved adding 1.5 equivalents of ethyl isocyanoacetate at -78°C. The reaction mixture was then allowed to reach room temperature and stirred for 12 hours, resulting in the formation of imidazodiazepine **7**. Purification of the product was achieved through column chromatography. However, in the new route, there were modifications made to the procedure. First, 1.3 equivalents of ethyl isocyanoacetate were added at -30°C. Subsequently, 1.3 equivalents of potassium t-butoxide were added, and the reaction mixture was allowed to reach room temperature and stirred for 6 hours. This yielded imidazodiazepine **7**. In terms of purification, the previous method employed column chromatography. In the new method, the crude product was washed with *t*-butyl methyl ether, resulting in the isolation of a pure imidazodiazepine product (**7**). These changes in the procedure aimed to streamline the synthesis and purification process, offering an alternative approach with comparable yield and improved efficiency.

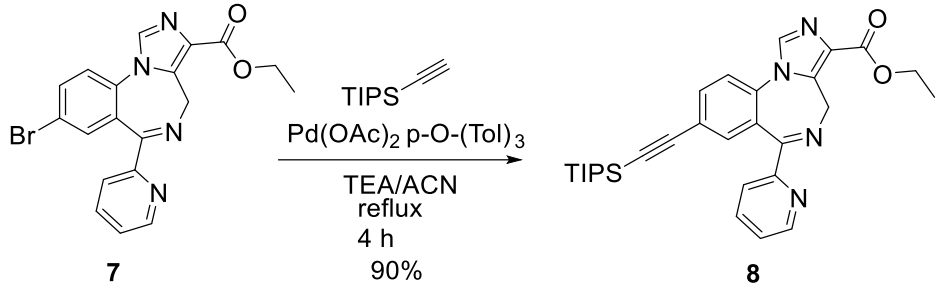
The proposed imidazole top reaction mechanism, as depicted in **Scheme 7**, provides a visual representation of the series of steps involved in the formation of imidazodiazepine. This mechanism serves as a valuable guide for understanding the reaction pathway and the key intermediates and transitions states involved in the transformation. It provides insights into the molecular-level details of the imidazole top reaction and aids in elucidating the chemical transformations that occur during the synthesis of imidazodiazepine.

Scheme 7: Possible mechanism of imidazole top installation on benzodiazepine



In the subsequent step of the reaction sequence, the copper-free Sonogashira coupling [155-156] was employed to convert the aryl bromide 4 into the silyl-protected Hz-166. The Sonogashira coupling reaction is a widely utilized method for the formation of carbon-carbon bonds, specifically between aryl halides and terminal alkynes. By using this coupling reaction, the desired transformation of aryl bromide **7** into the silyl-protected acetylene was achieved (**Scheme 8**).

Scheme 8: Copper free Sonogashira coupling: earlier chemistry

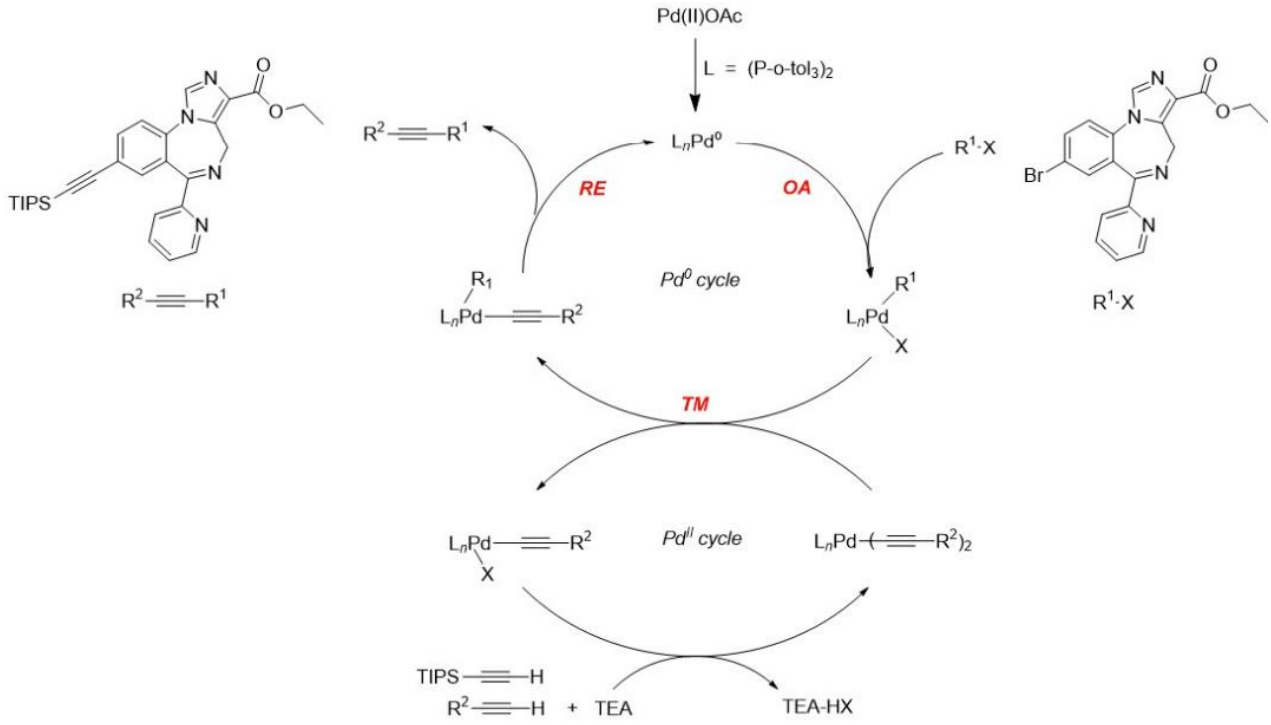


7 **8**

In the previous method, a trimethyl silyl group was used for the silyl-protection of the acetylene intermediate. However, it was found to be less stable. In the new method, a tri-isopropyl silyl group was employed instead. This modification provided two advantages. Firstly, the product obtained with the tri-isopropyl silyl group had a significantly higher R_f value compared to the starting bromo compound. This facilitated the purification process, as the product could be separated more easily from the impurities during chromatography.

Additionally, chromatographic purification was performed in this step for both the previous and new methods. This was done to remove palladium salts, which are often used as catalysts in Sonogashira coupling reactions. By purifying the compounds through chromatography, the palladium salts could be effectively removed, ensuring the purity of the final product.

Scheme 9: Probable mechanism for copper free Sonogashira coupling

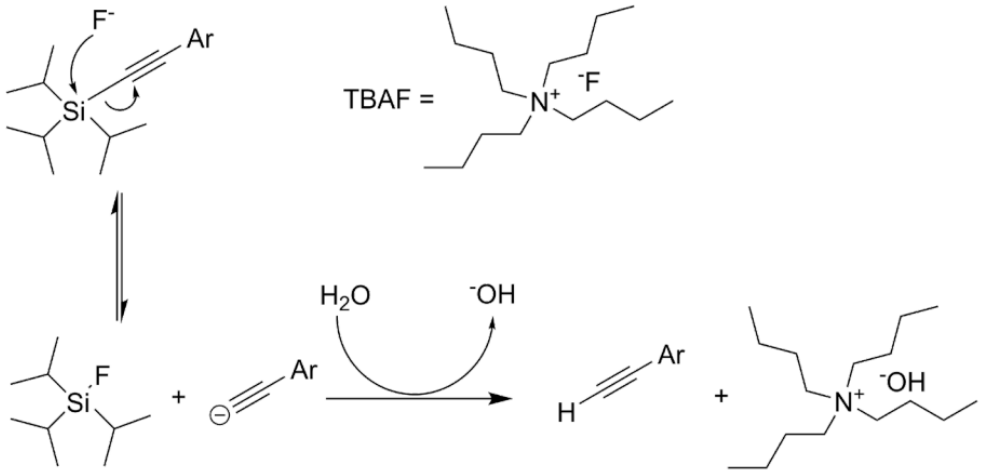


In the subsequent step of the development process, the key intermediate HZ-166 was obtained through the deprotection of the TIPS (tri-isopropylsilyl) acetylene group using a fluoride anion. This deprotection step was crucial for the final formation of HZ-166. Significant improvements were made to this process. Firstly, the reaction temperature was optimized to ensure efficient and selective deprotection of the TIPS-acetylene function. By carefully controlling the reaction temperature, the desired deprotection reaction could be achieved with high yield and minimal side reactions. Furthermore, the previous method involving chromatographic purification was replaced with crystallization. Crystallization was employed as a purification technique to isolate Hz-166. This modification not only simplified the purification process but also improved the overall efficiency of the synthesis. The compounds were subjected to an IPA-water mixture, with

a ratio of 50:50. This wash solution effectively removed impurities and unwanted byproducts, resulting in a purified compound.

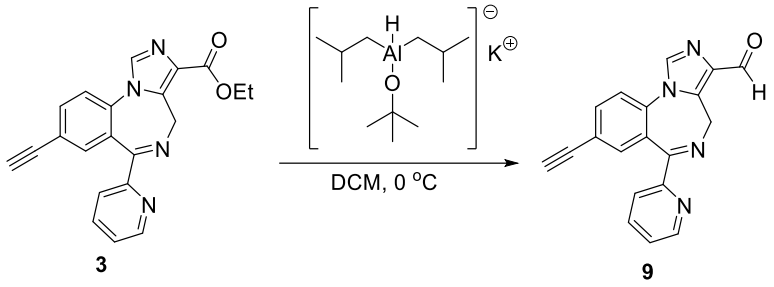
By utilizing this IPA-water wash purification method, the compounds could be efficiently purified, leading to improved yield and purity of the final product. This alternative purification approach offered advantages over the previous chromatographic purification method, simplifying the overall process and increasing the efficiency of the synthesis. The proposed mechanism for the cleavage of the TIPS (tri-isopropylsilyl) group is outlined in **Scheme 10**, illustrating the step-by-step process involved in the cleavage reaction.

Scheme 10: Probable mechanism for fluoride mediated deprotection of TIPS group



The subsequent step in both the old and new methods involves the reduction of the ester to an aldehyde by PDBBA (Potassium *t*-butoxide-DIBAL-H complex) (Li et al 2019, Knutson et al 2020).[151,142]

Scheme 10: Reduction of Hz-166 by PDBBA

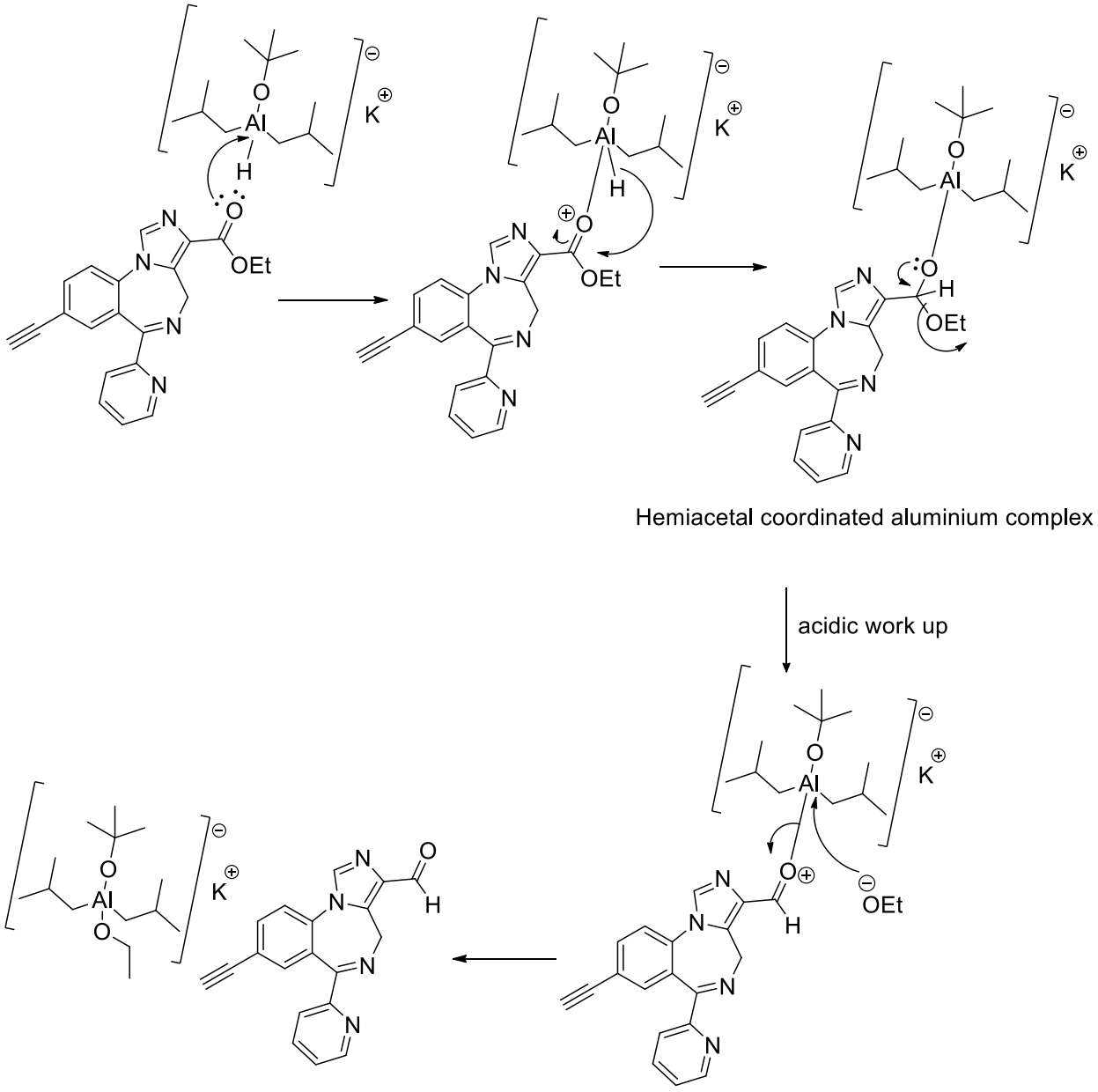


PDBBA (Potassium t-butoxide-DIBAL-H complex) can be conveniently prepared by slowly adding DIBAL in hexane to a solution of equimolar amounts of potassium t-butoxide in THF at 0°C for a period of 2 hours (161). The design of PDBBA takes advantage of its three bulky groups, which theoretically prevent it from attacking the imine double bond. Additionally, it can provide only one hydride atom during the reduction process, making it potentially easier to control and stop the reaction at the aldehyde stage compared to LiAlH4, which offers four hydride units. The proposed mechanism for the reduction reaction is straightforward.[162-163] The hydride from PDBBA attacks the carbonyl carbon, forming a tetrahedral intermediate, and subsequent elimination of the ethoxy group leads to the desired aldehyde formation (**Scheme 11**).

The reduction reaction proceeded rapidly, reaching completion in under 30 minutes. TLC analysis revealed the presence of alcohol by-products, indicating the conversion of a aldehyde function into an alcohol group. The formation of these by-products may be attributed to incomplete conversion or side reactions occurring during the reduction process. Despite the reaction's short duration, it is feasible to implement this procedure on a larger scale by employing TLC monitoring every 5-10 minutes. The optimized reaction conditions have been

successfully employed on a substantial scale, with a maximum quantity of 80 grams. The reaction achieved an 70% yield.

Scheme 11: Probable mechanism of reduction of Hz-166 by PDBBA



In an effort to enhance yield and minimize side reactions leading to alcohol formation, a flow chemistry approach was attempted for the synthesis of Hz-166 aldehyde. The procedure involved adding the HZ-166 solution in DCM and the PDBBA complex to an empty round bottom flask with vigorous stirring. Both reagents were being added gradually and slowly at 0 °C (**Scheme 12**). However, contrary to expectations, the attempted flow chemistry method resulted in a higher production of alcohol compared to the conventional reduction reaction.

The increased formation of alcohol in the flow chemistry approach could be attributed to various factors. It is possible that the reaction conditions, such as temperature, flow rate, or reagent concentrations, were not optimized appropriately. The reaction setup in the flow system might have contributed to the undesired outcome. It is also worth considering the residence time of the reactants in the flow system, as a longer residence time could lead to increased alcohol formation.

To improve the flow chemistry method and achieve higher yields of aldehyde while minimizing alcohol by-products, further investigation is necessary. It would be beneficial to carefully evaluate and adjust the reaction conditions, catalyst selection, flow rates, and other parameters. By systematically optimizing these factors, it may be possible to overcome the challenges encountered in the initial attempt and achieve a more favorable outcome in terms of aldehyde yield.

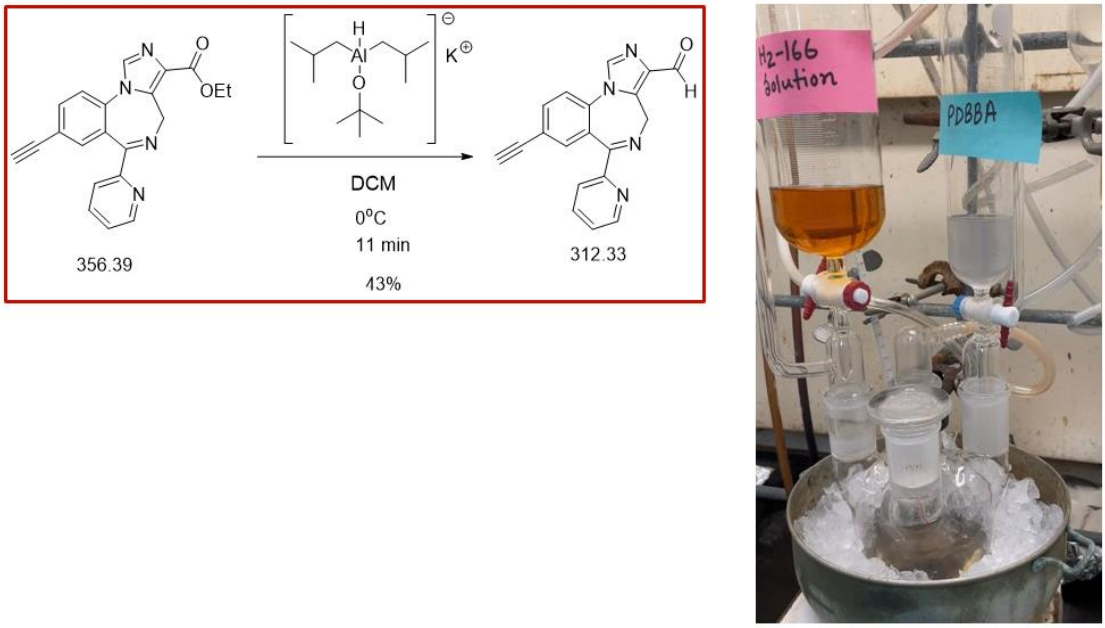
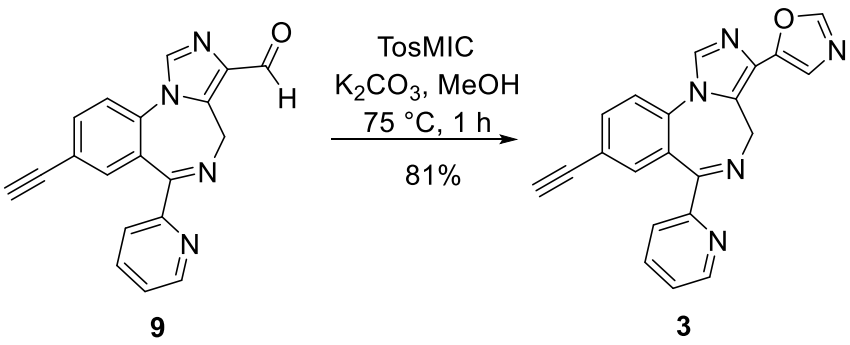


Figure 6. Flow reaction to synthesize Hz-166 aldehyde.

The Hz-166 aldehyde obtained from the reduction reaction was subsequently transformed into an oxazole compound, leading to the synthesis of KRM-II-81 via the Van Leusen reaction (**Scheme 13**).

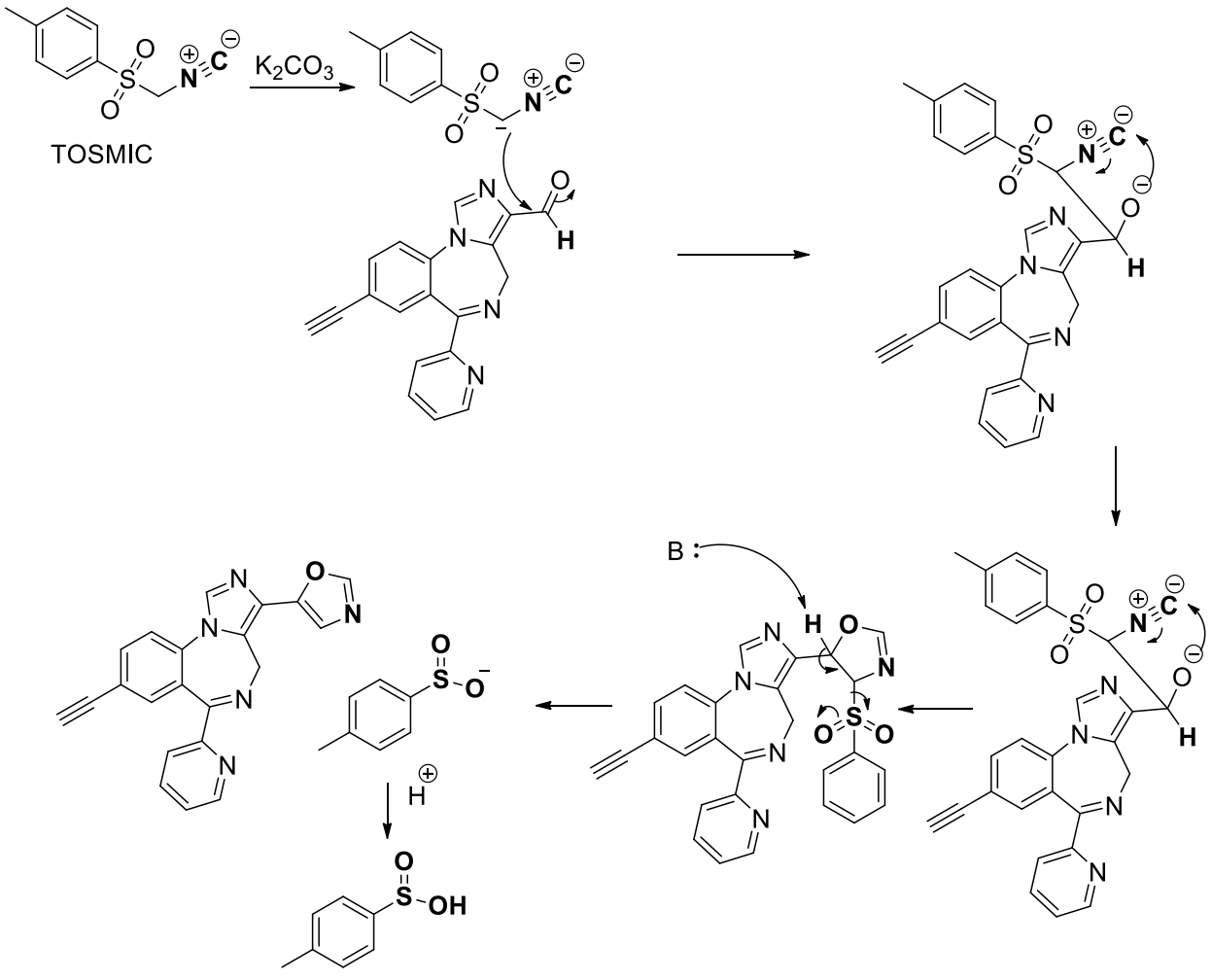
Scheme 13: Synthesis of KRM-II-81



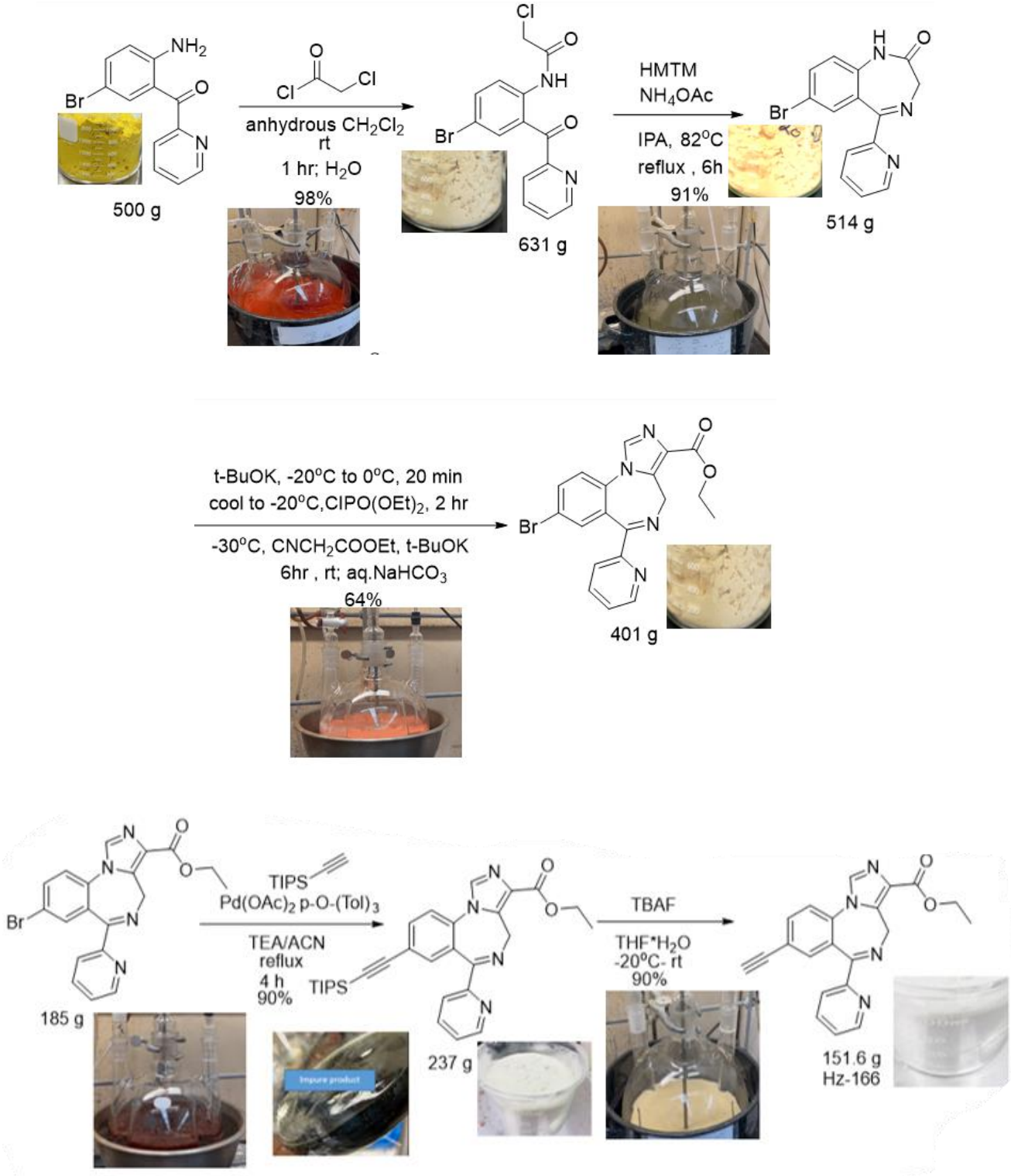
This conversion proceeded with a high yield, meaning that a significant amount of the desired product was obtained relative to the starting material. The Van Leusen reaction is a well-known

method for the synthesis of oxazoles and has proven to be effective in this case, resulting in the successful formation of KRM-II-81(**3**). The oxazole, KRM-II-81 was purified through a two-step process involving crystallization in a mixture of ethyl acetate and hexane, followed by flash chromatography. This method allows for the isolation of a purified form of the compound. The optimized reaction conditions have proven effective on a large scale, producing a maximum quantity of 60 grams. The reaction exhibited a yield of 81%, indicating a significant success in obtaining the desired product. The proposed mechanism of oxazole formation was depicted on **Scheme 14**. The improved and scalable synthesis of Hz-166, to date, is depicted in **Scheme 15**.

Scheme 14: Possible mechanism for the conversion of aldehyde function to oxazole



Scheme 15. Improved and scalable synthesis of Hz-166 by Sharmin



3.2.2. Synthesis of DS-II-73, a brominated analog of KRM-II-81

In the pursuit of developing treatments for pharmacoresistant epilepsy and other neurological and psychiatric disorders, KRM-II-81 (**3**) has shown promise as described earlier.[137-142,150-151] To ensure progress in this area, medicinal chemistry has focused on creating alternative compounds as structural backups. Several analogs have been synthesized and characterized, including compounds **13**, **14**, and **15** (**Figure 7**).

Compound **13**, which features a 2'Cl-substitution, exhibited reduced oral exposure in the brain and plasma of rats compared to KRM-II-81.[157] Similarly, compound **15** also demonstrated decreased brain and plasma exposure following oral administration. Compound **14**, the bromine analog of compound **15**, displayed the highest concentration levels in these compartments, as indicated by the areas under the curve.[157] Molecular docking studies with the α1β3γ2L configured GABAAR revealed that the bromine atom in compound **14** exhibited the least interaction with α1His102, an observation associated with its low sedating activity. Additionally, compound **14** exhibited favorable antiseizure activity in various rodent models when administered orally.[157]

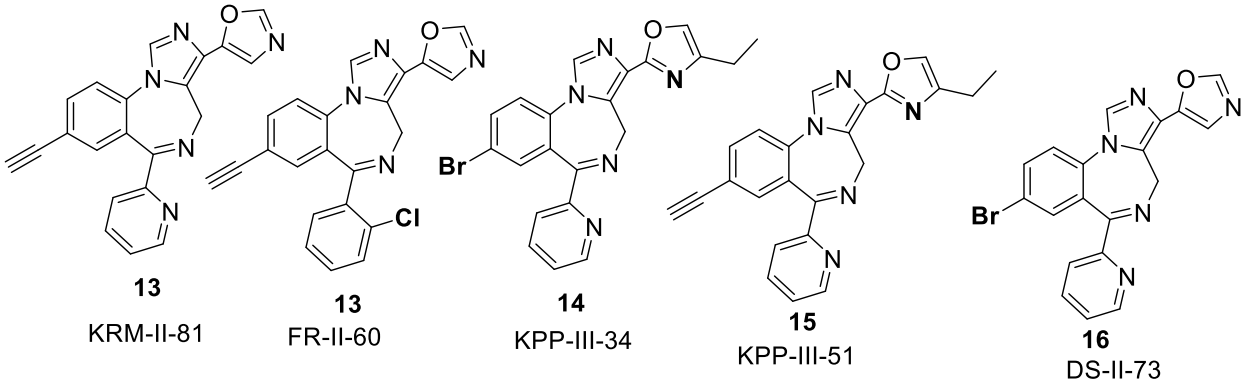
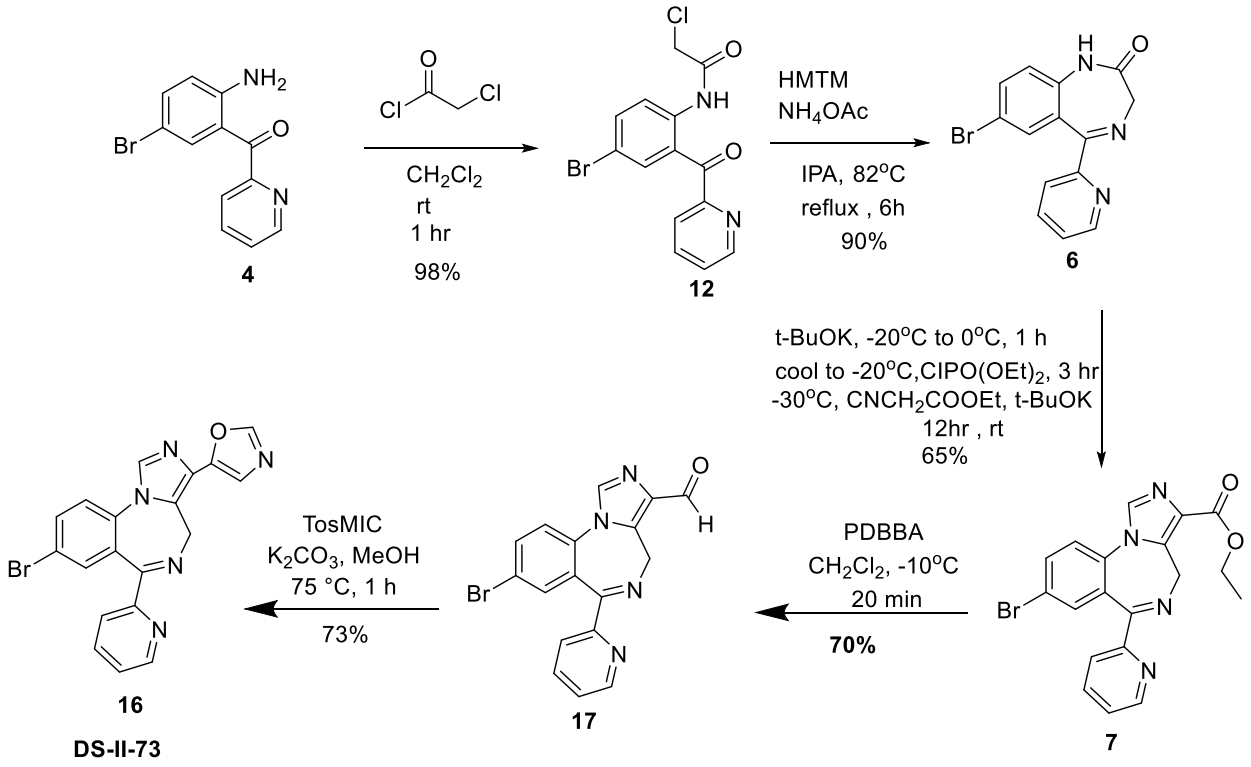


Figure 7. **Structures of KRM-II-81 (3) and some structural analogs**

Building upon the favorable oral pharmacokinetics and low sedation potential observed in the bromine-substituted analog of KRM-II-81, we postulated that a direct substitution of bromine with an ethynyl group in KRM-II-81 would yield another promising compound to serve as a potential structural backup. To investigate this hypothesis, we conducted the present study, which aimed to synthesize DS-II-73 (**16**) and evaluate its pharmacological properties. The characterization included ligand site binding and selectivity profiling, selectivity for various α-containing GABAARs, oral pharmacokinetics, oral anticonvulsant activity, and the ability to attenuate epileptic activity in cortical brain slices obtained from a patient with intractable mesial temporal lobe seizures.

The experimental findings revealed that DS-II-73(**16**) retained its ability to penetrate the brain and plasma following oral administration, displayed anticonvulsant activity when administered orally, and effectively suppressed the frequency of local field potentials in epileptic brain slices. Notably, DS-II-73(**16**) selectivity for GABAARs containing α2/3/5 subunits and had minimal impact on sensorimotor function even at a dose 12 times higher than the effective anticonvulsant dose. Similarly to compound **14**, DS-II-73 demonstrated low interaction with the α1His102 residue in α1β3γ2L configured GABAARs, suggesting a reduced sedation potential. The synthesis of DS-II-73 was a simplified two-step process compared to that of KRM-II-81, resulting in good yield without the need for a metal catalyst. The synthesis of DS-II-73(**16**) is depicted on **Scheme 16**. The yield of different steps are almost similar to that of KRM-II-81. The synthesis was efficient with 5 steps, each with yields of 65% or greater and generating an overall yield of 38%.

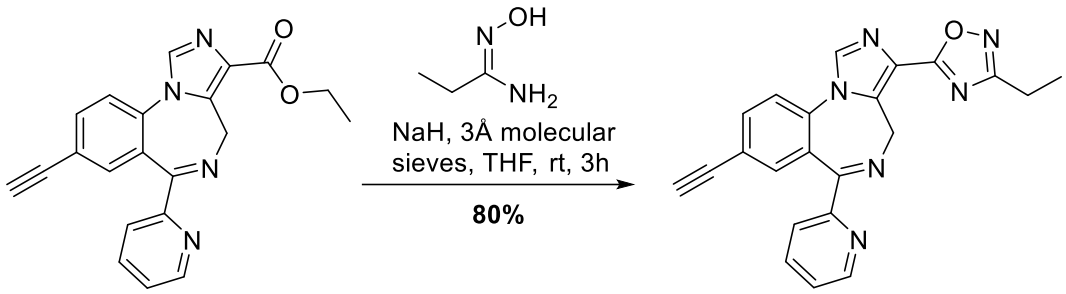
Scheme 16. Synthesis of DS-II-73 [158]



3.2.3. Synthesis of MP-III-080 (1, 2, 4-oxadizole bioisostere of HZ-166)

MP-III-80, a structural analog of KRM-II-81 and a 1,2,4-oxadizole bioisostere of HZ-166, exhibited significant efficacy in various pain and anxiolytic models. To proceed with further pre-clinical investigations, a substantial quantity of this compound was required. The synthesis of MP-III-080 (151) involved treating the ethyl ester Hz-166 with ethyl amidoxime and sodium hydride at room temperature, utilizing 3Å molecular sieves as catalysts.[119] The reaction was completed within a span of 3 hours, yielding an 80% product yield.

Scheme 17: **Synthesis of MP-III-080**



Hz-166

3

MP-III-080

2

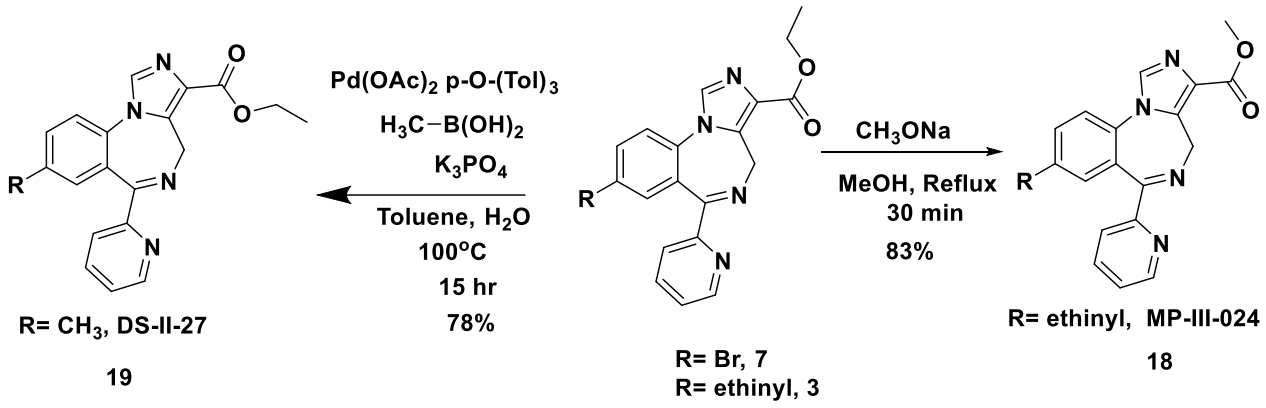
3.2.4. Synthesis of MP-III-24 and DS-II-27

MP-III-024 is a closely related analog of HZ-166 (ethyl ester), which has been previously demonstrated to possess non-sedating anxiolytic properties in rhesus monkeys (Fischer et al., 2010). Studies conducted by Paul et al. (2014) and Di Lio et al. (2011) also revealed that MP-III-024 exhibited antinociceptive effects in rodents. At a concentration of 1 μM, MP-III-024 exhibited functional selectivity for α2GABAA and α3GABAA receptors, with a stimulation of 220-240% of the control current. In contrast, its activity at α1GABAA and α5GABAA subtypes resulted in a stimulation of 110-130% of the control current. These findings were observed in recombinant GABAA-expressing oocytes (Fischer et al., 2017). This selective activity led to antihyperalgesic effects with minimal off-target effects, as assessed through operant responding and locomotor activity measurements. These results are consistent with the effects of other structurally related ligands with α2GABAA and α3GABAA preference, such as HZ-166 (Di Lio et al., 2011) and KRM-II-81 (Witkin et al., 2019; Biggerstaff et al., 2020). In metabolic studies, MP-III-024 (ester) exhibited a longer duration of activity compared to other compounds. Specifically, it demonstrated a time course and duration of action similar to the prototypical μ-opioid receptor agonist, morphine. This characteristic makes MP-III-024 suitable for

combination studies, particularly in exploring potential synergistic effects when used in conjunction with morphine (Fischer et al., 2017). MP-III-024 was synthesized specifically for the purpose of conducting dose-addition assays to assess α2GABAA/α3GABAA receptor-opioid interactions. The study aimed to investigate the effects of combining MP-III-024 and morphine in male CD1 mice, utilizing two distinct classical pain assays. The synthetic strategy employed for the synthesis of MP-III-024 is illustrated in **Scheme 18**.

Furthermore, in order to conduct a comparative study involving the substitution of a bromo group with a methyl group at the 8-position of the imidazodiazepine moiety in Hz-166, another analog named DS-II-27 was designed and synthesized. This comparison aimed to examine the impact of this substitution on the compound's properties and activities.

Scheme 18: **Synthesis of MP-III-024 and DS-II-27**

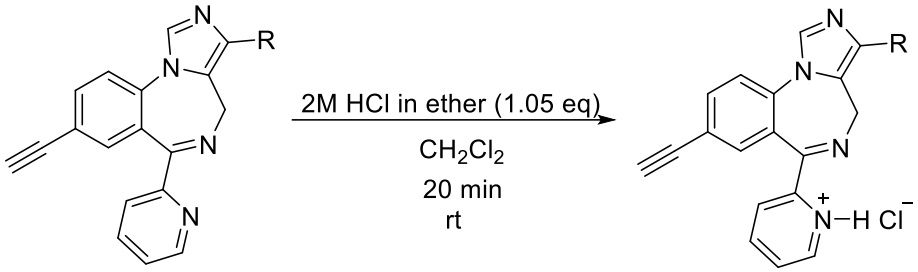


3.2.5. Synthesis of salt analogs of Hz-166

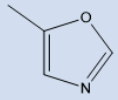
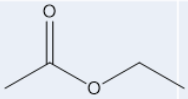
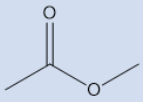
To improve solubility and enhance bioavailability, a hydrochloride salt of KRM-II-81 was synthesized. By converting KRM-II-81 into its hydrochloride salt form, its solubility in aqueous solutions was increased, allowing for improved dissolution and absorption in the body,

ultimately leading to enhanced bioavailability. Building upon the results obtained, a series of salt analogs of HZ-166 were synthesized. These analogs were designed with the aim of exploring their biological properties and conducting further analysis. The synthesis of these salt analogs provides an opportunity to investigate their potential effects and evaluate their efficacy in various biological systems or assays.

Scheme 19. Synthesis of MYM-V-26, DS-II-47, and DS-II-48



MYM-V-26, **20**
DS-II-47, **21**
DS-II-48, **22**

R	Code	Yield	Biological evaluation
	MYM-V-26	81%	Completed PTZ assay, PK
	DS-II-47	78%	In-progress
	DS-II-48	72%	

3.3. Biological studies of α2/3-selective imidazodiazepines: Results and discussions

3.3.1. Biological studies of KRM-II-81

3.3.1.1. Exploring the anxiolytic effects of KRM-II-81 and MP-III-080 (Marble-burying model in mice, A. Biggerstaff, J.M. Witkin and co-workers)

The marble burying assay is a commonly utilized method to evaluate the potential anxiolytic effects of test compounds, particularly in rodents and mice, without requiring prior training. This assay capitalizes on the innate behavior of the animals, whereby they tend to bury objects, regardless of their harmful or harmless nature, when experiencing fear or anxiety. The reduction in burying behavior indicates the anxiolytic properties of a ligand. In this assay, a marble is considered buried if 2/3 of it is covered.

The marble burying assay has proven to be effective in assessing the anxiolytic effects of traditional benzodiazepines (BZDs) such as chlordiazepoxide . To evaluate the anxiolytic effects of MP-III-080 and KRM-II-81, this assay was employed alongside chlordiazepoxide as a comparator. Swiss mice (N=10) were administered either vehicle (1% carboxymethyl cellulose), 30 mg/kg of chlordiazepoxide, MP-III-080, or KRM-II-81 intraperitoneally. Following a motor impairment test, the mice were placed in a chamber containing 20 marbles on sawdust bedding. The results, as shown in Figure 7, revealed a significant treatment effect on marble burying for both KRM-II-81 and MP-III-080 ($F_{5,59} = 54.1$, $p < 0.001$). At the dose of 30 mg/kg, both compounds significantly decreased marble burying, which was comparable to the effects observed with chlordiazepoxide at the same dose (**Figure 8**).

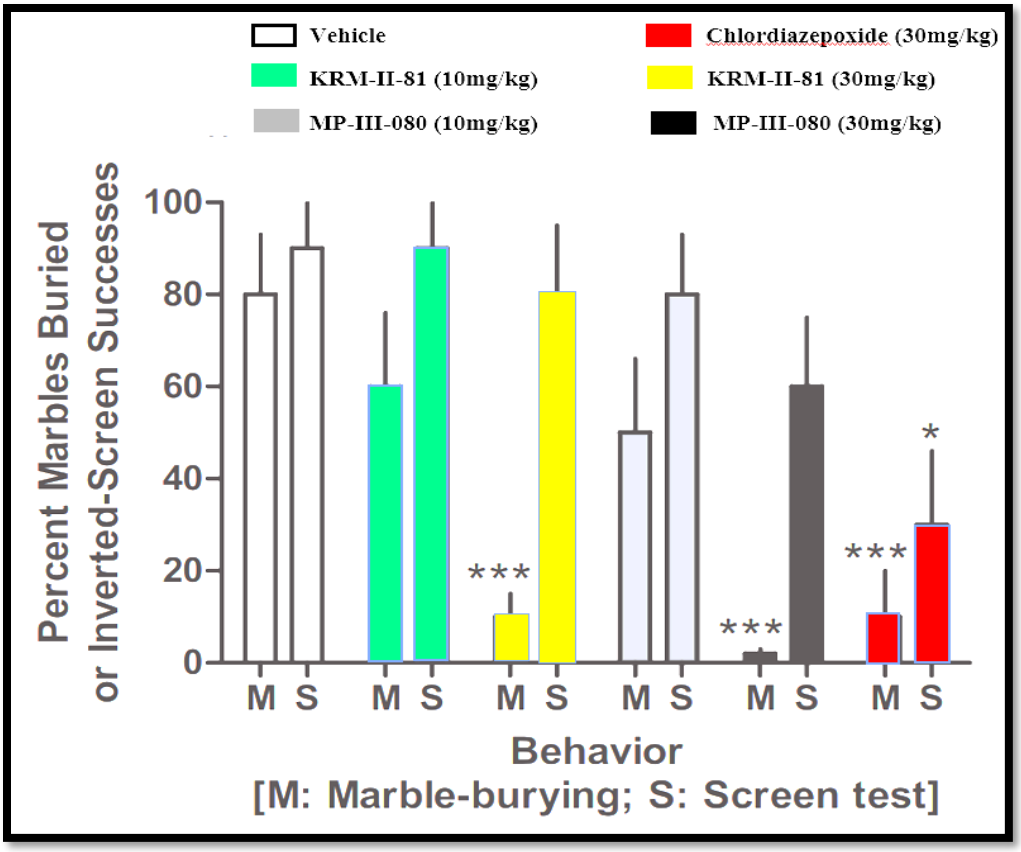


Figure 8. The anxiolytic and motor impairment effects of KRM-II-81 and MP-III-80, compared to the reference anxiolytic drug, chlordiazepoxide. The figure shows the results of two behavioral assays conducted in mice: the marble-burying behavior and the inverted-screen performance. The experiment involved using the same group of 10 mice for both tests. The inverted-screen test was conducted first, followed immediately by the marble-burying test. Each mouse received either the vehicle or one of the drugs (KRM-II-81, MP-III-80, or chlordiazepoxide). The figure includes statistical analysis, showing significance levels denoted by asterisks ($*p < 0.05$; $***p < 0.001$) based on Dunnett's test following a one-way ANOVA for each behavioral assay. Error bars indicating the standard error of the mean (± SEM) are also included in the figure. The figure presented in this text is adapted from the study conducted by Biggerstaff Witkin et al. in 2020.

3.3.1.2. Motor impairment effects of KRM-II-81 and MP-III-080 (Inverted screen test, A. Biggerstaff, J.M. Witkin and others)

To evaluate the potential motor-impairing effects of KRM-II-81, MP-III-80, and chlordiazepoxide, the mice were first subjected to an inverted screen test before the marble burying test. **Figure 8** displays the outcomes of these tests. The findings revealed that neither KRM-II-81 nor MP-III-80 had a significant impact on motor performance in the inverted screen test. However, the sedating anxiolytic drug, chlordiazepoxide, resulted in a decrease in the percentage of mice successfully completing the task ($F_{5,59} = 3.00$, $p < 0.05$).

3.3.1.3. Effects of KRM-II-81 and MP-III-080 on acute and chronic neuropathic pain (Paclitaxel induced pain, A. Biggerstaff, J.M. Witkin and others)

To evaluate the pain behaviors of KRM-II-81 and MP-III-80, a series of experiments were conducted using C57BL/6 mice. Pain was induced by administering the chemotherapeutic agent paclitaxel. As a comparator, gabapentin was used to examine the effects. The mice were divided into two cohorts: the first cohort consisted of 16 mice, and the second cohort had 18 mice. Each cohort was further subdivided into four groups.

On the initial day (day 0), the mice were assigned to either the paclitaxel pre-treatment group (n = 27) or the vehicle pre-treatment group (n = 7). The paclitaxel pre-treatment group received paclitaxel (4 mg/kg) in vehicle, while the vehicle pre-treatment group received vehicle alone (intraperitoneal injection) on days 0, 2, 4, and 6. Mechanical hyperalgesia and thermal allodynia measurements were taken on days 0, 2, and 4 (prior to paclitaxel injections), as well as on days 7, 11, 13, and 15 (prior to the dose response).

For the paclitaxel-treated groups, a total of six injections were administered, with each injection given every 30 minutes to achieve cumulative doses of 0.1, 1, 5, 10, 20, and 30 mg/kg of MP-III-080 (n = 6) and KRM-II-81 (n = 7), as well as gabapentin (n = 7), on day 15. Mechanical hyperalgesia (two measurements) and thermal allodynia (one measurement) were assessed for each hind paw, conducted 30 minutes after each injection.

Significant differences in the dose response curves for mechanical hyperalgesia were observed among the different treatment groups, as indicated by a sum of squares F-test ($F(8,108) = 10.63$, $p < 0.0001$). Additionally, there was a significant difference in mean Emax (maximum effect) between the treatment groups. Gabapentin demonstrated a slightly higher Emax compared to KRM-II-81 but was similar to MP-III-080 (**Table 4, Figure 9**).

Table 4 : $E_{max/min}$ and ED50 values for KRM-II-81, MP-III-80 and gabapentin from acute neuropathic pain dose response experiments

	KRM-II-81	MP-III-080	Gabapentin
Emax mechanical (g)	1.88 ± 0.19	8.14 ± 1.33	2.59 ± 0.22
ED_{50} mechanical (mg/kg)	8.86 ± 1.20	8.91 ± 1.15	8.12 ± 1.15
Emin thermal (s)	1.18 ± 1.08	0.95 ± 0.50	0.90 ± 0.58
ED_{50} thermal (mg/kg)	8.14 ± 1.33	7.09 ± 1.13	6.41 ± 1.12

***Table is modified from Biggerstaff et al. 2020.**

For thermal allodynia, significant differences were observed in the dose response curves among the different treatment groups, as determined by a sum of squares F-test ($F(8,108) = 2.15$, $p =$

0.037). However, there were no significant differences observed between the treatments for mean ED50 (effective dose for 50% of maximum effect) ($F(2,17) = 0.515$, $p = 0.606$) or Emax (maximum effect) ($F(2,17) = 1.731$, $p = 0.207$). Both KRM-II-81 and MP-III-080 exhibited equal potency and efficacy compared to gabapentin (**Figure 10, Table 4**).

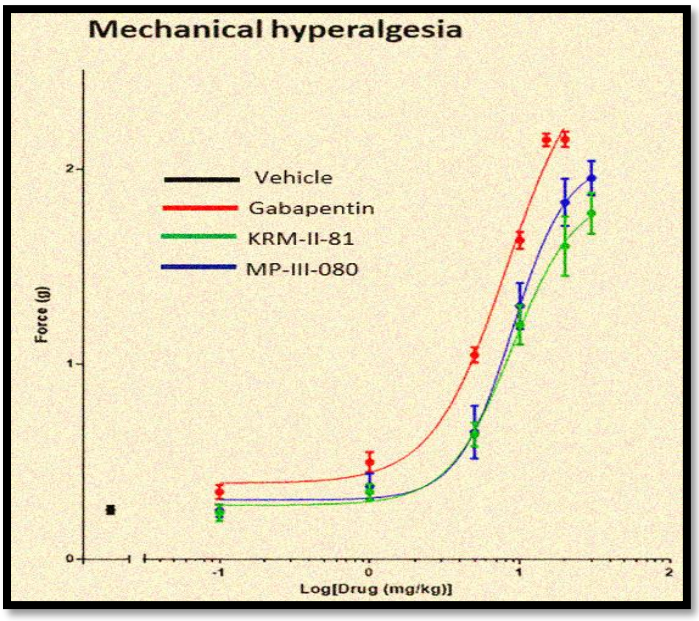


Figure 9. The dose response curves for mechanical hyperalgesia in paclitaxel-treated mice are depicted in the figure. The antinociceptive effects of KRM-II-81 are shown in green, MP-III-80 in blue, gabapentin in red, and vehicle in black. The analysis was performed on experimental day 15, with a sample size (n) ranging from 6 to 7. The error bars represent the standard error of the mean (± SEM), indicating the variability of the measurements around the mean values. The figure presented in this text is adapted from the study conducted by Biggerstaff Witkin et al. in 2020.

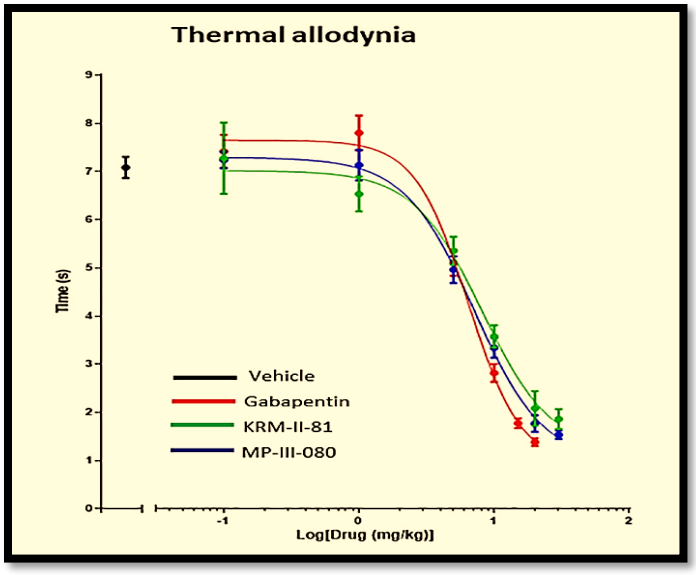


Figure 10. The figure presents the dose response curves for thermal allodynia in paclitaxel-treated mice. The antinociceptive effects of KRM-II-81 are depicted in green, MP-III-80 in blue, gabapentin in red, and vehicle in black. The analysis, with a sample size (n) of 6-7, was conducted on experimental day 15. The figure illustrates the varying responses of the different treatments in mitigating thermal allodynia. The error bars represent the standard error of the mean (± SEM), indicating the variability of the measurements around the mean values. The figure presented in this text is adapted from the study conducted by Biggerstaff Witkin et al. in 2020.

For the assessment of chronic neuropathic pain, a two-way ANOVA analysis was conducted on mechanical hyperalgesia measures performed from days 18 to 40. The analysis revealed significant differences among the treatment groups ($F(4,29) = 211.7$, $p < 0.0001$) as well as across different days ($F(11,319) = 5.925$, $p < 0.0001$). In comparison to the paclitaxel/vehicle treated mice, all treatment groups required a greater mechanical force to elicit a reaction, indicating potent antinociceptive effects that brought the response closer to non-disease levels.

Notably, the mice pre-treated with KRM-II-81, MP-III-80, and vehicle also exhibited a higher threshold of mechanical force to initiate a reaction, as shown in **Figure 11**.

Further analysis using Post hoc Tukey tests revealed significant differences between the gabapentin treatment group and the KRM-II-81, MP-III-80, and vehicle-vehicle treatment groups at individual time points, as illustrated in **Figure 11.**

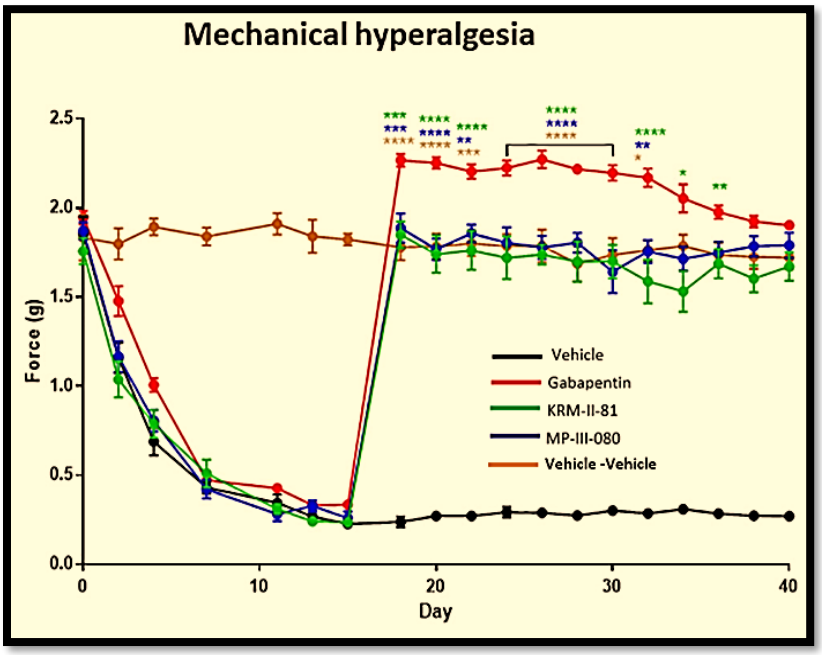


Figure 11. In the chronic neuropathic pain study conducted from days 18 to 40, mechanical hyperalgesia data were collected and analyzed for the effects of KRM-II-81, MP-III-80, gabapentin, and vehicle treatments. The data, obtained from a sample size of 6-7 mice, were measured 30 minutes after the administration of the respective treatments. In the figure, KRM-II-81 is represented by green, MP-III-80 by blue, gabapentin by red, and vehicle by black. Additionally, there is a Vehicle-Vehicle group shown in brown, which did not undergo paclitaxel pretreatment. The error bars in the figure represent the standard error of the mean (± SEM). Above the data points, any significant differences are indicated

with asterisks corresponding to the respective significance levels: * < 0.05, ** < 0.01, * < 0.001, **** < 0.0001. The figure presented in this text is adapted from the study conducted by Biggerstaff Witkin et al. in 2020.**

In the assessment of thermal allodynia conducted from days 18 to 40, a two-way ANOVA analysis revealed a significant difference between treatment groups ($F(4,29) = 533.7$, $p < 0.0001$) as well as across different days ($F(11,319) = 3.794$, $p < 0.0001$). These findings indicate that the treatment interventions had a significant impact on thermal allodynia, and there were also temporal variations observed throughout the study period.

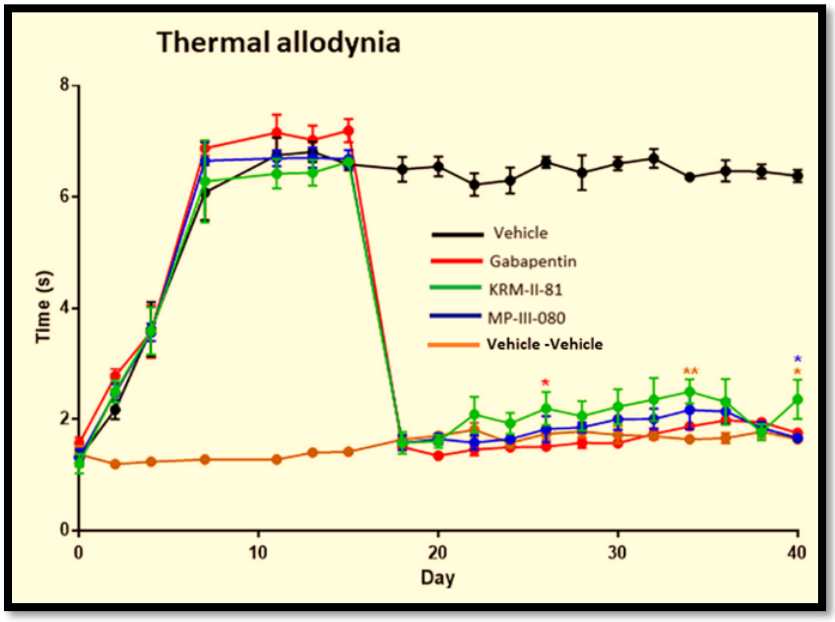


Figure 12. In the chronic neuropathic pain study conducted from days 18 to 40, thermal allodynia data were collected and analyzed for the effects of KRM-II-81, MP-III-80, gabapentin, and vehicle treatments. The data were collected from a sample size of 6-7 mice and measured 30 minutes after the administration of the respective treatments. The color green represents KRM-II-81, blue represents MP-III-80, red represents gabapentin, and black represents the vehicle. Additionally, there is a Vehicle-Vehicle group shown in brown, which did not undergo paclitaxel pretreatment. The error bars in the figure

represent the standard error of the mean (± SEM). Above the data points, any significant differences are indicated with asterisks corresponding to the respective significance levels: * < 0.05, ** < 0.01, * < 0.001, **** < 0.0001. The figure presented in this text is adapted from the study conducted by Biggerstaff Witkin et al. in 2020.**

Significant findings were observed in the time to cold stimulus in the treatment groups compared to the paclitaxel and vehicle-treated control group, as depicted in **Figure 12**. Both the paclitaxel and compound treatment groups exhibited a significantly shorter time to respond to the cold stimulus. Additionally, KRM-II-81 demonstrated a significantly longer time to respond compared to the gabapentin-treated mice. Post hoc Tukey tests further revealed significant differences at specific time points. The ligands targeting α2/3-containing GABAA receptors, KRM-II-81 and MP-III-80, exhibited notable efficacy in reducing pain behaviors in a chemotherapy-induced pain model using paclitaxel. Notably, over the course of 22 days of dosing, no tolerance to the reduction in hyperalgesia was observed with KRM-II-81 and MP-III-80. However, in contrast, the data showed that tolerance was developing to gabapentin during the latter part of the study.

3.3.1.4. Effects of KRM-II-81 (p.o., bid) on the cumulative handling-induced seizure burden in mice inoculated with TMEV (

with Jeff Witkin, Rok Cerne, and others)

In the study, viral injection on day 0 led to a progressive increase in handling-induced seizure burden, as assessed on experimental days 3-7, as shown in Figure 1. At a dosage of 15 mg/kg, KRM-II-81 demonstrated a significant reduction in seizure burden from days 3 to 7 ($F_{4,185} = 2.92$, $P < 0.05$). The administration of KRM-II-81 resulted in a decrease in overall seizure burden ($F_{1,185} = 47.9$, $P < 0.0001$), and there was also a significant interaction between experimental day and treatment ($F_{4,185} = 2.81$, $P < 0.05$).

Similarly, in the study using 30 mg/kg of KRM-II-81, handling-induced seizure burden showed an escalating increase over consecutive test days 3 to 7 ($F_{4,180} = 3.17$, $P < 0.05$). However, the

administration of KRM-II-81 reduced the cumulative seizure burden to zero ($F_{1,180} = 57.2$, $P < 0.0001$). Furthermore, a significant interaction between experimental day and treatment was observed ($F_{4,180} = 3.17$, $P < 0.05$), as illustrated in **Figure 13**.

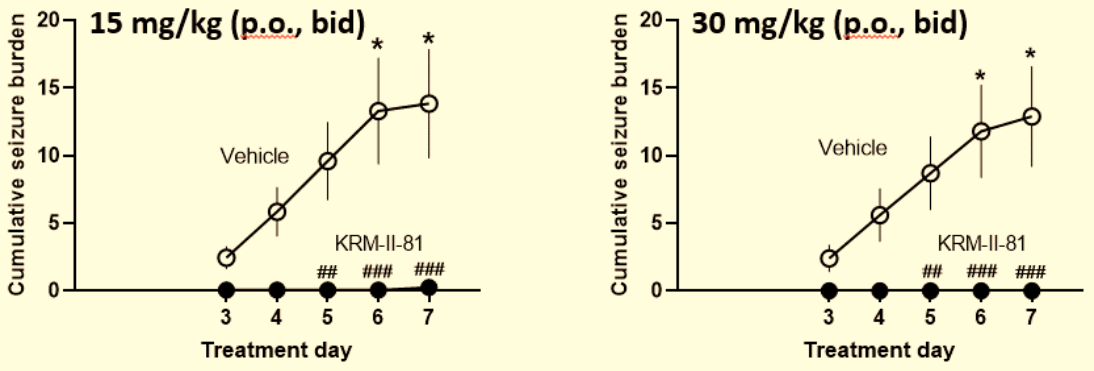


Figure 13. Effects of KRM-II-81 (p.o., bid) on the cumulative handling-induced seizure burden in mice inoculated with TMEV on day 0. Data for the occurrence of seizures in the vehicle and KRM-II-81 groups are shown for the time periods 2 h post injection. Each data point represents the cumulative mean + SEM for N = 16-20 mice due to attrition in the initial N=20 due to criteria weight loss or death (see Results). * P < 0.05 compared to day 3 values; ## P < 0.01, ### P < 0.0001 by ANOVA and Šidák's multiple comparison test. (Unpublished data)

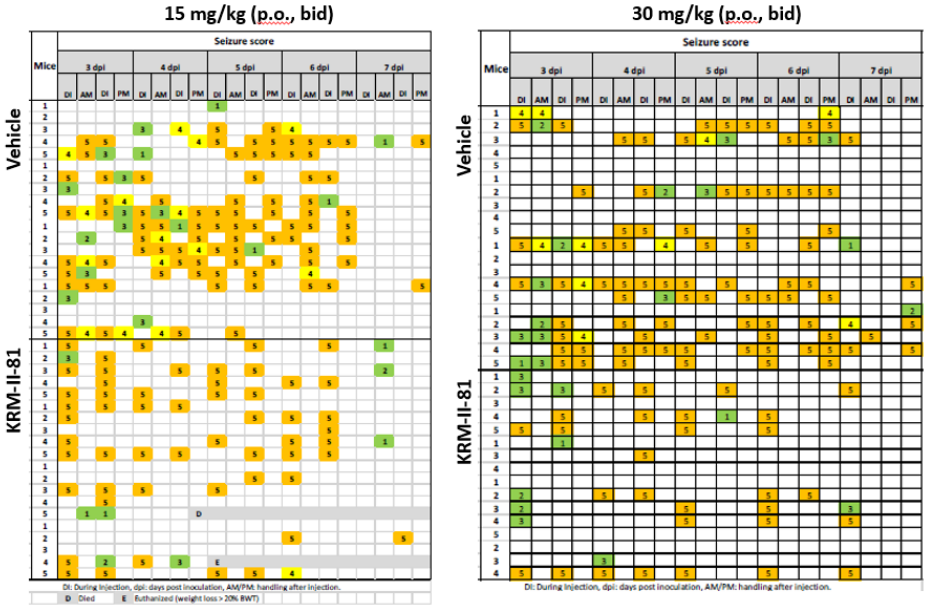


Figure 14. Heat map characterization of handling-induced behavioral seizure observations following TMEV inoculation. Effects of 15 mg/kg (left) and 30 mg/kg (right) KRM-II-81 are shown relative to vehicle with dosing bid. DI represents seizures observed during dosing and AM and PM designate handling-induced seizures observed 2 h post dosing for days 3-7 post viral inoculation on day 0. Behavioral seizures are illustrated according to the Racine seizure score (Racine, 1972) with stages 1-3 (green), 4 (yellow), 5 (orange), and no seizure (blank cell). Only the highest scoring seizure during each observation period is shown. On average in such studies, 70-80% of all animals infected with TMEV experience handling-induced seizures. (Unpublished data)

The effects of KRM-II-81 on seizure severity were compared to their respective vehicle control values, as shown in **Table 4**. Both the 15 mg/kg and 30 mg/kg doses of KRM-II-81 significantly suppressed seizures when measured 2 hours after dosing. However, no significant reduction in seizure severity was observed during the dosing period.

To specifically assess the impact of KRM-II-81 on the most severe tonic/clonic convulsions (stage 5 seizures), a separate evaluation was conducted. The comparison of the number of stage 5 seizures revealed a significant reduction with KRM-II-81 at both dose levels when measured 2 hours after dosing. However, there was no significant reduction in seizure severity when measured during the dosing period.

Table 5. Mean seizure severity during injection (DI) periods and in the AM or PM 2 h after injections.

DI: Vehicle	**DI: KRM-II-81 (15 mg/kg)**	**ANOVA**
1.18 $\pm$ 0.35	1.34 $\pm$ 0.36	$F_{1,369} = 1.13$, $P = 0.29$
AM/PM: Vehicle	**AM/PM: KRM-II-81 (15 mg/kg)**	
1.39 $\pm$ 0.39	0.03 $\pm$ 0.01	$F_{1,369} = 114$, $P < 0.0001$

DI: Vehicle	**DI: KRM-II-81 (30 mg/kg)**	
1.22 ± 0.38	0.87 ± 0.29	$F_{1,359} = 2.47$, P = 0.12
AM/PM: Vehicle	**AM/PM: KRM-II-81 (30 mg/kg)**	
1.36 ± 0.40	0.00 ± 0.00	$F_{1,359} = 124$, P < 0.0001

Seizure severity values in this table include scores for all mice including those that scored zero.

Values shown are means ± SEM for observations of all mice on days 3-7 post viral inoculation.

ANOVA values are for KRM-II-81 data compared to its respective vehicle control. **(Unpublished data)**

Table 6. Number of stage 5 seizures during injection (DI) periods and in the AM or PM 2 h after injections

DI: Vehicle	**DI: KRM-II-81 (15 mg/kg)**	**P value**
40	51	= 0.12
AM/PM: Vehicle	**AM/PM: KRM-II-81 (15 mg/kg)**	
40	0	< 0.0001
DI: Vehicle	**DI: KRM-II-81 (30 mg/kg)**	
40	30	= 0.60
AM/PM: Vehicle	**AM/PM: KRM-II-81 (30 mg/kg)**	
42	0	< 0.0001

Values shown are the total number of Stage 5 seizures that occurred in each observation period across days 3-7 post viral inoculation. Statistical values are from Fisher's Exact Probability test.

(Unpublished data)

3.3.1.5. Effects of KRM-II-81 Dravet syndrome (with Dr Kyoshi, ETSP, and others)

Dravet syndrome (DS) is a severe form of epilepsy that typically begins in early childhood and is considered an epileptic encephalopathy. It was first described by Charlotte Dravet in 1978 as severe myoclonic epilepsy in infancy, and later recognized as a distinct syndrome by the International League Against Epilepsy in 1989. DS is a rare genetic disorder with an estimated incidence ranging from 1 in 16,000 to 1 in 40,000 individuals.

The initial symptom of DS is typically a convulsive seizure that occurs between 1 and 18 months of age, with the majority of cases occurring between 4 and 8 months. These seizures are often fever-induced, prolonged, and generalized or hemiclonic in nature. The presence of alternating unilateral seizures helps to differentiate DS from focal epilepsy. In the early stages of the disease, electroencephalography (EEG) and magnetic resonance imaging (MRI) studies often appear normal. As the disease progresses, children between the ages of 1 and 5 years develop pharmaco-resistant seizures of various types, including focal seizures, atypical absences, myoclonic seizures, and atonic seizures. Although the duration of the seizures may become shorter over time, their frequency tends to increase. [1,2,3,4,5]

Over time, the interictal electroencephalography (EEG) of individuals with Dravet syndrome (DS) typically shows a progression towards background slowing and the presence of focal or generalized epileptiform discharges. In older children and adults, neuroimaging studies may reveal signs of generalized brain atrophy or focal abnormalities, such as hippocampal sclerosis [6]. In addition to drug-resistant epilepsy, individuals diagnosed with DS commonly experience comorbidities such as intellectual disability, behavioral issues, language impairments, sleep disorders, and gait abnormalities [7,8,9]. While adults with DS may have less frequent seizures,

often occurring predominantly during nighttime, their overall quality of life is significantly impacted.

The majority of Dravet syndrome cases, around 80-90%, are attributed to de novo mutations in the SCN1A gene, which encodes the voltage-gated sodium channel Nav1.1. These mutations lead to haploinsufficiency of Nav1.1, the alpha-1 subunit of the sodium channel. However, mutations in other genes, such as GABRA1, STXBP1, SCN9A, SCN1B, GABRG2, HCN1, and CHD2, have also been identified in some cases [10,11]. It is important to note that not all SCN1A mutations result in Dravet syndrome; certain variants have been associated with familial febrile seizures (FS), genetic epilepsy with febrile seizures plus (GEFS+), epilepsy of infancy with migrating focal seizures (EIMFS), or familial hemiplegic migraine type 3 (FHM3) [12,13,14].

A genotype-phenotype model developed by Brunklaus et al. provides a means of predicting the likelihood of developing Dravet syndrome versus GEFS+ in individuals with SCN1A mutations [15]. This model takes into account factors such as age at seizure onset and utilizes a newly developed SCN1A genetic score. By employing this model, early identification of patients who are at risk of developing Dravet syndrome or GEFS+ can be achieved, enabling targeted precision therapies and facilitating appropriate family counseling.

The emergence of genetic testing presents new opportunities for facilitating early diagnosis, which can contribute to improved developmental outcomes in individuals with Dravet syndrome (DS) [16,17]. However, despite the increasing accessibility of genetic testing and the potential for early diagnosis, DS remains one of the most challenging forms of epilepsy to manage, often resulting in poor neurodevelopmental outcomes. The impact of DS extends beyond the individual affected, as it places significant social and financial burdens on caregivers and

healthcare systems. Furthermore, DS is associated with an elevated risk of premature mortality, primarily due to complications arising from status epilepticus and sudden unexpected death in epilepsy (SUDEP) [18,19]. KRM-II-81 showed promising results on mouse model of Dravet syndrome.

3.3.1.5a. Effects of KRM-II-081 on inhibitory neurotransmission

KRM-II-81 had an impact on the decay time of miniature inhibitory postsynaptic currents (mIPSCs) rather than their amplitude. Specifically, mIPSCs with longer decay times were more significantly affected by KRM-II-81, suggesting a preference for targeting α2/3 subunits expressed in distal regions such as dendrites or axons, rather than the cell soma (**Figure 15**).

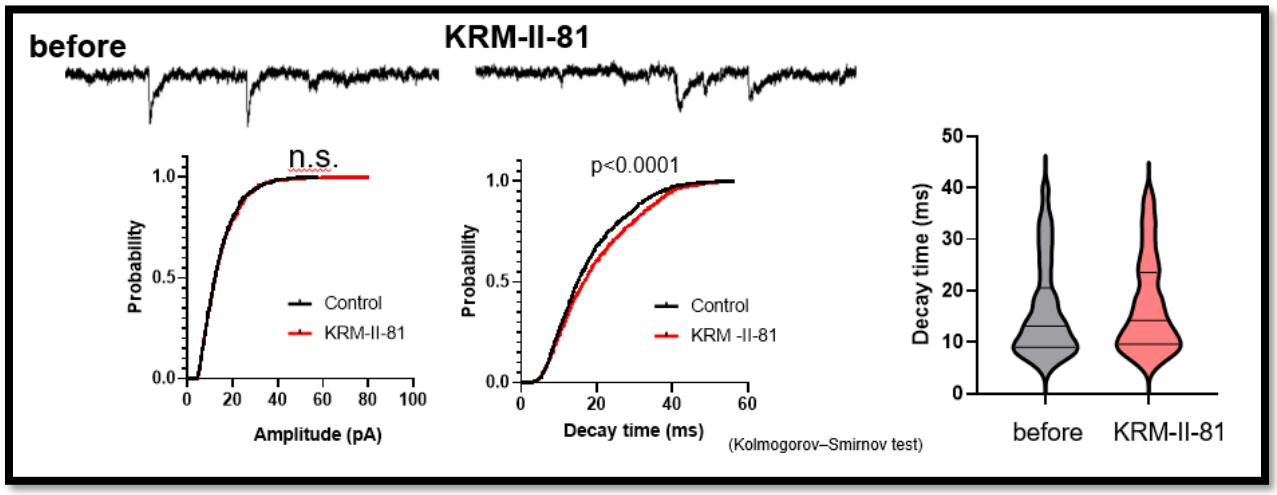


Figure 15. Miniature IPSCs. Voltage-clamp whole-cell patch clamp recordings were performed on CA1 pyramidal neurons in acute slices obtained from wild-type (WT) mice. mIPSCs with longer decay times were more significantly affected by KRM-II-81. (Unpublished data)

3.3.1.4b. Effects of KRM-II-081 on hyperthermia-induced seizure in DS mice

The acute administration of KRM-II-081 showed a protective effect against hyperthermia-induced seizures in mice with Dravet syndrome (DS). This finding suggests that KRM-II-081 has the potential to mitigate seizure susceptibility under conditions of increased body temperature, which is known to trigger seizures in individuals with DS. The protective effect observed in this study highlights the therapeutic potential of KRM-II-081 as a potential treatment option for managing seizures in DS, particularly in situations where hyperthermia is a contributing factor. Further research and investigation are needed to fully understand the underlying mechanisms and to assess the long-term efficacy and safety of KRM-II-081 in treating hyperthermia-induced seizures in individuals with DS.

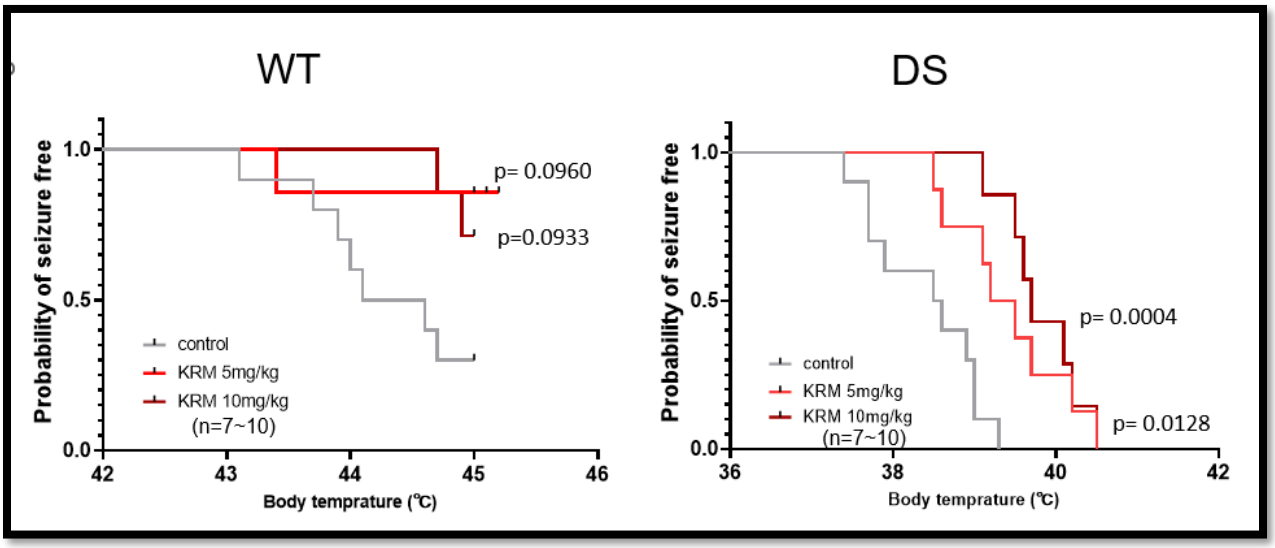


Figure 16. Effects of KRM-II-081 on hyperthermia-induced seizure in DS mice. Acute administration of KRM-II-081 demonstrated protective effect against hyperthermia-induced seizure in DS mice. (Unpublished data)

3.3.1.4c. Effects of chronic administration of KRM-II-081 on DS mice

In a chronic administration study, where KRM-II-081 was administered at a dose of 10mg/kg once per day, there was no observed improvement in the mortality rate in individuals with Dravet syndrome (DS) (**Figure 17**). This suggests that the chosen dosing regimen and dosage of KRM-II-081 did not effectively impact the overall survival of DS patients. Furthermore, the study found that increasing the frequency of administration to twice per day or implementing continuous infusion of KRM-II-081 was deemed unfeasible or impractical. These findings indicate that alternative dosing strategies or higher doses of KRM-II-081 may need to be explored in order to evaluate their potential efficacy in improving mortality rates in DS.

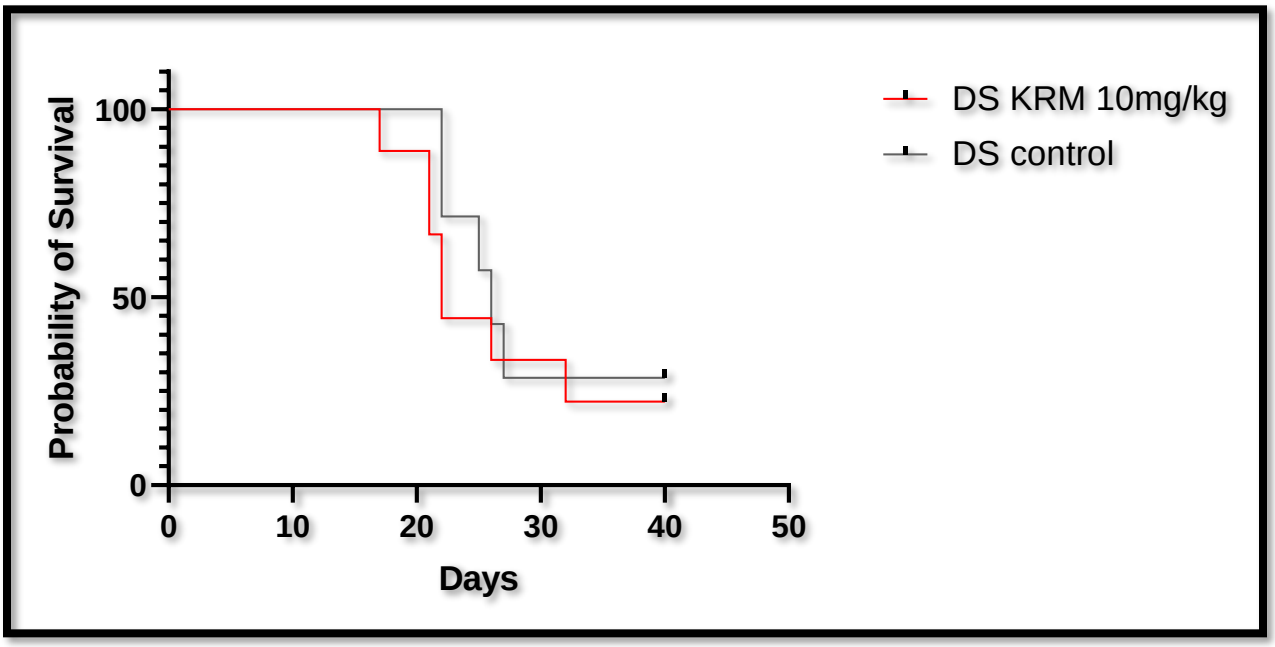


Figure 17. Chromic administration of KRM-II-081 (10mg/kg, once per day) did not improve mortality rate in DS. (Unpublished data)

3.3.1.4d. Effects of KRM-II-081 on DS mice by ETSP

The genetic mouse model of Dravet Syndrome is used to screen compounds for the ability to elevate the temperature threshold that initiates hyperthermia-induced seizures. **Table 6** shows each individual animal's (i) post-injection baseline temperature taken at time-of-peak effect (TPE) after drug or vehicle administration and just prior to turning on the heat lamp; and (ii) end temperature, i.e., temperature at first seizure. If the animal did not have a seizure during the testing period, the end temperature will read as 42.5°C, the experimental upper limit of temperature for hyperthermia induction, and it will be noted that there was no seizure during testing. Observed adverse events are also described in the tolerability column in **Table 6**.

Figure 18 shows a survival curve representing the percentage of animals that are not seizing as the core body temperature is increased. **Table 7** shows the median (± standard deviation; SD) temperature when seizures are induced and compares the vehicle group to the drug-administered group. The ability of the investigational compound to protect from seizures at temperatures below and at the endpoint temperature of 42.5°C is shown in **Table 8**.

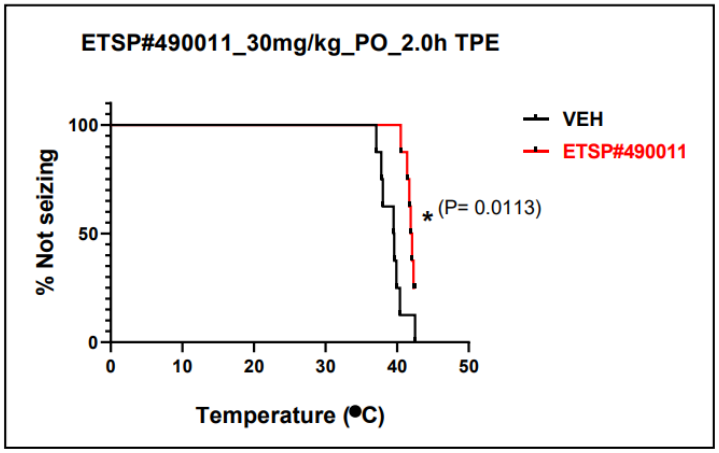


Figure 18. Survival curve evaluating percentage of animals not seizing as core temperature increases. There was a significant difference (Log-rank (Mantel-Cox) (P= 0.0113) between the vehicle and drug groups. (Unpublished data)

Table 7: Baseline and End Temperatures for ETSP #490011 tested at 30mg/kg for 2.0 hours in the Dravet Hyperthermia Assay

Note: The average (mean) post-injection baseline temperature of the Dravet syndrome mouse model following injection of either vehicle or ETSP#490011 (KRM-II-81) used in this study is = 33.78OC (vehicle) and 32.31OC (ETSP#490011)

Dose tested: 30mg/kg

Timepoint tested: 2.0h

Group	Animal #[a]	Post-injection baseline temperature[b]	End temperature	Seizure during testing	Tolerability Comments[c]
vehicle	2 (M)	34.9°C	39.9°C	Y	
vehicle	3 (M)	35.0°C	39.6°C	Y	
vehicle	4 (F)	35.6°C	42.5°C	Y	
vehicle	5 (F)	32.5°C	37.1°C	Y	
vehicle	8 (F)	33.7°C	40.4°C	Y	
vehicle	11 (F)	31.8°C	39.5°C	Y	
vehicle	13 (F)	31.7°C	37.8°C	Y	
vehicle	14 (F)	35.0°C	38.0°C	Y	
ETSP#490011	1 (M)	31.0°C	42.5°C	N	
ETSP#490011	6 (F)	33.3°C	42.5°C	N	
ETSP#490011	7 (F)	31.2°C	41.9°C	Y	19 (lethargic post-dosing)
ETSP#490011	9 (F)	32.8°C	42.3°C	Y	
ETSP#490011	10 (F)	32.9°C	41.7°C	Y	
ETSP#490011	12 (F)	32.1°C	42.1°C	Y	
ETSP#490011	15 (F)	33.0°C	40.5°C	Y	
ETSP#490011	16 (F)	32.2°C	41.4°C	Y	

[a] Animal number refers to numbers obtained from GraphPad QuickCalcs random number generator.

[b] There was no significant difference (unpaired two tailed t-test) (P= 0.0999) between the postinjection baseline temperatures for the drug and vehicle groups.

[c] Tolerability describes signs of adverse events observed during the testing period.

(Unpublished data)

Table 8. Ability of ETSP #490011 to Elevate the Temperature Threshold of Induced Seizures

Compound	Dose (mg/kg)	Timepoint[a]	Induced Seizure Temperature Threshold (°C) Median ± SD	Significance Log-rank (Mantel-Cox)
Vehicle	--	2.0h	39.55 ± 1.720	P = 0.0113
ETSP #490011	30mg/kg	2.0h	42.00 ± 0.6718	

[a] Timepoint when testing begins post drug administration.

(Unpublished data)

Table 9. Ability of ETSP#490011 to Prevent Hyperthermia-Induced Seizures

Compound	Dose (mg/kg)	Timepoint[a]	Induced Seizure Temperature Threshold (°C) Median ± SD	Significance Log-rank (Mantel-Cox)
Vehicle	--	2.0h	39.55 ± 1.720	P = 0.0113
ETSP #490011	30mg/kg	2.0h	42.00 ± 0.6718	

[b] Seizure protection is shown as number of animals protected from hyperthermia-induced seizures /number of animals tested in the group.

[a] There was no significant difference (Fisher's exact test) (P= 0.4771) in seizure protection when comparing the drug and vehicle groups.

(Unpublished data)

3.3.2. Biological studies of DS-II-73

3.3.2.1. Receptor binding studies of DS-II-73 (5) (PDSP, Dr Bryan Roth)

The receptor binding profile of DS-II-73 (**16**) was evaluated by ligand binding inhibition studies using a concentration of 10 mM DS-II-73. The binding was characterized by interaction with the benzodiazepine binding site (BZP), the adrenergic a2B binding site, kappa opioid receptors (KORs), and peripheral benzodiazepine receptor binding sites (PBR) (**Table 9**). There was no inhibition at the other binding sites assessed that was > 50% including a marker for cardiotoxicity (HERG) where DS-II-73 was tested up to 100 mM. K_i values for binding are shown in **Table 9**. The selectivity of interaction with the benzodiazepine (BZP) binding site was shown by the higher binding affinity of DS-II-73 for the BZP site than for the other binding sites with selectivity values of 2-14 observed (**Table 10**). Binding at all other 37 screened sites showed < 50% inhibition at the 10 mM concentration of **16** (DS-II-73).

Table 10. Primary and secondary binding data for DS-II-73 (Unpublished data)

Receptor	Primary (mean % inhibition)	Secondary (K_i in nM)	Fold Selectivity
BZP	93.4	150 ± 31.8	NA
PBR	93.4	331 ± 294	2.2
a2B	79.5	834 ± 341	5.6
KOR	61.6	2102 ± 203	14

Secondary binding was determined only for primary binding sites for which > 50% inhibition was achieved at the screening concentration of 10 mM. Only these sites are reported in the table. The secondary binding data are the means ± S.D. of 3 determinations except for KOR (n=2).

a2B: noradrenergic receptor binding site assessed by inhibition of [3H]-rauwolscine binding in rat brain homogenates

BZP: Benzodiazepine binding site assessed by inhibition of [3H]-flunitrazepam binding in rat brain

homogenates.

KOR: Kappa opioid receptor was assessed by inhibition of [3H]-U69593 binding in rat brain homogenates.

PBR: Peripheral benzodiazepine receptor sites were assessed by inhibition of [3H]-PK11195 in rat brain homogenates

3.3.2.2. Cytotoxicity study of DS-II-73 (16) (with Dr Arnold, Molly Elizabeth, and others)

Cytotoxicity of DS-II-73 was studied in cells where the LD_{50} was > 240 mM. In contrast, 3-dibutylamino-1-(4- hexyl-phenyl)-propan-1-one (150 μM in DMSO), used as a positive control, was toxic in these cell systems at 150 μM. The solvent, DMSO, was not cytotoxic.

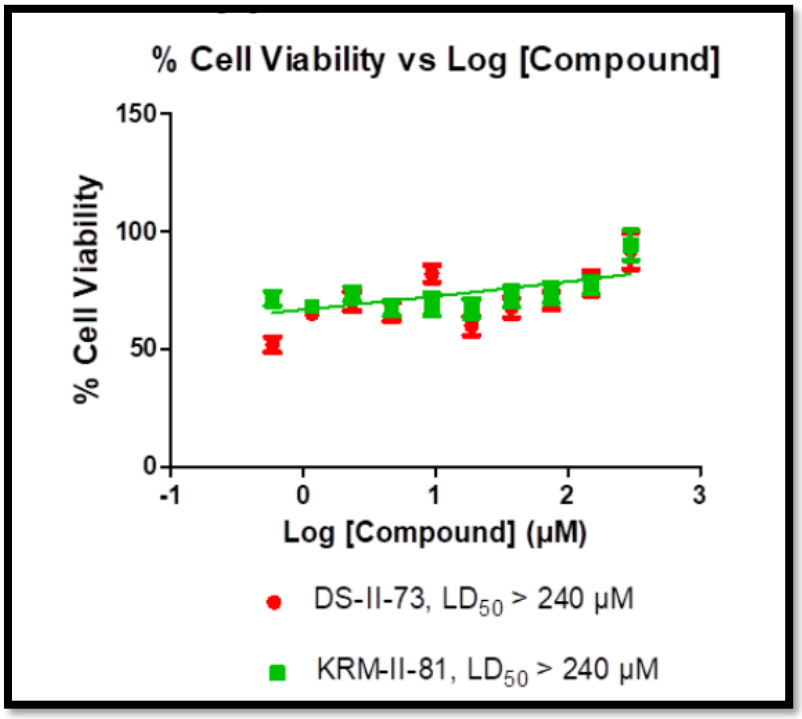


Figure 19. Cytotoxicity data of DS-II-73 (Unpublished data)

4.3.2.3. Sub-type selectivity of DS-II-73 (16) (with Dr Petra, and others)

The selectivity of DS-II-73 for GABAARs configured with specific alpha subtypes was determined in engineered cell lines expressing each subtype. DS-II-73 displayed selectivity for α2/3/5-containing GABAARs over α1-containing GABAARs (**Figure 20**). The binding parameters for cerebellar binding and for each cell line are shown in **Table 11**. DS-II-73 displayed IC50 values for inhibition of [3H]-flunitrazepam binding with cerebellum (225 nM) > α2 (320 nM) > α3 (381 nM) > α5 (616 nM), in order of potency.

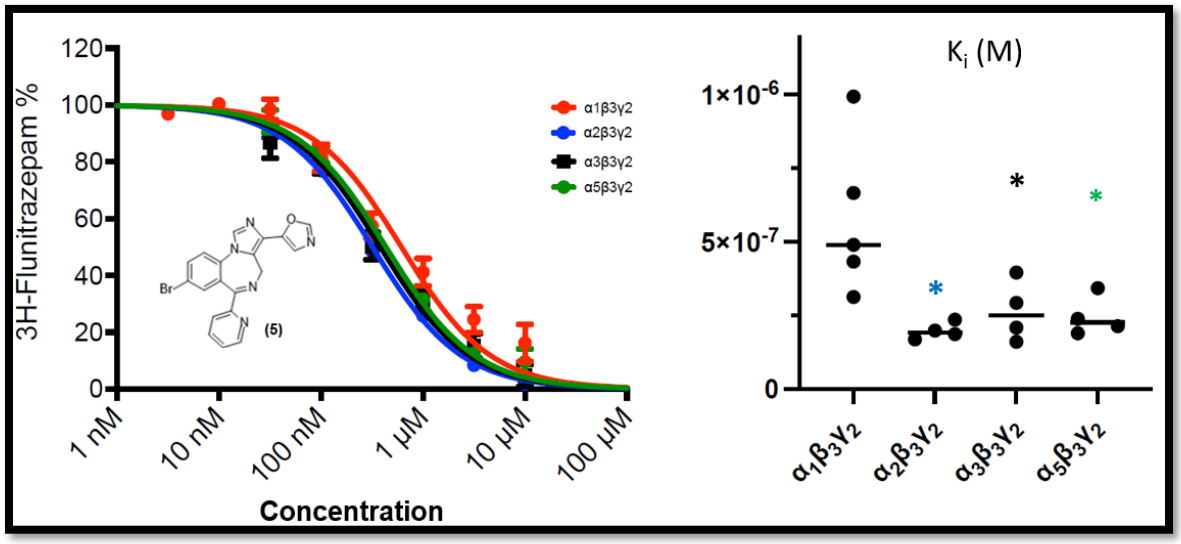


Figure 20. Selectivity of DS-II-73 for α2/3/5-containing GABAARs over that of α1-containing GABAARs. Data are means + S.E.M. for N = 5 (a1) or N = 4 (other cell lines). *P < 0.05 by Dunnett's post-hoc test. (Unpublished data)

Table 11. Binding concentration-inhibition functions for DS-II-73 (**16**)

	Cerebellum	α1β3γ2	α2β3γ2	α3β3γ2
Bottom	= 0.000	= 0.000	= 0.000	= 0.000
Top	= 100.0	= 100.0	= 100.0	= 100.0
LogIC50	-6.648	-6.211	-6.495	-6.419
HillSlope	= -1.000	= -1.000	= -1.000	= -1.000
IC50	2.249e-007	6.158e-007	3.201e-007	3.809e-007

Concentrations are molar **(Unpublished data)**

3.3.2.4. Oral dosing pharmacokinetics of DS-II-73 (16) (with Dr Savic, Brianka, and others)

In order to determine the oral exposures that can be achieved by DS-II-73 (5), a study was conducted in rats after oral dosing with 2 mg/kg. Oral exposure in both plasma and brain was relatively rapid with peak levels achieved at 60 min. Relatively long durations of exposure in both compartments were observed (**Figure 21**). The brain/plasma ratio for DS-II-73 was 0.52 based on areas under the curve (AUC) over 24 h**.**

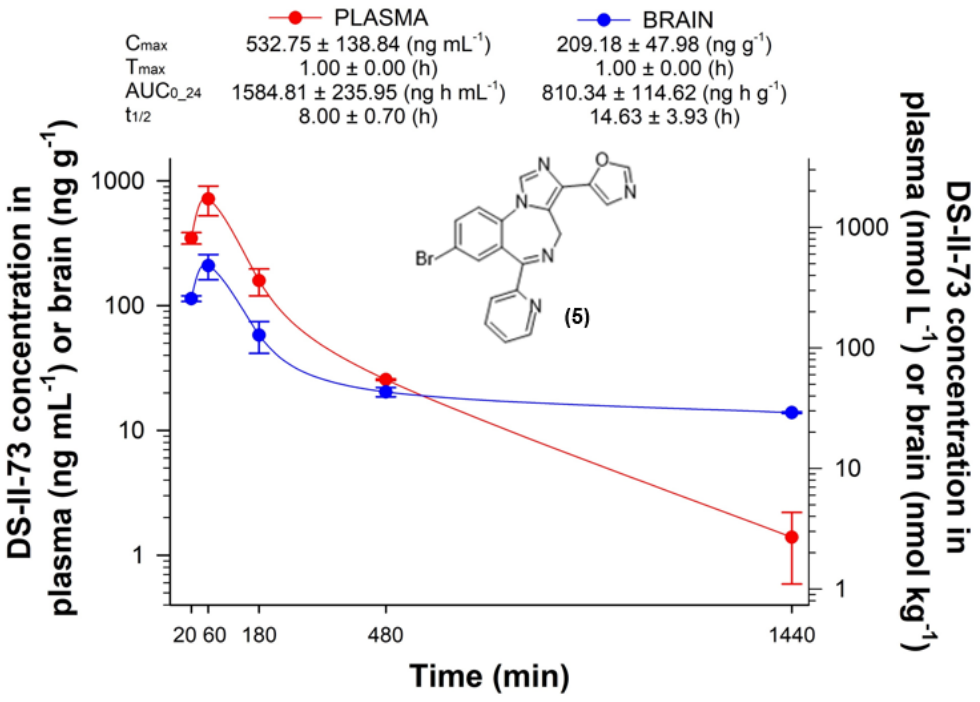


Figure 21. Concentrations of DS-II-73 in plasma and brain of rats after oral dosing of 2 mg/kg. Each point represents the mean + S.E.M. of 3 rats. Left Axis: ng/mL or ng/g; Right

Axis: nmol/L or nmol/Kg. AUC: area under the curve for concentration from 0-24 h; Cmax: maximum concentration achieved; T_{max}: time of maximum concentration; $T_{1/2}$: half life. (Unpublished data)

3.3.2.5. Anti-seizure effects of DS-II-73 (with Dr Witkin, Xingjie Ping, and others)

The oral bioavailability of DS-II-73 encouraged investigation of the anti-seizure effects of the compound after oral dosing. In this study, the GABAAR convulsant, pentylenetetrazol (PTZ, 70 mg/kg, s.c.) produced clonic and tonic seizures in and lethality in mice. DS-II-73 (10 mg/kg, p.o.), given 60 min prior to PTZ, significantly protected mice against tonic seizures and lethality but not against clonus (**Table 12**). DS-II-73 also significantly increased the latency to produce both clonic and tonic convulsions (**Figure 22**).

Table 12. Effects of DS-II-73 (16) against PTZ-induced seizures and lethality after oral administration in mice.

Treatment	Clonic seizures	Tonic seizures	Lethality
Vehicle	6/6 (100%)	6/6 (100%)	4/6 (67%)
DS-II-73	9/11 (82%)	3/11 (27%)**	0/11 (0%)**

P <0.01 by Fisher's Exact probability test. **(Unpublished data)

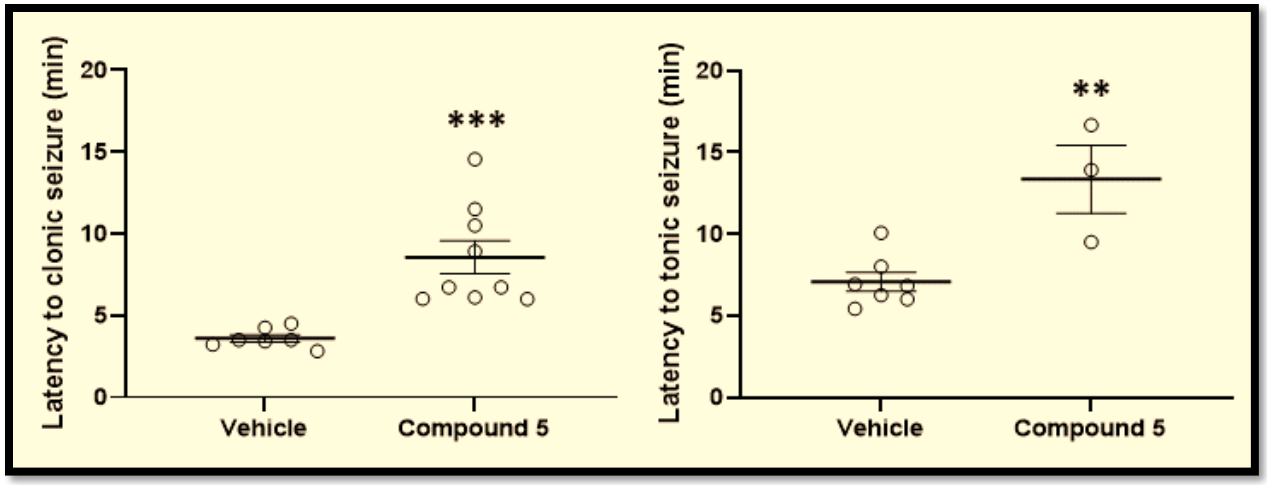


Figure 22. Effects of DS-II-73 (5) on PTZ-induced seizure latencies. Data were evaluated by un-paired Student's t-test. ** P < 0.01; *** P < 0.001. (Unpublished data)

Cortical tissue freshly transected from a pharmacoresistant epilepsy patient was studied for its electrical properties across a 60-microelectrode array. In this study, DS-II-73 applied by bath application at 30 mM, produced nearly complete suppression of activity in the slice. When DS-II-73 was removed from the tissue batch (washout), a return to activity was observed (**Figure 23**). This result was replicated in a second tissue slice from this patient although DS-II-73 suppressed activity less than in the first tissue slice. As with the first slice, washout of DS-II-73 from the tissue bath resulted in a return to baseline activity levels.

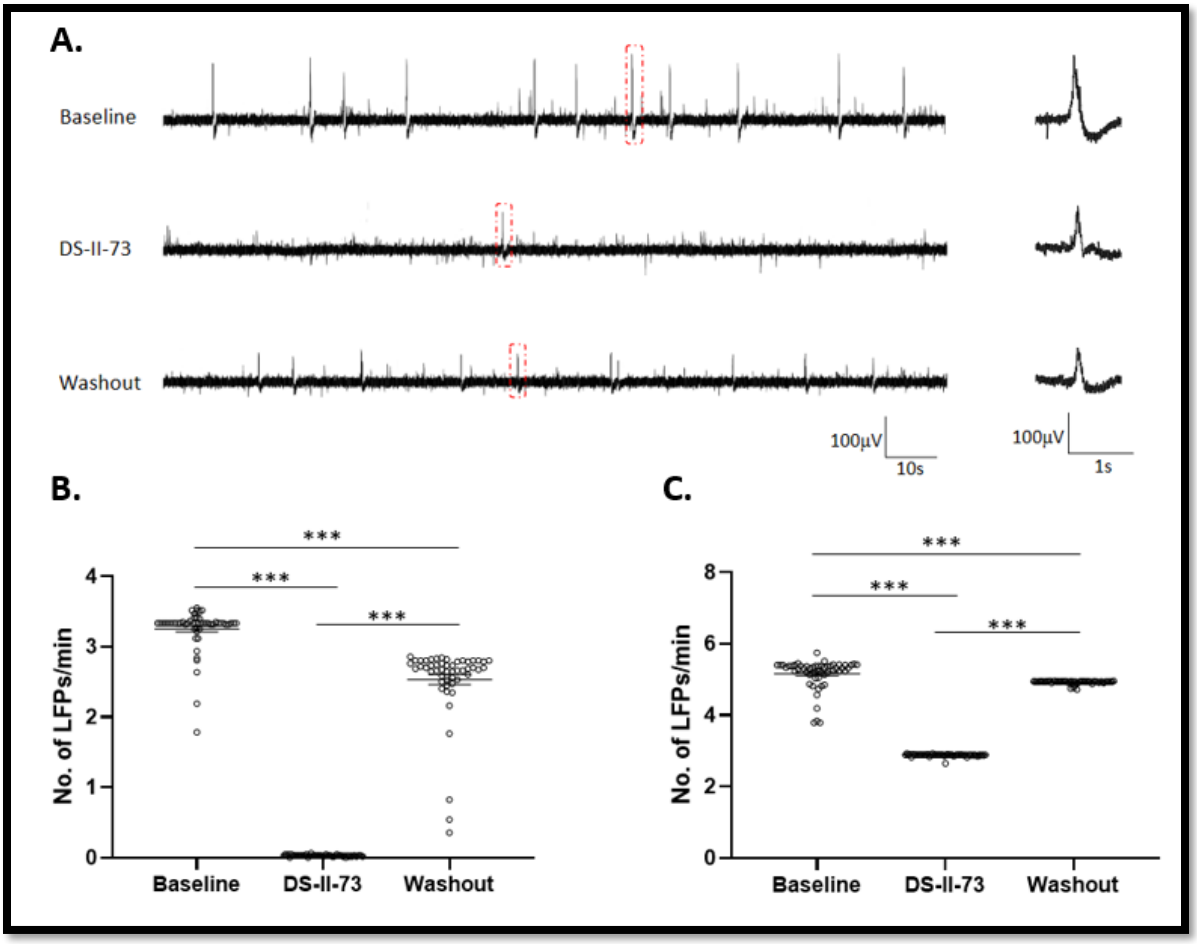


Figure 23. Effects of DS-II-73 on electrical activity in a slice from freshly transected cortical tissue from a patient with pharmacoresistant epilepsy. A. Representative tracings showing the local field potentials (LFPs) on 10 s and 1 s time scale. B. Quantification of the LFP frequency across the 60 m periods of Baseline, DS-II-73 application, and washout. C. Data as per Panel B. with a second independent tissue slice from the same patient. ***, $p < 0.001$, Kruskal-Wallis test followed by Dunn's multiple comparisons test. (Unpublished data)

3.2.3.6. Rotarod assay of DS-II-73 (with Dr Arnold, Michelle Meyer, and others)

Effects of DS-II-73 on sensorimotor performance of mice after oral dosing was assessed on a rotating rod and compared to that of diazepam. Diazepam significantly reduced rotorod performances of mice compared to vehicle controls. Effects of DS-II-73 differentiated significantly from effects of diazepam at all doses tested (**Figure 24**).

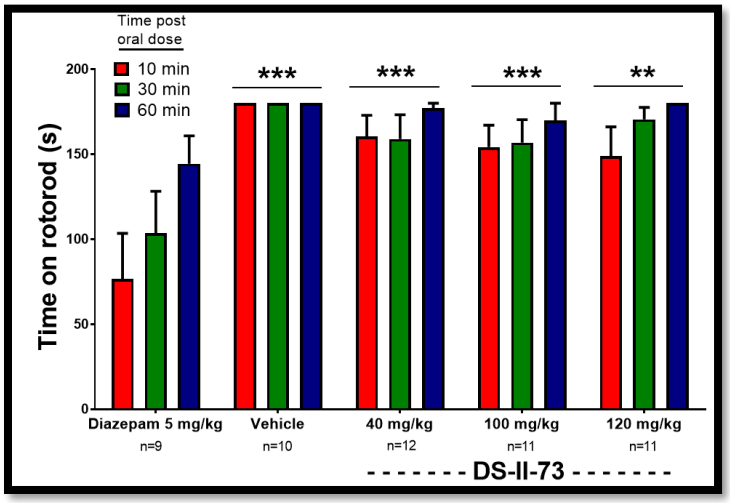


Figure 24. Comparative effects of diazepam and DS-II-73 on rotorod performance of mice. *** P < 0.001 compared to diazepam; ** P < 0.01 compared to diazepam by Tukey's multiple comparison test after ANOVA. The overall effect of treatment was significant ($F_{4,144}$ = 12.6, P < 0.0001) as was the effect of time ($F_{2,144}$ = 5.42, P <0.01). There was not a significant treatment x time interction ($F_{8,144}$ = 1.00, P = 0.44). (Unpublished data)

3.2.3.7. Molecular docking studies of DS-II-73 (16)

Molecular docking studies of DS-II-73 with the α1β3γ2L GABAAR 6HUO were conducted. Results of these in silico studies demonstrated reduced binding of DS-II-73 (5) to a1His102 (**Figures 25, 26**) as shown by the relative distances of the compounds from the ethynyl of **1** or the Br atom of **5** to the His102 residue of the α1 subunit. These data were confirmed by the

docking score values for these two compounds (**Figure 26**) where they were calculated to differ by 0.5.

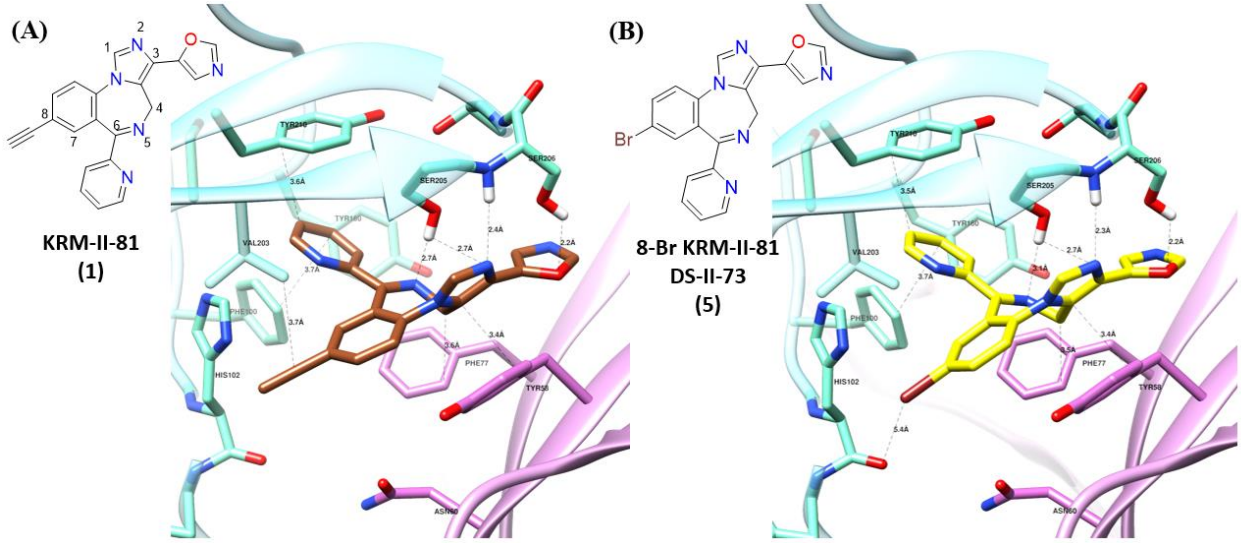


Figure 25. KRM-II-81 (1) vs. DS-II-73 (5) at the $\alpha^{+}\gamma^{-}$ interface of GABAAR. A. KR-II-81 (1) (brown) in complex with α1 (aquamarine) and γ2 (orchid) subunits of α1β3γ2L $GABA_A$ receptor 6HUO. B. Docked DS-II-73 (5) (yellow) in complex with α1 (aquamarine) and γ2 (orchid) subunits of α1β3γ2L $GABA_A$ receptor 6HUO. Dashed lines indicate π–π interactions, hydrogen bonds and halogen bonds.

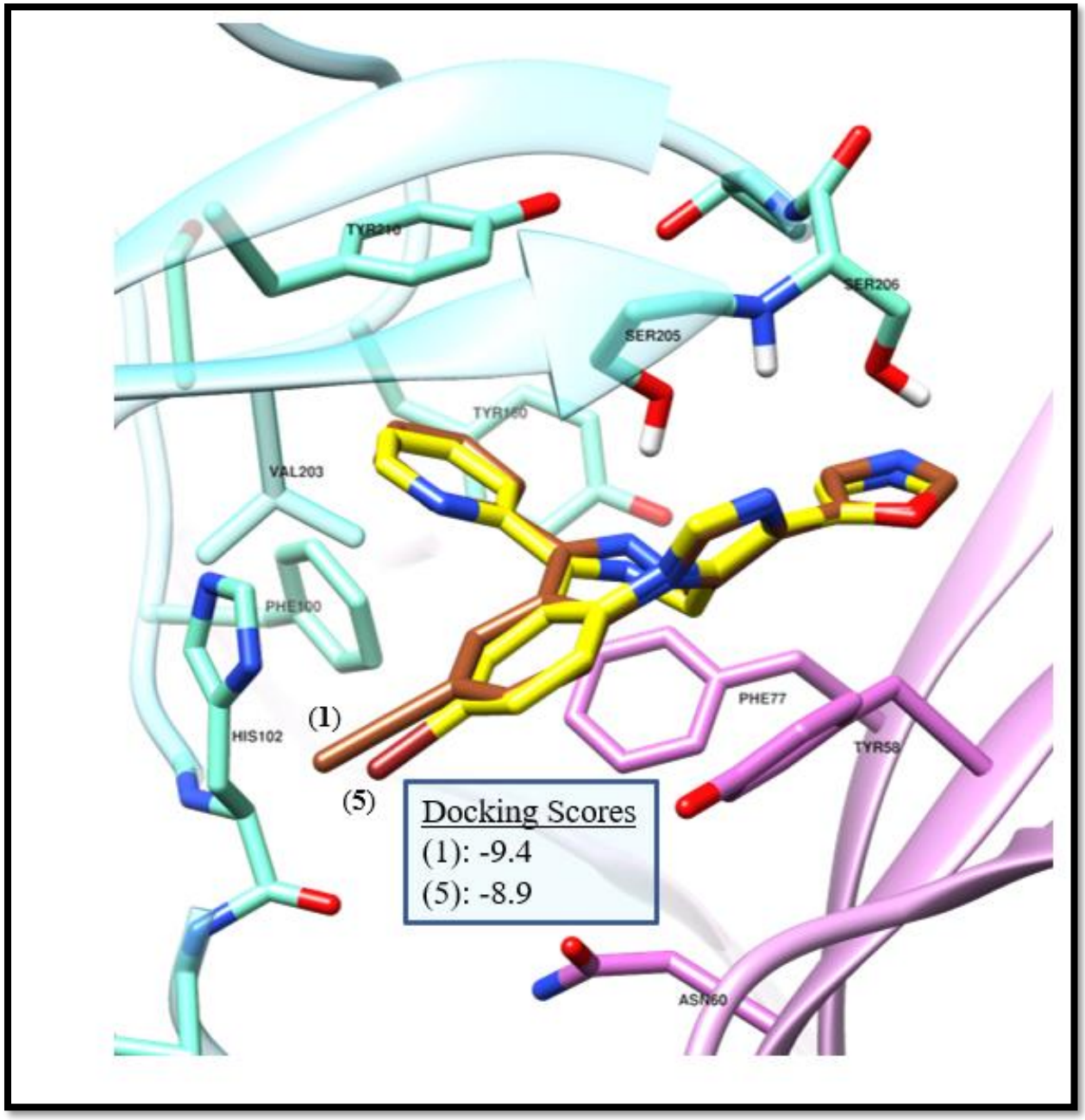


Figure 26. Overlay of KRM-II-81 (1) vs. DS-II-73 (5) at the $\alpha^{+}\gamma^{-}$ interface of $GABA_AR$.

Other details are described as in **Figure 25**.

3.3.3. Biological studies of MP-III-024 (18)

3.3.3.1. Exploring the Tremor-Reducing Effects of MP-III-024 and Its Impact on Locomotor Activity (with Dr Kuter, Barbara, and others)[159]

In this study, the aim was to investigate the potential of the GABA-A α2/3 subunit specific positive allosteric modulator (PAM) MP-III-024 in reducing tremors associated with Essential Tremor (ET). To assess its effects, the experiments were conducted involving harmaline-induced tremors and locomotor activity in rats. Administering harmaline at a dose of 15 mg/kg induced generalized tremors in the rats, leading to a significant increase in the AP2 parameter (power in the frequency range of 8–15 Hz) (**Figure 28B**) and the tremor index (**Figure 28C**) when compared to the control group. These changes persisted throughout the entire 60-minute tremor measurement period.

Additionally, harmaline affected the locomotor activity of rats, as evidenced by a decrease in the total distance traveled in the first 30 minutes, followed by an increase in walking activity between 30 and 60 minutes post-administration, in comparison to the control rats (**Figure 28E**). Moreover, within the first 30 minutes of measurement, harmaline reduced AP1 (power within the 0–8 Hz frequency band) (**Figure 28D**). The duration of the experiment was set at 60 minutes post-harmaline injection to observe the longevity of the effects (**Figure 27**) .

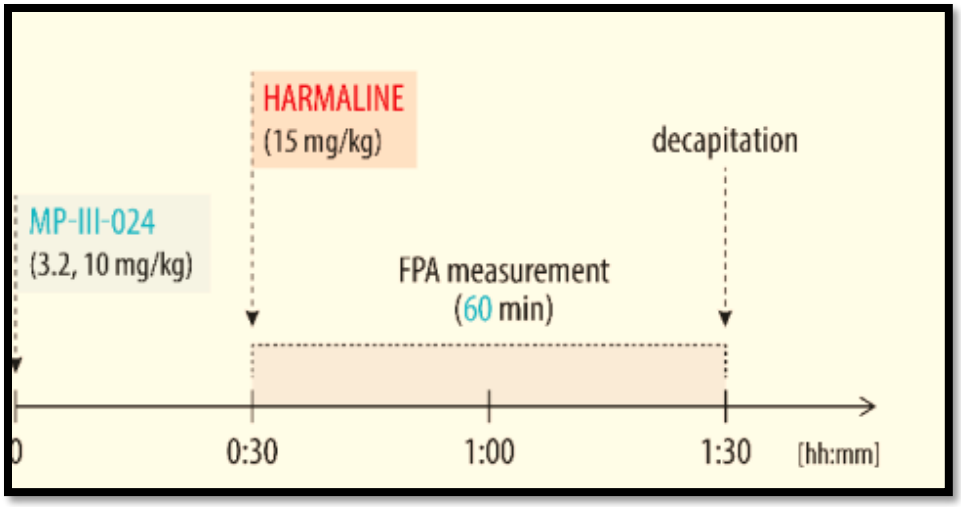


Figure 27. Timelines of drug administration and harmaline-induced tremor measurement

MP-III-024, a positive allosteric modulator targeting α2/3 subunit-containing GABA-A receptors, exhibited no significant effect on AP2 and distance parameters when administered alone. However, a noteworthy trend was observed, indicating a potential decrease in the tremor index at both doses compared to the solvent control. Moreover, MP-III-024 demonstrated an increase in animal mobility. The lower dose (3.2 mg/kg) led to an extension of the total distance traveled by the animals during the initial 30 minutes of measurement, coinciding with an elevation in the AP1 parameter during the same period. Additionally, the higher dose (10 mg/kg) also resulted in an increase in the AP1 parameter compared to the solvent control (**Figure 28D**).

MP-III-024, administered at both doses of 3.2 mg/kg and 10 mg/kg, exhibited significant tremor-reducing effects in response to harmaline administration, as evident from the power spectrum and AP2 graphs (Figure 2B). At the higher dose, MP-III-024's anti-tremor effect was somewhat weaker, impacting AP2 without significant changes in the tremor index parameter, and this effect persisted throughout the 60-minute measurement period. Conversely, at the lower dose, the effect was more pronounced, leading to reductions in both AP2 and the tremor index, but it was limited to the first 30 minutes after administration.

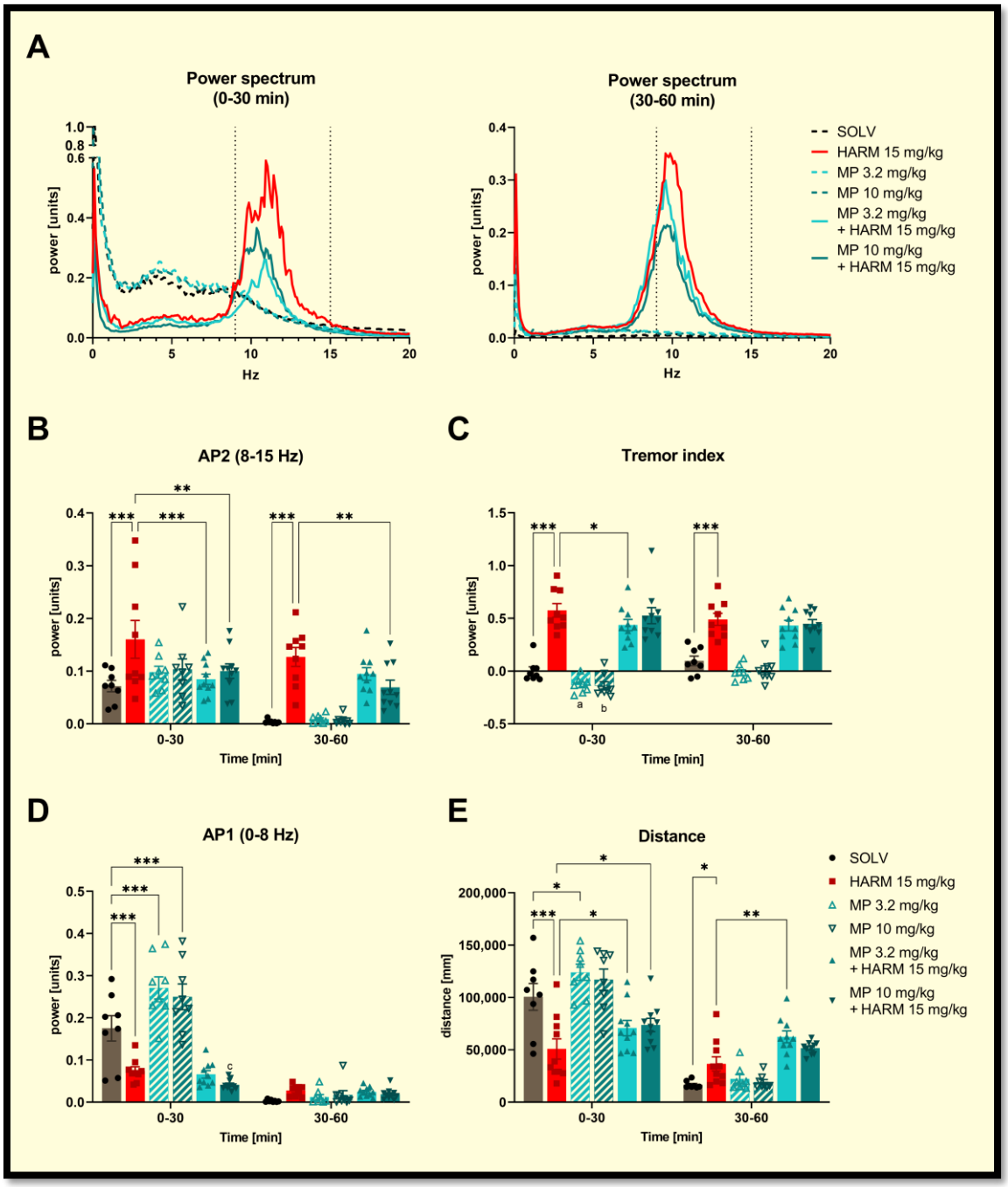


Figure 28. Effects of MP-III-024 at different doses (3.2 mg/kg and 10 mg/kg) on harmaline-induced tremors in rats. The graph (A) displays the power spectrum, averaged over two intervals (0-30 and 30-60 min) for all animals in each group within a frequency range of 0-20 Hz. The specific tremor parameters are represented as means ± SEM: (B) AP2, (C) tremor index, and (D) AP1, along with (E) locomotor activity (distance) of the rats. The

results show that both doses of MP-III-024 (3.2 mg/kg and 10 mg/kg) significantly reduced harmaline-induced tremors, as indicated by the effects on AP2 in graph (B). However, the anti-tremor effect of the higher dose (10 mg/kg) was comparatively weaker, as it only affected AP2 and did not show a significant impact on the tremor index parameter. Nonetheless, this effect lasted for the entire 60-minute measurement period. On the other hand, the lower dose (3.2 mg/kg) had a stronger and more observable effect on both AP2 and the tremor index but was limited to the initial 30 minutes after administration. Regarding locomotor activity (graph E), MP-III-024 at both doses increased the distance parameter compared to animals treated with harmaline alone. The effect was observed in the first 30 minutes after administration for the 3.2 mg/kg dose and throughout the 60-minute measurement period for the 10 mg/kg dose. The statistical analysis was performed using ANOVA for repeated measures, taking into account the effects of harmaline and MP-III-024 on AP2, tremor index, AP1, and distance parameters, as well as the impact of time. LSD post-hoc tests were conducted, with * indicating $p \leq 0.05$, ** $p \leq 0.01$, and *** $p \leq 0.001$ significance levels. Additionally, 'a' represented $p = 0.077$, 'b' denoted $p = 0.060$ compared to SOLV, and 'c' indicated $p = 0.090$ compared to HARM 15 mg. The figure was modified from Barbara et al. 2023.

Furthermore, following harmaline treatment, both doses of MP-III-024 increased locomotor activity (distance parameter) compared to the animals treated with harmaline alone, with the effect lasting from 0 to 30 minutes for the 3.2 mg/kg dose and for the entire 60-minute measurement period for the 10 mg/kg dose (**Figure 28E**). Interestingly, the observed effects of MP-III-024 on harmaline-induced tremor did not show a clear dose-dependent relationship within the tested dose range.

3.3.3.2. Exploring the Inhibitory Effects of MP-III-024 on Pimozide-Induced TJMs

To investigate the efficacy of a GABA-A α2/3 subunit specific positive allosteric modulator (PAM) in reducing tremors in different types of tremor, pimozide was administered at a dose of 1 mg/kg once a day for 7 days. Pimozide treatment induced tremulous jaw movements (TJMs) in all animals. There were no notable differences in the effects of MP-III-024 when given alone compared to the solvent (SOLV) control group. However, both doses of MP-III-024 used (3.2 and 10 mg/kg) significantly inhibited pimozide-induced TJMs (**Figure 29**).

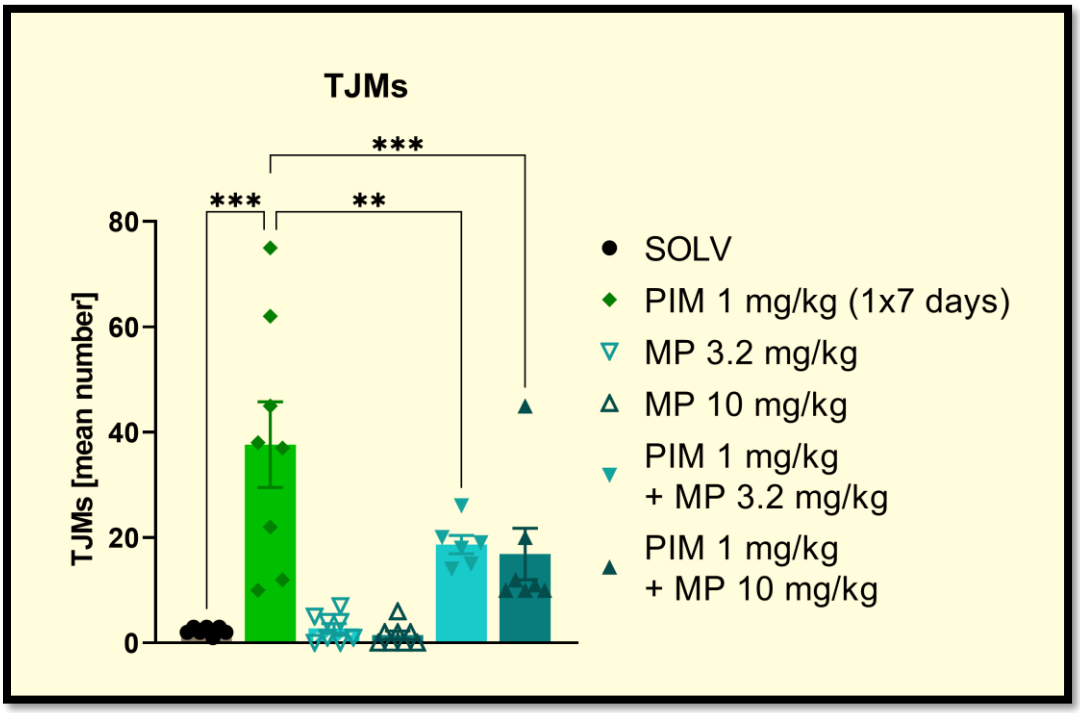


Figure 29. MP-III-024 (at doses of 3.2 mg/kg and 10 mg/kg) effectively reversed the pimozide-induced tremulous jaw movements (TJMs). The data are presented as the mean (± SEM) number of tremulous jaw movements per 10-minute observation period. The study included the following number of animals in each group: SOLV, n = 7; PIM 1 mg/kg, n = 8; MP 3.2 mg/kg, n = 8; MP 10 mg/kg, n = 8; PIM 1 mg/kg + MP 3.2 mg/kg, n = 6; PIM

1 mg/kg + MP 10 mg/kg, n = 7. Statistical analysis using Factorial ANOVA revealed significant effects of pimozide (PIM effect: $F[1,38] = 41.736$, $p = 0.001$) and MP-III-024 (MP effect: $F[2,38] = 3.919$, $p = 0.028$) on the number of TJMs. LSD post-hoc test further confirmed the significance of the results ($p \leq 0.01$, *** $p \leq 0.001$).**

3.3.3.3. Synergistic effects of morphine and MP-III-024 on Von Frey analgesia test and hot plate analgesia test [160]

In this study, a dose-addition analysis was employed to examine interactions between α2GABAA/α3GABAA receptors and opioids. The investigation focused on the combined effects of MP-III-024 and morphine in male CD1 mice, using two classical pain assays. To evaluate interactive effects on inflammatory pain, the zymosan A model of mechanical hyperalgesia was utilized. Additionally, the acute thermal antinociceptive effects of MP-III-024, morphine, and their combinations were evaluated using the hot plate procedure. A fixed-proportion design was employed to assess drug interactions, as it is recommended for studying drug interactions and has been previously used to investigate similar drug mixtures on similar endpoints**.**

Dose-effect curves for MP-III-024, morphine, and MP-III-024/morphine (**Figure 30**) combinations were constructed using a cumulative dosing procedure. After recording baseline latency measurements, mice received intraperitoneal injections of the lowest dose of either a drug or drug mixture. Antihyperalgesic or antinociceptive measurements were taken 30 minutes after the injection. Following each measurement, a subsequent injection was administered to increase the cumulative dose to the next 0.5 log unit, allowing for the generation of a dose-effect curve.

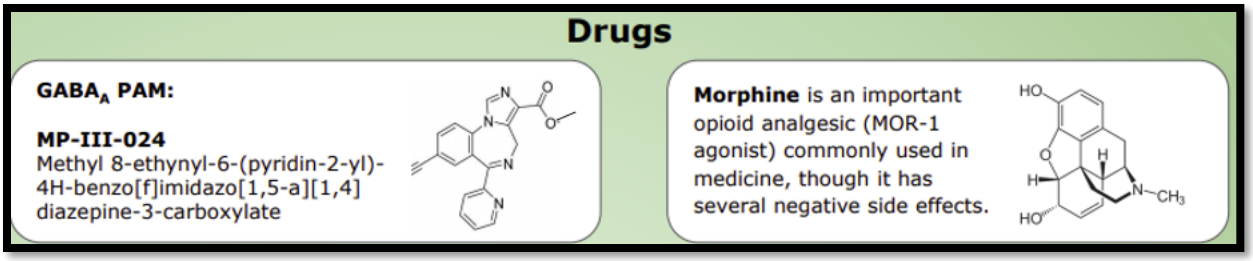


Figure 30. Structures of MP-III-024 and morphine

In this study, the dose of each drug, whether administered alone or in combination, required to produce a 50% Maximum Possible Effect (MPE) was determined using log-linear interpolation through linear regression. Individual ED50 (Effective Dose 50) values were converted to their log values for calculation of means and 95% confidence limits, and then converted back to linear values for presentation.

Interactions between MP-III-024 and morphine were assessed using both graphical and statistical approaches, following the methods described by Tallarida (2000) and Fischer et al. (2011). The graphical approach involved the use of isobolograms to differentiate between subadditive, additive, or supra-additive (synergistic) interactions. Isobolograms were constructed by connecting the ED_{50} of MP-III-024 when administered alone on the abscissa with the ED50 of morphine when administered alone on the ordinate, forming an additivity line. The additivity line represents dose pairs that produce an ED_{50} equal to the ED_{50} of MP-III-024 or morphine alone. Dose pairs falling below or to the left of the additivity line suggest an ED_{50} reached with lesser quantities of the drugs, indicating synergism. Conversely, experimental points representing dose pairs that fall above or to the right of the line suggest subadditivity.

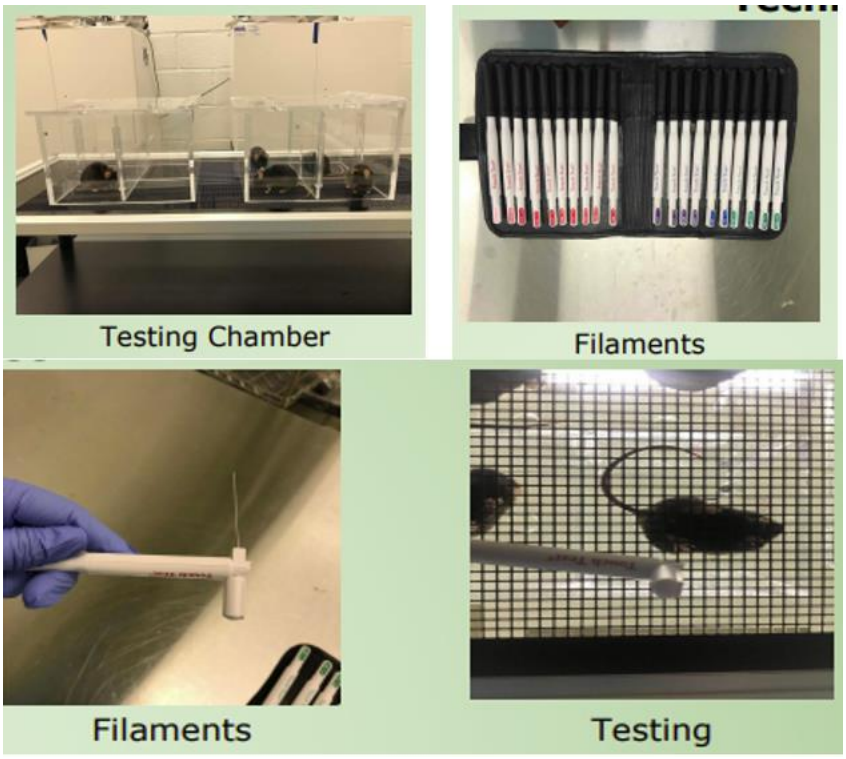


Figure 30. Von-Frey analgesia test

Figure 31. The dose-response curves for both morphine and MP-III-024 when administered individually in the von Frey mechanical hyperalgesia and thermal nociception procedures. In the mechanical hyperalgesia assay (panel A), injection of zymosan A into the right hind paw resulted in increased mechanical sensitivity compared to the non-injected left hind paw. The paw withdrawal thresholds of the non-injected paw were not affected by drug administration (data not shown). Each compound demonstrated dose- and time-dependent increases in mechanical sensitivity, expressed as %MPE (Maximum Possible Effect). The mean ED50 (Effective Dose 50) values for MP-III-024 and morphine were 9.96 (8.81–11.26) mg/kg and 10.72 (9.68–11.86) mg/kg, respectively. These potency values were used to determine the relative proportions of the compounds in subsequent studies that assessed MP-III-024/morphine mixtures. In panel B, the antinociceptive effects of MP-III-024 and

morphine in the thermal nociceptive assay are shown. Morphine induced dose-dependent increases in latency to respond on the hotplate, resulting in an ED50 value of 14.98 (14.39–15.60) mg/kg. On the other hand, MP-III-024 had no effect in this assay. Thus, the relative potencies determined in the von Frey procedure were also used to determine the proportions of the compounds in each MP-III-024/morphine mixture for subsequent combination studies in the hotplate test.

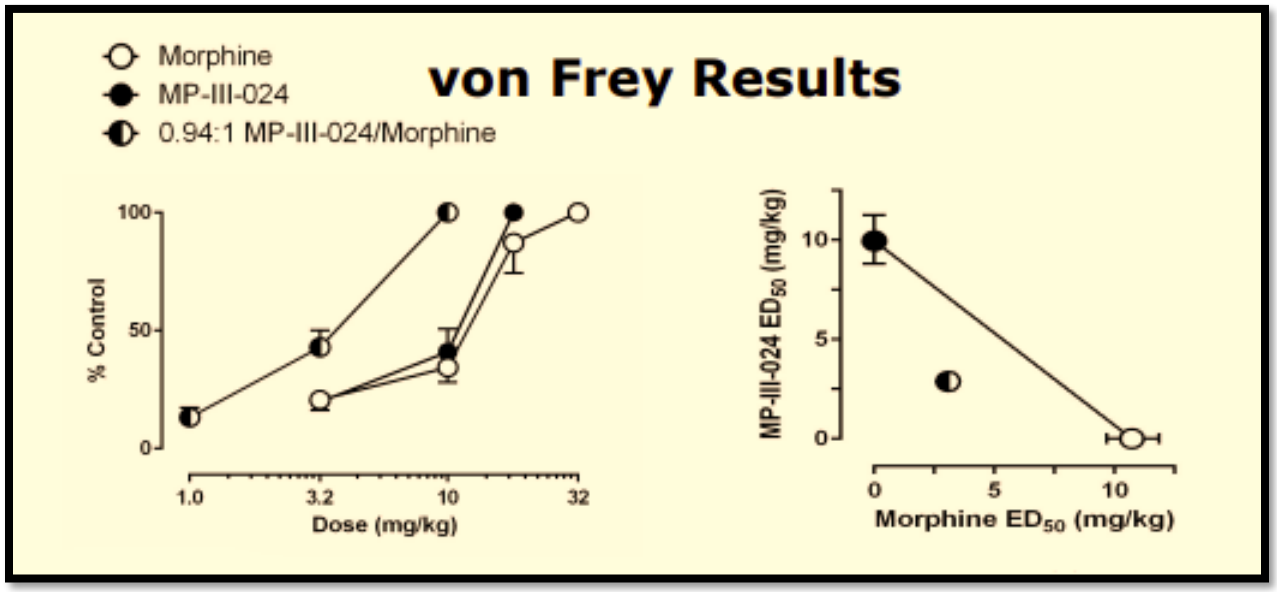


Figure 31. Dose-response curves for morphine alone, MP-III-024 alone and a 0.94:1 mixture of MP-III-024:morphine for both the von Frey. Figure is modified from Atiqur Rahman et al. 2021.

In **Figure 32**, the mechanical antihyperalgesic effects of morphine administered alone and in combination with MP-III-024 are shown. Each drug mixture demonstrated dose-dependent increases in antihyperalgesic %MPE. The addition of MP-III-024 resulted in concentration-dependent leftward shifts in the morphine dose-effect curve.

Similarly, the thermal antinociceptive effects of morphine administered alone and in combination with MP-III-024 are illustrated. In this procedure, each drug mixture exhibited dose-dependent increases in antinociception. Once again, the addition of MP-III-024 caused leftward shifts in the morphine dose-effect curve.

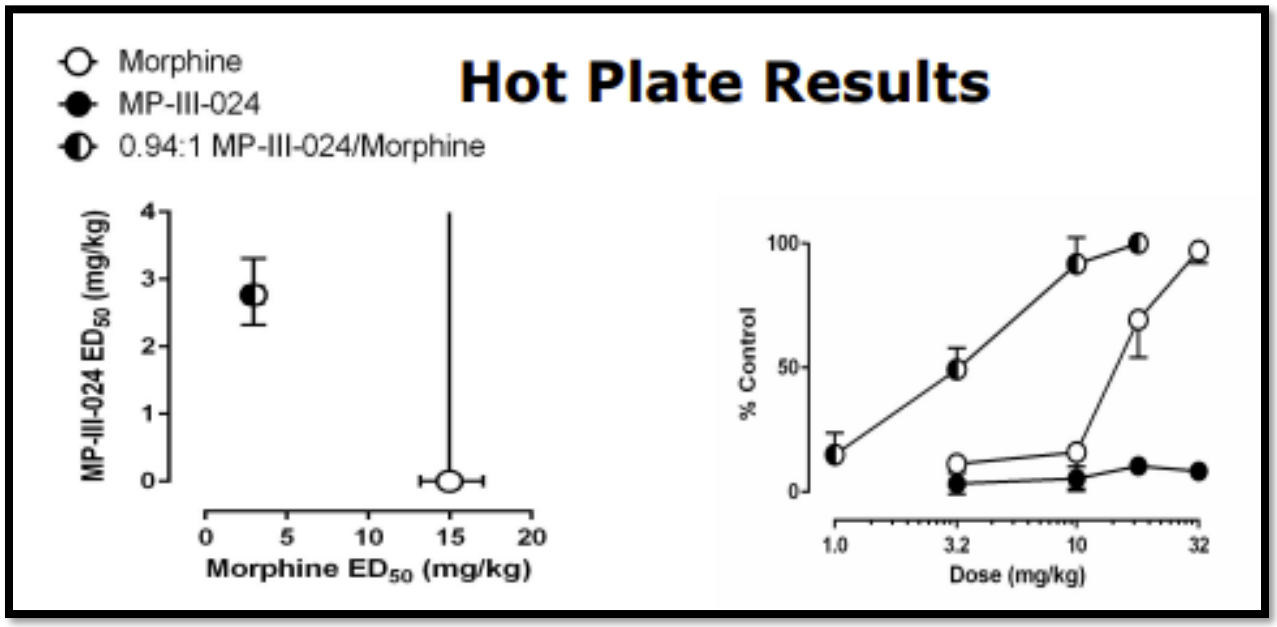


Figure 32: MP-III-024 alone and a 0.94:1 mixture of MP-III-024: morphine for hot plate

The isobolographic graphical analysis of the drug combinations is presented in **Figure 33**. In the mechanical hyperalgesia assay (panel A), the 0.31:1 MP-III-024/morphine mixture exhibited additive effects, as its ED50 values were closely aligned with the line of additivity. This finding was further confirmed by statistical comparison, where the experimentally determined ED50 values (Zmix) were similar to the predicted additive ED50 values (Zadd) (**Table 4**).

However, in contrast, the 0.92:1 and 2.8:1 MP-III-024/morphine mixtures produced supra-additive (synergistic) effects in the mechanical hyperalgesia assay. Their ED50 values fell below the line of additivity, and this observation was also supported by statistical dose-addition analysis (**Table 4**). In the thermal nociception assay (panel B), the graphical analysis of the MP-III-024/morphine mixtures indicated that each mixture produced supra-additive effects, as their ED50 values fell to the left of the line

of additivity. Statistical comparisons confirmed that the experimentally determined ED50 values for these mixtures (Zmix) were significantly lower than the predicted additive ED50 values (Zadd) (**Table 4**).

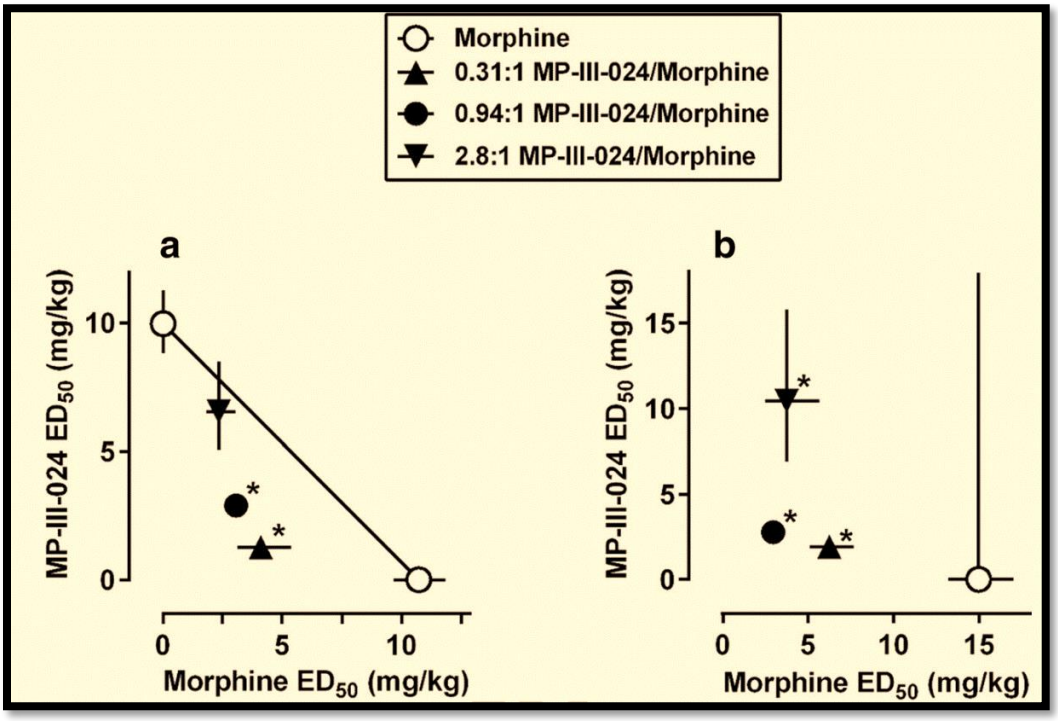


Figure 33. Isobolograms for MP-III024/morphine mixtures, mechanical hyperalgesia (panel a) and in the assay of thermal nociception (panel b). The abscissae represent the ED50 value for morphine in mg/kg, while the ordinates represent the ED50 value for MP-III024 in mg/kg. Each point in the isobolograms represents the mean (± S.E.M.) from 8 mice. In the mechanical hyperalgesia assay (panel a), some points fall above the line of additivity (marked as *), indicating supra-additive (synergistic) effects. These points demonstrate that the combination of MP-III024 and morphine produces stronger antihyperalgesic effects than would be expected if their effects were merely additive. In the thermal nociception assay (panel b), all points fall to the left of the line of additivity (marked as *), indicating supra-additive effects. This implies that the combination of MP-III024 and morphine produces more potent antinociceptive effects than predicted based on

additivity. The asterisks (*) indicate that the observed effects of the drug combinations are significantly different from additivity, further confirming the presence of synergistic interactions.

3.4. Methods

3.4.1. *In vivo* studies

a. Rodent assays: All rodent assays were conducted following the guidelines set forth by the national government and adhering to the recommendations of the local animal care and use committees. The welfare and ethical treatment of the animals were prioritized throughout the studies. The local animal care and use committee, along with the veterinary staff, played a crucial role in ensuring the well-being of the animals. Their oversight included regular inspections, reviews of experimental protocols, on-site visits to the laboratory, and continuous monitoring of animal health to ensure that the research was conducted ethically and responsibly. These measures were taken to safeguard the animals' welfare and to comply with the highest standards of animal care during the research process.

b. Oral dose pharmacokinetics with Dr Miroslav Savic and coworkers

Animals: For the pharmacokinetic study, adult male Sprague Dawley rats from the vivarium of the Faculty of Pharmacy, Belgrade, Serbia, were used. The rats were housed in groups of five and kept under standard laboratory conditions, including a controlled temperature of 21±2 °C, relative humidity maintained at 40-45%, and an illumination of 120 lx. They were provided with free access to pellet food and tap water.

The rats were maintained on a 12:12 h light/dark cycle, with lights on at 06.00 h. All handling and testing procedures were conducted during the light phase of the diurnal cycle. The study was conducted in compliance with the guidelines and regulations of the Ethical Council for the Protection of Experimental Animals of the Ministry of Agriculture, Forestry, and Water Management of the Republic of Serbia, ensuring the ethical treatment and well-being of the animals throughout the experiment.

c. Pharmacokinetic study: To determine the pharmacokinetic parameters and concentration-time profiles of the selected ligands after oral administration using the cassette method, the compounds were divided into two sets of three cohorts, each consisting of five groups of animals. Each group of animals corresponded to predetermined time intervals (15 minutes, 40 minutes, 2 hours, 6 hours, and 24 hours). All ligands were administered at a dose of 2.0 mg/kg in a 0.4 mg/ml concentration, dissolved in 0.25% methylcellulose in distilled water. At the specified time intervals, the animals were anesthetized with ketamine hydrochloride (90 mg/kg) and xylazine hydrochloride (10 mg/kg) administered intraperitoneally. Blood samples were collected via cardiac puncture using heparinized syringes, and brain tissue samples were obtained. Plasma was obtained from the blood samples after centrifugation, while brain tissue samples were homogenized in methanol using an ultrasonic probe. Supernatants were collected after centrifugation, and both plasma and supernatants were further processed using solid-phase extraction with Oasis HLB cartridges.

The concentration of the compounds in the plasma and supernatants was determined using ultraperformance liquid chromatography-tandem mass spectrometry (UPLC-MS/MS) with a Thermo Scientific Accela 600 UPLC system connected to a Thermo Scientific TSQ Quantum Access MAX triple quadrupole mass spectrometer. The non-compartmental pharmacokinetic

analysis was conducted using PK functions for Microsoft Excel software, while graphs were generated using commercial statistical software Sigma Plot 12.

The study was conducted in accordance with the guidelines and regulations of the Ethical Council for the Protection of Experimental Animals of the Ministry of Agriculture, Forestry, and Water Management of the Republic of Serbia, ensuring ethical treatment and welfare of the animals during the study (Obradović et al., 2014).

d. Oral Dose – PTZ seizures with Dr Jeffrey M Witkin and coworkers

PTZ seizures.

In the evaluation of PTZ seizures, male C57BL/6N mice from Charles River, Indianapolis, IN, were used. The potential anticonvulsant compounds were dissolved in 1% carboxymethylcellulose, while pentylenetetrazole (PTZ) was dissolved in 0.9% NaCl. The compounds were administered orally at a dose of 10 ml/kg.

The experimental procedure involved giving the mice the test compound via oral gavage, and they were then returned to their home cages for the pretreatment period. Afterward, PTZ was administered to the mice via subcutaneous injection at a dose of 70 mg/kg. A trained observer measured the latency to produce clonic seizures and tonic seizures using a stopwatch with precision to the second. The time to death was also recorded over a 60-minute observation period. The latencies to clonus and tonus were analyzed separately using one-way ANOVA, followed by Tukey's test with a priori probabilities of 0.05 to determine the statistical significance. For lethality assessment, the mice were observed for a 60-minute period after PTZ administration, and the latency to death was recorded. The number of mice that died in the PTZ-

alone group (vehicle + 70 mg/kg PTZ) was compared to each compound dose using Fisher's Exact Probability test, with a significance level of $p < 0.05$ considered statistically significant.

3.4.2. Receptor binding studies with PDSP program (Dr Bryan Roth)

The interactions of DS-II-73 (6) were evaluated by the National Institute of Mental Health Psychoactive Drug Screening Program. The compound was subjected to screening across 41 protein targets at a concentration of 10 mM. In cases where the compound exhibited inhibition of 50% or greater, concentration-inhibition studies were conducted to determine Ki values. The NIMH Psychoactive Drug Screening Program is overseen by Dr. Bryan Roth from the University of North Carolina (UNC).

3.4.3. Electrophysiology studies with Dr Jeffrey M Witkin and coworkers

For the electrophysiological studies, brain tissue was obtained and delivered to the laboratory in oxygenated artificial cerebral spinal fluid. The tissue was then sliced and prepared for recording following the methods described in a previous study conducted by Witkin et al. in 2018. These procedures ensured the appropriate handling and preparation of brain tissue for electrophysiological recordings.

3.4.4. Theiler's murine encephalomyelitis virus (TMEV) model handling-induced seizures with Dr Jeffrey M Witkin and coworkers

Animal: The study utilized male C57BL/6J mice, aged 5-6 weeks, obtained from The Jackson Laboratories located in Bar Harbor, ME, USA. The mice were provided with ad libitum access to food (TEKLAD GLOBAL 2920X-011620M) and water throughout the study. The housing and experimental procedures were conducted in accordance with the guidelines and recommendations outlined by the National Research Council in 2011. Additionally, the study

received approval from the Institutional Animal Care and Use Committee at the University of Utah, ensuring that all ethical considerations and standards for animal welfare were met during the research process.

TMEV model: For the study, forty male C57BL/6J mice were briefly anesthetized using a mixture of isoflurane and compressed air (1.5-3% isoflurane). The mice were initially injected with 20 μl of the Daniels strain of TMEV (3 x 105) plaque-forming units intra-cortically to a depth of 2 mm in the temporal region of the right hemisphere, posterior and medial to the right eye. This inoculation typically took place on a Friday (day 0), with monitoring occurring from day 3 to day 7, Monday to Friday of the following week.

Two separate studies were conducted, one using 15 mg/kg of KRM-II-81 and the other using 30 mg/kg. Each study involved dividing the mice into two groups: one group received KRM-II-81, and the other group received the drug vehicle, serving as the control group. From days 1 to 7, either the vehicle or KRM-II-81 was administered to the respective groups twice a day (at approximately 0900 and 1500 h) via oral gavage. Mice that experienced body weight loss of 20% or more were eliminated from the study.

Handling-induced seizures were evaluated during vehicle or KRM-II-81 injections (twice daily) and 2 hours after injections on days 3 to 7, using the methods previously described in Barker-Haliski et al. (2015). By comparing drug effects during the dosing period and 2 hours post-dosing, the study aimed to demonstrate that the presence of KRM-II-81 at its receptors was responsible for driving the anti-seizure efficacy. The choice of the 2-hour time period was based on prior pharmacokinetic and anti-seizure data from Mian et al. (2022) and Witkin et al. (2020), respectively.

Data Analysis: During the study, the following data were collected:

1. Presence or absence of seizures: Each mouse was monitored to determine if seizures occurred or not during the observation periods.
2. Severity of each seizure: Seizure severity was measured using a modified Racine scoring system, with scores ranging from 1 to 5 (Racine, 1972). This scoring system helps to assess the severity of seizures, with higher scores indicating more severe seizures.
3. Body weight: Daily measurements of the mice's body weight were taken throughout the experiment.

Seizure monitoring was conducted twice daily, during dosing and 2 hours after dosing. The person handling the mice during the experiment was blinded to the treatment to minimize bias. The cumulative seizure burden on days 3, 4, 5, 6, and 7 for the two observation periods/day that occurred 2 hours post-dosing was calculated. The seizure burden is defined as the sum of seizure scores for all seizures during an observation period (counted only for mice that exhibited a seizure) divided by the number of observation periods in which a seizure occurred. The seizure burden can range from 0 to 5. These data provide a comprehensive analysis combining both the frequency and severity of seizures. The mean + SEM cumulative score over these experimental days was evaluated using ANOVA to compare the vehicle-treating group with the KRM-II-81-treated group. Post-hoc comparisons of results from all days were evaluated using Šidák's multiple comparison test.

Seizure severity was assessed in two ways:

i. The mean seizure severity score was obtained by averaging all scores, including zeros, for each treatment period and condition. Vehicle vs. KRM-II-81 values were then assessed using ANOVA.

ii. A separate analysis was conducted for the severe stage 5 type seizures. Stage 5 seizures for the vehicle vs. KRM-II-81-treated groups were compared using Fisher's Exact Probability test.

All statistical comparisons were considered significant based on the a priori setting of $P < 0.05$ using two-tailed tests. The GraphPad Prism software version 9.4.1 (San Diego, CA) was used for statistical analyses.

Subunit composition:

Transfected mammalian cells. In this study, mammalian GABAA receptors were expressed in human embryonic kidney cells (HEK-293T) through transfection. Full-length cDNAs encoding the mammalian GABAA receptor subunits were inserted into pCMVNeo expression vectors and co-transfected into the cells (2 mg of each subunit) using calcium phosphate precipitation. Subunit clones were provided by Dr. Robert Macdonald from Vanderbilt University and Dr. David Weiss from the University of Texas Health Science Center.

To select the transfected cells, a plasmid containing cDNA encoding the surface antibody sFv (pHookTM-1) was also co-transfected into the cells. After incubating the cells with 15% glycerol solution in BBS buffer for 30 seconds, they were maintained in Dulbecco's modified Eagle medium (DMEM) supplemented with 10% fetal bovine serum, 100 IU/ml penicillin, and 100 mg/ml streptomycin.

The selection procedure for pHook expression was performed 44-52 hours later. This involved incubating the cells with magnetic beads coated with the antigen for the pHook antibody. The beads would bind to the positively transfected cells. After a 30-60 minute incubation, the bead-coated cells were isolated using a magnetic stand. The selected cells were then resuspended in DMEM, plated onto glass coverslips treated with poly L-lysine and coated with collagen, and used for recordings 18-28 hours later. This method allowed the researchers to express specific combinations of GABAA receptor subunits in the HEK-293T cells, enabling them to study the functional properties of the receptors.

Recording of GABA currents:

In this study, whole-cell GABA currents were recorded using a voltage-clamp mode on an Axon 200B patch clamp amplifier. For recordings from GABA-transfected HEK-293T cells, the external solution consisted of the following concentrations (in mM): 142 NaCl, 8.1 KCl, 6 MgCl2, 1 CaCl2, and 10 HEPES (4-(2-hydroxyethyl)-1-piperazineethanesulfonic acid), with pH adjusted to 7.4 and osmolarity adjusted to 295 - 305 mOsm. The recording electrodes were filled with an internal solution containing the following concentrations (in mM): 153 KCl, 1 MgCl2, 5 K-EGTA (ethylene glycol-bis(β-aminoethyl ether) N,N,N',N'-tetraacetate), 2 MgATP, and 10 HEPES, with pH adjusted to 7.4 and osmolarity adjusted to 295 - 305 mOsm.

GABA was diluted into the external solution from freshly made or frozen stocks in water. Test compounds were diluted from stocks in DMSO (dimethyl sulfoxide), and the final DMSO concentration for these experiments was no greater than 0.01%. Patch pipettes were pulled from borosilicate glass with an internal filament on a two-stage puller to achieve a resistance of 5-10 MΩ. For whole-cell recordings, GABA was applied to the cells using a stepper solution exchanger with a complete exchange time of less than 50 ms (open tip, SF-77B, Warner

Instruments, Hamden CT). This setup allowed for precise and rapid application of GABA and test compounds to the cells during the recordings.

Whole-cell currents were digitized at a sampling rate of 10 kHz and analyzed using the pClamp suite of programs (Molecular Devices Corporation, Sunnyvale, CA). The data are presented as the mean + SEM (standard error of the mean) based on a minimum of four replicates. Statistical analysis was performed using two-way ANOVA (analysis of variance) with Bonferroni multiple comparisons tests to assess differences between experimental groups. The Prism 5.0 software (GraphPad Prism, San Diego, CA) was used for conducting the statistical analyses. The significance level was set at $p < 0.05$, indicating that differences with a p-value below 0.05 were considered statistically significant.

3.4.6. Experimental procedures for Harmaline-Induced Tremor and Locomotor Activity Analysis with Dr Kuter, Barbara, and others

Animals. The study involved adult male Wistar Han rats obtained from Charles River, Germany, with an initial weight ranging from 250 to 340 grams. The rats were housed in an animal room under controlled conditions, including a 12-hour dark/light cycle (with lights on from 7 AM to 7 PM), a temperature of 22 ± 2 °C, and a relative humidity of 55 ± 5%. The rats were kept in cages with 4 to 5 rats per cage and had free access to food and water throughout the experiment.

All experimental procedures were conducted during the light period, specifically between 8 AM and 4 PM. The study was conducted in accordance with the Act on Experiments on Animals of 21 January 2005, amended on 15 January 2015, published in the Journal of Laws no. 23/2015 item 266, Poland. Additionally, the study adhered to the guidelines provided by the Directive of the European Parliament and the Council of Europe 2010/63/EU of 23 September 2010, which

regulates the protection of animals used for scientific purposes. Furthermore, the study was approved by the Local Ethics Committee at the Maj Institute of Pharmacology, Polish Academy of Sciences, Cracow. The ethical approval numbers for the study were 271/2018, 89/2020, and 90/2021. The researchers made every effort to minimize the suffering of the animals and reduce the number of animals used in the experiments.

Compounds. In the study, the following compounds were used, and their administration methods are described:

Harmaline hydrochloride dihydrate: It was obtained from Sigma-Aldrich, Merck & Co. Inc., Rahway, NJ, USA. Harmaline was dissolved in sterile redistilled water and administered acutely at a dose of 15 mg/kg intraperitoneally (ip).

Pimozide: Pimozide is an antagonist of dopamine receptors, mainly D2, but also D3 and D4 receptors. It was obtained from Sigma-Aldrich, Merck & Co. Inc., Rahway, NJ, USA. Pimozide was dissolved in warm 0.3% tartaric acid and administered subchronically, with 7 injections given once a day, at a dose of 1 mg/kg.

Tetrabenazine (TBZ): TBZ is a reversible type 2 vesicular monoamine transporter (VMAT) inhibitor. It was dissolved in 20% dimethyl sulfoxide (DMSO) in 0.9% NaCl, with 1N hydrochloric acid (HCl) added to ensure complete drug solubility (final pH = 3.5). TBZ was given acutely at a dose of 2 mg/kg.

Zolpidem hemitartarate: Zolpidem is a positive allosteric modulator of GABA-A receptors containing α1 subunits. It was synthesized and provided by Dr. M. Marcinkowska from Jagiellonian University, Medical College, Kraków, Poland. Zolpidem was dissolved in sterile redistilled water and administered acutely at doses of 0.34, 0.67, and 1.01 mg/kg.

MP-III-024: MP-III-024 is a positive allosteric modulator selective for α2/3 subunits of the GABA-A receptor. It was synthesized in Cook group laboratory by Sharmin at the University of Wisconsin-Milwaukee, Milwaukee, WI, USA. MP-III-024 was suspended in 0.5% methyl cellulose in 0.9% NaCl and given at doses of 3.2 and 10 mg/kg in a volume of 2 mL/kg.

Control animals received appropriate vehicles: water, 0.3% tartaric acid, 20% DMSO in 0.9% NaCl (pH = 3.5), or 0.5% methyl cellulose in 0.9% NaCl, instead of the respective compounds mentioned above. The administration times of the compounds are provided in the **Figure 34** of the study.

In the study, the administration timing of MP-III-024, Zolpidem, Harmaline, Pimozide, and TBZ is as follows:

MP-III-024: It was administered 30 minutes prior to harmaline.

Zolpidem: Zolpidem was administered subsequently with harmaline. The timing was either 3 hours and 45 minutes after the last pimozide injection or 1 hour and 45 minutes after TBZ administration.

Harmaline: Harmaline was administered acutely, likely after the administration of MP-III-024 and Zolpidem.

Pimozide: Pimozide was administered subchronically, with 7 injections given once a day, but the specific timing is not mentioned in the provided information.

TBZ: TBZ was administered acutely, and it was given before Zolpidem in the case of the experiment involving Zolpidem and TBZ.

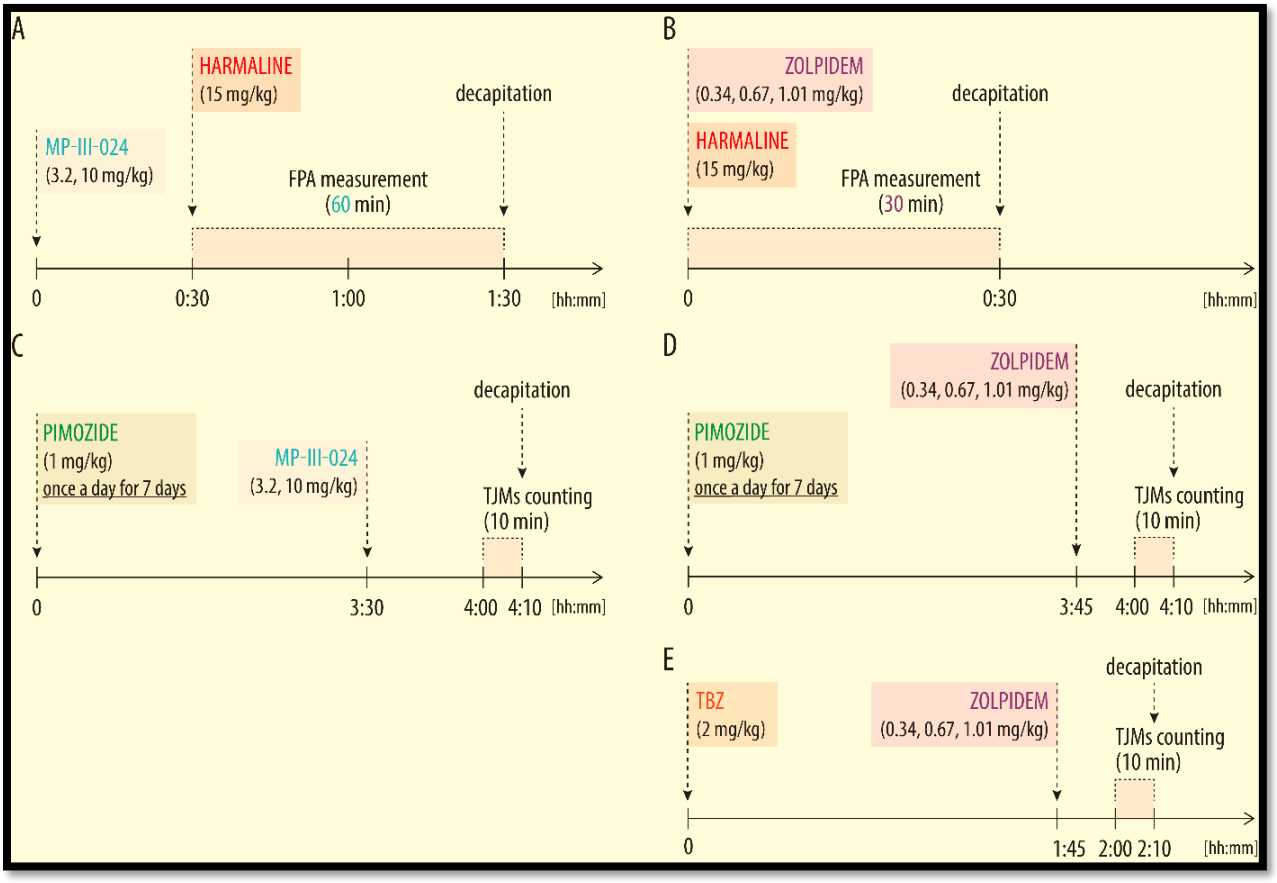


Figure 34. The timelines of drug administration and the measurement or observation of tremor induced by different compounds. The timelines are as follows: (A, B) For harmaline-induced tremor measurement using the Force Plate Actimeter (FPA), the measurement duration was 30 minutes. (C, D) For observation and counting of Tremulous Jaw Movements (TJMs) induced by pimozide, the observation period was not specified in the provided information. (E) For observation and counting of Tremulous Jaw Movements (TJMs) induced by TBZ, the observation period was not specified in the provided information. The abbreviations used in the figure are FPA for Force Plate Actimeter, TBZ

for tetrabenazine, and TJMs for Tremulous Jaw Movements. Figure is modified from Barbara et al.2023.

Harmaline-Induced Tremor and Locomotor Activity Analysis:

The measurement of tremor and locomotor activity was performed using Force Plate Actimeters (FPA) manufactured by BASi (West Lafayette, IN, USA). The FPA system consists of a measuring cage placed inside a sound-attenuating chamber. Four force transducers positioned under the corners of the measuring cage's floor allowed for recording the position and movement of the animals on a Cartesian plane, as well as measuring the force exerted on the plate.

Data were collected at a sampling frequency of 100 points per second, with each time unit (frame) lasting 10.24 seconds. Tremor was automatically analyzed using Fast Fourier Transform on each frame of the experiment. The power spectra obtained were then subjected to a logarithmic transformation (log10) and averaged over specific time intervals. For experiments with zolpidem, the averaging was done over one consecutive 180-frame series (0-30.72 min). In the study with MP-III-024, averaging was performed over two consecutive 180-frame series (0-30.72 min and 30.73-61.44 min), resulting in two intervals (0-30 min and 30-60 min).

The parameters obtained from the power spectra analysis were as follows:

AP1: Averaged power in frequency band I (0-8 Hz).

AP2: Averaged power in frequency band II (9-15 Hz).

Tremor Index (TI): The difference in power between AP2 and AP1.

In addition to tremor measurement, the total distance traveled by the animals during one or two intervals was also recorded as a measure of locomotor activity. The distance traveled was

measured in millimeters. These parameters were used to assess the effects of the compounds on tremor and locomotor activity in the experimental animals.

Tremulous Jaw Movements (TJMs) Analysis:

The measurement of Tremulous Jaw Movements (TJMs) in rats started at different time points depending on the treatment received:

i. For rats treated with pimozide: The measurement of TJMs began 4 hours after the last dose of subchronic pimozide administration.
ii. For rats treated with TBZ: The measurement of TJMs began 2 hours after TBZ administration.

All rats used in these experiments responded to TBZ and subchronic pimozide with TJMs, indicating that both compounds induced tremulous jaw movements in the animals. During the TJMs observation, the rats were placed in a clear Plexiglass cylinder (30 cm diameter, 40 cm high) positioned in front of an angled mirror. Tremulous jaw movements were defined as rapid vertical deflections of the lower jaw that resembled chewing behavior but were not directed at any specific stimulus. Each individual deflection of the jaw was recorded for 10 minutes using a mechanical hand counter by a trained observer who was blind to the experimental condition of the rat being observed. Additionally, the observation was video recorded for later verification and live counting. By recording and counting the TJMs in this manner, researchers could assess the effects of the tested compounds on tremulous jaw movements in the rats.

Statistical analysis:

The results of the experiments are presented as means ± standard errors of the mean (SEM). Statistical analysis of the data was performed using STATISTICA v. 13 software (StatSoft Inc., Tulsa, OK, USA). A p-value of ≤ 0.05 was considered statistically significant, and p-values between 0.1 and 0.05 were considered trends. For the results obtained using the Force Plate Actimeter (FPA) to measure harmaline-induced tremor and locomotor activity, factorial ANOVA was used for the zolpidem experiments. For experiments with MP-III-024, which involved two time points (0–30 min and 30–60 min), ANOVA for repeated measures was used. The Tremulous Jaw Movements (TJMs) were analyzed using factorial ANOVA. For individual comparisons between groups, the Least Significant Difference (LSD) post hoc test was used, allowing researchers to identify specific differences between treatment groups. Overall, these statistical methods were employed to determine the significance of the effects of the tested compounds on harmaline-induced tremor, locomotor activity, and TJMs in the rats.

3.4.7. Synergistic antihyperalgesic and antinociceptive effects of morphine and MP-III-024 with Atiqur Rahman, Dr Fisher, and others

Animal. The study involved adult male CD-1 mice, approximately 10 weeks old, obtained from Charles River Laboratories in Wilmington, MA. The mice were housed in a vivarium with controlled temperature and humidity, and they had constant access to air and water. The light/dark cycle was set to 12 hours, with lights on at 7:00 AM. The mice were group-housed in polycarbonate cages and provided with ad libitum food and water. Enrichment was provided in the form of paper Bio-Huts and/or nestlets. Prior to any experimental manipulation, the mice were habituated to the colony room environment for 2 weeks. They were also exposed to the testing environment and handled for 2 days before the start of the experiments. All testing procedures were conducted between 11:00 AM and 3:00 PM. The care and handling of the

animals were in accordance with the guidelines set by the Institutional Animal Care and Use Committee of Rowan University. This information provides details about the housing, handling, and care of the mice used in the study, ensuring that appropriate ethical considerations were followed throughout the experimental process.

Mechanical hyperglasia. The antihyperalgesic effects were investigated after inducing inflammation by injecting 0.06 mg of zymosan A suspended in 20 µl of 0.9% NaCl into the plantar surface of the right hind paw. The left hind paw, which was not injected, served as the control. After 24 hours of zymosan A injection, mechanical sensitivity was assessed. Mechanical sensitivity was measured using von Frey filaments of increasing stiffness (ranging from 5 to 26 grams) applied to the mid plantar surface of the hind paws. The filaments were applied until they bent. A positive response, indicated by paw withdrawal behavior, was considered as a response to the mechanical stimulation. The mechanical threshold was defined as the minimum force required to elicit a positive withdrawal response.

To assess the antihyperalgesic effects of the drugs, the mechanical threshold following drug administration was normalized to the baseline measurement of the non-injected left hind paw. The effect was expressed as a percentage of the maximal possible effect (%MPE) using the following formula:

%MPE = [(post-drug right paw threshold in grams) - (baseline right paw threshold in grams)] / [(baseline left paw threshold in grams) - (baseline right paw threshold in grams)]

This calculation allowed was used to quantify the antihyperalgesic effects of the drugs tested and compare them to the baseline mechanical threshold of the non-injected left hind paw.

Thermal nociception. The antinociceptive effects during the hot-plate procedure were assessed using a hot-plate analgesia meter. The hot-plate surface was maintained at a constant temperature of 56 ± 0.1 °C. To evaluate the antinociceptive response, the latency to lick or shuffle the hind paw(s) and/or to jump from the hot-plate surface was recorded. A predetermined cutoff time of 20 seconds was set as the maximal response to prevent tissue damage. If the animal did not show a response within this cutoff time, the test was terminated.

To evaluate the antinociceptive response, the latency to respond on the hot plate was measured twice, 30 minutes and 15 minutes prior to the beginning of drug administration. These two baseline measurements were averaged to yield a single baseline value. After administering the drug, the latency to respond on the hot plate was measured again, and the antinociceptive response was calculated as a percentage of maximal possible effect (%MPE) using the following formula:

%MPE = [(post-drug latency in seconds) - (baseline latency in seconds)] / (cutoff time in seconds - baseline latency in seconds)

Isobolographic and dose-addition analysis. In this study, the dose of each drug (MP-III-024 and morphine) required to produce a 50% maximal possible effect (%MPE) was determined using log-linear interpolation by linear regression. Individual ED50 values were calculated for each drug and then converted to their log values for calculation of means and 95% confidence limits. The values were then converted back to linear values for presentation.

Drug interactions between MP-III-024 and morphine were assessed using both graphical and statistical approaches. Isobolograms were constructed by connecting the ED50 of MP-III-024

alone (plotted on the abscissa) with the ED50 of morphine alone (plotted on the ordinate) to obtain an additivity line. The additivity line represents dose pairs that produce an ED50 equal to the ED50 of each drug alone. Dose pairs falling below or to the left of the additivity line suggest synergism, indicating that the combination of the drugs produces a stronger effect than each drug alone. Conversely, dose pairs falling above or to the right of the line suggest subadditivity, indicating that the combination of the drugs produces a weaker effect than each drug alone.

Statistical analysis of drug interactions involved comparing the experimentally determined ED50 values for each drug mixture (Zmix) with the predicted additive ED50 values (Zadd) using the formula described by Tallarida (2000). Zmix represents the total drug dose (i.e., dose of MP-III-024 + dose of morphine) that produced a 50%MPE. For mixtures where both drugs were equieffective, Zadd values were calculated individually for each mouse based on the ED50 values of each drug. The proportion of MP-III-024 to morphine in each mixture was determined using a specific formula based on the values of f (0.25, 0.5, or 0.75). These mixtures resulted in different ratios of MP-III-024 to morphine, ranging from 0.31:1 to 2.8:1 on a mg/kg basis. The purpose of these analyses was to understand the nature of the interactions between MP-III-024 and morphine and to determine whether their combined effect is additive, synergistic, or subadditive.

In the hot plate assay, it was found that MP-III-024 alone did not produce any antinociceptive effects. The hypothesis of additivity suggests that MP-III-024 would not contribute to the antinociceptive effects of any mixture of MP-III-024 in combination with morphine (Tallarida 2000). To test this hypothesis, the Zadd values were calculated by dividing the ED50 of morphine by the proportion of morphine in each mixture. Mean experimentally determined ED50 values (Zmix) and predicted additive ED50 values (Zadd) for each mixture were compared

using Student's t-test. All statistical analyses, including the comparison of Zmix and Zadd values, were performed using the GraphPad Prism software version 6 (Graphpad Software, San Diego, CA). This analysis aimed to determine whether the combination of MP-III-024 and morphine in the hot plate assay showed an additive effect or if MP-III-024 did not contribute to the antinociceptive effects of the mixture.

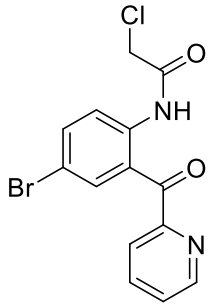
3.5. Experimental

3.5.1. General procedure:

The reactions were conducted in oven-dried round-bottom flasks equipped with magnetic stir bars or overhead mechanical stirrers, and all procedures were carried out under an argon atmosphere to maintain an inert environment. Organic solvents and chemicals used in the reactions were either purified by standard methods or obtained from reputable suppliers such as Sigma-Aldrich, Admiral Chemical Company, or Acros Organic.

The nuclear magnetic resonance (NMR) spectral data, including proton and 13C NMR, were obtained using a Bruker Avance III 500 MHz spectrometer. The chemical shifts in the NMR spectra are reported in units of δ (parts per million). High-resolution mass spectrometry (HRMS) spectral data were obtained using a Shimadzu Scientific LCMS-IT-TOF instrument. HRMS is a technique that provides precise mass measurements, allowing for the determination of molecular formulae and accurate determination of molecular weights.

3.5.2. *N*-(4-Bromo-2-picolinoylphenyl)-2-chloroacetamide (10)

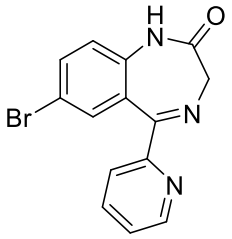


10

Chloroacetyl chloride (215.25 mL, 2706 mmol) was added dropwise to a stirred solution of (2-amino-5-bromophenyl) (pyridine-2yl)methanone (**6**, 500 g, 1804 mmol), sodium bicarbonate (303.1 g, 3608 mmol), and anhydrous DCM (5000 mL) over a period of 60 min while keeping the temperature between 25−30 °C. The bright red solution, which resulted, during the addition of chloroacetyl chloride turned to a light-yellow colored solution indicating the consumption of starting material. The completion of the reaction was confirmed by silica gel TLC (EtOAc: hexane = 20:80 with 1% triethylamine). The reaction mixture was quenched slowly by adding water (3000 mL) over a 30 min period as carbon dioxide gas evolved. The biphasic mixture, which resulted, was allowed to stand for 25 min and the layers were separated. The organic layer was separated and the aq layer was extracted with DCM (2x1000 mL) and the combined organic layers were washed with 5% aq sodium bicarbonate solution (1x 2500 mL), 10% aq sodium chloride solution (2x 2500 mL) and dried (Na_2SO_4). The solvents were removed under reduced pressure and the residue was stirred with ethanol (2000 mL) at 50−55 °C for 30 min. The mixture was cooled to rt and kept at that temperature for 3 h. The solid was filtered, washed with ethanol (300 mL × 3) and dried under vacuum at 40 °C to afford the *N*-(4-Bromo-2-picolinoylphenyl)-2-chloroacetamide **(10)** as an off-white powder (599.7 g, 93.5%). Additional product was isolated as a second crop by concentrating the filtrate (31.3 g, 4.9%). **^{1}H NMR** (500 MHz, $CDCl_3$) δ 11.65 (s, 1H), 8.76 (ddd, 1H), 8.58 (d, J = 9.0 Hz, 1H), 8.02 (dd, J = 9.5, 5.1 Hz,

2H), 7.96 (ddd, J = 7.7, 1.6, 0.8 Hz, 1H), 7.71 (dd, J = 9.0, 2.3 Hz, 1H), 7.58 – 7.53 (m, 1H), 4.21 (s, 2H). **^{13}C NMR** (126 MHz, $CDCl_3$) δ 195.26 (s), 165.33 (s), 154.74 (s), 148.81 (s), 138.78 (s), 137.42 (s), 137.17 (s), 136.86 (s), 126.69 (s), 124.98 (s), 124.61 (s), 122.98 (s), 115.80 (s), 43.15 (s). HRMS (ESI/ITTOF): m/z $[M + H]^+$ calcd for $C_{14}H_{11}BrClN_2O_2$: 352.9693; found: 352.9691

3.5.3. 7-Bromo-5-(pyridin-2-yl)-1,3-dihydro-2H-benzo[e][1,4]diazepin-2-one (6)

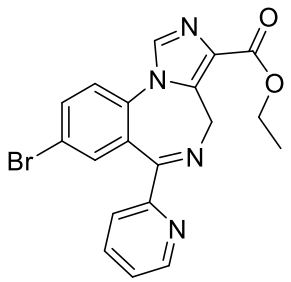


6

A 12 L 3-neck round bottom flask was charged with N-(4-bromo-2-picolinoylphenyl)-2-chloroacetamide (**10**, 630 g, 1781.6 mmol), isopropanol (6000 mL) hexamethylenetetramine (HMTM, 549.5 g, 3919.6 mmol), ammonium acetate (302.11 g, 3919.6 mmol), and was heated to reflux (82 °C) with continuous stirring with an overhead stirrer. The reaction mixture was held at reflux for 5 h at which point the reaction was deemed complete by analysis by silica gel TLC (EtOAc: hexane = 50:50 with 1 % triethylamine). The reaction mixture was then cooled to 0−5 °C using an ice bath. The solid, which resulted, was filtered, and washed with cold isopropanol (500 mL × 2) and then water (1000 mL × 4). The solid was dried under vacuum at 50 °C for 6 hours to afford the 7-Bromo-5-(pyridin-2-yl)-1,3-dihydro-2H-benzo[e][1,4]diazepin-2-one **(6)** as an off-white solid (451.16 g, 80%). The isopropanol filtrate was concentrated, and cold water (500mL) was added with stirring over a period of 30 min. The solid residue was filtered, washed with IPA-water (50:50, 300 mL) and water (3x300mL). The solid was then dried under vacuum at 50^{o}C for 4 hours to obtain additional product **6** (53.4 g, 9.5%). **^{1}H NMR** (500 MHz, $CDCl_3$) δ

9.47 (s, 1H), 8.66 (ddd, J = 4.8, 1.6, 0.9 Hz, 1H), 8.01 (dt, 1H), 7.84 (td, J = 7.7, 1.8 Hz, 1H), 7.57 (dd, J = 8.6, 2.3 Hz, 1H), 7.49 (d, J = 2.2 Hz, 1H), 7.40 (ddd, J = 7.6, 4.8, 1.1 Hz, 1H), 7.02 (d, J = 8.7 Hz, 1H), 4.38 (s, 2H). **^{13}C NMR** (126 MHz, $CDCl_3$) δ 171.21 (s), 168.43 (s), 156.13 (s), 148.94 (s), 137.83 (s), 136.93 (s), 134.69 (s), 134.09 (s), 127.78 (s), 124.82 (s), 124.12 (s), 122.93 (s), 116.17 (s), 56.82 (s). HRMS (ESI/IT-TOF): m/z [M + H]+ calcd for $C_{14}H_{11}BrN_3O$: 316.0080; found: 316.0076

3.5.4. Ethyl 8-bromo-6-(pyridin-2-yl)-4H-benzo[f]imidazo[1,5-a][1,4]diazepine-3-carboxylate (7)

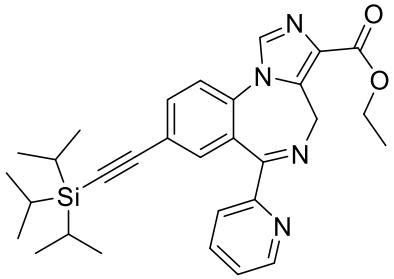


The 7-bromo-5-(pyridin-2- yl)-1,3-dihydro-2H-benzo[e][1,4]diazepin-2-one (**6**, 200 g, 632.5 mmol) was dissolved in anhydrous THF (1500 mL) and cooled to −20 °C using a dry ice/IPA bath. A solution of potassium t-butoxide (92.28 g, 822.3 mmol in 600mL anhydrous THF) was added dropwise to the reaction mixture over a 30 min period, while maintaining the temperature at −25 to −20 °C. The reaction mixture was allowed to stir for an additional 1 hour at −20 °C after the addition of base. Then diethyl chlorophosphate (127.8 mL, 884.3mmol) was added dropwise to the reaction mixture over 20 min at −20 to −15 °C. Upon completion of the addition, the reaction mixture was allowed to stir for 4 h at rt and the consumption of starting material was confirmed by silica gel TLC (1% triethylamine/ethyl acetate). At that point, ethyl isocyanoacetate (89.9 mL, 822.3 mmol) was then added dropwise to the reaction mixture at −20

to −15 °C for a period of 15 min followed by addition of potassium t-butoxide solution (92.28 g, 822.3 mmol in 600mL anhydrous tetrahydrofuran) over 30 min while maintaining the temperature at −20 to −15 °C. Upon completion of the addition, the reaction mixture was allowed to warm to rt and stirred for an additional 12 h, at which point the reaction was deemed complete by analysis by TLC (silica gel and 1% triethylamine/ethyl acetate). The reaction mixture was quenched with 5% aq sodium bicarbonate (2000 mL) and diluted with ethyl acetate (3000mL). The biphasic mixture, which resulted, was allowed to stand for 15 min and the layers were separated. The organic layer was separated and the aq layer was extracted with ethyl acetate (1000 mL x 2). The combined organic layers washed with 5% aq sodium bicarbonate solution (2x 1000 mL), 10% aq sodium chloride solution (2x 2000 mL) and dried (Na_2SO_4). The solvents were removed under reduced pressure and the gummy residue was stirred with t-butyl methyl ether (2000 mL) at 50−55 °C for 30 min. After cooling to rt and kept for 10 hr, the solid was filtered and washed with t-butyl methyl ether (200 mL x 3). The solid was heated in refluxing ethanol (500 mL) for 1h, cooled to −20 °C and kept for 12 h at −20 °C for maximizing precipitation. The solid residue, which resulted, was filtered and washed with cold ethanol (100 mL x 2). The residue was dried under vacuum at 45 °C for 6 hours to afford the product **7** as a light brown powder (143.5 g, 55%). **^{1}H NMR** (500 MHz, $CDCl_3$) δ 8.58 (ddd, J = 4.7, 1.5, 0.8 Hz, 1H), 8.09 (d, J = 7.9 Hz, 1H), 7.90 (s, 1H), 7.82 (td, J = 7.8, 1.7 Hz, 1H), 7.78 (dd, J = 8.6, 2.2 Hz, 1H), 7.60 (d, J = 2.2 Hz, 1H), 7.47 (d, J = 8.6 Hz, 1H), 7.37 (ddd, J = 7.5, 4.8, 1.1 Hz, 1H), 6.12 (d, J = 11.7 Hz, 1H), 4.43 (q, J = 13.2, 6.6 Hz, 2H), 4.15 (d, J = 11.9 Hz, 1H), 1.44 (t, J = 7.1 Hz, 3H). **^{13}C NMR** (126 MHz, $CDCl_3$) δ 167.08 (s), 162.93 (s), 156.18 (s), 148.73 (s), 138.41 (s), 136.94 (s), 135.30 (s), 134.99 (s), 134.56 (s), 134.45 (s), 129.35 (s), 128.53 (s),

124.90 (s), 124.28 (s), 123.98 (s), 120.57 (s), 60.82 (s), 45.02 (s), 14.44 (s). **HRMS** (ESI/IT-TOF): m/z $[M + H]^+$ calcd for $C_{19}H_{16}BrN_4O_2$: 411.0451; found: 411.0454

3.5.5. Ethyl 6-(pyridin-2-yl)-8-((triisopropylsilyl)ethynyl) 4H benzo[f]imidazo[1,5a][1,4] diazepine-3-carboxylate (8)

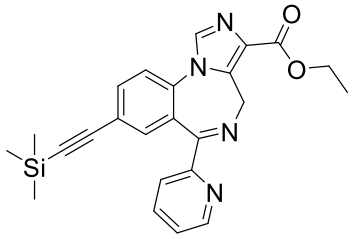


8

Palladium acetate (9.2 g, 40.8 mmol) and tri-o-tolylphosphine (24.85 g, 81.6 mmol) were taken up in a 3-L round-bottom flask, and acetonitrile (2400 mL) was added. The mixture was stirred for 30 minutes at room temperature (rt). Ethyl 8-bromo-6-(pyridin-2-yl)-4H-benzo[f]imidazo[1,5-a][1,4]diazepine-3-carboxylate (**7**, 240 g, 583.2 mmol) was added to the reaction mixture, followed by the addition of triethylamine (243.2 mL, 1749.6 mmol) and (triisopropylsilyl)acetylene (170 mL, 758.2 mmol). The reaction mixture was then heated to reflux (75 °C) and stirred for 6 hours. The reaction was monitored and deemed complete by silica gel TLC analysis using a solvent mixture of ethyl acetate and hexane (50:50) with 1% triethylamine as the mobile phase. The reaction mixture was cooled to room temperature (rt) and exposed to the air. Silica gel (100 g) was added to the mixture, and it was stirred for 20 minutes. The reaction mixture was then filtered through a pad of celite, and the residue was washed with dichloromethane (3x 500 mL).

The solvents were removed under reduced pressure, and the residue was dissolved in dichloromethane (2500 mL). To this solution, 5% aqueous sodium bicarbonate (1000 mL) was added, resulting in a biphasic mixture. The mixture was allowed to stand for 15 minutes, and the organic and aqueous layers were separated. The organic layer was collected, and the aqueous layer was further extracted with dichloromethane (2x 1000 mL). The combined organic layers were washed with 10% aqueous sodium chloride solution (2x 1500 mL) and dried using anhydrous sodium sulfate (Na_2SO_4). The solvents were removed under reduced pressure, and the residue was purified by flash chromatography using silica gel (750 g) and a solvent mixture of 50% ethyl acetate and hexanes with 5% triethylamine. The desired fractions were collected, and the solvents were removed under reduced pressure. The resulting semi-solid was dried under reduced pressure at 40 °C for 2 hours to obtain the product **8** as a clear, light brown semi-solid solid (268.8 g, 90%). $\boldsymbol{R_f}$ = 0.7 (EtOAc-hexanes, 1:1 and 1% of TEA) **^{1}H NMR** (500 MHz, $CDCl_3$) δ 8.58 (ddd, J = 4.6, 1.5, 0.8 Hz, 1H), 8.08 (d, J = 7.9 Hz, 1H), 7.90 (s, 1H), 7.82 (td, J = 7.6, 1.1 Hz, 1H), 7.72 (dd, J = 8.4, 1.5 Hz, 1H), 7.53 – 7.51 (m, 2H), 7.37 (dd, J = 7.5, 4.8 Hz, 1H), 6.11 (d, J = 11.2 Hz, 1H), 4.44 (q, 2H), 4.14 (d, J = 11.2 Hz, 1H), 1.44 (t, J = 7.1 Hz, 3H), 1.12 (d, J = 3.6 Hz, 21H). **^{13}C NMR** (126 MHz, $CDCl_3$) δ 167.78 (s), 162.96 (s), 156.48 (s), 148.72 (s), 138.51 (s), 136.82 (s), 135.71 (s), 135.33 (s), 134.93 (s), 134.47 (s), 129.28 (s), 126.99 (s), 124.77 (s), 124.02 (s), 122.67 (s), 122.65 (s), 104.87 (s), 93.86 (s), 60.78 (s), 45.05 (s), 18.61 (s), 14.45 (s), 11.23 (s).

3.5.6. Ethyl-6-(pyridin-2-yl)-8-((trimethylsilyl)ethynyl)-4*H*-benzo[*f*] imidazo[1,5*a*]-[1,4]dia zepine-3-carboxylate (7a)

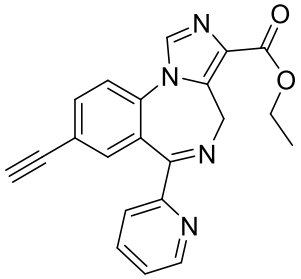


7a

In a 3-neck round-bottom flask equipped with a reflux condenser, the imidazodiazepine ethyl ester (**7**, 50 g, 121.55 mmol) was dissolved in triethylamine (TEA) (52 mL, 364.7 mmol) and dry acetonitrile (CH_3CN) (500 mL). The solution was degassed three times under vacuum and argon. Then, trimethylsilylacetylene (18 g, 182.4 mmol) and bis(triphenyl phosphine)-palladium (II) acetate (5.1 g, 6.68 mmol) were added to the solution under argon, and the mixture was degassed four times. The reaction mixture was heated to reflux under argon and stirred overnight. The reaction progress was monitored using TLC (silica gel, ethyl acetate/hexanes, 7:3, and 1% TEA), and after 15 hours, the reaction was completed. The mixture was then cooled to rt and filtered through celite. After washing with ethyl acetate and drying with Na_2SO_4, the filtrate was concentrated under reduced pressure. The resulting black residue was loaded onto a silica plug and purified by flash chromatography to yield **7a** as an off-white solid with a total yield of 47.8 g (92%). $\boldsymbol{R_f}$ = 0.5 (EtOAc-hexanes, 1:1 and 1% of TEA); **^{1}H NMR** (300 MHz, $CDCl_3$): δ = 8.58 (d, *J* = 4.1 Hz, 1H), 8.06 (d, *J* = 7.8 Hz, 1H), 7.91 (s, 1H), 7.78 (t, *J* = 7.7 Hz, 1H), 7.71 (d, *J* = 8.3 Hz, 1H), 7.51 (d, *J* = 9.2 Hz, 2H), 7.34 (t, *J* = 5.9 Hz, 1H), 6.08 (d, *J* = 9.2 Hz, 1H), 4.47 – 4.31 (m, 2H), 4.10 (d, *J* = 6.9 Hz, 1H), 1.41 (t, *J* = 7.0 Hz, 3H), 0.21(s, 9H); **^{13}C NMR** (75 MHz, $CDCl_3$): δ = 167.8, 162.7, 156.8, 148.8, 138.5, 136.8, 135.7, 135.2, 135.1, 134.5, 129.3,

127.0, 124.7, 124.0, 122.7, 122.2, 102.8, 97.0, 60.7, 45.0, 14.4, 0.2; **HRMS** (ESI/IT-TOF): m/z $[M + H]^+$ calcd for $C_{24}H_{25}N_4O_2Si$: 429.1742; found: 429.1747.

3.5.7. Ethyl 8-ethynyl-6-(pyridin-2-yl)-4H-benzo[f]imidazo[1,5-a][1,4]diazepine-3-carboxylate (Hz-166, 1)

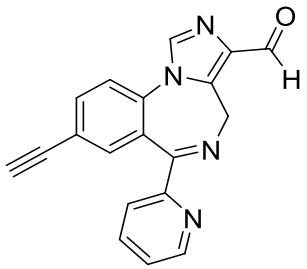


Hz-166, 1

The tri-isopropyl ethyl ester, ethyl 6-(pyridin-2-yl)-8-((triisopropylsilyl)ethynyl)-4H-benzo[f]imidazo[1,5-a][1,4]-diazepine-3-carboxylate (**8**, 198.0 g, 386.16 mmol) was dissolved in tetrahydrofuran (THF) (2000 mL), and 10 mL of water was added to the mixture. The temperature of the reaction mixture was lowered to 0 °C using an ice bath, and tetrabutylammonium fluoride hydrate, 1 M in THF (456.2 mL, 456.2 mmol), was added dropwise over 10 minutes while maintaining the temperature at 0 °C. The reaction mixture was allowed to warm to room temperature upon addition of the TBAF solution and stirred for 2 hours. The completion of the reaction was confirmed by analysis using silica gel TLC (ethyl acetate: hexane = 80:20 with 1% triethylamine). Then, dichloromethane (1500 mL) was added, followed by 10% aqueous sodium chloride (1500 mL). The mixture was stirred for 20 min. After standing for 15 min, the biphasic mixture was separated into organic and aqueous layers. The organic layer was collected, and the aqueous layer was further extracted with dichloromethane (2x 1000 mL). The combined organic layers were washed with 10% aqueous sodium chloride solution (1500 mL) and dried with sodium sulfate (Na_2SO_4). The solvents were evaporated under

reduced pressure, and the residue was stirred with isopropanol (IPA, 500 mL) at 60−65 °C for 30 minutes. Upon cooling to room temperature, cold water (500 mL) was added to the mixture, which was stirred for an additional 30 minutes and left for 2 hours. The solid formed was filtered and washed with cold IPA: water (50:50, 3x100 mL). The resulting solid was dried under vacuum at 40 °C for 4 hours, yielding **HZ-166** as a white crystalline solid (123.6 g, 90%). $\boldsymbol{R_f}$ = 0.3 (EtOAc-hexanes, 1:1 and 1% of TEA). **^{1}H NMR** (500 MHz, $CDCl_3$) δ 8.52 (d, J = 4.2 Hz, 1H), 8.02 (d, J = 7.9 Hz, 1H), 7.89 (s, 1H), 7.76 (td, J = 7.8, 1.7 Hz, 1H), 7.70 (dd, J = 8.3, 1.7 Hz, 1H), 7.54 – 7.50 (m, 2H), 7.31 (ddd, 1H), 6.06 (d, J = 10.4 Hz, 1H), 4.39 (q, J = 16.9 Hz, 2H), 4.12 (d, J = 10.5 Hz, 1H), 3.16 (s, 1H), 1.38 (t, J = 7.1 Hz, 3H). **^{13}C NMR** (126 MHz, $CDCl_3$) δ 167.7 (s), 162.94 (s), 156.45 (s), 148.77 (s), 138.48 (s), 136.87 (s), 136.23 (s), 135.46 (s), 135.26 (s), 134.49 (s), 129.36 (s), 127.10 (s), 124.79 (s), 124.40 (d, J = 99.3 Hz), 124.00 (s), 122.84 (s), 121.19 (s), 81.69 (s), 79.49 (s), 60.81 (s), 45.05 (s), 14.44 (s). **HRMS (ESI/IT-TOF**): m/z [M + H]+ calcd for $C_{21}H_{17}N_4O_2$: 357.1346; found: 357.1344.

3.5.8. 8-Ethynyl-6-(pyridin-2-yl)-4*H*-benzo[*f*]imidazo[1,5-*a*][1,4] diazepine-3-carbaldehyde (9)



9

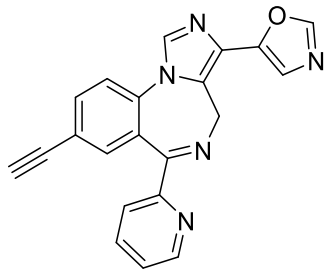
Preparation of PDBBA: The preparation of PDBBA started with the suspension of potassium tert-butoxide (47.1 g, 420 mmol) in dry THF (400 mL). Then, DIBALH (400 mL, 1.0 M in cyclohexane, 400 mmol) was added dropwise to the solution of potassium tert-butoxide at 0 °C

using an ice-water bath. The mixture was allowed to stir at room temperature for 2 hours, resulting in the formation of a colorless homogeneous solution.

Reduction: The Hz-166, ethyl 8-ethynyl-6-(pyridin-2-yl)-4H-benzo[f]imidazo[1,5-a][1,4]diazepine-3-carboxylate (**1,** 80 g, 224.5 mmol), was dissolved in anhydrous dichloromethane (DCM) (1000 mL), and the mixture was cooled to -10°C using an ice-methanol bath. The PDBBA solution (718.4 mL, 359.2 mmol in THF-cyclohexane) was added dropwise with vigorous stirring. The reaction progress was monitored by TLC (silica gel) every 2 minutes, and the reaction was completed within 20 minutes. The reaction mixture was then quenched with a 3% aqueous HCl solution (150 mL) at 0°C, followed by the addition of water (300 mL). The mixture was stirred for 30 minutes, and the resulting aluminum salt was filtered offand the DCM layer was passed through a pad of celite. It was washed with DCM. The filtrate was extracted with DCM (3 x 30 mL). The combined organic layers were washed with a 10% aqueous NaCl solution (2 x 40 mL) and dried with sodium sulfate (Na_2SO_4). The solvents were evaporated, and the solid residue was purified by silica gel flash chromatography using ethyl acetate: hexane = 80:20 with 2% triethylamine. The desired fractions were pooled, and the solvents were removed under reduced pressure. The residue was dried at 40°C for 2 h, resulting in the isolation of pure aldehyde **9** as a white powder (49.5 g, 70% yield). $\boldsymbol{R_f}$ = 0.35 (EtOAc-hexanes, 1:1 and 1% of TEA). ^{1}H NMR (500 MHz, CDCl3) δ 10.05 (s, 1H), 8.56 (ddd, J = 4.8, 1.6, 0.8 Hz, 1H), 8.06 (d, J = 7.9 Hz, 1H), 7.98 (s, 1H), 7.83 (td, J = 7.8, 1.7 Hz, 1H), 7.77 (dd, J = 8.4, 1.8 Hz, 1H), 7.58 (dd, J = 5.1, 3.2 Hz, 2H), 7.37 (ddd, J = 7.5, 4.8, 1.1 Hz, 1H), 6.01 (d, 1H), 4.18 (d, J = 5.9 Hz, 1H), 3.18 (s,1H). **^{13}C NMR** (126 MHz, CDCl3) δ 186.92 (s), 167.84 (s), 156.36 (s), 148.75 (s), 137.85 (s), 136.97 (s), 136.73 (s), 136.34 (s), 135.49 (s), 135.35 (s), 135.00 (s), 127.22 (s),

124.91 (s), 124.00 (s), 122.85 (s), 121.48 (s), 81.59 (s), 79.73 (s), 44.44 (s). **HRMS** (ESI/IT-TOF): m/z $[M + H]^+$ calcd for $C_{19}H_{13}N_4O$: 313.1084; found: 313.1086.

3.5.9. 5-(8-Ethynyl-6-(pyridin-2-yl)-4H-benzo[f]imidazo[1,5-a][1,4] diazepin-3-yl)oxazole (KRM-II-81, 3)

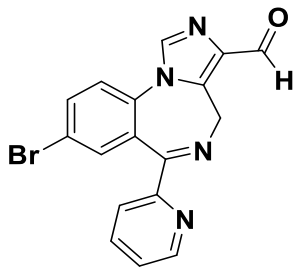


3

The Hz-166 aldehyde or 8-ethynyl-6-(pyridin-2-yl)-4H-benzo[f]imidazo[1,5-a][1,4]diazepine-3-carbaldehyde (75 g, 240.12 mmol) was charged into a round bottom flask, and toluenesulfonylmethyl isocyanide (TosMIC, 60.9 g, 312.3 mmol), K_2CO_3 (99.5 g, 720.3 mmol), and anhydrous methanol (800 mL) were added to the flask. The mixture was then heated to reflux at 65-70°C and held at reflux for 2 hours. After completion of the reaction, confirmed by TLC analysis using silica gel and EtOAc with 1% triethylamine (TEA), the solvent was removed under reduced pressure. The reaction mixture was diluted with cold water (500 mL), and chloroform (800 mL) was added. The organic layer was separated, and the aqueous layer was extracted with chloroform (2x250 mL). The combined organic layers were washed with 10% aqueous NaCl solution (2x500 mL) and dried with Na_2SO_4. The solvents were removed under reduced pressure, and the residue was purified by silica gel flash chromatography using 100% ethyl acetate with 2% TEA and 1% methanol. The appropriate fractions were collected, and the solvents were removed under reduced pressure. The resulting residue was dried under vacuum at 40°C for 3 hours to afford KRM-II-81 (**3**) as an off-white solid (55.4 g, 75% yield).): $\boldsymbol{R_f}$ = 0.3

(EtOAc and 1% each of MeOH and TEA). **^{1}H NMR** (500 MHz, DMSO) δ 8.51 (ddd, J = 4.8, 1.7, 0.9 Hz, 1H), 8.48 (d, J = 8.0 Hz, 2H), 8.08 (dt, J = 8.0, 1.0 Hz, 1H), 7.94 (td, J = 7.7, 1.8 Hz, 1H), 7.88 (d, J = 8.4 Hz, 1H), 7.83 (dd, J = 8.4, 1.8 Hz, 1H), 7.48 (ddd, J = 7.5, 4.8, 1.2 Hz, 1H), 7.44 (s, 2H), 5.53 (d, J = 8.4 Hz, 1H), 4.36 (d, J = 10.0 Hz, 1H), 4.36 (s, 1H). **^{13}C NMR** (126 MHz, DMSO) δ 167.68 (s), 156.78(s), 151.58 (s), 148.78 (s), 146.53 (s), 137.60 (s), 137.10 (s), 136.04 (s), 135.75 (s), 135.24 (s), 129.89 (s), 127.05 (s), 126.55 (s), 125.45 (s), 124.01 (s), 123.86 (s), 122.31 (s), 120.12 (s), 82.88 (s), 82.47 (s), 45.02 (s). **HRMS** (ESI/IT-TOF): m/z [M + H]$^{+}$ calcd for $C_{21}H_{14}N_5O$: 352.1193; found: 352.1194.

3.5.10. 8-bromo-6-(pyridin-2-yl)-4H-benzo[f]imidazo[1,5-a][1,4]diazepine-3-carbaldehyde (17)

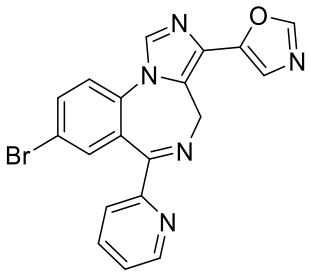


17

Ethyl 8-bromo-6-(pyridin-2-yl)-4H-benzo[f]imidazo[1,5-a][1,4] diazepine-3-carboxylate (**7**, 100 g, 93.37 mmol) was dissolved in anhydrous DCM (1000 mL) and the mixture was cooled to -10 ^{o}C using an ice-methanol bath. The PDBBA solution (927 mL, 1000 mmol in THF-cyclohexane) was added dropwise with vigorous stirring while maintaining the temperature at -10 ^{o}C to 0 ^{o}C. The reaction was monitored by TLC (silica gel) after each 2 minutes and was completed in 30 min. The reaction mixture was quenched with 3% *aq* HCl (500 mL) solution at 0 °C and then water (500 mL) was added. The mixture was stirred for 30 min and the aluminum salt, which resulted, was filtered off through a pad of celite. The filtrate was extracted with DCM (3 x 300

mL). The combined organic layers were washed with 10% aq NaCl solution (2x 500 mL) and dried (Na_2SO_4). The solvents were evaporated, and the solid residue was slurried in 30% EtOAC-hexane (500 mL) and stirred for 30 min at 50°C. The residue was filtered, washed with 30% EtOAc-hexane (2x 200 mL) and dried to obtain the crude aldehyde which was purified by a silica gel flash (short column) chromatography (EtOAc: hexane = 80:20 with 2% triethylamine). The collected fractions were evaporated, the residue was dried at 45°C for 6 hours to afford pure aldehyde **17** as a white powder (65.2 g, 70%). **^{1}H NMR** (500 MHz, $CDCl_3$) δ 10.05 (s, 1H), 8.57 (ddd, *J* = 4.8, 1.6, 0.8 Hz, 1H), 8.10 (d, *J* = 7.9 Hz, 1H), 7.97 (s, 1H), 7.84 (dd, *J* = 7.7, 1.7 Hz, 1H), 7.82 – 7.79 (m, 1H), 7.61 (d, *J* = 2.2 Hz, 1H), 7.50 (d, *J* = 8.6 Hz, 1H), 7.39 (ddd, *J* = 7.5, 4.8, 1.1 Hz, 1H), 6.02 (d, *J* = 9.2 Hz, 1H), 4.18 (d, *J* = 9.5 Hz, 1H). **^{13}C NMR** (126 MHz, $CDCl_3$) δ 186.86 (s), 167.17 (s), 155.98 (s), 148.64 (s), 137.74 (s), 137.11 (s), 136.69 (s), 135.45 (s), 135.42 (s), 135.14 (s), 134.11 (s), 128.59 (s), 125.04 (s), 124.29 (s), 124.02 (s), 120.88 (s), 44.40 (s). **HRMS** (ESI/IT-TOF): m/z $[M + H]^+$ calcd for $C_{17}H_{11}BrN_4O$:367.0189 ; found: 367.0177.

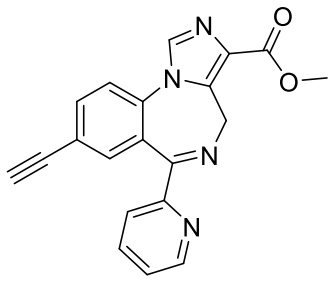
3.5.11. 5-(8-Bromo-6-(pyridin-2-yl)-4H-benzo[f]imidazo[1,5-a][1,4]diazepin-3-yl)oxazole (DS-II-73, 16)



DS-II-73 (16)

A two neck round bottom flask was charged with 8-bromo-6-(pyridin-2-yl)-4H-benzo[f]imidazo[1,5-a][1,4] diazepine-3-carbaldehyde (**17**, 9.0 g, 245 mmol), toluenesulfonylmethyl isocyanide (TosMIC, 6.22 g g, 31.8 mmol), K_2CO_3 (10.16 g, 73.5 mmol) and anhydrous methanol (200 mL) and the mixture was heated to reflux . The reaction mixture was then held at reflux for 3 h. The solvent was removed under reduced pressure after completion of the reaction on analysis by TLC (silica gel, EtOAc and 1% each of TEA). Then reaction mixture was diluted with cold water (300 mL) and $CHCl_3$ (300 mL) was added. The organic layer was separated, and the aqueous layer was extracted with $CHCl_3$ (2x50 mL). The combined organic layers were washed with 10% aq. NaCl (2x50 mL) and dried (Na_2SO_4). The solvents were evaporated, and the residue was purified by silica gel flash chromatography (100% EtOAc with 2% triethylamine and 1% methanol). The fractions were collected, the solvents were removed under reduced pressure. The residue was dried under vacuum at 45^{o}C for 8 h to afford DS-II-73 (**16**) as white solid (7.75 g, 73 %). **^{1}H NMR** (500 MHz, $CDCl_3$) δ 8.60 (ddd, *J* = 4.8, 1.6, 0.8 Hz, 1H), 8.18 (s, 1H), 8.07 (dt, *J* = 8.0, 0.9 Hz, 1H), 7.95 (s, 1H), 7.84 (td, *J* = 7.8, 1.8 Hz, 1H), 7.81 (dd, *J* = 8.6, 2.2 Hz, 1H), 7.57 (dd, *J* = 7.2, 5.4 Hz, 2H), 7.53 (s, 1H), 7.40 (ddd, *J* = 7.5, 4.8, 1.1 Hz, 1H), 5.76 (d, *J* = 12.5 Hz, 1H), 4.31 (d, *J* = 12.6 Hz, 1H). **^{13}C NMR** (126 MHz, $CDCl_3$) δ 167.19 (s), 156.05 (s), 149.98 (s), 148.75 (s), 145.80 (s), 137.13 (s), 135.37 (s), 135.26 (s), 135.12 (s), 134.62 (s), 129.66 (s), 128.36 (s), 126.67 (s), 125.03 (s), 124.37 (s), 124.02 (s), 123.16 (s), 120.61 (s), 45.03 (s). **HRMS** (ESI/IT-TOF): m/z $[M + H]^+$ calcd for $C_{19}H_{12}BrN_5O$: 406.0298; found: 406.0314

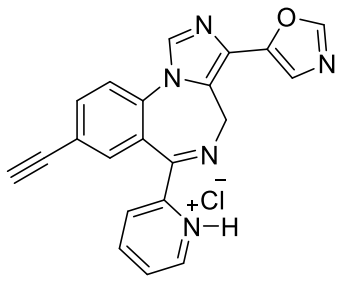
3.5.12. Methyl 8-ethynyl-6-(pyridin-2-yl)-4H-benzo[f]imidazo[1,5-a][1,4]diazepine-3-carboxylate (MP-III-024,18)



To prepare the methyl ester of Hz-166, ethyl ester HZ-166 (**1**, 7.5 g, 21 mmol) was dissolved in anhydrous methanol (150 mL). Sodium methoxide (4.55 g, 84.15 mmol) was added in one portion, and the solution was heated to reflux. The reaction mixture was monitored by TLC analysis using silica gel and a mixture of ethyl acetate (EtOAc) and hexanes (4:1) until the starting material had been consumed, which took approximately 30 minutes. The reaction solution was then cooled to room temperature (rt) and quenched with a saturated aqueous solution of sodium bicarbonate (100 mL). Water (150 mL) was added to the solution, and the methanol was removed under reduced pressure. The resulting product was then extracted with ethyl acetate (3 x 200 mL), and the organic layers were combined, washed with brine, and dried with Na_2SO_4. The solution was concentrated under reduced pressure, yielding a solid product. The solid was purified by refluxing with 30% EtOAc-hexane for 30 min followed by cooling to rt for 2 h. The solids were filtered and washed with 30% EtOAc-hexane (2x50 mL). The solids were dried at 45 °C overnight to afford pure MP-III-024 (**19**) as an off-white powder (5.61 g, 78%). **^{1}H NMR** (300 MHz, $CDCl_3$) δ 8.61 (d, J = 4.7 Hz, 1H), 8.08 (d, J = 7.9 Hz, 1H), 7.99 (s, 1H), 7.90 – 7.81 (m, 1H), 7.76 (dd, J = 8.4, 1.6 Hz, 1H), 7.59 – 7.54 (m, 1H), 7.42 (dd, J = 6.9, 5.4 Hz, 1H), 7.28 (s, 1H), 6.10 (s, 1H), 4.20 (s, 1H), 3.96 (s, 3H), 3.18 (s, 1H); **^{13}C NMR** (75

MHz, $CDCl_3$) δ 167.52, 163.15, 155.91, 148.49, 138.38, 137.36, 136.16, 135.49, 135.37, 134.69, 128.94, 126.94, 125.04, 124.25, 122.97, 121.41, 81.59, 79.67, 51.94, 44.95; **HRMS** (LCMS-IT-TOF) Calc. for $C_{20}H_{15}N_4O_2$ $(M + H)^+$ 343.1150, found 343.1146.

3.5.13. 2-(8-ethynyl-3-(oxazol-5-yl)-4H-benzo[f]imidazo[1,5-a][1,4]diazepin-6-yl)pyridin-1-ium chloride (MYM-V-26, KRM-II-81·HCl, 20)

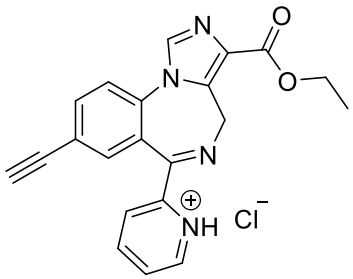


20

KRM-II-81 **3** (5.0, 14.2 mmol) was dissolved in 50 mL of anhydrous DCM under an argon atmosphere at 30-35°C. The resulting light yellow clear solution was then cooled to room temperature, and a 2M solution of HCl in ether (7.5 mL, 14.9 mmol) was added dropwise to the reaction mixture over 10 minutes. During the addition of HCl, a light-yellow cloudy suspension formed. The reaction mixture was stirred for 30 minutes until the starting material was completely consumed, as confirmed by TLC analysis. The residue from the reaction mixture was filtered and washed with anhydrous DCM (2x 20 mL) to remove any unreacted starting material. The residue was then dried under vacuum at 30-35°C, resulting in pure compound KRM-II-81·HCl (**20**) as a light yellow colored amorphous solid, with a yield of 4.6 g (85%). ^{1}**H NMR** (500 MHz, DMSO) δ 8.68 (ddd, J = 4.9, 1.3, 0.8 Hz, 1H), 8.59 (d, J = 4.0 Hz, 1H), 8.51 (s, 1H), 8.09 – 7.99 (m, 2H), 7.93 (d, J = 8.4 Hz, 1H), 7.89 (dd, J = 8.4, 1.7 Hz, 1H), 7.62 (td, 1H), 7.55 (s, 1H), 7.51 (s, 1H), 5.56 (d, J = 3.4 Hz, 1H), 4.44 (d, J = 7.8 Hz, 1H), 4.39 (s, 1H). **^{13}C NMR** (126 MHz, DMSO) δ 167.11 (s), 151.88 (s), 148.12 (s), 148.10 (s), 145.73 (s), 139.19 (s), 137.27

(s), 136.06 (s), 135.76 (s), 135.72 (s), 129.65 (s), 126.47 (s), 126.27 (s), 124.99 (s), 124.33 (s), 122.85 (s), 120.58 (s), 83.26 (s), 82.34 (s), 44.78 (s).

3.5.14. 2-(3-(Ethoxycarbonyl)-8-ethynyl-4H-benzo[f]imidazo[1,5-a][1,4]diazepin-6-yl)pyridin-1-ium hydrochloride (DS-II-47, 21)

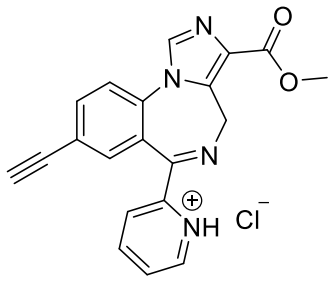


DS-II-47, 21

The starting material Hz-166 (3.0 g, 7.7 mmol) was dissolved in 50 mL of anhydrous DCM under an argon atmosphere. The mixture was stirred at a temperature range of 20-25°C to form a clear light-yellow solution. Then 2M HCl solution in ether (4.25 mL , 8.5 mmol) was added dropwise to the reaction mixture over a 10-minute period. The addition of HCl resulted in the formation of a light-yellow cloudy suspension. The reaction mixture was then stirred for 30 minutes until TLC analysis confirmed complete consumption of the starting material. Subsequently, the residue from the reaction mixture was filtered and washed with anhydrous DCM (2x 20 mL) to remove any unreacted starting material. Afterward, the residue was dried under vacuum at 30-35°C, yielding 2.8 grams (85%) of pure **DS-II-47 (21)** as an off-white solid. **^{1}H NMR** (500 MHz, DMSO) δ 8.55 (dd, *J* = 5.6, 4.3 Hz, 2H), 8.06 (td, *J* = 7.8, 1.3 Hz, 1H), 7.96 (d, *J* = 7.9 Hz, 1H), 7.86 (d, *J* = 8.4 Hz, 1H), 7.83 (dd, *J* = 8.4, 1.7 Hz, 1H), 7.64 – 7.59 (m, 1H), 7.52 (s, 1H), 6.29 (d, *J* = 11.1 Hz, 1H), 5.74 (d, *J* = 13.2 Hz, 1H), 4.29 – 4.22 (m, 2H), 1.25 (t, *J* = 7.1 Hz, 3H). **^{13}C NMR** (126 MHz, DMSO) δ 166.68 (s), 162.43 (s), 154.45 (s), 147.61 (s), 140.17 (s), 138.18 (s), 136.87 (s), 135.88 (s), 135.81 (s), 135.47 (s), 127.62 (s), 126.67 (s),

126.40 (s), 125.56 (s), 124.63 (s), 83.48 (s), 82.21 (s), 60.81 (s), 55.40 (s), 44.80 (s), 14.74 (s).

3.5.15.2-(8-Ethynyl-3-(methoxycarbonyl)-4H-benzo[f]imidazo[1,5-a][1,4]diazepin-6-yl)pyridin-1-ium chloride (DS-II-48, 22)



DS-II-48, 22

The starting material MP-III-024 (3.0 g, 8.08 mmol) was dissolved in 50 mL of anhydrous DCM under an argon atmosphere. The mixture was stirred at a temperature range of 20-25°C to form a clear light-yellow solution. Then 2M HCl solution in ether (4.4 mL , 8.9 mmol) was added dropwise to the reaction mixture over a 10-minute period. The addition of HCl resulted in the formation of a light-yellow cloudy suspension. The reaction mixture was then stirred for 30 minutes until TLC analysis confirmed complete consumption of the starting material. Subsequently, the residue from the reaction mixture was filtered and washed with anhydrous DCM (2x 20 mL) to remove any unreacted starting material. Afterward, the residue was dried under vacuum at 30-35°C, yielding 2.9 grams (87%) of pure **DS-II-48 (22)** as an off-white solid. **^{1}H NMR** (500 MHz, DMSO) δ 8.50 (d, *J* = 4.9 Hz, 1H), 8.46 (s, 1H), 8.00 – 7.94 (m, 2H), 7.84 (d, *J* = 8.4 Hz, 1H), 7.80 (dd, *J* = 8.4, 1.8 Hz, 1H), 7.53 (ddd, *J* = 7.0, 5.0, 2.2 Hz, 1H), 7.47 (d, *J* = 1.6 Hz, 1H), 5.73 (d, *J* = 9.6 Hz, 1H), 4.31 (s, 1H), 4.21 (d, *J* = 8.5 Hz, 1H), 3.76 (s, 3H). **^{13}C NMR** (126 MHz, DMSO) δ 167.08 (s), 163.16 (s), 154.94 (s), 148.08 (s), 139.16 (s), 138.44 (s), 136.81 (s), 135.86 (s), 135.59 (s), 135.47 (s), 127.83 (s), 126.72 (s), 126.20 (s), 124.88 (s), 124.47 (s), 120.77 (s), 83.31 (s), 82.30 (s), 55.39 (s), 44.91 (s).

Chapter 4

The Design and Synthesis of Chiral α5 Subtype BzR/GABAAR Modulators for Treating Anxiety, Depression, and Schizophrenia as well as Asthma

4.1. Introduction and Background

Dysregulation of GABAergic neurotransmission in the CNS has been implicated in several psychiatric disorders.[164] For instance, post-mortem studies have revealed lower expression of GABAergic interneurons [165] and reduced levels of the GABA synthesizing enzyme GAD67 [166] in the brains of individuals with schizophrenia. Depression and anxiety are also associated with alterations in GABA levels and signaling. [167-168] It is well known that the same gene(s) are involved in bipolar disorder, depression as well as schizophrenia. The etiology of both are similar.

While benzodiazepines are commonly used to treat anxiety disorders, their non-selectivity at GABAAR with different subunits often leads to undesirable side effects, including sedation and ataxia.[169] To overcome these limitations, selective targeting of GABAAR, particularly potentiating α2, α3, and α5 subunit-containing GABAAR, has been proposed to achieve the desired therapeutic effects while avoiding benzodiazepine-related side effects.

Schizophrenia, a complex mental disorder, manifests with a range of symptoms including positive symptoms characterized by disorganized thought, hallucinations, delusions, and

psychosis, as well as negative symptoms marked by diminished emotional expression, anhedonia, and social withdrawal.[170-171] In addition to these symptomatic presentations, individuals with schizophrenia often experience cognitive deficits, such as impairments in working memory, learning reversal, and executive function.[170-171]

The pathophysiology of schizophrenia remains multifaceted, and researchers have long sought to understand its origins. One prevailing hypothesis suggests that the hyperactivity of the mesolimbic dopamine system is implicated in mediating the positive symptoms observed in patients, such as hallucinations and delusions.[172-173] However, the exact mechanisms underlying this dopamine dysregulation have yet to be unequivocally identified. Consequently, it is believed that disruptions in upstream brain regions may contribute to the aberrant activity of the dopamine system. Among the brain regions implicated in schizophrenia, the hippocampus has garnered significant attention due to its role in regulating dopamine neuron activity.[174-178] Alterations in the structure and function of the hippocampus have been observed in individuals with schizophrenia, suggesting its involvement in the pathophysiology of the disorder.[174-178] Notably, heightened baseline hippocampal activity has been correlated with the presence of positive symptoms in patients, further highlighting its significance in the disease process.[174,178-179]

Schizophrenia-related pathophysiology has been extensively studied using rodent models, and numerous reports have documented findings in this area.[179-184] Through various mechanisms, these rodent studies have demonstrated the involvement of a multi-synaptic pathway comprising the nucleus accumbens (NAc), ventral pallidum (VP), and ventral tegmental area (VTA) in driving hippocampal hyperactivity. [179-184] This aberrant hippocampal activity, in turn, contributes to dysregulated dopamine system function.

To address these abnormalities, researchers have explored different approaches in rodent models. Pharmacological interventions, neurosurgical techniques, and cell-based therapies have shown promise in restoring normal dopamine system function and mitigating hippocampal hyperactivity.[182-185] Collectively, the growing body of evidence supports the notion that hippocampal hyperactivity plays a pivotal role in the pathophysiology of schizophrenia. Furthermore, reducing hippocampal hyperactivity emerges as a potential beneficial factor in the treatment of this complex disorder.

Post-traumatic stress disorder (PTSD) is a debilitating mental disorder triggered by exposure to traumatic events such as assault or combat. Research findings indicate that a substantial portion of the United States population, approximately 8% of the general population, and a staggering 20% of US combat veterans, suffer from PTSD.[186-187] The hallmark symptoms of PTSD encompass hyperarousal, cognitive deficits, avoidance of trauma-related stimuli, and sleep disturbances, all of which contribute to the profound impact on daily functioning and overall well-being of individuals affected by the disorder.[188-189]

Notably, the presence of comorbid psychotic symptoms, such as hallucinations and delusions, is also observed in individuals with PTSD, further complicating their clinical presentation.[188] Unfortunately, the treatment of PTSD has faced challenges due to the limited efficacy and undesirable side effects associated with commonly prescribed antipsychotic medications, resulting in the discontinuation or withdrawal of certain pharmacological interventions.[171] To develop more effective therapeutic approaches for individuals with PTSD, it is imperative to delve into the intricate pathophysiology underlying the psychosis that accompanies the disorder. By gaining a deeper understanding of the mechanisms involved in the development and manifestation of psychosis in PTSD, researchers can pave the way for targeted and innovative

interventions that address the specific needs of this complex and heterogeneous patient population.

Major Depressive Disorder (MDD) is a significant mental disorder that ranks among the leading causes of disability worldwide. It affects more than 322 million people across the globe.[190] Individuals suffering from MDD exhibit a wide range of symptoms, including anxiety, low mood, anhedonia, and cognitive dysfunctions. Unfortunately, current therapeutic options may not always provide suitable treatment outcomes.[191-192] The underlying pathologies of MDD involve dysfunctions in the GABAergic and monoaminergic systems, reduced neuronal complexity, and neuroendocrinology dysfunctions.[193-196]

Despite the complex nature of MDD, current treatments primarily focus on reversing the monoaminergic imbalance. However, these interventions have limited efficacy in alleviating mood symptoms and do not effectively target cognitive symptoms or other underlying pathologies, including anxiety.[197] Cognitive dysfunctions often persist even when mood symptoms improve. There is a proposed interconnection between mood and cognitive symptoms, as relapses in mood symptoms can be predicted based on persistent cognitive symptoms.[198-201] Therefore, understanding the molecular pathology of MDD is crucial for developing new therapeutic approaches.

Developing therapies for psychiatric disorders, including MDD, poses significant challenges but also presents extensive opportunities to improve the lives of millions of patients worldwide. In the case of depression, connectivity between neurons is decreased, potentially contributing to the severity of the disease.[202] Postmortem research has suggested that individuals with MDD exhibit a lower number of synapses and decreased expression of genes related to synaptic function in the dorsolateral prefrontal cortex (PFC).[202,203-204] Similar effects on neuronal morphology and

connectivity are observed in animal models of chronic stress-related disorders.[205-209] Chronic stress induces changes in dendritic length, spine density, and connectivity between neurons in various brain regions of the limbic system, such as the PFC, hippocampus (HPC), and amygdala.[210] In the PFC and HPC, chronic stress reduces dendritic length and spine density, while increasing various subnuclei of the amygdala.[211] These alterations in neuronal morphology and connectivity partially contribute to cognitive deficits associated with chronic stress, whereas increased connectivity in the amygdala is associated with heightened anxiety episodes observed in chronic stress-related disorders.

Altered GABAergic (inhibitory) function leads to an impaired excitation/inhibition balance in individuals with Major Depressive Disorder (MDD).[193] Reports indicate that untreated depressed patients exhibit reduced levels of GABA in various biological samples, including cerebrospinal fluid[211], plasma [212-217], and specific brain regions such as the occipital cortex[218-222], prefrontal cortex (PFC) [224], and anterior cingulate cortex (ACC) [218,221, 223-226]. However, there are currently no available treatment options targeting this GABA imbalance in MDD patients.

Selective targeting to modulate the activity of α2/3 GABAA receptors (GABAARs) has shown benefits in treating mood and anxiety symptoms[227], while α5 GABAARs are believed to play a role in anxiety and cognitive performance.[228-229] Interestingly, the hippocampus, a brain region crucially involved in MDD, is the primary location of α5-GABAAR subtype in the central nervous system (CNS).[230-231] Within the hippocampus, α5-containing GABAARs constitute approximately 25% of all hippocampal GABAARs[14]. Moreover, the ventral subregions of the hippocampus exhibit higher expression of α5 GABAARs compared to the dorsal subregions, making it an ideal target for activity manipulation within the hippocampus.[232-233]

Extensive research has revealed intriguing findings regarding the role of α5-GABAARs in cognitive functioning and psychiatric disorders. Knockdown of α5-GABAARs in healthy animals has been shown to elicit psychosis-like deficits in sensorimotor gating, as measured by pre-pulse inhibition (PPI).[234] Conversely, the overexpression of the α5 subunit specifically in the ventral hippocampus (vHipp) has demonstrated the potential to reverse dopamine system dysfunction and behavioral deficits in a rodent model of psychosis.[235] Moreover, the development of selective ligands targeting the α5-GABAAR subtype has yielded promising results in various procognitive assays, highlighting their potential for addressing cognitive impairments across a range of disorders. These disorders encompass Alzheimer's disease, Huntington's disease, Down syndrome, schizophrenia [226, 236-239], and depression, all of which are characterized by cognitive disturbances).[240] The α5-GABAAR modulation appears to hold considerable therapeutic promise in mitigating cognitive deficits associated with these conditions. The intricate interplay between α5-GABAARs and cognitive functioning as well as their implications in psychiatric disorders signifies the importance of further exploring and understanding their underlying mechanisms. Continued investigation in this field holds great potential for the development of novel therapeutic strategies aimed at ameliorating cognitive impairments and improving the lives of individuals affected by these challenging disorders.

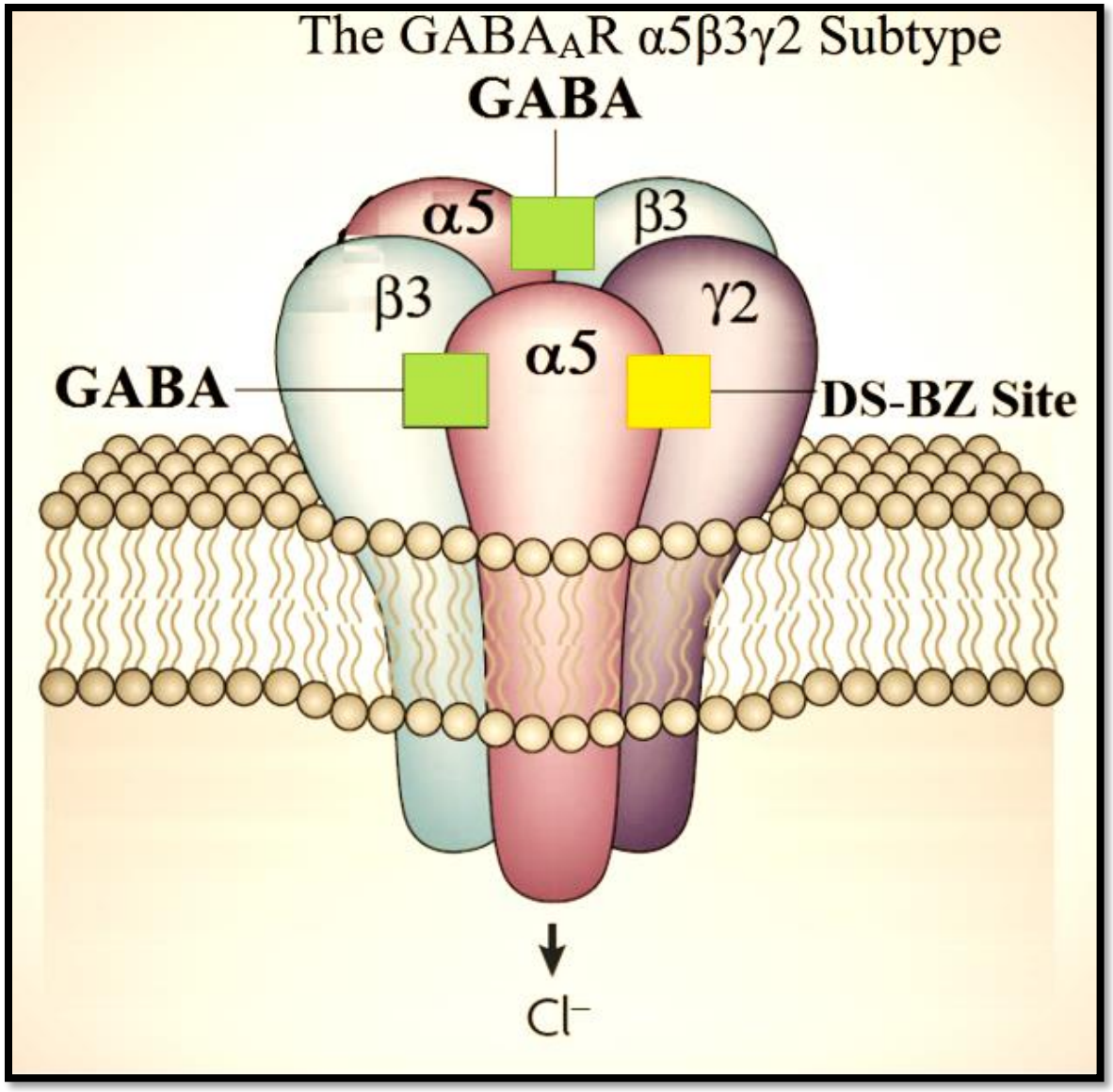


Figure 1: The α5β3γ2 subtype GABAAR. Several IBDZs such as SH-2'F-R-CH3, GL-II-73, and MP-III-22 have been identified as positive allosteric modulators (PAMs) that exert their effects specifically at the α5+γ2- interface (Jacob et al., Nature Reviews Neuroscience, 2008). These compounds have shown the ability to enhance the activity of α5β3γ2 GABAARs through allosteric modulation, leading to potential therapeutic applications. The modified image can be referred to in Jacob et al., Nature Reviews Neuroscience, 2008,

to visually explore the α5β3γ2 subtype GABAAR and its interaction with the identified IBDZs.

The Cook group in Milwaukee has made significant advancements in the development of novel α5-selective ligands (**Figure 2**). Among these ligands, SH-053-2'F-R-CH3, GL-II-73, and MP-III-022 have demonstrated remarkable effectiveness in various preclinical models associated with memory loss, cognitive disorders, depression, Angelman's syndrome, and schizophrenia. These ligands exhibit selectivity towards the α5 subtype of GABAAR and have shown promising potential for therapeutic interventions in a range of neurological and psychiatric conditions. The research conducted by the Cook group represents a significant contribution to the field, offering potential avenues for the development of targeted therapies for these challenging disorders.

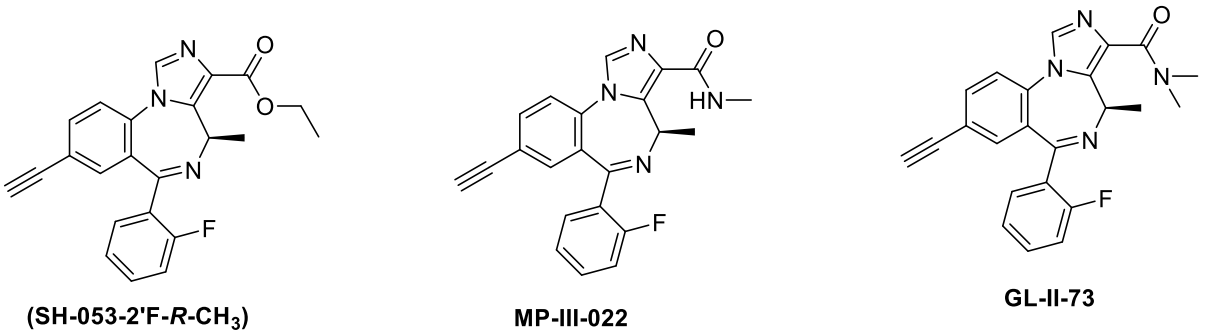


Figure 2: Lead α5-Selective Ligands of this Work

The positive allosteric modulator (PAM) ligand SH-053-2'F-R-CH_3, which selectively targets the α5-subtype of GABAAR, exhibits increased potency at α5 GABAAR subtypes while simultaneously showing decreased potency at the α1, α2, and α3 subtypes. In Table 1, the in vitro binding affinity data illustrates the higher selectivity of SH-053-2'F-R-CH_3 for α5 GABAAR receptors compared to other GABAAR subtypes. Furthermore, **Table 2** presents in

vitro efficacy data, demonstrating that the efficacy of SH-053-2'F-R-CH_3 at α5 GABAAR receptors increases with concentration .[128]

SH-053-2'F-R-CH_3 has demonstrated its potential in preclinical models. It has been shown to reduce the hyperactivity of the dopamine system induced by amphetamine in a maternal immune activation (MAM) model of schizophrenia .[237-238] Additionally, this ligand has exhibited anxiolytic and antidepressant effects in a mouse model of chronic stress, with the effects varying depending on the sex of the subjects.[241]

Related compounds, such as MP-III-022 (a monomethyl amide analog)[242] and SH-053-2'F-R-CH_3-acid (the carboxylic acid analog)[243], which have higher potency at α5-subtypes compared to SH-053-2'F-R-CH_3, have also been investigated in various behavioral studies.[244-245] These studies further highlight the potential of these ligands for therapeutic applications in the field of neuroscience.

Table 1: Binding affinity of SH-053-2'F-R-CH_3 at αxβ3γ2 $GABA_A$/benzodiazepine site subtypes. Measurements were made in duplicate. Ki values are reported in nM

Subtype	Ki (nM)
α1	759.1
α2	948.2
α3	768.8
α4	ND[a,b]

α5	95.2
α6	ND[a],[b]
[a]ND, not determined. [b]Binding at α_4GABAA and α_6GABAA receptors have not been determined. Because ligands which contain pendent phenyl ring do not bind to α_4 and α_6 diazepam insensitive BzR. The Table is modified from Fisher et al. 2010 [128]	

The enantiomer SH-053-2'F-S-CH_3 was evaluated for its pro-cognitive effects using a spatial-recognition working-memory test in the Y-maze, which was induced by prenatal immune activation. It was found that prenatal poly (I:C) exposure did not affect the distance moved during the Y-maze test. However, the administration of SH-053-2'F-S-CH3 resulted in an increase in the total distance moved.[246] Notably, this ligand demonstrated high efficacy in mitigating the amphetamine hypersensitivity phenotype induced by poly (I:C), without causing side effects in control offspring.[246]

Moreover, the ligand SH-053-2'F-R-CH_3 exhibited anxiolytic-like effects in the elevated plus maze (EPM) and facilitated fear memory extinction in male mice.[246] Additionally, it attenuated MK-801-induced hyperlocomotion and pre-pulse inhibition (PPI) disruption in female mice, while not producing the same effects in male mice.[246] These findings suggest a sex-dependent response to the ligand's effects. Overall, the evaluation of the enantiomers SH-053-2'F-S-CH_3 and SH-053-2'F-R-CH_3 has revealed their potential in improving cognitive function, mitigating amphetamine hypersensitivity, and producing anxiolytic-like effects in preclinical models. The ligands' effects vary based on sex, indicating the importance of considering sex-dependent responses in their therapeutic applications.

The distribution of the α5-subunit of GABAAR in the brain is particularly noteworthy, as it is predominantly found in brain regions that are highly involved in cognitive processes, such as the hippocampus and prefrontal cortex (PFC).[247] Importantly, studies analyzing preclinical and postmortem data have indicated that the α5-subunit is downregulated in the aging brain.[248-249] In addition, recent research has demonstrated that the synaptic localization of α5-containing GABAARs contributes to dendritic outgrowth and spine maturation.[251] This evidence strongly suggests that the α5-containing GABAAR subunit plays a critical role in the regulation of cognitive function mediated by the GABAergic system. Reversing the decreased activity of this receptor during aging or indirectly through dendritic growth mechanisms are directly involved in this regulatory process. These findings highlight the significance of the α5-subunit in cognitive function and its potential as a therapeutic target for addressing cognitive deficits associated with aging and other cognitive disorders.

Table 2: Efficacy of SH-053-2'F-R-CH3 at αxβ3γ2GABAA receptor subtypes as % of control current at 100 nM and 1 mM concentrations.

Subtype	% of control current
α1	111/154
α2	124/185
α3	125/220
α4	
α5	183/387

α6	
Data were presented as 100 nM/ 1mM. The table is adopted from Fischer et al. 2010	

GL-II-73, a lead α5-positive allosteric modulator (α5-PAM) developed in Milwaukee, has shown promising effects in improving working memory in mouse models of chronic stress and aging.[229] This ligand exhibits a preferential binding affinity for α5-containing GABAA receptors, with 6 times tighter affinity for α2 subtype, 11 times tighter affinity for α1 subtype, and 12.5 times tighter affinity for α3 subtypes, as indicated in **Table 3** .[229] Notably, the efficacy of GL-II-73 is significantly more potent at α5 subtypes compared to other benzodiazepine receptor (BZR) subtypes, as depicted in **Figure 2**.[229] Importantly, the observed biological effects of GL-II-73 can be attributed to its selectivity for α5 subtypes or its preference for this specific subtype, rather than actions at other subtypes. Comprehensive screening, such as the 47-panel PDSP screen, conducted by PDSP, ROTH, UNC, revealed that no other central nervous system (CNS) receptors, including HERG channels, are involved (PhD thesis Guanguan Li).

Table 3: Binding affinity of GL-II-73 at αxβ3γ2 $GABA_A$/benzodiazepine site subtypes

Subtype	Ki (μM)
α1	55 ± 4
α2	30 ± 5
α3	63 ± 7
α4	ND

α5	5 ± 2
α6	ND
Ki values are reported in μM. This table is adopted from Fisher et al. 2010[128] and Prevot et al. 2019[229]	

In comparison with other α5-PAMs, GL-II-73 has demonstrated improved cognitive functions in aged rats, as demonstrated by research conducted with Etienne Sibille and Thomas Prevot.[252] Furthermore, in vivo testing of this ligand in elderly mice has shown promising results in improving cognitive deficits and reversing dendritic shrinkage.[253] These findings hold significant implications for conditions such as major depressive disorder (MDD), schizophrenia, and Alzheimer's disease, where improving cognitive function is a key therapeutic target.

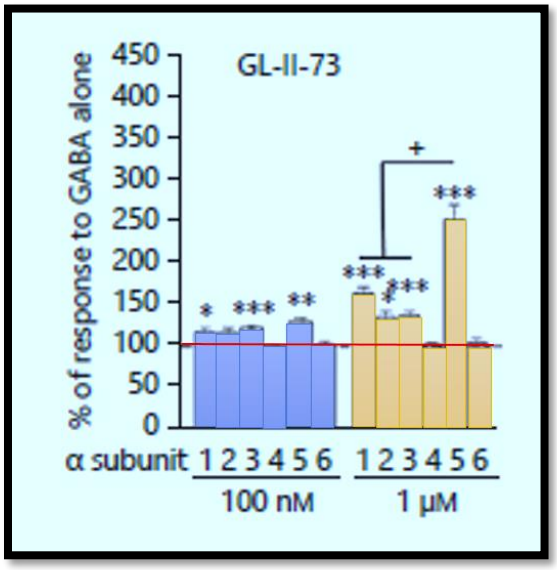


Figure 3: The figure visually represents the relative potentiation of GL-II-73 at different GABAA receptor subtypes, highlighting its greater affinity for the α5 subtype compared to

α1, α2, and α3 subtypes. At a concentration of 1 μM, the potentiation of GL-II-73 at α1, α2, and α3 subtypes was comparatively lower than its potentiation at the α5 subtype, suggesting that this ligand exhibits a preference for α5-containing GABAA receptors. This modified figure provides a graphical representation of GL-II-73's α5 preference, as supported by the experimental data presented in the PhD thesis of Guanguan Li, University of Wisconsin – Milwaukee, 2019.

The GABAergic system has been recognized to have a significant impact on the aging process, and reduced GABAergic function is known to play a crucial role in aging-related cognitive decline. GL-II-73, by targeting α5-GABAA receptors, has shown potential in mitigating these deficits and reversing age-related cognitive decline.[229] In a study conducted on aged mice, chronic treatment with GL-II-73 demonstrated the ability to reverse cognitive decline and counteract dendritic shrinkage and spine atrophy in the prefrontal cortex and CA region of the brain. Remarkably, chronic treatment with GL-II-73 led to an increase in dendritic length, spine count, and spine density in these important brain regions, signifying its neurotrophic effects.[229] This is a significant finding, as commonly used benzodiazepines have been associated with a decrease in spine density in cortical pyramidal neurons.[254]

Interestingly, recent reports have indicated that ketamine, an antidepressant, acts through the NMDA receptor of GABA neurons to exert its therapeutic effects.[255-256] Ongoing studies are exploring the mechanism of action underlying the neurotrophic effects of GL-II-73 and investigating any potential connections with the mechanism of action of ketamine. These investigations aim to shed light on the pathways and processes involved in the neurotrophic effects of GL-II-73, further expanding our understanding of its therapeutic potential for age-

related cognitive decline and potentially uncovering novel approaches for treating related conditions.

The pronounced neurotrophic effects of GL-II-73 were observed primarily in the apical segment of pyramidal neuron dendrites, which coincides with the location of α5-GABAA receptors (394). These findings strongly suggest that the neurotrophic effects of GL-II-73 are mediated through the activation of α5-GABAA receptors. Furthermore, GL-II-73 demonstrated an increase in spine counts and spine density in the basal segment of pyramidal neurons in the CA1 region.

Notably, when animals were discontinued from the administration of GL-II-73, the cognitive effects diminished, while the neurotrophic effects remained. This implies that continuous administration of GL-II-73 is necessary for sustaining the improvement in cognitive performance. It is worth highlighting that GL-II-73 is the first agent to exhibit neurotrophic effects by targeting an inhibitory system, providing a unique approach to alleviate symptoms of depression and cognitive deficits. Additionally, GL-II-73 has demonstrated anxiolytic and antidepressant effects, making it a potential therapeutic option for patients experiencing cognitive decline associated with GABAergic downregulation.[229]

Considering the excellent results of these α5-GABAA receptor subtype selective ligands in animal models, it becomes crucial to develop an improved scalable synthesis method for these compounds. This would be an essential step in advancing this technology toward clinical trials, opening up possibilities for potential therapeutic interventions in humans suffering from cognitive decline associated with GABAergic dysregulation. To support further ADME (absorption, distribution, metabolism, and excretion) toxicity studies and facilitate the

advancement of GL-II-73 as a potential therapeutic agent, a large-scale synthesis method was developed. This approach enables the production of a greater quantity of GL-II-73 for extensive testing, ensuring an ample supply of the compound for preclinical investigations. The large-scale synthesis of GL-II-73 allows collaborators at CAMH to conduct comprehensive studies on its pharmacokinetic properties, including its absorption and distribution within the body, metabolism processes, and excretion pathways. These studies are crucial for understanding how GL-II-73 interacts with biological systems and how it may be further optimized for therapeutic use.

By scaling up the synthesis process, scientists can generate enough GL-II-73 to support its continued evaluation, moving closer to potential clinical trials and the eventual development of a safe and effective therapeutic agent for the treatment of relevant conditions.

4.7.Chemistry: Results and Discussion

4.7.1. Improved scalable synthesis of SH-053-2'F-*R*-CH_3 and SH-053-2'F-*S*-CH_3

In order to facilitate structure-activity relationship (SAR) analysis and explore the potential of analogs, a large-scale synthesis of the R ethyl ester, ethyl (R)-8-ethynyl-6-(2-fluorophenyl)-4-methyl-4H-benzo[f]imidazo[1,5-a][1,4]diazepine-3-carboxylate (SH-053-2'F-R-CH3), and its enantiomer, SH-053-2'F-S-CH3, was undertaken. This synthetic approach enables the production of larger quantities of these compounds, thereby facilitating further SAR studies and expanding the scope for exploring their pharmacological properties. By synthesizing these compounds on a larger scale, a broader range of analogs can be designed, which can be systematically modified to investigate the relationship between chemical structure and biological activity. This SAR

analysis is crucial for identifying key molecular features responsible for the compounds' effects and guiding future drug development efforts. SH-053-2'F-R-CH3 was synthesized at 300 g scale while its enantiomer, SH-053-2'F-S-CH3 was synthesized at 50 g scale. Both compounds were synthesized according to the following description.

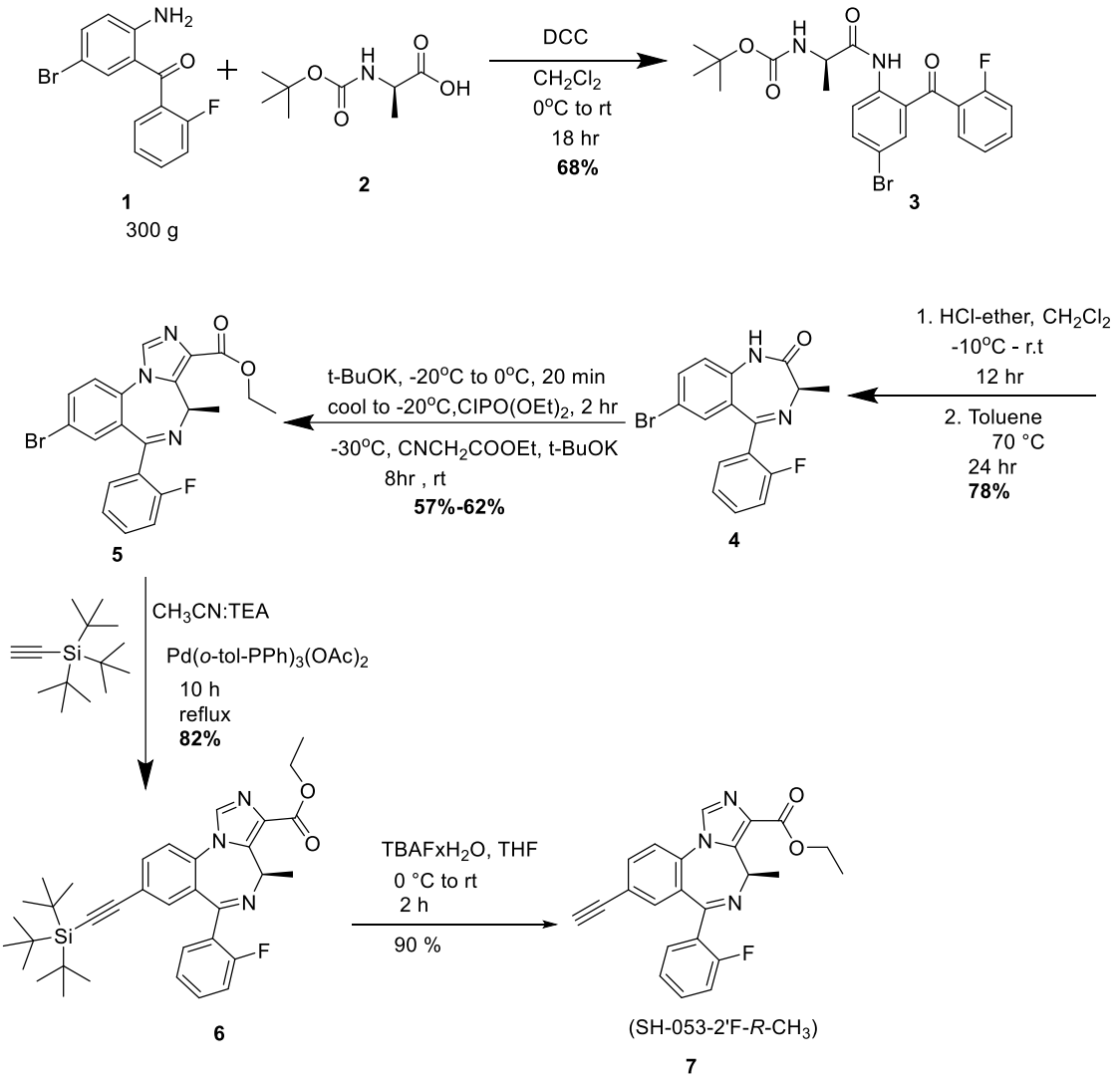
The difference in chirality between the two enantiomers, SH-053-2'F-R-CH3 and SH-053-2'F-S-CH_3, originates from the choice of starting amino acids during the synthesis process. **Scheme 1** illustrates the synthesis of SH-053-2'F-R-CH_3, wherein the R-enantiomer of the amino acid (tert-butoxycarbonyl)-D-alanine was utilized as the starting material. On the other hand, **Scheme 2** demonstrates the synthesis of SH-053-2'F-S-CH_3, which employed the S-enantiomer of the amino acid (tert-butoxycarbonyl)-L-alanine. The peptide coupling reaction between the starting amine, 2-amino-5-bromophenyl)(2'-fluorophenyl)methanone (**1**), and the respective chiral amino acids was carried out using the peptide coupling reagent *N*,*N'*-dicyclohexylcarbodiimide (DCC).

For the synthesis of SH-053-2'F-R-CH_3, the starting amine was treated with the R-amino acid, *N*-Boc-D-alanine, in the presence of DCC. This reaction resulted in the formation of the amide compound 85, with a yield of 77%, on a scale of 300 grams. Similarly, for the synthesis of SH-053-2'F-S-CH3, the same synthetic strategy was followed. However, in this case, the starting amine was treated with the S-amino acid, *N*-Boc-L-alanine, instead of *N*-Boc-D-alanine. The reaction yield for the S-enantiomer was similar to that of the R-enantiomer. The use of *N*-Boc-D-alanine or *N*-Boc-L-alanine in conjunction with DCC enables the successful coupling of the starting amine and the respective amino acid to form the target amide compounds. It is important to note that during the peptide coupling reaction, a homogenous solution of N,N'-dicyclohexylcarbodiimide (DCC) dissolved in dichloromethane (DCM) should be added dropwise to the mixture of the chiral amino acid and the starting benzophenone (3) in DCM at 0

˚C. It is crucial to perform this addition at a lower temperature and in a controlled manner to prevent the dimerization of DCC into a dimer of DCC urea. This dimerization can occur when DCC is added in one portion at room temperature, as higher concentrations of DCC favor the formation of the dimer. To avoid this side reaction and maintain the desired reaction conditions, the dropwise addition of DCC at 0 ˚C helps to ensure a successful and efficient peptide coupling reaction.

The next step is the deprotection of Boc group. For the deprotection of the Boc-group, two different acid solutions were employed: 2M HCl in ether and 4M HCl in dioxane. The deprotection process involved the addition of the acid solution dropwise to the mixture of amides (**3,10**) in dichloromethane (DCM), while maintaining a temperature range of -10 to 0 ˚C for an hour. Subsequently, the mixture was stirred at room temperature for 12 hours. Both 2M HCl in ether and 4M HCl in dioxane proved to be effective for the deprotection of the Boc-group. However, it was observed that the use of 4M HCl in dioxane yielded better results in terms of Boc-group deprotection. The higher concentration of acid in the 4M HCl solution might contribute to the improved efficiency of Boc-group deprotection. By carefully controlling the reaction conditions and selecting the appropriate acid solution, successful deprotection of the Boc-group was achieved, allowing for the further progression of the synthesis.

Scheme 2. Synthesis of SH-053-2'F-R-CH3

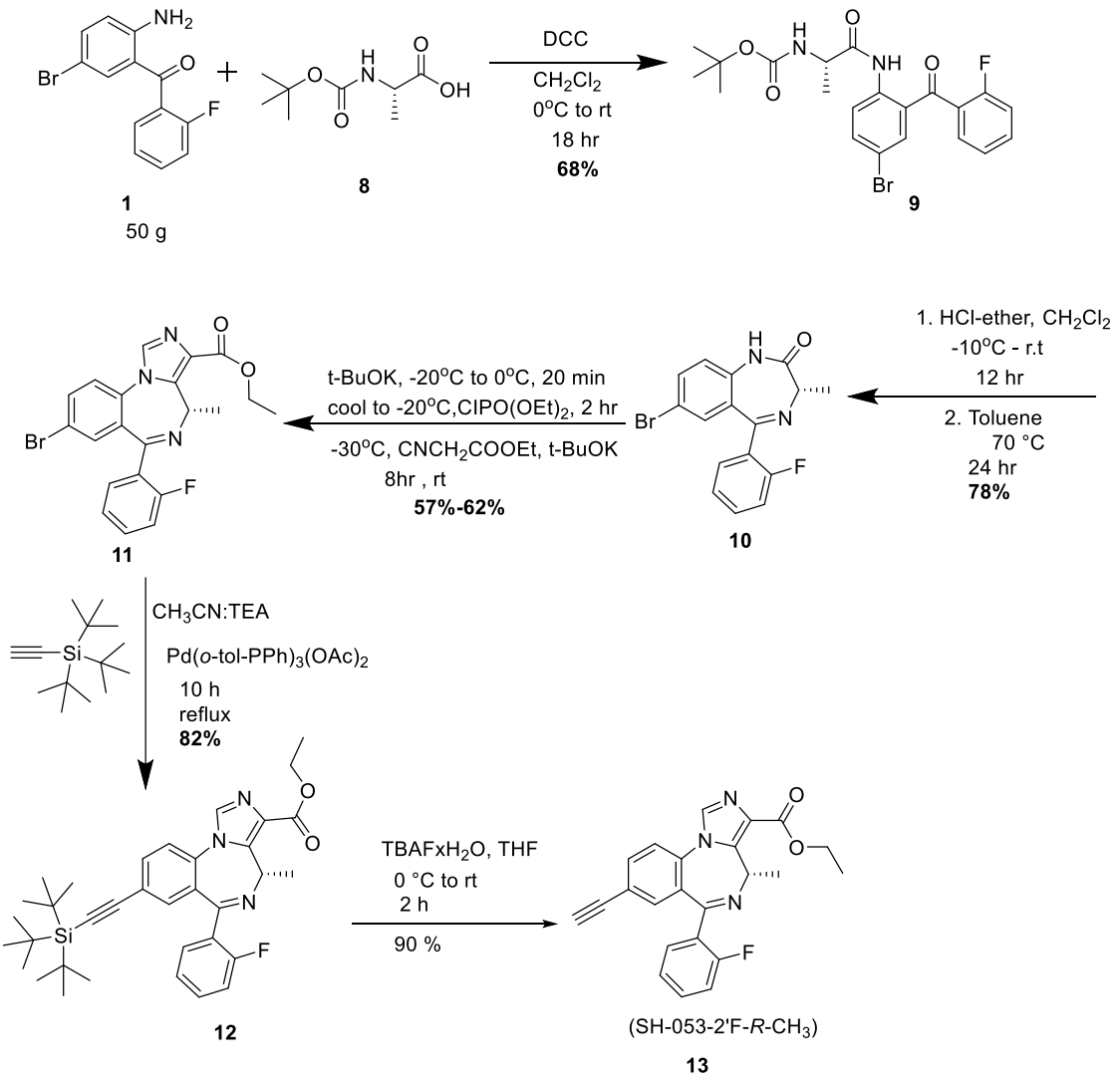


After the deprotection step, the remaining acid was neutralized by adding an aqueous sodium bicarbonate ($NaHCO_3$) solution. Upon addition of the $NaHCO_3$ solution, a mild exothermic reaction was observed. This neutralization step helps to adjust the pH and ensure a more controlled reaction environment. Subsequently, the cyclization of the deprotected amine was accomplished by dissolving the amine in methanol under neutral conditions and stirring the

mixture for 24 hours. This allows for the completion of the cyclization reaction, leading to the formation of the desired 1,4-benzodiazepine intermediates (**4,11**).

In some cases of the cyclization reaction performed in methanol, a light polar spot was observed on thin-layer chromatography (TLC), appearing just below the product spot. To address this issue, the cyclization reaction was subsequently carried out in anhydrous toluene, offering several advantages. Firstly, the use of toluene as a solvent resulted in the absence of polar impurities, eliminating the observed polar spot on TLC. Additionally, the reaction no longer required an aqueous workup step. Moreover, the use of anhydrous toluene as the solvent during the cyclization reaction did not have any impact on the chirality of the molecule, as confirmed by chiral high-performance liquid chromatography (HPLC) analysis. This is crucial for maintaining the desired stereochemistry of the synthesized compound. Overall, the use of anhydrous toluene as the solvent for the cyclization reaction provided improved results, including the absence of polar impurities, simplified workup procedure, and preservation of chirality. These optimizations contribute to the overall efficiency and quality of the synthetic process. After the removal of the Boc protecting group, the deprotected amine was dissolved in anhydrous toluene and heated at a temperature range of 60-70 °C for a period of 12-24 hours, which varied depending on the reaction scale. Following completion of the reaction, the toluene solvent was evaporated, and the resulting product was purified using a solvent mixture of 10% ethyl acetate (EtOAc) and hexane. The yield for the R-benzodiazepine intermediate **(4**) was 80% while S-benzodiazepine intermediate (**11**) was formed in 79% yield.

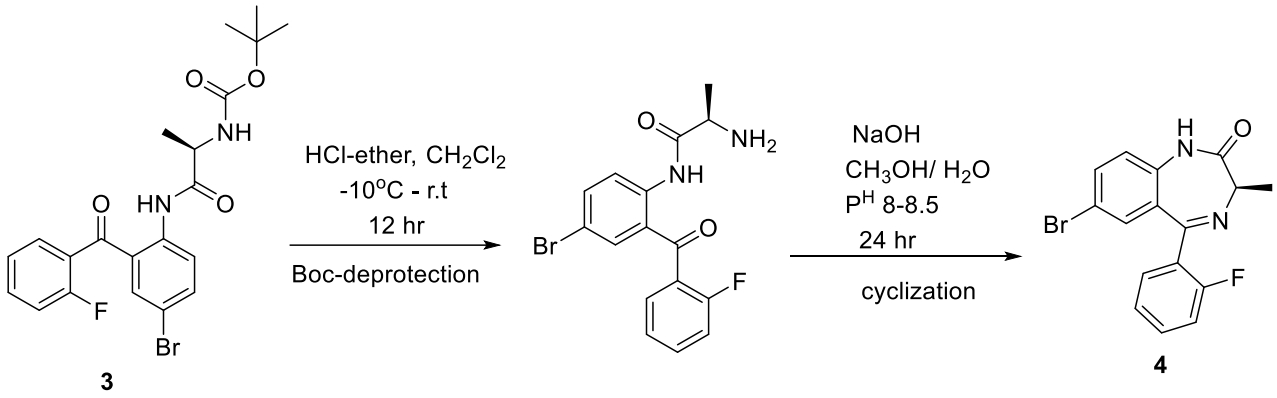
Scheme 2. Synthesis of SH-053-2'F-S-CH$_3$



During the earlier benzodiazepine ring closure step (highlighted in **Scheme 3**), an unexpected epimerization of the chiral methyl group was observed under the basic condensation conditions. Initially, the pH was adjusted to 8-8.5 using 0.1 equivalent of aqueous sodium hydroxide (NaOH). To increase the reaction rate, the equivalent of NaOH was increased to 1 equivalent, and the reaction time was reduced from 24 hours to 12 hours. While these modifications improved the reaction rate, they also led to the undesired epimerization of the chiral methyl group. This epimerization issue, along with considering the overall reaction yield of the peptide

coupling step, prompted the design of a new synthetic method for the synthesis of GL-II-73. By reevaluating the reaction conditions and considering the challenges encountered, a new synthetic method was developed by Daniel Knutson, a former graduate student, to address the epimerization issue and optimize the overall yield of the desired product. This new method aimed to minimize epimerization while maintaining a high reaction yield, ensuring the successful synthesis of GL-II-73.

Scheme 3: Cyclization of free amine to form benzodiazepine 4 using NaOH as base

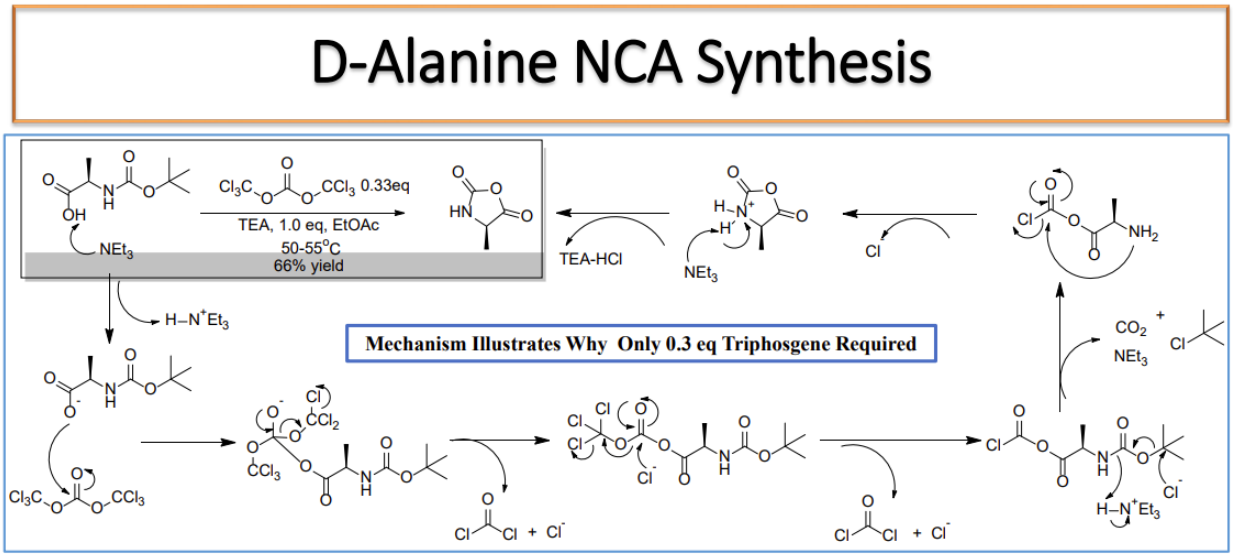


A novel synthetic procedure was developed based on the work of Fier and Whitakker at Merck and Co, which involved the synthesis of N-carboxyanhydrides (NCAs) from optically pure amino acids. In this method, the condensation step was carried out in non-polar solvents under neutral conditions, providing a safer and more controlled environment for the reaction (Fier and Whitakker).[257]

To synthesize N-carboxy-D-alanine anhydride, the Boc-protected amino acid was reacted with triphosgene in the presence of triethylamine. Triphosgene was chosen as an alternative to phosgene due to safety concerns (Fier and Whitakker[257]; Phosgene, [258-259]; Triphosgene[260]). A

possible mechanism of NCA formation is depicted in **Scheme 4**. The reaction yielded N-carboxy-D-alanine anhydride (NCA) in a moderate yield of 65% on a 50 g scale. Purification of the crude oily mass was achieved by recrystallization using a mixture of dichloromethane (DCM) and hexane (Fier and Whitakker).[257]

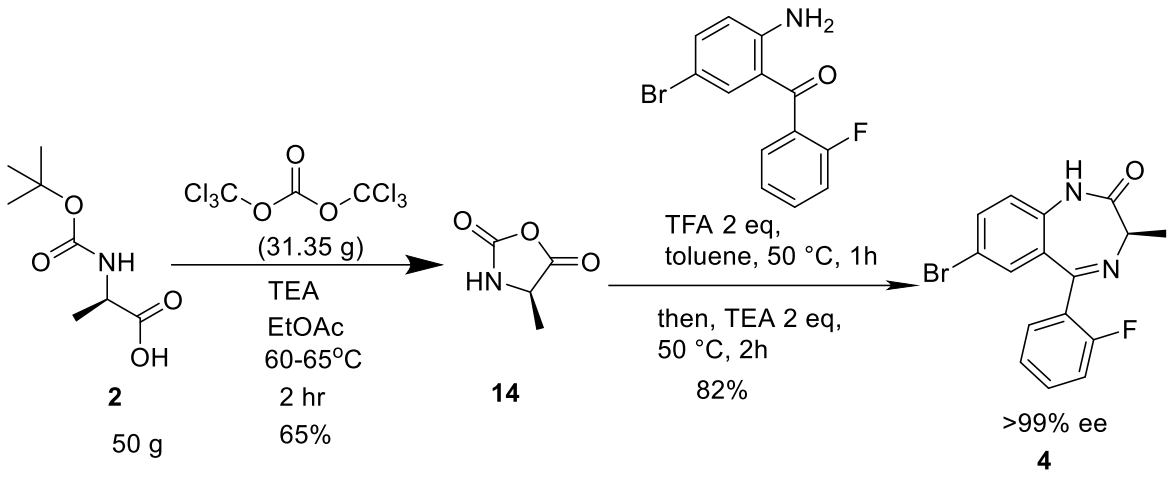
Scheme 4. Probable mechanism of NCA formation



Subsequently, the Boc-D-alanine NCA and amino benzophenone (3) were reacted in toluene with the addition of trifluoroacetic acid (TFA). Trifluoroacetic acid was utilized to form the trifluoroacetate salt of the amide intermediate, preventing oligomer formation. The reaction was then induced by the addition of triethylamine, leading to the condensation between the primary amine and the benzophenone carbonyl group. This process resulted in the formation of the optically pure (>99% ee) benzodiazepine (**4**) with a yield of 82%. The solid benzodiazepine intermediate was easily purified by washing with a mixture of ethyl acetate and hexanes (Fier and Whitakker).[107] I synthesized several 50 g batches of benzodiazepine intermediate following

NCA route (**Scheme 4**) and gave to our former graduate student, Daniel Knutson, to make optically pure GL-II-73.

Scheme 5: Synthesis of benzodiazepine intermediate by NCA route



The newly developed method represents a robust and higher yielding process compared to the previous approach. However, it is important to note that the first two steps, involving NCA formation and cyclization (**Scheme 4**), require extremely anhydrous conditions. This includes the use of anhydrous reagents, anhydrous solvents, and dry flasks, with careful monitoring throughout the process. Any traces of moisture can have a detrimental impact on the reaction. These steps can be challenging, particularly in environments with higher humidity, such as during the summer season. Additionally, the use of anhydrous solvents and reagents in this method may incur higher costs compared to standard ACS grade reagents. It is necessary to carefully consider these factors, including the availability and cost of anhydrous materials, when implementing this synthetic approach.

In order to develop an industrial-friendly process, the decision was made to revisit the Boc-route and focus on increasing the yield of the peptide coupling reaction. Additionally, it was crucial to

address the issue of racemization during the cyclization step. Extensive efforts were dedicated to optimizing the reaction conditions and exploring different strategies to enhance the yield of the peptide coupling reaction. Various reaction parameters, such as temperature, solvent, catalysts, and reaction times, were carefully examined to identify the optimal conditions that would maximize the desired product yield. Furthermore, innovative approaches were explored to prevent racemization during the cyclization step. Special attention was given to identifying suitable protecting groups and choosing appropriate solvents and reaction conditions that would minimize racemization and preserve the stereochemistry of the desired compound.

Our senior colleagues, Dan Knutson and Md Yeunus Mian, conducted a series of trials to enhance the peptide coupling reaction. These efforts were aimed at optimizing the reaction conditions and identifying strategies to improve the overall efficiency and yield. Throughout their investigations, various parameters were explored, including reaction temperature, choice of solvents, catalysts, and reaction times. They systematically varied these factors to evaluate their impact on the reaction outcome and identify the most favorable conditions for achieving improved results. The findings of their trials were carefully documented and compiled, resulting in valuable insights into the optimization of the peptide coupling reaction. The collected data and observations were summarized and presented in **Table 4**, providing a comprehensive overview of the different approaches and their corresponding outcomes.

Based on the findings presented in **Table 4**, a slightly higher yield was observed when using 1.6 equivalents of the peptide coupling reagent, N,N'-Dicyclohexylcarbodiimide (DCC), and 1.4 equivalents of the amino acid (**Entry 10**). To achieve this, the addition of DCC was carefully performed at a temperature of -10°C over a period of 30 minutes. Subsequently, the reaction was

stirred for a longer duration of 42 hours to ensure complete conversion and maximize the yield of the desired product.

Scheme 6: Peptide coupling and cyclization for formation of benzodiazepine, 4

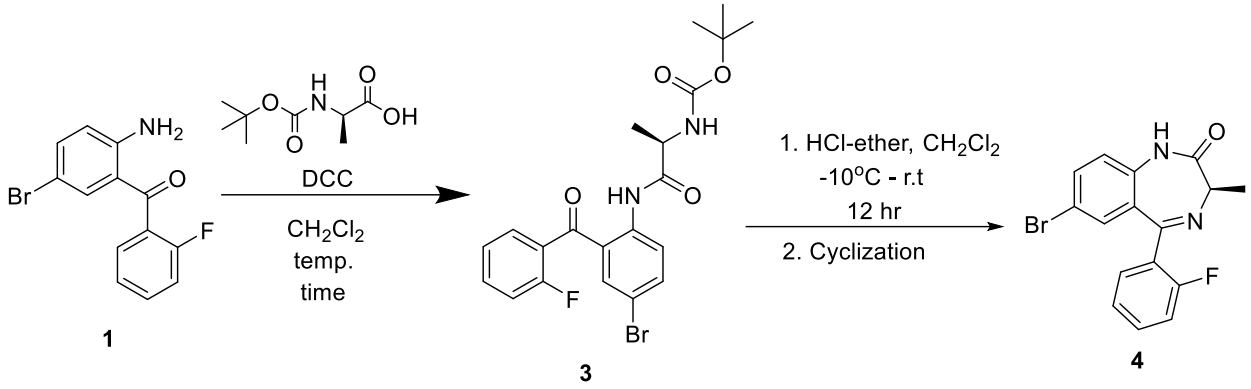


Table 4: Peptide coupling trials

Entry	Coupling reagent	Boc-D-Ala-OH	Additive	Solvent	Temp	Time	Yield
1	DCC, 1.2 equiv	1.0 equiv		CH_2Cl_2	rt	24h	60%
2	DCC, 1.2 equiv	1.0 equiv		CH_2Cl_2	rt	48h	55%
3	DCC, 1.2 equiv	1.0 equiv	DMAP, 0.1eq	CH_2Cl_2	rt	24h	62%
4	DCC, 2.0 equiv	2.0 equiv		CH_2Cl_2	rt	24h	59%
5	EDCI, 1.2 equiv	1.0 equiv	TEA, 1.2 eq	CH_2Cl_2	rt	24h	10%
6	EDCI, 1.2 equiv	2.0 equiv	TEA, 1.2 eq	CH_2Cl_2	rt	24h	39%

7	DCC, 1.4 equiv*	1.2 equiv		CH_2Cl_2	rt	36 hr	68%
9	DCC, 1.5 equiv*	1.5equiv		CH_2Cl_2	rt	36 hr	64%
9	DCC, 1.6 equiv*	1.4 equiv		CH_2Cl_2	rt	36 hr	65%
10	DCC, 1.6 equiv*	1.4 equiv		CH_2Cl_2	-10 addition, rt	42 hr	73%

Entries **1-6** of the trials mentioned in **Table 4** were conducted by Dr. Knutson (Knutson et al., 2020). Subsequently, entries 7-10 were carried out by Md Yeunus Mian (PhD Thesis 2022,Md Yeunus Mian, University of Wisconsin-Milwaukee), further building upon the work of Dr. Knutson.

Building upon these promising results, Md Yeunus Mian successfully scaled up the peptide coupling reaction to a larger scale of 170 grams. This successful scale-up demonstrates the reproducibility and potential applicability of the optimized conditions to achieve higher yields in a larger production setting. Following the successful optimization of the peptide coupling reaction, I scaled up the process to a larger quantity of 300 grams. In this scaled-up synthesis, a modification was made to the cyclization method, specifically regarding the choice of solvent. While the previous cyclization method employed methanol (MeOH) as the reaction solvent, the scaled-up synthesis utilized toluene, as previously described (**Scheme 1**).

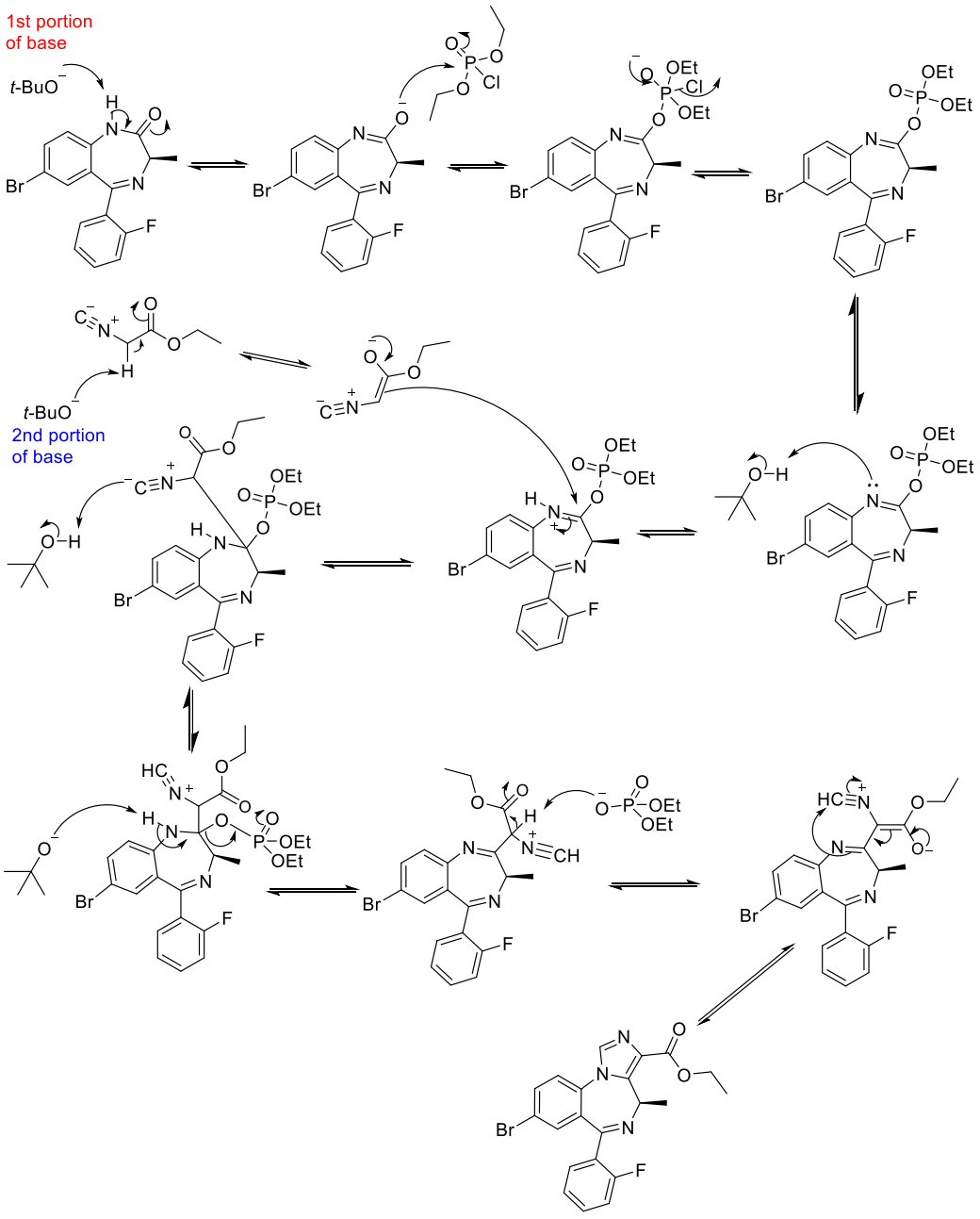
The decision to switch to toluene as the solvent in the cyclization step was likely made based on considerations such as reaction kinetics, solubility, and process compatibility for a larger-scale synthesis. Toluene, being a non-polar solvent, can offer advantages such as improved solubility of the reactants and products, as well as better control over reaction conditions during the cyclization process. By employing toluene as the reaction solvent in the scaled-up synthesis, it is

expected that the process can be conducted more efficiently and reliably on a larger scale. This modification allows for better scalability and compatibility with industrial processes, facilitating the production of a larger quantity of the desired compound while maintaining the desired quality and purity.

The successful scale-up of the peptide coupling reaction to 300 grams demonstrates the feasibility and applicability of the optimized conditions and the use of toluene as the reaction solvent for cyclization reaction. This advancement in the synthetic process paves the way for potential industrial applications and the production of the desired compound in larger quantities.

The third step of the synthesis involved the installation of the imidazole ring on the seven-member ring of benzodiazepines to form the imidazodiazepine intermediate (**5**) [261]. This step is crucial for introducing additional structural features and modifying the pharmacological properties of the compound. In order to improve the overall condition of the reaction, several modifications were made. One such modification involved the deprotonation of the benzodiazepine using solid potassium t-butoxide in the previous procedure. In the new procedure, a solution of potassium t-butoxide (1.3 equivalents) in tetrahydrofuran (THF) was used to carry out the deprotonation step. The use of a potassium t-butoxide solution in THF offers several advantages over the previous solid form. Firstly, the use of a solution allows for better control over the deprotonation process, ensuring more efficient and uniform reaction conditions. Secondly, the use of THF as a solvent can enhance the solubility and reactivity of the reagents, facilitating better mixing and faster reaction kinetics. Under the basic condition using the potassium *t*-butoxide solution in THF, effective deprotonation of the benzodiazepine occurred. Following this step, diethylchlorophosphate was added to generate the iminophosphate intermediate, as depicted in **Scheme 6**.

Scheme 7: Possible mechanism of imidazole top installation on benzodiazepine



The reaction progress was monitored by TLC, and once all the starting material was consumed, the second portion of base and ethyl isocyanoacetate were added. In this procedure, a lower quantity of ethyl isocyanoacetate (1.3 equivalents) was used compared to the previous method. This adjustment was made to optimize the reaction conditions and achieve the desired outcome.

The use of a lower quantity of ethyl isocyanoacetate can help avoid excessive or wasteful usage of the reagent, while still ensuring efficient conversion to the desired product.

In the purification step of the synthesis, chromatography was not necessary to purify the product. Instead, the crude solid containing the imidazodiazepine (**5**) was subjected to a washing step using t-butyl methyl ether. The use of hot t-butyl methyl ether as the washing solvent allowed for the removal of any residual impurities, particularly byproducts related to the phosphate intermediates. The choice of t-butyl methyl ether as the washing solvent is advantageous due to its ability to dissolve impurities and facilitate their removal from the solid product. The use of hot solvent further enhances the dissolution and extraction process, ensuring a more thorough removal of any remaining impurities. By washing the crude solid with hot t-butyl methyl ether, a pure form of the imidazodiazepine (**5**) was obtained. This purification step helps to improve the overall quality and purity of the final product, ensuring that it meets the desired specifications for further characterization and use in subsequent steps of the synthesis or in subsequent studies. The omission of chromatography in the purification process can save time and resources, providing a more efficient and streamlined approach to obtaining a pure form of the imidazodiazepine compound. The yield of the reaction for the synthesis of the imidazodiazepine compounds (R and S enantiomers) varied within the range of 59-68% on a scale-wise basis. The yield can vary depending on several factors, including the specific reaction conditions, reaction scale, and variations in the starting materials or procedures.

In the subsequent step of the reaction sequence, the aryl bromide 88 was transformed into the silyl-protected acetylene using a copper-free Sonogashira coupling method.[262-263] This transformation involved the use of palladium catalyst, which played a crucial role in facilitating the coupling reaction. The copper-free Sonogashira coupling of the imidazodiazepine

intermediate with TIPS-acetylene resulted in the formation of the TIPS-protected SH-053-2'F-R-CH_3 product with a yield of 88%. This step played a crucial role in introducing the desired silyl-protected acetylene moiety into the molecule. The TIPS-protected SH-053-2'F-S-CH_3 was synthesized in a similar fashion. The compounds obtained from the reaction were subjected to purification using column chromatography. In this case, column chromatography was employed to remove any residual Pd salts that might be present in the reaction mixture.

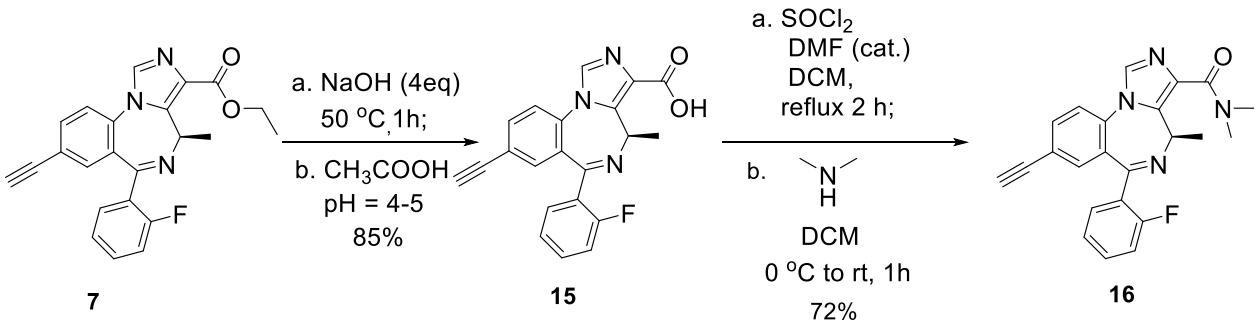
In the final step of the synthesis, the silyl protecting group of the compound was removed through a fluoride-mediated deprotection process. This was achieved by carefully adding a 1M solution of TBAF in THF at a temperature of -10°C. Under these conditions, the TIPS group was successfully cleaved, resulting in the formation of SH-053-2'F-R-CH_3 with an impressive enantiomeric excess of 99%. To ensure the purity of the final product, a new purification method was developed. Instead of relying on chromatographic purification as in the previous approach, a methanol-water mixture was employed to remove impurities associated with tetrabutyl ammonium salts. This modified purification method proved to be effective in obtaining a highly pure sample of the R-enantiomer, SH-053-2'F-R-CH_3 (**7**), without the need for chromatographic separation. A highly pure sample of the S-enantiomer, SH-053-2'F-S-CH_3(**13**), was also synthesized by employing the same protocol. The careful execution of the deprotection step and the implementation of the new purification technique contributed to the high enantiomeric purity and improved overall efficiency of the synthesis.

4.2.2. Synthesis of GL-II-73

In the synthesis of GL-II-73, the starting material, SH-053-2'F-R-CH_3 (**7**), was first converted to its corresponding acid form, SH-053-2'F-R-CH_3 acid (**15**), through a base hydrolysis reaction. To achieve this, a solution of aqueous sodium hydroxide (NaOH) was added dropwise to the THF

solution of SH-053-2'F-R-CH_3. It is crucial to dilute the reaction mixture with water after the ester hydrolysis to prevent the formation of a thick, jelly-like mass during the evaporation of THF. In a subsequent modification, the use of NaOH as the base in the ester hydrolysis step was replaced with LiOH. This change resulted in the prevention of gel formation during the reaction. Instead of a gel-like mass, a smoother reaction mixture was observed, facilitating the subsequent steps of the synthesis process. The substitution of NaOH with LiOH provided improved reaction conditions for the conversion of the ethyl ester to the corresponding acid, leading to a more efficient synthesis of GL-II-73. Excess base was neutralized by the addition of acetic acid to adjust the pH to approximately 4-5, which resulted in the precipitation of the acid (**15**) from the acidic water solution. (**Scheme 9**).

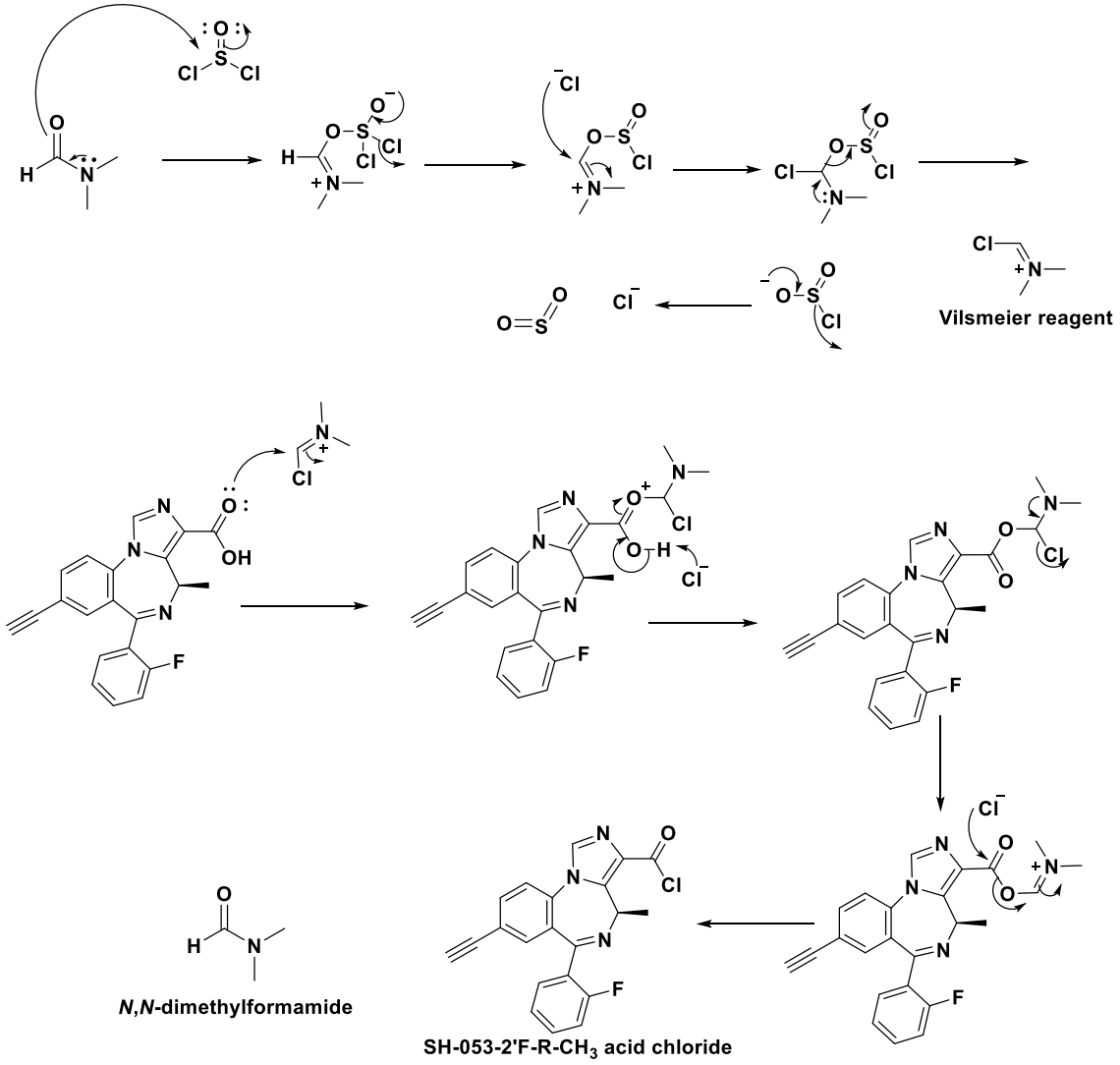
Scheme 8: Synthesis of GL-II-73



To purify the acid, hot ethanol recrystallization was employed, ensuring the removal of impurities and obtaining a highly pure product. To synthesize GL-II-73, the Vilsmeier chlorination reaction was employed starting from SH-053-2'F-R-CH3 acid (**15**). First, the acid was converted into the corresponding acid chloride using anhydrous dichloromethane (DCM) and thionyl chloride. The reaction was facilitated by the presence of catalytic N,N-dimethyl

formamide, which reacted with thionyl chloride to generate the Vilsmeier reagent, N,N-dimethyliminium chloride.

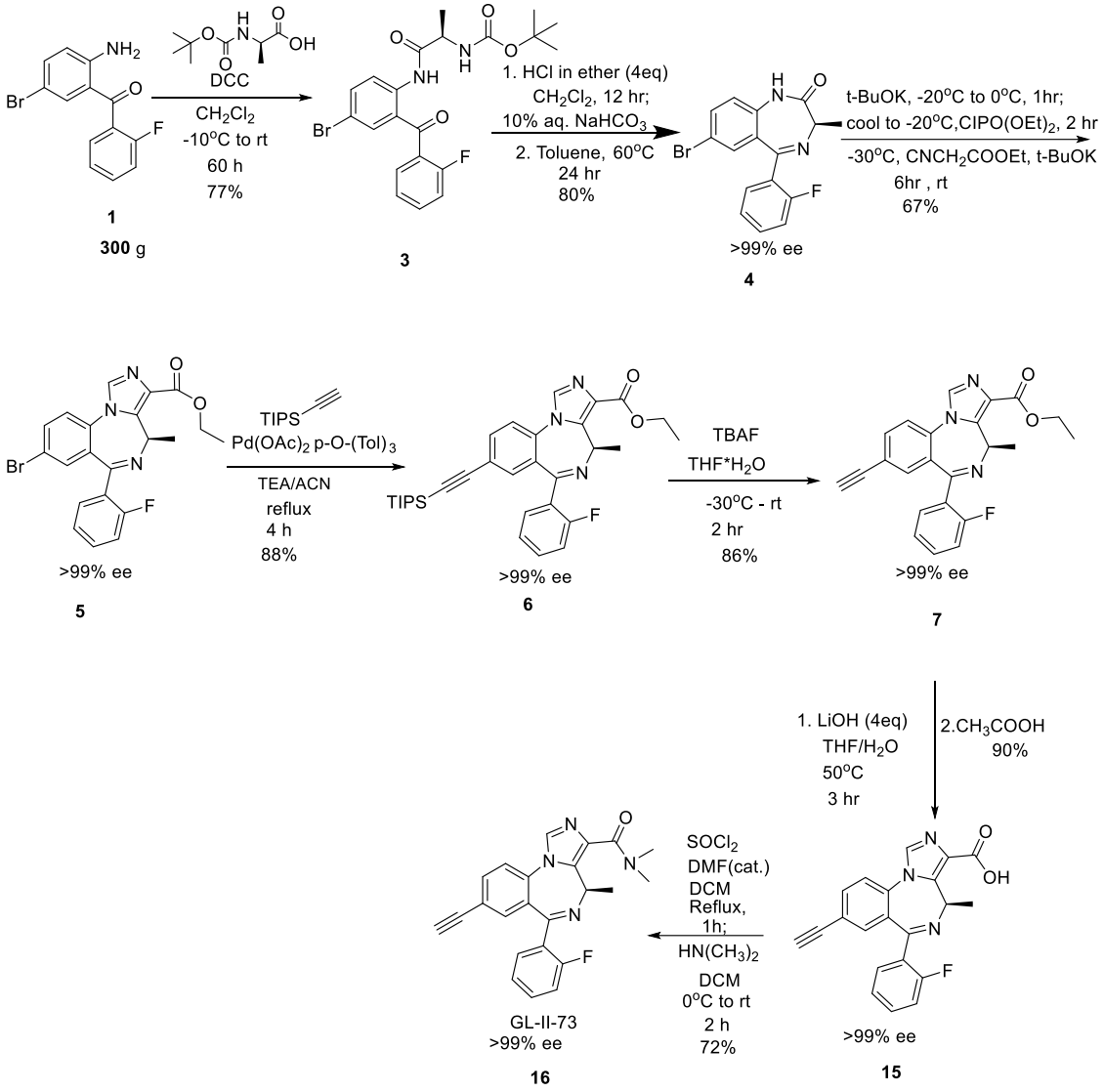
Scheme 8A: Possible mechanism of chlorination of SH-053-2'F-*R*-CH$_3$ acid



This reagent played a crucial role in the subsequent Vilsmeier chlorination reaction. After Vilsmeier chlorination step, N,N-dimethyl amine (2M solution in THF) acted as a nucleophile, attacking the SH-053-2'F-R-CH3 acid chloride to yield GL-II-73. The obtained GL-II-73 was purified by column chromatography using a silica gel column and eluting with ethyl acetate

containing 1% methanol. The overall yield of the reaction was 72%. The improved scalable synthesis of GL-II-73 is depicted on **Scheme 9**.

Scheme 9: Improved scalable synthesis of GL-II-73 by the modified Boc-route



4.2.3. Synthesis of analogs of GL-II-73

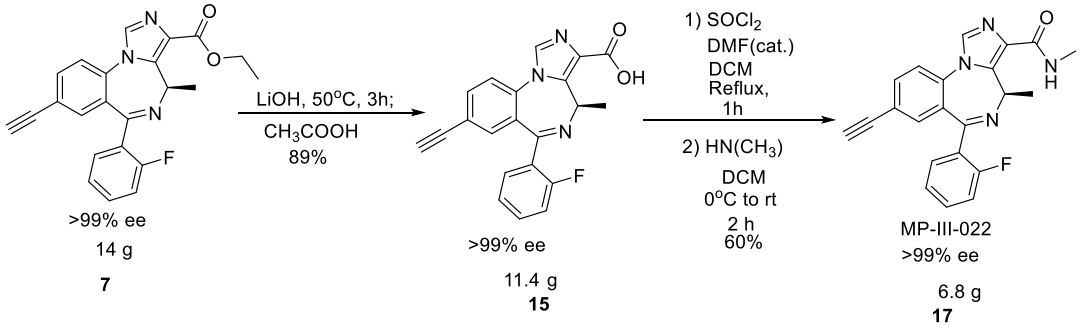
Research findings have indicated that subtle alterations in the structure of imidazodiazepines can have a profound impact on the subtype selectivity of benzodiazepine/GABA(A) receptors.[20] For instance, the presence or absence of the chiral methyl group at the C(4) position of

imidazodiazepines can significantly influence the α5-subtype selectivity, as well as the efficacy at α2/α3-β3γ2 subtypes. Removal of the chiral methyl group at C(4) results in a decrease in α5 selectivity, while showing an opposite trend in the selectivity at α2/α3-β3γ2 subtypes. Moreover, modifications of the lipophilic groups at the C(8) position have demonstrated the ability to modify α5 selectivity. In order to achieve improved ligands with enhanced antipsychotic or procognitive profiles, several structural modifications have been explored on GL-II-73 and its derivatives**.**

4.2.3.1. Synthesis of MP-III-022

MP-III-022, a monomethyl amide and a selective ligand for α5-GABAAR subtypes, has demonstrated activity at low doses in various psychiatric disorders, including autism[264], antipsychotic activity[265] , and cognitive disorders[266]. MP-III-022 was synthesized using a similar synthetic approach as GL-II-73 from SH-053-2'F-R-CH_3. After the Vilsmeier chlorination step, MP-III-022 was synthesized by reacting the SH-053-2'F-R-CH3 acid chloride with a 1M solution of monomethylamine in THF. The resulting MP-III-022 product was purified using column chromatography on a silica gel column, with elution using a mixture of 80% ethyl acetate and hexane containing 1% methanol. The reaction yielded 68% of the desired product.

Scheme 10: Synthesis of MP-III-022



4.2.3.2. Analogs of GL-II-73

Several modifications were made to the core structure of imidazodiazepine 1 to synthesize different amide analogs in order to obtain alternate active ligands with distinct or improved antipsychotic or procognitive profiles (**Figure 4**). These novel analogs were characterized and tested in different animal models to evaluate their bioactivity or a lack thereof, as regards the SAR.

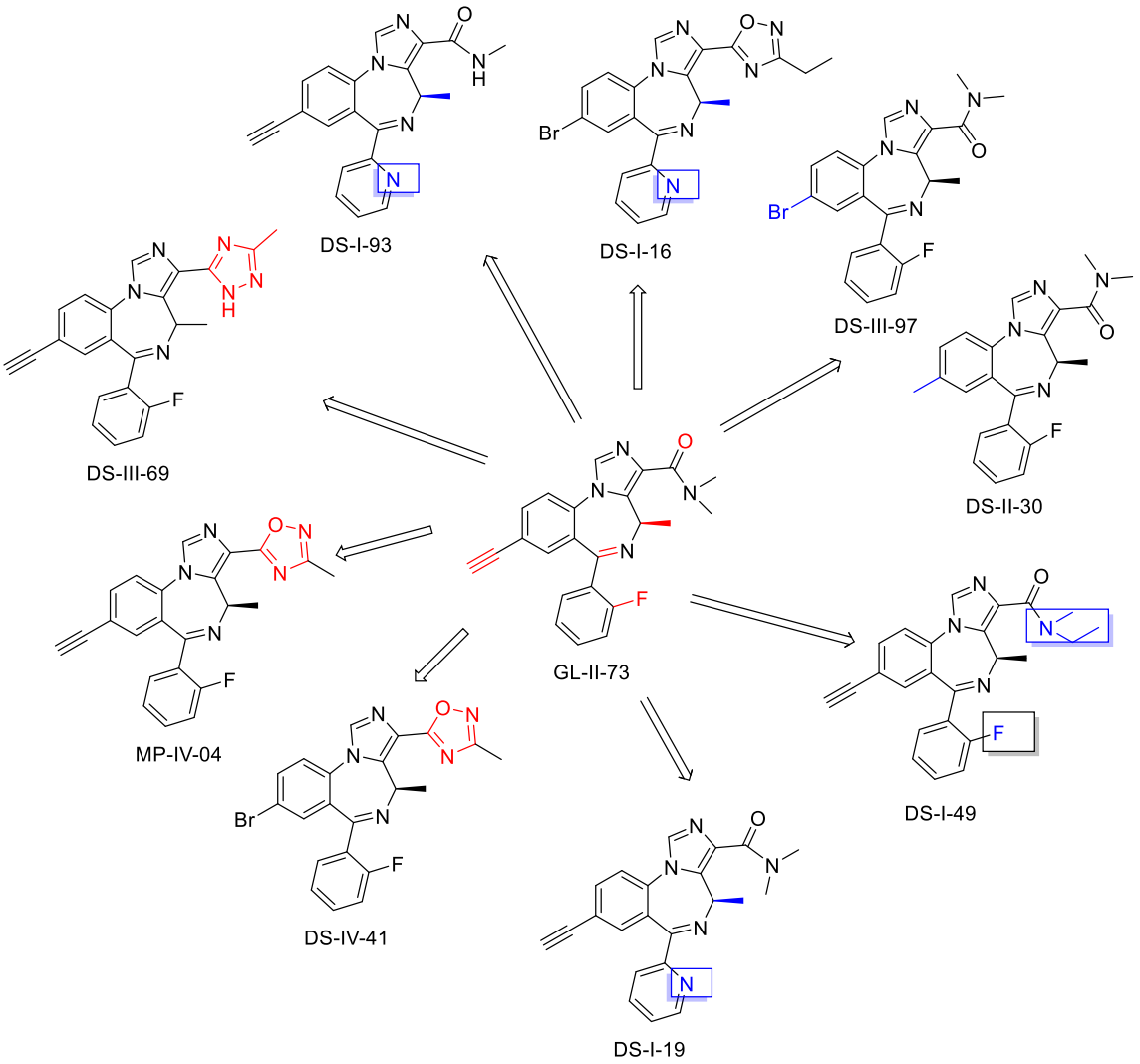
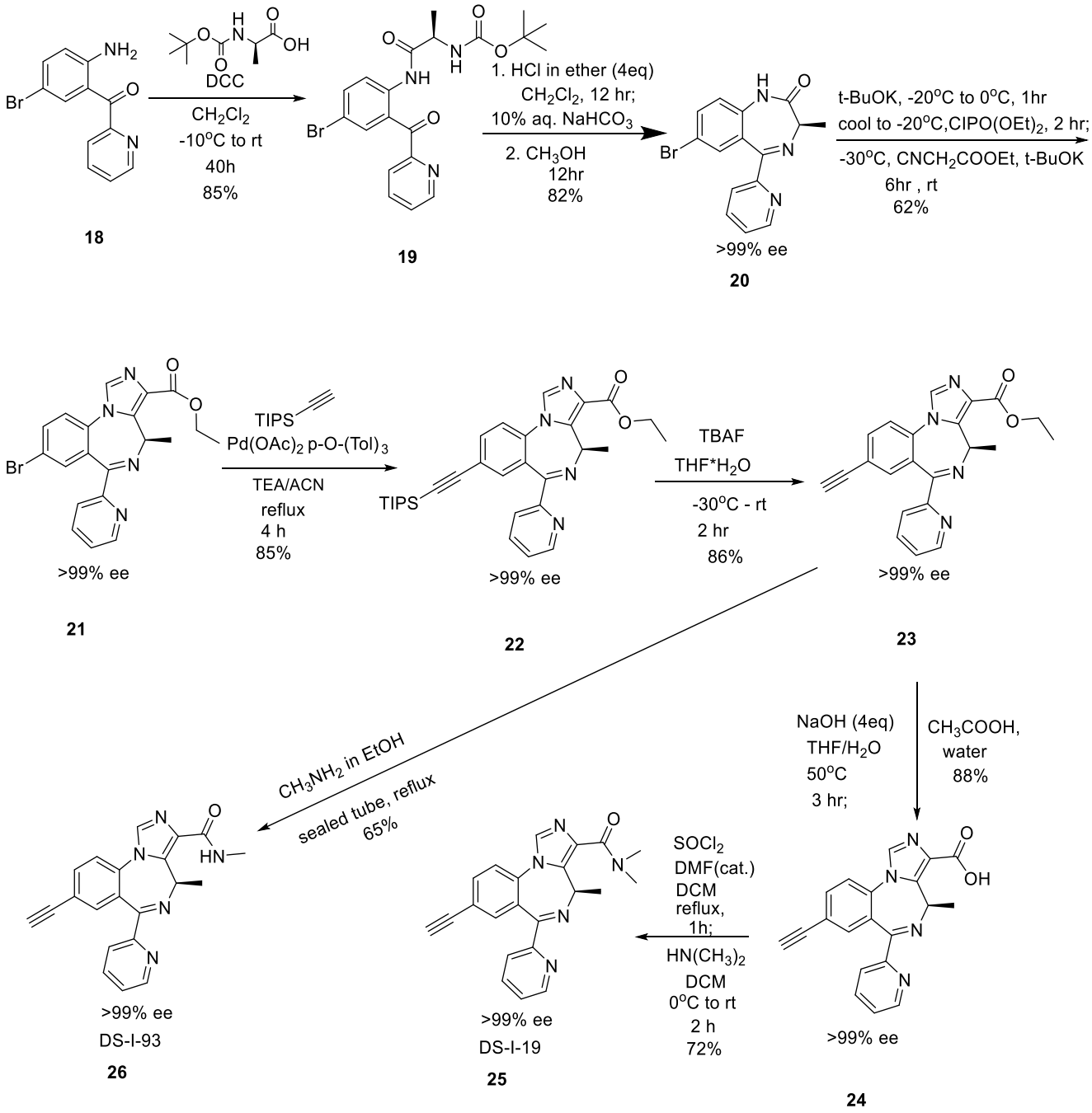


Figure 4. Analogs of GL-II-73

Based on the observed anxiolytic-like behavior of the 2′ N-pyridine analog in the Marble burying assay (Biggerstuff et al., 2020), further investigations were conducted to explore the potential of developing analogs of GL-II-73 and MP-III-022 with similar properties. With this objective in mind, a 2′ N-pyridine analog of both GL-II-73 and MP-III-022 was synthesized. The synthesis involved modifying the structure of the parent compounds to incorporate the desired pyridine moiety at the 2′ position.

The synthesis of 2′ N-GL-II-73 amide analogs was carried out using the Boc-route of peptide coupling reaction, followed by cyclization in methanol under neutral conditions (**Scheme 11**). In this synthetic approach, the Boc-protected amino acid was coupled with the appropriate amine to form the amide intermediate. The cyclization step was then performed in methanol, which provided a suitable environment for the formation of the desired analogs. The reaction conditions were carefully controlled to ensure optimal yield and purity of the final products.

Scheme 11. Synthesis of DS-I-19 and DS-I-93



The 2′N-pyridino benzophenone (**18**) was reacted with Boc-L-Ala-OH to form the amide intermediate **19.** The Boc protecting group was then removed under acidic conditions, followed

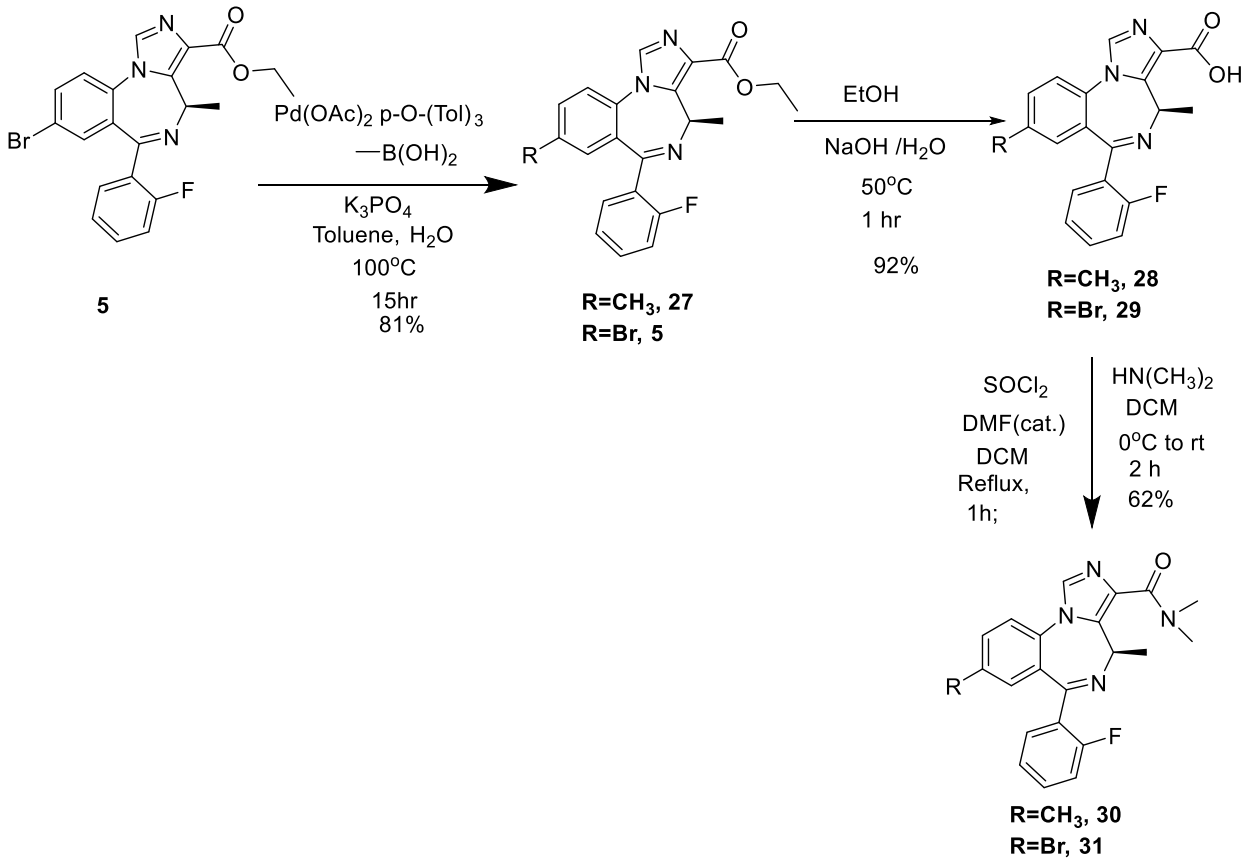
by cyclization in methanol to yield the 2′N-pyridino benzodiazepine **20** with a high yield of 88%. The purification of these compounds was performed using the same method as described earlier for the 2′F analogs. Interestingly, it was observed that the yield of the peptide coupling reaction for the 2′N-pyridino benzophenone was higher compared to the 2′F benzophenone.

Following the same procedure as described earlier, the imidazole group was introduced onto the benzodiazepine **21** to yield the imidazodiazepine **21**. The 8-bromo imidazodiazepine **21** was then converted to the 8-TIPS-acetylene imidazodiazepine intermediate. Finally, the TIPS group was selectively removed through fluoride-mediated deprotection, resulting in the formation of **23**. The next step involved the hydrolysis of the ethyl ester to yield the corresponding acid, **24**. Careful attention should be paid during the addition of water to dilute the reaction mixture and acetic acid to neutralize the excess base. It is important to maintain the appropriate pH (around 4-5) by regularly checking the pH using pH strips. Excessive amounts of acid or water can hinder the precipitation of the acid product and result in it remaining in solution.

The precipitated carboxylic acid **24** was further converted into the corresponding acid chloride. Subsequently, dimethylamine underwent nucleophilic attack on the acid chloride, resulting in the formation of DS-I-19 (**25**). The final product was purified using silica gel flash chromatography, employing an ethyl acetate solvent mixture with 1% methanol. To synthesize the monomethyl amide, direct amination of the ethyl ester **23**, was carried out (**Scheme 11**). The ethyl ester **23** was placed in a sealed tube under an argon atmosphere, and a solution of methylamine (88% methylamine in ethanol) was added to the tube at a temperature ranging from -10 to -15^{o}C. The tube was tightly sealed, and the reaction mixture was gradually allowed to warm to room temperature. The solution was refluxed for a duration of 14 hours, resulting in the formation of DS-I-93 (**26)** with a yield of 65%.

The synthesis of the 8-methyl ligand **27** was accomplished by following a literature procedure.[267] The Suzuki coupling between the methyl boronic acid and the aryl bromide **5** was carried out in the presence of a palladium catalyst, potassium phosphate, palladium acetate, and tri-O-tolyl phosphine. The reaction was allowed to proceed for 12 hours, resulting in the formation of the 8-methyl imidazodiazepine ester. Purification of the product was achieved using silica gel flash chromatography with an EtOAc:Hexane solvent mixture. The coupling reaction yielded 81% of the desired product with an optical purity of 99% ee.

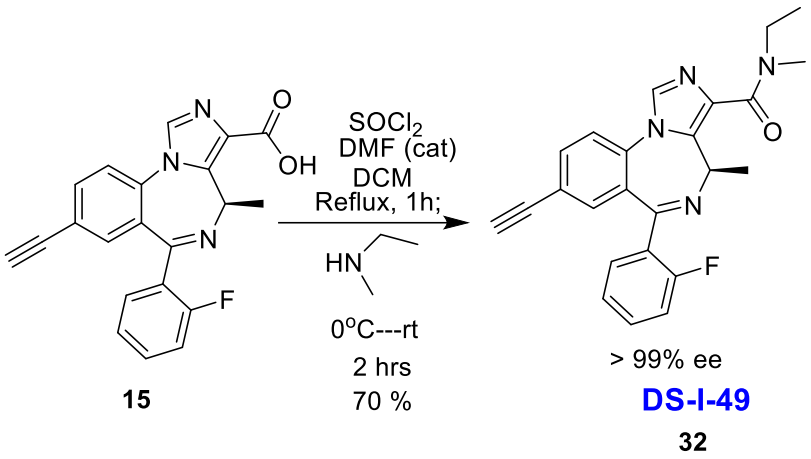
Scheme 12. Synthesis of DS-II-30



The 8-methyl imidazodiazepine ethyl ester was subjected to base hydrolysis to convert the ester group into a carboxylic acid group. The esters hydrolysis reaction proceeded smoothly, yielding

the carboxylic acids (**28** and **29**). The carboxylic acid was purified using hot ethanol as previously described. Next, the carboxylic acids (**28, 29**) were then converted into the acid chloride through Vilsmeier chlorination. The resulting acid chloride intermediates were then subjected to nucleophilic attack by dimethylamine (2M solution in THF) to produce DS-II-30 (**30**) and DS-III-97 (**31**). The compound was purified using silica gel column chromatography. Several other modifications were made to the parent structure of the active compound GL-II-73. One of these modifications involved the synthesis of DS-I-49, which is the ethyl methyl amide analog of GL-II-73. The synthesis of DS-I-49 followed a similar protocol to that of GL-II-73 (**Scheme 13**).

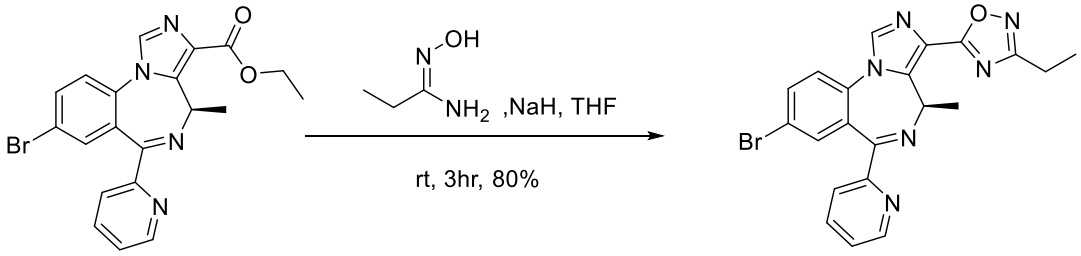
Scheme 13. Synthesis of DS-I-49



Bioisosteric replacements of ester functions have been extensively utilized in drug discovery and medicinal chemistry to improve metabolic stability, minimize side effects, and enhance the development of promising clinical candidates.[268] In the case of ligand SH-053-2'F-R-CH3, the substitution of ester functions with substituted 1,2,4-oxadiazoles led to notable improvements in hydrophilicity, as well as enhanced in vitro and in vivo stability[269-270] . Furthermore, the selective enhancement of ligand efficacy at BZD receptors was observed when compared to the

corresponding ester ligands. Oxadiazole rings have demonstrated significant utility in the field of drug discovery and have been incorporated into various programs due to their ability to contribute to ligand binding as an essential component of the pharmacophore.[271] Oxadiazole moieties often serve as planar, aromatic-like linkers, allowing for the appropriate orientation of substituents in the molecule.[272] Incorporating oxadiazoles at the periphery of the molecule can also modulate molecular properties.[273] Furthermore, oxadiazoles have been widely used as bioisosteric replacements for carbonyl-containing compounds such as esters and amides.[274-276] Oxadiazole rings can exist in different regioisomeric forms, including two 1,2,4-isomers (if asymmetrically substituted), a 1,3,4-isomer, and a 1,2,5-isomer, with the 1,2,4-regioisomer being more common than the others. Different regioisomers of oxadiazoles exhibit varying hydrogen bond acceptor properties, resulting in distinct hydrogen bonding potentials.[277-278] Based on these considerations, DS-I-86 and DS-IV-41 were synthesized and MP-IV-04 was resynthesized for more biological studies (**Scheme 14 and 15**).

Scheme 14: Synthesis of DS-I-16

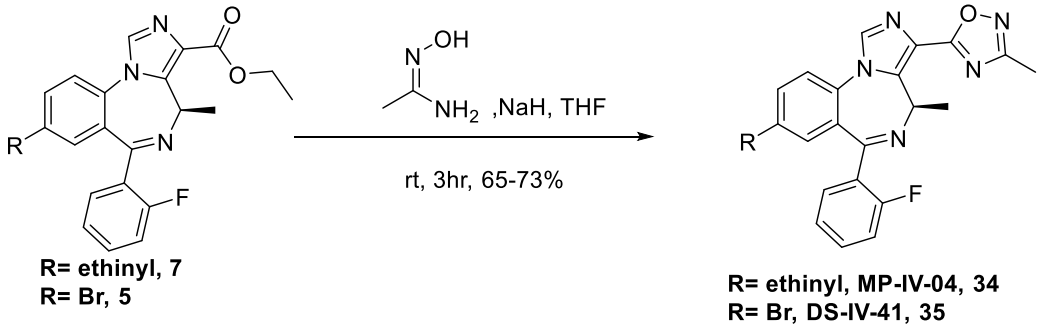


DS-I-16 (33)

DS-I-86 was synthesized by treating the corresponding imidazodiazepine ethyl ester bearing an 8-bromo substituent with ethyl oximes in the presence of sodium hydride. This reaction resulted in the formation of DS-I-86. The oxime was treated with sodium hydride in THF for an hour, followed by the addition of a solution of the ethyl ester in THF. Care should be taken with the

amount of sodium hydride used in the reaction. Insufficient hydride may result in incomplete reaction, while excessive hydride (equivalents higher than 1.3) can lead to the formation of an undesired olefinic migrated by-product. This by-product, being non-polar, can separate from the corresponding oxadiazole product and be detected on top of the desired product on a silica gel TLC plate.

Scheme 15. Synthesis of DS-IV-41 and MP-IV-04

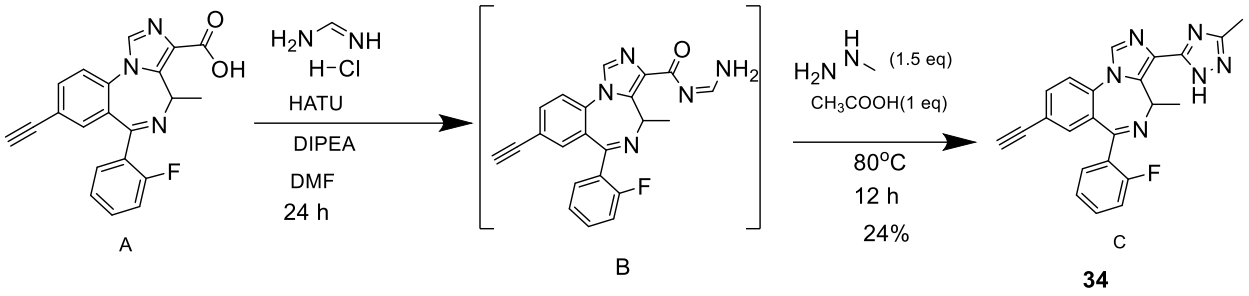


R= ethinyl, 7
R= Br, 5

R= ethinyl, MP-IV-04, 34
R= Br, DS-IV-41, 35

1,2,3-triazoles have gained significant recognition as versatile isosteres for amide bonds in the field of medicinal chemistry. These compounds exhibit structural features that enable them to effectively mimic the amide-binding motifs. Although there may be subtle variations in terms of dipolar moment and inter-substituent distances, the overall similarities make 1,2,3-triazoles suitable replacements for amide moieties. In particular, 1,4-disubstituted 1,2,3-triazoles demonstrate remarkable resemblance to amide isosteres, wherein the C-4 atom assumes an electrophilic role. Furthermore, the presence of a C-H bond within the triazole ring allows it to act as a hydrogen bond donor (HBD), while the lone pair of electrons on the N-3 atom serves as a hydrogen bond acceptor. This unique combination of properties makes 1,2,3-triazoles valuable tools for designing and optimizing bioactive compounds. [279] DS-III-69, a triazole analog of GL-II-73 was synthesized after several attempts.

Scheme 16 : Synthesis of DS-III-69



The trials are tabulated in **Table 5.** Among the various attempts, DS-III-69 was synthesized with a yield of 24% when 3 equivalents of the peptide coupling reagent HATU and 2 equivalents of formamidine hydrochloride were utilized (**Table 5, Entry 5**).

Table 5. Attempts to synthesize DS-III-69

Entry	Fromamidine HCl (eq)	HATU (eq)	DIPEA (eq)	DMF (M)	Temp. (°C)	Time (h)	Conversion from A to B
1	1	1	4	0.2	25	12-24 h	<2% by LCMS
2	1.1	1.5	4	0.2	25	24	<10% by LCMS
3	1.1	2	4	0.2	25	36	<14% by LCMS
4	1.5	2	4	0.2	25	48	<20% by LCMS
5	**2**	**3**	**4**	**0.2**	**25**	**48-54**	**~50% conversion by LCMS** **Conversion from B to C (~100%)**

4.3. Results and Discussion: Biological Activity

4.3.1. Systemic administration of selective α5-PAM, MP-III-022, reverses hippocampal activity impairments in AAV-AD rats by S.M Perez, Daniel Lodge and colleagues

No significant difference in ventral hippocampal firing frequency was observed compared to control rats **(Figure 2B)** in the case of AAV-AD rats. Furthermore, the firing rates of both control and AAV-AD rats were unaffected by the selective α5-PAM, MP-III-022 (**Figure 2C**). Spontaneous oscillatory activity recordings in the ventral hippocampus revealed an overall decrease in oscillatory activity in AAV-AD rats compared to controls. Interestingly, this decrease was reversed when MP-III-022 was systemically administered, indicating its potential therapeutic effect (**Figure 4 C, D**). These findings were statistically significant, as determined by three-way ANOVA and Holm Sidak post hoc analysis.

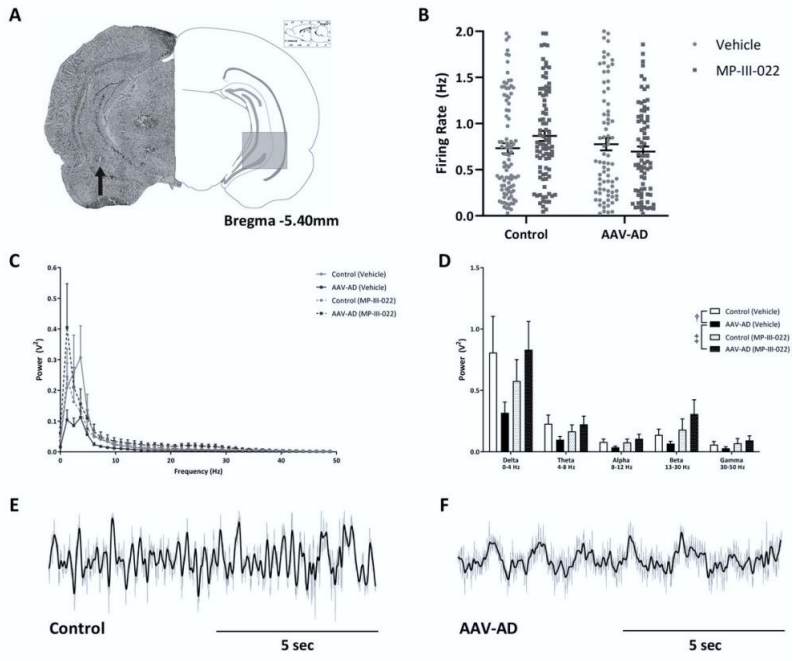


Figure 5. Impaired ventral hippocampal oscillatory activity reversed by MP-III-022 in AAV-AD rats. In Figure A (left), a representative brain slice is shown with an electrode

track indicated by a black arrow, targeting the ventral hippocampus (vHipp). The corresponding schematic of the brain section is depicted in Figure A (right). The average firing rate of spontaneously active putative pyramidal neurons in the vHipp remains unchanged between different treatment groups and is not affected by treatment with the selective α5-GABAA positive allosteric modulator (PAM), MP-III-022, as illustrated in Figure B. AAV-AD rats exhibit a significant decrease in oscillatory power compared to eGFP controls, which is then reversed by the systemic administration of MP-III-022, as depicted in Figures C and D. Figure E shows a representative trace of spontaneous local field potential oscillations filtered for delta frequency in the vHipp of a control rat, while Figure F shows the same for an AAV-AD rat. It is noteworthy that the symbol "†" denotes a significant main effect with p=0.014, and the symbol "‡" denotes another significant main effect with p=0.006. The figure was modified from Eassa et al. 2023.[280]

4.3.2. Systemic administration of the selective α5-PAM, MP-III-022, effectively reverses the aberrant dopamine system function observed in AAV-AD rats by S.M Perez, Daniel Lodge and colleagues

In AAV-AD rats, the population activity (n=10; 1.60 ± 0.13 cells per track) was significantly higher compared to control rats (n=10; 1.05 ± 0.08 cells per track), as determined by a two-way ANOVA ($F_{Strain}(1,34)=6.61$; $p=0.02$; $F_{Treatment}(1,34)=9.48$; $p=0.004$; $F_{Strain \times Treatment}(2,34)=8.25$; $p=0.007$; Holm-Sidak; $t=4.16$; $p<0.001$; **Figure 5B**). Notably, systemic administration of the selective α5-PAM, MP-III-022, reversed the increased population activity in AAV-AD rats (n=8 rats; 1.00 ± 0.06 cells per track; $t=4.29$; $p<0.001$), while no significant effect was observed in control rats (n=7 rats; 1.03 ± 0.08 cells per track). There were no

significant differences in average firing rate (n=44-98 dopamine neurons per group; **Figure 5C**) or bursting pattern (n=44-98 dopamine neurons per group; **Figure 5D**) among any of the groups.

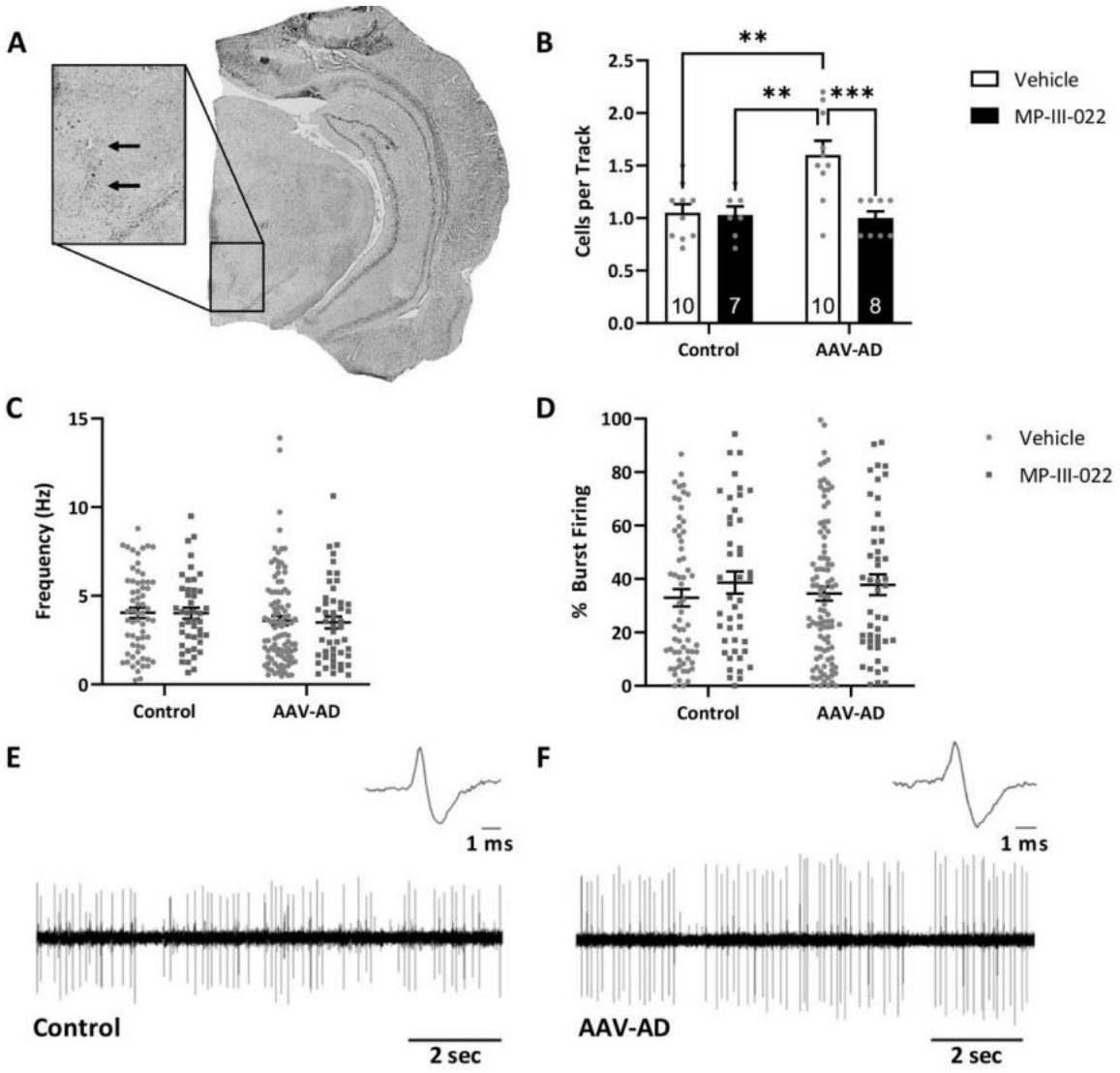


Figure 6. Aberrant ventral tegmental area activity is restored by MP-III-022 in AAV-AD rats. In Figure A, a representative brain slice is shown with electrode tracks indicated by black arrows targeting the ventral tegmental area (VTA). The dopamine neuron population activity, represented by the average number of spontaneously active dopamine neurons per electrode track, is significantly increased in AAV-AD rats compared to

controls. However, this increase is reversed by systemic administration of the selective α5-GABAA positive allosteric modulator (PAM), MP-III-022, as demonstrated in Figure B. Notably, there were no alterations observed in the average firing rate (Figure C) or bursting pattern (Figure D) in either control or AAV-AD rats, nor were there any effects of systemic MP-III-022 administration on these parameters. Figure E presents a representative dopamine recording and action potential from a control rat, while Figure F shows the same from an AAV-AD rat. The figure was modified from Eassa et al. 2023.[280]

4.3.3. AAV-AD Rats Exhibit Intact Cognitive Function but Selective Impairment in Dopamine-Dependent Behavior, Reversed by Systemic Administration of the Selective α5-PAM, MP-III-022 by S.M Perez, Daniel Lodge and colleagues

Cognitive deficits are a common observation in rodent models of AD. However, as this model specifically targets the vHipp, spatial learning and memory deficits were not detected. Our assessment of percent spontaneous alternations in the Y-maze revealed no significant differences between groups (n= 9-11 rats per group; **Figure 6A**), indicating the absence of working memory deficits in this context. Sensorimotor gating deficits, seen in both psychosis and AD models, were not evident in our comparison of PPI between groups (n= 10-11 rats per group; **Figure 6B**).

Psychosis-related rodent models frequently exhibit impairments in dopamine-dependent measures, often displaying exaggerated responses to acute systemic administration of psychotomimetic drugs. Interestingly, our study demonstrated consistent baseline locomotor activity across all groups (n= 10-11 rats per group). However, AAV-AD rats exhibited heightened MK-801-induced locomotor activity compared to control rats (evaluated using a

three-way ANOVA; FStrain(1,385)= 0.008; FTreatment(1,385)= 0.67; FTime(8,385)= 3.35; p= 0.001; FStrain X Treatment(1,385)= 10.85; p= 0.001; Holm Sidak; t= 2.23; p= 0.026; **Figure 6C**). Notably, this increase was reversed upon systemic administration of the selective α5-PAM, MP-III-022 (validated by Holm-Sidak; t= 2.87; p= 0.004).

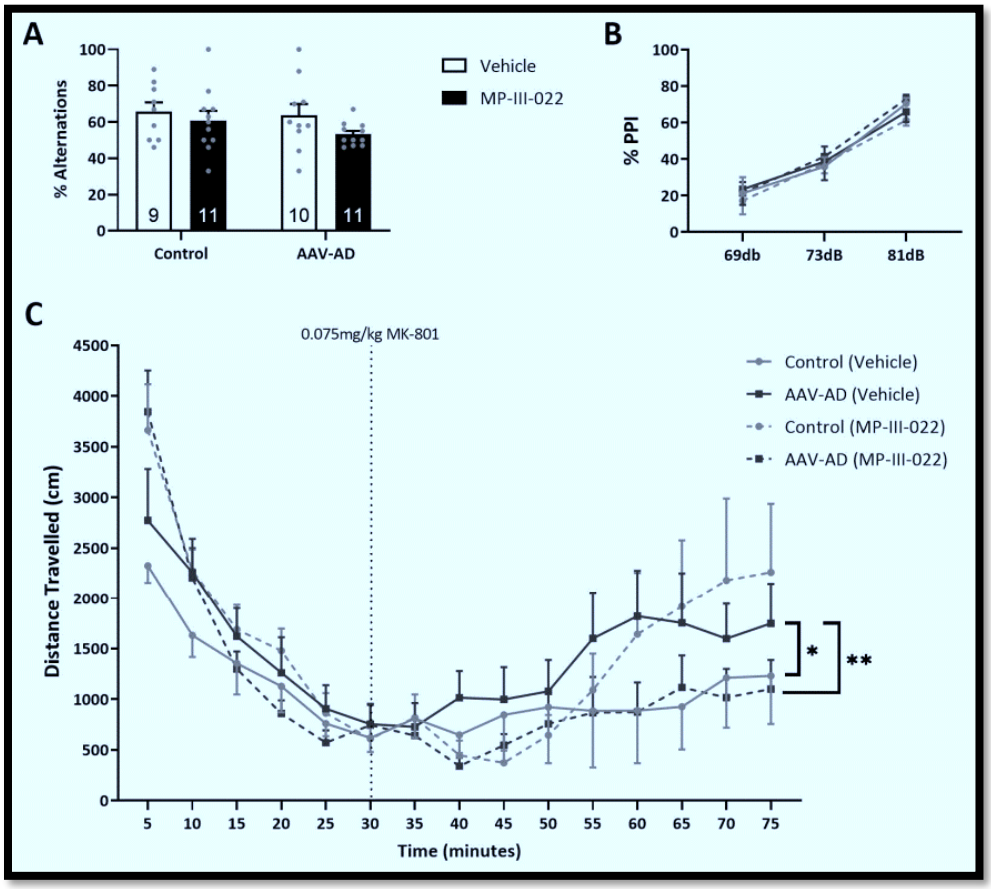


Figure 6. In AAV-AD rats, an increased sensitivity to the locomotor-boosting effects of MK-801 was noted, and this heightened response was subsequently counteracted by MP-II-022. Notably, no significant working memory deficits were observed among the various groups in the Y-maze test (A). Furthermore, there were no notable differences in sensorimotor gating, as evidenced by the lack of substantial distinctions in pre-pulse inhibition of startle responses (B). Interestingly, AAV-AD rats exhibited an amplified

locomotor reaction to MK-801, a reaction that was effectively mitigated through systemic administration of the selective α5-GABAA positive allosteric modulator, MP-III-022 (C). * p = 0.026, ** p = 0.004

4.3.4. Reduction of Parvalbumin-Positive Interneurons in AAV-AD Rats by MP-III-022 with S.M Perez, Daniel Lodge and colleagues

A decline in the number of parvalbumin interneurons (PV interneurons) has been previously documented in rodent models employed for the study of psychosis.[281, 283] This reduction has been linked to the activity of the ventral tegmental area (VTA) dopamine neuron population.[282] In our investigation, a substantial decrease in the count of PV neurons within the ventral hippocampus (vHipp) was evident in AAV-AD rats (n= 13 rats; 5.79 ± 0.62 PV cells/mm2) compared to control rats (n= 13 rats; 7.82 ± 0.64 PV cells/mm2; determined via a t-test; t= 2.28 with 24 degrees of freedom; p= 0.03; **Figure 7A**). Furthermore, an emerging trend suggests that the reduction in vHipp PV interneurons is associated with an elevation in the activity of the VTA dopamine neuron population (n= 13; evaluated using linear regression; R= 0.40; r2 = 0.16; analysis of variance; FRegression(1,12)= 2.10; p= 0.18; **Figure 7C**).

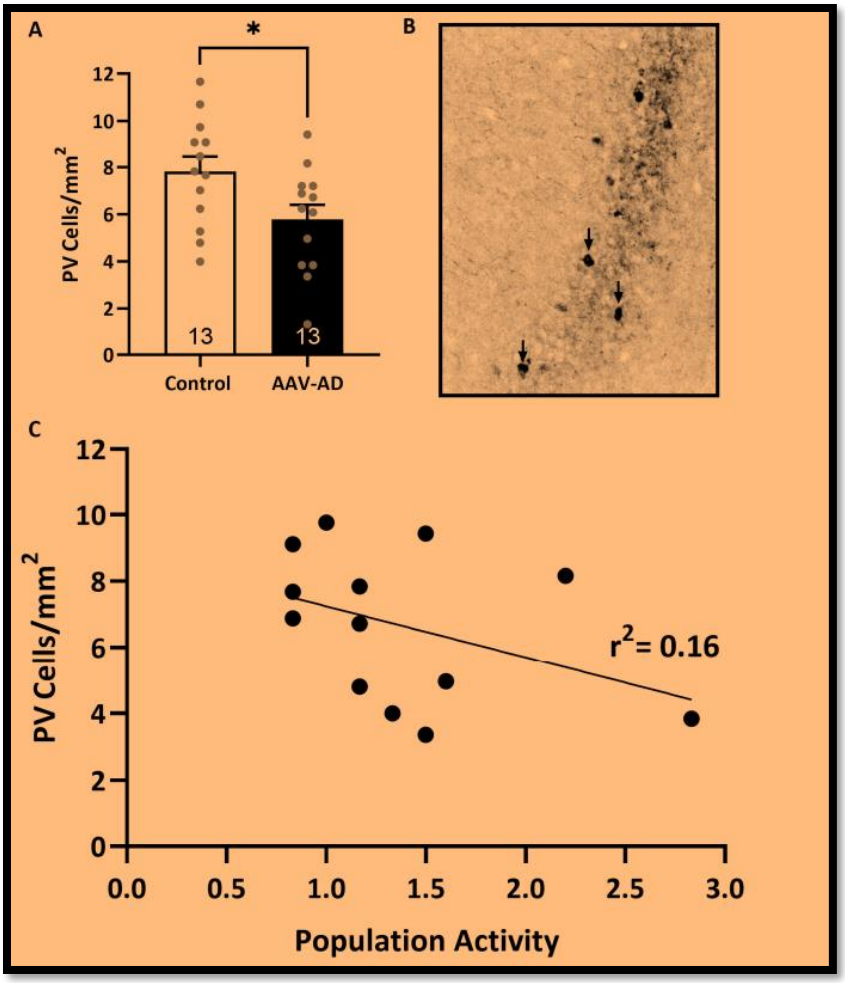


Figure 7. AAV-AD rats distinctly manifest a notable reduction in the count of parvalbumin-positive (PV) interneurons within the ventral hippocampus (vHipp). The AAV-AD rat group demonstrates a considerably lower presence of inhibitory interneurons that are parvalbumin-positive in the vHipp (A). A representative coronal brain section highlighting the ventral hippocampus (vHipp) showcases the presence of parvalbumin (rendered in greyscale and indicated by black arrows; (B)). Furthermore, a scatterplot illustrates the correlation between the activity of the dopamine neuron population and the quantity of PV interneurons in the vHipp. The black dots on the plot represent individual rats (C). * p = 0.032

4.3.5. Significant amelioration of social impairments in VPA animals achieved by MP-III-022 with Anja Santrac, Dr Miroslav Savic, and colleagues

In the context of allogrooming, VPA VEH males exhibited reduced time engagement (depicted in **Figure 8A**) compared to CTRL VEH males. Yet, the administration of MP0.3 to VPA males led to an increase in the time spent in allogrooming, surpassing both VPA VEH males and CTRL MP0.3. Further comparison between males and females unveiled that males generally spent more time crawling over/under the conspecific (illustrated in **Figure 8B**), particularly notable in the VPA VEH group. Furthermore, VPA VEH males displayed an elevation in this parameter relative to CTRL VEH. Overall, both doses of MP-III-022 curtailed the time spent in crawling, an effect primarily attributed to the influence of treatment on VPA males.

Differences were also noted in the "following the conspecific" behavior (**Figure 8C**), with VPA animals allocating less time to this activity compared to CTRL, particularly evident among VEH- and MP0.3-treated females. However, MP-III-022 did not demonstrate an ability to reverse this specific behavior. Turning attention to tail manipulation (**Figure 8D**), females outpaced males in this activity overall, evident across all groups and especially within the VPA MP1 group. Notably, VPA VEH females spent less time in tail manipulation relative to CTRL VEH females. This distinct prenatal administration disparity was reversed in MP1-treated females, as the application of MP1 to VPA females brought about an increase in this activity when compared to VPA VEH females.

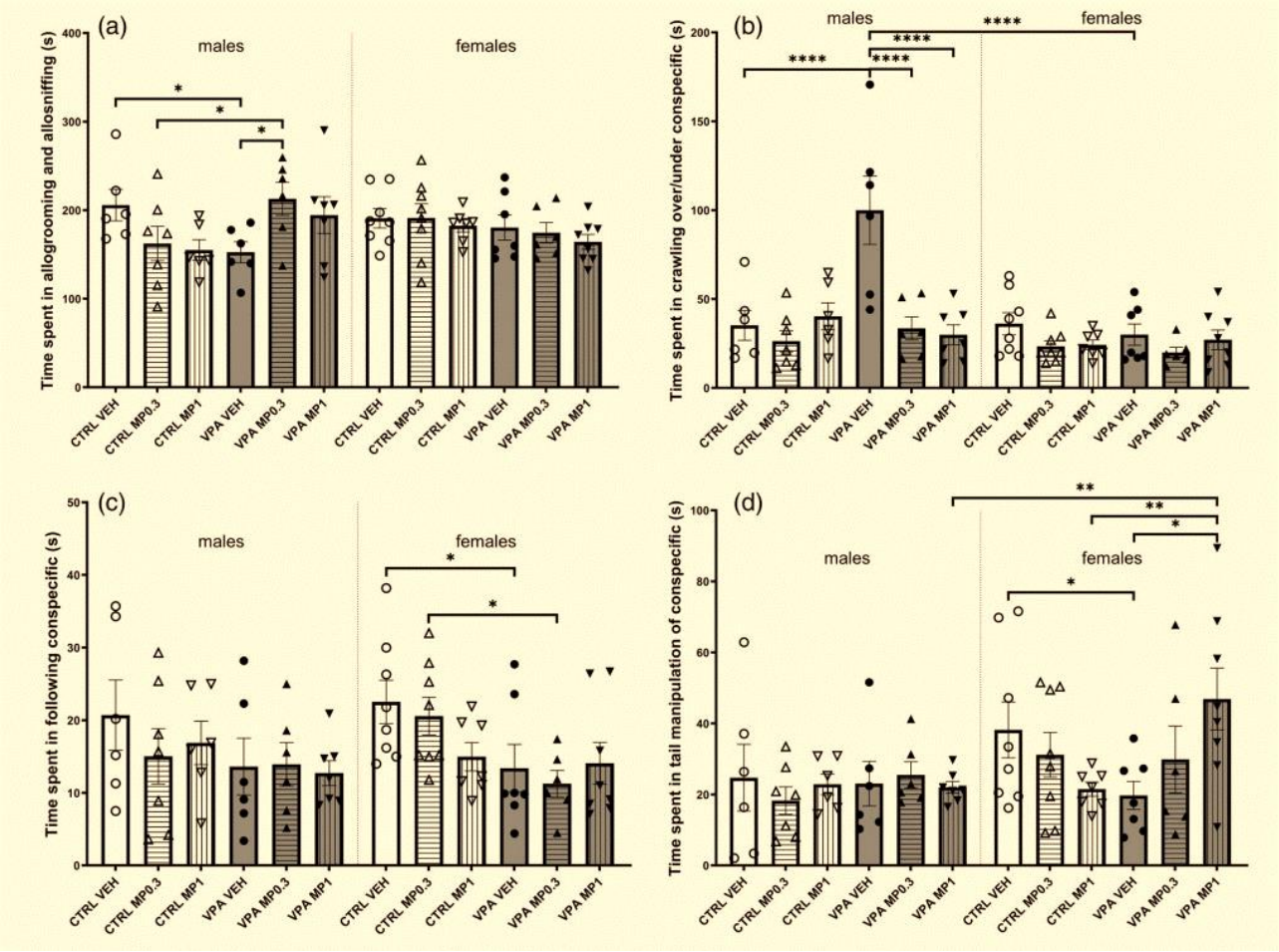


Figure 8. Impact of Treatment (Vehicle [VEH], MP-III-022 0.33 mg/kg [MP0.3], or MP-III-022 1 mg/kg [MP1]) on Social Behavior in Prenatally Treated Animals (Control [CTRL] or Valproate [VPA]):(A) Time dedicated to allogrooming and allosniffing;(B) Time spent in crawling over/under a conspecific;(C) Time allocated to following a conspecific;(D) Time devoted to tail manipulation of a conspecific. Group Pair Count: Males CTRL VEH 6, CTRL MP0.3 7, CTRL MP1 6, VPA VEH 6, VPA MP0.3 6, VPA MP1 7; females CTRL VEH 8, CTRL MP0.3 8, CTRL MP1 7, VPA VEH 7, VPA MP0.3 6, VPA MP1 8. *p < 0.05, **p < 0.01, ***p < 0.001. Figure was modified from Anja *et al*. 2021. [284]

4.3.6. MP-III-022 demonstrated efficacy in ameliorating hyperactivity and repetitive behavior, with notable effects observed particularly in male VPA animals with Anja Santrac, Dr Miroslav Savic, and colleagues

In terms of activity, VPA VEH males exhibited increased active time (**Figure 9a**) compared to CTRL VEH males. This discrepancy was partially attenuated in MP0.3-treated males due to MP0.3's impact on VPA males, leading to reduced active time relative to VPA VEH males. On the contrary, both doses of MP administered to CTRL males resulted in augmented active time compared to CTRL VEH males. Among female rats, a similar hyperactivity effect of VPA relative to CTRL was observed within the VEH group.

As for rotations (**Figure 9b**), VPA animals displayed more rotations overall compared to CTRL counterparts, notably pronounced in both VEH-treated males and females. Administering MP1 to CTRL animals yielded a similar trend, increasing the number of rotations relative to CTRL VEH, both for males and females. In VPA males, MP0.3 treatment led to a reduction in the number of rotations in comparison to VPA VEH males (at a trend level), as well as VPA MP0.3 females. Regarding clockwise rotations (**Figure 9c**), VPA animals exhibited a higher number of such rotations in comparison to CTRL, a trend evident across both sexes in the VEH group. Treatment with MP yielded a decrease in this number in VPA animals relative to VPA VEH. MP0.3 manifested an effect on males, while MP1 impacted females. Furthermore, within the VPA MP1-treated group, males demonstrated more clockwise rotations compared to females.

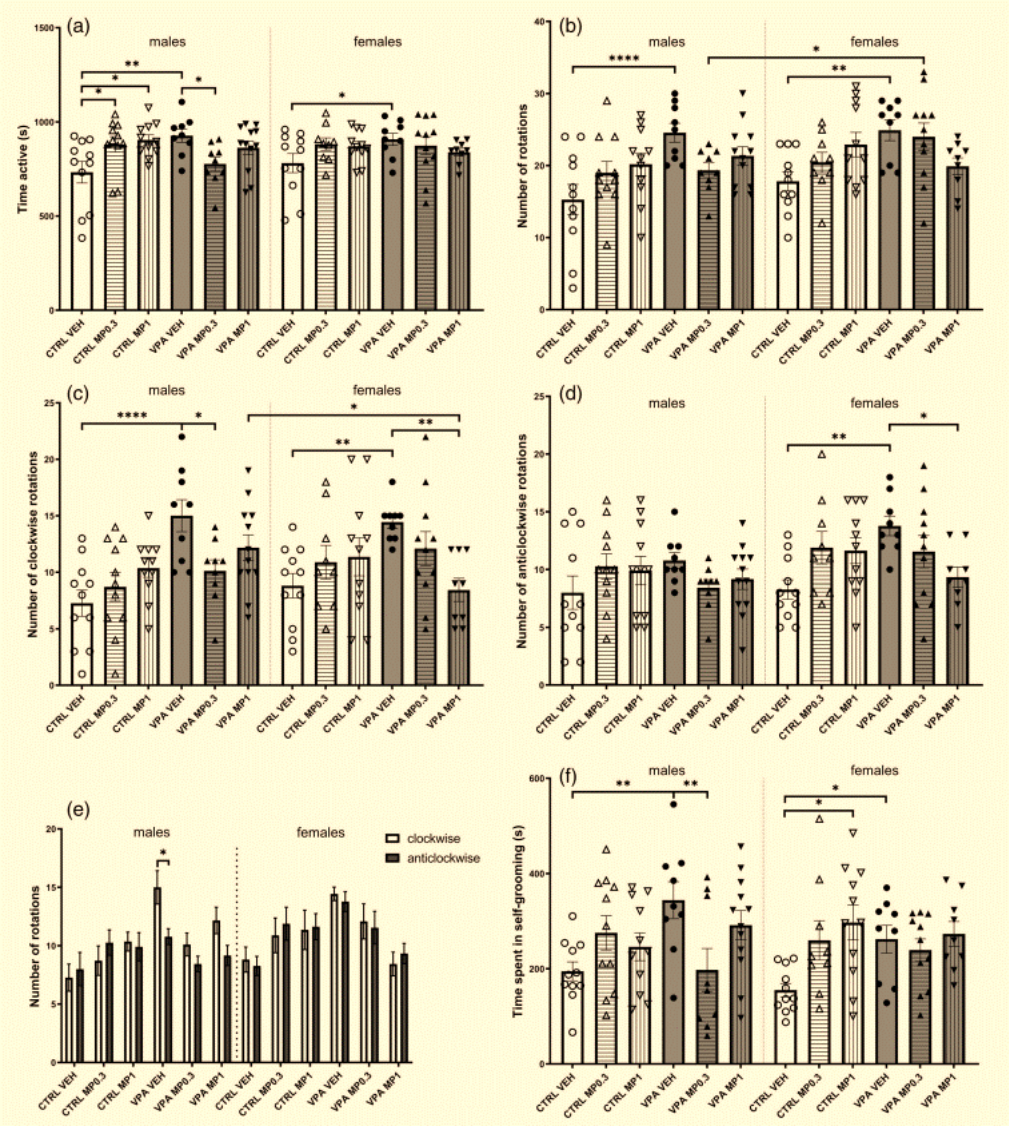


Figure 9. Effect of Treatment (Vehicle [VEH], MP-III-022 0.33 mg/kg [MP0.3], or MP-III-022 1 mg/kg [MP1]) on Spontaneous Locomotor Activity in Prenatally Treated Animals (Control [CTRL] or Valproate [VPA]):(a) Duration of activity; (b) Count of rotations; (c) Count of clockwise rotations; (d) Count of anticlockwise rotations; (e) Comparison between clockwise and anticlockwise rotations - statistical analysis conducted via paired t-test (solely significant difference observed in VPA VEH males: p = 0.011). (f) Time allocated to self-grooming. Group Size: Males CTRL VEH 11, CTRL MP0.3 11, CTRL MP1 11, VPA VEH 9, VPA MP0.3 9, VPA MP1 12; females CTRL VEH 11, CTRL MP0.3 9, CTRL MP1

11, VPA VEH 9, VPA MP0.3 11, VPA MP1 9. *p < 0.05, **p < 0.01, ***p < 0.001, ~ 0.05 < p < 0.01. Figure was modified from Anja *et al*. 2021. [284]

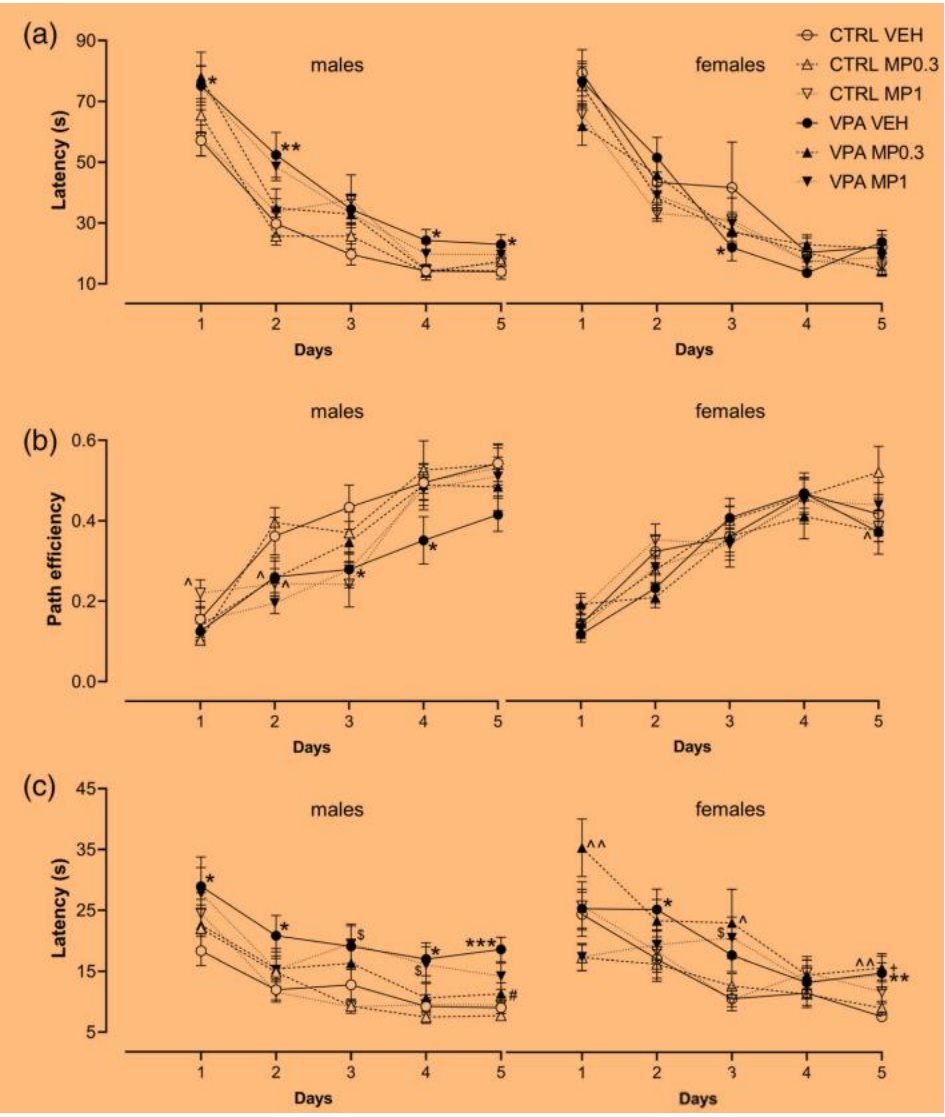
In terms of anti-clockwise rotations (**Figure 9d**), females had a higher number compared to males overall. VPA VEH females also displayed more anti-clockwise rotations compared to CTRL VEH females. For VPA females, MP1 treatment resulted in a decrease in this parameter relative to VPA VEH. Conversely, in CTRL females, the same MP1 treatment had the opposite effect, increasing the number of anti-clockwise rotations compared to CTRL VEH. Concerning self-grooming (**Figure 9f**), VPA animals allocated more time to this behavior compared to CTRL, observed in VEH-treated males and females. MP0.3 treatment administered to VPA males decreased this parameter compared to VPA VEH. Conversely, MP1 treatment in CTRL females led to an increased time spent in self-grooming compared to CTRL VEH.

4.3.7. The efficacy of MP-III-022 was demonstrated in enhancing cognitive flexibility in male VPA animals with Anja Santrac, Dr Miroslav Savic, and colleagues

During the acquisition phase of the Morris Water Maze (MWM), VPA animals displayed a learning deficit, evident through their extended latency (**Figure 10a**) and reduced path efficiency (**Figure 10b**) relative to CTRL animals. This pattern was observed across all groups and was particularly pronounced in VEH-treated males. Moving on to the reverse acquisition phase, VPA animals exhibited an increased latency (**Figure 10c**) and diminished path efficiency (**Figure 10d**) compared to CTRL animals. This trend was consistent overall and extended to VEH-treated males, MP1-treated males, VEH-treated females, and MP0.3-treated females. Among VPA males, administration of MP0.3 led to a decrease in latency and an increase in path efficiency when contrasted with VPA VEH-treated males. Additionally, a sex difference emerged in VPA

MP0.3 treated animals, with males achieving lower latency and higher path efficiency in comparison to females.

Regarding the number of previous platform entries (**Figure 10e**), VPA animals displayed a higher count relative to CTRL animals overall. This trend held true for VEH-treated males and females, as well as MP0.3-treated females. When VPA animals were treated with MP0.3 (males) or MP1 (females), this parameter decreased, with a trend level significance in the latter case.



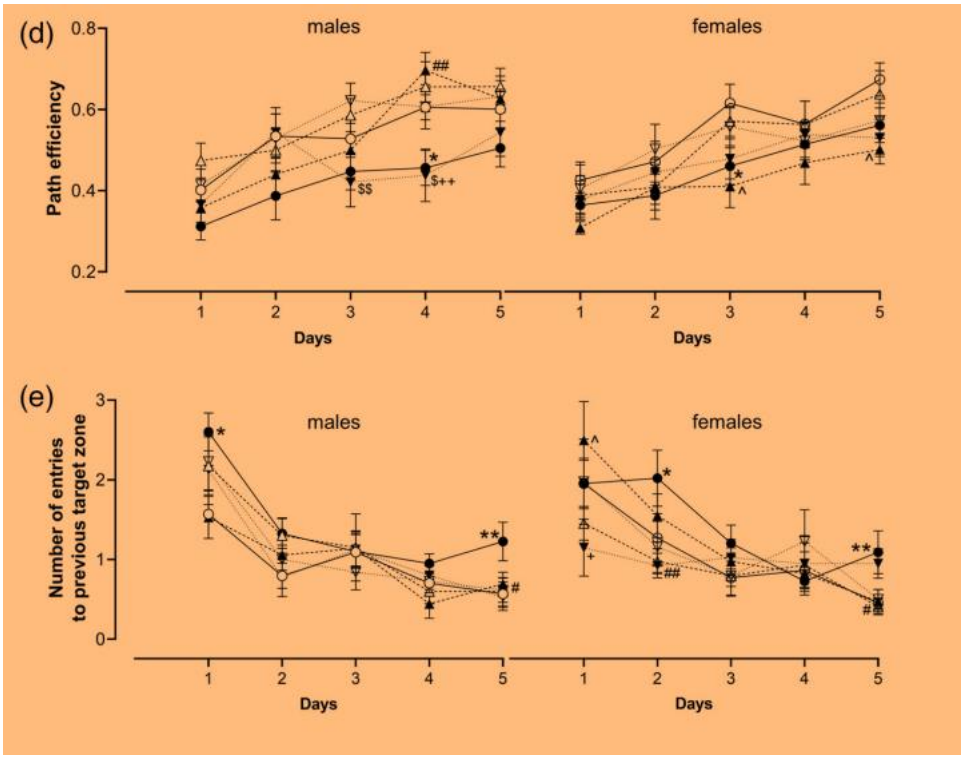


Figure 10. Effect of Treatment (Vehicle [VEH], MP-III-022 0.33 mg/kg [MP0.3], or MP-III-022 1 mg/kg [MP1]) on Morris Water Maze (MWM) Performance in Prenatally Treated Animals (Control [CTRL] or Valproate [VPA]):(a) Latency during standard MWM; (b) Path efficiency during standard MWM; (c) Latency during reverse MWM; (d) Path efficiency during reverse MWM; (e) Count of entries to the previous target zone during reverse MWM. Group Size: Males CTRL VEH 11, CTRL MP0.3 10, CTRL MP1 10, VPA VEH 10, VPA MP0.3 9, VPA MP1 10; females CTRL VEH 11, CTRL MP0.3 11, CTRL MP1 11, VPA VEH 11, VPA MP0.3 10, VPA MP1 10. *p < 0.05, **p < 0.01, ***p < 0.001 compared to CTRL VEH; ^ p < 0.05, ^^p < 0.01 compared to CTRL MP0.3, $ p < 0.05, $$ p < 0.01 compared to CTRL MP1, #p < 0.05, ##p < 0.01 compared to VPA VEH, + p < 0.05, ++ p < 0.01 compared to VPA MP0.3. Figure was modified from Anja *et al*. 2021. [284]

4.3.8. Neurons affected by VPA exhibited compromised GABA-switch functionality and altered spontaneous neuronal activity, both of which were restored to normal levels following treatment with MP-III-022 with Anja Santrac, Dr Miroslav Savic, and colleagues

Upon conducting initial calcium measurements, it became evident that the majority of cultures at DIV 13 displayed neuronal spontaneous activity. In the case of CTRL cultures, no GABA-evoked calcium transient was observed (**Figure 11 e**). Interestingly, a distinction was noticeable within VPA cultures—those exhibiting relatively low amplitude of spontaneous oscillations demonstrated a GABA-evoked calcium transient. However, VPA cultures characterized by higher frequency and larger amplitudes of spontaneous oscillations did not exhibit an increase in GABA-induced [Ca2+]i.

Further exploration revealed that VPA neurons had reduced frequency (**Figure 11a**) and amplitude (**Figure 11b**) of spontaneous oscillations in comparison to CTRL neurons. Those VPA neurons that lacked spontaneous calcium oscillations showed excitatory responses to GABA (designated as GABA responders) (**Figure 11e**). Among VPA animals, 38 out of 65 neurons exhibited a higher amplitude GABA-induced calcium transient (**Figure 11c**) compared to the 17 out of 49 CTRL neurons.

By DIV 15, all CTRL cultures (comprising 35 neurons) had developed spontaneous activity without GABA-induced calcium transients. The application of GABA during a spontaneous [Ca2+]i surge resulted in its immediate inhibition (**Figure 11e**). VPA cultures at this stage echoed the findings at DIV 13, ranging from no spontaneous activity accompanied by minor GABA-evoked calcium transients (23 out of 51 neurons) to spontaneous oscillations of lesser amplitude compared to CTRL, coupled with the absence of GABA-evoked calcium transients. CTRL neurons treated with MP exhibited reduced amplitude of spontaneous oscillations

compared to untreated CTRL. Intriguingly, some CTRL MP-treated neurons demonstrated a [Ca2+]i increase in response to GABA (14 out of 32 neurons). Conversely, VPA MP-treated neurons (24 in total) exhibited inhibition of spontaneous activity in response to GABA, along with an increased amplitude of spontaneous spikes compared to VPA neurons (**Figure 11d**).

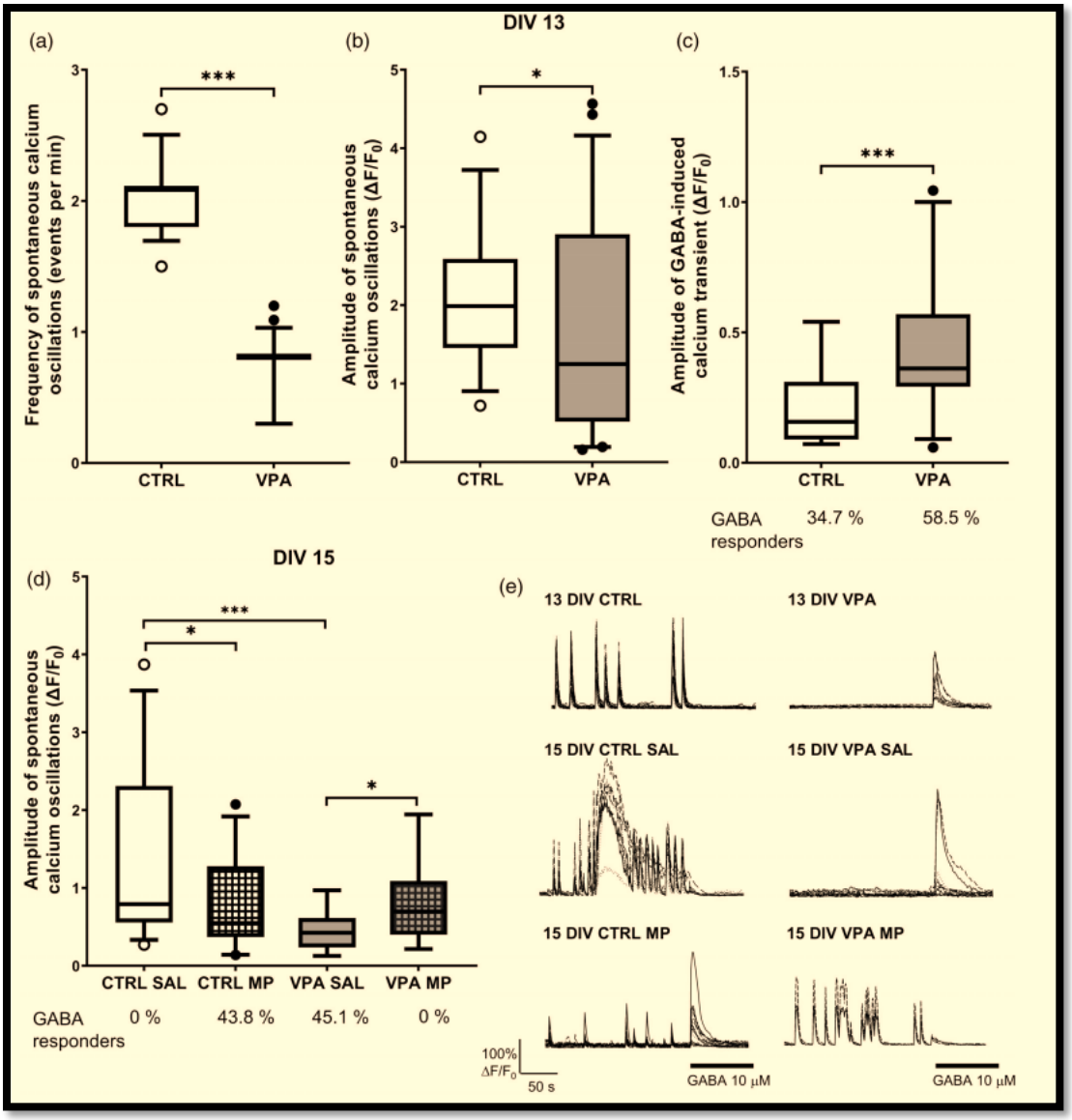


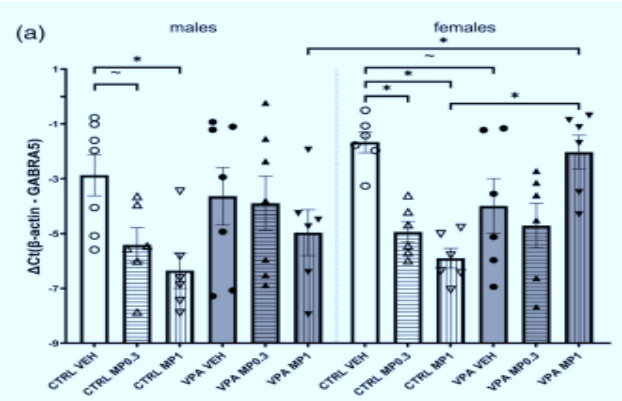
Figure 11. MP-III-022 at a concentration of 30 nM (referred to as "MP") exhibited the ability to enhance the timing of the GABA switch, as well as improve spontaneous neuronal activity which had been disrupted by the administration of valproate (referred to as

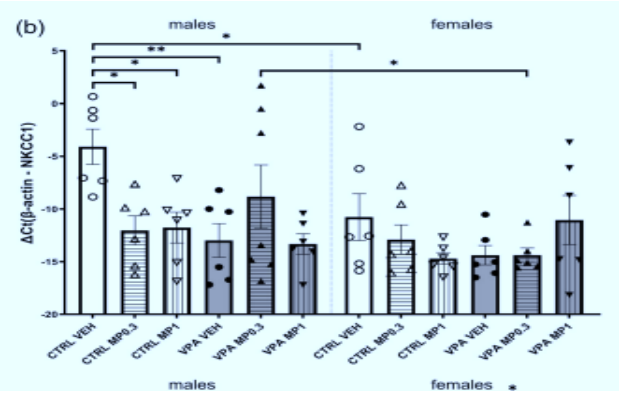
"VPA"). This improvement was observed through various parameters: (a) the frequency and (b) amplitude of spontaneous calcium oscillations, (c) the amplitude of GABA-induced calcium transient at day in vitro (DIV) 13, and (d) the amplitude of spontaneous calcium oscillations at DIV 15. Additionally, (e) representative recordings of all experimental groups were obtained during constant perfusion and GABA application. The cells were loaded with Fluo-4 AM at a concentration of 5 μM and subsequently imaged at a frequency of 1 Hz. The data presented included comparisons with the control group (referred to as "CTRL") and the saline-treated group (referred to as "SAL"). Statistical significance was indicated as follows: *p < 0.05, ***p < 0.001. Figure was modified from Anja *et al*. 2021. [284]

4.3.9. The impact of MP-022 on the expression of GABRA5, NKCC1, and KCC2 genes exhibited variations depending on both the sex and prenatal administration conditions with Anja Santrac, Dr Miroslav Savic, and colleagues

Examination of the GABRA5 mRNA levels (**Figure 12a**) demonstrated an overall reduction in expression following treatment with both doses of MP compared to VEH. This effect was particularly pronounced in the hippocampus of control (CTRL) animals. In male subjects, treatment with MP0.3 showed a trend-level decrease, and MP1 treatment also led to reduced expression. Among female subjects, MP0.3 and MP1 treatments similarly caused a decrease in GABRA5 mRNA levels. Notably, in females exposed to VPA, the hippocampal GABRA5 mRNA level exhibited a near-significant reduction ($p = 0.05$) compared to CTRL VEH females. Conversely, in females treated with VPA and MP1, there was an elevated expression compared to both CTRL MP1-treated females and VPA MP1-treated males.

Sex emerged as a significant factor influencing NKCC1 expression (**Figure 12b**). Female subjects displayed lower expression compared to males across all groups, a trend observed in both CTRL VEH and VPA MP0.3 groups. Among males, NKCC1 expression was lower in the VPA VEH, CTRL MP0.3, and CTRL MP1 groups relative to CTRL VEH males. In terms of KCC2 expression (**Figure 12c**), VPA females demonstrated decreased levels compared to VPA males in the MP0.3 group. Additionally, VPA VEH females displayed lower KCC2 mRNA expression relative to the CTRL VEH group (approaching statistical significance). However, this trend was reversed in the MP1 group: VPA MP1 females exhibited heightened KCC2 expression in comparison to CTRL MP1 females. Furthermore, VPA females treated with MP1 displayed increased hippocampal KCC2 expression relative to both VPA VEH and VPA MP0.3 females.





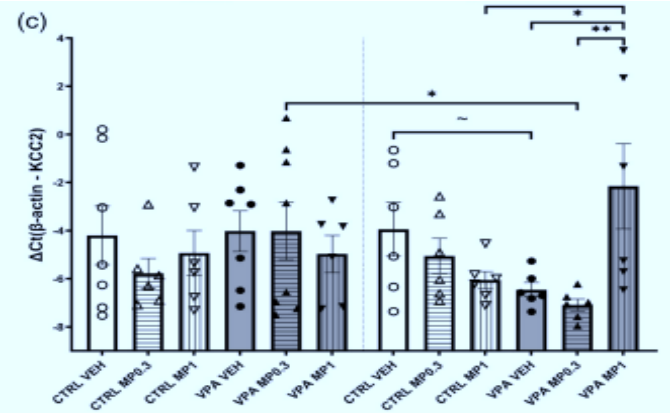


Figure 12. Hippocampal mRNA expression was assessed in response to different treatments (vehicle [VEH], MP-III-022 at 0.33 mg/kg [MP0.3], or MP-III-022 at 1 mg/kg [MP1]) administered to animals with prenatal exposure (control [CTRL] or valproate [VPA]). The expression levels of three genes were measured: (a) GABRA5, (b) NKCC1, and (c) KCC2. The sample sizes per group were as follows: For males in CTRL VEH and VPA VEH groups, there were 7 samples for GABRA5 and KCC2, and 6 samples for NKCC1. In the VPA MP0.3 group, there were 7 samples for GABRA5 and NKCC1, and 8 samples for KCC2. For males in CTRL MP0.3, CTRL MP1, VPA MP1, and females in each group, there were 6 samples for each gene expression. Statistical significance was denoted as follows: *p < 0.05, **p < 0.01, and 0.05 < p < 0.01. Figure was modified from Anja *et al*. 2021. [284]

4.3.10. In 5xFAD mice, both MP-III-022 and PWZ-029 were observed to negatively affect social recognition and social interaction, respectively with Jovana Abandelovic, Dr Miroslav M Savic, and colleagues

During the Social Interaction Test (SIT) and Social Recognition Test (SRT), both transgenic and non-transgenic males, when treated with the solvent, spent more time in the chamber containing a single unfamiliar animal or a new animal, respectively, in contrast to the chamber with an empty cage or an old animal, respectively (significant at $p = 0.036$ and $p = 0.028$, respectively, **Figure 13b**). In the SIT, transgenic and non-transgenic males treated with MP-III-022 exhibited a higher inclination to explore the cage with conspecifics compared to an empty cage (significant at $p = 0.013$ and $p = 0.012$, respectively, **Figure 13b**).

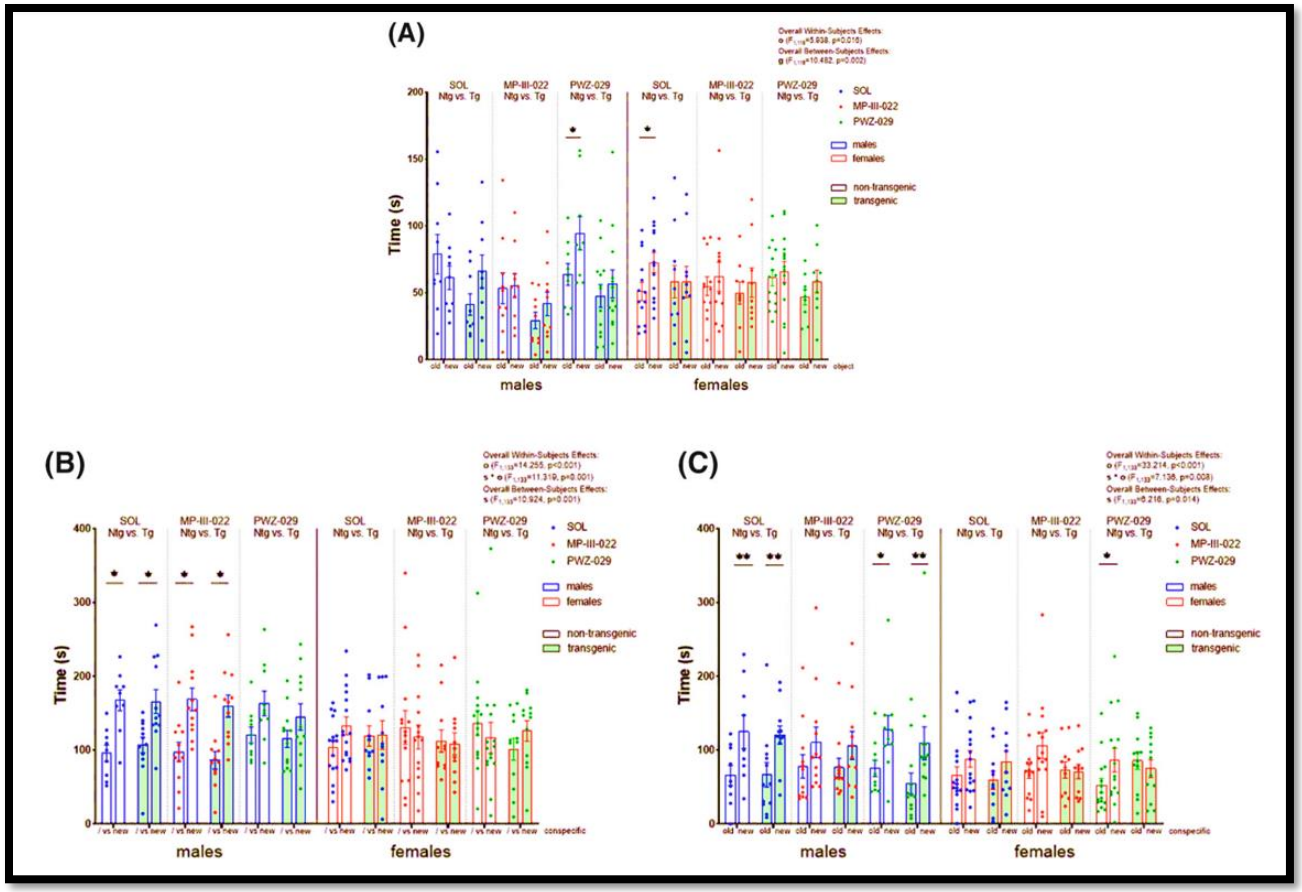


Figure 13. The outcomes of the Novel Object Recognition Test for short-term memory (NORT short-term), the Social Interaction Test (SIT), and the Social Recognition Test (SRT) are depicted for both transgenic and non-transgenic 5xFAD animals of both sexes, subjected to treatments with PWZ-029, MP-III-022, or solvent. The analysis involves evaluating the time spent with the new versus old object for NORT short-term, the time spent with an empty cage versus a cage with a conspecific in SIT, and the time spent with cages containing a new versus old mouse in SRT (designated as A, B, and C, respectively). The levels of statistical significance are indicated on the graphs: * signifies significance within the range of 0.01 < p < 0.05, ** indicates significance within the range of 0.001 < p < 0.01, and * signifies p < 0.001. Figure was modified from Arandelovic *et al.* 2022 [285]**

Conversely, in the SRT, transgenic and non-transgenic males treated with PWZ-029 displayed greater interest in the chamber with a new conspecific in comparison to the chamber with an old conspecific (significant at $p = 0.005$ and $p = 0.015$, respectively, **Figure 13c**). Furthermore, during the SRT, non-transgenic females treated with PWZ-029 demonstrated a heightened exploration of the chamber with a new conspecific in comparison to the chamber with an old conspecific (significant at $p = 0.046$, **Figure 13c**).

4.3.11. Treatment with MP-III-022 was found to hinder procedural learning specifically in transgenic females with Arandelovic, Dr Miroslav M Savic, and colleagues

In the regular Morris Water Maze (MWM) training, transgenic females treated with MP-III-022 exhibited a longer latency to locate the platform in comparison to solvent-treated transgenic females on day 3 ($p = 0.024$, **Table 6**). No significant differences in latencies were observed across training days in the regular MWM for any other transgenic or non-transgenic experimental groups (**Table 6**). During the probe trial, no significant distinctions in latency to find the platform zone were identified between groups.

In the probe trial, transgenic female controls spent less time in the peripheral zone compared to non-transgenic female controls ($p = 0.016$, **Figure 14A**). Transgenic females treated with MP-III-022 spent more time in the peripheral zone compared to those treated with the solvent ($p = 0.007$, **Figure 14A**). On the reversal cued day, transgenic female animals treated with MP-III-022 displayed shorter latencies to locate the new platform in trial 2 compared to trial 1 ($p = 0.031$, **Figure 14B**). In addition, transgenic male controls exhibited shorter latency to find the new platform in trial 1 compared to control non-transgenic male mice ($p = 0.013$, **Figure 14B**).

During the reversal probe, transgenic females treated with MP-III-022, PWZ-029, and the solvent had longer latencies to find the new platform zone compared to the old platform zone (p = 0.005, p = 0.012, and p = 0.002, respectively, **Figure 14C**). Moreover, PWZ-029-treated non-transgenic males displayed shorter latency to find the old platform zone compared to non-transgenic males treated with the solvent (p = 0.036, **Figure 14C**). Both transgenic and non-transgenic females treated with the solvent had fewer entries in the new platform zone compared to the old one (p = 0.011 and p = 0.029, respectively, **Figure 14D**). Similarly, PWZ-029-treated non-transgenic males exhibited more entries in the old platform zone compared to the new one (p = 0.001, **Figure 14d**), as well as more entries in the old platform zone compared to solvent-treated non-transgenic males (p = 0.014, **Figure 14d**).

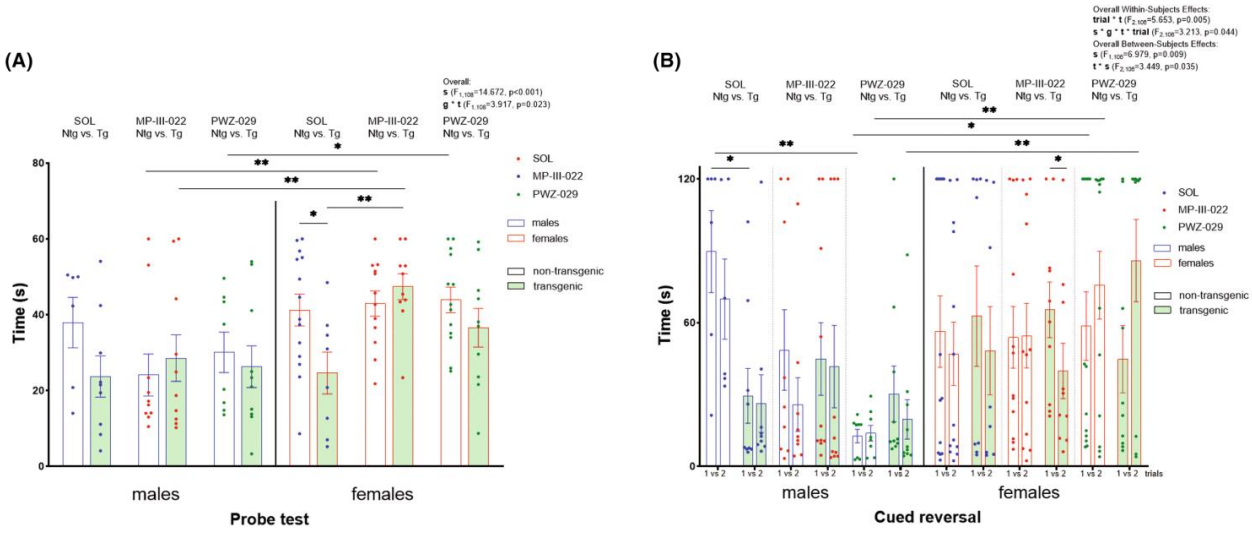
Table 6. Mean and standard error of latency to find the platform during regular Morris water maze (MWM) training

Sex	Genotype	Treatment	Mean of latency (s)	Standard error	*p* value (for all pairwise comparisons)
Males	Ntg	SOL	67.385	12.606	n.s.
		MP-III-022	49.902	9.765	n.s.
		PWZ-029	53.711	10.917	n.s.
	Tg	SOL	49.603	10.293	n.s.
		MP-III-022	59.683	9.765	n.s.
		PWZ-029	48.461	9.765	n.s.
Females	Ntg	SOL	66.955	8.253	n.s.
		MP-III-022	72.423	8.914	n.s.
		PWZ-029	71.899	8.564	n.s.
	Tg	SOL	52.234 (for day 3: 44.438)	10.917 (for day 3: 12.823)	Tg females treated with MP-III-022 vs SOL (overall) $p = 0.025$ * (Tg females treated with MP-III-022 vs SOL for day 3: $p = 0.024$ *)
		MP-III-022	85.544 (for day 3: 90.955)	9.765 (for day 3: 11.469)	
		PWZ-029	71.714	9.765	n.s.

****The notable outcomes from the Morris Water Maze (MWM) tests are outlined for both transgenic and non-transgenic 5xFAD animals of both sexes, subjected to treatments with**

PWZ-029, MP-III-022, or the solvent throughout the entire training procedure. Furthermore, any significant discrepancies detected during each training phase are indicated. Specifically, transgenic female animals treated with MP-III-022 or the solvent exhibited variations across all training days, and on training day 3, the mean values and standard errors for relevant latencies were incorporated within the table. The analyses were conducted using a three-way ANOVA with repeated measures, followed by Sidak's post hoc test. Statistical significances are denoted in the table using an asterisk (*) to indicate a significance level of 0.01 < p < 0.05.

Additionally, transgenic males treated with the solvent spent less time in the periphery compared to non-transgenic male controls (p = 0.009, Figure **14E**). Non-transgenic males treated with PWZ-029 and MP-III-022 also spent less time in the peripheral zone of the tank compared to non-transgenic males treated with the solvent (p = 0.003 and p = 0.006, respectively, **Figure 14E**).



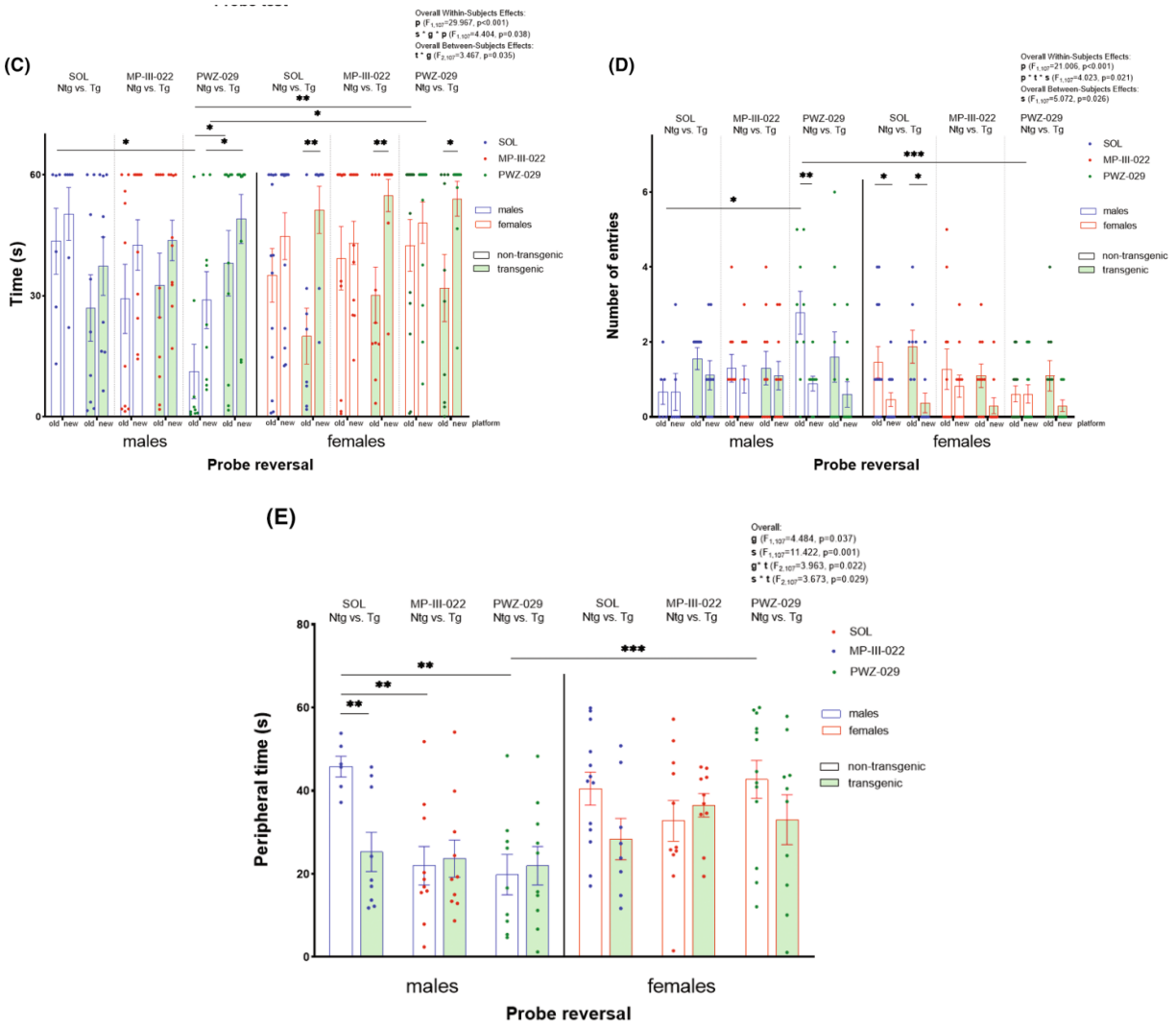


Figure 14. The results from the Morris Water Maze (MWM) are presented for both transgenic and non-transgenic 5xFAD animals of both sexes, subjected to treatments with PWZ-029, MP-III-022, or the solvent. The time spent in the peripheral zone during the probe test (Figure A); Latencies to reach the new platform in trials 1 vs. 2 during the reversal cued phase (Figure B); In the reversal probe, the latency to find the new platform zone vs. the old platform zone (Figure C); The number of entries in the new platform zone vs. the old platform zone (Figure D); The time spent in the peripheral zone (Figure E). For the analyses involving trials (B, C, D), a three-way ANOVA with repeated measures was used. For the analyses without repeated measures (A, E), a three-way ANOVA was

employed. In both cases, Sidak's post hoc test was applied. The levels of statistical significance are displayed on the graphs as follows: * for 0.01 < p < 0.05, ** for 0.001 < p < 0.01, and * for p < 0.001. The abbreviations used are: "g" for genotype, "s" for sex, "t" for treatment, and "p" for platform. Figure was modified from Arandelovic *et al.* 2022 [285]**

4.3.12. Effects of MP-III-022 on Angelman syndrome with Dr Kyoshi, and colleagues (Unpublished data)

Angelman syndrome (AS) is a neurodevelopmental disorder characterized by distinct clinical features. Individuals with AS typically exhibit severe learning difficulties, ataxia (loss of muscle control), a seizure disorder with a unique EEG pattern, subtle facial features that may appear dysmorphic, and a notably cheerful and sociable demeanor. Most children with AS experience delays in reaching developmental milestones, and their head growth slows during the first year of life. In the majority of cases, speech development does not occur. A hallmark behavioral phenotype is present, including jerky movements, frequent and sometimes inappropriate episodes of laughter, a fascination with water, and disturbances in sleep patterns.[286]

The facial features associated with AS are mild and include a broad, smiling mouth, a pronounced chin, and deep-set eyes. The disorder arises due to various genetic abnormalities affecting the chromosome 15q11-13 region, which undergoes genomic imprinting. These genetic anomalies encompass maternal deletion, paternal uniparental disomy, imprinting defects, and point mutations or small deletions within the UBE3A gene situated in this region. Notably, the UBE3A gene exhibits tissue-specific imprinting, meaning it is exclusively expressed from the maternal allele in the brain. The genetic mechanisms responsible for AS, identified thus far, are

present in approximately 85-90% of individuals with the clinical phenotype, all of which interfere with UBE3A expression. [136]



Figure 15. Patient with AS. Image was collected from google.

4.3.12.1 AS mice showed higher slow-wave power in awake EEG (Unpublished)

A subdural electrode was carefully positioned above the M1 cortex. During this procedure, the mice (6-12 months old) were awake, and their EEG (electroencephalogram) activity was recorded for a duration of 10 minutes. To ensure that the mice remained awake during the EEG recording, they were placed on a slowly rotating rotarod with a rotation rate of 2 ppm (rotations per minute).

For analysis, the EEG data was divided into 8 epochs, each lasting 9 seconds, with intervals of 20 seconds between them. The Fast Fourier Transform (FFT) results for each epoch were then averaged to obtain data for each trial. This approach helps in obtaining a consolidated view of

the EEG activity during these specific time intervals. The mice with Angelman syndrome (AS) exhibited greater power in the slow-wave frequencies during the awake EEG recordings (**Figure 17**).

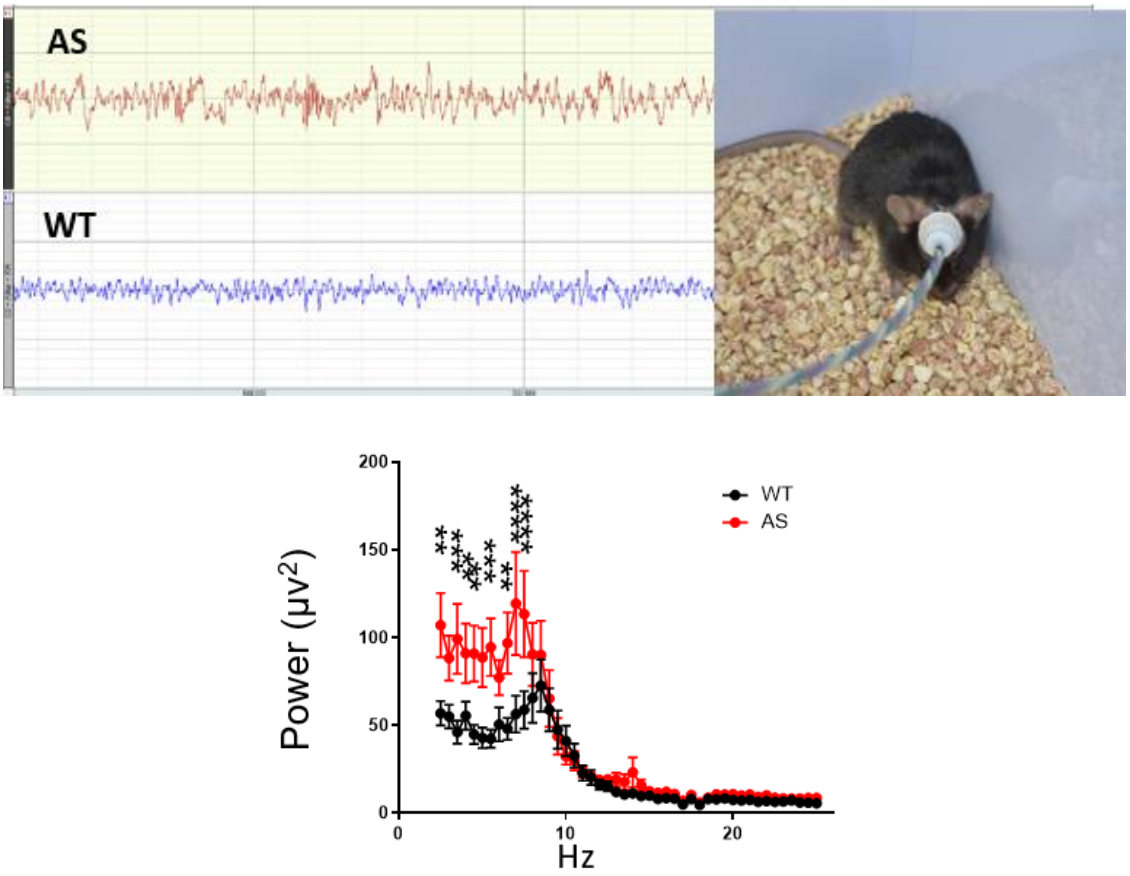


Figure 17. AS mice Vs WT mice. In mice with Angelman syndrome (AS), there was an observable increase in the power of slow-wave frequencies during their awake EEG recordings.

4.3.12.2 MP-III-022 at doses of 1.25 mg/kg, 2.5 mg/kg, or 5 mg/kg (but not at 0.5 mg/kg) resulted in a reduction in slow wave power in mice with Angelman syndrome (AS)

The impact of MP-III-022 on mice with Angelman syndrome (AS) was assessed at various dosage levels: 1.25 mg/kg, 2.5 mg/kg, 5 mg/kg, and 0.5 mg/kg. The results revealed that slow

wave power, a specific measurement of EEG activity associated with certain brain states, was affected by the administration of MP-III-022 in a dose-dependent manner. Specifically, when MP-III-022 was administered at doses of 1.25 mg/kg, 2.5 mg/kg, or 5 mg/kg, a significant reduction in slow wave power was observed (**Figure 18**). This indicates that the compound had a diminishing effect on the intensity of slow wave activity in the EEG recordings of AS mice. However, it's important to note that at the dosage of 0.5 mg/kg, no such reduction in slow wave power was observed(**Figure 18**). These findings suggest a potential dose-related relationship between MP-III-022 administration and its impact on the EEG activity of AS mice, particularly in relation to slow wave power.

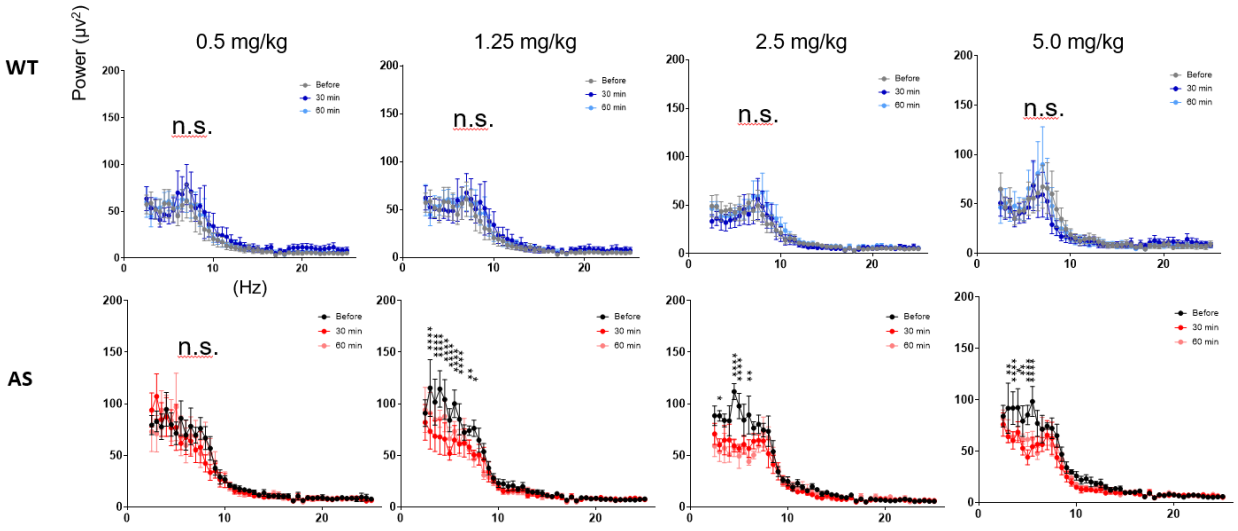


Figure 18. The varying doses of MP-III-022 (1.25 mg/kg, 2.5 mg/kg, and 5 mg/kg) exhibited a consistent trend of reducing slow wave power in mice with Angelman syndrome (AS), with the reduction being absent at the 0.5 mg/kg dose.

4.3.12.3. Higher seizure susceptibility of AS mice was improved by lower dose of MP-III-022

AS mice show higher seizure susceptibility induced by flurothyl inhalation. Induced seizures through flurothyl inhalation were conducted using male mice aged between 6 and 12 months. Each mouse was placed within a hermetically sealed glass chamber with a volume of approximately 2 liters. A solution comprising 10% flurothyl in 95% ethanol was administered at a rate of 200 µl/min onto a gauze pad suspended at the top of the chamber. Subsequent to the administration of the flurothyl solution, the latency period until the onset of myoclonic seizures (characterized by head-nodding and/or clonus of the body and forelimbs) or tonic posturing seizures (involving twitching of the body or tail, and forelimbs over a duration of at least 3 seconds) was measured and evaluated.

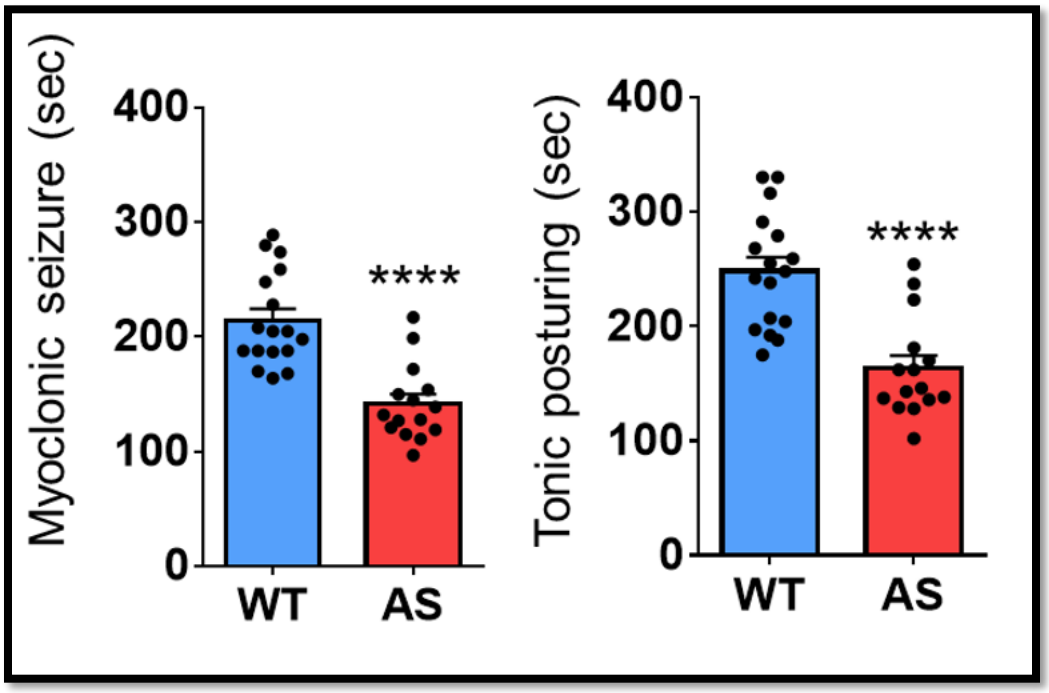


Figure 19. Induction of seizures by flurothyl inhalation

Through a series of tests involving different doses (0.5 mg/kg, 1.25 mg/kg, 2.5 mg/kg, and 5 mg/kg) of MP-III-022, the impact on the susceptibility to seizures in mice with Angelman

syndrome (AS) was examined. Interestingly, the results unveiled a distinct pattern: the mice exhibited a susceptibility to seizures associated with AS. However, when administered at a lower dose, specifically 0.5 mg/kg, MP-III-022 demonstrated a significant ability to ameliorate this heightened seizure susceptibility (**Figure 20**). This finding implies that the compound, at the lowest tested dose, effectively counteracted the tendency for AS mice to experience seizures. In essence, the lower dose of MP-III-022 exhibited a notable improvement in the seizure susceptibility of AS mice, as contrasted with the higher doses tested in the study.

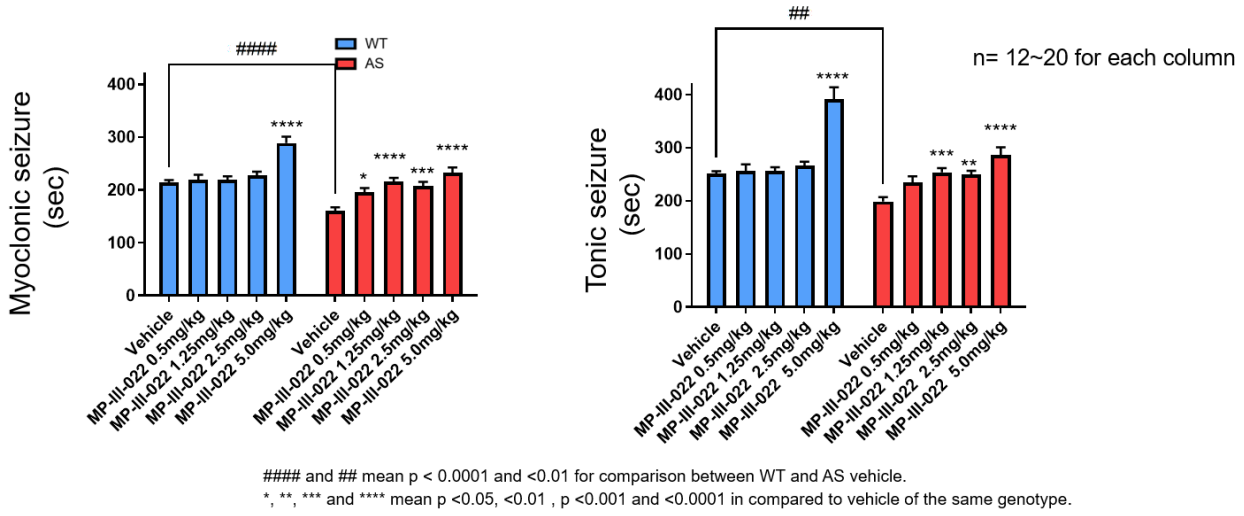


Figure 20. The susceptibility of AS mice to experiencing seizures was effectively reduced by administering a lower dose of MP-III-022. #### and ## mean p < 0.0001 and <0.01 for comparison between WT and AS vehicle. *, **, * and **** mean p <0.05, <0.01 , p <0.001 and <0.0001 in compared to vehicle of the same genotype.**

4.3.12.4. Lower dose MP-III-022 (0.5 > 1.25mg/kg i.p.) specifically improved anxiety-like behavior of AS mice

In the open field test, mice with Angelman syndrome (AS) demonstrate behaviors that resemble anxiety. This test involves placing the mice in an unfamiliar environment (the open field) and observing their responses. AS mice, in this context, exhibit behaviors that suggest heightened

anxiety, which could include reduced exploratory behavior, increased immobility, or other signs of discomfort. Mice aged between 6 and 12 months were placed within a 40cm x 40cm square field, and their distance covered during a 30-minute period of exploration was meticulously analyzed. Reduced exploration in center field represents higher anxiety of relevant mice (**Figure 21**).

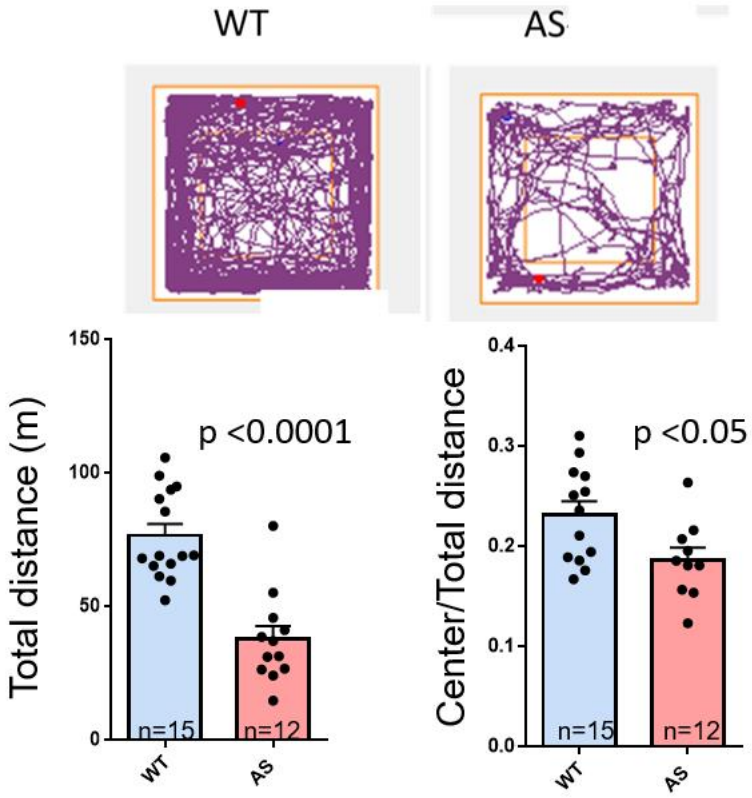


Figure 21. Open Field Test. Mice with Angelman syndrome (AS) exhibit behaviors that resemble anxiety-like behavior. A decreased tendency to explore the center field area is indicative of heightened anxiety in the mice under consideration.

In a comprehensive assessment aimed at evaluating anxiety-like behavior in mice with Angelman syndrome (AS), tests were conducted involving a range of doses: 0.0625 mg/kg, 1.25

mg/kg, 2.5 mg/kg, and 5 mg/kg. The focus was on determining how these different doses of MP-III-022 influenced the observed anxiety-related behaviors in the AS mice.

Remarkably, the study revealed that the impact of MP-III-022 was dose-dependent. Specifically, the lower doses of MP-III-022 showcased a significant and specific improvement in the anxiety-like behaviors exhibited by the AS mice (**Figure 22**). This improvement was distinct when compared to the responses elicited by the higher doses (1.25 mg/kg, 2.5 mg/kg, and 5 mg/kg) of the compound. These findings indicate that there exists a critical threshold at which the lower doses of MP-III-022 exert a notably beneficial effect on anxiety-like behavior in the context of Angelman syndrome.

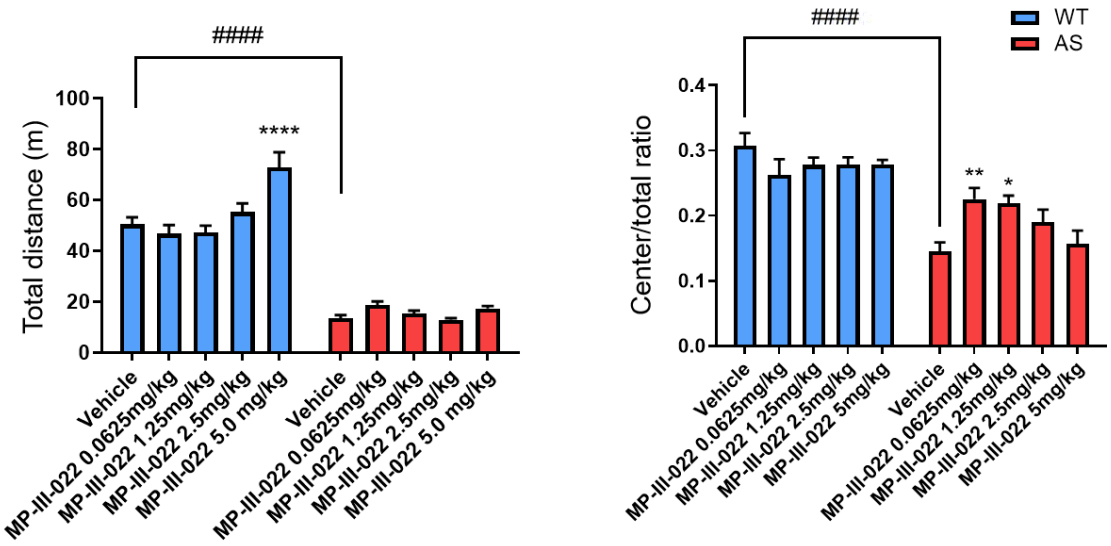


Figure 22. Improvement of anxiety-like behavior with MP-III-022. Specifically, the administration of a lower dose of MP-III-022 (0.5 mg/kg followed by 1.25 mg/kg intraperitoneal injection) led to a notable improvement in anxiety-like behavior in mice with Angelman syndrome (AS). This improvement was particularly evident when

compared to the response observed at the higher dose levels (1.25 mg/kg, 2.5 mg/kg, and 5 mg/kg). #### and ## mean p < 0.0001 and <0.01 for comparison between WT and AS vehicle. *, **, * and **** mean p <0.05, <0.01 , p <0.001 and <0.0001 in compared to vehicle of the same genotype.**

4.3.14. SH-053-2'F-R-CH_3 effectively reduces behavioral deficits in rats exposed to valproic acid (VPA), without inducing changes in the heightened activity of the ventral tegmental area dopamine (VTA DA) system with Adriana Souza, Felipe Gomes, and colleagues

Exposure to valproic acid (VPA) during prenatal development leads to an elevation in repetitive behavior during the early adolescent stage and induces impairments in sociability and cognitive function in both adult male and female rats

During the early adolescence phase, both male and female rats exposed to valproic acid (VPA) displayed an increase in self-grooming behavior (**Figure 23A**). Statistical analysis using a two-way ANOVA demonstrated significant effects of VPA exposure ($F_{1,32}=23.90$, $p<0.05$) and sex ($F_{1,32}=6.94$, $p<0.05$), with no notable interaction between them. Notably, spontaneous grooming behaviors were heightened in both male and female rats subjected to VPA exposure ($p<0.05$ compared to saline group; determined through Tukey's post-test). However, these alterations did not persist into adulthood (**Figure 23B**). Furthermore, no significant disparities in locomotor activity were observed among adolescent and adult VPA-exposed rats.

In terms of sociability, adult male and female rats that experienced in utero VPA exposure displayed reduced social interaction. A two-way ANOVA revealed a substantial influence of VPA exposure ($F_{1,32}=36.25$, $p<0.05$; **Figure 23C**), independent of sex, without any noticeable interaction. Across both sexes, rats exposed to VPA spent less time engaging in social

interactions with unfamiliar rats ($p<0.05$ compared to saline group; as determined by Tukey's post-test).

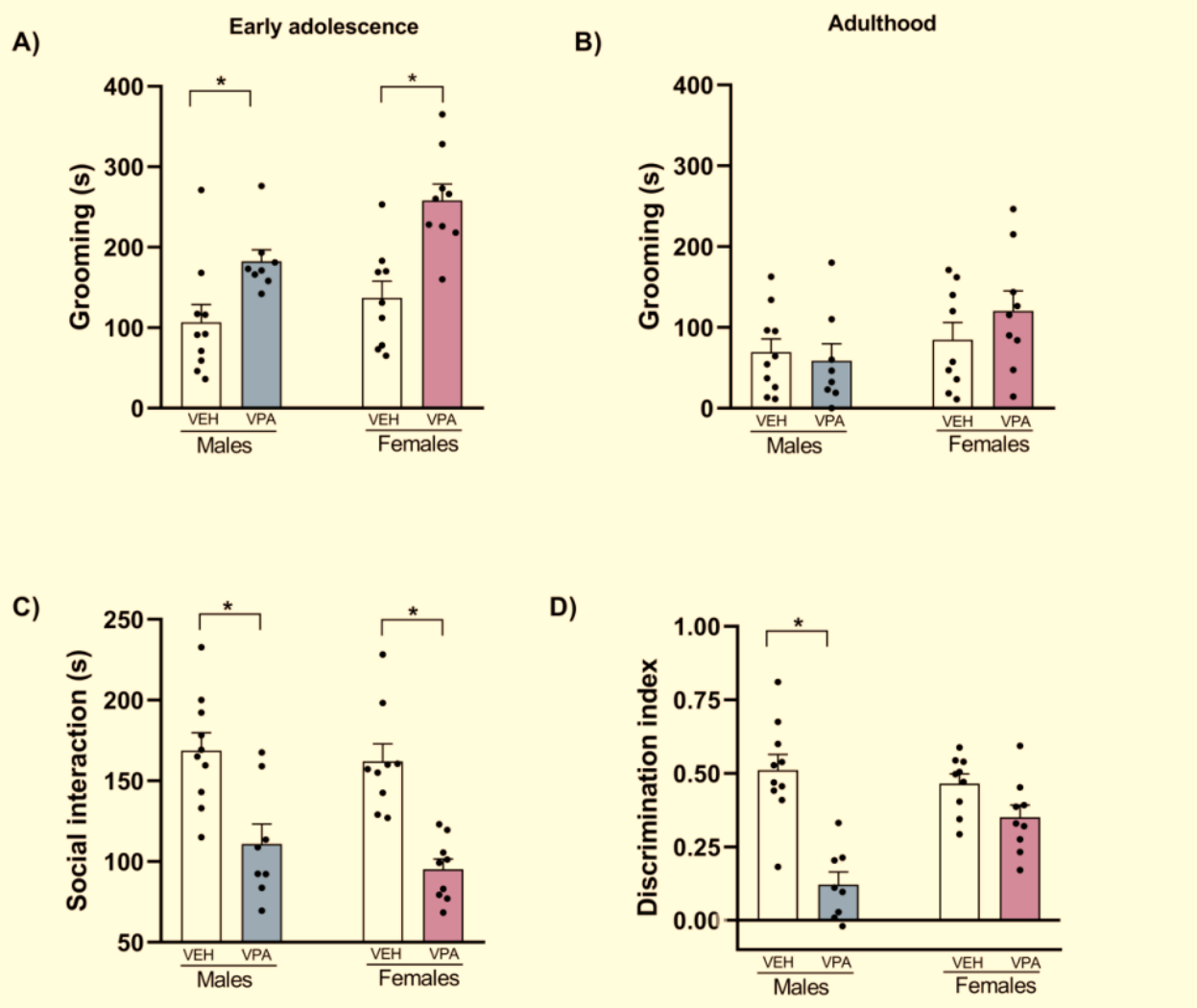


Figure 23. (A) Exposure to valproic acid (VPA) during prenatal development resulted in heightened self-grooming behavior among both male and female rats during early adolescence. (B) However, this increase in self-grooming behavior was not sustained into adulthood. (C) Notably, adult male and female rats exposed to VPA exhibited a notable reduction in social interaction. (D) In terms of cognitive function, only male rats exposed to VPA displayed a decline in recognition memory, as evidenced by their performance in the

Novel Object Recognition (NOR) test (n=8-10 rats per group). Statistical analysis using a two-way ANOVA followed by Tukey's post-test demonstrated statistical significance (*p<0.05) when comparing the results of the VPA-exposed rats to the saline-exposed rats. Image was modified from Adriana et al.2023 [287]

In the Novel Object Recognition (NOR) test, no disparities were observed in the exploration of identical objects placed on either side of the arena during the acquisition session for all groups, indicating a lack of spatial preference. However, during the retention session, increased exploration of the novel object was observed across all groups, except for male rats with in utero VPA exposure. These observations were consistent with the discrimination index (**Figure 23D**). Notably, a two-way ANOVA indicated substantial influences of VPA exposure ($F_{1,32}=32.52$, $p<0.05$) and sex ($F_{1,32}=4.27$, $p<0.05$), along with an interaction between the two ($F_{1,32}=9.66$, $p<0.05$). Further analysis indicated a reduction in the discrimination index among male rats exposed to VPA ($p<0.05$ compared to saline group; as determined by Tukey's post-test), whereas no such effect was observed in females. These findings suggest that the deficits in novel object recognition memory attributed to in utero VPA exposure appear to be sex-dependent, primarily affecting males.

In utero VPA increases VTA DA system activity in adult male and female rats

The day following the completion of the behavioral experiments, recordings of ventral tegmental area dopamine (VTA DA) neurons were initiated. Interestingly, an elevated activity within the population of VTA DA neurons were discovered in rats exposed to valproic acid (VPA), a pattern consistently observed regardless of the rats' sex (**Figure 24A**).

Utilizing a two-way ANOVA, we identified a significant influence of VPA exposure ($F_{1,20}=26.04$, $p<0.05$), while no notable effect of sex or interaction was observed. Both male and female rats with VPA exposure displayed an increased number of spontaneously active VTA DA neurons, exhibiting statistical significance when compared to the saline-exposed group ($p<0.05$).

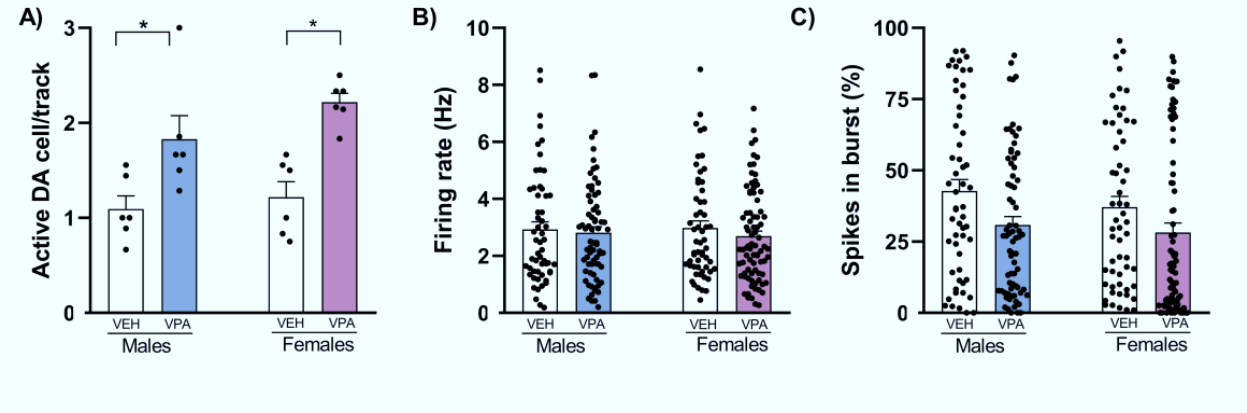


Figure 24. The effects of *in utero* valproic acid (VPA) exposure were observed in both male and female rats. (A) An augmented count of spontaneously active ventral tegmental area dopamine (VTA DA) neurons was evident, as indicated by significantly increased numbers in both males and females (n= 6 animals per group). (B) Importantly, despite the heightened activity, the firing rate of these VTA DA neurons remained unaffected. (C) Additionally, the percentage of spikes occurring within bursts of activity demonstrated no significant change. This analysis encompassed 56 DA neurons in male saline-exposed rats and 63 DA neurons in male VPA-exposed rats, as well as 57 DA neurons in female saline-exposed rats and 82 DA neurons in female VPA-exposed rats. Notably, statistical analysis was conducted using a two-way ANOVA followed by Tukey's post-test, with statistical significance indicated by *p<0.05 when comparing VPA-exposed rats to the saline-exposed rats. Image was modified from Adriana *et al*.2023 [287]

However, it's worth noting that we did not detect any alterations in the firing rate of these identified DA neurons (**Figure 24B**), nor did we observe any modifications in their burst activity (**Figure 24C**). These findings highlight that while VPA exposure led to heightened activity within the VTA DA neuron population, this effect did not extend to the individual firing rate or burst activity characteristics of these neurons.

SH-053-2'F-R-CH_3 effectively mitigates the behavioral deficits in rats exposed to valproic acid (VPA), yet it does so without causing alterations to the heightened activity of the ventral tegmental area dopamine (VTA DA) system

In order to assess the potential effects of SH-053-2'F-R-CH_3 in mitigating alterations seen in the social interaction and Novel Object Recognition (NOR) tests, as well as VTA DA system activity, several experiments were conducted on adult male and female rats with a history of valproic acid (VPA) exposure. The analyses involved a three-way ANOVA to account for potential interactions between sex, treatment, and VPA exposure.

In the social interaction realm, a noteworthy interaction between sex and treatment emerged ($F_{1,63}=4.59$, $p<0.05$), while another interaction encompassing sex, treatment, and VPA exposure was evident in the NOR test ($F_{1,63}=5.69$, $p<0.05$), implying the presence of sex-mediated effects. However, no interaction with sex was observed in the VTA recordings. Further analyses were performed using a two-way ANOVA approach. For male rats in the social interaction test, a significant interaction between VPA exposure and SH-053-2'F-R-CH3 treatment ($F_{1,22}=4.32$, $p<0.05$) was identified, along with a trend for a significant condition effect ($F_{1,22}=3.87$, $p=0.06$). Tukey's post-test indicated a significant reduction in social interaction behavior in

VPA-exposed rats treated with the vehicle ($p<0.05$ compared to vehicle-treated saline group), a reduction that was not observed in SH-053-2'F-R-CH3-treated VPA rats ($p>0.05$ compared to vehicle-treated saline; **Figure 25A**). On the other hand, among females, a significant effect of VPA exposure ($F_{1,32}=7.10$, $p<0.05$) was observed, but no effect of treatment or interaction was found.

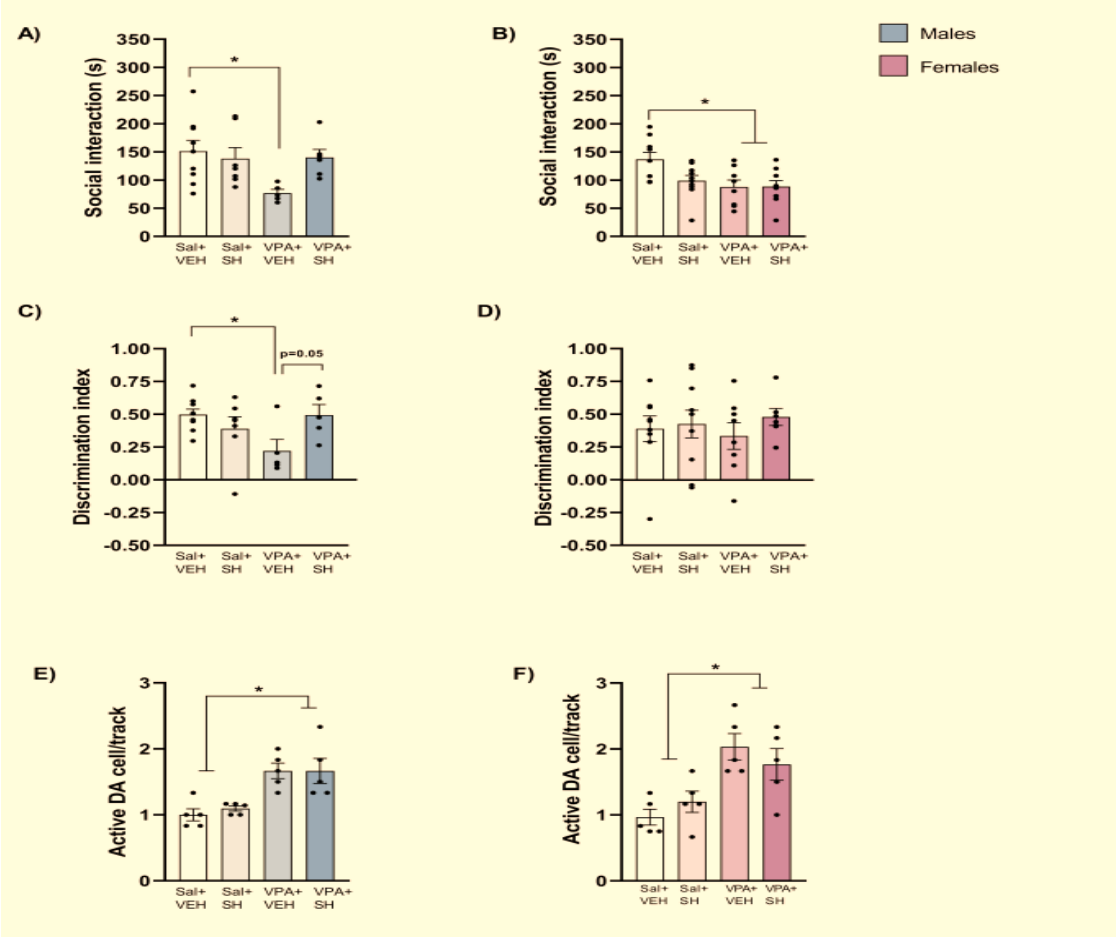


Figure 25. (A) SH-053-2'F-R-CH$_3$ effectively mitigated the impaired social interaction test performance in male rats exposed to VPA. (B) However, this ameliorating effect was not observed in female rats exposed to VPA. (C) Additionally, SH-053-2'F-R-CH$_3$ was capable of reversing deficits in novel object recognition memory specifically in male rats with VPA exposure. (D) Notably, female rats exposed to VPA did not exhibit deficits in the novel

object recognition test. (E) Despite these improvements, the heightened population activity of VTA DA neurons in (E) male and (F) female VPA-exposed rats remained unaltered by SH-053-2'F-R-CH_3 intervention. These findings were consistent across the behavioral tests (n=5-10 animals per group) and VTA recordings (n=5 animals per group). The statistical significance of these results was denoted by *p<0.05, as determined by a two-way ANOVA followed by Tukey's post-test. Image was modified from Adriana *et al*.2023 [287]

Tukey's post-test highlighted a notable reduction in social interaction in both female vehicle- and SH-053-2'F-R-CH_3-treated VPA rats ($p<0.05$ compared to vehicle-treated saline; **Figure 25B**). These results suggest that SH-053-2'F-R-CH_3 mitigated sociability deficits in male VPA rats, but not in females.

In the NOR test, no distinctions were found in object exploration during the acquisition session among all groups. However, during the retention session, greater exploration of the novel object was observed across all groups, except in male VPA rats treated with the. This trend was mirrored in the discrimination index (**Figures 25C and 25D**). For males, a significant interaction between SH-053-2'F-R-CH_3 treatment and VPA exposure ($F_{1,22}=9.45$, $p<0.05$) emerged, without observable treatment and interaction effects. Post hoc analysis demonstrated a decrease in the discrimination index in vehicle-treated VPA rats ($p<0.05$ compared to vehicle-treated saline; Tukey's post-test), with a tendency to be mitigated by SH-053-2'F-R-CH_3 treatment ($p=0.059$ compared to vehicle-treated VPA; Tukey's post-test). Consistent with previous findings, no deficits in the discrimination index were identified in female VPA rats (**Figure 25D**).

As for the VTA DA system activity, SH-053-2'F-R-CH_3 did not attenuate the heightened activity of the VTA DA neuron population in male and female VPA rats (**Figures 25E and F**). A two-

way ANOVA indicated a significant impact of VPA exposure in both males ($F_{1,16}=25.61$, $p<0.05$) and females ($F_{1,16}=19.38$, $p<0.05$), with no discernible treatment or interaction effects. Tukey's post-test indicated that irrespective of treatment and sex, VPA-exposed rats demonstrated a considerable increase in the number of spontaneously active VTA DA neurons ($p<0.05$ compared to vehicle-treated saline; Tukey's post-test). No significant alterations were observed in firing rate and burst activity.

4.3.5. Biological study of GL-II-73 with Alexandra McCoy, Dr Thomas Prevot, Dr Etienne Sibillie, and colleagues

4.3.5.1. Pilocarpine-induced seizures heightened the activity of the VTA dopamine neuron population, and this effect was reversed by GL-II-73

To establish a rodent model of temporal lobe epilepsy (TLE) [288-289], pilocarpine was unilaterally injected directly into the ventral hippocampus (vHipp). A brain slice depicting the cannula track is shown in **Figure 26A**. Consistent with previously reported findings [290], rats subjected to intra-vHipp pilocarpine injection exhibited significantly higher Racine ratings compared to control rats treated with saline (**Figure 26B**, t test; $t = 11.29$, $p < 0.0001$).

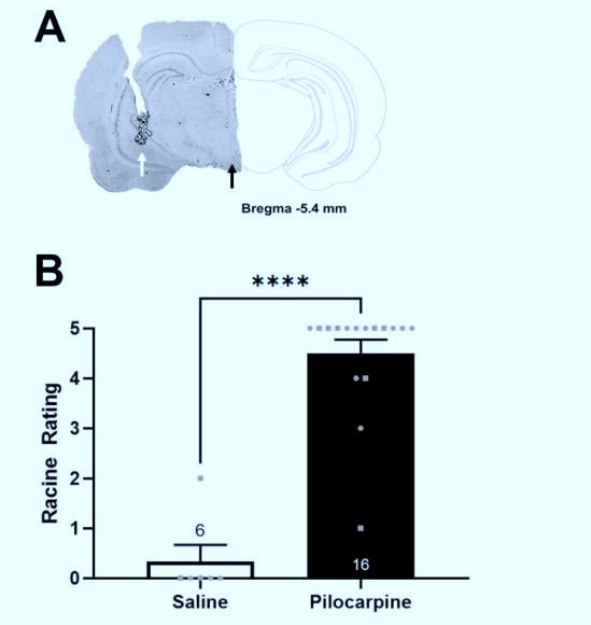


Figure 26. Verification of electrode placements and the response to pilocarpine. (A, Left) A representative brain slice displaying an electrode track within the ventral tegmental area (VTA; black arrow) and a cannula track within the ventral hippocampus (vHipp; white arrow) is presented, accompanied by the corresponding schematic of the brain section (right, positioned at -5.40 mm posterior to bregma. (B) Rats treated with pilocarpine exhibited a notably higher average Racine rating in comparison to controls treated with saline, **** $p < 0.0001$, n = 6–16/group; circles represent male subjects, while squares represent females. Image was modified from Alexandra *et al*.2023 [291]

A noteworthy increase in dopamine neuron activity was observed among rats treated with pilocarpine that received intra-vHipp vehicle (**Figure 27A**, n = 13 rats; 1.88 ± 0.10 cells per track; two-way ANOVA; $F_{Pilocarpine\ (1,33)} = 15.370$; $p < 0.001$; $F_{Drug\ (1,33)} = 7.121$; $p = 0.012$; Holm–Sidak; $t = 3.977$, $p = 0.002$) compared to saline-treated rats that were administered intra-vHipp vehicle (n = 6 rats; 1.13 ± 0.13 cells per track). Intriguingly, the elevation in dopamine

neuron activity triggered by pilocarpine was entirely reversed with the intra-vHipp administration of GL-II-73 (n = 12 rats; 1.30 ± 0.13 cells per track; Holm–Sidak; t = 3.800, p = 0.002), with no impact observed in saline-treated rats (n = 6 rats; 1.00 ± 0.09 cells per track). Notably, a subset of rats (4 of 17), as seen previously [290], did not manifest a hyperdopaminergic phenotype (n = 4 rats; 1.05 ± 0.13 cells per track), classifying as non-responders (defined as >1.5 cells per track) and were consequently excluded from this dataset. As expected, there were no significant differences in the average firing rate (**Figure 27B**; $F_{Pilocarpine\ (1,228)} = 0.140$; p = 0.709; $F_{Drug\ (1,228)} = 0.039$; p = 0.844) or bursting pattern (**Figure 27C**; $F_{Pilocarpine}$ (1,228) < 0.001; p = 0.989; $F_{Drug\ (1,228)} = 0.034$; p = 0.853). It's important to note that while both male (circles) and female (squares) subjects were included, our study may not have sufficient statistical power to detect any potential sex differences.

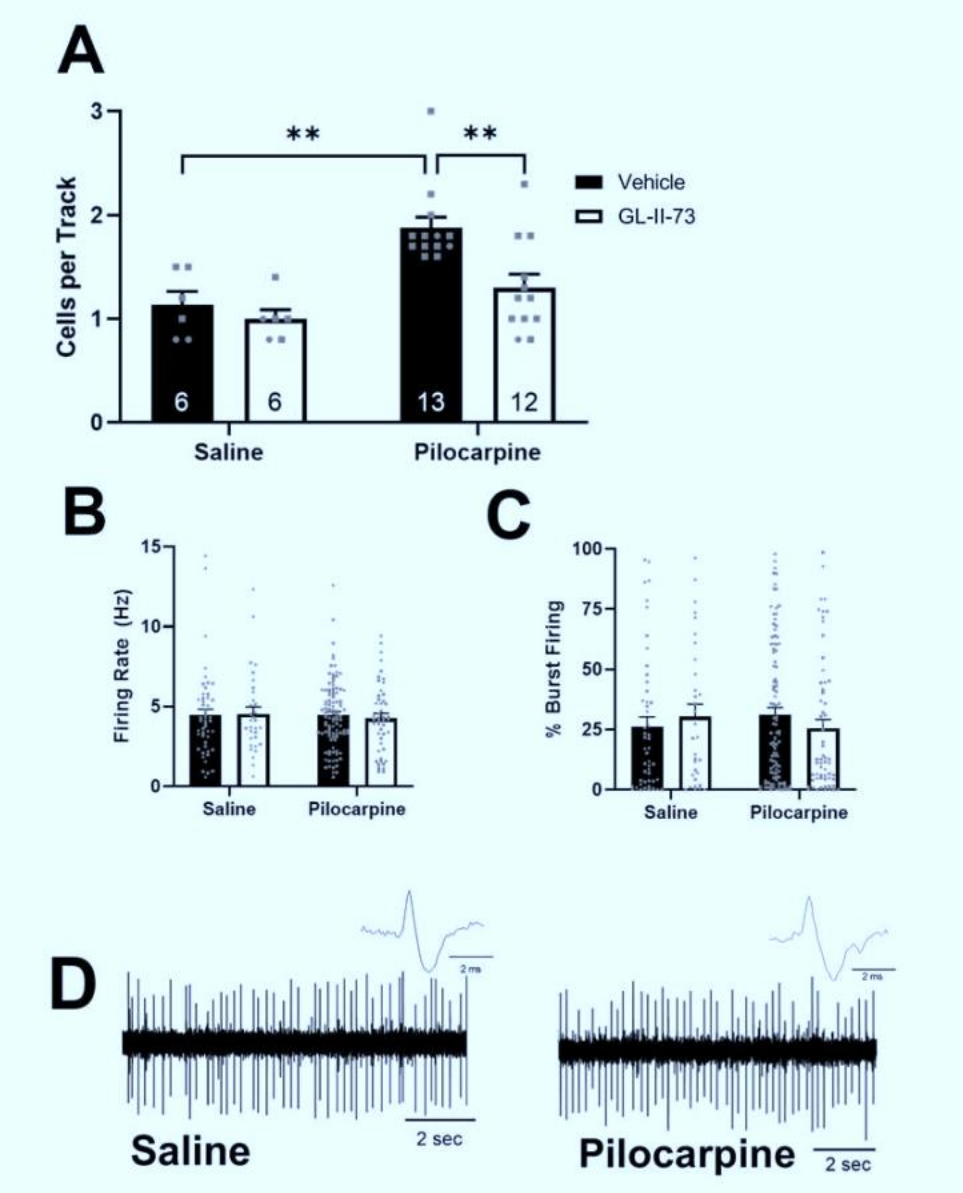


Figure 27. GL-II-73 effectively counteracts the heightened VTA dopamine neuron activity induced by pilocarpine. (A) Administration of intraventral hippocampal (vHipp) pilocarpine led to a substantial rise in the number of spontaneously active dopamine cells per track (population activity), which was then reversed through the intra-vHipp application of GL-II-73 (100 ng/µL; 0.75 µL). However, average firing rate (B) and percent burst firing (C) remained unaffected by pilocarpine or drug treatment. Additionally, (D) the representative trace of dopamine neuron firing and action potential for saline-treated

(left) and pilocarpine-treated (right) rats. ** p < 0.005, n = 6–13/group; circles represent male subjects and squares denote females. Figure was modified from Alexandra *et al.*2023 [144]

4.3.5.2. Radixin knockdown abolishes the therapeutic impact of intra-vHipp administration of GL-II-73 on dopamine system functionality

In the context of this experiment, it was focused on evaluating the functioning of the dopamine neuron system by utilizing *in vivo* extracellular electrophysiology to measure dopamine neuron activity within the ventral tegmental area (VTA). The outcomes of the study align with previous findings [292-293] and demonstrate that exposure to inescapable footshock stress prompts a substantial increase in the overall population activity of dopamine neurons. This effect was observed in shocked rats (n=6 rats; 1.733±0.109 cells per track) in comparison to non-shocked rats that received a vehicle (n=6 rats; 0.900±0.089 cells per track). Notably, this stress-induced elevation in dopamine neuron activity was entirely reversed when we introduced intra-hippocampal administration of GL-II-73 in shocked rats (n=7 rats; 1.071±0.078 cells per track). This intervention had no discernible impact on non-stressed rats treated with intra-hippocampal GL-II-73 (n=8 rats; 1.013±0.069 cells per track). Furthermore, knockdown of radixin in non-shocked rats did not influence the population activity in both vehicle-treated rats (n=6 rats; 0.967±0.061 cells per track) and GL-II-73-treated rats (n=8 rats; 1.113±0.088 cells per track). In alignment with findings from rats subjected to scrambled siRNA treatment, the footshock stress induced a significant increase in dopamine neuron activity in rats with radixin knockdown (n=7 rats; 1.571±0.121 cells per track). Intriguingly, the augmentation of synaptic α5GABAAR localization resulting from radixin knockdown obstructed the capacity of intra-hippocampal GL-

II-73 to reinstate dopamine system functionality in shocked rats (n=8 rats; 1.788±0.081 cells per track).

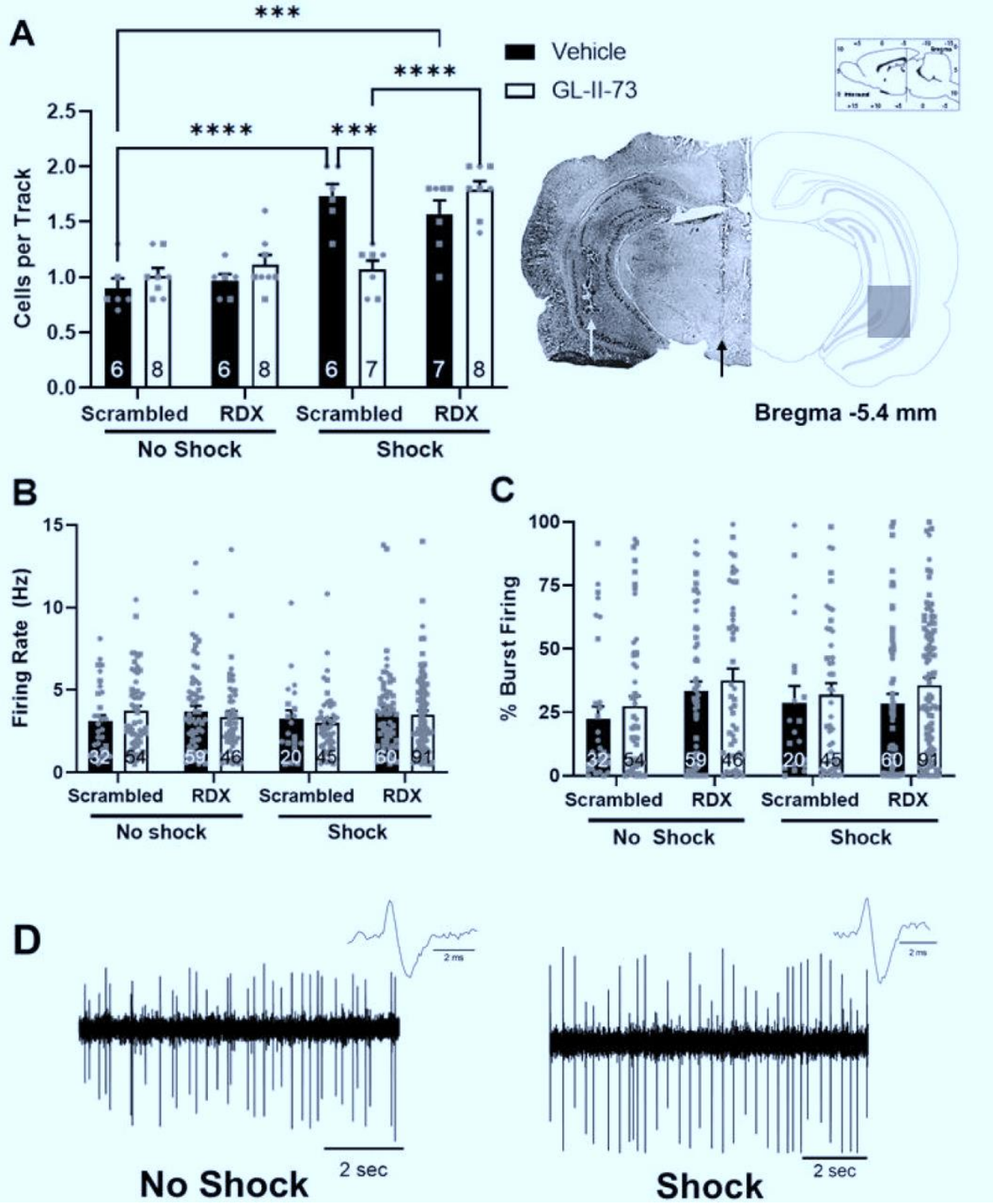


Figure 28. GL-II-73 exhibited an inability to reinstate proper dopamine system function in situations where radixin had been knocked down. In panel A, on the left, exposure to inescapable shock was observed to markedly elevate the count of spontaneously active cells per track, indicating an increase in population activity. However, this effect was counteracted by the administration of GL-II-73 (100ng/µL; 0.75 µL) into the ventral hippocampus, but this restoration was not observed in cases where radixin had been knocked down. On the right of panel A, a representative brain slice was displayed, with electrode placement highlighted in the ventral tegmental area (VTA) (marked by a black arrow), and the cannula's position for drug delivery in the ventral hippocampus (vHipp, indicated by a white arrow). Corresponding brain section schematics were provided for the region -5.40 mm posterior to bregma, with a box outlining the specific area containing the tracks. Analysis of (B) firing rate and (C) burst firing showed no significant effects resulting from siRNA, shock exposure, or drug treatment. Finally, panel (D) featured representative traces from both control (on the left) and shocked (on the right) rats. The study consisted of 6 to 8 individuals per group, with males represented by circles and females by squares. Statistical significance was denoted as ***P = 0.0001 and ****P < 0.0001. "RDX" refers to radixin. Figure was modified from Alexandra *et al.*2023 [294]

It's important to note that the analysis did not reveal any significant differences in the average firing rate (**Figure 28B**) with regard to shock ($F_{Shock(1,404)}$ = 0.953; p = 0.330), siRNA ($F_{siRNA(1,404)}$ = 0.304; p = 0.582), or drug effects ($F_{drug(1,404)}$ = 0.033; p = 0.856), nor in burst firing (**Figure 28C**) due to shock ($F_{Shock(1, 404)}$ = 3.427; p = 0.065), siRNA ($F_{siRNA(1, 404)}$ = 0.044; p = 0.833), or drug effects ($F_{drug(1, 404)}$ = 2.200; p = 0.139, **Figure 28D**).

4.3.5.3. Enhanced synaptic expression of α5GABAAR does not mitigate the impact of GL-II-73 in modulating the prepulse inhibition of startle response

In order to assess sensorimotor gating, measurements of prepulse inhibition (PPI) were conducted in response to the acoustic startle (**Figure 29**). Earlier investigations that examined PPI in rats subjected to inescapable stress (IS) indicated a noteworthy reduction in the percentage of PPI following exposure to inescapable footshock stress.[142] In this study, it was observed considerable overall effect stemming from the shock factor (with a sample size of 9 to 11 rats per group), as evidenced by a three-way ANOVA ($F_{shock\ (1,\ 71)} = 14.310$; $p = 0.0003$). Furthermore, an additional significant effect was noted concerning the intra-ventral hippocampus (intra-vHipp) administration of GL-II-73 ($F_{drug\ (1,\ 71)} = 8.765$; $p = 0.004$). However, upon conducting post hoc assessments, no statistically significant distinctions were detected between the various groups under consideration.

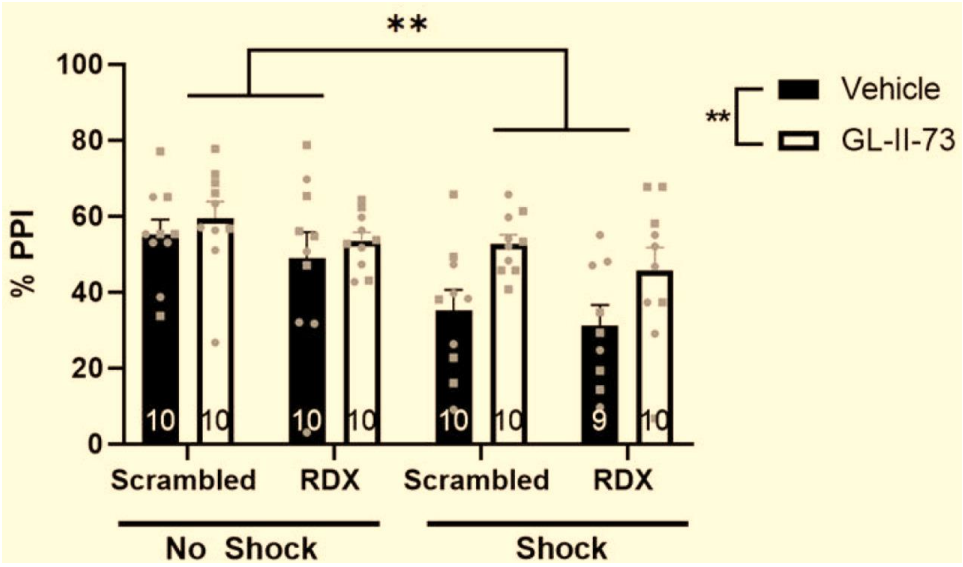


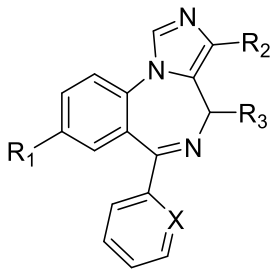
Figure 29. The reduction of radixin expression does not bring about any changes in prepulse inhibition. A period of two days involving inescapable shock demonstrated a

notable overall impact on prepulse inhibition, as did the administration of GL-II-73 (with a significance level of p = 0.0042). Nevertheless, when subsequent detailed examinations were conducted, no significant differences among the groups were observed. Each group encompassed a total of 9 to 11 individuals, with males and females represented by circles and squares, respectively. **P < 0.005, and RDX= radixin. Figure was modified from Alexandra *et al.*2023 [294]

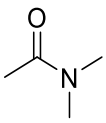
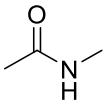
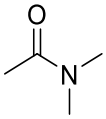
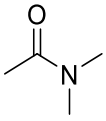
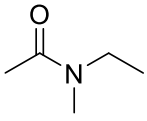
4.3.6. Biological study of analogs of GL-II-73 with Michael Marcotte, Dr Thomas Prevot, Dr Etienne Sibillie (CAMH)

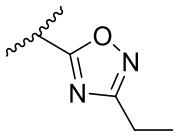
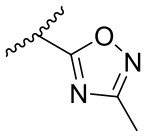
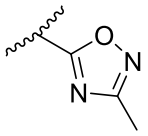
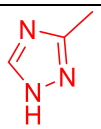
The analogs of GL-II-73 were tested in the Y-maze test to determine their pro-cognitive efficacy. While some of the compounds demonstrated positive activity in the Y-maze test, there were instances where certain compounds from the screening panel had no impact on the % alteration rate, even with drug treatments at 5, 10 mg/kg, and even 30 mg/kg. The data for some compounds is still in progress. The remaining active compounds in the Y-maze assay will be evaluated in the FST or EPM tests. It's noteworthy that none of the compounds displayed any adverse effects in the maximum tolerated dose (MTD) assay. For those active compounds that haven't undergone FST evaluation, their potential antidepressant effects will be investigated initially. Subsequent decisions will be made based on the outcomes of these evaluations. Additionally, a pharmacokinetic study will be conducted for certain compounds to ascertain their pharmacokinetic parameters. The overarching objective is to determine the anxiolytic, antidepressant, and cognitive-enhancing effects of the compounds, aiming to achieve levels that are comparable to, or even surpass, the effects of GL-II-73, GL-I-54, and the racemic mixture.

Table 7 : Pro-cognitive activity of GL-II-73 analogues in the Y-maze assay



Core structure of α5 imidazodiazepines

Genus	X	R_1	R_2	R_3	Code	Admin. Route	Cognition Y-maze
Amide	N	≡—H		R-CH_3	DS-I-19	i.p.	N
	N	≡—H		R-CH_3	DS-I-93	i.p.	N
	C-F	Br		R-CH_3	DS-III-97	i.p.	In-progress
	C-F	CH_3		R-CH_3	DS-II-30	i.p.	N
	C-F	≡—H		R-CH_3	DS-I-49	i.p.	N

Oxadiazoles and triazole	N	Br		$R\text{-}CH_3$	DS-I-86	i.p.	N
	C-F	Br		$R\text{-}CH_3$	DS-IV-41	i.p.	Y
	C-F			$R\text{-}CH_3$	MP-IV-04	_	resynthesized
	C-F			CH_3	DS-III-69	_	_

4.4. Methods

4.4.1. Animals for AD model with SM Perez, Eassa NE, and colleagues

To establish a rodent model of Alzheimer's disease (AD), specifically targeting pathological changes in the ventral hippocampus (vHipp), we employed high-titer adeno-associated viruses (AAV) in the AAV-AD model. Surgical procedures for survival were carried out under semi-

sterile conditions and general anesthesia. Male Sprague-Dawley rats (~325-350 g) obtained from Envigo in Indianapolis, IN, USA were administered anesthesia using Fluriso™ (2-5% Isoflurane, USP, along with oxygen at a flow of 1 L/min), and they were secured in a stereotaxic apparatus (Kopf, Tujunga, CA, USA) with the aid of gentle, non-traumatic ear bars. The rats' core body temperature was maintained at 37°C throughout the procedure. The viral vectors, containing GFP reporter and the mutated version of human amyloid precursor protein (hAPP) (at a titer of 2.09 x 1013 GC/ml; using pAAV[Exp]-CMV>{mutant hAPP}:WPRE) as well as human Presenilin-1 (hPSEN1) (with a titer of 6.28 x 1013 GC/ml; using pAAV[Exp]-CMV>{hPSEN1}:T2A:TurboGFP:WPRE), were injected bilaterally (0.5 µl each) into the vHipp. The coordinates used for injection were A/P: -5.3 mm, M/L: ±5.0 mm from Bregma, and D/V: -9.0 mm ventral from the brain surface. In the control group, AAV expressing eGFP (with a titer of 2.09 x 1013 GC/ml; pAAV[Exp]-CMV>EGFP:WPRE) was bilaterally administered.

Post-surgery, rats were given ketoprofen (5 mg/kg, subcutaneously) and were housed in groups of 2-3 animals until reaching approximately 8 months of age, prior to behavioral and electrophysiological assessments. As part of the experimental design, a subset of both control and AAV-AD rats received systemic treatment, either with vehicle (consisting of 1% Tween 80, 14% propylene glycol, in distilled water) or with the selective α5-positive allosteric modulator (PAM) named MP-III-022 (at a dose of 10 mg/kg), administered 20 minutes before any electrophysiological or behavioral testing.

4.4.2. *In Vivo* Extracellular Electrophysiology Recordings [295-296] with SM Perez, Eassa NE, and colleagues

For non-survival surgeries, rats were anesthetized using chloral hydrate (400 mg/kg; administered intraperitoneally) prior to being positioned within a stereotaxic apparatus (Kopf; Tujunga, CA). The use of chloral hydrate is necessary for dopamine neuron physiology, as it does not induce significant alterations in dopamine activity when compared to recordings from animals that are freely moving. During the procedure, the rats' core body temperature was maintained at 37°C, and additional anesthesia was administered as needed to ensure the suppression of the limb withdrawal reflex.

Extracellular glass microelectrodes with an impedance range of 6-10 MΩ were carefully lowered into either the ventral hippocampus (vHipp) or the ventral tegmental area (VTA). For vHipp recordings, the coordinates used were A/P: -5.3 mm and M/L: ±5.0 mm from Bregma, with a D/V range of -4.5 to -9.0 mm ventral from the brain surface. In the case of VTA recordings, the coordinates were A/P: -5.3 mm and M/L: ±0.6 mm from Bregma, with a D/V range of -6.5 to -9.0 mm ventral from the brain surface. The firing frequency of spontaneously active putative pyramidal neurons within the vHipp was quantified, and these neurons were identified following previously established criteria (neurons displaying firing frequencies of less than 2 Hz). Local field potential (LFP) oscillatory activity within the vHipp was generated and recorded for a minimum of ten minutes using open filter settings (Low Pass Filter: 0.3 Hz; High Pass Filter: 1000 Hz). Oscillations were quantified using commercially available computer software.

Spontaneously active dopamine neurons were identified according to well-established criteria: (1) action potential duration exceeding 2 ms and (2) a frequency range between 0.5 and 15 Hz. Three specific parameters of dopamine activity were measured: (1) population activity (indicating the count of spontaneously active dopamine neurons encountered per track), (2) basal

firing rate, and (3) the proportion of action potentials occurring in bursts (defined as spikes with intervals of less than 80 ms between them; termination of a burst occurs when spikes are separated by more than 160 ms). Recording sessions typically extended for approximately 2 to 4 hours. The electrophysiological recordings were subjected to analysis using a two-way ANOVA (strain x frequency) and were subsequently followed by a Holm-Sidak post-hoc test.

4.4.3. Y-maze Spontaneous alternation assay with SM Perez, Eassa NE, and colleagues

The Y-maze utilized in this study comprises three plastic arms, each measuring 81 cm in length, 20.32 cm in width, and 20 cm in height. These arms are separated by 120-degree angles. During experimentation, rats were positioned just within one of the arms, facing the central area of the maze. They were then allowed to move freely within the maze for a duration of 10 minutes. Throughout this period, both the number and sequence of arm entries were documented. An "arm entry" was defined as a situation where at least 80% of the front part of the rat moved into an arm starting from the central region of the maze.

To calculate the percentage of alternations, the number of alternations (which entails entering all three arms in a sequence) was divided by the total number of entries minus 2, and then multiplied by 100. Subsequently, the data collected from the Y-maze experiments were subjected to analysis using a two-way ANOVA, followed by a Holm-Sidak post hoc test for further investigation of significant results.

4.4.4. Pre-Pulse Inhibition of Startle (PPI) with SM Perez, Eassa NE, and colleagues

Rats were introduced into a sound-attenuated chamber provided by SD Instruments (San Diego, CA, USA). Before being subjected to any trials, they were given a period of 5 minutes to acclimate to a background noise level of 65 dB. Subsequently, the rats were exposed to a series of trials, starting with 10 "startle-only" trials. These trials involved a 40 ms duration pulse at a

sound intensity of 120 dB, with an average inter-trial interval (ITI) of 15 seconds. Following the startle-only trials, the rats experienced 24 additional trials. In these trials, a pre-pulse lasting 20 ms was introduced at varying sound intensities of 69 dB, 73 dB, and 81 dB. The pre-pulse was delivered 100 ms prior to the startle pulse. Each pre-pulse was presented 6 times in a pseudo-random order, with an ITI of 15 seconds between trials. Startle responses were recorded within a time frame of 10 to 80 ms from the initiation of the startle-only pulse. The SR-Lab Analysis Software was employed to capture and document these startle responses. The collected data from the prepulse inhibition (PPI) experiments were analyzed using a three-way ANOVA, involving the factors of strain, treatment, and pre-pulse sound intensity (dB). After the ANOVA, a Holm-Sidak post hoc test was applied to delve deeper into any statistically significant findings.

4.4.5. Stimulant-induced Locomotor Activity with SM Perez, Eassa NE, and colleagues

Rats were introduced into an open field arena, provided by Med Associates (VT, USA), to assess their spontaneous locomotor activity in the x-y plane. This activity was determined based on the occurrence of beam breaks, and the data was meticulously recorded using the Open Field Activity software. The experiment began with a 30-minute period of baseline recording, during which the rats' locomotor activity was monitored. Subsequently, all rats were administered the NMDA receptor antagonist, MK-801 (at a dose of 75 μg/kg, intraperitoneally), following which their locomotor activity was recorded for an additional 45 minutes.

The collected locomotor data were subjected to analysis using two separate three-way ANOVAs, one for the baseline period and another for the period following MK-801 administration. These ANOVAs incorporated the factors of strain, treatment (MK-801 injection), and time. To explore any statistically significant findings further, a Holm-Sidak post hoc test was applied after the ANOVA analysis.

4.4.6. Immunohistochemistry with SM Perez, Eassa NE, and colleagues

Upon the completion of all experimental procedures, the rats underwent transcardial perfusion with saline (150 mL). Subsequently, their brains were carefully extracted, followed by a post-fixation period of at least 24 hours in a solution of 4% formaldehyde dissolved in 0.1M phosphate-buffered saline (PBS). Following this, cryoprotection was achieved by immersing the brains in a solution of 10% sucrose diluted in PBS. The brains were then coronally sectioned at a thickness of 50 µm using a cryostat obtained from Leica (Buffalo Grove, IL, USA). For a subset of slices encompassing the ventral hippocampus (vHipp), specific actions were taken. These slices were mounted and cover-slipped with Prolong™ Gold anti-fade mountant to verify the expression of the virus using the GFP fluorescent reporter (as illustrated in Figure 2B and 2C). To ascertain the presence of amyloid plaques within the vHipp, another subset of slices underwent silver staining using the FD NeuroSilver Kit II following the manufacturer's instructions. These slices were then cover-slipped with Permount® (as shown in Figure 1C). Additionally, a separate subset of slices containing the vHipp was utilized for the detection of the expression of Parvalbumin (PV). This involved washing the slices three times for a duration of 10 minutes each in PBS, followed by blocking with a mixture of 2% normal goat serum and 0.3% Triton Tx 100 in PBS for a duration of 30 minutes at room temperature. The slices were then incubated with a primary antibody (rabbit anti-parvalbumin) at a dilution of 1:1000 overnight at 4°C. After washing the slices three times with PBS for 10 minutes each, they were exposed to AlexaFluor® 594 goat anti-rabbit immunoglobulin G (H+L) at a dilution of 1:1000 for a period of 1 hour at room temperature. Subsequently, the slices were wet-mounted and cover-slipped using ProLong™ Gold anti-fade mountant.

For imaging purposes, sections were observed utilizing an AxioCam ICc 1 camera (attached to a Zeiss microscope). The imaging was conducted on an Axio Lab.A1 microscope from Zeiss. To quantify the number of PV-positive cells within the vHipp, counts were performed on 6 sections from each animal. These sections were in an area approximately -6.0 to -8.5 mm ventral from the brain surface and within ±4.0 to 6.0 mm lateral of the midline.

4.4.7. Statistical analysis with SM Perez, Eassa NE, and colleagues

Electrophysiological analysis of both ventral hippocampus (vHipp) and dopamine neuron activity was conducted using LabChart version 8, which is a commercially available computer software provided by ADInstruments in Chalgrove, Oxfordshire, UK. Locomotor activity data were collected using Activity Monitor software obtained from MED Associates in St. Albans, VT, USA. For the prepulse inhibition (PPI) data, SR-Lab™ Analysis Software from SD Instruments in San Diego, CA, USA, was utilized. The analysis of all data was carried out using Prism software, which is available from GraphPad Software Inc. in San Diego, CA, USA. The presented data in the study are represented as mean ± standard error of the mean (SEM), with the 'n' values indicating the number of animals in each experimental group, unless otherwise specified. During analysis, a range of statistical methods was employed, including t-tests, linear regression, as well as two- or three-way analysis of variance (ANOVA). In instances where significant interactions were detected, the Holm-Sidak post hoc test was applied. The statistical calculations were performed using SigmaPlot, a software provided by Systat Software Inc. in Chicago, IL, USA. A significance level of $p < 0.05$ was used to determine the statistical significance of the findings.

4.4.8. Social interaction test with Anja Santrac, Miroslav M Savic, and colleagues

During the initial day of the experiment, rats were placed in separate individual small cages and remained isolated for a period of 3.5 hours, as per the methodology established by Schneider and Przewłocki in 2005. Subsequently, each rat was individually habituated in transparent Plexiglas chambers, with dimensions of 40 cm x 25 cm x 35 cm, for a duration of 10 minutes.

On the following day, the experimental protocol was adjusted for pair interactions. Rats were paired up in pairs of two, with the pairing being based on factors such as sex, prenatal administration, postnatal treatment, and their approximate size (with a maximum difference of 10 grams between partners). It's important to note that pairs were constituted using rats from distinct litters. During the observation phase, the behavior of these paired rats was recorded for a total of 10 minutes. The recorded videos were subsequently subjected to analysis. Specifically, the behaviors under scrutiny included allosniffing/grooming, instances of crawling over/under the conspecific, following the conspecific, tail manipulation (such as biting or grabbing the tail of the partner), instances of boxing and wrestling, as well as pinning. This analysis was carried out by two researchers, and it was performed in a manner that maintained blindness to the experimental conditions.

4.4.9. Spontaneous locomotor activity with Anja Santrac, Miroslav M Savic, and colleagues

The animals were introduced into a test arena constructed from plexiglass, measuring 40 cm x 25 cm x 35 cm. Notably, no prior habituation was conducted. This arena was illuminated by red light, maintained at an intensity of 20 lux. The freely moving behavior of the animals was recorded over a period of 20 minutes. Several parameters were automatically quantified during this recording. These included the measurement of the time during which the animals were

active, as well as the total count of rotations. Furthermore, rotations were classified into clockwise and anticlockwise rotations for separate analysis. On a different note, self-grooming behavior was manually tracked, and this tracking was performed by researchers in a blind manner.

4.4.10. Morris water maze (MWM) test with Anja Santrac, Miroslav M Savic, and colleagues

The testing protocol involved both a standard and reverse version, each comprising an acquisition phase and a probe test. The primary distinction between the two tests was the position of the platform in the pool. Specifically, in the reverse test, the platform was relocated diagonally opposite to its position during the standard test. In both the standard and reverse tests, various parameters were analyzed. These included the latency of the subjects, the efficiency of their paths during the acquisition phases, the count of entries into the target zone during both probe tests, as well as the number of entries into the previous target zone during both the acquisition phase and the probe test of the reverse version of the Morris Water Maze (MWM).

For the assessment of path efficiency, a crucial factor in understanding restrictive behavioral patterns observed in subjects, the ratio of the optimal path (the shortest distance between the start point and the target) to the actual path taken by the subjects was computed. This analysis was particularly chosen to shed light on restrictive behavioral patterns that are a significant characteristic of Autism Spectrum Disorder (ASD).

4.4.11. Primary hippocampal cell cultures and intracellular calcium imaging with Anja Santrac, Miroslav M Savic, and colleagues

Hippocampal neurons obtained from both the control (CTRL) and valproic acid (VPA) exposed pups were employed in our in vitro experiments. The process of cell culture preparation and the subsequent intracellular calcium measurements were described in-depth in a prior study (Kapadia et al., 2017).[297]

Preliminary data derived from our initial experimental setup, where tests were conducted every 2 days starting from Day In Vitro (DIV) 3, corroborated previously established findings indicating that a substantial number of neurons undergo a GABA switch around DIV 13 (as demonstrated by Ganguly et al., 2001).[298] Consequently, we designated this particular time point (DIV 13) for establishing the fundamental distinctions between VPA and CTRL neurons. These differences were assessed based on the frequency and amplitude of spontaneous calcium oscillations, as well as the amplitude and area under the curve of GABA-induced calcium transients. Furthermore, at DIV 13, we implemented a treatment involving the application of 30 nM MP-III-022, a compound that exhibited selectivity for α5GABAARs and was dissolved in saline (SAL). The control group received an equivalent volume of saline. We then examined the effects of this treatment at DIV 15, resulting in four distinct experimental conditions at this later time point (CTRL SAL, CTRL MP, VPA SAL, VPA MP).

The procedure was standardized across all experimental conditions. We initiated by recording baseline fluorescence intensities over a span of 3 minutes, while consistently perfusing the cells with an external solution. Subsequently, we introduced 10 μM of GABA to the solution and

recorded the ensuing response for an additional 100 seconds. This was succeeded by a wash step, followed by the addition of 50 mM KCl to the solution to observe the neurons' reaction to depolarization. For each specific experimental condition, we utilized 3–5 distinct cultures. On average, the number of regions of interest (cells' somas) we observed within each frame was 13 ± 2 (mean ± standard error of the mean).

4.4.12. Repetitive behavior (spontaneous grooming) with Adriana Souja, Felipe Gomes, and colleagues

Grooming behavior duration was assessed at two distinct life stages: early adolescence and adulthood. Specifically, evaluations were conducted on postnatal day (PND) 30 for males and PND 32 for females during early adolescence, as well as on PND 62 for males and PND 64 for females during adulthood. The assessment was carried out by placing the animals within a circular arena measuring 60 cm in diameter and 65 cm in height. This arena was designated for a 15-minute testing period. The entire test was recorded using video recording equipment, and the duration of grooming behavior exhibited by the animals was manually measured. In addition to grooming behavior assessment, locomotor activity was also evaluated during these testing periods. For this, the Any-Maze software provided by Stoelting in the USA was utilized to capture and quantify locomotor activity patterns.

4.4.13. Novel object recognition (NOR) test with Adriana Souja, Felipe Gomes, and colleagues

After the Social Interaction (SI) test, animals underwent assessment in the Novel Object Recognition (NOR) test. This evaluation took place on postnatal day (PND) 63 for males and PND 65 for females. The NOR test was executed through a well-defined procedure. Initially, animals were introduced to a circular arena with a diameter of 60 cm and a height of 65 cm for a habituation period lasting 15 minutes. Following a 24-hour interval, each animal was subjected to two distinct trials: the acquisition trial (T1) and the retention trial (T2).

In the acquisition trial (T1), individual rats were placed within the arena containing two identical objects for a duration of 10 minutes. Subsequently, one hour later, the animals were placed back into the arena for the retention trial (T2), lasting 5 minutes. Notably, in the retention trial, one of the objects that had been presented during T1 was substituted with a novel, unfamiliar object. Throughout both trials, the behavior of the animals was meticulously recorded using video equipment, enabling subsequent blind scoring of object exploration. The time spent by the animals in directing their attention toward an object, up to a distance of 2 cm, was measured. This encompassed activities such as observing, licking, sniffing, or employing their forepaws to touch the object.

The evaluation of recognition memory hinged on the calculation of the discrimination index. This index was derived from the difference between the time spent exploring the novel object and the familiar object. This difference was then normalized by the total time spent exploring both objects. In mathematical terms, the discrimination index was calculated as follows: Discrimination Index = (Novel Object Exploration Time - Familiar Object Exploration Time) / (Novel Object Exploration Time + Familiar Object Exploration Time).

4.4.13. *In vivo* recordings of VTA DA neurons with Adriana Souja, Felipe Gomes, and colleagues

Following the completion of behavioral tests, animals at postnatal days 66 to 80 were anesthetized using chloral hydrate administered intraperitoneally at a dose of 400 mg/kg. Once anesthetized, the animals were secured onto a stereotaxic frame. Periodic administration of chloral hydrate was carried out to sustain suppression of the hindlimb withdrawal reflex. Throughout the procedure, the body temperature of the animals was meticulously maintained at 37°C through the use of a temperature-controlled heating pad.

For in vivo single-cell extracellular recordings of ventral tegmental area (VTA) dopamine (DA) neurons, single glass microelectrodes were employed. These microelectrodes were filled with a solution containing 2% Chicago Sky Blue in 2 M NaCl. The placement of the electrodes in the VTA was accomplished utilizing a hydraulic positioner, with specific coordinates being anteroposterior: −5.3 mm from the bregma; mediolateral: +0.6 mm lateral to the midline; and −6.5 to −9.0 mm ventral from the brain surface. The identification of dopamine neurons was executed based on well-established electrophysiological criteria (as detailed in Ungless and Grace 2012). Three distinct parameters were quantified during the recording process. The population activity of DA neurons was ascertained by tallying the number of spontaneously firing DA neurons encountered during the creation of 6–9 vertical passes within the VTA, all executed in accordance with a predefined pattern. Additionally, the average firing rate of these neurons was measured, along with the percentage of action potentials occurring in bursts (burst activity). Each identified DA neuron was recorded for a duration ranging from 1 to 3 minutes. At the conclusion of the recording session, the sites of electrode insertion were marked. This was accomplished through the iontophoretic ejection of Chicago Sky Blue dye from the electrode,

employing a constant negative current of 20 μA for a period of 15 to 20 minutes. This marking process served as a reference for subsequent histological verification.

4.4.13. siRNA mediated knockdown of Radixin with Alexandra McCoy, Thomas D Prevot, and colleagues

Rats were administered anesthesia using 2-4% isoflurane prior to being secured in a stereotaxic apparatus using gentle, atraumatic ear bars. Bilateral indwelling cannulas (Protech International, Roanoke, VA, C317G, positioned at a depth of -6 mm below the skull's surface) were surgically implanted in the ventral hippocampus (vHipp). The coordinates for implantation were as follows: anteroposterior -5.3 mm, mediolateral ±5.0 mm from the Bregma, and dorsoventral -6.0 mm from the brain surface. The cannulas were anchored in place using dental cement along with four anchor screws. Following the procedure, the animals were administered the analgesic ketoprofen at a dose of 5 mg/kg subcutaneously. Subsequently, they were allowed to recover, individually housed, for at least one week before the commencement of experimentation.

For the purpose of microinjections, injectors extending 1 mm past the end of the guide cannula were employed. The guide cannulas were kept clear with the utilization of dummy cannulas. Injections were performed using either small interfering RNA (siRNA) targeting the radixin gene (RDX) at a concentration of 0.2 μg/μL, with a total volume of 0.75 μL, or a non-targeting, scrambled siRNA that served as a control. The injection rate was maintained at approximately 0.5 μL/min. The siRNA SMARTpool targeting the RDX gene was composed of four specific sequences:GAAUCAGUUAUAACGUUUA;CCAAUAAAUGUAAGAGUAA; CCUUAUUGC UAAAAGAAUC; CUCUAAUUUUGGAUAAUAU. The selection of Accell siRNA (Dharmacon, Lafayette, CO, USA) was deliberate due to its design to effectively enter

challenging-to-transfect cells like neurons, eliminating the need for a transfection agent. Additionally, it has been shown to achieve peak knockdown within 3-4 days after administration.

4.4.14. Inescapable foot shock stress with Alexandra McCoy, Thomas D Prevot, and colleagues

Rats were subjected to random assignment, either to the control group (no shock) or to the shock groups that underwent a two-day regimen of inescapable foot shock stress (IS). The IS protocol encompassed placing the rats within a conditioning chamber measuring 30.5 × 25.4 × 30.5 cm, which was equipped with a stainless-steel grid shock floor (provided by Coulbourn Instruments, Whitehall, PA, USA). Each IS session consisted of a sequence of 60 episodes of 15-second foot shocks at 0.8 mA intensity. The average inter-trial interval (ITI) was 30 seconds, allowing for a 25% variance of ±7.5 seconds. The complete IS session lasted approximately 40 minutes. In contrast, rats in the control group underwent daily handling procedures but were not subjected to exposure within the conditioning chambers. The electrophysiology and behavioral experiments were executed 24 hours after the conclusion of the two-day IS protocol.

4.4.15. *In vivo* extracellular dopamine recordings with Alexandra McCoy, Thomas D Prevot, and colleagues

Rats were anesthetized using an 8% chloral hydrate solution (at a dose of 400 mg/kg, administered intraperitoneally) and were positioned within a stereotaxic apparatus (manufactured by Kopf Instruments, Tujunga, CA, USA). Extracellular glass microelectrodes, characterized by an impedance of approximately 6-10 MΩ, were gradually inserted into the ventral tegmental area (VTA) using a hydraulic micro-positioner (Model 640, Kopf), with the following stereotaxic coordinates: anteroposterior -5.3 mm from bregma, mediolateral ±0.6 mm, and dorsoventral -6.5

to -9.0 mm from the brain surface. Employing open filter settings (low-frequency cutoff: 30 Hz; high-frequency cutoff: 30 kHz), spontaneously active dopamine neurons were identified, employing well-established electrophysiological criteria.

Analysis of dopamine neuron activity included measurement and evaluation of three distinct parameters: 1.) the count of spontaneously firing dopamine neurons per track (referred to as population activity), 2.) the firing rate of these neurons, and 3.) the proportion of action potentials that occurred in bursts. Bursts were defined by the occurrence of spikes with inter-spike intervals of less than 80 ms, while the termination of a burst was characterized by inter-spike intervals greater than 180 ms. The software utilized for the analysis of dopamine neuron activity was LabChart (developed by ADInstruments, Sydney, Australia). Following these electrophysiological procedures, the rats were promptly decapitated and their brains were removed. A subset of these brains was utilized for the purpose of confirming the placement of electrodes and cannulas, while the remaining brains were employed for subsequent molecular analyses.

4.4.16. Elevated plus-maze (EPM)

The Elevated Plus Maze (EPM) was positioned within a room specially designed to attenuate external sounds. This room contained an incandescent light source with an intensity of 60 lux, placed at a distance of 1.3 meters from the maze. To conduct the experiment, animals were allowed to explore the EPM freely for a duration of 5 minutes. This exploration was initiated by placing the animals on the central platform of the maze, with their head facing one of the enclosed arms. For the purpose of data collection, Any Maze software (manufactured by Stoelting, USA) was employed. This software recorded several key parameters of the animals' behavior during their time in the maze. Specifically, it captured the percentage of entries into the

open arms and the corresponding time spent within these open arms, which are indicative of anti-anxiety responses. Additionally, the number of entries into the enclosed arms was recorded, serving as an index of locomotor activity.

4.5. Experimental section

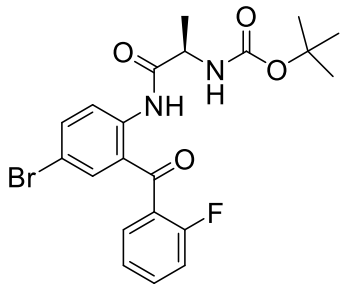
4.5.1. General

All chemical reactions were conducted in round-bottom flasks, utilizing magnetic stir bars or an overhead stirrer, and were carried out under an argon atmosphere. Whenever necessary, organic solvents were purified using standard methods or obtained from Sigma-Aldrich Chemicals. Reagents and other chemicals were procured from reputable sources, including Sigma-Aldrich, Oakwood Chemical, Alfa Aesar, Matrix Scientific, Admiral Chemical Company, or Acros Organic. To track the progress of reactions, Thin Layer Chromatography (TLC) plates from Dynamic Adsorbents, Inc. were employed, and visualization was achieved under UV light. In some cases, LCMS 2020 was utilized to monitor reaction progress. For purification of specific analogs, flash column chromatography was performed using silica gel (230-400 mesh, Dynamic Adsorbents). A normal phase Agilent High-Performance Liquid Chromatography (HPLC) system was used to determine the ratio of optically active enantiomers and to calculate the percentage of enantiomeric excess (%ee).

Nuclear Magnetic Resonance (NMR) spectroscopy was conducted using a Bruker Spectrospin 500 MHz instrument, with $CDCl_3$, DMSO-d6, Methanol-d4 as the solvent. Chemical shifts were reported in δ (ppm), and multiplet patterns were represented as singlet (s), broad signal (br), doublet (d), triplet (t), quartet (q), doublet of doublets (dd), and multiplet (m). High-Resolution

Mass Spectrometry (HRMS) analysis was carried out using an LCMS-IT-TOF instrument at the Milwaukee Institute for Drug Discovery in the Shimadzu Laboratory for Advanced and Applied Analytical Chemistry.

4.5.2. *Tert*-Butyl-(*R*)-(1-((4-bromo-2-(2-fluorobenzoyl)phenyl)amino)-1-oxopropan-2-yl) carbamate (3)

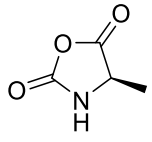


3

A 5-L round bottom flask was charged with commercially available bezophenone, (2-amino-5-bromophenyl)(2-fluorophenyl)methanone **1** (300 g, 1020 mmol) and dry DCM (2000 mL). The *N*-Boc-protected amino acid, *N*-Boc-D-alanine (250.8 g, 1326 mmol), was introduced to the stirred solution of (2-amino-5-bromophenyl)(2-fluorophenyl)methanone **1** in dry DCM. The reaction mixture was cooled down to -10°C using an ice-methanol bath. A solution of dicyclohexylcarbodiimide (DCC; 336.8 g, 1632 mmol dissolved in 1000 mL of DCM) was added dropwise to the mixture over the course of 1 hour at -10°C. The solution was allowed to gradually reach room temperature and was stirred for 41 hours at that temperature. The resulting white-colored dicyclohexyl urea byproduct that formed during the reaction was separated by filtration and washed with DCM (3x300 mL). The combined organic layers were then concentrated under reduced pressure, resulting in a gummy, yellow-colored semi-solid mass. A mixture of ethyl acetate (EtOAc) and hexane (0.5:9.5, 2500 mL) was added to this mass, and the

mixture was stirred at 60°C for 30 minutes. During this EtOAc-hexane stirring, the semi-solid mass transformed into an off-white-colored powder. Subsequently, the mixture was cooled to room temperature and left undisturbed for 5 hours to facilitate maximum precipitation. The solid was then isolated by filtration, washed with an EtOAc-hexane mixture (0.5:9.5, 2x300 mL), and dried under vacuum at 45°C for 12 h. This yielded amide **3** as an off-white powder (351.1 g, 74% yield). $\mathbf{R_f}$ = 0.4 (silica gel TLC, EtOAc-hexane=1:4). **^{1}H NMR** (500 MHz, $CDCl_3$) δ 11.692 (s, 1H), 8.7 (d, J = 9.0 Hz, 1H), 7.70 (dd, J = 9.0, 2.3 Hz, 1H), 7.60 – 7.54 (m, 2H), 7.48 (t, J = 6.7 Hz, 1H), 7.32 (dd, J = 8.5, 6.5 Hz, 1H), 7.19 (t, J = 9.0 Hz, 1H), 5.27 (s, 1H), 4.34 (dd, J = 27.8 Hz, 1H), 1.53 (d, J = 7.0 Hz, 3H), 1.47 (s, 9H); **^{13}C NMR** (126 MHz, $CDCl_3$) δ 195.40 (s), 172.46 (s), 159.52 (d, $^1J_{C\text{-}F}$ = 253.2 Hz), 155.31 (s), 139.66 (s), 137.92 (s), 135.92 (d, $J_{C\text{-}F}$ = 1.5 Hz), 133.61 (d, $^3J_{C\text{-}F}$ = 8.3 Hz), 130.29 (d, $^4J_{C\text{-}F}$ = 2.2 Hz), 126.74 (d, $^2J_{C\text{-}F}$ = 14.5 Hz), 124.49 (s), 124.46 (s), 122.59 (s), 116.52 (d, $^2J_{C\text{-}F}$ = 21.4 Hz), 114.91 (s), 80.36 (s), 51.85 (s), 28.27 (s), 18.49 (s); **HRMS** (ESI/IT-TOF) m/z: $[M + Na]^+$ Calcd for $C_{21}H_{23}BrFN_2O_4$ 487.0639 found 487.0675.

4.5.2. *N*-Carboxy-D-Alanine Anhydride (14)

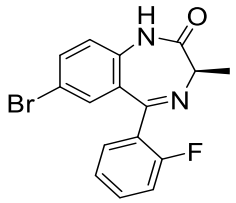


14

In a three-neck round-bottom flask, Boc-*D*-Alanine (50g, 264.25 mmol) was combined with anhydrous ethyl acetate (2000 mL) under an argon atmosphere. The mixture was stirred to form

a solution. Subsequently, triphosgene (31.35g, 105.7 mmol) was introduced into the reaction mixture. This was followed by the gradual dropwise addition of triethylamine (40.5 mL, 290.72 mmol) over a period of 60 minutes while maintaining a temperature of 25 – 30°C. During the addition of triethylamine, both CO_2(g) and HCl(g) evolved. The resulting reaction mixture was allowed to stir for an additional hour at 25 – 30°C. After this one-hour stirring at room temperature, the mixture was refluxed at 65 – 70°C for 2 h. At this point, the reaction was considered complete as the evolution of gas had ceased. A white slurry was formed as a result. The reaction mixture was then cooled to room temperature and left to stand for 5 h. The white TEA-HCl salt, which resulted, was removed from the mixture by filtration, and the remaining residue was washed with anhydrous ethyl acetate (2 x 100 mL). The pale-yellow colored filtrates were concentrated under reduced pressure, resulting in a semi-solid mass. This residue was then dissolved in anhydrous DCM (200 mL). Subsequently, anhydrous hexane (200 mL) was slowly added dropwise over the course of 1 h while vigorously stirring the mixture. To ensure the proper precipitation of the product, the mixture was placed in a freezer at -20°C overnight. *It is important to note that the addition of hexane to the dichloromethane solution should be done very slowly. Rapid addition of hexane may result in an oily product that doesn't precipitate effectively.* The resulting white crystalline solid was filtered and washed with anhydrous hexanes (150 mL x 2). The solid was then dried under vacuum at room temperature for 3 h, yielding product **14** as an off-white solid (20.1 g, 68.0% yield). **^{1}H NMR** (500 MHz, DMSO-d_6) δ 9.01 (s, 1H), 4.48 (qd, J = 7.0, 1.1 Hz, 1H), 1.34 (d, J = 7.1 Hz, 3H); **^{13}C NMR** (126 MHz, DMSO-d_6) δ 172.88, 152.15, 53.28, 17.23.

4.5.3. (*R*)-7-Bromo-5-(2-fluorophenyl)-3-methyl-1,3-dihydro-2*H*-benzo[*e*][1,4]diazepin-2-one (4)



4

Boc procedure: A solution of 4M hydrochloric acid (HCl) in dioxane (640 mL, 2560 mmol) was added to a stirred solution of the protected amide, *tert*-butyl-(*R*)-(1-((4-bromo-2-(2-fluorobenzoyl)phenyl)amino)-1-oxopropan-2-yl) carbamate **3** (300 g, 640 mmol) in DCM (3000 mL) at a temperature of -10°C. The mixture was allowed to reach room temperature and stirred for 12 h at that temperature. The completion of the reaction and consumption of the starting material was confirmed by TLC (using a silica gel plate with a solvent mixture of 50% ethyl acetate and 50% hexane). Following the reaction, the mixture was neutralized (pH ~7, by pH paper) with a 10% aqueous solution of sodium bicarbonate ($NaHCO_3$) (3000 mL). The layers were separated, and the aqueous layer was extracted with DCM (2x500 mL). The combined organic layers were then washed with a 10% aqueous solution of sodium bicarbonate (1x 700 mL), followed by a 10% aqueous sodium chloride (NaCl) solution (2x1000 mL). The organic layer was then dried using sodium sulfate (Na_2SO_4). The solvents were subsequently removed under reduced pressure. The resulting yellow-colored oil was dissolved in anhydrous toluene, and the solution was stirred at internal temperature of 60-70°C for 24 h. The disappearance of the deprotected amide was monitored using TLC (using a silica gel plate with a solvent mixture of 50% ethyl acetate and 50% hexane). The solution was then concentrated under reduced pressure, and a mixture of water (1500 mL) and DCM (2500 mL) was added. The layers were

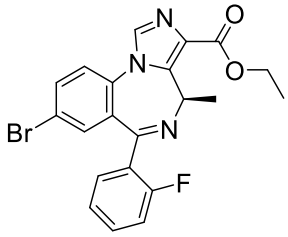
separated, and the aqueous layer was extracted with DCM (2x300 mL). The combined organic layers were washed with a 10% aqueous sodium chloride solution (2x800 mL) and then dried using sodium sulfate. The solvents were again removed under reduced pressure. The resulting light, yellow-colored residue was slurried with a 10% mixture of ethyl acetate and hexane (1000 mL) and stirred at 60°C for 40 minutes. The mixture was then cooled and left to stand at room temperature for 12 h. The solid that formed was filtered, washed with the 10% ethyl acetate-hexane mixture (2x200 mL), and dried under vacuum at 45°C for 12h, yielding the off-white solid product, benzodiazepine **4** (181.5 g, 81%). %). **R_f** = 0.4 (Silica gel TLC, EtOAc-hexane=1:1). **^{1}H NMR** (500 MHz, $CDCl_3$) δ 10.07 (s, 1H), 7.58 (ddd, J = 8.7, 6.3, 2.0 Hz, 2H), 7.47 – 7.42 (m, 1H), 7.35 (d, J = 2.1 Hz, 1H), 7.23 (td, J = 7.6, 1.0 Hz, 1H), 7.14 (d, J = 8.7 Hz, 1H), 7.08 – 7.02 (m, 1H), 3.80 (q, J = 6.5 Hz, 1H), 1.79 (d, J = 6.5 Hz, 3H); **^{13}C NMR** (126 MHz, $CDCl_3$) δ 172.46 (s), 164.51 (s), 160.41 (d, $^1J_{C-F}$ = 252.1 Hz), 136.59 (s), 134.70 (s), 132.14 (d, $^3J_{C-F}$ = 8.3 Hz), 132.01 (s), 131.57 (d, J_{C-F} = 2.1 Hz), 130.05 (s), 127.11 (d, $^2J_{C-F}$ = 12.3 Hz), 124.40 (d, $^4J_{C-F}$ = 3.5 Hz), 122.99 (s), 116.43 (s), 116.28 (d, $^2J_{C-F}$ = 21.5 Hz), 58.88 (s), 16.96 (s). **HRMS (ESI/IT-TOF**): m/z [M + H]+ calcd for $C_{16}H_{13}BrFN_2O$: 347.0190; found: 347.0181; Optical purity, >99% EE (Whelk-01 column (4.6 mm x 25 cm, 5 μm particle size).

***N*-Carboxy alanine anhydride (NCA) procedure**: Anhydrous trifluoroacetic acid (78 mL, 1020 mmol) was added to a stirred solution of commercially available 2-amino-5-bromo-2'-fluorobenzophenone (**1**, 150 g, 510 mmol) in anhydrous toluene (1500 mL) under an argon atmosphere. The mixture was allowed to stir at room temperature for 30 minutes to dissolve the starting material, resulting in a yellow-colored solution. Next, the *N*-carboxy-*D*-alanine anhydride **15** (70.42 g, 612 mmol) was added to the reaction mixture all at once. The reaction

mixture was then stirred for 1 h at an internal temperature of 50 – 55°C, monitoring the consumption of the starting material by TLC. The formation of the trifluoroacetic acid (TFA) salt intermediate was confirmed by TLC using a silica gel plate with a solvent mixture of 30% ethyl acetate and 70% hexanes. After 1 h, it was observed that less than 5% of the 2-amino-5-bromo-2'-fluorobenzophenone remained (as indicated by TLC). Then, anhydrous triethylamine (142.8 mL, 1020 mmol) was added dropwise slowly to the reaction mixture over a period of 30 minutes while maintaining an internal temperature of 50 – 55°C. Once the addition was complete, the reaction mixture was stirred for 4 h to 5 h at 50 – 55°C. The disappearance of the TFA salt intermediate was confirmed by TLC using a silica gel plate with a solvent mixture of 50% ethyl acetate and 50% hexanes. The reaction mixture was then cooled to room temperature, and the solvents were concentrated under reduced pressure. The residue was diluted with ethyl acetate (1500 mL) and water (1500 mL). The biphasic mixture was stirred for 15 minutes, allowed to stand for 20 minutes, and then transferred to a separatory funnel. The layers were separated, and the aqueous layer was extracted with ethyl acetate (2x450 mL). The combined organic layers were washed with a 10% aqueous sodium chloride solution (2x300 mL) and then dried using sodium sulfate (Na_2SO_4). The solvents were removed under reduced pressure, and the resulting residue was slurried in a mixture of 10% ethyl acetate and hexane (600 mL). The slurry was then stirred at an internal temperature of 60 – 65°C for 30 minutes. The mixture was cooled to room temperature and left to stand for 2-3 h to precipitate the product. The solid product was filtered, washed with a 10% mixture of ethyl acetate and hexane (150 mL x 2), and collected by filtration. The collected solid was further washed with heptane (300 mL x 2) and then dried under vacuum at 35 – 40°C to yield compound **4** as an off-white solid (92.9 g, 82.0%). **^{1}H NMR** (500 MHz, $CDCl_3$) δ 10.07 (s, 1H), 7.58 (ddd, J = 8.7, 6.3, 2.0 Hz, 2H), 7.47 – 7.42 (m, 1H),

7.35 (d, J = 2.1 Hz, 1H), 7.23 (td, J = 7.6, 1.0 Hz, 1H), 7.14 (d, J = 8.7 Hz, 1H), 7.08 – 7.02 (m, 1H), 3.80 (q, J = 6.5 Hz, 1H), 1.79 (d, J = 6.5 Hz, 3H); **^{13}C NMR** (126 MHz, $CDCl_3$) δ 172.46 (s), 164.51 (s), 160.41 (d, $^{1}J_{C\text{-}F}$ = 252.1 Hz), 136.59 (s), 134.70 (s), 132.14 (d, $^{3}J_{C\text{-}F}$ = 8.3 Hz), 132.01 (s), 131.57 (d, $J_{C\text{-}F}$ = 2.1 Hz), 130.05 (s), 127.11 (d, $^{2}J_{C\text{-}F}$ = 12.3 Hz), 124.40 (d, $^{4}J_{C\text{-}F}$ = 3.5 Hz), 122.99 (s), 116.43 (s), 116.28 (d, $^{2}J_{C\text{-}F}$ = 21.5 Hz), 58.88 (s), 16.96 (s). **HRMS (ESI/IT-TOF)**: m/z [M + H]+ calcd for $C_{16}H_{13}BrFN_2O$: 347.0190; found: 347.0181; Optical purity, >99% EE (Whelk-01 column (4.6 mm x 25 cm, 5 μm particle size).

4.5.4 Ethyl (*R*)-8-bromo-6-(2-fluorophenyl)-4-methyl-4*H*-benzo[*f*]imidazo[1,5-*a*][1,4] diazepine-3-carboxylate (5)



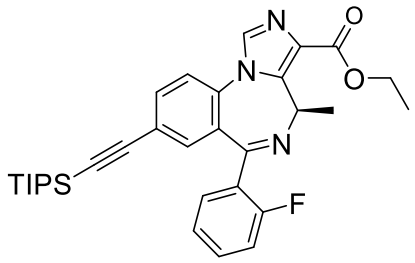
5

The benzodiazepine (*R*)-7-bromo-5-(2-fluorophenyl)-3-methyl-1,3-dihydro-2H-benzo[e][1,4] diazepin-2-one **4** (100.0 g, 288.0 mmol) was dissolved in anhydrous THF (1500 mL). The mixture was cooled to -20°C using a dry ice and isopropanol (IPA) bath. A solution of potassium *t*-butoxide (42.02 g, 374.0 mmol) in dry THF (250 mL) was added dropwise to the reaction mixture over a period of 30 minutes while maintaining an internal temperature of -25°C to -20°C with continuous stirring. A mild exotherm was observed during the addition of potassium *t*-butoxide, causing the temperature to rise from -20°C to -15°C. The reaction mixture was allowed to stir for 1 h upon complete addition of the base while maintaining the temperature between -

20°C and -10°C. Then, the reaction mixture was cooled again to -20°C, and diethyl chlorophosphate (58.27 mL, 403 mmol) was added dropwise over a period of 15 minutes. The reaction mixture was stirred for 3 h, and the consumption of starting material was monitored by TLC analysis using a silica gel TLC plate with a solvent mixture of 50% ethyl acetate and 50% hexane. Following this, ethyl isocyanoacetate (31.5 mL, 374.0 mmol) was added dropwise to the reaction mixture at -30°C. Subsequently, a solution of potassium *t*-butoxide (42.02 g, 374.0 mmol) in THF (350 mL) was added dropwise at the same temperature. The reaction mixture was allowed to warm to room temperature and stirred for 8 h. At this point, analysis by TLC (silica gel plate with a solvent mixture of 60% ethyl acetate and 40% hexane) confirmed the consumption of the starting material. The reaction mixture was then quenched by the addition of a 5% aqueous solution of sodium bicarbonate (2500 mL). The resulting mixture was diluted with ethyl acetate (2500 mL). After stirring for 15 minutes, the biphasic mixture was allowed to stand to allow the layers to separate for 30 minutes. The layers were separated, and the aqueous layer was extracted with ethyl acetate (2x1000 mL). The combined organic layers were then washed successively with a 5% aqueous solution of sodium bicarbonate (1x1500 mL) and a 10% aqueous solution of sodium chloride (2x2000 mL). Afterward, the organic layer was dried using sodium sulfate (Na_2SO_4). The solvents were subsequently removed under reduced pressure, yielding a blackish-orange colored residue. To this residue, *t*-butyl methyl ether (800 mL) was added, and the mixture was stirred for 30 minutes at 50–55°C. The mixture was then cooled to room temperature and left to stand at that temperature for 8 h to maximize precipitation. The solid residue was filtered, washed with *t*-butyl methyl ether (3x150 mL), and dried under vacuum at 40°C for 12 h to yield product **5** as an off-white powder (86.6 g, 68%). %). $\mathbf{R_f}$ = 0.3 (Silica gel TLC, EtOAc-hexane=3:2); **^{1}H NMR** (500 MHz, CDCl3) δ 7.92 (s, 1H), 7.72 (dd, 1H), 7.61 (t, J

= 7.0 Hz, 1H), 7.49 – 7.41 (m, 3H), 7.26 (td, J = 7.6, 0.9 Hz, 1H), 7.05 (t, J = 9.3 Hz, 1H), 6.70 (q, J = 7.2 Hz, 1H), 4.40 (q, J = 16.1, 7.2 Hz, 2H), 1.41 (t, J = 7.1 Hz, 3H), 1.28 (d, J = 7.3 Hz, 3H); **^{13}C NMR** (126 MHz, CDCl3) δ 162.93 (s), 162.66 (s), 160.09 (d, $^{1}J_{C\text{-}F}$ = 250.8 Hz), 141.58 (s), 134.85 (s), 134.76 (s), 133.68 (s), 133.04 (s), 132.11 (d, $^{4}J_{C\text{-}F}$ = 8.2 Hz), 131.19 (s), 129.59 (s), 128.42 (d, $^{3}J_{C\text{-}F}$ = 12.3 Hz), 124.58 (s), 124.56 (s), 123.66 (s), 120.95 (s), 116.24 (d, $^{2}J_{C\text{-}F}$ = 21.4 Hz), 60.80 (s), 50.11 (s), 14.87 (s), 14.44 (s). **HRMS (ESI/IT-TOF)**: m/z $[M + H]^+$ calcd for $C_{21}H_{18}BrFN_3O_2$: 442.0560; found: 442.0590; % EE= >99% on a chiral column (Whelk-01 column (4.6 mm x 25 cm, 5 μm particle size).

4.5.5. Ethyl (*R*)-6-(2-fluorophenyl)-4-methyl-8-((triisopropylsilyl)ethynyl)-4*H*-benzo[*f*]imidazo[1,5-*a*][1,4]diazepine-3-carboxylate (6)



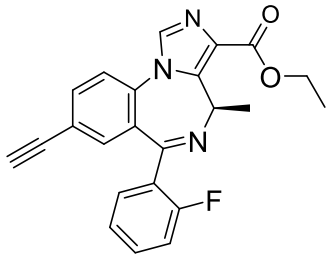
6

In a three-neck round-bottom flask, tri(*o*-tolyl)phosphine (18.28 g, 37.08 mmol) and $Pd(OAc)_2$ (4.16 g, 18.5 mmol) were added to dry ACN (300 mL). The mixture was stirred for 30 minutes under an argon atmosphere. The initially orange cloudy solution turned yellow, indicating the formation of a Pd catalyst *in situ*. Subsequently, the imidazodiazepine compound ethyl (*R*)-8-bromo-6-(2-fluorophenyl)-4-methyl-4H-benzo[f]imidazo[1,5-a][1,4]diazepine-3-carboxylate **5** (82 g, 185.4 mmol), was added to the reaction mixture. To this mixture, triethylamine (77.5 mL, 556 mmol), (triisopropylsilyl)acetylene (49.9 mL, 222 mmol), and additional ACN (500 mL) were sequentially added under an argon atmosphere. The reaction mixture was then refluxed for

4 hours. The consumption of the starting material was confirmed by TLC analysis using a silica gel plate with a solvent mixture of 60% ethyl acetate and 40% hexane. Following this, the reaction mixture was cooled to room temperature and exposed to air. Subsequently, silica gel (150 g) was added to the flask, and the contents were stirred for 30 minutes. The mixture was then filtered through a pad of celite, and the residue was washed with DCM (2x250 mL). The solvents were removed under reduced pressure. To the resulting black oily mass, DCM (1000 mL) and water (500 mL) were added to dissolve the contents. After stirring for 5 minutes, the mixture was allowed to stand for 20 minutes to facilitate the separation of layers. The layers were separated, and the aqueous layer was extracted with DCM (2x250 mL). The combined organic layers were then washed with a 10% aqueous sodium chloride (NaCl) solution (2x350 mL) and dried using sodium sulfate (Na2SO4). The DCM solvent was subsequently removed under reduced pressure. The resulting residue was purified by flash chromatography on silica gel (1200 g) using a solvent mixture of 50% ethyl acetate and 50% hexane as the eluent. The appropriate fractions were collected and pooled. The solvents were removed, and the semi-solid residue was dried under vacuum for 12 h at 45°C to afford the product **6** as golden colored fluffy semi-solid (88.7 g, 88%). **R_f** = 0.6 (silica gel, 60% EtOAc-hexane); **^{1}H NMR** (500 MHz, $CDCl_3$) δ 7.98 (s, 1H), 7.68 (d, J = 7.4 Hz, 1H), 7.62 (t, J = 7.0 Hz, 1H), 7.55 (d, J = 8.3 Hz, 1H), 7.45 (td, J = 13.2, 6.8 Hz, 1H), 7.32 (d, J = 8.4 Hz, 1H), 7.25 (dd, J = 11.0, 4.0 Hz, 1H), 7.06 (dd, J = 19.8, 10.3 Hz, 1H), 6.69 (q, J = 7.3 Hz, 1H), 4.40 (q, J = 15.4Hz, 3H), 1.41 (t, J = 7.1 Hz, 3H), 1.29 (d, J = 7.3 Hz, 3H), 1.10 (s, 18H), 1.09 (s, 3H). **^{13}C NMR** (126 MHz, CDCl3) δ 163.78 (s), 162.83 (s), 160.15 (d, J = 251.3 Hz), 141.5 (s), 135.54 (s), 134.91 (s), 134.01 (s), 133.51 (s), 132.13 (d, J = 7.9 Hz), 131.29 (s), 129.40 (s), 129.30 (s), 128.30 (d, J = 10.6 Hz), 124.45 (d, J = 3.3 Hz), 123.12 (s), 122.17 (s), 116.17 (d, J = 21.5 Hz), 104.46 (s), 94.32 (s), 60.36 (s), 49.96 (s),

18.58 (s), 14.87 (s), 14.42 (s), 11.20 (s); **HRMS (ESI/IT-TOF)**: m/z $[M + H]^+$ calcd for $C_{32}H_{39}FN_3O_2Si$: 544.27901; found: 544.28330; %EE >99.9% on a chiral column (Whelk-01 column (4.6 mm x 25 cm, 5 μm particle size).

4.5.6. Ethyl (*R*)-8-ethynyl-6-(2-fluorophenyl)-4-methyl-4*H*-benzo[*f*]imidazo[1,5-*a*][1,4] diazepine-3-carboxylate (SH-053-2'F-*R*-CH_3, 7)

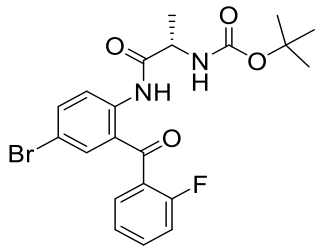


7

The TIPS-protected imidazodiazepine ethyl (*R*)-6-(2-fluorophenyl)-4-methyl-8-((triisopropylsilyl)ethynyl)4H-benzo[f]imidazo[1,5-a][1,4]diazepine-3-carboxylate **6** (108 g, 199 mmol) was dissolved in THF (1000 mL), and water (10 mL) was added. The resulting mixture was cooled to -20°C using a dry ice / isopropanol (IPA) bath. Subsequently, tetrabutylammonium fluoride hydrate, 1M in THF (240 mL, 240 mmol) was added dropwise to the reaction mixture over a period of 20 minutes. The reaction mixture was then allowed to reach room temperature and stirred for 2 h at that temperature. At this point, the reaction was deemed complete, which was confirmed by TLC analysis using a silica gel plate with a solvent mixture of 70% ethyl acetate and 30% hexane ($\mathbf{R_f}$ values: SH-053-2'F-R-CH_3-TIPS (**6**) = 0.5, SH-053-2'F-R-CH_3 = 0.3). To quench the reaction, water (500 mL) was added, and the resulting mixture was then diluted with ethyl acetate (1000 mL). After stirring for 5 minutes, the biphasic mixture was allowed to stand for 15 minutes. The organic layer was separated, and the aqueous layer was extracted with ethyl acetate (2x500 mL). The combined organic layers were washed with a 10%

aqueous sodium chloride solution (2x700 mL) and dried using sodium sulfate (Na_2SO_4). The solvents were then removed under reduced pressure, resulting in an orange-colored residue. The residue was then slurried with methanol (300 mL) and stirred for 30 minutes at 60°C. Subsequently, water (300 mL) was added to the methanol slurry, and the mixture was stirred for an additional 30 minutes at 50–55°C. The mixture was then cooled to 20–25°C and left for 5 h to maximize the precipitation of the product. The solid residue was filtered, washed with a mixture of 50% methanol and water (100 mL x 3), followed by washing with hexanes (80 mL x 2). The solid residue was then dried under vacuum at 45°C for 12 h, resulting the product **7** as a white powder (69.2 g, 90%). **R_f**= 0.3 (silica gel; 70% ethyl acetate-hexane); 1H NMR (500 MHz, CDCl3) δ 8.00 (s, 1H), 7.71 (d, J = 7.8 Hz, 1H), 7.60 (dd, J = 7.4, 6.3 Hz, 2H), 7.49 – 7.38 (m, 2H), 7.26 (t, J = 7.4 Hz, 1H), 7.05 (t, J = 9.1 Hz, 1H), 6.71 (q, J = 6.6 Hz, 1H), 4.47 (q, J = 14.0 Hz, 1H), 4.41 (q, J = 14.2, 7.1 Hz, 2H), 3.16 (s, 1H), 1.41 (t, J = 7.1 Hz, 3H), 1.29 (d, J = 7.0 Hz, 3H). **^{13}C NMR** (126 MHz, CDCl3) δ 163.68 (s), 162.76 (s), 160.10 (d, $^1J_{CF}$ = J = 251.1 Hz), 141.43 (s), 135.45 (s), 134.95 (s), 134.51 (s), 134.10 (s), 132.28 (s), 131.29 (s), 129.47 (s), 129.33 (s), 128.18 (d, $^3J_{CF}$ = 5.2 Hz), 124.54 (d, J = 3.2 Hz), 122.34 (s), 121.77 (s), 116.24 (d, $^2J_{CF}$ = 21.3 Hz), 81.33 (s), 79.86 (s), 60.86 (s), 49.93 (s), 14.91 (s), 14.42 (s); **HRMS** (ESI/IT-TOF) m/z: $[M + H]^+$ Calcd for $C_{23}H_{19}FN_3O_2$ 388.1455; found 388.1487. %EE >99.0% on a chiral column (Whelk-01 column (4.6 mm x 25 cm, 5 μm particle size).

4.5.7. *Tert*-Butyl (*S*)-(1-((4-bromo-2-(2-fluorobenzoyl)phenyl)amino)-1-oxopropan-2-yl) carbamate (9)

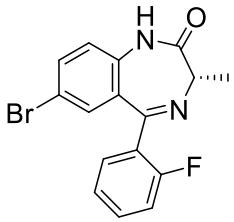


9

The benzophenone (2-amino-5-bromophenyl)(2-fluorophenyl)methanone **1** (75 g, 253.5 mmol) was dissolved in DCM (500 mL). To this DCM solution, the amino acid Boc-L-alanine (67.8 g, 357 mmol) was added, and the mixture was cooled to -10°C using an ice-methanol bath. A solution of dicyclohexylcarbodiimide (DCC, 83.7 g, 405 mmol) in DCM (300 mL) was then added dropwise to the mixture over a period of 30 minutes. The solution was stirred for 24 hours at room temperature. The white-colored byproduct dicyclohexyl urea that formed during the reaction was filtered off and washed with DCM (3x50 mL). The filtrate was then concentrated under reduced pressure. The resulting yellow oil was subjected to a slurry in a mixture of 5% ethyl acetate and hexane (300 mL), and the mixture was stirred for 30 minutes at 55°C. During this stirring, the yellow oil gradually transformed into an off-white powder. The mixture was then cooled to room temperature and left at that temperature for 12 h. The resulting solid residue was filtered, washed with 5% EtOAc-hexane (2x50 mL), and dried under vacuum at 40°C for 12 h to afford amide **9** as an off-white powder (85.4 g, 72% yield). $\mathbf{R_f}$ = 0.4 (Silica gel TLC, EtOAc-hexane=1:4). **^{1}H NMR** (500 MHz, $CDCl_3$) δ 11.67 (s, 1H), 8.72 (d, J = 9.0 Hz, 1H), 7.69 (d, J = 9.0 Hz, 1H), 7.62 – 7.56 (m, 2H), 7.46 (t, J = 7.2 Hz, 1H), 7.31 (td, J = 7.5, 1.2 Hz, 1H), 7.21 (t, J = 9.0 Hz, 1H), 5.16 (s, 1H), 4.37 (q, 1H), 1.52 (d, J = 7.0 Hz, 3H), 1.46 (s, 9H). **^{13}C NMR** (126 MHz, $CDCl_3$) δ 195.44 (s), 172.41 (s), 159.54 (d, $^1J_{CF}$ = 253.2 Hz), 155.30 (s), 139.69 (s), 137.95 (s), 135.96 (s), 133.61 (d, J = 8.3 Hz), 130.30 (d, J = 2.3 Hz), 126.77 (d, $^3J_{CF}$ = 14.5 Hz), 124.48 (d, $^4J_{CF}$ = 3.6 Hz), 124.44 (s), 122.61 (s), 116.55 (d, $^2J_{CF}$ = 21.4 Hz), 114.93 (s), 80.40 (s), 51.84

(s), 28.27 (s), 18.56 (s). **HRMS** (ESI/IT-TOF) m/z: $[M + H]^+$ Calcd for $C_{21}H_{23}BrFN_2O_4$ 465.0820; found 465.0841.

4.5.8. (*S*)-7-Bromo-5-(2-fluorophenyl)-3-methyl-1,3-dihydro-2*H*-benzo[*e*][1,4]diazepin-2-one (10)

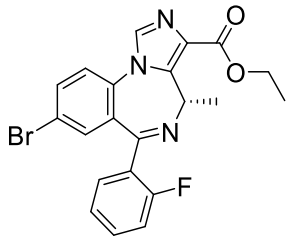


10

The *N*-Boc protected amide *tert*-butyl (*S*)-(1-((4-bromo-2-(2-fluorobenzoyl)phenyl)amino)-1-oxopropan-2-yl)carbamate **9** (112 g, 240 mmol) was dissolved in DCM (500 mL), and a 4M hydrochloric acid (HCl) solution in dioxane (240.6 mL, 962 mmol) was added dropwise to the DCM solution at -10°C. The solution was allowed to stir for 12 h at room temperature. The completion of the reaction was confirmed by TLC analysis (silica gel, EtOAc-hexane = 1:1). At the end of the reaction, the mixture was neutralized using a 5% aqueous sodium bicarbonate ($NaHCO_3$) solution (500 mL), and the organic layer was extracted with DCM (2x500 mL). The combined organic layers were then washed with a 5% aqueous $NaHCO_3$ solution (500 mL) and a 10% aqueous sodium chloride (NaCl) solution (2x500 mL). The organic layer was concentrated under reduced pressure, resulting in an oily mass. This oily mass was dissolved in anhydrous toluene (600 mL), and the solution was stirred at 60 °C for 7 h. The confirmation of the completion of the reaction was again verified by TLC (EtOAc: hexane = 1:1). After evaporation of all the methanol, a light-yellow gummy mass remained. A mixture of 10% ethyl acetate in hexane (300 mL) was added to the gummy mass, and the mixture was stirred for 30 minutes at 50°C. Subsequently, the mixture was cooled to room temperature and allowed to stand for 3 h.

The resulting solid residue was filtered, washed with 10% ethyl acetate in hexane (2x80 mL), and then dried in a vacuum oven for 12 h at 40°C to afford compound **10** as a white powder (43 g, 85%). $\mathbf{R_f}$ = 0.4 (silica gel, EtOAc: hexane = 1:1). **^{1}H NMR** (500 MHz, $CDCl_3$) δ 9.62 (s, 1H), 7.59 (ddd, J = 7.1, 5.0, 2.0 Hz, 2H), 7.48 – 7.43 (m, 1H), 7.36 (d, J = 2.1 Hz, 1H), 7.25 (t, J = 7.5 Hz, 1H), 7.12 (d, J = 8.6 Hz, 1H), 7.09 – 7.05 (m, 1H), 3.80 (q, J = 6.5 Hz, 1H), 1.79 (d, J = 6.5 Hz, 3H**). ^{13}C NMR** (126 MHz, $CDCl_3$) δ 172.4 (s), 164.5 (s), 160.44 (d, J = 252.1 Hz), 136.47 (s), 134.74 (s), 132.18 (d, J = 8.3 Hz), 132.08 (s), 131.56 (d, J = 1.6 Hz), 130.07 (s), 127.06 (d, J = 12.2 Hz), 124.42 (d, J = 3.6 Hz), 122.90 (s), 116.51 (s), 116.28 (d, J = 21.5 Hz), 58.85 (s), 16.94 (s). **HRMS** (ESI/IT-TOF) m/z: $[M + H]^+$ Calcd for $C_{16}H_{13}BrFN_2O$ 347.01898; found 347.01901. %EE= >99% on a chiral column (Whelk-01 column (4.6 mm x 25 cm, 5 μm particle size).

4.5.9. Ethyl (*S*)-8-bromo-6-(2-fluorophenyl)-4-methyl-4*H*-benzo[*f*]imidazo[1,5-*a*][1,4] diazepine-3-carboxylate (11)

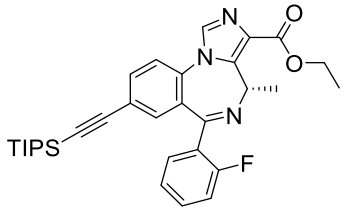


11

A three-neck round-bottom flask was charged with the 1,4-benzodiazepine **61** (70 g, 200.1 mmol) and dry THF(250 mL). The mixture was stirred until the compound was completely dissolved. The solution was then cooled to -20°C using a mixture of isopropyl alcohol (IPA) and dry ice. A solution of *t*-BuOK (29.4 g, 262 mmol) in THF (100 mL) was added dropwise to the reaction mixture over a period of 20 minutes, and the temperature was maintained at -20°C during the entire addition. The mixture was stirred for 1.5 h, and then diethyl chlorophosphate (40.8 mL, 282.2 mmol) was added dropwise at -30°C. The solution was

allowed to warm to room temperature (rt) and was held at that temperature for 2 h. The reaction mixture was then cooled again to -20°C, and ethyl isocyanoacetate (28.6 mL, 262 mmol) was added, followed by the dropwise addition of a second portion of *t*-BuOK (29.4 g, 262 mmol) dissolved in THF (100 mL). The reaction mixture was allowed to warm to rt and stirred overnight. The progress of the reaction was monitored by TLC (EtOAc: hexane = 60:40). The reaction mixture was quenched by adding a cold 10% aqueous solution of sodium bicarbonate (300 mL) and extracted with ethyl acetate (3x300 mL). The organic layers were combined, washed with brine (2x150 mL), and then dried with sodium sulfate (Na_2SO_4). The solvent was removed under reduced pressure, resulting in a brown solid. To purify the impure brown solid, 400 mL of *tert*-butyl methyl ether was added, and the mixture was stirred for 30 minutes at 55°C. The mixture was then cooled to room temperature and allowed to stand for 3 h. The solid residue was filtered, washed with *tert*-butyl methyl ether (2x80 mL), and dried under vacuum to obtain the pure imidazodiazepine **11** as an off-white powder (56.1 g, 63%). $\mathbf{R_f}$ = 0.4,(EtOAc: hexane = 60:40). **^{1}H NMR** (500 MHz, $CDCl_3$) δ 7.92 (s, 1H), 7.73 (d, J = 8.3 Hz, 1H), 7.60 (t, J = 7.4 Hz, 1H), 7.48 (d, J = 8.6 Hz, 1H), 7.47 – 7.37 (m, 2H), 7.26 (dd, J = 13.9, 6.4 Hz, 1H), 7.05 (t, J = 9.3 Hz, 1H), 6.71 (q, J = 7.2 Hz, 1H), 4.48-4.36 (m, 2H),1.41 (td, J = 7.1 Hz,1.1Hz, 3H), 1.29 (d, J = 7.3 Hz, 3H). **^{13}C NMR** (126 MHz, $CDCl_3$) δ 162.91 (s), 162.65 (s), 160.08 (d, J = 250.8 Hz), 141.53 (s), 134.90 (s), 134.78 (s), 133.66 (s), 133.06 (s), 132.16 (d, J = 8.4 Hz), 131.20 (s), 131.08 (s), 129.54 (s), 128.32 (d, J = 12.2 Hz), 124.57 (d, J = 3.2 Hz), 123.68 (s), 120.97 (s), 116.24 (d, J = 21.4 Hz), 60.81 (s), 50.08 (s), 14.87 (s), 14.44 (s). **HRMS (ESI/IT-TOF)** m/z: [M + H]+ Calcd for $C_{21}H_{18}BrFN_3O_2$ 442.0560; found 442.0563. %EE = >99%. (Chiral pak IBN3-4.6mmx150mm, 3µm).

4.5.10. Ethyl(S)-6-(2-fluorophenyl)-4-methyl-8-((triisopropylsilyl)ethynyl)-4Hbenzo[f] imidazo [1,5-a][1,4]diazepine-3-carboxylate (12)



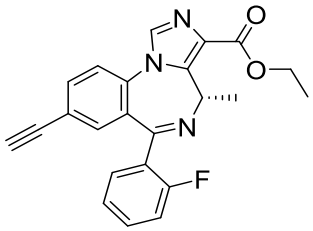
12

Tri-(*o*-tolyl) phosphine (2.48 g, 8.1 mmol) and $Pd(OAc)_2$ (0.92 g, 48 mmol) were dissolved in acetonitrile (ACN, 30 mL), and the mixture was stirred for 10 minutes under an argon atmosphere to generate the Pd catalyst in-situ. Then, the intermediate ethyl (*S*)-8-bromo-6-(2-fluorophenyl)-4-methyl-4H-benzo[f]imidazo[1,5-a][1,4]diazepine-3-carboxylate **10** (30 g, 68 mmol), triethylamine (29 mL, 204 mmol), (triisopropylsilyl)acetylene (18.2 mL, 82 mmol), and additional acetonitrile (200 mL) were added sequentially to the previous reaction mixture under an argon atmosphere. The reaction mixture was then refluxed for 4 h, and the consumption of the starting material was confirmed by thin-layer chromatography (TLC) using silica gel plates and a solvent system of 60% ethyl acetate and 40% hexane. The mixture was then cooled to room temperature and opened to air. Silica gel (30 g) was added to the flask. The mixture was stirred for 15 minutes, and the contents were filtered through a pad of celite. The residue was washed with DCM (2x100 mL). The solvents were removed under reduced pressure. To the resulting black oily mass, DCM (200 mL) and water (100 mL) were added to dissolve the contents. The mixture was stirred for 5 minutes and allowed to stand to separate into layers for 10 minutes. The layers were separated, and the aqueous layer was extracted with DCM (2x50 mL). The combined organic layers were washed with a 10% aqueous sodium chloride (NaCl) solution (2x50 mL) and

then dried over sodium sulfate (Na_2SO_4). The DCM solvent was removed under reduced pressure.

The residue was purified by silica gel (400 g) flash chromatography using a solvent mixture of 50% ethyl acetate and 50% hexane. The desired fractions containing the product were collected, and the solvents were removed under reduced pressure. The resulting oil was dried under vacuum for 4 h to afford an orange-colored oil of compound **12** (30.2 g, 82% yield). $\mathbf{R_f}$ = 0.6 (silica gel, 60% EtOAc-hexane); **^{1}H NMR** (500 MHz, $CDCl_3$) δ 7.97 (s, 1H), 7.67 (d, J = 7.4 Hz, 1H), 7.62 (t, J = 7.0 Hz, 1H), 7.55 (d, J = 8.3 Hz, 1H), 7.45 (td, J = 13.2, 6.8 Hz, 1H), 7.32 (d, J = 8.4 Hz, 1H), 7.25 (dd, J = 11.0, 4.0 Hz, 1H), 7.06 (dd, J = 19.8, 10.3 Hz, 1H), 6.69 (q, J = 7.3 Hz, 1H), 4.40 (q, J = 15.4Hz, 3H), 1.41 (t, J = 7.1 Hz, 3H), 1.29 (d, J = 7.3 Hz, 3H), 1.10 (s, 18H), 1.08 (s, 3H). **^{13}C NMR** (126 MHz, $CDCl_3$) δ 163.54 (s), 162.88 (s), 160.13 (d, *J* = 250.9 Hz), 141.58 (s), 135.42 (s), 134.88 (s), 134.01 (s), 133.42 (s), 131.97 (d, *J* = 10.1 Hz), 131.22 (s), 129.43 (d, *J* = 4.9 Hz), 128.52 (d, *J* = 12.1 Hz), 124.42 (d, *J* = 3.1 Hz), 123.06 (s), 122.16 (d, *J* = 9.5 Hz), 116.14 (d, *J* = 21.5 Hz), 104.52 (s), 94.22 (s), 60.87 (d, *J* = 26.6 Hz), 50.03 (s), 18.57 (d, *J* = 3.8 Hz), 14.85 (s), 14.42 (s), 11.20 (s).**HRMS** m/z: [M + H]+ calculated for $C_{32}H_{38}N_3O_2FSi$ 544.2790; found 544.2772.

4.5.12. Ethyl (*S*)-8-ethynyl-6-(2-fluorophenyl)-4-methyl-4*H*-benzo[*f*]imidazo[1,5-*a*][1,4] diazepine-3-carboxylate (SH-053-2'F-*S*-CH_3, 13)

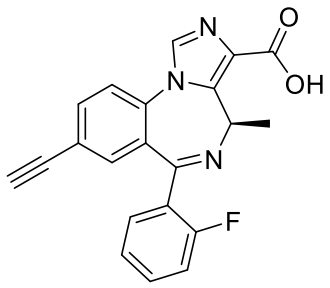


13 (SH-053-2'F-*S*-CH_3)

A round bottom flask was charged with ethyl (S)-6-(2-fluorophenyl)-4-methyl-8-((triisopropylsilyl)ethynyl)4H-benzo[f]imidazo[1,5-a][1,4]diazepine-3-carboxylate **12** (14 g, 27.5 mmol), THF (50 mL), and water (5 mL). The mixture was cooled to -10°C using a dry ice / isopropyl alcohol (IPA) bath. Then, tetrabutylammonium fluoride hydrate, 1M in THF (30.0 mL, 30.0 mmol), was added dropwise to the reaction mixture over a period of 10 minutes. The reaction mixture was allowed to warm to rt and stirred for 1-2 h while maintaining an internal temperature of 20-25°C. At that point, the reaction was completed, and the consumption of the starting material was confirmed by thin-layer chromatography (TLC) using silica gel TLC plates and a solvent system of 70% ethyl acetate and 30% hexane. The TLC analysis showed Rf values of 0.5 for **12** and 0.3 for compound **13**. To quench the reaction, water (100 mL) was added, and the mixture was then diluted with ethyl acetate (200 mL). The resulting biphasic mixture was stirred for 5 minutes and allowed to stand for 10 minutes. The organic layer was separated, and the aqueous layer was extracted with ethyl acetate (3x50 mL). The combined organic layers were washed with a 10% aqueous sodium chloride (NaCl) solution (2x100 mL) and then dried over sodium sulfate (Na_2SO_4). The residue was slurried with methanol (50 mL) and stirred for 30 min at 60 ^oC. At that point water (50 mL) was added to the methanol slurry and stirred for additional 30 min at 50 – 55^oC. The mixture was cooled to 20-25 ^oC and kept for 5h to maximize precipitation. The solid residue was filtered and washed with 50% methanol/water (10 mL x 3) followed by washing with hexanes (40 mL x 2). The solid residue was dried under vacuum at 45^oC for 12h to afford the product **13** as a white powder (8.2 g, 81%). $\mathbf{R_f}$= 0.3 (silica gel; 70% ethyl acetate-hexane); **^{1}H NMR** (500 MHz, CDCl3) δ 7.98 (s, 1H), 7.72 (d, J = 7.4 Hz, 1H), 7.60 (t, J = 6.0 Hz, 2H), 7.49 – 7.38 (m, 2H), 7.25 (t, J = 7.3 Hz, 1H), 7.04 (t, J = 8.5 Hz, 1H), 6.70 (q, J = 6.9 Hz, 1H), 4.40 (q, J = 14.4, 7.1 Hz, 2H), 3.16 (s, 1H), 1.41 (t, 3H), 1.28 (d, J = 6.7 Hz,

3H); **^{13}C NMR** (126 MHz, CDCl3) δ 163.71 (s), 162.79 (s), 160.10 (d, J = 251.2 Hz), 141.46 (s), 135.40 (s), 134.95 (s), 134.51 (s), 134.07 (s), 133.44 (s), 132.27 (d, J = 10.3 Hz), 131.28 (d, J = 3.5 Hz), 129.46 (s), 128.31 (d, J = 12.2 Hz), 124.54 (s), 122.33 (s), 121.76 (d, J = 2.7 Hz), 116.23 (d, J = 21.4 Hz), 81.34 (s), 79.85 (s), 60.85 (s), 49.95 (s), 14.90 (s), 14.43 (s); **HRMS (ESI/IT-TOF)** m/z: [M + H]+ Calcd for $C_{23}H_{19}FN_3O_2$ 388.1456; found 338.1448. %EE = >99%. (Chiral pak IBN3-4.6mmx150mm, 3µm).

4.5.13. (*R*)-8-ethynyl-6-(2-fluorophenyl)-4-methyl-4H-benzo[f]imidazo[1,5-a][1,4]diazepine-3-carboxylic acid (15)

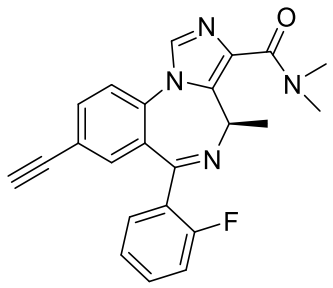


15

A round bottom flask was charged with the ester ,ethyl (*R*)-8-ethynyl-6-(2-fluorophenyl)-4-methyl-4H-benzo[f]imidazo[1,5-a][1,4]diazepine-3-carboxylate **7** (56.0 g, 144.5 mmol), THF (1000 mL), and stirred to make a solution. A solution of lithium hydroxide (13.84 g, 578 mmol) in water (100 mL) was added dropwise to the reaction mixture over a period of 15 minutes at 25 – 30°C. The reaction mixture was stirred at 50 – 55°C for 3 h. The progress of the reaction was monitored by thin-layer chromatography (TLC) using silica gel TLC plates and a solvent system of 100% ethyl acetate. After the reaction was complete, the mixture was cooled to room temperature (rt) and diluted with water (500 mL). Glacial acetic acid (41.4 mL, 720 mmol) was

then added dropwise to the reaction mixture with continuous stirring. This step was performed to break the lithium salt of the carboxylic acid **15**. The THF was removed under reduced pressure which resulted in a semi-solid slurry. To homogenize the mixture, methanol (200 mL) was added to the semi-solid slurry, and the contents were stirred at 40 – 45°C for 30 minutes. Additional water (100 mL) was added to dilute the mixture. The mixture was then allowed to stand at room temperature for 12 h to maximize the precipitation of the product. The solid product was filtered, and the residue was washed with water (4x 150 mL). The residue was then slurried in ethanol, and the slurry was stirred at 50 – 55°C for 30 minutes. The mixture was cooled to room temperature and placed in a freezer at -20°C overnight. The resulting solid was filtered, washed with cold ethanol (2x30 mL), and dried under vacuum at 45°C for 12 h to afford pure compound **15** as a white powder (46.7 g, 90% yield). **^{1}H NMR** (500 MHz, DMSO) δ 8.46 (s, 1H), 7.95 (d, J = 8.4 Hz, 1H), 7.84 (dd, J = 29.4, 8.3 Hz, 1H), 7.57 (t, J = 7.3 Hz, 1H), 7.51 (dd, J = 13.2, 6.1 Hz, 1H), 7.29 (dd, J = 20.1, 12.6 Hz, 2H), 7.19 (t, J = 9.4 Hz, 1H), 6.53 (q, J = 7.0 Hz, 1H), 4.30 (s, 1H), 1.95 (d, J = 13.2 Hz, 1H), 1.16 (d, J = 7.2 Hz, 3H); **^{13}C NMR** (126 MHz, DMSO) δ 164.63 (s), 162.92 (s), 159.82 (d, $^{1}J_{C\text{-}F}$ = 248.2 Hz), 141.11 (s), 136.72 (s), 135.58 (s), 134.68 (s), 133.21 (s), 132.58 (d, $^{4}J_{C\text{-}F}$ = 7.9 Hz), 131.86 (s), 129.36 (s), 128.87 (d, $^{3}J_{C\text{-}F}$ = 12.8 Hz), 125.10 (d, J = 2.6 Hz), 123.95 (s), 121.18 (s), 116.35 (d, $^{2}J_{C\text{-}F}$ = 21.2 Hz), 83.31 (s), 81.97 (s), 49.82 (s), 15.02 (s). **HRMS** (ESI/IT-TOF) m/z: $[M + H]^{+}$ Calcd for $C_{21}H_{15}FN_3O_2$ 360.1142; found 360.1171

4.5.14. *(R)*-8-Ethynyl-6-(2-fluorophenyl)-*N*,*N*,4-trimethyl-4*H*-benzo[*f*]imidazo[1,5 *a*][1,4]diazepine-3-carboxamide [GL-II-73,16]

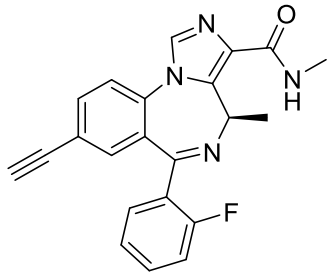


GL-II-73, 16

The acid, (*R*)-8-bromo-6-(2-fluorophenyl)-4-methyl-4H-benzo[f]imidazo[1,5-a][1,4]diazepine-3-carboxylic acid **15** (40.0 g, 111 mmol) was charged in a round bottom flask. A catalytic amount of anhydrous *N*,*N*-dimethylformamide (0.85 mL, 1.1 mmol) and anhydrous DCM (600 mL) were added to the flask and stirred the mixture. An off-white slurry resulted. The mixture was heated to 35 – 40°C under an argon atmosphere. Thionyl chloride (80.74 mL, 1110 mmol) was then added dropwise to the reaction mixture over a 30-minute period. During the addition of thionyl chloride, evolution of sulfur dioxide (SO_2) and hydrogen chloride (HCl) gases was observed. *It's crucial to add thionyl chloride gradually to avoid overflowing of the reaction mixture due to the gas evolution.* The resulting reaction mixture was refluxed for 2 h. The consumption of the starting material was confirmed by thin-layer chromatography (TLC) using silica gel plates and a solvent system of 100% ethyl acetate. For the TLC analysis, a test tube was prepared with 1 mL of methanol and 1 mL of triethylamine (TEA), and 0.5 mL of the reaction mixture was added. The TLC analysis of the methyl ester of **15** was then performed. After the reaction was completed, the reaction mixture was allowed to cool, and the solvents were removed under reduced pressure. To remove residual thionyl chloride, anhydrous DCM was added and removed six times (6x150 mL). The resulting, yellow-colored residue was dissolved in anhydrous DCM (400 mL), and the mixture was cooled to 0°C. A solution of dimethylamine (2M in THF, 333 mL, 666 mmol) was then added dropwise to the reaction mixture at 0°C. The mixture was

allowed to warm to room temperature and stirred for 2 h. At the end of the reaction, the reaction mixture was diluted with a 10% aqueous solution of sodium bicarbonate (300 mL) and additional DCM (300 mL). The biphasic mixture was allowed to stand for 15 minutes to allow the layers to separate. The organic layer was separated, and the aqueous layer was extracted with DCM (2x150 mL). The combined organic layers were washed with a 10% aqueous solution of sodium bicarbonate (1x250 mL), a 10% aqueous solution of sodium chloride (NaCl, 2x400 mL), and dried using sodium sulfate (Na_2SO_4). The solvents were removed under reduced pressure, and the residue was purified using flash chromatography (silica gel) with a solvent system of 100% ethyl acetate containing 5% methanol and 1% triethylamine (TEA). The purified fractions were combined, and the solvents were removed under reduced pressure. The resulting solid residue was dried under vacuum at 45°C for 4 h to yield pure compound **16** as an off-white colored powder (29.8 g, 71%). $\mathbf{R_f}$ = 0.2 (silica gel, 100% EtOAc). **^{1}H NMR** (500 MHz, $CDCl_3$) δ 7.92 (s, 1H), 7.71 (d, J = 8.0 Hz, 1H), 7.60 (td, J = 7.4 Hz, 1.7 Hz,1H), 7.50 (d, J = 8.2 Hz, 1H), 7.46 – 7.39 (m, 3H), 7.24 (ddd, J = 7.5 Hz, 1H), 7.02 (t, J = 9.3 Hz, 1H), 6.22 (q, 1H), 4.32 (q, J = 14.7 Hz, 1H), 3.29 (s, 1H), 3.15 (s, 1H), 3.11 (s, 3H), 3.07 (s, 1H), 2.99 (s, 3H), 1.92 (d, J = 6.4 Hz, 3H), 1.28 (d, J = 6.7 Hz, 1H). **^{13}C NMR** (126 MHz, $CDCl_3$) δ 166.1 (s), 162.54 (s), 160.15 (d, $^1J_{C\text{-}F}$ = 251.2 Hz), 135.28 (s), 134.60 (d, J = 5.8 Hz), 133.87 (s), 133.63 (s), 133.00 (s), 132.56 (s), 132.04 (d, $^3J_{C\text{-}F}$ = 8.1 Hz), 131.26 (s), 129.13 (s), 127.62 (d, $^2J_{C\text{-}F}$ = 11.9 Hz), 124.45 (d, $^4J_{C\text{-}F}$ = 1.9 Hz), 122.87 (s), 121.44 (s), 116.10 (d, $^2J_{C\text{-}F}$ = 21.5 Hz), 81.50 (s), 79.66 (s), 52.13 (s), 39.02 (s), 34.95 (s), 18.40 (s). **HRMS (ESI/IT-TOF)** m/z: [M + H] Calcd for $C_{23}H_{20}FN_4O$ 387.16157; found 387.1637; %EE = >99%. (Chiral pak IBN3-4.6mmx150mm, 3µm).

4.5.15. *(R)*-8-ethynyl-6-(2-fluorophenyl)-N,4-dimethyl-4H-benzo[f]imidazo[1,5-a][1,4] diazepine-3-carboxamide [MP-III-022,17]

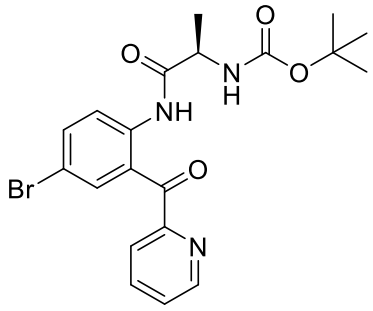


MP-III-022, 17

The carboxylic acid, **15** (5.5 g, 15.3 mmol) was charged in a round bottom flask. A catalytic amount of anhydrous *N,N*-dimethylformamide (0.1 mL, 0.15 mmol) and anhydrous DCM (60 mL) were added to the flask and stirred the mixture. An off-white slurry resulted. The mixture was heated to 35 – 40°C under an argon atmosphere. Thionyl chloride (10.8 mL, 153 mmol) was then added dropwise to the reaction mixture over a 30-minute period. During the addition of thionyl chloride, evolution of sulfur dioxide (SO_2) and hydrogen chloride (HCl) gases was observed. *It's crucial to add thionyl chloride gradually to avoid overflowing of the reaction mixture due to the gas evolution.* The resulting reaction mixture was refluxed for 2 h. The consumption of the starting material was confirmed by thin-layer chromatography (TLC) using silica gel plates and a solvent system of 100% ethyl acetate. For the TLC analysis, a test tube was prepared with 1 mL of methanol and 1 mL of triethylamine (TEA), and 0.5 mL of the reaction mixture was added. The TLC analysis of the methyl ester of **15** was then performed. After the reaction was completed, the reaction mixture was allowed to cool, and the solvents were removed under reduced pressure. To remove residual thionyl chloride, anhydrous DCM was added and removed six times (6x15 mL). The resulting, yellow-colored residue was dissolved in anhydrous DCM (40 mL), and the mixture was cooled to 0°C. A solution of methylamine (2M in

THF, 53.5 mL, 107 mmol) was then added dropwise to the reaction mixture at 0°C. The mixture was allowed to warm to room temperature and stirred for 2 h. At the end of the reaction, the reaction mixture was diluted with a 10% aqueous solution of sodium bicarbonate (30 mL) and additional DCM (30 mL). The biphasic mixture was allowed to stand for 15 minutes to allow the layers to separate. The organic layer was separated, and the aqueous layer was extracted with DCM (2x15 mL). The combined organic layers were washed with a 10% aqueous solution of sodium bicarbonate (1x25 mL), a 10% aqueous solution of sodium chloride (NaCl, 2x40 mL), and dried using sodium sulfate (Na_2SO_4). The solvents were removed under reduced pressure, and the residue was purified using flash chromatography (silica gel) with a solvent system of 80% ethyl acetate-hexane containing 1% triethylamine (TEA). The purified fractions were combined, and the solvents were removed under reduced pressure. The resulting solid residue was dried under vacuum at 45°C for 4 h to yield pure compound **17** as an off-white colored powder (3.87 g, 68%). $\mathbf{R_f}$ = 0.3 (silica gel, 100% EtOAc). **^{1}H NMR** (500 MHz, $CDCl_3$) δ 7.83 (s, 1H), 7.68 (d, *J* = 8.1 Hz, 1H), 7.64 (t, *J* = 7.1 Hz, 1H), 7.53 (d, *J* = 8.3 Hz, 1H), 7.47 – 7.40 (m, 2H), 7.25 (td, *J* = 7.6, 1.0 Hz, 1H), 7.17 (s, 1H), 7.05 – 7.00 (m, 1H), 6.90 (dd, *J* = 14.1, 6.9 Hz, 1H), 3.14 (d, *J* = 8.8 Hz, 1H), 2.97 (d, *J* = 5.0 Hz, 3H), 1.30 (d, *J* = 4.1 Hz, 3H). **^{13}C NMR** (126 MHz, $CDCl_3$) δ 163.30 (s), 162.80 (s), 160.12 (d, *J* = 250.1 Hz), 138.75 (s), 134.95 (s), 134.70 (s), 133.92 (s), 133.42 (s), 131.81 (d, *J* = 2.5 Hz), 131.75 (s), 131.35 (s), 129.79 (s), 128.85 (d, *J* = 11.4 Hz), 124.44 (d, *J* = 3.3 Hz), 122.02 (s), 121.38 (s), 116.07 (d, *J* = 21.5 Hz), 81.55 (s), 79.50 (s), 49.89 (s), 31.59 (s), 15.07 (s). **HRMS** (LCMS-IT-TOF) Calc. for $C_{22}H_{18}FN_4O$ $(M + H)^+$ 373.1459, found: 373.1462; %EE = >99%. (Chiral pak IBN3-4.6mmx150mm, 3µm).

4.5.16. *Tert*-butyl-(*R*)-(1-((4-bromo-2-picolinoylphenyl)amino)-1-oxopropan-2-yl)carbamate (19)

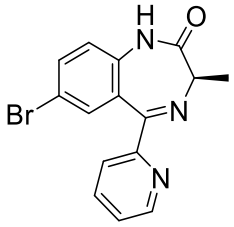


19

The benzophenone starting material (2-amino-5-bromophenyl)(pyridin-2'-yl)methanone **18** (50 g, 180 mmol) and BOC-*D*-alanine (44.5 g, 234 mmol) were dissolved in DCM (400 mL) and cooled the solution to -10 °C using an ice-methanol bath. A solution of the peptide coupling reagent DCC (59.4 g, 288 mmol) in DCM (200 mL) is then incrementally added to the mixture over 60 minutes while maintaining the temperature at -10 °C to -5 °C. Once the DCC addition is complete, the reaction mixture is allowed to gradually warm to room temperature (rt) and is stirred for a prolonged period of 30 h. The consumption of starting material was monitored by TLC (silica gel, 30% EtOAc-hexane, 1% TEA). Once the reaction was done, the white dicyclohexyl urea byproduct was filtered off and the residue was washed with DCM (3 × 100 mL). The combined DCM layers were removed under reduced pressure and a yellow-colored oil resulted. The oil was slurried with 5% EtOAc-hexane (250 mL) and stirred for 30 min at 55 °C. The yellow-colored oil turned into a white-colored powder floating on the flask during this stirring. The mixture was cooled to rt and held for 2 h. The solid, which formed, was filtered, washed with 5% EtOAc-hexane (3 × 50 mL), and dried under vacuum for 2 h at 40 °C to afford pure **19** as a white powder (68.2 g, 85%). $\mathbf{R_f}$ = 0.4 (silica gel, 30% EtOAc-hexane). **^{1}H NMR**

(500 MHz, $CDCl_3$) δ 11.40 (s, 1H), 8.78 (dd, *J* = 25.2, 6.7 Hz, 1H), 8.64 (d, *J* = 9.0 Hz, 1H), 7.99 (d, *J* = 1.8 Hz, 1H), 7.95 (d, *J* = 4.3 Hz, 2H), 7.69 (dd, *J* = 9.0, 1.9 Hz, 1H), 7.54 (dd, *J* = 8.9, 4.6 Hz, 1H), 5.12 (s, 1H), 4.37 (q, *J* = 24.3 Hz, 1H), 1.49 (d, *J* = 7.2 Hz, 3H), 1.46 (s, 9H). **^{13}C NMR** (126 MHz, $CDCl_3$) δ 195.41 (s), 172.01 (s), 155.06 (s), 148.72 (s), 139.86 (s), 137.31 (s), 136.87 (s), 126.45 (s), 124.79 (s), 123.71 (s), 122.80 (s), 114.82 (s), 80.31 (s), 51.66 (s), 28.30 (s), 18.67 (s). **HRMS (ESI/IT-TOF**) m/z: [M + H] + Calcd for $C_{20}H_{22}N_3O_4Br$ 448.0866; found 448.0877.

4.5.17. (*R*)-7-bromo-3-methyl-5-(pyridin-2-yl)-1,3-dihydro-2H-benzo[e][1,4]diazepin-2-one (20)

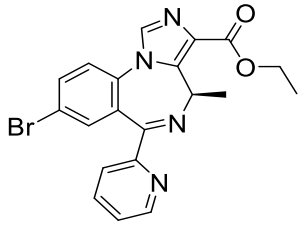


20

Under controlled conditions, a solution of 4M hydrochloric acid (HCl) in dioxane (168 mL, 671.4 mmol) was added dropwise a stirred solution containing the *N*-Boc protected amide *tert*-butyl (*R*)-(1-((4-bromo-2-picolinoylphenyl)amino)-1-oxopropan-2-yl)carbamate **19** (75 g, 167.8 mmol) in DCM (500 mL) while maintaining a temperature of -10 °C. As the mixture transitioned to room temperature (rt), it was stirred for a period of 12 h at that temperature. The progress of the reaction was monitored by TLC (silica gel, 60% EtOAc-hexane with 1% triethylamine) to confirm the consumption of the starting material. Upon completion, the reaction mixture was neutralized using an aqueous solution of 5% sodium bicarbonate (600 mL). The organic layer was extracted with DCM (2x500 mL), and it was followed by washing with aqueous 5% $NaHCO_3$ solution (250 mL) and aqueous 10% sodium chloride (NaCl) solution (2x350 mL). The

solvents were then evaporated under reduced pressure, yielding an oily mass. This residue was dissolved in methanol (500 mL) and stirred for 20 hours at rt to ensure the completion of the reaction. Afterward, solvents were evaporated, and the remaining residue was dissolved in DCM (1000 mL), followed by the addition of water (500 mL) for dilution. After allowing the biphasic mixture to separate into layers for 5 minutes, the organic layer was collected, and the aqueous layer was extracted with DCM (2x250 mL). The combined organic layers were then washed with brine (2x200 mL) and dried (Na_2SO_4). After removing solvents under reduced pressure, the resulting residue was subjected to slurry in 10% EtOAc-hexane (300 mL) and stirred at 50°C for 30 minutes. Subsequent cooling to rt and a 3-h period of standing maximized the precipitation of the solid residue. This residue was filtered and washed with 10% EtOAc-hexane (2x50 mL) and finally dried under vacuum at 40°C for 12 h to afford compound **20** as a white-colored powder (45.4 g, 81). $\mathbf{R_f}$ = 0.5 (silica gel, 60% EtOAc-hexane with 1% TEA). **^{1}H NMR** (500 MHz, $CDCl_3$) δ 9.26 (s, 1H), 8.62 (d, *J* = 4.8 Hz, 1H), 8.03–8.00 (m, 1H), 7.81 (t, *J* = 7.7 Hz, 1H), 7.60–7.55 (m, 1H), 7.52 (s, 1H), 7.36 (dd, *J* = 8.7, 3.7 Hz, 1H), 7.05 (d, *J* = 8.6 Hz, 1H), 3.83 (q,*J* = 11.9 Hz, 1H), 1.77 (d, *J* = 6.5 Hz, 3H).. **^{13}C NMR** (126 MHz, $CDCl_3$) δ 172.24 (s), 166.39 (s), 156.07 (s), 148.91 (s), 137.49 (s), 136.85 (s), 134.55 (s), 133.80 (s), 128.32 (s), 124.63 (s), 124.14 (s), 122.88 (s), 116.02 (s), 59.05 (s), 16.93 (s). **HRMS (ESI/IT-TOF)** *m/z*: [M + H] + Calcd for $C_{15}H_{12}N_3OBr$ 330.0236; found 330. 330.0214. %ee >99% (HPLC).

4.5.18. Ethyl (*R*)-8-bromo-4-methyl-6-(pyridin-2'-yl)-4H-benzo[f]imidazo[1,5-a][1,4] diazepine-3-carboxylate(21)

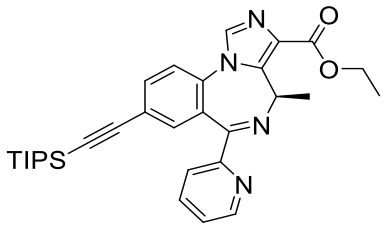


21

A solution of *t*-BuOK (19.44 g, 173 mmol) in anhydrous THF (150 mL) was added dropwise over a period of 20 min to a stirred solution of 1,4-benzodiazepine **20** (44 g, 133 mmol) in anhydrous THF (400 mL) at −20 °C. The mixture was then stirred for 1.5 h, after which diethyl chlorophosphate (26.9 mL, 186.2 mmol) was added dropwise at −20 °C to the reaction mixture. The solution was allowed to warm to rt, and the temperature was held there for 2 h. The consumption of starting material was confirmed by TLC (silica gel, 60% EtOAc-hexane, 1% TEA). A small amount of starting material remained unreacted even after increasing the stirring time. Then the reaction was again cooled to −20 °C and ethyl isocyanoacetate (18.9 mL, 173 mmol) was added, and this was followed by a dropwise addition of a second portion of *t*-BuOK (19.44 g, 173 mmol) in THF (100 mL) solution at −20 °C. The reaction mixture was allowed to warm to rt and stirred for 8 h. The consumption of starting material was determined on analysis by TLC (silica gel, 70% EtOAc-hexane with 1% TEA). The reaction was quenched by addition of a cold 10% aq solution of $NaHCO_3$ (300 mL) and extracted with EtOAc (3 × 300 mL). The combined organic layer was washed with brine (2 × 150 mL), dried (Na_2SO_4) and the solvent was removed under reduced pressure to afford a brown solid. Then *t*-butyl methyl ether (250 mL) was added to the brown impure solid and stirred for 30 min at 55 °C. The mixture was then cooled to rt, and stirred at rt for 3 h. The residue was filtered and washed with *t*-butyl methyl

ether (2 × 40 mL). The solid residue was then slurried again with ethanol (200 mL) and stirred for 30 min at 60 °C. The mixture was cooled to rt and kept at −20 °C in the freezer for 5 h to maximize precipitation. The solid residue was filtered, washed with cold ethanol (2 × 50 mL), and dried under vacuum at 45 °C for 3 h to obtain pure imidazodiazepine **21** as an off-white powder (35.5 g, 62.1%). R_f = 0.4 (70% EtOAc-hexane with 2% TEA). **^{1}H NMR** (500 MHz, $CDCl_3$) δ 8.58 (d, *J* = 4.7 Hz, 1H), 8.03 (d, *J* = 7.9 Hz, 1H), 7.87 (s, 1H), 7.83 (td, *J* = 7.9, 1.5 Hz, 1H), 7.74 (dd, *J* = 8.6, 2.0 Hz, 1H), 7.50 (d, *J* = 2.0 Hz, 1H), 7.46 (d, *J* = 8.6 Hz, 1H), 7.38 (dd, *J* = 6.9, 5.1 Hz, 1H), 6.72 (q, *J* = 7.3 Hz, 1H), 4.56–4.29 (m, 3H), 1.43 (t, *J* = 7.1 Hz, 3H), 1.29 (d, *J* = 7.4 Hz, 3H). **^{13}C NMR** (126 MHz, $CDCl_3$) δ 164.56 (s), 163.03 (s), 157.28 (s), 148.59 (s), 141.67 (s), 136.96 (s), 135.00 (s), 134.90 (s), 134.73 (s), 129.43 (s), 124.87 (s), 124.71 (s), 124.60 (s), 124.04 (s), 123.83 (s), 120.36 (s), 60.79 (s), 49.86 (s), 14.58 (s), 14.43 (s). **HRMS (ESI/IT-TOF)** *m/z*: [M + H]+ Calcd for $C_{20}H_{17}N_4O_2Br$ 425.0607; found 425.0610. %ee >99% (Chiral pak IBN3-4.6 mm × 150 mm, 3 µm).

4.5.19. Ethyl (R)-4-methyl-6-(pyridin-2-yl)-8-((triisopropylsilyl)ethynyl)-4H-benzo[f] imidazo[1,5-a][1,4]diazepine-3-carboxylate (22)

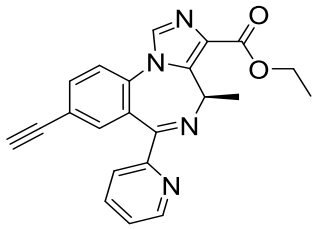


22

A round bottom flask was charged with tri-(*o*-tolyl) phosphine (3.31 g, 10.88 mmol), $Pd(OAc)_2$ (1.22 g, 5.4 mmol), ACN (30 mL), and the mixture was stirred for 10 min under an argon atmosphere to generate the Pd catalyst in situ. Then ethyl (*S*)-8-bromo-4- methyl-6-(pyridin-2′-

yl)-4H-benzo[f]imidazo[1,5-a] [1,4] diazepin-3-carboxylate (**21**, 29 g, 68 mmol), triethylamine (28.7 mL, 204 mmol), (triisopropylsilyl)acetylene (16.82 mL, 75 mmol) and additional acetonitrile (230 mL) were added sequentially to the previous reaction mixture under argon. The reaction mixture was allowed to stir at reflux for 4 h. At the end of the reaction period the mixture was then cooled to rt, and silica gel (30 g) was added to the flask, and the mixture was allowed to stir for 15 min. The contents were filtered through a pad of celite, and the residue was washed with DCM (3 × 300 mL). The solvents were removed under reduced pressure. After which DCM (400 mL) and water (200 mL) were added to the resulting black oily mass to dissolve the contents. The mixture was stirred for 5 min and then allowed to stand to separate the layers for 10 min. The layers were separated and the aq layer was extracted with DCM (2 × 100 mL). The combined organic layers were washed with 10% aqueous NaCl (2 × 50 mL) and dried (Na_2SO_4). The DCM was removed under reduced pressure, and the residue was purified by silica gel (400 g) flash chromatography using 60% EtOAc-hexane with 2% TEA. The desired fractions were collected, and the solvents were removed under reduced pressure. The oil, which resulted, was then dried under vacuum for 4 h to afford an orange-colored oil of **22** (30 g, 83.5%). R_f = 0.6 (silica gel, 70% EtOAc-hexane with 1% TEA **^{1}H NMR** (500 MHz, $CDCl_3$) δ 8.59 (d, *J* = 4.2 Hz, 1H), 8.01 (d, *J* = 7.9 Hz, 1H), 7.88 (s, 1H), 7.83 (dd, *J* = 11.0, 4.4 Hz, 1H), 7.68 (d, *J* = 8.3 Hz, 1H), 7.51 (d, *J* = 8.4 Hz, 1H), 7.41 (s, 1H), 7.37 (dd, *J* = 6.9, 5.2 Hz, 1H), 6.70 (q, *J* = 7.3 Hz, 1H), 4.49–4.35 (m, 2H), 1.42 (t, *J* = 7.1 Hz, 3H), 1.29 (d, *J* = 7.3 Hz, 3H), 1.11 (s, 21H).. **^{13}C NMR** (126 MHz, CDCl3) δ 165.26 (s), 163.05 (s), 157.58 (s), 148.54 (s), 141.76 (s), 136.82 (s), 135.40 (s), 135.34 (s), 135.12 (s), 134.95 (s), 129.33 (s), 127.83 (s), 124.55 (s), 124.05 (s), 122.43 (s), 122.24 (s), 104.88 (s), 93.72 (s), 60.73 (s), 49.86 (s), 18.60 (s), 14.55 (s), 14.44 (s), 11.23 (s). HRMS (ESI/IT-TOF) *m/z*: [M + H] Calcd for $C_{25}H_{27}N_4O_2Si$ 443.1898; found 443.1901

4.5.20. Ethyl (S)-8-ethynyl-4-methyl-6-(pyridin-2-yl)-4H-benzo[f]imidazo [1,5-a][1,4] diazepine-3-carboxylate(23)

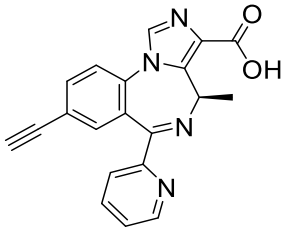


23

The ethyl ester, ethyl (*S*)-4-methyl-6-(pyridin-2′-yl)-8-((triisopropylsilyl)ethynyl)-4Hbenzo[f]imidazo[1,5-a][1,4]diazepine-3-carboxylate **22** (48 g, 91 mmol) was dissolved in THF(250 mL) and water (20 mL) was added. The mixture was cooled to −20 °C by using IPA/dry ice bath. A solution of tetrabutylammonium fluoride hydrate, [1 M in THF (95.6 mL, 95.6 mmoL)] was added dropwise to the reaction mixture over a period of 10 min while maintain an internal temperature of −10 °C. The reaction mixture was allowed to warm to rt and stir for 1 h at that temperature. The consumption of starting material was confirmed by analysis by TLC (silica gel; 80% ethyl acetate-hexane with 2% TEA). Water (200 mL) was then added to quench the reaction and the mixture was then diluted with DCM (500 mL). The biphasic mixture, which resulted, was stirred for 5 min, and allowed to stand for 10 min. The organic layer was separated and the aqueous layer was then extracted with DCM (2 × 200 mL). The combined organic layers were washed with a 10% aq sodium chloride solution (2 × 150 mL) and dried (Na_2SO_4). The solvents were removed under reduced pressure, which resulted, in an orange-colored residue. The residue was slurried with IPA (350 mL) and allowed to stir for 30 min at 55 °C. Then water (300 mL) was added to the mixture, and it was stirred for an additional 20 min. The mixture was allowed to cool to rt and kept overnight. The solid residue was filtered, washed with IPA-water

(1:1, 2 × 50 mL), and dried under vacuum at 45 °C for 12 h to afford the product as a white powder of **23** (27.5 g, 89%). R_f = 0.4 (silica gel; 80% ethyl acetate-hexane with 2% TEA); **^{1}H NMR** (500 MHz, $CDCl_3$) δ 8.58 (d, *J* = 4.2 Hz, 1H), 8.00 (d, *J* = 7.9 Hz, 1H), 7.89 (s, 1H), 7.82 (td, *J* = 7.8, 1.5 Hz, 1H), 7.71 (dd, *J* = 8.3, 1.5 Hz, 1H), 7.55 (d, *J* = 8.3 Hz, 1H), 7.47 (t, *J* = 7.3 Hz, 1H), 7.37 (dd, *J* = 6.7, 5.1 Hz, 1H), 6.71 (q, *J* = 7.3 Hz, 1H), 4.41 (m, 2H), 3.16 (s, 1H), 1.42 (t, *J* = 7.1 Hz, 3H), 1.26 (d, *J* = 21.4 Hz, 3H). **^{13}C NMR** (126 MHz, $CDCl_3$) δ 165.17 (s), 163.04 (s), 157.56 (s), 148.63 (s), 141.76 (s), 136.89 (s), 135.87 (s), 135.06 (s), 134.98 (s), 134.44 (s), 129.41 (s), 127.96 (s), 124.60 (s), 124.04 (s), 122.41 (s), 120.98 (s), 81.70 (s), 79.41 (s), 60.77 (s), 49.85 (s), 14.58 (s), 14.43 (s). **HRMS (ESI/IT-TOF)** *m/z*: [M + H]+ Calcd for $C_{22}H_{18}N_4O_2$ 371.1505; found 371.1502.

4.5.21. (*R*)-8-Ethynyl-4-methyl-6-(pyridin-2-yl)-4H-benzo[f]imidazo[1,5-a][1,4]diazepine-3-carboxylic acid (24)

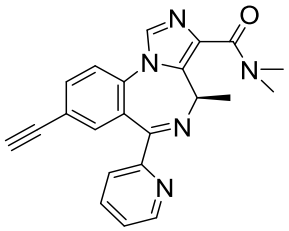


24

The ethyl ester, ethyl (*S*)-8-ethynyl-4-methyl-6-(pyridin-2′-yl)-4H-benzo[f]imidazo [1,5-a][1,4] diazepine-3-carboxylate **23** (12 g, 32.4 mmol) was stirred in ethanol (30 mL) and a slurry resulted. A solution of lithium hydroxide (5.2 g, 129.6 mmol) in water (15 mL) was added dropwise to that mixture at rt. The mixture was then heated to 50 °C and stirred for 1 h while maintaining an internal temperature of 50 °C . The reaction was deemed to be completed on analysis by TLC (silica gel, 100% EtOAc with 2% TEA) after 1 h. The mixture was then allowed

to cool to rt, and water (80 mL) was added to dilute the mixture. Then glacial acetic acid (10 mL) was added to adjust the pH to 5 (pH paper). Then ethanol was removed under reduced pressure and a white precipitation formed. *Caution: Addition of too much water or acetic acid needs to be avoided, otherwise the acid will go back into the water solution, and it will be difficult to make it precipitate*. The solid residue was filtered, washed with water (4× 20 mL), and dried under vacuum. The residue was then suspended in 100% EtOAc (50 mL) and stirred for 10 min at 45 °C. The mixture was cooled to rt and held there for 1 h. The solid was filtered, washed (EtOAc, 2 × 10 mL), and dried under vacuum at 50 °C for 8 h to afford a white powder of **24** (10 g, 90%). **^{1}H NMR** (300 MHz, DMSO-d^{6}) δ 8.51 (d, *J* = 4.5 Hz, 1H), 8.38 (s, 1H), 8.00 (d, *J* = 7.4 Hz, 1H), 7.96 (dd, *J* = 7.3, 1.7 Hz, 1H), 7.91 (d, *J* = 3.1 Hz, 1H), 7.88 (s, 1H), 7.80 (d, *J* = 8.2 Hz, 1H), 7.52–7.46 (m, 1H), 7.34 (s, 1H), 6.52 (q, *J* = 7.2 Hz, 1H), 4.34 (s, 1H), 1.16 (d, *J* = 7.2 Hz, 3H). **^{13}C NMR** (126 MHz, DMSO-d^{6}) δ 165.43(s), 164.72 (s), 157.59(s), 148.55 (s), 141.20 (s), 137.54 (s), 136.75 (s), 135.8 (s), 135.45 (s), 134.94 (s), 129.29 (s), 128.08 (s), 125.34 (s), 124.06 (s), 123.80 (s), 120.32 (s), 82.96 (s), 82.08 (s), 49.58 (s), 14.63 (s). **HRMS (ESI/IT-TOF)** *m/z*: [M + H]+ Calcd for $C_{22}H_{18}N_4O_2$ 343.1189; found 343.1211.

4.5.22. (*R*)-8-Ethynyl-N,N,4-trimethyl-6-(pyridin-2-yl)-4H-benzo[f]imidazo[1,5-a][1,4] diazepine-3-carboxamide (25)

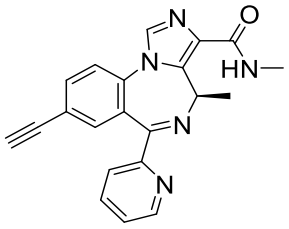


DS-I-19, 25

A round bottom flask was charged with (*S*)-8-ethynyl-4-methyl-6-(pyridin-2′-yl)-4H-benzo[f]imidazo[1,5-a][1,4]diazepine-3-carboxylic acid **24** (9 g, 25.8 mmol), anhydrous *N*,*N*-dimethylformamide (0.1 mL, 0.43 mmol), anhydrous DCM (30 mL) under an atmosphere of argon and the mixture was stirred to make a solution. The reaction mixture was then heated to 35 to 40 °C. Thionyl chloride (19.1 mL, 258 mmol) was added dropwise to the stirred solution of mixture while maintaining an internal temperature of 35 to 40 °C. and stirred for 1 h at reflux temperature. Evolution of SO_2 (g) and HCl (g) was observed during the addition of thionyl chloride. The completion of reaction was confirmed by TLC (silica gel, 100% EtOAc with 2% TEA). To perform TLC, a test tube was filled with 1 mL of methanol and 1 mL of triethylamine. Then, 0.5 mL of the reaction mixture was added to the test tube. The methyl ester, which resulted was analyzed by TLC. The reaction mixture was cooled at the end of the reaction and the solvents were removed under reduced pressure. The residual thionyl chloride was removed by adding and flash evaporating anhydrous DCM (6 × 50 mL) under vacuum. A yellow-colored residue was obtained. The solid residue was dissolved in anhydrous DCM (60 mL) and the mixture was cooled to 0 °C. A solution of dimethylamine (2 M in THF, 77.4 mL, 150.5 mmol) was added dropwise to the reaction mixture at 0 °C. The mixture was allowed to warm to rt and allowed to stir for 1 h until the consumption of starting material was finished (TLC). The reaction mixture was diluted with aq 10% $NaHCO_3$ (50 mL) and additional DCM (150 mL) was added. The biphasic mixture, which resulted, was allowed to stand 3 min to separate the layers. The organic layer was separated and the aq layer was extracted with DCM (2 × 100 mL). The combined organic layers were washed with aq 10% $NaHCO_3$ solution (1 × 50 mL), aqueous 10% NaCl solution (2 × 50 mL) and dried (Na_2SO_4). After removing the solvents under reduced pressure, the residue was purified by flash chromatography (silica gel, 100% EtOAC with 2%

MeOH and 2% TEA). The desired fractions were pooled, and the solvents were evaporated under reduced pressure. The solid was dried under vacuum at 45 °C for 12 h to afford compound **25** as a light, yellow-colored powder (4.32 g, 67.2%). **^{1}H NMR** (500 MHz, MeOD) δ 8.52 (d, *J* = 4.5 Hz, 1H), 8.32 (s, 1H), 8.04 (d, *J* = 7.8 Hz, 1H), 7.98 (t, *J* = 7.4 Hz, 1H), 7.82 (s, 2H), 7.57–7.50 (m, 1H), 7.42 (s, 1H), 4.45 (q, *J* = 6.6 Hz, 1H), 3.68 (s, 1H), 3.15 (s, 3H), 2.97 (s, 3H), 1.86 (d, *J* = 6.7 Hz, 3H). **^{13}C NMR** (126 MHz, MeOD) δ 166.73 (s), 165.44 (s), 156.39 (s), 148.17 (s), 137.42 (s), 135.48 (s), 135.22 (s), 135.15 (s), 135.03 (s), 133.95 (s), 130.84 (s), 127.28 (s), 124.98 (s), 124.11 (s), 123.32 (s), 121.34 (s), 81.08 (s), 79.73 (s), 51.89 (s), 37.96 (s), 33.89 (s), 16.88 (s). **HRMS (ESI/IT-TOF)** *m/z*: $[M + H]^+$ Calcd for $C_{22}H_{19}N_5O$ 370.1662; found 370.1624. %ee > 99%.

4.5.23. (*R*)-8-Ethynyl-N,N,4-trimethyl-6-(pyridin-2-yl)-4H-benzo[f]imidazo[1,5-a][1,4] diazepine-3-carboxamide (26)

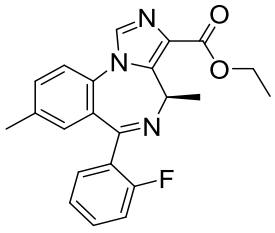


DS-I-96, 26

The ethyl ester (*S*)-8-ethynyl-4-methyl-6-(pyridin-2′-yl)-4H-benzo[f]imidazo[1,5-a][1,4] diazepine-3-carboxylate **23** (1 g, 2.69 mmol) was charged into a sealed vessel fitted with a septum equipped with a magnetic stir bar. Then methyl amine (20 mL, 33% wt solution in EtOH) was added to the sealed tube at −30 °C. The vessel was secured with a screwcap and stirred at 60 °C for 12 h. The solution was then cooled to rt, and the methyl amine and ethanol were removed under reduced pressure. The residue, which resulted, was purified by flash column

chromatography (silica gel, EtOAc) to afford the pure methyl amide **26** as an off- white colored powder (0.60 g, 62%). **^{1}H NMR** (500 MHz, $CDCl_3$) δ 8.56 (dd, *J* = 4.7, 0.6 Hz, 1H), 8.06 (d, *J* = 7.9 Hz, 1H), 7.82 (td, *J* = 7.8, 1.7 Hz, 1H), 7.76 (s, 1H), 7.69 (dd, *J* = 8.3, 1.4 Hz, 1H), 7.52 (d, *J* = 8.3 Hz, 1H), 7.47 (d, *J* = 1.1 Hz, 1H), 7.35 (ddd, *J* = 7.4, 4.8, 0.9 Hz, 1H), 7.18 (d, *J* = 4.3 Hz, 1H), 6.90 (q, *J* = 7.3 Hz, 1H), 3.15 (s, 1H), 2.96 (s, 3H), 1.28 (d, *J* = 7.1, 4.2 Hz, 3H). **^{13}C NMR** (126 MHz, $CDCl_3$) δ 164.72 (s), 163.42 (s), 157.73 (s), 148.39 (s), 138.74 (s), 136.84 (s), 136.08 (s), 135.96 (s), 134.85 (s), 133.65 (s), 131.57 (s), 128.02 (s), 124.47 (s), 124.08 (s), 123.09 (s), 122.26 (s), 81.84 (s), 79.20 (s), 49.64 (s), 25.57 (s), 14.74 (s). **HRMS** (ESI/IT-TOF) *m/z*: [M + H] + Calcd for C_{21} $H_{17}N_5O$ 356.1506; found 356.1504**;** %ee => 99% (HPLC).

4.5.24. Ethyl (*R*)-6-(2'-fluorophenyl)-4-methyl-8-methyl-4H-benzo[f]imidazo[1,5-a][1,4] diazepine-3-carboxylate (27)

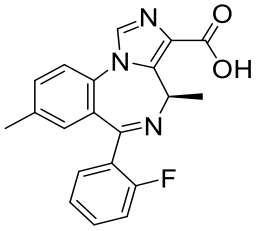


27

Palladium acetate ($Pd(OAc)_2$, 0.28 g, 1.27 mmol) and tri-(*o*-tolyl) phosphine (0.77 g, 2.5 mmol) were dissolved in toluene (20 mL), and the mixture was stirred for 10 minutes under an argon atmosphere to generate the $Pd(OAc)_2$-p-*O*-$(tol)_3$-phosphine catalyst *in situ*. Subsequently, the imidazodiazepine ethyl (*R*)-8-bromo-6-(2-fluorophenyl)-4-methyl-4H-benzo[f]imidazo[1,5-a][1,4]diazepine-3-carboxylate **5** (8.0 g, 18.1 mmol), methyl boronic acid (5.4 g, 90.4 mmol), tri-basic potassium phosphate (K_3PO_4, 17.2 g, 81.4 mmol), water (1.4 mL, 81.4 mmol), and additional toluene (50 mL) were sequentially introduced into the previous reaction mixture under

an argon atmosphere. The resulting reaction mixture was stirred at 100°C for 12 h, and the progress of the reaction was confirmed by LCMS 2020 (single quadrupole mass analyzer) due to the nearly identical $\mathbf{R_f}$ values of both the reactant and product on TLC (silica gel; neutral alumina; 60% ethyl acetate-hexane). After the completion of the reaction, indicated by the consumption of starting material, the reaction mixture was cooled and exposed to air. It was then passed through a celite pad to eliminate any palladium salts. Following this, the filtrate was combined with water (50 mL) and ethyl acetate (100 mL). The biphasic mixture thus obtained was allowed to separate, with the organic layer being collected and the aqueous layer subjected to extraction (2x30 mL). The combined organic layer was washed with 10% aqueous sodium chloride (NaCl) solution (3x30 mL) and subsequently dried with sodium sulfate (Na_2SO_4). The solvents were removed under reduced pressure, leading to an orange-colored residue. This residue was purified through flash chromatography (silica gel 200 g, 80% EtOAc-hexane). The desired fractions were combined, and solvents were evaporated. The resulting solid residue was dried under vacuum at 45°C for 8 h, to afford compound **27** as an off-white colored powder (4.9 g, 72%). **^{1}H NMR** (500 MHz, DMSO-d6) δ 8.39 (s, 1H), 7.80 (d, *J* = 8.2 Hz, 1H), 7.61 – 7.49 (m, 3H), 7.31 (t, *J* = 7.5 Hz, 1H), 7.20 (t, *J* = 9.4 Hz, 1H), 7.02 (s, 1H), 6.44 (q, *J* = 7.1 Hz, 1H), 4.29 (dd, *J* = 13.7, 6.8 Hz, 2H), 2.29 (s, 3H), 1.30 (t, *J* = 7.1 Hz, 3H), 1.15 (d, *J* = 7.2 Hz, 3H). **^{13}C NMR** (126 MHz, DMSO-d6) δ 163.96 (s), 163.23 (s), 159.86 (d, *J* = 247.4 Hz), 141.41 (s), 137.66 (s), 136.76 (s), 133.36 (s), 132.32 (s), 132.30 (s), 131.76 (s), 130.20 (s), 129.35 (d, *J* = 13.1 Hz), 129.00 (s), 128.28 (s), 125.02 (d, *J* = 2.3 Hz), 123.21 (s), 116.33 (d, *J* = 21.4 Hz), 60.40 (s), 49.76 (s), 20.85 (s), 14.73 (s). **HRMS** (ESI/IT-TOF) *m/z*: [M + H] + Calcd for $C_{22}H_{20}FN_3O_2$ 377.1506; found 377.1504.

4.5.25. Ethyl (*R*)-6-(2'-fluorophenyl)-4-methyl-8-methyl-4H-benzo[f]imidazo[1,5-a][1,4] diazepine-3-carboxylic acid (28)

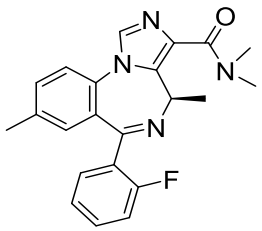


28

The ethyl ester, ethyl (*R*)-6-(2-fluorophenyl)-4-methyl-8-methyl-4H-benzo[f]imidazo[1,5-a][1,4]diazepine-3-carboxylate **27** (3.3 g, 8.7 mmol) was dissolved in ethanol (20 mL), and a solution of NaOH (1.4 g, 34.9 mmol) in water (5 mL) was added dropwise to the solution. The resulting mixture was stirred for 1 hour at 50°C. The completion of the reaction was verified through TLC (silica gel, 100% EtOAc; R_f for DS-II-28 (**27**) = 0.5, R_f for sodium salt of DS-II-29 (**28)**= 0). At the end of the reaction, the mixture was allowed to cool to room temperature. To dilute the mixture, water (20 mL) was introduced, and the pH was adjusted to 4-5 by adding acetic acid (2.75 mL, 48 mmol). After removing ethanol under reduced pressure, the mixture was allowed to stand for 5 h to maximize the precipitation of the solid residue. The resulting solid was filtered, washed with water (4x10 mL), and dried under vacuum. This residue was then subjected to slurry with EtOAc (10 mL) and stirred at 50°C for 10 minutes. Following this, the mixture was cooled to room temperature and held there for 3 h. The solid product was filtered, washed with EtOAc (2x10 mL), and subsequently dried under vacuum at 40°C for 12 h, yielding a white powder of **28** (2.44 g, 80%). **^{1}H NMR** (500 MHz, DMSO) δ 8.31 (s, 1H), 7.78 (d, *J* = 8.2 Hz, 1H), 7.53 (dd, *J* = 15.3, 7.2 Hz, 3H), 7.31 (t, *J* = 7.5 Hz, 1H), 7.23 – 7.17 (m, 1H), 7.00 (s, 1H), 6.56 (q, *J* = 6.8 Hz, 1H), 2.29 (s, 3H), 1.12 (d, *J* = 7.2 Hz, 3H). **^{13}C NMR** (126 MHz, DMSO) δ 165.24 (s), 163.70 (s), 159.86 (d, J = 247.8 Hz), 140.19 (s), 137.31 (s), 135.88 (s),

133.25 (s), 132.60 (s), 132.22 (d, J = 8.0 Hz), 131.76 (s), 130.16 (s), 130.16 (s), 129.51 (d, J = 12.7 Hz), 129.00 (s), 125.00 (d, J = 2.2 Hz), 123.09 (s), 116.32 (d, J = 21.3 Hz), 49.71 (s), 20.85 (s), 14.91 (s).

4.5.26. (*R*)-6-(2'-fluorophenyl)-*N*,*N*,4,8-tetramethyl-4H-benzo[f]imidazo[1,5-a][1,4] diazepine-3-carboxamide (30)

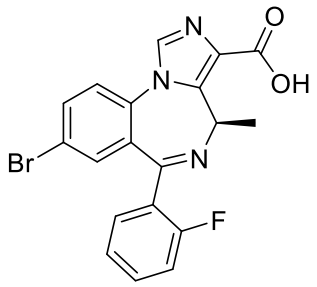


30, DS-II-30

A round bottom flask was charged with ethyl (*R*)-6-(2'-fluorophenyl)-4-methyl-8-methyl-4H-benzo[f]imidazo[1,5-a][1,4] diazepine-3-carboxylic acid **24** (1 g, 2.86 mmol), anhydrous *N*,*N*-dimethylformamide (0.02 mL, 0.28 mmol), anhydrous DCM (20 mL) under an atmosphere of argon and the mixture was stirred to make a solution. The reaction mixture was then heated to 35 to 40 °C. Thionyl chloride (2 mL, 2.8 mmol) was added dropwise to the stirred solution of mixture while maintaining an internal temperature of 35 to 40 °C. and stirred for 1 h at reflux temperature. The completion of reaction was confirmed by TLC (silica gel, 100% EtOAc with 2% TEA). To perform TLC, a test tube was filled with 1 mL of methanol and 1 mL of triethylamine. Then, 0.5 mL of the reaction mixture was added to the test tube. The methyl ester, which resulted was analyzed by TLC. The reaction mixture was cooled at the end of the reaction and the solvents were removed under reduced pressure. The residual thionyl chloride was removed by adding and flash evaporating anhydrous DCM (6 × 10 mL) under vacuum. A yellow-colored residue was obtained. The solid residue was dissolved in anhydrous DCM (20

mL) and the mixture was cooled to 0 °C. A solution of dimethylamine (2 M in THF, 14.3 mL, 28.6 mmol) was added dropwise to the reaction mixture at 0 °C. The mixture was allowed to warm to rt and allowed to stir for 1 h until the consumption of starting material was finished (TLC). The reaction mixture was diluted with aq 10% $NaHCO_3$ (10 mL) and additional DCM (50 mL) was added. The biphasic mixture, which resulted, was allowed to stand 3 min to separate the layers. The organic layer was separated and the aq layer was extracted with DCM (2 × 10 mL). The combined organic layers were washed with aq 10% $NaHCO_3$ solution (1 × 5 mL), aqueous 10% NaCl solution (2 × 10 mL) and dried (Na_2SO_4). After removing the solvents under reduced pressure, the residue was purified by flash chromatography (silica gel, 100% EtOAC with 2% MeOH and 2% TEA). The desired fractions were pooled, and the solvents were evaporated under reduced pressure. The solid was dried under vacuum at 45 °C for 12 h to afford compound **30** as a light, yellow-colored powder (700 mg, 65%). **^{1}H NMR** (500 MHz, $CDCl_3$) δ 7.91 (s, 1H), 7.61 (td, J = 7.5, 1.8 Hz, 1H), 7.46 – 7.40 (m, 3H), 7.24 (td, J = 7.5, 1.0 Hz, 1H), 7.08 (d, J = 9.6 Hz, 1H), 7.05 – 7.00 (m, 1H), 4.31 (q, J = 6.7 Hz, 1H), 3.13 (s, 3H), 3.01 (s, 3H), 2.37 (s, 3H), 1.93 (d, J = 6.8 Hz, 3H). **^{13}C NMR** (126 MHz, $CDCl_3$) δ 166.45 (s), 163.49 (s), 160.25 (d, J = 252.8 Hz), 137.28 (s), 134.81 (s), 133.76 (d, J = 2.1 Hz), 132.77 (s), 132.20 (s), 131.68 (d, J = 7.7 Hz), 131.33 (s), 131.31 (s), 130.26 (s), 128.96 (s), 128.26 (d, J = 12.1 Hz), 124.36 (d, J = 3.4 Hz), 122.46 (s), 116.04 (d, J = 21.5 Hz), 52.20 (s), 39.14 (s), 35.03 (s), 21.01 (s), 18.60 (s). **HRMS** (ESI/IT-TOF) *m/z*: [M + H] + Calcd for $C_{22}H_{20}FN_4O$

4.5.27. (*R*)-8-bromo-6-(2'-fluorophenyl)-4-methyl-4H-benzo[f]imidazo[1,5-a][1,4]diazepine-3-carboxylic acid (29)

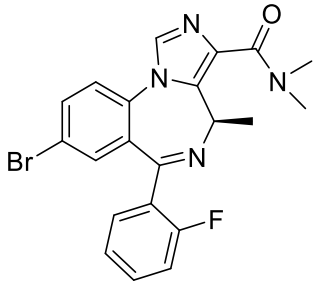


29

A round bottom flask was charged with the ester , ethyl (*R*)-8-bromo-6-(2-fluorophenyl)-4-methyl-4H-benzo[f]imidazo[1,5-a][1,4]diazepine-3-carboxylate **5** (5.0 g, 11.3 mmol), THF (50 mL), and stirred to make a solution. A solution of lithium hydroxide (1.1 g, 45.2 mmol) in water (10 mL) was added dropwise to the reaction mixture over a period of 15 minutes at 25 – 30°C. The reaction mixture was stirred at 50 – 55°C for 1 h. The progress of the reaction was monitored by thin-layer chromatography (TLC) using silica gel TLC plates and a solvent system of 100% ethyl acetate. After the reaction was complete, the mixture was cooled to room temperature (rt) and diluted with water (100 mL). Glacial acetic acid (3.7 mL, 65 mmol) was then added dropwise to the reaction mixture with continuous stirring. This step was performed to break the lithium salt of the carboxylic acid **29**. The THF was removed under reduced pressure which resulted in a semi-solid slurry. To homogenize the mixture, methanol (30 mL) was added to the semi-solid slurry, and the contents were stirred at 40 – 45°C for 30 minutes. Additional water (30 mL) was added to dilute the mixture. The mixture was then allowed to stand at room temperature for 12 h to maximize the precipitation of the product. The solid product was filtered, and the residue was washed with water (4x 15 mL). The residue was then slurried in ethanol, and the slurry was stirred at 50 – 55°C for 30 minutes. The mixture was cooled to room temperature

and placed in a freezer at -20°C overnight. The resulting solid was filtered, washed with cold ethanol (2x5 mL), and dried under vacuum at 45°C for 12 h to afford pure compound **29** as a white powder (3.74 g, 80% yield). **^{1}H NMR** (500 MHz, DMSO-d6) δ 12.83 (s, 1H), 8.43 (s, 1H), 7.92 (dd, J = 25.8, 8.1 Hz, 2H), 7.56 (dd, J = 13.6, 6.5 Hz, 2H), 7.32 (d, J = 7.5 Hz, 2H), 7.23 (t, J = 9.2 Hz, 1H), 6.52 (q, J = 6.8 Hz, 1H), 1.97 (d, J = 20.4 Hz, 1H), 1.17 (d, J = 6.5 Hz, 2H). **^{13}C NMR** (126 MHz, DMSO-d6) δ 164.68 (s), 162.37 (s), 159.85 (d, J = 248.2 Hz), 140.87 (s), 136.64 (s), 135.49 (s), 134.01 (s), 132.73 (d, J = 7.9 Hz), 132.38 (s), 131.93 (s), 130.88 (s), 129.36 (s), 128.68 (d, J = 12.2 Hz), 125.64 (s), 125.18 (s), 120.28 (s), 116.42 (d, J = 21.2 Hz), 49.82 (s), 15.05 (s). **HRMS** (ESI/IT-TOF) m/z: $[M + H]^+$ Calcd for $C_{19}H_{14}BrFN_3O_2$ 414.0248 and 416.0230; found 414.0247 and 416.0242.

4.5.28. *(R)*-8-Bromo-6-(2-fluorophenyl)-*N*,*N*,4-trimethyl-4*H*-benzo[*f*]imidazo[1,5][1,4] diazepine-3-carboxamide [DS-III-97, 31]



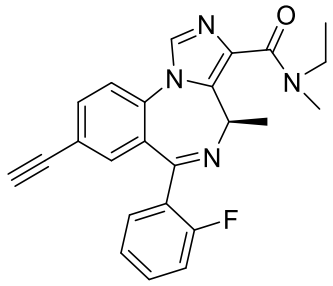
DS-III-97, 16

The acid, (*R*)-8-bromo-6-(2'-fluorophenyl)-4-methyl-4H-benzo[f]imidazo[1,5-a][1,4]diazepine-3-carboxylic acid **29** (3.2 g, 7.7 mmol) was charged in a round bottom flask. A catalytic amount of anhydrous *N*,*N*-dimethylformamide (0.1 mL, 0.77 mmol) and anhydrous DCM (50 mL) were added to the flask and stirred the mixture. An off-white slurry resulted. The mixture was heated to 35 – 40°C under an argon atmosphere. Thionyl chloride (5.6 mL, 77 mmol) was then added dropwise to the reaction mixture over a 5-minute period. During the addition of thionyl chloride,

evolution of sulfur dioxide (SO_2) and hydrogen chloride (HCl) gases was observed. *It's crucial to add thionyl chloride gradually to avoid overflowing of the reaction mixture due to the gas evolution.* The resulting reaction mixture was refluxed for 2 h. The consumption of the starting material was confirmed by thin-layer chromatography (TLC) using silica gel plates and a solvent system of 100% ethyl acetate. For the TLC analysis, a test tube was prepared with 1 mL of methanol and 1 mL of triethylamine (TEA), and 0.5 mL of the reaction mixture was added. The TLC analysis of the methyl ester of **29** was then performed. After the reaction was completed, the reaction mixture was allowed to cool, and the solvents were removed under reduced pressure. To remove residual thionyl chloride, anhydrous DCM was added and removed six times (6x50 mL). The resulting, yellow-colored residue was dissolved in anhydrous DCM (40 mL), and the mixture was cooled to 0°C. A solution of dimethylamine (2M in THF, 23.1 mL, 46.2 mmol) was then added dropwise to the reaction mixture at 0°C. The mixture was allowed to warm to room temperature and stirred for 2 h. At the end of the reaction, the reaction mixture was diluted with a 10% aqueous solution of sodium bicarbonate (30 mL) and additional DCM (30 mL). The biphasic mixture was allowed to stand for 15 minutes to allow the layers to separate. The organic layer was separated, and the aqueous layer was extracted with DCM (2x15 mL). The combined organic layers were washed with a 10% aqueous solution of sodium bicarbonate (1x25 mL), a 10% aqueous solution of sodium chloride (NaCl, 2x20 mL), and dried using sodium sulfate (Na_2SO_4). The solvents were removed under reduced pressure, and the residue was purified using flash chromatography (silica gel) with a solvent system of 100% ethyl acetate containing 5% methanol and 1% triethylamine (TEA). The purified fractions were combined, and the solvents were removed under reduced pressure. The resulting solid residue was dried under vacuum at 45°C for 4 h to yield pure compound **31** as an off-white-colored powder (3.02 g,

88%). **^{1}H NMR** (500 MHz, $CDCl_3$) δ 7.91 (s, 1H), 7.74 (d, J = 8.4 Hz, 1H), 7.62 (dd, J = 10.7, 4.2 Hz, 1H), 7.49 – 7.40 (m, 4H), 7.26 (t, J = 7.5 Hz, 1H), 7.07 – 6.98 (m, 1H), 4.31 (q, J = 6.6 Hz, 1H), 3.12 (s, 3H), 3.00 (s, 3H), 1.93 (d, J = 6.8 Hz, 3H). **^{13}C NMR** (126 MHz, $CDCl_3$) δ 166.09 (s), 162.02 (s), 160.21 (d, J = 251.6 Hz), 135.00 (s), 134.74 (s), 133.75 (s), 132.95 (d, J = 3.1 Hz), 132.74 (s), 132.22 (d, J = 8.3 Hz), 131.31 (s), 131.29 (s), 130.74 (s), 127.42 (d, J = 12.7 Hz), 124.58 (d, J = 3.0 Hz), 124.33 (s), 120.84 (s), 116.20 (d, J = 21.4 Hz), 67.97 (s), 39.09 (s), 35.04 (s), 25.61 (s), 18.47 (s).

4.5.29. *(R)-N*-ethyl-8-ethynyl-6-(2-fluorophenyl)-N,4-dimethyl-4H-benzo[f]imidazo[1,5-a][1,4]diazepine-3-carboxamide (DS-I-49, 32)



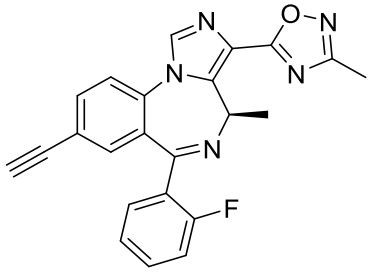
DS-I-49, 32

The acid, (*R*)-8-bromo-6-(2-fluorophenyl)-4-methyl-4H-benzo[f]imidazo[1,5-a][1,4]diazepine-3-carboxylic acid **15** (1.8 g, 5 mmol) was charged in a round bottom flask. A catalytic amount of anhydrous *N*,*N*-dimethylformamide (0.1 mL, 1.1 mmol) and anhydrous DCM (30 mL) were added to the flask and stirred the mixture. An off-white slurry resulted. The mixture was heated to 35 – 40°C under an argon atmosphere. Thionyl chloride (3.6 mL, 50 mmol) was then added dropwise to the reaction mixture over a 30-minute period. The resulting reaction mixture was refluxed for 2 h. The consumption of the starting material was confirmed by thin-layer

chromatography (TLC) using silica gel plates and a solvent system of 100% ethyl acetate. For the TLC analysis, a test tube was prepared with 1 mL of methanol and 1 mL of triethylamine (TEA), and 0.5 mL of the reaction mixture was added. The TLC analysis of the methyl ester of **15** was then performed. After the reaction was completed, the reaction mixture was allowed to cool, and the solvents were removed under reduced pressure. To remove residual thionyl chloride, anhydrous DCM was added and removed six times (6x15 mL). The resulting, yellow-colored residue was dissolved in anhydrous DCM (30 mL), and the mixture was cooled to 0°C. A solution of dimethylamine (2.5 mL, 50 mmol) was then added dropwise to the reaction mixture at 0°C. The mixture was allowed to warm to room temperature and stirred for 2 h. At the end of the reaction, the reaction mixture was diluted with a 10% aqueous solution of sodium bicarbonate (10 mL) and additional DCM (20 mL). The biphasic mixture was allowed to stand for 15 minutes to allow the layers to separate. The organic layer was separated, and the aqueous layer was extracted with DCM (2x15 mL). The combined organic layers were washed with a 10% aqueous solution of sodium bicarbonate (1x 10 mL), a 10% aqueous solution of sodium chloride (NaCl, 2x20 mL), and dried using sodium sulfate (Na_2SO_4). The solvents were removed under reduced pressure, and the residue was purified using flash chromatography (silica gel) with a solvent system of 100% ethyl acetate containing 5% methanol and 1% triethylamine (TEA). The purified fractions were combined, and the solvents were removed under reduced pressure. The resulting solid residue was dried under vacuum at 45°C for 4 h to yield pure compound **32** as an off-white colored powder (1.2 g, 62%). **^{1}H NMR** (500 MHz, $CDCl_3$) δ 7.96 – 7.85 (m, 1H), 7.71 (d, *J* = 8.0 Hz, 1H), 7.62 (t, *J* = 6.5 Hz, 1H), 7.50 (d, *J* = 8.3 Hz, 1H), 7.44 (dd, *J* = 13.2, 6.9 Hz, 2H), 7.25 (t, *J* = 7.5 Hz, 1H), 7.03 (t, *J* = 9.3 Hz, 1H), 4.32 (q, *J* = 5.6 Hz, 1H), 3.23 (dd, *J* = 4.3, 3.3 Hz, 1H), 3.14 (s, 1H), 3.10 (s, 1H), 2.96 (s, 1H), 1.92 (t, *J* = 6.3 Hz,

3H), 1.20 (d, *J* = 1.0 Hz, 3H). **^{13}C NMR** (126 MHz, MeOD) δ 166.56 (s), 163.54 (s), 160.15 (d, *J* = 249.5 Hz), 135.38 (s), 135.04 (d, *J* = 15.5 Hz), 134.23 (s), 133.80 (d, *J* = 23.2 Hz), 133.33 (s), 132.32 (s), 131.13 (s), 128.95 (s), 127.41 (d, *J* = 9.4 Hz), 124.34 (s), 123.35 (s), 121.99 (s), 115.66 (d, *J* = 21.4 Hz), 80.88 (s), 80.13 (s), 51.68 (s), 45.93 (s), 35.56 (s), 31.31 (s), 31.31 (s), 16.92 (s). **HRMS** (ESI/IT-TOF) m/z: $[M + H]^+$ Calcd for $C_{24}H_{21}FN_4O$ 401.1772 and found 401.1759

4.5.30. (*R*)-5-(8-ethynyl-6-(2-fluorophenyl)-4-methyl-4*H*-benzo[*f*]imidazo[1,5-*a*][1,4]diazepin-3-yl)-3-methyl-1,2,4-oxadiazole (34)

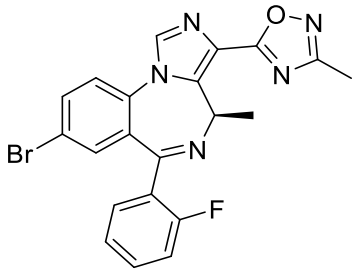


34

The ethyl ester SH-053-2'F-R-CH_3 **7** (1 g, 2.6 mmol) was dissolved in dry THF (30 mL) at room temperature under an argon atmosphere. In a separate flask containing 3Å molecular sieves, *N*-hydroxyacetimidamide (0.91 g, 10 mmol) was dissolved in dry THF (30 mL) under argon and treated with sodium hydride (60% dispersion in mineral oil, 254 mg, 6.5 mmol). After stirring the resulting mixture for 15 minutes, the solution containing compound **7** was added. The reaction mixture was stirred at room temperature for 3 h until the starting material was consumed, as indicated by TLC on silica gel. The reaction was quenched with a saturated aqueous $NaHCO_3$ solution (5 mL). Subsequently, water (50 mL) was added, and the product was extracted with ethyl acetate (3 x 100 mL). The combined organic layers were washed with brine, dried over Na_2SO_4, and the solvent was removed under reduced pressure. The resulting solid was purified by flash chromatography on silica gel, using an EtOAc:hexane ratio of 4:1, yielding pure methyl oxadiazole **34** as a white powder (0.47 g, 45.0%). **^{1}H NMR** (500 MHz, $CDCl_3$)

δ 8.08 (s, 1H), 7.74 (d, J = 8.1 Hz, 1H), 7.62 (t, J = 7.0 Hz, 2H), 7.50 – 7.43 (m, 2H), 7.26 (dd, J = 7.5, 0.8 Hz, 1H), 7.05 (t, J = 9.3 Hz, 1H), 6.75 (q, J = 7.2 Hz, 1H), 3.18 (s, 1H), 2.47 (s, 3H), 1.35 (d, J = 7.3 Hz, 3H). **^{13}C NMR** (126 MHz, $CDCl_3$) δ 170.67 (s), 167.45 (s), 163.68 (s), 160.11 (d, J = 251.2 Hz), 139.13 (s), 136.29 (s), 135.47 (s), 134.20 (s), 132.27 (d, J = 6.1 Hz), 131.27 (s), 129.48 (s), 128.23 (d, J = 4.0 Hz), 125.46 (d, J = 12.7 Hz), 124.94 (s), 124.53 (d, J = 3.3 Hz), 122.21 (s), 121.96 (s), 116.27 (d, J = 18.6 Hz), 81.30 (s), 79.96 (s), 50.09 (s), 14.99 (s), 11.66 (s).

4.5.31. (*R*)-5-(8-ethynyl-6-(2-fluorophenyl)-4-methyl-4*H*-benzo[*f*]imidazo[1,5-*a*][1,4]diazepin-3-yl)-3-methyl-1,2,4-oxadiazole (DS-IV-41, 35)

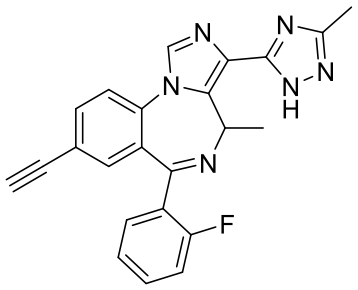


DS-IV-41, 35

The ethyl ester **5** (10 g, 22.6 mmol) was dissolved in dry THF (50 mL) at room temperature under an argon atmosphere. In a separate flask containing 3Å molecular sieves, *N*-hydroxyacetimidamide (6.7 g, 90.4 mmol) was dissolved in dry THF (50 mL) under argon and treated with sodium hydride (60% dispersion in mineral oil, 0.81 g, 33 mmol). After stirring the resulting mixture for 1 h, the solution containing compound **5** was added. The reaction mixture was stirred at room temperature for 3 h until the starting material was consumed, as indicated by TLC on silica gel. The reaction was quenched with a saturated aqueous $NaHCO_3$ solution (50 mL). Subsequently, water (100 mL) was added, and the product was extracted with ethyl acetate (3 x 150 mL). The combined organic layers were washed with brine, dried over Na_2SO_4, and the solvent was removed under reduced pressure. The resulting solid was purified by flash chromatography on silica gel, using an EtOAc:hexane ratio of 4:1, yielding pure methyl

oxadiazole **35** as a white powder (5.72 g, 56.0%). **^{1}H NMR** (500 MHz, $CDCl_3$) δ 8.07 (s, 1H), 7.77 (d, *J* = 8.4 Hz, 1H), 7.63 (t, *J* = 7.1 Hz, 1H), 7.55 (d, *J* = 8.6 Hz, 1H), 7.51 – 7.44 (m, 2H), 7.26 (d, *J* = 7.5 Hz, 1H), 7.06 (t, *J* = 9.3 Hz, 1H), 6.75 (q, *J* = 7.1 Hz, 1H), 2.46 (s, 3H), 1.36 (d, *J* = 7.3 Hz, 3H). **^{13}C NMR** (126 MHz, $CDCl_3$) δ 170.62 (s), 167.45 (s), 163.21 (s), 160.10 (d, *J* = 251.0 Hz), 139.00 (s), 136.25 (s), 135.24 (s), 133.40 (s), 133.34 (s), 132.48 (d, *J* = 7.7 Hz), 131.29 (s), 130.89 (s), 127.91 (d, *J* = 15.2 Hz), 124.96 (s), 124.61 (d, *J* = 3.3 Hz), 123.68 (s), 121.26 (s), 116.29 (d, *J* = 21.4 Hz), 50.08 (s), 15.00 (s), 11.66 (s).

4.5.32. 8-Ethynyl-6-(2-fluorophenyl)-4-methyl-3-(3-methyl-1H-1,2,4-triazol-5-yl)-4H-benzo[f]imidazo[1,5-a][1,4]diazepine (DS-III-69, 36)



DS-III-69, 36

A round bottom flask was charged with racemic SH-2'F-CH_3-053 acid (1 g, 2.7 mmol), formamidine hydrochloride (0.43 g, 5.4 mmol), HATU (3.1 g, 8.4 mmol), *N*,*N*-diisopropylethylamine (1.9 mL, 10.8 mmol), DMF (6.5 mL), and the mixture was stirred for 41 h at an internal temperature 20-25 °C. The progress of the reaction was monitored by LCMS (single quadrupole analyzer). Then methyl hydrazine (2.2 mL, 4.2 mmol) and acetic acid (0.16 mL, 2.7 mmol) were added. The mixture was then heated to 80 °C and stirred for 3 h at that temperature. After that the reaction mixture was cooled to rt and diluted with DCM (200 mL) and saturated aqueous sodium bi-carbonate solution (100 mL). The mixture was stirred for 15 min and allowed to stand to separate layers. The aqueous layer was separated and discarded. The organic layer was washed with 10% aqueous solution of sodium chloride (50 mL) and dried ($MgSO_4$). The solvents were removed under reduced pressure. The residue was purified by silica

gel column chromatography (40% EtOAc-hexane to 70% EtOAc-hexane). The desired fractions were pooled, and the solvents were evaporated under reduced pressure to afford compound **36** as an off-white powder (110 mg, 12%). **^{1}H NMR** (500 MHz, $CDCl_3$) δ 8.00 (t, *J* = 13.5 Hz, 1H), 7.73 (d, *J* = 8.1 Hz, 1H), 7.67 (t, *J* = 7.1 Hz, 1H), 7.60 (d, *J* = 8.3 Hz, 1H), 7.52 – 7.46 (m, 1H), 7.43 (s, 1H), 7.26 (d, *J* = 7.5 Hz, 1H), 7.05 (t, *J* = 9.2 Hz, 1H), 6.88 (q, *J* = 7.1 Hz, 1H), 3.17 (s, 1H), 2.97 (s, 3H), 1.28 (d, *J* = 14.0, 6.9 Hz, 3H). **^{13}C NMR** (126 MHz, $CDCl_3$) δ 164.36 (s), 162.52 (s), 160.13 (d, *J* = 250.7 Hz), 139.43 (s), 135.52 (s), 134.54 (s), 134.24 (s), 133.72 (s), 132.40 (s), 132.34 (s), 131.51 (d, *J* = 1.7 Hz), 130.72 (s), 129.26 (d, *J* = 2.6 Hz), 127.95 (d, *J* = 11.1 Hz), 124.58 (s), 122.33 (s), 121.81 (s), 116.18 (d, *J* = 21.5 Hz), 81.34 (s), 79.85 (s), 49.57 (s), 36.48 (s), 15.01 (s).

4.6. α5 Subtype $GABA_AR$ Modulators and Asthma

4.6.1. Introduction

The Greek term 'asthma,' signifying a condition characterized by shortness of breath, was initially utilized by the ancient Greek poet Homer around 800 BC in his renowned work 'The Iliad' .[299] It wasn't until the era of Hippocrates, an esteemed Greek physician from around 400 BC, that asthma was formally defined in the Corpus Hippocraticum, a collection of his medical writings.[299] This historical context underscores that asthma is far from being a novel ailment; it has existed for centuries. In the contemporary landscape, asthma has evolved into a global concern, impacting over 350 million individuals worldwide .[300] This condition is not confined by age, affecting both the young and elderly populations, with more than 6 million children grappling with its effects. [301] Multiple factors, encompassing genetics, environment, and lifestyle choices, contribute to the increasing prevalence of asthma. Such a multifaceted approach is essential in comprehending and addressing this complex respiratory ailment.

In asthma, a notable phenomenon involves the inflammation and swelling of the airway lining within the lungs during acute episodes. This inflammatory response leads to the production of mucus within the airways, and this mucus production is also observed in the muscles that encircle the airway, contributing to constriction. These combined factors result in reduced airflow and breathing difficulties. Asthma's defining features encompass airway inflammation, obstruction, and hyperresponsiveness.[302] The inflammation leads to a narrowing of the airway lining, causing it to become red, swollen, and constricted. Muscle tightening around the airway contributes to its obstruction, making the inhalation and exhalation of air challenging. Airway hyperresponsiveness causes the muscles surrounding the airway to react more sensitively to

small amounts of allergens and irritants. This heightened sensitivity can trigger rapid responses and exacerbate the condition. Clinical manifestations of asthma include shortness of breath, involuntary wheezing, coughing, increased respiratory rate, and difficulty breathing during both physical activity and rest. Additional symptoms encompass chest or abdominal pain, chest tightness, fatigue, increased heart rate, restlessness, and an inability to partake in sports.

The severity of asthma can escalate during acute episodes, with some individuals experiencing extreme symptoms such as the inability to form coherent sentences and a preference for sitting or leaning forward to alleviate breathing difficulties.[303] Asthma poses a significant impact on individuals' lives, contributing to missed workdays, school absences, doctor visits, emergency room admissions, and even hospitalizations, especially among the younger population.[303-305] Recognized as a major noncommunicable disease by the World Health Organization (WHO), asthma's triggers can vary from person to person. Allergic reactions to environmental allergens like pollen, molds, dust mites, and animal dander are common triggers, some of which may be seasonal. Viral respiratory infections and colds can also induce asthma symptoms, while irritants including tobacco smoke, air pollution, strong odors, and perfumes can exacerbate the condition.[306-308]

Asthma management guidelines often classify the disease based on its severity and aim to control symptoms and address underlying airway inflammation.[30-311] Identifying specific inflammatory patterns may provide valuable insights for individualized asthma management.[312-313] As a chronic condition with multifaceted triggers and implications, understanding the mechanisms and triggers of asthma is crucial for effectively managing and improving the quality of life for those affected.

Gamma-aminobutyric acid type A receptors (GABAARs) are not confined solely to the brain and spinal neurons; they are also present in peripheral tissues and cells, including the liver, heart, and lungs. Emerging evidence suggests that the expression of GABAARs in the lungs is associated with the inhibition of cholinergic outflow.[314-315] This hypothesis points towards a potential mechanism for the muscle-relaxant effects observed in asthma. The presence of GABAARs in the lung introduces a promising avenue for research into the development of alternative treatments for asthma.

Dr. Charles Emala and his research team were pioneers in this field, reporting the functional expression of specific GABAAR subtypes, namely α4, α5, β3, and γ2, in the airway smooth muscle (ASM) of human lungs and guinea pigs (citations not provided). Their studies conducted using organ bath techniques revealed that ASM in precontracted human and guinea pig tracheal rings experienced relaxation upon activation of GABAARs through a β-agonist-regulated mechanism. This activation was linked to enhanced muscle relaxation, thereby suggesting a potential therapeutic avenue for managing asthma symptoms.[316-319]

The α5β3γ2-containing receptors present in the airway smooth muscle (ASM) of the lungs have been targeted for the development of asthma treatments. It's worth noting that while the primary location of α5-GABAAR is the hippocampus, this receptor subtype is also found in other locations within the central nervous system (CNS) as well as in peripheral tissues and cells. This includes the airway smooth muscle (ASM) within the lungs , airway leucocytes like CD4+ T cells[320], airway epithelia [321-322], and alveolar macrophages[323].

The ligand SH-053-2'F-R-CH_3 (**7**), recognized for its α5 subtype selectivity, was subjected to an initial assessment in an ASM relaxation assay.[323] This compound displayed the capability to induce relaxation in precontracted airway smooth muscle, evident in both human ASM strips and guinea pig tracheal rings.[324] However, at a dosage of 200 mg/kg, sedation was observed due to the activation of other benzodiazepine (BZD) receptor subtypes.[237] This outcome was anticipated, given that the original intent behind designing this ligand was to facilitate passage across the blood-brain barrier (BBB) to exert central nervous system (CNS) effects. Notably, this design focus aimed to address conditions such as schizophrenia and major depressive disorder (MDD).[238, 325-326] The ligand's efficacy and side effects prompted the synthesis of a series of structurally similar compounds, including Hz-166, SH-I-048A, SH-053-2'F-R-CH3-acid, MP-III-004, and MP-III-058 (**Figure 30**).

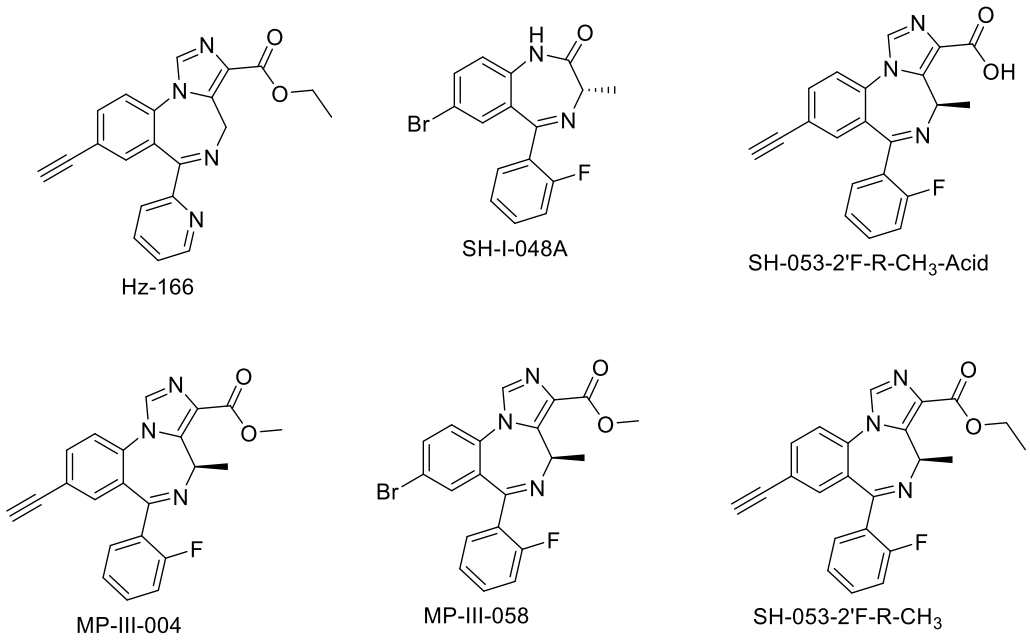


Figure 30. The structures of Hz-166, SH-I-048A, SH-053-2'F-*R*-CH_3-acid, MP-III-004, and MP-III-058, and SH-053-2'F-*R*-CH_3.

The pharmacokinetic (PK) analysis conducted on MP-III-058, MP-III-004, and SH-053-2'F-R-CH3-acid revealed intriguing findings regarding their blood-brain barrier (BBB) penetration capabilities. The ester compounds, MP-III-058 and MP-III-004, were shown to effectively cross the BBB, while the acid form, SH-053-2'F-R-CH_3-acid, demonstrated minimal brain presence, suggesting a lack of central nervous system (CNS) effects. This outcome underscores the distinct pharmacological behavior of these compounds, particularly the absence of CNS-related activity from the acid form.

Among these compounds, SH-053-2'F-R-CH_3 emerges as a promising candidate for further development in asthma treatment due to its potential to induce airway smooth muscle relaxation. A notable observation arises from a comparison between the ASM relaxation effects of MP-III-004 (8-ethinyl methyl ester) and MP-III-058 (8-bromo methyl ester). The 8-bromo analog, MP-III-058, exhibited significantly superior activity compared to its 8-ethinyl counterpart (which was also studied previously). This distinction prompted the exploration of GL-II-93, the 8-bromo carboxylic acid derived from SH-053-2'F-R-CH_3-acid. The intention behind this screening was to identify a compound with optimized airway relaxation effects while avoiding CNS-related side effects. The result of this investigation culminated in the discovery of GL-II-93, the 8-bromo carboxylic acid, which displayed excellent properties as an asthma treatment candidate. Subsequently designated as MIDD0301, this compound emerges as a prime contender for further development in the pursuit of novel and effective treatments for asthma.

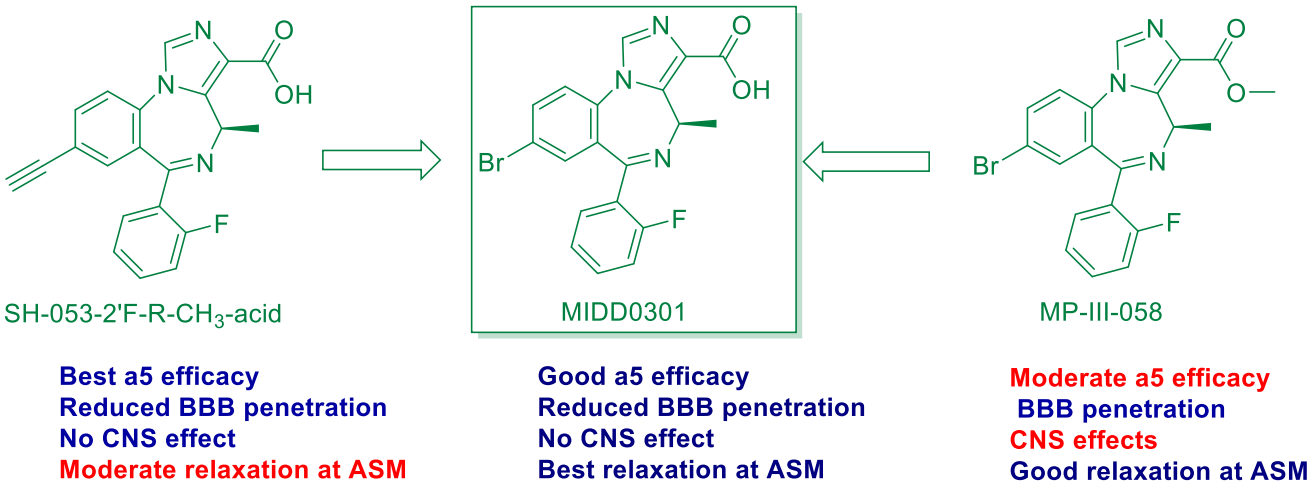


Figure 31. Discovery of GL-II-93 (MIDD0301)

The lead compound, MIDD0301, has demonstrated promising effects both in vitro and in vivo. Its efficacy was observed in relaxing airway smooth muscle (ASM) across human, guinea pig, and mouse models, all of which express distinct GABAARs.[327-328] In vivo studies revealed that MIDD0301 effectively mitigated airway hyperresponsiveness (AHR) in various rodent asthma models when administered orally[327] as well as in nebulized form [327-328]. In a model of ovalbumin-sensitized and challenged mice, MIDD0301 administration at 100 mg/kg orally led to a reduction in eosinophil, CD4+ T cell, and macrophage numbers in the lungs, along with a decrease in airway hyper-responsiveness to methacholine challenge.[327] Moreover, MIDD0301 exhibited the capacity to lower the levels of IL-17A, IL-4, and TNFα in the lungs of these asthmatic mice, indicating its potential anti-inflammatory activity.

MIDD0301 possesses a distinct and pH-dependent structural and bioavailability property.[329] Investigating the therapeutic efficacy of nebulized MIDD0301 revealed significant reductions in airway resistance upon methacholine-induced bronchoconstriction. This effect was evident in ovalbumin and house dust mite allergic asthma models, as well as in normal mice.[328] Notably, in

a steroid-resistant asthma mouse model induced by intratracheal installation of lipopolysaccharide and interferon-gamma, nebulized MIDD0301 demonstrated comparable or superior therapeutic efficacy in reducing airway bronchoconstriction when compared to the marketed drugs nebulized albuterol and oral montelukast.

Crucially, minimal brain exposure was noted even with high doses of nebulized MIDD0301, consistent with prior studies on acids (citation not provided). Furthermore, nebulized MIDD0301, administered at 100 mg/kg, exhibited no adverse cardiovascular effects.[328] These findings collectively highlight the potential of MIDD0301 as a promising candidate for asthma treatment, showcasing its dual benefits of airway relaxation and anti-inflammatory activity, while also addressing concerns regarding adverse effects and central nervous system exposure. Inspired by the promising result of GL-II-93, a number of analogs were synthesized and evaluated in guinea pig model of airway smooth muscle relaxant assay.

4.6.2. Chemistry

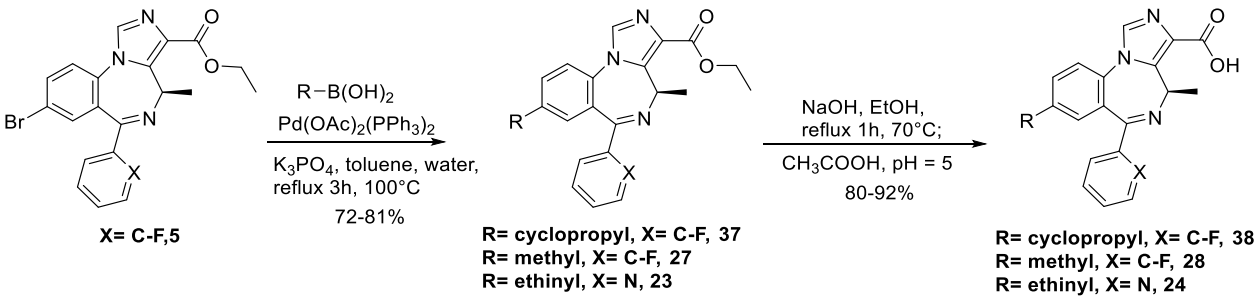
In pursuit of a deeper understanding of the structure-activity relationship (SAR) associated with the lead compound Gl-II-93 for asthma treatment, a comprehensive exploration was undertaken. This involved the design and synthesis of a series of carboxylic acid analogs of MIDD0301.

To optimize the compound's structure for improved therapeutic activity, a deliberate approach was taken to introduce a cyclopropyl group at the C(8) position. This choice was motivated by the fact that the cyclopropyl group possesses a van der Waals radii similar to that of an ethinyl function. This similarity in molecular size prompted the incorporation of the cyclopropyl group at C(8). Importantly, the cyclopropyl group's ability to freely rotate at the C(8) position contributes to a closely aligned electron density map when compared to the ethinyl moiety and

bromine atom. Consequently, this similarity suggests that a C(8)-cyclopropyl group could interact favorably within the binding pocket, akin to an acetylene group. This strategic modification aimed to harness similar interactions in the binding pocket, possibly leading to the desired biological activity. An added advantage of introducing the C(8)-cyclopropyl group is the potential avoidance of reactive metabolite formation, a concern with acetylene or bromine substitutions. Diverse metabolic pathways could prevent the generation of such metabolites. As a result, the C(8)-cyclopropyl analog of MIDD0301 was synthesized based on this hypothesis.

The synthesis process involved the treatment of the aryl-bromide ethyl ester intermediate **5** with cyclopropyl boronic acid in the presence of a palladium catalyst through a Suzuki cross-coupling reaction (**Scheme 17**). This reaction yielded the C(8)-cyclopropyl ethyl ester. Subsequently, the ester at the C(3) position was saponified, resulting in the production of the corresponding carboxylic acid **38**. DS-II-29 (**28**) was also synthesized in a similar way. Another carboxylic acid analog of MIDD0301, DS-I-95 was synthesized from its corresponding ester by saponification (**Scheme 17**)

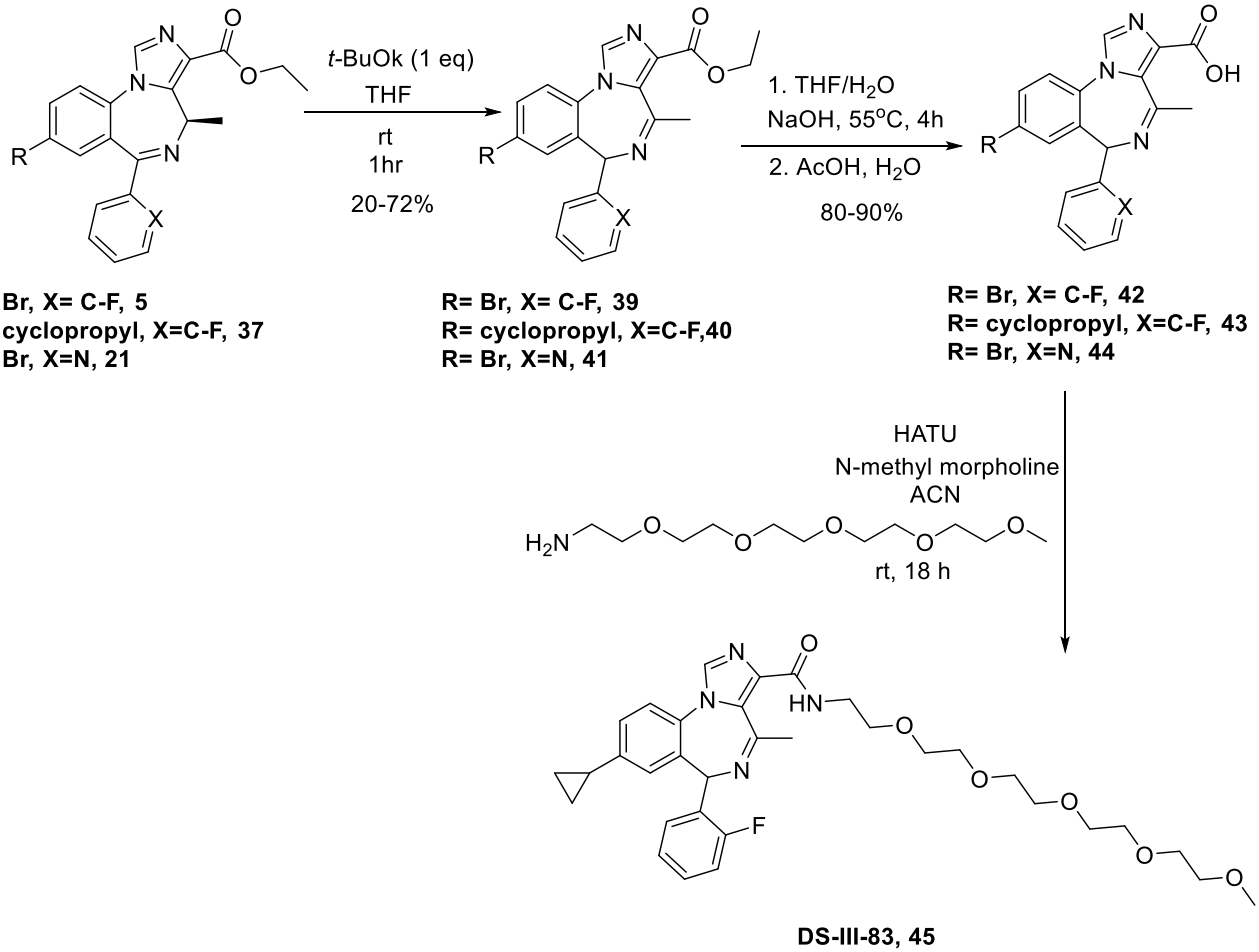
Scheme 17. Synthesis of 8-cyclopropyl carboxylic acid 38



As both *S*-MIDD0301 and *R*-MIDD0301 showed activity in animal model of asthma [330], an imine migrated MIDD0301, MYM-III-100 was constructed to lock the methyl group in fix

position in order to have good activity. Luckily this compound turned as the best compound to date in guinea pig model of airway smooth muscle relaxant assay (unpublished data). Based on this hypothesis several analogs were designed and synthesized. The synthesis of the imine migrated compounds involved treating imidazodiazepines esters with potassium *t*-butoxide, followed by ester hydrolysis, employing a methodology previously described (**Scheme 18**)

Scheme 18. Synthesis of imine migrated analogs of GL-II-93



R= Br, X= C-F, 5
R= cyclopropyl, X=C-F, 37
R= Br, X=N, 21

R= Br, X= C-F, 39
R= cyclopropyl, X=C-F,40
R= Br, X=N, 41

R= Br, X= C-F, 42
R= cyclopropyl, X=C-F, 43
R= Br, X=N, 44

DS-III-83, 45

However, a challenge arose during the synthesis of the imine migrated isomer, particularly for substrates bearing an 8-ethinyl group. The presence of the carboxylic acid and acetylene groups posed an interference during the reaction with potassium t-butoxide, resulting in a low-yield reaction. To enhance the purity of the crude compound, a purification step was implemented using flash chromatography on a silica gel column, with a solvent mixture of 2% methanol and dichloromethane (DCM), supplemented with 0.5% acetic acid. Dr Arnold research group showed that conjugation of MIDD0301 at the carboxyl group can generate amides that retain GABAAR affinity.[183] An imine migrated long chain amide analog of MIDD0301 was synthesized according to the published procedure (**Scheme 17**). [331]

4.6.3. Evaluation of *ex vivo* ASM relaxation of analogs of MIDD0301 with Dr Charles Emala, Gene T. Yocum, and coworkers (unpublished data)

In the pursuit of enhancing the understanding of MIDD0301's structure-activity relationship (SAR), a range of analogs were subjected to investigation using an airway smooth muscle (ASM) relaxation assay. MIDD0301 was employed as a comparator compound in this study. Among all the analogs examined, MYM-III-100 emerged as the most promising candidate based on the assay results (**Figure 31**). The ASM relaxation assay showcased that MYM-III-100 exhibited significant relaxation effects on guinea pig trachea rings constricted by substance P. This relaxation activity was observed when the compound was tested at a concentration of 100 µM in an organ bath setup. Strikingly, MYM-III-100's activity outperformed that of MIDD0301 and the vehicle control, showcasing a notably higher degree of relaxation in comparison to the comparator compound. The compounds **DS-II-19, DS-II-29,** and **DS-I-95** did not produce comparable outcomes in the same assay (**Figure 31 and 32**).

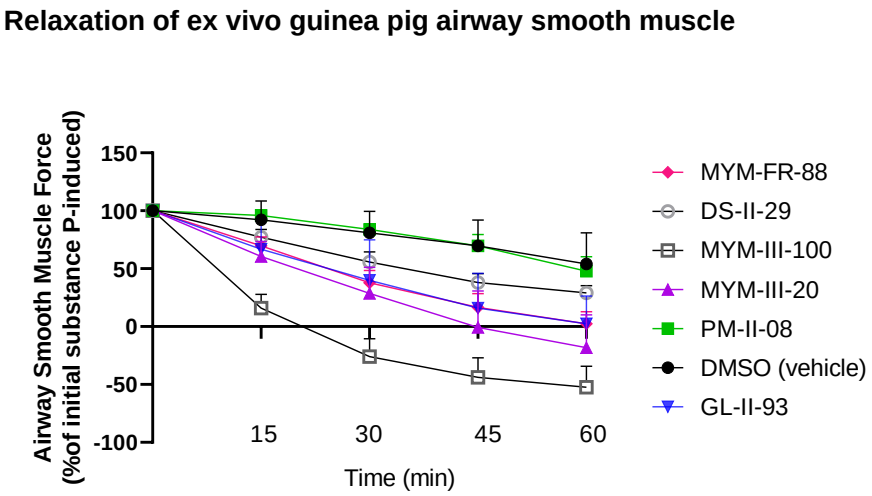


Figure 31: *Ex vivo* smooth muscle force in guinea pig tracheal rings. Rings were pre-contracted with 1 µM substance P and then treated with vehicle (0.1% DMSO) or 100 µM of indicated compounds and resulting relaxation was measured at 15 min, 30 min, 45 min, and 60 min. Data is expressed as the amount of muscle force remaining at indicated time points (n=4-7). Unpublished data (confidential)

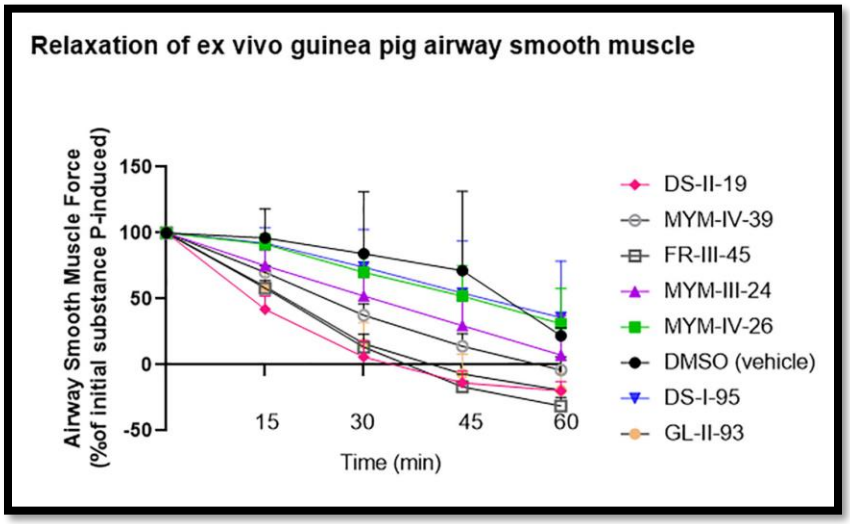


Figure 32: *Ex vivo* smooth muscle force in guinea pig tracheal rings. Rings were pre-contracted with 1 µM substance P and then treated with vehicle (0.1% DMSO) or 100 µM

of indicated compounds and resulting relaxation was measured at 15 min, 30 min, 45 min, and 60 min. Data is expressed as the amount of muscle force remaining at indicated time points (n=3). Unpublished data (confidential). No comparable effects were produced by DS-II-19 and DS-I-95.

The imine migrated 8-cyclopropyl carboxylic acid, DS-II-67 showed little better activity than MIDD0301 (**Figure 33 and Table 7**).

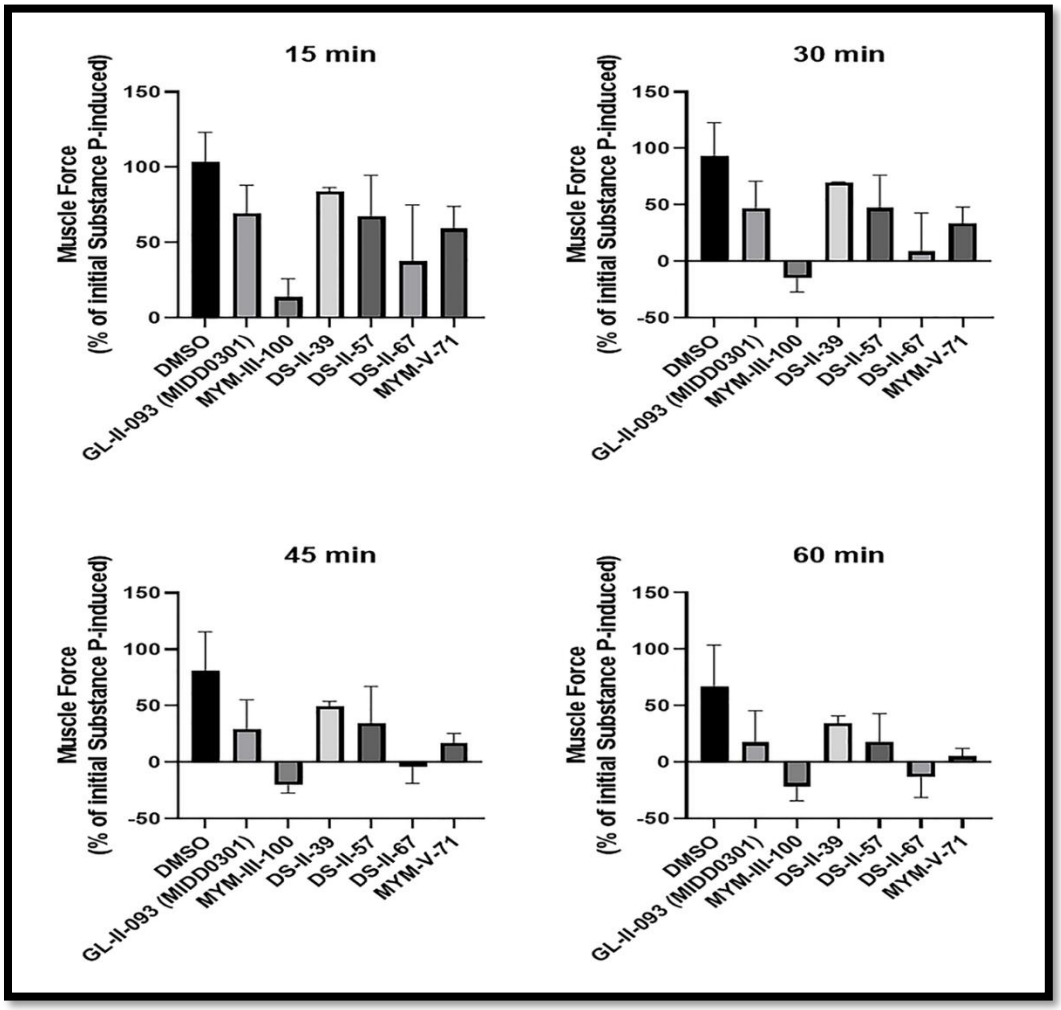
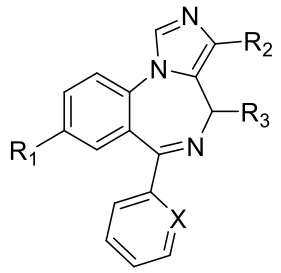


Figure 33. Relaxation of *Ex vivo* guinea pig smooth muscle. Rings were pre-contracted with 1 µM substance P and then treated with vehicle (0.1% DMSO) or 100 µM of indicated compounds and resulting relaxation was measured at 15 min, 30 min, 45 min, and 60 min.

Data is expressed as the amount of muscle force remaining at indicated time points (n=3). DS-II-67 produced comparable activity with MIDD0301.

Table 7: Summary of *ex vivo* ASM relaxation of analogs of MIDD0301. Unpublished data.



Core structure of α5 imidazodiazepines

SL	X	R_1	R_2	R_3	Code	*Ex vivo* relaxation activity
1	C-F	Br	COOH	R-CH_3	MIDD0301	active
2	C-F	≡	COOH	CH_3	DS-II-57 Olefinic migrated	No comparable activity like MIDD0301
3	C-F	CH_3	COOH	R-CH_3	DS-II-19	Not active
4	C-F	▷	COOH	CH_3	DS-II-29	No comparable activity like MIDD0301

5	C-F		COOH	CH_3	DS-II-67 Olefinic migrated	Active, higher than MIDD0301
6	N	Br	COOH	CH_3	DS-II-39 Olefinic migrated	Not active
MIDD0301 was used as a comparator, three compounds showed similar activity profile in relaxation of ASM like MIDD0301, two compounds showed little higher activity, one compound showed much higher activity						

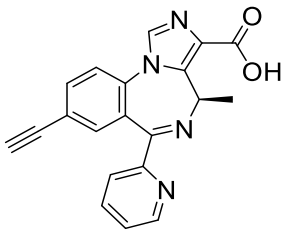
4.6.4. Methods and Experimental

4.6.4.1. Relaxation of *ex vivo* airway smooth muscle with Dr Charles Emala, Gene Yocum and coworkers

The *ex vivo* experiments involving the relaxation of airway smooth muscles were conducted at Columbia University under the supervision of Dr. Emala and her research group. Approval was granted by Columbia University IACUC to carry out the studies on animals, adhering to the necessary methods for the ethical use of laboratory animals. For the experiments, adult male Hartley guinea pigs were selected and euthanized using an intraperitoneal injection of pentobarbital at a dose of 100 mg/kg. Subsequently, the tracheas were extracted and two cartilage rings were isolated after transection. To ensure proper cleansing, the tracheas underwent five rinses with a phosphate buffer (0.5 M, pH 7.4) to eliminate any residual pentobarbital. Following the removal of the epithelium with a cotton swab, the strips were suspended in a 4 mL jacketed organ bath from Radnoti Glass Technology. One strip was affixed

to a stationary hook while the other was connected to an FT-03 force transducer (Grass-Telefactor, West Warwick, RI). Facilitating computer linkage, Acknowledged 7.3.3 software from Biopac Systems (Goleta, CA) was employed to monitor the FT-03 force. The composition of the buffer solution in the organ bath, where the tracheal rings were immersed, consisted of 5.6 mM KCl, 1.3 mM NaH2PO4, 118 mM NaCl, 0.2 mM MgSO4, 0.5 mM CaCl2, 25 mM NaHCO3, and 5.6 mM D-glucose. Additionally, 10 μM indomethacin (with a final concentration of 0.01% DMSO vehicle) was present, and the mixture was maintained at a pH of 7.4 with a continuous supply of 5% CO2 and 95% O2, all at a temperature of 37°C. Prior to commencing the experiments, tracheal rings were equilibrated at 1 g of isotonic tension for one hour, with periodic replenishment of new KH buffer every 15 minutes. The process included precontracting all tracheal rings using 10 μM N-vanillylnonanamide, followed by two cycles of incremental ACh concentrations (ranging from 0.1 to 100 μM). Buffer washes were performed extensively between and after the two cycles at a resting tension of 1.0 g. The influence of airway nerves and histamine receptors was negated using pyrilamine (10 μM) and tetrodotoxin (1 μM). Upon achieving a stable peak contraction line at 1.0 g resting tension, the tracheal ring contraction was initiated using 1 μM of substance P. The experimental compound or vehicle (0.1% DMSO) was introduced into the organ bath mixture once a steady contraction was established. The percentage of the initial contractile force remaining at specific time points was then calculated by comparing it to the percentage of remaining force in tissues exposed to the vehicle after compound exposure.

4.6.4.2. (*R*)-8-Ethynyl-4-methyl-6-(pyridin-2-yl)-4H-benzo[f]imidazo[1,5-a][1,4]diazepine-3-carboxylic acid (24)

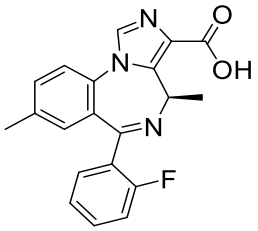


24

The ethyl ester, ethyl (*S*)-8-ethynyl-4-methyl-6-(pyridin-2′-yl)-4H-benzo[f]imidazo [1,5-a][1,4] diazepine-3-carboxylate **23** (12 g, 32.4 mmol) was stirred in ethanol (30 mL) and a slurry resulted. A solution of lithium hydroxide (5.2 g, 129.6 mmol) in water (15 mL) was added dropwise to that mixture at rt. The mixture was then heated to 50 °C and stirred for 1 h while maintaining an internal temperature of 50 °C . The reaction was deemed to be completed on analysis by TLC (silica gel, 100% EtOAc with 2% TEA) after 1 h. The mixture was then allowed to cool to rt, and water (80 mL) was added to dilute the mixture. Then glacial acetic acid (10 mL) was added to adjust the pH to 5 (pH paper). Then ethanol was removed under reduced pressure and a white precipitation formed. *Caution: Addition of too much water or acetic acid needs to be avoided, otherwise the acid will go back into the water solution, and it will be difficult to make it precipitate*. The solid residue was filtered, washed with water (4× 20 mL), and dried under vacuum. The residue was then suspended in 100% EtOAc (50 mL) and stirred for 10 min at 45 °C. The mixture was cooled to rt and held there for 1 h. The solid was filtered, washed (EtOAc, 2 × 10 mL), and dried under vacuum at 50 °C for 8 h to afford a white powder of **24** (10 g, 90%). **^{1}H NMR** (300 MHz, DMSO-d^{6}) δ 8.51 (d, *J* = 4.5 Hz, 1H), 8.38 (s, 1H), 8.00 (d, *J* = 7.4 Hz, 1H), 7.96 (dd, *J* = 7.3, 1.7 Hz, 1H), 7.91 (d, *J* = 3.1 Hz, 1H), 7.88 (s, 1H), 7.80 (d, *J* = 8.2 Hz, 1H), 7.52–7.46 (m, 1H), 7.34 (s, 1H), 6.52 (q, *J* = 7.2 Hz, 1H), 4.34 (s, 1H), 1.16 (d, *J* = 7.2 Hz, 3H). **^{13}C NMR** (126 MHz, DMSO-d^{6}) δ 165.43(s), 164.72 (s), 157.59(s), 148.55 (s), 141.20 (s), 137.54 (s), 136.75 (s), 135.8 (s), 135.45 (s), 134.94 (s), 129.29 (s), 128.08 (s), 125.34 (s), 124.06

(s), 123.80 (s), 120.32 (s), 82.96 (s), 82.08 (s), 49.58 (s), 14.63 (s). **HRMS (ESI/IT-TOF)** *m/z*: [M + H]+ Calcd for $C_{22}H_{18}N_4O_2$ 343.1189; found 343.1211.

4.6.4.11. Ethyl (*R*)-6-(2'-fluorophenyl)-4-methyl-8-methyl-4H-benzo[f]imidazo[1,5-a][1,4] diazepine-3-carboxylic acid (28)

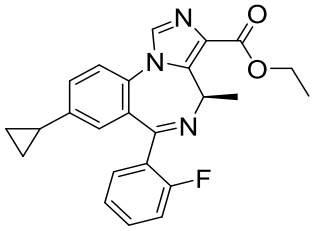


28

The ethyl ester, ethyl (*R*)-6-(2-fluorophenyl)-4-methyl-8-methyl-4H-benzo[f]imidazo[1,5-a][1,4]diazepine-3-carboxylate **27** (3.3 g, 8.7 mmol) was dissolved in ethanol (20 mL), and a solution of NaOH (1.4 g, 34.9 mmol) in water (5 mL) was added dropwise to the solution. The resulting mixture was stirred for 1 hour at 50°C. The completion of the reaction was verified through TLC (silica gel, 100% EtOAc; R_f for DS-II-28 (**27**) = 0.5, R_f for sodium salt of DS-II-29 (**28)**= 0). At the end of the reaction, the mixture was allowed to cool to room temperature. To dilute the mixture, water (20 mL) was introduced, and the pH was adjusted to 4-5 by adding acetic acid (2.75 mL, 48 mmol). After removing ethanol under reduced pressure, the mixture was allowed to stand for 5 h to maximize the precipitation of the solid residue. The resulting solid was filtered, washed with water (4x10 mL), and dried under vacuum. This residue was then subjected to slurry with EtOAc (10 mL) and stirred at 50°C for 10 minutes. Following this, the mixture was cooled to room temperature and held there for 3 h. The solid product was filtered, washed with EtOAc (2x10 mL), and subsequently dried under vacuum at 40°C for 12 h, yielding

a white powder of **28** (2.44 g, 80%). **^{1}H NMR** (500 MHz, DMSO) δ 8.31 (s, 1H), 7.78 (d, *J* = 8.2 Hz, 1H), 7.53 (dd, *J* = 15.3, 7.2 Hz, 3H), 7.31 (t, *J* = 7.5 Hz, 1H), 7.23 – 7.17 (m, 1H), 7.00 (s, 1H), 6.56 (q, *J* = 6.8 Hz, 1H), 2.29 (s, 3H), 1.12 (d, *J* = 7.2 Hz, 3H). **^{13}C NMR** (126 MHz, DMSO) δ 165.24 (s), 163.70 (s), 159.86 (d, J = 247.8 Hz), 140.19 (s), 137.31 (s), 135.88 (s), 133.25 (s), 132.60 (s), 132.22 (d, J = 8.0 Hz), 131.76 (s), 130.16 (s), 130.16 (s), 129.51 (d, J = 12.7 Hz), 129.00 (s), 125.00 (d, J = 2.2 Hz), 123.09 (s), 116.32 (d, J = 21.3 Hz), 49.71 (s), 20.85 (s), 14.91 (s).

4.6.4.12. (*R*)-Ethyl-cyclopropyl-6-(2-fluorophenyl)-4-methyl-4*H*-benzo[*f*]imidazo[1,5-*a*][1,4]diazepine-3-carboxylate (37)

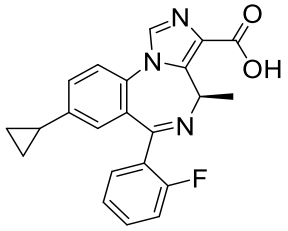


37

Palladium acetate ($Pd(OAc)_2$, 0.17 g, 0.8 mmol) and tri-(*o*-tolyl) phosphine (0.48 g, 1.6 mmol) were dissolved in toluene (50 mL), and the mixture was stirred for 10 minutes under an argon atmosphere to generate the $Pd(OAc)_2$-p-*O*-$(tol)_3$-phosphine catalyst *in situ*. Subsequently, the imidazodiazepine ethyl (*R*)-8-bromo-6-(2-fluorophenyl)-4-methyl-4H-benzo[f]imidazo[1,5-a][1,4]diazepine-3-carboxylate **5** (5.0 g, 11.3 mmol), cyclopropyl boronic acid (2.92 g, 33.9 mmol), tri-basic potassium phosphate (K_3PO_4, 10.78 g, 50 mmol), water (1.0 mL, 50 mmol), and additional toluene (50 mL) were sequentially introduced into the previous reaction mixture under an argon atmosphere. The resulting reaction mixture was stirred at 100°C for 12 h, and the

progress of the reaction was confirmed by LCMS 2020 (single quadrupole mass analyzer) due to the nearly identical $\mathbf{R_f}$ values of both the reactant and product on TLC (silica gel; neutral alumina; 60% ethyl acetate-hexane). After the completion of the reaction, indicated by the consumption of starting material, the reaction mixture was cooled and exposed to air. It was then passed through a celite pad to eliminate any palladium salts. Following this, the filtrate was combined with water (50 mL) and ethyl acetate (100 mL). The biphasic mixture thus obtained was allowed to separate, with the organic layer being collected and the aqueous layer subjected to extraction (2x30 mL). The combined organic layer was washed with 10% aqueous sodium chloride (NaCl) solution (3x30 mL) and subsequently dried with sodium sulfate (Na_2SO_4). The solvents were removed under reduced pressure, leading to an orange-colored residue. This residue was purified through flash chromatography (silica gel 200 g, 80% EtOAc-hexane). The desired fractions were combined, and solvents were evaporated. The resulting solid residue was dried under vacuum at 45°C for 8 h, to afford compound **27** as an off-white colored powder (3.2 g, 70%). **^{1}H NMR** (500 MHz, $CDCl_3$) δ 7.89 (s, 1H), 7.56 (t, *J* = 7.1 Hz, 1H), 7.44 (d, *J* = 8.3 Hz, 1H), 7.42 – 7.32 (m, 1H), 7.19 (dd, *J* = 12.9, 6.1 Hz, 2H), 6.98 (dd, *J* = 18.9, 9.9 Hz, 2H), 6.64 (q, *J* = 7.2 Hz, 1H), 4.55 – 4.14 (m, 2H), 1.92 – 1.73 (m, 1H), 1.38 (t, *J* = 7.1 Hz, 3H), 1.24 (d, *J* = 7.3 Hz, 3H), 1.03 – 0.87 (m, 2H), 0.68 – 0.48 (m, 2H); **^{13}C NMR** (126 MHz, DMSO) δ 164.4 (s), 162.70 (s), 159.86 (d, J = 247.8 Hz), 140.19 (s), 137.31 (s), 135.88 (s), 133.25 (s), 132.72 (s), 132.22 (d, J = 8.0 Hz), 131.78 (s), 130.16 (s), 130.16 (s), 129.51 (d, J = 12.7 Hz), 129.00 (s), 125.00 (d, J = 2.2 Hz), 123.09 (s), 116.32 (d, J = 21.3 Hz), 50.72 (s),15.04 (s), 14.64 (s), 14.44 (s), 9.91 (s), 9.8 (s). **HRMS** (ESI/IT-TOF) m/z: $[M + H]^+$ Calcd for $C_{24}H_{23}FN_3O_2$ 404.1769; found 404.1763.

4.6.4.13. (*R*)-8-cyclopropyl-6-(2-fluorophenyl)-4-methyl-4H-benzo[f]imidazo[1,5-a][1,4] diazepine-3-carboxylic acid (38)

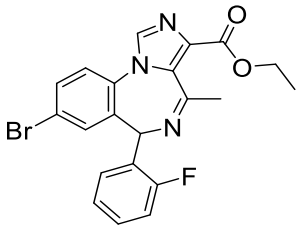


38

The ethyl ester, ethyl (*R*)-6-(2-fluorophenyl)-4-methyl-8-cyclopropyl-4H-benzo[f]imidazo[1,5-a][1,4]diazepine-3-carboxylate **37** (2.7 g, 6.6 mmol) was dissolved in ethanol (20 mL), and a solution of NaOH (0.18 g, 4.45 mmol) in water (5 mL) was added dropwise to the solution. The resulting mixture was stirred for 1 hour at 50°C. The completion of the reaction was verified through TLC (silica gel, 100% EtOAc; R_f for **37** = 0.5, R_f for sodium salt of **38**=0). At the end of the reaction, the mixture was allowed to cool to room temperature. To dilute the mixture, water (20 mL) was introduced, and the pH was adjusted to 4-5 by adding acetic acid (1.78 mL, 5.5 mmol). After removing ethanol under reduced pressure, the mixture was allowed to stand for 5 h to maximize the precipitation of the solid residue. The resulting solid was filtered, washed with water (4x10 mL), and dried under vacuum. This residue was then subjected to slurry with EtOAc (10 mL) and stirred at 50°C for 10 minutes. Following this, the mixture was cooled to room temperature and held there for 3 h. The solid product was filtered, washed with EtOAc (2x10 mL), and subsequently dried under vacuum at 40°C for 12 h, yielding a white powder of **38** (2.1 g, 86%). **^{1}H NMR** (500 MHz, $CDCl_3$) δ 8.01 – 7.98 (m, 1H), 7.63 (s, 1H), 7.51 (d, *J* = 7.9 Hz, 1H), 7.47 – 7.40 (m, 1H), 7.25 (dd, *J* = 13.6, 6.7 Hz, 2H), 7.03 (dd, *J* = 19.1, 10.1 Hz, 2H), 6.73 (q, *J* = 7.2 Hz, 1H), 3.96 (s, 1H), 1.95 – 1.76 (m, *J* = 25.4 Hz, 1H), 1.27 (d, *J* = 3.1

Hz, 3H), 1.02 (d, *J* = 7.8 Hz, 2H), 0.65 (d, *J* = 26.9 Hz, 2H); **HRMS** (ESI/IT-TOF) m/z: [M + H]$^+$ Calcd for $C_{22}H_{19}FN_3O_2$ 376.1456; found 376.1454.

4.6.4.5.Ethyl 8-bromo-6-(2-fluorophenyl)-4-methyl-6H-benzo[f]imidazo[1,5-a][1,4] diazepine -3-carboxylate (39)

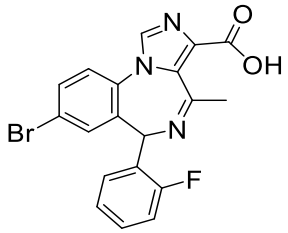


39

A solution containing potassium *t*-butoxide (0.5 g, 5.16 mmol) in THF (10 mL) was gradually added drop by drop to the stirred solution of imidazodiazepine ethyl ester **5** (2 g, 4.52 mmol) at room temperature (rt) over a span of 3 minutes. The resulting solution turned black and was stirred for an additional hour, during which the completion of the reaction was confirmed through TLC analysis using a silica gel plate and a solvent mixture of 60% EtOA-hexane. Once this stage was reached, the reaction was stopped by introducing aqueous solution of 100% $NaHCO_3$, after which the mixture was diluted with 20 mL of ethyl acetate. The layers were separated, and the organic layer was collected. This organic layer was subjected to washing with brine twice (2 x 10 mL) and was subsequently dried using Na_2SO_4.The solvents were evaporated and the residue was purified by a flash chromatography (silica gel, 40% EtOAc-hexane) to afford pure **39** as an off white powder (1.4 g, 70%). **^{1}H NMR** (500 MHz, $CDCl_3$) δ 8.29 (td, *J* = 7.3, 1.6 Hz, 1H), 8.08 (s, 1H), 7.59 (dd, *J* = 8.4, 2.0 Hz, 1H), 7.44 – 7.37 (m, 3H), 7.13 – 7.08 (m, 1H), 6.97 (d, *J* = 1.6 Hz, 1H), 5.47 (s, 1H), 4.47 (q, *J* = 7.1 Hz, 2H), 2.59 (s, 3H), 1.45 (t, *J* = 7.1 Hz, 3H). **^{13}C NMR** (126 MHz, $CDCl_3$) δ 162.3 (s), 160.17 (d, *J* = 246.9 Hz), 159.31 (s), 139.09 (s), 136.50 (s), 132.98 (s), 132.83 (s), 132.39 (s), 132.06 (s), 130.66 (d, *J* = 3.6 Hz), 129.92 (s),

129.75 (d, *J* = 8.2 Hz), 125.49 (d, *J* = 12.6 Hz), 124.67 (d, *J* = 3.3 Hz), 123.72 (s), 123.12 (s), 115.52 (d, *J* = 21.0 Hz), 61.49 (s), 57.94 (d, *J* = 3.2 Hz), 26.05 (s), 14.37 (s). **HRMS (ESI/IT-TOF):** m/z $[M + H]^+$ calcd for $C_{21}H_{18}BrFN_3O_2$: 442.056; found: 442.059.

4.6.4.6. 8-bromo-6-(2-fluorophenyl)-4-methyl-6H-benzo[f]imidazo[1,5-a][1,4]diazepine-3-carboxylic acid (42)

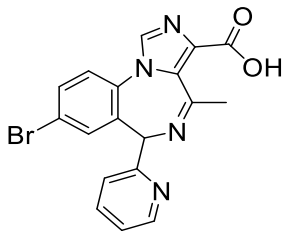


42

The ethyl ester, ethyl 8-bromo-6-(2-fluorophenyl)-4-methyl-6H-benzo[f]imidazo[1,5-a][1,4]diazepine-3-carboxylate **39** (1.2 g, 2.7 mmol), was dissolved in 10 mL of ethanol. A solution of sodium hydroxide (0.4 g, 10.2 mmol) in 4 mL of water was gradually added dropwise to the solution at room temperature (rt). The resulting reaction mixture was then heated to 55°C for 30 min. Verification of the consumption of the starting material was achieved through TLC analysis using a silica gel plate with 100% EtOAc as the solvent. To the mixture, 10 mL of water was added to dilute it, followed by the addition of acetic acid (0.8 mL, 13.2 mmol). Subsequently, the ethanol was removed under reduced pressure. The mixture was left at room temperature for 1 h. The resulting solid residue was filtered, washed with water four times (4 x 6 mL), and dried under vacuum. This solid residue was then mixed with 10 mL of 100% EtOAc and stirred at 55°C for 10 min. The mixture was allowed to cool to room temperature and held at that temperature for 2 h. The final residue was filtered, washed with ethyl acetate twice (2 x 5

mL), and dried under vacuum for 2 h. This process yielded pure acid **42** as an off-white powder (1.0 g, 88% yield).**^{1}H NMR** (500 MHz, DMSO) δ 8.59 (s, 1H), 8.21 (d, J = 25.0 Hz, 1H), 7.83 (dd, J = 30.5, 8.2 Hz, 2H), 7.48 (d, J = 32.4 Hz, 2H), 7.27 (t, J = 17.6 Hz,1H), 6.73 (s, 1H), 5.41 (s, 1H), 2.47 (s, 3H). **HRMS (ESI/IT-TOF):** m/z $[M - H]^-$ calcd for $C_{19}H_{13}BrFN_3O_2$: 412.0102; found: 412.0094.

4.6.4.7. 8-Bromo-4-methyl-6-(pyridin-2'-yl)-6H-benzo[f]imidazo[1,5-a][1,4]diazepine-3-carboxylic acid (44)

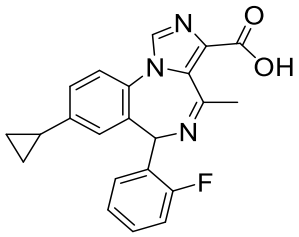


44

The ethyl ester, ethyl 8-bromo-6-(pyridin-2'-yl)-4-methyl-6H-benzo[f]imidazo[1,5-a][1,4]diazepine-3-carboxylate **41** (2.0 g, 5.6 mmol), was dissolved in 10 mL of ethanol. A solution of sodium hydroxide (0.9 g, 22.2 mmol) in 4 mL of water was gradually added dropwise to the solution at room temperature (rt). The resulting reaction mixture was then heated to 55°C for 30 min. Verification of the consumption of the starting material was achieved through TLC analysis using a silica gel plate with 100% EtOAc as the solvent. To the mixture, 10 mL of water was added to dilute it, followed by the addition of acetic acid (1.7 mL, 30.8 mmol). Subsequently, the ethanol was removed under reduced pressure. The mixture was left at room temperature for 1 h. The resulting solid residue was filtered, washed with water four times (4 x 6 mL), and dried under vacuum. This solid residue was then mixed with 10 mL of 100% EtOAc

and stirred at 55°C for 10 min. The mixture was allowed to cool to room temperature and held at that temperature for 2 h. The final residue was filtered, washed with ethyl acetate twice (2 x 5 mL), and dried under vacuum for 2 h. This process yielded pure acid **44** as an off-white powder (1.6 g, 86% yield). ^{1}H NMR (500 MHz, DMSO) δ 8.48 (s, 1H), 8.20 (t, J = 6.9 Hz, 1H), 7.66 (d, J = 8.1 Hz, 1H), 7.51 (dt, J = 18.0, 6.6 Hz, 1H), 7.47 – 7.40 (m, 1H), 7.26 (t, J = 7.0 Hz, 1H), 7.14 (d, J = 7.6 Hz, 1H), 6.98 (dd, J = 14.0, 7.0 Hz, 1H), 6.39 (s, 1H), 2.38 (s, 3H), 1.85 – 1.73 (m, 1H), 0.89 (d, J = 8.4 Hz, 2H), 0.48 (dd, J = 13.5, 8.5 Hz, 2H). **HRMS (ESI/IT-TOF):** m/z $[M - H]^-$ calcd for $C_{21}H_{16}BrN_4O_2$: 328.3302; found

4.6.4.8. 8-cyclopropyl-6-(2-fluorophenyl)-4-methyl-6H-benzo[f]imidazo[1,5-a][1,4]diazepine-3-carboxylic acid (43)

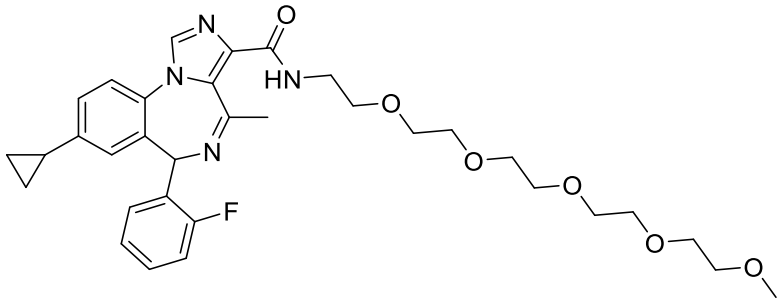


DS-II-67, 43

The ethyl ester, ethyl 8-bromo-6-(2'-fluorophenyl)-4-methyl-6H-benzo[f]imidazo[1,5-a][1,4]diazepine-3-carboxylate **40** (2.0 g, 4.9 mmol), was dissolved in 10 mL of ethanol. A solution of sodium hydroxide (0.8 g, 19.8 mmol) in 4 mL of water was gradually added dropwise to the solution at room temperature (rt). The resulting reaction mixture was then heated to 55°C for 30 min. Verification of the consumption of the starting material was achieved through TLC analysis using a silica gel plate with 100% EtOAc as the solvent. To the mixture, 10 mL of water was added to dilute it, followed by the addition of acetic acid (1.6 mL, 27.2 mmol). Subsequently, the ethanol was removed under reduced pressure. The mixture was left at room temperature for 1 h. The resulting solid residue was filtered, washed with water four times (4 x 6

mL), and dried under vacuum. This solid residue was then mixed with 10 mL of 100% EtOAc and stirred at 55°C for 10 min. The mixture was allowed to cool to room temperature and held at that temperature for 2 h. The final residue was filtered, washed with ethyl acetate twice (2 x 5 mL), and dried under vacuum for 2 h. This process yielded pure acid **DS-II-67 (43)** as an off-white powder (1.5 g, 82% yield). ^{1}H NMR (500 MHz, DMSO) δ 8.48 (s, 1H), 8.20 (t, *J* = 6.9 Hz, 1H), 7.66 (d, *J* = 8.1 Hz, 1H), 7.51 (dt, *J* = 18.0, 6.6 Hz, 1H), 7.47 – 7.40 (m, 1H), 7.26 (t, *J* = 7.0 Hz, 1H), 7.14 (d, *J* = 7.6 Hz, 1H), 6.98 (dd, *J* = 14.0, 7.0 Hz, 1H), 6.39 (s, 1H), 2.38 (s, 3H), 1.85 – 1.73 (m, 1H), 0.89 (d, *J* = 8.4 Hz, 2H), 0.48 (dd, *J* = 13.5, 8.5 Hz, 2H). **^{13}C NMR** (126 MHz, DMSO-d6) δ 164.62 (s), 160.19 (d, *J* = 245.2 Hz), 159.76 (s), 144.75 (s), 142.91 (s), 142.86 (s), 132.67 (s), 132.43 (d, *J* = 8.4 Hz), 131.89 (s), 131.31 (s), 130.99 (s), 130.51 (s), 130.15 (d, *J* = 6.1 Hz), 126.30 (d, *J* = 12.4 Hz), 125.57 (s), 125.11 (s), 123.72 (s), 123.36 (s), 115.82 (d, *J* = 21.0 Hz), 58.25 (s), 21.78 (s), 15.09 (s), 10.28 (s), 10.09 (s). **HRMS** (ESI/IT-TOF) m/z: $[M + H]^+$ Calcd for $C_{22}H_{19}FN_3O_2$ 376.1456; found 376.1455.

4.6.5.7.**8-cyclopropyl-6-(2'-fluorophenyl)-N-(2,5,8,11,14-pentaoxahexadecan-16-yl)-4-methyl-6H-benzo[f]imidazo[1,5-a][1,4]diazepine-3-carboxamide** (**45**)



DS-III-83, 45

A round bottom flask was charged with **43** (200 mg, 0.53 mmol), HATU (222 mg, 0.58 mmol), and *N*-methylmorpholine (0.23 mL, 2.0 mmol) were stirred in dry acetonitrile (6 mL) under

nitrogen at room temperature for 10 min, resulting in an almost clear solution. 2,5,8,11,14-Pentaoxahexadecan-16-amine (140 mg, 0.5 mmol) was added, and stirring was continued for 18 h. The solvent was removed under reduced pressure and the residue was dissolved in chloroform (15 mL) and treated with a saturated solution of ammonium chloride (10 mL, pH 7.0). After separation, the aqueous layer was again extracted with chloroform (15 mL). The combined organic layers were washed with brine and dried over MgSO4. The residue was purified by column chromatography with a gradient of EtOAc. The product was obtained as a viscous oil (199 mg, 60%). **^{1}H NMR** (500 MHz, $CDCl_3$) δ 8.26 (t, *J* = 6.4 Hz, 1H), 7.96 (s, 1H), 7.82 (s, 1H), 7.34 (dd, *J* = 14.4, 7.6 Hz, 3H), 7.04 (dd, *J* = 17.0, 8.4 Hz, 2H), 6.52 (s, 1H), 5.45 (s, 1H), 3.69 – 3.62 (m, 18H), 3.55 – 3.52 (m, 2H), 3.35 (s, 3H), 2.63 (s, 3H), 1.75 (dd, *J* = 10.9, 6.4 Hz, 1H), 0.89 (d, *J* = 8.2 Hz, 2H), 0.53 (dd, *J* = 16.8, 4.6 Hz, 2H). **^{13}C NMR** (126 MHz, $CDCl_3$) δ 162.25 (s), 161.17 (s), 159.45 (d, *J* = 61.9 Hz), 145.18 (s), 136.94 (s), 135.52 (s), 135.21 (s), 131.50 (s), 130.84 (d, *J* = 3.5 Hz), 129.80 (s), 129.24 (d, *J* = 8.1 Hz), 126.41 (d, *J* = 12.6 Hz), 125.24 (s), 124.37 (d, *J* = 2.9 Hz), 124.18 (s), 122.12 (s), 115.17 (d, *J* = 21.2 Hz), 71.77 (s), 70.40 (s), 70.38 (s), 70.29 (s), 70.20 (s), 58.95 (s), 58.15 (s), 38.99 (s), 29.67 (s), 26.28 (s), 15.18 (s), 9.76 (s).

References

1. Watanabe, M.; Maemura, K.; Kanbara, K.; Tamayama, T.; Hayasaki, H. GABA and GABA receptors in the central nervous system and other organs. In *Int. Rev. Cytol.*, Jeon, K. W., Ed. Academic Press: **2002**; Vol. 213, pp 1-47.
2. Sieghart, W. Structure and pharmacology of gamma-aminobutyric acid A receptor subtypes. *Pharmacol. Rev.* **1995,** *47* (2), 181.
3. Twyman, R. E.; Rogers, C. J.; Macdonald, R. L., Differential regulation of gamma-aminobutyric acid receptor channels by diazepam and phenobarbital. *Ann. Neurol.* **1989,** *25* (3), 213-20.
4. Hyland, N. P.; Cryan, J. F., A gut feeling about gaba: focus on GABA(B) receptors. *Front. Pharmacol.* **2010,** *1*, 124-124.
5. Luscher, B.; Shen, Q.; Sahir, N., The GABAergic deficit hypothesis of major depressive disorder. *Mol. Psychiatry* **2011,** *16* (4), 383-406.
6. Guidotti, A.; Auta, J.; Davis, J. M.; Dong, E.; Grayson, D. R.; Veldic, M.; Zhang, X.; Costa, E., GABAergic dysfunction in schizophrenia: new treatment strategies on the horizon. *Psychopharmacology (Berl.)* **2005,** *180* (2), 191-205.
7. Sieghart, W.; Ernst, M., Heterogeneity of GABAA receptors: revived interest in the development of subtype-selective drugs. *Current Medicinal Chemistry - Central Nervous System Agents* **2005,** *5* (3), 217-242.
8. Otani, K.; Ujike, H.; Tanaka, Y.; Morita, Y.; Katsu, T.; Nomura, A.; Uchida, N.; Hamamura, T.; Fujiwara, Y.; Kuroda, S. The GABA type A receptor alpha 5 subunit gene is associated with bipolar I disorder. Neuroscience Letters 2005, 381, 108 - 113.

9. Dean, B.; Scarr, E.; McLeod, M. Changes in hippocampal GABA(A) receptor subunit composition in bipolar I disorder. Brain Res. Mol. Brain Res. 2005, 138, 145 - 155.
10. Bowser, D. N.; Wagner, D. A.; Czajkowski, C.; Cromer, B. A.; Parker, M. W.; Wallace, R. H.; Harkin, L. A.; Mulley, J. C.; Marini, C.; Berkovic, S. F.; Williams, D. A.; Jones, M. V.; Petrou, S., Altered kinetics and benzodiazepine sensitivity of a GABAA receptor subunit mutation [gamma 2(R43Q)] found in human epilepsy. *Proc. Natl. Acad. Sci. U. S. A.* **2002,** *99* (23), 15170-5.
11. Munro, G.; Hansen, R. R.; Mirza, N. R., GABAA receptor modulation: Potential to deliver novel pain medicines? *Eur. J. Pharmacol.* **2013,** *716* (1), 17-23.
12. Maubach, K. GABA(A) receptor subtype selective cognition enhancers. *Drug Targets-CNS & Neuro. Disorders*, **2003**, 233 - 239.
13. Simon, J.; Wakimoto, H.; Fujita, N.; Lalande, M.; Barnard, E. A. Analysis of the set of GABAA receptor genes in the human genome. *J. Biol. Chem.* **2004**, 279, 41422 - 41435.
14. Olsen, R. W.; Sieghart, W. GABAA receptors: Subtypes provide diversity of function and pharmacology. *Neuropharmacology* **2009**, 56, 141 - 148.
15. Sieghart, W.; Sperk, G. Subunit composition, distribution and function of GABAA receptor subtypes. *Curr. Topics Med. Chem.* **2002**, 2, 785 - 816.
16. Olsen, R. W.; Tobin, A. J. Molecular biology of GABAA receptors. *FASEB J.* **1990**, 4, 1469 - 1480.
17. Wisden, W.; Laurie, D. J.; Monyer, H.; Seeburg, P. H., The distribution of 13 GABAA receptor subunit mRNAs in the rat brain. I. Telencephalon, diencephalon, mesencephalon. *J. Neurosci.* **1992,** *12* (3), 1040-62.

18. Fritschy, J. M.; Mohler, H., GABAA-receptor heterogeneity in the adult rat brain: differential regional and cellular distribution of seven major subunits. *J. Comp. Neurol.* **1995,** *359* (1), 154-94.
19. Nutt, D., GABAA receptors: subtypes, regional distribution, and function. *J. Clin. Sleep Med.* **2006,** *2* (2), S7-11.
20. Pirker, S.; Schwarzer, C.; Wieselthaler, A.; Sieghart, W.; Sperk, G., GABA(A) receptors: immunocytochemical distribution of 13 subunits in the adult rat brain. *Neuroscience* **2000,** *101* (4), 815-50.
21. Burt, D. R.; Kamatchi, G. L. GABAA receptor subtypes: from pharmacology to molecular biology. *FASEB J.* **1991**, 5, 2916 - 2923.
22. Clayton, T.; Chen, J. L.; Ernst, M.; Richter, L.; Cromer, B. A.; Morton, C. J.; Ng, H.; Kaczorowski, C. C.; Helmstetter, F. J.; Furtmuller, R.; Ecker, G.; Parker, M. W.; Sieghart, W.; Cook, J. M. An updated unified pharmacophore model of the benzodiazepine binding site on g-aminobutyric acida receptors: Correlation with comparative models. *Curr. Med. Chem.* **2007**, 14, 2755 – 2775
23. Keramidas, A.; Moorhouse, A.; Schofield, P. C.; Barry, P. Ligand-gated ion channels: mechanisms underlying ion selectivity. *Prog. Biophys. Mol. Biol*. **2004**, 86, 161 - 204.
24. MacDonald, R. L. Benzodiazepine mechanisms of action. In Antiepileptic Drugs, Levy, R. H.; Mattson, R. H.; Meldrum, B. S.; Perucca, E., Eds. *Lippincott Williams and Wilkins: Philadelphia*, **2002**; pp 179 - 186.
25. Sigel, E.; Luscher, B. P. A closer look at the high affinity benzodiazepine binding site on GABA(A) receptors. *Curr. Topics Med. Chem*. **2011**, 11, 241 - 246.

26. Ramerstorfer, J.; Furtmuller, R.; Sarto-Jackson, I.; Varagic, Z.; Sieghart, W.; Ernst, M. The GABAA receptor a+b- interface: A novel target for subtype selective drugs. *J. Neurosci.* **2011**, 31, 870 - 877.
27. Varagic, Z.; Ramerstorfer, J.; Huang, S.; Rallapalli, S.; Sarto-Jackson, I.; Cook, J.; Sieghart, W.; Ernst, M. Subtype selectivity of a+b- site ligands of GABAA receptors: identification of the first highly specific positive modulators at a6b2/3g2 receptors *Br. J. Pharmacol.* **2013,** 169, 384 - 399.
28. Sigel, E. Mapping of the benzodiazepine recognition site of GABAA receptors. *Curr. Topics Med. Chem*. **2002**, 2, 833-839.
29. Belelli, D.; Lambert, J. J. Neurosteriods: endogenous regulators of the GABA(A) receptor. *Nat. Rev. Neurosci.* **2005**, 6, 565 - 575.
30. Harris, R. A. Ethanol actions on multiple ion channels: which are important? *Alcohol Clin. Exp. Res.* **1999**, 23, 1563 - 1570.
31. Lobo, I. A.; Harris, R. A. GABAA receptors and alcohol. *Pharmacol. Biochem. Behav*. **2008**, 90, 90 - 94.
32. Olsen, R. W.; Hanchar, H. J.; Meera, P.; Wallner, M. GABAA receptor subtypes: the "one glass of wine" receptors. *Alcohol* **2007**, 41, 201 - 209.
33. Sawyer, E.; Moran, C.; Sirbu, M. H.; Szafir, M.; Van Linn, M.; Namjoshi, O.; Tiruveedhula, V. V. N. P. B.; Cook, J. M.; Platt, D. M. Little evidence of a role for the a1 GABAA subunit-containing receptor in rhesus monkey model of alcohol drinking. *Alcohol Clin. Exp. Res*. **2014**, 38, 1108 - 1117.
34. Ernst, M.; Brauchart, D.; Boresch, S.; Sieghart, W. Comparative modeling of GABAA receptors: Limits, insights, future developments. *Neurosci.* **2003**, 119, 933 - 943.

35. Haefely, W., The biological basis of benzodiazepine actions. *J. Psychoactive Drugs* **1983,** *15* (1-2), 19-39.
36. Haefely, W.; Facklam, M.; Schoch, P.; Martin, J. R.; Bonetti, E. P.; Moreau, J. L.; Jenck, F.; Richards, J. G., Partial agonists of benzodiazepine receptors for the treatment of epilepsy, sleep, and anxiety disorders. *Advances in biochemical psychopharmacology* **1992,** *47*, 379-394.
37. Garattini, S.; Mussini, E.; Marucci, F.; Guaitani, A., Metabolic studies on benzodiazepines in various animal species. In *The Benzodiazepines*, Garattini, S.; Mussini, E.; Randall, L. O., Eds. Raven Press: New York, 1973; pp 75 - 97.
38. Rutherford, D. M.; Okoko, A.; Tyrer, P. J., Plasma concentrations of diazepam and desmethyldiazepam during chronic diazepam therapy. *Br. J. Clin. Pharmacol.* **1978,** *1978* (6).
39. Bond, A. J.; Hailey, D. M.; Lader, M. H., Plasma concentrations of benzodiazepines. *Br. J. Clin. Pharmacol.* **1977,** *4*, 51 - 56.
40. Moss, G. P., Nomenclature of fused and bridged fused ring systems (IUPAC Recommendations 1998). In *Pure Appl. Chem.*, **1998**; Vol. 70, p 143.
41. Killam, E. K.; Suria, A. Benzodiazepines. In Antiepileptic Drugs: Mechanisms of Action, Glaser, G. H.; Penry, J. K.; Woodbury, D. M., *Eds. Raven Press: New York*, **1980**; pp 597 - 615.
42. Rogawski, M. A. Principles of antiepileptic drug action. In Antiepileptic Drugs, 5th ed.; Levy, R. H.; Mattson, R. H.; Meldrum, B. S.; Perucca, E., Eds. *Lippincott Williams and Wilkins: Philadelphia*, **2002**; pp 3 - 22.

43. Vicini, S.; Ferguson, C.; Prybylowski, K.; Kralic, J.; Morrow, A. L.; Homanics, G. E. GABAA receptor a1 subunit deletion prevents developmental changes of inhibitory synaptic currents in cerebellar neurons. *J. Neurosci*. **2001**, 21, 3009 – 3016

44. Sur, C.; Wafford, K. A.; Reynolds, D. S.; Hadingham, K. L.; Bromidge, F.; Macaulay, A.; Collinson, N.; O'Meara, G.; Howell, O.; Newman, R.; Myers, J.; Atack, J. R.; Dawson, G. R.; McKernan, R. M.; Whiting, P. J.; Rosahl, T. W. Loss of the major GABAA receptor subtype in the brain is not lethal in mice. *J. Neurosci*. **2001**, 21, 3409 - 3418.

45. Rudolph, U.; Crestani, F.; Benke, D.; Brunig, I.; Benson, J. A.; Fritschy, J. M.; Martin, J. R.; Bluethmann, H.; Mohler, H., Benzodiazepine actions mediated by specific gamma-aminobutyric acid(A) receptor subtypes. *Nature* **1999,** *401* (6755), 796-800.

46. McKernan, R. M.; Rosahl, T. W.; Reynolds, D. S.; Sur, C.; Wafford, K. A.; Atack, J. R.; Farrar, S.; Myers, J.; Cook, G.; Ferris, P.; Garrett, L.; Bristow, L.; Marshall, G.; Macaulay, A.; Brown, N.; Howell, O.; Moore, K. W.; Carling, R. W.; Street, L. J.; Castro, J. L.; Ragan, C. I.; Dawson, G. R.; Whiting, P. J., Sedative but not anxiolytic properties of benzodiazepines are mediated by the GABAA receptor α1 subtype. *Nat. Neurosci.* **2000,** *3*, 587.

47. Low, K.; Crestani, F.; Keist, R.; Benke, D.; Brunig, I.; Benson, J. A.; Fritschy, J. M.; Rulicke, T.; Bluethmann, H.; Mohler, H.; Rudolph, U., Molecular and neuronal substrate for the selective attenuation of anxiety. *Science* **2000,** *290* (5489), 131-4.

48. Morris, H. V.; Dawson, G. R.; Reynolds, D. S.; Atack, J. R.; Stephens, D. N., Both alpha2 and alpha3 GABAA receptor subtypes mediate the anxiolytic properties of

benzodiazepine site ligands in the conditioned emotional response paradigm. *Eur. J. Neurosci.* **2006,** *23* (9), 2495-504.

49. Paul, J.; Yévenes, G. E.; Benke, D.; Di Lio, A.; Ralvenius, W. T.; Witschi, R.; Scheurer, L.; Cook, J. M.; Rudolph, U.; Fritschy, J.-M.; Zeilhofer, H. U., Antihyperalgesia by α2-GABAA receptors occurs via a genuine spinal action and does not involve supraspinal sites. *Neuropsychopharmacology : official publication of the American College of Neuropsychopharmacology* **2014,** *39* (2), 477-487.
50. Ralvenius, W. T.; Benke, D.; Acuna, M. A.; Rudolph, U.; Zeilhofer, H. U., Analgesia and unwanted benzodiazepine effects in point-mutated mice expressing only one benzodiazepine-sensitive GABAA receptor subtype. *Nature communications* **2015,** *6*, 6803.
51. Dias, R.; Sheppard, W. F.; Fradley, R. L.; Garrett, E. M.; Stanley, J. L.; Tye, S. J.; Goodacre, S.; Lincoln, R. J.; Cook, S. M.; Conley, R.; Hallett, D.; Humphries, A. C.; Thompson, S. A.; Wafford, K. A.; Street, L. J.; Castro, J. L.; Whiting, P. J.; Rosahl, T. W.; Atack, J. R.; McKernan, R. M.; Dawson, G. R.; Reynolds, D. S., Evidence for a significant role of alpha 3-containing GABAA receptors in mediating the anxiolytic effects of benzodiazepines. *J. Neurosci.* **2005,** *25* (46), 10682-8.
52. Yee, B. K.; Keist, R.; von Boehmer, L.; Studer, R.; Benke, D.; Hagenbuch, N.; Dong, Y.; Malenka, R. C.; Fritschy, J. M.; Bluethmann, H.; Feldon, J.; Möhler, H.; Rudolph, U., A schizophrenia-related sensorimotor deficit links α3-containing GABAA receptors to a dopamine hyperfunction. *Proc. Natl. Acad. Sci. U. S. A.* **2005,** *102* (47), 17154.
53. Gallos, G.; Yim, P.; Chang, S.; Zhang, Y.; Xu, D.; Cook, J. M.; Gerthoffer, W. T.; Emala, C. W., Sr., Targeting the restricted alpha-subunit repertoire of airway smooth

muscle GABAA receptors augments airway smooth muscle relaxation. *Am. J. Physiol. Lung Cell Mol. Physiol.* **2012,** *302* (2), L248-56.

54. Collinson, N.; Kuenzi, F. M.; Jarolimek, W.; Maubach, K. A.; Cothliff, R.; Sur, C.; Smith, A.; Otu, F. M.; Howell, O.; Atack, J. R.; McKernan, R. M.; Seabrook, G. R.; Dawson, G. R.; Whiting, P. J.; Rosahl, T. W., Enhanced learning and memory and altered GABAergic synaptic transmission in mice lacking the alpha 5 subunit of the GABAA receptor. *J. Neurosci.* **2002,** *22* (13), 5572-80.
55. Crestani, F.; Keist, R.; Fritschy, J. M.; Benke, D.; Vogt, K.; Prut, L.; Blüthmann, H.; Möhler, H.; Rudolph, U., Trace fear conditioning involves hippocampal alpha5 GABA(A) receptors. *Proc. Natl. Acad. Sci. U. S. A.* **2002,** *99* (13), 8980-8985.
56. Yang, W.; Drewe, J. A.; Lan, N. C., Cloning and characterization of the human GABAA receptor alpha 4 subunit: identification of a unique diazepam-insensitive binding site. *Eur. J. Pharmacol.* **1995,** *291* (3), 319-25.
57. Korpi, E. R.; Seeburg, P. H., Natural mutation of GABAA receptor alpha 6 subunit alters benzodiazepine affinity but not allosteric GABA effects. *Eur. J. Pharmacol.* **1993,** *247* (1), 23-27.
58. Cook, J. M.; Edwankar, R.; Poe, M. M.; Tiruveedhula, V. V. N. P. B.; Witzigmann, C., Synthesis of natural products and related heterocyclic compounds. Search for agents to treat neuropathic pain, epilepsy and anxiety disorders as well as simple molecules to treat TB and MRSA infections. In *Mona Symposium on Natural Products and Medicinal Chemistry*, Kingston, Jamaica, 2014.

59. Davies, M.; Bateson, A. N.; Dunn, S. M. J., Structural requirements for ligand interactions at the benzodiazepine recognition site of the GABAA receptor. *J. Neurochem.* **1998,** *70* (5), 2188-2194.
60. Mizuta, K.; Xu, D.; Pan, Y.; Comas, G.; Sonett, J. R.; Zhang, Y.; Panettieri, R. A., Jr.; Yang, J.; Emala, C. W., Sr., GABAA receptors are expressed and facilitate relaxation in airway smooth muscle. *Am. J. Physiol. Lung Cell Mol. Physiol.* **2008,** *294* (6), L1206-16.
61. Gallos, G.; Yim, P.; Chang, S.; Zhang, Y.; Xu, D.; Cook, J. M.; Gerthoffer, W. T.; Emala, C. W., Sr., Targeting the restricted alpha-subunit repertoire of airway smooth muscle GABAA receptors augments airway smooth muscle relaxation. *Am. J. Physiol. Lung Cell Mol. Physiol.* **2012,** *302* (2), L248-56.
62. Gallos, G.; Yocum, G. T.; Siviski, M. E.; Yim, P. D.; Fu, X. W.; Poe, M. M.; Cook, J. M.; Harrison, N.; Perez-Zoghbi, J.; Emala, C. W., Sr., Selective targeting of the alpha5-subunit of GABAA receptors relaxes airway smooth muscle and inhibits cellular calcium handling. *Am. J. Physiol. Lung Cell Mol. Physiol.* **2015,** *308* (9), L931-42.
63. Chiou, L.-C.; Tzeng, H.-R.; Fan, P.-C.; Sieghart, W.; Ernst, M.; Knutson, D. E.; Cook, J., A novel drug target for migraine: The GABAA receptor α6 subtype in trigeminal ganglia. *The FASEB Journal* **2019,** *33* (1_supplement), lb78-lb78.
64. Knutson, D. E.; Kodali, R.; Divović, B.; Treven, M.; Stephen, M. R.; Zahn, N. M.; Dobričić, V.; Huber, A. T.; Meirelles, M. A.; Verma, R. S.; Wimmer, L.; Witzigmann, C.; Arnold, L. A.; Chiou, L.-C.; Ernst, M.; Mihovilovic, M. D.; Savić, M. M.; Sieghart, W.; Cook, J. M., Design and synthesis of novel deuterated ligands functionally selective for the γ- aminobutyric acid type a receptor (GABAAR) α6 subtype with improved metabolic stability and enhanced bioavailability. *J. Med. Chem.* **2018,** *61* (6), 2422-2446.

65. Vasović, D.; Divović, B.; Treven, M.; Knutson, D. E.; Steudle, F.; Scholze, P.; Obradović, A.; Fabjan, J.; Brković, B.; Sieghart, W.; Ernst, M.; Cook, J. M.; Savić, M. M., Trigeminal neuropathic pain development and maintenance in rats are suppressed by a positive modulator of α6 GABAA receptors. *European Journal of Pain* **2019,** *23* (5), 973-984.

66. Hagen, T. J.; Guzman, F.; Schultz, C.; Cook, J. M., Synthesis of 3,6-disubstituted b-carbolines which possess either benzodiazepine antagonist or agonist activity. *Heterocycles* **1986,** *24*, 2845 - 855.

67. Clayton, T. S. Ph.D. Thesis, Part I. Unified Pharmacophoric Protein Models of the Benzodiazepine Receptor Subtypes. Part II. Subtype Selective Ligands for a5 GABAA/Bz Receptors. University of Wisconsin-Milwaukee, 2011.

68. García-Nafría, J.; Tate, C. G., Cryo-Electron Microscopy: Moving beyond x-ray crystal structures for drug receptors and drug development. *Annual Review of Pharmacology and Toxicology* **2020,** *60* (1), null. https://doi.org/10.1146/annurev-pharmtox-010919-023545

69. Laverty, D.; Desai, R.; Uchanski, T.; Masiulis, S.; Stec, W. J.; Malinauskas, T.; Zivanov, J.; Pardon, E.; Steyaert, J.; Miller, K. W.; Aricescu, A. R., Cryo-EM structure of the human alpha1beta3gamma2 GABAA receptor in a lipid bilayer. *Nature* **2019,** *565* (7740), 516-520. doi: 10.1038/s41586-018-0833-4

70. Liu, S.; Xu, L.; Guan, F.; Liu, Y. T.; Cui, Y.; Zhang, Q.; Zheng, X.; Bi, G. Q.; Zhou, Z. H.; Zhang, X.; Ye, S., Cryo-EM structure of the human alpha5beta3 GABAA receptor. *Cell Res* **2018,** *28* (9), 958-961. DOI: 10.1038/s41422-018-0077-8

71. Phulera, S.; Zhu, H.; Yu, J.; Claxton, D. P.; Yoder, N.; Yoshioka, C.; Gouaux, E., Cryo-EM structure of the benzodiazepine-sensitive alpha1beta1gamma2S tri-heteromeric

GABAA receptor in complex with GABA. *Elife* **2018,** *7*. https://doi.org/10.7554/eLife.39383.001

72. Zhu, S.; Noviello, C. M.; Teng, J.; Walsh, R. M.; Kim, J. J.; Hibbs, R. E., Structure of a human synaptic GABA A receptor. *Nature* **2018,** *559* (7712), 67-72. DOI: 10.1038/s41586-018-0255-3
73. Masiulis, S.; Desai, R.; Uchanski, T.; Serna Martin, I.; Laverty, D.; Karia, D.; Malinauskas, T.; Zivanov, J.; Pardon, E.; Kotecha, A.; Steyaert, J.; Miller, K. W.; Aricescu, A. R., GABAA receptor signalling mechanisms revealed by structural pharmacology. *Nature* **2019,** *565* (7740), 454-459. DOI: 10.1038/s41586-018-0832-5
74. Wongsamitkul, N.; Maldifassi, M. C.; Simeone, X.; Baur, R.; Ernst, M.; Sigel, E., α subunits in GABAA receptors are dispensable for GABA and diazepam action. *Sci Rep* **2017,** *7* (1), 15498. https://doi.org/10.1038/s41598-017-15628-7
75. Golani, L.K. †; Mian, M.Y. †; Ahmed, T.; Pandey, K.P.; Mondal, P.; Sharmin, D.; Rezvanian, S.; Witkin, J.M.; Cook, J.M., Rationalizing the Binding and α Subtype Selectivity of Synthesized Imidazodiazepines and Benzodiazepines at GABAA Receptors by Using Molecular Docking Studies. *Biorganic and medicinal chemistry letters*, **2022**, 62, 128637. https://doi.org/10.1016/j.bmcl.2022.128637
76. Witkin, J. M.; Cerne, R.; Davis, P. G.; Freeman, K. B.; do Carmo, J. M.; Rowlett, J. K.; Methuku, K. R.; Okun, A.; Gleason, S. D.; Li, X.; Krambis, M. J.; Poe, M.; Li, G.; Schkeryantz, J. M.; Jahan, R.; Yang, L.; Guo, W.; Golani, L. K.; Anderson, W. H.; Catlow, J. T.; Jones, T. M.; Porreca, F.; Smith, J. L.; Knopp, K. L.; Cook, J. M., The alpha2,3-selective potentiator of GABAA receptors, KRM-II-81, reduces nociceptive-

associated behaviors induced by formalin and spinal nerve ligation in rats. *Pharmacol Biochem Behav* **2019,** *180*, 22-31. https://doi.org/10.1016/j.pbb.2019.02.013

77. Smith, J. L.; Ping, X.; Jin, X.; Golani, L. K.; Li, G.; Rashid, F.; Jahan, R.; Cook, J. M.; Witkin, J. M., The positive allosteric modulator of alpha-2/3-containing γ-aminobutyric acid type a receptors, KRM-II-81, is active in pharmacoresistant models of epilepsy and in human epileptic tissue. *Neurosurgery* **2019,** *66* (Supplement_1). DOI: 10.1093/neuros/nyz310_697
78. Methuku, K. R.; Li, X.; Cerne, R.; Gleason, S. D.; Schkeryantz, J. M.; Tiruveedhula, V. V. N. P. B.; Golani, L. K.; Li, G.; Poe, M. M.; Rahman, M. T.; Cook, J. M.; Fisher, J. L.; Witkin, J. M., An antidepressant-related pharmacological signature for positive allosteric modulators of alpha2/3-containing GABAA receptors. *Pharmacol Biochem Behav* **2018,** *170*, 9-13. DOI: 10.1016/j.pbb.2018.04.009
79. Berro, L. F.; Rüedi-Bettschen, D.; Cook, J. E.; Golani, L. K.; Li, G.; Jahan, R.; Rashid, F.; Cook, J. M.; Rowlett, J. K.; Platt, D. M., GABAA receptor subtypes and the abuse-related effects of ethanol in rhesus monkeys: experiments with selective positive allosteric modulators. *Alcoholism: Clinical and Experimental Research* **2019,** *43* (5), 791-802. DOI: 10.1111/acer.14000
80. Moerke, M. J.; Li, G.; Golani, L. K.; Cook, J.; Negus, S. S., Effects of the α2/α3-subtype-selective GABAA receptor positive allosteric modulator KRM-II-81 on pain-depressed behavior in rats: comparison with ketorolac and diazepam. *Behavioural Pharmacology* **2019,** *30* (5), 452-461. DOI: 10.1097/FBP.0000000000000464
81. Witkin, J. M.; Li, G.; Golani, L. K.; Xiong, W.; Smith, J. L.; Ping, X.; Rashid, F.; Jahan, R.; Cerne, R.; Cook, J. M.; Jin, X., The positive allosteric modulator of alpha2/3-

containing GABAA receptors, KRM-II-81, is active in pharmaco-resistant models of epilepsy and reduces hyperexcitability after traumatic brain injury. *J Pharmacol Exp Ther* **2019**. DOI: 10.1124/jpet.119.260968

82. Golani, L.; Witkin, J.; Cook, J., Novel imidazobenzodiazepine GABAA receptor alpha 2/alpha 3 selective PAM for the treatment of refractory/resistance epilepsy. In *Abstr Pap Am Chem S*, American Chemical Society: Orlando, Florida, **2019**; Vol. 257.
83. Ciardiello, F.; Tortora, G., A novel approach in the treatment of cancer: targeting the epidermal growth factor receptor. *Clin Cancer Res* **2001,** *7* (10), 2958-70. PMID: 11595683
84. Yun, C. H.; Boggon, T. J.; Li, Y.; Woo, M. S.; Greulich, H.; Meyerson, M.; Eck, M. J., Structures of lung cancer-derived EGFR mutants and inhibitor complexes: mechanism of activation and insights into differential inhibitor sensitivity. *Cancer Cell* **2007,** *11* (3), 217-27. DOI: 10.1016/j.ccr.2006.12.017
85. Park, J. H.; Liu, Y.; Lemmon, M. A.; Radhakrishnan, R., Erlotinib binds both inactive and active conformations of the EGFR tyrosine kinase domain. *Biochem J* **2012,** *448* (3), 417-23. DOI: 10.1042/BJ20121513
86. Parks, D. J.; Lafrance, L. V.; Calvo, R. R.; Milkiewicz, K. L.; Gupta, V.; Lattanze, J.; Ramachandren, K.; Carver, T. E.; Petrella, E. C.; Cummings, M. D.; Maguire, D.; Grasberger, B. L.; Lu, T., 1,4-Benzodiazepine-2,5-diones as small molecule antagonists of the HDM2-p53 interaction: discovery and SAR. *Bioorg Med Chem Lett* **2005,** *15* (3), 765-70. DOI: 10.1016/j.bmcl.2004.11.009
87. Cook, J. M.; Huang, Q.; He, X.; Li, X.; Yu, J.; Han, D.; Lelas, S.; McElroy, J. F. Anxiolytic agents with reduced sedative and ataxic effects. US 7119196 B2, 2006.

88. Cook, J. M.; Li, G.; Poe, M. M.; Savic, M.; Sibille, E. Preparation of substituted benzo[f] imidazo[1,5-a][1,4]diazepine-3-carboxamides as α5-containing GABAA receptor agonists for treatment of cognitive and mood symptoms in neurodegenerative and neuropsychiatric disorders. WO 2017161370 A1, 2017.

89. Obradovic, A.; Joksimovic, S.; Poe, M. M.; Ramerstorfer, J.; Varagic, Z.; Namjoshi, O.; Batinic, B.; Radulovic, T.; Markovic, B.; Roth, B. L.; Sieghart, W.; Cook, J. M.; Savic, M. M., Sh-I-048A, an in vitro non-selective super-agonist at the benzodiazepine site of GABAA receptors: the approximated activation of receptor subtypes may explain behavioral effects. *Brain Res* **2014,** *1554*, 36-48. DOI: 10.1016/j.brainres.2014.01.036

90. Olsen, R. W.; Sieghart, W., International Union of Pharmacology. Lxx. Subtypes of Gamma-Aminobutyric Acid(a) Receptors: Classification on the Basis of Subunit Composition, Pharmacology, and Function. *Update. Pharmacol*. Rev. **2008**, 60 (3), 243-260.

91. Mortensen, M.; Patel, B.; Smart, T. G., Gaba Potency at Gaba(a) Receptors Found in Synaptic and Extrasynaptic Zones. *Front. Cell. Neurosci*. **2011**, 6, 1-10.

Sieghart, W.; Ramerstorfer, J.; Sarto-Jackson, I.; Varagic, Z.; Ernst, M., A Novel Gaba(a) Receptor Pharmacology: Drugs Interacting with the Alpha(+) Beta(-) Interface. Br. *J. Pharmacol.* **2012**, 166 (2), 476-485.

92. Varagic, Z.; Wimmer, L.; Schnurch, M.; Mihovilovic, M. D.; Huang, S.; Rallapalli, S.; Cook, J. M.; Mirheydari, P.; Ecker, G. F.; Sieghart, W.; Ernst, M., Identification of Novel Positive Allosteric Modulators and Null Modulators at the Gabaa Receptor Alpha+Beta- Interface. Br. *J. Pharmacol*. **2013,** 169 (2), 371-383

93. Nusser, Z.; Sieghart, W.; Somogyi, P., Segregation of Different Gabaa Receptors to Synaptic and Extrasynaptic Membranes of Cerebellar Granule Cells. *J. Neurosci*. **1998**, 18 (5), 1693-1703.

94. Gutiérrez, A.; Khan, Z. U.; De Blas, A. L., Immunocytochemical Localization of the A6 Subunit of the Γ-Aminobutyric Acida Receptor in the Rat Nervous System. *J. Comp. Neuro*. **1996**, 365 (3), 504-510.

95. Yang, L.; Xu, T.; Zhang, K.; Wei, Z.; Li, X.; Huang, M.; Rose, G. M.; Cai, X., The Essential Role of Hippocampal Alpha6 Subunit-Containing Gabaa Receptors in Maternal Separation Stress-Induced Adolescent Depressive Behaviors. *Behav. Brain Res*. **2016**, 313, 135-143.

96. Chiou, L. C.; Wu, C. Y.; Lee, H. J.; Du, J. C.; Hor, C. C.; Ernst, M.; Sieghart, W.; Cook, J., The Cerebellar Alpha6-Containing Gaba-a Receptor: A Novel Target for Neuropsychiatric Disorders. *In Neuroscience*, San Diego, CA, USA, **2016**.

97. Liao, Y. H.; Lee, H. J.; Huang, W. J.; Fan, P. C.; Chiou, L. C., Hispidulin Alleviated Methamphetamine-Induced Hyperlocomotion by Acting at Alpha6 Subunit-Containing Gabaa Receptors in the Cerebellum. *Psychopharmacology***. 2016,** 233 (17), 3187-3199.

98. Fan, P. C.; Huang, M.; Sieghart, W.; Ernst, M.; Knutson, D. E.; Cook, J. M.; Chiou, L. C., The A6 Subunit-Containing Gabaa Receptors: A Novel Target for Migraine Therapy. In The 18th Congress of International Headache Society (IHC2017), Vancouver, BC, Canada, **2017**.

99. Kramer, P. R.; Bellinger, L. L., Reduced Gabaa Receptor Alpha6 Expression in the Trigeminal Ganglion Enhanced Myofascial Nociceptive Response. *Neurosci*. **2013**, 245, 1-11.

100. Czernik, A. J.; Petrack, B.; Kalinsky, H. J.; Psychoyos, S.; Cash, W. D.; Tsai, C.; Rinehart, R. K.; Granat, F. R.; Lovell, R. A.; Brundish, D. E.; Wade, R., Cgs 8216: Receptor Binding Characteristics of a Potent Benzodiazepine Antagonist. *Life Sci.* **1982**, 30 (4), 363-372.

101. Boast, C. A.; Snowhill, E. W.; Simke, J. P., Cgs 8216 and Cgs 9896, Novel Pyrazoloquinoline Benzodiazepine Ligands with Benzodiazepine Agonist and Antagonist Properties. Pharmacol. Biochem. *Behav.* **1985**, 23 (4), 639-644.

102. Li, X.; Ma, C.; He, X.; Yu, J.; Han, D.; Zhang, C.; Atack, J. R.; Cook, J. M., Studies in Search of Diazepam-Insensitive Subtype Selective Agents for Gabaa/Bz Receptors. *Med. Chem. Res.* **2003,** 11 (9), 504-537

103. Wong, G.; Gu, Z. Q.; Fryer, R. I.; Skolnick, P., Pyrazolo(4,3-C)Quinolines with High Affinities for “Diazepam- Insensitive” (Di)Gabaa/Benzodiazepine Receptors. Med. Chem. Res. **1992**, 2 (4), 217-224.

104. Clayton, T.; Poe, M. M.; Rallapalli, S.; Biawat, P.; Savic, M. M.; Rowlett, J. K.; Gallos, G.; Emala, C. W.; Kaczorowski, C. C.; Stafford, D. C.; Arnold, L. A.; Cook, J. M., A Review of the Updated Pharmacophore for the Alpha 5 Gaba(a) Benzodiazepine Receptor Model. Int. *J. Med. Chem.* **2015**, 2015, 1-54

105. Zhang, P.; Zhang, W.; Liu, R.; Harris, B.; Skolnick, P.; Cook, J. M., Synthesis of Novel Imidazobenzodiazepines as Probes of the Pharmacophore for "Diazepam-Insensitive" Gabaa Receptors. *J. Med. Chem.* **1995**, 38 (10), 1679-1688.

106. He, X.; Huang, Q.; Yu, S.; Ma, C.; McKernan, R.; Cook, J. M., Studies of Molecular Pharmacophore/Receptor Models for Gabaa/Bzr Subtypes: Binding Affinities of Symmetrically Substituted Pyrazolo[4,3-C]Quinolin-3-Ones at Recombinant Axβ3γ2

Subtypes and Quantitative Structure-Activity Relationship Studies Via a Comparative Molecular Field Analysis. *Drug. Des. Discov.* **1999**, 16 (1), 77-91.

107. Huang, Q.; He, X.; Ma, C.; Liu, R.; Yu, S.; Dayer, C. A.; Wenger, G. R.; McKernan, R.; Cook, J. M., Pharmacophore/Receptor Models for Gabaa/Bzr Subtypes (A1β3γ2, A5β3γ2, and α6β3γ2) Via a Comprehensive Ligand-Mapping Approach. *J. Med. Chem*. **2000**, 43 (1), 71-95.

108. Treven, M.; Siebert, D. C. B.; Holzinger, R.; Bampali, K.; Fabjan, J.; Varagic, Z.; Wimmer, L.; Steudle, F.; Scholze, P.; Schnurch, M.; Mihovilovic, M. D.; Ernst, M., Towards Functional Selectivity for Alpha6beta3gamma2 Gabaa Receptors: A Series of Novel Pyrazoloquinolinones. Br. *J. Pharmacol*. **2018**, 175 (3), 419-428.

109. Chiou, L.-C.; Cook, J.; Ernst, M.; Fan, P.-C.; Knutson, D.; Meirelles, M.; Mihovilovic, M.; Sieghart, W.; Varagic, Z.; Verma, R.; Wimmer, L.; Weizigmann, C.; Siebert, D. C. B.; Savic, M. M. Preparation of Ligands Selective to Alpha 6 Subunit-Ccontaining Gabaa Receptors and Their Methods of Use. WO2016196961, 2016.

110. Mirheydari, P.; Ramerstorfer, J.; Varagic, Z.; Scholze, P.; Wimmer, L.; Mihovilovic, M. M.; Sieghart, W.; Ernst, M., Unexpected Properties of Delta-Containing Gabaa Receptors in Response to Ligands Interacting with the Alpha+ Beta- Site. *Neurochem. Res.* **2014**, 39 (6), 1057-1067.

111. Gould, R. G.; Jacobs, W. A., The Synthesis of Certain Substituted Quinolines and 5,6-Benzoquinolines. *J. Am. Chem. Soc*. **1939**, 61 (10), 2890-2895

112. Malvacio, I.; Moyano, E. L.; Vera, D. M. A., Gas-Phase Synthesis of 3-Carboethoxy-quinolin-4-Ones. A Comprehensive Computational Mechanistic Study to

Uncover the Dark Side of the Gould–Jacobs Reaction. *RSC Advances* **2016**, 6 (87), 83973-83981.

113. Knutson, D. E.; Kodali, R.; Divovic, B.; Treven, M.; Stephen, M. R.; Zahn, N. M.; Dobricic, V.; Huber, A. T.; Meirelles, M. A.; Verma, R. S.; Wimmer, L.; Witzigmann, C.; Arnold, L. A.; Chiou, L. C.; Ernst, M.; Mihovilovic, M. D.; Savic, M. M.; Sieghart, W.; Cook, J. M., Design and Synthesis of Novel Deuterated Ligands Functionally Selective for the GammaAminobutyric Acid Type a Receptor (Gabaar) Alpha6 Subtype with Improved Metabolic Stability and Enhanced Bioavailability. *J. Med. Chem.* **2018**, 61 (6), 2422-2446.

114. Fryer, R. I.; Zhang, P.; Rios, R.; Gu, Z. Q.; Basile, A. S.; Skolnick, P., Structure-Activity Relationship Studies at Benzodiazepine Receptor (Bzr): A Comparison of the Substituent Effects of Pyrazoloquinolinone Analogs. *J. Med. Chem*. **1993**, 36 (11), 1669-1673.

115. Yokoyama, N.; Ritter, B.; Neubert, A. D., 2-Arylpyrazolo[4,3-C]Quinolin-3-Ones: A Novel Agonist, a Partial Agonist and an Antagonist of Benzodiazepines. *J. Med. Chem*. **1982**, 25(4), 337-339

116. Ya-Hsien Huang, Ming Tatt Lee, Daniel E. Knutson**,** Dishary Sharmin, James M Cook, LC Chiou. Positive modulation of cerebellar α6GABAA receptors for treating essential tremor: a proof-of-concept study in harmaline-treated mice. 2021. DOI: 10.1101/2021.04.19.440397

117. Richter, L.; de Graaf, C.; Sieghart, W.; Varagic, Z.; Morzinger, M.; de Esch, I. J.; Ecker, G. F.; Ernst, M., Diazepam-bound GABAA receptor models identify new benzodiazepine binding-site ligands. *Nat. Chem. Biol.* **2012,** *8* (5), 455-64.

118. Rudolph, U.; Mohler, H., GABA-based therapeutic approaches: GABAA receptor subtype functions. *Curr. Opin. Pharmacol.* **2006,** *6* (1), 18-23.

119. Poe, M. M.; Methuku, K. R.; Li, G.; Verma, A. R.; Teske, K. A.; Stafford, D. C.; Arnold, L. A.; Cramer, J. W.; Jones, T. M.; Cerne, R., Synthesis and Characterization of a Novel γ-Aminobutyric Acid Type A (GABA A) Receptor Ligand That Combines Outstanding Metabolic Stability, Pharmacokinetics, and Anxiolytic Efficacy. *J. Med. Chem*. 2016, 59, 10800

120. Li, G.; Golani, L. K.; Jahan, R.; Rashid, F.; Cook, J. M., Improved Synthesis of Anxiolytic, Anticonvulsant, and Antinociceptive α2/α3-GABA(A)-ergic Receptor Subtype Selective Ligands as Promising Agents to Treat Anxiety, Epilepsy, and Neuropathic Pain. *Synthesis* 2018, 50, 4124.

121. Sieghart, W.; Ernst, M.. Heterogeneity of GABAA Receptors: Revived Interest in the Development of Subtype-selective Drugs *Curr. Med. Chem.* **2005**, *5*, 217

122. Löw, K.; Crestani, F.; Keist, R.; Benke, D.; Brünig, I.; Benson, J. A.; Fritschy, J.-M.;Rülicke, T.; Bluethmann, H.; Möhler, H., Molecular and Neuronal Substrate for the Selective Attenuation of Anxiety. *Science* **2000**, 290, 131

123. Mendelson, W.; Owen, C.; Skolnick, P.; Paul, S.; Martin, J.; Ko, G.; Wagner, R., Quantitative description of sleep stage electrophysiology using digital period analytic techniques. *Sleep* **1984**, 7, 64.

124. Ninan, P. T.; Insel, T. M.; Cohen, R. M.; Cook, J. M.; Skolnick, P.; Paul, S. M., Benzodiazepine receptor-mediated experimental "anxiety" in primates. *Science* **1982,** 218, 1332.

125. Rudolph, U.; Crestani, F.; Benke, D.; Brünig, I.; Benson, J. A.; Fritschy, J.-M.; Martin, J. R.; Bluethmann, H.; Möhler, H. Benzodiazepine actions mediated by specific gamma-aminobutyric acid(A) receptor subtypes. *Nature* **2000**, 404, 629.

126. Cook, J. M.; Huang, Q.; He, X.; Li, X.; Yu, J.; Han, D.; Lelas, S.; McElroy, J. F. Anxiolytic agents with reduced sedative and ataxic effects. Patent: US7119196 B2. Date: Oct. 10, 2006.

127. Cook, J. M.; Zhou, H.; Huang, S.; Sarma, P. V. V. S.; Zhang, C., Stereospecific anxiolytic and anticonvulsant agents with reduced muscle-relaxant, sedative-hypnotic and ataxic effects. Patent: US 7618958 B2. Date: Nov. 17, 2009.

128. Fischer, B. D.; Licata, S. C.; Edwankar, R. V.; Wang, Z. J.; Huang, S.; He, X.; Yu, J.; Zhou, H.; Johnson, E. M., Jr.; Cook, J. M.; Furtmuller, R.; Ramerstorfer, J.; Sieghart, W.; Roth, B. L.; Majumder, S.; Rowlett, J. K., Anxiolytic-like effects of 8-acetylene imidazobenzodiazepines in a rhesus monkey conflict procedure. *Neuropharmacology* **2010,** *59* (7-8), 612-8.

129. Witkin, J. M.; Cerne, R.; Wakulchik, M.; S, J.; Gleason, S. D.; Jones, T. M.; Li, G.; Arnold, L. A.; Li, J. X.; Schkeryantz, J. M.; Methuku, K. R.; Cook, J. M.; Poe, M. M., Further evaluation of the potential anxiolytic activity of imidazo[1,5-a][1,4]diazepin agents selective for α2/3-containing GABAA receptors. *Pharmacology Biochemistry and Behavior* 2017, 157 (Supplement C), 35-40

130. Atack, J. R.; Wafford, K. A.; Street, L. J.; Dawson, G. R.; Tye, S.; Van Laere, K.; Bormans, G.; Sanabria-Bohorquez, S. M.; De Lepeleire, I.; de Hoon, J. N.; Van Hecken, A.; Burns, H. D.; McKernan, R. M.; Murphy, M. G.; Hargreaves, R. J., MRK-409 (MK-0343), a GABAA receptor subtype-selective partial agonist, is a non-sedating anxiolytic

in preclinical species but causes sedation in humans. *Journal of psychopharmacology (Oxford, England)* **2011,** *25* (3), 314-28.

131. Mirza, N. R.; Larsen, J. S.; Mathiasen, C.; Jacobsen, T. A.; Munro, G.; Erichsen, H. K.; Nielsen, A. N.; Troelsen, K. B.; Nielsen, E. O.; Ahring, P. K., NS11394 [3'-[5-(1-hydroxy-1-methyl-ethyl)-benzoimidazol-1-yl]-biphenyl-2-carbonitrile], a unique subtype-selective GABAA receptor positive allosteric modulator: in vitro actions, pharmacokinetic properties and in vivo anxiolytic efficacy. *J. Pharmacol. Exp. Ther.* **2008,** *327* (3), 954-68.

132. Munro, G.; Lopez-Garcia, J. A.; Rivera-Arconada, I.; Erichsen, H. K.; Nielsen, E. O.; Larsen, J. S.; Ahring, P. K.; Mirza, N. R., Comparison of the novel subtype-selective GABAA receptor-positive allosteric modulator NS11394 [3'-[5-(1-hydroxy-1-methyl-ethyl)-benzoimidazol-1-yl]-biphenyl-2-carbonitrile] with diazepam, zolpidem, bretazenil, and gaboxadol in rat models of inflammatory and neuropathic pain. *J. Pharmacol. Exp. Ther.* **2008,** *327* (3), 969-81.

133. Fischer, B. D.; Schlitt, R. J.; Hamade, B. Z.; Rehman, S.; Ernst, M.; Poe, M. M.; Li, G.; Kodali, R.; Arnold, L. A.; Cook, J. M., Pharmacological and antihyperalgesic properties of the novel α2/3 preferring GABAA receptor ligand MP-III-024. *Brain Res. Bull.* **2017,** *131*, 62-69.

134. Biggerstaff. A.; Kivell B.; Smith, J.L.; Mian, M.Y.; Golani, L.K.; Rashid, F.; Sharmin, D.; Knutson, D.E.; Cerne, R.; Cook, J.M.; Witkin, J.M., The α2,3-selective potentiators of GABAA receptors, KRM-II-81 and MP-III-80, produce anxiolytic-like effects and block chemotherapy-induced hyperalgesia in mice without tolerance development. *Pharmacology, Biochemistry and Behavior* **2020**, 196 172996

135. Kannampalli, P.; Babygirija, R.; Zhang, J.; Poe, M. M.; Li, G.; Cook, J. M.; Shaker, R.; Banerjee, B.; Sengupta, J. N., Neonatal bladder inflammation induces long-term visceral pain and altered responses of spinal neurons in adult rats. *Neuroscience* **2017,** *346* (Supplement C), 349-364

136. Jacob, T.; Moss, S.; Jurd, R., GABAA receptor trafficking and its role in the dynamic modulation of neuronal inhibition. *Nat Rev Neurosci* **2008**, 9, 331–343

137. Witkin, J. M.; Smith, J. L.; Ping, X.; Gleason, S. D.; Poe, M. M.; Li, G.; Jin, X.; Hobbs, J.; Schkeryantz, J. M.; McDermott, J. S.; Alatorre, A. I.; Siemian, J. N.; Cramer, J. W.; Airey, D. C.; Methuku, K. R.; Tiruveedhula, V.; Jones, T. M.; Crawford, J.; Krambis, M. J.; Fisher, J. L.; Cook, J. M.; Cerne, R., Bioisosteres of ethyl 8-ethynyl-6-(pyridin-2-yl)-4H-benzo[f]imidazo [1,5-a][1,4]diazepine-3-carboxylate (HZ-166) as novel alpha 2,3 selective potentiators of GABAA receptors: Improved bioavailability enhances anticonvulsant efficacy. *Neuropharmacology* **2018,** *137*, 332-343.

138. Lewter, L. A.; Fisher, J. L.; Siemian, J. N.; Methuku, K. R.; Poe, M. M.; Cook, J. M.; Li, J.-X., Antinociceptive effects of a novel α2/α3-subtype selective GABAA receptor positive allosteric modulator. *ACS Chem. Neurosci.* **2017,** *8* (6), 1305-1312.

139. Cerne, R.; Smith, J.L.; Fisher, J.L.; Golani, L.K.; Knutson, D.E.; Cook, J.M; Witkin, J.M., Chapter 11 - The orally bioavailable imidazodiazepine, KRM-II-81, is a novel potentiator of α2/3-containing GABAA receptors with analgesic efficacy. *The Neurobiology, Physiology, and Psychology of Pain,* Academic Press, **2022**, 117-127

140. Witkin, J. M.; Li, G.; Golani, L.K.; Xiong, W.; Smith, J. L.; Ping, X.; Rashid, F.; Jahan, R.; Cerne, R., Cook, J. M.; Jin, X., The Positive Allosteric Modulator of α2/3-Containing GABAA Receptors, KRM-II-81, Is Active in Pharmaco-Resistant Models of

Epilepsy and Reduces Hyperexcitability after Traumatic Brain Injury. *Journal of Pharmacology and Experimental Therapeutics* January **2020**, 372 (1) 83-94.

141. Moerke, M.J.; Li, G.; Golani, L.K.; Cook, J.M.; and Negus, S.S., Effects of the α2/α3-subtype-selective GABAA receptor positive allosteric modulator KRM-II-81 on pain-depressed behavior in rats: comparison with ketorolac and diazepam. *Behav Pharmacol* **2019**, 30: 452-461.

142. Knutson D.E.; Smith, J.L.; Ping, P.; Jin, X.; Golani, L.K.; Li, G.; Tiruveedhula, V.V.N.P.B.; Rashid, F.; Mian, M.Y.; Jahan, R.; Sharmin, D.; Cerne, R.; Cook, J.M.; Witkin, J.M., The Imidazodiazepine Anticonvulsant, KRM-II-81, Produces Novel, Non-diazepam-like Antiseizure Effects. *ACS Chem. Neurosci.* **2020**. 11, 2624−2637

143. Gardner, C.R.; Walsh, C.T.; Almarsson, O., Drugs as materials: valuing physical form in drug discovery. *Nat. Rev. Drug Discovery*, **3**, 926−934

144. Lipinski, C.A., Poor aqueous solubility-An industry wide problem in drug discovery. *Am. Pharm. Rev*. **2002,** 5, 82−85

145. Serajuddin, A.T., Salt formation to improve drug solubility. *Adv. Drug Delivery Rev*. **2007**, 59, 603−616

146. Hawley, M.; Morozowich, W., Modifying the diffusion layer of soluble salts of poorly soluble basic drugs to improve dissolution performance. *Mol. Pharm.* **2010**, **7**, 1441−1449

147. Paulekuhn, G.S.; Dressman, J.B.; Saal, C., Salt screening and characterization for poorly soluble, weak basic compounds: case study albendazole. *Pharmazie*, **2013**, 68, 555−56

148. Mukesh, S.; Joshi, P.; Bansal, A.K.; Kashyap, M.C.; Mandal, S.K.; Sathe, V.;

Sangamwar, A.T., Amorphous Salts Solid Dispersions of Celecoxib: Enhanced Biopharmaceutical Performance and Physical Stability. *Molecular Pharmaceutics*, **2021**, 18 (6**)**, 2334-2348

149. Kumar, V.; Bharate, S.B.; Vishwakarma, R.A.; Bharate, S.S., Selection of a Water-Soluble Salt Form of a Preclinical Candidate, IIIM-290: Multiwell-Plate Salt Screening and Characterization. *ACS Omega*, **2018**, **7**, 8365-8377

150. Mian, M.Y.; Sharmin, D.; Pandey, K.P.; Divović, B.; Golani, L.K.; Cerne, R.; Smith, J.L.; Ping, X.; Jin, X.; Imler, G.H.; Deschamp, J.; Lippa, A.; Cook, J.M. Savić, M.M.; Witkin, J.M. A hydrochloride salt of the GABAkine KRM-II-81. *ACS Omega* **2022** 7 (31), 27550-27559. DOI: 10.1021/acsomega.2c03029

151. Li, G**.**; Golani, L. K.; Jahan, R.; Rashid, F.; Cook, J. M., Improved Synthesis of Anxiolytic, Anticonvulsant, and Antinociceptive alpha 2/alpha 3-GABA(A)-ergic Receptor Subtype Selective Ligands as Promising Agents to Treat Anxiety, Epilepsy, and Neuropathic. *Synthesis-Stuttgart* **2018,** *50* (20), 4124-4132

152. Delépine, M., Bull. *Soc. Chim. Fr.* **1895**, 13, 352-361.

153. Blažević, N.; Kajfež, F., A New Ring Closure Synthesis of 1,4-Benzodiazepines. *Ii. J. Heterocycl. Chem.* **1971**, 8 (5), 845-846.

154. Cepanec, I.; Litvić, M.; Pogorelić, I., Efficient Synthesis of 3-Hydroxy-1,4-Benzodiazepines Oxazepam and Lorazepam by New Acetoxylation Reaction of 3-Position of 1,4- Benzodiazepine Ring. *Organic Process Research & Development* **2006**, 10 (6), 1192-1198.

155. Cassar, L., Synthesis of Aryl- and Vinyl-Substituted Acetylene Derivatives by the Use of Nickel and Palladium Complexes. *J. Organomet. Chem*. **1975**, 93 (2), 253-257.

156. Dieck, H. A.; Heck, F. R., Palladium Catalyzed Synthesis of Aryl, Heterocyclic and Vinylic Acetylene Derivatives. *J. Organomet. Chem*. **1975**, 93 (2), 259-263.

157. Pandey, K. P.; Divović, B.; Rashid, F.; Golani, L. K.; Cerne, R.; Zahn, N. M.; Meyer, M. J.; Arnold, L. A.; Sharmin, D.; Mian, M. Y.; Smith, J. L.; Ping, X.; Jin, X.; Lippa, A.; Tiruveedhula, V. V. N. P. B.; Cook, J. M.; Savić, M. M.; Witkin, J. M. Structural Analogs of the GABAkine KRM-II-81 Are Orally Bioavailable Anticonvulsants without Sedation. *J. Pharmacol. Exp. Ther*. **2023**, *385* (1), 50–61. https://doi.org/10.1124/jpet.122.001362.

158. Dishary Sharmin, Branka Divović, Xingjie Ping, Rok Cerne, Jodi L. Smith, Sepideh Revanian, Prithu Mondal, Michelle J. Meyer, Molly E. Kiley, Leggy A. Arnold, Md Yeunus Mian, Kamel P. Pandey, Xiaoming Jin, Jelena R. Mitrović, Djordje Djorović, Arnold Lippa, James M. Cook, Lalit K. Golani, Petra Scholze, Miroslav M. Savić, and Jeffrey M. Witkin. A Brominated Analog of the Anti-seizure Compound KRM-II-81 has Anti-seizure Efficacy in Rodents, and Anti-epileptogenic Activity in Neural Networks of Brain Slices from a Patient with Mesial Temporal Lobe Epilepsy. *ACS Chem. Neuo. Sci.* **2023** (under review)

159. Kosmowska, B.; Paleczna, M.; Biała, D.; Kadłuczka, J.; Wardas, J.; Witkin, J.M.; Cook, J.M.; Sharmin, D.; Marcinkowska, M.; Kuter, K.Z. GABA-A Alpha 2/3 but Not Alpha 1 Receptor Subunit Ligand Inhibits Harmaline and Pimozide-Induced Tremor in Rats. *Biomolecules* **2023**, *13*, 197. https://doi.org/10.3390/biom13020197

160. Atiqur Rahman, Thomas M. Keck, Michael M. Poe, Dishary Sharmin, James M. Cook, Bradford D. Fischer. Synergistic antihyperalgesic and antinociceptive effects of morphine and methyl 8- ethynyl-6-(pyridin-2-yl)-4H-benzo[f]imidazo [1,5-

a][1,4]diazepine-3-carboxylate (MP-III024), a positive allosteric modulator at α2GABAA and α3GABAA receptors. *Psychopharmacology* **2021**, 238, 1585–1592. https://doi.org/10.1007/s00213-021-05791-1

161. Clerinx, J.; Bottieau, E.; Wichmann, D.; Tannich, E.; Van Esbroeck, M. Acute schistosomiasis in a cluster of travelers from Rwanda: diagnostic contribution of schistosome DNA detection in serum compared to parasitology and serology. *J Travel Med.* **2011,** 18:367–372. http://dx.doi.org /10.1111/j.1708-8305.2011.00552.x

162. Lawrence, N. J.; Drew, M. D.; Bushell, S. M. Polymethylhydrosiloxane: a versatile reducing agent for organic synthesis. *J. Chem. Soc., Perkin Trans*. 1 **1999**, 3381–3391 https://doi.org/10.1039/A903662H

163. Chandrasekhar, S.; Chandraiah, L.; Reddy, R.; Reddy, M.V. Direct Conversion of Azides and Benzyl Carbamates to t-Butyl Carbamates Using Polymethylhydrosiloxane and Pd-C. *Chemistry Letters*. **2000**, 29(7): 780–781. https://doi.org/10.1246/cl.2000.780

164. Bast, T.; Pezze, M.; McGarrity, S. Cognitive deficits caused by prefrontal cortical and hippocampal neural disinhibition. *Br J Pharmacol* **2017**, 174(19), 3211-3225.

165. Zhang, Z.J.; Reynolds, G.P. A selective decrease in the relative density of parvalbumin-immunoreactive neurons in the hippocampus in schizophrenia. *Schizophr Res* **2002**, 55(1-2), 1-10

166. Benes, F.M.; Lim, B.; Matzilevich, D.; Walsh, J.P.; Subburaju, S.; Minns, M. Regulation of the GABA cell phenotype in hippocampus of schizophrenics and bipolars. *Proc Natl Acad Sci U S A* **2007**, 104(24), 10164-10169.

167. Fee, C.; Banasr, M.; Sibille, E. Somatostatin-positive gamma-aminobutyric acid interneuron deficits in depression: cortical microcircuit and therapeutic perspectives. *Biol Psychiatry* **2017**, 82(8), 549-559.

168. Petty, F.; Schlesser, M.A. Plasma GABA in affective illness. A preliminary investigation. *J Affect Disord* **1981**, 3(4), 339-343.

169. Griffin, C.E.; Kaye, A.M.; Bueno, F.R.; Kaye, A.D. Benzodiazepine pharmacology and central nervous system-mediated effects. *Ochsner J* **2013**, 13(2), 214-223.

170. Perez, S. M.; Lodge, D. J. New approaches to the management of schizophrenia: focus on aberrant hippocampal drive of dopamine pathways. *Drug Des. Dev. Therapy* **2014**, 8, 887 - 896.

171. Lieberman, J. A.; Stroup, T. S.; McEvoy, J. P.; Swartz, M. S.; Rosenheck, R. A.; Perkins, D. O.; Keefe, R. S. E.; Davis, S. M.; Davis, C. E.; Lebowitz, B. D.; Severe, J.; Hsiao, J. K. Effectiveness of antipsychotic drugs in patients with chronic schizophrenia. *N. Engl. J. Med.* **2005,** 353, 1209 - 1223.

172. Dargham, A. Do we still believe in the dopamine hypothesis? New data bring new evidence. *Int J Neuropsychopharmacol* **2004**, 7 Suppl 1:S1-5.

173. Laruelle, M.; Dargham, A. Dopamine as the wind of the psychotic fire: new evidence from brain imaging studies. *J Psychopharmacol* **1999**, 13, 358-371.

174. Heckers, S.; Konradi, C. Hippocampal pathology in schizophrenia. *Curr Top Behav Neurosci* **2010**, 4,529-553.

175. Nelson, M.D.; Saykin, A.J.; Flashman, L.A.; Riordan, H.J. Hippocampal volume reduction in schizophrenia as assessed by magnetic resonance imaging: A meta-analytic study. *Archives of General Psychiatry* **1998**, 55, 433-440.

176. Tamminga, C.A.; Stan, A.D.; Wagner, A.D. The hippocampal formation in schizophrenia. *Am J Psychiatry* **2010**, 167,1178-1193.

177. Wright, I.C.; Rabe-Hesketh, S.; Woodruff, P.W.R.; David, A.S.; Murray, R.M.; Bullmore, E. T. Meta-analysis of regional brain volumes in schizophrenia. *American Journal of Psychiatry* **2000,** 157, 16-25.

178. Heckers, S. Neuroimaging studies of the hippocampus in schizophrenia. *Hippocampus* **2001**, 11,520-528.

179. Schobel, S.A.; Lewandowski, N.M.; Corcoran, C.M.; Moore, H.; Brown, T.; Malaspina, D. Differential targeting of the CA1 subfield of the hippocampal formation by schizophrenia and related psychotic disorders. *Arch Gen Psychiatry* **2009**, 66, 938-946.

180. Lodge, D.J.; Grace, A.A. Aberrant hippocampal activity underlies the dopamine dysregulation in an animal model of schizophrenia. *J Neurosci*. **2007**, 27, 11424-11430.

181. Perez, S.M.; Lodge, D.J. Convergent Inputs from the Hippocampus and Thalamus to the Nucleus Accumbens Regulate Dopamine Neuron Activity. *J Neurosci* **2018**, 38, 10607-10618.

182. Perez, S.M.; Carreno, F.R.; Frazer, A.; Lodge, D.J. Vagal nerve stimulation reverses aberrant dopamine system function in the methylazoxymethanol acetate rodent model of schizophrenia. *J Neurosci*. **2014**, 34, 9261-9267.

183. Perez, S.M.; Lodge, D.J. Hippocampal interneuron transplants reverse aberrant dopamine system function and behavior in a rodent model of schizophrenia. *Mol Psychiatry*. **2013,** 18, 1193-1198.

184. Perez, S.M.; Shah, A,; Asher, A.; Lodge, D.J. Hippocampal deep brain stimulation reverses physiological and behavioural deficits in a rodent model of schizophrenia. *Int J Neuropsychopharmacol*. **2013**, 16, 1331-1339.

185. Donegan, J.J.; Lodge, D.J. Cell-based therapies for the treatment of schizophrenia. *Brain Res*. **2017,** 1655, 262-269.

186. Kilpatrick, D. G.; Resnick, H. S.; Milanak, M. E.; Miller, M. W.; Keyes, K. M.; & Friedman, M. J. National estimates of exposure to traumatic events and PTSD prevalence using DSM-IV and DSM-5 criteria. *Journal of Traumatic Stress*, **2013**, 26(5), 537–547. https://doi.org/10.1002/jts.21848

187. Kilpatrick, D. G.; Ruggiero, K. J.; Acierno, R.; Saunders, B. E.; Resnick, H. S.; Best, C. L. Violence and risk of PTSD, major depression, substance abuse/dependence, and comorbidity: Results from the National Survey of Adolescents. *Journal of Consulting and Clinical Psychology* **2003**, 71(4), 692–700. https://doi.org/10.1037/0022-006X.71.4.692

188. Battle, D. E. Diagnostic and Statistical Manual of Mental Disorders (DSM). *CoDAS* 2013, 25(2), 191–192. https://doi.org/10.1590/s2317-17822013000200017

189. Braakman, M. H.; Kortmann, F. A. M.; van den Brink, W. Validity of "post-traumatic stress disorder with secondary psychotic features": A review of the evidence. *Acta Psychiatrica Scandinavica* **2009**, 119(1), 15–24. https://doi.org/10.1111/j.1600-0447.2008.01252.x

190. Prevalence, Global, regional, and national incidence, prevalence, and years lived with disability for 328 diseases and injuries for 195 countries, 1990-2016: a systematic analysis for the Global Burden of Disease Study 2016. *Lancet,* **2017**, 390(10100): p. 1211-1259.

191. Malhi, G.S; Mann, J.J. Depression. *The Lancet*, **2018**, 392(10161): p. 2299-2312

192. Gartlehner, G. Pharmacological and non-pharmacological treatments for major depressive disorder: review of systematic reviews. *BMJ Open*, **2017**, 7(6): p. e014912

193. Fogaca, M.V. and R.S. Duman, Cortical GABAergic Dysfunction in Stress and Depression: New Insights for Therapeutic Interventions. *Front Cell Neurosci*, **2019**. 13: p. 87.

194. Hirschfeld, R.M.A., History and evolution of the monoamine hypothesis of depression. *The J. of Clin. Psych.*, **2000**. 61(Suppl6): p. 4-6

195. Chávez-Castillo, M., et al., Depression as a Neuroendocrine Disorder: Emerging Neuropsychopharmacological Approaches beyond Monoamines. *Adv. in Pharm. Sci.*, **2019**, 7943481

196. Duman, C.H. and R.S. Duman, Spine synapse remodeling in the pathophysiology and treatment of depression. *Neurosci Lett*, **2015**, 601, 20-9

197. Conradi, H.J., J. Ormel, and P. De Jonge, Presence of individual (residual) symptoms during depressive episodes and periods of remission: a 3-year prospective study. *Psychological Medicine*, **2011**. 41(6): p. 1165-1174

198. Fossati, P., A.M. Ergis, and J.F. Allilaire. Executive functioning in unipolar depression: a review. *Encephale*, **2002,** 28(2), 97-107

199. Bortolato, B. Cognitive remission: a novel objective for the treatment of major depression? *BMC Med*, **2016**, 14, 9

200. Lee, R.S.C., et al., A meta-analysis of cognitive deficits in first-episode Major Depressive Disorder. *Journal of Affective Disorders*, **2012,** 140(2), 113-124

201. Majer, M. Impaired divided attention predicts delayed response and risk to relapse in subjects with depressive disorders. *Psychological Medicine*, **2004,** 34(8), 1453-1463

202. Kang, H.J., et al., Decreased expression of synapse-related genes and loss of synapses in major depressive disorder. *Nat Med*, **2012**. 18(9), 1413-7.

203. Kang, H.J., et al., Decreased expression of synapse-related genes and loss of synapses in major depressive disorder. *Nature Medicine*, **2012**, 18(9), 1413-1417

204. Feyissa, A.M., et al., Reduced levels of NR2A and NR2B subunits of NMDA receptor and PSD-95 in the prefrontal cortex in major depression. *Progress in Neuro-Psychopharmacology and Biological Psychiatry*, **2009**. 33(1), 70-75.

205. Holmes, S.E., et al., Lower synaptic density is associated with depression severity and network alterations. *Nature Communications*, **2019,** 10(1), 1529

206. Christoffel, D.J., S.A. Golden, and S.J. Russo, Structural and synaptic plasticity in stress-related disorders. *Reviews in the neurosciences*, **2011**, 22(5), 535-549

207. Izquierdo, A., C.L. Wellman, and A. Holmes, Brief uncontrollable stress causes dendritic

retraction in infralimbic cortex and resistance to fear extinction in mice. *J Neurosci*, **2006**. 26(21), 5733-8

208. Liston, C., et al., Stress-induced alterations in prefrontal cortical dendritic morphology predict selective impairments in perceptual attentional set-shifting. *J Neurosci*, **2006**, 26(30), 78704

209. Shansky, R.M., et al., Stress-Induced Dendritic Remodeling in the Prefrontal Cortex is Circuit Specific. *Cerebral Cortex*, **2009**, 19(10), 2479-2484

210. Qiao, H., et al., Dendritic Spines in Depression: What We Learned from Animal Models. *Neural plasticity*, **2016**. 2016: p. 8056370-8056370

211. Newton, D.F. Chapter 28 - Altered GABAergic Function, Cortical Microcircuitry, and Information Processing in Depression, in *Neurobiology of Depression*, J. Quevedo, A.F. Carvalho, and C.A. Zarate, Editors. **2019**, Academic Press. p. 315-329

212. Berrettini, W.H., et al., Reduced plasma and CSF gamma-aminobutyric acid in affective illness: effect of lithium carbonate. *Biological psychiatry*, **1983**. 18(2): p. 185-194.

213. Petty, F., et al., Plasma GABA in mood disorders. *Psychopharmacology bulletin*, **1990**. 26(2), 157-61.

214. Petty, F., et al., Stability of plasma GABA at four-year follow-up in patients with primary unipolar depression. *Biological psychiatry*, **1995**, 37(11), 806-810.

215. Petty, F., et al., Low plasma γ-aminobutyric acid levels in male patients with depression. *Biological Psychiatry*, **1992**, 32(4), 354-363

216. Petty, F. and A.D. Sherman, Plasma GABA in psychiatric illness. *J Affect Disorder*, **1984**. 6, 131-138.

217. Petty, F., et al., Low plasma GABA is a trait-like marker for bipolar illness. *Neuropsychopharmacol.*, **1993**. 9(2), 125-32

218. Bhagwagar, Z., et al., Low GABA concentrations in occipital cortex and anterior cingulate cortex in medication-free, recovered depressed patients. *The international journal of neuropsychopharmacology*, **2008**, 11(2), 255-60

219. Goddard, A.W., et al., Reductions in Occipital Cortex GABA Levels in Panic Disorder Detected With 1H-Magnetic Resonance Spectroscopy. *Archives of General Psychiatry*, **2001**, 58(6), 556-556.

220. Price, R.B., et al., Amino acid neurotransmitters assessed by proton magnetic resonance

spectroscopy: relationship to treatment resistance in major depressive disorder. *Biol Psychiatry*, **2009**. 65(9), 792-800

221. Sanacora, G., et al., Subtype-specific alterations of gamma-aminobutyric acid and glutamate in patients with major depression. *Arch Gen Psychiatry*, **2004**. 61(7), 705-13

222. Sanacora, G., et al., Increased occipital cortex GABA concentrations in depressed patients after therapy with selective serotonin reuptake inhibitors. *Am J Psychiatry*, **2002**, 159(4), 663-5

223. Sanacora, G., et al., Reduced Cortical γ-Aminobutyric Acid Levels in Depressed Patients

Determined by Proton Magnetic Resonance Spectroscopy. *Archives of General Psychiatry*, **1999**, 56(11), 1043-1043

224. Hasler, G., et al., Reduced prefrontal glutamate/glutamine and gamma-aminobutyric acid levels in major depression determined using proton magnetic resonance spectroscopy. *Archives of general psychiatry*, **2007**, 64(2), 193-200

225. Gabbay, V., et al., Anterior Cingulate Cortexγ-Aminobutyric Acid in Depressed Adolescents. *Archives of General Psychiatry*, **2012,** 69(2), 139-139

226. Plante, D.T., et al., Reduced gamma-aminobutyric acid in occipital and anterior cingulate cortices in primary insomnia: a link to major depressive disorder? *Neuropsychopharmacology*, **2012**, 37(6), 1548-57.

227. Engin, E., J. Liu, and U. Rudolph, α2-containing GABA(A) receptors: a target for the development of novel treatment strategies for CNS disorders. *Pharmacology & therapeutics***, 2012**. 136(2), 142-152.

228. Koh, M.T., S. Rosenzweig-Lipson, and M. Gallagher, Selective GABA(A) alpha5 positive allosteric modulators improve cognitive function in aged rats with memory impairment. *Neuropharmacology*, **2013**. 64, 145-52

229. Prevot, T.D., et al., Novel Benzodiazepine-Like Ligands with Various Anxiolytic, Antidepressant, or Pro-Cognitive Profiles. *Mol Neuropsychiatry*, **2019**. 5(2): p. 84-97

230. Collinson, N.; Kuenzi, F. M.; Jarolimek, W.; Maubach, K. A.; Cothliff, R.; Sur, C.;

Smith, A.; Otu, F. M.; Howell, O.; Atack, J. R.; McKernan, R. M.; Seabrook, G. R.; Dawson, G. R.; Whiting, P. J.; Rosahl, T. W., Enhanced Learning and Memory and Altered Gabaergic Synaptic Transmission in Mice Lacking the Alpha 5 Subunit of the Gabaa Receptor. *J. Neurosci*. **2002**, 22 (13), 5572-80.

231. Korpi, E. R.; Mattila, M. J.; Wisden, W.; Luddens, H., Gaba(a)-Receptor Subtypes: Clinical Efficacy and Selectivity of Benzodiazepine Site Ligands. *Ann Med* **1997**, 29 (4), 275-82.161.

232. Fritschy, J. M., & Mohler, H. (1995). GABAA-receptor heterogeneity in the adult rat brain: Differential regional and cellular distribution of seven major subunits. *The Journal of Comparative Neurology*, **1995**, *359*(1), 154–194. https://doi.org/10.1002/cne.903590111

233. Sur, C., Fresu, L., Howell, O., McKernan, R. M., & Atack, J. R. (1999). Autoradiographic localization of alpha5 subunit-containing GABAA receptors in rat brain. *Brain Research*, **1999**, 822(1–2), 265–270.

234. Hauser, J., Rudolph, U., Keist, R., Möhler, H., Feldon, J., & Yee, B. K. Hippocampal α5 subunit-containing GABAA receptors modulate the expression of prepulse inhibition. *Molecular Psychiatry*, **2005**, *10*(2), 201–207. https://doi.org/10.1038/sj.mp.4001554

235. Donegan, J. J., Tyson, J. A., Branch, S. Y., Beckstead, M. J., Anderson, S. A., & Lodge, D. J. Stem cell-derived interneuron transplants as a treatment for schizophrenia: Preclinical validation in a rodent model. *Molecular Psychiatry*, **2017**, *22*(10), 1492–1501. https://doi.org/10.1038/mp.2016.121

236. Lodge, D. J.; Grace, A. A., Hippocampal Dysfunction and Disruption of Dopamine System Regulation in an Animal Model of Schizophrenia. *Neurotox Res* **2008**, 14 (2-3), 97-104.

237. Gill, K. M.; Lodge, D. J.; Cook, J. M.; Aras, S.; Grace, A. A., A Novel Alpha5$GABA_AR$ Positive Allosteric Modulator Reverses Hyperactivation of the Dopamine System in the Mam Model of Schizophrenia. *Neuropsychopharmacology* **2011**, 36 (9), 1903-11.

238. Gill, K. M.; Cook, J. M.; Poe, M. M.; Grace, A. A., Prior Antipsychotic Drug Treatment Prevents Response to Novel Antipsychotic Agent in the Methylazoxymethanol Acetate Model of Schizophrenia. *Schizophr Bull* **2014**, 40 (2), 341-50.

239. Benes, F. M., A New Paradigm for Understanding Gamma-Aminobutyric Acid Cell Pathology in Schizophrenia? *Biol Psychiatry* **2012**, 72 (9), 712-3.

240. Papadimitriou, G. N.; Dikeos, D. G.; Karadima, G.; Avramopoulos, D.; Daskalopoulou, E. G.; Vassilopoulos, D.; Stefanis, C. N., Association between the Gaba(a) Receptor Alpha5 Subunit Gene Locus (Gabra5) and Bipolar Affective Disorder. *Am J Med Genet* **1998**, 81 (1), 73- 80.

241. Piantadosi, S. C.; French, B. J.; Poe, M. M.; Timic, T.; Markovic, B. D.; Pabba, M.; Seney, M. L.; Oh, H.; Orser, B. A.; Savic, M. M.; Cook, J. M.; Sibille, E., Sex-dependent anti-stress effect of an alpha5 subunit containing gabaa receptor positive allosteric modulator. *Front. Pharmacol.* **2016,** *7*, 446.

242. Batinic, B.; Santrac, A.; Jancic, I.; Li, G.; Vidojevic, A.; Markovic, B.; Cook, J. M.; Savic, M. M., Positive modulation of alpha5 GABAA receptors in preadolescence prevents reduced locomotor response to amphetamine in adult female but not male rats prenatally exposed to lipopolysaccharide. *Int. J. Dev. Neurosci.* **2017,** *61*, 31-39.

243. Forkuo, G. S.; Nieman, A. N.; Yuan, N. Y.; Kodali, R.; Yu, O. B.; Zahn, N. M.; Jahan, R.; Li, G.; Stephen, M. R.; Guthrie, M. L.; Poe, M. M.; Hartzler, B. D.; Harris, T. W.; Yocum, G. T.; Emala, C. W.; Steeber, D. A.; Stafford, D. C.; Cook, J. M.; Arnold, L. A., Alleviation of multiple asthmatic pathologic features with orally available and subtype selective GABAA receptor modulators. *Mol. Pharm.* **2017,** *14* (6), 2088-2098.

244. Mizuta, K.; Xu, D.; Pan, Y.; Comas, G.; Sonett, J. R.; Zhang, Y.; Panettieri, R. A., Jr.; Yang, J.; Emala, C. W., Sr., GABAA receptors are expressed and facilitate relaxation in airway smooth muscle. *Am. J. Physiol. Lung Cell Mol. Physiol.* **2008,** *294* (6), L1206-16.

245. Gallos, G.; Yim, P.; Chang, S.; Zhang, Y.; Xu, D.; Cook, J. M.; Gerthoffer, W. T.; Emala, C. W., Sr., Targeting the restricted alpha-subunit repertoire of airway smooth muscle GABAA receptors augments airway smooth muscle relaxation. *Am. J. Physiol. Lung Cell Mol. Physiol.* **2012,** *302* (2), L248-56.

246. Richetto J, Labouesse MA, Poe MM, Cook JM, Grace AA, Riva MA, Meyer U. Behavioral effects of the benzodiazepine-positive allosteric modulator SH-053-2'F-S-CH_3 in an immune-mediated neurodevelopmental disruption model. Int J *Neuropsychopharmacol*. **2015** ,18(4), 055. doi: 10.1093/ijnp/pyu055. PMID: 25636893; PMCID: PMC4360215.

247. Hortnagl, H.; Tasan, R. O.; Wieselthaler, A.; Kirchmair, E.; Sieghart, W.; Sperk, G.,Patterns of mRNA and Protein Expression for 12 GABAA receptor subunits in the mouse brain. *Neuroscience* **2013,** 236, 345-72.

248. Howell, O.; Atack, J. R.; Dewar, D.; McKernan, R. M.; Sur, C., Density and Pharmacology of α5 Subunit-Containing gabaa receptors are preserved in hippocampus of alzheimer's disease patients. *Neuroscience* **2000**, 98 (4), 669-675

249. Rissman, R. A.; Mishizen-Eberz, A. J.; Carter, T. L.; Wolfe, B. B.; De Blas, A. L.;

Miralles, C. P.; Ikonomovic, M. D.; Armstrong, D. M., Biochemical Analysis of Gabaa

Receptor Subunits α1, α 5, β1, β 2 in the hippocampus of patients with alzheimer's disease neuropathology. *Neuroscience* **2003**, 120 (3), 695-704.

250. Rissman, R. A.; Bennett, D. A.; Armstrong, D. M., Subregional Analysis of GABAA receptor subunit mrnas in the hippocampus of older persons with and without cognitive impairment. *J Chem Neuroanat* **2004**, 28 (1-2), 17-25.

251. Brady, M. L.; Jacob, T. C., Synaptic Localization of α5 GABAA receptors via gephyrin interaction regulates dendritic outgrowth and spine maturation. Dev *Neurobiol* **2015**, 75 (11), 1241-51

252. Koh, M. T.; Rosenzweig-Lipson, S.; Gallagher, M., Selective GABAA alpha5 positive allosteric modulators improve cognitive function in aged rats with memory impairment. *Neuropharmacology* **2013**, 64, 145-52.

253. Prevot, T. D.; Sumitomo, A.; Tomoda, T.; Knutson, D. E.; Li, G.; Cook, J. M.; Sibille,E., Chronic administration of a positive allosteric modulator at the α5-gabaa receptor reverses age-related dendritic shrinkage. **2020,** https://doi.org/10.1101/2020.02.28.964742

254. Curto, Y.; Garcia-Mompo, C.; Bueno-Fernandez, C.; Nacher, J., Chronic Benzodiazepine Treatment Decreases Spine Density in Cortical Pyramidal Neurons. *Neurosci Lett* **2016**, 613, 41-6

255. Gerhard, D. M.; Pothula, S.; Liu, R. J.; Wu, M.; Li, X. Y.; Girgenti, M. J.; Taylor, S.R.; Duman, C. H.; Delpire, E.; Picciotto, M.; Wohleb, E. S.; Duman, R. S., GABA interneurons are the cellular trigger for ketamine's rapid antidepressant actions. *J Clin Invest* **2020**, 130 (3), 1336-1349.

256. Ghosal, S.; Duman, C. H.; Liu, R. J.; Wu, M.; Terwilliger, R.; Girgenti, M. J.; Wohleb, E.; Fogaca, M. V.; Teichman, E. M.; Hare, B.; Duman, R. S., Ketamine rapidly reverses stress induced impairments in gabaergic transmission in the prefrontal cortex in male rodents. *Neurobiol Dis* **2020**, 134, 104669

257. Fier, P. S.; Whittaker, A. M., An Atom-Economical Method to Prepare Enantiopure Benzodiazepines with N-Carboxyanhydrides. *Org. Lett*. **2017**, 19 (6), 1454-1457

258. Bailey, J. L., 679. The Synthesis of Simple Peptides from Anhydro-N-Carboxyamino Acids. *Journal of the Chemical Society* , **1950**, 3461.

259. Brenner, M.; Photaki, I., Zur Herstellung Der Chlorid-Hydrochloride Der ?-Aminos  Uren. *Helv. Chim. Acta* **1956,** *39* (6), 1525-1528

260. Daly, W. H.; Poché, D., The Preparation of N-Carboxyanhydrides of A-Amino Acids Using Bis(Trichloromethyl)Carbonate. *Tetrahedron Lett.* **1988**, 29 (46), 5859-5862

261. Yang, J.; Teng, Y.; Ara, S.; Rallapalli, S.; Cook, J. M., An Improved Process for the Synthesis of 4h-Imidazo[1,5-a][1,4]Benzodiazepines. *Synthesis* **2009**, 40 (32), 145687

262. Cassar, L., Synthesis of Aryl- and Vinyl-Substituted Acetylene Derivatives by the Use of Nickel and Palladium Complexes. *J. Organomet. Chem*. **1975**, 93 (2), 253-257

263. Dieck, H. A.; Heck, F. R., Palladium Catalyzed Synthesis of Aryl, Heterocyclic and Vinylic Acetylene Derivatives. *J. Organomet. Chem*. **1975**, 93 (2), 259-263

264. Santrač, A.; Bijelić, D.; Stevanović, V.; Banićević, M.; Aranđelović, J.; Batinić, B.; Sharmin, D.; Cook, J.M.; Savić M., M. Postweaning positive modulation of

α5GABAA receptors improves autism-like features in prenatal valproate rat model in a sex-specific manner. *Autism Res.* **2022**, *15*, 806–820

265. Perez, S.M.; McCoy, A.M.; Prevot, T.D.; Mian, M.Y.; Carreno, F.R.; Frazer, A.; Cook, J.M.; Sibille, E.; Lodge D., J. Hippocampal α5-GABAA Receptors Modulate Dopamine Neuron Activity in the Rat Ventral Tegmental Area. *Biol. Psychiatry Glob Open Sci.* **2022**, *3*, 78–86. [Google Scholar] [CrossRef] [PubMed]

266. Santrac, A.; Stamenić, T.T.; Batinić, B.; Matović, B.D.; Stanković, T.; Poe, M.; Cook, J.; Savić, M.M.P. 225 Effect of MP-III-022, positive modulator of alpha 5 containing GABAA receptors, on learning and memory. *Eur. Neuropsychopharmacol.* **2019**, *29*, S173–S174.

267. Wallace, D. J.; Chen, C.-y., Cyclopropylboronic acid: synthesis and Suzuki cross-coupling reactions. *Tetrahedron Lett.* **2002,** *43* (39), 6987-6990.

268. Patani, G. A.; LaVoie, E. J., Bioisosterism: A rational approach in drug design. *Chemical Reviews* **1996,** *96* (8), 3147-3176.

269. Batinic, B.; Santrac, A.; Jancic, I.; Li, G.; Vidojevic, A.; Markovic, B.; Cook, J. M.; Savic, M. M., Positive modulation of alpha5 GABAA receptors in preadolescence prevents reduced locomotor response to amphetamine in adult female but not male rats prenatally exposed to lipopolysaccharide. *Int. J. Dev. Neurosci.* **2017,** *61*, 31-39.

270. Namjoshi, O. A.; Wang, Z.-j.; Rallapalli, S. K.; Johnson, E. M.; Johnson, Y.-T.; Ng, H.; Ramerstorfer, J.; Varagic, Z.; Sieghart, W.; Majumder, S.; Roth, B. L.; Rowlett, J. K.; Cook, J. M., Search for α3β2/3γ2 subtype selective ligands that are stable on human liver microsomes. *Bioorganic & Medicinal Chemistry* **2013,** *21* (1), 93-101

271. Ohmoto, K.; Yamamoto, T.; Horiuchi, T.; Imanishi, H.; Odagaki, Y.; Kawabata, K.; Sekioka, T.; Hirota, Y.; Matsuoka, S.; Nakai, H.; Toda, M.; Cheronis, J. C.; Spruce, L. W.; Gyorkos, A.; Wieczorek, M. Design and synthesis of new orally active nonpeptidic inhibitors of human neutrophil elastase. *J. Med. Chem*. **2000**, 43, 4927−4929

272. Ono, M.; Haratake, M.; Saji, H.; Nakayama, M. Development of novel β-amyloid probes based on 3,5-diphenyl-1,2,4-oxadiazole. *Bioorg. Med. Chem*. **2008**, 16, 6867−6872

273. Orlek, B. S.; Blaney, F. E.; Brown, F.; Clark, M. S. G.; Hadley, M. S.; Hatcher, J.; Riley, G. J.; Rosenberg, H. E.; Wadsworth, H. J.; Wyman, P. Comparison of azabicyclic esters and oxadiazoles as ligands for the muscarinic receptor. *J. Med. Chem.* **1991**, 34, 2726−2735

274. Patani, G. A.; LaVoie, E. J. Bioisosterism: A rational approach in drug design. *Chem. Rev*. **1996**, 96, 3147−3176

275. Warmus, J. S.; Flamme, C.; Zhang, L. Y.; Barrrett, S.; Bridges, A.; Kaufman, M.; Tecle, H.; Gowan, R.; Sebolt-Leopold, J.; Leopold, W.; Merriman, R.; Przybranowski, S.; Valik, H.; Chen, J.; Ohren, J.; Pavlovsky, A.; Whithead, C.; Ahang, E. 2-Alkylamino- and alkoxysubstituted 2-amino-1,3,4-oxadiazoles-O-Alkyl benzohydroxamate esters replacements retain the desired inhibition and selectivity against MEK (MAP ERK kinase). *Bioorg. Med. Chem. Lett*. **2008**, 18, 6171− 6174

276. McBriar, M. D.; Clader, J. W.; Chu, I.; Del Vecchio, R. A.; Favreau, L.; Greenlee, W. J.; Hyde, L. A.; Nomeir, A. A.; Parker, E. M.; Pissarnitski, D. A.; Song, L.; Zhang, L.; Zhao, Z. Discovery of amide and heteroaryl isosteres as carbamate replacements in a

series of orally active γ-secretase inhibitors. *Bioorg. Med. Chem. Lett*. **2008**, 18, 215−219

277. Bostrom, J.; Hogner, A.; Schmitt, S. Do structurally similar ligands bind in a similar fashion? *J. Med. Chem***. 2006**, 49, 6716−6725

278. Jonas Boström,* Anders Hogner, Antonio Llinas, Eric Wellner, and Alleyn T. Plowright. Oxadiazoles in Medicinal Chemistry. *J. Med. Chem*. **2012**, 55, 5, 1817–1830

279. Bonandi, Elisa, Michael S. Christodoulou, Gaia Fumagalli, Dario Perdicchia, Giulio Rastelli, and Daniele Passarella. "The 1,2,3-Triazole Ring as a Bioisostere in Medicinal Chemistry." *Drug Discovery Today* , **2017,** 22 (10): 1572–81. https://doi.org/10.1016/j.drudis.2017.05.014.

280. Eassa, N.E.; Perez, S.M.; Boley, A.M.; Elam, H.B.; Sharmin, D.; Cook, J.M.; Lodge, D.J. α5-GABAA Receptor Modulation Reverses Behavioral and Neurophysiological Correlates of Psychosis in Rats with Ventral Hippocampal Alzheimer's Disease-like Pathology. *Int. J. Mol. Sci*. **2023**, *24*, 11788. https://doi.org/10.3390/ijms241411788

281. Boley AM, Perez SM, Lodge DJ. A fundamental role for hippocampal parvalbumin in the dopamine hyperfunction associated with schizophrenia. *Schizophr Res* 2014; **157**(1-3)**:** 238-243.

282. Lodge DJ, Behrens MM, Grace AA. A loss of parvalbumin-containing interneurons is associated with diminished oscillatory activity in an animal model of schizophrenia. *The Journal of neuroscience : the official journal of the Society for Neuroscience* 2009; **29**(8)**:** 2344-2354.

283. Perez SM, Aguilar DD, Neary JL, Carless MA, Giuffrida A, Lodge DJ. Schizophrenia-Like Phenotype Inherited by the F2 Generation of a Gestational Disruption Model of Schizophrenia. *Neuropsychopharmacology* 2016; **41**(2)**:** 477-486.

284. Santrač, A.; Bijelić, D.; Stevanović, V.; Banićević, M.; Aranđelović, J.; Batinić, B.; Sharmin, D.; Cook, J. M.; Savić, M. M. Postweaning Positive Modulation of α5GABAA Receptors Improves Autism-like Features in Prenatal Valproate Rat Model in a Sex-specific Manner. *Autism Res*. **2022**, *15* (5), 806–820. https://doi.org/10.1002/aur.2699.

285. Aranđelović J, Santrač A, Batinić B, Todorović L, Stevanović V, Tiruveedhula VVNPB, Sharmin D, Rashid F, Stanojević B, Cook JM, Savić MM. Effects of α5 $GABA_A$ receptor modulation on social interaction, memory, and neuroinflammation in a mouse model of Alzheimer's disease. *CNS Neurosci Ther*. **2022**, 28(11):1767-1778. doi: 10.1111/cns.13914

286. J Clayton-Smith, L Laan. Angelman syndrome: a review of the clinical and genetic aspects. *J Med Genet* **2003**;40:87–95

287. Adriana Jesus Souza; Dishary Sharmin; James M. Cook; Francisco S. Guimarães, Felipe Gomes. An alpha 5-GABAa receptor positive allosteric modulator attenuates social and cognitive deficits without changing dopamine system hyperactivity in an animal model for autism. *European Neuropsychopharmacology*, under review, 2**023**

288. Cavalheiro, E.A. The Pilocarpine Model of Epilepsy. *Ital. J. Neurol. Sci*. **1995,** 16, 33–37.

289. Curia, G.; Longo, D.; Biagini, G.; Jones, R.S.G.; Avoli, M. The pilocarpine model of temporal lobe epilepsy. *J. Neurosci. Methods* **2008**, 172, 143–157.

290. Cifelli, P.; Grace, A.A. Pilocarpine Induced Temporal Lobe Epilepsy in the Rat Is Associated with Increased Dopamine Neuron Activity. *Int. J. Neuropsychopharmacol*. Off. Sci. J. Coll. Int. i. CINP **2012**, 15, 957–964.

291. McCoy, A.M.; Prevot, T.D.; Sharmin, D.; Cook, J.M.; Sibille, E.L.; Lodge, D.J. GL-II-73, a Positive Allosteric Modulator of α5GABA$_A$ Receptors, Reverses Dopamine System Dysfunction Associated with Pilocarpine-Induced Temporal Lobe Epilepsy. *Int. J. Mol. Sci.* **2023**, *24*, 11588. https://doi.org/10.3390/ijms241411588

292. McCoy, A. M. et al. Positive allosteric modulation of α5-GABAA receptors reverses stress-induced alterations in dopamine system function and prepulse inhibition of startle. *Int. J. Neuropsychopharmacol*. **2022**, 42 doi:10.1093/ijnp/pyac035

293. Van Dijken, H. H., Van der Heyden, J. A., Mos, J. & Tilders, F. J. Inescapable footshocks induce progressive and long lasting behavioural changes in male rats. *Physiol. Behav*. **1992**, 51, 787–794.

294. Alexandra M. McCoy, Thomas D. Prevot, Md Yeunus Mian, Dishary Sharmin, Adeeba N. Ahmad, James M. Cook, Etienne L. Sibille, Daniel J. Lodge. Extrasynaptic localization is essential for α5GABAA receptor modulation of dopamine system function. 2023. doi: https://doi.org/10.1101/2023.07.12.548744

295. Grace AA, Bunney BS. Intracellular and extracellular electrophysiology of nigral dopaminergic neurons--1. Identification and characterization. *Neuroscience* 1983; **10**(2)**:** 301-315.

296. Ungless MA, Grace AA. Are you or aren't you? Challenges associated with physiologically identifying dopamine neurons. *Trends in Neurosciences* **2012**; **35**(7)**:** 422-430.

297. Kapadia, M., Bijelic, D., Zhao, H., Ma, D., Stojanovich, L., Miloševic, M., Andjus, P., & Šakic, B. Effects of sustained i.c.v. infusion of lupus CSF and autoantibodies on behavioral phenotype and neuronal calcium signaling. *Acta Neuropathologica Communications,* **2017,** 5(1), 70. https://doi.org/10.1186/s40478-017-0473-1

298. Ganguly, K., Schinder, A. F., Wong, S. T., & Poo, M. GABA itself promotes the developmental switch of neuronal GABAergic responses from excitation to inhibition. *Cell* **2001**,105(4), 521–532. https://doi.org/10.1016/s0092-8674(01)00341-5

299. Saunders, K. Identification of sleep disruption and sleep disordered breathing from the systolic blood pressure profile. Thorax 1993, 48, 647.

300. Papi, A.; Brightling, C.; Pedersen, S. E.; Reddel, H. K., Asthma. *The Lancet* **2018,** *391* (10122), 783-800.

301. Nunes, C.; Pereira, A. M.; Morais-Almeida, M. Asthma costs and social impact. *Asthma Res. Pract*. **2017**, 3

302. Pascual, R. M.; Peters, S. P. Asthma Exacerbations: Pathogenesis, Prevention, and Treatment. *J. Allergy Clin. Immunol***. 2005**, 116, 477

303. Jahan, R.; Stephen, M. R.; Forkuo, G. S.; Kodali, R.; Guthrie, M. L.; Nieman, A. N.;Yuan, N. Y.; Zahn, N. M.; Poe, M. M.; Li, G. *Eur. J. Med. Chem*. **2017**, 126, 550.

304. American_Asthma_Foundation, Impact of Asthma, **2016**. Available at: americanasthmafoundation.org/impact-asthma

305. Barnett, S. B. L.; Nurmagambetov, T. A. Costs of asthma in the United States: 2002-2007 *J. Allergy Clin. Immunol*. **2011**, 127, 145

306. https://www.who.int/news-room/fact-sheets/detail/asthma; Last visited: May 05, 2019

307. Asher, M. I. Effect of urbanisation on asthma, allergy and airways inflammation in a developing country setting. *Thorax* **2011**, 66, 1025

308. Robinson, C. L.; Baumann, L. M.; Romero, K.; Combe, J. M.; Gomez, A.; Gilman, R. H.;Cabrera, L.; Gonzalvez, G.; Hansel, N. N.; Wise, R. A. *Thora*x **2011**, 66, 1051

309. Guarnieri, M.; Balmes, J. R. Outdoor air pollution and asthma. *Lancet* **2014**, 383, 1581

310. Global Initiative for Asthma. Global strategy for asthma management and prevention. **2005**; www.ginasthma.com.

311. Wenzel, S. E.; Schwartz, L. B.; Langmack, E. L.; Halliday, J. L.; Trudeau, J. B.; Gibbs, R. L.; Chu, H. W. Am J. Respir. *Crit. Care Med*. **1999**, 160, 1001

312. Wardlaw, A. J.; Silverman, M.; Siva R.; Green, R. *Clin. Exp. Allergy* **2005**, 35, 1254. https://doi.org/10.1016/S0140-6736(02)11679-5

313. Green, R. H.; Brightling, C. E.; McKenna,S.; Hargadon, B.; Parker, D.; Bradding, P.; Wardlaw, A. J.; Pavord, I. D. *Lancet* **2002**, *360*, 1715

314. Moore, C. T.; Wilson, C. G.; Mayer, C. A.; Acquah, S. S.; Massari, V. J.; Haxhiu, M. A., A GABAergic inhibitory microcircuit controlling cholinergic outflow to the airways. *Journal of applied physiology* **2004,** *96* (1), 260-70.

315. Mizuta, K.; Xu, D.; Pan, Y.; Comas, G.; Sonett, J. R.; Zhang, Y.; Panettieri, R. A., Jr.; Yang, J.; Emala, C. W., Sr., GABAA receptors are expressed and facilitate relaxation

in airway smooth muscle. *Am. J. Physiol. Lung Cell Mol. Physiol.* **2008,** *294* (6), L1206-16.

316. Gallos, G.; Yim, P.; Chang, S.; Zhang, Y.; Xu, D.; Cook, J. M.; Gerthoffer, W. T.; Emala, C. W., Sr., Targeting the restricted α-subunit repertoire of airway smooth muscle GABAA receptors augments airway smooth muscle relaxation. *American journal of physiology. Lung cellular and molecular physiology* **2012,** *302* (2), L248-L256.

317. Gallos, G.; Townsend, E.; Yim, P.; Virag, L.; Zhang, Y.; Xu, D.; Bacchetta, M.; Emala, C. W., Airway epithelium is a predominant source of endogenous airway GABA and contributes to relaxation of airway smooth muscle tone. *Am. J. Physiol. Lung Cell Mol. Physiol.* **2013,** *304* (3), L191-7.

318. Gallos, G.; Gleason, N. R.; Zhang, Y.; Pak, S. W.; Sonett, J. R.; Yang, J.; Emala, C. W., Activation of endogenous GABAA channels on airway smooth muscle potentiates isoproterenol-mediated relaxation. *Am. J. Physiol. Lung Cell Mol. Physiol.* **2008,** *295* (6), L1040-7.

319. Yocum, G. T.; Gallos, G.; Zhang, Y.; Jahan, R.; Stephen, M. R.; Varagic, Z.; Puthenkalam, R.; Ernst, M.; Cook, J. M.; Emala, C. W., Targeting the gamma-aminobutyric acid a receptor alpha4 subunit in airway smooth muscle to alleviate bronchoconstriction. *Am. J. Respir. Cell Mol. Biol.* **2016,** *54* (4), 546-53.

320. Fu, X. W.; Wood, K.; Spindel, E. R., Prenatal Nicotine Exposure Increases Gaba Signaling and Mucin Expression in Airway Epithelium. *Am. J. Respir. Cell Mol. Biol.* **2011**, 44 (2), 222-9.

321. Xiang, Y. Y.; Wang, S.; Liu, M.; Hirota, J. A.; Li, J.; Ju, W.; Fan, Y.; Kelly, M. M.; Ye, B.; Orser, B.; O'Byrne, P. M.; Inman, M. D.; Yang, X.; Lu, W. Y., A Gabaergic

System in Airway Epithelium Is Essential for Mucus Overproduction in Asthma. Nat Med 2007, 13 (7), 862-7.

322. Sanders, R. D.; Grover, V.; Goulding, J.; Godlee, A.; Gurney, S.; Snelgrove, R.; Ma,D.; Singh, S.; Maze, M.; Hussell, T., Immune Cell Expression of Gabaa Receptors and the Effects of Diazepam on Influenza Infection. J Neuroimmunol 2015, 282, 97-103

323. Gallos, G.; Yim, P.; Chang, S.; Zhang, Y.; Xu, D.; Cook, J. M.; Gerthoffer, W. T.; Emala, C. W., Sr., Targeting the restricted alpha-subunit repertoire of airway smooth muscle GABAA receptors augments airway smooth muscle relaxation. *Am. J. Physiol. Lung Cell Mol. Physiol.* **2012,** *302* (2), L248-56.

324. Stamenic, T. T.; Poe, M. M.; Rehman, S.; Santrac, A.; Divovic, B.; Scholze, P.; Ernst, M.; Cook, J. M.; Savic, M. M., Ester to amide substitution improves selectivity, efficacy and kinetic behavior of a benzodiazepine positive modulator of GABAA receptors containing the alpha5 subunit. *Eur. J. Pharmacol.* **2016,** *791*, 433-443

325. Piantadosi, S. C.; French, B. J.; Poe, M. M.; Timic, T.; Markovic, B. D.; Pabba, M.; Seney, M. L.; Oh, H.; Orser, B. A.; Savic, M. M.; Cook, J. M.; Sibille, E., Sex-dependent anti-stress effect of an alpha5 subunit containing gabaa receptor positive allosteric modulator. *Front. Pharmacol.* **2016,** *7*, 446.

326. Obradovic, A. L.; Joksimovic, S.; Batinic, B.; Radulovic, T.; Poe, M. M.; Namjoshi, O. A.; Cook, J. M.; Ramerstorfer, J.; Varagic, Z.; Sieghart, W.; Karovic, B.; Roth, B.; Savic, M. M., SH-I-048A, an *in vitro* nonselective super-agonist at the benzodiazepine site of $GABA_A$ receptors: the approximated activation of receptor subtypes may explain behavioral effects. *Brain Res.* **2014,** *1554*, 36 - 48.

327. Forkuo, G. S.; Nieman, A. N.; Kodali, R.; Zahn, N. M.; Li, G.; Rashid Roni, M. S.; Stephen, M. R.; Harris, T. W.; Jahan, R.; Guthrie, M. L.; et al. A Novel Orally Available Asthma Drug Candidate That Reduces Smooth Muscle Constriction and Inflammation by Targeting GABAA Receptors in the Lung. *Mol Pharm* **2018**, *15* (5), 1766-1777. DOI: 10.1021/acs.molpharmaceut.7b01013.

328. Zahn, N. M.; Mikulsky, B. N.; Roni, M. S. R.; Yocum, G. T.; Mian, M. Y.; Knutson, D. E.; Cook, J. M.; Emala, C. W.; Stafford, D. C.; Arnold, L. A. Nebulized MIDD0301 Reduces Airway Hyperresponsiveness in Moderate and Severe Murine Asthma Models. *ACS Pharmacol Transl Sci* **2020**, *3* (6), 1381-1390. DOI: 10.1021/acsptsci.0c00180.

329. Roni, M. S. R.; Li, G.; Mikulsky, B. N.; Knutson, D. E.; Mian, M. Y.; Zahn, N. M.;Cook, J. M.; Stafford, D. C.; Arnold, L. A., The Effects of Ph on the Structure and Bioavailability of Imidazobenzodiazepine-3-Carboxylate Midd0301. *Mol Pharm* **2020**.

330. Rashid Roni, M. S.; Zahn, N. M.; Yocum, G. T.; Webb, D. A.; Mian, M. Y.; Meyer, M. J.; Tylek, A. S.; Cook, J. M.; Emala, C. W.; Stafford, D. C.; Arnold, L. A. Comparative Pharmacodynamic and Pharmacokinetic Study of MIDD0301 and Its (S) Enantiomer. *Drug Dev. Res.* **2022**, *83* (4), 979–992. https://doi.org/10.1002/ddr.21926

331. Nicolas M. Zahn, M. S. Rashid Roni, Gene T. Yocum, Michelle J. Meyer, Daniel A. Webb, Md Yeunus Mian, James M. Cook, Douglas C. Stafford, Charles W. Emala, and Leggy A. Arnold. Development of Inhaled GABAA Receptor Modulators to Improve Airway Function in Bronchoconstrictive Disorders. *ACS Pharmacology & Translational Science* **2022** *5* (2), 80-88. DOI: 10.1021/acsptsci.1c00238

5. Appendix

5.1. PDSP data

Compound list

PDSP Code	Compound code	M.W.	Chemical formula
58277	DS-I-71	296.12	$C_{12}H_{10}BrNO_3$
58278	DS-I-72	235.21	$C_{12}H_{10}FNO_3$
58279	DS-I-74	235.21	$C_{12}H_{10}FNO_3$
58280	DS-I-75	247.25	$C_{13}H_{13}NO_4$
58281	DS-I-76	314.56	C12H9BrClNO2
58282	DS-I-77	265.69	C13H12ClNO3
58283	DS-1-78	370.21	C17H12BrN3O2
58284	DS-1-80	253.66	C12H9ClFNO2
58285	DS-1-81	253.66	C12H9ClFNO2
58286	DS-1-82	342.36	C20H14N4O2
58287	DS-1-83	309.3	C17H12FN3O2
58288	DS-1-84	309.3	C17H12FN3O2
58289	DS-1-93	355.4	C21H17N5O
58290	DS-1-96	369.43	C22H19N5O
58291	LAU 165	325.75	C17H12ClN3O2
58215	DS-I-16	449.31	C21H17BrN6O
58217	DS-I-49	400.46	C24H21FN4O
72510	DS-II-73	406.24	C19H12BrN5O
72512	DS-II-67	375.4	C22H18FN3O2
72513	DS-III-83	608.71	C33H41FN4O6

Compound #	Receptor	Inhibition 1	Inhibition 2	Inhibition 3	Inhibition 4	Mean %
58277	5-HT1A	0.87	-1.06	-9.08	15.57	1.58
58277	5-HT1B	-0.36	-5.06	-4.09	-10.87	-5.1
58277	5-HT1D	-15.7	24.11	-6.04	5.94	2.08
58277	5-HT1E	22.73	27.95	39.57	19.18	27.36
58277	5-HT2A	17.48	-18.54	-14.02	-13.32	-7.1
58277	5-HT2B	-4.12	-27.41	-31.83	-20.98	-21.09
58277	5-HT2C	6.9	-6.15	0.81	12.12	3.42
58277	5-HT3	34.12	35.97	24.33	9.75	26.04
58277	5-HT4	1.09	-2.39	-16.32	-6.75	-6.09
58277	5-HT5A	-14.06	-15.65	4.72	12.04	-3.24

58277	5-HT6	6.6	-6.36	-4.65	16.65	3.06
58277	5-HT7A	-0.86	7.08	-17.8	-2.45	-3.51
58277	A1	27.12	8.52	18.32	22.12	19.02
58277	A2A	15.72	33.61	47.42	24.79	30.39
58277	Alpha1A	3.7	-7.25	-11.86	0.28	-3.78
58277	Alpha1B	22.66	27.36	35.08	-0.88	21.06
58277	Alpha1D	38.2	14.72	-10.04	18.3	15.3
58277	Alpha2A	-11.23	-30.09	-26.35	-28.89	-24.14
58277	Alpha2B	10.39	-7.3	-5.94	-7.55	-2.6
58277	Alpha2C	37.94	29.28	15.98	1.02	21.06
58277	Beta1	21.7	29.41	20.62	42.37	28.53
58277	Beta2	-10.65	-14.45	-6.21	-24.97	-14.07
58277	Beta3	57.72	39.73	23.85	37.96	39.82
58277	AT2	1.73	3.35	6.86	-3.29	2.16
58277	BZP Rat Brain Site	97.56	99.96	100.41	99.04	99.24
58277	D1	28.64	28.09	-9.18	34.39	20.49
58277	D2	-24.98	-16.65	-25.94	29.03	-9.64
58277	D3	-21.48	24.53	5.77	15.87	6.17
58277	D4	-6.02	4.87	-7.17	10.76	0.61
58277	D5	84.05	73.9	55.23	32.72	61.48
58277	DAT	-56.51	-55.56	-40.23	-31.22	-45.88
58277	DOR	8.03	-14.7	-23.37	-11.19	-10.31
58277	GABAA	25.58	32.92	14.92	32.92	26.59
58277	H1	26.43	29.01	32.52	35.41	30.84
58277	H2	12.5	8.09	-2.02	4.04	5.65
58277	H3	-17.71	0.98	1.18	2.76	-3.2
58277	H4	25.63	6.02	2.27	8.87	10.7
58277	KOR	-15.12	-8.12	-20.91	-6.31	-12.62
58277	M1	38.79	-10.09	15.68	23.19	16.89
58277	M2	32.28	-7.52	-14.74	-15.95	-1.48
58277	M3	3.86	-0.85	5.97	15.77	6.19
58277	M4	-3.6	-5.52	-11.61	-7.69	-7.11
58277	M5	2.3	-8.52	-16.08	1.77	-5.13
58277	MOR	8.01	7.31	0.35	0.43	4.03
58277	NET	4.07	10.53	-6.35	-13.27	-1.26
58277	PBR	-1.76	7.21	-1.85	-11	-1.85
58277	SERT	8.96	-3.35	-9.72	-16.52	-5.16
58277	Sigma 1	-3.21	17.9	-9.89	7.48	3.07
58277	Sigma 2	3.01	8.24	-1.55	-9.02	0.17
58277	AMPA	32.42	-34.31	0.32	9.92	2.09
58277	Kainate (Rat Brain)	37.47	30.31	18.23	68.34	38.59

58277	NMDA	86.54	47.86	32.39	18.71	46.38
58277	NR2B	8.25	24.04	10.35	12.17	13.7
58277	HCA2	29.64	10.55	36.13	33.84	27.54
58277	Ca channel human	25.4	2.82	7.66	-6.85	7.26
58277	HERG	-9.06	1.47	-36.95	0.85	-10.92
58277	M3D	36.16	19.96	21.5	-7.81	17.45
58277	M4 D	13.61	3.04	8.06	9.88	8.65
58277	NTS1	3.25	5.71	1.9	3.02	3.47
58277	Alpha2Beta2	-1.96	-0.76	-0.39	10	1.72
58277	Alpha2Beta4	-5.3	-2.36	-4.18	7.27	-1.14
58277	Alpha3Beta2	-1.39	-1.19	-7.63	-6.26	-4.12
58277	Alpha3Beta4	1.63	2.24	-7.95	11.06	1.75
58277	Alpha4Beta2	9.9	5.69	-2.16	31.48	11.23
58277	Alpha4Beta2 (Rat Brain)	-1.19	2.4	-6.53	4.15	-0.29
58277	Alpha4Beta4	3.4	10.34	11.55	18.19	10.87
58277	Alpha7	1.88	4.43	-1.76	15.01	4.89
58277	NOP	-1.35	29.99	8.56	6.38	10.9
58277	OT	-13.51	-14.9	-6.01	1.49	-8.23
58277	V1A	-7.51	3.2	6.65	66.41	17.19
58277	V1B	34.54	5.42	15.87	27.2	20.76
58277	V2	0.09	-21.28	-18.43	-31.26	-17.72
58277	PBR	26.12	4.8	5.96	1.58	9.62
58277	SERT	21.33	-0.68	-10.97	-17.71	-2.01
58277	GABAA	24.53	8.58	0.36	21.63	13.78
58277	Oxytocin	3.78	-5.76	-15.57	-16.89	-8.61
58278	5-HT1A	-8.93	-20.95	0.58	6.96	-5.59
58278	5-HT1B	4.2	-7.27	-11.83	4.34	-2.64
58278	5-HT1D	-9.52	4.01	6.71	6.71	1.98
58278	5-HT1E	30.08	20.12	23.21	27.24	25.16
58278	5-HT2A	-14.54	3.21	-3.23	13.82	-0.19
58278	5-HT2B	2.31	-12.95	-25	-15.36	-12.75
58278	5-HT2C	12.33	10.16	-16.37	1.24	1.84
58278	5-HT3	17.23	24.02	26.1	29.65	24.25
58278	5-HT4	17.63	12.4	7.18	28.94	16.54
58278	5-HT5A	31.45	-14.06	13.31	-20.74	2.49
58278	5-HT6	6.99	-3.85	-11.92	-10.6	-4.85
58278	5-HT7A	-7.48	-9.59	8.53	-3.37	-2.98
58278	A1	7.52	-20.27	30.12	29.32	11.67
58278	A2A	21.13	49.5	27.45	9.73	26.95
58278	Alpha1A	10.54	-11.18	-8.1	-11.86	-5.15
58278	Alpha1B	20.57	41.44	29.52	-2.97	22.14

58278	Alpha1D	33.62	29.9	22.31	21.6	26.86
58278	Alpha2A	10.48	-10.33	-22.9	-34.88	-14.41
58278	Alpha2B	17.44	-3.96	-2.16	-5.13	1.55
58278	Alpha2C	12.77	35.32	7.53	13.14	17.19
58278	Beta1	20.62	15.54	27.26	28.49	22.98
58278	Beta2	-19.98	-17.92	-6.32	-14.88	-14.78
58278	Beta3	53.48	26.32	65.83	32.67	44.58
58278	AT2	4.07	-0.92	6.14	5.01	3.58
58278	BZP Rat Brain Site	97.21	97.33	99.5	97.9	97.99
58278	D1	32.91	18.63	11.96	0.65	16.04
58278	D2	-10.4	-35.24	-32.19	-13.12	-22.74
58278	D3	-0.48	0.48	8.34	7.05	3.85
58278	D4	1.54	-2.95	8.58	1.02	2.05
58278	D5	7.76	3.91	4.72	2.74	4.78
58278	DAT	-38.6	-38.79	-24.32	-28.25	-32.49
58278	DOR	2.87	-12.36	-15.88	-8.61	-8.5
58278	GABAA	39.58	44.25	10.92	-11.75	20.75
58278	H1	26.74	20.85	-6.09	16.21	14.43
58278	H2	36.58	26.72	-7.33	22.61	19.65
58278	H3	1.38	-6.3	0.98	9.64	1.43
58278	H4	25.63	-6.82	8.51	7.44	8.69
58278	KOR	-17.75	-12.48	-13.99	-5.18	-12.35
58278	M1	-7.06	-5.49	24.4	28.27	10.03
58278	M2	15.16	-1.78	-13.63	-9.56	-2.45
58278	M3	2.45	4.51	29.26	17.18	13.35
58278	M4	10.92	-11.35	-13.15	-13.07	-6.66
58278	M5	4.85	16.1	4.67	9.15	8.69
58278	MOR	2.98	7	2.13	7	4.78
58278	NET	-0.27	2.17	-3.61	-3.69	-1.35
58278	PBR	39.73	-12.94	-21.9	-16.45	-2.89
58278	SERT	6.91	-12.04	-2.54	-3.19	-2.72
58278	Sigma 1	15.37	-9.49	-2.87	4.81	1.96
58278	Sigma 2	11.5	-9.23	-5.56	3.82	0.13
58278	AMPA	24.83	-1.71	22.56	26.6	18.07
58278	Kainate (Rat Brain)	24.34	40.06	43.08	64.25	42.93
58278	NMDA	65.41	26.74	24.06	9.19	31.35
58278	NR2B	29.18	78.21	18.36	14.99	35.19
58278	HCA2	25.44	12.84	45.3	20.48	26.02
58278	Ca channel human	-10.08	-6.85	22.18	-8.47	-0.81
58278	HERG	23.99	-17.74	-38.19	8.7	-5.81

58278	M3D	32.3	13.02	15.33	23.82	21.12
58278	M4 D	-1.01	10.83	87.94	3.95	25.43
58278	NTS1	9.74	3.02	9.74	2.13	6.16
58278	Alpha2Beta2	4.68	1.06	3.47	3.47	3.17
58278	Alpha2Beta4	5.24	0.48	-5.19	2.91	0.86
58278	Alpha3Beta2	2.8	0.27	8.94	7.58	4.9
58278	Alpha3Beta4	2.7	2.4	-0.34	4.37	2.28
58278	Alpha4Beta2	7.35	0.29	3.73	5.98	4.34
58278	Alpha4Beta2 (Rat Brain)	5.99	-4.11	11.59	8.58	5.51
58278	Alpha4Beta4	12.45	13.96	11.25	9.13	11.7
58278	Alpha7	-7.23	19.99	6.14	7.96	6.72
58278	NOP	8.85	18.47	10.31	6.67	11.08
58278	OT	-12.4	-2.12	-22.4	-5.17	-10.52
58278	V1A	17.7	-0.95	40.16	61.23	29.54
58278	V1B	-1.03	-6.14	-10.81	20.98	0.75
58278	V2	21.46	-23.42	-51.91	-33.39	-21.82
58278	PBR	14.97	13.64	11.58	5.63	11.46
58278	SERT	24.28	-0.2	-5.32	-14.34	1.11
58278	GABAA	33.23	21.15	16.31	2.78	18.37
58278	Oxytocin	-22.46	-29.61	-5.76	6.96	-12.72
58279	5-HT1A	5.92	3.99	-4.47	8.3	3.44
58279	5-HT1B	4.61	9.45	-0.09	-2.99	2.75
58279	5-HT1D	4.4	-3.33	-2.56	8.26	1.69
58279	5-HT1E	20.6	33.17	35.06	31.51	30.09
58279	5-HT2A	-12.63	-18.02	28.09	18.52	3.99
58279	5-HT2B	1.51	-22.99	-36.65	-34.64	-23.19
58279	5-HT2C	4.72	21.03	-1.15	-3.54	5.27
58279	5-HT3	2.51	34.97	28.72	38.43	26.16
58279	5-HT4	15.02	1.96	5.44	15.89	9.58
58279	5-HT5A	-7.69	-3.87	-5.46	-8.96	-6.5
58279	5-HT6	18.5	-3.59	-10.6	-10.6	-1.57
58279	5-HT7A	4.43	-4.83	-3.51	2.71	-0.3
58279	A1	27.92	27.32	29.92	38.92	31.02
58279	A2A	28.28	41.84	37.1	40.1	36.83
58279	Alpha1A	-1.43	-4.17	-4	-8.44	-4.51
58279	Alpha1B	16.67	3.24	-2.32	-2.32	3.82
58279	Alpha1D	29.61	-7.75	-1.74	-14.19	1.48
58279	Alpha2A	-2.69	0	0	-6.74	-4.72
58279	Alpha2B	-3.04	-11.85	0.02	-0.49	-3.84
58279	Alpha2C	11.22	8.82	6.25	5.98	8.07
58279	Beta1	39.59	11.84	23.71	44.53	29.92
58279	Beta2	-17.81	-12.06	7.35	-0.24	-5.69

58279	Beta3	25.26	30.56	45.02	40.08	35.23
58279	AT2	0.48	-1.86	7.65	-11.74	-1.37
58279	BZP Rat Brain Site	80.06	74.46	75.83	81.89	78.06
58279	D1	27.35	2.87	25.68	6.58	15.62
58279	D2	18.45	-8.31	-7.99	-17.45	-3.83
58279	D3	11.38	3.69	18.12	8.5	10.42
58279	D4	9.86	-4.48	-3.59	14.86	4.16
58279	D5	8.11	6.47	5.54	19.31	9.86
58279	DAT	-25.95	-17.71	-33.33	-10.91	-21.98
58279	DOR	-2.05	-2.75	-30.64	-5.1	-10.14
58279	GABAA	15.58	23.58	-0.42	2.25	10.25
58279	H1	5.68	20.13	-12.49	-12.59	0.18
58279	H2	47.14	39.28	-5.08	13.7	23.76
58279	H3	7.87	-1.38	3.54	14.17	6.05
58279	H4	5.84	1.92	6.55	9.76	6.02
58279	KOR	-20.38	-20.01	-14.66	-22.72	-19.44
58279	M1	-23.15	0.08	-4.28	21.61	-1.44
58279	M2	13.21	-19.09	-20.85	-3.08	-7.45
58279	M3	8.84	6.02	23.84	7.92	11.66
58279	M4	-1.2	-22.53	-9.2	-14.87	-11.95
58279	M5	-7.46	16.19	16.36	4.41	7.38
58279	MOR	10.41	5.45	-2.05	4.91	4.68
58279	NET	-0.8	-10.46	-20.65	-8.71	-10.16
58279	PBR	18.57	-2.49	10.44	-21.25	1.32
58279	SERT	-0.76	5.29	-14.36	6.48	-0.84
58279	Sigma 1	18.71	-15.37	5.61	3.74	3.17
58279	Sigma 2	17.62	24.35	24.62	14.7	20.32
58279	AMPA	59.97	28.37	-3.22	23.32	27.11
58279	Kainate (Rat Brain)	-35.47	-7.79	-18.86	0.52	-15.4
58279	NMDA	51.73	27.04	21.98	15.43	29.05
58279	NR2B	86.38	82.57	2.02	14.93	46.48
58279	HCA2	-0.14	9.79	31.17	30.79	17.9
58279	Ca channel human	17.34	12.5	17.34	12.5	14.92
58279	HERG	20.89	1.88	-32.4	-28.89	-9.63
58279	M3D	27.68	-7.81	13.79	9.16	10.71
58279	M4 D	-8.87	6.4	0.69	-7.04	-2.21
58279	NTS1	18.69	13.09	19.14	5.48	14.1
58279	Alpha2Beta2	-3.9	9.03	9.76	3.71	4.65
58279	Alpha2Beta4	2.91	10.31	4.54	-4.99	3.19
58279	Alpha3Beta2	10.02	0.85	1.15	5.34	4.34

58279	Alpha3Beta4	-10.08	-7.19	-3.99	-10.53	-7.95
58279	Alpha4Beta2	7.35	4.22	8.24	3.92	5.93
58279	Alpha4Beta2 (Rat Brain)	-5.37	-1.69	0.73	0.98	-1.34
58279	Alpha4Beta4	16.98	18.19	7.62	17.28	15.02
58279	Alpha7	28.98	13.06	7.47	24	18.38
58279	NOP	3.61	11.77	27.66	18.91	15.49
58279	OT	-12.12	-9.9	-5.17	7.05	-5.04
58279	V1A	-8.89	12.18	5.61	85.06	23.49
58279	V1B	0.08	6.75	-32.37	8.53	-4.25
58279	V2	48.53	80.59	77.74	69.19	69.01
58279	PBR	13.64	10.09	23.31	19.01	16.51
58279	SERT	27.29	-2.37	-11.03	-6.7	1.8
58279	GABAA	6.16	11.48	-2.05	20.18	8.94
58279	Oxytocin	5.9	-4.44	-3.11	-4.44	-1.52
58280	5-HT1A	-0.76	-12.19	-1.95	-9.97	-6.22
58280	5-HT1B	21.06	10.97	4.47	0.19	9.17
58280	5-HT1D	4.01	2.08	-4.11	0.14	0.53
58280	5-HT1E	30.08	40.04	42.41	28.66	35.3
58280	5-HT2A	-15.41	-8.97	1.29	32.61	2.38
58280	5-HT2B	3.11	-31.02	-19.78	-18.57	-16.57
58280	5-HT2C	9.51	5.37	-7.46	-2.89	1.13
58280	5-HT3	-7.29	2.74	13.38	44.91	13.44
58280	5-HT4	18.5	9.79	25.46	28.07	20.46
58280	5-HT5A	3.77	-0.05	-27.11	-3.55	-6.74
58280	5-HT6	26.57	-6.5	-3.72	-4.78	2.89
58280	5-HT7A	11.31	0.86	-13.83	-5.49	-1.79
58280	A1	34.12	23.32	7.92	97.3	40.67
58280	A2A	33.19	45.67	48.25	53.99	45.28
58280	Alpha1A	-13.57	-8.27	-8.44	-10.84	-10.28
58280	Alpha1B	9.95	-10.26	0.57	-4.7	-1.11
58280	Alpha1D	6.99	-3.03	-4.74	-1.74	-0.63
58280	Alpha2A	31.59	34.13	54.19	25.6	36.38
58280	Alpha2B	20.69	14.39	26.82	17.57	19.87
58280	Alpha2C	22.5	22.34	16.51	22.34	20.92
58280	Beta1	40.66	17.47	9.86	10.02	19.5
58280	Beta2	33.16	26.22	1.27	-7.73	13.23
58280	Beta3	58.42	36.2	34.79	10.8	35.05
58280	AT2	3.58	13.54	18.33	13.57	12.26
58280	BZP Rat Brain Site	65.19	61.88	68.62	72.51	67.05
58280	D1	35.32	10.85	9.36	-10.1	11.36
58280	D2	15.31	17.96	5.4	7.59	11.57

58280	D3	11.54	23.57	17.96	6.25	14.83
58280	D4	13.32	-1.67	-0.64	2.31	3.33
58280	D5	10.79	8.22	10.44	24.44	13.47
58280	DAT	-4.08	-25.59	-29.01	-21.81	-20.12
58280	DOR	0.29	-15.88	1.93	-21.73	-8.85
58280	GABAA	14.25	11.58	-8.42	2.92	5.08
58280	H1	-2.58	-8.98	-35.2	-14.55	-15.33
58280	H2	38.78	26.82	16.55	10.44	23.15
58280	H3	8.27	-1.38	-0.39	-6.3	0.05
58280	H4	9.23	3.7	-0.4	-1.83	2.68
58280	KOR	-14.44	-18.73	-29.26	52.32	-2.53
58280	M1	66.38	11.21	33.23	17.86	32.17
58280	M2	7.2	-12.43	-2.06	-20.85	-7.04
58280	M3	4.29	10.47	3.26	5.16	5.8
58280	M4	7.31	-6.02	-8.6	-8.77	-4.02
58280	M5	-8.78	3.35	7.22	-0.08	0.43
58280	MOR	15.9	22.32	8.01	3.91	12.54
58280	NET	-0.8	-13.35	-13.35	-31.52	-14.76
58280	PBR	17.65	9.79	3.6	2.03	8.27
58280	SERT	18.09	1.73	-11.18	2.92	2.89
58280	Sigma 1	13.66	-6.57	7.66	12.01	6.69
58280	Sigma 2	0.77	-20.13	2.62	-12.17	-7.23
58280	AMPA	5.88	19.53	-9.29	32.92	12.26
58280	Kainate (Rat Brain)	-23.01	-7.79	-17.47	-16.09	-16.09
58280	NMDA	60.95	22.57	-0.04	25.25	27.18
58280	NR2B	37.27	1.15	-9.22	24.28	13.37
58280	HCA2	-32.22	-48.26	19.33	18.95	-10.55
58280	Ca channel human	38.31	-2.02	6.05	-10.08	8.07
58280	HERG	19.44	-51.82	-6.17	-7.41	-11.49
58280	M3D	16.88	-10.13	-7.04	9.16	2.22
58280	M4 D	-5.69	-7.35	-20.41	-10	-10.86
58280	NTS1	12.87	11.08	12.87	14.66	12.87
58280	Alpha2Beta2	1.66	2.27	5.53	7.1	4.14
58280	Alpha2Beta4	3.72	3.93	-1.24	-7.93	-0.38
58280	Alpha3Beta2	5.44	5.53	4.56	9.63	6.29
58280	Alpha3Beta4	24.14	0.72	-1.1	-2.02	5.44
58280	Alpha4Beta2	-8.34	-9.32	-1.08	4.12	-3.66
58280	Alpha4Beta2 (Rat Brain)	-1.36	-2.19	-4.36	-5.11	-3.26
58280	Alpha4Beta4	13.66	16.08	2.79	19.7	13.06
58280	Alpha7	4.68	-19.99	0.55	19.5	1.19

58280	NOP	14.98	5.36	26.05	27.07	18.37
58280	OT	2.05	8.99	-0.45	19.27	7.47
58280	V1A	10.79	22.88	8.72	79.53	30.48
58280	V1B	-8.14	-8.59	-5.25	-3.7	-6.42
58280	V2	59.93	70.61	62.78	58.5	62.96
58280	PBR	-8.91	-25.52	-0.9	7.2	-7.03
58280	SERT	31.56	13.93	-19.09	-1.83	6.14
58280	GABAA	33.23	14.86	-1.57	18.73	16.31
58280	Oxytocin	-0.2	-7.88	-3.38	-18.48	-7.49
58281	5-HT1A	-5.96	-5.36	-2.99	-14.27	-7.15
58281	5-HT1B	9.73	7.65	-7.96	0.05	2.37
58281	5-HT1D	-5.27	-13.77	-8.74	2.08	-6.43
58281	5-HT1E	31.74	34.59	24.87	29.13	30.08
58281	5-HT2A	-8.28	-12.28	-1.84	-11.76	-8.54
58281	5-HT2B	2.71	-28.21	-29.02	-12.15	-16.67
58281	5-HT2C	-11.59	5.37	30.6	-9.2	3.8
58281	5-HT3	-6.82	-11.3	-1.43	55.01	8.87
58281	5-HT4	3.7	8.92	4.57	-5.88	2.83
58281	5-HT5A	-14.06	-6.42	-29.01	-12.15	-15.41
58281	5-HT6	12.94	-6.36	-15.23	4.74	-0.98
58281	5-HT7A	3.11	-2.18	-7.21	6.02	-0.07
58281	A1	24.12	18.52	-12.67	29.52	14.87
58281	A2A	32.61	31.36	23.62	15.39	25.75
58281	Alpha1A	-10.66	0.79	-4.17	-9.64	-5.92
58281	Alpha1B	-12.72	-2.47	-15.82	5.55	-6.37
58281	Alpha1D	17.3	15.73	10.86	-2.88	10.25
58281	Alpha2A	-0.45	5.99	39.52	7.63	13.17
58281	Alpha2B	9.11	-2.7	2.35	6.21	3.74
58281	Alpha2C	21.32	7.91	26.45	7.64	15.83
58281	Beta1	13.5	9.69	11.51	15.82	12.63
58281	Beta2	47.47	28.17	8.76	-10.76	18.41
58281	Beta3	61.24	53.48	47.13	39.37	50.31
58281	AT2	-1.37	-2.16	13.65	0.14	2.57
58281	BZP Rat Brain Site	60.16	50.21	61.31	60.96	58.16
58281	D1	24.38	-16.04	9.73	16.96	8.76
58281	D2	19.45	8.97	5.28	2.17	8.97
58281	D3	8.34	9.94	4.17	10.74	8.3
58281	D4	12.17	-18.96	1.92	-0.64	-1.38
58281	D5	7.87	20.94	6.36	31.44	16.65
58281	DAT	-1.97	-23.92	-36.86	-24.14	-21.72
58281	DOR	2.87	-36.5	-20.56	-14.47	-17.17
58281	GABAA	18.92	1.58	20.92	36.92	19.59

58281	H1	-6.61	-21.68	-29.52	-14.76	-18.14
58281	H2	32.67	46.29	29.97	5.89	28.71
58281	H3	-1.57	-4.53	-4.33	-0.2	-2.66
58281	H4	3.16	-5.93	-13.42	10.83	-1.34
58281	KOR	-12.48	-23.54	-9.62	-15.27	-15.23
58281	M1	8.18	-2.47	17.74	37.1	15.14
58281	M2	22.19	-10.39	3.86	-6.23	2.36
58281	M3	-3.81	2.15	-2.26	2.93	-0.25
58281	M4	2.41	-5.24	-3.78	-18.83	-6.36
58281	M5	-4.65	19.44	9.59	17.33	10.43
58281	MOR	-0.58	9.71	6.07	-1.2	3.5
58281	NET	-3.92	-15.78	-11.52	-17.61	-12.21
58281	PBR	7.85	16.72	6.38	15.8	11.69
58281	SERT	11.99	-2.27	3.67	2.38	3.94
58281	Sigma 1	-14.63	-13.36	-4.94	8.15	-6.2
58281	Sigma 2	15.58	15.85	23.8	18.98	18.55
58281	AMPA	26.6	-48.21	-19.65	11.94	-7.33
58281	Kainate (Rat Brain)	-5.02	-28.55	-65.92	-41	-35.12
58281	NMDA	68.98	31.2	18.11	20.19	34.62
58281	NR2B	36.82	23.88	21.77	31.52	28.5
58281	HCA2	-12.74	-50.93	-14.27	2.91	-18.76
58281	Ca channel human	12.5	1.21	25.4	4.44	10.89
58281	HERG	0.65	-19.39	-7.41	-24.14	-12.57
58281	M3D	23.82	9.93	8.39	-5.5	9.16
58281	M4 D	-0.36	-1.35	-18.24	18.89	-0.27
58281	NTS1	4.59	21.82	11.98	6.6	11.25
58281	Alpha2Beta2	0.57	-2.2	3.96	0.69	0.76
58281	Alpha2Beta4	3.52	5.55	1.9	-1.04	2.48
58281	Alpha3Beta2	6.31	6.31	5.14	11.87	7.41
58281	Alpha3Beta4	-6.27	-6.27	3.16	-4.6	-3.5
58281	Alpha4Beta2	0.39	3.14	6.28	10.89	5.18
58281	Alpha4Beta2 (Rat Brain)	0.9	4.07	3.24	-2.36	1.46
58281	Alpha4Beta4	-0.23	15.77	8.53	9.74	8.45
58281	Alpha7	-5.41	13.67	10.75	12.09	7.78
58281	NOP	7.4	5.94	3.32	34.07	12.68
58281	OT	13.99	14.55	9.27	0.66	9.62
58281	V1A	31.52	18.39	6.3	83.33	34.89
58281	V1B	-17.25	-7.7	-1.92	3.2	-5.92
58281	V2	20.75	39.27	85.57	42.12	46.93
58281	PBR	7.69	21.08	37.52	9.26	18.89

58281	SERT	29.15	-2.43	0.22	-3.27	5.92
58281	GABAA	14.86	-14.62	14.38	36.62	12.81
58281	Oxytocin	-5.5	-0.99	-22.19	-9.74	-9.61
58282	5-HT1A	2.36	-11.45	-15.91	-8.63	-8.41
58282	5-HT1B	2.54	-2.44	6.13	-2.44	0.95
58282	5-HT1D	10.97	14.06	7.49	7.49	10
58282	5-HT1E	27	16.33	19.89	31.74	23.74
58282	5-HT2A	3.73	-22.2	-0.45	-4.1	-5.76
58282	5-HT2B	14.36	7.13	-7.33	6.33	5.12
58282	5-HT2C	9.94	11.9	23.21	17.12	15.54
58282	5-HT3	-18.23	-0.66	-2.66	40.98	4.86
58282	5-HT4	14.15	-5.01	3.7	20.24	8.27
58282	5-HT5A	-2.28	-12.15	-14.06	-22.33	-12.71
58282	5-HT6	7.79	-5.17	-16.81	-14.7	-7.22
58282	5-HT7A	-4.7	-4.7	-49.82	-4.7	-15.98
58282	A1	50.11	29.12	20.52	34.72	33.62
58282	A2A	26.62	33.11	18.55	38.35	29.16
58282	Alpha1A	10.88	-8.1	-5.54	0.45	-0.58
58282	Alpha1B	-2.61	-3.04	-8.53	-3.19	-4.34
58282	Alpha1D	18.88	12.72	26.32	8	16.48
58282	Alpha2A	0.3	-27.99	34.43	15.12	5.47
58282	Alpha2B	17.51	6.78	6.44	9.9	10.16
58282	Alpha2C	4.76	13.2	1.02	6.57	6.39
58282	Beta1	18.96	15.49	13.66	9.03	14.29
58282	Beta2	26.11	31.75	2.47	-16.19	11.04
58282	Beta3	34.08	48.54	47.84	31.26	40.43
58282	AT2	-8.39	-3.63	-0.73	-17.82	-7.64
58282	BZP Rat Brain Site	56.96	57.42	63.02	63.36	60.19
58282	D1	-15.11	4.36	25.49	8.62	5.84
58282	D2	10.01	3.33	6.78	1.37	5.37
58282	D3	6.57	7.7	7.7	12.51	8.62
58282	D4	-9.99	-8.2	-7.3	1.54	-5.99
58282	D5	16.39	10.09	9.74	36.57	18.2
58282	DAT	9.37	-5.95	-16.23	7.21	-1.4
58282	DOR	3.57	-19.16	-17.52	-16.34	-12.36
58282	GABAA	16.25	4.92	26.25	-25.08	5.59
58282	H1	-18.79	-27.56	-24.88	-32.52	-25.94
58282	H2	16.8	30.87	51	28.52	31.8
58282	H3	2.95	12.79	-0.59	12.99	7.04
58282	H4	14.4	-10.21	-8.07	7.62	0.94
58282	KOR	1.44	11.23	-11.35	-6.91	-1.4
58282	M1	-4.76	8.79	-3.68	10.84	2.8

58282	M2	1.83	1.74	-17.98	-10.39	-6.2
58282	M3	-6.13	-13.23	4.48	-4.05	-4.73
58282	M4	-5.93	-8.68	-4.56	-0.26	-4.86
58282	M5	12.41	9.86	7.57	24.98	13.71
58282	MOR	-1.12	5.38	0.81	4.06	2.28
58282	NET	-17.3	-12.28	-16.62	-7.19	-13.35
58282	PBR	16.63	-9.33	9.33	13.86	7.62
58282	SERT	25.54	12.2	12.91	10.37	15.26
58282	Sigma 1	-6.81	-23.25	-13.49	12.69	-7.72
58282	Sigma 2	9.19	-0.73	8.78	-0.12	4.28
58282	AMPA	20.28	2.34	-17.88	-0.95	0.95
58282	Kainate (Rat Brain)	-7.79	-3.63	-13.32	-0.87	-6.4
58282	NMDA	76.42	24.95	30.9	32.09	41.09
58282	NR2B	38.18	11.52	30.72	27.76	27.05
58282	HCA2	17.8	-23.05	9.02	10.17	3.49
58282	Ca channel human	-3.63	-10.08	-13.31	2.82	-6.05
58282	HERG	-11.13	-15.88	5.6	23.16	0.44
58282	M3D	6.85	2.99	22.28	38.48	17.65
58282	M4 D	-1.31	11.34	21.91	26.57	14.63
58282	NTS1	21.82	18.24	-1.01	7.95	11.75
58282	Alpha2Beta2	7.7	6.49	-3.05	2.14	3.32
58282	Alpha2Beta4	7.98	10.31	2.51	-9.25	2.89
58282	Alpha3Beta2	6.31	2.71	10.8	2.22	5.51
58282	Alpha3Beta4	7.26	-1.41	1.48	1.63	2.24
58282	Alpha4Beta2	11.28	-2.84	-2.26	1.47	1.91
58282	Alpha4Beta2 (Rat Brain)	-1.52	1.73	1.98	-1.69	0.13
58282	Alpha4Beta4	13.06	23.62	-4.75	13.66	11.4
58282	Alpha7	21.2	4.07	-13.43	16.22	7.02
58282	NOP	2.59	5.65	12.5	32.46	13.3
58282	OT	14.83	18.72	17.05	-6.84	10.94
58282	V1A	-5.89	-5.59	10.6	-7.36	-2.06
58282	V1B	-16.81	-3.92	-6.59	-3.7	-7.76
58282	V2	59.93	75.6	75.6	68.48	69.9
58282	PBR	29.1	9.51	23.89	19.68	20.55
58282	SERT	21.39	-1.77	7.68	14.84	10.54
58282	GABAA	13.9	1.81	9.55	25.02	12.57
58282	Oxytocin	4.57	-4.17	-4.7	8.28	1
58283	5-HT1A	14.09	5.92	2.21	10.82	8.26
58283	5-HT1B	22.3	10.14	-0.64	3.64	8.86
58283	5-HT1D	29.9	24.88	5.17	23.33	20.82

58283	5-HT1E	-8.57	-56.46	-7.85	-8.57	-20.36
58283	5-HT2A	25.13	-10.89	-7.93	40.27	11.65
58283	5-HT2B	38.05	34.44	14.36	-6.93	19.98
58283	5-HT2C	4.18	6.43	8.67	-11.73	1.89
58283	5-HT3	-6.75	3.05	8.91	62.95	17.04
58283	5-HT4	-14.58	-9.36	21.98	-38.08	-10.01
58283	5-HT5A	-2.28	-35.38	-23.6	-13.42	-18.67
58283	5-HT6	12.55	-6.23	-9.27	-13.51	-4.12
58283	5-HT7A	6.42	12.9	24.02	-9.99	8.34
58283	A1	74.51	55.11	67.91	67.91	66.36
58283	A2A	25.37	42.59	26.62	37.77	33.09
58283	Alpha1A	5.07	-1.09	-20.58	-8.27	-6.22
58283	Alpha1B	14.72	-2.03	-11.06	6.92	2.14
58283	Alpha1D	26.61	13.44	8.14	28.32	19.13
58283	Alpha2A	19.61	30.09	35.03	16.47	25.3
58283	Alpha2B	16.71	-4.24	-2.7	-5.2	1.14
58283	Alpha2C	43.56	-0.65	-3.24	-9.43	7.56
58283	Beta1	-2.73	-3.73	-19.96	-10.68	-9.28
58283	Beta2	14.4	22.75	10.71	-3.5	11.09
58283	Beta3	-50.22	15.04	33.73	33.02	7.89
58283	AT2	2.37	2.93	0.86	-12.73	-1.64
58283	BZP Rat Brain Site	97.56	96.87	96.76	95.84	96.76
58283	D1	-3.8	8.44	6.77	29.2	10.15
58283	D2	20.72	3.44	3.67	8.97	9.2
58283	D3	6.89	11.38	-3.21	27.41	10.62
58283	D4	6.66	8.2	2.18	5.12	5.54
58283	D5	23.62	18.37	10.91	39.25	23.04
58283	DAT	35.6	12.87	15.13	13.49	19.27
58283	DOR	39.43	15.99	-19.39	-0.41	8.91
58283	GABAA	-2.42	22.25	-5.75	9.58	5.92
58283	H1	-29.63	-17.96	-31.69	-12.8	-23.02
58283	H2	7.59	26.67	43.99	19.11	24.34
58283	H3	11.22	0	6.49	2.56	5.07
58283	H4	11.37	-2.01	-0.22	15.29	6.11
58283	KOR	8.22	-7.59	7.69	14.16	5.62
58283	M1	19.07	-5.13	16.89	44.72	18.89
58283	M2	20.99	-6.6	-4.28	-1.87	2.06
58283	M3	2.51	8.95	5.67	-10.31	1.71
58283	M4	1.55	-22.27	-9.72	2.58	-6.97
58283	M5	2.21	17.6	12.32	20.76	13.22
58283	MOR	43.44	31.76	20.69	18.76	28.66
58283	NET	23.69	2.47	-24.91	5.36	1.65

58283	PBR	42.78	13.77	19.5	-6.93	17.28
58283	SERT	-10.69	-13.72	-9.23	-6.05	-9.92
58283	Sigma 1	0.6	-12.89	-5.41	13.16	-1.14
58283	Sigma 2	39.64	19.11	12.66	28.15	24.89
58283	AMPA	42.02	0.06	-31.79	11.94	5.56
58283	Kainate (Rat Brain)	21.28	-6.4	-10.55	-14.71	-2.6
58283	NMDA	95.46	59.76	54.41	64.22	68.46
58283	NR2B	33.8	25.08	34.71	37.16	32.69
58283	HCA2	42.24	72.03	49.88	22	46.54
58283	Ca channel human	41	11.88	16.48	19.54	22.23
58283	HERG	-5.96	-6.79	-3.9	20.68	1.01
58283	M3D	10.7	-6.27	37.7	7.62	12.44
58283	M4 D	-18.16	17.54	13.18	32.22	11.2
58283	NTS1	-11.53	-14.21	-8.39	-1.9	-9.01
58283	Alpha2Beta2	6.13	9.39	4.68	1.06	5.32
58283	Alpha2Beta4	4.64	4.64	13.76	11.12	8.54
58283	Alpha3Beta2	16.16	3.49	7.87	7.58	8.78
58283	Alpha3Beta4	-3.23	6.2	0.87	9.24	3.27
58283	Alpha4Beta2	2.26	-1.27	12.55	8.83	5.59
58283	Alpha4Beta2 (Rat Brain)	7.08	5.82	-1.02	-3.7	2.05
58283	Alpha4Beta4	4.3	9.13	16.08	14.26	10.94
58283	Alpha7	21.81	19.62	-18.41	22.78	11.45
58283	NOP	17.02	15.41	1.57	17.16	12.79
58283	OT	23.16	10.94	9.83	14.55	14.62
58283	V1A	-20.6	2.06	-7.06	-14.72	-10.08
58283	V1B	-18.14	-17.03	-10.36	-14.37	-14.98
58283	V2	28.58	4.36	27.16	69.9	32.5
58283	PBR	30.5	20.17	17.44	28.19	24.08
58283	SERT	-3.87	2.68	-4.05	4.79	-0.11
58283	GABAA	9.06	19.7	8.1	45.32	20.55
58283	Oxytocin	16.76	-3.11	18.09	18.35	12.52
58284	5-HT1A	0.13	-9.22	-5.36	13.05	-0.35
58284	5-HT1B	15.25	1.85	1.85	-4.51	3.61
58284	5-HT1D	5.02	-14.48	12.41	12.71	3.92
58284	5-HT1E	28.19	23.68	24.63	24.63	25.28
58284	5-HT2A	-8.97	-2.19	3.9	-12.8	-5.02
58284	5-HT2B	-21.79	-17.77	-17.77	10.74	-11.65
58284	5-HT2C	-0.92	34.99	7.04	15.61	14.18
58284	5-HT3	15.15	8.29	10.37	63.42	24.31
58284	5-HT4	7.18	-15.45	12.4	32.43	9.14

58284	5-HT5A	12.04	17.77	18.09	7.59	13.87
58284	5-HT6	-4.51	-7.82	-10.46	-13.51	-9.08
58284	5-HT7A	-2.58	2.32	-7.48	-20.58	-7.08
58284	A1	18.52	29.52	-2.87	9.92	13.77
58284	A2A	26.54	19.63	15.89	19.88	20.49
58284	Alpha1A	-8.27	6.77	-22.12	-9.3	-8.23
58284	Alpha1B	6.63	0.71	-4.7	-10.12	-1.87
58284	Alpha1D	6.13	7.14	4.13	46.22	15.91
58284	Alpha2A	0.6	-14.07	31.59	40.72	14.71
58284	Alpha2B	4.73	8.14	2.75	0.36	4
58284	Alpha2C	10.09	9	-14.6	-18.81	-3.58
58284	Beta1	12.17	-1.9	-4.06	12.34	4.64
58284	Beta2	-7.08	11.9	1.17	0.84	1.71
58284	Beta3	48.19	30.2	46.43	16.8	35.41
58284	AT2	3.69	1.16	-10.16	-16.84	-5.54
58284	BZP Rat Brain Site	100.47	98.85	97.98	97.23	98.63
58284	D1	31.61	-4.91	4.17	19	12.47
58284	D2	4.25	13.92	10.93	11.27	10.09
58284	D3	-10.9	10.9	11.7	7.37	4.77
58284	D4	-1.92	-12.68	3.59	14.09	0.77
58284	D5	12.42	15.46	12.77	24.09	16.19
58284	DAT	27.06	32.41	38.27	21.61	29.84
58284	DOR	-0.88	-27.12	-17.75	-14.24	-15
58284	GABAA	-1.08	30.92	28.25	26.25	21.09
58284	H1	-10.69	-17.07	-18.97	-16.64	-15.84
58284	H2	14.45	9.94	34.23	32.22	22.71
58284	H3	18.89	17.52	14.56	20.66	17.91
58284	H4	7.44	35.44	16.71	24.74	21.08
58284	KOR	2.42	-6.23	99.36	5.66	25.3
58284	M1	13.99	5.64	1.65	13.38	8.67
58284	M2	0.44	10.16	6.36	-8.82	2.04
58284	M3	-4.05	2.03	-4.35	-7.74	-3.53
58284	M4	11.78	-6.71	-11.26	-4.81	-2.75
58284	M5	-5.79	4.76	13.29	17.16	7.36
58284	MOR	4.45	0.97	9.71	8.86	6
58284	NET	5.67	-7.19	-15.17	-10.61	-6.83
58284	PBR	5.17	12.94	-1.57	-7.85	2.17
58284	SERT	-3.08	-9.29	-15.34	-3.73	-7.86
58284	Sigma 1	5.81	-6.95	-2.74	9.29	1.35
58284	Sigma 2	1.92	3.42	7.7	2.87	3.98
58284	AMPA	-2.72	5.62	-16.87	2.34	-2.91
58284	Kainate (Rat	-6.4	-36.85	0	-3.63	-15.63

	Brain)					
58284	NMDA	28.82	-5.69	-5.69	25.55	10.75
58284	NR2B	37.5	6.5	15.51	26.33	21.46
58284	HCA2	20.86	52.55	56.75	59.05	47.3
58284	Ca channel human	19.54	4.21	-38.7	18.01	0.77
58284	HERG	-14.64	7.26	6.84	33.08	8.14
58284	M3D	33.85	18.42	30.76	38.48	30.38
58284	M4 D	-4.63	-16.78	-18.95	6.32	-8.51
58284	NTS1	16.9	7.95	12.65	13.54	12.76
58284	Alpha2Beta2	15.31	13.02	9.88	12.65	12.72
58284	Alpha2Beta4	17.2	10.72	1.19	10.92	10.01
58284	Alpha3Beta2	16.35	17.13	19.08	20.64	18.3
58284	Alpha3Beta4	-2.78	-2.02	-7.49	4.83	-1.87
58284	Alpha4Beta2	17.75	20.5	12.36	15	16.4
58284	Alpha4Beta2 (Rat Brain)	10.75	11.25	10.08	4.49	9.14
58284	Alpha4Beta4	12.15	16.38	27.55	9.74	16.46
58284	Alpha7	26.18	27.64	17.44	16.59	21.96
58284	NOP	7.4	1.28	1.86	9.44	5
58284	OT	3.99	4.55	-2.4	19.27	6.35
58284	V1A	6.77	2.35	7.95	-13.25	0.96
58284	V1B	13.95	19.95	9.35	-4.45	9.7
58284	V2	32.86	11.49	64.2	37.85	36.6
58284	PBR	12.9	12.16	-0.15	-0.4	6.13
58284	SERT	-8.08	-17.83	-24.57	0.7	-12.45
58284	GABAA	13.9	34.2	29.37	39.03	29.13
58284	Oxytocin	-10	14.64	4.57	0.6	2.45
58285	5-HT1A	1.61	4.58	-16.95	-17.98	-7.19
58285	5-HT1B	14.01	-8.38	4.89	-0.78	2.44
58285	5-HT1D	-16.25	-0.59	18.03	1.48	0.67
58285	5-HT1E	33.4	27.24	41.23	13.96	28.96
58285	5-HT2A	10.69	-1.14	-13.15	-12.98	-4.15
58285	5-HT2B	-42.67	-14.16	-18.57	-12.15	-21.89
58285	5-HT2C	19.48	5.2	-2.96	1.53	5.81
58285	5-HT3	18.23	-10.83	29.26	60.02	24.17
58285	5-HT4	3.7	-1.52	7.18	7.18	4.14
58285	5-HT5A	-4.19	9.18	3.45	5.99	3.61
58285	5-HT6	-14.43	-14.04	-26.33	-20.52	-18.83
58285	5-HT7A	-0.86	2.45	18.19	-4.83	3.74
58285	A1	39.32	44.11	17.92	45.71	36.77
58285	A2A	14.39	17.3	4.74	21.88	14.58
58285	Alpha1A	0.11	-1.77	-5.36	6.26	-0.19

58285	Alpha1B	8.37	2.81	-7.52	-4.34	-0.17
58285	Alpha1D	3.27	7.14	13.72	14.72	9.71
58285	Alpha2A	-82.63	2.84	-25.9	-24.7	-32.6
58285	Alpha2B	5.36	3.94	7.06	9.16	6.38
58285	Alpha2C	22.67	1.11	-22.28	-7.73	-1.56
58285	Beta1	13	14.99	-7.7	-8.86	2.86
58285	Beta2	-7.62	0.62	-23.67	-15.32	-11.5
58285	Beta3	55.25	30.2	33.02	18.92	34.35
58285	AT2	9.24	8.37	-6.12	-10.08	0.35
58285	BZP Rat Brain Site	91.38	82.94	80.56	81.21	84.02
58285	D1	6.4	16.22	9.55	21.97	13.54
58285	D2	15.19	2.17	5.28	9.55	8.05
58285	D3	13.47	23.25	9.46	4.65	12.71
58285	D4	2.05	3.97	11.53	18.19	8.94
58285	D5	12.89	26.77	6.71	26.07	18.11
58285	DAT	26.34	4.54	2.59	13.38	11.71
58285	DOR	6.85	-23.14	-22.67	-9.78	-12.19
58285	GABAA	32.25	44.92	14.25	20.25	27.92
58285	H1	-12.59	-16.98	-24.4	-17.07	-17.76
58285	H2	-11.93	15.4	38.28	35.23	19.25
58285	H3	21.65	17.12	10.43	21.06	17.57
58285	H4	14.04	9.94	9.23	32.94	16.54
58285	KOR	8.07	-13.83	-11.4	-20.39	-9.39
58285	M1	2.37	5.16	2.98	14.47	6.25
58285	M2	-1.5	-5.48	3.77	4.33	0.28
58285	M3	2.99	0.01	4.9	-1.6	1.58
58285	M4	-12.29	-4.99	-0.52	-8.17	-6.49
58285	M5	-2.27	22.17	36.23	20.76	19.22
58285	MOR	-6.85	8.7	5.14	7.54	3.63
58285	NET	-13.96	-11.6	-1.86	-1.79	-7.3
58285	PBR	-11.83	3.6	-4.9	-6.1	-4.81
58285	SERT	-12.37	-18.36	-9.88	1.78	-9.71
58285	Sigma 1	-18.84	-7.75	-6.21	3.81	-7.25
58285	Sigma 2	1.04	-11.94	-17.93	12.11	-4.18
58285	AMPA	13.21	-5.24	-0.44	-2.72	1.2
58285	Kainate (Rat Brain)	11.59	19.9	17.13	-18.86	7.44
58285	NMDA	28.23	-10.45	28.52	46.08	23.1
58285	NR2B	19.84	5.19	15.79	4.39	11.3
58285	HCA2	32.7	66.3	69.36	36.13	51.12
58285	Ca channel human	14.94	-4.98	-63.22	10.34	-10.73

58285	HERG	9.53	5.19	-6.17	26.67	8.81
58285	M3D	9.93	26.9	38.48	52.36	31.92
58285	M4 D	-4.98	-10.99	-12.85	2.15	-6.67
58285	NTS1	4.14	11.3	15.78	19.14	12.59
58285	Alpha2Beta2	-1.84	-1.12	6.01	-3.17	-0.03
58285	Alpha2Beta4	17.91	15.28	2.1	2.91	9.55
58285	Alpha3Beta2	3.39	11.19	10.21	-1.78	5.75
58285	Alpha3Beta4	-2.17	-0.49	-4.3	-9.01	-3.99
58285	Alpha4Beta2	8.24	12.45	15.4	10.98	11.77
58285	Alpha4Beta2 (Rat Brain)	-5.2	3.82	2.23	-0.27	0.15
58285	Alpha4Beta4	27.25	14.57	12.15	16.98	17.74
58285	Alpha7	-6.26	22.3	-23.27	27.16	4.98
58285	NOP	6.67	8.71	0.69	-2.95	3.28
58285	OT	9.55	9.83	6.49	7.6	8.37
58285	V1A	19.72	-30.02	-1.77	12.66	0.15
58285	V1B	43.55	-2.65	1.35	-1.45	10.2
58285	V2	33.57	1.51	57.79	59.22	38.02
58285	PBR	2.32	-12.3	-10.48	4.14	-4.08
58285	SERT	-9.59	-11.87	-2.37	2.32	-5.38
58285	GABAA	37.58	32.27	19.21	40.97	32.51
58285	Oxytocin	5.1	11.99	18.88	2.19	9.54
58286	5-HT1A	13.49	-2.84	-29.71	19.43	0.09
58286	5-HT1B	7.38	-0.5	-6.17	-8.1	-1.85
58286	5-HT1D	22.76	-2.66	11.53	18.62	12.56
58286	5-HT1E	33.4	40.28	37.67	43.36	38.68
58286	5-HT2A	-10.54	-6.36	3.38	-21.5	-8.76
58286	5-HT2B	-22.99	-6.12	-21.79	3.92	-11.75
58286	5-HT2C	11.73	-17.04	-10.71	-16.83	-8.21
58286	5-HT3	-21.01	-2.43	13.45	69.74	14.94
58286	5-HT4	-22.42	-11.1	28.94	-5.01	-2.4
58286	5-HT5A	15.86	38.14	3.77	-12.47	11.33
58286	5-HT6	-10.33	-21.71	-14.96	-7.82	-13.71
58286	5-HT7A	-14.49	4.43	8.14	30.5	7.15
58286	A1	10.72	23.32	1.12	54.31	22.37
58286	A2A	36.05	2.75	37.2	24.57	25.14
58286	Alpha1A	-25.2	5.75	9.34	-6.56	-4.17
58286	Alpha1B	25.62	9.67	-3.62	0.5	8.04
58286	Alpha1D	10.43	25.03	24.17	-1.74	14.47
58286	Alpha2A	-30.69	-25.9	15.57	23.8	-4.31
58286	Alpha2B	2.63	-3.04	-3.16	6.95	0.85
58286	Alpha2C	20.36	23.42	12.34	-7.39	12.18
58286	Beta1	-37.35	4.55	4.39	11.84	-4.14

58286	Beta2	-10	-6.97	-21.17	-11.96	-12.53
58286	Beta3	60.89	42.9	6.57	-7.19	25.79
58286	AT2	-3.67	-8.42	-13.56	-1.63	-6.82
58286	BZP Rat Brain Site	82.18	86.51	82.94	83.92	83.89
58286	D1	7.14	-1.02	13.81	22.9	10.71
58286	D2	6.55	9.55	9.89	10.47	9.12
58286	D3	7.31	-30.25	-30.43	-27.21	-20.15
58286	D4	-1.02	2.95	8.58	21.65	8.04
58286	D5	17.56	5.77	16.97	12.07	13.09
58286	DAT	-8.21	-12.02	-22.92	-17.26	-15.1
58286	DOR	-2.52	-10.25	-3.46	-20.56	-9.2
58286	GABAA	22.25	25.58	12.92	28.25	22.25
58286	H1	3.28	-1.38	-2.76	2.33	0.37
58286	H2	3.79	18.46	29.97	15.3	16.88
58286	H3	29.32	24.99	16.33	26.77	24.35
58286	H4	0.31	4.59	16	30.62	12.88
58286	KOR	15.42	-10.62	-19.9	-24.46	-9.89
58286	M1	0.44	5.76	8.67	19.56	8.61
58286	M2	-12.15	-10.58	-6.78	-3.91	-8.36
58286	M3	-6.61	-1.78	-15.73	-4.64	-7.19
58286	M4	1.89	-7.57	-1.81	4.3	-0.8
58286	M5	11.88	17.16	18.47	24.63	18.04
58286	MOR	2.44	13.73	1.43	0.97	4.64
58286	NET	-21.26	6.65	20.57	3.23	2.3
58286	PBR	26.06	25.5	22.73	17.46	22.94
58286	SERT	-15.71	-14.63	-9.4	-1.4	-10.29
58286	Sigma 1	-15.57	-27.86	-17.9	-6.21	-16.89
58286	Sigma 2	-8.41	-23.29	-21.32	-29.41	-20.61
58286	AMPA	12.45	0.57	-3.98	4.87	3.48
58286	Kainate (Rat Brain)	30.97	-20.24	-14.71	-18.86	-5.71
58286	NMDA	37.45	-30.09	-8.07	41.02	10.08
58286	NR2B	9.35	9.64	16.42	20.52	13.98
58286	HCA2	33.46	82.72	56.37	17.04	47.4
58286	Ca channel human	27.2	13.41	-3.45	19.54	14.18
58286	HERG	-17.33	-14.23	-33.44	-8.86	-18.47
58286	M3D	29.99	14.56	36.93	67.02	37.13
58286	M4 D	7.43	-18.5	-5.18	-4.51	-5.19
58286	NTS1	8.39	8.84	8.84	5.93	8
58286	Alpha2Beta2	1.06	2.27	4.32	8.43	4.02
58286	Alpha2Beta4	9.8	5.04	-0.23	16.29	7.73

58286	Alpha3Beta2	6.7	1.54	4.66	10.21	5.78
58286	Alpha3Beta4	1.33	-1.25	-4.3	5.44	0.31
58286	Alpha4Beta2	10.89	9.41	2.26	11.08	8.41
58286	Alpha4Beta2 (Rat Brain)	2.99	-1.86	-4.36	-3.36	-1.65
58286	Alpha4Beta4	13.96	13.96	13.66	18.79	15.09
58286	Alpha7	20.35	7.35	-18.29	19.14	7.14
58286	NOP	5.45	6.59	-11.74	0.05	0.09
58286	OT	9.83	17.33	-1.01	-5.73	5.11
58286	V1A	20.6	-14.72	15.89	13.83	8.9
58286	V1B	13.35	-2.05	-17.45	-18.85	-6.25
58286	V2	-1.34	21.46	49.96	94.84	41.23
58286	PBR	40.42	29.76	29.43	23.72	30.83
58286	SERT	-27.15	-20.12	-0.8	-4.47	-13.14
58286	GABAA	36.13	21.63	13.41	36.13	26.83
58286	Oxytocin	-11.33	-15.3	1.92	-8.15	-8.22
58287	5-HT1A	28.04	-3.14	8.15	-1.8	7.81
58287	5-HT1B	25.89	25.89	32.11	38.33	30.56
58287	5-HT1D	34.28	27.19	9.75	22.76	23.5
58287	5-HT1E	-38.44	-10.46	-45.32	0	-31.41
58287	5-HT2A	-5.49	-6.36	-1.49	-15.93	-7.32
58287	5-HT2B	-4.12	-15.36	-11.35	-1.31	-8.04
58287	5-HT2C	15.81	18.06	22.14	5.81	15.46
58287	5-HT3	11.96	-12.83	4.4	2.55	1.52
58287	5-HT4	-20.67	10.66	32.43	26.33	12.19
58287	5-HT5A	41	-1.01	4.08	-17.56	6.63
58287	5-HT6	-22.5	-3.46	-14.83	-0.94	-10.43
58287	5-HT7A	-1.65	-2.45	7.61	23.09	6.65
58287	A1	88.18	68.4	51.3	65.2	68.27
58287	A2A	21.94	11.44	24.57	51.48	27.36
58287	Alpha1A	2.16	-14.77	7.97	26.61	5.49
58287	Alpha1B	12.7	9.81	6.92	-0.88	7.14
58287	Alpha1D	7.14	3.99	-7.46	14.72	4.6
58287	Alpha2A	-11.38	8.83	0.6	15.12	3.29
58287	Alpha2B	1.33	-15.51	12.74	-1.66	-0.78
58287	Alpha2C	17.23	2.41	-9.56	3.09	3.29
58287	Beta1	21.28	-0.91	7.2	14.33	10.48
58287	Beta2	-10.33	-10.22	-10.55	-14.88	-11.5
58287	Beta3	37.96	31.26	18.92	30.91	29.76
58287	AT2	-0.29	-13.92	-4.96	-13.64	-8.2
58287	BZP Rat Brain Site	102.75	101.23	102.21	98.96	101.29
58287	D1	20.67	8.62	2.5	20.12	12.98

58287	D2	16.34	18.07	3.67	10.93	12.25
58287	D3	2.12	-11.29	-31.14	-11.29	-12.9
58287	D4	14.22	6.4	4.61	13.7	9.73
58287	D5	23.16	7.17	19.54	8.57	14.61
58287	DAT	-29.91	-46.37	-14.38	-13.15	-25.95
58287	DOR	5.92	1.93	-12.36	6.39	0.47
58287	GABAA	26.25	9.58	18.25	7.58	15.42
58287	H1	-5.52	-0.52	8.45	27.76	7.54
58287	H2	11.65	22.31	24.41	20.61	19.75
58287	H3	6.3	8.27	-1.57	-17.71	-1.18
58287	H4	6.73	8.51	-1.29	29.55	10.88
58287	KOR	19.63	15.49	-11.48	-21.39	0.56
58287	M1	7.61	-7.3	-0.53	9.91	2.42
58287	M2	-2.89	-6.13	-5.76	0.16	-3.66
58287	M3	-9.12	-11.08	-14.84	-10.37	-11.35
58287	M4	5.42	7.48	-8.17	6.88	2.9
58287	M5	11.18	22.08	10.74	35.36	19.84
58287	MOR	20.38	12.65	7.93	8.86	12.46
58287	NET	10.46	-10.99	1.94	22.09	5.88
58287	PBR	1.48	-1.66	-0.09	2.03	0.44
58287	SERT	-8.21	5.08	-11.18	-0.32	-3.66
58287	Sigma 1	-17.44	-3.14	-31.87	-8.02	-15.12
58287	Sigma 2	2.53	1.99	-16.77	-2.23	-3.62
58287	AMPA	10.17	30.9	13.71	-2.46	13.08
58287	Kainate (Rat Brain)	19.9	-0.87	-9.17	-41	-7.79
58287	NMDA	-17.3	39.89	38.59	-37.02	6.04
58287	NR2B	31.8	34.25	43.08	36.19	36.33
58287	HCA2	36.13	68.59	52.94	23.15	45.2
58287	Ca channel human	51.72	2.68	-15.71	-29.5	2.3
58287	HERG	-1.01	-2.87	4.78	15.1	4
58287	M3D	13.79	17.65	26.9	51.59	27.48
58287	M4 D	-4.25	0.73	-2	2.01	-0.88
58287	NTS1	0.11	0.11	-5.04	9.74	1.23
58287	Alpha2Beta2	11.45	2.27	-6.07	3.96	2.9
58287	Alpha2Beta4	17.61	13.86	14.77	15.48	15.43
58287	Alpha3Beta2	3.39	7.48	10.41	13.82	8.78
58287	Alpha3Beta4	3	-2.17	-1.25	3.31	0.72
58287	Alpha4Beta2	5.88	9.32	13.73	9.02	9.49
58287	Alpha4Beta2 (Rat Brain)	-4.03	14.59	-4.28	0.56	1.71
58287	Alpha4Beta4	11.85	3.4	20.3	31.77	16.83

58287	Alpha7	1.64	-2.61	20.47	18.53	9.51
58287	NOP	14.4	1.33	5.74	1.62	5.77
58287	OT	15.66	14.27	1.49	-2.67	7.19
58287	V1A	24.14	-16.78	-8.83	-1.18	-0.66
58287	V1B	-3.45	-16.45	-27.25	-24.05	-17.8
58287	V2	-1.34	7.21	4.36	91.27	25.38
58287	PBR	14.55	18.44	9.18	14.06	14.06
58287	SERT	-9.17	-4.23	1.96	-7.84	-4.82
58287	GABAA	24.53	5.2	23.56	30.82	21.03
58287	Oxytocin	16.23	-8.68	21	0.6	7.29
58288	5-HT1A	-22.44	-4.62	-8.18	8.59	-6.66
58288	5-HT1B	15.81	15.25	13.46	33.22	19.44
58288	5-HT1D	39.6	28.96	10.05	11.23	22.46
58288	5-HT1E	-23.74	-11.89	-0.98	-11.89	-12.13
58288	5-HT2A	38.45	0.14	-3.48	7.54	10.66
58288	5-HT2B	-0.9	-44.68	-15.36	-2.91	-15.96
58288	5-HT2C	10.3	1.33	-5	-9.08	-0.61
58288	5-HT3	13.73	-2.36	-10.09	-3.17	-0.47
58288	5-HT4	-6.75	21.11	28.07	22.85	16.32
58288	5-HT5A	9.81	8.54	-13.1	-2.92	0.58
58288	5-HT6	-8.08	-21.44	-18.27	-6.76	-13.64
58288	5-HT7A	-6.68	16.08	-8.4	19.65	5.16
58288	A1	68.94	40.61	38.48	47.56	48.9
58288	A2A	-22.03	-17.76	24.08	-1.19	-4.23
58288	Alpha1A	-19.21	-3.48	0.96	20.62	-0.28
58288	Alpha1B	-30.27	3.24	14.29	-5.14	-4.47
58288	Alpha1D	-9.33	-19.35	9.43	0.27	-4.75
58288	Alpha2A	13.92	32.49	-22.46	42.66	16.65
58288	Alpha2B	11.08	2.33	15.01	-8.03	5.1
58288	Alpha2C	-3.99	4.92	4.65	3.63	2.3
58288	Beta1	23.44	2.73	-11.68	-1.24	3.31
58288	Beta2	13.96	15.59	-1	-2.74	6.45
58288	Beta3	35.49	-59.04	-10.36	1.28	-8.16
58288	AT2	-17.83	-7.54	21.65	-5.55	-2.32
58288	BZP Rat Brain Site	102.42	97.44	98.09	97.33	98.82
58288	D1	63.13	13.26	49.59	12.33	34.58
58288	D2	7.93	11.85	-0.82	-1.63	4.33
58288	D3	3.73	-18.98	-9.86	-6.46	-7.89
58288	D4	9.73	7.17	4.61	33.81	13.83
58288	D5	-6.23	-22.72	-33.41	-4.55	-16.73
58288	DAT	-38.96	-65.49	-9.45	-21.38	-33.82
58288	DOR	3.57	2.4	-2.99	-0.88	0.53

58288	GABAA	44.25	24.92	20.25	18.92	27.09
58288	H1	6.47	15.78	31.29	43.97	24.38
58288	H2	20.16	0.63	10.18	16.09	11.77
58288	H3	9.45	2.16	-9.25	-16.73	-3.59
58288	H4	0.31	8.87	21.53	32.23	15.74
58288	KOR	16.63	2.36	-12.48	-12.48	-1.49
58288	M1	-2.02	-3.28	18.97	-1.91	2.94
58288	M2	0.62	-22.61	-6.32	-9.56	-9.47
58288	M3	-2.74	6.51	-9.65	10.14	1.07
58288	M4	-4.56	-11.35	6.28	-8.43	-4.52
58288	M5	17.64	-22.38	-2.56	10.65	0.84
58288	MOR	19.61	19.22	13.27	6.23	14.58
58288	NET	-3.76	-13.35	1.03	14.72	-0.34
58288	PBR	5.45	-14.78	-5.08	-0.65	-3.77
58288	SERT	-12.74	-10.42	-11.45	-4.97	-9.9
58288	Sigma 1	7.08	6.21	-16.7	8.02	1.15
58288	Sigma 2	19.18	-11.54	4.37	-22.14	-2.53
58288	AMPA	28.88	14.98	11.69	23.57	19.78
58288	Kainate (Rat Brain)	-13.32	-16.09	-3.63	-5.02	-9.52
58288	NMDA	-21.2	-16	39.89	24.29	6.75
58288	NR2B	24.51	25.02	46.39	41.72	34.41
58288	HCA2	47.21	23.53	4.44	-17.71	14.37
58288	Ca channel human	16.48	22.61	4.21	19.54	15.71
58288	HERG	27.5	20.68	45.26	45.47	34.73
58288	M3D	21.5	19.19	14.56	63.93	29.8
58288	M4 D	-0.5	-12.49	-9.03	3.14	-4.72
58288	NTS1	3.69	19.59	13.54	13.54	12.59
58288	Alpha2Beta2	5.16	5.29	6.86	5.77	5.77
58288	Alpha2Beta4	7.17	7.37	5.75	12.95	8.31
58288	Alpha3Beta2	0.56	1.34	-4.41	0.85	-0.42
58288	Alpha3Beta4	-2.32	3	1.48	-3.99	-0.46
58288	Alpha4Beta2	4.81	1.67	6.67	5.2	4.59
58288	Alpha4Beta2 (Rat Brain)	-1.02	4.91	0.98	-5.7	-0.21
58288	Alpha4Beta4	13.96	1.58	8.83	17.58	10.49
58288	Alpha7	4.92	13.79	11	7.96	9.42
58288	NOP	9.43	6.45	13.12	10.14	9.79
58288	OT	9.83	0.66	0.66	22.33	8.37
58288	V1A	28.26	0.88	-13.54	-13.54	0.52
58288	V1B	-16.65	-10.05	0	-25.65	-17.45
58288	V2	10.06	0.09	27.87	53.52	22.89

58288	PBR	22.98	12.4	7.36	19.92	15.67
58288	SERT	3.29	-5.92	-11.87	-12.11	-6.65
58288	GABAA	35.17	18.25	31.78	25.02	27.56
58288	Oxytocin	-11.86	1.39	-12.92	-18.22	-10.4
58289	5-HT1A	-1.8	-18.13	0.43	-1.95	-5.36
58289	5-HT1B	21.33	3.64	-1.74	27.14	12.59
58289	5-HT1D	15.96	19.8	0	5.91	10.42
58289	5-HT1E	27	24.63	27.95	42.65	30.56
58289	5-HT2A	30.56	4.25	1.95	-3.97	8.2
58289	5-HT2B	-7.73	-22.99	-40.26	-11.35	-20.58
58289	5-HT2C	3.98	3.37	-9.28	1.12	-0.2
58289	5-HT3	13.01	3.35	-6.31	-13.95	-0.98
58289	5-HT4	3.7	25.46	22.85	24.59	19.15
58289	5-HT5A	-8.65	-18.51	-15.33	-12.47	-13.74
58289	5-HT6	13.08	-11.39	-14.3	-17.74	-7.59
58289	5-HT7A	-7.08	-1.52	-3.11	1.26	-2.61
58289	A1	25.12	-27.79	-27.79	-1.6	-8.02
58289	A2A	8	-0.04	17.68	-4.96	5.17
58289	Alpha1A	-11.52	-18.53	3.7	14.47	-2.97
58289	Alpha1B	13.02	-4.61	2.24	-9.94	0.18
58289	Alpha1D	-1.6	32.04	-17.2	11.43	6.17
58289	Alpha2A	-4.19	16.92	-29.64	22.31	1.35
58289	Alpha2B	31.41	-7.98	0.66	-6.37	4.43
58289	Alpha2C	-14.6	-21.54	-8.27	8.53	-8.97
58289	Beta1	15.65	-8.2	9.19	-1.08	3.89
58289	Beta2	7.35	12.66	-3.5	-13.69	0.71
58289	Beta3	39.37	22.8	44.66	55.95	40.7
58289	AT2	11.32	-17.24	10.98	-21.21	-4.04
58289	BZP Rat Brain Site	98.85	95.06	93.22	94.41	95.39
58289	D1	26.23	32.35	20.12	49.41	32.03
58289	D2	-8.88	6.44	-6.58	-0.13	-2.29
58289	D3	-4.31	-25.96	-16.48	-25.6	-18.09
58289	D4	20.37	22.41	6.92	28.18	19.47
58289	D5	-18.75	-21.5	-32.95	-13.41	-21.65
58289	DAT	-32.48	-41.64	-29.6	-22.1	-31.46
58289	DOR	14.12	-9.08	3.81	18.1	6.74
58289	GABAA	31.09	-0.54	8.14	26.12	16.2
58289	H1	37.41	30.43	46.55	58.97	43.34
58289	H2	10.66	1.11	24.72	23.89	15.1
58289	H3	12.6	-0.59	-8.46	10.23	3.45
58289	H4	9.94	-3.25	6.37	31.16	11.06
58289	KOR	26.91	8	6.72	-0.7	10.23

58289	M1	8.53	-0.99	11.28	15.3	8.53
58289	M2	-10.3	-5.3	-5.48	-12.98	-8.52
58289	M3	-9.59	-8.46	-13.71	-9.89	-10.41
58289	M4	-23.04	-6.79	-9.97	-13.15	-13.24
58289	M5	-25.88	-20.53	-5.96	11.23	-10.29
58289	MOR	0.58	1.12	5.38	8.24	3.83
58289	NET	-34.95	-18.67	4.98	16.47	-8.04
58289	PBR	89.35	79	81.96	77.89	82.05
58289	SERT	0.27	-9.23	7.29	-7.13	-2.2
58289	Sigma 1	-8.89	-2.67	8.28	10.42	1.79
58289	Sigma 2	21.43	11.71	-4.81	-12.42	3.98
58289	AMPA	22.05	10.93	12.2	12.2	14.35
58289	Kainate (Rat Brain)	-7.79	-2.25	6.06	48.96	11.25
58289	NMDA	-77.09	-29.65	20.61	32.52	-13.4
58289	NR2B	24.62	13.51	27.02	16.02	20.29
58289	HCA2	19.33	9.79	-14.27	-5.11	2.44
58289	Ca channel human	13.41	8.81	1.15	-14.18	2.3
58289	HERG	-9.68	-18.98	-26.83	21.51	-8.5
58289	M3D	8.39	26.13	32.3	73.96	35.2
58289	M4 D	-17.82	-19.48	-17.86	-11.03	-16.55
58289	NTS1	20.48	16.9	4.81	11.53	13.43
58289	Alpha2Beta2	-0.51	0.09	1.54	-1.72	-0.15
58289	Alpha2Beta4	6.26	5.45	3.93	19.13	8.69
58289	Alpha3Beta2	9.82	1.24	5.92	12.16	7.29
58289	Alpha3Beta4	1.18	1.79	1.48	-5.21	-0.19
58289	Alpha4Beta2	1.86	0.2	1.86	5.1	2.26
58289	Alpha4Beta2 (Rat Brain)	-2.86	-2.36	-6.12	-1.94	-3.32
58289	Alpha4Beta4	13.66	0.98	7.02	11.55	8.3
58289	Alpha7	-18.29	-6.87	-10.63	3.95	-7.96
58289	NOP	20.23	13.27	6.16	12.98	13.16
58289	OT	5.94	13.16	-22.12	2.88	-0.03
58289	V1A	29.14	2.94	-27.37	-11.48	-1.69
58289	V1B	-15.65	1.15	-26.45	-16.45	-14.35
58289	V2	26.78	-8.47	4.18	16.84	9.83
58289	PBR	84.54	82.56	85.36	89.74	85.55
58289	SERT	-11.09	-5.14	-14.04	28.49	-0.45
58289	GABAA	6.32	-1.15	-19.53	-5.74	-5.03
58289	Oxytocin	-1.26	-1.26	6.16	-2.85	0.2
58290	5-HT1A	-4.32	-8.63	16.46	13.05	4.14
58290	5-HT1B	9.59	10.42	14.56	25.62	15.05

58290	5-HT1D	23.64	23.05	-10.64	16.85	13.23
58290	5-HT1E	38.62	30.56	28.9	35.06	33.29
58290	5-HT2A	30.06	15.92	13.46	4.09	15.88
58290	5-HT2B	-9.34	-23.8	-18.17	-15.76	-16.77
58290	5-HT2C	3.37	1.53	-19.69	9.9	-1.22
58290	5-HT3	16.31	5.44	-11.7	-12.34	-0.57
58290	5-HT4	7.18	21.98	13.28	21.11	15.89
58290	5-HT5A	-17.88	-16.28	-19.47	-16.28	-17.48
58290	5-HT6	5.14	-1.6	-16.68	-10.2	-5.84
58290	5-HT7A	-3.64	-13.3	-0.86	9.33	-2.12
58290	A1	53.44	2.14	-12.83	40.08	20.71
58290	A2A	13.41	-11.03	10.13	4.55	4.27
58290	Alpha1A	1.13	0.45	-5.88	14.98	2.67
58290	Alpha1B	15.41	11.17	-3.41	9.1	8.07
58290	Alpha1D	17.44	2.56	1.98	-5.46	4.13
58290	Alpha2A	-1.78	-14.79	-9.15	8.78	-4.24
58290	Alpha2B	60.11	61.78	52.47	53.91	57.07
58290	Alpha2C	-10.38	-14.39	0.16	-0.65	-6.32
58290	Beta1	13.17	4.06	11.68	28.9	14.45
58290	Beta2	-7.1	-20.39	-28.58	13.37	-10.68
58290	Beta3	49.6	-51.98	22.8	52.07	18.12
58290	AT2	-4.47	-6.6	-10.37	-2.24	-5.92
58290	BZP Rat Brain Site	63.24	53.18	53.72	53.18	55.83
58290	D1	-4.91	33.46	12.7	13.81	13.77
58290	D2	7.24	1.48	8.16	1.14	4.51
58290	D3	7.67	-12.01	-22.02	-35.26	-15.41
58290	D4	-1.15	5	21.01	24.21	12.27
58290	D5	-20.74	-8.83	-16.31	-6.08	-12.99
58290	DAT	-18.19	-52.54	-41.43	-51.3	-40.87
58290	DOR	11.54	2.87	5.92	14.12	8.61
58290	GABAA	44.11	8.76	-27.21	18.68	11.09
58290	H1	51.29	46.9	57.33	57.16	53.17
58290	H2	3.44	4.22	5.43	22.34	8.86
58290	H3	-1.57	6.49	13.78	10.04	7.19
58290	H4	7.27	1.03	0.31	34.01	10.66
58290	KOR	45.03	15.56	16.21	13.71	22.63
58290	M1	3.48	21.38	1.19	7.27	8.33
58290	M2	-28.63	-11.13	-19.19	-18.35	-19.33
58290	M3	-10.49	-8.22	-10.07	-4.7	-8.37
58290	M4	-21.75	-18.66	-22.27	-18.83	-20.38
58290	M5	-21.12	-8.97	7.74	13.66	-2.17
58290	MOR	1.2	2.67	1.97	3.67	2.38

58290	NET	-18.44	-10	-3.92	37.99	1.41
58290	PBR	61.51	48.73	41.37	44.37	49
58290	SERT	-5.18	14.26	-5.24	1.84	1.42
58290	Sigma 1	9.69	9.11	9.98	3.79	8.14
58290	Sigma 2	47.41	46.91	60.14	45.7	50.04
58290	AMPA	23.57	7.39	-1.2	23.32	13.27
58290	Kainate (Rat Brain)	-10.55	-41	28.2	14.36	-2.25
58290	NMDA	-9.5	9.13	2.84	19.52	5.5
58290	NR2B	6.16	32.2	14.71	14.31	16.85
58290	HCA2	-5.11	23.91	-19.62	-46.35	-11.79
58290	Ca channel human	-1.92	19.54	7.28	1.15	6.51
58290	HERG	-0.8	23.16	3.33	53.52	19.8
58290	M3D	4.53	19.96	25.36	49.28	24.78
58290	M4 D	-18.06	-13.38	-11.11	-0.04	-10.65
58290	NTS1	29.21	20.93	16	16.68	20.71
58290	Alpha2Beta2	3.11	10.6	13.38	10.36	9.36
58290	Alpha2Beta4	13.15	9.7	19.84	11.02	13.43
58290	Alpha3Beta2	12.55	5.92	5.63	6.6	7.68
58290	Alpha3Beta4	1.03	3.46	2.24	1.33	2.02
58290	Alpha4Beta2	16.18	13.63	14.91	14.22	14.74
58290	Alpha4Beta2 (Rat Brain)	6.08	10.33	6.24	4.74	6.85
58290	Alpha4Beta4	14.87	27.55	10.94	10.34	15.93
58290	Alpha7	-13.43	15.98	4.92	22.66	7.53
58290	NOP	14.69	9.57	12.27	9	11.38
58290	OT	4.55	5.1	12.33	25.38	11.84
58290	V1A	45.92	30.02	25.61	2.06	25.9
58290	V1B	-11.05	2.15	-23.25	2.15	-7.5
58290	V2	43.95	-30.17	-27.46	-12.99	-6.67
58290	PBR	48.9	39.42	37.25	40.78	41.59
58290	SERT	-5.56	-2.19	3.89	4.25	0.1
58290	GABAA	20.1	5.17	-2.3	-8.61	3.59
58290	Oxytocin	-0.73	-9.74	-3.38	-7.88	-5.43
58290	M2	1.68	6.58	-0.28	4.86	3.21
58291	5-HT1A	-22.59	6.37	-15.46	-3.14	-8.71
58291	5-HT1B	13.18	10.55	3.64	32.8	15.04
58291	5-HT1D	32.8	10.93	5.32	0	12.26
58291	5-HT1E	-39.86	-23.27	-12.12	-14.97	-22.56
58291	5-HT2A	34.67	20.03	5.73	9.02	17.36
58291	5-HT2B	19.58	-21.39	-5.32	-18.17	-6.33
58291	5-HT2C	24.79	6.63	14.59	8.67	13.67

58291	5-HT3	6.57	7.53	8.58	4.8	6.87
58291	5-HT4	3.7	15.89	5.44	17.63	10.67
58291	5-HT5A	-12.78	-18.51	-8.01	-8.96	-12.07
58291	5-HT6	-5.04	-2.93	-15.62	-13.51	-9.28
58291	5-HT7A	49.82	35	26.66	40.16	37.91
58291	A1	70.54	32.6	28.32	31.53	40.75
58291	A2A	-12.18	5.05	29.98	11.61	8.62
58291	Alpha1A	-8.61	-3.14	-14.08	24.04	-0.45
58291	Alpha1B	10.4	7.9	17.04	16.17	12.88
58291	Alpha1D	-13.76	-14.48	21.74	12.72	1.56
58291	Alpha2A	-14.79	-22.53	-5.34	13.69	-7.24
58291	Alpha2B	17.95	-1.94	-1.44	3.82	4.6
58291	Alpha2C	0.23	3.22	2.27	9.14	3.72
58291	Beta1	4.06	4.55	-18.47	29.57	4.93
58291	Beta2	-33.51	-22.23	-26.66	15.46	-16.74
58291	Beta3	45.72	33.73	30.91	52.78	40.79
58291	AT2	-41.26	23.84	-7.44	-5.59	-7.61
58291	BZP Rat Brain Site	100.04	96.14	96.36	95.28	96.96
58291	D1	0.09	-5.47	24.57	43.85	15.76
58291	D2	6.21	-2.09	-3.93	-11.76	-2.89
58291	D3	-7.18	-12.36	-21.31	-14.87	-13.93
58291	D4	30.74	22.29	25.49	16.52	23.76
58291	D5	-8.68	14.22	13.31	19.11	9.49
58291	DAT	-5.95	-37.01	-42.25	-40.2	-31.35
58291	DOR	-5.8	-0.41	1	-15.41	-5.16
58291	GABAA	39.15	53.41	34.81	19.92	36.82
58291	H1	56.98	72.16	59.74	63.19	63.02
58291	H2	5.23	5.48	10.81	2.04	5.89
58291	H3	13.19	11.41	13.38	15.15	13.28
58291	H4	11.19	-0.4	7.62	16.18	8.65
58291	KOR	20.56	7.79	-1.84	1.79	7.08
58291	M1	3.37	24.7	24.13	33.42	21.41
58291	M2	-20.3	-14	-31.03	-24.74	-22.52
58291	M3	-0.83	4.06	9.49	11.52	6.06
58291	M4	-13.58	-4.99	-0.43	-4.9	-5.98
58291	M5	1.71	2.88	-2.85	16.48	4.56
58291	MOR	18.06	3.44	6.23	16.59	11.08
58291	NET	-6.81	-9.92	6.88	29.62	4.94
58291	PBR	54.47	21.4	12.92	37.33	31.53
58291	SERT	4.27	9.29	0.27	11.93	6.44
58291	Sigma 1	16.09	-0.62	-13.15	-9.42	-1.78
58291	Sigma 2	27.38	16.47	2.18	-0.62	11.35

58291	AMPA	-3.48	5.37	41.01	34.19	19.27
58291	Kainate (Rat Brain)	24.05	-0.87	36.51	14.36	18.51
58291	NMDA	-11.02	-3.22	11.51	19.96	4.31
58291	NR2B	30.15	69.24	20.86	20.58	35.21
58291	HCA2	-4.73	62.86	16.28	-13.89	15.13
58291	Ca channel human	13.41	-21.84	11.88	-34.1	-7.66
58291	HERG	-10.51	25.64	-5.76	51.46	15.21
58291	M3D	-3.18	19.96	7.62	33.85	14.56
58291	M4 D	6.34	5.21	15.49	18.45	11.37
58291	NTS1	5.48	12.65	7.05	27.42	13.15
58291	Alpha2Beta2	25.58	-1.12	5.89	3.23	8.4
58291	Alpha2Beta4	16.8	15.38	6.97	6.06	11.3
58291	Alpha3Beta2	10.31	5.92	-0.32	-5.58	2.58
58291	Alpha3Beta4	0.57	-1.56	4.37	-1.41	0.49
58291	Alpha4Beta2	13.43	7.16	14.42	16.28	12.82
58291	Alpha4Beta2 (Rat Brain)	1.4	-3.28	-0.77	-4.53	-1.8
58291	Alpha4Beta4	13.36	12.75	20.3	26.34	18.19
58291	Alpha7	-14.64	12.7	6.26	-0.06	1.07
58291	NOP	9	0.76	1.76	20.23	7.94
58291	V1A	27.08	43.27	28.26	30.91	32.38
58291	V1B	-18.05	2.35	-21.85	-8.45	-11.5
58291	V2	54.8	14.12	23.16	7.8	24.97
58291	PBR	50.34	33.07	27.45	39.26	37.53
58291	SERT	5.09	13.27	10.14	4.55	8.26
58291	GABAA	51.11	42.5	22.97	25.27	35.46
58291	OT	-7.88	-12.65	-4.17	0.33	-6.09
58291	OT	-1.56	6.18	-3.49	-7.79	-1.67
72510	Alpha2Beta2	17.26	9.07	9.38	10.33	11.51
72510	Alpha2Beta4	25.35	7.13	2.69	-5.26	7.48
72510	Alpha3Beta2	5.5	-19.16	14.79	-6.43	-1.33
72510	Alpha3Beta4	1.84	0.08	5.04	-6.97	0
72510	Alpha4Beta2	8.94	12.59	-8.14	2.56	3.99
72510	Alpha4Beta2 (Rat Brain)	10.71	13.46	0.25	5.94	7.59
72510	Alpha4Beta4	-7.94	-6	-33.11	-23.43	-17.62
72510	Alpha7	-12.99	0.6	-56.54	12.99	-13.99
72511	Alpha2Beta2	1.18	1.02	10.01	-0.55	2.92
72511	Alpha2Beta4	-15.3	-68.81	3.86	19.28	-15.24
72511	Alpha3Beta2	-10.94	1.79	11.6	19.3	5.44
72511	Alpha3Beta4	9.69	17.05	4.4	-1.84	7.33

72511	Alpha4Beta2	9.17	23.97	9.17	-7	8.83
72511	Alpha4Beta2 (Rat Brain)	13.27	4.43	9.28	9.34	9.08
72511	Alpha4Beta4	-31.95	12.97	2.9	26.52	2.61
72511	Alpha7	5.79	3.8	12.19	17.78	9.89
72512	Alpha2Beta2	18.37	17.74	11.43	16.32	15.97
72512	Alpha2Beta4	8.06	17.17	22.55	-21.85	6.48
72512	Alpha3Beta2	-9.88	-7.76	1.26	11.6	-1.2
72512	Alpha3Beta4	5.2	6.65	-19.14	-22.66	-7.49
72512	Alpha4Beta2	12.36	7.57	-3.13	-1.99	3.7
72512	Alpha4Beta2 (Rat Brain)	6.92	10	8.62	-4.34	5.3
72512	Alpha4Beta4	-24.59	-23.04	0.19	-10.65	-14.52
72512	Alpha7	-17.78	-17.38	-10.99	7.39	-9.69
72513	Alpha2Beta2	12.38	12.22	19.94	12.85	14.35
72513	Alpha2Beta4	-11.1	19.04	-28.39	31.19	2.69
72513	Alpha3Beta2	13.46	-2.72	-21.02	-35.88	-11.54
72513	Alpha3Beta4	-4.08	4.56	6.33	-38.35	-7.89
72513	Alpha4Beta2	-9.05	4.84	-6.09	-6.09	-4.1
72513	Alpha4Beta2 (Rat Brain)	12.02	13.79	14.18	4.11	11.03
72513	Alpha4Beta4	-16.84	-4.45	-16.07	19.17	-4.55
72513	Alpha7	6.59	5.39	-0.6	4.2	3.9
58217	5-HT1A	-0.55	-1.69	-7.54	-10.63	-5.1
58217	5-HT1B	60.41	27.1	12.42	24.05	31
58217	5-HT1D	-8.48	-12.5	-10.71	-4.02	-8.93
58217	5-HT1E	-1.56	9.8	-1.56	25.72	8.1
58217	5-HT2A	18.6	14.1	11.17	13.76	14.41
58217	5-HT2B	15.43	1.49	2.51	16.46	8.97
58217	5-HT2C	3.65	17.23	-15.13	-5.6	0.04
58217	5-HT3	11.94	8.52	-11.9	-3.56	1.25
58217	5-HT4	8.24	-11.93	17.56	9.02	5.72
58217	5-HT5A	7.17	-11.03	-1.31	-3.3	-2.12
58217	5-HT6	5.1	-11.61	11.29	-2.39	0.6
58217	5-HT7A	-14.27	-23.24	-5.03	10.46	-8.02
58217	A1	8.9	13.87	14.55	46.41	20.93
58217	A2A	-9.69	-9.69	18.83	33.35	8.2
58217	Alpha1A	9.36	7.04	-10.25	11.68	4.46
58217	Alpha1B	-4.95	5.18	1.16	7.91	2.33
58217	Alpha1D	21.86	-1.83	-15.83	5.02	2.31
58217	Alpha2A	28.86	-2.84	-8.52	15.23	8.18
58217	Alpha2B	31.09	21.75	12.41	14.09	19.84
58217	Alpha2C	31.17	17.46	-5.71	28.65	17.89

58217	Beta1	37.43	41.57	7.26	0.28	21.64
58217	Beta2	-4.39	17.05	22.52	34.18	17.34
58217	Beta3	31.06	12.38	26.33	35.55	26.33
58217	AT2	0	2.27	-3.8	-6.84	-2.09
58217	BZP Rat Brain Site	46.56	50.78	53.97	58.3	52.4
58217	D1	8.37	-23.45	-20.29	19.98	-3.85
58217	D2	-4.81	-3.1	2.46	38.08	8.16
58217	D3	-11.41	-13.78	-11.41	-6.88	-10.87
58217	D4	-3.76	-41.36	-2.43	-6.82	-13.59
58217	D5	-16.46	-22.48	-26.62	8.56	-14.25
58217	DAT	87.07	67.78	52.12	14.49	55.37
58217	DOR	23.2	14.81	17.8	5.22	15.26
58217	GABAA	5.83	1.65	-28.26	11.39	-2.35
58217	H1	-11.52	-20.85	6.81	-21.19	-11.69
58217	H2	25.99	23.91	-9.9	5.16	11.29
58217	H3	7.81	2.88	-15.88	-13.12	-4.58
58217	H4	-5.71	-8.29	-2.41	15	-0.35
58217	KOR	89.08	84.17	78.8	70.7	80.69
58217	M1	2.13	-5.69	-10.1	-13.51	-6.79
58217	M2	-2.23	-8.08	-20.55	-8.08	-9.74
58217	M3	4.67	23.61	11.66	10.21	12.54
58217	M4	65.02	45.31	32.2	26.04	42.14
58217	M5	16.36	-0.05	1.3	6.03	5.91
58217	MOR	14.66	6.23	3.3	6.99	7.8
58217	NET	52.46	38.77	36.31	20.54	37.02
58217	PBR	25.81	13.02	3.71	9.18	12.93
58217	SERT	-0.44	-5.7	-11.09	-16.78	-8.5
58217	Sigma 1	-0.26	5.08	-5.72	15.88	3.75
58217	Sigma 2	13.73	1.5	-22.74	23.09	3.9
58217	AMPA	16.3	-14.3	-3.47	20.54	4.77
58217	Kainate (Rat Brain)	45.7	24.77	29.63	24.39	31.12
58217	NMDA	89.56	93.93	96.66	100.3	95.11
58217	NR2B	24.63	26.71	24.91	-3.71	18.14
58217	HCA2	25.32	-5.95	24.77	28.64	18.2
58217	Ca channel human	49.71	38.92	21.97	37.38	37
58217	HERG	0.54	11.98	2.91	-19.97	-1.14
58217	M3D	26.79	23.42	-6.96	-11.18	8.02
58217	M4 D	16.89	-10.45	12.21	37.21	13.97
58217	NTS1	-20.53	-32.62	-41.68	-17.05	-27.97
58217	Alpha2Beta2	1.44	-2.73	-6.9	-3.53	-2.93

58217	Alpha2Beta4	-0.87	7.72	-0.75	5.05	2.79
58217	Alpha3Beta2	-11.22	-3.26	-4.51	-5.88	-6.22
58217	Alpha3Beta4	-1.4	-7.42	3.78	-1.26	-1.58
58217	Alpha4Beta2	3.67	-3.67	7.51	8.49	4
58217	Alpha4Beta2 (Rat Brain)	-7.89	-14.92	-6.07	-2.78	-7.92
58217	Alpha4Beta4	8.42	2.2	-6.87	1.17	1.23
58217	Alpha7	-7.09	-11.56	-2.75	4.36	-4.26
58217	NOP	35.3	46.33	-5.36	-36.4	9.97
58217	OT	2.86	-13.79	-1.38	-6.17	-4.62
58217	V1A	13.11	13.99	18.62	10.02	13.94
58217	V1B	6.12	-1.89	-10.58	10.7	1.09
58217	V2	63.49	-3.24	-1.63	52.44	27.77
58217	NET	-35.32	-39.8	-44.72	-63.18	-45.76
58217	PBR	5.97	-9.46	-22.4	8.36	-4.38
58217	SERT	-9.72	-18.33	-16.37	-35.07	-19.87
58217	GABAA	16.01	9.19	-3.41	19.69	10.37
58217	Oxytocin	15.85	-12.24	-10.75	-7.77	-3.73
58219	5-HT1A	17.18	-2.01	7.58	0.43	5.8
58219	5-HT1B	-20.6	10.38	8.78	24.34	5.73
58219	5-HT1D	28.57	12.95	-2.68	16.96	13.95
58219	5-HT1E	-62.1	-69.2	-41.63	-69.2	-60.53
58219	5-HT2A	26.89	23.43	27.75	30.17	27.06
58219	5-HT2B	-4.46	9.89	4.97	10.31	5.18
58219	5-HT2C	1.91	7.11	9.71	10.29	7.26
58219	5-HT3	43.27	37.77	4.02	6.69	22.94
58219	5-HT4	70.32	53.25	57.9	62.56	61.01
58219	5-HT5A	1.43	-8.29	-3.8	10.9	0.06
58219	5-HT6	28.15	21.07	4.95	13.15	16.83
58219	5-HT7A	-31.39	-16.71	-5.84	10.46	-10.87
58219	A1	17.03	15	28.56	69.92	32.63
58219	A2A	-9.86	-16.95	-7.36	31.28	-0.72
58219	Alpha1A	20.05	2.58	-9.89	6.15	4.72
58219	Alpha1B	0.51	-8.68	7.7	16.17	3.93
58219	Alpha1D	32.88	20.07	16.94	16.94	21.71
58219	Alpha2A	12.61	-8.52	2.05	-4.89	0.31
58219	Alpha2B	2.54	8.34	5.41	26.66	10.74
58219	Alpha2C	41.95	-11.73	12.24	42.12	21.15
58219	Beta1	33.28	5.94	-15.18	60.05	21.02
58219	Beta2	6.69	-0.36	3.09	37.78	11.8
58219	Beta3	88.34	54.37	72.55	44.41	64.92
58219	AT2	4.4	30.68	22.55	19.48	19.28
58219	BZP Rat	36.86	16.79	6.3	22.15	20.53

	Brain Site					
58219	D1	57.6	46.35	61.65	54.44	55.01
58219	D2	12.72	27.97	31.67	43.21	28.89
58219	D3	6.53	-5.1	5.74	27.03	8.55
58219	D4	-3.04	8.92	-8.66	13.72	2.74
58219	D5	39.41	45.05	36.02	55.02	43.88
58219	DAT	71.42	61.95	58.07	55.88	61.83
58219	DOR	2.82	-8.96	-14.56	-18.95	-9.91
58219	GABAA	21.13	16.96	-9.48	-0.43	7.05
58219	H1	28.7	19.71	32.44	32.1	28.24
58219	H2	20.47	26.34	24.2	16.29	21.83
58219	H3	20.73	12.12	8.12	13.35	13.58
58219	H4	-2.18	-0.29	-12.29	-3.12	-4.47
58219	KOR	4.73	-4.28	0.64	-14.65	-3.39
58219	M1	12.56	5.94	12.36	8.15	9.75
58219	M2	-18.77	-16.73	-12.4	-12.4	-15.08
58219	M3	11.52	12.03	-1.37	8.24	7.61
58219	M4	-8.74	1.8	-8.93	8.69	-1.8
58219	M5	-3.72	-11.82	-10.96	-11.53	-9.51
58219	MOR	13.24	9.92	5.67	-0.58	7.06
58219	NET	-3.53	-10.22	-13.3	12.62	-3.61
58219	PBR	35.56	21.97	16.57	8.96	20.77
58219	SERT	13.52	7.46	12.17	11.38	11.13
58219	Sigma 1	29.23	31.82	35.76	58.19	38.75
58219	Sigma 2	73.24	76.7	89.25	76.64	78.96
58219	AMPA	55.37	22.65	10.65	-1.59	21.77
58219	Kainate (Rat Brain)	35.76	7.92	0	11.35	18.34
58219	NMDA	100.84	94.47	96.11	94.47	96.47
58219	NR2B	36.85	32	36.96	24.01	32.46
58219	HCA2	22.83	-21.72	13.42	-1.52	3.25
58219	Ca channel human	58.96	60.5	28.13	55.88	50.87
58219	HERG	33.78	32.27	9.39	22.99	24.61
58219	M3D	31.86	18.35	-9.49	1.48	10.55
58219	M4 D	32.08	-51.52	0	-55.41	-24.95
58219	NTS1	21.99	21.06	24.08	22.22	22.34
58219	Alpha2Beta2	-1.76	2.57	-4.65	2.89	-0.24
58219	Alpha2Beta4	9.7	20.85	2.15	22.01	13.68
58219	Alpha3Beta2	3.57	10.66	2.83	-0.4	4.17
58219	Alpha3Beta4	-4.62	5.74	-3.5	-4.9	-1.82
58219	Alpha4Beta2	8.25	4.98	1.22	0.65	3.78
58219	Alpha4Beta2	-22.75	-20.71	-21.73	-16.28	-20.37

	(Rat Brain)					
58219	Alpha4Beta4	5.31	8.16	12.82	0.13	6.61
58219	Alpha7	22.29	18.77	25.81	18.58	21.36
58219	NOP	30.25	50.9	40.97	-4.25	29.47
58219	OT	2.86	6.81	29.95	22.05	15.42
58219	V1A	12.89	28.09	19.72	19.72	20.11
58219	V1B	21.22	-8.98	-11.5	-11.5	-2.69
58219	V2	8.82	5.6	22.29	26.51	15.81
58219	NET	21.71	21.49	23.53	35.97	25.68
58219	PBR	8.96	-5.48	15.43	1.29	5.05
58219	SERT	10.02	2.93	9.2	10.73	8.22
58219	GABAA	20.73	21.78	1.84	-26.51	4.46
58219	Oxytocin	21.81	-21.94	6.15	12.37	4.6

5.2. Publications

molecules

MDPI

Article

Synthesis and Receptor Binding Studies of α5 $GABA_AR$ Selective Novel Imidazodiazepines Targeted for Psychiatric and Cognitive Disorders

Dishary Sharmin [1,*], Md Yeunus Mian [1], Michael Marcotte [2], Thomas D. Prevot [2,3], Etienne Sibille [2,3,4], Jeffrey M. Witkin [1,5] and James M. Cook [1,*]

[1] Department of Chemistry and Biochemistry, Milwaukee Institute of Drug Discovery, University of Wisconsin Milwaukee, Milwaukee, WI 53201, USA
[2] Campbell Family Mental Health Research Institute of CAMH, Toronto, ON M5S 2S1, Canada
[3] Department of Psychiatry, University of Toronto, Toronto, ON M5T 1R8, Canada
[4] Department of Pharmacology and Toxicology, University of Toronto, Toronto, ON M5T 1R8, Canada
[5] Laboratory of Antiepileptic Drug Discovery, Ascension, St. Vincent, Indianapolis, IN 46260, USA
* Correspondence: dsharmin@uwm.edu (D.S.); capncook@uwm.edu (J.M.C.)

Abstract: GABA mediates inhibitory actions through various $GABA_A$ receptor subtypes, including 19 subunits in human GABAAR. Dysregulation of GABAergic neurotransmission is associated with several psychiatric disorders, including depression, anxiety, and schizophrenia. Selective targeting of α2/3 GABAARs can treat mood and anxiety, while α5 GABAA-Rs can treat anxiety, depression, and cognitive performance. GL-II-73 and MP-III-022, α5-positive allosteric modulators have shown promising results in animal models of chronic stress, aging, and cognitive disorders, including MDD, schizophrenia, autism, and Alzheimer's disease. Described in this article is how small changes in the structure of imidazodiazepine substituents can greatly impact the subtype selectivity of benzodiazepine GABAAR. To investigate alternate and potentially more effective therapeutic compounds, modifications were made to the structure of imidazodiazepine **1** to synthesize different amide analogs. The novel ligands were screened at the NIMH PDSP against a panel of 47 receptors, ion channels, including hERG, and transporters to identify on- and off-target interactions. Any ligands with significant inhibition in primary binding were subjected to secondary binding assays to determine their K_i values. The newly synthesized imidazodiazepines were found to have variable affinities for the benzodiazepine site and negligible or no binding to any off-target profile receptors that could cause other physiological problems.

Keywords: γ-Aminobutyric acid (GABA); positive allosteric modulator; cognitive disorders; imidazodiazepine; PDSP; off-target profile

check for updates

Citation: Sharmin, D.; Mian, M.Y.; Marcotte, M.; Prevot, T.D.; Sibille, E.; Witkin, J.M.; Cook, J.M. Synthesis and Receptor Binding Studies of α5 $GABA_AR$ Selective Novel Imidazodiazepines Targeted for Psychiatric and Cognitive Disorders. *Molecules* **2023**, *28*, 4771. https://doi.org/10.3390/molecules28124771

Academic Editors: Chiara Brullo, Rosa Amoroso, Olga Yarovaya, Sophia S. Borisevich and Vladimir V. Zarubaev

Received: 24 April 2023
Revised: 9 June 2023
Accepted: 12 June 2023
Published: 14 June 2023

Copyright: © 2023 by the authors. Licensee MDPI, Basel, Switzerland. This article is an open access article distributed under the terms and conditions of the Creative Commons Attribution (CC BY) license (https://creativecommons.org/licenses/by/4.0/).

1. Introduction

γ-Aminobutyric acid (GABA) acts as an inhibitory neurotransmitter through various subtypes of GABA receptors [1–3]. Nineteen subunits of GABAAR have been identified in humans, including α1-6, β1-3, γ1-3, δ, ε, θ, π, and ρ1-3 subunits, although only a few subunit combinations form a functional receptor [4,5]. The GABAAR ion channel comprises α1-6β1-3γ2 subunits in a 2:2:1 stoichiometric ratio to form a fully functional benzodiazepine-mediated chloride ion channel [6]. Dysregulation of GABAergic neurotransmission has been linked to several psychiatric disorders, including schizophrenia, depression, autism, and anxiety [7–11]. Non-selective targeting of GABAAR with different subunits by benzodiazepines, commonly used to treat anxiety disorders, can result in side effects such as sedation, ataxia, [12] and dependence. Therefore, selective targeting of GABAAR, specifically by potentiating α2, α3, and α5 subunits containing GABAAR, can produce the desired therapeutic effects [7,12].

International Journal of
Molecular Sciences

MDPI

Article

α5-GABAA Receptor Modulation Reverses Behavioral and Neurophysiological Correlates of Psychosis in Rats with Ventral Hippocampal Alzheimer's Disease-like Pathology

Nicole E. Eassa [1,2], Stephanie M. Perez [1,2,*], Angela M. Boley [1,2], Hannah B. Elam [1,2], Dishary Sharmin [3], James M. Cook [3] and Daniel J. Lodge [1,2]

[1] Department of Pharmacology and Center for Biomedical Neuroscience, UT Health San Antonio, San Antonio, TX 78229, USA; eassa@livemail.uthscsa.edu (N.E.E.); boley@uthscsa.edu (A.M.B.); elamh@livemail.uthscsa.edu (H.B.E.); lodged@uthscsa.edu (D.J.L.)
[2] South Texas Veterans Health Care System, Audie L. Murphy Division, San Antonio, TX 78229, USA
[3] Department of Chemistry and Biochemistry, Milwaukee Institute of Drug Discovery, University of Wisconsin-Milwaukee, Milwaukee, WI 53211, USA; dsharmin@uwm.edu (D.S.); capncook@uwm.edu (J.M.C.)
* Correspondence: perezsm@uthscsa.edu

Abstract: Of the 35 million people in the world suffering from Alzheimer's Disease (AD), up to half experience comorbid psychosis. Antipsychotics, used to treat psychosis, are contraindicated in elderly patients because they increase the risk of premature death. Reports indicate that the hippocampus is hyperactive in patients with psychosis and those with AD. Preclinical studies have demonstrated that the ventral hippocampus (vHipp) can regulate dopamine system function, which is thought to underlie symptoms of psychosis. A viral-mediated approach was used to express mutated human genes known to contribute to AD pathology: the Swedish (K670N, M671L), Florida (I716V), and London (V717I) mutations of amyloid precursor protein and two mutations (M146L and L286V) of presenilin 1 specifically in the vHipp, to investigate the selective contribution of AD-like pathology in this region. We observed a significant increase in dopamine neuron population activity and behavioral deficits in this AD-AAV model that mimics observations in rodent models with psychosis-like symptomatologies. Further, systemic administration of MP-III-022 (α5-GABAA receptor selective positive allosteric modulator) was able to reverse aberrant dopamine system function in AD-AAV rats. This study provides evidence for the development of drugs that target α5-GABAA receptors for patients with AD and comorbid psychosis.

Keywords: Alzheimer's disease; psychosis; dopamine; ventral hippocampus; parvalbumin; α5-GABAA

check for updates

Citation: Eassa, N.E.; Perez, S.M.; Boley, A.M.; Elam, H.B.; Sharmin, D.; Cook, J.M.; Lodge, D.J. α5-GABAA Receptor Modulation Reverses Behavioral and Neurophysiological Correlates of Psychosis in Rats with Ventral Hippocampal Alzheimer's Disease-like Pathology. *Int. J. Mol. Sci.* **2023**, *24*, 11788. https://doi.org/10.3390/ijms241411788

Academic Editor: Alberto Pérez-Mediavilla

Received: 6 July 2023
Revised: 18 July 2023
Accepted: 20 July 2023
Published: 22 July 2023

Copyright: © 2023 by the authors. Licensee MDPI, Basel, Switzerland. This article is an open access article distributed under the terms and conditions of the Creative Commons Attribution (CC BY) license (https://creativecommons.org/licenses/by/4.0/).

1. Introduction

Alzheimer's Disease (AD) is the most common neurodegenerative disease, affecting an estimated 6.7 million Americans age 65 and older [1] and is known to cause a progressive cognitive decline, but it is less appreciated that half of these patients also suffer with comorbid psychosis (hallucinations and delusions) [2]. Elderly patients are unable to be treated with antipsychotics (the standard-of-care) given that the Food and Drug Administration issued a black box warning contraindicating their use in the elderly due to an increased risk of premature death. AD patients suffering from comorbid psychosis are clearly in need of novel therapeutic options.

Dopamine system dysfunction has been demonstrated to underlie symptoms of psychosis and is likely attributable to aberrant regulation by afferent brain regions [3,4]. The hippocampus is one such region upstream of the dopamine system that is a key site of pathology in patients with AD [5] and displays aberrant activity in psychosis [6]. In preclinical studies, our laboratory, along with others, has shown that hyperactivity of the ventral hippocampus (vHipp) drives dopamine system dysfunction in the ventral tegmental area

International Journal of
Molecular Sciences

MDPI

Communication

GL-II-73, a Positive Allosteric Modulator of α5GABA$_A$ Receptors, Reverses Dopamine System Dysfunction Associated with Pilocarpine-Induced Temporal Lobe Epilepsy

Alexandra M. McCoy [1,2], Thomas D. Prevot [3,4], Dishary Sharmin [5], James M. Cook [5], Etienne L. Sibille [3,4,6] and Daniel J. Lodge [1,2,*]

[1] Department of Pharmacology and Center for Biomedical Neuroscience, UT Health San Antonio, San Antonio, TX 78229, USA; mccoya1@livemail.uthscsa.edu
[2] South Texas Veterans Health Care System, Audie L. Murphy Division, San Antonio, TX 78229, USA
[3] Campbell Family Mental Health Research Institute of CAMH, Toronto, ON M5S 2S1, Canada; thomas.prevot@camh.ca (T.D.P.); etienne.sibille@camh.ca (E.L.S.)
[4] Department of Psychiatry, University of Toronto, Toronto, ON M5T 1R8, Canada
[5] Department of Chemistry and Biochemistry, University of Wisconsin-Milwaukee, Milwaukee, WI 53201, USA; dsharmin@uwm.edu (D.S.); capncook@uwm.edu (J.M.C.)
[6] Department of Pharmacology and Toxicology, University of Toronto, Toronto, ON M5T 1R8, Canada
* Correspondence: lodged@uthscsa.edu

Abstract: Although seizures are a hallmark feature of temporal lobe epilepsy (TLE), psychiatric comorbidities, including psychosis, are frequently associated with TLE and contribute to decreased quality of life. Currently, there are no defined therapeutic protocols to manage psychosis in TLE patients, as antipsychotic agents may induce epileptic seizures and are associated with severe side effects and pharmacokinetic and pharmacodynamic interactions with antiepileptic drugs. Thus, novel treatment strategies are necessary. Several lines of evidence suggest that hippocampal hyperactivity is central to the pathology of both TLE and psychosis; therefore, restoring hippocampal activity back to normal levels may be a novel therapeutic approach for treating psychosis in TLE. In rodent models, increased activity in the ventral hippocampus (vHipp) results in aberrant dopamine system function, which is thought to underlie symptoms of psychosis. Indeed, we have previously demonstrated that targeting α5-containing γ-aminobutyric acid receptors (α5GABA$_A$Rs), an inhibitory receptor abundant in the hippocampus, with positive allosteric modulators (PAMs), can restore dopamine system function in rodent models displaying hippocampal hyperactivity. Thus, we posited that α5-PAMs may be beneficial in a model used to study TLE. Here, we demonstrate that pilocarpine-induced TLE is associated with increased VTA dopamine neuron activity, an effect that was completely reversed by intra-vHipp administration of GL-II-73, a selective α5-PAM. Further, pilocarpine did not alter the hippocampal α5GABA$_A$R expression or synaptic localization that may affect the efficacy of α5-PAMs. Taken together, these results suggest augmenting α5GABA$_A$R function as a novel therapeutic modality for the treatment of psychosis in TLE.

Keywords: dopamine; temporal lobe epilepsy; electrophysiology

check for updates

Citation: McCoy, A.M.; Prevot, T.D.; Sharmin, D.; Cook, J.M.; Sibille, E.L.; Lodge, D.J. GL-II-73, a Positive Allosteric Modulator of α5GABA$_A$ Receptors, Reverses Dopamine System Dysfunction Associated with Pilocarpine-Induced Temporal Lobe Epilepsy. *Int. J. Mol. Sci.* **2023**, *24*, 11588. https://doi.org/10.3390/ijms241411588

Academic Editor: Alexandre Hiroaki Kihara

Received: 25 June 2023
Revised: 15 July 2023
Accepted: 16 July 2023
Published: 18 July 2023

Copyright: © 2023 by the authors. Licensee MDPI, Basel, Switzerland. This article is an open access article distributed under the terms and conditions of the Creative Commons Attribution (CC BY) license (https://creativecommons.org/licenses/by/4.0/).

1. Introduction

Temporal lobe epilepsy (TLE) is a disorder characterized by the presence of spontaneous seizures, or uncontrolled neural activity, involving the temporal lobe, typically the hippocampal formation. Given that seizures are the hallmark feature of TLE, other neuropsychiatric comorbidities, such as psychosis, are often overlooked, despite the well-established relationship between TLE and psychotic symptoms [1–4]. TLE patients are 6–12 times more likely than the general population to suffer from psychosis [5,6]; however, the management of psychosis for patients with TLE is currently inadequate. Both first- and second-generation antipsychotics are associated with an increase in seizure incidence,

Research Square

Preprints are preliminary reports that have not undergone peer review.
They should not be considered conclusive, used to inform clinical practice,
or referenced by the media as validated information.

α5-GABAA receptor modulation reverses behavioral and neurophysiological correlates of psychosis in rats with ventral hippocampal Alzheimer's Disease-like pathology

Stephanie Perez (PerezSM@uthscsa.edu)
UTHSCSA https://orcid.org/0000-0002-3258-4456
Nicole Eassa
UTHSCSA
Angela Boley
University of Texas Health Science Center at San Antonio https://orcid.org/0000-0003-0253-1481
Hannah Elam
UT Health San Antonio https://orcid.org/0000-0002-6106-4011
Dishary Sharmin
James Cook
Daniel Lodge
University of Texas Health Science Center at San Antonio https://orcid.org/0000-0002-6772-1748

Article

Keywords: Alzheimer's Disease, psychosis, dopamine, ventral hippocampus, parvalbumin, α5-GABAA

Posted Date: May 23rd, 2023

DOI: https://doi.org/10.21203/rs.3.rs-2809328/v1

License: This work is licensed under a Creative Commons Attribution 4.0 International License.
Read Full License

Additional Declarations: The authors have declared there is **NO** conflict of interest to disclose

Comparative anticonvulsant activity of the GABAkine KRM-II-81 and a deuterated analog

Xingjie Ping, Michelle J. Meyer, Nicolas M. Zahn, Lalit K. Golani, Dishary Sharmin, Kamal P. Pandey, Sepideh Revanian, Prithu Mondal, Xiaoming Jin, Leggy A. Arnold, Rok Cerne, James M. Cook, Branka Divović, Miroslav M. Savić, Arnold Lippa, Jodi L. Smith, Jeffrey M. Witkin ... See fewer authors

First published: 07 February 2023 | https://doi.org/10.1002/ddr.22042 | Citations: 1

Read the full text > PDF TOOLS SHARE

Abstract

A series of imidazodiazepines has been developed that possess reduced sedative liabilities but retain efficacy in anticonvulsant screening models. The latest of these compounds, (5-(8-ethynyl-6-(pyridin-2-yl)-4H-benzo[*f*]imidazole[1,5-α][1,4]diazepin-3-yl) oxazole known as KRM-II-81) is currently awaiting advancement into the clinic. A deuterated structural analog (D5-KRM-II-81) was made as a potential backup compound and studied here in comparison to KRM-II-81. In the present study, both compounds significantly prevented seizures in mice induced by 6 Hz (44 mA) electrical stimulation without significantly altering motoric function on a rotarod after intraperitoneal administration. Both compounds also significantly prevented clonic seizures, tonic seizures, and lethality induced by pentylenetetrazol in mice when given orally. D5-KRM-II-81 had a slightly longer duration of action against clonic and tonic seizures than KRM-II-81. Oral administration of 100 mg/kg of either KRM-II-81 or D5-KRM-II-81 was significantly less disruptive of sensorimotor function in mice than diazepam (5 mg/kg, p.o.). The present report documents that D5-KRM-II-81 represents another in this series of

THE JOURNAL OF PHARMACOLOGY AND EXPERIMENTAL THERAPEUTICS

Research Article | Neuropharmacology

Structural Analogs of the GABAkine KRM-II-81 Are Orally Bioavailable Anticonvulsants without Sedation

Kamal P. Pandey, Branka Divović, Farjana Rashid, Lalit K. Golani, Rok Cerne, Nicolas M. Zahn, Michelle Jean Meyer, Leggy A. Arnold, Dishary Sharmin, Md Yeunus Mian, Jodi L. Smith, Xingjie Ping, Xiaoming Jin, Arnold Lippa, V.V.N. Phani Babu Tiruveedhula, James M. Cook, Miroslav M. Savić, and Jeffrey M. Witkin

Journal of Pharmacology and Experimental Therapeutics April 2023, 385 (1) 50-61; DOI: https://doi.org/10.1124/jpet.122.001382

Abstract

To provide back-up compounds to support the development of the $GABA_A$ receptor (GABAAR) potentiator KRM-II-81, three novel analogs were designed: replacing the pyridinyl with 2′-Cl-phenyl (FR-II-60), changing the positions of the N and O atoms in the oxazole ring with addition of an ethyl group (KPP-III-34 and KPP-III-51), or substituting a Br atom for the ethynyl of KRM-II-81 (KPP-III-34). The compounds bound to brain GABAARs. Intraperitoneal administration of FR-II-60 and KPP-III-34 produced anticonvulsant activity in mice [maximal electroshock (MES)-induced seizures or 6 Hz-induced seizures], whereas KPP-III-51 did not. Although all compounds were orally bioavailable, structural changes reduced the plasma and brain (FR-II-60 and KPP-III-51) exposures relative to KRM-II-81. Oral administration of each compound produced dose-dependent increases in the latency for both clonic and tonic seizures and the lethality induced by pentylenetetrazol (PTZ) in mice. Since KPP-III-34 produced the highest brain area under the curve (AUC) exposures, it was selected for further profiling. Oral administration of KPP-III-34 suppressed seizures in corneal-kindled mice, hippocampal paroxysmal discharges in mesial temporal lobe epileptic mice, and PTZ-induced convulsions in rats. Only transient sensorimotor impairment was observed in mice, and doses of KPP-III-34 up to 500 mg/kg did not produce impairment in rats. Molecular docking studies demonstrated that all compounds displayed a reduced propensity for binding to α1His102 compared with the sedating compound alprazolam; the bromine-substituted KPP-III-34 achieved the least interaction. Overall, these findings document the oral bioavailability and anticonvulsant efficacy of three novel analogs of KRM-II-81 with reduced sedative effects.

SIGNIFICANCE STATEMENT A new non-sedating compound, KRM-II-81, with reduced propensity for tolerance is moving into clinical development. Three new analogs were orally bioavailable, produced anticonvulsant effects in rodents, and displayed low sensorimotor impairment. KPP-III-34 demonstrated efficacy in models of pharmacoresistant epilepsy. Docking studies demonstrated a low propensity for compound binding to the α1His102 residue implicated in sedation. Thus, three additional structures have been added to the list of non-sedating imidazodiazepine anticonvulsants that could serve as backups in the clinical development of KRM-II-81.

In this issue



Journal of Pharmacology and Experimental Therapeutics
Vol. 385, Issue 1
1 Apr 2023
Table of Contents
Table of Contents (PDF)
About the Cover
Index by author
Editorial Board (PDF)
Front Matter (PDF)

Download PDF
Article Alerts
Email Article
Citation Tools
Request Permissions
Share
Tweet
Like 0

Jump to section

- Article
  - Abstract
  - Introduction
  - Materials and Methods
  - Results
  - Discussion
  - Acknowledgments
  - Authorship Contributions
  - Footnotes
  - Abbreviations
  - References
- Figures & Data
- Info & Metrics
- eLetters

Drug and Alcohol Dependence
Volume 243, 1 February 2023, 109735



Modeling cue-exposure therapy for alcohol use disorder in rhesus monkeys: Effects of putative cognitive enhancers

Tanya Pareek [a], John S. Overton [a], Luat T. Nguyen [a], Md. Toufiqur Rahman [c], Dishary Sharmin [c], James M. Cook [c], Donna M. Platt [a b]

Show more
+ Add to Mendeley Share Cite

https://doi.org/10.1016/j.drugalcdep.2022.109735 Get rights and content

Abstract

Background

Cue-exposure therapy (CET) is an effective approach for anxiety-related disorders, but its effectiveness for substance use disorders is less clear. One potential means of improving CET outcomes is to include a cognitive-enhancing pharmacotherapy. This study evaluated D-cycloserine (DCS) and RY-023, putative cognitive enhancers targeting glutamate and GABA systems, respectively, in a monkey model of CET for alcohol use disorder.

Methods

Male rhesus monkeys (n=4) underwent multiple cycles of the CET procedure. During baseline (Phase 1), monkeys self-administered an ethanol solution under a fixed-ratio schedule and limited access conditions such that every 5th response in a 3-h session resulted in 30-s access to a drinking spout and a change in ethanol-paired cue lights from white to red. Behavior then was extinguished (Phase 2) by omitting the ethanol solution yet retaining the ethanol-paired stimulus lights. Monkeys also received injections of vehicle, DCS (3mg/kg), a partial agonist at the glycine modulatory site on glutamatergic NMDA receptors, or the $\alpha5GABA_A$ receptor-selective inverse agonist RY-023 (0.03 or 0.3mg/kg). Once responding declined, monkeys underwent a cue reactivity test (Phase 3), and then returned to self-administration the following day to assess reacquisition (Phase 4).

Results

Through multiple cycles, self-administration remained stable. Compared to vehicle, DCS facilitated extinction of ethanol seeking (Phase 2) and delayed reacquisition of ethanol self-administration (Phase 4). In contrast, RY-023 facilitated extinction (Phase 2) and reduced cue reactivity (Phase 3).

biomolecules

MDPI

Article

GABA-A Alpha 2/3 but Not Alpha 1 Receptor Subunit Ligand Inhibits Harmaline and Pimozide-Induced Tremor in Rats

Barbara Kosmowska [1], Martyna Paleczna [1], Dominika Biała [1], Justyna Kadłuczka [1], Jadwiga Wardas [1], Jeffrey M. Witkin [2,3], James M. Cook [2,3], Dishary Sharmin [2], Monika Marcinkowska [4] and Katarzyna Z. Kuter [1,*]

[1] Department of Neuropsychopharmacology, Maj Institute of Pharmacology, Polish Academy of Sciences, 12 Smetna St., 31-343 Krakow, Poland
[2] Department of Chemistry and Biochemistry, University of Wisconsin-Milwaukee, Milwaukee, WI 53211, USA
[3] RespireRx Pharmaceuticals Inc., Glen Rock, NJ 07452, USA
[4] Department of Pharmaceutical Chemistry, Jagiellonian University, Medical College, 9 Medyczna St., 30-688 Krakow, Poland
* Correspondence: kuter@if-pan.krakow.pl; Tel.: +48-12-662-32-26

Abstract: Treatment of tremors, such as in essential tremor (ET) and Parkinson's disease (PD) is mostly ineffective. Exact tremor pathomechanisms are unknown and relevant animal models are missing. GABA-A receptor is a target for tremorolytic medications, but current non-selective drugs produce side effects and have safety liabilities. The aim of this study was a search for GABA-A subunit-specific tremorolytics using different tremor-generating mechanisms. Two selective positive allosteric modulators (PAMs) were tested. Zolpidem, targeting GABA-A α1, was not effective in models of harmaline-induced ET, pimozide- or tetrabenazine-induced tremulous jaw movements (TJMs), while the novel GABA-A α2/3 selective MP-III-024 significantly reduced both the harmaline-induced ET tremor and pimozide-induced TJMs. While zolpidem decreased the locomotor activity of the rats, MP-III-024 produced small increases. These results provide important new clues into tremor suppression mechanisms initiated by the enhancement of GABA-driven inhibition in pathways controlled by α2/3 but not α1 containing GABA-A receptors. Tremor suppression by MP-III-024 provides a compelling reason to consider selective PAMs targeting α2/3-containing GABA-A receptors as novel therapeutic drug targets for ET and PD-associated tremor. The possibility of the improved tolerability and safety of this mechanism over non-selective GABA potentiation provides an additional rationale to further pursue the selective α2/3 hypothesis.

Keywords: resting tremor; action tremor; GABAA alpha 1; GABAA alpha 2/3; Parkinson's disease; essential tremor; MP-III-024; zolpidem; positive allosteric modulator; tetrabenazine

check for updates

Citation: Kosmowska, B.; Paleczna, M.; Biała, D.; Kadłuczka, J.; Wardas, J.; Witkin, J.M.; Cook, J.M.; Sharmin, D.; Marcinkowska, M.; Kuter, K.Z. GABA-A Alpha 2/3 but Not Alpha 1 Receptor Subunit Ligand Inhibits Harmaline and Pimozide-Induced Tremor in Rats. *Biomolecules* **2023**, *13*, 197. https://doi.org/10.3390/biom13020197

Academic Editor: Katarina Vukojević

Received: 29 November 2022
Revised: 11 January 2023
Accepted: 15 January 2023
Published: 18 January 2023

Copyright: © 2023 by the authors. Licensee MDPI, Basel, Switzerland. This article is an open access article distributed under the terms and conditions of the Creative Commons Attribution (CC BY) license (https://creativecommons.org/licenses/by/4.0/).

1. Introduction

Tremors are uncontrollable, rhythmic, and oscillating movements produced by alternating or synchronous contractions of antagonistic muscles in different parts of the body. Tremor is a common symptom of many neurological diseases, such as Parkinson's disease (PD), or can constitute an independent disease, such as essential tremor (ET). Tremor significantly hinders daily functioning and has a direct negative impact on the patient's quality of life. Besides some progress in the treatment of those diseases, tremor remains their key, but still untreated, symptom. Currently, there are no specific and effective enough anti-tremor pharmacotherapies and we still do not understand the exact mechanism underlying tremor pathology. Therefore, there is an immediate need to focus attention on exploring new molecular pathways and searching for improved tremorolytics drug targets.

An alpha 5-GABAa receptor positive allosteric modulator attenuates social and cognitive deficits without changing dopamine system hyperactivity in an animal model for autism

Adriana Jesus Souza[1]; Dishary Sharmin[2]; James M. Cook[2]; Francisco S. Guimarães[1]; Felipe V. Gomes[1*]

[1]Department of Pharmacology, Ribeirao Preto Medical School, University of São Paulo, Ribeirão Preto, Brazil;
[2] Department of Chemistry and Biochemistry, Milwaukee Institute of Drug Discovery, University of Wisconsin-Milwaukee, Milwaukee, USA.

ABSTRACT

Autism Spectrum Disorders (ASD) are characterized by core behavioral symptoms in the domains of sociability, language/communication, and repetitive or stereotyped behaviors. Deficits in the prefrontal and hippocampal excitatory/inhibitory balance due to a functional loss of GABAergic interneurons are proposed to underlie these symptoms. Increasing the postsynaptic effects of GABA with compounds that selectively modulate GABAergic receptors could be a potential target for treating ASD symptoms. In addition, deficits in GABAergic interneurons have been linked to dopamine (DA) system dysregulation, and, despite conflicting evidence, abnormalities in the DA system activity may underly some ASD symptoms. Here, we

investigated whether the positive allosteric modulator of α5-containing GABAA receptors (α5-GABAARs) SH-053-2'F-R-CH3 (10 mg/kg) attenuates behavioral abnormalities in a rat model for autism based on in utero VPA exposure. We also evaluated if animals exposed to VPA in utero present changes in the ventral tegmental area (VTA) DA system activity using in vivo electrophysiology and if SH-053-2'F-R-CH3 could attenuate these changes. In utero VPA exposure caused male and female rats to present increased repetitive behavior (self-grooming) in early adolescence and deficits in social interaction in adulthood. Male, but not female VPA rats, also presented deficits in recognition memory as adults. SH-053-2'F-R-CH3 attenuated the impairments in sociability and cognitive function in male VPA-exposed rats without attenuating the decreased social interaction in females. Male and female adult VPA-exposed rats also showed an increased VTA DA neuron population activity, which was not changed by SH-053-2'F-R-CH3. Despite sex differences, our findings indicate α5-GABAARs positive allosteric modulators may effectively attenuate some core ASD symptoms.

Extrasynaptic localization is essential for α5GABA$_A$ receptor modulation of dopamine system function

Alexandra M. McCoy, Thomas D. Prevot, Md Yeunus Mian, Dishary Sharmin, Adeeba N. Ahmad, James M. Cook, Etienne L. Sibille, Daniel J. Lodge

doi: https://doi.org/10.1101/2023.07.12.548744

This article is a preprint and has not been certified by peer review [what does this mean?].

0 0 0 0 0 0 2

Abstract Full Text Info/History Metrics Preview PDF

Abstract

Dopamine system dysfunction, observed in animal models with psychosis-like symptomatology, can be restored by targeting Gamma-Aminobutyric Acid type A receptors (GABA$_A$R) containing the α5, but not α1, subunit in the ventral hippocampus (vHipp). The reason for this discrepancy in efficacy remains elusive; however, one key difference is that α1GABA$_A$Rs are primarily located in the synapse, whereas α5GABA$_A$Rs are mostly extrasynaptic. To test whether receptor location is responsible for this difference in efficacy, we injected a small interfering ribonucleic acid (siRNA) into the vHipp to knock down radixin, a scaffolding protein that holds α5GABA$_A$Rs in the extrasynaptic space. We then administered GL-II-73, a positive allosteric modulator of α5GABA$_A$Rs (α5-PAM) known to reverse shock-induced deficits in dopamine system function, to determine if shifting α5GABA$_A$Rs from the extrasynaptic space to the synapse would prevent the effects of α5-PAM on dopamine system function. As expected, knockdown of radixin significantly decreased radixin-associated α5GABA$_A$Rs

Effects of alpha 5 GABA (A) receptor modulation on social interaction, memory, and neuroinflammation in a mouse model of Alzheimer's disease

Authors Jovana Arandelovic, Anja Santrac, Bojan Batinic, Lidija Todorovic, Vladimir Stevanovic, Veera Venkata Naga Phani Babu Tiruveedhula, Dishary Sharmin, Farjana Rashid, Boban Stanojevic, James M Cook, Miroslav M Savic

Publication date 2022/11/1

Journal CNS NEUROSCIENCE & THERAPEUTICS

Volume 28

Issue 11

Pages 1767-1778

Publisher WILEY

Description Aims: GABAergic modulation involved in cognitive processing appears to be substantially changed in Alzheimer's disease (AD). In a widely used 5xFAD model of AD, we aimed to assess if negative and positive allosteric modulators of alpha 5 GABA(A) receptors (NAM and PAM, respectively) would affect social interaction, social, object and spatial memory, and neuroinflammation.

Methods: After 10-day treatment with PAM, NAM, or solvent, 6-month-old transgenic and non-transgenic 5xFAD mice underwent testing in a behavioral battery. Gene expressions of iL-1 beta, IL-6, TNF-alpha, GFAP, and IBA-1 were determined in hippocampus and prefrontal cortex by qPCR.

Results: PAM treatment impaired spatial learning in transgenic females compared to solvent-treated transgenic females, and social recognition in transgenic and non-transgenic males. NAM treatment declined social interaction in transgenic and non …

ARTICLE

Check for updates

Symptomatic and neurotrophic effects of GABAA receptor positive allosteric modulation in a mouse model of chronic stress

Ashley Bernardo[1], Philip Lee[2], Michael Marcotte[1], Md Yeunus Mian[3], Sepideh Rezvanian[3], Dishary Sharmin[3], Aleksandra Kovačević[4], Miroslav M. Savić[4], James M. Cook[3], Etienne Sibille[1,2,5]✉ and Thomas D. Prevot[1,5]✉

© The Author(s), under exclusive licence to American College of Neuropsychopharmacology 2022

Chronic stress is a risk factor for Major Depressive Disorder (MDD), and in rodents, it recapitulates human behavioral, cellular and molecular changes. In MDD and after chronic stress, neuronal dysfunctions and deficits in GABAergic signaling are observed and responsible for symptom severity. GABA signals predominantly through GABAA receptors (GABAA-R) composed of various subunit types that relate to downstream outcomes. Activity at α2-GABAA-Rs contributes to anxiolytic properties, α5-GABAA-Rs to cognitive functions, and α1-GABAA-Rs to sedation. Therefore, a therapy aiming at increasing α2- and α5-GABAA-Rs activity, but devoid of α1-GABAA-R activity, has potential to address several symptomologies of depression while avoiding side-effects. This study investigated the activity profiles and behavioral efficacy of two enantiomers of each other (GL-II-73 and GL-I-54), separately and as a racemic mixture (GL-RM), and potential disease-modifying effects on neuronal morphology. Results confirm GL-I-54 and GL-II-73 exert positive allosteric modulation at the α2-, α3-, α5-GABAA-Rs and α5-containing GABAA-Rs, respectively, and separately reduces immobility in the forced swim test and improves stress-induced spatial working memory deficits. Using unpredictable chronic mild stress (UCMS), we show that acute and chronic administration of GL-RM provide pro-cognitive effects, with mild efficacy on mood symptoms, although at lower doses avoiding sedation. Morphology studies showed reversal of spine density loss caused by UCMS after chronic GL-RM treatment at apical and basal dendrites of the PFC and CA1. Together, these results support using a racemic mixture with combined α2-, α3-, α5-GABAA-R profile to reverse chronic stress-induced mood symptoms, cognitive deficits, and with anti-stress neurotrophic effects.

Neuropsychopharmacology (2022) 47:1608–1619; https://doi.org/10.1038/s41386-022-01360-y

ACS OMEGA

http://pubs.acs.org/journal/acsodf

Article

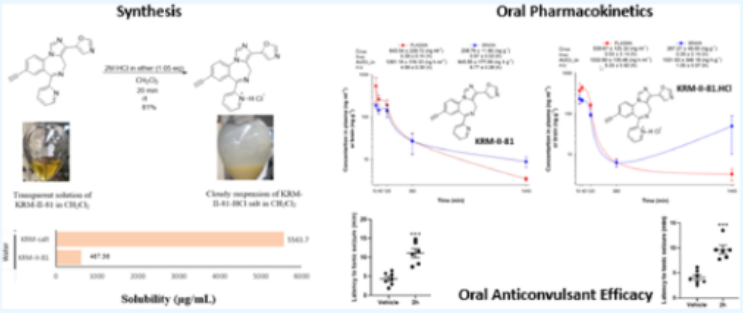
Hydrochloride Salt of the GABAkine KRM-II-81

Md Yeunus Mian,* Branka Divović, Dishary Sharmin, Kamal P. Pandey, Lalit K. Golani, V. V. N. Phani Babu Tiruveedhula, Rok Cerne, Jodi L. Smith, Xingjie Ping, Xiaoming Jin, Gregory H. Imler, Jeffrey R. Deschamps, Arnold Lippa, James M. Cook, Miroslav M. Savić, James Rowlett, and Jeffrey M. Witkin

Cite This: *ACS Omega* 2022, 7, 27550−27559

Read Online

ACCESS | Metrics & More | Article Recommendations | Supporting Information



ABSTRACT: Imidazodiazepine (5-(8-ethynyl-6-(pyridin-2-yl)-4*H*-benzo[*f*]imidazole[1,5-α][1,4]diazepin-3-yl) oxazole or KRM-II-81) is a potentiator of $GABA_A$ receptors (a GABAkine) undergoing preparation for clinical development. KRM-II-81 is active against many seizure and pain models in rodents, where it exhibits improved pharmacological properties over standard-of-care agents. Since salts can be utilized to create opportunities for increased solubility, enhanced absorption, and distribution, as well as for efficient methods of bulk synthesis, a hydrochloride salt of KRM-II-81 was prepared. KRM-II-81·HCl was produced from the free base with anhydrous hydrochloric acid. The formation of the monohydrochloride salt was confirmed by X-ray crystallography, as well as ^{1}H NMR and ^{13}C NMR analyses. High water solubility and a lower partition coefficient (octanol/water) were exhibited by KRM-II-81·HCl as compared to the free base. Oral administration of either KRM-II-81·HCl or the free base resulted in high concentrations in the brain and plasma of rats. Oral dosing in mice significantly increased the latency to both clonic and tonic convulsions and decreased pentylenetetrazol-induced lethality. The increased water solubility of the HCl salt enables intravenous dosing and the potential for higher concentration formulations compared with the free base without impacting anticonvulsant potency. Thus, KRM-II-81·HCl adds an important new compound to facilitate the development of these imidazodiazepines for clinical evaluation.

Behavioural Brain Research
Volume 428, 25 June 2022, 113832

Distinct sex-dependent behavioral responses induced by two positive allosteric modulators of alpha 5 subunit-containing $GABA_A$ receptors

Adriana Jesus Souza [a], Isadora L. Cortez [a], Nicole R. Silva [a], João Francisco C. Pedrazzi [b], Luana B. Domingos [a], Matheus Silva Braga [a], Thamyris Santos-Silva [a], Elaine A. Del-Bel [c], Leonardo B.M. Resstel [a], Guanguan Li [d], Md Yeunus Mian [d], Dishary Sharmin [d], Francisco S. Guimarães [a], James M. Cook [d], Felipe V. Gomes [a]

Show more

+ Add to Mendeley Share Cite

https://doi.org/10.1016/j.bbr.2022.113832

Get rights and content

Abstract

Dysregulation of GABAergic neurotransmission has long been implicated in several psychiatric disorders, including schizophrenia, depression, and anxiety disorders. Alpha 5 subunit-containing $GABA_A$ receptors (α5-$GABA_A$R), which are expressed mainly by pyramidal neurons in the hippocampus, have been proposed as a potential target to treat these psychiatric disorders. Here, we evaluated the effects produced by GL-II-73 and SH-053–2′F-R-CH3 (1, 5, and 10mg/kg), two positive allosteric modulators of α5-$GABA_A$R in behavioral tests sensitive to drugs with anxiolytic, antidepressant, and antipsychotic properties in male and female C57BL/6 mice. In both males and females, GL-II-73 produced an anxiolytic-like effect in the elevated plus-maze (EPM) and novelty-suppressed feeding and a rapid and sustained antidepressant-like effect in the forced swim test. GL-II-73 also induced antipsychotic-like effects in males indicated by attenuating MK-801-induced hyperlocomotion and prepulse inhibition (PPI) disruption. However, GL-II-73 *per se* increased locomotor activity and impaired fear memory extinction in males and females and PPI in males. On the other hand, SH-053–2′F-R-CH3 induced anxiolytic-like effects in the EPM and facilitated fear memory extinction in males. Contrary to GL-II-73, SH-053–2′F-R-CH3 attenuated MK-801-induced hyperlocomotion and PPI disruption in females but not in males. Neither of these drugs induced rewarding effects or impaired motor coordination. These findings suggest that GL-II-73 and SH-053–2′F-R-CH3 cause distinct sex-dependent behavioral responses and support continued preclinical research on the potential of positive allosteric modulators of α5-$GABA_A$R for the treatment of psychiatric disorders.

The FASEB Journal

Pharmacology | Free Access

Assessing the synergistic effects of morphine and MP-III-024 co-administration: enhanced antinociception with reduced side effects

Sara Uribe, Eric J. DiDomenico, Christa M. Donegan, Yulista Tapia, Jason Conviser, Rohit R. Nambiar, Amy A. Juarez, Christine M. Side, Danya Aldaghma, Michael M. Poe, Dishary Sharmin ... See all authors

First published: 13 May 2022 | https://doi.org/10.1096/fasebj.2022.36.S1.R5946

Research support: NIH (DA041560, DA043204, NS076517), NSF (CHE-1625735), Camille and Henry Dreyfus Foundation (BL-19-004), Milwaukee Institute for Drug Discovery, University of Wisconsin-Milwaukee's Shimadzu Laboratory for Advanced and Applied Analytical Chemistry, and internal funds from Rowan University and Cooper Medical School of Rowan University

TOOLS SHARE

Abstract

Opioid analgesics are critical for acute and chronic pain management, but important side effects—including tolerance, constipation, respiratory depression, and abuse liability—limit their safety and utility. To provide patients with safer analgesic options, it is critically important to identify of new pharmacotherapeutic strategies to treat pain. Activation of μ-opioid receptors (MORs) in central and peripheral nociceptive pathways mediates opioid analgesia and their critical side effects. Antinociception can also be achieved via selective enhancement of GABAergic signaling at ionotropic $GABA_A$ receptors. α2 and α3 subunit-containing $GABA_A$ receptors (α2/α3$GABA_A$), which are co-expressed with MORs in dorsal horn spinal pathways important to nociceptive transmission, can be selectively targeted with novel imidazodiazepine positive allosteric modulators (PAMs), such as MP-III-024, which produces antinociceptive effects with limited behavioral disruption. MP-III-024 co-administered with morphine produces synergistic antinociceptive and anti-hyperalgesic effects. In this study, we evaluated whether MP-III-024/morphine co-administration produces sub-additive or synergistic effects in behavioral tests sensitive to morphine side effects. Herein we report that co-administration of MP-III-024/morphine at a 0.94/1 ratio (synergistic in models of antinociception) produced sub-additive effects in morphine-induced hyperlocomotion and in measures of behavioral disruption in food-maintained operant responding. Ongoing studies are evaluating the effects of MP-III-024/morphine co-administration on tolerance in the hot plate test and in conditioned place preference. These experiments are the first comprehensive preclinical analyses of a dual MOR-α2/α3$GABA_A$ pharmacotherapy strategy which may increase the therapeutic window between desirable opioid analgesic effects and side effects.

RESEARCH ARTICLE

Postweaning positive modulation of α5GABAA receptors improves autism-like features in prenatal valproate rat model in a sex-specific manner

Anja Santrač, Dunja Bijelić, Vladimir Stevanović, Marija Banićević, Jovana Arančelović, Bojan Batinić, Dishary Sharmin, James M. Cook, Miroslav M. Savić

First published: 10 March 2022 | https://doi.org/10.1002/aur.2699 | Citations: 1

Funding information: Ministarstvo Prosvete, Nauke i Tehnološkog Razvoja, Grant/Award Number: 451-03-9/2021-14/200161; National Institutes of Health, Grant/Award Numbers: DA-043204, R01NS076517; National Science Foundation, Division of Chemistry, Grant/Award Number: CHE-1625735

Read the full text > PDF TOOLS SHARE

Abstract

Autism spectrum disorder (ASD), as a common neurodevelopmental disorder that encompasses impairments in social communication and interaction, as well as repetitive and restrictive behavior, still awaits an effective treatment strategy. The involvement of GABAergic neurotransmission, and especially a deficit of $GABA_A$ receptors that contain the α5 subunits, were implicated in pathogenesis of ASD. Therefore, we tested MP-III-022, a positive allosteric modulator (PAM) selective for α5GABAA receptors, in Wistar rats prenatally exposed to valproic acid, as an animal model useful for studying ASD. Postweaning rats of both sexes were treated for 7 days with vehicle or MP-III-022 at two doses pharmacokinetically determined as selective, and thereafter tested in a behavioral battery (social interaction test, elevated plus maze, spontaneous locomotor activity, and standard and reverse Morris water maze). Additional rats were used for establishing a primary neuronal culture and performing calcium imaging, and determination of hippocampal mRNA levels of GABRA5, NKCC1, and KCC2. MP-III-022 prevented impairments in many parameters connected with social, repetitive and restrictive behavioral domains. The lower and higher dose was more effective in males and females, respectively. Intriguingly, MP-III-022 elicited certain changes in control animals similar to those manifested in valproate animals themselves. Behavioral results were mirrored in GABA switch and spontaneous neuronal activity, assessed with calcium imaging, and also in expression changes of three genes analyzed. Our data support a role of α5GABAA receptors in pathophysiology of ASD, and suggest a potential application of selective PAMs in its treatment, that needs to be researched in a sex-specific manner.

Bioorganic & Medicinal Chemistry Letters
Volume 62, 15 April 2022, 128637



Rationalizing the binding and α subtype selectivity of synthesized imidazodiazepines and benzodiazepines at GABAA receptors by using molecular docking studies

Lalit K Golani [a 1], Md Yeunus Mian [a 1], Taukir Ahmed [a], Kamal P Pandey [a], Prithu Mondal [a], Dishary Sharmin [a], Sepideh Rezvanian [a], Jeffrey M Witkin [a b], James M Cook [a]

Show more

+ Add to Mendeley Share Cite

https://doi.org/10.1016/j.bmcl.2022.128637

Get rights and content

Abstract

The pharmacological actions exerted by benzodiazepines are dependent on the discrete α protein subunits of the γ-aminobutyric acid type A receptor ($GABA_A$ R). Recent developments *via* a cryo-EM structure of the α1β3γ2L $GABA_A$ R ion channel provide crucial insights into ligand efficacy and binding affinity at this subtype. We investigated the molecular interactions of diazepam and alprazolam bound $GABA_A$ R structures (6HUP and 6HUO) to determine key binding interaction domains. A halogen bond between the chlorine atoms of diazepam and alprazolam with the group on the backbone of the α1 histidine amino acid 102 is important to the positive allosteric modulatory actions of diazepam and alprazolam in the α1β3γ2L $GABA_A$ R ion channel. In order to gain insight into α subtype selectivity we designed and synthesized close structural analogs of diazepam and alprazolam. These compounds were then docked into the recently publish cryo-EM structures of $GABA_A$ Rs (6HUP and 6HUO). This modeling along with radio-ligand binding data resulted in the conclusion that the non-classical bioisosteric replacement of the chlorine atom at C7 with an ethinyl group (compound **5**) resulted in an 11-fold gain in α5 binding selectivity over the α1 subtype. Moreover, the potency of compound **5** resulted in a ligand with less sedation than diazepam, while still maintaining the same anxiolytic potency. These modeling data extend our understanding of the structural requirements for α-subtype-selective compounds that can be utilized to achieve improved medical treatments. It is clear that the ethinyl group in place of a halogen atom decreases the affinity and efficacy of benzodiazepines and imidazodiazepines at α1 subtypes, which results in less sedation and ataxia.

Biopharmaceutics & Drug Disposition



ORIGINAL ARTICLE

Metabolism, pharmacokinetics, and anticonvulsant activity of a deuterated analog of the α2/3-selective GABAkine KRM-II-81

Lalit K. Golani, Branka Divović, Dishary Sharmin, Kamal P. Pandey, Md Yeunus Mian, Rok Cerne, Nicolas M. Zahn, Michelle J. Meyer, Veera V. N. P. B. Tiruveedhula, Jodi L. Smith ... See all authors

First published: 22 February 2022 | https://doi.org/10.1002/bdd.2313 | Citations: 3

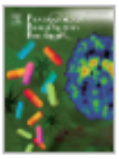
Lalit K. Golani, Branka Divović, and Dishary Sharmin contributed equally to this work.

Read the full text > PDF TOOLS SHARE

Abstract

The imidazodiazepine, (5-(8-ethynyl-6-(pyridin-2-yl)-4H-benzo [*f*]imidazole[1,5-α] [1,4]diazepin-3-yl) oxazole or KRM-II-81) is a new α2/3-selective GABAkine (gamma aminobutyric acid A receptor potentiator) with anticonvulsant, anxiolytic, and antinociceptive activity in preclinical models. Reducing metabolism was utilized as a means of potentially extending the half-life of KRM-II-81. *In vitro* and *in vivo* studies were conducted to evaluate metabolic liabilities. Incubation of KRM-II-81 in hepatocytes revealed sites of potential metabolism on the oxazole and the diazepine rings. These sites were targeted in the design of a deuterated analog (D5-KRM-II-81) that could be evaluated as a potentially longer-acting analog. In contrast to computer predictions, peak plasma concentrations of D5-KRM-II-81 in rats were not significantly greater than those produced by KRM-II-81 after oral administration. Furthermore, brain disposition of KRM-II-81 was higher than that of D5-KRM-II-81. The half-life of the two compounds in either plasma or brain did not statistically differ from one another but the t_{max} for D5-KRM-II-81 occurred slightly earlier than for KRM-II-81. Non-metabolic considerations might be relevant to the lack of increases in exposure by D5-KRM-II-81. Alternative sites of metabolism on KRM-II-81, not targeted by the current deuteration process, are also possible. Despite its lack of augmented exposure, D5-KRM-II-81, like KRM-II-81, significantly prevented seizures induced by pentylenetetrazol when given orally. The present findings introduce a new orally active anticonvulsant GABAkine, D5-KRM-II-81.

Pharmacology Biochemistry and Behavior
Volume 213, February 2022, 173321



Review

The imidazodiazepine, KRM-II-81: An example of a newly emerging generation of GABAkines for neurological and psychiatric disorders ☆, ☆☆

Jeffrey M. Witkin [a b c], Arnold Lippa [b], Jodi L. Smith [a], Xiaoming Jin [d], Xingjie Ping [d], Andrew Biggerstaff [e], Bronwyn M. Kivell [e], Daniel E. Knutson [c], Dishary Sharmin [c], Kamal P. Pandey [c], Md Yeunus Mian [c], James M. Cook [b c], Rok Cerne [a b d f]

Show more

+ Add to Mendeley Share Cite

https://doi.org/10.1016/j.pbb.2021.173321

Get rights and content

Abstract

GABAkines, or positive allosteric modulators of γ-aminobutyric acid-A ($GABA_A$) receptors, are used for the treatment of anxiety, epilepsy, sleep, and other disorders.

The search for improved GABAkines, with reduced safety liabilities (e.g., dependence) or side-effect profiles (e.g., sedation) constituted multiple discovery and development campaigns that involved a multitude of strategies over the past century. Due to the general lack of success in the development of new GABAkines, there had been a decades-long draught in bringing new GABAkines to market. Recently, however, there has been a resurgence of efforts to bring GABAkines to patients, the FDA approval of the neuroactive steroid brexanolone for post-partum depression in 2019 being the first. Other neuroactive steroids are in various stages of clinical development (ganaxolone, zuranolone, LYT-300, Sage-324, PRAX 114, and ETX-155). These GABAkines and non-steroid compounds (GRX-917, a TSPO binding site ligand), darigabat (CVL-865), an α2/3/5-preferring GABAkine, SAN711, an α3-preferring GABAkine, and the α2/3-preferring GABAkine, KRM-II-81, bring new therapeutic promise to this highly utilized medicinal target in neurology and psychiatry. Herein, we also discuss possible conditions that have enabled the transition to a new age of GABAkines.

Positive allosteric modulation of α5-GABA A Receptor in the 5XFAD mouse model has cognitive and neurotrophic benefits

Ashley M. Bernardo, Michael Marcotte, Kayla Wong, Dishary Sharmin, Kamal Prandey, James M. Cook, Etienne Sibille, Thomas D. Prevot

doi: https://doi.org/10.1101/2022.09.30.510361

This article is a preprint and has not been certified by peer review [what does this mean?].

0 0 0 0 0 0 1

Abstract Full Text Info/History Metrics Preview PDF

Abstract

Alzheimer's disease (AD) clinically presents with significant cognitive deficits in memory and executive function while pathologically displaying neuronal atrophy, the buildup of amyloid beta plaques and the presence of neurofibrillary tangles. Current therapies have modest effects on cognition and no effect on neurodegeneration. In AD, the GABAergic system shows reduced neuron populations, less GABA release and altered GABAA receptor (GABAAR) functioning. GABAergic somatostatin (SST) interneurons are particularly vulnerable. These SST cells target GABAAR's containing the α5 subunit which are linked to cognition, but remain untargeted for therapeutic interventions. When lost, SST interneurons no longer coordinate signals and this presents as cognitive impairment. Using α5-GABAAR positive allosteric modulation (α5-PAM), there is the potential to restore their signaling and improve cognitive performance despite the presence of amyloid. Here we tested a selective α5-PAM (GL-II-73) at early (2 months) and late (5 months) stages of amyloid progression using the 5XFAD model for cognitive benefits, neurotrophic effects and amyloid clearance ability (N=48/study; 50% female). We found age-dependent deficits in spatial working memory and GL-II-73 dose dependently improves this deficit at 5 months of age. Chronic treatment with GL-II-73 showed spine density, spine count and dendritic length recovery at both time points. However, amyloid deposition progressed with age, and GL-II-73 did not have an effect on amyloid build up, suggesting that the effects observed are directly due to the impact of GL-II-73 on α5-GABAARs, and not related to amyloid plaques. These results show that despite the presence of amyloid GL-II-73's α5-PAM activity overcomes cognitive deficits even at later stages of amyloid progression and demonstrates neurotrophic effects. Overall, results support GL-II-73 and its selective α5-PAM activity as a promising therapeutic option for cognitive deficits in AD.

Drug and Alcohol Dependence
Volume 228, 1 November 2021, 108985

Tolerance and dependence following chronic alprazolam treatment in rhesus monkeys: Role of $GABA_A$ receptor subtypes

Angela N. Duke [a 1], V.V.N. Phani Babu Tiruveedhula [b], Dishary Sharmin [b], Daniel E. Knutson [b], James M. Cook [b], Donna M. Platt [a c], James K. Rowlett [a c]

Show more
+ Add to Mendeley Share Cite

https://doi.org/10.1016/j.drugalcdep.2021.108985 Get rights and content

Abstract

Background

To assess $GABA_A$ receptor subtypes involved in benzodiazepine tolerance and dependence, we evaluated the ability of subtype-selective and non-selective ligands to substitute for (i.e., produce "cross-tolerance") or precipitate withdrawal during chronic alprazolam treatment.

Methods

Four female rhesus monkeys (*Macaca mulatta*) were implanted with chronic intravenous catheters and administered alprazolam (1.0 mg/kg every 4 h). Following 14+ days of chronic alprazolam, acute administration of selected doses of non-selective and subtype-selective ligands were substituted for, or administered with, alprazolam, followed by quantitative behavioral observations. The ligands included alprazolam and midazolam (positive modulators, non-selective), zolpidem (positive modulator, preferential affinity for α1-containing $GABA_A$ receptors), HZ-166 (positive modulator, preferential efficacy at α2- and α3-containing $GABA_A$ receptors), and βCCT (antagonist, preferential affinity for α1-containing $GABA_A$ receptors).

Results

Acutely, alprazolam and midazolam both induced observable ataxia along with a mild form of sedation referred to as "rest/sleep posture" at a lower dose (0.1 mg/kg, i.v.), whereas at a higher dose (1.0 mg/kg, i.v.), induced deep sedation and observable ataxia. With chronic alprazolam treatment, observable ataxia and deep sedation were reduced significantly, whereas rest/sleep posture was unchanged or emerged. Zolpidem showed a similar pattern of effects, whereas no behaviors engendered by HZ-166 were changed by chronic alprazolam. Administration of βCCT, but not HZ-166, resulted in significant withdrawal signs.

Original Investigation | Published: 13 February 2021

Synergistic antihyperalgesic and antinociceptive effects of morphine and methyl 8-ethynyl-6-(pyridin-2-yl)-4*H*-benzo[*f*]imidazo[1,5-*a*][1,4]diazepine-3-carboxylate (MP-III-024): a positive allosteric modulator at α2GABA$_A$ and α3GABA$_A$ receptors

Mohammad A. Rahman, Thomas M. Keck, Michael M. Poe, Dishary Sharmin, James M. Cook & Bradford D. Fischer ✉

Psychopharmacology **238**, 1585–1592 (2021) | Cite this article

428 Accesses | **5** Citations | **2** Altmetric | Metrics

Abstract

Rationale

Opioid and GABA$_A$ receptors are both located in central nociceptive pathways, and compounds that activate these receptors have pain-relieving properties. To date, the interactive effects of concurrent administration of these compounds in preclinical models of pain-like behaviors have not been assessed.

Objective

The purpose of this study was to examine the interactive effects of the μ-opioid agonist morphine and the α2GABA$_A$ and α3GABA$_A$ receptor positive allosteric modulator methyl 8-ethynyl-6-(pyridin-2-yl)-4*H*-benzo[*f*]imidazo[1,5-*a*][1,4]diazepine-3-carboxylate (MP-III-024) in preclinical models of mechanical hyperalgesia and thermal nociception.

Methods

European Journal of Pharmacology
Volume 899, 15 May 2021, 174023

Vasodilatory effects of a variety of positive allosteric modulators of $GABA_A$ receptors on rat thoracic aorta

Milica Gajić Bojić [a], Lidija Todorović [b], Anja Santrač [c], Md Yeunus Mian [d], Dishary Sharmin [d], James M. Cook [d], Miroslav M. Savić [c]

Show more
+ Add to Mendeley Share Cite

https://doi.org/10.1016/j.ejphar.2021.174023
Get rights and content

Abstract

Different subtypes of $GABA_A$ (gamma-aminobutyric acid A) receptors, through their specific regional and cellular localization, are involved in the manifestation of various functions, both at the central and peripheral levels. We hypothesized that various non-neuronal $GABA_A$ receptors are expressed on blood vessels, through which positive allosteric modulators of $GABA_A$ receptors exhibit vasodilatory effects.

This study involved two parts: one to determine the presence of α1-6 subunit $GABA_A$ receptor mRNAs in the rat thoracic aorta, and the other to determine the vasoactivity of the various selective and non-selective positive $GABA_A$ receptor modulators: zolpidem (α1-selective), XHe–III–074 (α4-selective), MP–III–022 (α5-selective), DK-I-56-1 (α6-selective), SH-I-048A and diazepam (non-selective).

Reverse transcription-polymerase chain reaction (RT-PCR) analysis data demonstrated for the first time the expression of α1, α2, α3, α4 and α5 subunits in the rat thoracic aorta tissue. Tissue bath assays on isolated rat aortic rings revealed significant vasodilatory effects of diazepam, SH-I-048A, XHe–III–074, MP–III–022 and DK-I-56-1, all in terms of achieved relaxations (over 50% of relative tension decrease), as well as in terms of preventive effects on phenylephrine (PE) contraction. Diazepam was the most efficient ligand in the present study, while zolpidem showed the weakest vascular effects. In addition, diazepam-induced relaxations in the presence of antagonists PK11195 or bicuculline were significantly reduced ($P<0.001$ and $P<0.05$, respectively) at lower concentrations of diazepam (10^{-7}M and 3×10^{-7}M).

Positive modulation of cerebellar α6GABA$_A$ receptors for treating essential tremor: a proof-of-concept study in harmaline-treated mice

Ya-Hsien Huang, Ming Tatt Lee, Werner Sieghart, Daniel E. Knutson, Laurin R. Wimmer, Dishary Sharmin, James Cook, Marko D. Mihovilovic, Lih-Chu Chiou

doi: https://doi.org/10.1101/2021.04.19.440397

This article is a preprint and has not been certified by peer review [what does this mean?].

0 0 0 0 0 0 1

Abstract Full Text Info/History Metrics Preview PDF

Abstract

Background The etiology of essential tremor (ET) remains unclear but may involve abnormal firing of Purkinje cells, which receive excitatory inputs from granule cells in the cerebellum. Since α6 subunit-containing GABA$_A$ receptors (α6GABA$_A$Rs) are abundantly expressed in granule cells, we validated a hypothesis that α6GABA$_A$R-selective positive allosteric modulators (PAMs) are promising pharmacological interventions for ET therapy.

Methods Employing the harmaline-induced ET model in male ICR mice, we evaluated the possible anti-tremor effects of four α6GABA$_A$R-selective PAMs, the pyrazoloquinolinones Compound 6 and LAU-463 and their respective deuterated derivatives. Propranolol, a clinical anti-tremor agent, was employed as positive control. To investigate the involvement of cerebellar α6GABA$_A$Rs in the antitremor effect of intraperitoneal (*i.p.*) Compound 6, furosemide, an α6GABA$_A$R antagonist, was intracerebellarly (*i.cb.*) co-administered with Compound 6. The burrowing activity, an indicator of wellbeing in rodents, was measured concurrently.

Pharmacology Biochemistry and Behavior
Volume 196, September 2020, 172996

The α2,3-selective potentiators of $GABA_A$ receptors, KRM-II-81 and MP-III-80, produce anxiolytic-like effects and block chemotherapy-induced hyperalgesia in mice without tolerance development

A. Biggerstaff [a 1], B. Kivell [a 1], J.L. Smith [b], Md Y. Mian [c], L.K. Golani [c], F. Rashid [c], D. Sharmin [c], D.E. Knutson [c], R. Cerne [b d], J.M. Cook [c], J.M. Witkin [b c e]

Show more
+ Add to Mendeley Share Cite

https://doi.org/10.1016/j.pbb.2020.172996
Get rights and content

Abstract

Opiate analgesics are one of the treatment options for severe chronic pain, including late-stage cancer, chronic back pain and other disorders. The recent resurgence in opioid overdose has highlighted the serious need for alternative medicines for pain management. While a role for potentiators of α2/3-containing $GABA_A$ receptors in the modulation of pain has been known for several years, advancements in this area required data from selective compounds. KRM-II-81(5-(8-ethynyl-6-(pyridin-2-yl)-4*H*-benzo[*f*]imidazo[1,5-*a*][1,4]diazepin-3- yl)oxazole) and analogs selectively potentiate $GABA_A$ receptors containing α2/3 subunits and have recently been shown to attenuate pain behaviors in several acute and chronic pain models in rodents. The present study was designed to ascertain whether KRM-II-81 and the structural analog MP-III-80 (3-ethyl-5-(8-ethynyl-6-(pyridin-2-yl)-4H-benzo[*f*]imidazo[1,5-a][1,4]diazepin-3-yl)-1,2,4-oxadiazole) would block chemotherapeutic agent paclitaxel-induced pain in male, C57BL/6 mice. Both compounds significantly inhibited pain behaviors evoked by cold and tactile stimulation in paclitaxel-treated mice as did the neuropathic pain drug gabapentin. Subchronic dosing for 22 days with KRM-II-81 and MP-III-80 demonstrated enduring analgesic efficacy without tolerance development, while the effects of gabapentin showed evidence of tolerance development. KRM-II-81 and MP-III-80 also decreased marble-burying behavior in this mouse strain as did the anxiolytic drug chlordiazepoxide. In contrast to KRM-II-81 and MP-III-80, chlordiazepoxide had motor-impairing effects at anxiolytic-like doses. The data add to the literature documenting that

ACS Chemical Neuroscience

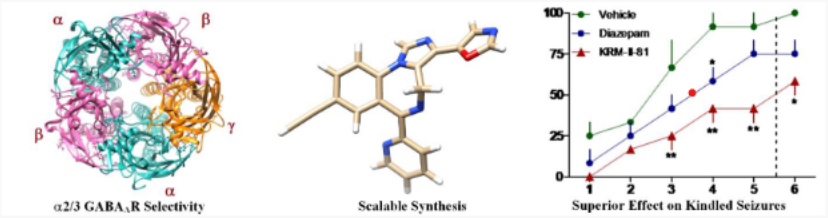
pubs.acs.org/chemneuro Research Article

Imidazodiazepine Anticonvulsant, KRM-II-81, Produces Novel, Non-diazepam-like Antiseizure Effects

Daniel E. Knutson,* Jodi L. Smith, Xingjie Ping, Xiaoming Jin, Lalit K. Golani, Guanguan Li, V. V. N. Phani Babu Tiruveedhula, Farjana Rashid, Md Yeunus Mian, Rajwana Jahan, Dishary Sharmin, Rok Cerne, James M. Cook, and Jeffrey M. Witkin*

Cite This: ACS Chem. Neurosci. 2020, 11, 2624–2637 Read Online

ACCESS | Metrics & More | Article Recommendations | Supporting Information



ABSTRACT: The need for improved medications for the treatment of epilepsy and chronic pain is essential. Epileptic patients typically take multiple antiseizure drugs without complete seizure freedom, and chronic pain is not fully managed with current medications. A positive allosteric modulator (PAM) of α2/3-containing $GABA_A$ receptors (5-(8-ethynyl-6-(pyridin-2-yl)-4*H*-benzo[*f*]imidazole[1,5-α][1,4]diazepin-3-yl) oxazole or KRM-II-81 (**8**) is a lead compound in a series of imidazodiazepines. We previously reported that KRM-II-81 produces broad-based anticonvulsant and antinociceptive efficacy in rodent models and provides a wider margin over motoric side effects than that of other $GABA_A$ receptor PAMs. The present series of experiments was designed to fill key missing gaps in prior preclinical studies assessing whether KRM-II-81 could be further differentiated from nonselective $GABA_A$ receptor PAMs using the anticonvulsant diazepam (DZP) as a comparator. In multiple chemical seizure provocation models in mice, KRM-II-81 was either equally or more efficacious than DZP. Most strikingly, KRM-II-81 but not DZP blocked the development of seizure sensitivity to the chemoconvulsants cocaine and pentylenetetrazol in seizure kindling models. These and predecessor data have placed KRM-II-81 into consideration for clinical development requiring the manufacture of kilogram amounts of good manufacturing practice material. We describe here a novel synthetic route amenable to kilogram quantity production. The new biological and chemical data provide key steps forward in the development of KRM-II-81 (**8**) as an improved treatment option for patients suffering from epilepsy.

KEYWORDS: *KRM-II-81, $GABA_A$ receptor PAMs, α2/3-containing $GABA_A$ receptors, diazepam, epilepsy, seizure kindling*

European Journal of Pharmaceutical Sciences
Volume 189, 1 October 2023, 106557

Freeze-dried nanocrystal dispersion of novel deuterated pyrazoloquinolinone ligand (DK-I-56-1): Process parameters and lyoprotectant selection through the stability study

Jelena R. Mitrović [a], Maja Bjelošević Žiberna [b], Aleksandar Vukadinović [c], Daniel E. Knutson [d], Dishary Sharmin [d], Aleksandar Kremenović [e], Pegi Ahlin Grabnar [b], Odon Planinšek [b], Dominique Lunter [f], James M. Cook [d], Miroslav M. Savić [g], Snežana D. Savić [a]

Show more

+ Add to Mendeley Share Cite

https://doi.org/10.1016/j.ejps.2023.106557

Get rights and content

Under a Creative Commons license

open access

Abstract

Recently, nanocrystal dispersions have been considered as a promising formulation strategy to improve the bioavailability of the deuterated pyrazoloquinolinone ligand DK-I-56-1 (7-methoxy-2-(4-methoxy-d3-phenyl)-2,5-dihydro-3H-pyrazolo[4,3-c]quinolin-3-one). In the current study, the freeze-drying process (formulation and process parameters) was investigated to improve the storage stability of the previously developed formulation. Different combinations of lyoprotectant (sucrose or trehalose) and bulking agent (mannitol) were varied while formulations were freeze-dried under two conditions (primary drying at -10 or -45 °C). The obtained lyophilizates were characterized in terms of particle size, solid state properties and morphology, while the interactions within the samples were analyzed by Fourier transform infrared spectroscopy. In the preliminary study, three formulations were selected based on the high redispersibility index values (around 95%). The temperature of primary drying had no significant effect on particle size, but stability during storage was impaired for samples dried at -10 °C. Samples dried at lower temperature were more homogeneous and remained stable for three months. It was found that the optimal ratio of sucrose or trehalose to mannitol was 3:2 at a total concentration of 10% to achieve the best stability (particle size < 1.0μm, polydispersity index < 0.250). The amorphous state of lyoprotectants probably provided a high degree of interaction with nanocrystals, while the crystalline mannitol provided an elegant cake structure. Sucrose was superior to trehalose in maintaining particle size during freeze-drying, while trehalose was more effective in keeping particle size within limits during storage. In conclusion, results demonstrated that the appropriate combination of sucrose/trehalose and mannitol

Meeting Report | ASPET 2023 Annual Meeting Abstract - Central Nervous System Pharmacology - Behavioral

Widening the Opioid Analgesia Therapeutic Window with a Dual Pharmacology Strategy

Indu Mithra Madhuranthakam, Sarah Uribe, Danya Aldaghma, Drew Kwitchoff, Jonathan Philip, Aela A. Williams, Rohit A. Nambiar, Dishary Sharmin, James Cook, Bradford Fischer, and Thomas Keck

Journal of Pharmacology and Experimental Therapeutics June 2023, 385 (S3) 405; DOI: https://doi.org/10.1124/jpet.122.269240

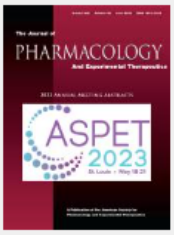
Abstract

Abstract ID 26924

Poster Board 405

Opioids are effective in managing acute and chronic pain but have serious side effects like constipation, tolerance, abuse liability, and respiratory depression. To provide safer analgesic options to patients, it is critical to identify new pharmacotherapeutic strategies to treat pain. In addition to central and peripheral nociceptive pathways, antinociception can also be achieved by selective enhancement of GABAergic signaling at ionotropic $GABA_A$ receptors. These receptors can be selectively targeted by MP-III-024, a novel α2/α3 subunit-selective positive allosteric modulator (PAMs). We previously demonstrated that morphine/MP-III-024 co-administration produced synergistic antinociceptive and antihyperalgesic effects. In this follow-up study, we investigated whether co-administration of MP-III-024 with morphine generates synergistic effects in behavioral tests susceptible to morphine side effects. Herein, we report that co-administration of MP-III-024 with morphine at a 0.94:1 ratio (synergistic in antinociception models) induced only additive or sub-additive effects on morphine-induced hyperlocomotion, behavioral disruption measures in food-maintained operant responding, and conditioned place preference. Co-administration of MP-III-024 also does not affect the development of analgesic tolerance caused by chronic morphine. Studies evaluating the effects on respiratory depression are ongoing. These findings suggest that a dual medication strategy may widen the therapeutic window for opioid analgesia and lower the risk of negative effects, including opioid dependence.

In this issue



Journal of Pharmacology and Experimental Therapeutics
Vol. 385, Issue S3
1 Jun 2023
Complete Issue (PDF)
Table of Contents
Table of Contents (PDF)

Download PDF
Article Alerts
Email Article
Citation Tools
Request Permissions

Share
Tweet
Like 0

Jump to section

- Article
- Info & Metrics
- eLetters
- PDF

ABSTRACT | VOLUME 93, ISSUE 9, SUPPLEMENT , S5, MAY 01, 2023

Improvement of Cognitive Functions and Neurotrophic Effects Across Animal Models Mediated by A5-GABAA Receptor Positive Allosteric Modulation

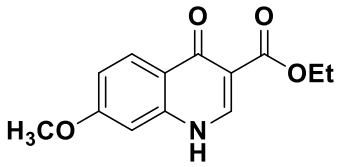
Thomas Prevot • Ashley Bernardo • Kayla Wong • ... Dishary Sharmin • James Cook • Etienne Sibille •
Show all authors

DOI: https://doi.org/10.1016/j.biopsych.2023.02.033

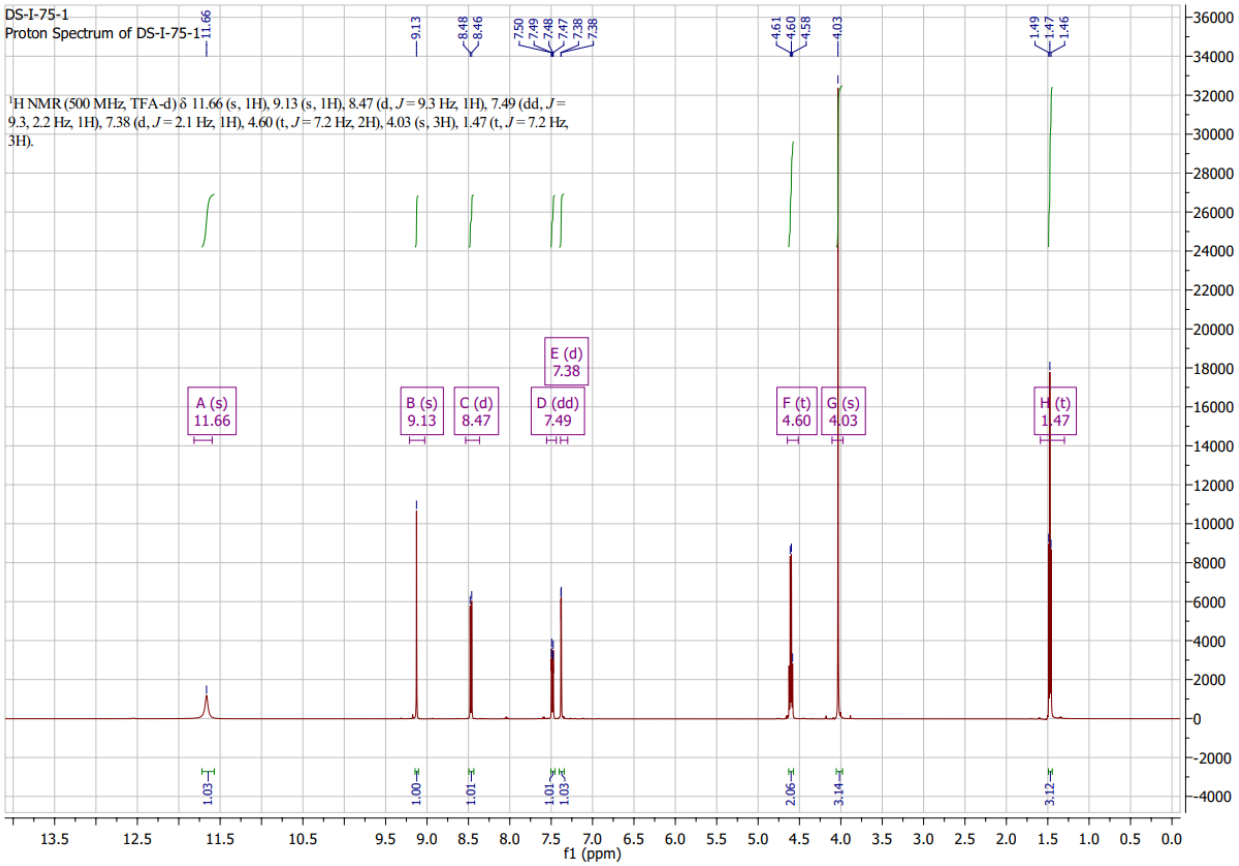
Reduced GABA/somatostatin (SST) signaling is reported in psychiatric, stress-related, and neurodegenerative disorders. SST+ interneurons within cortex and hippocampus inhibit the dendrites of excitatory neurons, largely through α5-containing GABAA receptors (α5-GABAAR). We showed that an α5-positive allosteric modulator (α5-PAM, GL-II-73) alleviates working memory deficits and reverses neuronal atrophy in old mice. We then investigated the behavioral and neurotrophic effects of this α5-PAM in animal models of aging, chronic stress, β-amyloid load, and tauopathy.

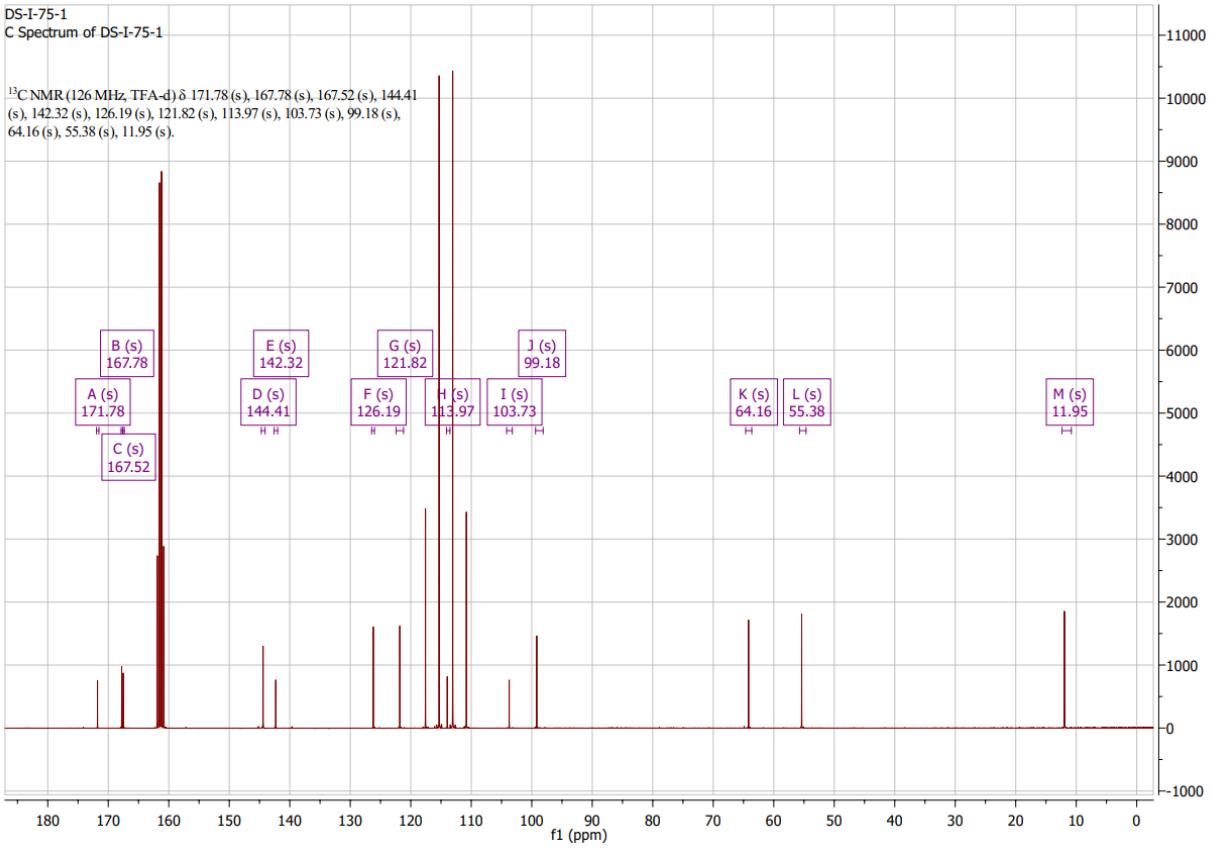
5.3. Spectra (^{1}HNMR and ^{13}C NMR)

Ethyl 7-methoxy-4-oxo-1,4-dihydroquinoline-3-carboxylate (14)

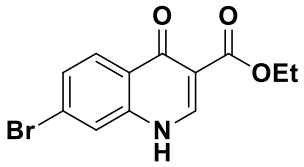


14

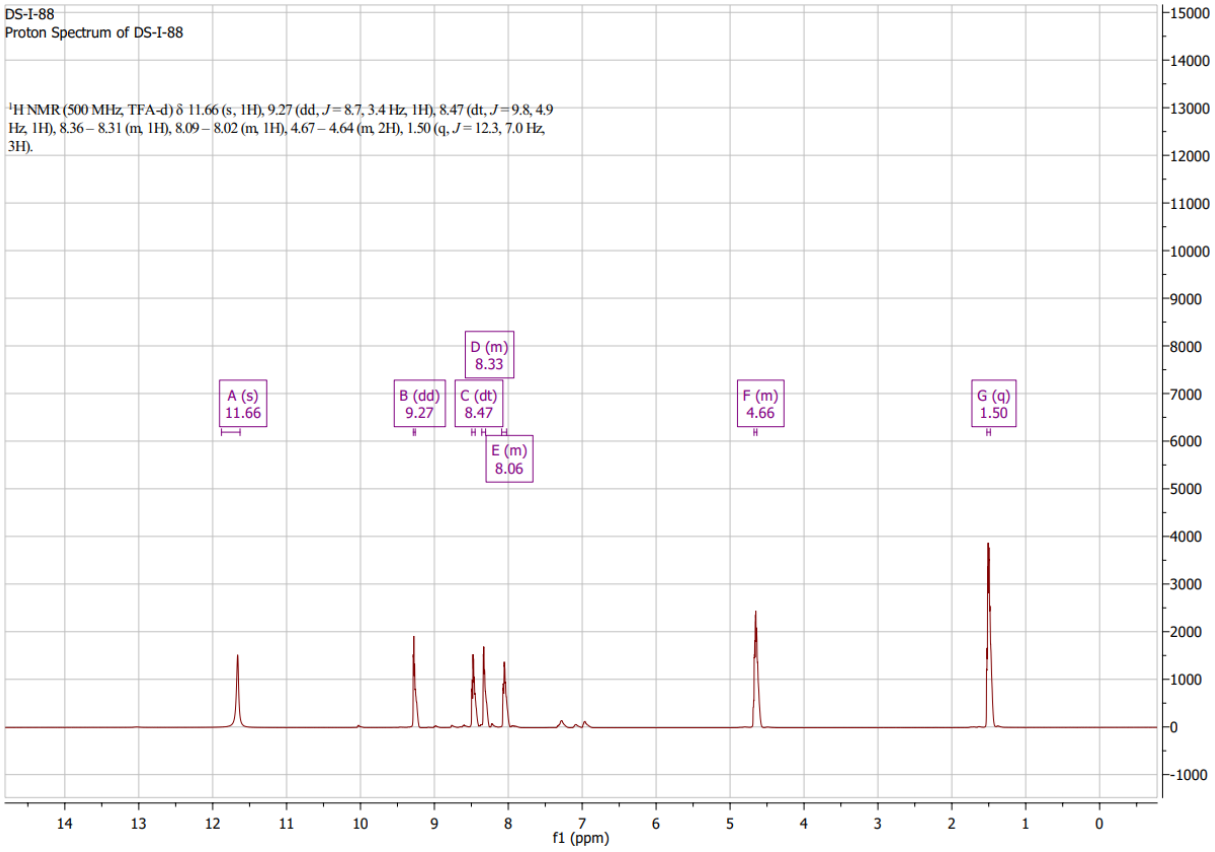


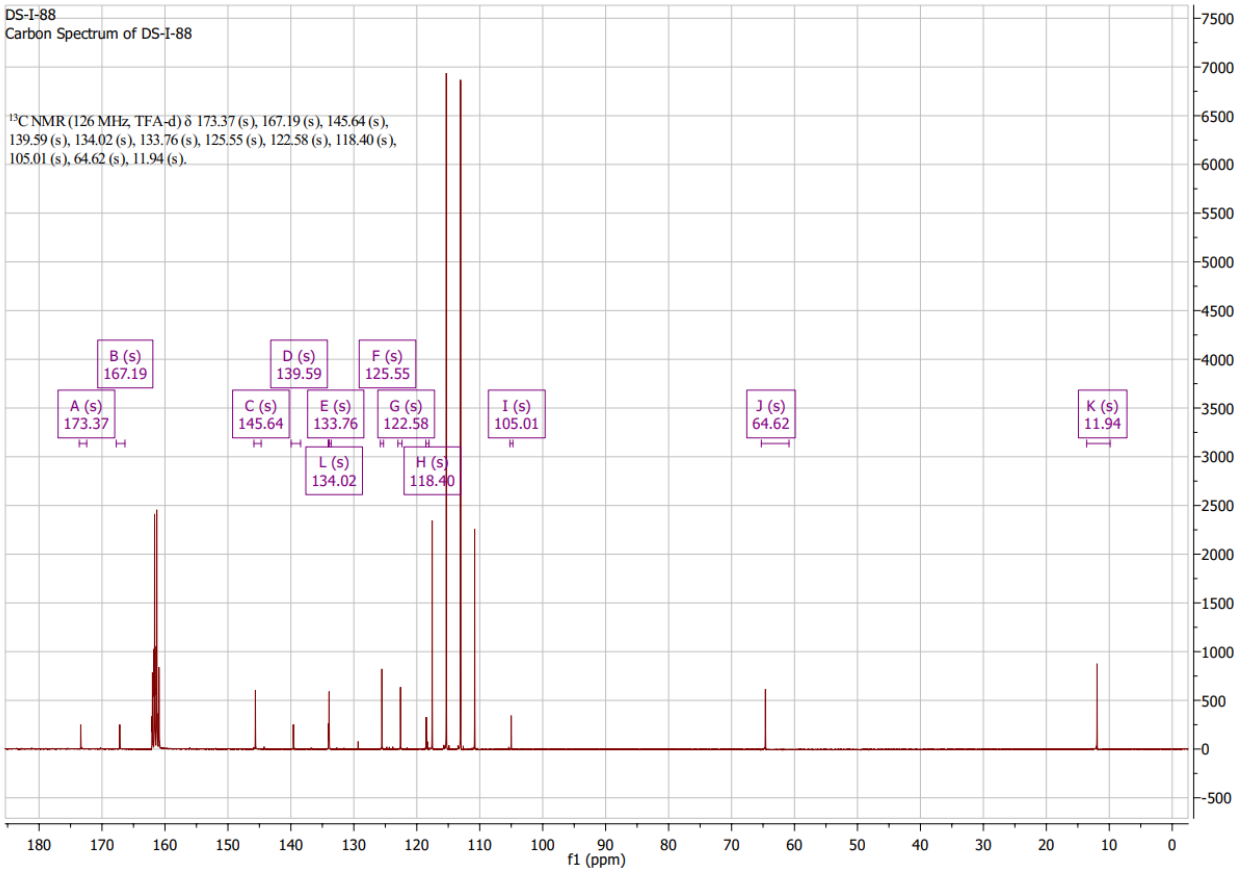

DS-I-75-1
C Spectrum of DS-I-75-1
^{13}C NMR (126 MHz, TFA-d) δ 171.78 (s), 167.78 (s), 167.52 (s), 144.41 (s), 142.32 (s), 126.19 (s), 121.82 (s), 113.97 (s), 103.73 (s), 99.18 (s), 64.16 (s), 55.38 (s), 11.95 (s).
B (s) 167.78
A (s) 171.78
C (s) 167.52
E (s) 142.32
D (s) 144.41
G (s) 121.82
F (s) 126.19
H (s) 113.97
J (s) 99.18
I (s) 103.73
K (s) 64.16
L (s) 55.38
M (s) 11.95
f1 (ppm)

Ethyl 7-bromo-4-oxo-1,4-dihydroquinoline-3-carboxylate (15)

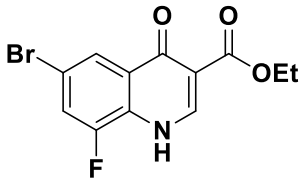


15

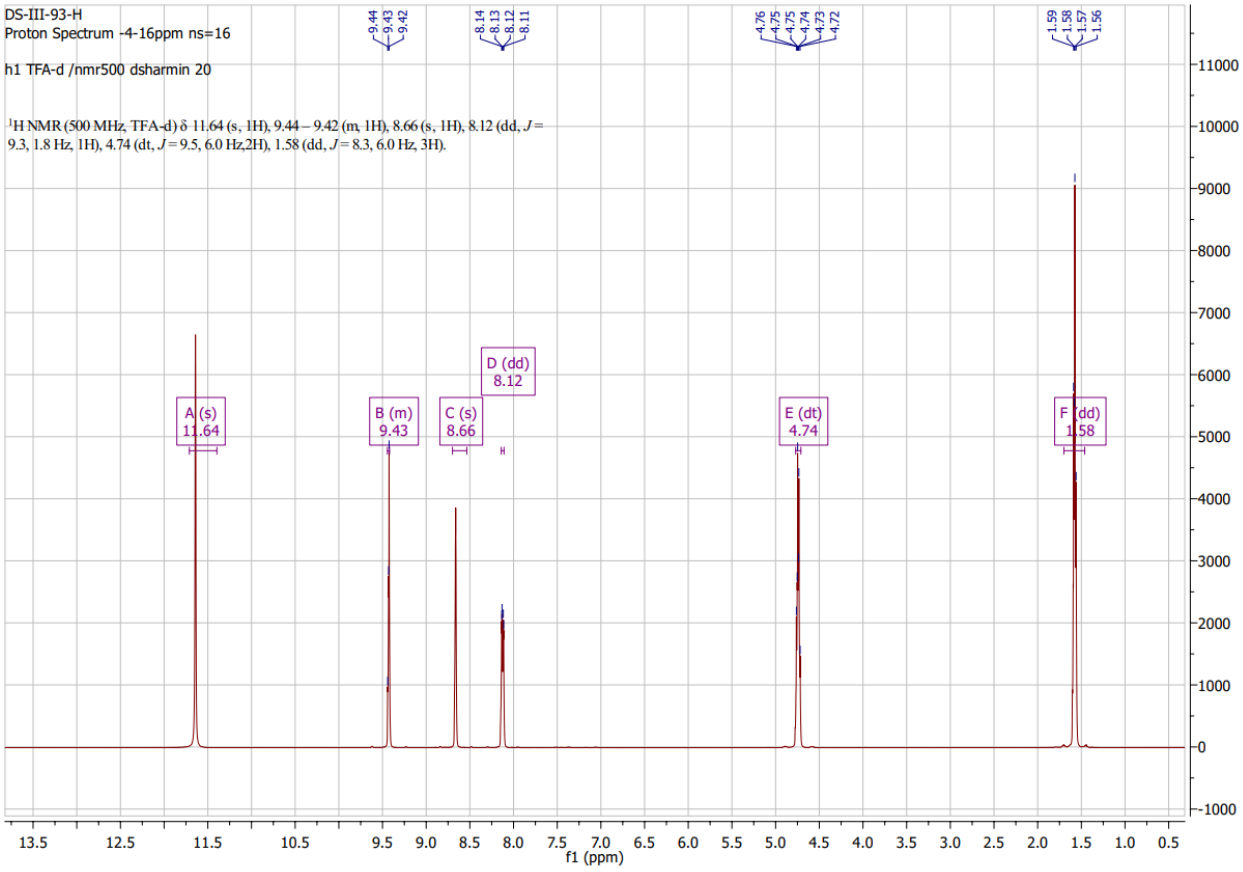


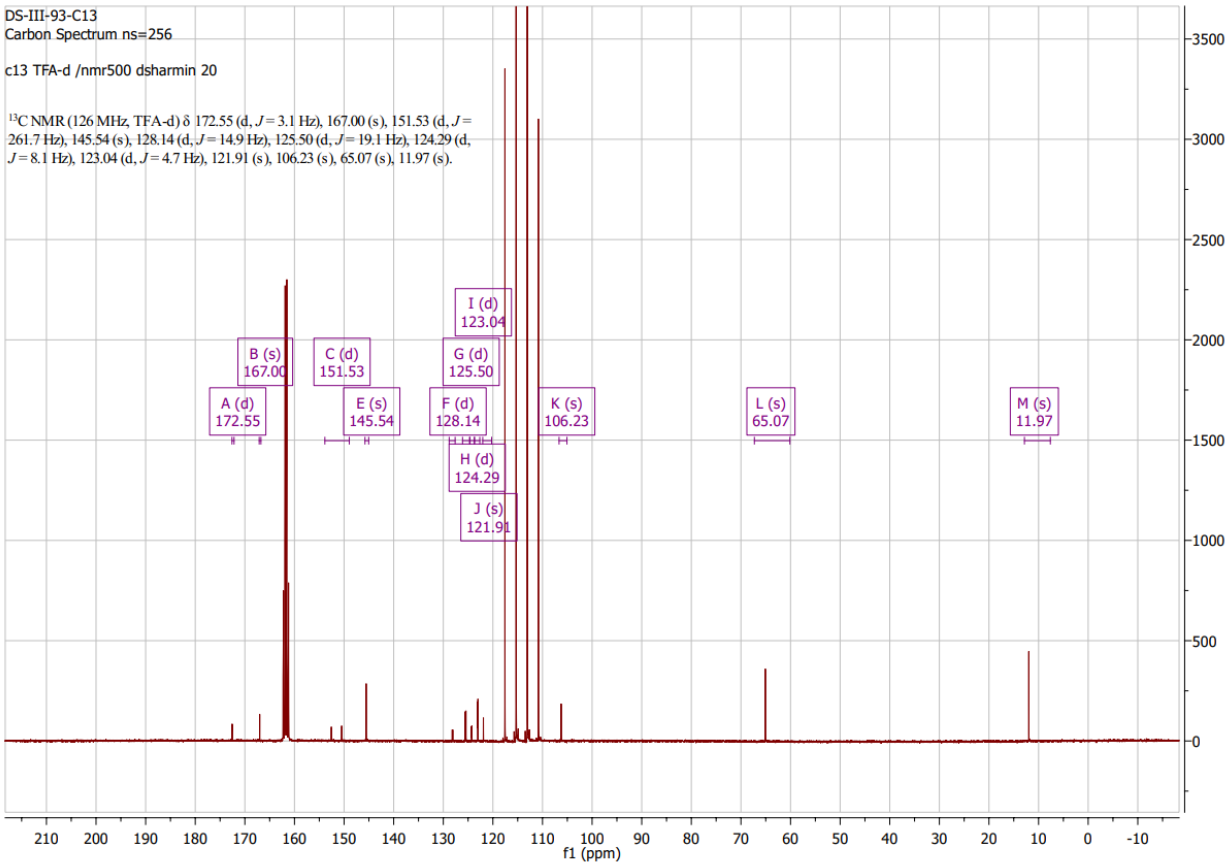

DS-I-88
Carbon Spectrum of DS-I-88
^{13}C NMR (126 MHz, TFA-d) δ 173.37 (s), 167.19 (s), 145.64 (s), 139.59 (s), 134.02 (s), 133.76 (s), 125.55 (s), 122.58 (s), 118.40 (s), 105.01 (s), 64.62 (s), 11.94 (s).
A (s) 173.37
B (s) 167.19
C (s) 145.64
D (s) 139.59
E (s) 133.76
F (s) 125.55
G (s) 122.58
H (s) 118.40
I (s) 105.01
J (s) 64.62
K (s) 11.94
L (s) 134.02
f1 (ppm)

Ethyl 6-bromo-8-fluoro-4-oxo-1,4-dihydroquinoline-3-carboxylate (16)

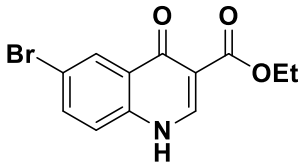


16

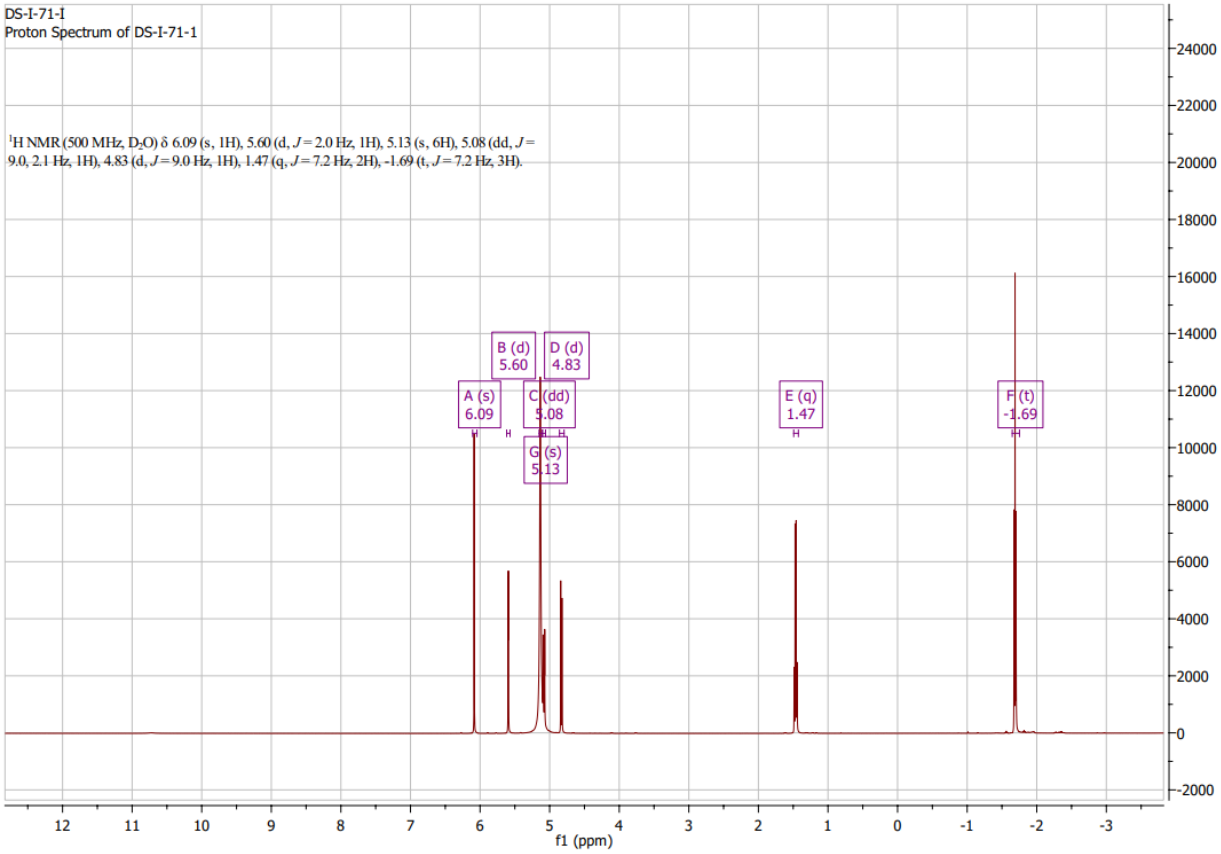


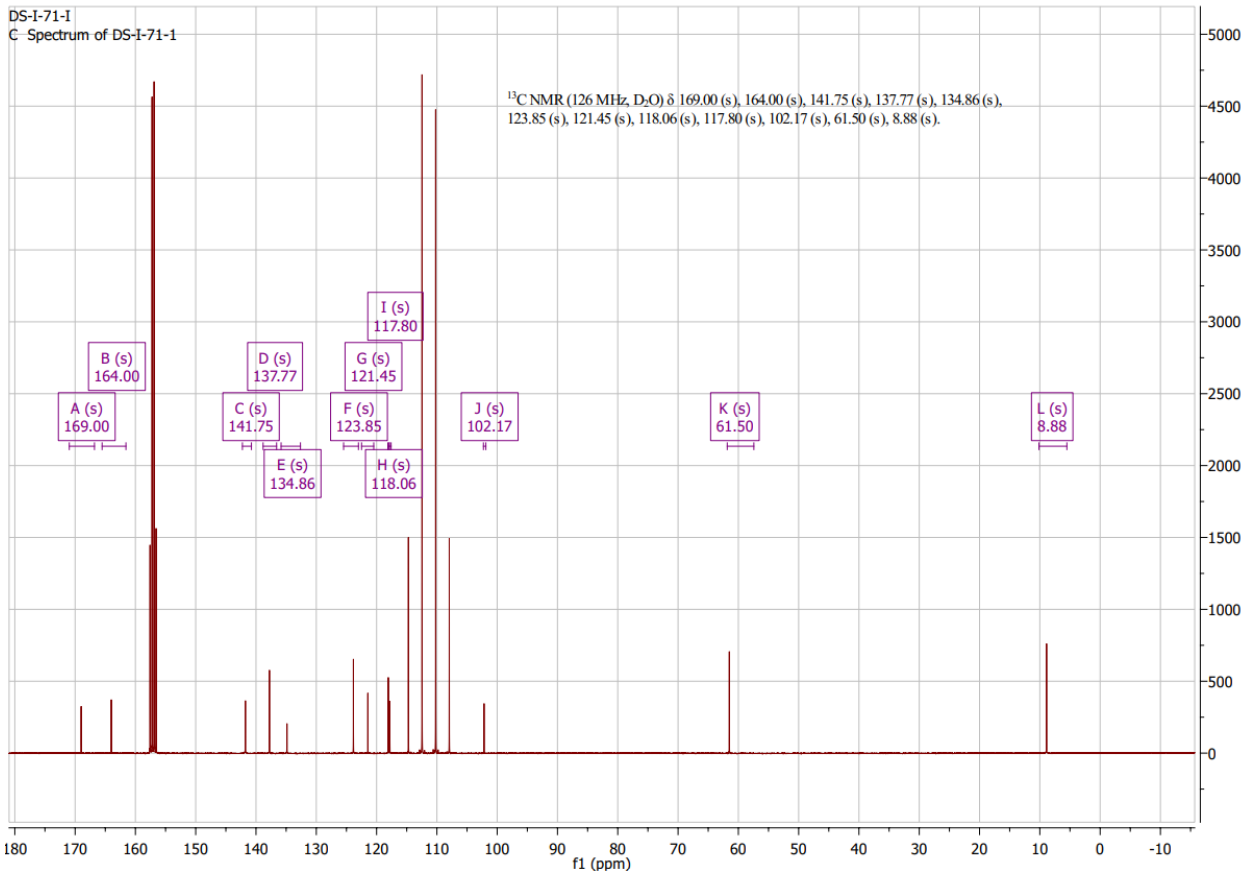

DS-III-93-C13
Carbon Spectrum ns=256
c13 TFA-d /nmr500 dsharmin 20
^{13}C NMR (126 MHz, TFA-d) δ 172.55 (d, J = 3.1 Hz), 167.00 (s), 151.53 (d, J = 261.7 Hz), 145.54 (s), 128.14 (d, J = 14.9 Hz), 125.50 (d, J = 19.1 Hz), 124.29 (d, J = 8.1 Hz), 123.04 (d, J = 4.7 Hz), 121.91 (s), 106.23 (s), 65.07 (s), 11.97 (s).
I (d) 123.04
B (s) 167.00
C (d) 151.53
G (d) 125.50
A (d) 172.55
E (s) 145.54
F (d) 128.14
K (s) 106.23
L (s) 65.07
M (s) 11.97
H (d) 124.29
J (s) 121.91
f1 (ppm)

Ethyl 6-bromo-4-oxo-1,4-dihydroquinoline-3-carboxylate (17)

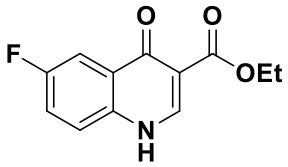


17

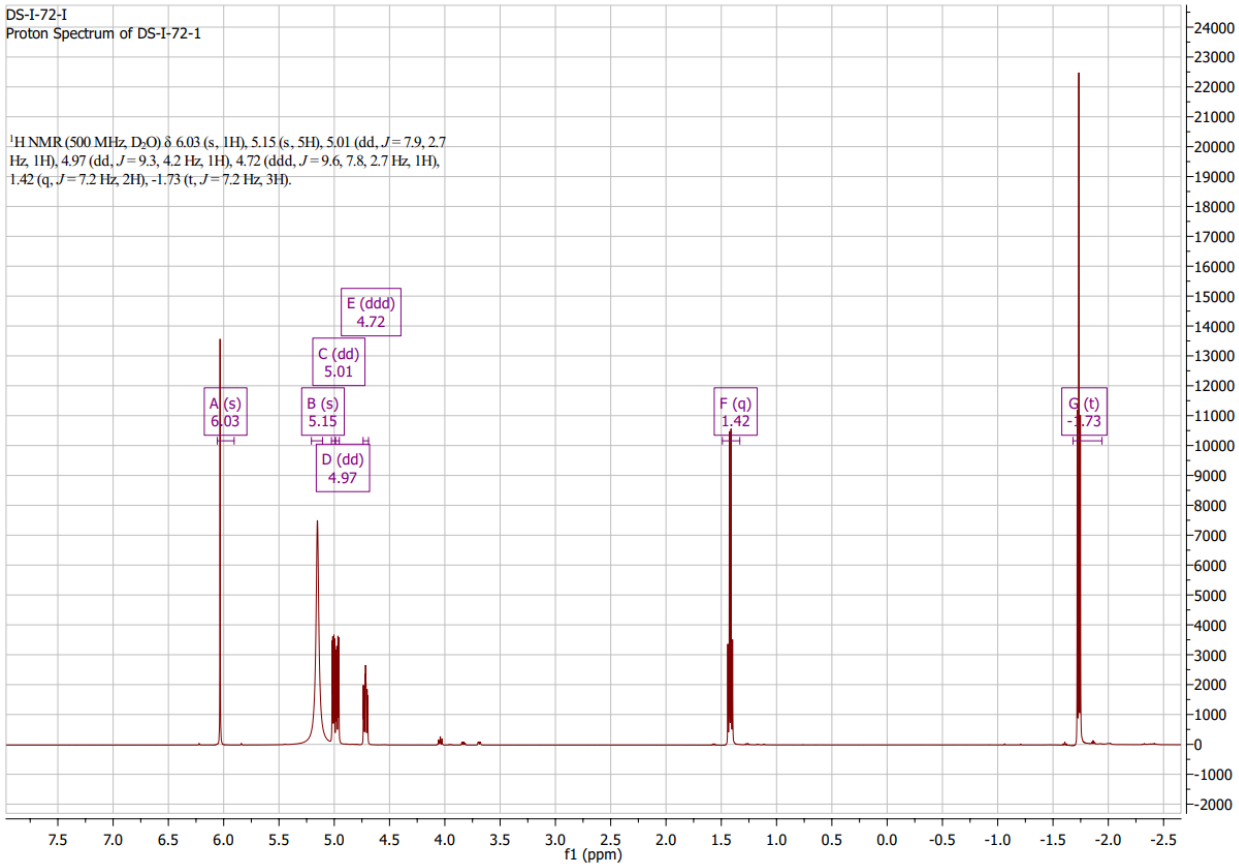


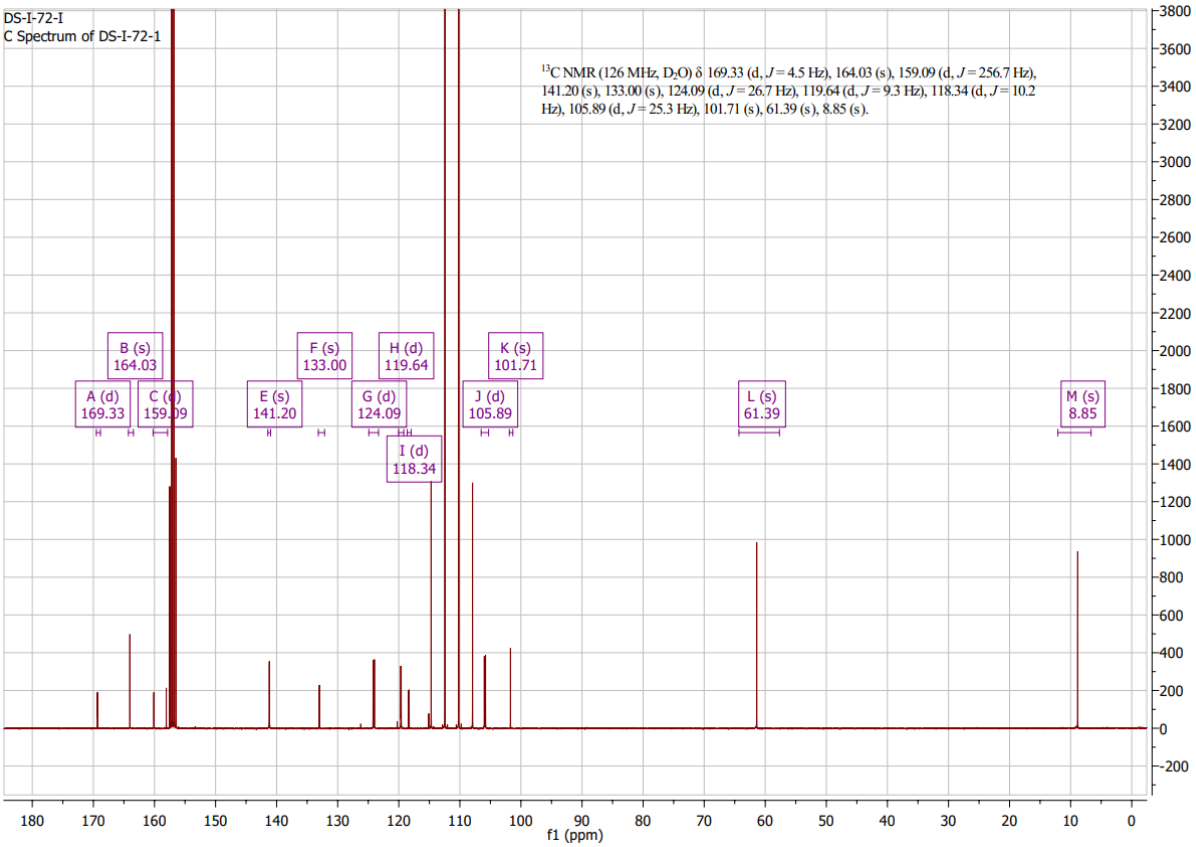

DS-I-71-I
C Spectrum of DS-I-71-1
^{13}C NMR (126 MHz, D_2O) δ 169.00 (s), 164.00 (s), 141.75 (s), 137.77 (s), 134.86 (s), 123.85 (s), 121.45 (s), 118.06 (s), 117.80 (s), 102.17 (s), 61.50 (s), 8.88 (s).
A (s) 169.00
B (s) 164.00
C (s) 141.75
D (s) 137.77
E (s) 134.86
F (s) 123.85
G (s) 121.45
H (s) 118.06
I (s) 117.80
J (s) 102.17
K (s) 61.50
L (s) 8.88
f1 (ppm)

Ethyl 6-fluoro-4-oxo-1,4-dihydroquinoline-3-carboxylate (18)

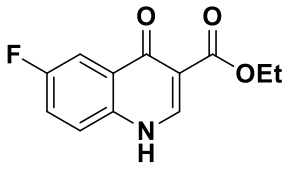


18

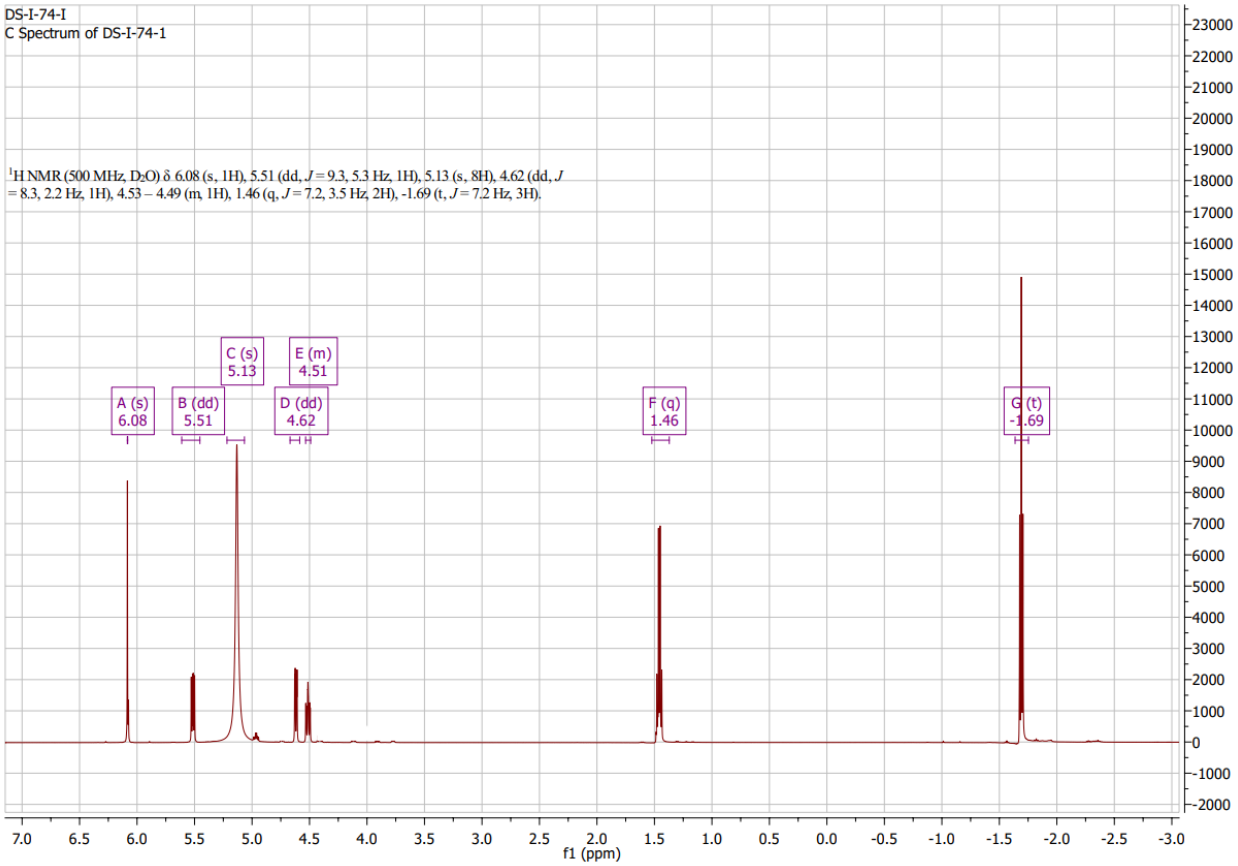




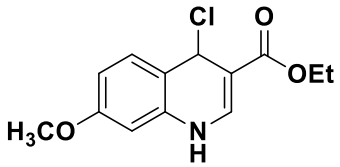
Ethyl 6-fluoro-4-oxo-1,4-dihydroquinoline-3-carboxylate (19)



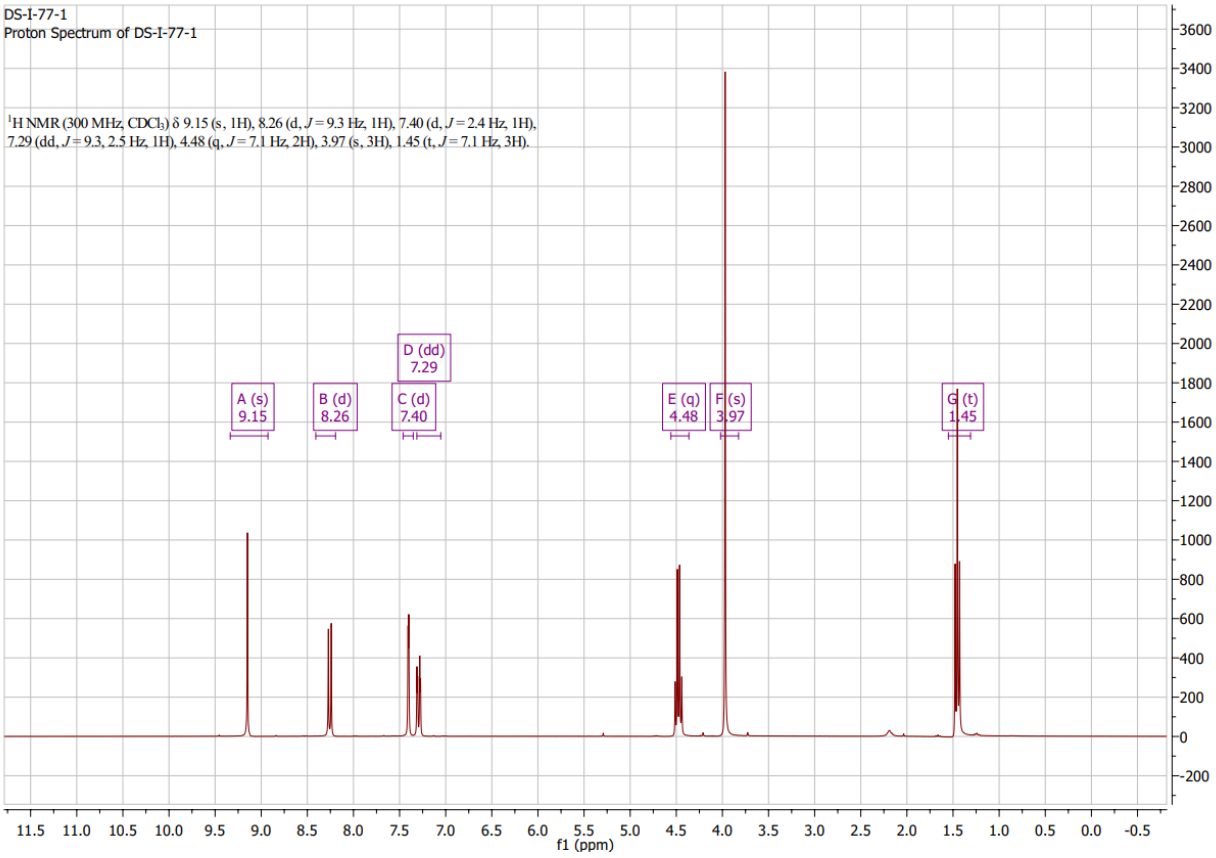
19

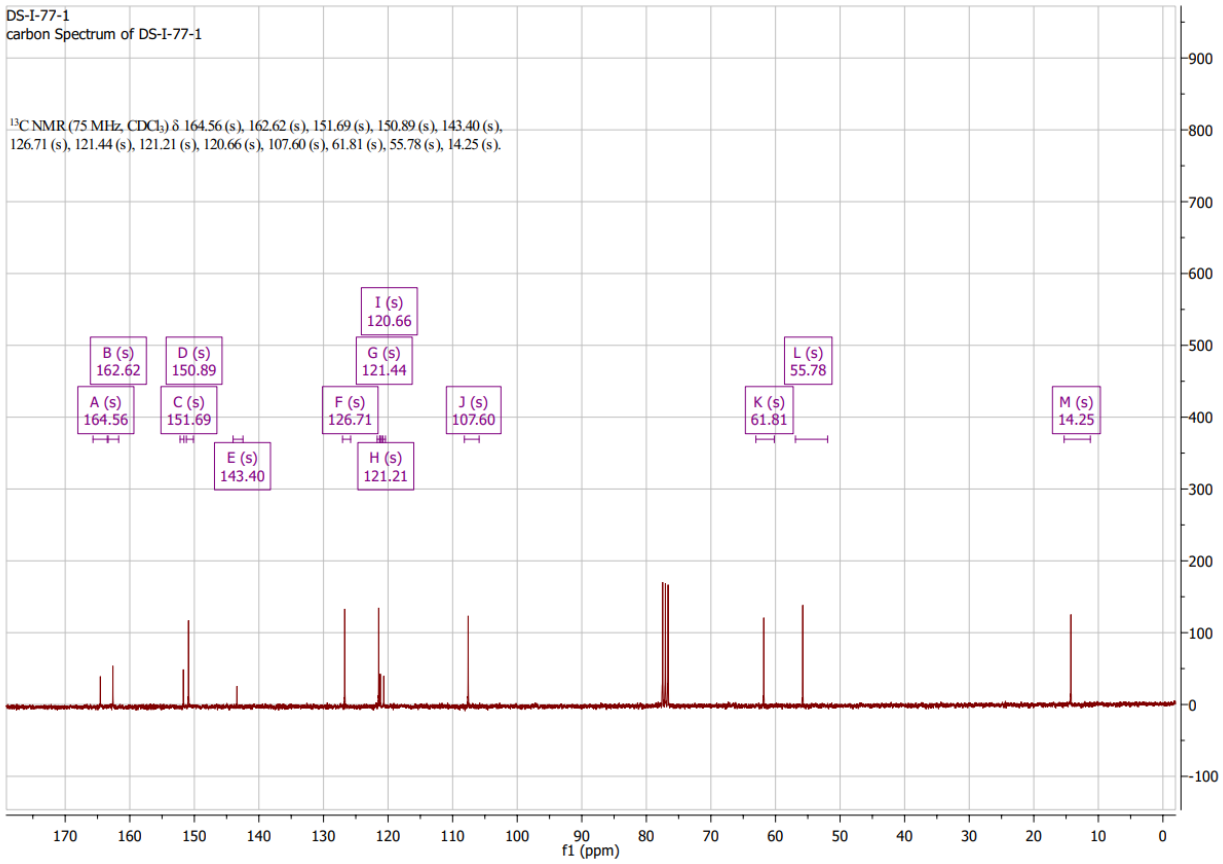

DS-I-74-I
C Spectrum of DS-I-74-1
^{1}H NMR (500 MHz, D_2O) δ 6.08 (s, 1H), 5.51 (dd, J = 9.3, 5.3 Hz, 1H), 5.13 (s, 8H), 4.62 (dd, J = 8.3, 2.2 Hz, 1H), 4.53 – 4.49 (m, 1H), 1.46 (q, J = 7.2, 3.5 Hz, 2H), -1.69 (t, J = 7.2 Hz, 3H).
A (s) 6.08
B (dd) 5.51
C (s) 5.13
D (dd) 4.62
E (m) 4.51
F (q) 1.46
G (t) -1.69
f1 (ppm)

Ethyl 4-chloro-7-methoxyquinoline-3-carboxylate (20)

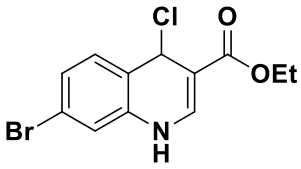


20

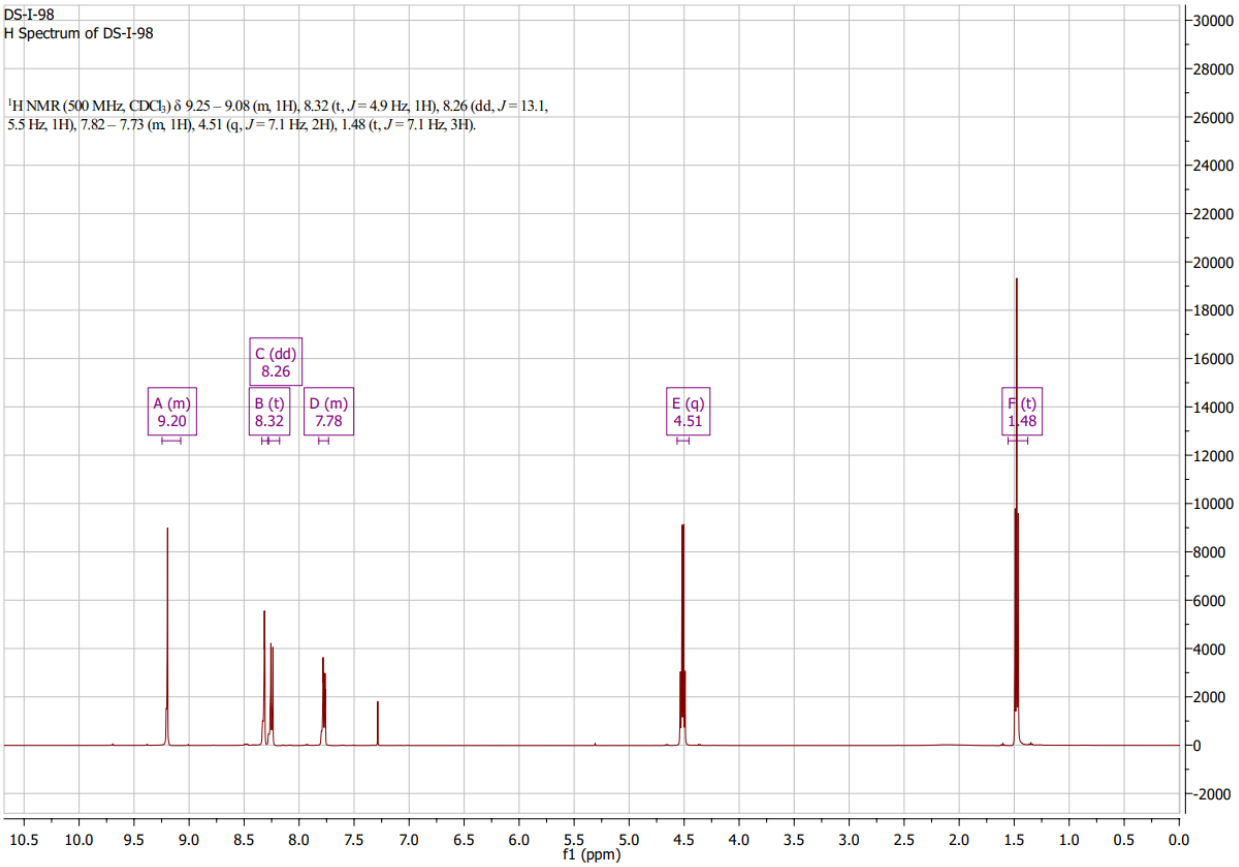


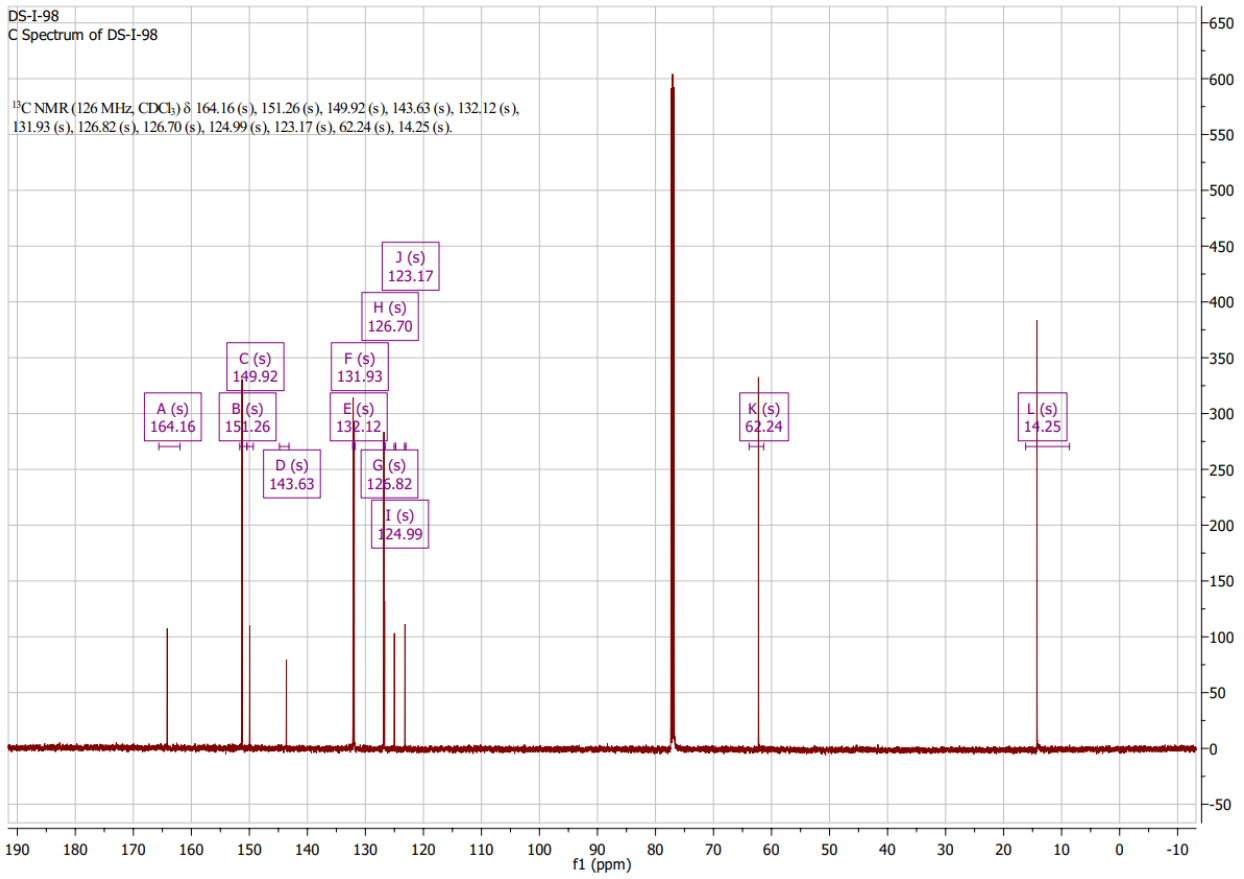

DS-I-77-1
carbon Spectrum of DS-I-77-1
^{13}C NMR (75 MHz, $CDCl_3$) δ 164.56 (s), 162.62 (s), 151.69 (s), 150.89 (s), 143.40 (s), 126.71 (s), 121.44 (s), 121.21 (s), 120.66 (s), 107.60 (s), 61.81 (s), 55.78 (s), 14.25 (s).
A (s) 164.56
B (s) 162.62
C (s) 151.69
D (s) 150.89
E (s) 143.40
F (s) 126.71
G (s) 121.44
H (s) 121.21
I (s) 120.66
J (s) 107.60
K (s) 61.81
L (s) 55.78
M (s) 14.25
f1 (ppm)

Ethyl 4-chloro-7-bromoquinoline-3-carboxylate (21)

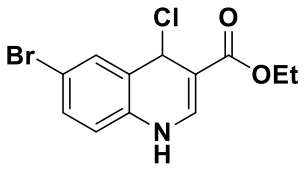


21



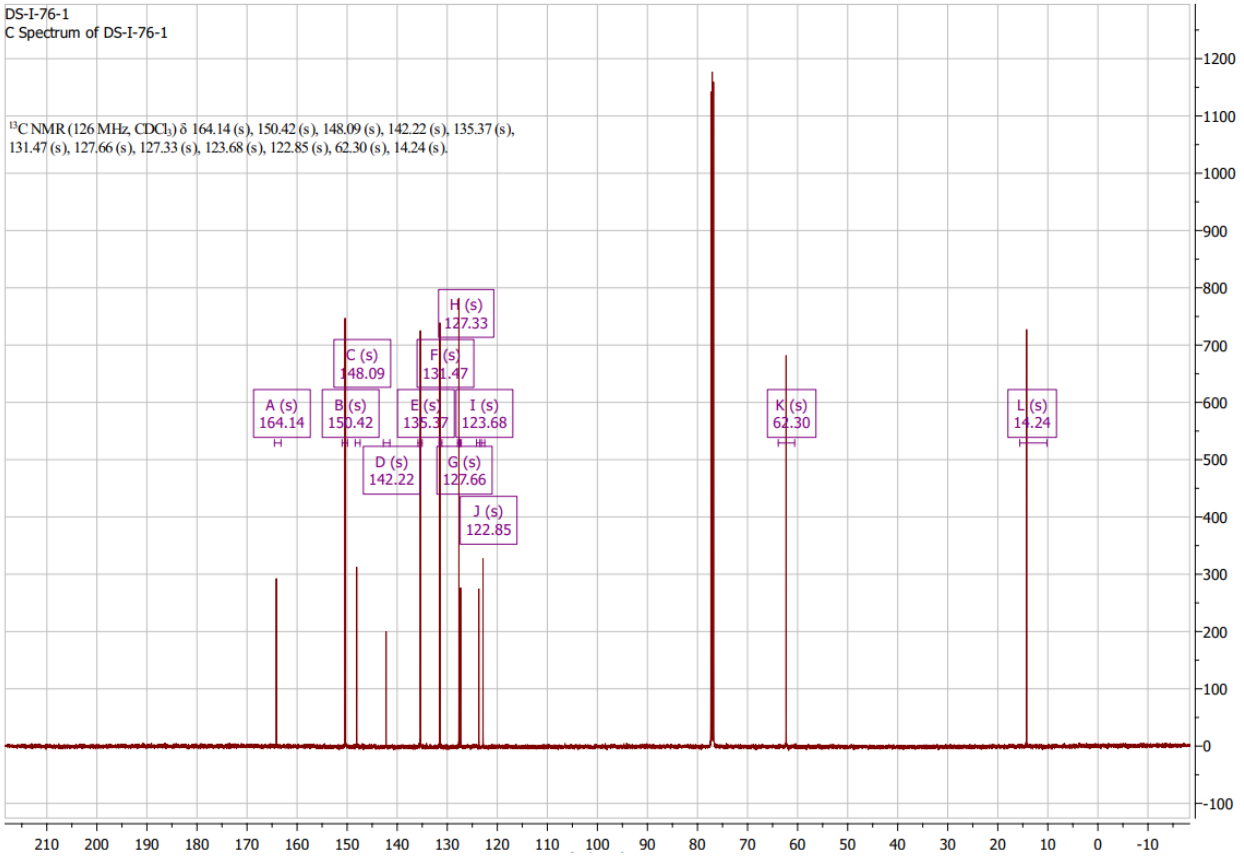

DS-I-98
C Spectrum of DS-I-98
^{13}C NMR (126 MHz, $CDCl_3$) δ 164.16 (s), 151.26 (s), 149.92 (s), 143.63 (s), 132.12 (s), 131.93 (s), 126.82 (s), 126.70 (s), 124.99 (s), 123.17 (s), 62.24 (s), 14.25 (s).
J (s) 123.17
H (s) 126.70
C (s) 149.92
F (s) 131.93
A (s) 164.16
B (s) 151.26
E (s) 132.12
K (s) 62.24
L (s) 14.25
D (s) 143.63
G (s) 126.82
I (s) 124.99
f1 (ppm)

Ethyl 6-bromo-4-chloro-1,4-dihydroquinoline-3-carboxylate (23)

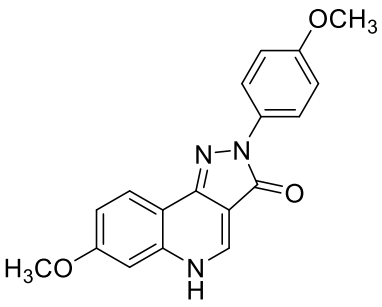


23

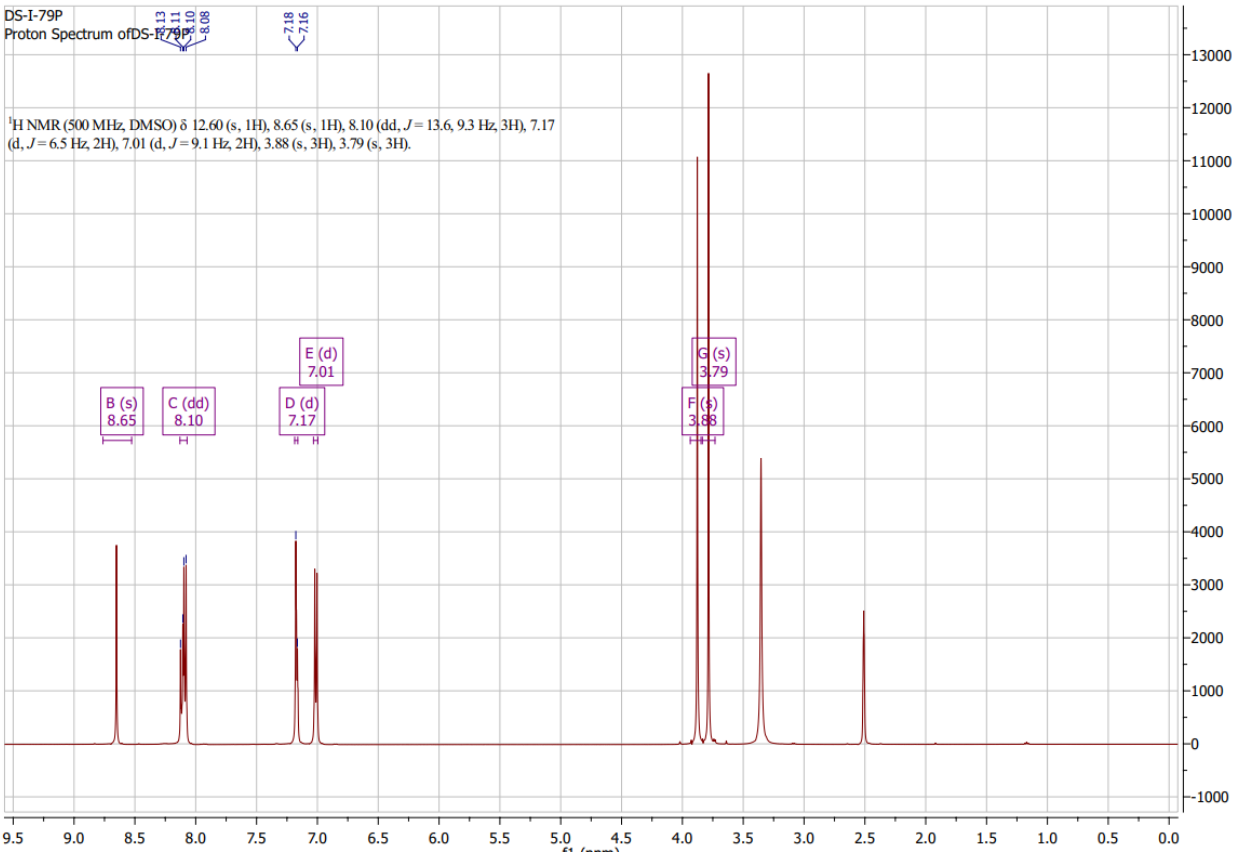


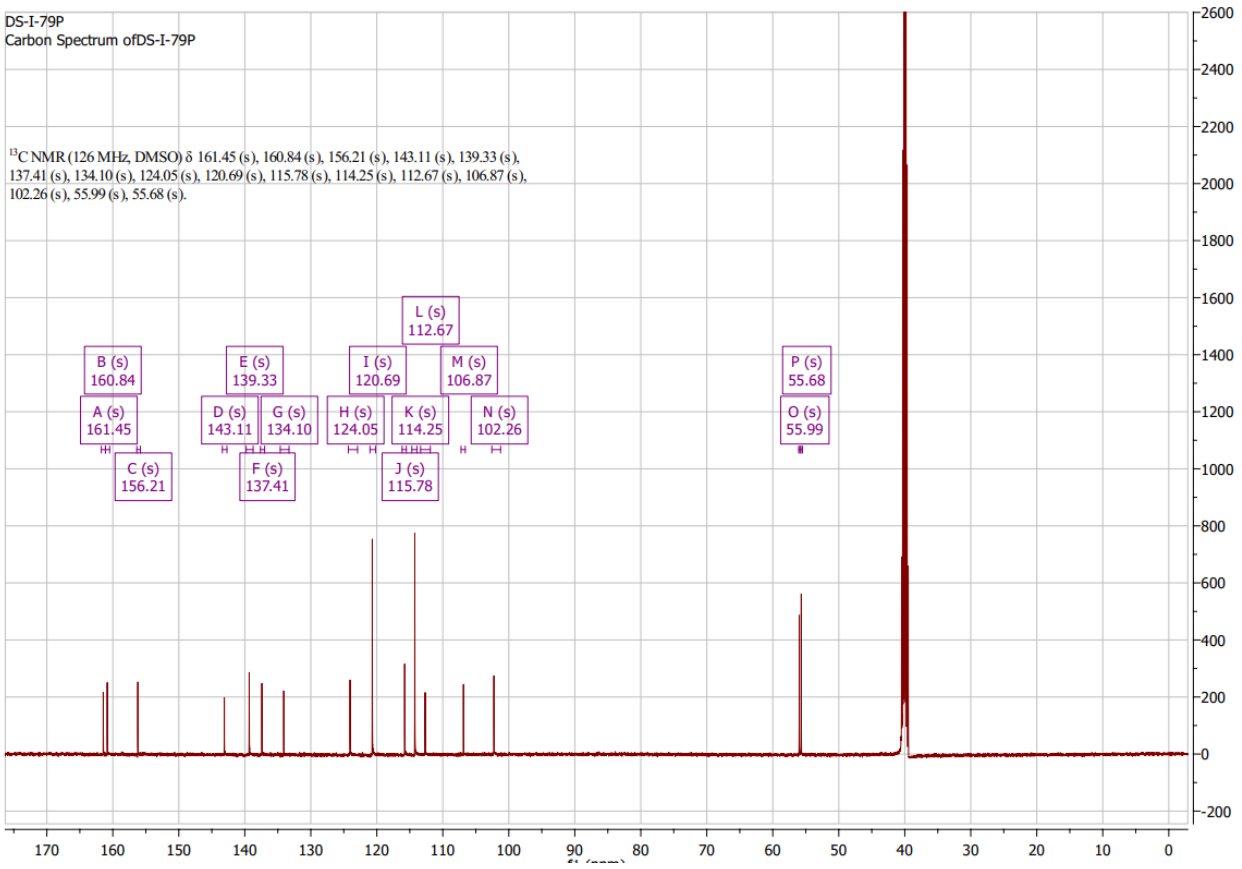

DS-I-76-1
C Spectrum of DS-I-76-1
^{13}C NMR (126 MHz, $CDCl_3$) δ 164.14 (s), 150.42 (s), 148.09 (s), 142.22 (s), 135.37 (s), 131.47 (s), 127.66 (s), 127.33 (s), 123.68 (s), 122.85 (s), 62.30 (s), 14.24 (s).
A (s) 164.14
B (s) 150.42
C (s) 148.09
D (s) 142.22
E (s) 135.37
F (s) 131.47
G (s) 127.66
H (s) 127.33
I (s) 123.68
J (s) 122.85
K (s) 62.30
L (s) 14.24

7-Methoxy-2-(4-methoxyphenyl)-2,5-dihydro-3H-pyrazolo[4,3-c]quinolin-3-one (PZ-II-029, 3)



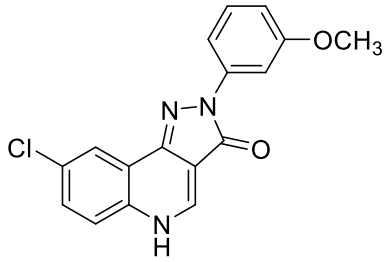
PZ-II-029 (3)



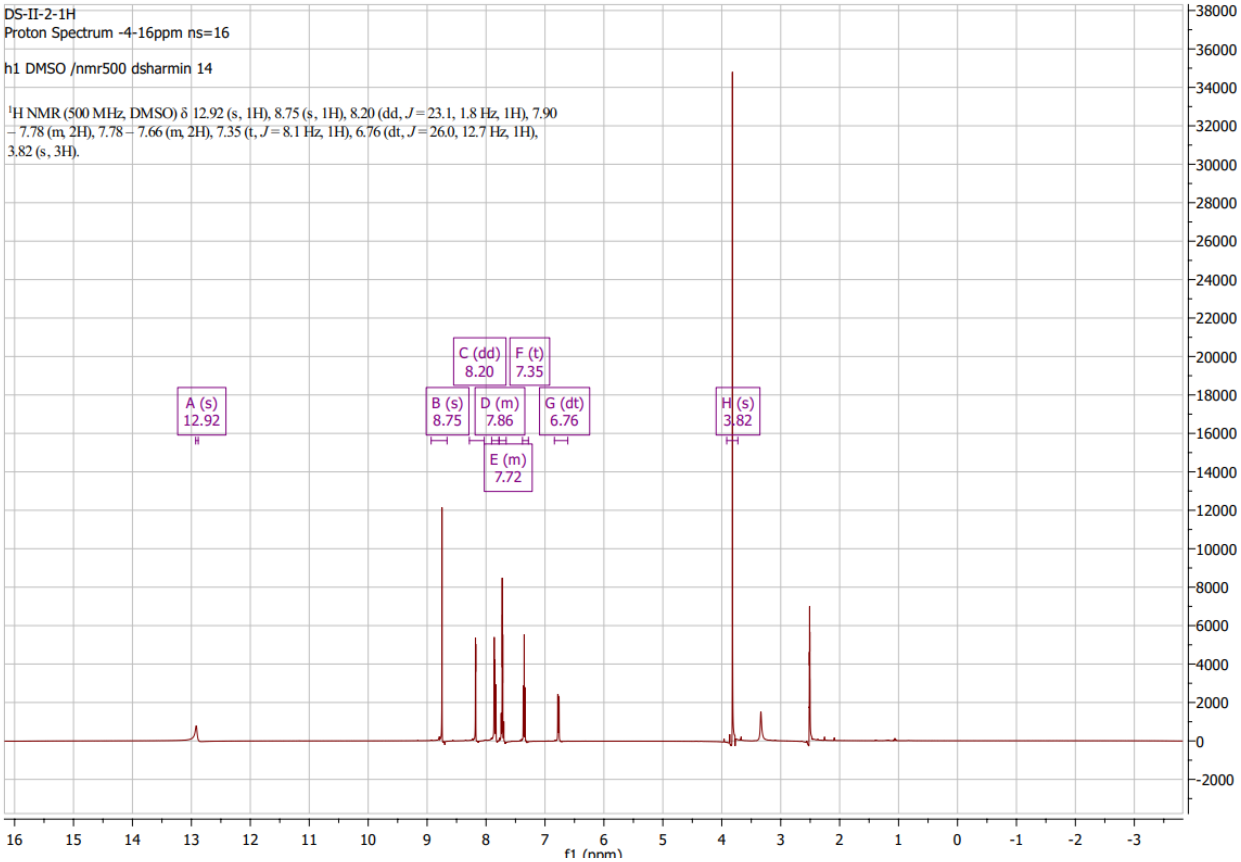

DS-I-79P
Carbon Spectrum ofDS-I-79P
13C NMR (126 MHz, DMSO) δ 161.45 (s), 160.84 (s), 156.21 (s), 143.11 (s), 139.33 (s), 137.41 (s), 134.10 (s), 124.05 (s), 120.69 (s), 115.78 (s), 114.25 (s), 112.67 (s), 106.87 (s), 102.26 (s), 55.99 (s), 55.68 (s).
L (s) 112.67
B (s) 160.84
E (s) 139.33
I (s) 120.69
M (s) 106.87
P (s) 55.68
A (s) 161.45
D (s) 143.11
G (s) 134.10
H (s) 124.05
K (s) 114.25
N (s) 102.26
O (s) 55.99
C (s) 156.21
F (s) 137.41
J (s) 115.78
2600
2400
2200
2000
1800
1600
1400
1200
1000
800
600
400
200
0
-200
170
160
150
140
130
120
110
100
90
80
70
60
50
40
30
20
10
0

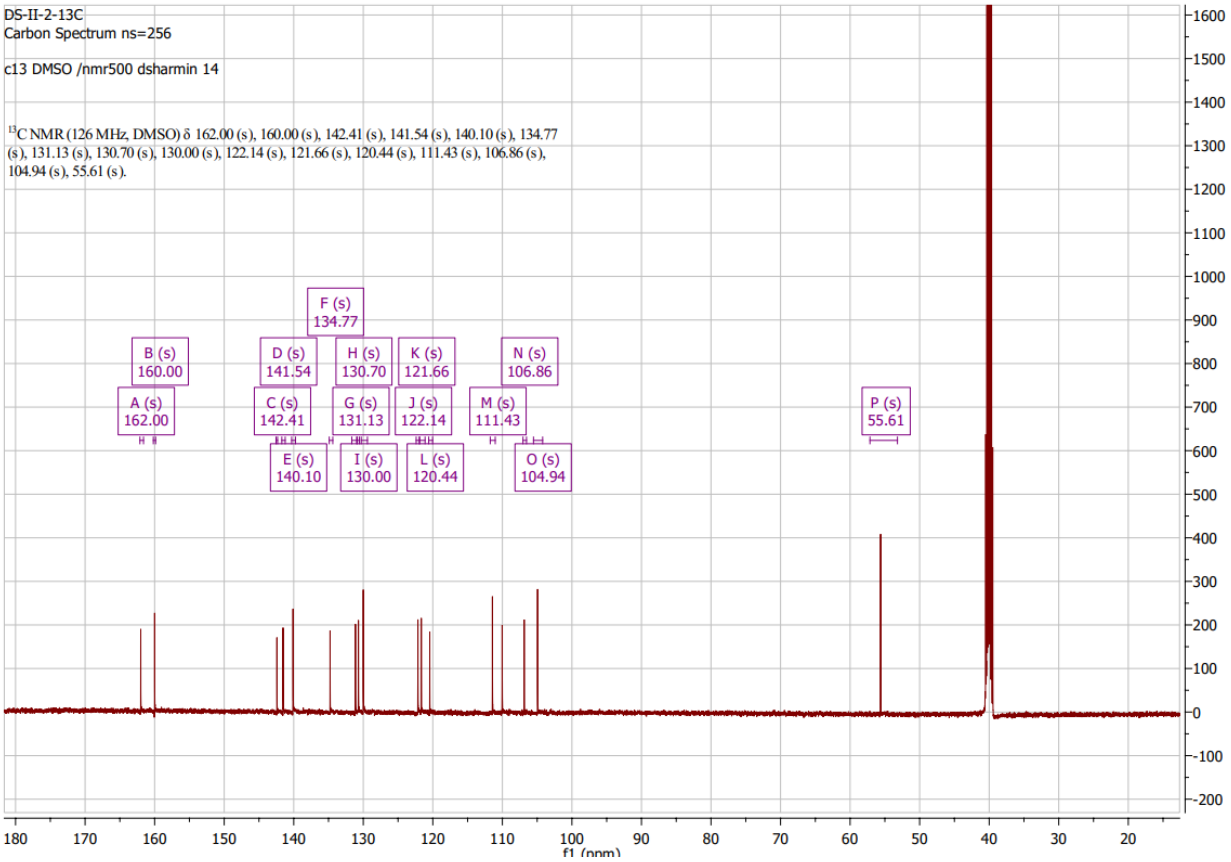
8-Chloro-2-(3-methoxyphenyl)-2,5-dihydro-3H-pyrazolo[4,3-c]quinolin-3-one

(LAU 159, 5)

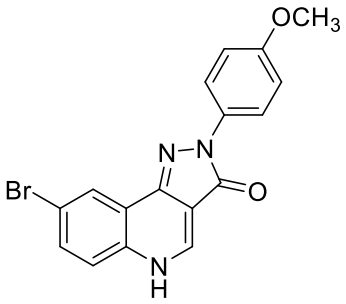


LAU 159 (5)

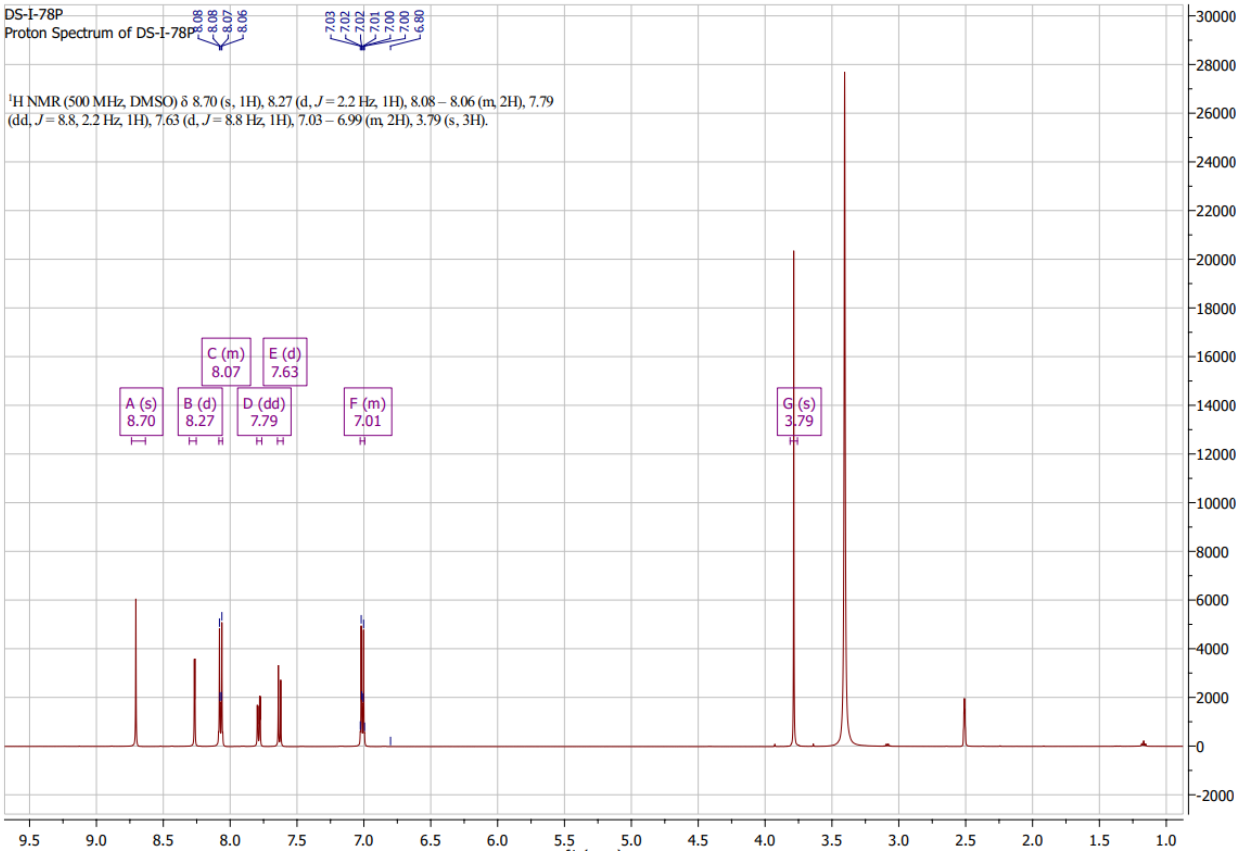


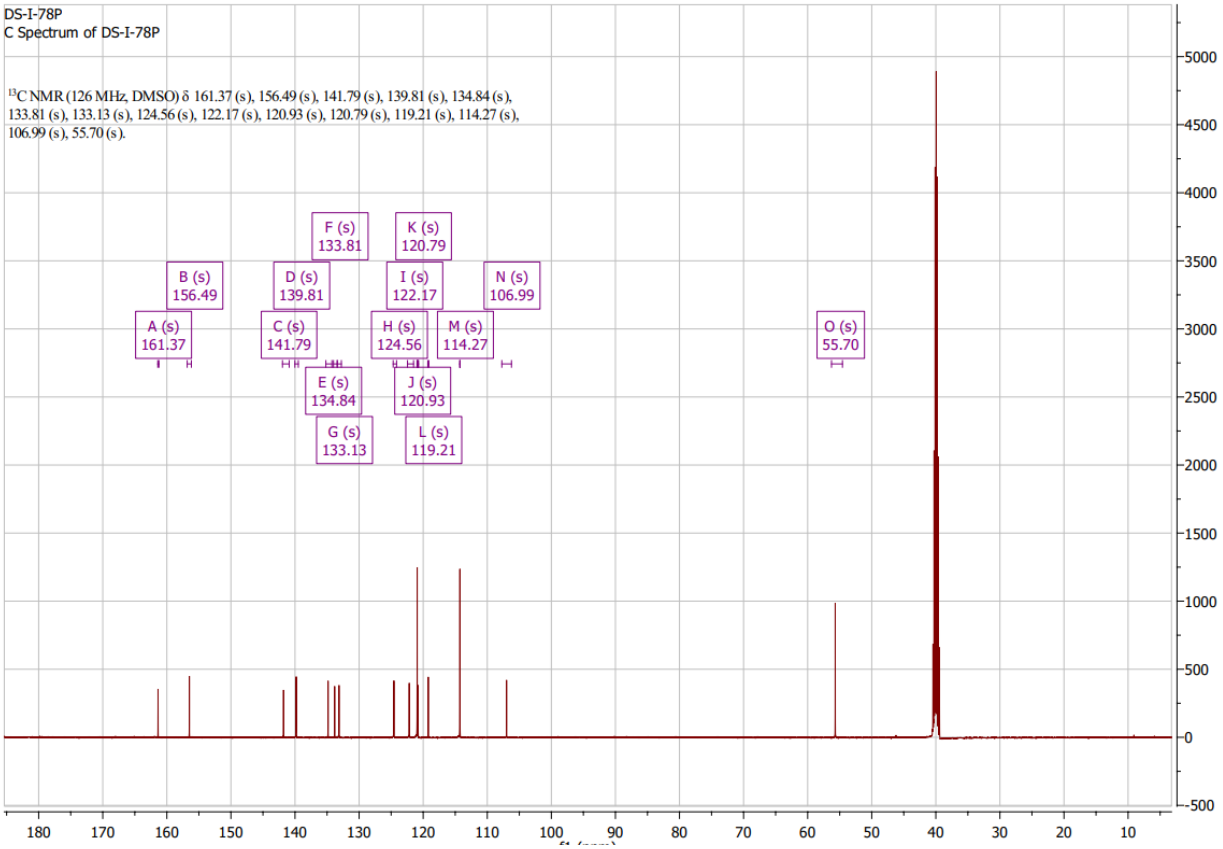

DS-II-2-13C
Carbon Spectrum ns=256
c13 DMSO /nmr500 dsharmin 14
13C NMR (126 MHz, DMSO) δ 162.00 (s), 160.00 (s), 142.41 (s), 141.54 (s), 140.10 (s), 134.77 (s), 131.13 (s), 130.70 (s), 130.00 (s), 122.14 (s), 121.66 (s), 120.44 (s), 111.43 (s), 106.86 (s), 104.94 (s), 55.61 (s).
F (s) 134.77
B (s) 160.00
D (s) 141.54
H (s) 130.70
K (s) 121.66
N (s) 106.86
A (s) 162.00
C (s) 142.41
G (s) 131.13
J (s) 122.14
M (s) 111.43
P (s) 55.61
E (s) 140.10
I (s) 130.00
L (s) 120.44
O (s) 104.94
f1 (ppm)

8-Bromo-2-(4-methoxyphenyl)-2,5-dihydro-3H-pyrazolo[4,3-c]quinolin-3-one (DS-I-78, 33)

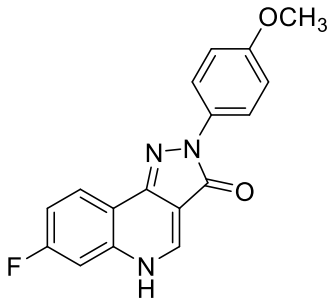


DS-I-78 (33)

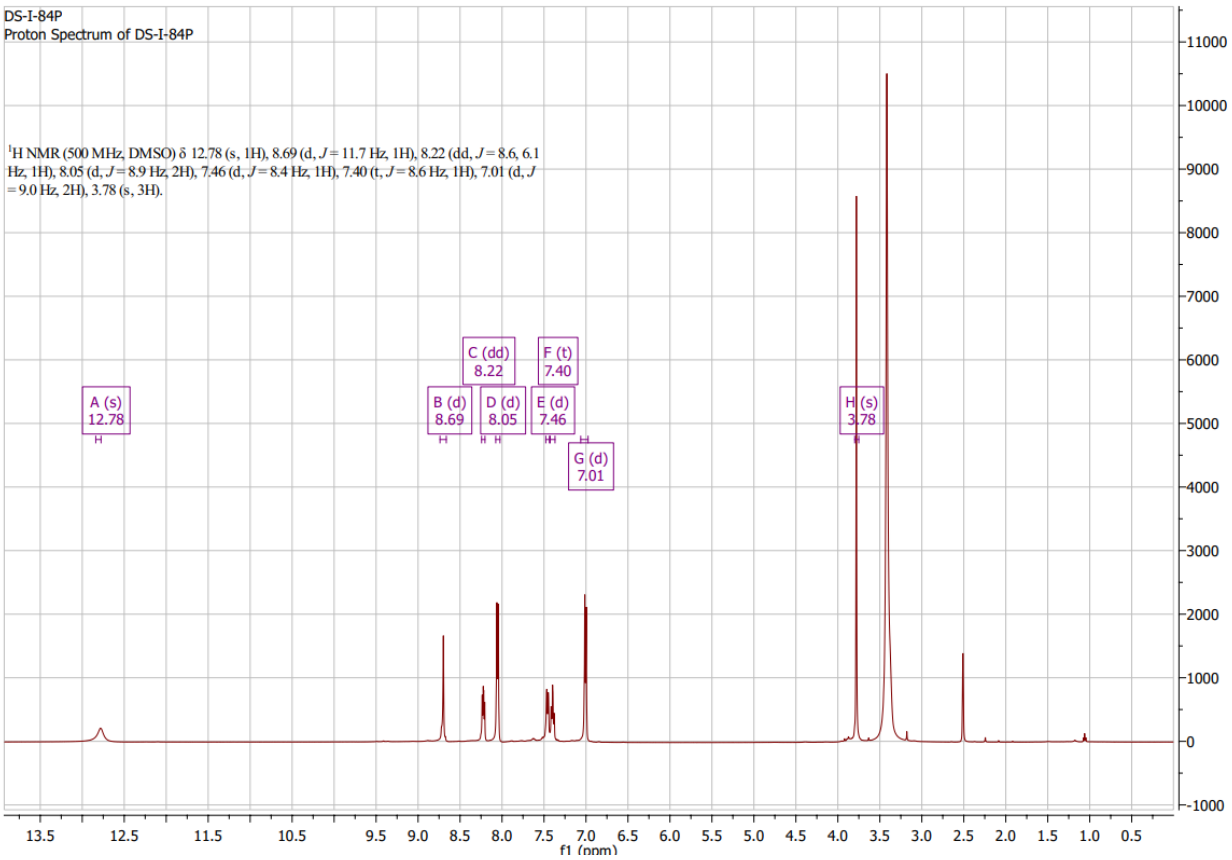


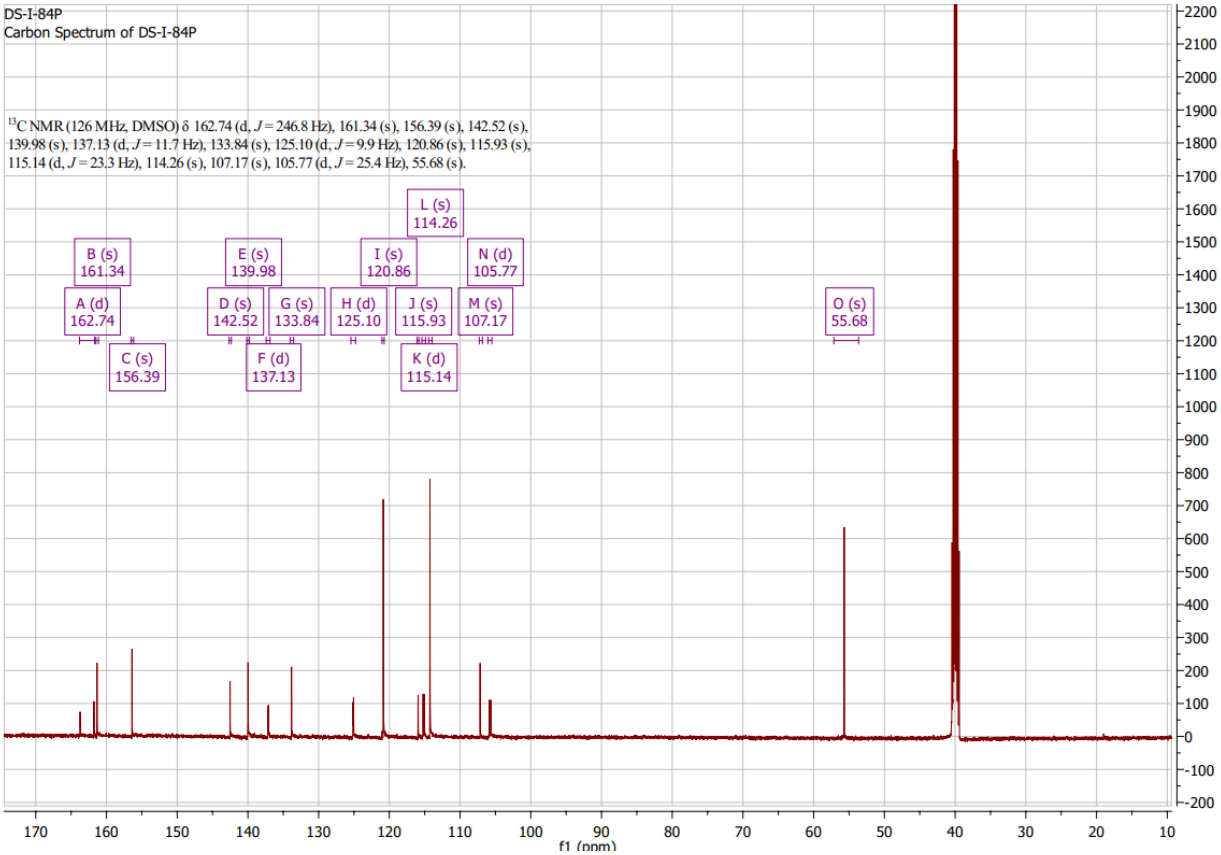

DS-I-78P
C Spectrum of DS-I-78P
^{13}C NMR (126 MHz, DMSO) δ 161.37 (s), 156.49 (s), 141.79 (s), 139.81 (s), 134.84 (s), 133.81 (s), 133.13 (s), 124.56 (s), 122.17 (s), 120.93 (s), 120.79 (s), 119.21 (s), 114.27 (s), 106.99 (s), 55.70 (s).
A (s) 161.37
B (s) 156.49
C (s) 141.79
D (s) 139.81
E (s) 134.84
F (s) 133.81
G (s) 133.13
H (s) 124.56
I (s) 122.17
J (s) 120.93
K (s) 120.79
L (s) 119.21
M (s) 114.27
N (s) 106.99
O (s) 55.70
5000
4500
4000
3500
3000
2500
2000
1500
1000
500
0
-500
180
170
160
150
140
130
120
110
100
90
80
70
60
50
40
30
20
10

7-fluoro-2-(4-methoxyphenyl)-2,5-dihydro-3H-pyrazolo[4,3-c]quinolin-3-one (DS-I-84, 34)

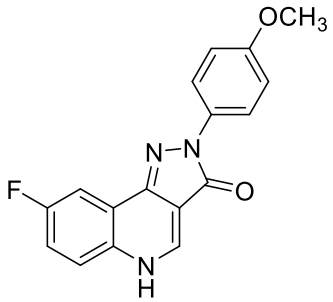


DS-I-84 (34)

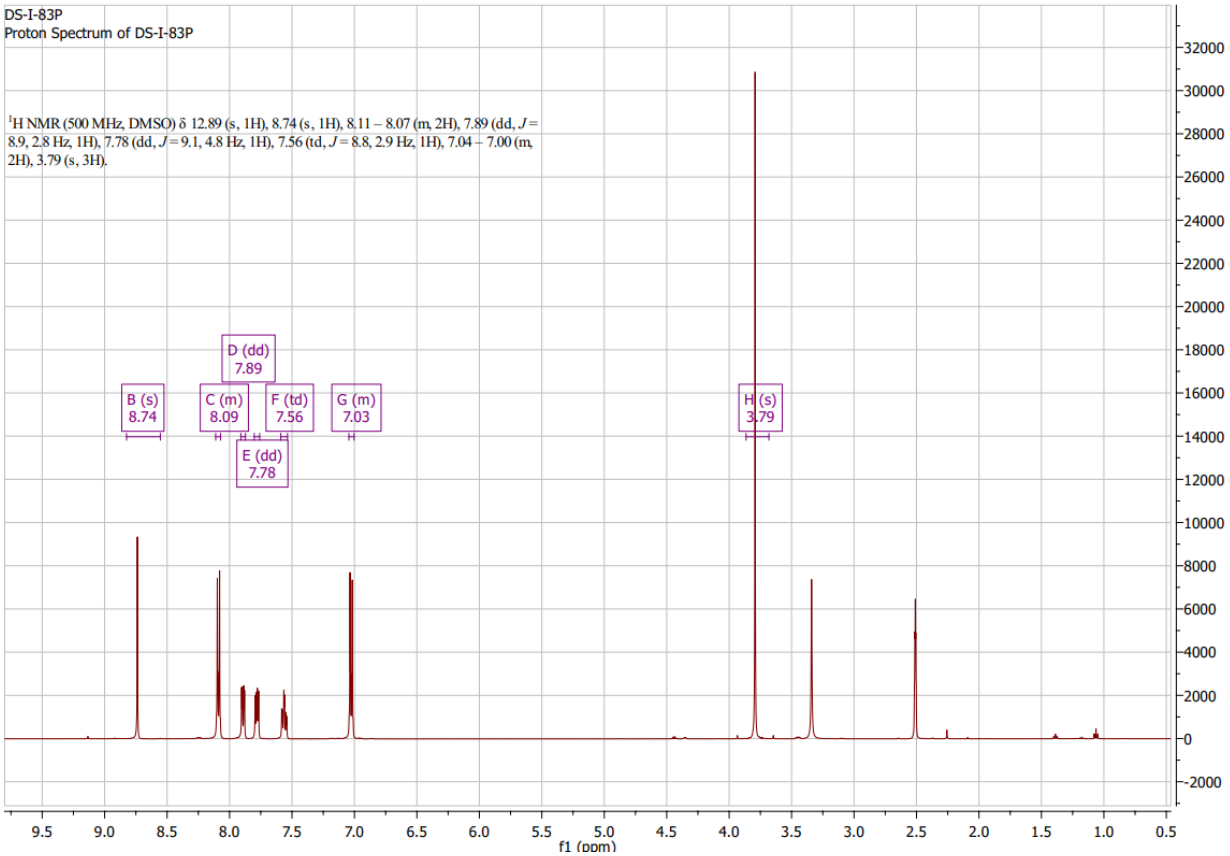


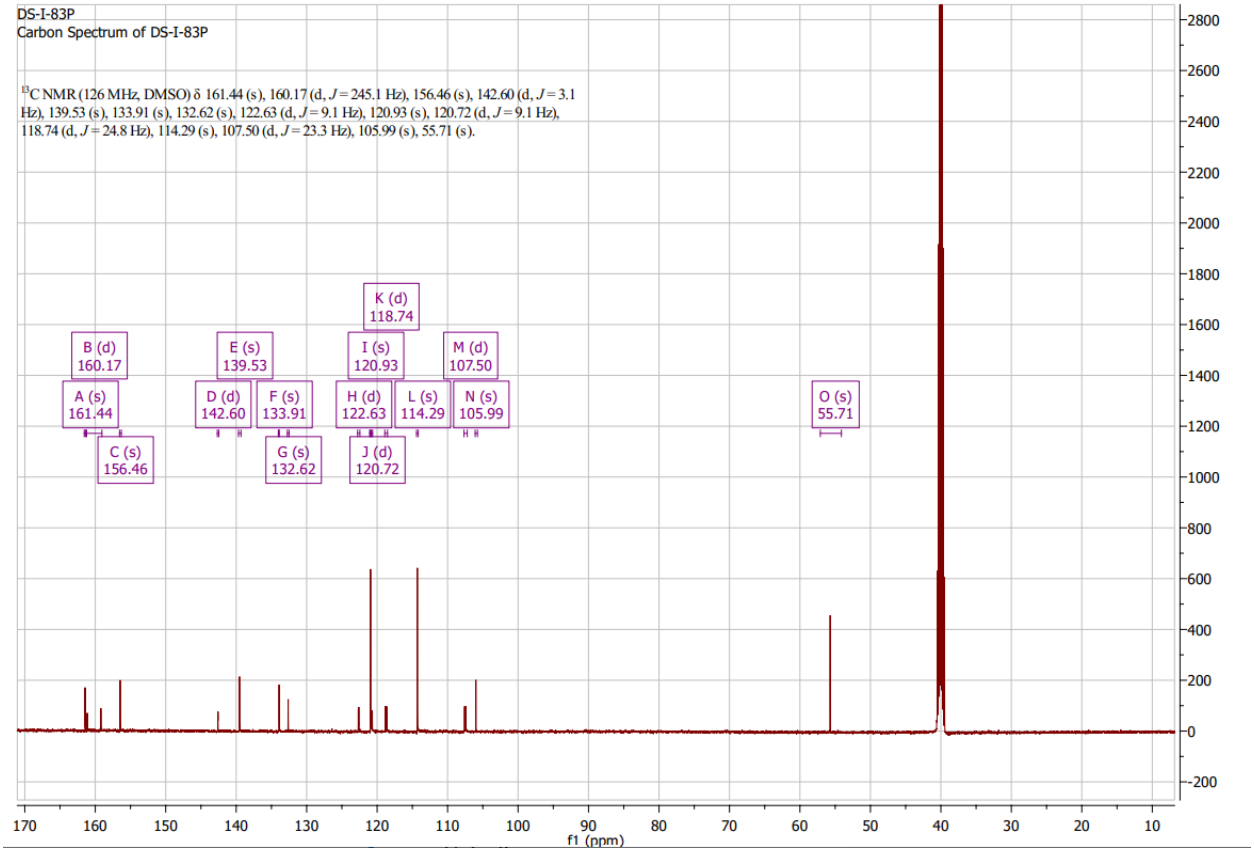

DS-I-84P
Carbon Spectrum of DS-I-84P
^{13}C NMR (126 MHz, DMSO) δ 162.74 (d, J = 246.8 Hz), 161.34 (s), 156.39 (s), 142.52 (s), 139.98 (s), 137.13 (d, J = 11.7 Hz), 133.84 (s), 125.10 (d, J = 9.9 Hz), 120.86 (s), 115.93 (s), 115.14 (d, J = 23.3 Hz), 114.26 (s), 107.17 (s), 105.77 (d, J = 25.4 Hz), 55.68 (s).
L (s) 114.26
B (s) 161.34
E (s) 139.98
I (s) 120.86
N (d) 105.77
A (d) 162.74
D (s) 142.52
G (s) 133.84
H (d) 125.10
J (s) 115.93
M (s) 107.17
O (s) 55.68
C (s) 156.39
F (d) 137.13
K (d) 115.14
f1 (ppm)

. 8-Fluoro-2-(4-methoxyphenyl)-2,5-dihydro-3H-pyrazolo[4,3-c]quinolin-3-one (DS-I-83, 35)



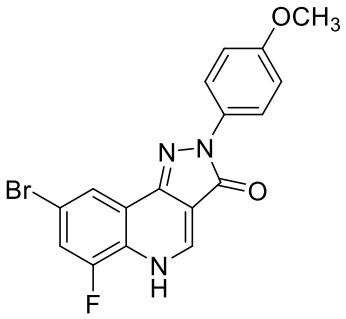
DS-I-83 (35)



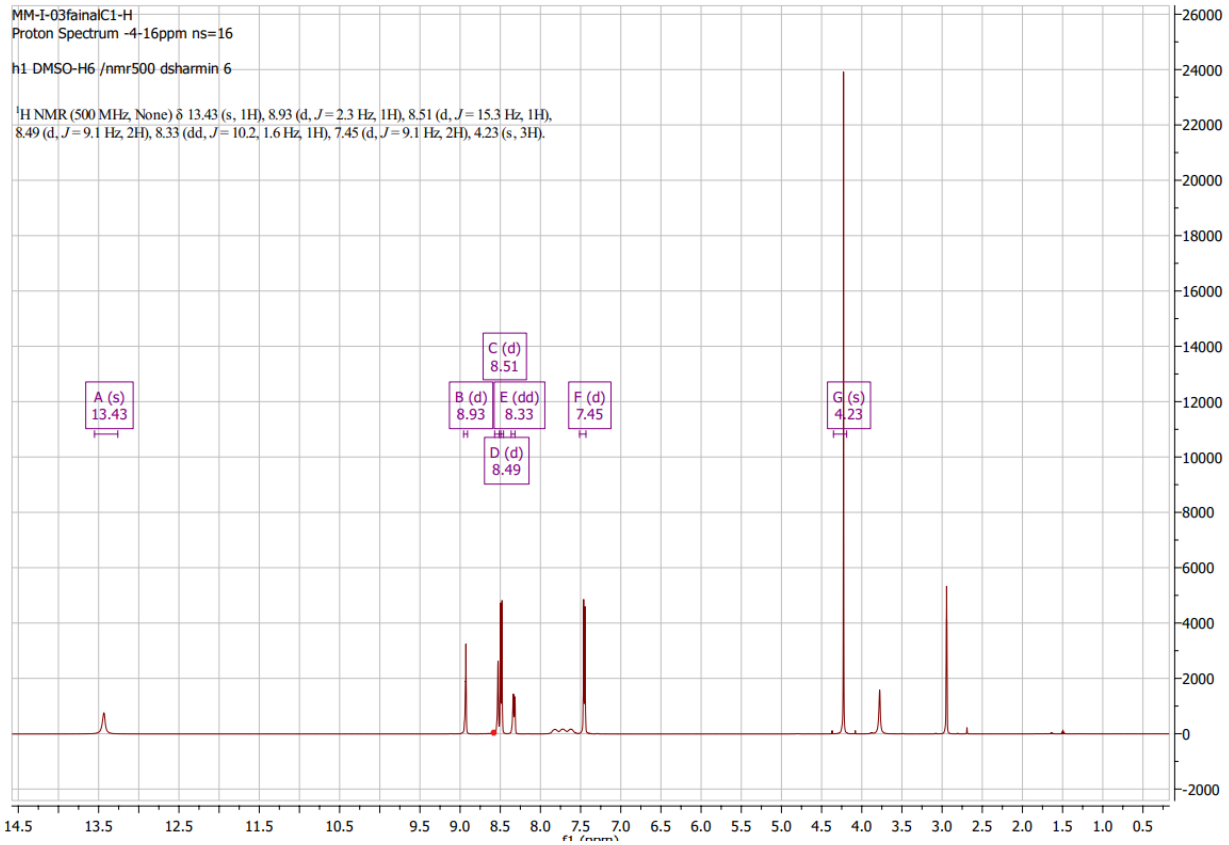

DS-I-83P
Carbon Spectrum of DS-I-83P
13C NMR (126 MHz, DMSO) δ 161.44 (s), 160.17 (d, J = 245.1 Hz), 156.46 (s), 142.60 (d, J = 3.1 Hz), 139.53 (s), 133.91 (s), 132.62 (s), 122.63 (d, J = 9.1 Hz), 120.93 (s), 120.72 (d, J = 9.1 Hz), 118.74 (d, J = 24.8 Hz), 114.29 (s), 107.50 (d, J = 23.3 Hz), 105.99 (s), 55.71 (s).
K (d) 118.74
B (d) 160.17
E (s) 139.53
I (s) 120.93
M (d) 107.50
A (s) 161.44
D (d) 142.60
F (s) 133.91
H (d) 122.63
L (s) 114.29
N (s) 105.99
O (s) 55.71
C (s) 156.46
G (s) 132.62
J (d) 120.72
f1 (ppm)

8-Bromo-6-fluoro-2-(4-methoxyphenyl)-2,5-dihydro-3H-pyrazolo[4,3-c]quinolin-3-one

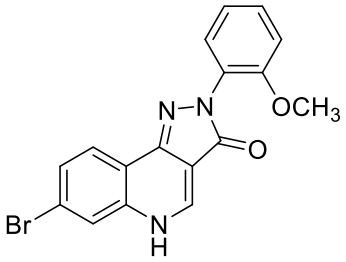
(MM-I-03, 36)



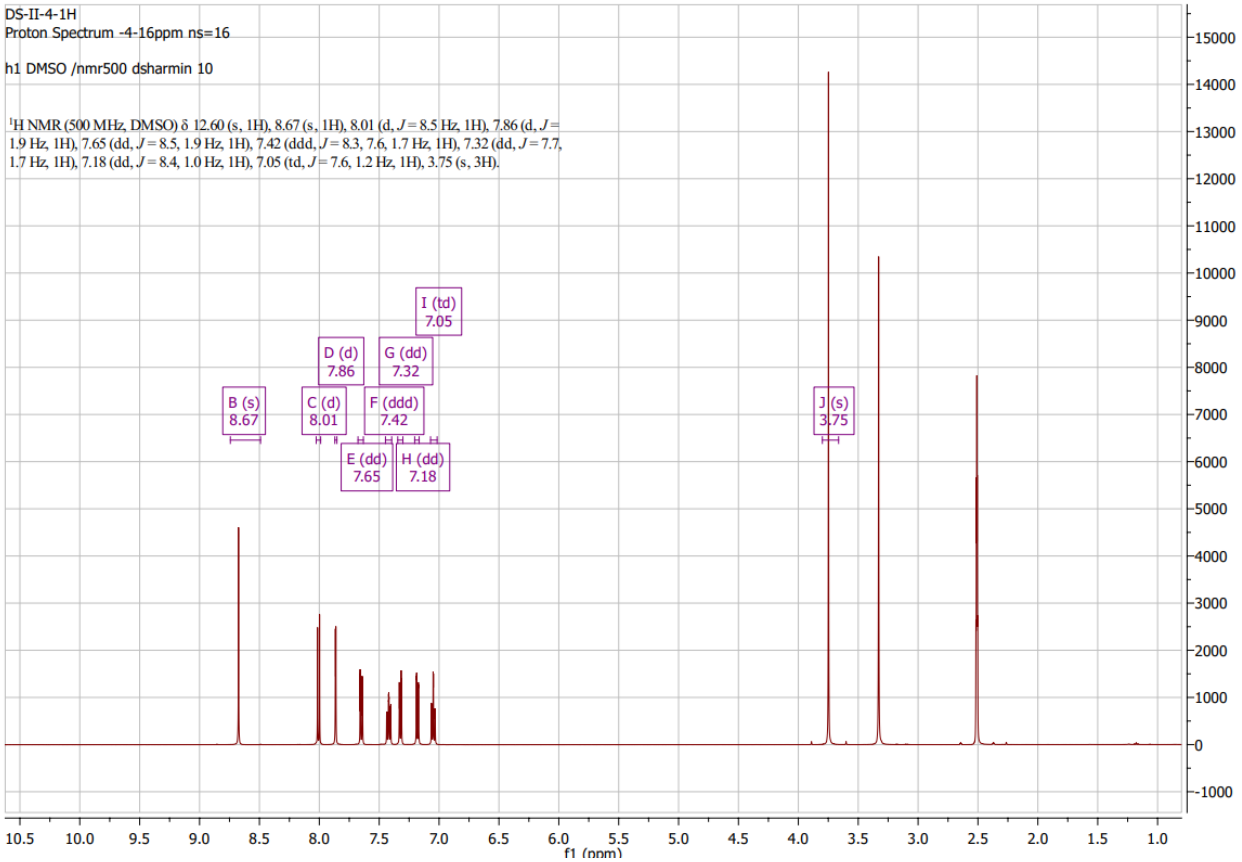
MM-I-03 (36)

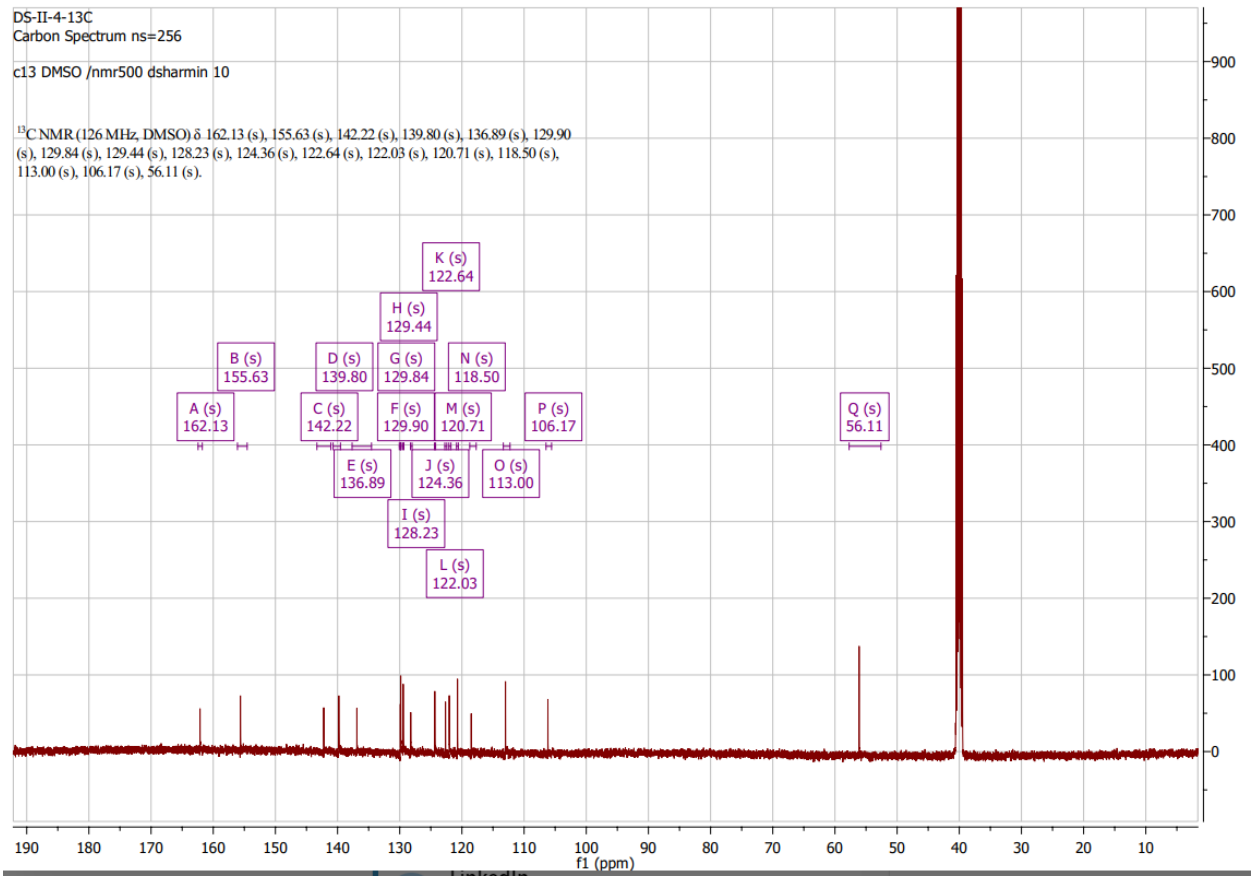


7-Bromo-2-(2-methoxyphenyl)-2,5-dihydro-3H-pyrazolo[4,3-c]quinolin-3-one (DS-II-04, 37)

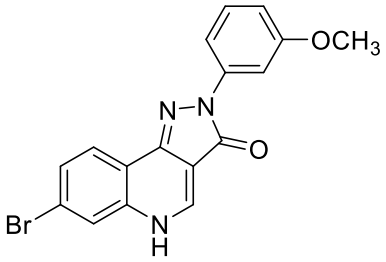


DS-II-04 (37)

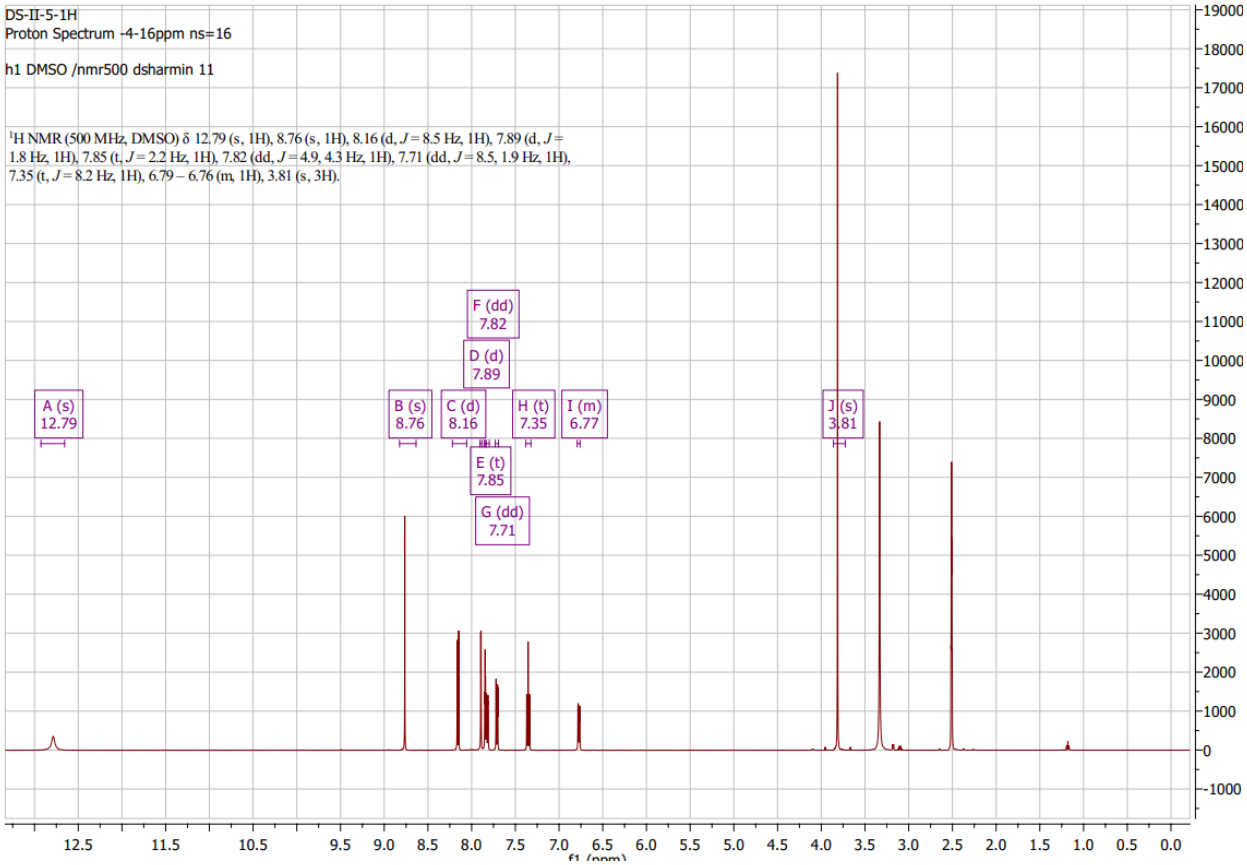


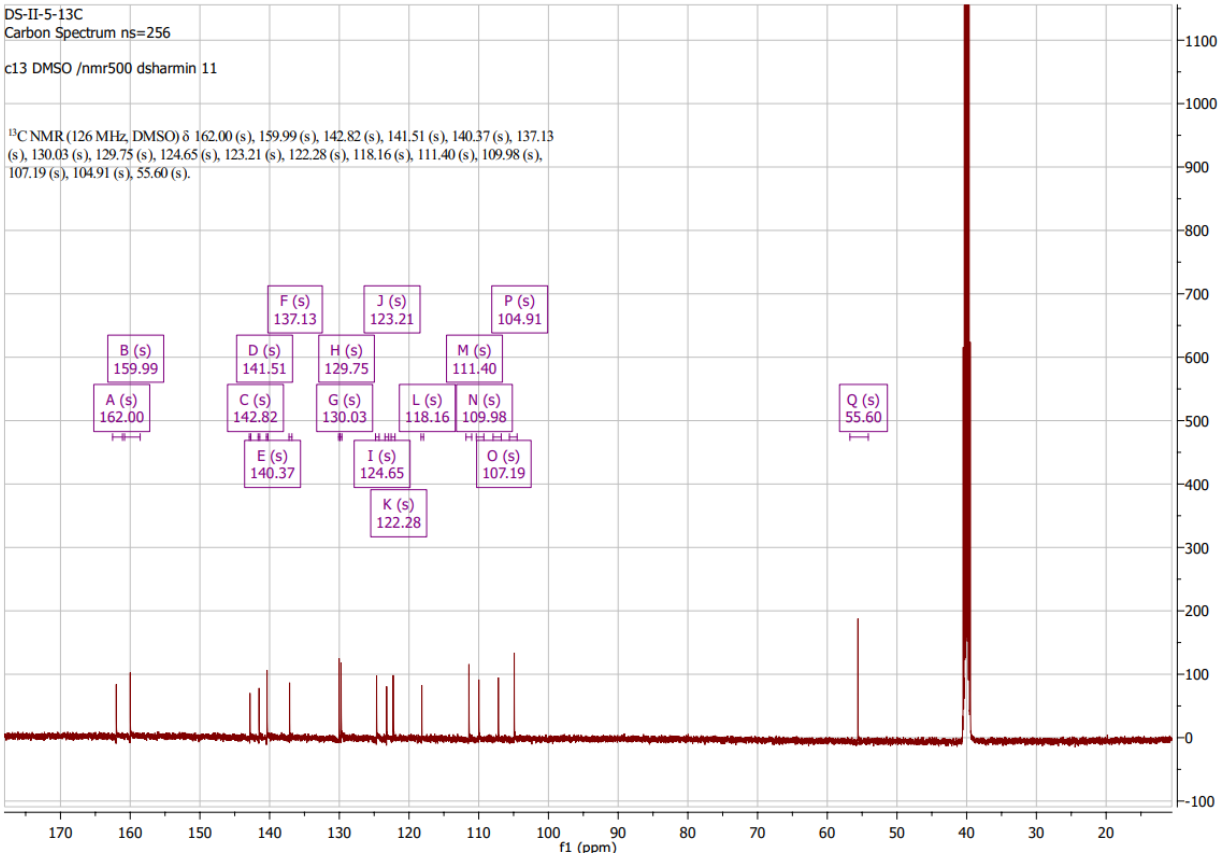

DS-II-4-13C
Carbon Spectrum ns=256
c13 DMSO /nmr500 dsharmin 10
^{13}C NMR (126 MHz, DMSO) δ 162.13 (s), 155.63 (s), 142.22 (s), 139.80 (s), 136.89 (s), 129.90 (s), 129.84 (s), 129.44 (s), 128.23 (s), 124.36 (s), 122.64 (s), 122.03 (s), 120.71 (s), 118.50 (s), 113.00 (s), 106.17 (s), 56.11 (s).
K (s) 122.64
H (s) 129.44
B (s) 155.63
D (s) 139.80
G (s) 129.84
N (s) 118.50
A (s) 162.13
C (s) 142.22
F (s) 129.90
M (s) 120.71
P (s) 106.17
Q (s) 56.11
E (s) 136.89
J (s) 124.36
O (s) 113.00
I (s) 128.23
L (s) 122.03
f1 (ppm)

7-Bromo-2-(3-methoxyphenyl)-2,5-dihydro-3H-pyrazolo[4,3-c]quinolin-3-onene (DS-II-05, 38)

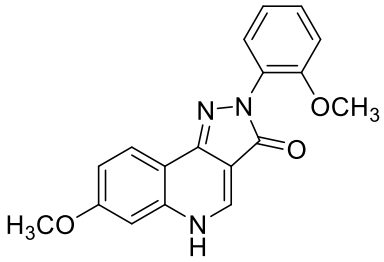


DS-II-05 (38)

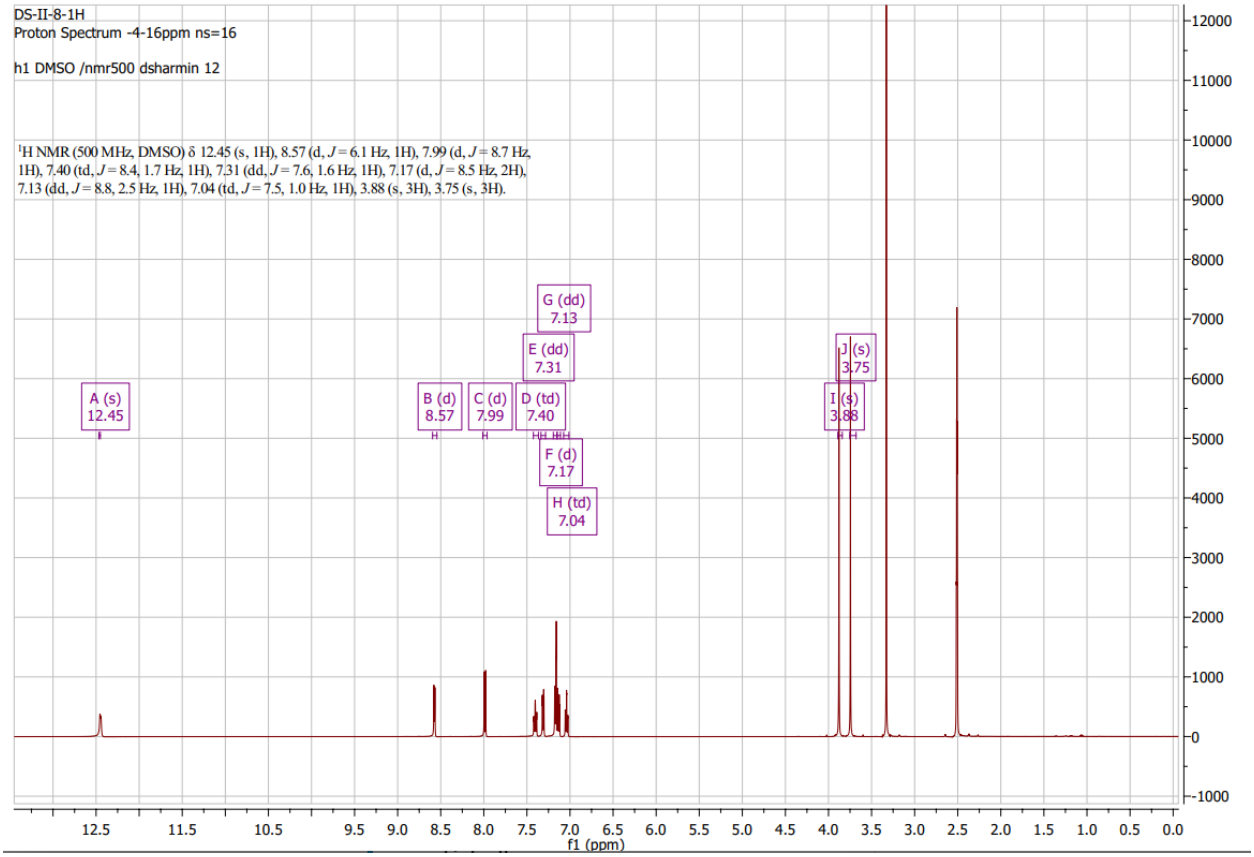


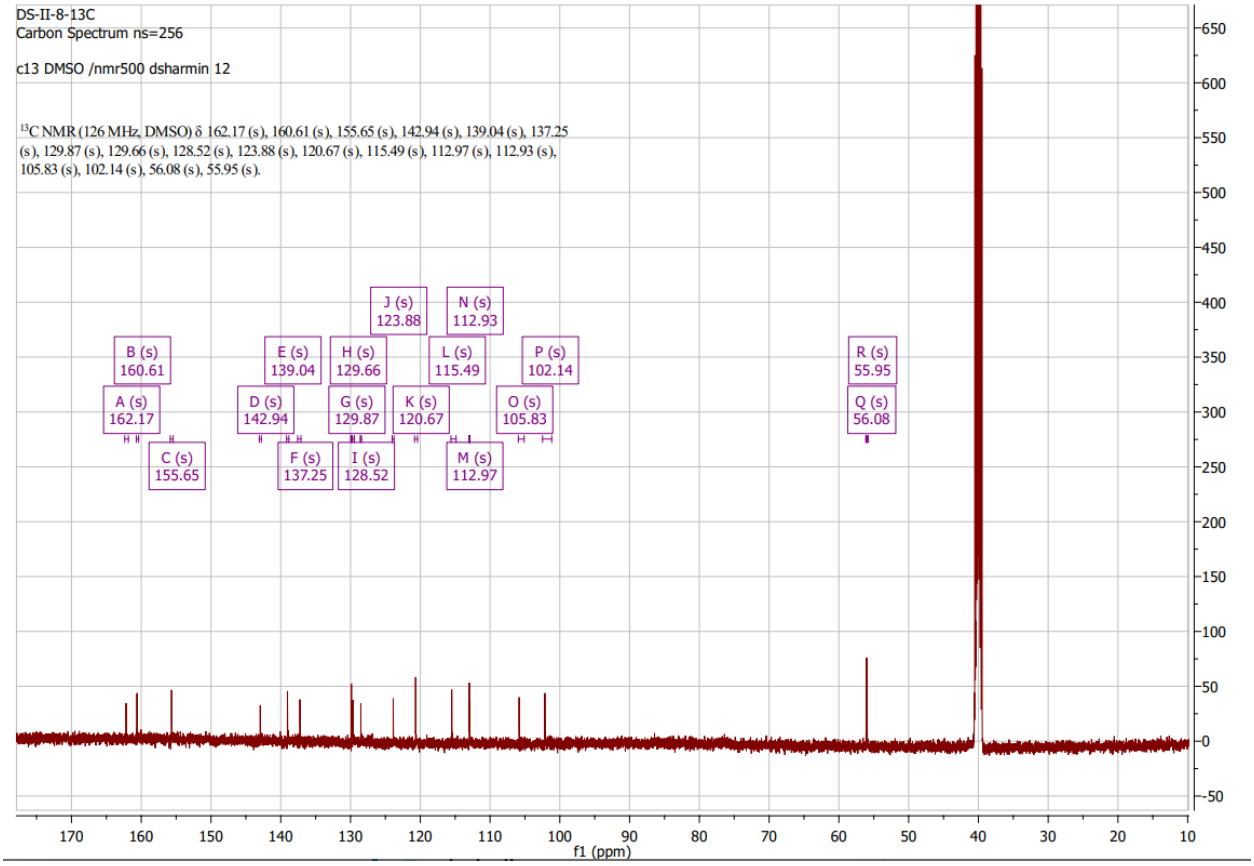

DS-II-5-13C
Carbon Spectrum ns=256
c13 DMSO /nmr500 dsharmin 11
13C NMR (126 MHz, DMSO) δ 162.00 (s), 159.99 (s), 142.82 (s), 141.51 (s), 140.37 (s), 137.13 (s), 130.03 (s), 129.75 (s), 124.65 (s), 123.21 (s), 122.28 (s), 118.16 (s), 111.40 (s), 109.98 (s), 107.19 (s), 104.91 (s), 55.60 (s).
F (s) 137.13
J (s) 123.21
P (s) 104.91
B (s) 159.99
D (s) 141.51
H (s) 129.75
M (s) 111.40
A (s) 162.00
C (s) 142.82
G (s) 130.03
L (s) 118.16
N (s) 109.98
Q (s) 55.60
E (s) 140.37
I (s) 124.65
O (s) 107.19
K (s) 122.28
f1 (ppm)

7-Methoxy-2-(2-methoxyphenyl)-2,5-dihydro-3H-pyrazolo[4,3-c]quinolin-3-one (DS-II-08, 39)



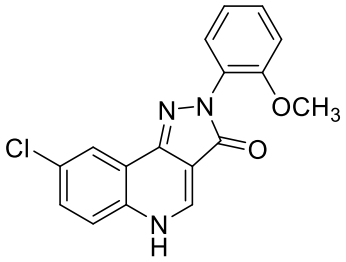
DS-II-08 (39)



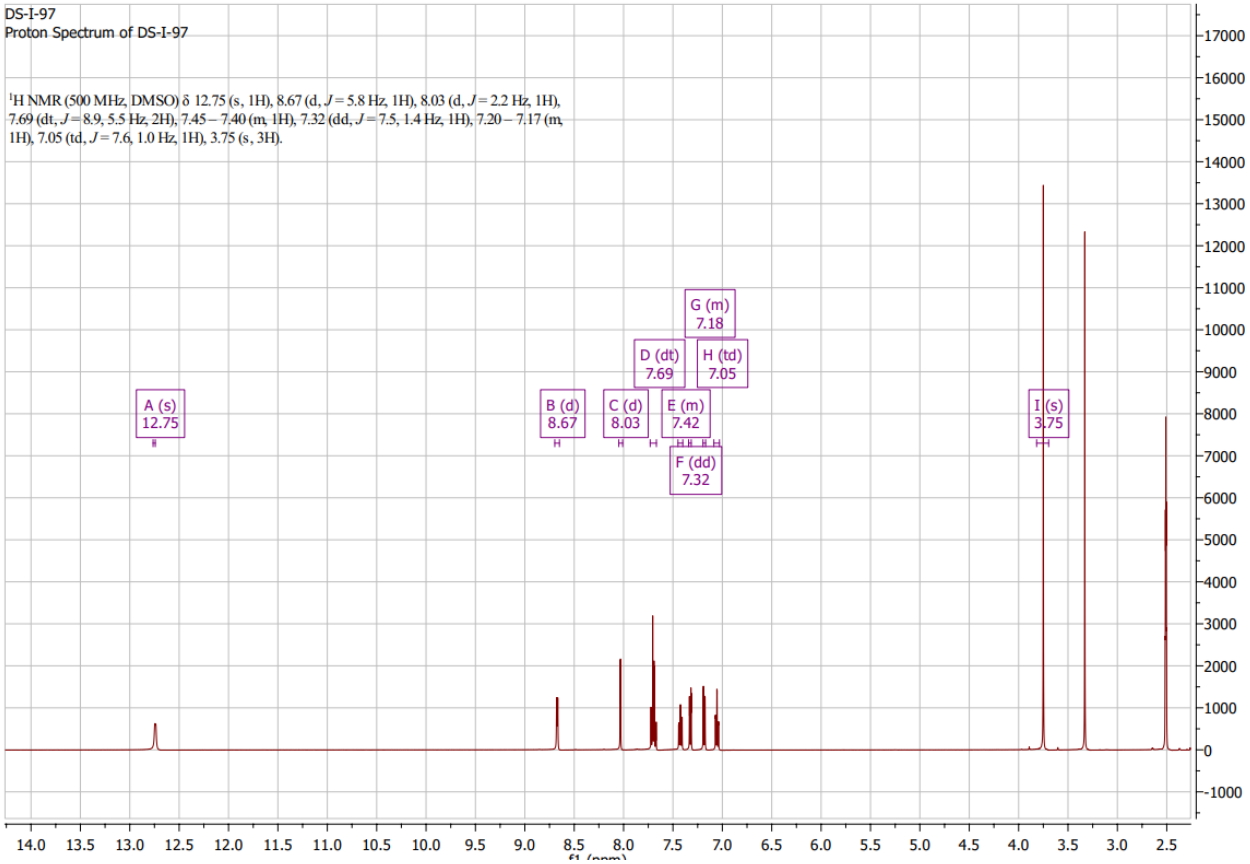

DS-II-8-13C
Carbon Spectrum ns=256
c13 DMSO /nmr500 dsharmin 12
13C NMR (126 MHz, DMSO) δ 162.17 (s), 160.61 (s), 155.65 (s), 142.94 (s), 139.04 (s), 137.25 (s), 129.87 (s), 129.66 (s), 128.52 (s), 123.88 (s), 120.67 (s), 115.49 (s), 112.97 (s), 112.93 (s), 105.83 (s), 102.14 (s), 56.08 (s), 55.95 (s).
J (s) 123.88
N (s) 112.93
B (s) 160.61
E (s) 139.04
H (s) 129.66
L (s) 115.49
P (s) 102.14
R (s) 55.95
A (s) 162.17
D (s) 142.94
G (s) 129.87
K (s) 120.67
O (s) 105.83
Q (s) 56.08
C (s) 155.65
F (s) 137.25
I (s) 128.52
M (s) 112.97
f1 (ppm)

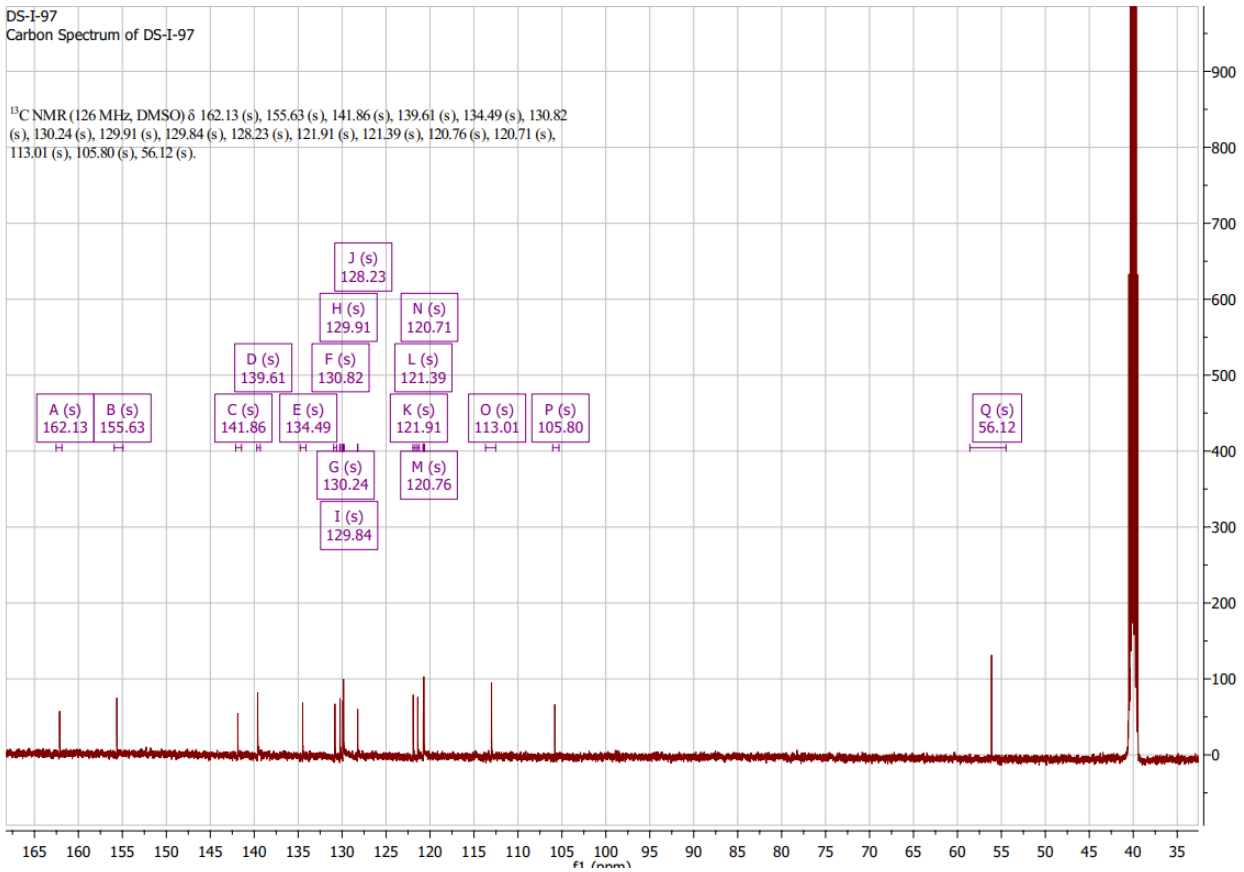
8-Chloro-2-(2-methoxyphenyl)-2,5-dihydro-3H-pyrazolo[4,3-c]quinolin-3-one

(DS-I-97, 41)

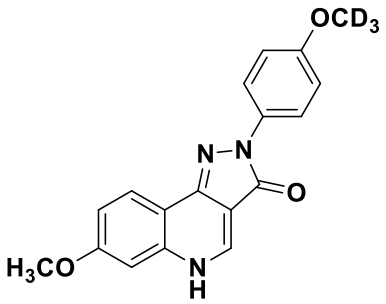


DS-I-97 (41)

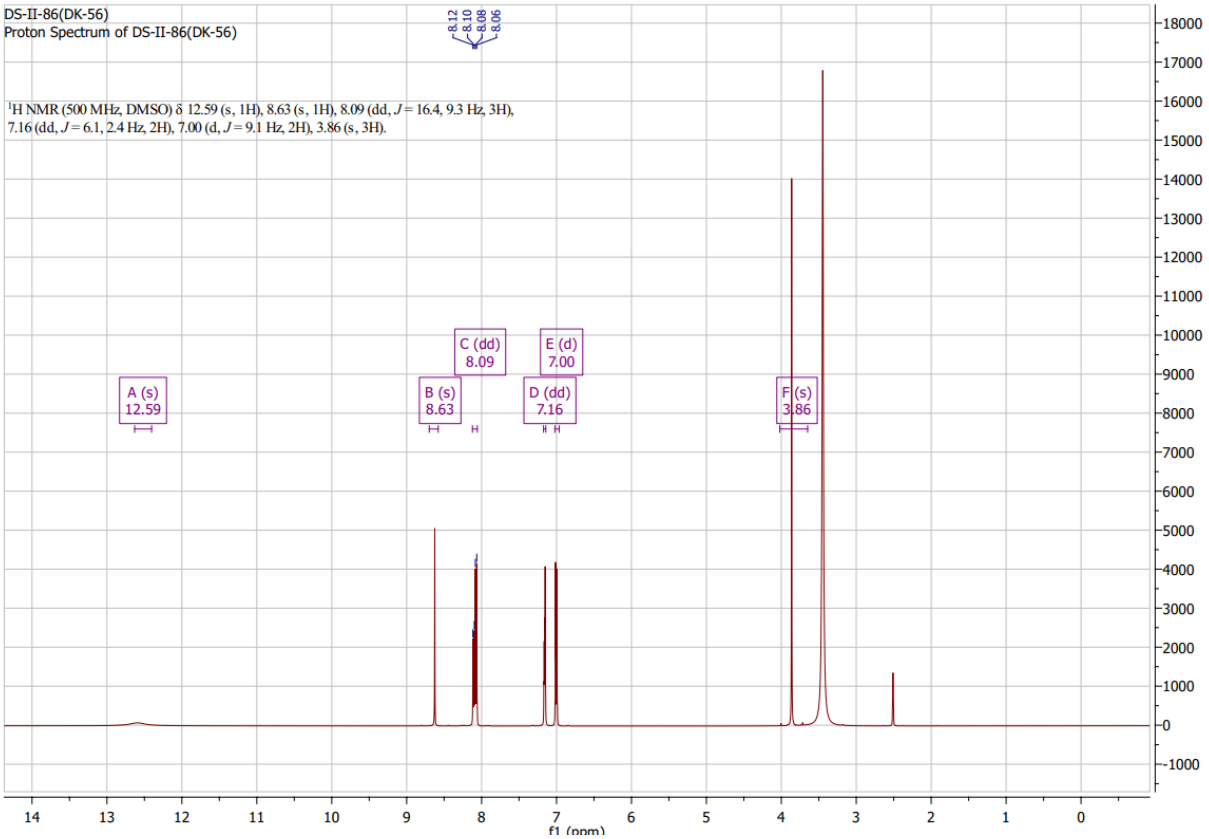


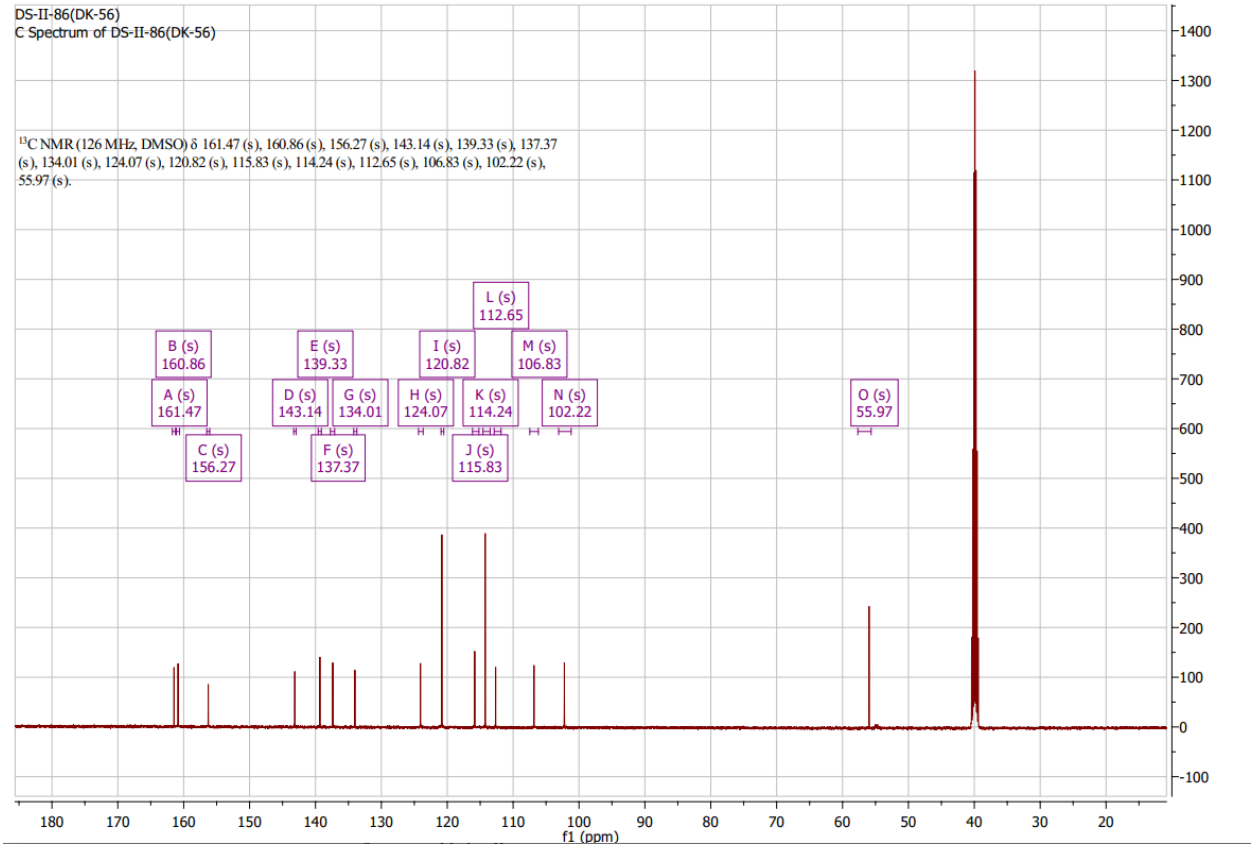

DS-I-97
Carbon Spectrum of DS-I-97
^{13}C NMR (126 MHz, DMSO) δ 162.13 (s), 155.63 (s), 141.86 (s), 139.61 (s), 134.49 (s), 130.82 (s), 130.24 (s), 129.91 (s), 129.84 (s), 128.23 (s), 121.91 (s), 121.39 (s), 120.76 (s), 120.71 (s), 113.01 (s), 105.80 (s), 56.12 (s).
J (s) 128.23
H (s) 129.91
N (s) 120.71
D (s) 139.61
F (s) 130.82
L (s) 121.39
A (s) 162.13
B (s) 155.63
C (s) 141.86
E (s) 134.49
K (s) 121.91
O (s) 113.01
P (s) 105.80
Q (s) 56.12
G (s) 130.24
M (s) 120.76
I (s) 129.84
f1 (ppm)

7-Methoxy-2-(4-methoxy-d3-phenyl)-2,5-dihydro-3H-pyrazolo[4,3-c]quinoline-3-one (DK-I-56-1, 44)

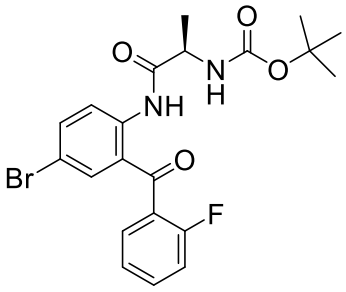


DK-I-56-1 (44)

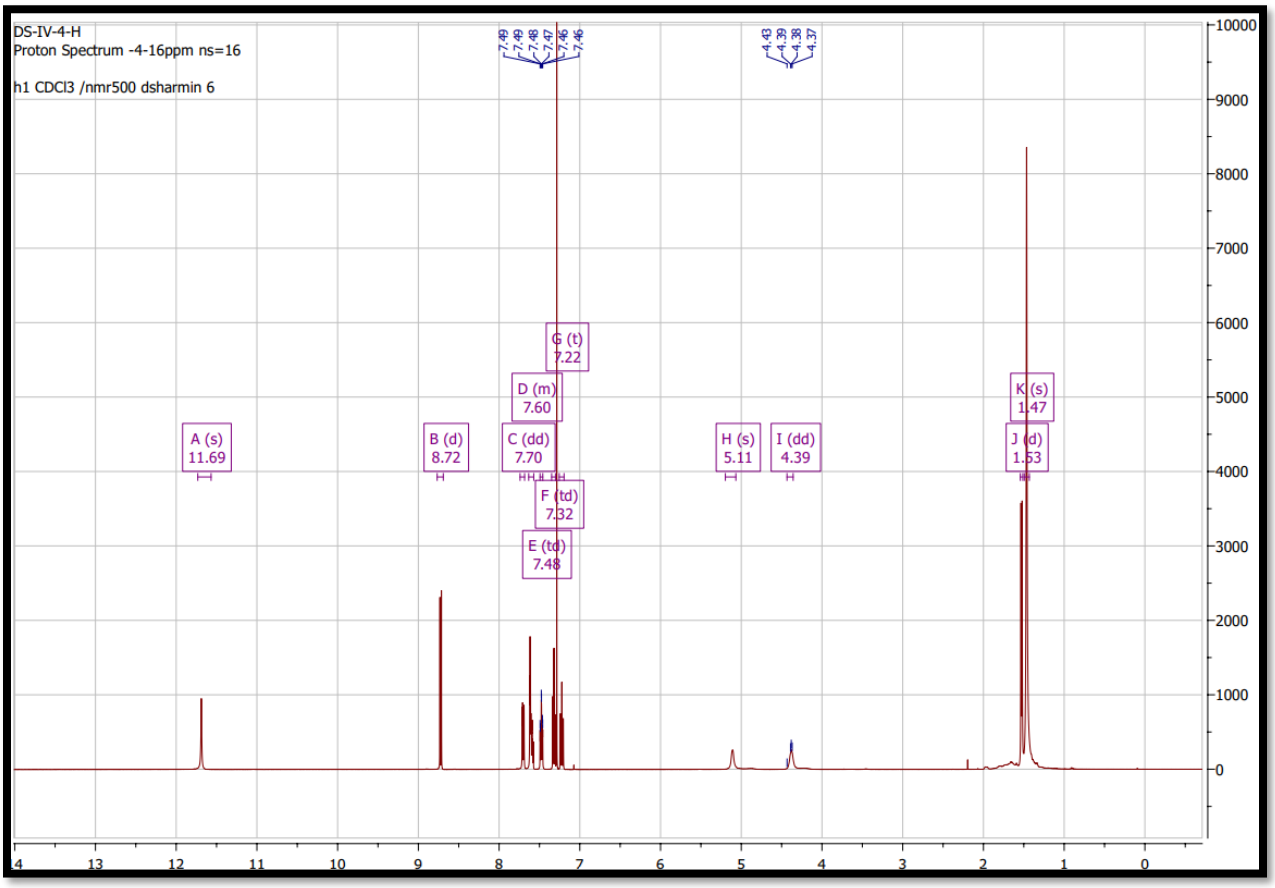


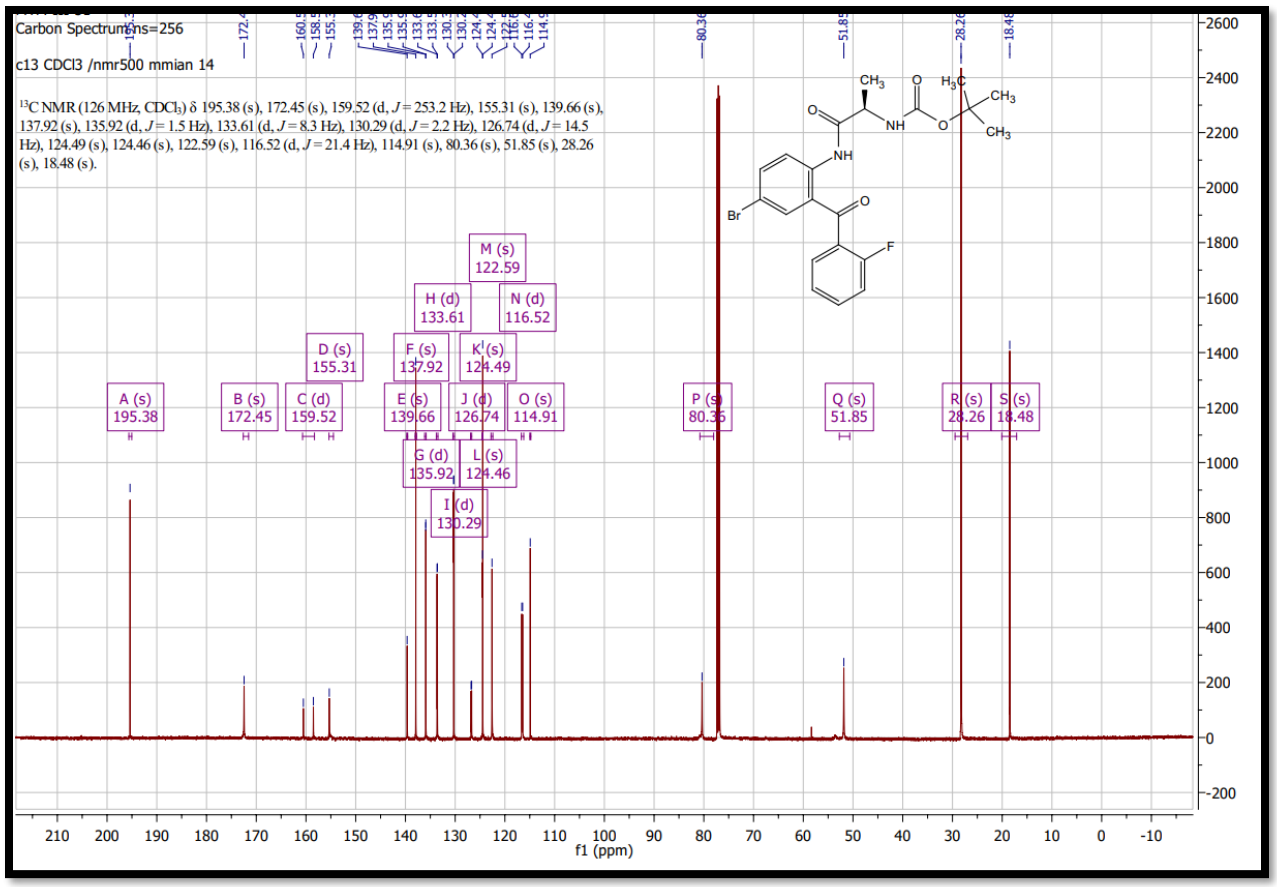

DS-II-86(DK-56)
C Spectrum of DS-II-86(DK-56)
13C NMR (126 MHz, DMSO) δ 161.47 (s), 160.86 (s), 156.27 (s), 143.14 (s), 139.33 (s), 137.37 (s), 134.01 (s), 124.07 (s), 120.82 (s), 115.83 (s), 114.24 (s), 112.65 (s), 106.83 (s), 102.22 (s), 55.97 (s).
L (s) 112.65
B (s) 160.86
E (s) 139.33
I (s) 120.82
M (s) 106.83
A (s) 161.47
D (s) 143.14
G (s) 134.01
H (s) 124.07
K (s) 114.24
N (s) 102.22
O (s) 55.97
C (s) 156.27
F (s) 137.37
J (s) 115.83
f1 (ppm)

Tert-Butyl-(_R_)-(1-((4-bromo-2-(2-fluorobenzoyl)phenyl)amino)-1-oxopropan-2-yl) carbamate (3)

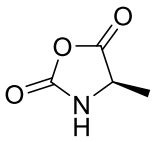


3

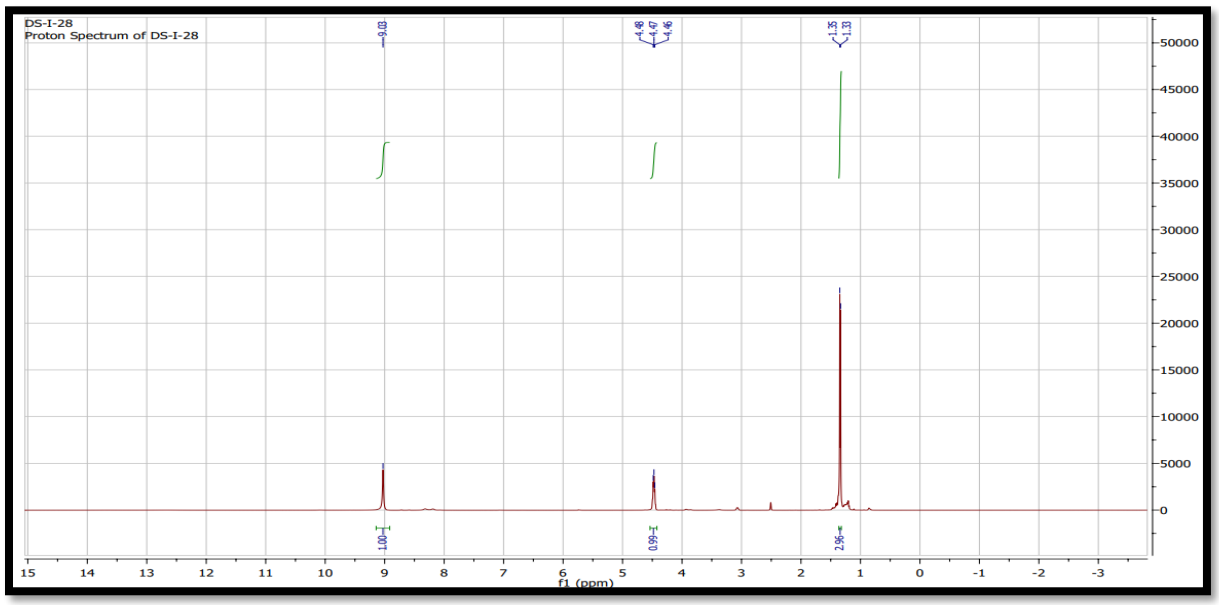


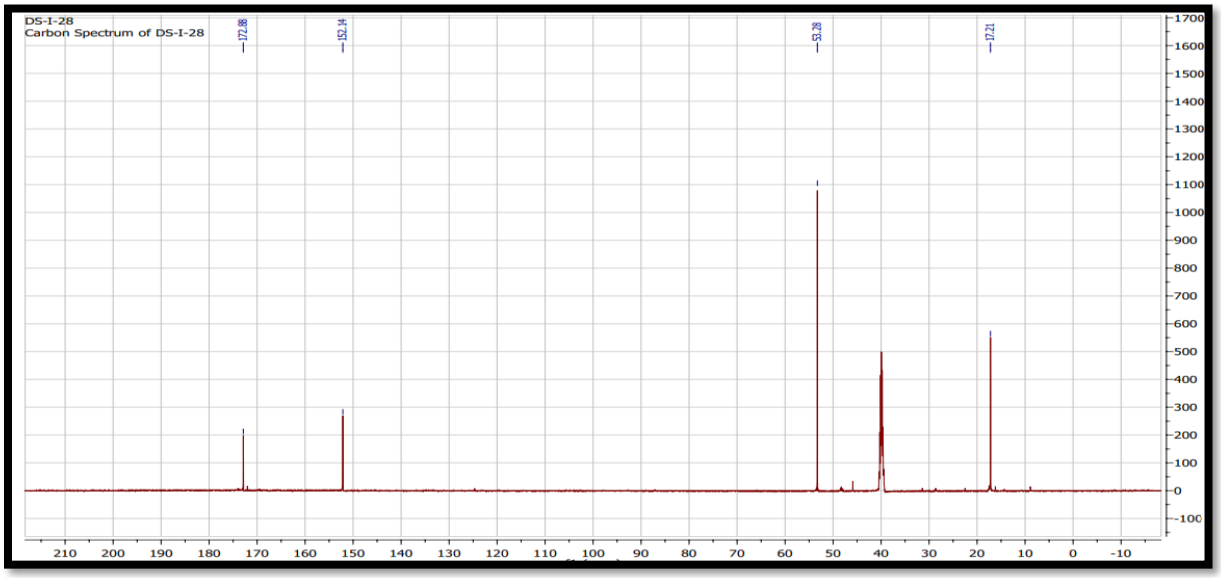

Carbon Spectrum ns=256
c13 CDCl3 /nmr500 mmian 14
13C NMR (126 MHz, CDCl3) δ 195.38 (s), 172.45 (s), 159.52 (d, J = 253.2 Hz), 155.31 (s), 139.66 (s), 137.92 (s), 135.92 (d, J = 1.5 Hz), 133.61 (d, J = 8.3 Hz), 130.29 (d, J = 2.2 Hz), 126.74 (d, J = 14.5 Hz), 124.49 (s), 124.46 (s), 122.59 (s), 116.52 (d, J = 21.4 Hz), 114.91 (s), 80.36 (s), 51.85 (s), 28.26 (s), 18.48 (s).
A (s) 195.38
B (s) 172.45
C (d) 159.52
D (s) 155.31
E (s) 139.66
F (s) 137.92
G (d) 135.92
H (d) 133.61
I (d) 130.29
J (d) 126.74
K (s) 124.49
L (s) 124.46
M (s) 122.59
N (d) 116.52
O (s) 114.91
P (s) 80.36
Q (s) 51.85
R (s) 28.26
S (s) 18.48
f1 (ppm)

N-Carboxy-D-Alanine Anhydride (15)

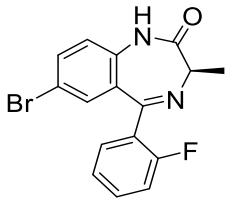


15

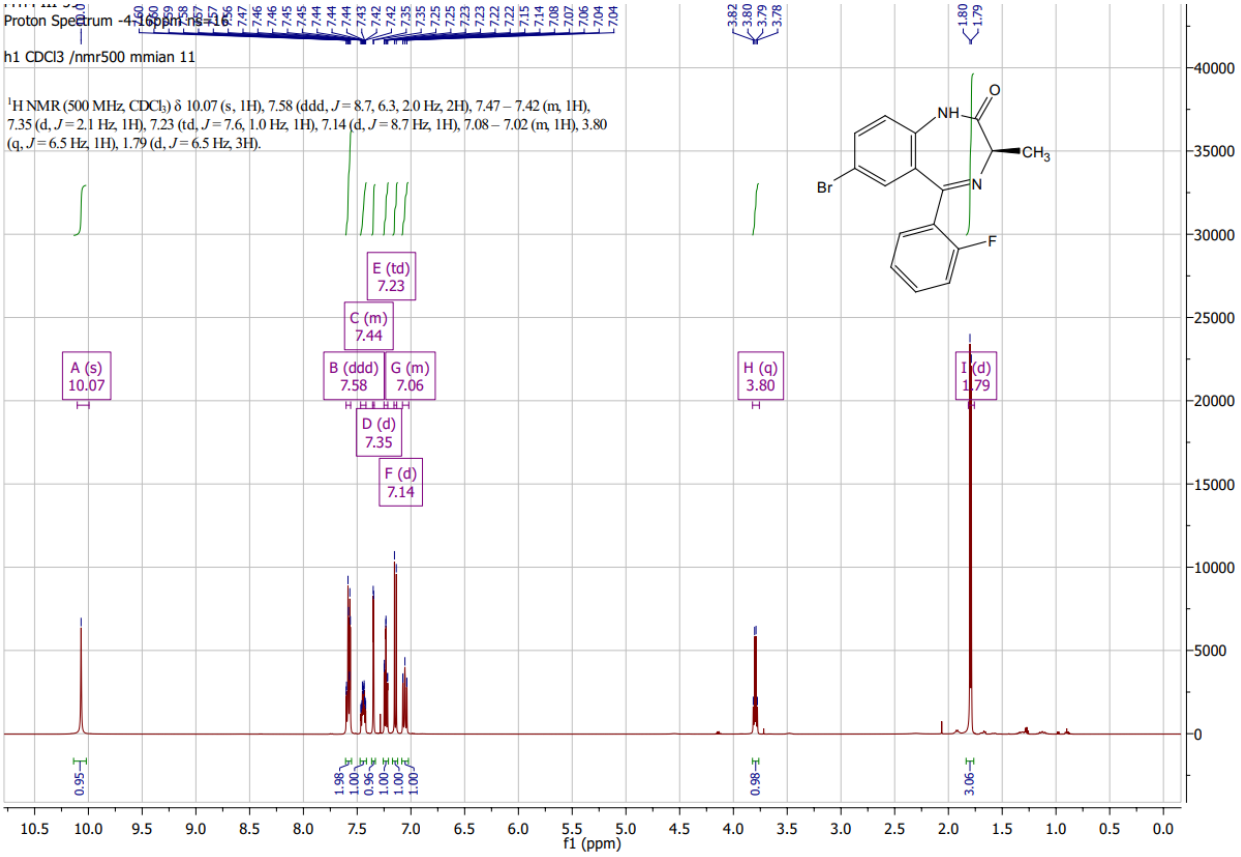


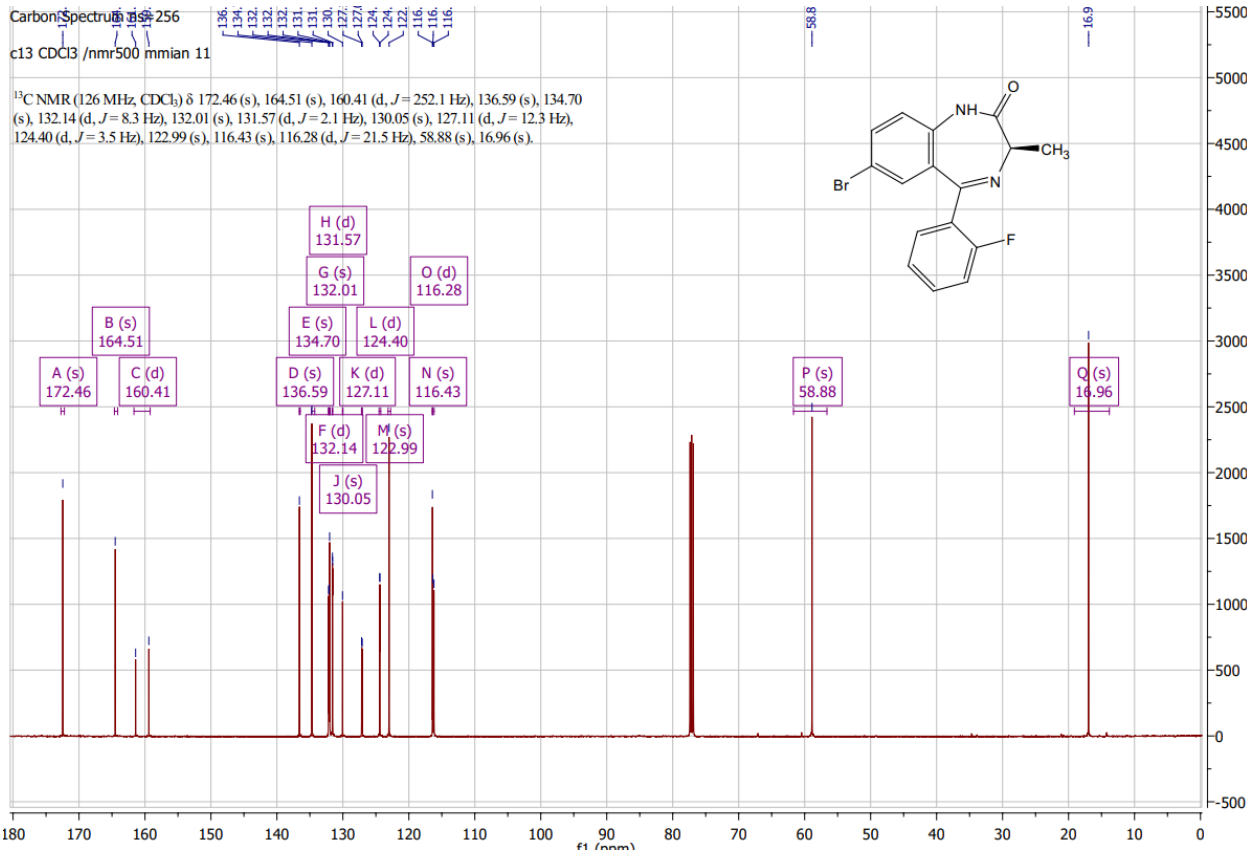


(*R*)-7-Bromo-5-(2-fluorophenyl)-3-methyl-1,3-dihydro-2*H*-benzo[*e*][1,4]diazepin-2-one (87)

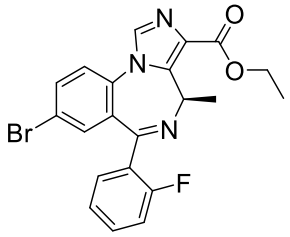


87

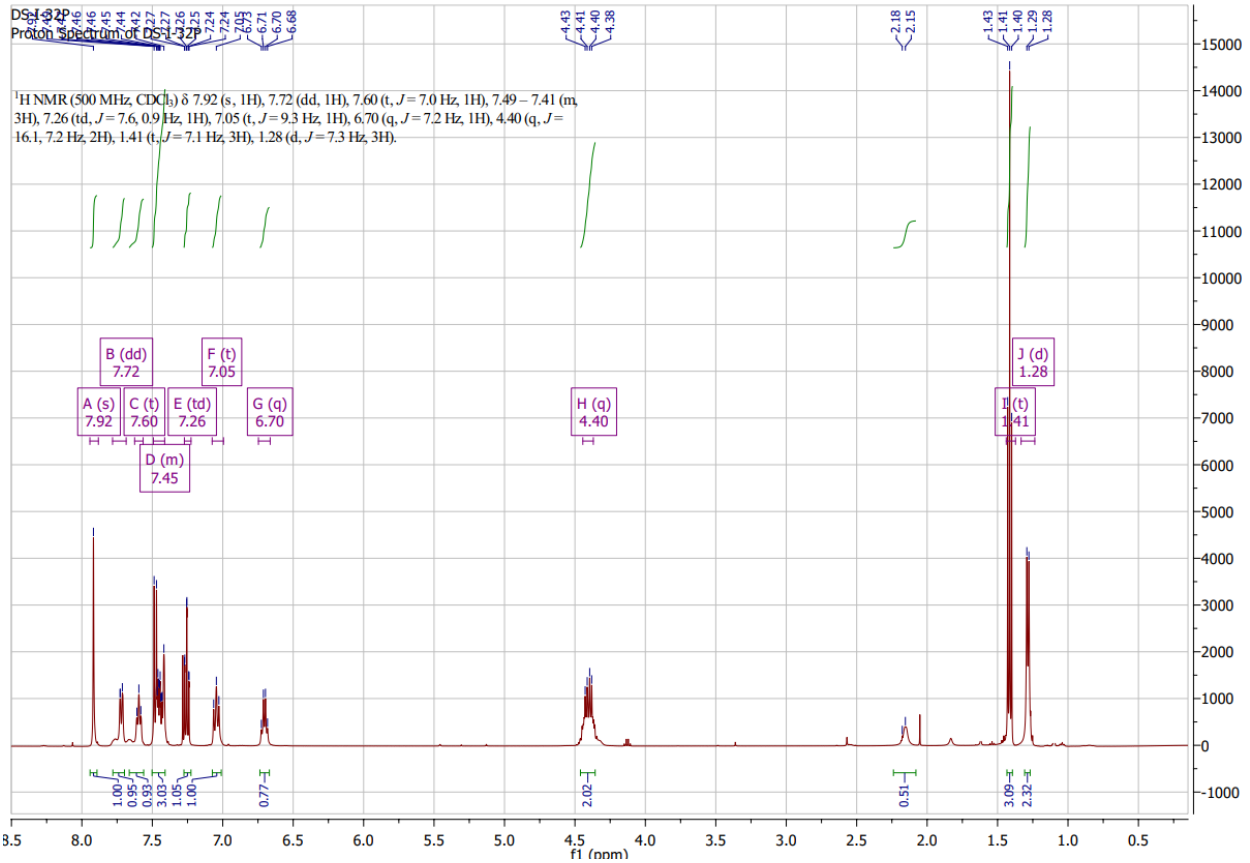


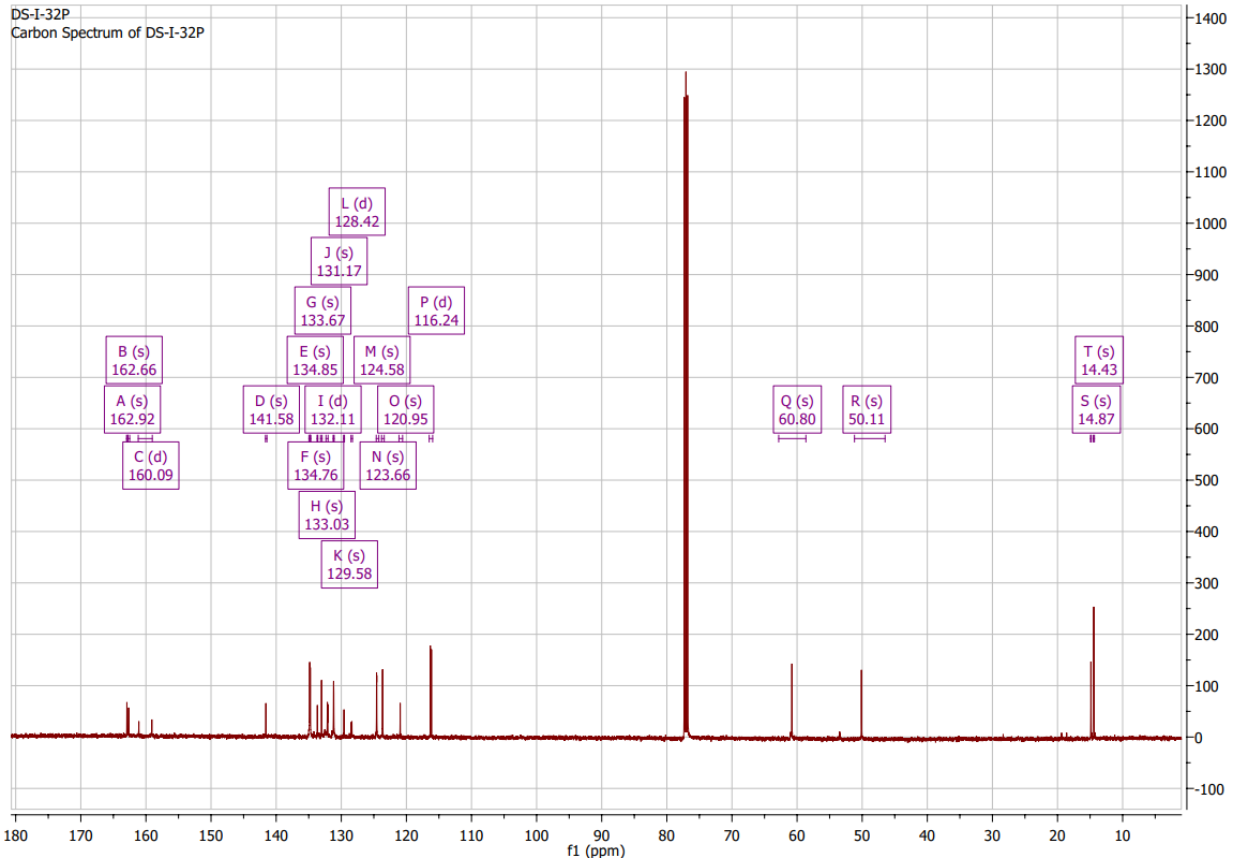

Carbon Spectrum bs 256
c13 CDCl3 /nmr500 mmian 11
13C NMR (126 MHz, CDCl3) δ 172.46 (s), 164.51 (s), 160.41 (d, J = 252.1 Hz), 136.59 (s), 134.70 (s), 132.14 (d, J = 8.3 Hz), 132.01 (s), 131.57 (d, J = 2.1 Hz), 130.05 (s), 127.11 (d, J = 12.3 Hz), 124.40 (d, J = 3.5 Hz), 122.99 (s), 116.43 (s), 116.28 (d, J = 21.5 Hz), 58.88 (s), 16.96 (s).
A (s) 172.46
B (s) 164.51
C (d) 160.41
D (s) 136.59
E (s) 134.70
F (d) 132.14
G (s) 132.01
H (d) 131.57
J (s) 130.05
K (d) 127.11
L (d) 124.40
M (s) 122.99
N (s) 116.43
O (d) 116.28
P (s) 58.88
Q (s) 16.96
NH
O
CH3
N
Br
F
f1 (ppm)

Ethyl (*R*)-8-bromo-6-(2-fluorophenyl)-4-methyl-4*H*-benzo[*f*]imidazo[1,5-*a*][1,4] diazepine-3-carboxylate (5)

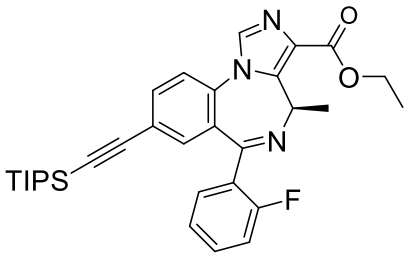


5

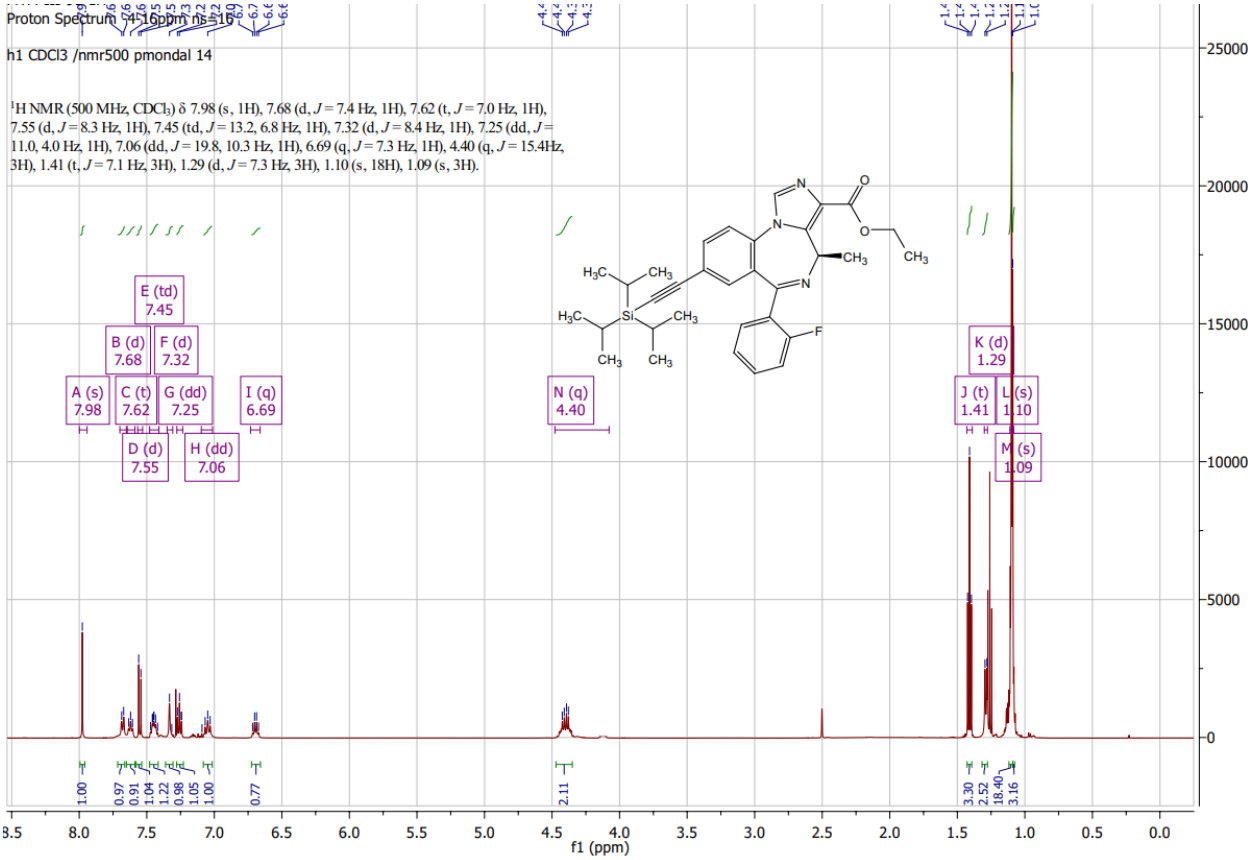


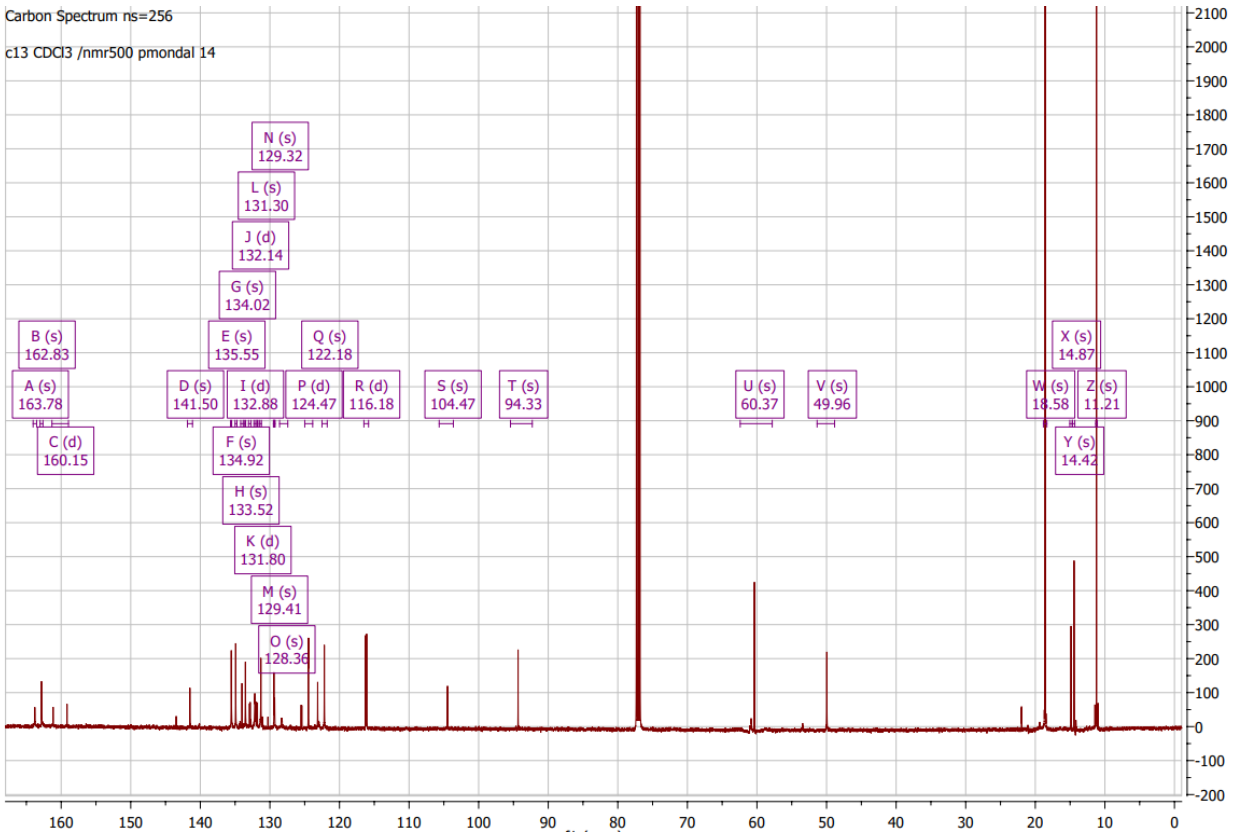

DS-I-32P
Carbon Spectrum of DS-I-32P
L (d)
128.42
J (s)
131.17
G (s)
133.67
P (d)
116.24
B (s)
162.66
E (s)
134.85
M (s)
124.58
A (s)
162.92
D (s)
141.58
I (d)
132.11
O (s)
120.95
C (d)
160.09
F (s)
134.76
N (s)
123.66
H (s)
133.03
K (s)
129.58
Q (s)
60.80
R (s)
50.11
T (s)
14.43
S (s)
14.87
f1 (ppm)

Ethyl (*R*)-6-(2-fluorophenyl)-4-methyl-8-((triisopropylsilyl)ethynyl)-4*H*-benzo[*f*] imidazo[1,5-*a*][1,4]diazepine-3-carboxylate (6)

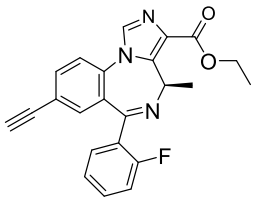


6

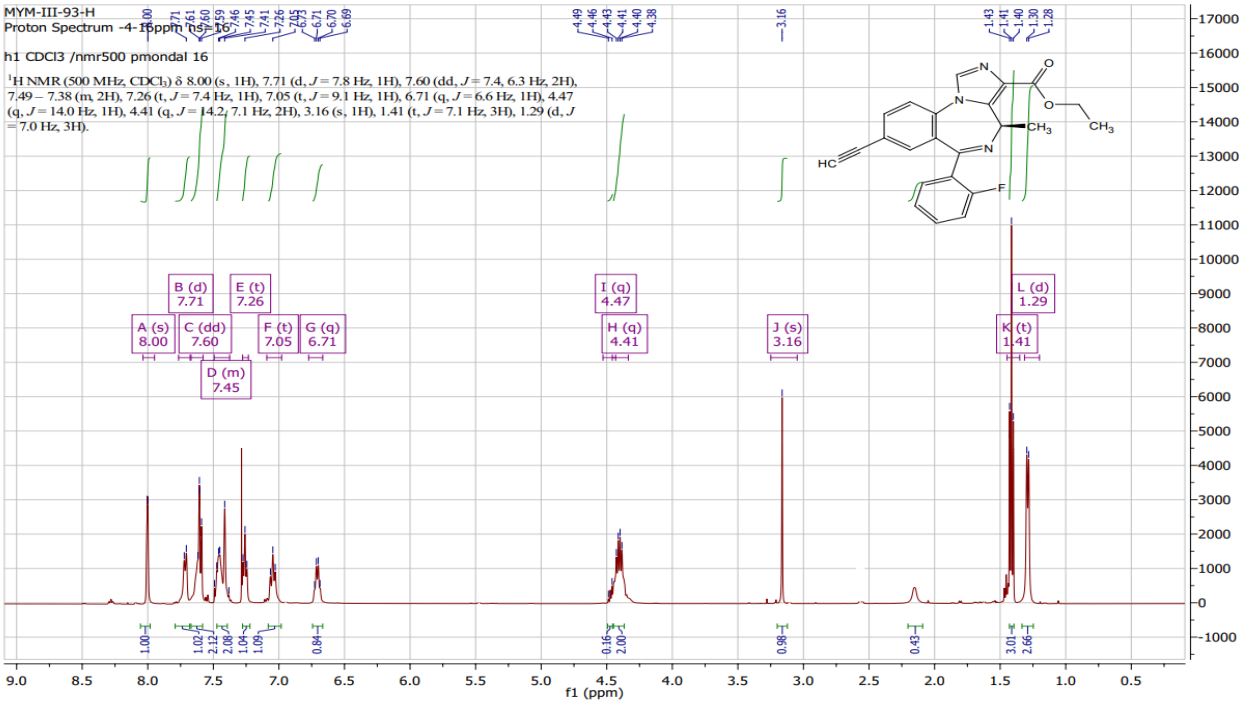


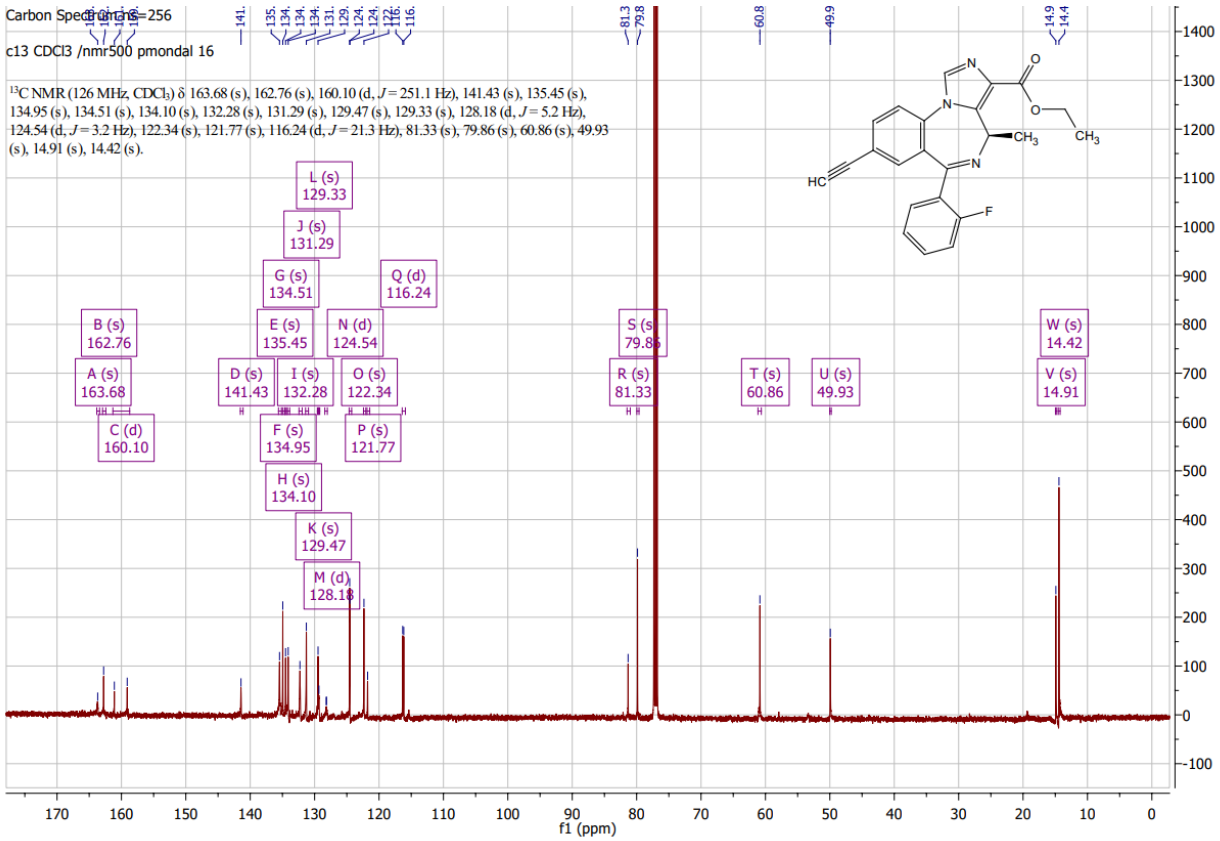

Carbon Spectrum ns=256
c13 CDCl3 /nmr500 pmondal 14
N (s) 129.32
L (s) 131.30
J (d) 132.14
G (s) 134.02
B (s) 162.83
E (s) 135.55
Q (s) 122.18
X (s) 14.87
A (s) 163.78
D (s) 141.50
I (d) 132.88
P (d) 124.47
R (d) 116.18
S (s) 104.47
T (s) 94.33
U (s) 60.37
V (s) 49.96
W (s) 18.58
Z (s) 11.21
C (d) 160.15
F (s) 134.92
Y (s) 14.42
H (s) 133.52
K (d) 131.80
M (s) 129.41
O (s) 128.36

Ethyl (*R*)-8-ethynyl-6-(2-fluorophenyl)-4-methyl-4*H*-benzo[*f*]imidazo[1,5-*a*][1,4] diazepine-3-carboxylate (SH-053-2'F-*R*-CH_3, 7)

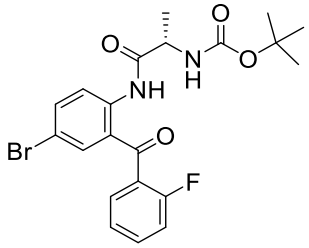


7

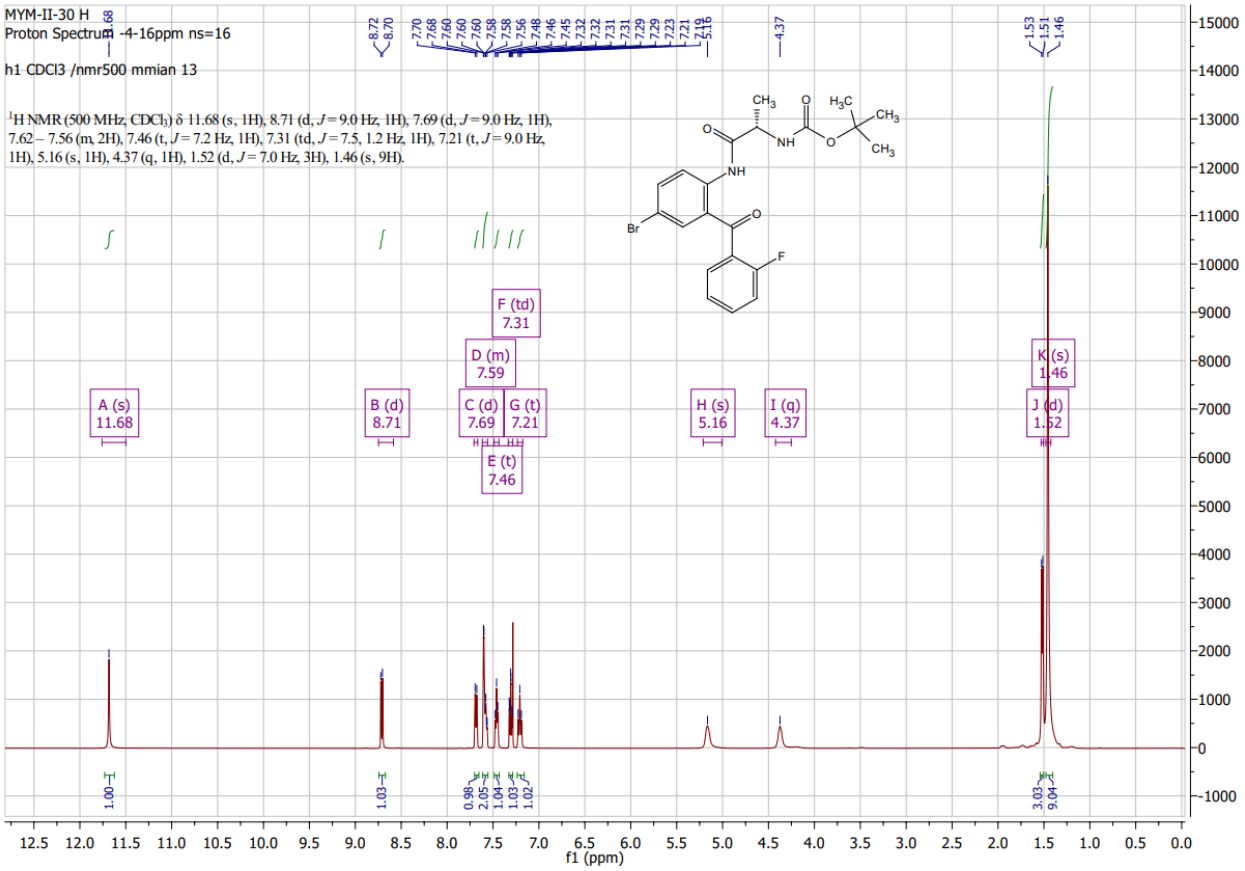


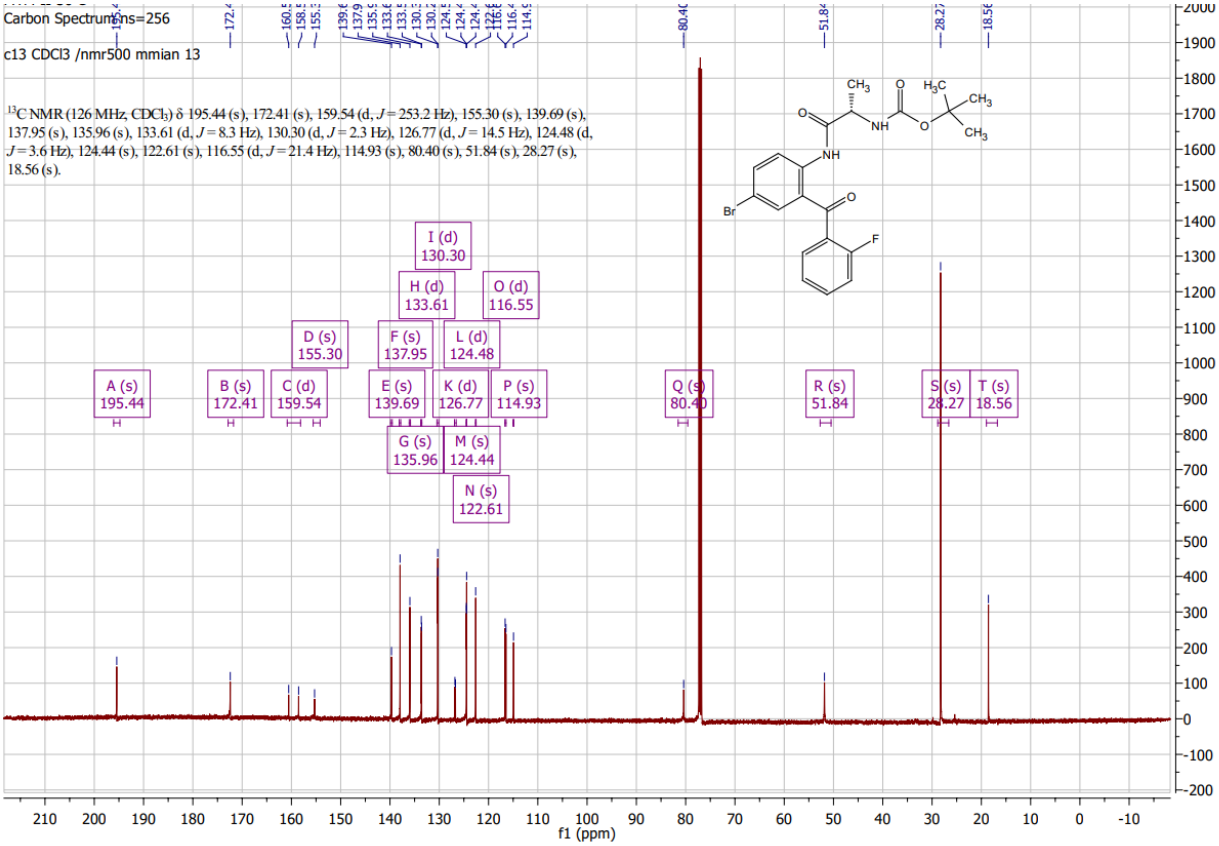

Carbon Spectrum Scans=256
c13 CDCl3 /nmr500 pmondal 16
^{13}C NMR (126 MHz, $CDCl_3$) δ 163.68 (s), 162.76 (s), 160.10 (d, J = 251.1 Hz), 141.43 (s), 135.45 (s), 134.95 (s), 134.51 (s), 134.10 (s), 132.28 (s), 131.29 (s), 129.47 (s), 129.33 (s), 128.18 (d, J = 5.2 Hz), 124.54 (d, J = 3.2 Hz), 122.34 (s), 121.77 (s), 116.24 (d, J = 21.3 Hz), 81.33 (s), 79.86 (s), 60.86 (s), 49.93 (s), 14.91 (s), 14.42 (s).
L (s) 129.33
J (s) 131.29
G (s) 134.51
Q (d) 116.24
B (s) 162.76
E (s) 135.45
N (d) 124.54
S (s) 79.86
W (s) 14.42
A (s) 163.68
D (s) 141.43
I (s) 132.28
O (s) 122.34
R (s) 81.33
T (s) 60.86
U (s) 49.93
V (s) 14.91
C (d) 160.10
F (s) 134.95
P (s) 121.77
H (s) 134.10
K (s) 129.47
M (d) 128.18
f1 (ppm)

Tert-Butyl (_S_)-(1-((4-bromo-2-(2-fluorobenzoyl)phenyl)amino)-1-oxopropan-2-yl) carbamate (9)

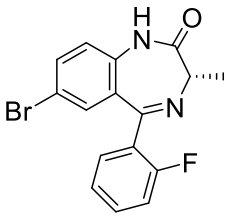


9

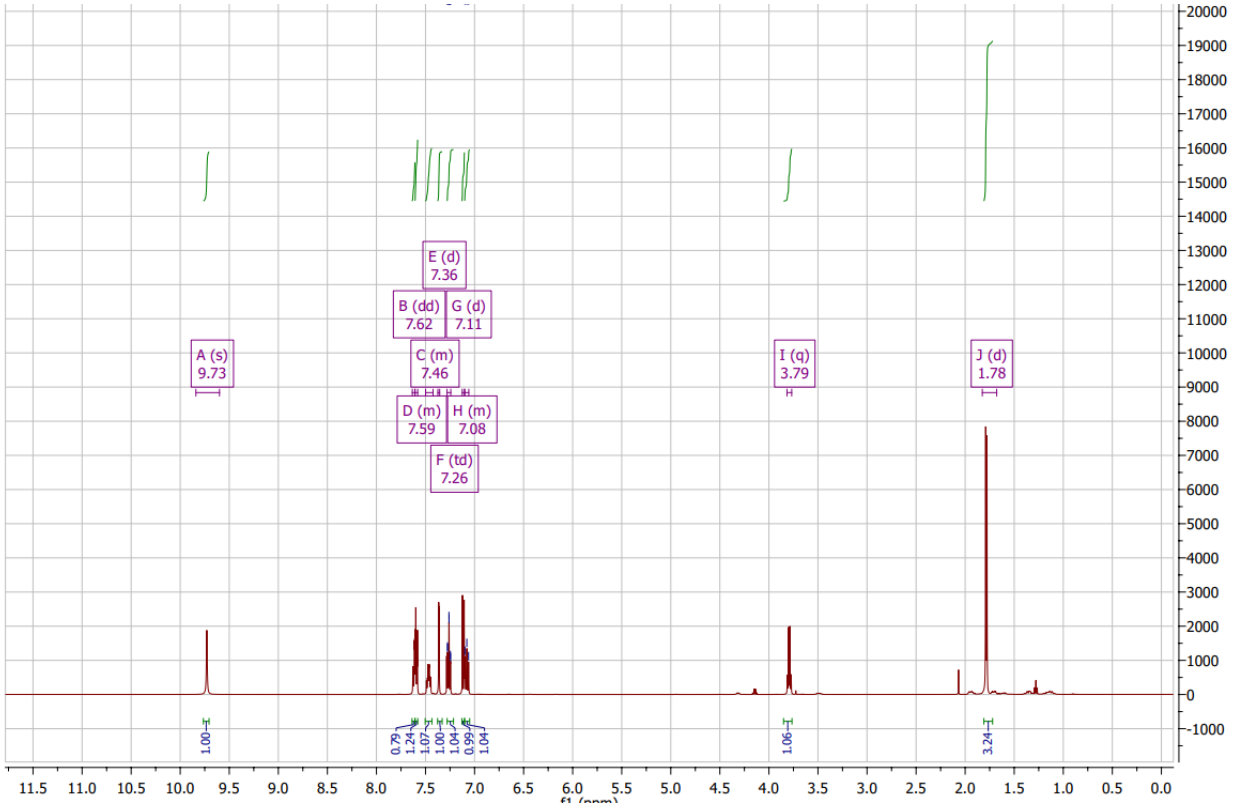


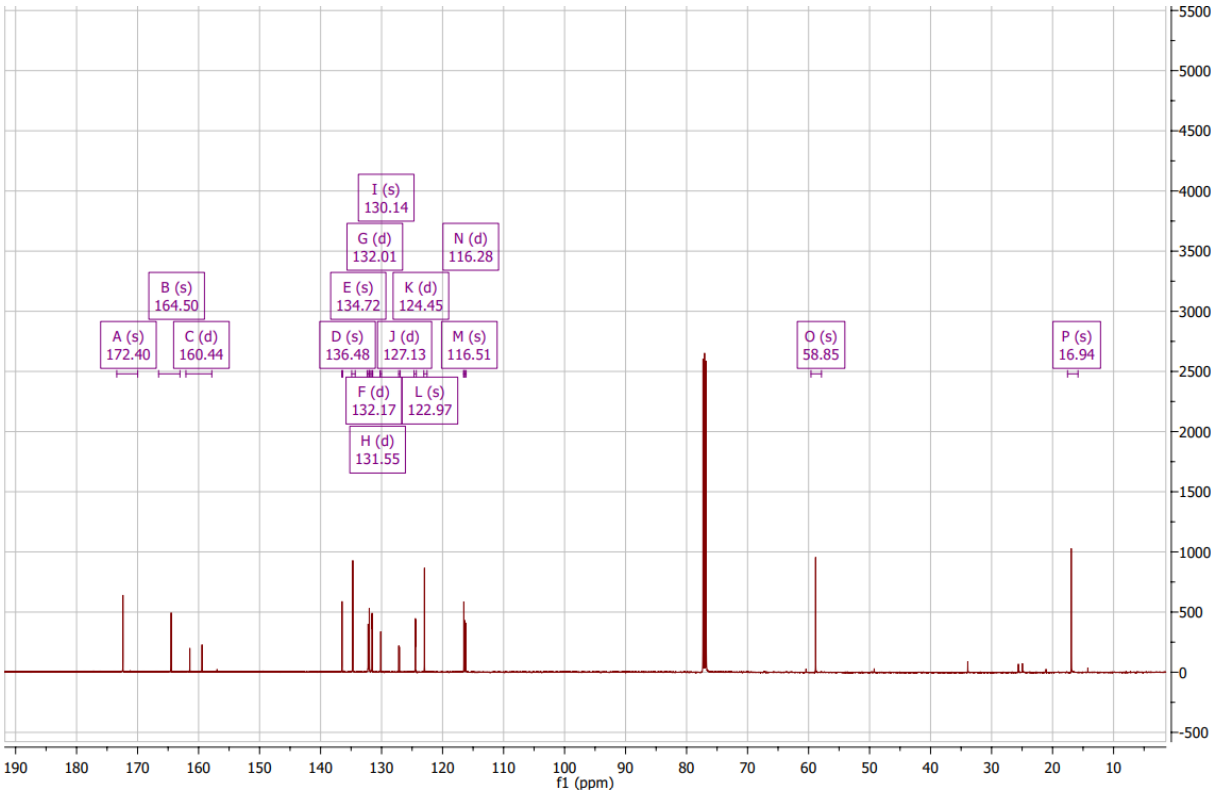

Carbon Spectrum ns=256
c13 CDCl3 /nmr500 mmian 13
^{13}C NMR (126 MHz, $CDCl_3$) δ 195.44 (s), 172.41 (s), 159.54 (d, J = 253.2 Hz), 155.30 (s), 139.69 (s), 137.95 (s), 135.96 (s), 133.61 (d, J = 8.3 Hz), 130.30 (d, J = 2.3 Hz), 126.77 (d, J = 14.5 Hz), 124.48 (d, J = 3.6 Hz), 124.44 (s), 122.61 (s), 116.55 (d, J = 21.4 Hz), 114.93 (s), 80.40 (s), 51.84 (s), 28.27 (s), 18.56 (s).
A (s) 195.44
B (s) 172.41
C (d) 159.54
D (s) 155.30
E (s) 139.69
F (s) 137.95
G (s) 135.96
H (d) 133.61
I (d) 130.30
K (d) 126.77
L (d) 124.48
M (s) 124.44
N (s) 122.61
O (d) 116.55
P (s) 114.93
Q (s) 80.40
R (s) 51.84
S (s) 28.27
T (s) 18.56
f1 (ppm)

(*S*)-7-Bromo-5-(2-fluorophenyl)-3-methyl-1,3-dihydro-2*H*-benzo[*e*][1,4]diazepin-2-one (10)

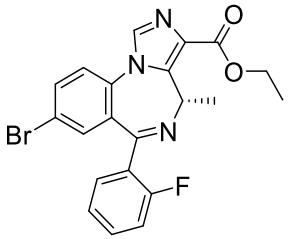


10

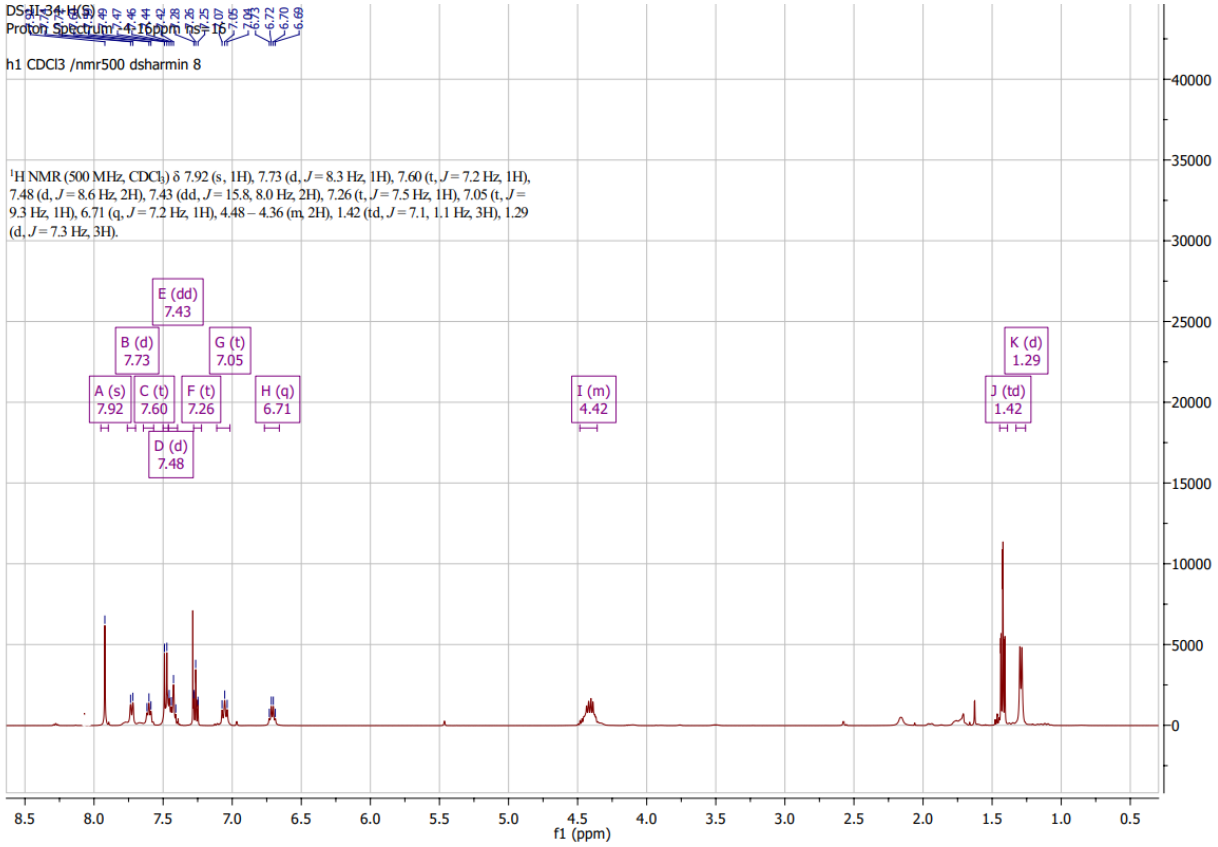


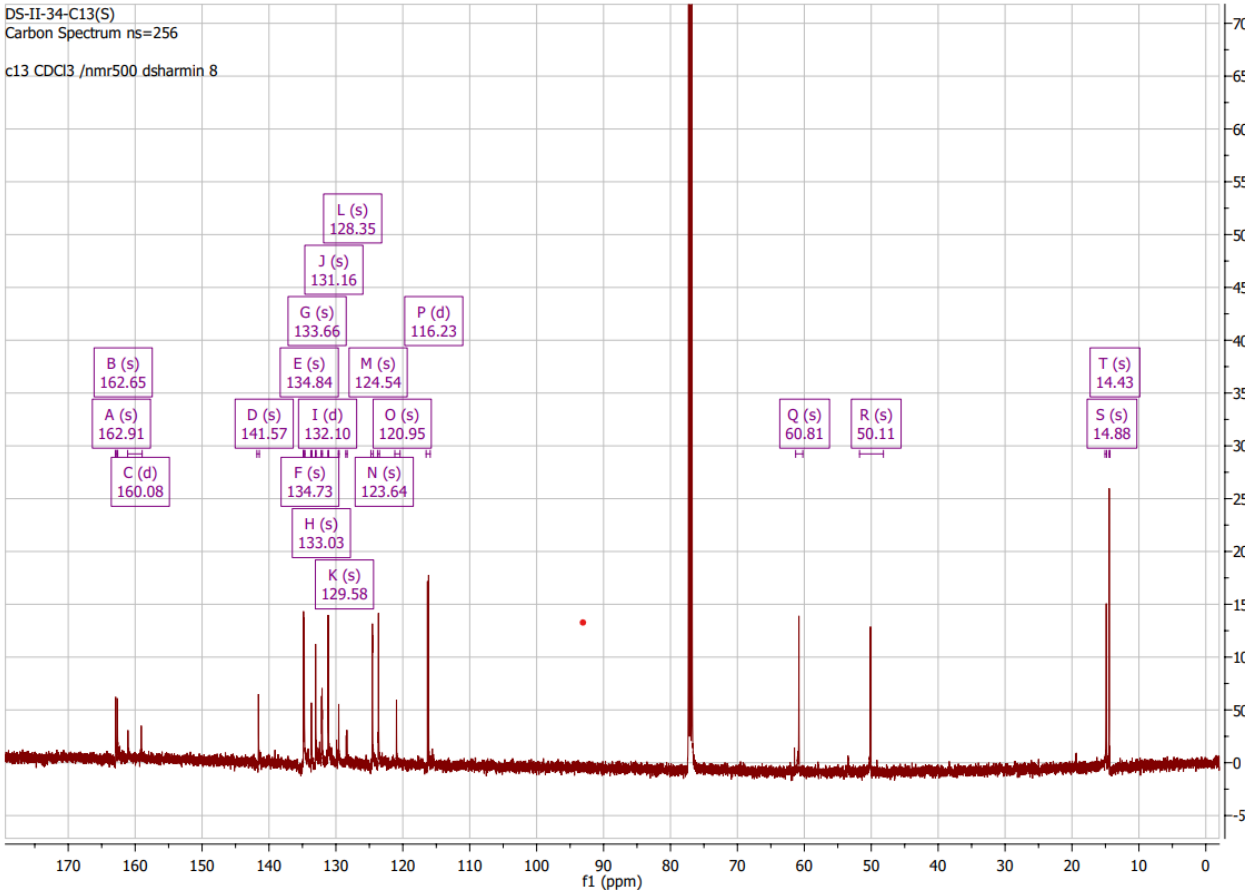

I (s)
130.14
G (d)
132.01
N (d)
116.28
B (s)
164.50
E (s)
134.72
K (d)
124.45
A (s)
172.40
C (d)
160.44
D (s)
136.48
J (d)
127.13
M (s)
116.51
O (s)
58.85
P (s)
16.94
F (d)
132.17
L (s)
122.97
H (d)
131.55
f1 (ppm)

Ethyl (*S*)-8-bromo-6-(2-fluorophenyl)-4-methyl-4*H*-benzo[*f*]imidazo[1,5-*a*][1,4] diazepine-3-carboxylate (11)

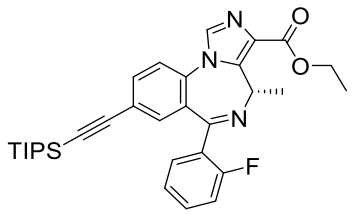


11

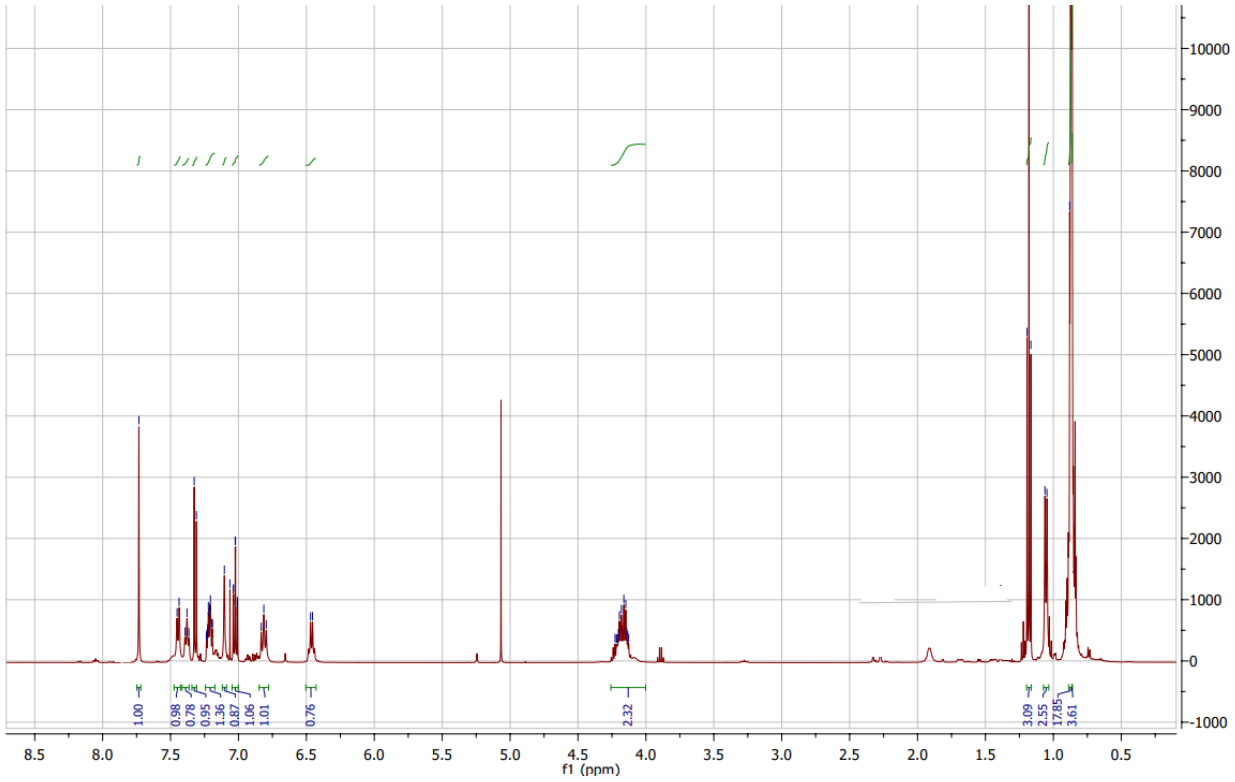


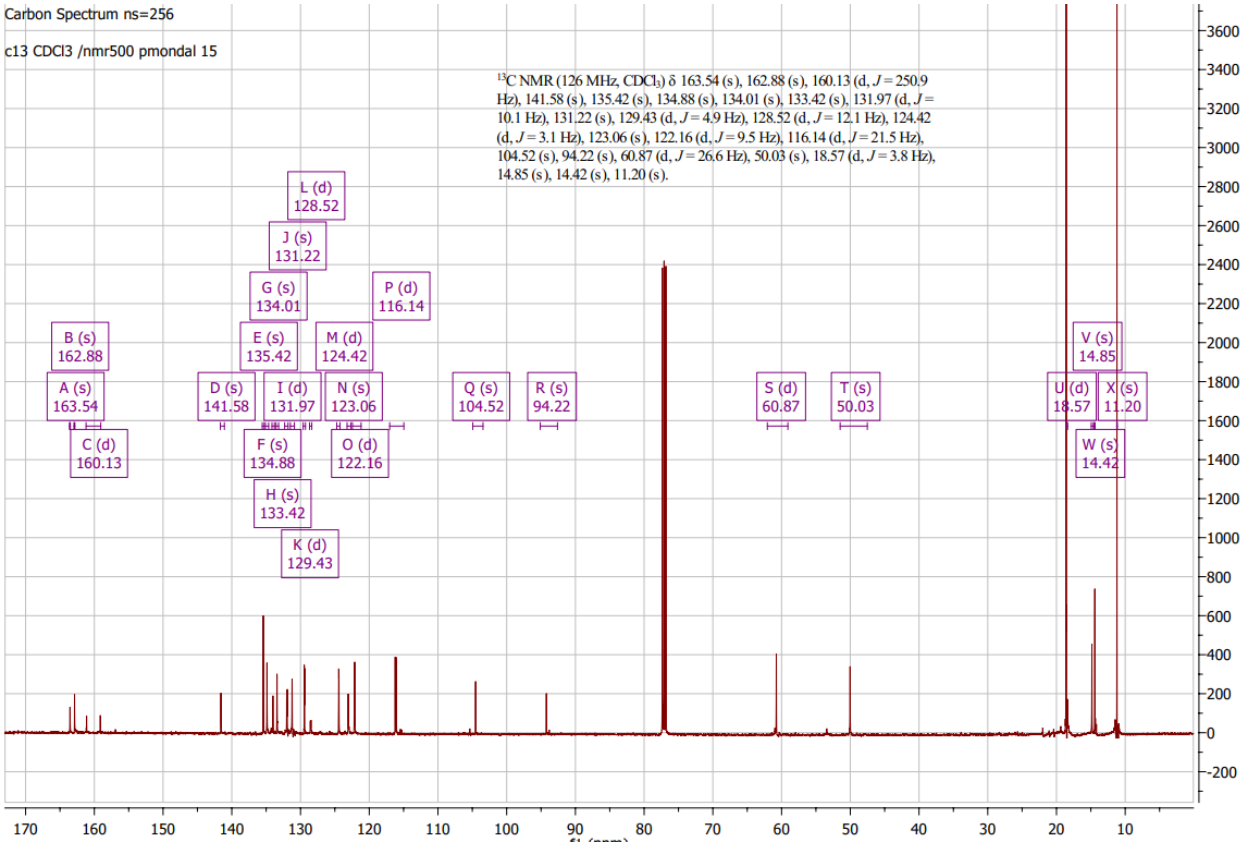

DS-II-34-C13(S)
Carbon Spectrum ns=256
c13 CDCl3 /nmr500 dsharmin 8
L (s) 128.35
J (s) 131.16
G (s) 133.66
P (d) 116.23
B (s) 162.65
E (s) 134.84
M (s) 124.54
T (s) 14.43
A (s) 162.91
D (s) 141.57
I (d) 132.10
O (s) 120.95
Q (s) 60.81
R (s) 50.11
S (s) 14.88
C (d) 160.08
F (s) 134.73
N (s) 123.64
H (s) 133.03
K (s) 129.58
f1 (ppm)

Ethyl(S)-6-(2-fluorophenyl)-4-methyl-8-((triisopropylsilyl)ethynyl)-4Hbenzo[f] imidazo [1,5-a][1,4]diazepine-3-carboxylate (12)

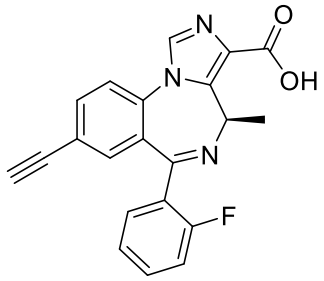


12



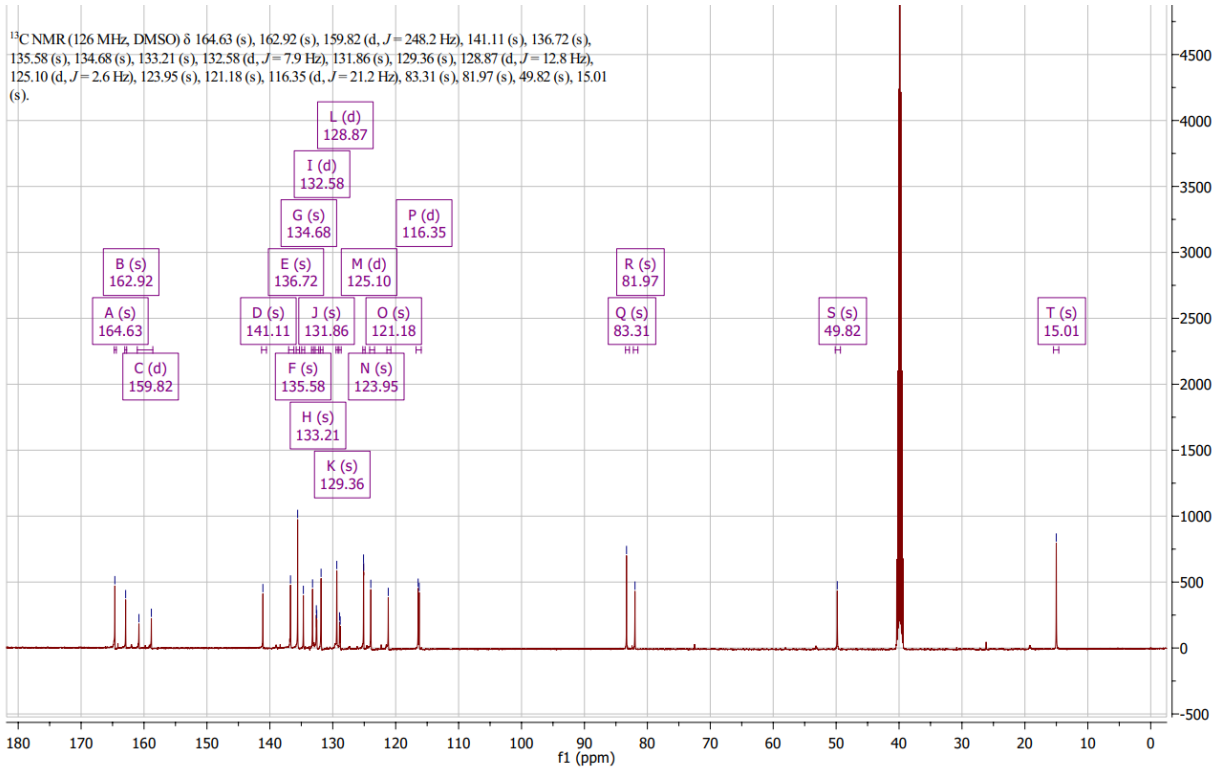

Carbon Spectrum ns=256
c13 CDCl3 /nmr500 pmondal 15
^{13}C NMR (126 MHz, $CDCl_3$) δ 163.54 (s), 162.88 (s), 160.13 (d, J = 250.9 Hz), 141.58 (s), 135.42 (s), 134.88 (s), 134.01 (s), 133.42 (s), 131.97 (d, J = 10.1 Hz), 131.22 (s), 129.43 (d, J = 4.9 Hz), 128.52 (d, J = 12.1 Hz), 124.42 (d, J = 3.1 Hz), 123.06 (s), 122.16 (d, J = 9.5 Hz), 116.14 (d, J = 21.5 Hz), 104.52 (s), 94.22 (s), 60.87 (d, J = 26.6 Hz), 50.03 (s), 18.57 (d, J = 3.8 Hz), 14.85 (s), 14.42 (s), 11.20 (s).
L (d) 128.52
J (s) 131.22
G (s) 134.01
P (d) 116.14
B (s) 162.88
E (s) 135.42
M (d) 124.42
V (s) 14.85
A (s) 163.54
D (s) 141.58
I (d) 131.97
N (s) 123.06
Q (s) 104.52
R (s) 94.22
S (d) 60.87
T (s) 50.03
U (d) 18.57
X (s) 11.20
C (d) 160.13
F (s) 134.88
O (d) 122.16
W (s) 14.42
H (s) 133.42
K (d) 129.43
3600
3400
3200
3000
2800
2600
2400
2200
2000
1800
1600
1400
1200
1000
800
600
400
200
0
-200
170
160
150
140
130
120
110
100
90
80
70
60
50
40
30
20
10

(*R*)-8-ethynyl-6-(2-fluorophenyl)-4-methyl-4H-benzo[f]imidazo[1,5-a][1,4]diazepine-3-carboxylic acid (15)

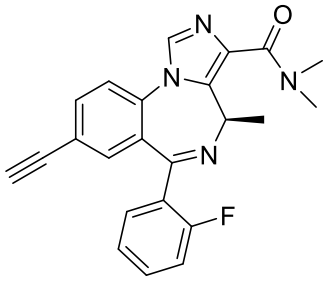


15

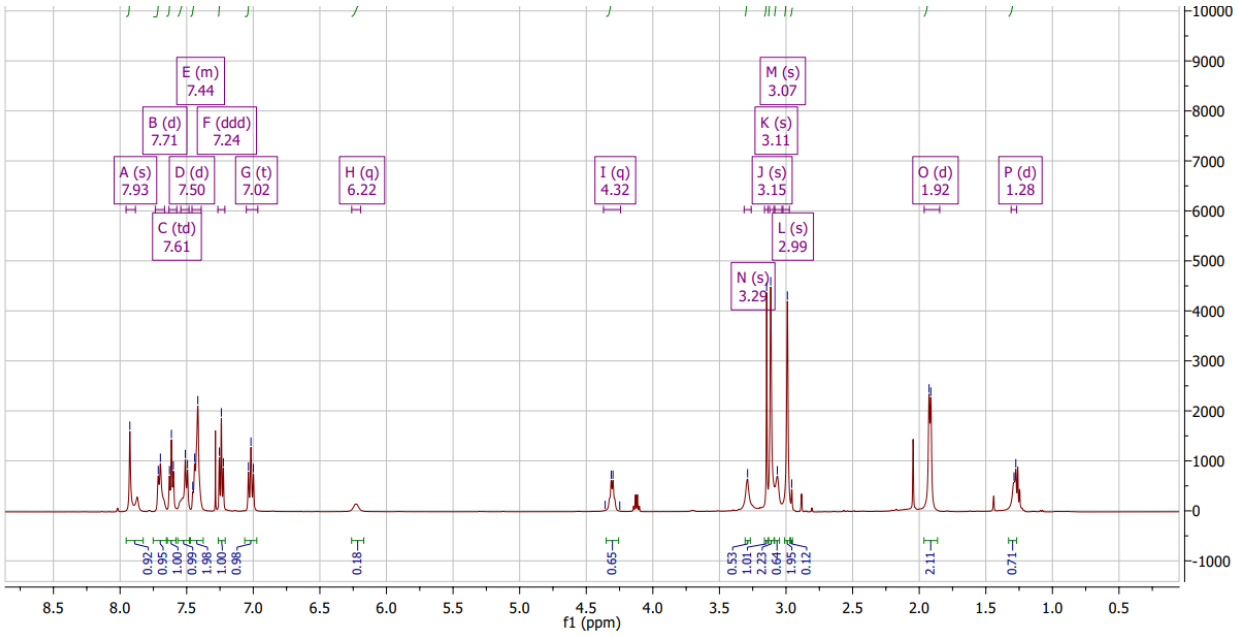


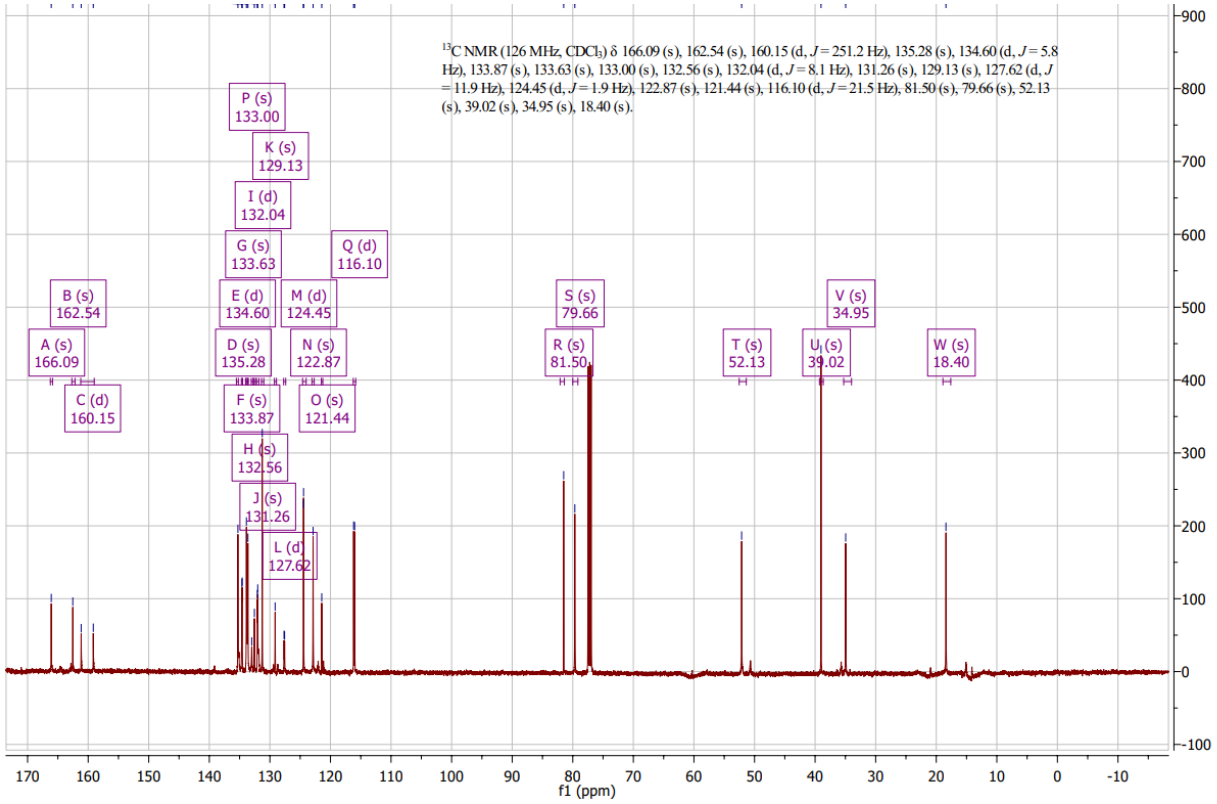

13C NMR (126 MHz, DMSO) δ 164.63 (s), 162.92 (s), 159.82 (d, J = 248.2 Hz), 141.11 (s), 136.72 (s), 135.58 (s), 134.68 (s), 133.21 (s), 132.58 (d, J = 7.9 Hz), 131.86 (s), 129.36 (s), 128.87 (d, J = 12.8 Hz), 125.10 (d, J = 2.6 Hz), 123.95 (s), 121.18 (s), 116.35 (d, J = 21.2 Hz), 83.31 (s), 81.97 (s), 49.82 (s), 15.01 (s).
L (d) 128.87
I (d) 132.58
G (s) 134.68
P (d) 116.35
B (s) 162.92
E (s) 136.72
M (d) 125.10
R (s) 81.97
A (s) 164.63
D (s) 141.11
J (s) 131.86
O (s) 121.18
Q (s) 83.31
S (s) 49.82
T (s) 15.01
C (d) 159.82
F (s) 135.58
N (s) 123.95
H (s) 133.21
K (s) 129.36
f1 (ppm)

(*R*)-8-Ethynyl-6-(2-fluorophenyl)-*N*,*N*,4-trimethyl-4*H*-benzo[*f*]imidazo[1,5 *a*][1,4]diazepine-3-carboxamide [GL-II-73,16]

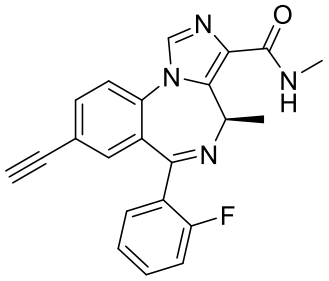


GL-II-73, 16

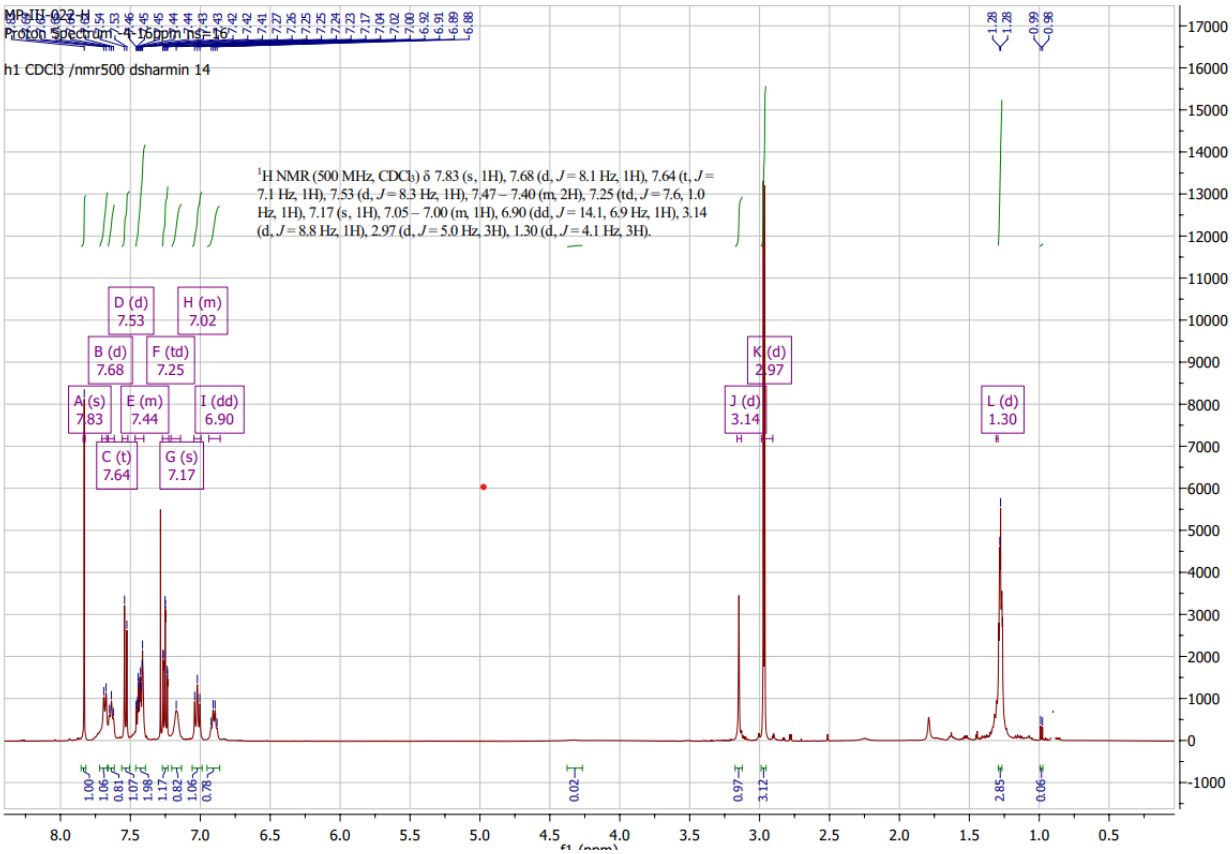


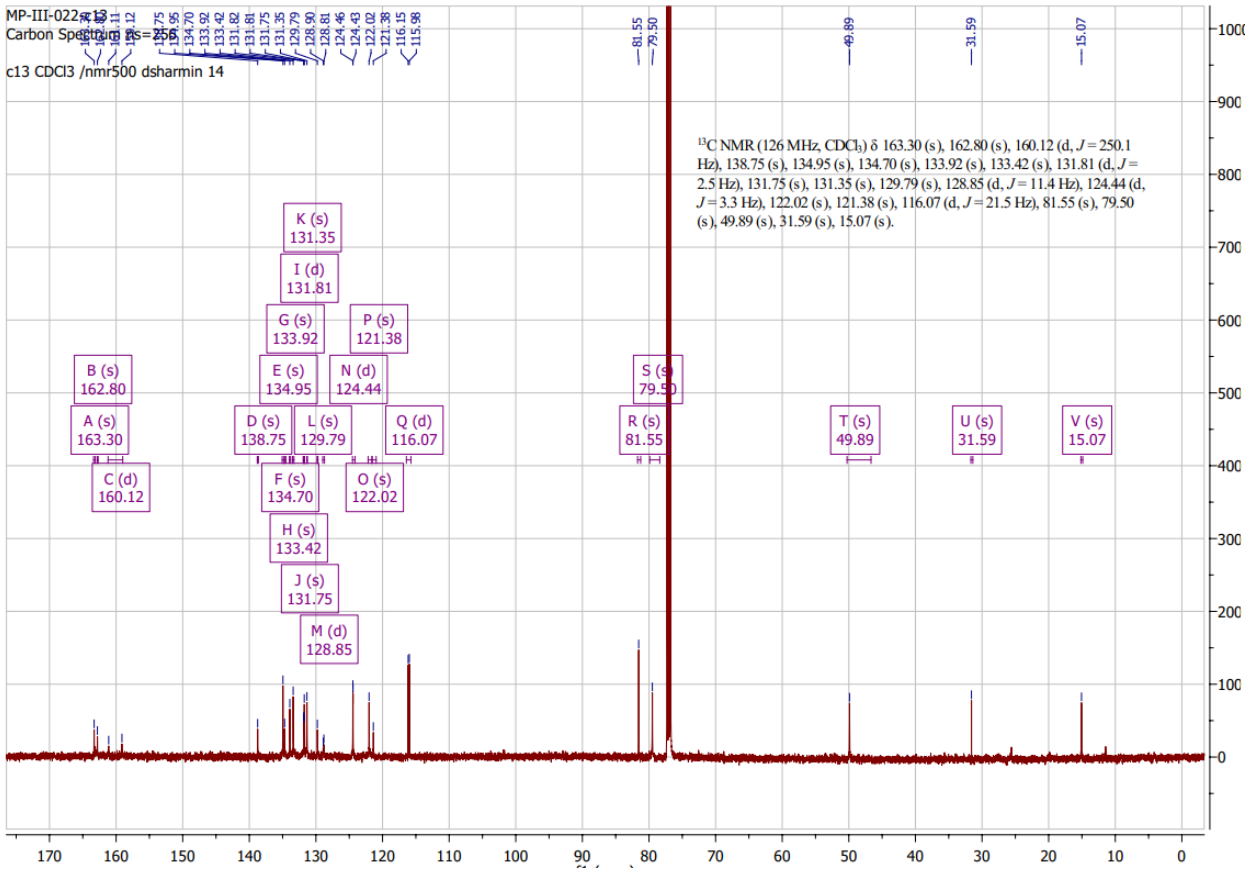

^{13}C NMR (126 MHz, $CDCl_3$) δ 166.09 (s), 162.54 (s), 160.15 (d, J = 251.2 Hz), 135.28 (s), 134.60 (d, J = 5.8 Hz), 133.87 (s), 133.63 (s), 133.00 (s), 132.56 (s), 132.04 (d, J = 8.1 Hz), 131.26 (s), 129.13 (s), 127.62 (d, J = 11.9 Hz), 124.45 (d, J = 1.9 Hz), 122.87 (s), 121.44 (s), 116.10 (d, J = 21.5 Hz), 81.50 (s), 79.66 (s), 52.13 (s), 39.02 (s), 34.95 (s), 18.40 (s).
P (s) 133.00
K (s) 129.13
I (d) 132.04
G (s) 133.63
Q (d) 116.10
B (s) 162.54
E (d) 134.60
M (d) 124.45
S (s) 79.66
V (s) 34.95
A (s) 166.09
D (s) 135.28
N (s) 122.87
R (s) 81.50
T (s) 52.13
U (s) 39.02
W (s) 18.40
C (d) 160.15
F (s) 133.87
O (s) 121.44
H (s) 132.56
J (s) 131.26
L (d) 127.62
f1 (ppm)

***(R)*-8-ethynyl-6-(2-fluorophenyl)-N,4-dimethyl-4H-benzo[f]imidazo[1,5-a][1,4] diazepine-3-carboxamide [MP-III-022,17]**

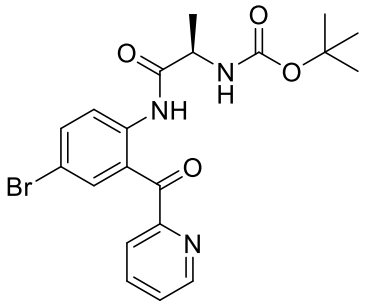


MP-III-022, 17

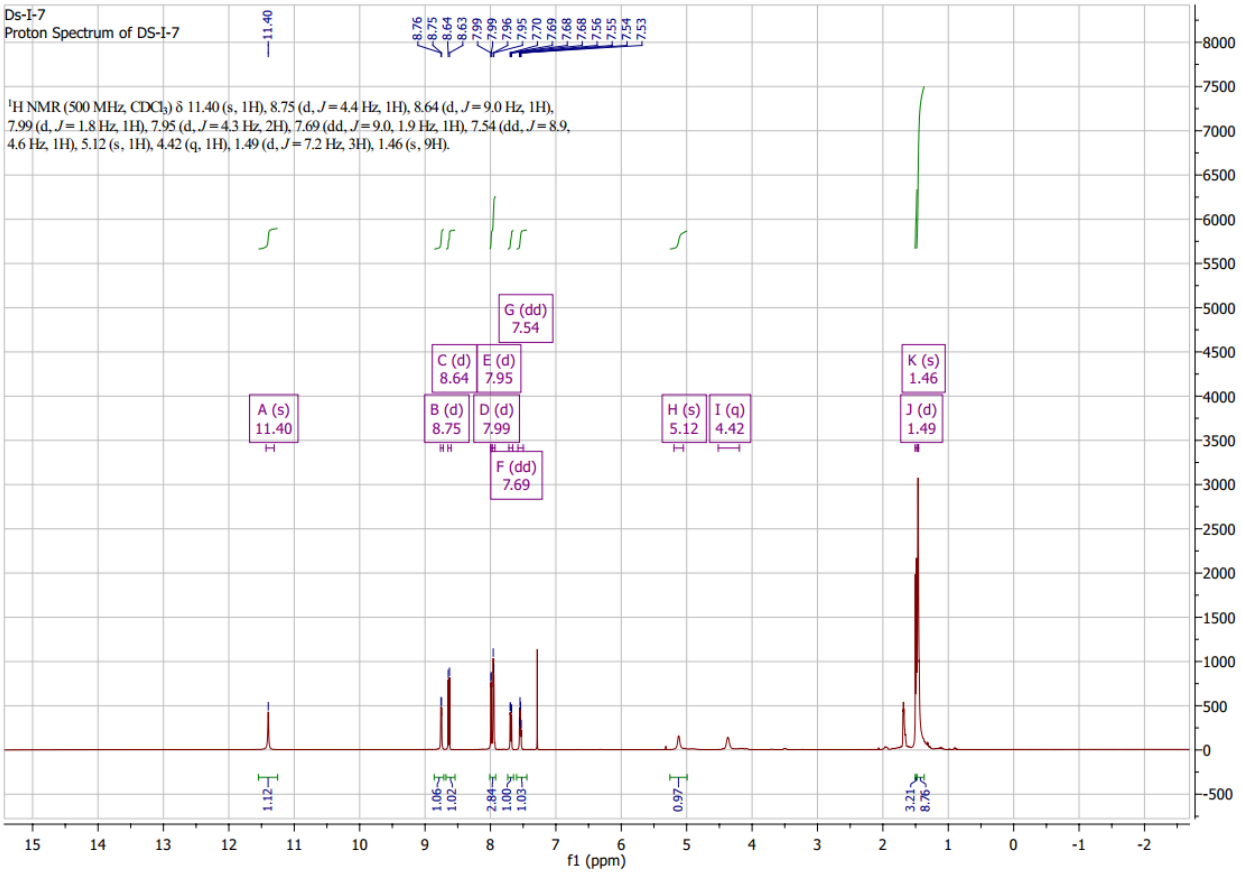


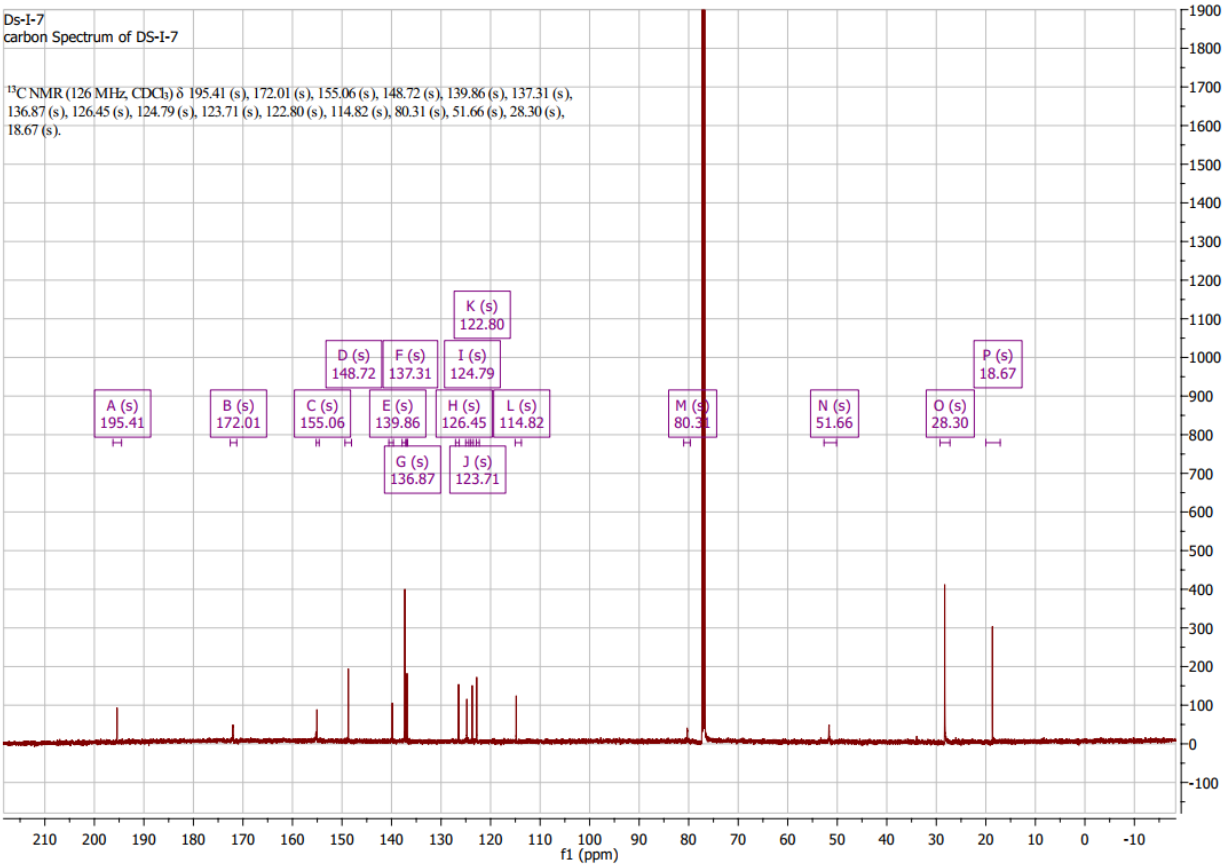

MP-III-022-c13
Carbon Spectrum ns=256
c13 CDCl3 /nmr500 dsharmin 14
^{13}C NMR (126 MHz, $CDCl_3$) δ 163.30 (s), 162.80 (s), 160.12 (d, J = 250.1 Hz), 138.75 (s), 134.95 (s), 134.70 (s), 133.92 (s), 133.42 (s), 131.81 (d, J = 2.5 Hz), 131.75 (s), 131.35 (s), 129.79 (s), 128.85 (d, J = 11.4 Hz), 124.44 (d, J = 3.3 Hz), 122.02 (s), 121.38 (s), 116.07 (d, J = 21.5 Hz), 81.55 (s), 79.50 (s), 49.89 (s), 31.59 (s), 15.07 (s).
A (s) 163.30
B (s) 162.80
C (d) 160.12
D (s) 138.75
E (s) 134.95
F (s) 134.70
G (s) 133.92
H (s) 133.42
I (d) 131.81
J (s) 131.75
K (s) 131.35
L (s) 129.79
M (d) 128.85
N (d) 124.44
O (s) 122.02
P (s) 121.38
Q (d) 116.07
R (s) 81.55
S (s) 79.50
T (s) 49.89
U (s) 31.59
V (s) 15.07

Tert-butyl-(*R*)-(1-((4-bromo-2-picolinoylphenyl)amino)-1-oxopropan-2-yl)carbamate (19)

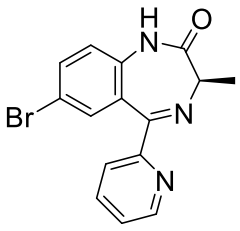


19

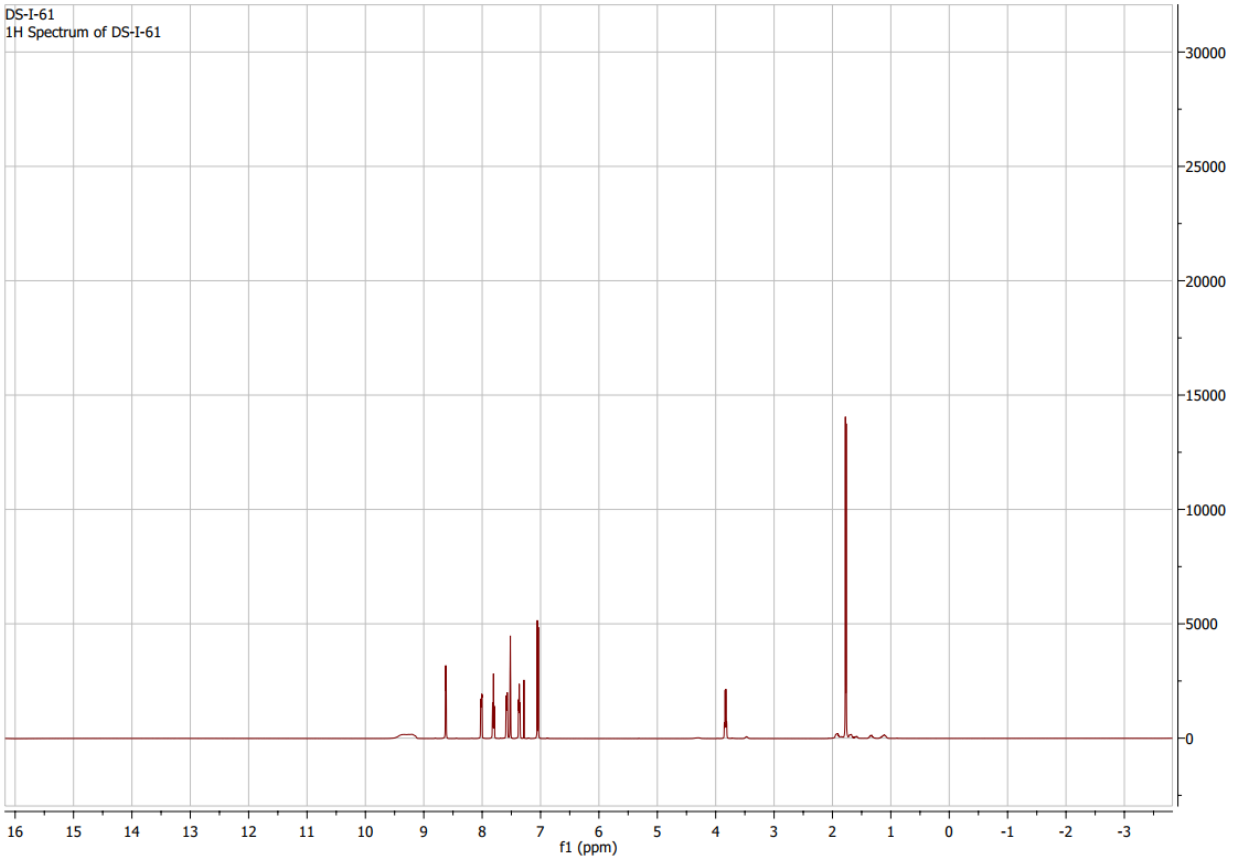


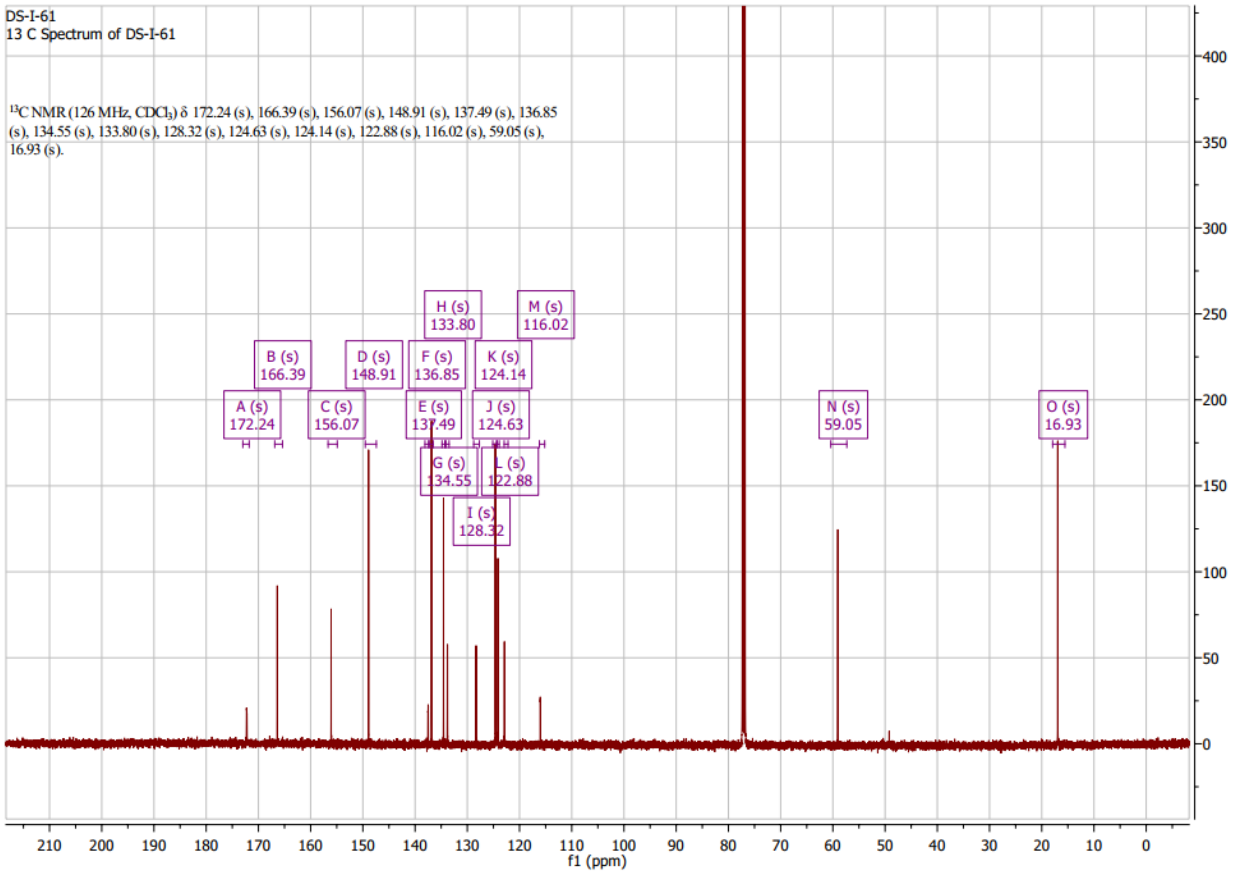

Ds-I-7
carbon Spectrum of DS-I-7
^{13}C NMR (126 MHz, $CDCl_3$) δ 195.41 (s), 172.01 (s), 155.06 (s), 148.72 (s), 139.86 (s), 137.31 (s), 136.87 (s), 126.45 (s), 124.79 (s), 123.71 (s), 122.80 (s), 114.82 (s), 80.31 (s), 51.66 (s), 28.30 (s), 18.67 (s).
A (s) 195.41
B (s) 172.01
C (s) 155.06
D (s) 148.72
E (s) 139.86
F (s) 137.31
G (s) 136.87
H (s) 126.45
I (s) 124.79
J (s) 123.71
K (s) 122.80
L (s) 114.82
M (s) 80.31
N (s) 51.66
O (s) 28.30
P (s) 18.67
f1 (ppm)

(*R*)-7-bromo-3-methyl-5-(pyridin-2-yl)-1,3-dihydro-2H-benzo[e][1,4]diazepin-2-one (20)

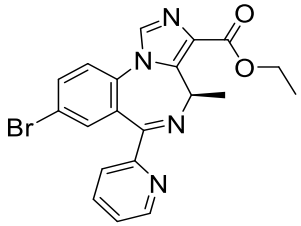


20

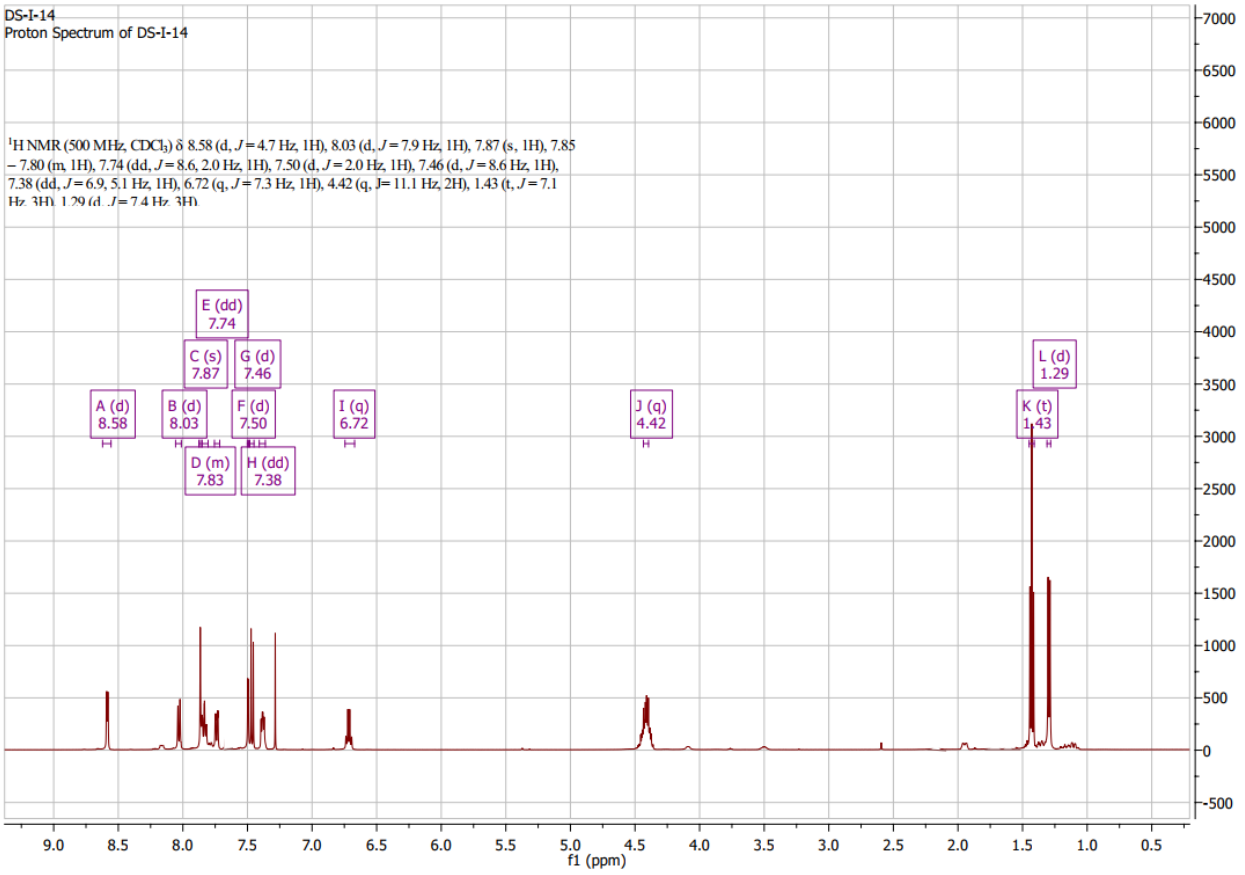


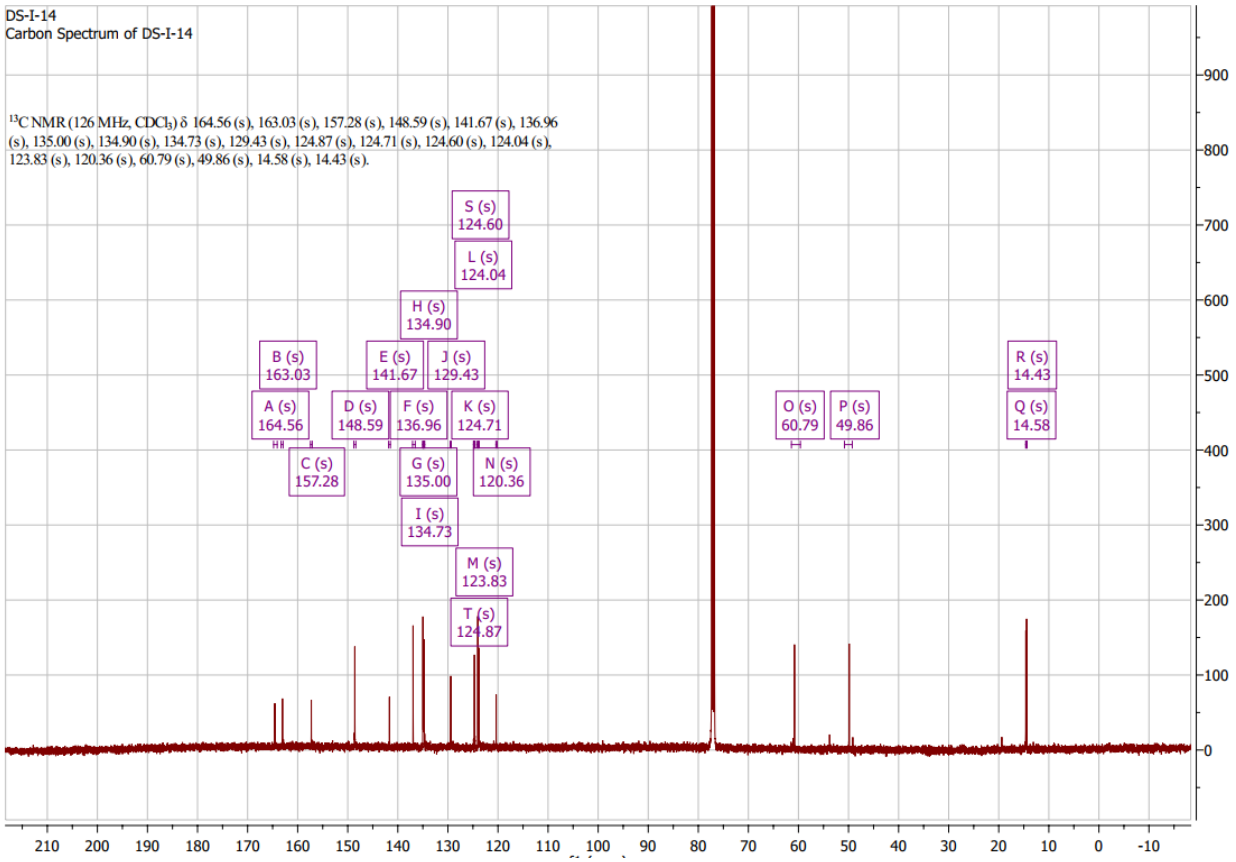

DS-I-61
13 C Spectrum of DS-I-61
^{13}C NMR (126 MHz, $CDCl_3$) δ 172.24 (s), 166.39 (s), 156.07 (s), 148.91 (s), 137.49 (s), 136.85 (s), 134.55 (s), 133.80 (s), 128.32 (s), 124.63 (s), 124.14 (s), 122.88 (s), 116.02 (s), 59.05 (s), 16.93 (s).
A (s) 172.24
B (s) 166.39
C (s) 156.07
D (s) 148.91
E (s) 137.49
F (s) 136.85
G (s) 134.55
H (s) 133.80
I (s) 128.32
J (s) 124.63
K (s) 124.14
L (s) 122.88
M (s) 116.02
N (s) 59.05
O (s) 16.93
f1 (ppm)

Ethyl (*R*)-8-bromo-4-methyl-6-(pyridin-2'-yl)-4H-benzo[f]imidazo[1,5-a][1,4] diazepine-3-carboxylate(21)

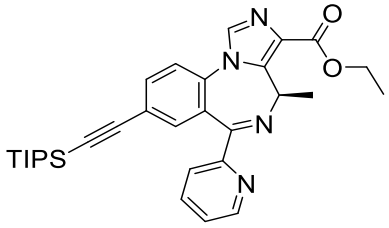


21

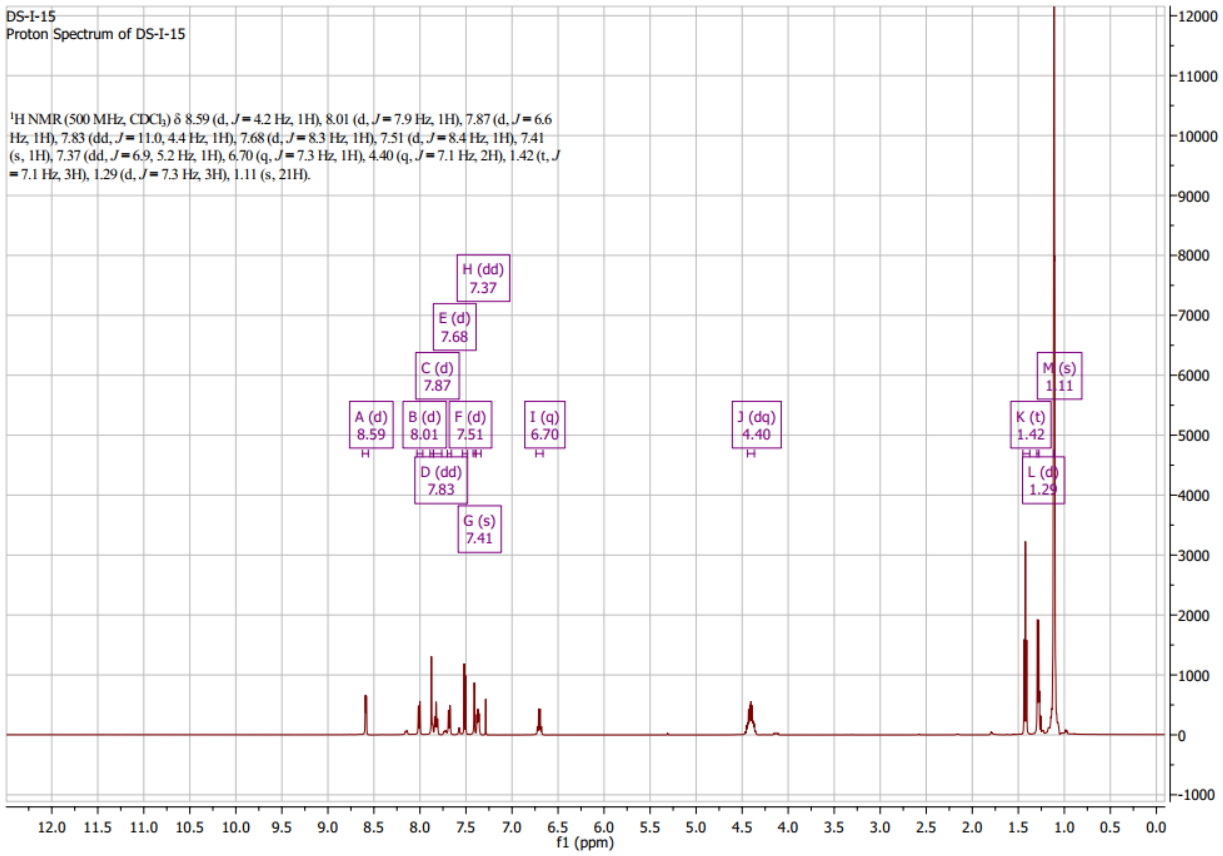


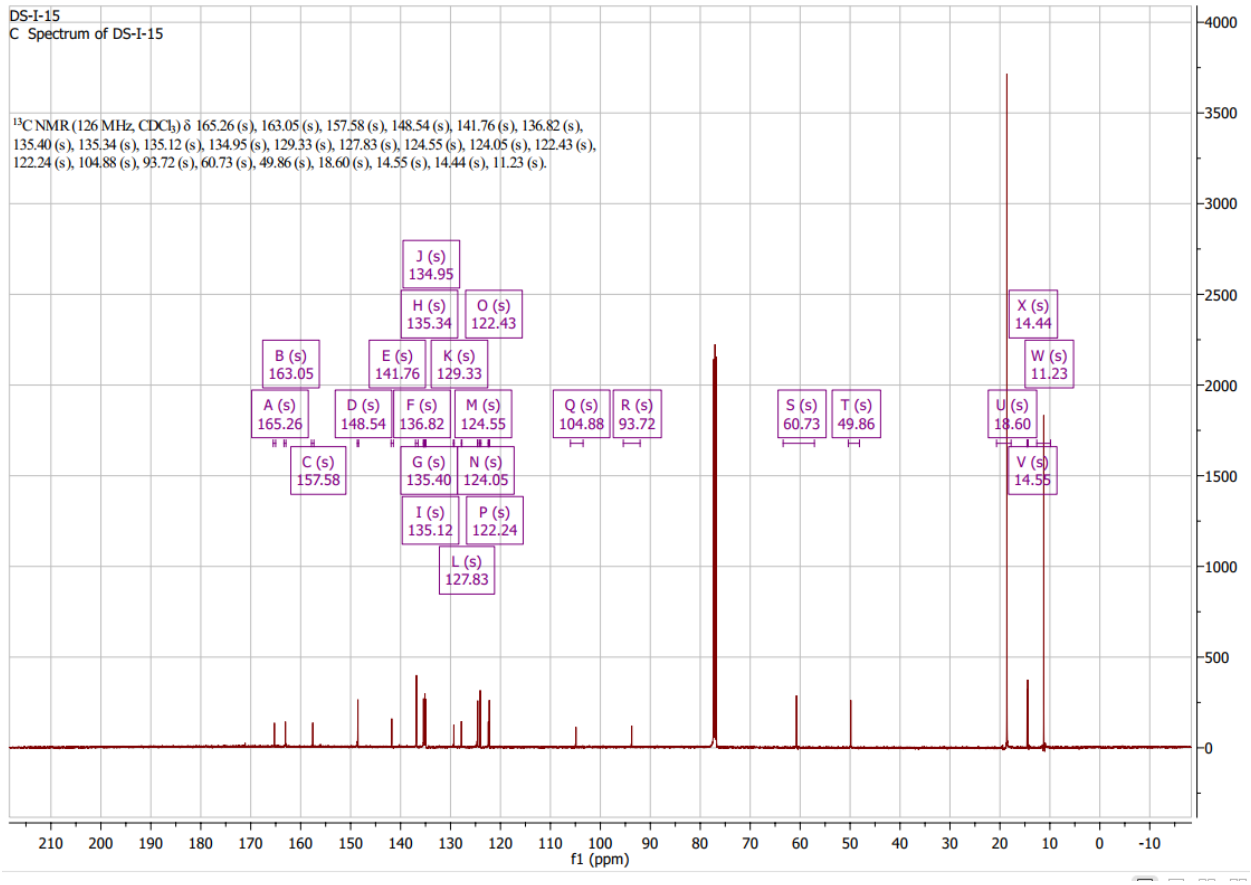

DS-I-14
Carbon Spectrum of DS-I-14
^{13}C NMR (126 MHz, $CDCl_3$) δ 164.56 (s), 163.03 (s), 157.28 (s), 148.59 (s), 141.67 (s), 136.96 (s), 135.00 (s), 134.90 (s), 134.73 (s), 129.43 (s), 124.87 (s), 124.71 (s), 124.60 (s), 124.04 (s), 123.83 (s), 120.36 (s), 60.79 (s), 49.86 (s), 14.58 (s), 14.43 (s).
S (s) 124.60
L (s) 124.04
H (s) 134.90
B (s) 163.03
E (s) 141.67
J (s) 129.43
R (s) 14.43
A (s) 164.56
D (s) 148.59
F (s) 136.96
K (s) 124.71
O (s) 60.79
P (s) 49.86
Q (s) 14.58
C (s) 157.28
G (s) 135.00
N (s) 120.36
I (s) 134.73
M (s) 123.83
T (s) 124.87

Ethyl (R)-4-methyl-6-(pyridin-2-yl)-8-((triisopropylsilyl)ethynyl)-4H-benzo[f] imidazo[1,5-a][1,4]diazepine-3-carboxylate (22)

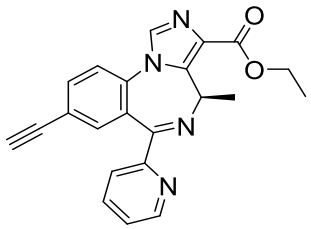


22

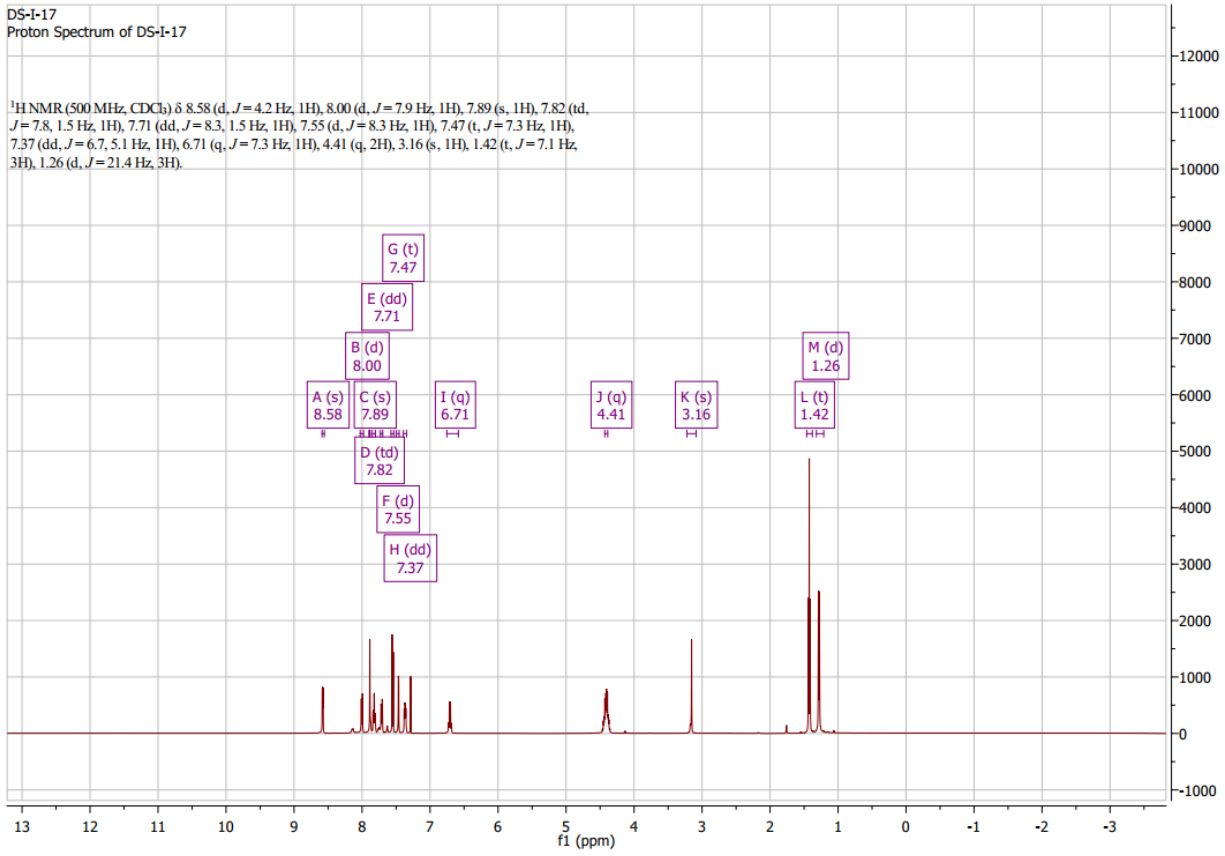


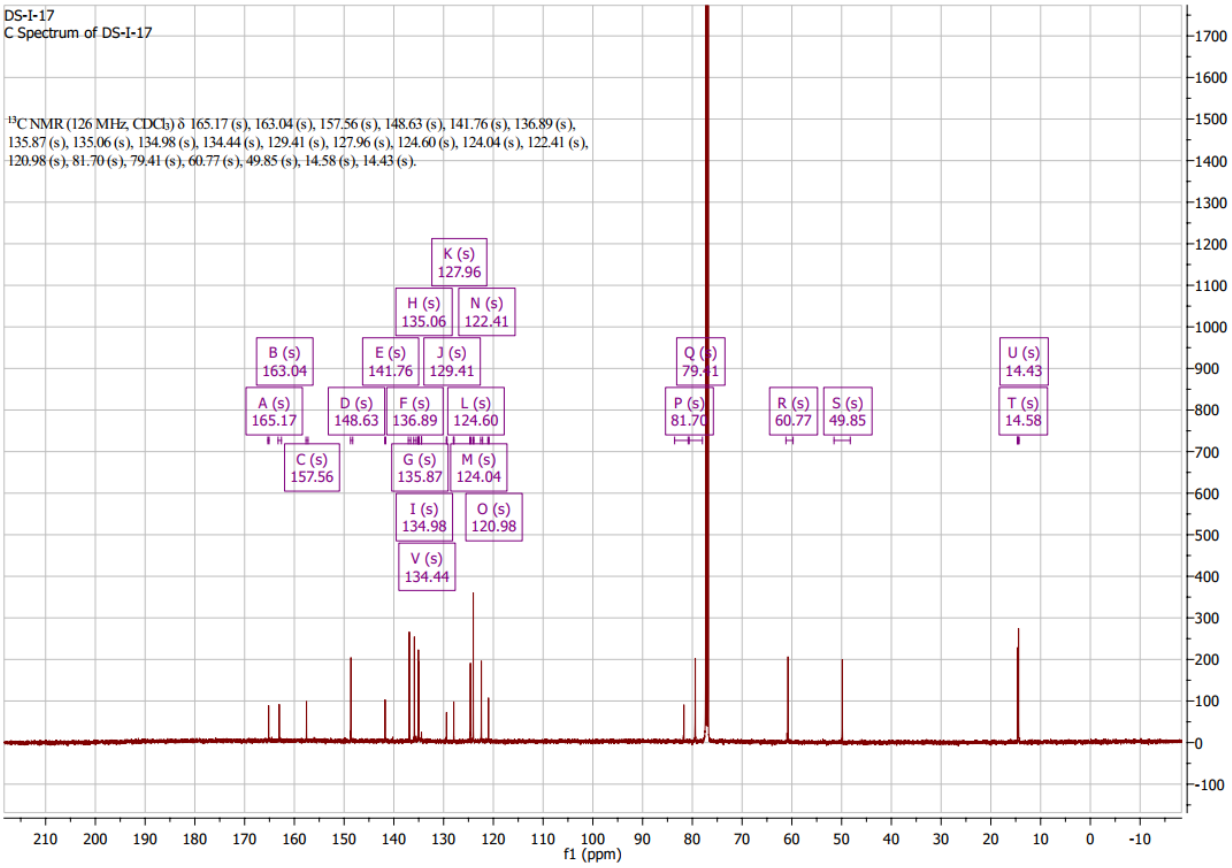

DS-I-15
C Spectrum of DS-I-15
13C NMR (126 MHz, CDCl3) δ 165.26 (s), 163.05 (s), 157.58 (s), 148.54 (s), 141.76 (s), 136.82 (s), 135.40 (s), 135.34 (s), 135.12 (s), 134.95 (s), 129.33 (s), 127.83 (s), 124.55 (s), 124.05 (s), 122.43 (s), 122.24 (s), 104.88 (s), 93.72 (s), 60.73 (s), 49.86 (s), 18.60 (s), 14.55 (s), 14.44 (s), 11.23 (s).
J (s) 134.95
H (s) 135.34
O (s) 122.43
B (s) 163.05
E (s) 141.76
K (s) 129.33
A (s) 165.26
D (s) 148.54
F (s) 136.82
M (s) 124.55
Q (s) 104.88
R (s) 93.72
S (s) 60.73
T (s) 49.86
X (s) 14.44
W (s) 11.23
U (s) 18.60
C (s) 157.58
G (s) 135.40
N (s) 124.05
V (s) 14.55
I (s) 135.12
P (s) 122.24
L (s) 127.83
4000
3500
3000
2500
2000
1500
1000
500
0
210 200 190 180 170 160 150 140 130 120 110 100 90 80 70 60 50 40 30 20 10 0 -10
f1 (ppm)

Ethyl (S)-8-ethynyl-4-methyl-6-(pyridin-2-yl)-4H-benzo[f]imidazo [1,5-a][1,4] diazepine-3-carboxylate(23)

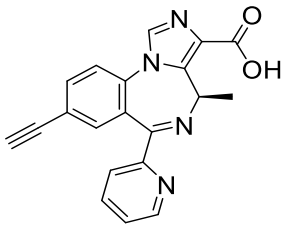


23

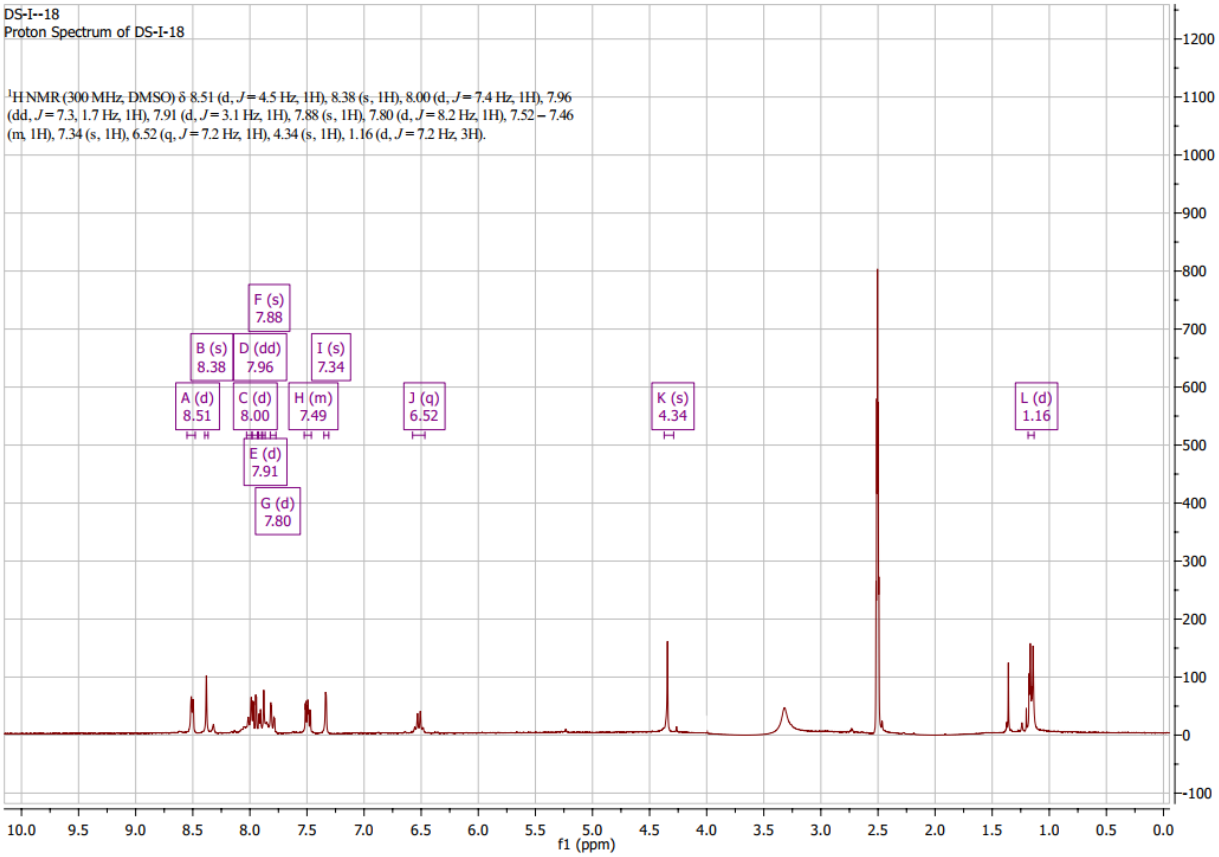


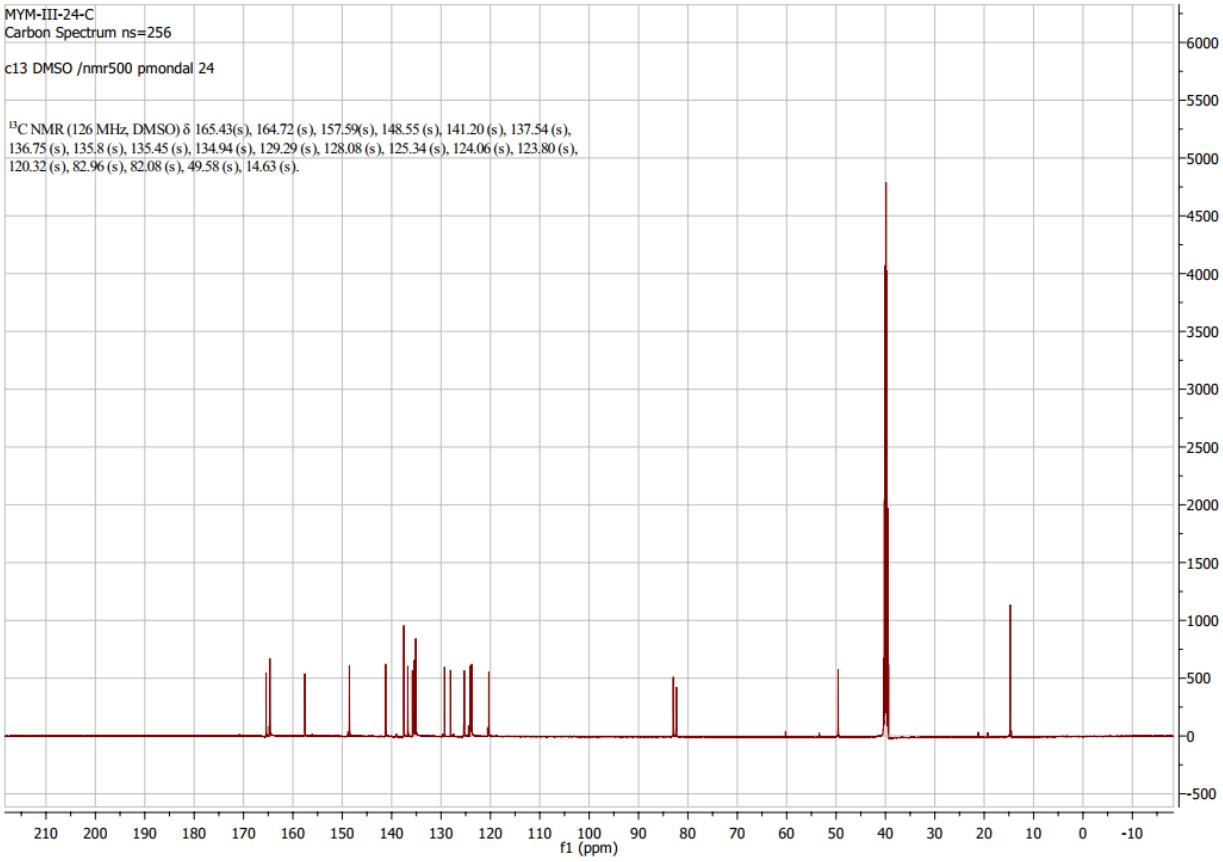

DS-I-17
C Spectrum of DS-I-17
^{13}C NMR (126 MHz, CDCl$_3$) δ 165.17 (s), 163.04 (s), 157.56 (s), 148.63 (s), 141.76 (s), 136.89 (s), 135.87 (s), 135.06 (s), 134.98 (s), 134.44 (s), 129.41 (s), 127.96 (s), 124.60 (s), 124.04 (s), 122.41 (s), 120.98 (s), 81.70 (s), 79.41 (s), 60.77 (s), 49.85 (s), 14.58 (s), 14.43 (s).
K (s) 127.96
H (s) 135.06
N (s) 122.41
B (s) 163.04
E (s) 141.76
J (s) 129.41
Q (s) 79.41
U (s) 14.43
A (s) 165.17
D (s) 148.63
F (s) 136.89
L (s) 124.60
P (s) 81.70
R (s) 60.77
S (s) 49.85
T (s) 14.58
C (s) 157.56
G (s) 135.87
M (s) 124.04
I (s) 134.98
O (s) 120.98
V (s) 134.44
f1 (ppm)

(*R*)-8-Ethynyl-4-methyl-6-(pyridin-2-yl)-4H-benzo[f]imidazo[1,5-a][1,4]diazepine-3-carboxylic acid (24)

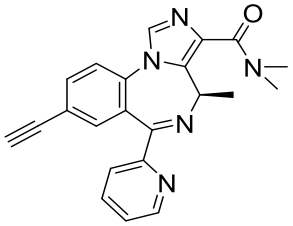


24

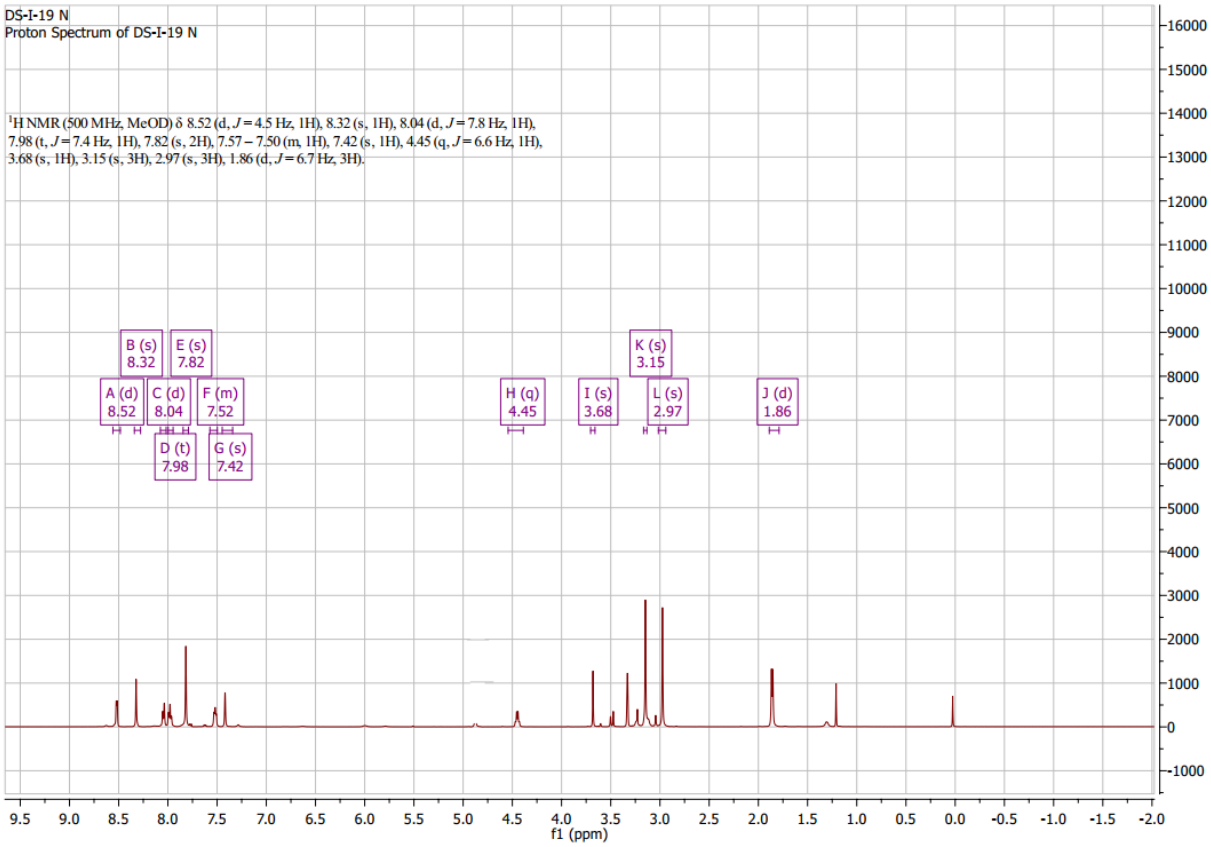


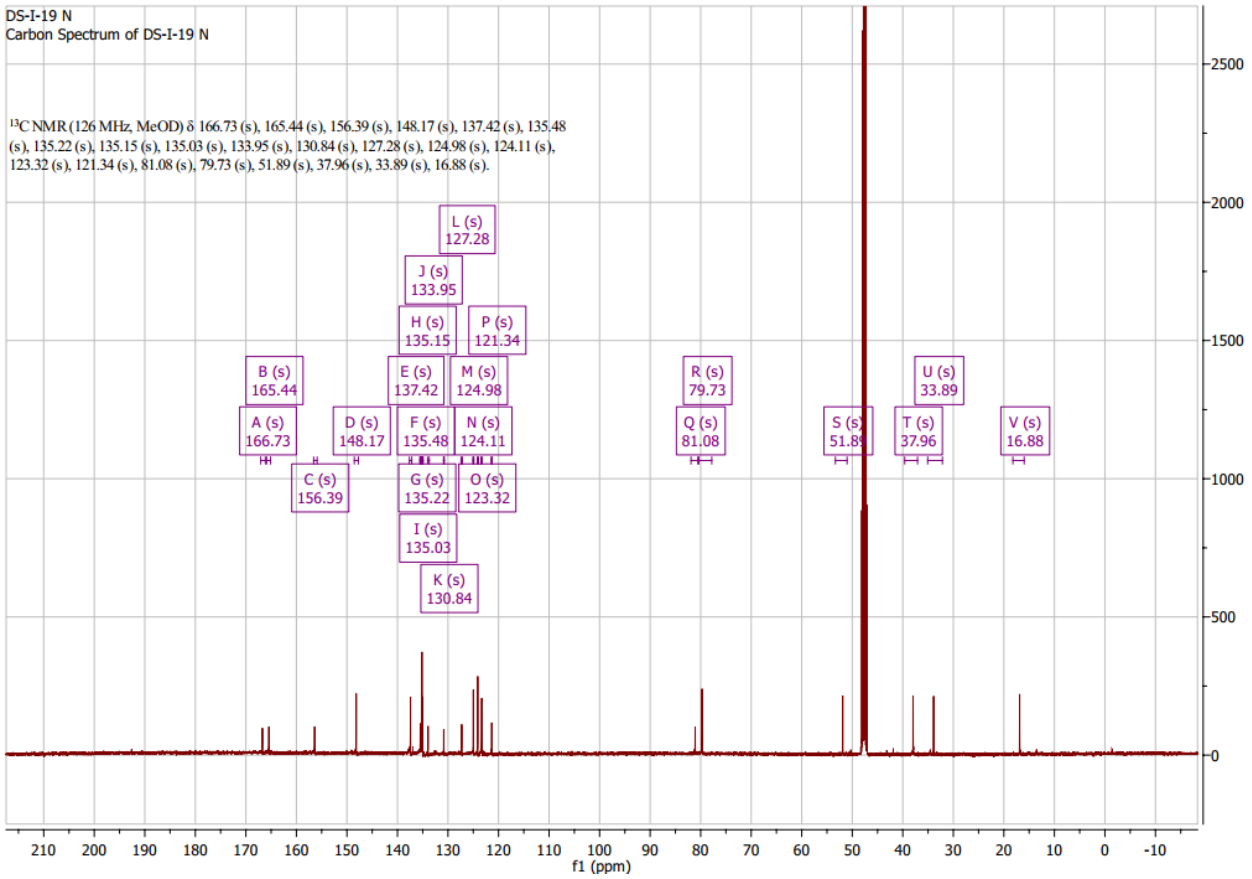

MYM-III-24-C
Carbon Spectrum ns=256
c13 DMSO /nmr500 pmondal 24
13C NMR (126 MHz, DMSO) δ 165.43(s), 164.72 (s), 157.59(s), 148.55 (s), 141.20 (s), 137.54 (s), 136.75 (s), 135.8 (s), 135.45 (s), 134.94 (s), 129.29 (s), 128.08 (s), 125.34 (s), 124.06 (s), 123.80 (s), 120.32 (s), 82.96 (s), 82.08 (s), 49.58 (s), 14.63 (s).
6000
5500
5000
4500
4000
3500
3000
2500
2000
1500
1000
500
0
-500
210 200 190 180 170 160 150 140 130 120 110 100 90 80 70 60 50 40 30 20 10 0 -10
f1 (ppm)

(*R*)-8-Ethynyl-N,N,4-trimethyl-6-(pyridin-2-yl)-4H-benzo[f]imidazo[1,5-a][1,4] diazepine-3-carboxamide (25)

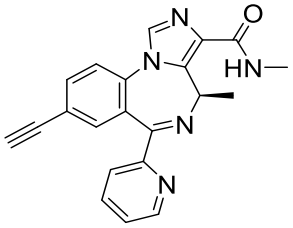


25

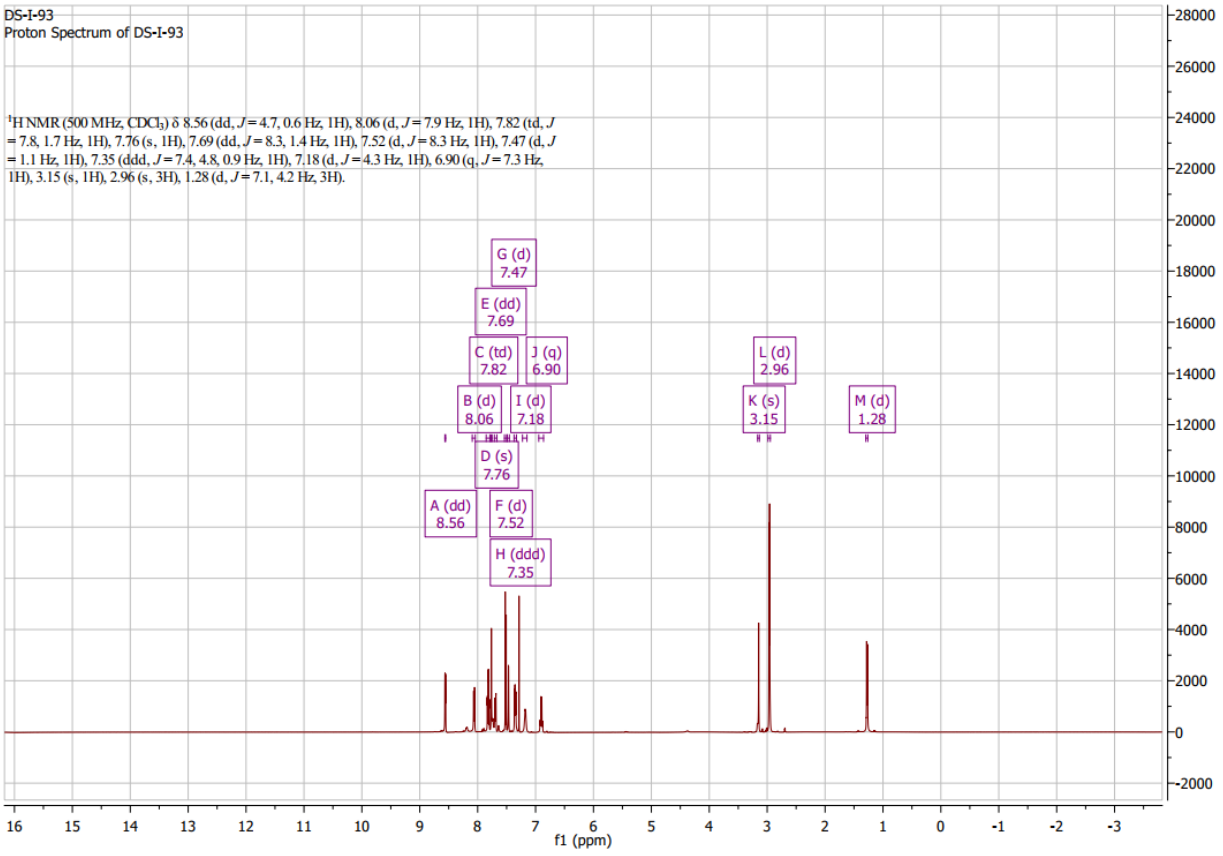



DS-I-19 N
Carbon Spectrum of DS-I-19 N
13C NMR (126 MHz, MeOD) δ 166.73 (s), 165.44 (s), 156.39 (s), 148.17 (s), 137.42 (s), 135.48 (s), 135.22 (s), 135.15 (s), 135.03 (s), 133.95 (s), 130.84 (s), 127.28 (s), 124.98 (s), 124.11 (s), 123.32 (s), 121.34 (s), 81.08 (s), 79.73 (s), 51.89 (s), 37.96 (s), 33.89 (s), 16.88 (s).
L (s) 127.28
J (s) 133.95
H (s) 135.15
P (s) 121.34
B (s) 165.44
E (s) 137.42
M (s) 124.98
R (s) 79.73
U (s) 33.89
A (s) 166.73
D (s) 148.17
F (s) 135.48
N (s) 124.11
Q (s) 81.08
S (s) 51.89
T (s) 37.96
V (s) 16.88
C (s) 156.39
G (s) 135.22
O (s) 123.32
I (s) 135.03
K (s) 130.84
2500
2000
1500
1000
500
0
210 200 190 180 170 160 150 140 130 120 110 100 90 80 70 60 50 40 30 20 10 0 -10
f1 (ppm)

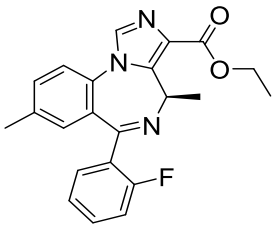
(*R*)-8-Ethynyl-N,N,4-trimethyl-6-(pyridin-2-yl)-4H-benzo[f]imidazo[1,5-a][1,4] diazepine-3-carboxamide (26)



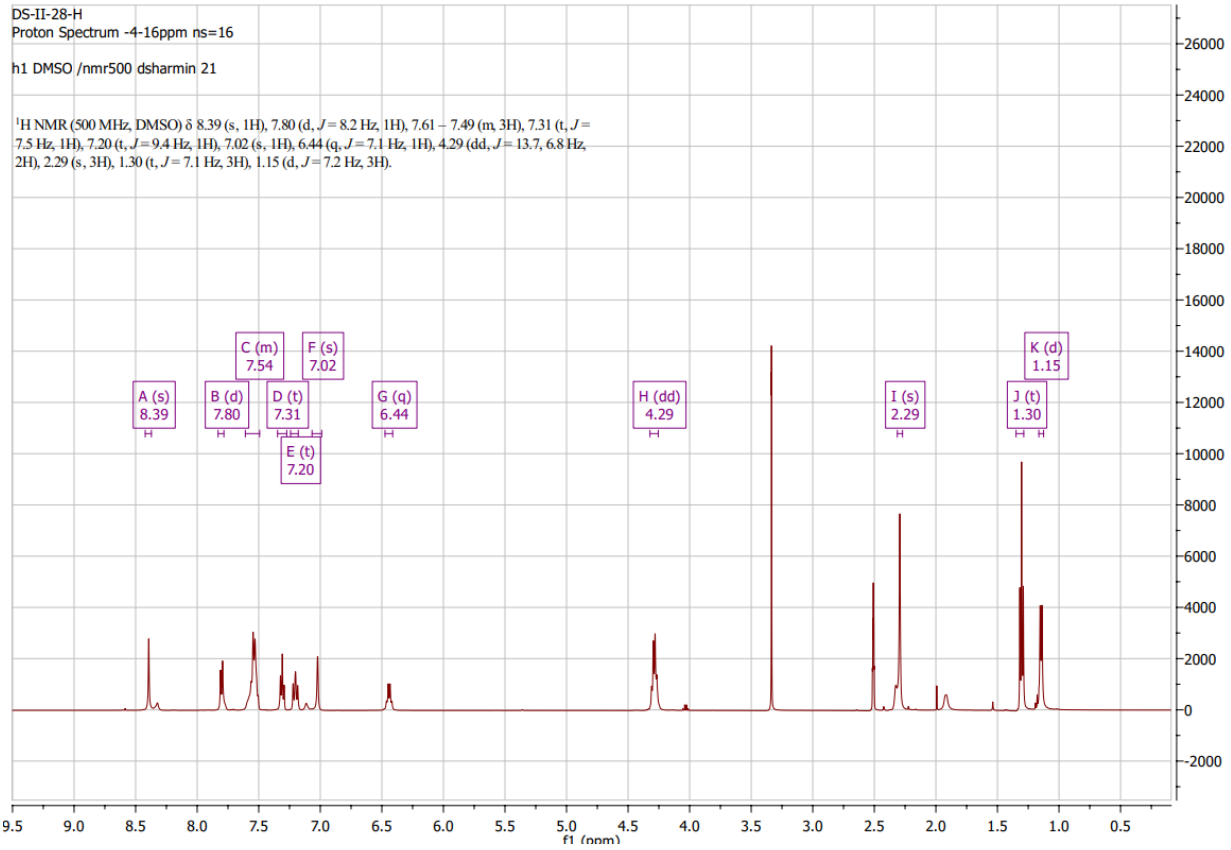
DS-I-96, 26

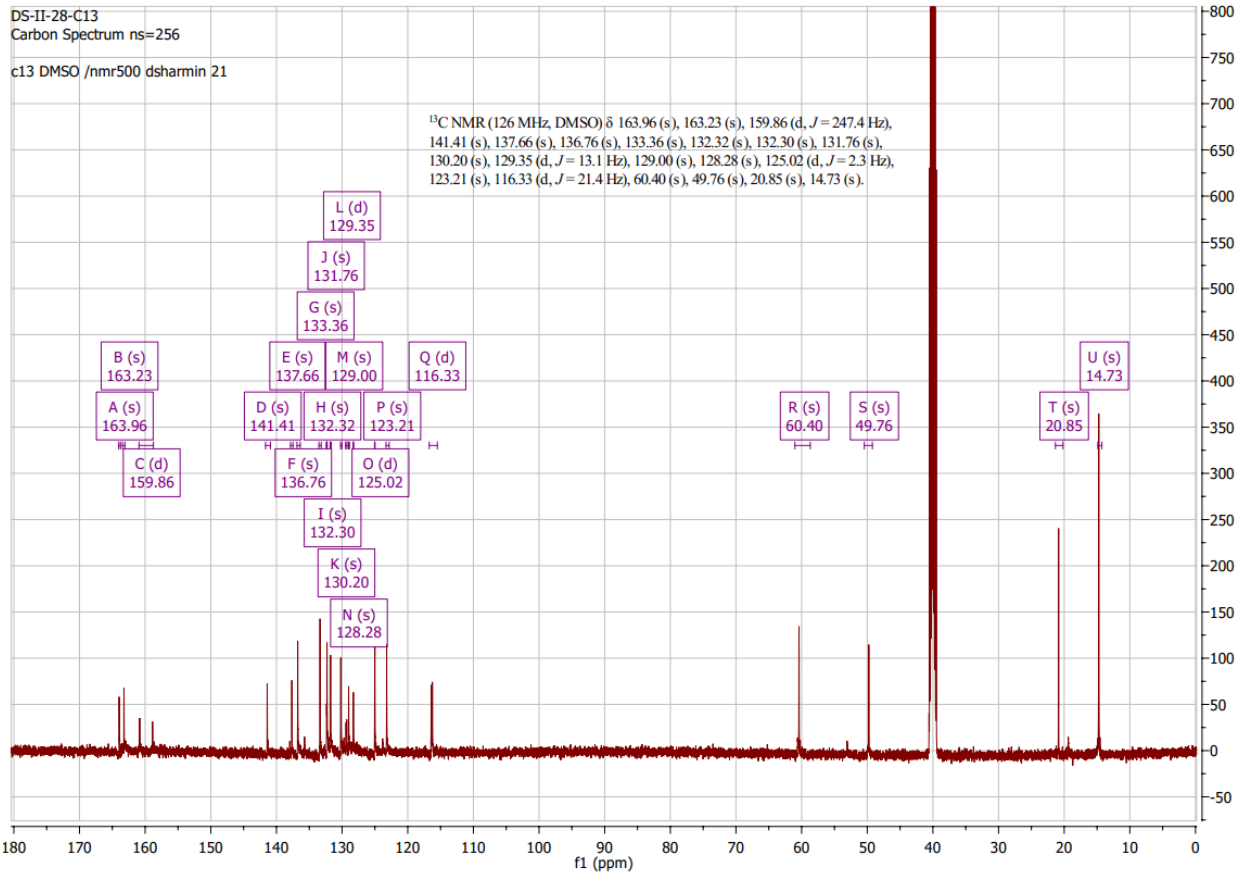


Ethyl (*R*)-6-(2'-fluorophenyl)-4-methyl-8-methyl-4H-benzo[f]imidazo[1,5-a][1,4] diazepine-3-carboxylate (27)

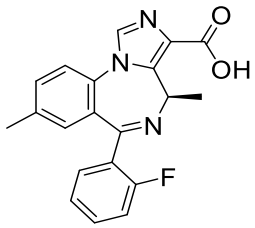


27

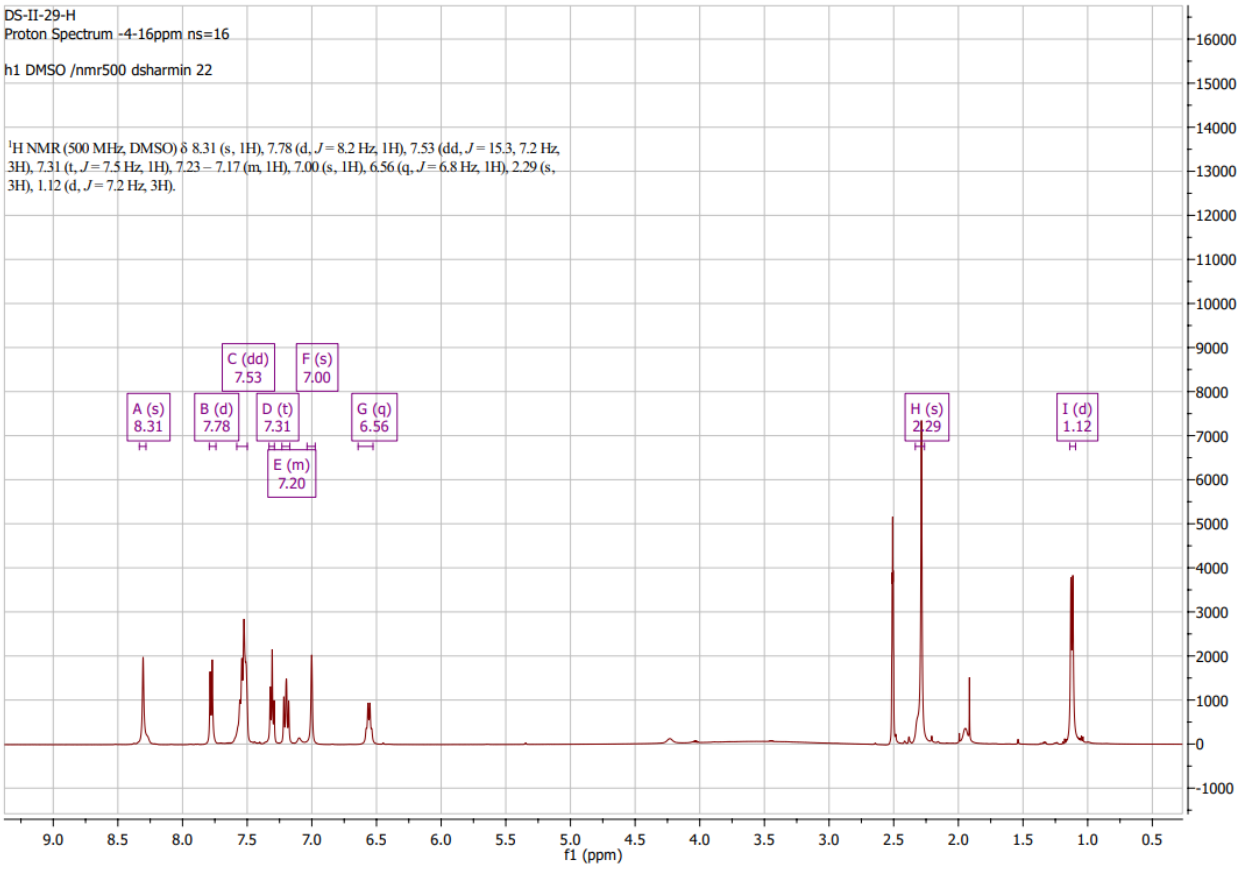


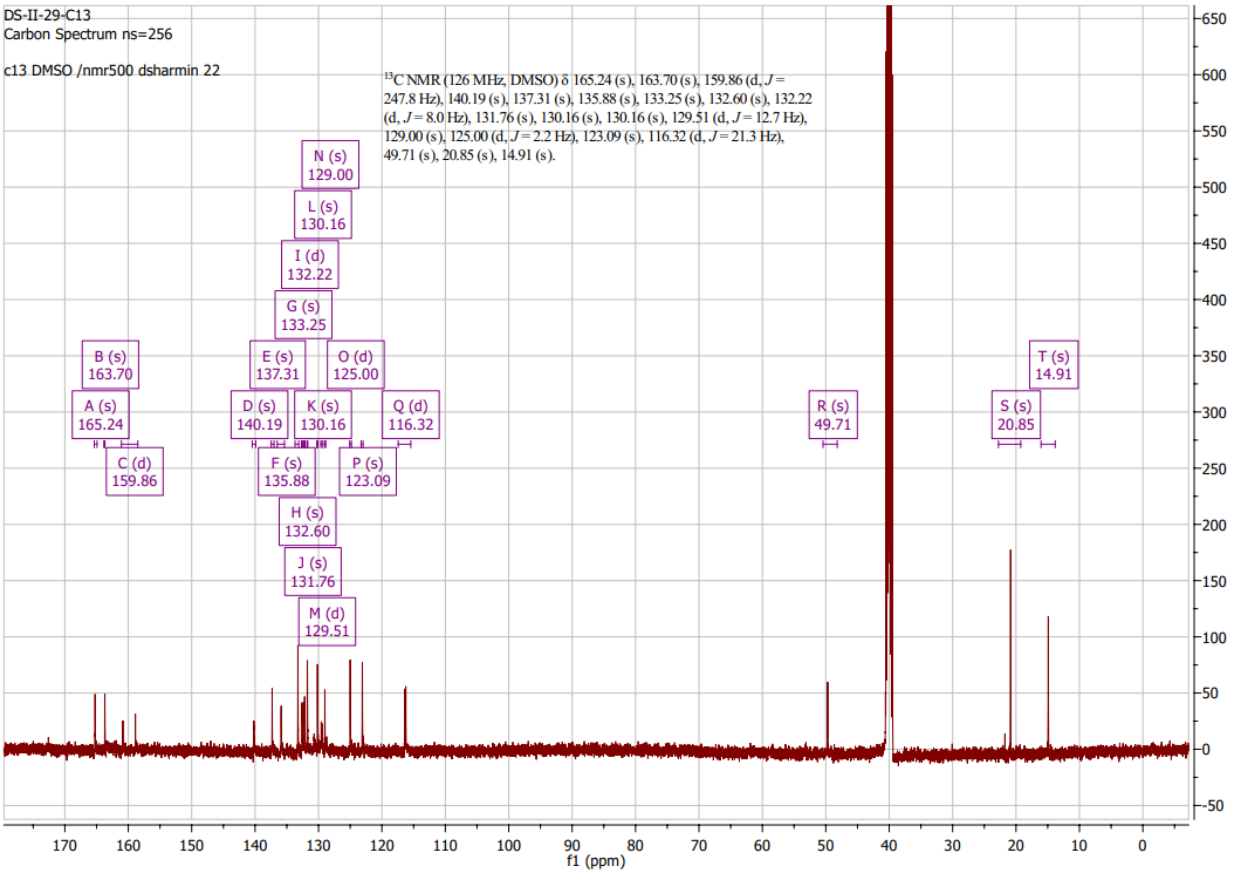

DS-II-28-C13
Carbon Spectrum ns=256
c13 DMSO /nmr500 dsharmin 21
^{13}C NMR (126 MHz, DMSO) δ 163.96 (s), 163.23 (s), 159.86 (d, J = 247.4 Hz), 141.41 (s), 137.66 (s), 136.76 (s), 133.36 (s), 132.32 (s), 132.30 (s), 131.76 (s), 130.20 (s), 129.35 (d, J = 13.1 Hz), 129.00 (s), 128.28 (s), 125.02 (d, J = 2.3 Hz), 123.21 (s), 116.33 (d, J = 21.4 Hz), 60.40 (s), 49.76 (s), 20.85 (s), 14.73 (s).
L (d) 129.35
J (s) 131.76
G (s) 133.36
B (s) 163.23
E (s) 137.66
M (s) 129.00
Q (d) 116.33
A (s) 163.96
D (s) 141.41
H (s) 132.32
P (s) 123.21
C (d) 159.86
F (s) 136.76
O (d) 125.02
I (s) 132.30
K (s) 130.20
N (s) 128.28
R (s) 60.40
S (s) 49.76
T (s) 20.85
U (s) 14.73
f1 (ppm)

Ethyl (*R*)-6-(2'-fluorophenyl)-4-methyl-8-methyl-4H-benzo[f]imidazo[1,5-a][1,4] diazepine-3-carboxylic acid (28)

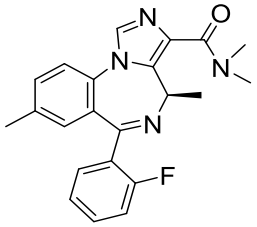


28

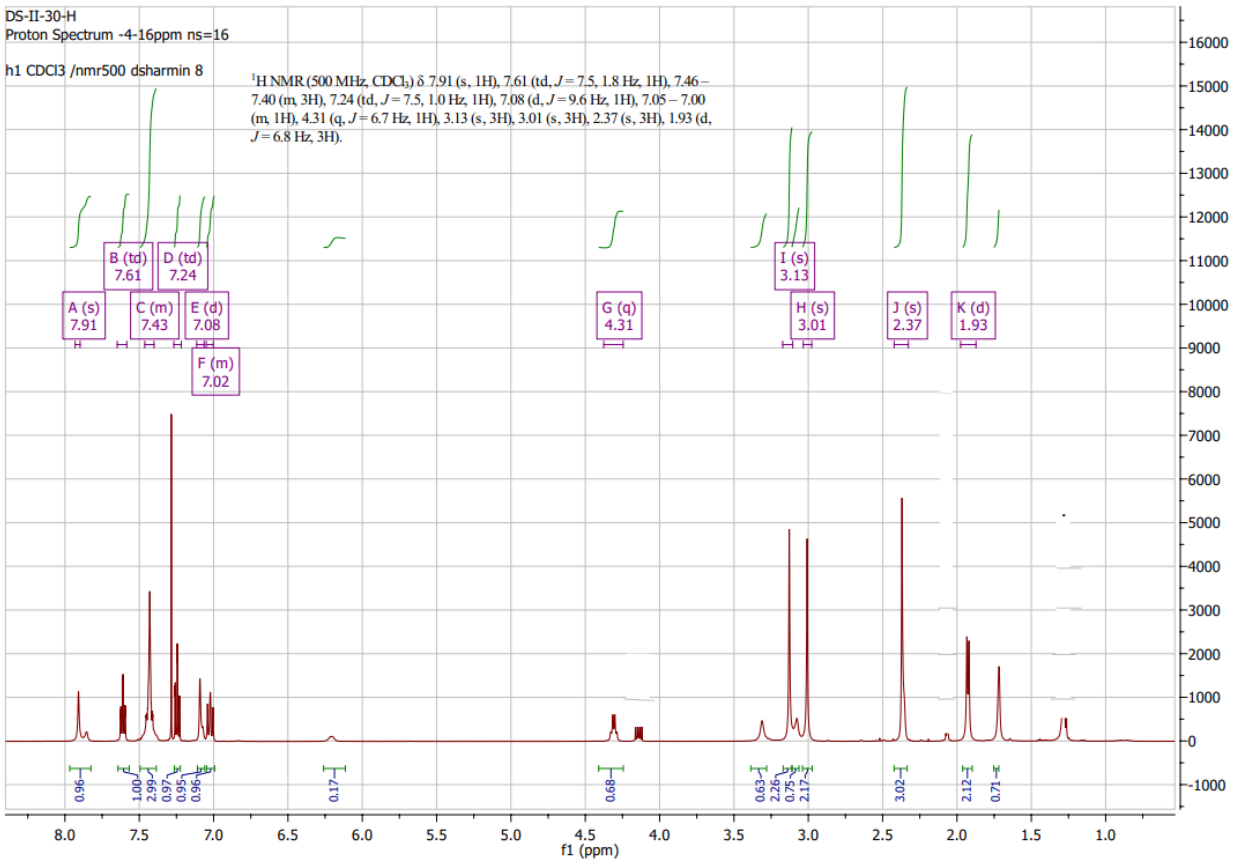


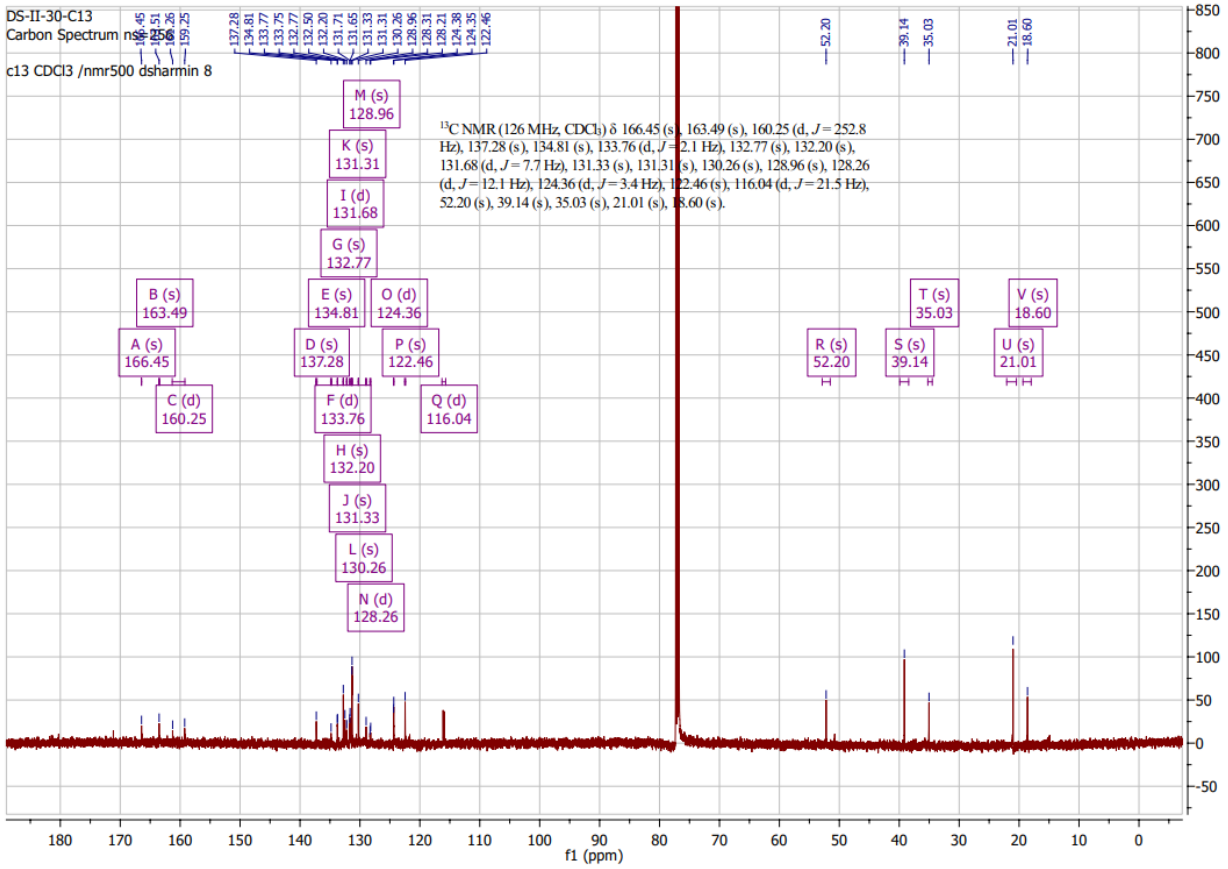

DS-II-29-C13
Carbon Spectrum ns=256
c13 DMSO /nmr500 dsharmin 22
^{13}C NMR (126 MHz, DMSO) δ 165.24 (s), 163.70 (s), 159.86 (d, J = 247.8 Hz), 140.19 (s), 137.31 (s), 135.88 (s), 133.25 (s), 132.60 (s), 132.22 (d, J = 8.0 Hz), 131.76 (s), 130.16 (s), 130.16 (s), 129.51 (d, J = 12.7 Hz), 129.00 (s), 125.00 (d, J = 2.2 Hz), 123.09 (s), 116.32 (d, J = 21.3 Hz), 49.71 (s), 20.85 (s), 14.91 (s).
N (s) 129.00
L (s) 130.16
I (d) 132.22
G (s) 133.25
B (s) 163.70
E (s) 137.31
O (d) 125.00
A (s) 165.24
D (s) 140.19
K (s) 130.16
Q (d) 116.32
R (s) 49.71
S (s) 20.85
T (s) 14.91
C (d) 159.86
F (s) 135.88
P (s) 123.09
H (s) 132.60
J (s) 131.76
M (d) 129.51
f1 (ppm)

(*R*)-6-(2'-fluorophenyl)-*N*,*N*,4,8-tetramethyl-4H-benzo[f]imidazo[1,5-a][1,4] diazepine-3-carboxamide (30)

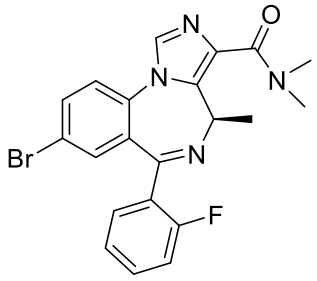


30, DS-II-30

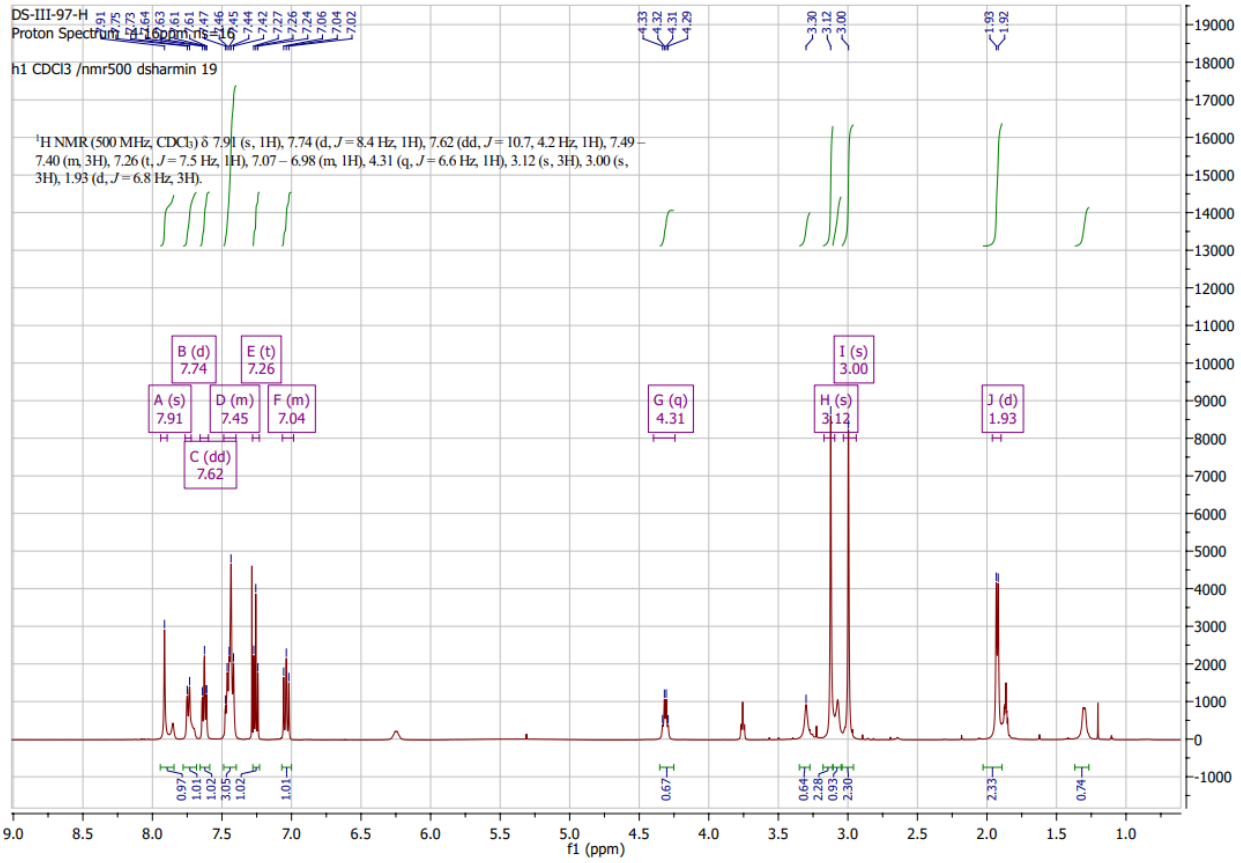


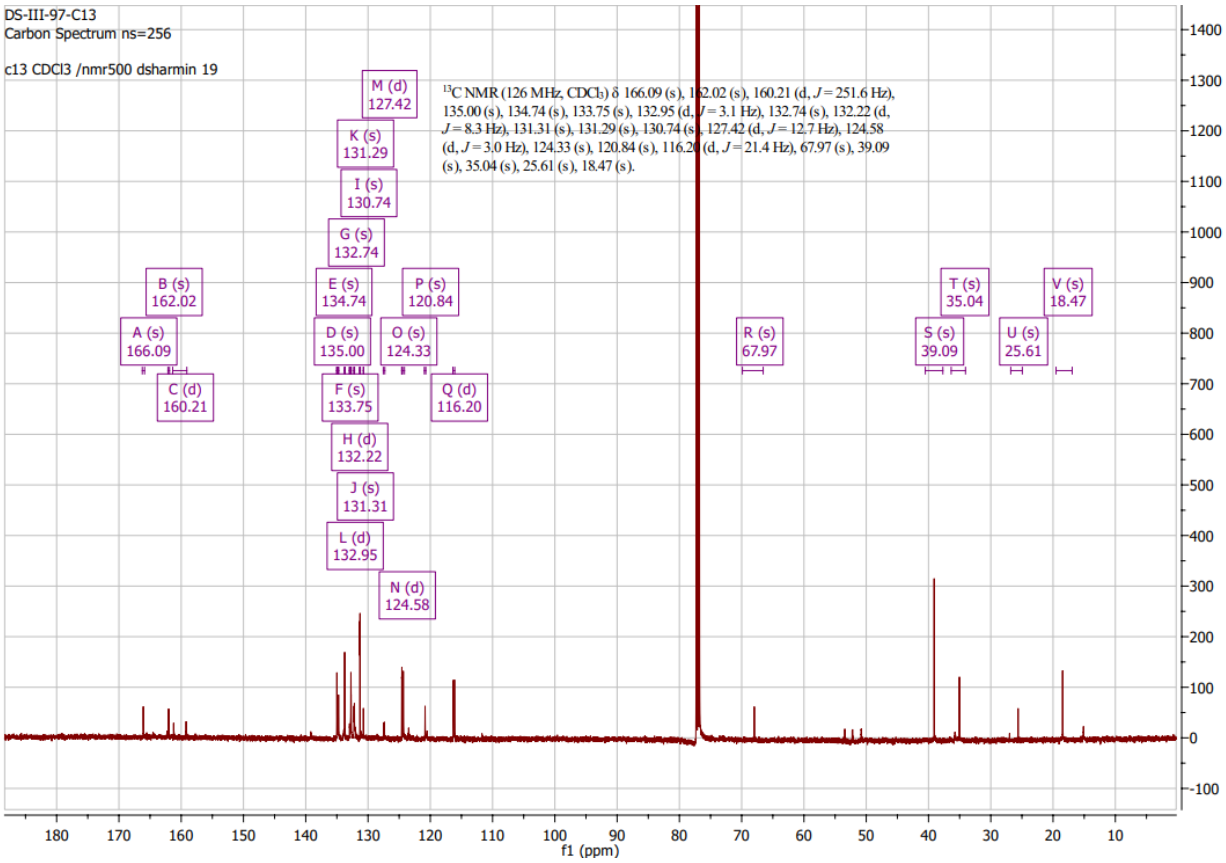

DS-II-30-C13
Carbon Spectrum nsc 256
c13 CDCl3 /nmr500 dsharmin 8
M (s) 128.96
K (s) 131.31
I (d) 131.68
G (s) 132.77
B (s) 163.49
E (s) 134.81
O (d) 124.36
A (s) 166.45
D (s) 137.28
P (s) 122.46
C (d) 160.25
F (d) 133.76
Q (d) 116.04
H (s) 132.20
J (s) 131.33
L (s) 130.26
N (d) 128.26
T (s) 35.03
V (s) 18.60
R (s) 52.20
S (s) 39.14
U (s) 21.01
^{13}C NMR (126 MHz, CDCl$_3$) δ 166.45 (s), 163.49 (s), 160.25 (d, J = 252.8 Hz), 137.28 (s), 134.81 (s), 133.76 (d, J = 2.1 Hz), 132.77 (s), 132.20 (s), 131.68 (d, J = 7.7 Hz), 131.33 (s), 131.31 (s), 130.26 (s), 128.96 (s), 128.26 (d, J = 12.1 Hz), 124.36 (d, J = 3.4 Hz), 122.46 (s), 116.04 (d, J = 21.5 Hz), 52.20 (s), 39.14 (s), 35.03 (s), 21.01 (s), 18.60 (s).
f1 (ppm)

(*R*)-8-Bromo-6-(2-fluorophenyl)-*N*,*N*,4-trimethyl-4*H*-benzo[*f*]imidazo[1,5][1,4] diazepine-3-carboxamide [DS-III-97, 31]

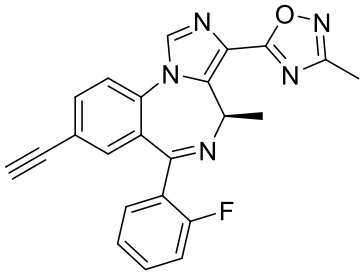


DS-III-97, 16

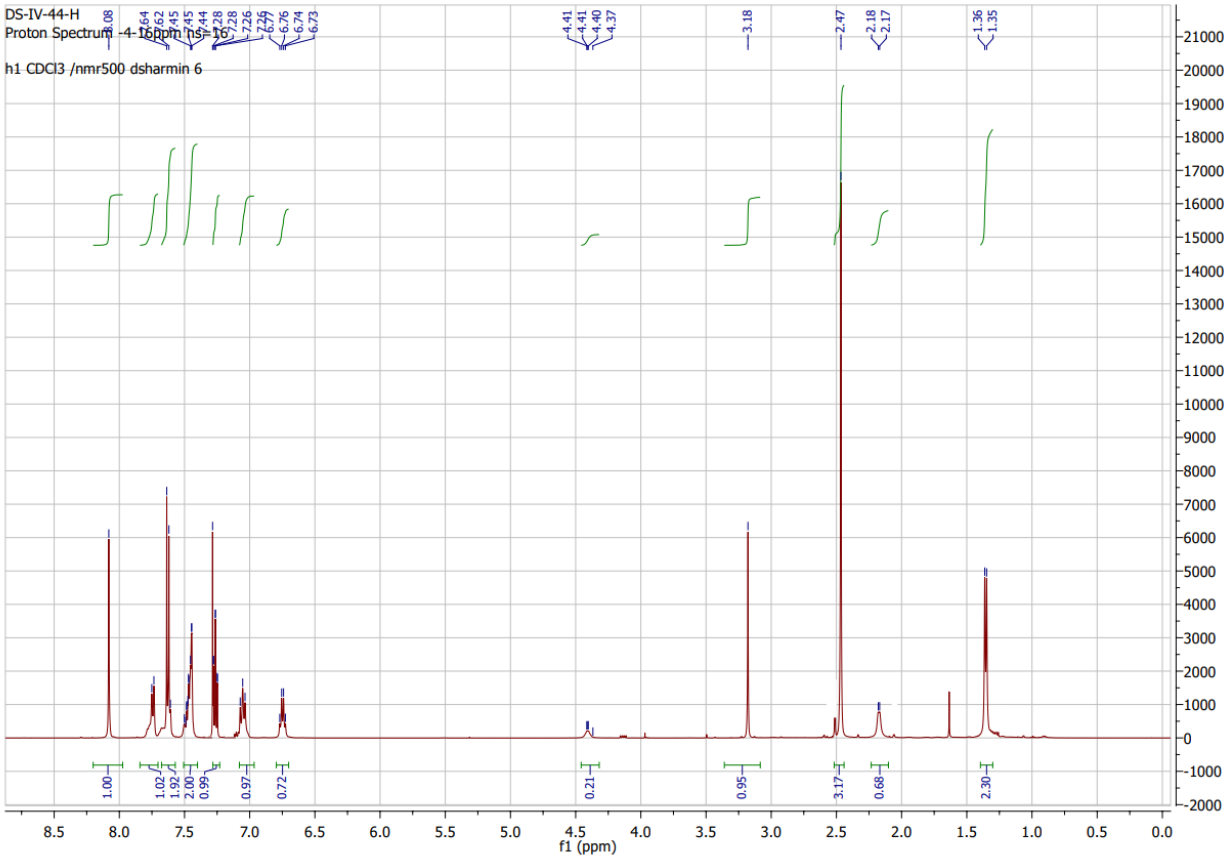


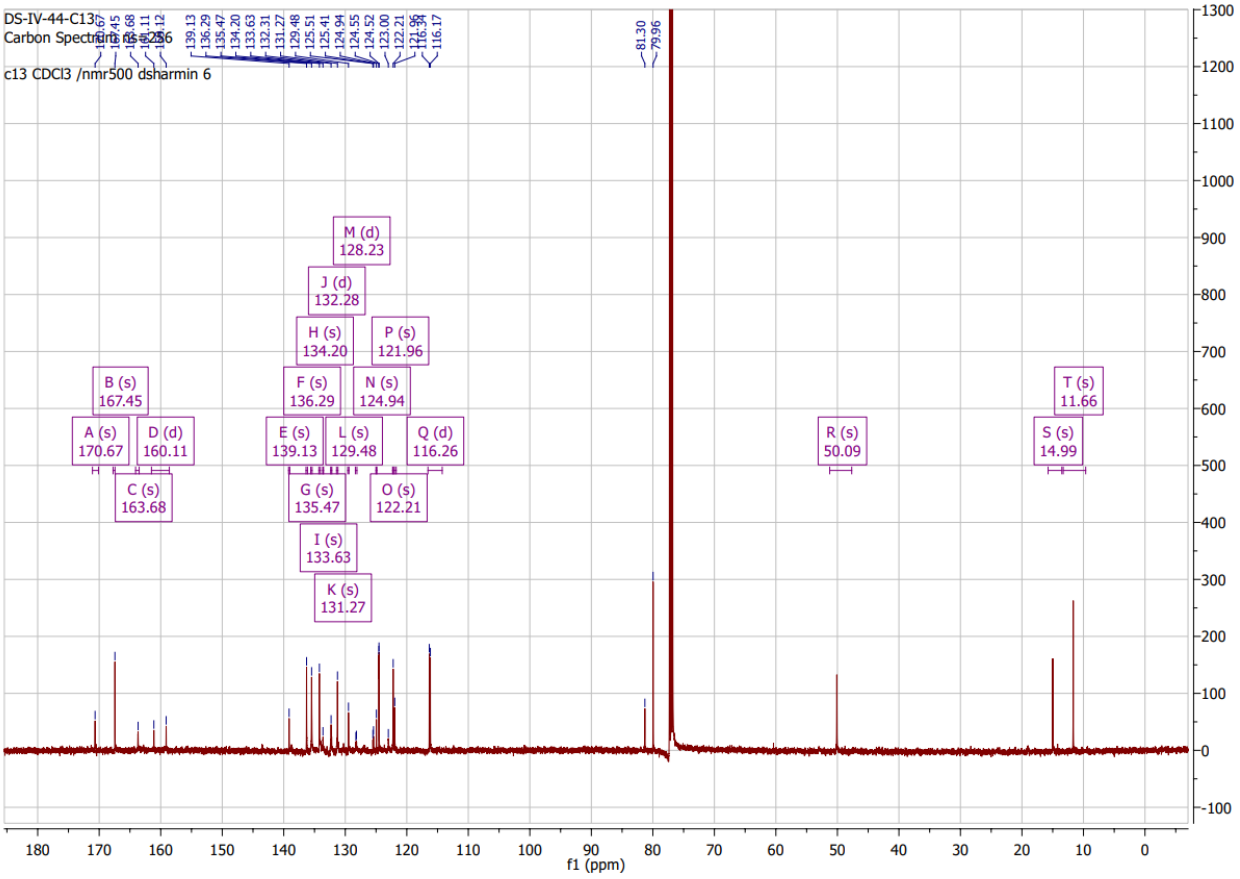

DS-III-97-C13
Carbon Spectrum ns=256
c13 CDCl3 /nmr500 dsharmin 19
13C NMR (126 MHz, CDCl3) δ 166.09 (s), 162.02 (s), 160.21 (d, J = 251.6 Hz), 135.00 (s), 134.74 (s), 133.75 (s), 132.95 (d, J = 3.1 Hz), 132.74 (s), 132.22 (d, J = 8.3 Hz), 131.31 (s), 131.29 (s), 130.74 (s), 127.42 (d, J = 12.7 Hz), 124.58 (d, J = 3.0 Hz), 124.33 (s), 120.84 (s), 116.20 (d, J = 21.4 Hz), 67.97 (s), 39.09 (s), 35.04 (s), 25.61 (s), 18.47 (s).
M (d) 127.42
K (s) 131.29
I (s) 130.74
G (s) 132.74
B (s) 162.02
E (s) 134.74
P (s) 120.84
A (s) 166.09
D (s) 135.00
O (s) 124.33
R (s) 67.97
T (s) 35.04
V (s) 18.47
S (s) 39.09
U (s) 25.61
C (d) 160.21
F (s) 133.75
Q (d) 116.20
H (d) 132.22
J (s) 131.31
L (d) 132.95
N (d) 124.58
f1 (ppm)

(*R*)-5-(8-ethynyl-6-(2-fluorophenyl)-4-methyl-4*H*-benzo[*f*]imidazo[1,5-*a*][1,4]diazepin-3-yl)-3-methyl-1,2,4-oxadiazole (34)

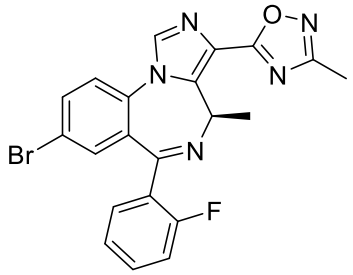


34

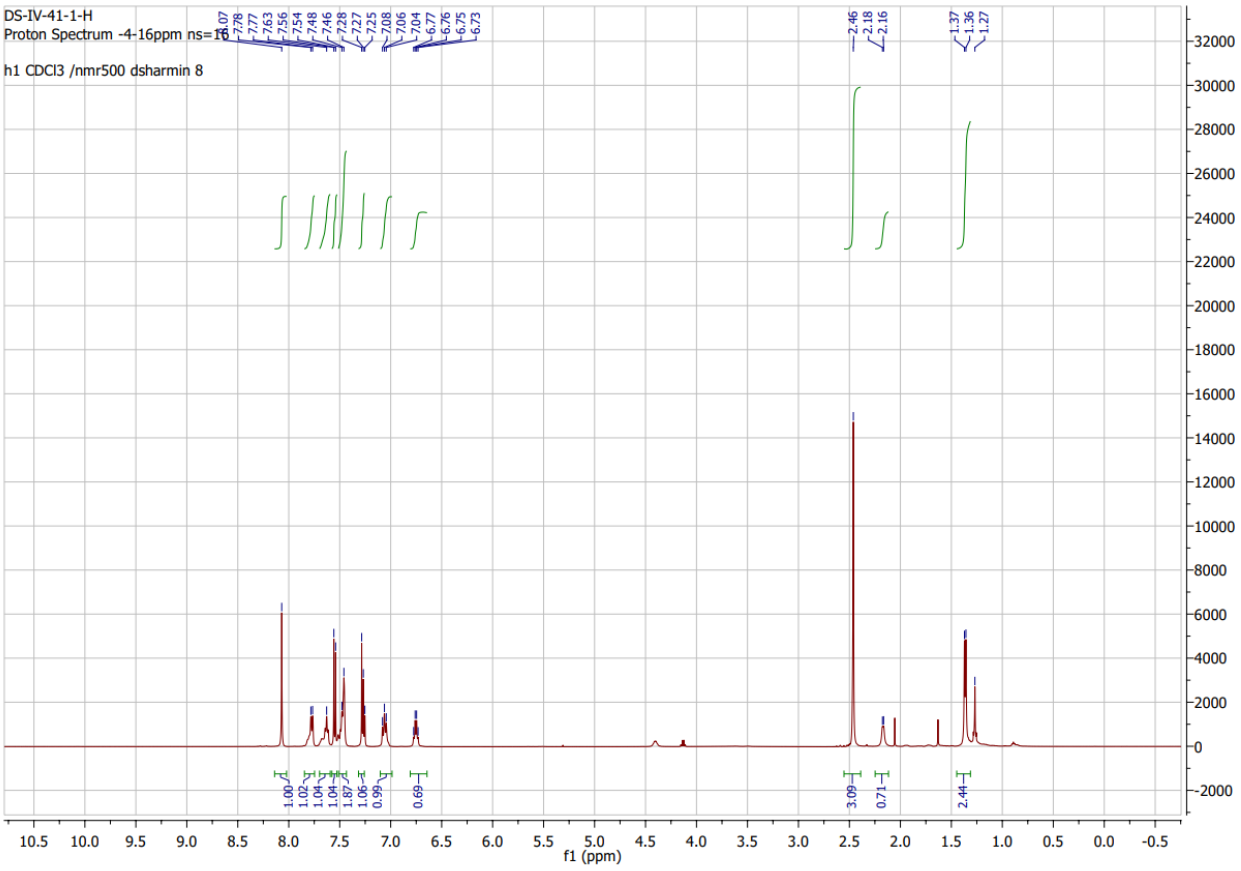


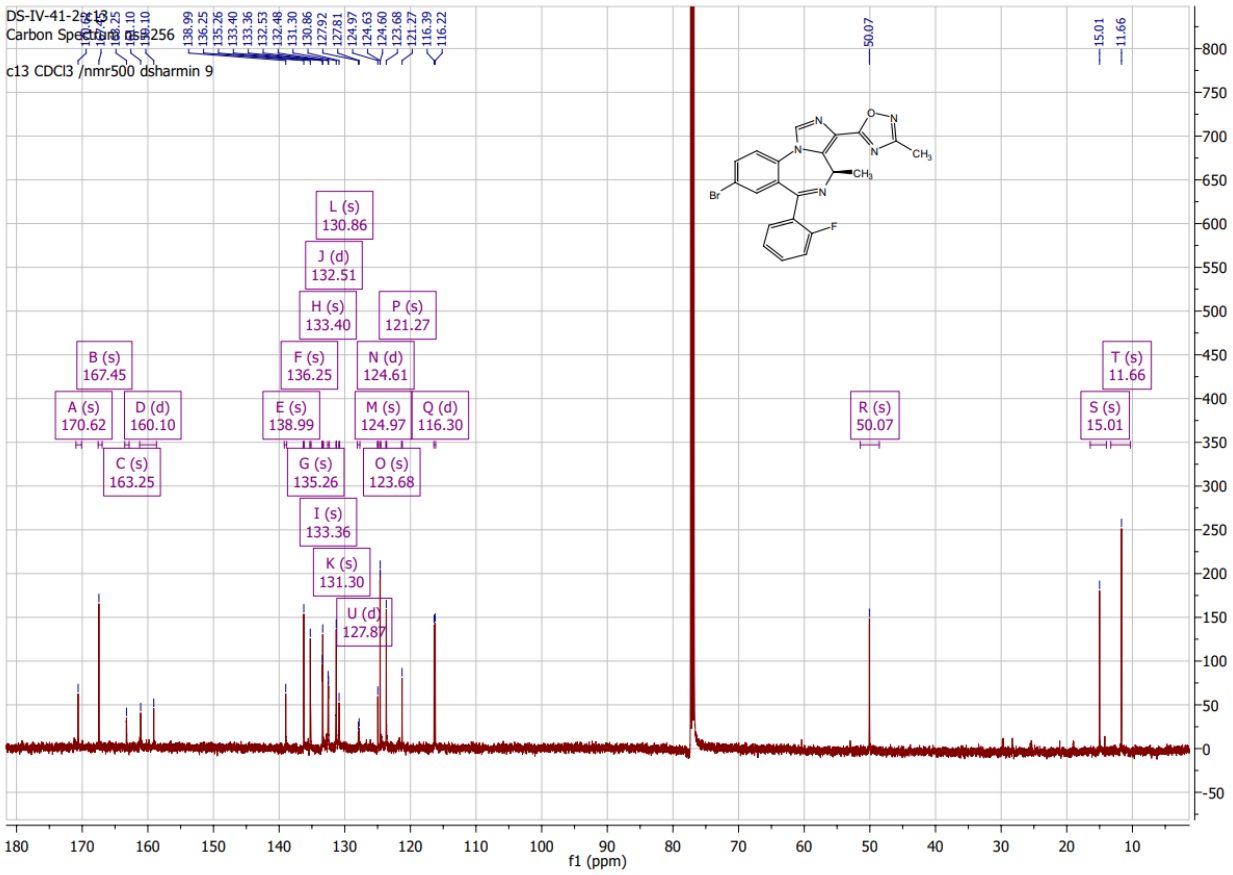

DS-IV-44-C13
Carbon Spectrum 6 s 256
c13 CDCl3 /nmr500 dsharmin 6
A (s) 170.67
B (s) 167.45
C (s) 163.68
D (d) 160.11
E (s) 139.13
F (s) 136.29
G (s) 135.47
H (s) 134.20
I (s) 133.63
J (d) 132.28
K (s) 131.27
L (s) 129.48
M (d) 128.23
N (s) 124.94
O (s) 122.21
P (s) 121.96
Q (d) 116.26
R (s) 50.09
S (s) 14.99
T (s) 11.66
f1 (ppm)

(*R*)-5-(8-ethynyl-6-(2-fluorophenyl)-4-methyl-4*H*-benzo[*f*]imidazo[1,5-*a*][1,4]diazepin-3-yl)-3-methyl-1,2,4-oxadiazole (DS-IV-41, 35)

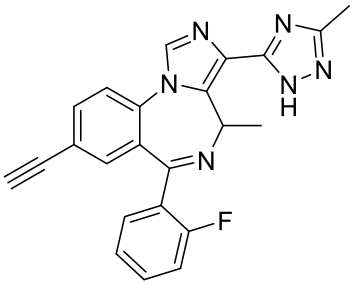


DS-IV-41, 35

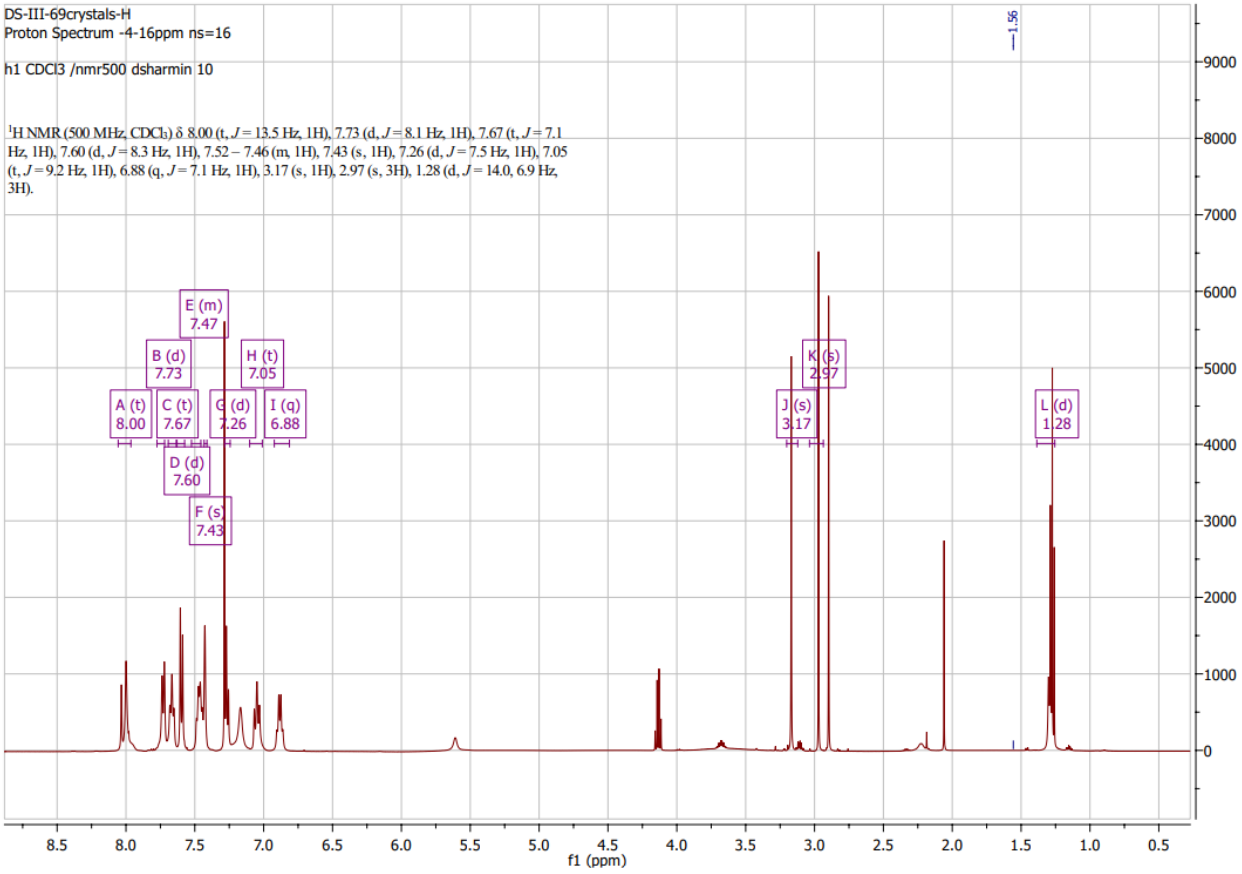


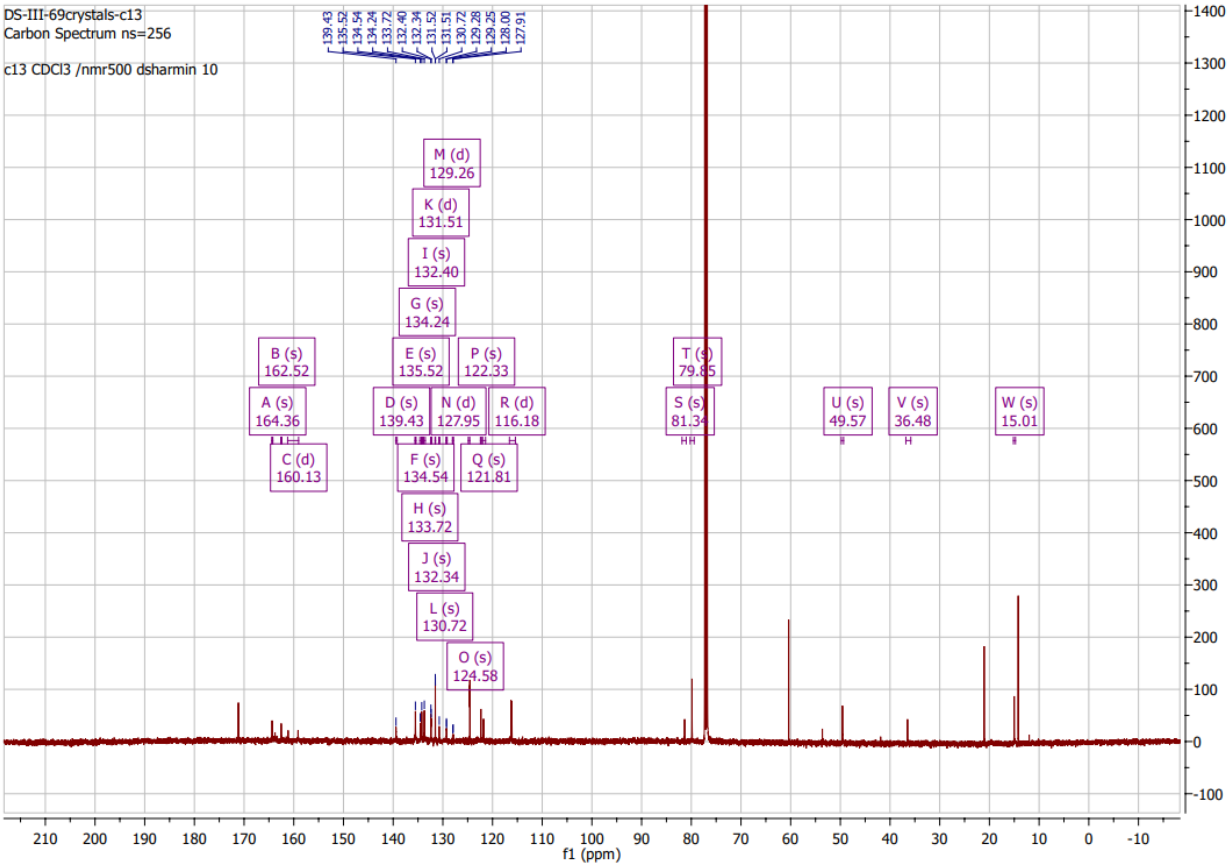

DS-IV-41-2-c13
Carbon Spectrum ds 256
c13 CDCl3 /nmr500 dsharmin 9
A (s) 170.62
B (s) 167.45
C (s) 163.25
D (d) 160.10
E (s) 138.99
F (s) 136.25
G (s) 135.26
H (s) 133.40
I (s) 133.36
J (d) 132.51
K (s) 131.30
L (s) 130.86
M (s) 124.97
N (d) 124.61
O (s) 123.68
P (s) 121.27
Q (d) 116.30
R (s) 50.07
S (s) 15.01
T (s) 11.66
U (d) 127.87
f1 (ppm)

8-ethynyl-6-(2-fluorophenyl)-4-methyl-3-(3-methyl-1H-1,2,4-triazol-5-yl)-4H-benzo[f]imidazo[1,5-a][1,4]diazepine (DS-III-69, 36)

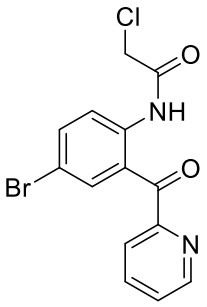


DS-III-69, 36

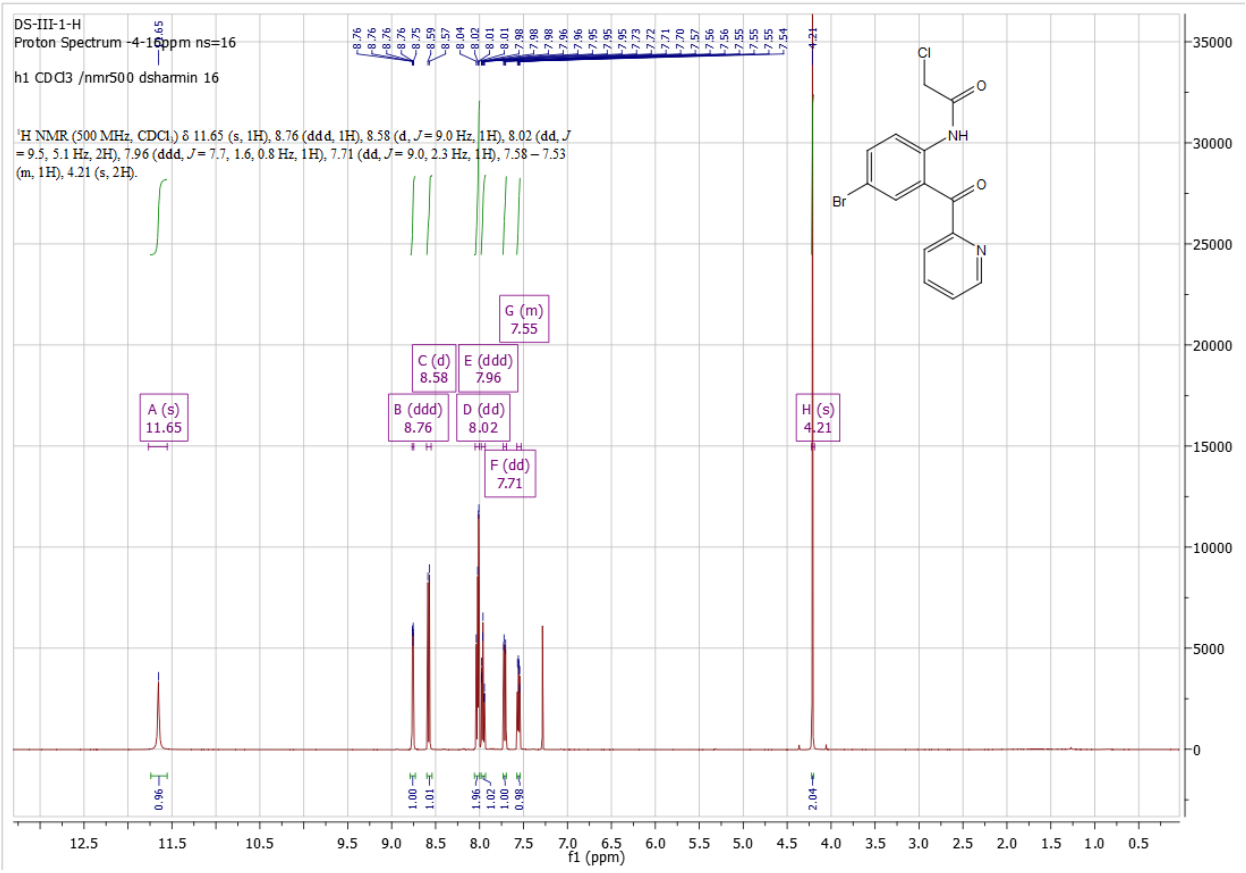



DS-III-69crystals-c13
Carbon Spectrum ns=256
c13 CDCl3 /nmr500 dsharmin 10
139.43
135.52
134.54
134.24
133.72
132.40
132.34
131.52
131.51
130.72
129.28
129.25
128.00
127.91
M (d) 129.26
K (d) 131.51
I (s) 132.40
G (s) 134.24
B (s) 162.52
E (s) 135.52
P (s) 122.33
T (s) 79.85
A (s) 164.36
D (s) 139.43
N (d) 127.95
R (d) 116.18
S (s) 81.34
U (s) 49.57
V (s) 36.48
W (s) 15.01
C (d) 160.13
F (s) 134.54
Q (s) 121.81
H (s) 133.72
J (s) 132.34
L (s) 130.72
O (s) 124.58
f1 (ppm)

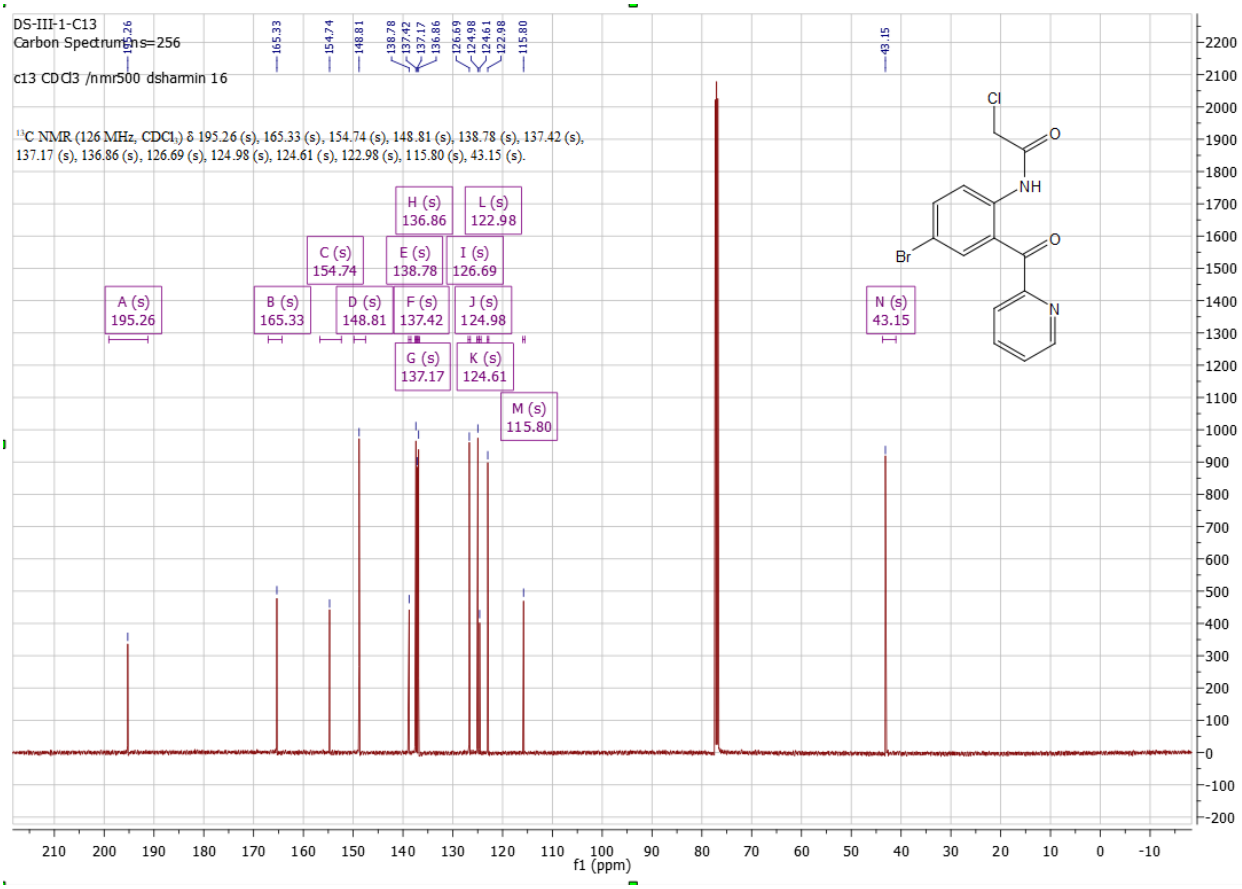
N-(4-bromo-2-picolinoylphenyl)-2-chloroacetamide (7)



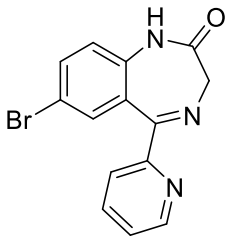
^{1}H NMR



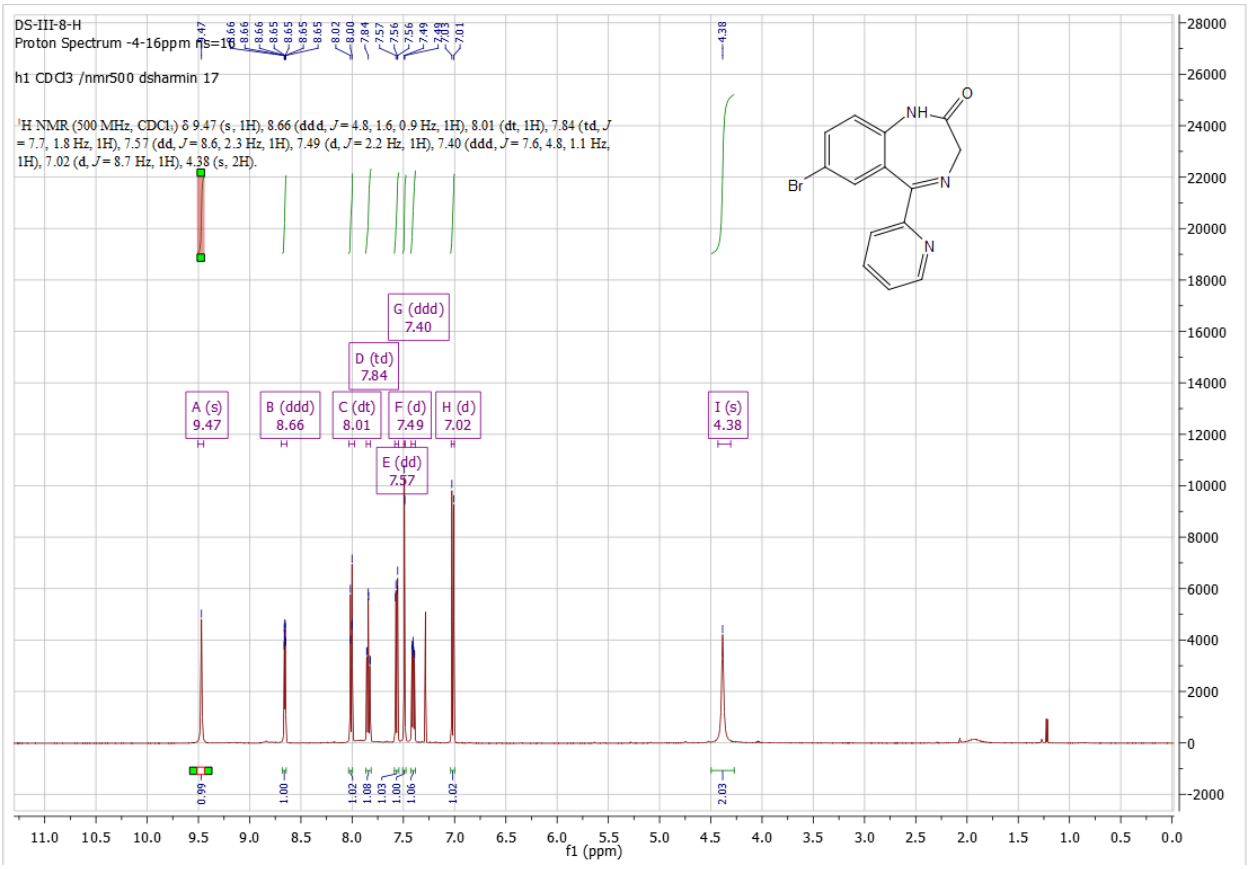
^{13}C NMR


DS-III-1-C13
Carbon Spectrum ns=256
c13 CDCl3 /nmr500 dsharmin 16
13C NMR (126 MHz, CDCl3) δ 195.26 (s), 165.33 (s), 154.74 (s), 148.81 (s), 138.78 (s), 137.42 (s), 137.17 (s), 136.86 (s), 126.69 (s), 124.98 (s), 124.61 (s), 122.98 (s), 115.80 (s), 43.15 (s).
A (s) 195.26
B (s) 165.33
C (s) 154.74
D (s) 148.81
E (s) 138.78
F (s) 137.42
G (s) 137.17
H (s) 136.86
I (s) 126.69
J (s) 124.98
K (s) 124.61
L (s) 122.98
M (s) 115.80
N (s) 43.15
Cl
O
NH
O
Br
N
f1 (ppm)

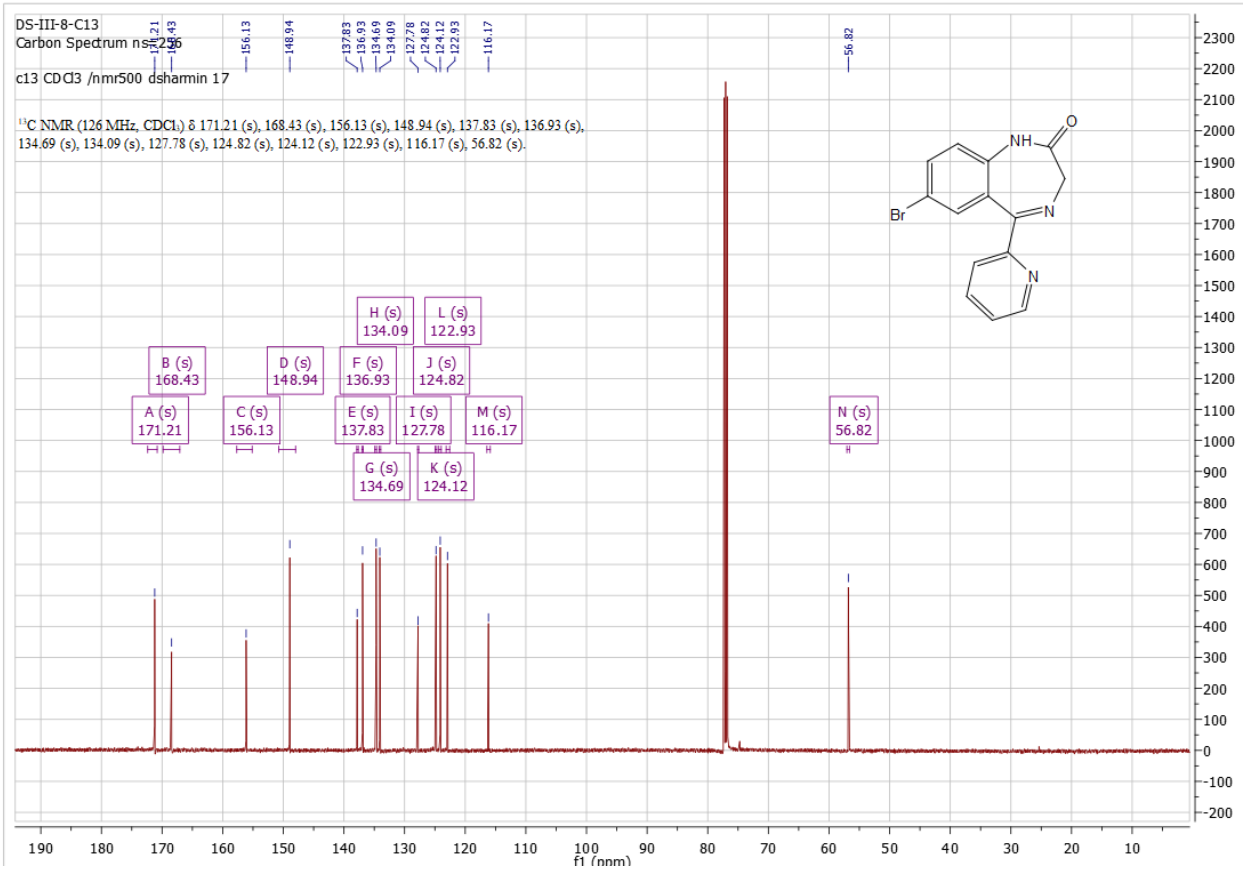
7-Bromo-5-(pyridin-2-yl)-1,3-dihydro-2H-benzo[e][1,4]diazepin-2-one (8)



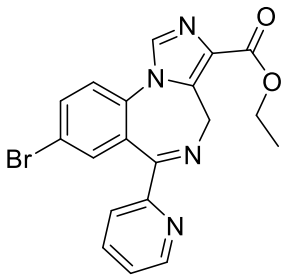
^{1}H NMR



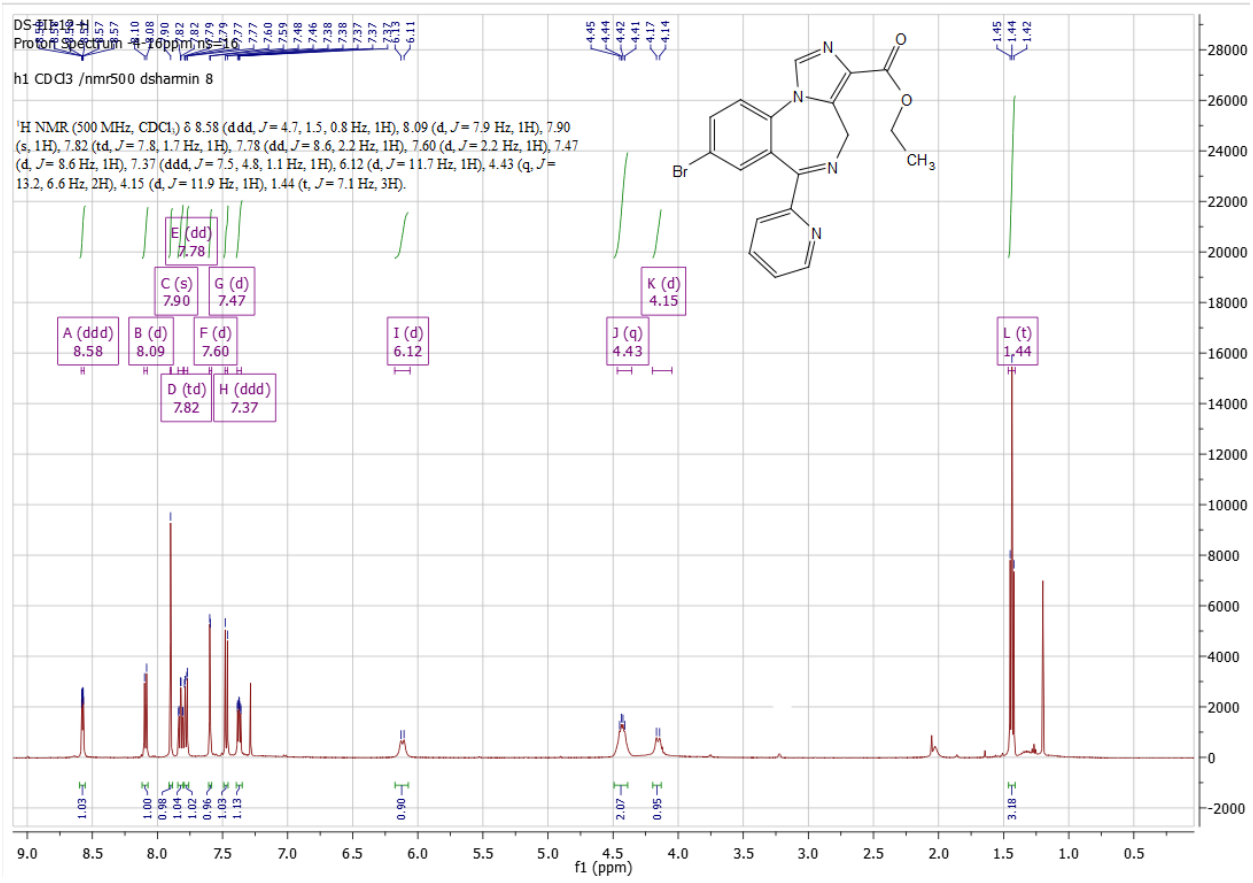
^{13}C NMR


DS-III-8-C13
Carbon Spectrum ns=2256
c13 CDCl3 /nmr500 dsharmin 17
13C NMR (126 MHz, CDCl3) δ 171.21 (s), 168.43 (s), 156.13 (s), 148.94 (s), 137.83 (s), 136.93 (s), 134.69 (s), 134.09 (s), 127.78 (s), 124.82 (s), 124.12 (s), 122.93 (s), 116.17 (s), 56.82 (s).
171.21
168.43
156.13
148.94
137.83
136.93
134.69
134.09
127.78
124.82
124.12
122.93
116.17
56.82
A (s) 171.21
B (s) 168.43
C (s) 156.13
D (s) 148.94
E (s) 137.83
F (s) 136.93
G (s) 134.69
H (s) 134.09
I (s) 127.78
J (s) 124.82
K (s) 124.12
L (s) 122.93
M (s) 116.17
N (s) 56.82
NH
O
Br
N
N
f1 (ppm)

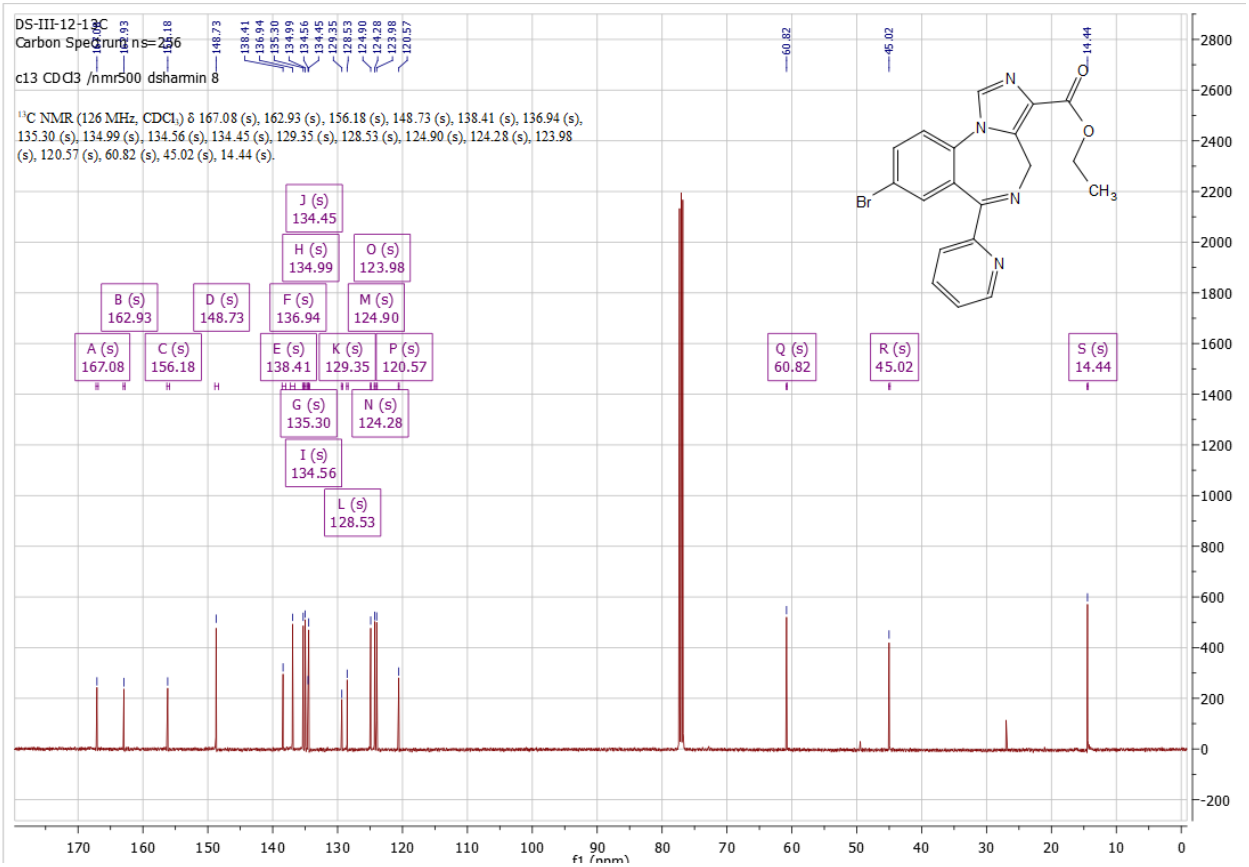
Ethyl 8-bromo-6-(pyridin-2-yl)-4H-benzo[f]imidazo[1,5-a][1,4]diazepine-3-carboxylate(9)



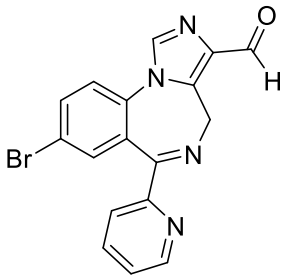
^{1}H NMR



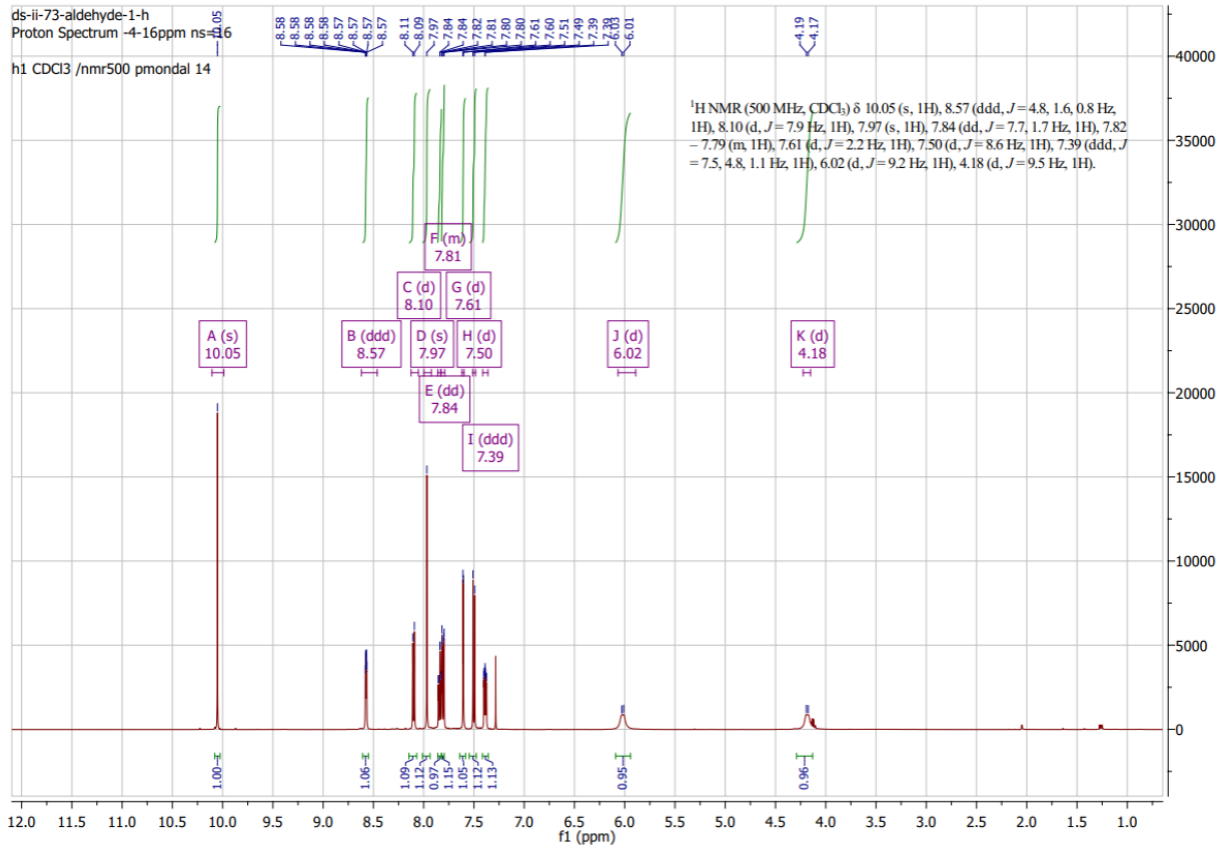
^{13}C NMR


DS-III-12-13C
Carbon Spectrum ns=256
c13 CDCl3 /nmr500 dsharmin 8
^{13}C NMR (126 MHz, $CDCl_3$) δ 167.08 (s), 162.93 (s), 156.18 (s), 148.73 (s), 138.41 (s), 136.94 (s), 135.30 (s), 134.99 (s), 134.56 (s), 134.45 (s), 129.35 (s), 128.53 (s), 124.90 (s), 124.28 (s), 123.98 (s), 120.57 (s), 60.82 (s), 45.02 (s), 14.44 (s).
A (s) 167.08
B (s) 162.93
C (s) 156.18
D (s) 148.73
E (s) 138.41
F (s) 136.94
G (s) 135.30
H (s) 134.99
I (s) 134.56
J (s) 134.45
K (s) 129.35
L (s) 128.53
M (s) 124.90
N (s) 124.28
O (s) 123.98
P (s) 120.57
Q (s) 60.82
R (s) 45.02
S (s) 14.44
Br
CH3
f1 (ppm)

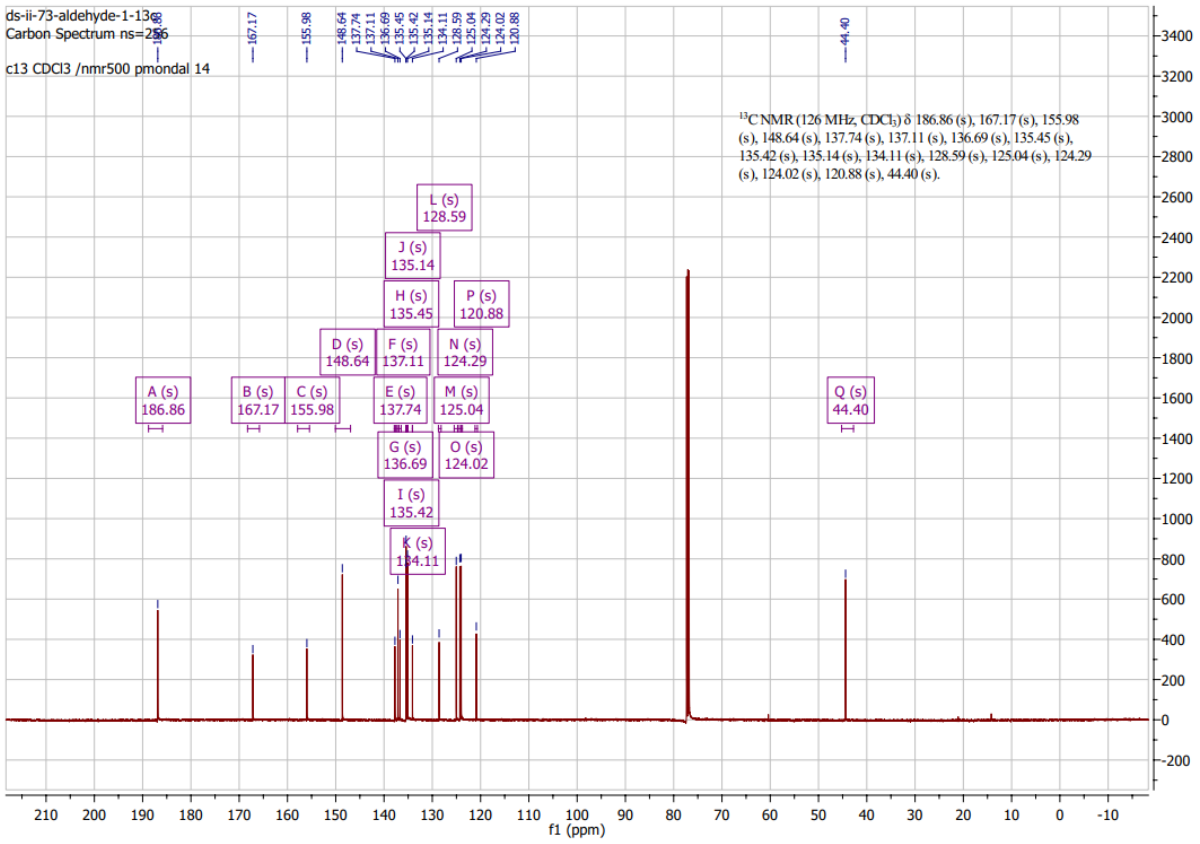
8-Bromo-6-(pyridin-2-yl)-4H-benzo[f]imidazo[1,5-a][1,4]diazepine-3-carbaldehyde (10)



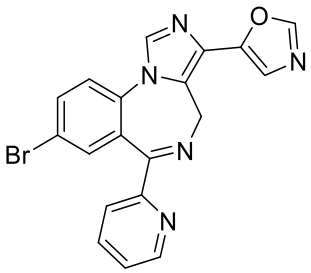
^{1}H NMR:



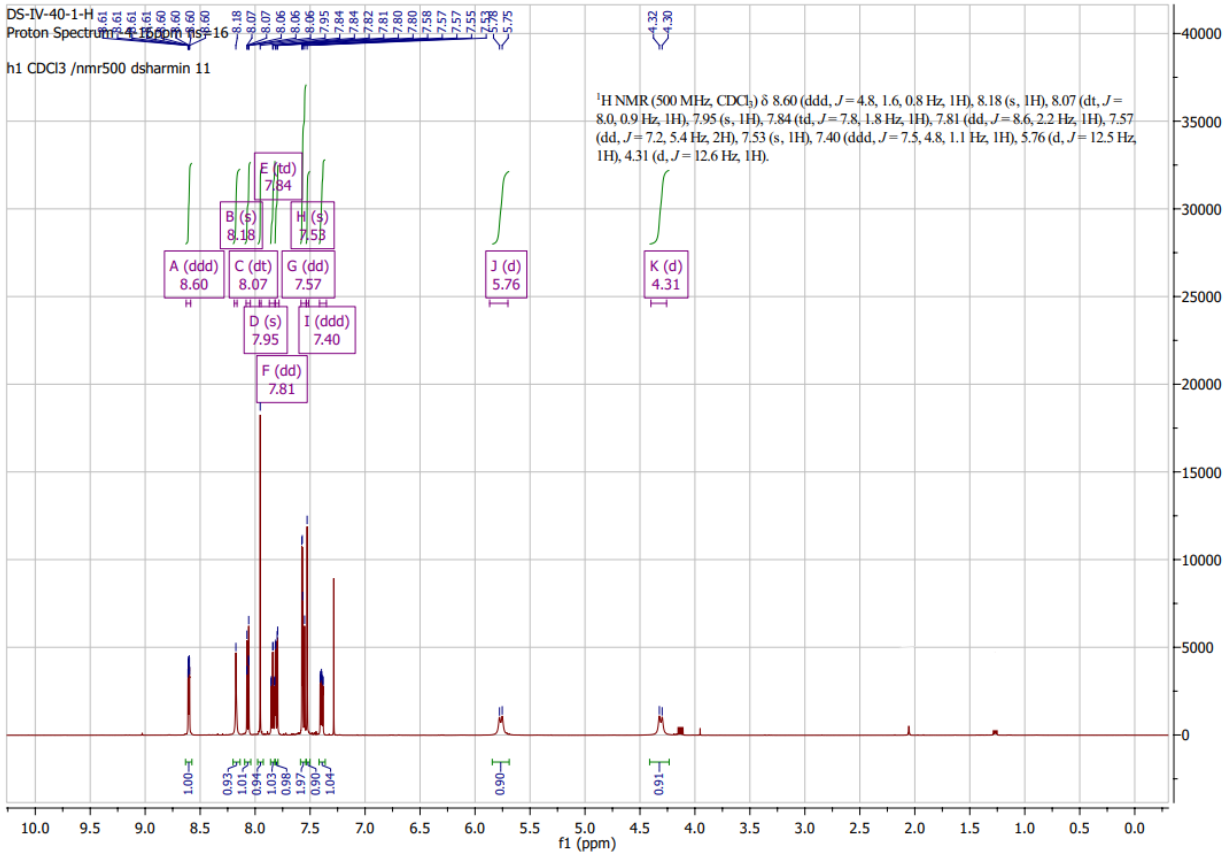
^{13}C NMR:


ds-ii-73-aldehyde-1-13c
Carbon Spectrum ns=256
c13 CDCl3 /nmr500 pmondal 14
^{13}C NMR (126 MHz, $CDCl_3$) δ 186.86 (s), 167.17 (s), 155.98 (s), 148.64 (s), 137.74 (s), 137.11 (s), 136.69 (s), 135.45 (s), 135.42 (s), 135.14 (s), 134.11 (s), 128.59 (s), 125.04 (s), 124.29 (s), 124.02 (s), 120.88 (s), 44.40 (s).
A (s) 186.86
B (s) 167.17
C (s) 155.98
D (s) 148.64
E (s) 137.74
F (s) 137.11
G (s) 136.69
H (s) 135.45
I (s) 135.42
J (s) 135.14
K (s) 134.11
L (s) 128.59
M (s) 125.04
N (s) 124.29
O (s) 124.02
P (s) 120.88
Q (s) 44.40
f1 (ppm)

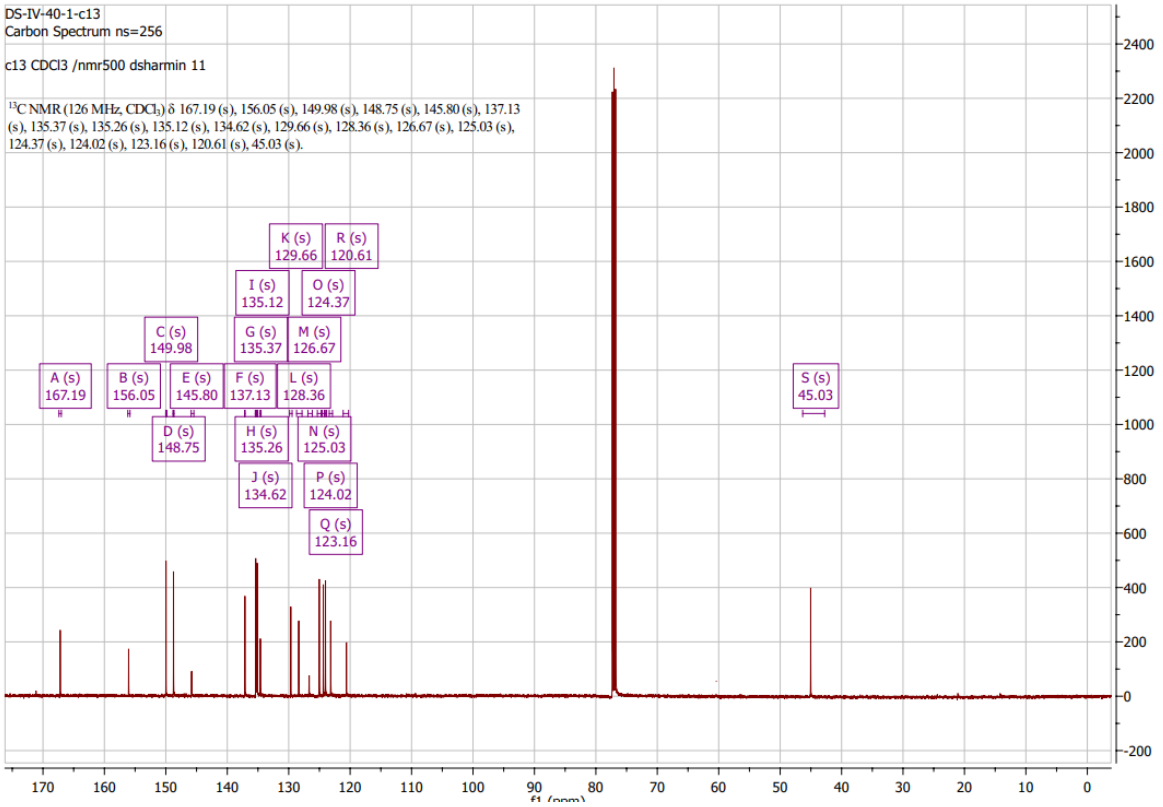
5-(8-Bromo-6-(pyridin-2-yl)-4H-benzo[f]imidazo[1,5-a][1,4]diazepin-3-yl)oxazole (DS-II-73, 5)



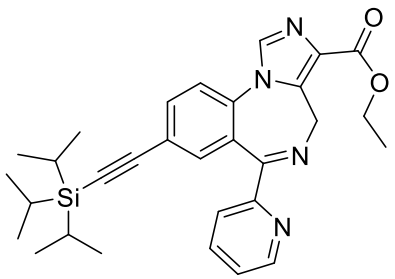
^{1}H NMR:

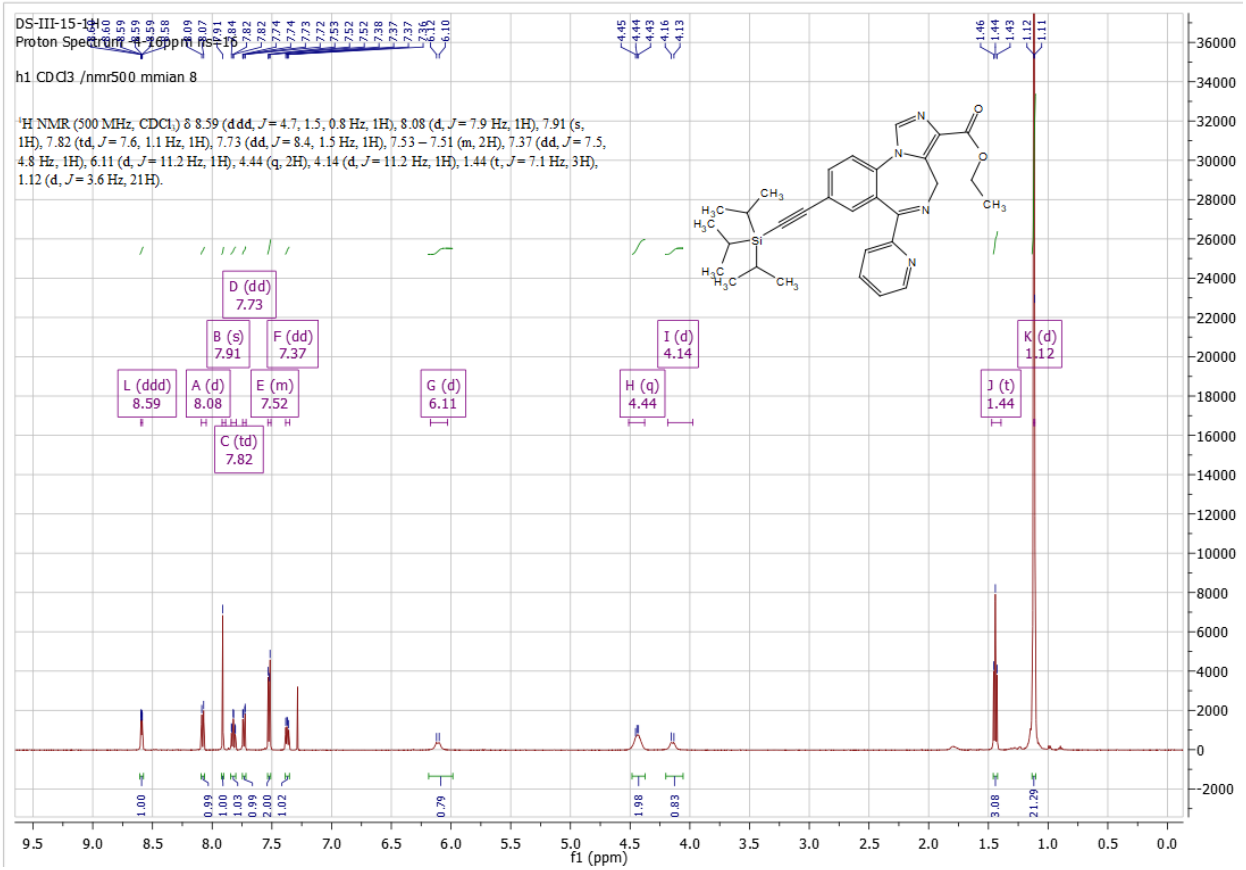


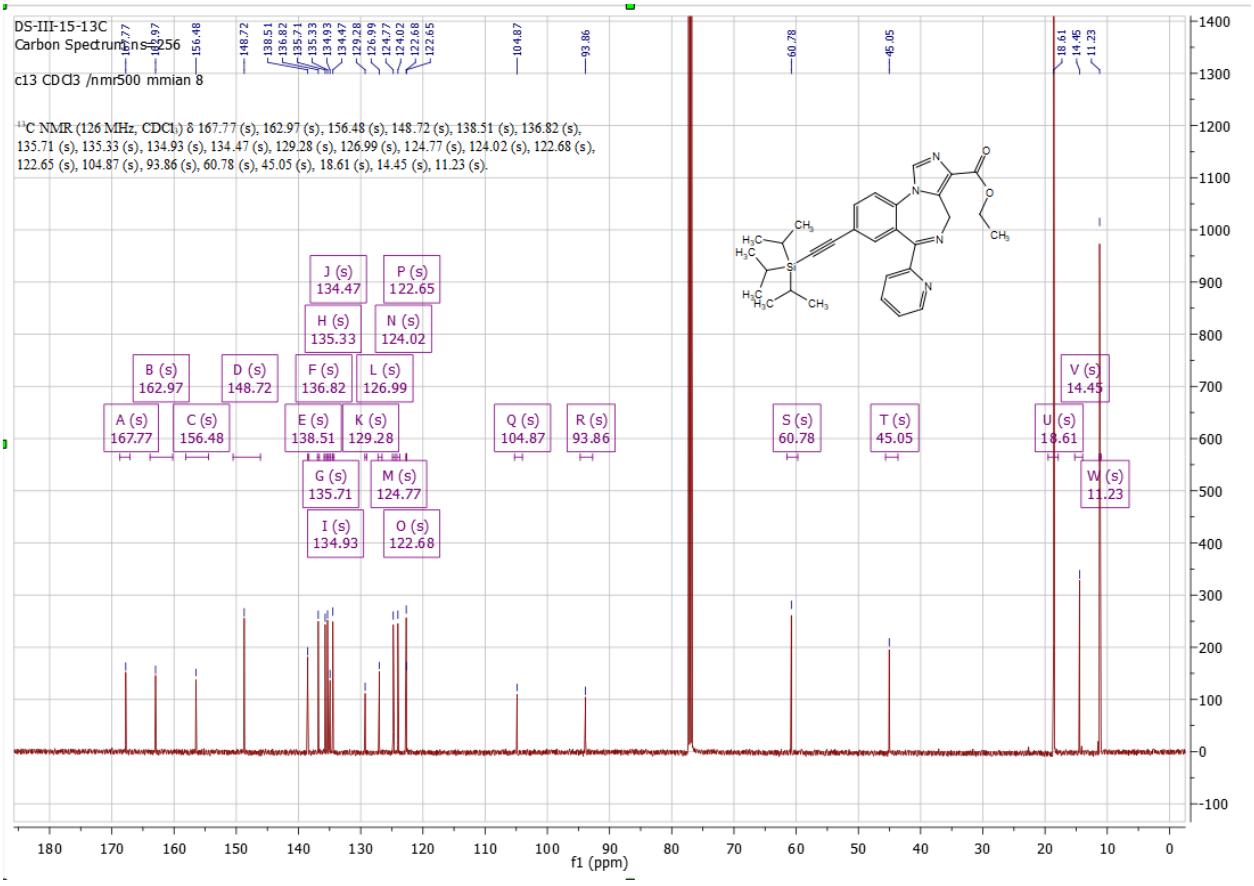
^{13}C NMR:


DS-IV-40-1-c13
Carbon Spectrum ns=256
c13 CDCl3 /nmr500 dsharmin 11
^{13}C NMR (126 MHz, $CDCl_3$) δ 167.19 (s), 156.05 (s), 149.98 (s), 148.75 (s), 145.80 (s), 137.13 (s), 135.37 (s), 135.26 (s), 135.12 (s), 134.62 (s), 129.66 (s), 128.36 (s), 126.67 (s), 125.03 (s), 124.37 (s), 124.02 (s), 123.16 (s), 120.61 (s), 45.03 (s).
A (s) 167.19
B (s) 156.05
C (s) 149.98
D (s) 148.75
E (s) 145.80
F (s) 137.13
G (s) 135.37
H (s) 135.26
I (s) 135.12
J (s) 134.62
K (s) 129.66
L (s) 128.36
M (s) 126.67
N (s) 125.03
O (s) 124.37
P (s) 124.02
Q (s) 123.16
R (s) 120.61
S (s) 45.03
2400
2200
2000
1800
1600
1400
1200
1000
800
600
400
200
0
-200
170
160
150
140
130
120
110
100
90
80
70
60
50
40
30
20
10
0
f1 (ppm)

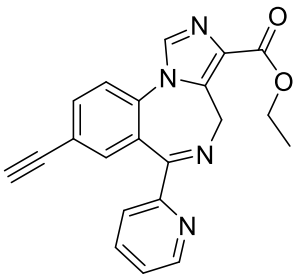
Ethyl 6-(pyridin-2-yl)-8-((triisopropylsilyl)ethynyl)-4Hbenzo[f]imidazo[1,5a][1,4]diazepine-3-carboxylate

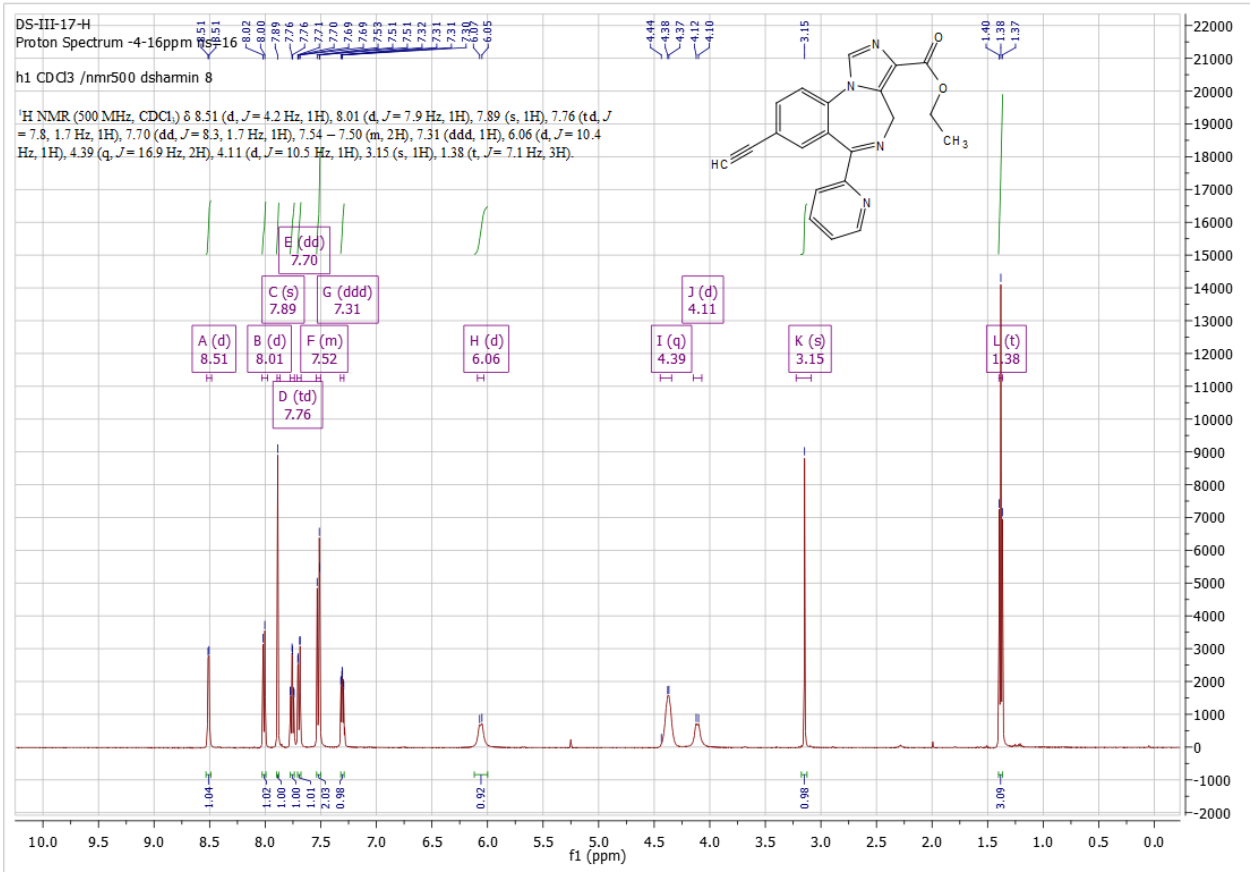


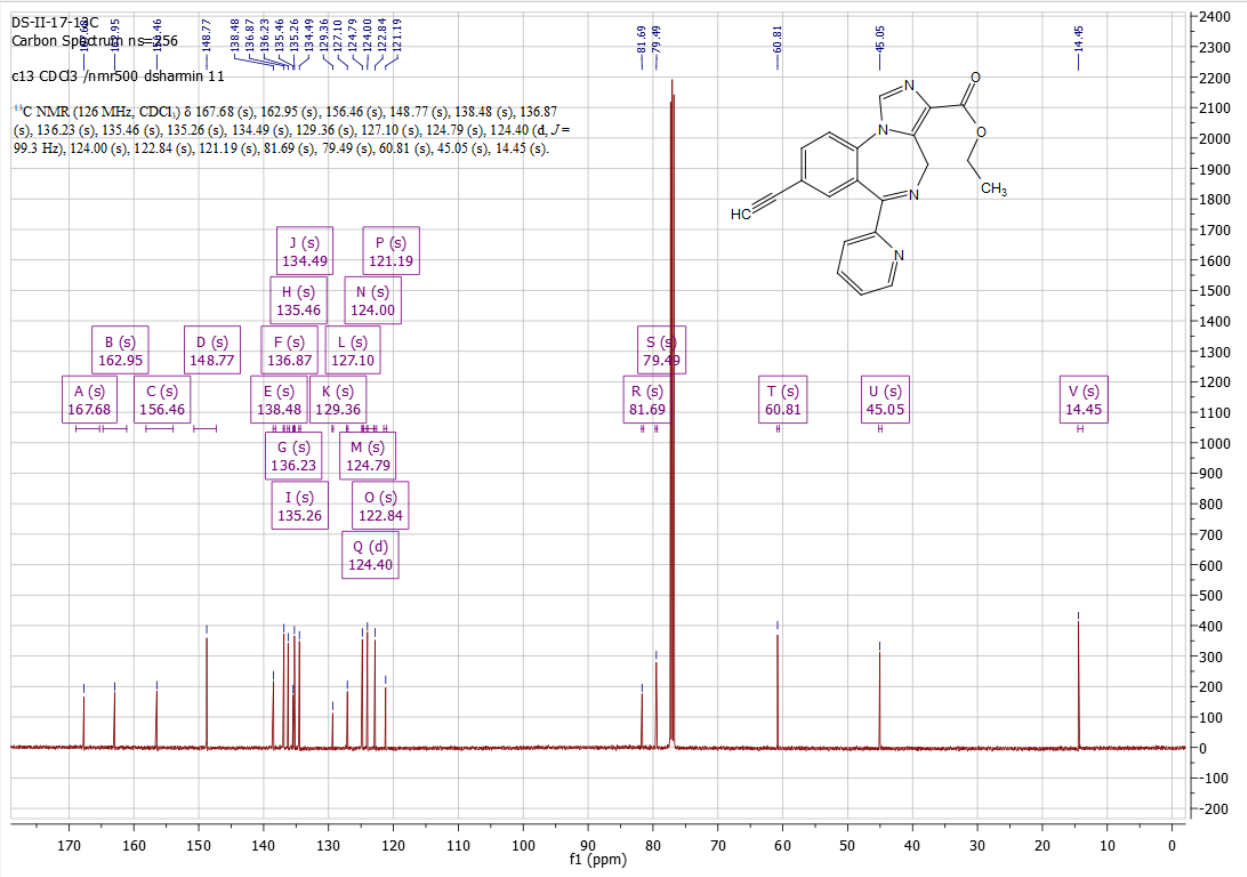



DS-III-15-13C
Carbon Spectrum ns=6256
c13 CDCl3 /nmr500 mmian 8
^{13}C NMR (126 MHz, CDCl$_3$) δ 167.77 (s), 162.97 (s), 156.48 (s), 148.72 (s), 138.51 (s), 136.82 (s), 135.71 (s), 135.33 (s), 134.93 (s), 134.47 (s), 129.28 (s), 126.99 (s), 124.77 (s), 124.02 (s), 122.68 (s), 122.65 (s), 104.87 (s), 93.86 (s), 60.78 (s), 45.05 (s), 18.61 (s), 14.45 (s), 11.23 (s).
A (s) 167.77
B (s) 162.97
C (s) 156.48
D (s) 148.72
E (s) 138.51
F (s) 136.82
G (s) 135.71
H (s) 135.33
I (s) 134.93
J (s) 134.47
K (s) 129.28
L (s) 126.99
M (s) 124.77
N (s) 124.02
O (s) 122.68
P (s) 122.65
Q (s) 104.87
R (s) 93.86
S (s) 60.78
T (s) 45.05
U (s) 18.61
V (s) 14.45
W (s) 11.23
f1 (ppm)

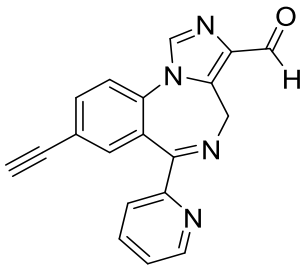
Ethyl 8-ethynyl-6-(pyridin-2-yl)-4H-benzo[f]imidazo[1,5-a][1,4]diazepine-3-carboxylate (HZ-166)

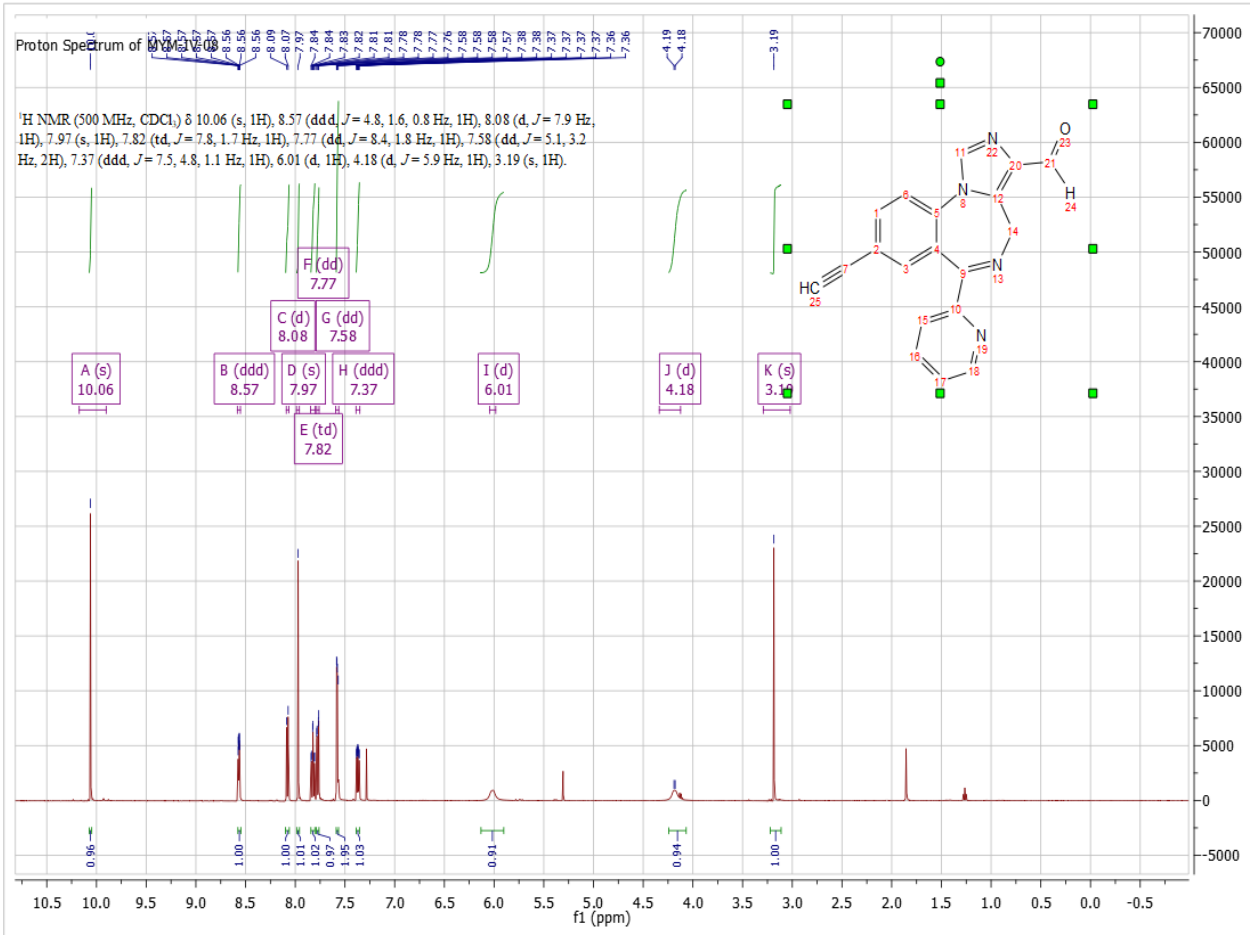


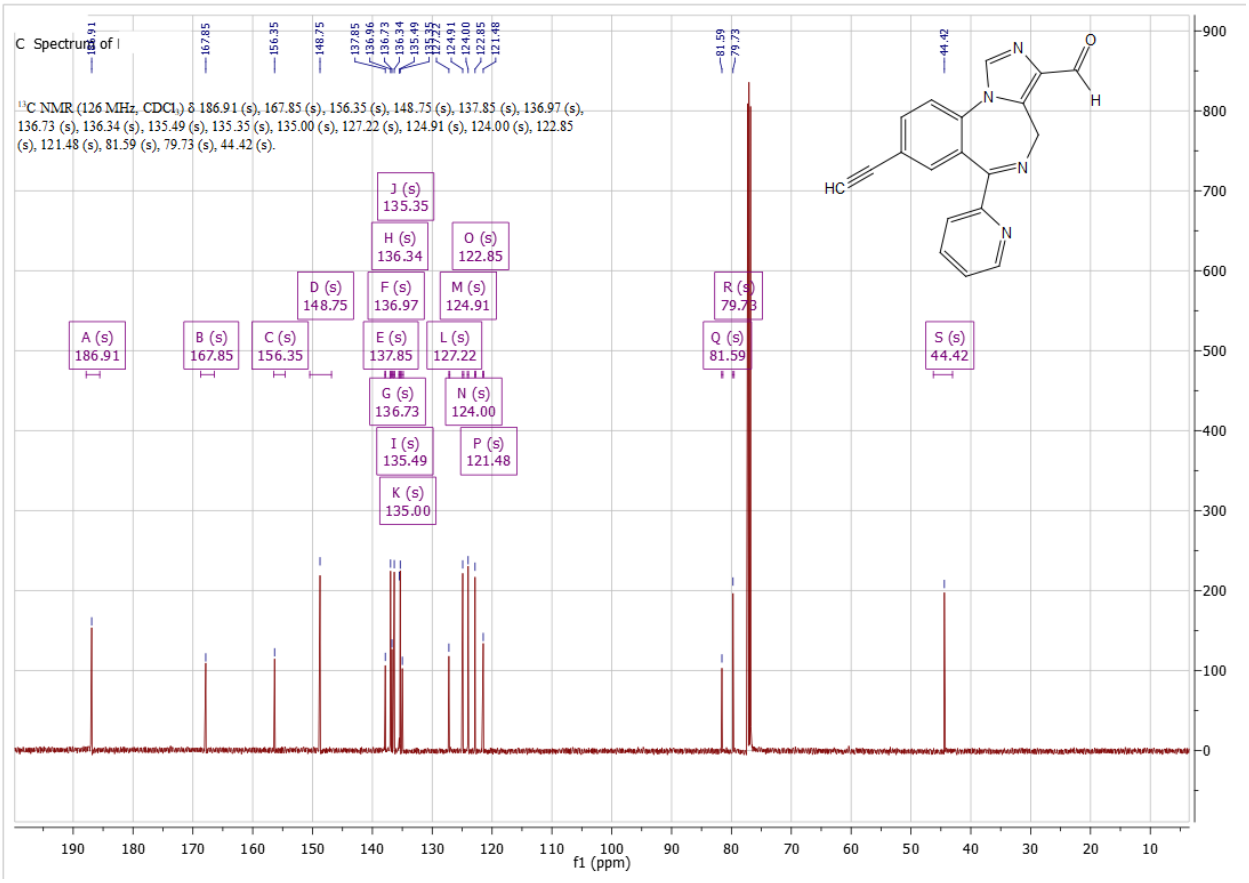



DS-II-17-13C
Carbon Spectrum ns=256
c13 CDCl3 /nmr500 dsharmin 11
^{13}C NMR (126 MHz, $CDCl_3$) δ 167.68 (s), 162.95 (s), 156.46 (s), 148.77 (s), 138.48 (s), 136.87 (s), 136.23 (s), 135.46 (s), 135.26 (s), 134.49 (s), 129.36 (s), 127.10 (s), 124.79 (s), 124.40 (d, J = 99.3 Hz), 124.00 (s), 122.84 (s), 121.19 (s), 81.69 (s), 79.49 (s), 60.81 (s), 45.05 (s), 14.45 (s).
A (s) 167.68
B (s) 162.95
C (s) 156.46
D (s) 148.77
E (s) 138.48
F (s) 136.87
G (s) 136.23
H (s) 135.46
I (s) 135.26
J (s) 134.49
K (s) 129.36
L (s) 127.10
M (s) 124.79
N (s) 124.00
O (s) 122.84
P (s) 121.19
Q (d) 124.40
R (s) 81.69
S (s) 79.49
T (s) 60.81
U (s) 45.05
V (s) 14.45
HC
N
O
CH3
f1 (ppm)

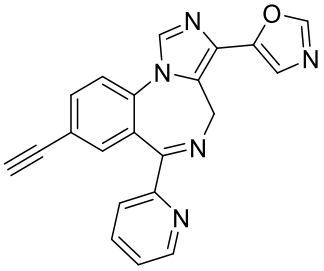
8-Ethynyl-6-(pyridin-2-yl)-4*H*-benzo[*f*]imidazo[1,5-*a*][1,4] diazepine-3-carbaldehyde (HZZ-166 aldehyde)

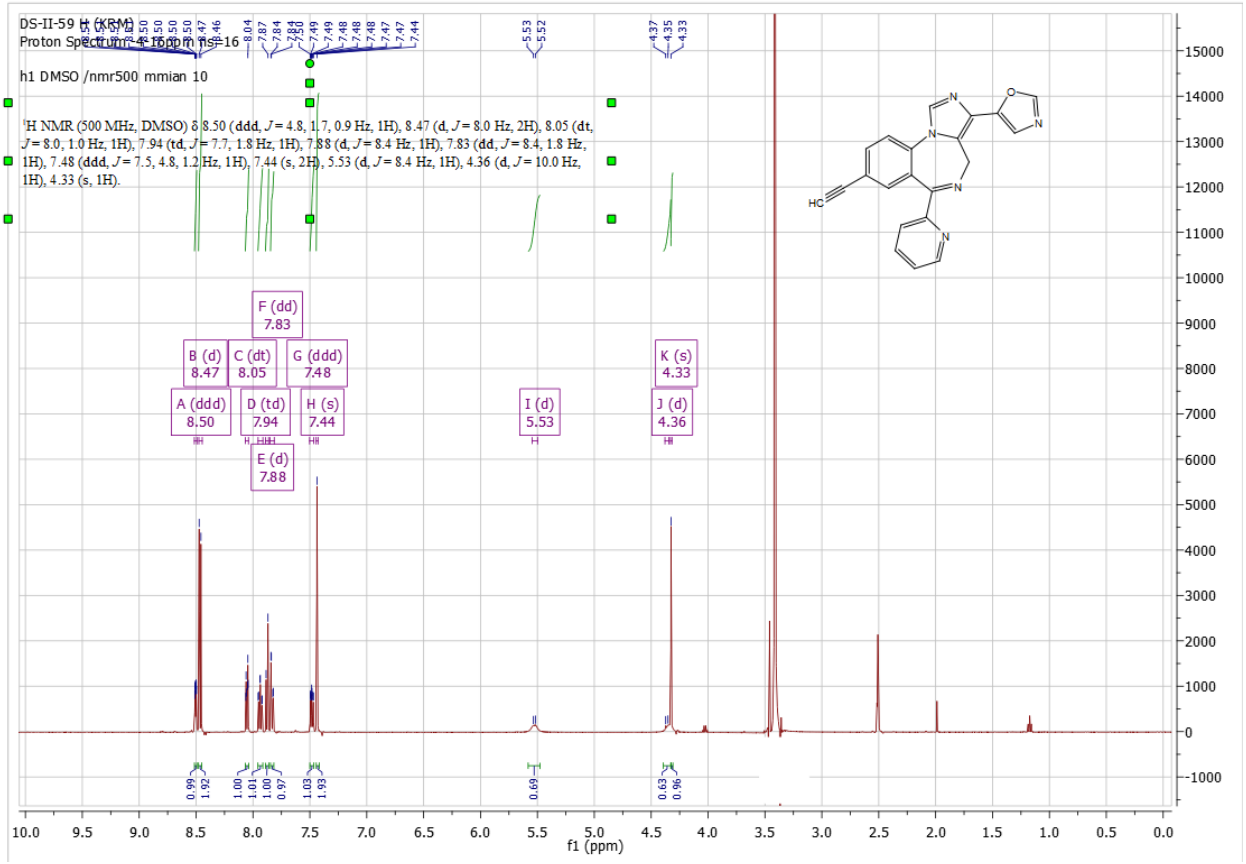


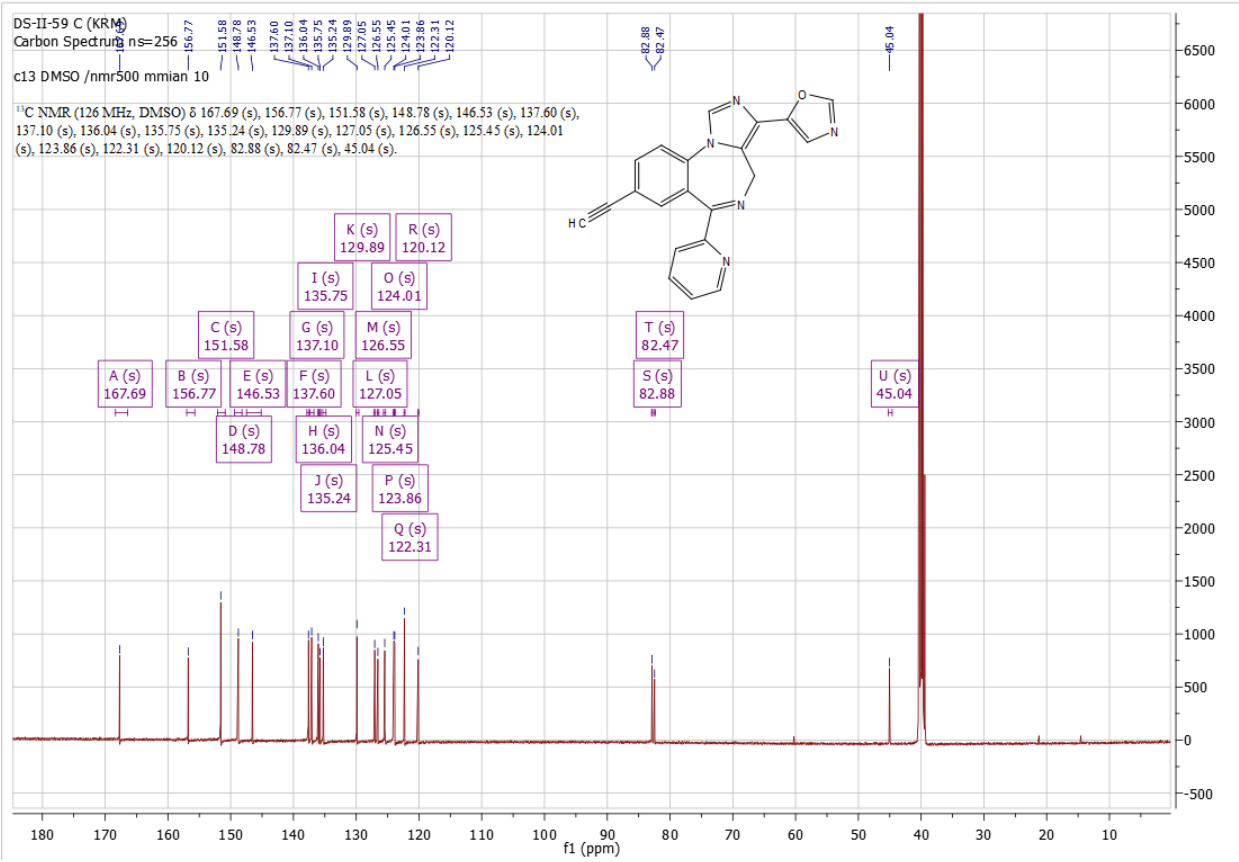



C Spectrum of I
^{13}C NMR (126 MHz, CDCl$_3$) δ 186.91 (s), 167.85 (s), 156.35 (s), 148.75 (s), 137.85 (s), 136.97 (s), 136.73 (s), 136.34 (s), 135.49 (s), 135.35 (s), 135.00 (s), 127.22 (s), 124.91 (s), 124.00 (s), 122.85 (s), 121.48 (s), 81.59 (s), 79.73 (s), 44.42 (s).
A (s) 186.91
B (s) 167.85
C (s) 156.35
D (s) 148.75
E (s) 137.85
F (s) 136.97
G (s) 136.73
H (s) 136.34
I (s) 135.49
J (s) 135.35
K (s) 135.00
L (s) 127.22
M (s) 124.91
N (s) 124.00
O (s) 122.85
P (s) 121.48
Q (s) 81.59
R (s) 79.73
S (s) 44.42
HC
N
O
H
f1 (ppm)

5-(8-Ethynyl-6-(pyridin-2-yl)-4*H*-benzo[*f*]imidazo[1,5-*a*][1,4] diazepin-3-yl)oxazole (KRM-II-81).






DS-II-59 C (KRM)
Carbon Spectrum ns=256
c13 DMSO /nmr500 mmian 10
13C NMR (126 MHz, DMSO) δ 167.69 (s), 156.77 (s), 151.58 (s), 148.78 (s), 146.53 (s), 137.60 (s), 137.10 (s), 136.04 (s), 135.75 (s), 135.24 (s), 129.89 (s), 127.05 (s), 126.55 (s), 125.45 (s), 124.01 (s), 123.86 (s), 122.31 (s), 120.12 (s), 82.88 (s), 82.47 (s), 45.04 (s).
A (s) 167.69
B (s) 156.77
C (s) 151.58
D (s) 148.78
E (s) 146.53
F (s) 137.60
G (s) 137.10
H (s) 136.04
I (s) 135.75
J (s) 135.24
K (s) 129.89
L (s) 127.05
M (s) 126.55
N (s) 125.45
O (s) 124.01
P (s) 123.86
Q (s) 122.31
R (s) 120.12
S (s) 82.88
T (s) 82.47
U (s) 45.04
f1 (ppm)

CURRICULUM VITAE

Dishary Sharmin

LinkedIn: https://www.linkedin.com/in/dishary-sharmin-02a009204/

SUMMARY OF TECHNICAL SKILLS

Medicinal chemist with strong synthetic organic chemistry skills, experienced in multi-step synthesis (milligram to multi-gram scale), knowledgeable with modern analytical techniques including NMR, LC-MS/MS, HPLC, IR and UV spectroscopy.

EDUCATION

PhD in Medicinal Chemistry **Spring 2019-August 2023**

Department of Chemistry and Biochemistry

University of Wisconsin-Milwaukee, Milwaukee, WI

Bachelor of Pharmacy

State University of Bangladesh, Bangladesh **September 2012- December 2016**

cGPA: 3.87 out of 4.0

RESEARCH EXPERIENCE

University of Wisconsin-Milwaukee, Milwaukee, WI **Spring 2019 – August 2023**

***Thesis**: DESIGN, SYNTHESIS, AND BIOLOGICAL EVALUATION OF $GABA_AR$ SUBTYPE SELECTIVE (α6, α2/3, AND α5) LIGANDS TO TREAT MIGRAINE, NEUROPATHIC PAIN, TRIGEMINAL PAIN, TOURETTE SYNDROME, EPILEPSY, ANXIETY AND COGNITIVE DISORDERS AS WELL AS ASTHMA*

Advisor: Prof. James M Cook, PhD

- Developed and optimized synthetic routes for 30+ novel ligands as treatments for migraine, trigeminal pain and Tourette syndrome, depression and epilepsy
- Performed 500g scale synthesis of HZ-166, a precursor of KRM-II-81 (a clinical candidate for epilepsy)
- Performed synthesis of the lead compounds in >100-gram quantities
- Determined overall and optical compound purities using LCMS and HPLC
- Determined physicochemical properties of active drugs, including solubility and hygroscopicity using UV spectroscopy and HPLC

State University of Bangladesh, Bangladesh **September 2012 – December 2016**

Evaluation of antimicrobial, antidiarrheal, analgesic activity of leaves of *Calotropis procera* plants in Bangladesh.

PEER REVIEWED PUBLICATIONS

1. **Sharmin, D**.; Mian, M.Y.; Marcotte, M.; Prevot, T.D.; Sibille, E.; Witkin, J.M.; Cook, J.M. Synthesis and Receptor Binding Studies of α5 $GABA_AR$ Selective Novel Imidazodiazepines Targeted for Psychiatric and Cognitive Disorders. *Molecules* **2023**, *28*, 4771. https://doi.org/10.3390/molecules28124771
2. **Dishary Sharmin**, Branka Divović , Rok Cerne, Jodi L. Smith, Sepideh Revanian, Prithu Mondal, Michelle J. Meyer, Leggy A. Arnold, Md Yeunus Mian, Kamel P. Pandey, Xiaoming Jin, Jelena R. Mitrović, Djordje Djorović, Arnold Lippa, James M. Cook, Xingjie Ping Lalit K. Golani, Miroslav M. Savić, and Jeffrey M. Witkin. A Brominated Analog of the Anti-seizure Compound KRM-II-81 has Anti-seizure Efficacy in Rodents, and Anti-epileptogenic Activity in Neural Networks of Brain Slices from a Patient with Intractable Mesial Temporal Lobe Epilepsy. *ACS Chem Neuroscience*, **2023 (**under review**)**
3. **Dishary Sharmin**, Kamal P. Pandey, Lalit K. Golani, Sepideh Revanian, Md Yeunus Mian, Janet L. Fisher, Arnold Lippa, James M. Cook, Jeffrey M. Witkin, Jodi L. Smith, Jeffrey M. Witkin, Hana Shafique, and Rok Cerne. KRM-II-81, a b3-preferring GABAA receptor potentiator, blocks handling-induced seizures in Theiler's murine encephalomyelitis virus-infected mice. *Psychopharmacology*, **2023** (under review)
4. Adriana Jesus Souza; **Dishary Sharmin**; James M. Cook; Francisco S. Guimarães; Felipe V. Gomes. An alpha 5-GABAa receptor positive allosteric modulator attenuates social and cognitive deficits without changing dopamine system hyperactivity in an animal model for autism. *Biological psychiatry.* **2023 (**under review**).**
5. Lalit K. Golani*, Branka Divović*, **Dishary Sharmin*,** Kamal P. Pandey, Md Yeunus Mian, Rok Cerne, Nicolas M. Zahn, Michelle J. Meyer, Jodi L. Smith, Xingjie Ping, Xiaoming Jin, Arnold Lippa, Jeffrey M. Schkeryantz, Leggy A. Arnold, James M. Cook, Miroslav M. Savić and Jeffrey M. Witkin. Metabolism, pharmacokinetics, and anticonvulsant activity of a deuterated analog of the alpha-2/3-selective GABAkine KRM-II-81. *Biopharmaceutics and drug disposition* **2022**, https://doi.org/10.1002/bdd.2313.

6. Mitrović, J. R.; Bjelošević Žiberna, M.; Vukadinović, A.; Knutson, D. E.; **Sharmin, D**.; Kremenović, A.; Ahlin Grabnar, P.; Planinšek, O.; Lunter, D.; Cook, J. M.; Savić, M. M.; Savić, S. D. Freeze-Dried Nanocrystal Dispersion of Novel Deuterated Pyrazoloquinolinone Ligand (DK-I-56-1): Process Parameters and Lyoprotectant Selection through the Stability Study. *Eur. J. Pharm. Sci.* **2023**, *189* (106557), 106557. https://doi.org/10.1016/j.ejps.2023.106557.

7. Eassa, N.E.; Perez, S.M.; Boley, A.M.; Elam, H.B.; **Sharmin, D**.; Cook, J.M.; Lodge, D.J. α5-GABAA Receptor Modulation Reverses Behavioral and Neurophysiological Correlates of Psychosis in Rats with Ventral Hippocampal Alzheimer's Disease-like Pathology. *Int. J. Mol. Sci.* **2023**, *24*, 11788. https://doi.org/10.3390/ijms241411788

8. McCoy, A.M.; Prevot, T.D.; **Sharmin, D.**; Cook, J.M.; Sibille, E.L.; Lodge, D.J. GL-II-73, a Positive Allosteric Modulator of α5GABA$_A$ Receptors, Reverses Dopamine System Dysfunction Associated with Pilocarpine-Induced Temporal Lobe Epilepsy. *Int. J. Mol. Sci.* **2023**, *24*, 11588. https://doi.org/10.3390/ijms241411588

9. Perez, S.; Eassa, N.; Boley, A.; Elam, H.; **Sharmin, D**.; Cook, J.; Lodge, D. A5-GABAA Receptor Modulation Reverses Behavioral and Neurophysiological Correlates of Psychosis in Rats with Ventral Hippocampal Alzheimer's Disease-like Pathology. *Research Square*, **2023**. https://doi.org/10.21203/rs.3.rs-2809328/v1.

10. Md Yeunus Mian, Branka Divović, **Dishary Sharmin**, Kamal P. Pandey, Lalit K. Golani, V. V. N. Phani Babu Tiruveedhula, Rok Cerne, Jodi L. Smith, Xingjie Ping, Xiaoming Jin, Gregory H. Imler, Jeffrey R. Deschamps, Arnold Lippa, James M. Cook, Miroslav M. Savić, James Rowlett, and Jeffrey M. Witkin. Hydrochloride Salt of the GABAkine KRM-II-81. *ACS Omega* **2022**, 7 (31), 27550-27559. DOI: 10.1021/acsomega.2c03029

11. Angela N Duke, VVN Phani Babu Tiruveedhula, **Dishary Sharmin**, Daniel E Knutson, James M Cook, Donna M Platt, James K Rowlett. Tolerance and dependence following chronic alprazolam treatment in rhesus monkeys: Role of GABAA receptor subtypes. ***2021***. Drug and Alcohol Dependence, 228,108985 https://doi.org/10.1016/j.drugalcdep.2021.108985

12. Md Yeunus Mian, Prithu Mondal, **Dishary Sharmin,** Kamal P. Pandey, Farjana Rashid, Sepideh Rezvanian, Lalit Golani, V.V.N Phani Babu Tiruveedhula, Vilashini Rajaratnam, Shama P Mirza, John D

Chan, James M Cook. An efficient debromination technique using PMHS with a number of ligands containing different functional groups. *Arkivoc* **2021**, 171-188. DOI: https://doi.org/10.24820/ark.5550190.p011.712

13. Atiqur Rahman, Thomas M. Keck, Michael M. Poe, **Dishary Sharmin**, James M. Cook, Bradford D. Fischer. Synergistic antihyperalgesic and antinociceptive effects of morphine and methyl 8-ethynyl-6-(pyridin-2-yl)-4H-benzo[f]imidazo [1,5-a][1,4]diazepine-3-carboxylate (MP-III024), a positive allosteric modulator at α2GABAA and α3GABAA receptors. ***2021***. *Psychopharmacology* 238, 1585–1592 https://doi.org/10.1007/s00213-021-05791-1
14. Xingjie Ping, Michelle J Meyer, Nicolas M Zahn, Lalit K Golani, **Dishary Sharmin**, Kamal P Pandey, Sepideh Revanian, Prithu Mondal, Xiaoming Jin, Leggy A Arnold, Rok Cerne, James M Cook, Branka Divović, Miroslav M Savić, Arnold Lippa, Jodi L Smith, Jeffrey M Witkin. Comparative anticonvulsant activity of the GABAkine KRM-II-81 and a deuterated analog. *Drug Development Research* **2023**. https://doi.org/10.1002/ddr.22042
15. Ashley M Bernardo, Michael Marcotte, Kayla Wong, **Dishary Sharmin**, Kamal Prandey, James M Cook, Etienne Sibille, Thomas Damien Prevot. Positive allosteric modulation of α5-GABA A Receptor in the 5XFAD mouse model has cognitive and neurotrophic benefits. bioRxiv **2022**, 09(30),510361. doi: https://doi.org/10.1101/2022.09.30.510361
16. Tanya Pareek, John S Overton, Luat T Nguyen, Md Toufiqur Rahman, **Dishary Sharmin**, James M Cook, Donna M Platt. Modeling cue-exposure therapy for alcohol use disorder in rhesus monkeys: Effects of putative cognitive enhancers. *Drug and Alcohol Dependence* **2023**, 243, 109735. https://doi.org/10.1016/j.drugalcdep.2022.109735
17. Milia Gajic Bojic,Lidija Todorovic, Anja Santrac, Md Yeunus Mian, **Dishary Sharmin**, James M Cook, Miroslav Savic. Vasodilatory effects of a positive allosteric modulators of GABAA receptors on rat thoracic aorta. *European Journal of Pharmacology* **2020**, 899,174023. https://doi.org/10.1016/j.ejphar.2021.174023
18. Anja Santrač, Bojan Batinić, Tamara Timić Stamenić, Jovana Aranđelović, **Dishary Sharmin**, Daniel E Knutson, James M Cook, Miroslav M Savić. Positive modulation of α5GABAA receptors leads to dichotomous effects in rats on memory pattern and GABRA5 expression in prefrontal cortex and hippocampus. *Behavioural Brain Research* **2022**, 416,113578. https://doi.org/10.1016/j.bbr.2021.113578

19. Ashley Bernardo, Philip Lee, Michael Marcotte, Yeunus Mian, Zubair A Khan, **Dishary Sharmin**, James M Cook, Etienne Sibille, Thomas Damien Prevot. Symptomatic and Disease-Modifying Effects of GABAA Receptor Positive Allosteric Modulation in a Mouse Model of Chronic Stress. bioRxiv **2021**. DOI: 10.1101/2021.03.22.436517

20. A. Biggerstaff, B. Kivella, J.L. Smith , Md Y. Mian , L.K. Golani , F. Rashid , D. Sharmin , D.E. Knutson, R. Cerne , J.M. Cook, J.M. Witkin. The α2,3-selective potentiators of GABAA receptors, KRM-II-81 and MP-III-80, produce anxiolytic-like effects and block chemotherapy-induced hyperalgesia in mice without tolerance development. *Pharmacology, Biochemistry and Behavior* **2020,** 196, 172996. https://doi.org/10.1016/j.pbb.2020.172996

21. Lalit K Golani† , Md Yeunus Mian† , Taukir Ahmed, Kamal Pandey, Prithu Mondal, **Dishary Sharmin**, Sepideh Rezvanian, Jeffrey M Witkin, James M Cook. Rationalizing the Binding and α Subtype Selectivity of Synthesized Imidazodiazepines and Benzodiazepines at GABAA Receptors by Using Molecular Docking Studies. *Biorganic and medicinal chemistry letters*, **2022**, 62, 128637. https://doi. org/10.1016/j.bmcl.2022.128637

22. Ashley Bernardo, Philip Lee, Michael Marcotte, Md Yeunus Mian, Sepideh Rezvanian, **Dishary Sharmin**, Aleksandra Kovačević, Miroslav M Savić, James M Cook, Etienne Sibille, Thomas D Prevot. Symptomatic and neurotrophic effects of GABAA receptor positive allosteric modulation in a mouse model of chronic stress. *Neuropsychopharmacology* **2022**, 47(9), 1608-1619. https://doi.org/10.1038/s41386-022-01360-

23. Kamal P. Pandey, Branka Divović, Farjana Rashid, Lalit K. Golani, Rok Cerne, Nicolas M. Zahn, Michelle Jean Meyer, Leggy A. Arnold, **Dishary Sharmin**, Md Yeunus Mian, Jodi L. Smith, Xingjie Ping, Xiaoming Jin, Arnold Lippa, V.V.N. Phani Babu Tiruveedhula, James M. Cook, Miroslav M. Savić, Jeffrey M. Witkin. Structural Analogs of the GABAkine KRM-II-81 Are Orally Bioavailable Anticonvulsants without Sedation. *Journal of Pharmacology and Experimental Therapeutics* **2023**, 385 (1), 50-61. https://doi.org/ 10.1124/jpet.122.001362

24. Barbara Kosmowska, Martyna Paleczna, Dominika Biała, Justyna Kadłuczka, Jadwiga Wardas, Jeffrey M Witkin, James M Cook, **Dishary Sharmin**, Monika Marcinkowska, Katarzyna Z Kuter. GABA-A Alpha 2/3 but Not Alpha 1 Receptor Subunit Ligand Inhibits Harmaline and PimozideInduced Tremor in Rats. *Biomolecules* **2023**, 13(2), 197; https://doi.org/10.3390/biom13

25. Jovana Arandelovic, Anja Santrac, Bojan Batinic, Lidija Todorovic, Vladimir Stevanovic, Veera Venkata Naga Phani Babu Tiruveedhula, **Dishary Sharmin**, Farjana Rashid, Boban Stanojevic, James M Cook, Miroslav M Savic. Effects of alpha 5 GABA (A) receptor modulation on social interaction, memory, and neuroinflammation in a mouse model of Alzheimer's disease. *CNS NEUROSCIENCE & THERAPEUTICS* **2022**, 28(11), 1767-1778. https://doi.org/10.1111/cns.13914

26. Adriana Jesus Souza; Isadora L. Cortez; Nicole R. Silva; João Francisco C. Pedrazzi; Luana B. Domingues; Matheus Silva Braga; Thamyris Santos-Silva; Elaine A. Del-Bel; Leonardo B. M. Resstel; Guanguan Li; Md Yeunus Mian; **Dishary Sharmin**; Francisco S. Guimarães; James Cook; Felipe V. Gomes. Distinct sex-dependent behavioral responses induced by two positive allosteric modulators of alpha 5 subunit-containing GABAA receptors. *Behavioural Brain Research* **2022**, 428, 113832. https://doi.org/10.1016/j.bbr.2022.113832

27. Anja Santrač, Dunja Bijelić, Vladimir Stevanović, Marija Banićević, Jovana Aranđelović, Bojan Batinić, **Dishary Sharmin,** James M Cook, Miroslav M Savić. Postweaning positive modulation of α5GABAA receptors improves autism-like features in prenatal valproate rat model in a sex-specific manner. *Autism Research* **2022**, 15(5), 806-820. https://doi.org/10.1002/aur.2699

28. Jeffrey M. Witkin, Arnold Lippa, Jodi L. Smith, Xiaoming Jin, Xingjie Ping, Andrew Biggerstaff, Bronwyn M. Kivell, Daniel E. Knutson, **Dishary Sharmin**, Kamal P. Pandey, Md Yeunus Mian, James M. Cook, Rok Cerne. The imidazodiazepine, KRM-II-81: An example of a newly emerging generation of GABAkines for neurological and psychiatric disorders. *Pharmacology Biochemistry and Behavior* **2022**, 213, 173321. https://doi.org/10.1016/j.pbb.2021.173321

29. Ya-Hsien Huang, Ming Tatt Lee, Werner Sieghart, Daniel E Knutson, Laurin R Wimmer, **Dishary Sharmin**, James Cook, Marko D Mihovilovic, Lih-Chu Chiou. Positive modulation of cerebellar α6GABAA receptors for treating essential tremor: a proof-of-concept study in harmaline-treated mice. **2021**. doi: https://doi.org/10.1101/2021.04.19.440397

30. Kamal P Pandey, Md Zubair Ahmed Khan, Lalit K Golani, Prithu Mondal, Md Yeunus Mian, Farjana Rashid, VVN Phani Babu Tiruveedhula, Daniel E Knutson, **Dishary Sharmin**, Taukir Ahmed, Sepideh Rezvanian,Nicolas M Zahn, Leggy A Arnold, Jeffrey M Witkin, James M Cook. Design, synthesis and

characterization of novel gamma-aminobutyric acid type A receptor ligands. *ARKIVOC* **2020**, (Pt 7), 242–256. doi:10.24820/ark.5550190.p011.398.

CONFERENCE PAPER

1. Thomas Prevot, Ashley Bernardo, Philip Lee, Michael Marcotte, Daniel Knutson, **Dishary Sharmin**, Yeunus Mian, James Cook, Etienne Sibille. Positive Allosteric Modulation at α5-GABAA Receptor Reverses Cognitive Dysfunctions and Neuronal Atrophy in Mouse Model of Chronic Stress. **2021**. *Biological psychiatry*. DOI:https://doi.org/10.1016/j.biopsych.2021.02.540
2. Bradford Fischer, Mohammad Rahman, Thomas Keck, Michael Poe, **Dishary Sharmin**, James Cook. 2021. Supra-additive effects of morphine and the α2/3 preferring GABAA receptor ligand MP-III-024 on mechanical hyperalgesia and thermal nociception. https://doi.org/10.1096/fasebj.2021.35.S1.03252
3. Sara Uribe, Eric J DiDomenico, Christa M Donegan, Yulista Tapia, Jason Conviser, Rohit R Nambiar, Amy A Juarez, Christine M Side, Danya Aldaghma, Michael M Poe, **Dishary Sharmin**, James M Cook, Thomas M Keck, Bradford D Fischer. Assessing the synergistic effects of morphine and MP-III-024 co-adminis. *The FASEB Journal* **2022**, 36. https://doi.org/10.1096/fasebj.2022.36.S1.R5946
4. Thomas Prevot, Ashley Bernardo, Michael Marcotte, Md Yeunus Mian, **Dishary Sharmin**, James Cook, Etienne Sibille. P99. Role of α5-GABAA Receptor Positive Allosteric Modulation on Cognitive Functions and Neurotrophic Effects Across Animal Models. *Biological Psychiatry* **2022**, 91 (9), S127. DOI: https://doi.org/10.1016/j.biopsych.2022.02.333
5. Prevot, T.; Bernardo, A.; Wong, K.; Pina-Leblanc, C.; Marcotte, M.; Mian, M. Y.; Sharmin, D.; Cook, J.; Sibille, E. Improvement of Cognitive Functions and Neurotrophic Effects across Animal Models Mediated by α5-GABAA Receptor Positive Allosteric Modulation. *Biol. Psychiatry* **2023**, *93* (9), S5. https://doi.org/10.1016/j.biopsych.2023.02.033.
6. Indu Mithra Madhuranthakam, Sarah Uribe, Danya Aldaghma, Drew Kwitchoff, Jonathan Philip, Aela A. Williams, Rohit A. Nambiar, **Dishary Sharmin**, James Cook, Bradford Fischer and Thomas Keck. Widening the Opioid Analgesia Therapeutic Window with a Dual Pharmacology Strategy. *Journal of*

Pharmacology and Experimental Therapeutics **2023**, 385 (S3) 405; DOI: https://doi.org/10.1124/jpet.122.269240.

POSTER PRESENTATION:

1. **Dishary Sharmin**, Kamal P. Pandey, Md Yeunus Mian, Sepideh Rezvanian , Prithu Mondal, Branka Divović , Xingjie Ping , Miroslav M. Savić, Jeffrey M. Witkin, James M. Cook. Synthesis, metabolism, pharmacokinetics, and anticonvulsant activity of a deuterated analog of the α2/3-selective GABAkine KRM-II-81. 264th ACS Fall 2022 Meeting & Exposition.(Paper ID: 3753553)
2. **Dishary Sharmin**, Daniel Knutson, Ming T. Lee, Werner Sieghart, Lih-Chu Chio, James Cook. Development of α6GABAA receptor positive allosteric modulators to treat migraine via compensating GABAergic deficits in Trigeminal Ganglia. 263rd ACS Spring 2022 Meeting & Expo. (Paper ID: 3641926)
3. **Dishary Sharmin**, Mohammad A. Rahman, Michael M. Poe, Thomas M. Keck, Bradford D. Fischer, James M. Cook. Synthesis of MP-III-024, a positive allosteric modulator at α2GABAA and α3GABAA receptors and its biological evaluation as combination therapy with morphine for antihyperalgesia. ACS Milwaukee, Fall 2021.
4. **Dishary Sharmin**, Mohammad A. Rahman, Michael M. Poe, Thomas M. Keck, Bradford D. Fischer, James M. Cook. Synthesis of MP-III-024, a positive allosteric modulator at α2GABAA and α3GABAA receptors and its biological evaluation as combination therapy with morphine for antihyperalgesia. Chemistry and Biochemistry Annual Research Symposium 2022, UW-Milwaukee.
5. Md Yeunus Mian, Prithu Mondal, **Dishary Sharmin**, Farjana Rashid, V.V.N Phani Babu Tiruveedhula, Lalit Golani , John D Chan , Ashley Bernardo, Philippe Lee, Michael Marcotte, Etienne Sibille, Thomas D. Prevot, James M Cook. Non-sedating anti-schistosomal imidazodiazepines cause disruption of the tegument of Schistosoma mansoni and GABAA receptor positive allosteric modulators show disease-modifying effects in a mouse model of chronic stress. 262nd ACS Fall 2021 Meeting & Expo, PAPER ID: 3593061

6. Md Yeunus Mian, Prithu Mondal, **Dishary Sharmin**, VVN Phani Babu Tiruveedhula, Lalit K Golani, Farjana Rashid, James M Cook, John D Chan. Design and synthesis of anti-schistosomal drug with decreased sedation. Chemistry and Biochemistry Research Symposium, UW Milwaukee, 2021
7. Md Yeunus Mian, Prithu Mondal, **Dishary Sharmin**, Sepideh Rezvanian, Farjana Rashid, Ashley Bernardo, Philippe Lee, Michael Marcotte, Etienne Sibille, Thomas D. Prevot, James M Cook. Synthesis of GL-RM, a GABAA receptor positive allosteric modulators and evaluation of its diseasemodifying effects in a mouse model of chronic stress. ACS Milwaukee, Fall 2021.
8. Sepideh Rezvanian, Farjana Rashid, Md Yeunus Mian, Pirthu Mondal**, Dishary Sharmin**, Kamal Pandey, Ashley Bernardo, Philippe Lee, Michael Marcotte, Etienne Sibille, Thomas D. Prevot, James M Cook. Synthesis and Analysis of the Anti-depressant Activity of GL-I-54, a Positive Allosteric GABAA Receptor Modulator. ACS Milwaukee, Fall 2021.
9. Prithu Mondal, Md Yeunus Mian, Kamal P Pandey, **Dishary Sharmin**, Thomas D. prevot, Akiko Sumimoto, Toshifumi Tomoda , Daniel Knutson, Guanguan Li, Mounira Banasr, Etienne Sibille , James M. Cook. Alpha-5 GABA-A receptor potentiation as a treatment for behavioral deficits. 263rd ACS Spring 2022 Meeting & Expo .
10. Prithu Mondal, Md Yeunus Mian, Kamal P Pandey, **Dishary Sharmin**, Thomas D. prevot, Akiko Sumimoto, Toshifumi Tomoda , Daniel Knutson, Guanguan Li, Mounira Banasr, James M. Cook. Synthesis of a ligand capable of binding to a GABAA receptor as a treatment for psychological disorders. 262nd ACS Fall 2021 Meeting & Expo
11. Kamal P. Pandey, Jeffrey M Witkin, Lalit K. Golani, Md Yeunus Mian, Prithu Mondal, V. V. N. Phani Babu Tiruveedhula, **Dishary Sharmin**, Sepideh Rezvanian, Kashi R. Methuku, Michael M. Poe, Nicolas M. Poe, Zahn, Michelle J. Meyer, Leggy A. Arnold, James M. Cook. Synthesis of analogs of KRM-II-81, Gamma Aminobutyric Acid Type A (GABAA) Receptor α2/α3 Subtype-selective Ligand, for Epilepsy Treatment without any adverse effects. ACS National Meeting and Exposition Fall-2022. https://doi.org/10.1021/scimeetings.2c00346
12. Kamal P. Pandey, Jeffrey M Witkin, Lalit K. Golani, Md Yeunus Mian, Prithu Mondal, V. V. N. Phani Babu Tiruveedhula, **Dishary Sharmin**, Sepideh Rezvanian, Kashi R. Methuku, Michael M. Poe, Nicolas M. Poe, Zahn, Michelle J. Meyer, Leggy A. Arnold, James M. Cook. Design, synthesis, and

characterization of novel analogs of clinically progressing gamma-aminobutyric acid type A (GABAA) receptor α2/α3 subtype-selective ligand KRM-II-81. 263rd ACS Spring 2022 Meeting & Expo. https://doi.org/10.1021/scimeetings.2c00059

13. S. Rezvanian, F. Rashid, M.Y. Mian, **D. Sharmin**, P. Mondal, K. Pandey, A. Bernardo, P. Lee, M. Marcotte, E. Sibille, T. D. Prevot, J. M. Cook. GL-I-54, a Non-selective α2/3/5-GABAA receptor positive allosteric modulator shows disease modifying effects in chronic stress of mouse models. 263rd ACS Spring 2022 Meeting & Expo.

ADDITIONAL EXPERIENCE

Department of Chemistry and Biochemistry, University of Wisconsin-Milwaukee, Milwaukee, WI

- Graduate Research Assistant (June 2021- present)
- Laboratory Preparation Technician (January 2021- May 2021)
    - Operating and maintaining chemical stockroom and instructional laboratories
    - Reporting any problems with the physical space to the Laboratory Technical Support Supervisor
    - Preparing, setting up, and taking down experiments for General, Physical and Organic Chemistry instructional laboratories
    - Maintaining a service counter for the distribution of chemicals, supplies and equipment to teaching assistants and faculty for instructional chemistry laboratories
    - Maintaining and operating laboratory instruments
    - Monitoring the inventory of chemicals and supplies for instructional laboratories and initiate ordering process as needed
    - Receiving chemical orders, entering, and removing materials from the chemical inventory system
    - Monitoring instructional lab activities to ensure that appropriate safety precautions are used
    - Coordinating the safe storage, handling, disposal, and recordkeeping of hazardous chemicals and chemical waste
    - Keeping laboratory benches and reagent shelves clean and orderly
    - Providing instructional support
- Graduate Teaching Assistant (January 2019- December 2020)
    - Aiding faculty members with lecture and laboratory instructions, exams and record keeping
    - Preparing laboratories activities on a weekly basis, and providing tutoring to enrolled students

Beximco Pharmaceuticals Limited, Dhaka, Bangladesh

- Industrial training in formulation and packaging, December 2016-January 2017

TEACHING EXPERIENCE

- CHEM 104 General Chemistry and Qualitative Analysis
- CHEM 344 Organic Chemistry Laboratory